

AGARD

ADVISORY GROUP FOR AEROSPACE RESEARCH & DEVELOPMENT

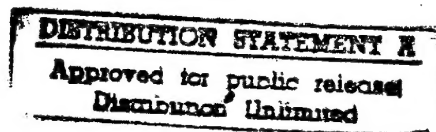
7 RUE ANCELLE, 92200 NEUILLY-SUR-SEINE, FRANCE

AGARD CONFERENCE PROCEEDINGS 585

Aerodynamics of Wind Tunnel Circuits and their Components

(l'Aérodynamique des circuits des souffleries et de leurs composants)

Papers presented and discussions recorded at the 79th Fluid Dynamics Panel Symposium held in Moscow, Russia, 30 September - 3 October 1996.



North Atlantic Treaty Organization
Organisation du Traité de l'Atlantique Nord

19970722 165

DTIC QUALITY INSPECTED 4

The Mission of AGARD

According to its Charter, the mission of AGARD is to bring together the leading personalities of the NATO nations in the fields of science and technology relating to aerospace for the following purposes:

- Recommending effective ways for the member nations to use their research and development capabilities for the common benefit of the NATO community;
- Providing scientific and technical advice and assistance to the Military Committee in the field of aerospace research and development (with particular regard to its military application);
- Continuously stimulating advances in the aerospace sciences relevant to strengthening the common defence posture;
- Improving the co-operation among member nations in aerospace research and development;
- Exchange of scientific and technical information;
- Providing assistance to member nations for the purpose of increasing their scientific and technical potential;
- Rendering scientific and technical assistance, as requested, to other NATO bodies and to member nations in connection with research and development problems in the aerospace field.

The highest authority within AGARD is the National Delegates Board consisting of officially appointed senior representatives from each member nation. The mission of AGARD is carried out through the Panels which are composed of experts appointed by the National Delegates, the Consultant and Exchange Programme and the Aerospace Applications Studies Programme. The results of AGARD work are reported to the member nations and the NATO Authorities through the AGARD series of publications of which this is one.

Participation in AGARD activities is by invitation only and is normally limited to citizens of the NATO nations.

The content of this publication has been reproduced
directly from material supplied by AGARD or the authors.

Published June 1997

Copyright © AGARD 1997
All Rights Reserved

ISBN 92-836-0042-8



*Printed by Canada Communication Group Inc.
(A St. Joseph Corporation Company)
45 Sacré-Cœur Blvd., Hull (Québec), Canada K1A 0S7*

Aerodynamics of Wind Tunnel Circuits and their Components

(AGARD CP-585)

Executive Summary

The aim of this Symposium was to gather and review both current knowledge and ongoing research on the aerodynamic design and evaluation of ground test facilities, focusing primarily on wind tunnels, in order to provide to the designers of experimental facilities an opportunity to exchange information, ideas, and visions. Shrinking budgets for new facilities have led to fewer facilities being developed and longer development times, which have in turn led to less opportunity for advances in the state-of-the-art and for the retention of the experts needed for the design of good experimental facilities.

The normal overriding user objectives, when conducting almost any kind of wind-tunnel test, are obtaining reliable and meaningful data in a timely and cost-effective manner. Principal requirements for obtaining reliable and meaningful data are an adequate Reynolds number, representative or satisfactory tunnel flow quality, and the avoidance of tunnel wall and support system effects. Factors which are important in satisfying the timeliness and cost effectiveness requirements include minimizing the time required for model installation and configuration changes, utilization of efficient data gathering systems, and the ability to use rapid techniques to account for tunnel wall and support system interference effects. Since the aerodynamic design of wind-tunnel circuits has a fundamental first order effect on tunnel flow quality, tunnel wall and support interference effects, and on tunnel construction costs, the adequacy of the circuit design is of crucial importance in meeting the user's objectives.

It should be noted that this was the first AGARD Symposium held in Russia, and that 50% of the papers were by Russian authors. Much information was shared by those who are involved in developing, operating, and utilizing experimental ground test facilities.

L'aérodynamique des souffleries et de leurs composants

(AGARD CP-585)

Synthèse

Le symposium avait pour objectif de recueillir et d'évaluer les connaissances actuelles et la recherche en cours dans le domaine de la conception aérodynamique et dans l'évaluation des installations d'essais au sol, en mettant l'accent sur les souffleries, afin de permettre aux concepteurs des installations expérimentales l'occasion d'échanger des informations, des idées et des projets futurs. De moins en moins de souffleries sont en cours de développement et leur délais de réalisation sont de plus en plus longs en raison des réductions budgétaires. Par conséquent, des possibilités moindres existent pour des percées dans l'état de l'art et pour la formation et le maintien des spécialistes demandés pour la conception d'installations expérimentales de bonne qualité.

L'objectif primordial de l'utilisateur chargé de la réalisation d'essai en soufflerie est d'obtenir des données fiables et significatives de façon rentable et en temps voulu. Les principales conditions requises pour l'obtention de données fiables et significatives sont de disposer d'un nombre de Reynolds adéquat, d'une qualité d'écoulement représentative ou du moins satisfaisante et d'éviter les effets de paroi et de bâti.

Les facteurs qui permettent d'obtenir la rentabilité et l'opportunité comprennent notamment la réduction au minimum du temps demandé pour l'installation de la maquette et pour les éventuels changements de la configuration, ainsi que l'emploi de systèmes efficaces de collecte de données et le recours à des techniques rapides pour la prise en compte des effets de paroi et de bâti.

La conception aérodynamique des circuits de soufflerie a un effet fondamental de premier ordre sur la qualité des écoulements, les effets de paroi et de bâti et les coûts de construction. La justesse de la conception des circuits est d'une importance capitale pour la satisfaction des desiderata de l'utilisateur.

Il est à noter qu'il s'agissait du premier symposium AGARD à être organisé en Russie, et que 50% des communications présentées ont été proposées par des auteurs russes. Un volume important d'informations a été échangé entre ceux qui, d'une part ont pour tâche de développer, et d'autre part d'exploiter et d'utiliser les installations expérimentales d'essais au sol.

Contents

	Page
Executive Summary	iii
Synthèse	iv
Recent Publications of the Fluid Dynamics Panel	viii
Fluid Dynamics Panel	x
	Reference
Technical Evaluation Report by F.W. Steinle, Jr.	T
Historical Review of the Creation and Improvement of Aerodynamic Test Facilities at TsAGI by E.L. Bedrzhitsky and V.P. Roukavets	1
Some Constraints Imposed on the Aerodynamic Development Process by Wind-Tunnel Circuit Design Characteristics by F.T. Lynch and R.C. Crites	2
General Design Aspects of Low Speed Wind Tunnels by F. Jaarsma	3
The Aerodynamic and Structural Design of the DRA 5-Metre and ONERA F1 Low-Speed Pressurised Wind Tunnels by D.S. Woodward, G. François and N.J. Taylor	4
Subsonic Wind Tunnel with Flow Speed Pulsation by M.P. Ryabokon and A.G. Malyk	5
Aerodynamic Design of a Civil-Aeronautical Low Speed Large Wind Tunnel by G. Gibertini, L. Gasparini and A. Zasso	6
Experimental and Computational Aerodynamics Applications for an Icing Wind Tunnel Design by F. De Gregorio, B. Esposito, G. Mingione and A. Vicini	7
Development of Boeing Research Aerodynamic Icing Tunnel Circuit by S. Chintamani, D. Delcarpio and G. Langmeyer	8
Paper 9 cancelled	
New Test Cell Design Methods Based on Integrated Usage of Calculated and Experimental Researches by I.I. Kabakov and A.N. Timoshin	10
ETW Aerodynamic Design -A Case Study- by X. Bouis, J. Prieur, J.A. Tizard and G. Hefer	11

Control and Mathematical Model of Transonic Wind Tunnels (<i>Modélisation et pilotage des souffleries transsoniques</i>) by J.L. Gobert	12
Elaboration of Cryogenic Transonic Short-Duration Wind Tunnel at ITAM by V.I. Zvegintsev and A.I. Omelaev	13
The Impulse Transonic Wind Tunnel U-11. New Effective Technology for Generation of Sub-, Trans- and Supersonic Gas Flow by V.V. Kislykh, V.V. Koudriavtsev, O.V. Petrova and V.V. Puchkov	14
A New Tool for Screen Integration in Internal Flow Systems and its Application to Wind Tunnel Design by M.M. Seltsam	15
Adaptive-Wall Perforated Test Section for Transonic Wind Tunnels by V.M. Neyland, A.I. Ivanov, A.V. Semenov, O.K. Semenova, and G.A. Amirjanz	16
Alleviation of Axial Static Pressure Gradients in 2D Perforated Test Section of IAR Blowdown Wind Tunnel by F.C. Tang and Y.Y. Chan	17
Evaluating Analytically and Experimentally the Gas Dynamics of Transonic Wind Tunnels with Devices for Air Evacuation from Plenum Chamber by V.P. Verkhovsky, O.V. Lyzhin and Z.G. Pasova	18
Adaptive Slots: An Alternative Concept to Reduce Wall Interference by J. Quest, W. Nitsche and A. Mignosi	19
Progress in Determining Wall-Induced Interference in Slotted-Liner Wind Tunnels Using Measured Wall Conditions by M.M. Freestone and D.M. Sykes	20
Aerodynamic Design of Axial-Flow Fans for Subsonic Wind Tunnels by I.V. Brusilovsky	21
Ejector-Driven Wind Tunnels by Yu. K. Arkodov and V.P. Roukavets	22
Improving Transonic Wind Tunnel Compressor Operation by Means of Guide Vane Angle Optimization by A.G. Kukinov, G.E. Dyadchenko, A.A. Lunyov and V.S. Panasenko	23
Development of Closed-Circuit Subsonic Wind Tunnel with Diametral Fan by A.G. Korovkin, V.D. Savchuk and V.K. Kuroles	24
Experimental Study of a Low-Speed Wind Tunnel Test Section with a Free Jet by V.P. Roukavets, A.P. Byrkin, A.L. Iskra, A.P. Filatov, V.V. Troitsky, V.C. Ponomaryova, D. Holzdeppe, H.D. Papenfuss, and D. Barbagallo	25A
Lowering the Turbulence Level in an Open-Jet Wind Tunnel by Novel Adjustable Jet-Exit Vanes by H.D. Papenfuss, D. Holzdeppe, W. Lorentz-Meyer, V.P. Roukavets and A.P. Filatov	25B
Model and Full Scale Investigations of the Low Frequency Vibration Phenomena of the DNW Open Jet by H. Holthausen and J.W. Kooi	26

Self-Oscillation Flow Control in Free-Jet Wind Tunnels by A.S. Ginevsky	27
Turbulence and Noise Criteria and their Implementation in NWTC-Type Wind Tunnels by E. Reshotko, W.S. Saric and H.M. Nagib	28
Conception et Qualification de la soufflerie Silencieuse R1Ch de l'ONERA <i>(Design & Validation of a Quiet Supersonic Wind Tunnel)</i> by O. Papirnyk, G. Rancarani, J. Délery and D. Arnal	29
Characteristics of the NASA-AMES Laminar Flow Supersonic Wind Tunnel for Unique Mach 1.6 Transition Studies by S.W.D. Wolf and J.A. Laub	30
Fluctuation Characteristics of Flows in Test Sections of High-Speed Wind Tunnels by V.A. Lebiga and V.N. Zinoviev	31
Aerodynamic Design of Nozzles for Subsonic and Transonic Wind Tunnels by A.P. Byrkin, S.P. Ponomaryov, V.S. Ponomaryova and A.P. Filatov	32
Method for the Calculation of 2D Supersonic Variable Nozzle Contours by V.P. Verkhovsky	33
General Discussion	GD

Recent Publications of the Fluid Dynamics Panel

AGARDOGRAPHS (AG)

Turbulent Boundary Layers in Subsonic and Supersonic Flow
AGARD AG-335, July 1996

Computational Aerodynamics Based on the Euler Equations
AGARD AG-325, September 1994

Scale Effects on Aircraft and Weapon Aerodynamics
AGARD AG-323 (E), July 1994

Design and Testing of High-Performance Parachutes
AGARD AG-319, November 1991

Experimental Techniques in the Field of Low Density Aerodynamics
AGARD AG-318 (E), April 1991

Techniques Expérimentales Liées à l'Aérodynamique à Basse Densité
AGARD AG-318 (FR), April 1990

A Survey of Measurements and Measuring Techniques in Rapidly Distorted Compressible Turbulent Boundary Layers
AGARD AG-315, May 1989

Reynolds Number Effects in Transonic Flows
AGARD AG-303, December 1988

REPORTS (R)

Advances in Cryogenic Wind Tunnel Technology
AGARD R-812, Special Course Notes, January 1997

Aerothermodynamics and Propulsion Integration for Hypersonic Vehicles
AGARD R-813, Special Course Notes, October 1996

Parallel Computing in CFD
AGARD R-807, Special Course Notes, October 1995

Optimum Design Methods for Aerodynamics
AGARD R-803, Special Course Notes, November 1994

Missile Aerodynamics
AGARD R-804, Special Course Notes, May 1994

Progress in Transition Modelling
AGARD R-793, Special Course Notes, April 1994

Shock-Wave/Boundary-Layer Interactions in Supersonic and Hypersonic Flows
AGARD R-792, Special Course Notes, August 1993

Unstructured Grid Methods for Advection Dominated Flows
AGARD R-787, Special Course Notes, May 1992

Skin Friction Drag Reduction
AGARD R-786, Special Course Notes, March 1992

Engineering Methods in Aerodynamic Analysis and Design of Aircraft
AGARD R-783, Special Course Notes, January 1992

ADVISORY REPORTS (AR)

Cooperative Programme on Dynamic Wind Tunnel Experiments for Manoeuvring Aircraft
AGARD AR-305, Report of WG-16, October 1996

Hypersonic Experimental and Computational Capability, Improvement and Validation
AGARD AR-319, Vol. I, Report of WG-18, May 1996

Aerodynamics of 3-D Aircraft Afterbodies
AGARD AR-318, Report of WG-17, September 1995

A Selection of Experimental Test Cases for the Validation of CFD Codes
AGARD AR-303, Vols. I and II, Report of WG-14, August 1994

Quality Assessment for Wind Tunnel Testing
AGARD AR-304, Report of WG-15, July 1994

Air Intakes of High Speed Vehicles
AGARD AR-270, Report of WG-13, September 1991

Appraisal of the Suitability of Turbulence Models in Flow Calculations

AGARD AR-291, Technical Status Review, July 1991

Rotary-Balance Testing for Aircraft Dynamics

AGARD AR-265, Report of WG11, December 1990

Calculation of 3D Separated Turbulent Flows in Boundary Layer Limit

AGARD AR-255, Report of WG10, May 1990

Adaptive Wind Tunnel Walls: Technology and Applications

AGARD AR-269, Report of WG12, April 1990

CONFERENCE PROCEEDINGS (CP)

The Characterization & Modification of Wakes from Lifting Vehicles in Fluids

AGARD CP-584, November 1996

Progress and Challenges in CFD Methods and Algorithms

AGARD CP-578, April 1996

Aerodynamics of Store Integration and Separation

AGARD CP-570, February 1996

Aerodynamics and Aeroacoustics of Rotorcraft

AGARD CP-552, August 1995

Application of Direct and Large Eddy Simulation to Transition and Turbulence

AGARD CP-551, December 1994

Wall Interference, Support Interference, and Flow Field Measurements

AGARD CP-535, July 1994

Computational and Experimental Assessment of Jets in Cross Flow

AGARD CP-534, November 1993

High-Lift System Aerodynamics

AGARD CP-515, September 1993

Theoretical and Experimental Methods in Hypersonic Flows

AGARD CP-514, April 1993

Aerodynamic Engine/Airframe Integration for High Performance Aircraft and Missiles

AGARD CP-498, September 1992

Effects of Adverse Weather on Aerodynamics

AGARD CP-496, December 1991

Manoeuvring Aerodynamics

AGARD CP-497, November 1991

Vortex Flow Aerodynamics

AGARD CP-494, July 1991

Missile Aerodynamics

AGARD CP-493, October 1990

Aerodynamics of Combat Aircraft Controls and of Ground Effects

AGARD CP-465, April 1990

Computational Methods for Aerodynamic Design (Inverse) and Optimization

AGARD CP-463, March 1990

Applications of Mesh Generation to Complex 3-D Configurations

AGARD CP-464, March 1990

Fluid Dynamics of Three-Dimensional Turbulent Shear Flows and Transition

AGARD CP-438, April 1989

Validation of Computational Fluid Dynamics

AGARD CP-437, December 1988

Aerodynamic Data Accuracy and Quality: Requirements and Capabilities in Wind Tunnel Testing

AGARD CP-429, July 1988

Aerodynamics of Hypersonic Lifting Vehicles

AGARD CP-428, November 1987

Aerodynamic and Related Hydrodynamic Studies Using Water Facilities

AGARD CP-413, June 1987

Fluid Dynamics Panel

Chairman: Prof. Dr. C. ÇIRAY
Aeronautical Eng. Department
Middle East Technical University
Inonu Bulvari PK: 06531
Ankara, Turkey

Deputy Chairman: Prof. B. CANTWELL
Stanford University
Dept. of Aeronautics &
Astronautics
Stanford, CA 94305
United States

PROGRAMME COMMITTEE

Mr. Ronald L. BENGELINK (Chairman)
Director, Ed Wells Initiative
The Boeing Company
PO Box 3707, MS 6Y-93
Seattle, WA 98112-2207 - USA

ICA Xavier BOUIS
Directeur des Grands Moyens d'Essais
ONERA
BP 72
92322 Châtillon Cedex - France

Ir Bram ELSENAAR
National Aerospace Laboratory NLR
Anthony Fokkerweg 2
1059 CM Amsterdam - Netherlands

Prof. Dipl. Ing. Bernd EWALD
Technische Hochschule Darmstadt
Fachgebiet Aerodynamik und Messtechnik
Petersenstr. 30
D-64287 Darmstadt - Germany

Ms. Galina KRYMASOVA
Central Aero-Hydrodynamic Institute (TsAGI)
Program Manager for International Scientific Affairs
Zhukovsky, Moscow Region - 140160 Russia

Dr. Norman D. MALMUTH
Rockwell International Science Center
P.O. Box 1085
1049 Camino Dos Rios
Thousand Oaks
California 91358 - USA

Prof. Alexander M. MATVEENKO
Rector of the Moscow Aviation Institute (MAI)
4, Volokolamskoe Shosse
Moscow - 125871 Russia

Mr. Fernando MONGE
INTA-DeptoDinamica de Fluidos
Div. de Aerodinamica y Vuelo
Carretera Torrejon Ajalvir, km. 4.5
28850 - Torrejon de Ardoz, Madrid - Spain

Mr. Jean M. MUYLAERT
ESTEC
Aerothermodynamic Section
Postbus 99
2200 AG Noordwijk - Belgium

Prof. Michele ONORATO
Politecnico di Torino
Dipartimento di Ingegneria
Aeronautica e Spaziale
C.so Duca degli Abruzzi 24
10129 Torino - Italy

Mr. Vasily RUKAVETS
Central Aero-Hydrodynamic Institute (TsAGI)
Chief of windtunnel Design Division
Zhukovsky, Moscow Region - 140160 Russia

Dr. David WOODWARD
Research Manager. Low Speed & Basic
Aerodynamics Dept
X80 Building
Defence Research Agency
Farnborough Hants GU14 6TD - U.K.

PANEL EXECUTIVE

Mr. J.K. MOLLOY

Mail from Europe:
AGARD-OTAN
Attn: FDP Executive
7, rue Ancelle
92200 Neuilly-sur-Seine
France

Mail from USA and Canada:
AGARD-NATO
Attn: FDP Executive
Unit PSC 116
APO AE 0977

Tel: 33 (1) 55 61 22 75
Fax: 33 (1) 55 61 22 98

TECHNICAL EVALUATION REPORT

Fluid Dynamics Panel Symposium on

AERODYNAMICS OF WIND TUNNEL CIRCUITS AND THEIR COMPONENTS

F.W. Steinle, Jr.

Sverdrup Technology - AEDC

Arnold Engineering Development Center, Arnold AFB, Tennessee 37389-9013, USA

SUMMARY

The topic of the 79th Fluid Dynamics Panel Symposium was titled "Aerodynamics of Wind Tunnel Circuits and Their Components" and was held at the Russian Finance Academy Congress Center, Moscow Russia on 30 September through 3 October, 1996. The sponsorship of the Symposium was by TsAGI whose organization and members are to be commended for their preparation and support in the hosting and conduct of the Symposium.

The aim of the Symposium was "*to gather and review both current knowledge and on-going research on the aerodynamic design and evaluation of ground test facilities, focusing primarily on wind tunnels, in order to provide to the designers of experimental facilities an opportunity to exchange information, ideas, and visions.*" Further, it was noted that "*The use of CFD and experimental methods in the design of wind tunnels, as well as, significant lessons learned in the design process of recently built tunnels is emphasized.*" The Keynote session comprised two invited papers. The first concerned a historical review of the aerodynamic facilities of TsAGI and the second addressed constraints the wind tunnel circuit design imposed on the aerodynamic development process. The remaining sessions of the Symposium were organized into topics pertaining to circuit design (low speed and high speed separately), test sections (ventilated & adaptive test sections separate from open jet test sections), drive systems, flow quality (laminar/turbulent flow considerations), and nozzles. Five other invited papers provided a highlight to the remaining sessions. These invited papers concerned the design of the DRA 5m and the ONERA F-1, and the ETW facilities, the adaptive-wall perforated test section (T-128), the design of axial flow fans for subsonic wind tunnels, and turbulence and noise

criteria for the design of the US National Wind Tunnel Complex (NWTC). The

Symposium was unclassified and the papers presented ranged from the application of conventional technology of years past to the present where CFD solutions employing Navier-Stokes codes are just beginning to be integrated into the design process. Thirty-two papers were presented at the Symposium, sixteen of which were from our colleagues from Russia. An overview of the Symposium in comparison with the indicated aim of the Symposium and some general conclusions and recommendations are provided.

1. INTRODUCTION

Interest in achieving a better answer from tests in wind tunnels has always been present and has served to provide the basis for major wind tunnel developments and improvements in testing technology that have occurred over the last twenty years and more. AGARD has long recognized the need to determine wind tunnel and testing technology requirements and to advance the state of the art in information quality through improvements to simulation capability, testing methodology and data quality. Consequently, over the years, the FDP has chartered studies in a broad range of topics relating to identification of these requirements and to making improvements. Within the last decade and a half, topics addressed have included flow quality¹, computer - wind tunnel integration², data accuracy versus wind tunnel requirements and capabilities³, data uncertainty assessment⁴, et cetera.

Organizations in the business of wind tunnel testing also have a history of recognizing the need to improve the quality of information derived from their wind tunnel facilities and there is a growing body of literature reporting improvements to facilities and test techniques,

calibration results of new facilities, plans for future wind tunnels, and progress reports for wind tunnel projects under way. The most recent major wind tunnel facility to come on line is the ETW, having completed its first commercial test in October of this year. The origins of that facility trace back at least 20 years when interested parties in Europe began to study cryogenic solutions to achieving high Reynolds numbers at transonic conditions. January of 1978 saw the MoU for the ETW between Germany, France, the United Kingdom, and The Netherlands become formalized. The Indonesian Transonic Wind Tunnel (ITST) is the next transonic wind tunnel to come on line (1999?) The ITST (designed by Sverdrup Technology) will have a Reynolds number capability at high subsonic speeds comparable to major non-cryogenic wind tunnels and is expected to have outstanding flow quality. In today's environment, the ability to secure funding for an ETW type project wherein high performance is sought is seen as virtually impossible. For instance, the most ambitious new project of the decade was to construct the US National Wind Tunnel Complex (NWTC). This project has now been deferred for an indeterminate time. The heart of that project as envisioned was to provide highly productive, high Reynolds number low speed and transonic test capability with extremely high flow quality suitable for both industrial and military aircraft development programs⁵.

The NWTC flow quality requirements were very ambitious and at the close of the project there were areas where significant gaps existed between what was desired and what was clearly achievable with conventional design methodology. One of the lessons learned in that project was the need to employ the best of CFD and experimental techniques practical in the development of a better design. This same challenge exists for any installation seeking to improve the quality of their respective facility through a modification. Consequently, with the challenge to the wind tunnel community for improved wind tunnel facilities and test information unabated, it is very timely that the aim of this symposium was *"to gather and review both current knowledge and on-going research on the aerodynamic design and evaluation of ground test facilities, focusing primarily on wind tunnels, in order to provide to the designers of experimental facilities and opportunity to exchange information, ideas,*

and visions." A further clarification of the aim of the symposium was the stated emphasis on *"The use of CFD and experimental methods in the design of wind tunnels, as well as, significant lessons learned in the design process of recently built tunnels ..."*

To help achieve the aim of the symposium, seven papers were invited which afforded an excellent range of opportunity to cover the full range of topics in the design and development of wind tunnels from a historical perspective to requirements for the future. These invited papers covered the facilities of TsAGI (Bedrzhitsky and Roukavets), a viewpoint from US industry on the interaction between the design of a wind tunnel circuit and the aerodynamic development process (Lynch and Crites), the development of the DRA 5m and the ONERA F-1 Pressurized Low Speed Wind Tunnels (Woodward and Francois), the aerodynamic design of the ETW (Bouis, Prieur, Tizard, and Hefer), adaptive wind tunnel walls (V. Neyland, Ivanov, Semenov, Semenova, and Amirjanz), the aerodynamic design of axial flow fans for subsonic wind tunnels (Brusilovsky), and turbulence and noise criteria for the NWTC (Reshotko, and Saric).

Thirty-three papers were on the program. Thirty-two of these were presented. Regrettably, paper number 9 concerning state of the art in performance analysis of wind tunnel circuits by T. Wolf, Technical University of Darmstadt was not presented. This topic is intriguing, useful, and would have added significantly to the breadth of the symposium. The Keynote and ensuing seven technical sessions spanned three and one-half days. Technical Sessions I through VII titles sequentially were: Circuit Design - Low Speed, Circuit Design - High Speed, Ventilated & Adaptive Test Sections, Drive Systems, Open Jet Test Sections, Laminar/Turbulent Flow Considerations, and Nozzles. The meeting concluded with Technical Evaluators' comments by Dr. V. P. Roukavets and the author, followed by a general discussion.

Despite the Symposium being organized into distinct sessions, the papers themselves are far ranging within each session. Consequently, it seems appropriate to treat each paper individually. Observations, conclusions, and/or recommendations included as

appropriate with the discussion for each paper. General observations and recommendations are presented in the final section of this report.

2. KEYNOTE SESSION

The first two papers of the symposium which constituted the keynote session served to broaden one's attention beyond focus on the mechanics of designing and evaluation of ground test facilities which is predominate in the stated theme. However, these papers were very appropriate for supplying information, ideas, and visions to the designer. Paper 1 by Bedrzhitsky and Roukavets could be viewed solely as interesting historical and technical information concerning the aerodynamic test facilities at TsAGI. However, it is more than that for the governing philosophy behind the establishment of the facilities of TsAGI is worthy of note. The method of N. E. Zhukovsky which consisted of a "*continuous combination of fundamental, searched-for and applied researches with experimental investigations in the wind tunnels*" was reported to have always remained of primary interest in the development of TsAGI. Further in discussing the development of the wind tunnels for the Chaplyguin laboratory, it was noted that "*the best results are achieved under close cooperation and reciprocity between the customers, designers, and operators.*" Zhukovsky's method is none other than what is currently referred to as a "continuous improvement process." In today's environment of budgetary restrictions, being able to sustain a meaningful continuous improvement process is generally very difficult. It is suggested that one of the difficulties of obtaining a budgetary consideration for improvement in capability is associated with a lack of understanding of the relative importance to a company, association, state, country, or nation providing the budget authority of the benefits of any improvement in relation to other needs clamoring for funding. Overcoming this situation is not guaranteed. However, it seems clear that to do so requires that those interested in making improvements establish a close cooperation with the users of the facilities to establish measures of product benefits (risk reduction, performance gains, cycle-time reduction, etc.) through any improvements. In addition, close cooperation with others in the economic chain is required to establish a benefit against overall

budgetary resources (aircraft sales, reduced operating expenses, profit margin, gross national product, reduced unemployment, increased tax revenues, etc.) is required. The point is, those in control of budget authority should be viewed as customers who generally speak a different language from the operators of wind tunnel facilities. To realize any gains, these customers must be shown in their terms why an action is in their best interest. The onus is sensibly on the operators to establish the necessary close working relationship involving the customers, designers, and themselves noted in Paper 1 that existed at the Chaplyguin Laboratory.

Paper 2 by Lynch and Crites provided a viewpoint from a wind tunnel test customer engaged in aerodynamic development as to how the wind tunnel design affected the aerodynamic product. Addressed were Reynolds number, tunnel flow quality, wall and support system effects, and other factors important to timeliness and cost effectiveness. Examples of impacts of various factors are cited along with the logical call for improvement in all technical areas as well as a more cost effective product.

Notably:

- Special efforts to minimize free stream turbulence and noise effects are called for (case wherein full scale Reynolds number does not give full scale results was cited and free stream unsteadiness is the prime suspect).
- A. B. Haines⁶ call for the user to have a thorough knowledge of the important flow physics involved in the simulation in relationship to the identification of flow quality and data accuracy requirements was echoed.
- The necessity of reduction of wall interference effects with large semispan models was seen as being necessary for Reynolds number requirements of transport aircraft to be met
- Concern was expressed for the adequacy of icing tunnel simulation because of lack of vertical velocity component for water droplets.
- The use of improved wind tunnel design through CFD techniques of inverse solutions and constrained optimization was seen as being very beneficial, particularly in the design of both the contraction and the diffuser.

- Pursuit of advanced test-section wall ventilation and control concepts to permit testing of larger models was advocated.

Lynch & Crites did not provide a set of design requirements that resulted from their perspective. However, they did provide information and recommendations as to what should be worked toward and why. Appropriate to the theme of this symposium, they saw the need to integrate CFD into the wind tunnel design process as is done in the aircraft industry today with inverse solutions and constrained-optimization techniques.

Experience of the writer working on the NWTC project has led to the conclusion that integration of CFD into the aerodynamic design of wind tunnel circuits in the same manner as designers of modern aircraft is essential to achieving any leap forward in wind tunnel design technology, particularly in the areas of stream uniformity and tunnel wall effects at low and high subsonic speed conditions. There is ample opportunity to apply this approach to a modernization of existing wind tunnels. In view of the high cost of acquiring a new facility, application of CFD in a constrained optimization design approach to a modernization project is much more likely.

3. SESSION I - CIRCUIT DESIGN - LOW SPEED

Seven papers (numbers 3 - 8, and 10) were presented in this session. The topics included design aspects in general, design of existing and proposed low speed wind tunnels, icing tunnels, and design of test cells using integrated computations and experiment.

Jaarsma discussed aspects of low-speed wind tunnel design that were generalized from experience gained with the DNW and LST facilities in The Netherlands and the Indonesia ILST wind tunnel. Featured topics included circuit lay-out, conical diffusers, turning vanes (with and without acoustic treatment), contractions, stilling chamber flow conditioning, test section shape (no corner fillets is preferred), and wall provisions (windows, adjustable slotted wall capability), model supports, and test section/model logistics with selected data. Data were presented which showed the benefit of screen tensioning on flow angle and the effect of acoustic treatment of corner vanes. Curves

were shown for the damping of turbulence as a function of contraction ratio. Jaarsma called for Navier-Stokes calculation of the flow in the contraction section to explore the effects of secondary flow and to improve on the contraction design. The use of variable slotted walls for the reduction of wall interference was discussed but not advocated for routine application because of the current difficulties associated with assessing the residual wall interference. Navier-Stokes calculations, coupled with the constrained optimization approach advocated by Lynch & Crites, to the design process for the contraction section is challenging and affords the best opportunity for advances in test section stream uniformity at the entrance of the test section. Exploration of the technology for achieving variable slotted walls is clearly warranted because of the potential for reduction in wall interference. If the difficulty impeding the use of this technology is in assessing the residual interference as Jaarsma indicates, then solving the assessment problem should be one of the near term focal points for research.

Paper 4 (invited) by Woodward and Francois concerned aerodynamic and structural design of the DRA 5metre and ONERA F-1 wind tunnels. Both of these facilities represent different design solutions to the same specifications. Although having been designed 25 years ago utilizing empiricism and experimental approaches in the design, the facilities produce excellent results. The approaches to the design are discussed, along with supporting model test results. Although the use of modern CFD tools in the design process are expected to lead to an improved result, the approaches outlined would form the basis of an excellent starting point for further optimization. Non-linear corner vane spacing, an integrated approach to the design of the screen - contraction arrangement, and the design of rapid diffuser configurations are particularly interesting.

The fifth paper of the Symposium (Ryabokon and Malyk) discussed their work to develop a low speed sinusoidal flow pulsation capability. Elliptical shaped rotating vanes downstream of the test section were employed. Frequency and amplitude control was demonstrated. Although the pulse shape was not truly sinusoidal, improvement in the shape over a single rotating pulser was gained

by a set of corrector pulsers rotating at twice the speed of the primary pulsers.

Paper 6 by Gilbertini, Gasparini, and Zasso gave an overview and a progress report on the Politecnico di Milano's project to develop a new Civil-Aeronautical Low Speed Large Wind Tunnel. The tunnel is to have two test sections on parallel legs of the tunnel circuit. The larger test section is to provide testing of civil structures such as bridges which requires simulation of Earth boundary-layer profile. The most notable feature of this paper is the discussion concerning the use of numerical optimization in the design of the contraction and corner vanes. The design of the corner vanes which are to function in very low Reynolds number conditions (down to 100,000) used a multi-point inverse method with coupled integral boundary layer. Pressure profiles similar to Eppler high lift airfoils were specified. Experimental results showed promise. The approach employed is an attractive one for future designs.

The requirements and statement of work for the CIRA icing tunnel were discussed in Paper 7 by De Gregorio, Esposito, Mingione, and Vicini. The use of Euler calculations for optimization of the contraction shape coupled with a droplet trajectory analysis to provide the best droplet distribution was featured. Boundary layer growth in the contraction section was not considered in the analysis. Calculations showed that droplet distribution could be significantly improved by proper shaping of the contraction.

Paper 8, Chintamani, Delcarpio, and Langmeyer, discussed development of the Boeing Research Aerodynamic Icing Tunnel circuit. Design requirements, design solutions, performance, and calibration results are discussed. Although details of the design process are lacking, the general features and test results presented, are very useful, particularly the discussion as to the development of the spraybar design.

The last paper of the session (Paper 10 by Kabakov, Timoshin, and Ciam) provided schematics of altitude and sea-level test cell components for testing of aviation engines. Featured is the use of jets for the control of test conditions. A very limited set of non-dimensional data is presented along with some general discussion which should be of interest to the designer of test cells. However,

geometrical details are lacking. There is no comparison of any theory with experimental results although the discussion presented indicates there is agreement. The main contribution of this paper is in the general discussion.

4. SESSION II - CIRCUIT DESIGN - HIGH SPEED

Five papers (11 -15) comprised this session. Paper 11 (invited) by Bouis, Prieur, Tizard, and Hefer presented an excellent overview of the development of the aerodynamic design of the ETW. Design specifications, design approaches involving the use of calculations and reliance on test rigs and the pilot facility (PETW), the control system, and calibration results are discussed. An eight year period prior to start of final design in which optimization efforts and pilot tests were carried out, a firm freeze on the major design specifications after the start of final design, and adequate authority of the ETW team to manage all aspects of the project were cited as being major contributors to the final success of the project. The latter two factors are what any design team wants to have. The eight year period for optimization is not to be desired although the outcome is. A challenge for today's developer of any new facility is to adequately plan for the technology development needed and the process for achieving the desired result in the shortest practical time.

Paper 12 by Gobert discussed a methodology for dynamic control of transonic wind tunnels. The method shown uses a math model composed of forty finite volumes with appropriate physics modeled in each volume and transfer functions between volumes in a time dependent solution to predict the system response. A key feature is the use of adaptive learning. Results were presented for application to the ONERA S2 and ETW facilities. Excellent control of test conditions is demonstrated and the use of this type of dynamic model to design or redesign control systems for improved responsiveness is indicated. Details of the adaptive learning method and gains are limited. Use of adaptive learning technology to improve both test information quality and productivity of any facility is well worth consideration.

Studies on two short-duration cryogenic transonic wind tunnel concepts for a low cost alternative to a high Reynolds number facility were presented as paper 13 by Zvegintsev and Omelaev of the Institute of Theoretical and Applied Mechanics, Siberian Branch of the Russian Academy of Sciences. A classic blow-down concept and a variant of the Ludwig tube tunnel with an expansion chamber reservoir at the upstream end of the tube, separated by a perforated plate are discussed. The purpose of the perforated plate and chamber is to extend the run time a factor of three or more by essentially eliminating the reflected rarefaction wave. Schematics are presented for both concepts along with predicted performance curves and test results from a small impulse facility used to examine the effects of perforation on reflected wave strength. Experimental values for low speed test conditions are shown to be close to predictions. No mathematical description of predictions is given. Several references to TsAGI reports are given which appear to relate to the predictions. It is hoped that the references cited can be readily obtained.

Paper 14 by Kislykh, Koudriavtsev, Petrova, and Puchkov, Central Research Institute of Machine Building (TSNIMASH), Russia, describe the impulse transonic wind tunnel, ITT U-11 which is capable of Mach numbers from approximately 0.1 to 2. The facility features control valves in the gas supply circuit and in the diffuser ahead of the vacuum reservoir. Other features include a multi-stage perforated plate nozzle with cylindrical channels, a circular (.8 meter diameter) slotted transonic test section with surrounding silencer, and the ability to vary the test gas. Turbulence and noise spectra are presented along with some comparable results from the T109 facility. In relation to high quality flow, the turbulence and noise levels are high. Run times cited range from less than a second (Helium) up to 2.5 seconds (Nitrogen). Geometric and tunnel calibration information is lacking. The authors suggest that the ITT U-11 concept could be improved through optimization of elements and systems and that such an optimized concept could be used to produce facilities with nozzle exit diameters of the order 5 to 10 meters.

The last paper of the session (15) by Seltsam, DLR, concerns the application of Navier Stokes calculations to the integration of

screen components in diffusers and stilling chambers. The screen characterization uses the $k-\epsilon$ model for the transport equations and treats the pressure drop as a source term. The method is applied to the improvement of flow in a wide angle diffuser with screen and is confirmed by experiment to result in improvement of flow. Turning of flow by the screen is only considered in terms of its effect on turbulence. The effects of a non-planar screen due to deflection under load are not considered. In an integrated design approach for the stilling chamber and contraction, it seems that the effect of non-planar screens and associated flow turning should be considered in the design process. This is an opportunity for further improvement on the Seltsam's work.

5. SESSION III - VENTILATED & ADAPTIVE TEST SECTIONS

Session III (papers 16 - 20) started with an invited paper by V.M. Neyland, et. al concerning adaptive-wall perforated test sections for transonic wind tunnels. Neyland presented information concerning the development and operation of the T-128 tunnel. Overall geometric dimensions of the facility are reported along with comparison test results from the AEDC 16T tunnel and a comparison performance chart with major European and US and the T-109 tunnels. The scale used in the comparison is fairly coarse such that finer details of agreement or disagreement is lost. A comparison of the ability to achieve a free air pressure profile at three pressure rail positions for a large Boeing half-model is shown. The general shape of the predicted curve is matched reasonably well. However, there is no assessment of the residual wall interference associated with not matching the predicted profile. Such an assessment would be useful. The major issue is the choice of the method to use in assessing wall interference and in achieving convergence in wall adaptation. Adaptation is cited as being "quite time consuming..." and in many cases, capable of being replaced by a less expensive method. Developing an improved process for wall adaptation is a technological challenge which was recognized by the NWTC project and remains to be solved.

Tang and Chan (paper 17) discuss the work at the IAR 1.5m Trisonic Wind Tunnel directed

toward reducing the adverse pressure gradient in the 2D test section. Extension of the side walls which included a short section with a 2-degree diffusion half-angle to reduce the amount of plenum flow entrained at the end of the test section was effective in alleviating the pressure gradient. Interestingly, the benefit of the extension was reported as being insensitive to Mach Number and Reynolds Number. The results of this work should be beneficial in adding to the body of knowledge concerning the design of plenum re-entry regions. Additional information, such as the state of the boundary layer approaching the re-entry region and at the mixing region would be helpful. One hopes that further analysis might be directed to the entrainment process and the coupling with the test section flow.

Experimental results of the effects of plenum suction on transonic test section flow are presented by Verkhovsky, Lyzhin, and Pasova in Paper 18. Use of a small blow-down tunnel (.18m x .18m) and the T-128 tunnels are cited. Geometrical information is minimal. The general trends are useful. However, the value of the information presented would be greatly enhanced by presenting more details concerning the geometry and the test conditions.

Paper 19 by Quest, Nitsche, and Mignosi examines the potential benefit of an adaptive wall slot which is formed by channels with a flexible plate to vary the cross-section area of the stream flow. Three-dimensional Navier Stokes calculations of local flow indicate that both 2-D and 3-D adaptation is feasible. In the 2-D mode, calculations showed that a wall with 6 adaptive slots gave the best results. Adaptation using this approach may well afford the best opportunity for a low-noise generating transonic test section. Further development is clearly warranted.

The final paper of the session (Paper 20) by Freestone and Sykes reports on the use of measured wall conditions (slat pressure and flow in the slot) to determine the effective inviscid boundary flow conditions in conjunction with the Ashill and Weeks method for assessing wall interference. Focus was on a two-dimensional application. However, the approach is applicable to 3-D. A key feature is the use of a three-hole probe for measurement of slot flow. The principal near term use is seen to be in post-test

processing to determine residual wall corrections. Results are encouraging. However, there is the concern for the impact of a mature boundary layer on the determination of the effective inviscid boundary condition. Further development is indicated and urged.

6. SESSION IV - DRIVE SYSTEMS

Papers 21 - 24, all by colleagues from TsAGI, comprised the fourth session. Paper 21 by Brusilovsky covered the aerodynamic design of fans for low speed wind tunnels. The general design methodology, in use and improved over the last 45 years, along with some supporting experimental results is presented. The mathematical representation is simple enough that it is easy to implement on a desk-top personal computer. Fan maps for the T-102 and T-124 tunnels are presented. However, the absence of fan blading details and fan blade airfoil characteristics prevents one from making full use of the information presented. The methodology is useful to the analysis and improvement of an existing fan.

Arkadov and Roukavets (Paper 22) have provided commentary, schematics of five ejector concepts, and supporting data on applications to ejector driven wind tunnels. Featured are ejectors with offset nozzles, a helical nozzle, a perforated nozzle, and parallel ejectors. Some geometric information is provided. More geometric detail would be useful. However, the data presented along with the discussion is of significant value to the designer.

Kukinov, et al (Paper 23) discuss the use of adjustable inlet guide vanes and speed control for the improvement of the efficiency of the T-128 compressor and the reduction of third mode vibratory stress in the last stage of the rotor (4th). A model of the T-128 compressor was constructed as part of the study. Model details are not provided. Supervisory monitoring of the stall margin for supersonic operation is discussed. Compressor maps are given along with tunnel operating lines for supersonic conditions. Some T-128 compressor geometric information is provided. However blading and blade aerodynamic characteristics information is lacking. The addition of compressor geometry and blade characteristics would greatly

enhance the value of this paper to the designer.

The last paper of the section (Paper 24) by Korovkin, Savchuk, and Kuroles characterizes the performance of diametral fans and discusses their application to specialized wind tunnels. A novel use is the simulation of a free surface flow of a liquid about a body. The compactness of the diametral fan is of particular value in the construction of small, wind tunnels where circuit length is restricted.

7. SESSION V - OPEN JET TEST SECTIONS

Papers 25 - 26 were presented in this session. Paper 25 was presented in two parts. Part 1 by Roukavets, et al reported on the use of the T-103 tunnel to examine investigate collector concepts with regards to jet flow quality. A substantial amount of data is presented which should be very useful to the designer. A one-piece contracting collector (nominally 14 degrees) whose exit matched the diffuser entrance with a gap whose area was about .2 of the area of the collector was found to be best. It is interesting to learn that in this study the use of a breather did not improve the flow quality.

Part 2 of Paper 25 by Papenfuss, et al concerns a new design of jet exit vanes that are adjustable. The arrangement investigated is an alternating series of inclined round flaps that point out of the flow and triangular end plates (pointing in to the flow) which are attached to the base of pyramidal wedges that point into the flow with their bases aligned with the nozzle flange. It was shown that up to a 50% reduction of core flow turbulence could be achieved from that of a base-line configuration having no vanes. A reduction in noise level over that achieved by the Seiferth wing configuration is alluded to, but not quantified. Overall, this line of work is very important to the improvement of open-jet flow quality. The NWTC project identified the need to have an open-jet test capability substantially higher than the 70m/s capability of the University of Kassel (Germany) wind tunnel used in this study. Test capability up to Mach Number 0.6 (about 205m/s) was strongly desired. To achieve a flow of acceptable stability, noise, and turbulence is a formidable challenge which has not been met. The work reported herein

is a valuable addition to any effort aimed at meeting higher Mach Number test capability.

Holthusen and Kooi (Paper 26) reported on the results of a study aimed at reducing low frequency pressure fluctuations in the DNW Open Jet test section which were producing unacceptably high structural vibrations of the test hall structure. A 10m/s gain in upper test speed to 90m/s was projected by using tetrahedrons pointing upstream along the nozzle at the exit. The gain was at the expense of a steeper longitudinal pressure gradient. Other modifications tested were not successful. It is encouraging to note that 1:10 pilot scale test results correlated well with the DNW so that further work at pilot scale prove to be successful. A thinner shear layer was associated with the tetrahedrons installed. Possibly, means of developing a thinner shear layer without generating unacceptable noise levels is indicated from this result.

Paper 27 by Ginevsky discussed the results of experiments using forced pulsations to reduce pressure and velocity pulsations in four wind tunnels with exhaust nozzle diameters ranging from 0.15 to 2.2m. The use of anti-sound appears to be most effective in suppression of pulsations in the return circuit. Periodic blowing/suction also was very beneficial. The results of this experimental program are encouraging and should be investigated in conjunction with other solutions that appear promising and at higher speeds.

8. SESSION VI - LAMINAR/TURBULENT FLOW CONSIDERATIONS

The first paper (Paper 28 by Reshotko and Saric) of the four papers in this session was invited. Paper 28 discussed the turbulence and noise criteria that were developed for the NWTC project and presented recommendations as to guidelines for turbulence management. The criteria were based on what was seen as being necessary to achieve natural laminar flow at high subsonic speeds. A notable point is their opinion that the contraction ratio should be no larger than 9:1 as opposed to the 12:1 that was planned for the NWTC. A secondary issue, but very important to the design-builder is the determination of turbulence and acoustic disturbances once the facility is constructed.

At the heart of this issue is the sensitivity of measuring devices to both disturbances. In that regard, the authors recommended a cross-correlation technique coupled with optimal filtering to reduce errors in separating velocity and pressure fluctuations. However, they noted that near Mach 1 where density fluctuations must be separated from mass flux fluctuations to obtain velocity fluctuations, it is unclear as how difficult it will be to employ optimal filtering. A validated technique for separating turbulence and pressure fluctuations is vital to the wind tunnel community, the designer-builder, the operator, and the user. A technique such as this does not exist.

Paper 29 by Rancarani, et al (ONERA) discusses the design and validation of a quiet supersonic wind tunnel. Noise suppression considerations included a silencer in the stilling chamber and the use of aspiration in the contraction. At Mach 3.0, pressure fluctuations of less than .1% dynamic pressure and transition Reynolds numbers of 6 million were achieved. The importance of laminar flow in the nozzle is noted. This work in the R1Ch, R2Ch, and R3Ch facilities essentially parallels the work by NASA Langley to develop a quiet supersonic wind tunnel.

The NASA Ames Laminar Flow Supersonic Wind Tunnel (LFSWT), commissioned at the Fluid Mechanics Laboratory in 1994 to support supersonic laminar flow research at Mach number 1.6 was represented in Paper 30 by Wolf and Laub. The tunnel has an 8-inch high x 16-inch wide test section and a contraction ratio of 12:1. It is powered by air from the NASA Ames high pressure air system. Schlieren visualization of flow with a 10 degree cone present shows the existence of weak waves which have been determined to originate from the window and test section joints (hand finished). Despite these disturbances, a convincing case is made that the flow in the test section is quiet. The authors noted the need for standardization of instrumentation and signal processing to determine flow quality. This is an interesting point. Changing technology argues that a standard won't be a permanent standard. Perhaps the important feature is the

methodology (e.g., as proposed by Reshotko and Saric) and a standard approach to reporting uncertainty.

The final paper of the session (Paper 31) by Lebiga and Zinoviev used hot wire measurements to characterize flows in the T-325 and MT-325 wind tunnels which cover transonic Mach numbers up to Mach 4.0. Use is made of hot-wire anemometry in conjunction with modal representations for vorticity, entropy, and acoustic waves to separate the various fluctuating components. A result is obtained. However, an assessment of the inherent errors associated with these measurements is lacking. This method should be validated.

9. SESSION VII - NOZZLES

Two papers were presented in this final session of the symposium. Paper 32 by Byrkin, Ponomaryova, and Filatov discussed the design of subsonic axisymmetric nozzles (contraction) and an octagonal nozzle that transitions to a square test section with corner fillets. Design guidelines for avoidance of separation in the contraction are discussed. Experimental results are presented. The design methodology presented does not measure up to a constrained numerical optimization method. However, the design methodology is useful for an initial starting point and it is possible that the recommended constraints would be useful for validation as part of a constrained optimization method.

Paper 33 by Verkhovsky discusses an influence coefficient method for establishing 2D nozzle contours that have minimum flow non-uniformity at the nozzle exit. The method of characteristics, coupled with a displacement thickness correction, is used to calculate the influence coefficients. The empirical results for displacement thickness correction are worth noting. What is relatively novel about the design is that it consists of a rigid curved plate through the throat region followed by a flexible plate. Only four control positions are shown. The level of non-uniformity from Mach number 1.2 to 4.0 varies between .2 to 1.5 %.

10. GENERAL OBSERVATIONS & RECOMMENDATIONS

General Observations:

The Symposium was unique because of its location and the hosting and extraordinary participation of our colleagues from Russia.

The Symposium's topics gave a broad opportunity for response. The scope and timeliness of the invited papers helped to set the theme for the symposium.

In many instances, the absence of information such as geometry detracted from the utility of the papers presented. Full access to references may solve any problems of this nature.

Very few papers actually captured modern use of CFD in the design of wind tunnels. On the other hand, the amount of information shared concerning experimental methods in the design of wind tunnels as well as lessons learned was substantial. A fair amount of current research on the aerodynamic design of wind tunnels was presented.

To the author, the purpose of the Symposium was oriented toward setting the tone for the future. In that regard, four challenges to the community of those in our profession are seen.

- Assurance of a continuation of scientists and engineers who are artists in the ground test facilities genre and as such, should be viewed as integral to the facilities;
- Achievement of fullest cooperation and reciprocity on the international level involving designers, operators, and customers for our mutual benefit;
- Forecast of technological requirements of the future with sufficient certainty that necessary enabling ground test facility technology development can be best advocated;
- Identifying changes in design philosophy and methodology needed to provide ground test based information that is of the quality necessary to satisfy customer requirements.

Recommendations:

The author believes that it is safe to assume that all interested in ground test facilities would prefer a process of continuous improvement and hence, no recommendation of that sort is offered. Specific recommendations that are an outcome of the review of each paper are not repeated here. Rather, it is deemed sufficient to recommend a general course of action to address the four challenges presented.

The first three challenges seem to be most appropriate for an ad-hoc gathering of interested parties to share views on the process that should be followed in assessing whether the challenges posed are indeed worthy and if so, how should they be attacked.

The fourth challenge is seen to be worthy of consideration as an AGARD working group activity whose central theme should be an *Integrated Design Process for Maximizing Information Quality* with the following sub topics:

- Design for low turbulence and noise (including measurement and signal processing techniques for quantification of turbulence and noise);
- Design for high stream mean flow uniformity;
- Design for low wall and support interference
- Design for flow quality and interference corrections;
- Design for optical-based measurements of surface flow conditions and model shape;
- Design for integration of CFD and experiment.

The methods employed in developing present tunnels are not viewed as sufficient if a significant gain is to be realized. The above sub topics are viewed by the author as critical technology issues.

At some point, these topics would be appropriate for a Symposium. Noting the wording of the call for this Symposium, it appears that the above items would fit well within the present Symposium.

11. REFERENCES

1. Steinle, F. & Stanewsky, E., "Wind Tunnel Flow Quality and Data Accuracy Requirements", AGARD-AR-184, Nov. 1982.
2. Wind Tunnel Testing Sub-Committee of the FDP, "Windtunnel Capability Related to Test Sections, Cryogenics, and Computer-Windtunnel Integration" AGARD - AR-174, April, 1982.
3. Various, "Aerodynamic Data Accuracy and Quality: Requirements and Capabilities in Wind Tunnel Testing," AGARD-CP-429, Oct., 1987.
4. Fluid Dynamics Panel Working Group 15, "Quality Assessment for Wind Tunnel Testing," AGARD-AR-304.
5. Ring, Leon, et. Al., "NWTC Final Report." NASA CR-198491, June 1996, Archives of the National Wind Tunnel Complex, CD-ROM Vol. No. 1, Electronic Document:nwtcfnl.htm, 1-3.
6. Haines, A.B., "Acale Effects on Aircraft and Weapon Aerodynamics," AGARDograph 323, July 1994.

HISTORICAL REVIEW OF THE CREATION AND IMPROVEMENT OF AERODYNAMIC TEST FACILITIES AT TsAGI

E.I. Bedrzhitsky, V.P. Roukavets
Central Aerohydrodynamic Institute (TsAGI), 1, Zhukovsky Street
140160 Zhukovsky, Moscow Region, Russia

ABSTRACT

Extract from the history of development of the wind tunnels of TsAGI and their main characteristics are cited.

INTRODUCTION

The Central Aerodynamic Institute named after Prof. N.E. Zhukovsky (TsAGI) was set up by a Resolution of the Scientific and Technical Department (Nauchno-Tekhnichesky Otdel – NTO) attached to the Supreme Council of the People's Economy (Vysshi Sovet Narodnogo Khozyaistva – VSNH) of the Russian Socialist Federative Soviet Republic (RSFSR) on December 1, 1918 with an aim of:

"... a) promoting the development of aero- and hydrodynamics in the direction of its practical use in various sectors of technology;

b) promoting individual establishments and workers in their scientific and practical researches and inventions in the field of aero- and hydrodynamics ...".

A team of young scholars, engineers and pilots possessing already a practical experience of researches in the area of aerohydrodynamics at the Computation and Research Bureau (CRB) established within the Moscow High Technical College (Moskovskoe Vysshee Tekhnicheskoe Uchilishe – MVTU) in 1916 formed the kernel of TsAGI headed by N.E. Zhukovsky. The foundation for these researches was laid by a methodology created by N.E. Zhukovsky and consisting in a continuous combination of fundamental, searched-for and applied researches with experimental investigations in the wind tunnels. This principle was preserved and developed through all stages of activities of TsAGI where the problems of creation of the experimental aerodynamic equipment and development of the scientifically grounded test methodology had always been of primary emphasis.

Two principal periods could be stood out against the history of creation and development of aerodynamic experimental facilities of TsAGI:

- the period from 1918 to 1933 (the city of Moscow);
- the period from 1933 up to now (the city of Zhukovsky).

The period from 1918 to 1933 (the city of Moscow)

At the early period after creation of TsAGI the experimental aerodynamic investigations were carried out in the laboratory named after N.E. Zhukovsky of the Moscow Higher Technical College that by that time possessed two low speed wind tunnels:

- wind tunnel #1 with a flat test section of 0.3×1.5 m built in 1910;
- wind tunnel #2 with a circular test section of 1.5 m in diameter built in 1916.

To expand the front of experimental investigations and improve the conditions of transition to full scale testing wind tunnel #3 with two test sections of 1.5 m and 2.25 m in diameter was built in the same laboratory in 1925.

However yet before this wind tunnel was built TsAGI appealed to VSNH with a proposal of building new laboratories. And already in August 1923 design works were launched to build such a laboratory (named after S.A. Chaplyguin) on Radio street, and in December 1925 the T-I-T-II wind tunnel was put into operation. For that time it was the largest wind tunnel in the world.

This wind tunnel had two closed test sections of octahedral section with diameters of the inscribed circle 3 m and 6 m and maximum flow velocities 60 m/s and 27 m/s, accordingly. During its construction and adjustment use of the results of investigations of the No.3 wind tunnel of the N.E. Zhukovsky's laboratory attached to MVTU was made, serving as the pilot tunnel for T-I-T-II. The test section of T-I equipped with a 4-component balance was basically used to test infinite span wing models, and the test section of T-II to test fuselages and other full scale aircraft elements. Since 1927 T-I-T-II became the principal wind tunnel of the aviation industry of Russia and was constantly re-equipped with the required experimental apparatus (rotor testing bench rig, spin testing devices and facility for determination of rotational derivatives etc.).

In 1926 wind tunnel T-III was built in the same laboratory equipped with test sections of 1.5 m in diameter in two variants:

- closed,
- with an Eiffel chamber.

The maximum flow velocity in this wind tunnel was, accordingly, 93 m/s and 82 m/s.

In 1931 closed circuit wind tunnel T-V was put into operation with a diameter of the nozzle exit section 2.20 m and maximum flow velocity 50 m/s. A particular feature of this wind tunnel was a six-component balance and a device to create slip angles of the models (turning wheel).

The laboratory named after S.A. Chaplyguin was equipped with up-to-date for that epoch wind tunnels with the required apparatus that not to a small extent contributed to achieving by Russia considerable progress in the field of aircraft aerodynamics and permitted in the 30 – 40s development of the airplanes that established some world records and performed long distance flights known throughout the world.

The principal characteristics of the wind tunnels of Chaplyguin's laboratory of TsAGI are given in Table 1 and the schematic of two of them in Figs. 1 and 2.

Along with this the experimental investigations in the wind tunnels of the Chaplyguin's laboratory revealed a remarkable influence of Reynolds numbers on the wind-tunnel results. Already at the end of the 20s it became clear that new very

large wind tunnels should be constructed with test conditions approached to real ones at their maximum. Therefore in 1931 following the suggestion put forward by TsAGI a government resolution was adopted to build a new large complex of wind tunnels outside Moscow.

The period from 1933 up to now
(the city of Zhukovsky)

In 1933 the Soviet Government approved a building site for construction of a new complex of wind tunnels in the area of the city of Zhukovsky.

The first phase implied the construction of large (full scale) wind tunnels T-101 and T-104 that would provide a reliable transition of the wind tunnel test results to real flight conditions. To determine the principal parameters of these wind tunnels versatile investigations were performed pertaining to the prospects of scientific researches and advancement in the field of aircraft construction, opportunities of the USSR industry. These investigations resulted in the determination of the following wind tunnel parameters:

- T-101, a closed circuit wind tunnel with an open test section of 25 m long of elliptical section with the ellipse axes dimensions 24 m and 14 m, maximum air flow velocity 65 – 70 m/s with two fans and two return circuits;
- T-104, a closed circuit wind tunnel with an open test section of 13 m long of circular section 7 m in diameter with the flow velocity up to 125 m/s and with one return circuit.

The experience of development of the wind tunnels for the Chaplyguin's laboratory has shown that the best results are achieved under close cooperation and reciprocity between the customers, designers and operators. This is why to solve multiple scientific, engineering and organizational problems associated with the construction of large wind tunnels a special team was formed within TsAGI aimed at working out the designs of the wind tunnels in cooperation with their customers and operators. This practice of designing new wind tunnels and improving the existing ones has been constantly preserved and is used by TsAGI up to now.

In order to reduce the technical risk linked with the construction of the unique T-101 and T-104 wind tunnels, performance of investigations and flow adjustment, development of techniques and methodology of testing, it was decided to build the pilot wind tunnel T-102, a pattern of T-101, to a scale of 1/6. Additionally, in order to increase the scope of the model investigations it was decided to build the T-103 wind tunnel with the same dimensions of the test section as for T-102, but with one return circuit and the maximum flow velocity 100 – 110 m/s.

So, the first industrial construction on the site of the new TsAGI was a complex of small wind tunnels put into service in November 1936. The main starting adjustment, research and methodological works in these wind tunnels were terminated by the end of 1937. The accumulated experience and scientific and technical results of these works laid the foundation to prepare the commissioning of the new large wind tunnels T-101 and T-104. The T-102 and T-103 wind tunnels, having performed their role of "pilot wind tunnels", were used further on and are used up to now to carry out tests of aircraft models.

Construction of the complex of the large wind tunnels was terminated in 1939. The first commissioning of T-101 occurred on the 15th of August, 1939, and T-104 on the 20th of August, 1939. Already during the first puttings in operation of these wind tunnels the highest in the world wind-tunnel Reynolds numbers were obtained. Fitting these wind tunnels with up-to-date for that epoch six-component balances provided integral aircraft characteristics close to real flight conditions.

These wind tunnels made a noticeable contribution to the development of the Russian aircraft building. Their special role during the years of the Great Patriotic War of 1941–1945 should be noted. At this time the investigations carried out at TsAGI (basically in the wind tunnels T-101 and T-104) resulted in improving the performance of combat airplanes, in particular maximum speeds of the military aviation airplanes were considerably increased (by 60 – 70 km/hour), and their characteristics of stability and controllability were perfected.

Among the first wind tunnels of the new TsAGI was also the free-spinning T-105 wind tunnel designed basically to study spin of the airplanes. The T-105 wind tunnel has an open test section 7 m in height with a diameter of the nozzle exit section 4.5 m; the maximum flow velocity in the test section is 35 m/s. The first start-up of this wind tunnel occurred in August, 1941, however because of the war the adjustment tests were suspended and renewed at the end of 1943. Further on besides the studies of spin the T-105 wind tunnel was used to perform tests of helicopter models, their rotors, parachute systems etc.

Among the whole complex of the first phase wind tunnels construction of the variable density T-106 wind tunnel, that provided investigation of the air compressibility impact on the aerodynamic characteristics of airplanes at high speeds, should be noted especially. The main parameters of this wind tunnel:

- range of variation of the flow Mach numbers, 0.15 – 0.9;
- test section diameter, 2.6 m;
- range of pressure variation, 0.15 – 6.7 kg/square cm,

surpassed in performance similar foreign facilities of that time. The wind tunnel construction was started in the summer of 1938 and completed at the end of 1942, and the first start-up took place in 1943.

In 1949 T-106 was modernized (the circular test section with solid walls was replaced with a polyhedral one with perforated walls, the one-stage compressor with a two-stage one) that provided Mach numbers up to 1.10 with a continuous transition through the sonic velocity.

With the construction of the T-106 wind tunnel the first phase of creation of wind tunnels of the new TsAGI was accomplished. The main characteristics of these wind tunnels are given in Table 2, and the schematics of some of them are presented in Figs. 3 – 7.

A swift development of aviation at the end of 1940 generated an acute necessity of designing trans- and supersonic wind tunnels. In the period from 1948 till 1953 the first supersonic wind tunnels were built at TsAGI. During these years a large complex of continuous flow and blowdown wind tunnels were built with various test section dimensions. The main characteristics of these wind tunnels are presented in

Table 3, and the schematics of some of them are given in Figs. 2-13.

Start-up of the large T-109 blowdown wind tunnel in 1953 was the final phase of creating a complex of trans- and supersonic wind tunnels.

This wind tunnel was designed for a range of Mach numbers from 0.5 to 3.5. It is equipped with pressure and suction ejectors, an adjustable supersonic diffuser and a square test section of 2.25×2.25 m with perforated walls of variable permeability (from 0 to 30%). In the range of Mach numbers from 0.5 to 1.3 the wind tunnel operates with the perforated test section and the pressure ejector placed in front of the settling chamber. The use of the pressure ejector at these modes makes it possible to reduce twice the compressed air rate from the balloons. Beginning from $M=1.7$ the wind tunnel operates with the solid test section in a direct-flow scheme. The suction ejector placed behind the supersonic diffuser ensures the required starting degrees of compression and also realizes $M=3.5$. The maximum pressure in the settling chamber is 6 kg/sm^2 . In this case Reynolds numbers of up to 60×10^6 (per 1 meter) may be obtained. To get such values of Reynolds numbers with a compressor drive unit for the same test section dimensions an electrical drive unit with a power of about 250 MW would have been needed. Initially the wind tunnel was equipped with replaceable supersonic nozzles, and after modernization in 1983 an adjustable nozzle was added for the range of Mach numbers from 0.5 to 4.0.

The complex of the supersonic wind tunnels of TsAGI has promoted considerably the development of the supersonic aviation of Russia. However the further growth of the airplane flight velocity and appearance of the space aircraft urgently necessitated the development of the appropriate wind tunnels.

In the mid-50s intensive researches were started at TsAGI to create large supersonic and hypersonic wind tunnels. These researches resulted in a complex of large supersonic and hypersonic wind tunnels the technical characteristics of which are presented in Table 4, and the schematics of some of them are given in Figs. 14, 15.

The most striking representatives of the large supersonic and hypersonic wind tunnels are the T-116 and T-117 wind tunnels covering the range of Mach numbers from 1.8 to 20 with a characteristic cross section of the test section 1 m.

In fact the T-116 wind tunnel is a complex of three wind tunnels with the following Mach number ranges: $M=1.75 - 4.0$; $M=4.5 - 7.0$; $M=7 - 10$, the common elements for which are: the test section, supersonic adjustable diffuser, exhaust duct with a three-stage ejector and also engineering and energetic systems. In order to minimize the losses in the wind tunnel and to reduce the time of the transient processes each of the three contours is equipped with its own systems of air supply, adjustment of parameters and heating.

To realize Mach numbers from 10 to 20 the T-117 wind tunnel is equipped with replaceable arc heaters and two systems of creating the required pressure difference:

- four-stage ejector,
- vacuum reservoir.

At the same period to study delicate physical phenomena the low-turbulence T-124 and T-125 wind tunnels are constructed with flow velocities in the test section up to 110 m/s and $M=0.3 - 4.0$, accordingly.

To solve specific problems linked with the space aircraft flights vacuum wind tunnels were built (see Table 5).

It should be noted that in 1962 a special scientific and research division (NIO-16) was formed at TsAGI with a mission of performing investigations pertaining to the creation of new and improving the existing wind tunnels. It played an important role in the development of the modern wind tunnels of TsAGI and the other enterprises of Russia and keeps on working in this direction up to now.

The principal characteristic of experimental facilities are presented in Table 6.

The growth of cruise flight velocities of civil aviation and appearance of highly maneuverable military airplanes necessitated the development of more perfect, highly efficient transonic wind tunnels.

This type of the wind tunnel, T-128, was commissioned at TsAGI in 1983 the schematic of which and the main technical characteristics are represented in Fig. 16.

Characteristic features of the wind tunnel are:

- availability of replaceable test sections with perforated walls of variable permeability (adaptive perforation);
- availability of an adjustable nozzle the range of Mach numbers $M=0.15 - 1.7$;
- availability of a forced suction of air from the pressure chamber and boundary layer suction from the test section walls.

To conclude this short historical review it should be noted that the investigations of TsAGI in the area of development and advancement of the wind tunnels had a remarkable impact on the creation of experimental bases of the kindred enterprises and organizations of Russia and other countries that formed the USSR.

Thus, under technical assistance and using the concepts of TsAGI the following facilities were built:

- wind tunnels of T-103-type: Moscow State University, Antonov design bureau (the city of Kiev), SibNIA (the city of Novosibirsk);
- wind tunnels of T-112-type: "Geodesia" institute (the city of Krasnoarmeysk), TsNIIMASH (the city of Kaliningrad);
- wind tunnels of T-113-type: ITPM CoRAN (the city of Novosibirsk), "Geodesia" institute (the city of Krasnoarmeysk), Moscow State university, TsNIIMASH (the city of Kaliningrad), TsKBMAH (the city of Reutovo);
- wind tunnels of T-114-type: KHAI (the city of Kharkov), TsKBMAH (the city of Reutovo), Moscow State University;
- wind tunnels of T-124, T-125-types: ITPM So RAN (the city of Novosibirsk).

Wind tunnels of Chaplyguin's laboratory of TsAGI

Table 1

Wind tunnel index	Test section dimensions, m	Velocity range, m/s	Stagnation pressure	Stagnation temperature,	Year of constr./ modernization
T-I	diam. 3	5 – 27	Atmospher.	Atmospher.	1925/1976
T-II	diam. 6	5 – 60	Atmospher.	Atmospher.	
T-III	diam. 1.5 (closed) diam. 1.5 (with an Eiffel chamber)	10 – 93 10 – 82	Atmospher. Atmospher.	Atmospher. Atmospher.	1926/1968
T-V	diam. 2.20	5 – 50	Atmospher.	Atmospher.	1931/1975

Note: All wind tunnels of Chaplyguin's laboratory were continuous-flow fan-driven wind tunnels.

Wind tunnels of the top priority of the new TsAGI

Table 2.

Wind tunnel index	Test section dimensions, m	Range of Mach numbers. Velocity range, m/s	Stagnation pressure	Stagnation temperature	Year of constr./ modernization
T-102	4.0 × 2.33 (ellipse)	20 – 50	Atmosph.	Atmosph.	1936/1950, 1964, 1976
T-103	4.0 × 2.33 (ellipse)	20 – 80	Atmosph.	Atmosph.	1936/1952, 1968, 1976
T-101	24.0 × 14.0 (ellipse)	up to 65	Atmosph.	Atmosph.	1939/1954, 1964, 1983
T-104	diam. 7.0	up to 125	Atmosph.	Atmosph.	1939/1956, 1960, 1969
T-105	diam. 4.5	2 – 35	Atmosph.	Atmosph.	1941/1949, 1965, 1979
T-106	diam. 2.6	0.1 – 1.1	0.5 – 5 tech. atm.	up to 330 K	1943/1949, 1962, 1982

Note: All wind tunnels are of continuous action

Wind tunnels of high subsonic and supersonic velocities

Table 3.

Wind tunnel index	Test section dimensions, m	Range of Mach numbers	Stagnation pressure, kPa	Stagnation temperature, K	Year of constr./ modernization
T-107*	diam. 2.7	0.1 – 0.92	Atmosph.	Atmosph.	1949/1970
T-108*	1 × 1	0.5 – 1.15; 1.3; 1.5; 1.7	30 – 150	290 – 330	1951/1968, 1978
T-112**	0.6 × 0.6	0.6 – 1.25; 1.5; 1.7	Atmosph.	Atmosph.	1947/1959, 1971
T-113**	0.6 × 0.6	1.75 – 5.0; 6.0	150 – 700	290 – 550	1948/1960, 1976
T-114**	0.6 × 0.6	0.6 – 1.2; 1.5 – 4	100 – 580	Atmosph.	1952/1960, 1970
T-109**	2.25 × 2.25	0.4 – 4.0	80 – 560	Atmosph.	1953/1968 1983
SVS-2	0.5 × 0.516 diam. 0.56	0.3 – 5; 5.0 – 6.0	20 – 1050	Atmosph. 290 – 500	1956/1968, 1995

Note: * – wind tunnel of continuous action; ** – intermittent wind tunnel

Hypersonic wind tunnels

Table 4

Wind tunnel index	Test section dimensions, m	Range of Mach numbers; velocities, m/s	Stagnation pressure, kPa	Stagnation temperature, K	Year of constr./ modernization
Small size wind tunnels					
T-33	diam. 0.3	3 – 5	350 – 900	290 – 770	1958/1968
GT-2	diam. 0.3	8; 16 – 22	100 – 4000	290 – 800	1962/1978
T-120	diam. 0.15	4 – 10	200 – 14000	290 – 980	1964/1973
T-121	diam. 0.2	4 – 9	200 – 9000	290 – 960	1958/1970
T-122	0.03 × 0.18 diam. 0.08 – 0.15	4.8 4.8 – 7.8	200 – 1000	up to 5000	1964/1981
T-123	diam. 0.02 – 0.08 diam. 0.3	1 – 7 7 – 20	up to 5000 up to 20000	up to 4000 up to 5000	1964/1976

Table 4 (continued)

Wind tunnel index	Test section dimensions, m	Range of Mach numbers; velocities, m/s	Stagnation pressure, kPa	Stagnation temperature, K	Year of constr./ modernization
Large size wind tunnels					
T-116	1 × 1	1.8 – 10	60 – 8000	290 – 1070	1960/1972
T-117	diam. 1	10 – 20	up to 16000	1100 – 3000	1978/1984
UT-1	diam. 0.3; 0.4; 0.5	5 – 15.5	up to 150000	up to 2200	1959/1972
IT-2	diam. 0.44 diam. 0.2; 0.53; 0.9	16.3 – 17.9; 10 – 22	12000 – 150000	1500 – 5000	1960/1980

Note: All the wind tunnels are of blowdown type

Table 5

Vacuum wind tunnels

Wind tunnel index	Test section dimensions, m	Range of Mach numbers; velocities, m/s	Stagnation pressure, kPa	Stagnation temperature, K	Year of constr./ modernization
VAT-3	diam. 0.15; 0.3; 0.4	12; 18; 20	500 – 6000	290 – 2000	1967/1982
VAT-102	diam. 0.18; 0.25; 0.38	0.2 – 1.0; 5; 8	1 – 30	290 – 1800	1980
VAT-103	diam. 0.1	7; 4000 – 8000	10 – 40	3000 – 6000	1968/1979
VAT-104	diam. 0.05	4 – 8; 4200	3 – 40	5000 – 8000	1983/1989

Table 6

Experimental facilities to study wind tunnel elements

Facility index	Test section dimensions, m	Range of Mach numbers; velocities, m/s	Stagnation pressure, kPa	Stagnation temperature, K	Purpose
T-03*	0.4 × 0.6	5 – 70	Atmosph.	Atmosph.	Study of nozzles, test sections, diffusers of subsonic wind tunnels
T-02**	0.12 × 0.18	0.1 – 1.3	20 – 300	Atmosph.	Study of transonic wind tunnels with ejector drives
T-04**	0.2 × 0.2	0.1 – 1.15	110 – 600	100 – 300	Study of cryogenic wind tunnels, their elements and systems
UVS**	0.18 × 0.18	0.2 – 1.7	100 – 200	Atmosph.	Study of elements of transonic wind tunnels
UGSD**	diam. 0.15 diam. 0.3	5 – 12 13 – 20	2 – 200 MPa	up to 2000	Study of high stagnation pressure wind tunnels
SMGDU**	from 0.025 × 0.025 to 0.25 × 0.25	8 – 15 2500 – 9000	up to 18000	up to 9000	Study of wind tunnels and their elements by magnetic and hydrodynamic gas acceleration

Note: * – wind tunnel of continuous action; ** – intermittent wind tunnel

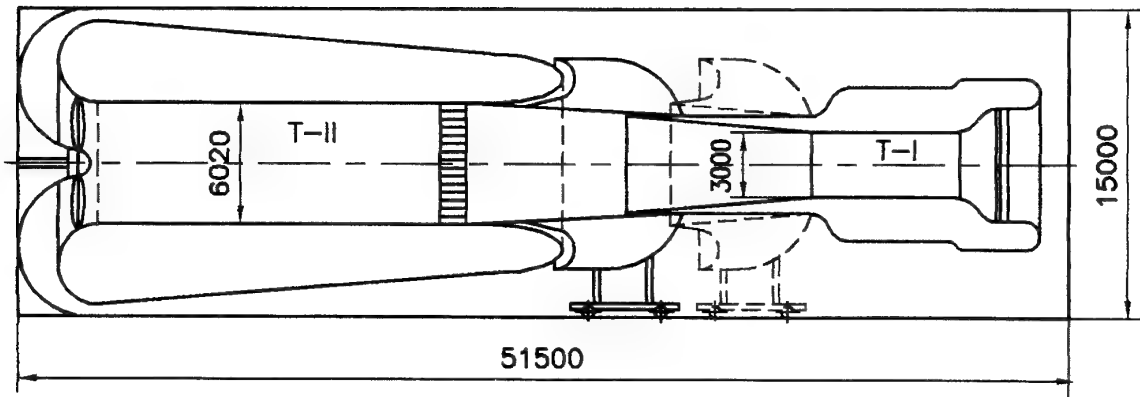


Figure 1. T-I - T-II wind tunnel schematic

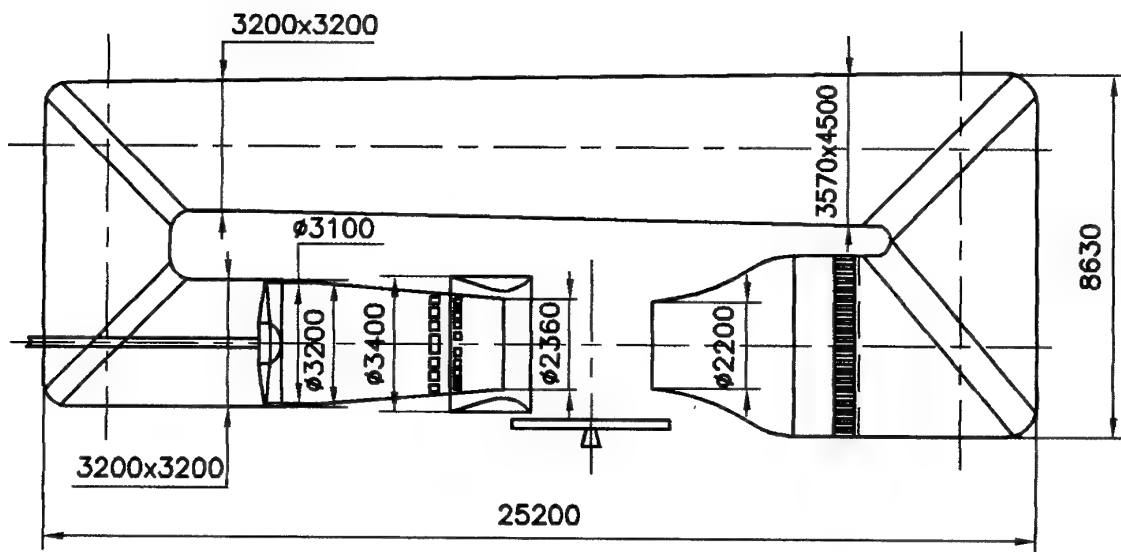


Figure 2. T-V wind tunnel schematic

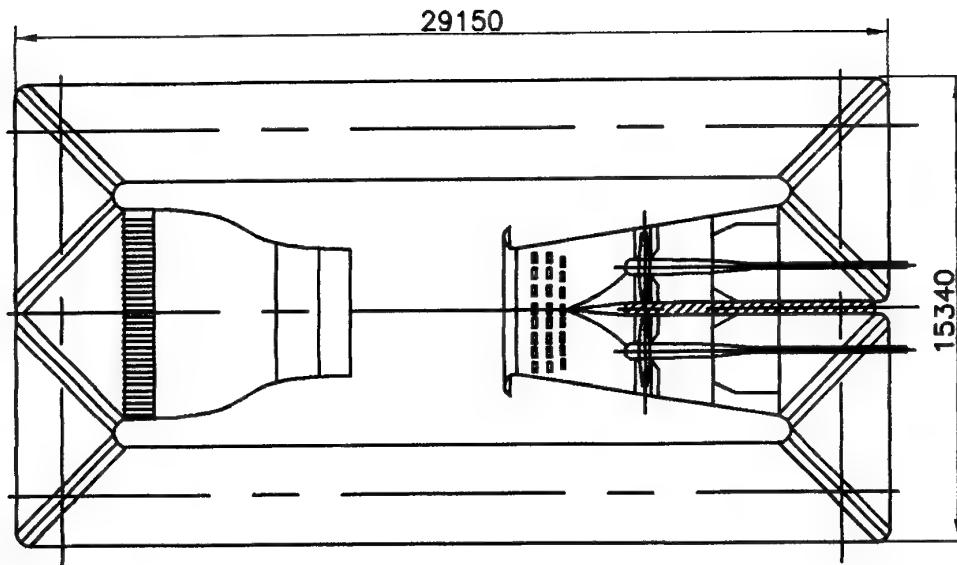


Figure 3. T-102 wind tunnel schematic

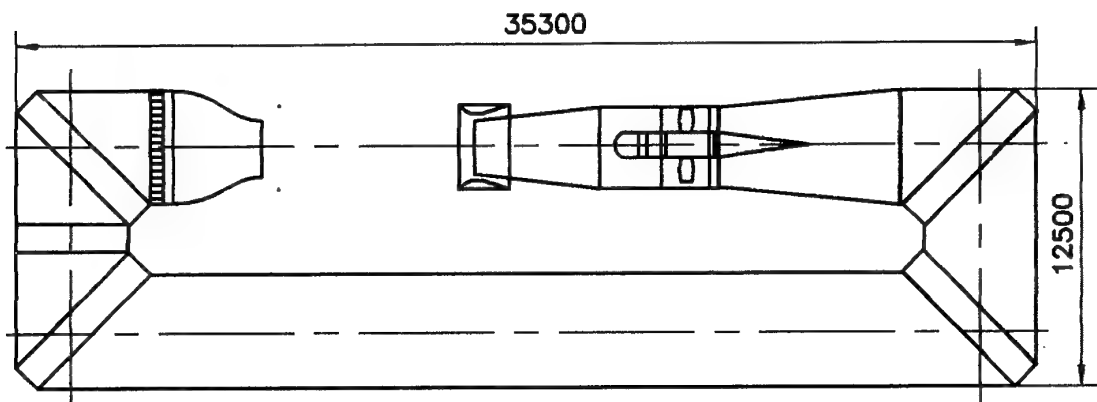


Figure 4. T-103 wind tunnel schematic

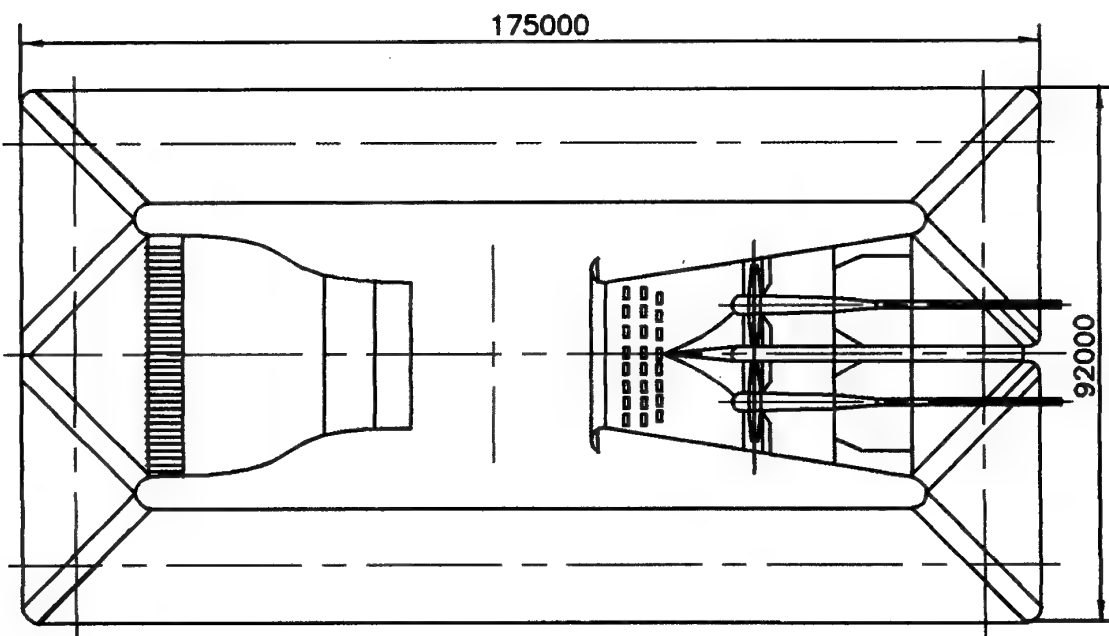


Figure 5. T-101 wind tunnel schematic

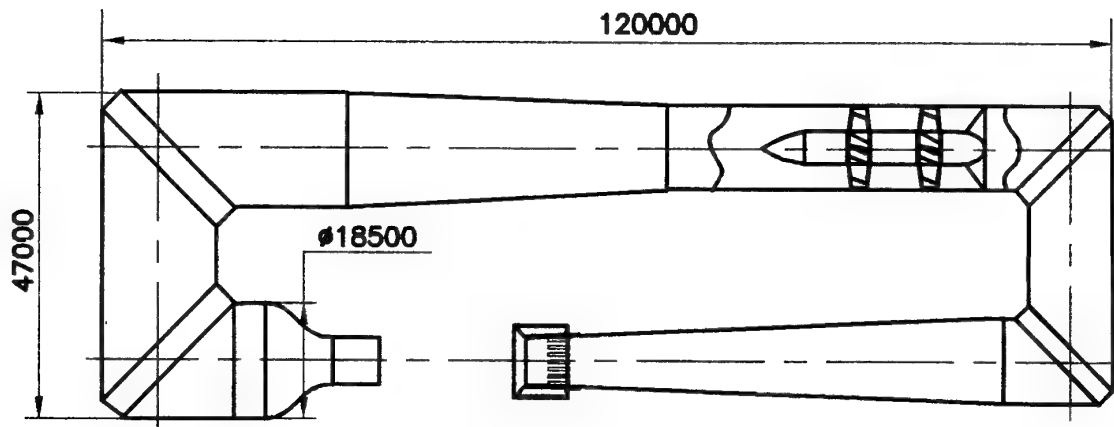


Figure 6. T-104 wind tunnel schematic

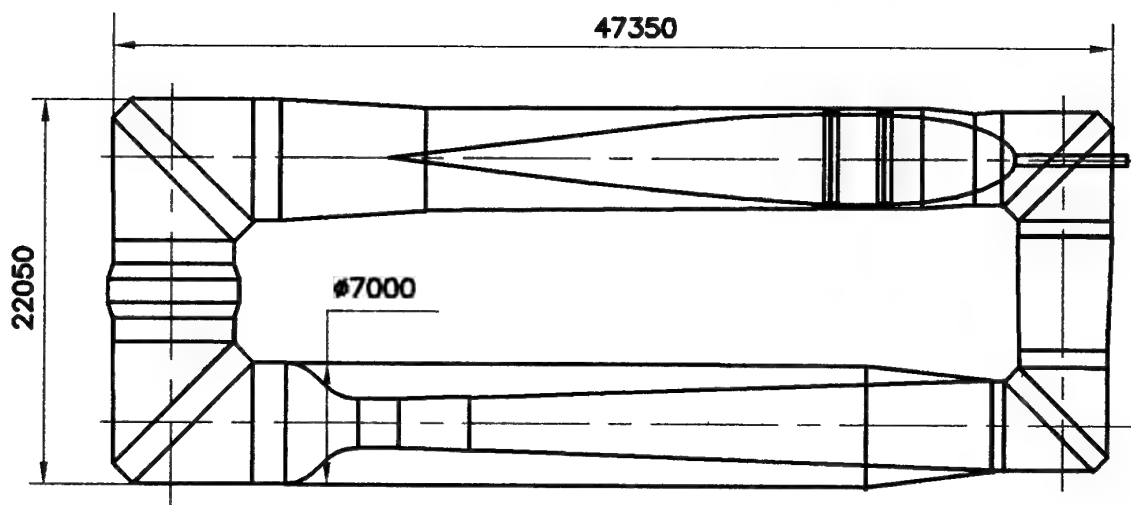


Figure 7. T-106 wind tunnel schematic

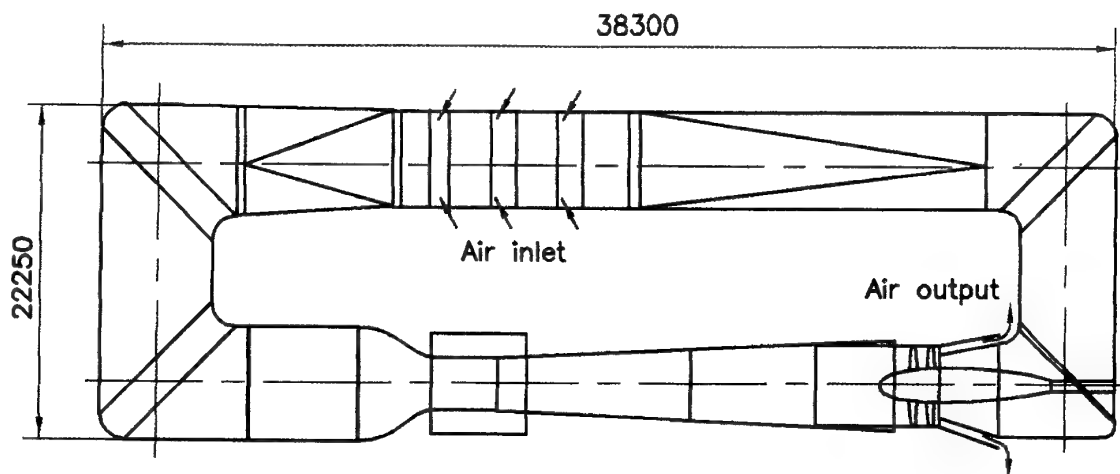


Figure 8. T-107 wind tunnel schematic

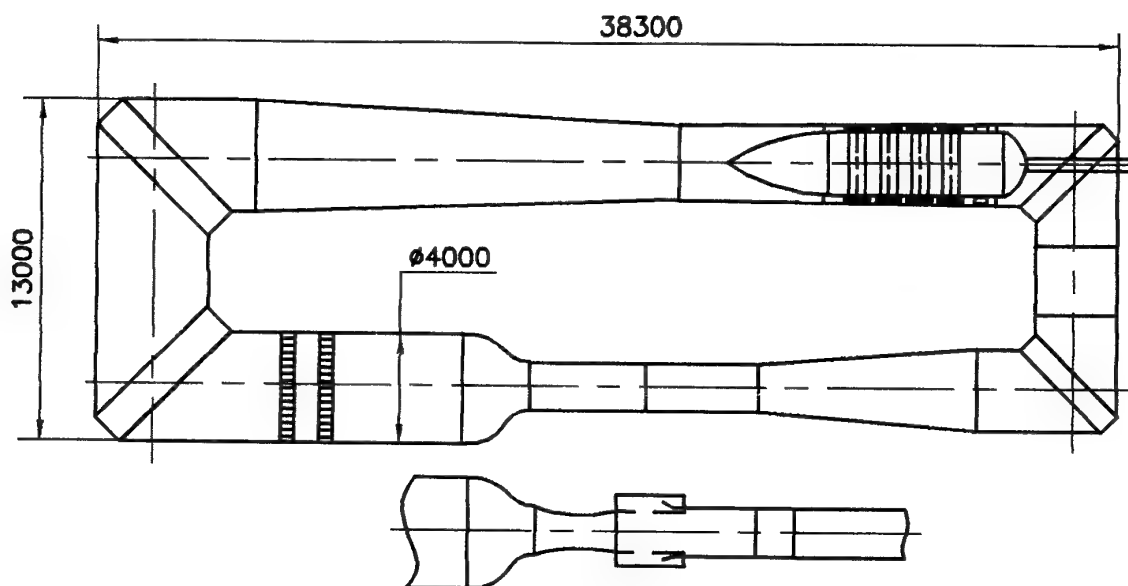


Figure 9. T-108 wind tunnel schematic

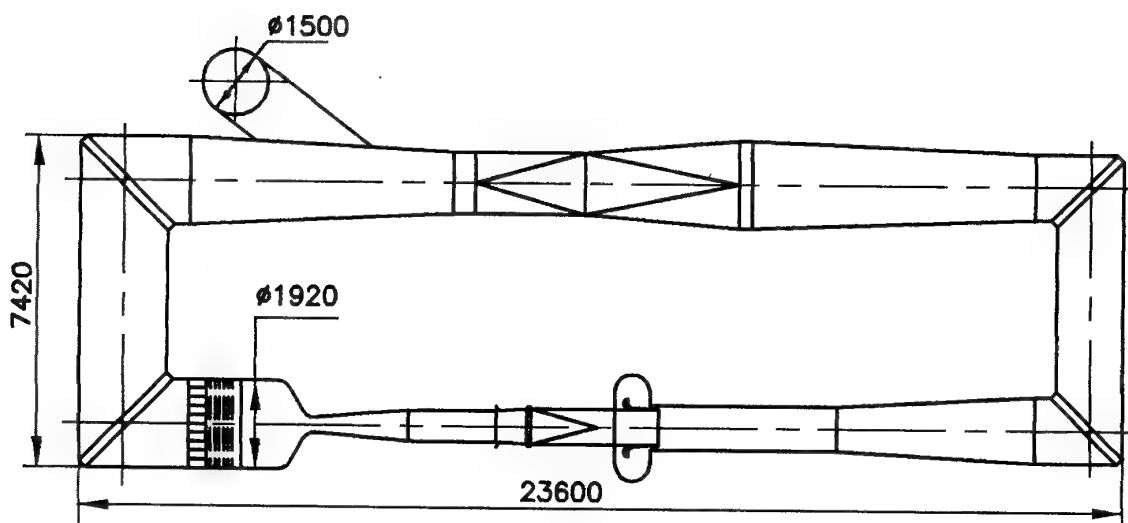
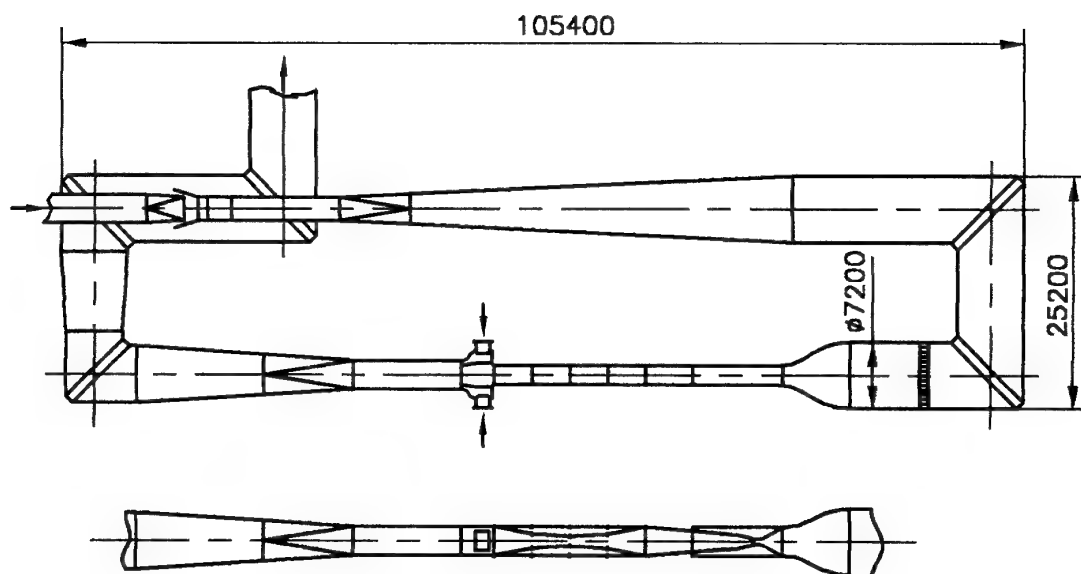
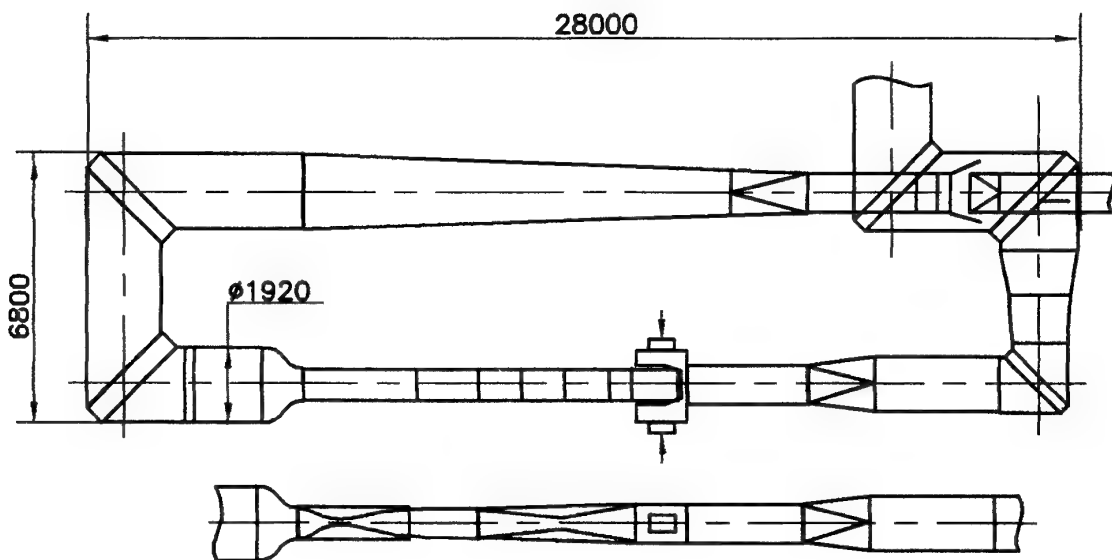
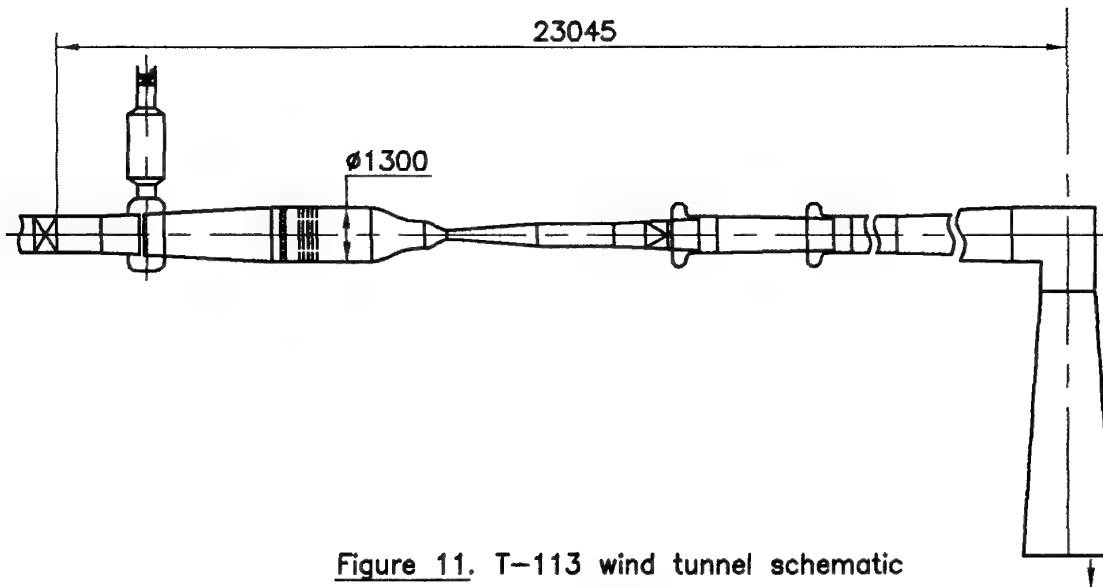


Figure 10. T-112 wind tunnel schematic



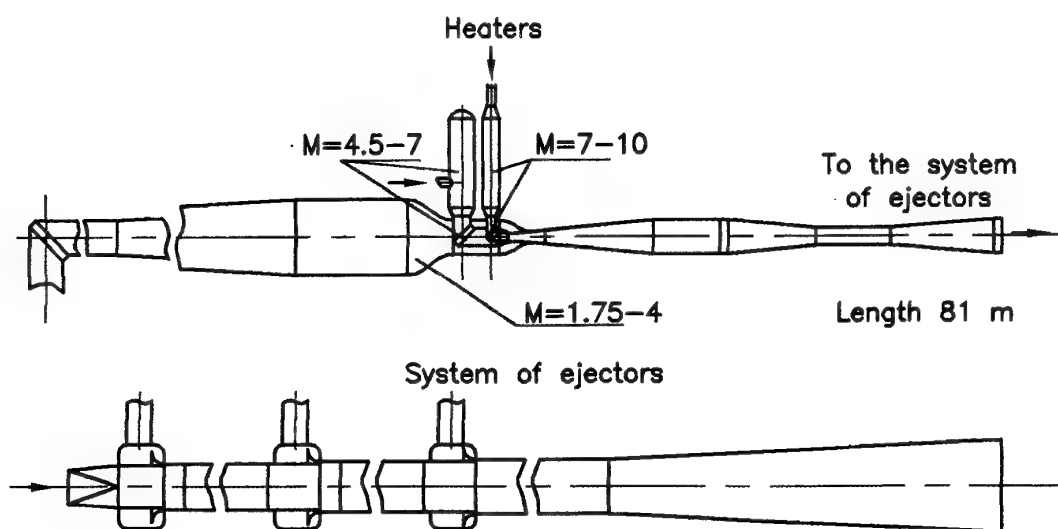


Figure 14. T-116 wind tunnel schematic

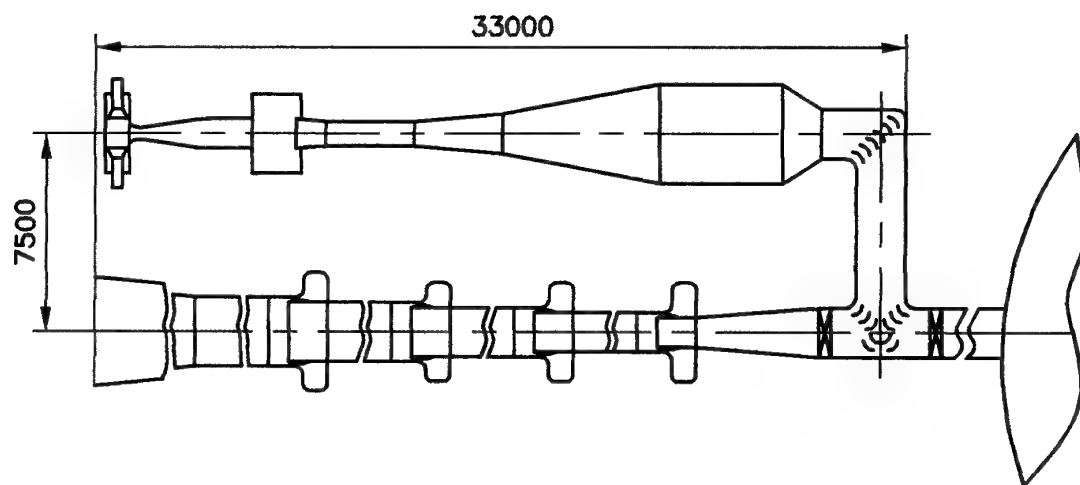
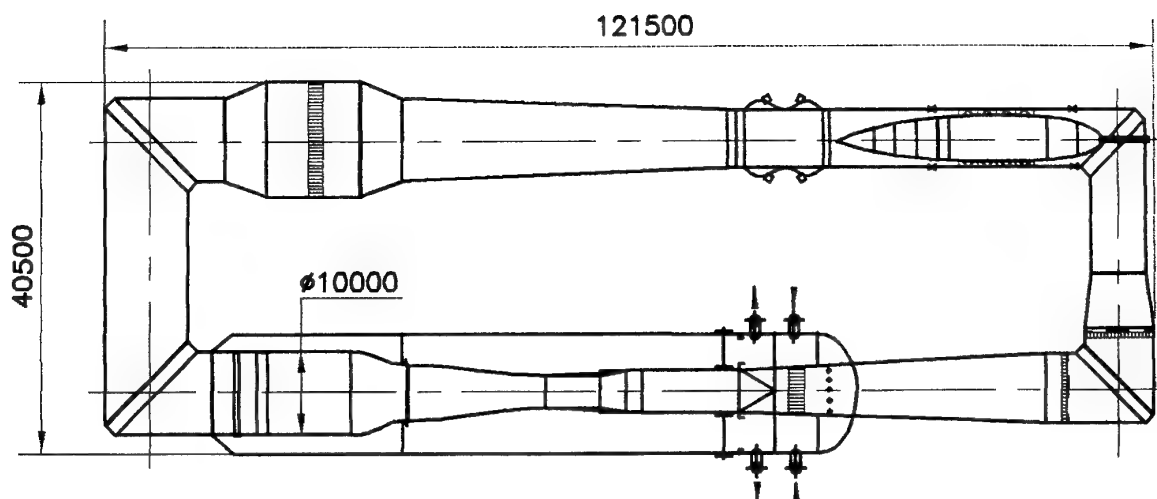


Figure 15. T-117 wind tunnel schematic



Test section (m),	2.75 x 2.75	Suction system power (MW),	45
Mach range,	0.15 to 1.7	Reynolds number ($\times 10^6/m$),	to 41
Total pressure (kPa),	0.5 to 400	Dynamic pressure (kPa),	to 105
Total temperature (K),	313	Run time,	continuous
Fan drive power (MW),	100		

Figure 16. T-128 wind tunnel schematic

Some Constraints Imposed on the Aerodynamic Development Process by Wind-Tunnel Circuit Design Characteristics

F.T. Lynch

R.C. Crites

McDonnell Douglas Corporation

Mail Code 71-35

2401 E. Wardlow Road

Long Beach, California 90807-4418

SUMMARY

Requirements for obtaining reliable and meaningful data in most wind tunnel test situations are addressed from an aircraft industry user's perspective. Factors considered are Reynolds number requirements, tunnel flow quality requirements, and tunnel wall and support system effects. Factors which are important in satisfying timeliness and cost effectiveness requirements are also identified. Important flow quality imperfections which exist with less-than-perfect wind-tunnel circuit aerodynamic design are considered, together with a review of the existing knowledge base for assessing the likely/potential effects of variations in these imperfections on the resultant test data. The need to have a thorough knowledge of the important flow physics features which are controlling the aerodynamic, aeroacoustic, and/or propulsion characteristics of the vehicle or flow situation under investigation at the associated test conditions is stressed in order to adequately understand and identify wind-tunnel flow quality requirements and effects on data quality, accuracy, and adequacy. The importance of not limiting the identification of potential data errors and measurement uncertainties to just those which can be currently quantified with existing analytical and computational methods is also stressed, as is the importance of understanding the aerodynamic design and validation process in which the data is being used, and the risk involved in the particular design being investigated. Additional considerations which need to be given attention when conducting some specialized types of tests (icing, semispan, open throat, etc.) are addressed. Examples of observed and easily-envisioned flow-quality-variation effects on measured aerodynamic characteristics are presented. Lastly, prospects for improving tunnel flow quality through application of current advanced CFD capabilities are highlighted, as well as prospects for incorporating advanced test-section wall ventilation concepts to enable more reliable and cost effective high Reynolds number testing capabilities.

1. INTRODUCTION

Outstanding progress has been made in the development and effective application of advanced CFD methods in the aerodynamic design process, thereby enabling significant reductions in the aerodynamic design cycle time for most aircraft categories^{1,2}. This is especially true for cruise configuration development^{3,4}, and this role will be expanding in the relatively near future to more complex geometries and flow situations such as high lift systems, control surfaces, etc. However, CFD is not about to

replace the wind tunnel as some have predicted, because their roles in the design process are truly complementary and unique. As illustrated by Rubbert², CFD is a very cost- and time-effective means of providing important configuration-setting simulations, since these relatively few simulations can be obtained in significantly less time and for less cost than it takes to build a wind tunnel model. But, as he also showed, wind-tunnel testing is much more effective (i.e., practical) in obtaining the additional, orders-of-magnitude greater number of simulations required to provide all the data needed in the total design process. So, even if future development of CFD capabilities achieves the accurate prediction of the wide range of flow conditions for which reliable data are needed, CFD will not replace the wind tunnel in any realistic design process.

Virtually all wind-tunnel-imposed constraints on the aircraft design process have their origin in the obvious, but often overlooked fact that wind-tunnel testing is only a simulation of flight. In flight, the air stands still (more or less) and the aircraft moves through it. In the wind tunnel, the aircraft model stands still (more or less) and the air is forced past it. The implied simple translation of reference frame misses the extremely important fact that the vast bulk of the air remains still, and only a comparatively small stream (compared to flight) can be forced past the model. This seemingly minor, but inescapable distinction is really the "root of all evil" in the simulation of flight commonly called wind tunnel testing.

Obtaining reliable and meaningful data in a timely and cost-effective manner are the normal overriding user objectives when conducting almost any kind of wind-tunnel test in almost any test facility. Principal requirements for obtaining reliable and meaningful data in most testing situations are an adequate Reynolds number, representative or satisfactory tunnel flow quality, and avoiding tunnel wall and support system effects which either alter important flow characteristics on the model, or cause effects which cannot be readily or accurately accounted for⁵⁻⁸. The definition of an adequate Reynolds number can be very different for differing applications⁹, while the definition of satisfactory flow quality involves several flow parameters and a multitude of potential impacts on data adequacy and accuracy⁵⁻⁷. Similarly, tunnel-test-section design requirements vary widely for different aircraft product categories, such as V/STOL versus transport aircraft. Failure in any one of the three identified requirements will likely preclude achievement of the desired and needed results. For example, testing at full scale Reynolds numbers is certainly attractive for

minimizing risk, but much of this advantage may well be lost if the tunnel flow quality is not representative of free air flight conditions, or if the wall effects or support system effects become too large in seeking these flight Reynolds numbers, or if the testing costs are too high.

Factors which are important in satisfying the timeliness and cost-effectiveness requirements include minimizing the time required for model installation and configuration changes, utilization of efficient data gathering systems, effective utilization of test time (i.e., time per data point) in data gathering/sampling¹⁰, and the ability to use rapid techniques to account for tunnel wall and support system interference effects. These requirements have led to the use of interchangeable carts and test section isolation systems, as well as the use of global optical measurement systems such as pressure sensitive paint (PSP), Doppler global velocimetry (DGV), particle image velocimetry (PIV), etc⁸. These capabilities are certainly major contributors to achieving cost effectiveness and timeliness objectives, but they are not, by themselves, sufficient. For example, if the user has to wait a considerable time for necessary data corrections to account for significant tunnel wall and support system interference effects, or poor tunnel flow quality effects (presuming they are correctable), then the timeliness requirements will not be met. It is also important to note that flow quality, in terms of flow steadiness, is a factor in the ability to effectively utilize rapid data gathering techniques such as the global optical measurement systems. Hence, the aerodynamic design of wind tunnel circuits, in that it has a fundamental first order effect on tunnel flow quality, tunnel wall and support system interference effects, and on tunnel construction and operating costs, is of crucial importance in meeting user objectives for obtaining reliable and meaningful test results in a timely and cost effective manner. However, it is essential to keep in mind that user objectives and requirements can vary widely for different aircraft or air vehicle types for a variety of reasons.

In order to adequately understand and identify wind-tunnel flow quality requirements and effects on data quality, accuracy, and adequacy, it is imperative that the user (either researcher or industry product designer) have a thorough knowledge of the important flow physics features which are controlling the aerodynamic, aeroacoustic, and/or propulsion characteristics of the vehicle or flow situation under investigation at the associated test conditions (i.e., Reynolds number, etc.)⁷. Without this understanding, it is not possible to properly identify and quantify the effects of potential or known flow quality characteristics and deviations on the quality or adequacy of the data being obtained. Examples supporting this contention will be presented. And, it is especially important that tunnel users and operators not limit the identification of potential data errors and measurement uncertainties to just those which can be currently predicted with existing analytical and computational (CFD) methods. Although this is a very typical approach, it can be a recipe for disaster. It would seem to be more logical to focus instead on minimizing the flow quality defects which cannot be adequately addressed with computational methods rather than those that can.

Another important prerequisite for establishing wind tunnel flow quality requirements and priorities is a

thorough understanding of both the aerodynamic design and validation process being utilized as well as the types of advanced aerodynamic technology (i.e., risk) being incorporated in the particular design being investigated. The design and validation process being employed typically depends on many factors including customer requirements, the skill and background of the aerodynamic designers, and upper management insights and requirements. For example, if the choice or purchase of an aircraft depends upon whether the customer has confidence in drag characteristics derived almost exclusively from wind tunnel measurements, then flow quality parameters which have the greatest effect on drag uncertainty are of utmost importance. However, if absolute drag measurements from the wind tunnel are not the cornerstone of the aircraft drag assessment, or if the focus is instead on minimizing the risk associated with the introduction of advanced aerodynamic concepts, then other flow quality parameters are of highest priority.

Tunnel flow quality characteristics, which are a result of the aerodynamic design of the wind tunnel circuit, can influence and alter the data being gathered in many ways. Obvious influences are the effects of freestream turbulence and background noise on the boundary-layer transition process, the existence (or absence) of laminar separation bubbles, and possible relaminarization phenomena. In addition, there are the freestream turbulence effects on the development of transitional boundary-layer characteristics, on skin friction and heat transfer levels, on separation onset/progression tendencies of turbulent boundary layers, and on the spreading characteristics of jets, merging wakes and shear layers. These effects in turn, have a major impact on almost (if not) all detailed and integrated vehicle aerodynamic, aeroacoustic, and propulsion characteristics or basic flow situations of interest, including the establishment of appropriate viscous scaling criteria, determination of drag characteristics, identifying separation onset in interference / juncture flow regions, establishing the viability of natural-laminar-flow-control concepts, determining control surface effectiveness characteristics, determining buffet onset/progression characteristics, in establishing the maximum lift and drag characteristics of candidate high lift systems at both takeoff and landing conditions, and in establishing airframe and jet exhaust noise levels. There are also other non-uniformities in the onset freestream flow which can have significant adverse effects on the value of the test data being gathered. For example, flow angularity and uniformity variations and gradients have very measurable effects on drag characteristics, and can also alter the (spanwise) development of separated flow characteristics, which, in turn, directly impacts buffet onset/progression and stall characteristics. In a similar manner, wall interference effects can drastically alter crucial aerodynamic characteristics, especially at subsonic and transonic conditions. Consequently, it is mandatory that the user thoroughly understand the possible ramifications which can arise from all of these potential modifications to measured aerodynamic characteristics, etc. This is true whether the test is being conducted for aircraft/vehicle configuration development and validation, to gather the large quantities of data needed in the detailed design process, for CFD calibration and validation, to

obtain data to guide CFD development effects, to establish empirical-type methods, or for any other purpose.

In order to provide some basis for assessing the relative importance of the various flow imperfections which are likely to exist with any relatively conventional wind tunnel due to less-than-perfect circuit aerodynamic design, important flow quality parameters are considered first in section 2 of this paper, together with a review of the existing knowledge base for assessing the likely/potential effects of variations in these parameters on the resultant test data. Additional considerations which need to be given tests, such as icing, semispan, 2-D, open throat, etc., are addressed in section 3. Following this, some examples of observed flow-quality-variation effects on measured aerodynamic characteristics are presented in section 4, along with some other easily-envisioned effects of tunnel- and wall-induced flow imperfections that users should be aware of. Lastly, prospects for improving tunnel flow quality and minimizing wall interference effects in future tunnel designs or modifications are addressed in section 5, with a special emphasis on application of current advanced CFD constrained-optimization methods (developed for aircraft design) to the design of some wind tunnel circuit components. Throughout this paper, due to practical limitations, emphasis is placed primarily on the requirements for continuous-flow subsonic and transonic production-testing-type tunnels, since this class of facilities certainly predominates in terms of number of tunnels and amount of usage. However, most of the lessons learned apply almost equally to other classes of facilities (i.e., supersonic, hypersonic, and research).

2. FLOW QUALITY ASSESSMENT

Model-in-tunnel test section flow quality is obviously of prime importance to the user, as compared to clear tunnel test section flow quality, although clear tunnel flow quality is an obvious (but not sufficient) prerequisite. The clear tunnel flow quality is determined by the effectiveness of the aerodynamic design of the non-test-section components in the wind tunnel circuit (i.e., diffusers, fan nacelles, heat exchangers, flow turning components, settling length, contraction/nozzle, acoustic treatment, etc.) in suppressing flow disturbances and subsequent interactions, but model installation effects can also easily impact the adequacy/performance of these components, and must be considered. For example, it is well known that onset flow conditions have a very strong influence on the aerodynamic performance or adequacy of subsonic diffusers. Therefore, possible flow disturbances emanating from the test section, either from model support system components, adverse flow interactions with the tunnel wall (boundary layer), or model wakes, must be addressed and accounted for in the design of the tunnel diffuser. Some of these influences are especially important for semispan and two-dimensional testing. Many other interactions are also likely and plausible, and must be considered.

Several figures of merit are normally used to describe and quantify wind tunnel flow quality characteristics. The most significant ones include:

- Test section turbulence characteristics (levels and spectral properties) - both axial and cross components

- Background noise levels/static pressure fluctuations (levels and spectral properties)
- Flow angle gradients - both axial and cross components
- Mach number uncertainty and gradients
- Total temperature - reference value, distribution, and rate change
- Tunnel steadiness - total and static pressure, total temperature.

In addition, the absence of small (hard) particles in the tunnel flow is important to avoid sandblasting the leading edges of models, and the absence of humidity in the flow is crucial for cryogenic tunnels to prevent problems with ice forming on the model or on components in the wind tunnel circuit. While all of these figures of merit are normally used in defining clear tunnel test section flow quality characteristics, many of them are, or can be, modified to various degrees by model installation effects. For example, in addition to the aforementioned effects on diffuser performance, with the subsequent effect on turbulence levels, flow gradients, and tunnel stability and control, wall interference can alter test section flow angle and Mach number levels and gradients, as can semispan model installation effects. Hence to be meaningful to the tunnel user, test section tunnel flow quality characteristics must be evaluated for the range of model installations likely to be utilized.

2.1 Turbulence and Background Noise

Test section turbulence (i.e., relatively high frequency, small scale velocity fluctuations in both axial and transverse directions), above the relatively low values which are believed to exist at normal inflight conditions, can have a most significant impact on a wide range of viscous characteristics typically encountered on wind tunnel models^{5,7}. To start with, elevated turbulence levels, especially at lower frequencies, are known to cause premature boundary-layer transition (upstream of where transition would occur if turbulence levels were below threshold values) on the model aerodynamic surfaces, although the tunnel background noise environment also plays an important role in triggering this premature transition. Knowledge of where boundary-layer transition occurs is always important, but it is particularly crucial in establishing appropriate viscous scaling criteria for any testing at less-than-full-scale flight Reynolds numbers, and it is certainly of great importance for any wing designs trying to incorporate natural laminar flow (NLF) benefits. Although the qualitative effects of elevated freestream turbulence (and background noise) on boundary-layer transition are well known, the current knowledge base for quantitative assessments of these effects accounting for both spectral content and amplitude of disturbances, is certainly not at an advanced state of readiness. In fact, transition predictions on swept wings at flight conditions (i.e., low freestream turbulence levels) are not yet very reliable with existing methods, let alone at elevated freestream turbulence (and background noise) levels. While an integrated effect of elevated freestream turbulence and background noise levels is often judged by transition measurements on a 10° cone, this indicator is not at all conclusive or reliable since it only addresses T-S wave instability, but does not address many of the other modes which can trigger transition on a swept wing. Considering

the range of model geometries and test Reynolds numbers which need to be considered, much additional research clearly remains to be done before it will be possible to either reliably specify threshold turbulence characteristics and background noise levels, etc. necessary to avoid premature transition, or provide meaningful quantitative predictions of the effects of a broad spectrum of turbulence and noise levels and characteristics above the threshold values on the transition process. One current school of thought has specified an RMS turbulence amplitude of 0.05 percent for axial (u/U_∞) and cross components (v/U_∞ and w/U_∞) as being sufficiently low to avoid premature transition¹¹. Unfortunately, corresponding values for current production-type transonic wind tunnels are several times higher than this level. A threshold level for static pressure fluctuations of 0.6 percent has likewise been specified for transonic conditions, but, again, levels present in current production-type transonic tunnels are significantly higher than this (see Figure 1).

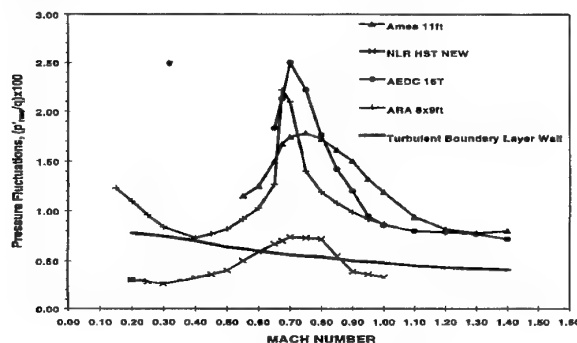


Figure 1: Noise Measurements in Major Transonic Wind Tunnels

Consequently, if these threshold values are at all realistic, then premature transition (at a given Reynolds number) due to elevated turbulence and background noise levels has existed for at least all transonic testing conducted in production-type transonic tunnels to date. Knowing (i.e., measuring) where transition is occurring under these circumstances is clearly mandatory for any intelligent interpretation of test data.

Although not gaining the notoriety that premature transition effects have, turbulent boundary layer characteristics are also modified in important ways by elevated freestream turbulence levels^{7,12}. In particular, boundary layer (thickness) growth rates, momentum thickness (and shape factors), skin friction and heat transfer levels, and propensity to separation are all altered. Elevated turbulence levels do lead to increased skin friction levels, and, in turn, thicker boundary layers. The mechanism which results in the higher skin friction levels is just the opposite of that which has been employed to reduce turbulent boundary layer skin friction levels. Riblets are an excellent case in point. In that case, riblets reduced skin friction levels by reducing near-wall turbulence levels. Hence, any increases in near-wall turbulence levels brought about by elevated freestream turbulence levels do result in higher skin friction levels. The higher skin friction levels and reduced shape factors, together with the attendant thicker boundary layer (which leads to reduced

adverse pressure gradients), result in a reduced tendency for boundary-layer separation onset in many flow situations. Again, as was the case for premature transition, these effects are well known qualitatively, but any quantitative predictions of these effects are not currently reliable. Much research needs to be accomplished in developing appropriate turbulence models to represent a wide range of separation onset/progression situations, especially with strong spanwise viscous components, before reliable quantitative estimates of these effects are possible. Model surface condition (i.e., smoothness) effects need to be quantified as well.

Elevated freestream turbulence and background noise levels can also influence many other aerodynamic, aeroacoustic, and propulsion flow characteristics which impact measured integrated vehicle characteristics. At low-speed high-lift conditions, the formation and bursting of laminar separation bubbles on leading-edge components, possible relaminarization on the main element of multielement designs with the leading-edge device extended, and the merging shear layers and wakes which often control the maximum lifting capability of multielement high lift systems, are all influenced to some degree by elevated freestream turbulence levels, and, in some cases, background noise levels. In a similar manner, the spreading characteristics of propulsive jets are also influenced. In every case, the direction or qualitative nature of the influence is known. For example, elevated turbulence and background noise levels can keep destructive laminar separation bubbles from forming, and will promote the harmful merging and spreading of the shear layers and wakes of multielement high lift systems. However, in every case, it is again not yet possible to provide meaningful quantitative predictions, and extensive research will be required before this situation will change.

Freestream turbulence also implies both dynamic angle of attack and time-varying dynamic pressure which provides a time-varying excitation of model and model-support system structural modes, which in turn translate into balance dynamics which affects the time required (i.e., tunnel productivity) to integrate/extract data of sufficiently low uncertainty.

2.2 Flow Angle Gradients

The evaluation of flow-angle gradient effects, either clear tunnel or model-installed values, is an area where the specification of allowable limits, and the identification of potential data errors and measurement uncertainties, typically tends to be established by what can be currently predicted with existing analytical and CFD methods. For example, the consequences of flow angle gradients along the span of the wing are normally evaluated in terms of an induced twist affecting lift, drag, and rolling moment at unseparated flow conditions. What is rarely considered is the potential impact on the stall- or buffet-onset characteristics of the wing, which are often the biggest unknowns requiring wind-tunnel testing due to limitations of current 3-D CFD capabilities. Flow angle gradients due to tunnel wall effects with large models are a major concern for these higher angle-of-attack conditions.

The same assess-what-you-can process is also normally used in evaluating the effects of axial flow angle gradients, again either clear tunnel or model-installed. In this case,

the typical assessment process addresses an induced camber and tail angle increment as they impact lift, drag, and pitching and yawing moments. Based on this approach, a typical limitation on axial flow angle gradients turns out to be around 0.03 deg/chord over the length of the model to keep the impact of these effects within target measurement uncertainties. However, additional analysis is needed as a minimum to determine the impact of such gradients on the flow characteristics of representative multielement high-lift wing designs at stall conditions, and for modern transonic wing designs at conditions where the flow development is very sensitive to small changes.

2.3 Mach Number Uncertainty and Gradients

Accuracy in establishing the reference Mach number is of utmost importance in minimizing drag level uncertainty. At typical transonic cruise conditions, it can be shown that a 0.003 uncertainty in Mach number by itself results in a one-drag-count uncertainty. However, since Mach number uncertainty is not the only contributor to drag level uncertainties, a realistic requirement is that a 0.001 Mach number increment must be recognizable at transonic cruise conditions in order to meet appropriate drag level uncertainty requirements¹¹.

Allowable axial Mach number gradients in the test section are often established by trying to restrict the buoyancy correction, with a typical goal being one drag count for most model configurations. However, an additional consideration which should be examined in establishing such limits is the impact of axial Mach number gradients on the ability to validate shock-free design concepts (wings, nacelles, etc.). Cross-stream Mach number gradients must also be considered, as these could be very important in determining the acceptability (or lack thereof), of buffet onset/progression characteristics at transonic conditions.

2.4 Total Temperature Uncertainty, Distribution, and Rate Change

Accuracy in establishing tunnel reference total temperature is necessary in that it influences the reference Mach number and Reynolds number, and affects skin friction levels, propulsion system characteristics, etc. Imposing typical criteria such as limiting Reynolds number uncertainty to no more than 0.2 percent, and (laminar) skin friction level uncertainty to a maximum of 0.1 percent, leads to establishing a maximum uncertainty level tolerable for the mean value of total temperature of approximately $\pm 1^\circ \text{F}$ throughout the Mach number and total pressure envelope of the tunnel. These same considerations also lead to the requirement that the temperature deviation from the mean value in a plane normal to the flow (i.e., along the span of a wing) should not be any greater than the uncertainty of the mean value¹¹. Tunnel control is also important along with stability, since rate change of stagnation temperature is needed for infrared transition detection systems.

3. UNIQUE TESTING CONSIDERATIONS

The flow quality characteristics just described are critical in almost all kinds of wind-tunnel testing conceivable. There are, however, various additional considerations which need to be addressed for some specialized types of wind-tunnel testing.

3.1 Icing Tunnels

Testing in icing tunnels is normally undertaken for any number of reasons, including:

- Determining ice-catch characteristics of unprotected areas of the vehicle
- Development/validation of more cost-effective anti-icing systems
- Development/evaluation of advanced deicing system concepts
- Calibration of ice-catch prediction methods
- Development of ice detectors

Providing representative onset flow conditions in the test section is important for all of these. For example, elevated onset disturbance levels impact the boundary layer characteristics on the leading edges of wings, empennages, nacelles, etc., which, in turn, influence the heat transfer rates achievable with anti-icing systems, etc. Consequently, it is important that the disturbances emanating from the apparatus dispensing the water droplets just upstream of the test section, and from other special components in the icing tunnel circuit, be minimized. However, a much more important consideration is a growing concern that the typical icing tunnel simulation of inflight water droplet "kinematics" may not be representative. The cause for this concern is the icing tunnel results (and corresponding analytical methods) for multielement high-lift airfoil/wing systems showing ice accretions on downstream elements such as the main element and flap (see Figure 2) which have not been observed in flight icing conditions. Likely culprits are the significant horizontal velocity component given to the water droplet, combined with the absence of any vertical velocity component for larger droplet sizes.

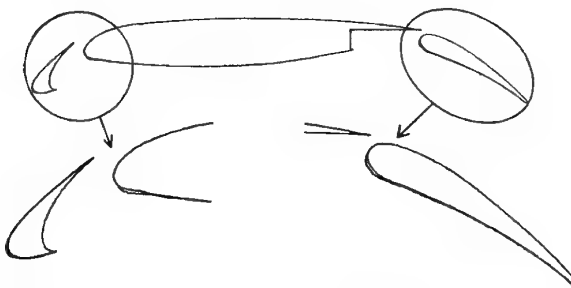


Figure 2: Icing Tunnel Measurements of Ice Accretion on Multielement High Lift Airfoil

3.2 Open Jet Tunnels

Testing wind tunnel models at atmospheric pressures in open jet test sections with a surrounding anechoic chamber is considered in much of the acoustics community to be a "proven, universally accepted technique" to provide the far field data needed to estimate flyover noise levels (even though the effects of sound propagation through the open jet shear layer must be dealt with). This position seems to be applicable for jet exhaust and large-scale rotorcraft noise testing. Similarly, the same is true for the normal specification of significantly higher allowable RMS turbulence levels for this kind of testing (as compared to aerodynamic high-lift development testing). However, both of these positions appear to be subject to challenge

for the determination of non-propulsive or airframe noise characteristics, including jet exhaust/airframe interactions. It is somewhat difficult to comprehend how test results obtained with poorer flow quality and at lower Reynolds numbers, with likely inadequate flow physics representation for establishing reliable quantitative high-lift performance trends, can properly represent the airframe aerodynamics from whence the airframe noise characteristics originate (i.e., doesn't anything matter?). Unfortunately, there is not yet a proven alternative method to the conventional, single-traversing far-field microphone measurement in an anechoic environment.

Major limitations that currently exist for open-jet testing are the maximum usable Mach number (~ 0.25) due to the onset of unacceptable flow and/or structural dynamics with increasing Mach number, and being limited to atmospheric test conditions. Acoustic testing up to a Mach number of 0.6 is being requested for future high-speed transport aircraft applications. Unfortunately, sufficient data or information does not exist to permit the basic understanding of the individual and interactive effects causing this Mach number limitation, including fundamental factors such as nozzle-to-collector spacing and area ratio, nozzle exit Mach number and Reynolds number, nozzle exit boundary layer characteristics, coupling of jet instabilities with surrounding plenum and duct resonances, etc. Development of an appropriate data base and understanding would increase prospects for perhaps using active control to suppress these limiting instabilities.

On the other hand, great interest exists in developing closed test section/phased microphone array testing techniques for the future so that good quality, quantitative acoustic measurements for product development (including identification of noise source locations) can be obtained in conjunction with performance testing. Two of the several technical issues which need to be pursued include the required positioning of the phased microphone arrays in order to get adequate signal to noise ratio for the resultant near-field measurements, and the potential need for acoustic treatment in the test section walls. Regarding the positioning of the phased microphone arrays, one concern is the possibility that a unique array design may be required for each test article in order to satisfy noise source measurement requirements in terms of resolution and upper frequencies.

3.3 V/STOL Tunnels

V/STOL aircraft using powered lift systems generate large downwash angles in the flow. The relatively thin layer of moving air between the model and the flow boundaries can easily be penetrated by the downwash, resulting in a strong interaction of the boundaries with the primary flowfield. V/STOL tunnels were developed to overcome this constraint by allowing a much larger test section for a given size model to reduce the interaction between powered lift systems and the tunnel flow boundary. The problem is particularly severe in transitional flight (i.e., the transition to forward flight), and moving ground boards or sophisticated wall boundary-layer conditioning systems are sometimes required.

3.4 Two-Dimensional Testing

With the advent of effective CFD methods (i.e., Navier Stokes), there has been a significant lessening of the need to conduct two-dimensional single-element transonic airfoil tests. This is particularly true for attached flow cruise conditions, but also holds as well for higher-angle-of-attack separated flow conditions, especially since the prime interest currently lies in understanding/predicting three-dimensional separated flows (i.e., flows with significant spanwise viscous content). However, this is certainly not the case for low speed multielement-high-lift airfoils where we still have quite a ways to go before CFD will be considered reliable enough to provide the understanding and guidance needed for overall and individual component optimization.

A major requirement for effective two-dimensional airfoil testing has always been in providing effective sidewall boundary-layer control so as to not contaminate the test results or cause downstream (diffuser) problems due to sidewall boundary layer separation. This is even more important for multielement high-lift airfoil testing, since the adverse pressure gradient experienced by the sidewall boundary layer is much greater. Whereas the (upper surface) adverse pressure gradient on each of the forward elements of the multielement airfoil is reduced by the so-called "dumping" phenomena, and the boundary layer history largely starts over on each of the downstream elements, the sidewall boundary layer is subjected to the total multielement airfoil adverse pressure gradient. Several types of sidewall boundary layer control have been attempted or utilized such as slot suction and blowing, but distributed suction in close proximity to the model is the most effective.

3.5 Semispan Testing

This type of testing which, at one time, was not looked upon very favorably, has received greatly renewed interest and use in the last several years for both subsonic and transonic testing, as it is a means of providing a significant increase in test Reynolds number for wing, high lift system, and propulsion integration development¹³. At the same time, semispan models tend to be simpler and cheaper, especially for configurations requiring power simulation. On the other hand, there are a number of additional tunnel flow quality and model installation requirements that must be carefully addressed to ensure that the test results obtained are representative. Included amongst these are the following:

- Flow quality requirements extend to the perimeter of the test section
- Need for an appropriate/representative (fuselage) standoff design accounting for the boundary layer on the "image" plane.
- Controlling/minimizing wind tunnel wall effects with the larger (chord) models needed to achieve high test Reynolds numbers.
- Presence of rear sting support strut.
- Ensuring representative onset flow conditions.

The latter is potentially a major issue with tunnels where the cross section of the test section is not rectangular, thereby necessitating the installation of an artificial reflection/image plane surface which has tunnel air passing below it. Adjustable control surfaces will likely

be necessary on this surface in order to provide appropriate (uniform) onset flow conditions. Success with this particular concept has not yet been demonstrated for large semispan models, although CFD predictions do justify some optimism. However, reducing wall effects to an acceptable/correctable level with large semispan models may well be the greatest challenge, necessitating some advanced test-section wall treatment/ventilation concepts.

3.6 Other

Other specialized types of tunnels with their own set of tunnel circuit aerodynamic design problems include propulsion tunnels, stability tunnels, and spin tunnels. Testing of aircraft engines at flight conditions requires simulation of flight velocity and the variation of atmospheric pressure and temperature. These propulsion tunnels must have means of scrubbing the engine exhaust gas, while controlling speed, pressure, and temperature -- a formidable challenge. Stability tunnels were developed since the conventional wind-tunnel simulation of flight doesn't model the characteristics of maneuvering flight crucial to aircraft stability. Two types of simulations are used, one utilizing rotating vanes to create a swirl, and the other a curved circuit to simulate turning flight. Similarly, spin tunnels were developed because the conventional simulation of flight in a wind tunnel cannot correctly model the unsteady and dynamic phenomena that are crucial to spin recovery. This led to the development of vertical wind tunnels with air moving upward, where dynamically similar models are inserted into the tunnel in a spinning attitude. It is important to note that each of these special types of wind tunnels, as well as some of the others, were developed to reduce the limitations imposed directly, or indirectly, by various constraints on the simulation of flight. Although successful to some extent in overcoming these limitations, they all generated new constraints in the process, thereby limiting their general applicability.

4. EXAMPLES OF FLOW QUALITY VARIATION EFFECTS

There are numerous recorded and easily envisioned examples of where less-than-desired tunnel flow quality has or could lead to non-representative and misleading test results, including cases where testing was conducted at full scale Reynolds numbers. Although some of the most intriguing cases cannot be discussed due to data restriction guidelines, the following three examples provide a glimpse of the type of data reliability issues due to tunnel flow quality variations that can arise from elevated freestream turbulence and background noise levels, onset flow angle gradients, and test-section-wall-induced gradients.

4.1 Transition Process on a 2-D Airfoil

More than one aircraft program has been beset by problems with high stall speeds and undesirable stall characteristics caused by the existence of laminar separation bubbles at flight conditions that did not appear during wind tunnel testing. A comparison of test results obtained for a two-dimensional airfoil design at low speed ($M_0=0.2$) conditions in two wind tunnels with different turbulence and background noise levels clearly illustrates how this can occur. The particular airfoil tested in this case was an 11.55-percent thick, aft-loaded-type airfoil,

while the two tunnels utilized were the Low Turbulence Pressure Tunnel (LTPT) at NASA Langley and the 5-Foot blow-down facility (with 2-D inserts) at IAR in Ottawa, Canada. Of the two tunnels, the latter is known to have higher freestream turbulence and background noise levels.

A comparison of the measured maximum lift characteristics for this airfoil from the two tunnels is shown in Figure 3

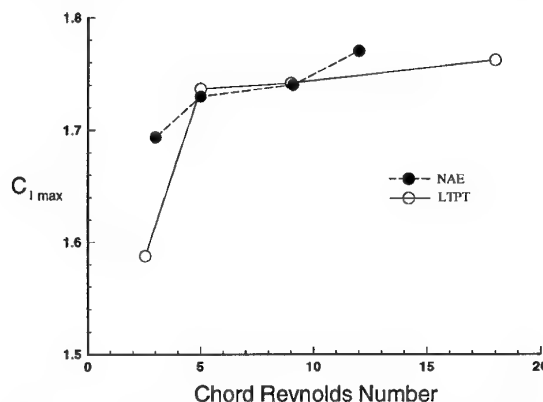


Figure 3: Effect of Freestream Turbulence and Background Noise on Single Element Airfoil Maximum Lift

for a range of (chord) Reynolds numbers. Of interest is the large drop in maximum lift capability observed at the lowest Reynolds number in the LTPT. This substantial reduction in maximum lift capability is due to the existence of a laminar separation bubble, indicated by the bulge in the chordwise pressure distribution seen just aft of the suction peak in Figure 4, which is not present at either

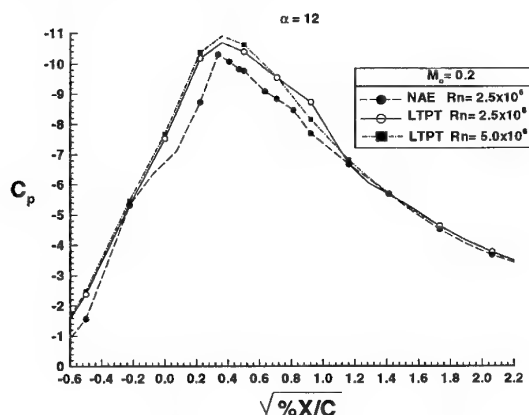


Figure 4: Turbulence Level and Reynolds Number Effects on Laminar Bubble Formation

the next highest Reynolds number in the LTPT or the same Reynolds number in the IAR facility. In this case, the acceleration of the transition process, brought about by higher freestream turbulence and background noise levels, effectively hides what could be a serious stall speed and characteristics problem due to the existence of laminar separation bubbles that can then catch the aircraft

developer by surprise in the flight test program. Furthermore, starting with this example, it is not difficult to envision how acceleration of the transition process in other ways due to elevated noise and turbulence levels could yield non-representative results for multielement high lift systems, winglet installations, etc.

4.2 Flow Angularity Effects on Installed Nacelle Characteristics

The aerodynamic design of low drag, cost effective nacelle geometries for large wing-mounted high-bypass-ratio (HBPR) engines is a high priority matter for transport aircraft developers. Even though modern CFD capabilities (i.e., 3-D Navier Stokes), especially constrained inverse applications, are the principal factor in establishing the aerodynamic lines for the nacelle, wind tunnel testing (and corresponding tunnel flow quality) still play an important part in the total design process. Typical roles for wind tunnel testing in this design process include calibration and validation of the CFD methods, validation of the effectiveness of the resulting external nacelle designs (and inlet lines), determination of aerodynamic loads, and determination of installation effects on nozzle performance characteristics. Unfortunately, poor tunnel flow quality can thwart the accomplishment of more than one of these test objectives.

Nacelle pressure data obtained from the test of a large HBPR (engine) nacelle installed in a representative underwing location on a full-span model of a $M=0.85$ transport wing/fuselage help illustrate this adverse effect for the case of a spanwise (wing) onset flow angularity (and Mach number) discrepancy/variation (which was not known to the industry users at the time of the test). The pressures measured on the top and both sides of the nacelle fan cowl are shown in Figure 5, compared to two sets of CFD predictions, the first assuming no flow angularity discrepancy, and the second using an average spanwise flow angle (i.e., sideslip) of 0.6° to approximate the effect of the (nonuniform) flow angularity discrepancy. It can be seen that, as expected, the spanwise flow angularity variation has essentially no effect on the predicted pressures on the top of the nacelle where, incidentally, the predictions match the test data quite well. Further, on the inboard side of the nacelle, where the measured pressures reflect velocities barely above sonic conditions, the pressures predicted using the indicated average onset flow angle also match the data quite well. However, on the

outboard side of the nacelle, the pressures predicted using the average onset flow angle did not match the measured peak velocities as well, likely indicating that using the average onset flow discrepancy for a more critical (i.e., sensitive) flow situation does not adequately represent the nonuniform onset flow discrepancy, which, incidentally, cannot be realistically modeled. Hence, in this case, due to the poor tunnel flow quality, it was not possible to either completely validate the CFD methods utilized nor the effectiveness of the resulting nacelle design. Consequently, the test objectives were not met. This example again illustrates why it is important for the user to thoroughly understand the flow physics features involved, since the average correction worked well for a non-critical flow situation, but not for a more critical (sensitive) flow situation.

4.3 Wall Effects on High-Lift Characteristics

The desire/need to attain high test Reynolds numbers at low-speed takeoff and landing conditions in order to reduce the aerodynamic risk associated with the development of more cost-effective multielement-high-lift systems for transport aircraft is leading to the use of large semispan models in subsonic tunnels which have solid test-section walls. One of the potential risks with this testing concept that needs to be addressed is the possibility that test-section wall effects may alter critical aerodynamic characteristics in ways that can not be adequately accounted for. An example of this type of effect would involve the reduction of suction pressure peaks on the slat (and an increase in the lift on the main element) at a given total lift, which could result in an underdeflection of the slat and/or an unrealistic delay in the onset of adverse compressibility effects on the stall speeds.

In order to visualize how these changes can occur, it is helpful to examine the pressures measured on a close-to-optimally-rigged 2-D three-element high-lift airfoil⁹, with a slat and single-segment flap, at conditions approaching maximum lift at 0.2 Mach number that are illustrated in Figure 6, and the panel-method-predicted reduction in slat peak suction pressures on relatively large 3-D semispan transport aircraft high-lift model installations in solid wall wind tunnels⁸ shown in Figure 7. For the slat rigging corresponding to the pressure distributions shown in Figure 6, the maximum lift level attainable is not controlled by any flow breakdown on the slat, even though the slat experiences significantly higher peak suction

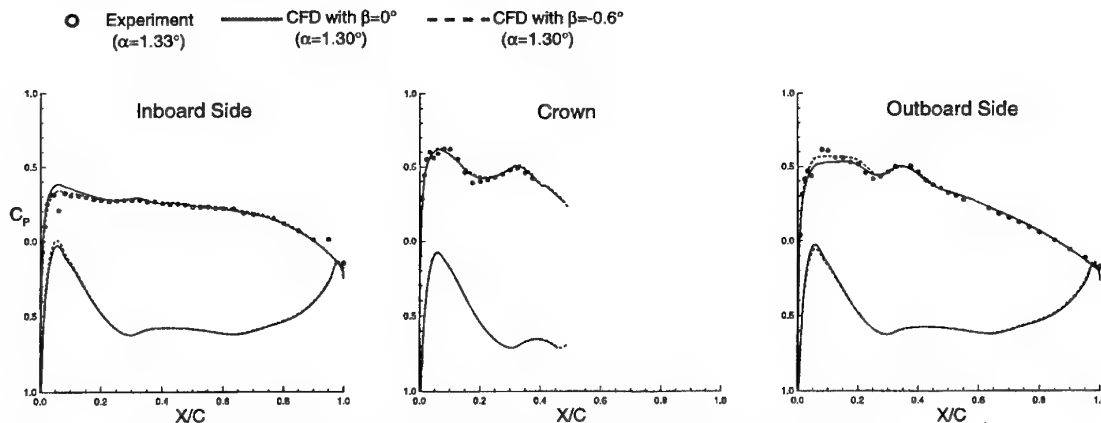


Figure 5: Spanwise Flow Angularity Effect on Installed Nacelle Pressures

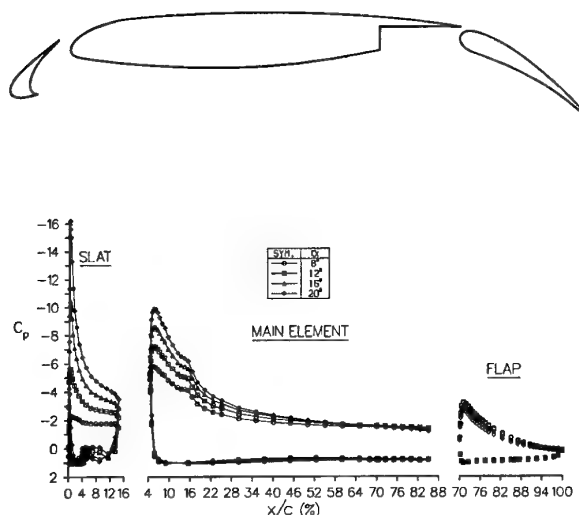


Figure 6: Multielement Airfoil Pressure Distributions

pressures⁹. Instead, the maximum lift is limited by a flow breakdown brought about by rapidly spreading and merging shear layers and wakes above the flap. However, it does not take much of a reduction in slat deflection (increased peak suction pressures), or increase in Mach number (reduced critical pressure coefficient), before a flow breakdown on the slat is limiting the maximum lift achievable. In these situations, the (predicted) reduction in slat peak suction pressures due to wall interference on large 3-D semispan models can become quite important. And, the real reductions in slat peak suction pressures are undoubtedly greater than the panel-method predicted values since the peak velocities on the slat at maximum lift conditions typically exceed sonic velocity values, a situation where panel methods are notorious for underpredicting peak suction pressures. This situation requiring testing of large semispan high-lift models strongly suggests that ventilated wind-tunnel wall concepts should be seriously considered for subsonic wind

tunnels in order to minimize these adverse tunnel-wall interference effects encountered with solid wall test sections. This particular situation provides even further testimony in support of the need for the tunnel users to have a thorough knowledge of the important flow physics features which are controlling the aerodynamic characteristics under investigation in order to adequately understand and identify wind-tunnel flow quality requirements and effects on data quality, accuracy, and adequacy.

5. TUNNEL CIRCUIT DESIGN CHALLENGES

In view of current and expected economic realities in aeronautics, justification for the construction of any major new wind tunnels for production-type testing will have to be based on a combination of many factors including improved Reynolds number capability, tunnel flow quality, and productivity, plus reduced operating costs. Minimizing tunnel construction costs will also be critical. Considering these requirements, two of the most important aerodynamic challenges which should be energetically pursued in order to enable any viable new tunnel design are the application of modern advanced CFD capabilities to provide more effective aerodynamic designs for several of the components in the tunnel circuit, and the development of more effective test-section wall ventilation and control concepts. The former is needed to concurrently enable significant improvements in both tunnel construction and operating costs, and, very importantly, test section flow quality. The improved test-section wall concepts are needed in order to enable more cost effective high Reynolds number testing capabilities.

5.1 Improved Tunnel Circuit Design via CFD

Current state-of-the-art CFD capabilities play a very major role in the aerodynamic configuration design process for air vehicles. For instance, the aerodynamic design of transport aircraft cruise geometries can now be confidently established using CFD methods before the first wind-tunnel test is ever undertaken. Initially, the use of standard direct CFD methods involved a repetitive process similar to the typical experimental process. However, with the subsequent introduction of inverse CFD design methods, and, more recently, constrained-optimization techniques,

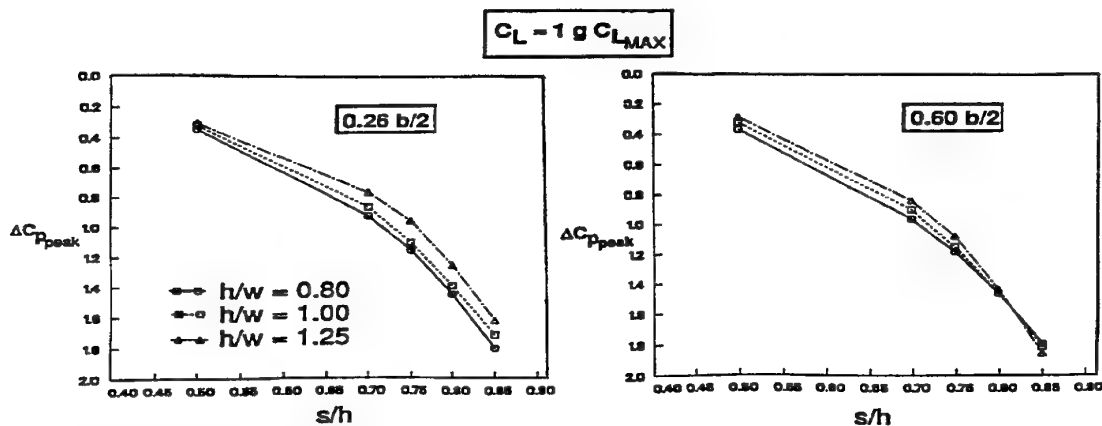


Figure 7: Predicted Reduction in Slat Peak Pressure Coefficient for Large Semispan High Lift Model in Solid Wall Tunnel

the role of CFD in the design process has expanded dramatically. Inverse CFD methods, i.e., designing the shape to achieve engineering objectives, was a major breakthrough which enabled solutions to many design problems which were heretofore unaddressable by either experimental or direct CFD methods. But, effective application of these inverse methods still required numerous iterations, and obstacles were often encountered in dealing with complex 3-D flow situations because of the difficulty involved in specifying achievable target pressure distributions in these situations. Now, however, the introduction and broadening use of constrained-optimization techniques essentially avoids these obstacles, and is allowing complex aircraft aerodynamic design problems to be addressed and solved in short time periods while simultaneously imposing manufacturing, structural, and other constraints on the geometry. A well known application of this technique is the design of subsonic transport aircraft wings accounting for the presence of large, wing-mounted engine installations^{1,4}.

Adaptations of this constrained-optimization process to the design of more effective components in the wind tunnel circuit could well provide large rewards in terms of improved flow quality and reduced tunnel fabrication and operating costs. Obvious potentially-beneficial applications include an integrated contraction/nozzle design, diffuser designs, flow turning components, and model support systems. For the contraction/nozzle design, application of this approach should result in a shorter (cheaper) contraction section which provides a velocity field at the nozzle exit that has minimal deviation from uniformity and a minimal amplification of cross-stream turbulence quantities. Similar improvements should be forthcoming from improved diffuser designs, etc. Improving component designs, by suppressing flow disturbances and subsequent interactions, should also permit reducing the number of turbulence screens (i.e., power) required.

5.2 Advanced Test-Section Wall Ventilation Concepts

As indicated previously, reducing test-section wall interference effects to acceptable and readily correctable levels with the large semispan models needed to achieve higher test Reynolds numbers is a high priority requirement at both subsonic high lift and transonic conditions. Accomplishing this in a cost-effective manner represents a significant challenge. The alternative of increasing tunnel size is certainly not cost effective, and the cryogenic option has some drawbacks for a production-testing-type tunnel. Various CFD studies have clearly indicated that wall effects with solid wall subsonic facilities are excessive for (floor-mounted) semispan model spans approaching 80-percent of the test section height, as are wall effects with fixed porosity walls at transonic conditions for similarly sized models^{8,14}. However, some of these same CFD studies have indicated that a spatially variable resistive (controllable variable porosity slots) wall can substantially reduce wall corrections at transonic conditions to levels where corrections may well be possible with a high degree of confidence¹⁴. A successful development and cost-effective implementation of this concept would represent a significant breakthrough in the pursuit of a practical high

Reynolds number testing capability. Key issues which need to be addressed for this proposed controllable variable porosity slot concept include the determination of the best placement and minimum number of control segments in the slot, establishing an appropriate active wall control strategy, and controlling noise generation sources. Furthermore, control of side wall angle is an important issue here as well, since it can play a significant role in reducing wall interference

6. CONCLUSIONS

Normal overriding user objectives when conducting almost any kind of wind-tunnel test in almost any test facility are obtaining reliable and meaningful data in a timely and cost-effective manner. Principal requirements for obtaining reliable and meaningful data in most testing situations are an adequate Reynolds number, representative or satisfactory tunnel flow quality, and avoiding tunnel wall and support system effects which either alter important flow characteristics on the model, or cause effects which cannot be readily or accurately accounted for. Factors which are important in satisfying the timeliness and cost-effectiveness requirements include minimizing the time required for model installation and configuration changes, utilization of efficient data gathering systems, effective utilization of test time in data gathering, etc., and the ability to use rapid techniques to account for tunnel wall and support system interference effects. Since the aerodynamic design of wind-tunnel circuits has a fundamental first order effect on tunnel flow quality, tunnel wall and support system interference effects, and on tunnel construction and operating costs, the adequacy of the circuit design is of crucial importance in meeting the user's objectives.

Both known and potential data discrepancies resulting from less-than-perfect circuit aerodynamic design (including test section wall effects) have been addressed from an aircraft industry user's perspective in order to provide some basis for assessing the relative importance of various flow quality parameters. Conclusions arising from this review include the following:

- In order to adequately understand and identify wind-tunnel flow quality requirements and effects on data quality, accuracy, and adequacy, it is imperative that the user have a thorough knowledge of the important flow physics features which are controlling the aerodynamic and other characteristics of the vehicle or flow situation under investigation at the test conditions, the design and validation process being utilized, and the level and type of risk involved in the technology being incorporated in the design.
- It is also especially important that tunnel users and operators not limit the identification of potential data errors and measurement uncertainties to just those which can be currently predicted with existing analytical and CFD methods. It would seem to be more logical to focus more heavily instead on minimizing the flow quality deficits which cannot be adequately addressed with computational methods rather than those that can.
- Special efforts should be made to minimize freestream turbulence and background noise levels since they can

have very significant, but, unfortunately, unquantifiable effects on critical viscous characteristics.

- Reducing test section wall interference effects with large semispan models is necessary in both subsonic and transonic tunnels if test Reynolds number requirements for transport aircraft are to be met.
- Minimizing tunnel flow quality defects which contribute to measured drag inaccuracy and uncertainty continues to be a very important consideration for some product categories and design/validation processes.
- The correctness and/or adequacy of the current icing tunnel simulations of inflight icing encounters which do not introduce any vertical (downward) velocity component for the water droplets is somewhat in doubt, and needs to be sorted out.
- Applications of current state-of-the-art CFD capabilities to the design of more effective components in the wind tunnel circuit could well provide large rewards in terms of improved flow quality and reduced tunnel fabrication and operating costs, and should hence be energetically pursued.
- Advanced test-section wall ventilation and control concepts offer substantial potential for enabling more reliable- and cost-effective high Reynolds number testing capabilities, and should also be energetically pursued.

ACKNOWLEDGMENT

Several very educational consultations with members of the National Wind Tunnel Complex (NWTc) study group enabled significant portions of this paper, and are sincerely appreciated.

REFERENCES

1. Rubbert, P. and Goldhammer, M., "CFD in Design: An Airframe Perspective," AIAA Paper No. 89-0092, Jan. 1989.
2. Rubbert, P.E., "CFD and the Changing World of Airplane Design," ICAS-94-0.2, Sept. 1994.
3. Lynch, F.T. and Intemann, G.A., "The Modern Role of CFD in Addressing Airframe/Engine Integration Issues for Subsonic Transports," ICAS-94-6.4.3, Sept. 1994.
4. Jou, W-H., "Status and Future Challenges of the Applications of Computational Fluid Dynamics (CFD) in Commercial Airplane Aerodynamic Configuration Development," NPU/AIAA AFM Conf., June 1996.
5. Elsenaar, A., Binion, T.W. Jr., Stanewsky, E., "Reynolds Number Effects in Transonic Flow," AGARDograph AG-303, December 1988.
6. Lynch, F.T., "Experimental Necessities for Subsonic Transport Configuration Development," AIAA Paper 92-058, Jan. 1992.
7. Haines, A.B., "Scale Effects on Aircraft and Weapon Aerodynamics," AGARDograph 323, July 1994.
8. Lynch, F.T., Crites, R.C., and Spaid, F.W., "The Crucial Role of Wall Interference, Support Interference, and Flow Field Measurements in the Development of Advanced Aircraft Configurations," AGARD-CP-535, Paper No. 1, Oct. 1993.
9. Lynch, F.T., "Subsonic Transport High-Lift Technology — Review of Experimental Studies," AIAA Overview of High Lift Aerodynamics, June 1995.
10. Muhlstein, L. and Coe, C.F., "Integration Time Required to Extract Accurate Static and Dynamic Data from Transonic Wind-Tunnel Tests," AIAA Paper 75-142, Jan. 1975.
11. NWTc Customer Performance Requirements Document, NAS3-27330, Doc. No. NWT-03-A-9100-05, May 1996.
12. Green, J.E., "On the Influence of Free Stream Turbulence on a Turbulent Boundary Layer, as it Relates to Wind Tunnel Testing at Subsonic Speeds," AGARD-R-602, 1973, Paper 4.
13. Goldhammer, M.I., Steinle, F.W. Jr., "Design and Validation of Advanced Transonic Wings Using CFD and Very High Reynolds Number Wind Tunnel Testing," ICAS-90-2.6.2, September 1990.
14. Sickles, W.L. and Steinle, F.W. Jr., "Global Wall Interference Correction and Control for the NWTc Transonic Test Section," AIAA paper to be published, Jan. 1997.

General Design Aspects of Low Speed Wind Tunnels

F. Jaarsma

National Aerospace Laboratory NLR
Voorsterweg 31, 8316 PR Marknesse, The Netherlands

SUMMARY

Since the sixties NLR was considering conceptional layouts and airline diagrams for the next generation low speed wind tunnels. This has resulted in the construction of a multi-purpose pilot facility in the early seventies. Based on the experiences gained from this facility, three major wind tunnels have been realized and are in full operation to great satisfaction of the operators and users: namely the DNW (1980) and LST (1983) facilities in the North East Polder in The Netherlands and the ILST (1987) near Jakarta in Indonesia.

In this report the general design considerations in terms of aerodynamic and testing requirements are reviewed and are compared with the actual achievements. Also other operational aspects, such as logistics, acoustics, local constraints, and model supports are considered. From these aspects some lessons learned are concluded and recommendations made.

LIST OF SYMBOLS

A	Area
b	width
c	cord
c_p	pressure coefficient
k	pressure loss coefficient
L	length
p	static pressure
q	dynamic pressure
r, R	radius
U	axial velocity
u	axial velocity perturbation
x, y, z	axial, horizontal, vertical axis
α	pitch angle
β	yaw angle
subscripts	
o	test section, entry diffuser
w	entry Wide angle diffuser

1. INTRODUCTION

In the last decades NLR has been involved in the design and realization of a few major atmospheric subsonic wind tunnels which have found their place in the aerospace development business. These wind tunnels involved in chronological order, the king size German

Netherlands Windtunnel DNW, the smaller Low Speed Tunnel LST of NLR, both located in the Northeastpolder near the former fishing village of Vollenhove, and in Indonesia near Jakarta (at Serpong) the interim size Indonesian Low Speed Tunnel ILST.

All three tunnels are based on the earlier aerodynamic design and development work done at NLR as presented at the AGARD Symposium on 'Windtunnel Design and Testing' in October 1975 (ref. 1). This work was based on the earlier plans at NLR to realize a large size low speed tunnel of 8 x 6 m test section (WxH) dimension. This project was then merged with simultaneous plans in Germany for the GUK (Gross Unterschall Kanal) with a specification of two test section sizes, namely 9.5 x 9.5 m and 6 x 6 m, for respectively low and high speeds. The combination of these specifications resulted in the present DNW with three exchangeable test sections and an open test section of 8 x 6 m size for aero-acoustic testing as well.

Tests in the available 1/10th scale model tunnel revealed that the initial circuit design of the 8 x 6 m test section configuration could also accommodate the 9.5 x 9.5 m, 6 x 6 m and open jet configuration meeting all requirements on flow quality as put forward for the GUK and initial NLR plans.

This result could be obtained thanks to a conservative circuit design. More background information on the aerodynamic design aspects of the DNW has been published by Mr. van Ditschuijn in 'Construction book of DNW' (ref. 2).

During the realization of DNW, NLR decided to replace its two small low speed tunnels in Amsterdam by a so-called 3 meter tunnel in the Northeastpolder based on the same circuit design as referred to in ref. 1 for both aeronautical and non-aeronautical testing. Non-aeronautical testing also contains wind-hindrance testing and this type of research requires some type of simulation of the earth natural boundary layer for some surface conditions (e.g. being a flat free field, urban environment etc.). This requires some distance downstream of the contraction to generate and develop the simulated boundary layer before the test article is struck by the wind. Hence a relatively long exchangeable test section arrangement was drafted and realized in the LST.

After completion of the DNW, NLR was approached by the Indonesian authorities for the assistance in the realization of an advanced low speed tunnel at the PUSPIPTK site near Serpong, West-Java. Size and complexity to be less as the DNW but sufficient for the near and long term needs for the envisaged Indonesian aerospace industry (now IPTN) in development by that time. This tunnel, the ILST, came on stream in 1987 and has since then been in full use for the CN235 and N250 programs. The circuit was slightly modified from the existing well proven design and the 4 x 3 m exchangeable test section arrangement can provide four different combinations for different test purposes and set-ups (ref. 3).

This paper reviews the various components and general aspects of low speed tunnel design and realization, not only from the aerodynamic point of view but also from the users and operations point of view and states, where appropriate, the lessons learned.

2. GENERAL CONSIDERATIONS

For the tunnel user an important parameter is cost vs quality. The cost factor is governed strongly by tunnel productivity and this factor in turn depends, amongst others, on tunnel logistics for interchangeability of model support and test section components. The quality of the wind tunnel data (defined as the degree of simulating free flight) can be expressed in four categories:

- Reynolds number
- Flow quality
- Interference effects (supports, walls)
- Instrumentation and data systems.

This paper deals mainly with the second issue. Interference effects are also linked with logistics and will be considered herein for the wind tunnel configuration concerned (classic, atmospheric). The needed Reynolds no. capability is not considered here. It is usually set beforehand based on aerodynamic considerations, available budgets and other requirements associated with the envisaged usage scenario, such as helicopter testing, noise testing, propulsion simulation, non-aeronautical testing etc. Sometimes, also the available space and/or other provisions dictate the tunnel size and/or type.

When large Reynolds numbers and variations thereof are required for aerospace use as the prime objective a pressurized, close return-tunnel is a good choice as is the DRA 5m tunnel and the ONERA F-1.

Similar characteristics can also be achieved going cryogenic, such as the DLR KKK or use of heavy-gases as was planned in the US recently, but in the latter case Re-variation is problematic. However, the majority of low speed tunnels are atmospheric meaning that either the total pressure or the static pressure in the test section is atmospheric. The test section size then determines the Reynolds number capability.

The maximum speed for low speed wind tunnels for aerospace use is related to the landing, take-off, and climb-out phases of airplanes and therefore should be at least 80 m/s but preferably in excess of 100 m/s. For high-lift systems duplication of the Mach number is of importance to simulate properly the compressibility effects on the wing surfaces. So this prefixes the air speed and hence unit Reynolds number.

The type of atmospheric tunnel for new developments are presently only of the closed-circuit return type what is called in Germany the Göttinger type. Open return tunnels, either via the outdoor environment (such as the added 80 x 120 ft leg to the NASA Ames 80 x 40 ft tunnel) or internally inside a building (DA/Bremen) are hardly considered anymore, because precise and predictably flow conditioning in the test section is not optimal and/or inhouse nuisance. Besides the test section is at sub atmospheric pressure causing sealing and operational problems or at least inconveniences.

3. FLOW QUALITY SPECIFICATION

The design of the airline diagram (internal shaping) of a wind tunnel and its inserts into the flow results from flow quality optimization in the test section versus construction and operational costs. In reference 1 flow quality requirements are defined based on acceptable mean flow variations. Compatible with this general requirement is a flow angularity better than 0,1 degree and a turbulence level of less than 0,1 percent.

In a more recent AGARD FDP effort (ref. 4) similar requirements were derived mainly based on the objective to measure drag with a repeatability of one drag count. From this requirement it is necessary to measure overall incidence with an accuracy of 0,01 degrees, local incidence variation along the wing span can be one order of magnitude larger.

In the past the majority of attention to flow quality was directed towards turbulence level with a uniform flow (speed, total head). In the last decades, also requirements are given for flow angularity, static pressure distribution, especially in longitudinal direction (buoyancy) and noise level. To this end various older wind tunnels have been equipped with flow rectifying honey combs in the settling chamber and longer and closed test sections to better meet the additional requirements.

4. DISCUSSION OF AIRLINE COMPONENTS

4.1 General airline lay out

The airline used for practically all new low speed wind tunnels is depicted in figure 1. It consists of moderately expanding diffusers, contraction ratio's close to 10 to 1 and a wide angle diffuser in front of the settling chamber. The fan is usually located opposite to the test section arrangement after the flow has passed twice a 90 degrees corner. Somewhere between the test section and

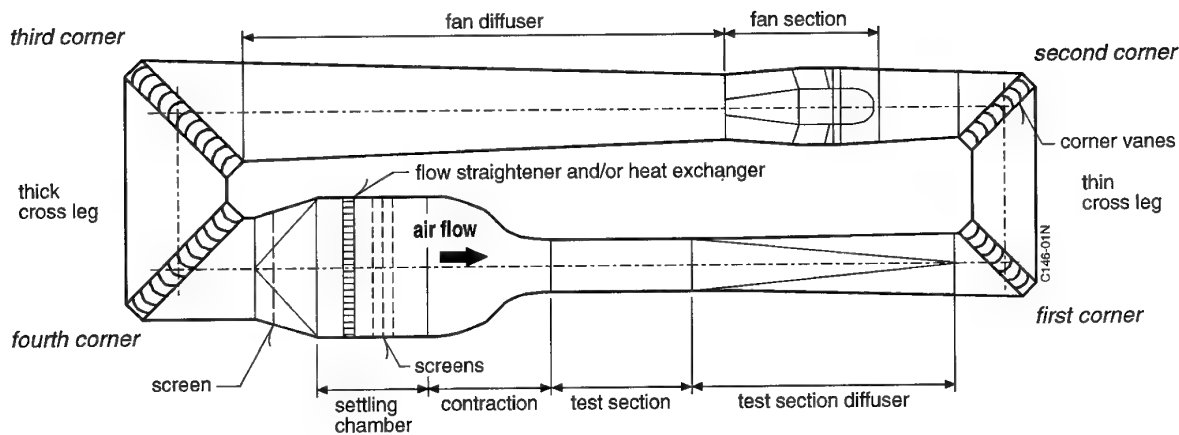


Fig. 1 General Airline Diagram of modern Low Speed Tunnel

the fan a fan blade protector is installed in the form of a screen or honeycomb grid to catch pieces travelling with the flow in case of a mishap with a model in the test section. Wind tunnel fans are practically solely of the axial type and low speed wind tunnels have only one stage with 4 to 10 blades. The combination of the rotating fan with the pre- or aft stator blading provides practically uniform flow to the second (fan) diffuser entry.

Turning the flow around the corner is now-a-days solely done using a cascade of vanes of 90 degrees. In the wide angle diffuser the flow is stabilized by one or two screens to promote uniform spreading. The settling chamber is used to install a heat-exchanger when deemed necessary and here the flow is conditioned as good as possible by installing honeycombs and/or screens.

The circuit is essentially closed but for an atmospheric wind tunnel the interior should be in contact with the environment to equalize pressure at one particular station. A good place for such a breather is at the downstream end of the test section so that it does not disturb the flow around the model but it allows some minor open penetrations in test section walls. This means that the remainder of the circuit is at over pressures and therefore shall be air tight for good efficiency and to prevent flow entry at the breather/test section locations.

4.2 Circuit losses, power requirements

The losses in a wind tunnel circuit, expressed as a decrease in total pressure, have to be compensated by the pressure rise to be generated by the fan. So, in order to establish the necessary power of a wind tunnel, estimates have to be made of the total pressure losses of the various components along the circuit. By adding the individual losses in terms of the dynamic head in the test section the total loss is obtained. Early work by Margoulis, Wattendorf, Parkhurst and Bradshaw should be mentioned in this respect. In a recent study by Wolf an excellent survey is given of the application of this

method for compressible flows as generated in transonic wind tunnels (ref. 5). This method is not elaborated further here since it is well established and it has proven its use in practice. In ref. 1, 2, and 5 examples are given of calculating the circuit losses and hence calculating the necessary power to drive the tunnel.

4.3 Diffusers

Diffusers in a wind tunnel are used to recover part of the kinetic energy of the flow in the test section in the form of potential energy finally leading to excess pressure in the settling chamber. To reduce fan drive power, efficient recovery without generating separation is needed. The basis for judgement whether separation may occur is depicted in fig. 2 and is valid for conical diffusers starting from a flat velocity profile at the diffuser entry (ref. 6). With increasing cone angle above a certain value the diffuser will exhibit increasing

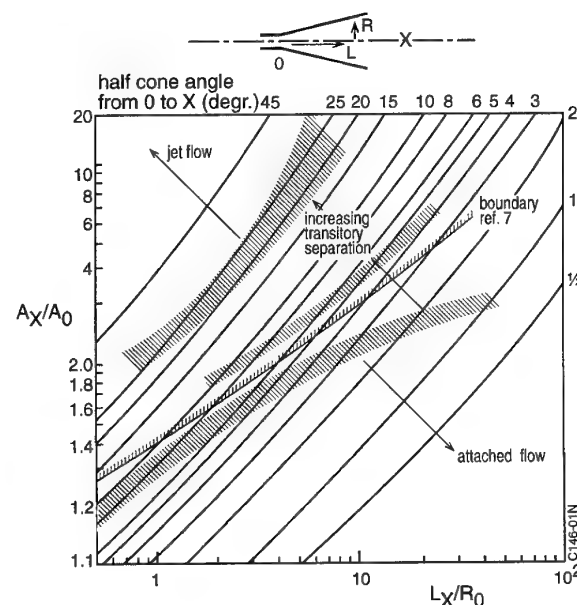


Fig. 2 Flow regime boundaries for conical diffusers

transitory stall causing vibrations and unsteady loading to the fan. At very large cone angles the flow will be continuously separated and the issuing flow can be distinguished as jet flow. Figure 2 also shows the boundary as presented by Wolf (ref. 7). For rectangular diffusers the equivalent cone angles should be 0,5 to 1,0 degrees smaller.

It is essential for the test section diffuser that it is designed very conservatively since the flow downstream of a heavily loaded model may trigger separation earlier than envisaged. In the NLR wind tunnel designs the test section diffusers have an area ratio of about 2 and a cone angle of about 4 degrees. It has been shown that this gave sufficient margin to introduce (insert) a 6 x 6 m test section into the 8 x 6 m test section although with this smaller test section the diffuser is more prone to instabilities.

Rectangular diffusers show strong thickening of the boundary layer in the corners. Therefore it is recommended to use circular, or as a compromise octagonal cross sections where applicable to eliminate unwanted flow phenomena.

Relative to turbulent pipe flow, the total head profile is usually more peaked at the center on leaving the diffuser. Therefore it is wise to make the corner sections cylindrical (parallel) so that some recovery to pipe flow is accomplished. This may allow some additional diffusing action between the first and second corner (in the thin cross leg) but this diffuser shall never be considered as being independent from the test section diffuser. Practice at the ILST has shown that a small diffuser having a 1.1 area ratio can be applied without causing separation problems in this cross leg.

The other item is pressure recovery of the diffuser. Calculations at NLR for the LST 8 x 6/DNW project revealed that optimum pressure recovery (90 - 95%) is obtained for diffuser opening angles close to the upper limit for attached flow as is shown in figure 2 (ref. 2). Besides, it was concluded that the opening angle for optimum pressure recovery decreases with increasing Reynoldsnumber; about one degree (of cone top angle) per one order of magnitude in the Reynoldsnumber.

Since the diffusers cover the majority of the circuit length their crosssectional shape is also determined by the construction material. For example, when steel is used it is easy and convenient to make a circular cross section (LST), but when (ply)wood or concrete is used flat surfaces are the more logical choice. At DNW and ILST prefabricated flat concrete slabs were used to construct the circuit having an octagonal cross section. In both cases the experiences were very good because good surface quality and precise and fast surface alignment were possible.

4.4 Corner vanes

The aerodynamic design of corner vanes of the wind tunnels in which NLR has been involved are based on the earlier work of Mr. Zwaaneveld of NLR (ref. 8). Older wind tunnels elsewhere have been modified with these turning vanes showing considerable performance improvements. Turning vanes should be designed for optimal turning effectiveness, rather than for minimal pressure loss.

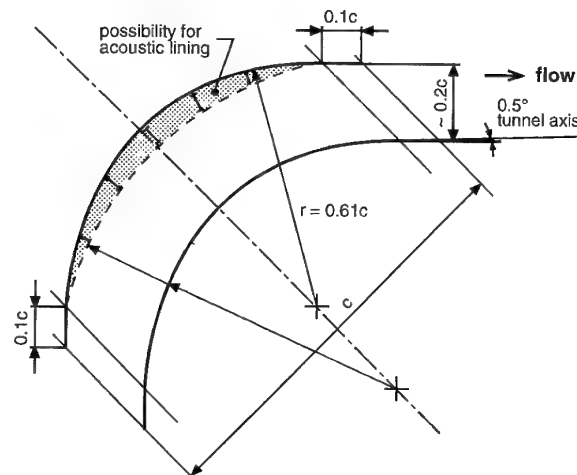


Fig. 3 General lay out of corner vanes

The turning vanes used by NLR consist of metal sheets bend circularly over 90 degrees with both straight leading and trailing edge extensions of 0.1 times cord length. Pitch/cord ratio is 0,2 and the average angle of incidence should be .5 degree. See figure 3. These vanes give room for acoustic treatment at the vane inner corner without sacrificing performances on turning effectiveness and pressure loss (as far as has been observed). To

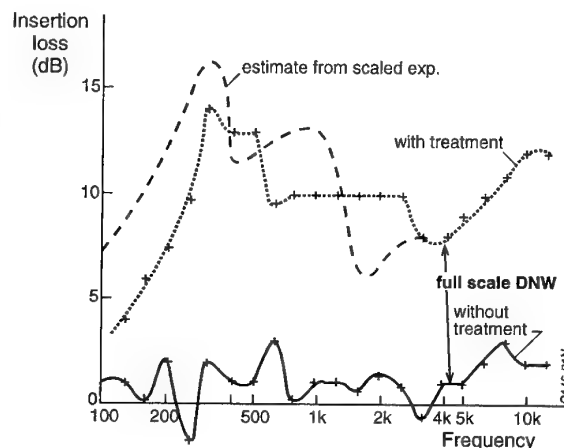


Fig. 4 Insertion loss of lined 1st corner and unlined 2nd corner; no flow

prevent air to flow through the lining material, strips normal to the vane surface should be installed. The noise reduction (insertion loss) due to such a lining is 8 to 13 dB depending on cord/wave length ratio, see figure 4. Such acoustic lining also improves the working comfort within the tunnel because it strongly suppresses reverberation.

One practical remark. From strength point of view the vanes could be made from relatively thin sheets. But from manufacturing, stability point of view a sheet thickness of 8 to 10 mm is recommended with pitch values large enough to pass through. Usually horizontal splitter plates are used to further improve stability to the vane structure.

Diffusing or contracting corner vanes are not or seldom used. Recent work at Boeing showed that both types can be used successfully in their particular application for transforming an existing tunnel into an icing tunnel and to provide additional cross sectional space in between the third and fourth corner (ref. 9).

4.5 Wide angle diffuser

Since efficient and stable diffusion (recompression) of the flow is only achievable in diffusers with limited area ratio's, as has been explained in section 4.3, and since basically only two diffusers are available (the test section and the fan diffuser), a wide-angle diffuser is needed to reduce the airspeed to the level as required in the settling chamber for achieving the desired contraction ratio. In ref. 2 it is argued that by increasing the area ratio of this wide diffuser the turbulence level will also increase at the entry of the settling chamber and this may ultimately increase the turbulence level in the test section with increasing contraction ratio. Figure 5, as taken from ref. 2 and based on empirical computation, clearly illustrates this effect.

A large cross sectional area of the settling chamber will also increase the construction costs considerably because of the large span to cover the (pressurised) chamber and the inserts (heat exchanger, screens, honey combs) to cover the cross section. So, there is a limit to the area ratio of the wide angle diffuser.

The design of this diffuser is based on empirical rules. Without a stabilizing screen the flow will be fully separated (jet flow). However, local separations can not be avoided but are acceptable as long as they are of a steady nature.

The early work of ref. 10 can be used as a guideline to design the screen/diffuser shape combinations. The aim will be to achieve zero pressure efficiency or in other words: the ideal gain in static pressure is used as pressure loss across the screen. It is recommended to confirm the design solution by a scaled model test when possible.

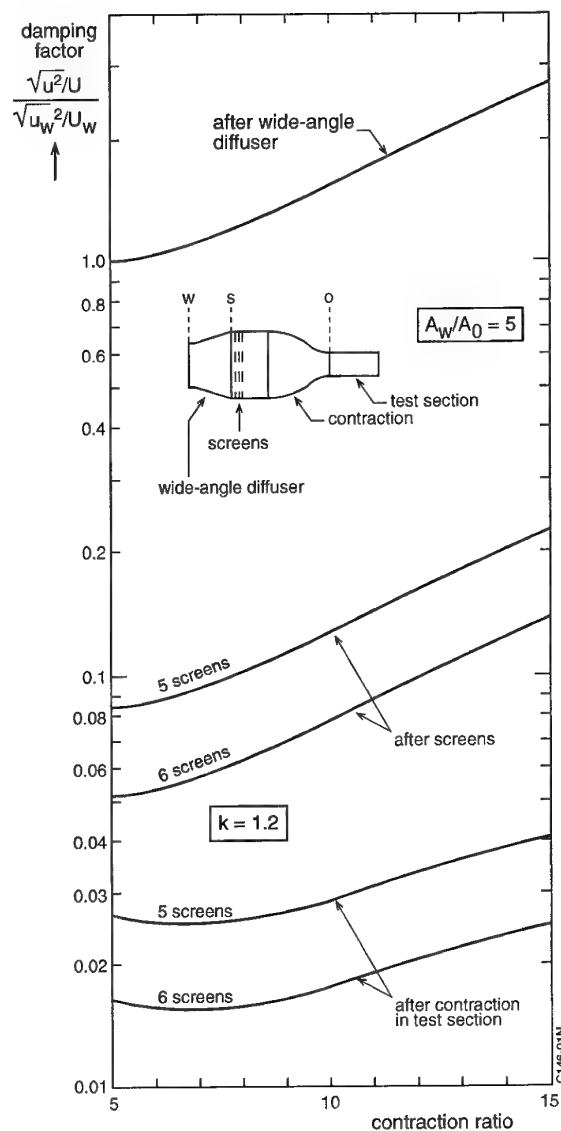


Fig. 5 Damping of Turbulence between 4th Corner and Test Section as a Function of the Contraction Ratio

The drag from the heat exchanger and screen package in the settling chamber will also help to stabilize and spread the flow over its entire cross section. It has been experienced in the model tunnel that when this drag is too large (in that particular case the pressure loss across all inserts was in excess of 6,5 times the local dynamic head) the flow spreading is overcompensated, meaning that the total pressure at the walls in the test section is larger than at the tunnel axis.

4.6 Contraction

For low speed wind tunnels the contraction ratio to be selected will usually be close to 10. With the modern means to condition the flow in the settling chamber in terms of total head, turbulence and flow angularity, a

smaller contraction ratio can be selected than was thought of in the early days. As explained in ref. 2, a contraction ratio of 9 to 1 for the 8 x 6 test section of DNW was selected. Therefore, the 9.5 x 9.5 m and 6 x 6 m test section have contraction ratios of 4.8 to 1 resp. 12 to 1.

In principle the design of a nozzle is easy, because essentially the flow goes down hill to lower pressures. The reality is different because:

- there are two potential areas of flow separations, namely at the nozzle entry and downstream of the inflection point;
- cross flow may occur in the boundary layer because of crosswise pressure gradients which may cause large vortices in the test section flow;
- it is desirable to have an uniform velocity and hence static pressure field at the entry of the effective test section;
- it is usually desirable to make the contraction short.

In case of the DNW the design of the contraction was even more difficult because it had to accommodate the three test sections with different cross section sizes and shapes (rectangular and square) starting from a 24 x 18 m settling chamber. Therefore, a special 3-D potential flow code was developed at NLR (ref. 11) to optimise for:

- short nozzles; equal length for all test sections;
- a common interface (as much downstream as possible) for the exchangeable contraction parts to be used;
- prevention of flow separation using the 2-D Stratford criterion.

Use was made of the Börger approach for contraction development (ref. 12). Fig. 6 gives a comparison of the initial 9.5 x 9.5 m contour design (as used with the model tunnel) and the final design in relation to the axial symmetric Börger contour. In recent work at T.U. Darmstadt, Mr. Wolf also used similar methods to cope with his space limitation problem (ref. 7).

An interesting discovery during the development of the DNW nozzle was that the wall pressure distribution in the vertical and horizontal plane of symmetry for the 8 x 6 m test section turned out to be almost equal for the width to height ratio along the contraction that was needed to accommodate the 9.5 x 9.5 test section (see figure 7). It is thought that this would have a beneficial effect on the suppression of secondary flows in the boundary layer. Therefore, at the ILST the same contours with varying width to height ratio were selected as well, scaled down from the DNW contour. At ILST the boundary layers at the test section entry were measured during the tunnel calibration program and it was observed that the velocity profiles were non-uniform but very symmetrical along the periphery; see figure 8. The thin boundary layers in the (x-y and x-z) planes of symmetry indicate that there is a secondary flow in the boundary layers from the centers towards the corners. One would estimate that the boundary layer thickness is of the order of the values as measured except for the planes of symmetry.

Contrary to the ILST, the LST has a nozzle with a constant width/height ratio. At the LST nozzle exit this phenomenon is not observed.

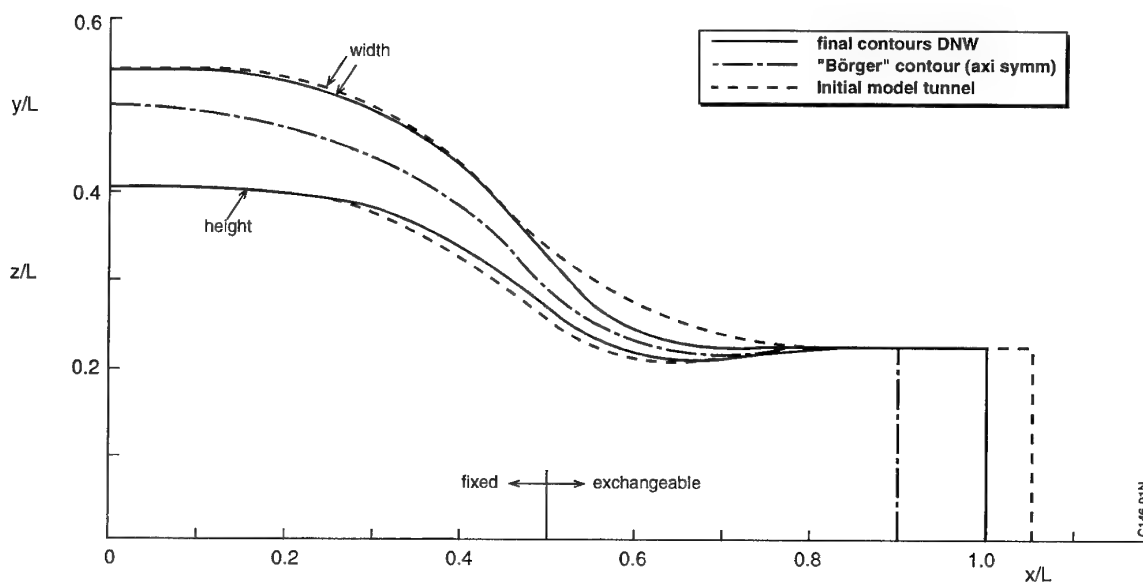


Fig. 6 Contours for the 9.5 x 9.5 m contraction of DNW

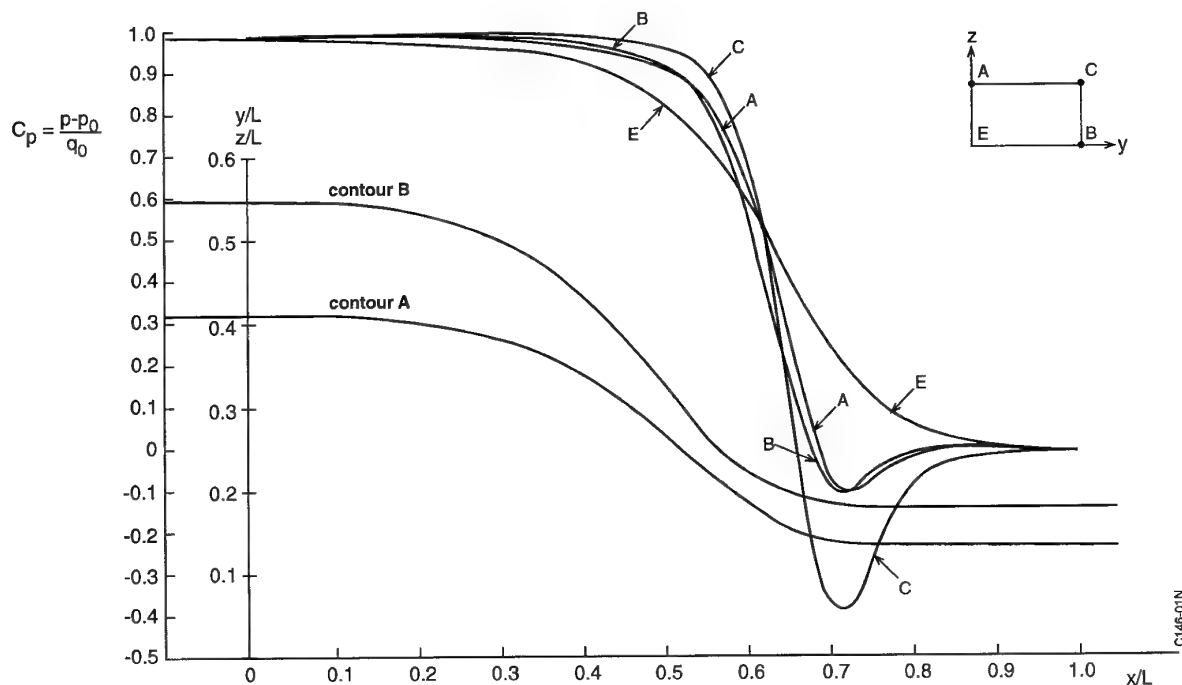


Fig. 7 Wall contours and pressure distribution, contraction $8 \times 6 \text{ m}^2$ of DNW

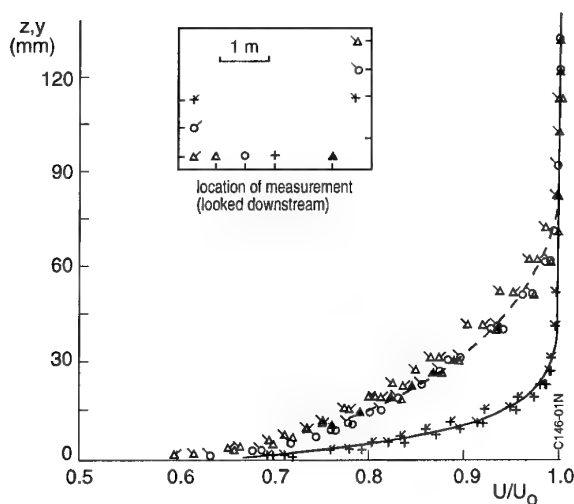


Fig. 8 Velocity profiles in boundary layer at end of ILST contraction

For both methods of Börger and NLR, the nozzles show at the exit a parallel part with a length of about the nozzle height/width in order to arrive at a sufficiently constant static pressure distribution ($\Delta p \leq 0.003$) at the test section entry. This parallel part gave the opportunity to install faired inserts in the $8 \times 6 \text{ m}$ DNW nozzle along the side walls to attain the $6 \times 6 \text{ m}$ exit for the smallest test section. In this configuration the static pressure field is within specification 3 m downstream of the contraction exit, but this is acceptable because the

smaller test section will accommodate also smaller models.

It is recommended to execute some contraction flow computations with modern N.S. codes in order to better understand the viscous flow along the walls and in the corners and to observe in how far secondary flows and/or even separations are a problem, and if so, how improvements can be made. This is even more opportune for designing transonic nozzles. There the shaping is inherently complex since part of the nozzle is two-dimensional in the sonic adjustable throat area. Maybe more data and experiences will be presented later in this symposium.

4.7 Settling chamber

In the settling chamber the flow is preconditioned to obtain the desired flow quality in the test section. Here the following inserts are usually placed into the flow

- heat exchanger, (when deemed necessary)
- flow rectifier,
- anti-turbulence screens and
- (as recently needed) smoke/seeding generator(s) for laser flow visualisation.

It is recommended to place first the heat exchanger in the flow (in downstream order). This device consists usually of finned tubes. For low speed tunnels a single row with about 10 cm long fins is usually sufficient. In the LST no heat exchanger is applied because the power level (or max. speed) is low (80 m/s). Since the steel

circular shell is mainly outdoors no running limitations are experienced except at hot, sunny days.

In order to limit the total pressure loss inside the settling chamber (below about 6,5 times local dynamic head), the tubes used in the DNW and ILST have an elliptical cross section.

The heat exchangers fins basically will have a (lateral) turbulence and flow angularity damping effect but the heat exchangers tubes will cause vortex shedding and when the fins are not placed fully parallel (and horizontal) new stable vortices will be generating behind the heat exchanger. Since the commercial production method of finned heat exchanger pipes is not intended for making perfectly straight fins and fins exactly normal the pipe axis, one should not strive to combine the flow rectifying and cooling function into one device.

Studies at NLR in the model tunnel have revealed that it is very effective to suppress vortex shedding of the heat exchanger pipes by placing the leading edge of the flow rectifier close to the heat exchanger. At DNW and ILST the same configuration was selected with only a gap of 5 mm between the fins and honey comb of the flow rectifier.

The design of the flow rectifier was mainly based on the early work by Humley (ref. 13). It was recommended to select a cell length to diameter ratio between 5 and 10. When the cells are short the flow rectifying function and lateral turbulence suppression function decrease, whereas for long cells the merging of the internal cell boundary layers causes new turbulence.

In all three tunnels, similar flow rectifying panels of about 1 x 2 m size (H x W) were used containing 115 mm deep honeycomb mesh of 1/2" cells. The cells are made of 0,2 mm aluminium sheet produced by an industrial expansion process. It is experienced in the model tunnel that both the leading and trailing edges of these honeycombs should be completely free of damages, blurs etc., because these minor deficiencies have a measurable effect on the flow in the test section and will not be damped by the downstream screens. It is, of course, also extremely important to inspect, install and align the honeycomb panels very carefully. The honeycomb panels were attached to the heat exchanger structure (DNW and ILST) and it was observed that the wakes from the extruding bolt heads and nuts (downstream from the flow rectifier) could not be traced back in the flow in the settling chamber.

Whereas a flow rectifier has a strong damping effect on lateral flows, screens have this effect on imperfections in the axial flow direction. Three to four anti-turbulence screens are applied in between the flow rectifier and contraction with an open area ratio of 0,57. Ref. 2 gives more details. Since much has been published in the past on screen turbulence damping (see also ref. 1) nothing will be said here about the specific screen characteristics (mesh, wire diameter, open area ratio, etc.).

Instead some practical remarks will be made.

- Since the screen weaving machines do not allow full width screen weaving in one cloth, seams have to be made. Modern plasma welding (wire by wire) or brazing techniques are sufficient (see fig. 9 of plasma welding example).

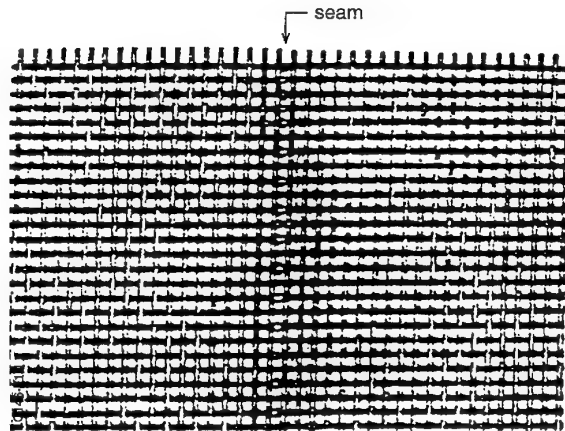


Fig. 9 Screen cloth with welded seam

- It has been shown that deviations in ideal flow direction (flow angularity) in the test section in both ILST and LST in pitch ($\Delta\alpha$) direction is larger than in yaw direction ($\Delta\beta$), see fig. 10. This may be attributed to the weaving direction of the screens. Therefore it is suggested to position the screens such that the waving direction is horizontal. In the on-going upgrading program of the NLR-HST, the new screens will be placed horizontal. The effect hereof will be published when the results are available, probably in 1997.
- During the commissioning process of the ILST the screens were (apart from being fixed and stretched somewhat to the ceiling and floor) fixed and stretched as well to the side walls. This had the effect that the maximum flow angularity in pitch decreased somewhat from 0,15 to 0,10 degrees (see fig. 10). This finding supports the previous statement on weaving direction. So, screens should be fixed and (slightly) stretched all around its periphery.
- Screens shall be completely free of kinks, sharp bends or other inhomogenities because such imperfections can be traced back in the flow and in particularly for flow angularity.
- The weaving direction of one screen shall be the same; e.g. on both sides of a seam the weaving shall be from left to right or visa versa.
- The distances between the screens shall be large enough to prevent vortex (turbulence) interaction and to allow human entry in between the screens for screen cleaning.

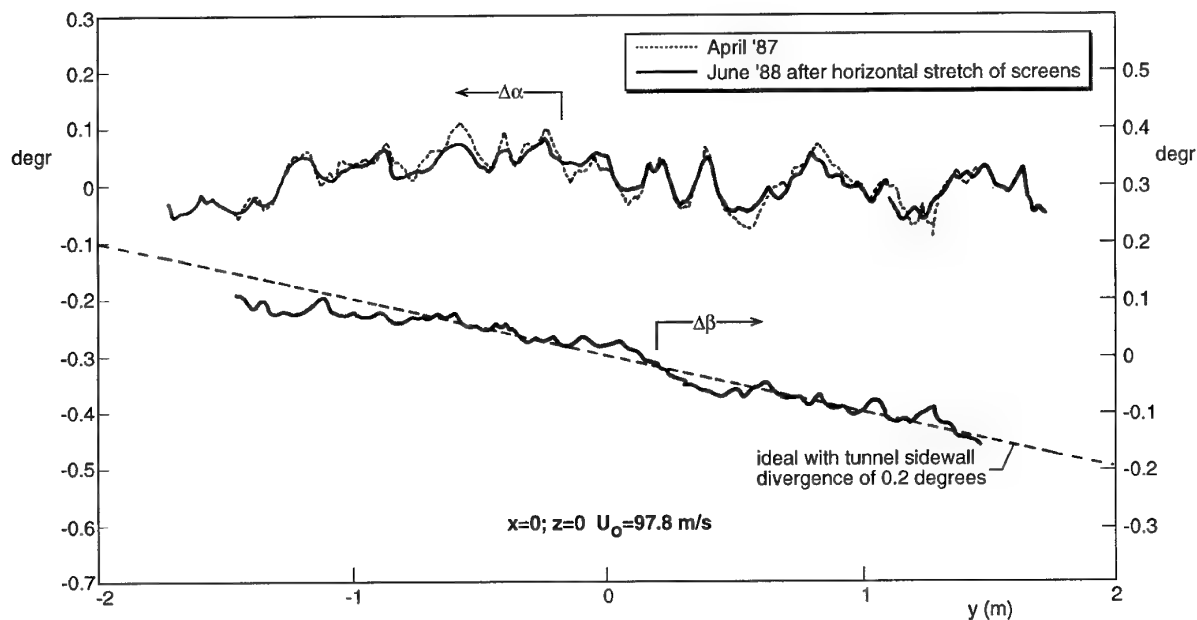


Fig. 10 Flow angularity in pitch ($\Delta\alpha$) and yaw ($\Delta\beta$) along y -axis and the effect of screen stretching in ILST

The turbulence levels in the DNW and LST test sections are very low (0,03 to 0,06 percent), as was established with special measuring techniques during the calibration programs. Since these values are so low, this special effort was not done in the ILST. In a comparative test campaign in the DNW and in free flight it has been shown that the turbulence level in the DNW is below a threshold value for affecting transition of a laminar boundary layer (ref. 14). This shows that the design efforts for the inserts in the settling chamber have been successful and no further optimizations are needed in this respect. This will also be valid for the two other tunnels, LST and ILST.

Recently a fourth item is occasionally introduced into the settling chamber: a smoke or seeding generator for laser flow visualisation studies. In order to pinpoint a certain streamline or streamtube, a traversing device and/or spatially distributed smoke/seeding injector can be used. Exploratory tests in a model tunnel at NLR have revealed that, for stability reasons, injection upstream of the heat exchanger is the most suitable place. Besides, the flow disturbances from these devices are best damped by the downstream heat exchanger, flow rectifier, and screen package. Similar experience is also attained at DNW. Therefore in the NLR's high speed tunnel, HST, a traversing smoke/seeding mechanism will be installed in front of the heat exchanger and whether this device will have to be removed when flow seeding is not needed, has still to be determined in practice by observing flow quality during a calibration campaign.

5. TEST SECTION

The flow within the test section and the test capabilities count for the aerodynamic researchers. Therefore, although the test section is part of the airline, it will be discussed here separately. The following topics will be discussed in this section:

- Test section shape
- Provisions in the walls
- Model supports and logistics.

These topics are interrelated but nevertheless it will be tried to describe them separately.

5.1 Test section shape

Modern wind tunnels have either a square- or a rectangular cross section. It is thought that for high lift testing such as for helicopters or for V/STOL planes, square shapes would be better than the rectangular ones. Experience in DNW has shown for the past 15 years of operation that the rectangular 8 x 6 m test section is used by far the most for aerospace testing relative to the available square 6 x 6 m and 9.5 x 9.5 m test sections, also for helicopter work and high lift devices.

Corner fillets are rarely used anymore. It will disturb the routinely applied wall correction methods and with properly designed contractions, flow separation in the corners can be prevented. Besides, without those fillets the full side walls height and floor/ceiling width are available for easy access and instrumentation.

The test section length should be at least about three times the average of width and height (or \sqrt{A}) (to

prevent buoyancy effects from the test section diffuser) with the model center at approximately one third from the test section entry under the conditions that the contraction is designed according to the Börger/NLR approach.

One set of walls should be parallel to accommodate a set of axially aligned turntables in these walls (in the three tunnels considered herein the floor and ceiling). The other set should be diverging somewhat to compensate for displacement due to boundary layer growth along all four walls.

In all three tunnels a value of 0,2 degrees divergence (relative to the test section axis) was selected but it was found that in all three tunnels this resulted in some overcompensation as is shown in table 1.

Table 1 Static pressure gradients at T.S. axis for DNW, LST and ILST

	DNW			LST	ILST	without BL
	8 × 6	6 × 6				
	closed	slotted	closed			
$\frac{dcp}{dx/b_0}$	0.004	0.0032	0.0046	0.003	0.0012	0.014

It may be concluded that a value of divergence of 0,18 or 0,17 degrees would have been a better average choice. Nevertheless, the effect of this buoyancy on drag measurements is only of the order of one drag count or less and therefore can be disregarded for most tests.

5.2 Provisions in the walls

Low speed aerodynamicists want to watch their model during tests. Also modern flow visualization techniques require good access to the flow field by passing laser light bundles inside the flow. Therefore all four walls should be equipped with removable windows where possible. Depending on the optical demands various glass qualities may be used. At DNW the windows consists of three sheets glued together to prevent scattering at accident whereas in LST and ILST plexiglas panels are used. Special glass is to be used when high power laser light bundles have to pass the windows. Window panels are usually removed when necessary to stick probes or traversing mechanisms into the floor. The side walls are further provided with entry doors for human access and at DNW also to enter a cherry picker to reach the model for adjustments or checks.

At ILST and LST a removable test section part is provided with a set of synchronous and axially aligned turntables in the floor and ceiling. Both tunnels also have a similar turn table at the downstream end of the test section for wind hinderance testing.

At LST and DNW sets of almost full test section length rulers with static pressure ports can be installed along the test section walls to measure the wall pressure distribution. They are used for wall interference assessment using methods based on measured boundary conditions. Having available such devices turns out to be very handsome and practical.

Wind tunnel walls are also often used to install a fast acting q-stopper in the form of fast opening doors or protruding panels. The walls of the tunnels under consideration herein are not designed to accommodate such devices. Instead, at DNW an extremely fast q-stopper was developed and designed consisting of a 1 m³ pressure vessel on the tunnel axis at the entry of the test section diffuser. At trigger a small fast acting valve is opened initiating a set of retro airjets opposing the flow. This causes a weak upstream travelling shockwave that passes over the model. See fig. 11. Model tunnel tests in

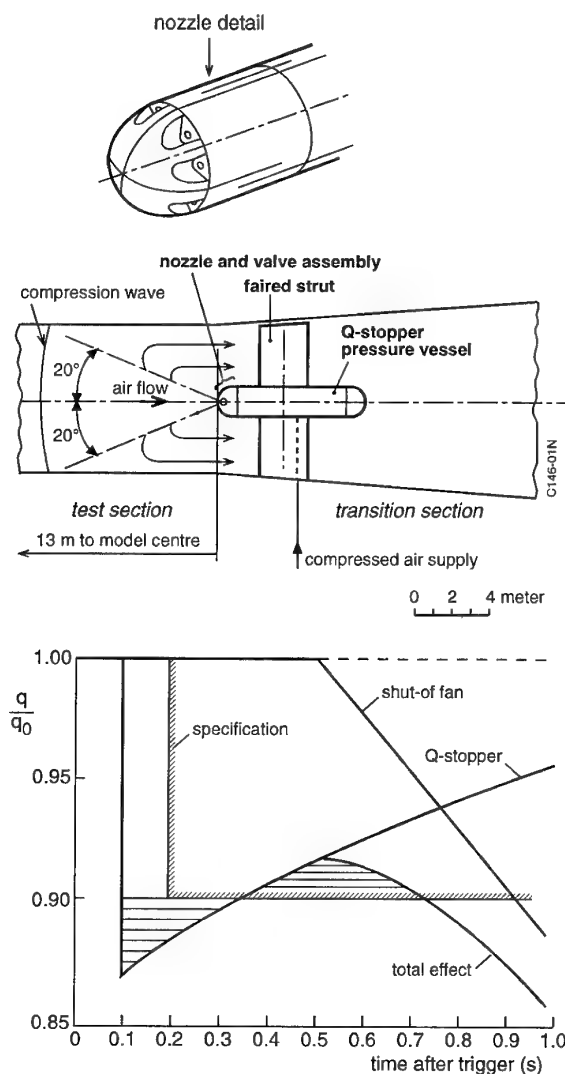


Fig. 11 Q-stopper design for DNW

the DLR MUK have shown that the q value can be reduced 10% or more within 0.2 seconds after trigger. Jet braking is only required for a few seconds when simultaneously the fan drive is turned off as well. However the q -stopper has not been realized yet because no use has shown up so far, but the interfaces with the first part of the test section diffuser have been included.

All four walls of the 8 x 6 and 6 x 6 test sections of the DNW are equipped with remotely adjustable slots (max. 12% open) at a pitch of 1 m in order to reduce wall interference. This provision was made in the seventies because it was assumed at that time that within the foreseeable future methods will become available to assess the residual wall interference. Although it has been demonstrated that the wall interference reduces with a slotted wall, the residual interference is still hard to determine. Therefore the slotted wall arrangement is not much used. Maybe future developments will change this picture. In the 9.5 x 9.5 m DNW test section and in the ILST provisions for a slotted wall arrangements are made, but not yet realized and it is felt that this was a good decision. Work is still going on in a joint effort at NLR, DNW and DLR to better understand and assess wall interferences with slotted walls. It should be remarked here that slotted walls consume much energy and that special reingestion measures have to be taken to prevent strong axial pressure gradients (and hence buoyancy) in the test section (ref. 2).

In the DNW test sections, the floors can be interchanged with a variety of floor hatches containing either turntables, slotted wall arrangement or a (moving) ground board provision for ground proximity testing (see fig. 12). In the smaller and less complex ILST and LST some of these provisions are fixed to the test section and for exchangeability the entire test section part is exchanged. It is felt after many years of testing experience that it has been a good decision, for reasons of costs and complexity, to provide the (large) DNW with exchangeable hatches and the smaller tunnels with exchangeable test section parts.

In all tunnels provisions are made to install an axial blowing slit for boundary layer energizing in front of a test object when needed. Every low speed wind tunnel should have such a provision. At DNW also boundary layer scooping is used.

5.3 Test section and model logistics

The last paragraph of the former section already refers to test section component exchangeability. To plan a test section, its provisions in and around it and the associated testing hall and related building arrangement, a clear view must be developed on the tunnel usage in the envisaged market segment. For example the predecessor of the DNW at NLR, the LST 8 x 6 was planned initially (late sixties) for V/STOL aircraft development testing. Then environmental issues became a hot item and noise testing at model scale was requested aiming

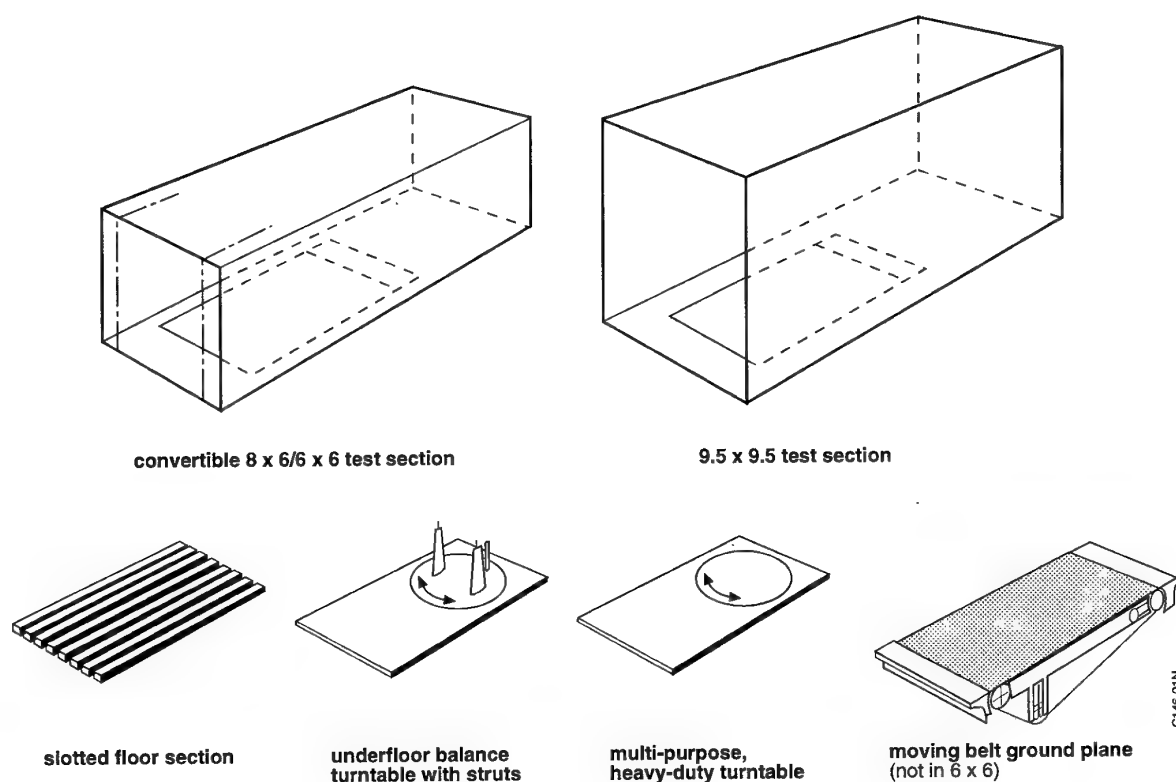


Fig. 12 Test section floor interchangeability at DNW

for an open test section. The DFVLR (now DLR) brought in high speed helicopter testing giving the 6 x 6 m test section arrangement and full scale component testing asking for the 9.5 x 9.5 m test section. So the DNW was set up for a multi purpose atmospheric test facility with many testing capabilities including extensive propulsion simulation. Studies between a tandem test section arrangement and a exchangeable test section arrangement soon revealed, for aerodynamic (possible flow separations) and productivity (preparation) reasons, that an exchangeable test section arrangement should be preferred. This has the additional advantage that a (removable) model support, can be installed of a fixed location to the foundation.

Feasibility studies showed that the 8 x 6 m and 6 x 6 m test sections could be combined in a single arrangement by moving the sidewalls inward and having at the downstream end the last 6 m hinged forming a steep but short diffuser.

Model tunnel tests further showed that for the open 8 x 6 m test section, the 13 m long 9.5 x 9.5 m transition piece to the test section diffuser could be used as a flow collector for the open 8 x 6 m test section arrangement. In total this required 6 pieces to be interchanged (2 movable contractions, 2 test sections, 2 transition pieces with the diffuser). Having this interchangeability done by a rail system, would require a complex system, huge halls and would give little flexibility. This was the reason why a transport system based on air cushions was selected. Although it was risky at that time for such large and heavy applications, the system has shown its value in practice. The (concrete) floor should be very flat, horizontal and air tight (cracks may cause problems

because air pressure then penetrates the concrete and may separate layers). The same transport system was selected for the LST. The selected ILST test section arrangement could be easily handled by a rail system and to ensure trouble free operations this system was selected in Indonesia (fig. 13).

Model entry into the test sections is relatively easy for exchangeable test sections either from downstream or from upstream. This can also be done when the test section to be used is in situ in the circuit by removing the adjacent component (e.g. the contraction at the DNW).

Whereas the model supports of the DNW are fixed to the foundation, at the LST and ILST these devices are fixed to a particular test section component. This gives the advantage at DNW to use the model support for any test section and also in the open test section arrangement. This requirement was not present at the other two smaller tunnels having both a single test section size. To this end at both tunnels the test section is split in an upstream and downstream part and at both tunnels the upstream part is executed in two configurations of which one configuration carries an external six component balance (see fig. 14a) on top of the turntable in the ceiling. The other upstream test section part of the LST contains a set of turntables in the ceiling and floor (for 2-D testing for example) and at the ILST this is simply an empty box. At ILST the downstream end is also executed in two fold of which one part carries a sting support mechanism (see fig. 14b) and the other part a turntable for industrial testing, similar as at the LST. So at the ILST by combining the two upstream and two downstream parts four test section configurations can be made for particular test purposes (see fig. 13).

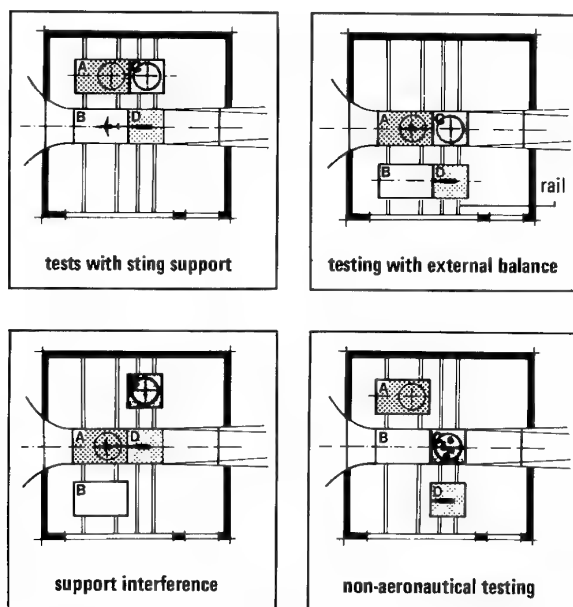


Fig. 13 Possible test section arrangements at ILST

At both DNW and ILST two model preparation rooms are available. Models can then be brought into the test section at DNW with the use of a movable (on air cushions) elevator. For the ILST an overhead crane is used either when these test sections are in situ or removed from the circuit. At the LST the test section parts can be moved in front of a workshop at the same floor level for easy model preparation, mounting and check-out prior to movement into the circuit. From experiences these three systems for model preparation, mounting and check-out are satisfactory for efficient use.

5.4 Model supports

All three tunnels have an external 6-component balance and a sting support mechanism for model support via an internal balance.

For multi-use requirements the DNW external balance is a floor balance (fig. 15). Although easy for use for floor mounted half models and full-scale cars and trucks the support of full airplane models is cumbersome because only strut supports can be used. In particular the tail strut (and especially the wind shield thereof) gives a

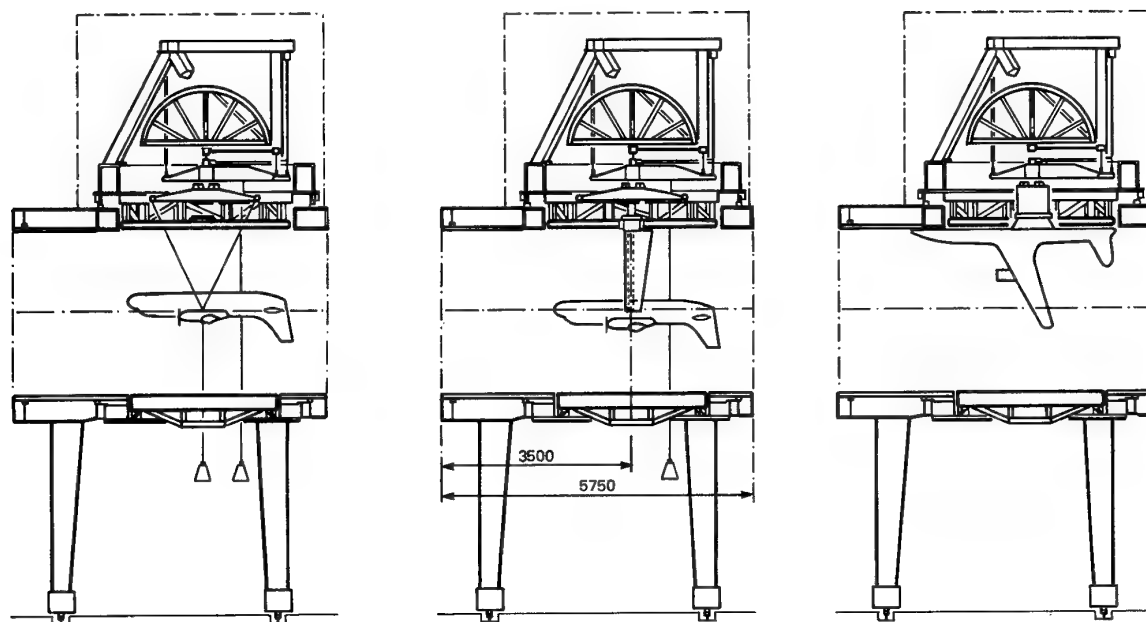


Fig. 14a ILST upstream test section part with external balance

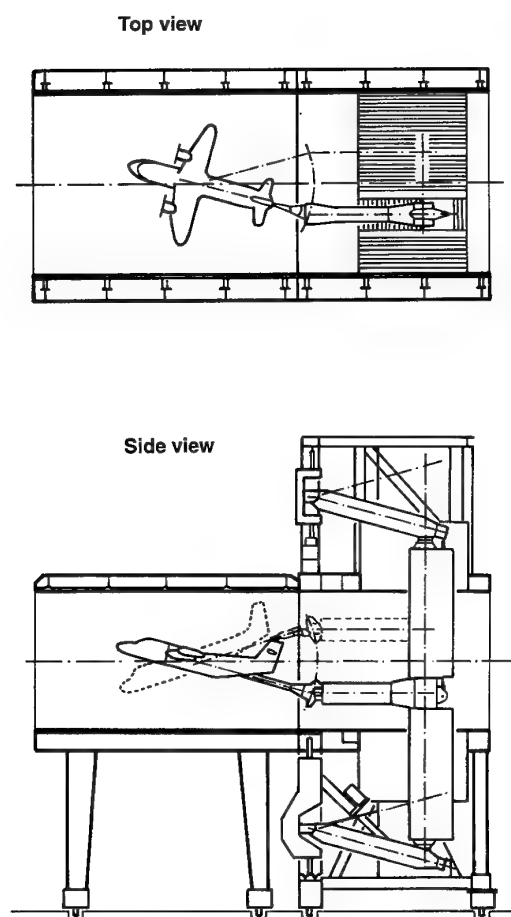


Fig. 14b ILST test section configuration with sting support mechanism

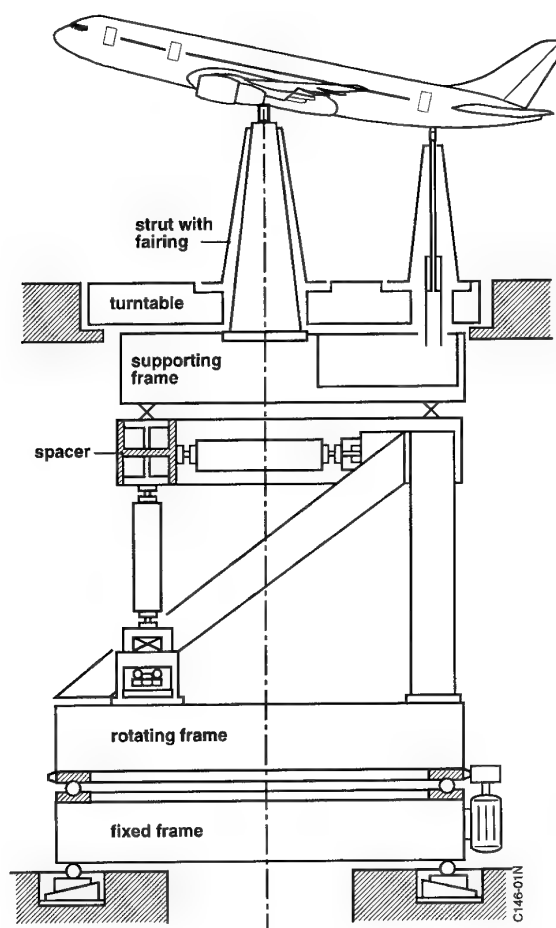


Fig. 15 External balance of DNW with a model supported by struts

substantial aerodynamic interference. Since the test section and the external balance are essentially uncoupled (both separately fixed to the foundation) the yaw and pitch movements have to be carefully synchronized. Since the external balance can be moved on air cushions as well, the balance can be calibrated in a special calibration hall, assuring that the (usually long-lasting) calibration process does not interfere with wind tunnel tests.

The LST and ILST have a similar overhead balance allowing both strut (wing and central) and wire suspension (see fig. 14a). Although wire suspension does not give accurate drag data, the other aerodynamic interferences are minimal and therefore it gives a good basis for interference free testing with the other model support systems. Pitching can be done either by a pre-loaded pitching wire or by an internal pitch mechanism. Both at ILST and LST the external balances showed to be real work horses and proved to be very stable in course of time. The external thermal covers and temperature controls of the ILST and DNW balances further improve stability in read-out.

The work horse at DNW is the sting support mechanism (fig. 16). DNW has developed an elaborate method for sting support interference corrections for the various

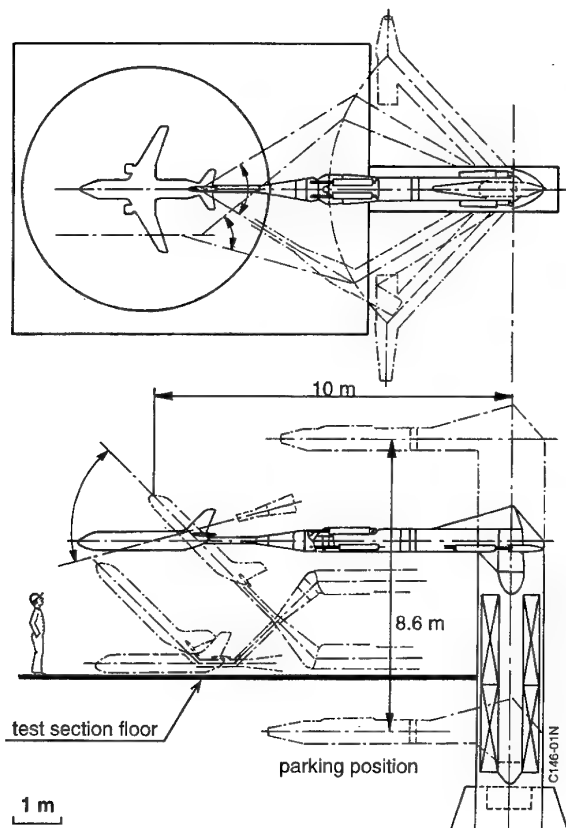


Fig. 16 Sting support mechanism of DNW

stings (dorsal, tail, ventral). The DNW sting support mechanism consists of a streamlined strut, that can move up and down on vertical rails in a 14 m deep pit. This strut supports an articulated boom for yaw and incidence movements. As a consequence the center of rotation moves back and forward. Because all movements are independent the system can also be used to position models just above the moving belt ground plane at the floor level. All movements are powered hydraulically and in the early phase it was problematic to take-over from the stationary brake position to live hydraulic power control without shaking the model and hence possibly damaging the balance. Now this phenomenon is well under control.

This last phenomenon was the main reason to select for the ILST an electromechanic drive and control and besides to have for pitch and yaw each only one single drive. By linkages and torsion tubes it was possible to transfer external movements to the sting movements such that the center of rotation remains at place. The vertical strut is moving laterally when yawing the model keeping the boom in flow direction (fig. 14b). This requires the use of rolling doors in the ceiling and floor of the downstream test section. The boom is relatively of similar size as the DNW boom that so it may be expected that interference effects are similar as well. Although it was planned to execute an extensive support/sting interference exercise in the ILST, this has not been done yet and LAGG (the ILST owner) mainly uses the external balance with strut supports, applying now and then a wire suspension for baseline data.

Recently the LST was equipped with a simple sting support mechanism by placing a segment pitch mechanism in the upstream turntable (fig. 17). From studies at DNW it was concluded that for models of transport aircraft, use of ventral stings is a good solution, for interference reasons, often better than tail stings. The LST sting support mechanism can be easily combined with ventral stings giving a good and cheap solution. However not much experience is available yet.

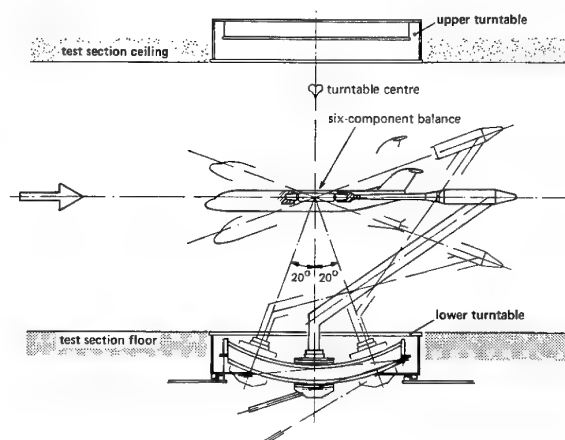


Fig. 17 Sting support mechanism of LST

6. CONCLUDING REMARKS

It has been tried to give an overview of the experiences gained since the mid seventies during the realization, and operation of three low speed wind tunnels in which NLR was strongly involved. Some explanations and backgrounds have been given on aerodynamics and operational issues and where possible experiences and recommendations stated. A selection has been made of topics without going into depth nor having the pretention of being complete. The following general conclusions can be drawn from the above:

- The airline as developed at NLR is a conservative but solid basis for subsonic wind tunnels giving data which are close to what the aerospace industry is aiming for. Of course further refinements will always be possible and certainly will come up in the symposium where this paper will be presented.
- It is wise to design a low speed facility for multi-purpose use. It is difficult to predict which testing capability will ultimately make the tunnel successful in operation and this will change in time. For example the aero-acoustic testing capability is one of the high- lights of DNW. The car industries used this facility extensively until they built their own facilities. Who would have thought that full scale truck testing would be a major application of the 9.5 x 9.5 m test section of the DNW?
- Great care must be devoted to the manufacture and installation of the inserts in the settling chamber. Almost non measureable deviations to the ideal screen properties have measureable effects on the flow angularity.
- It is believed that the sequence and relative distance of the inserts on the settling chamber as described in this paper contribute to high flow quality.
- More theoretical and experimental work should be done to better understand whether and how secondary flows in the contraction may effect the flow in the test section and which improvements may be useful.
- Tunnel operators and users have a tendency to stick to a model support system in which they have gained confidence by building up a data base. This is the case at DNW for the sting support system whereas in Indonesia the external balance is primarily used.
- Little has been said herein on the open test section of the DNW, because in a subsequent paper this item will be treated extensively.

Acknowledgement

Realisation of a wind tunnel is a matter of team work with colleagues and external consultants and contractors. The author feels grateful to have worked with so many of them in various teams in always a very enthusiastic atmosphere. For the writing of this paper the author wants to thank Messrs. van Ditschuijzen and Eckert for submission of some old unpublished DNW material and

Mr. Roßs and the LAGG staffmembers for their inputs on ILST operation experiences.

REFERENCES

1. J.C.A. van Ditschuijzen "Design and Calibration of the 1/10th scale Model of the NLR Low Speed Wind Tunnel LST 8 x 6", NLR MP 75031 U, 1975.
2. J.C.A. van Ditschuijzen and R. Ross "Aerodynamic and Aeroacoustic Design Aspects" Design, Manufacturing Calibration of the German-Dutch Windtunnel (DNW) CONSTRUCTION BOOK 1976-1980 (Published by DNW).
3. F. Jaarsma and M. Laihad "Indonesian Low Speed Tunnel ILST" Paper 19 of the International Symposium on Aeronautical Science and Technology Indonesia - ISASTI, June 1986.
4. F. Steinle and E. Stanewsky "Wind Tunnel Flow Quality and Data Accuracy Requirements" AGARD-AR-184 1982.
5. T. Wolf "Berechnung des Leistungsbedarfs von Unterschall- und Transsonik- Windkanälen" Dissertation, Technical University Darmstadt, 1995.
6. Ann "Performance of Conical Diffusers in Incompressible Flow", Engineering Science Data Unit, Ian nr. 73024.
7. T. Wolf "On the Possibilities for Improvement and Modernization of Subsonic Wind Tunnels" AIAA 90-1423, June 1990.
8. I. Zwaaneveld, "Investigation of Sheet Metal Vane Cascades for 90°C Corners with 0,10 and 20% Extension, NLR (formerly NLL) report A1118, 1950 (in Dutch).
9. S.H. Chintamani and R.S. Sawyer, "Experimental Design of Expanding Third Corner for the Boeing Research Aerodynamic Icing Tunnel" AIAA 92-0031, January 1992.
10. G.B. Schubauer and W.G. Spangenberg, "Effect of Screens in Wide-Angle Diffusers" NACA Report 949 1949.
11. J. v.d. Vooren and A. Sanderse, "Finite Difference Calculation of Incompressible Flow through a Straight Channel of Varying Rectangular Cross Sections, with Applications to Low Speed Wind Tunnels" NLR TR 77109 U 1977.
12. G.G. Börger, "Optimierung von Windkanaldüsen für den Unterschallbereich" Zeitschrift Flugwissenschaften 23, pp. 45-50 1975.
13. J.L. Lumley and J.F. McMahon "Reducing Water Tunnel Turbulence by Means of a Honeycomb" Transactions of the ASME Journal of Basic Engineering, Dec. 1967, pp. 764.
14. K.H. Horstmann, A. Quast and G. Redeker, "Flight and Wind Tunnel Investigations on Boundary Layer Transition" Journal of Aircraft 27, 1990.

THE AERODYNAMIC AND STRUCTURAL DESIGN OF THE DRA 5-METRE AND ONERA F1 LOW-SPEED PRESSURISED WIND TUNNELS

D S Woodward (Defence Research Agency, Farnborough, Hants GU14 6TD, UK)

G Francois (ONERA, France)

N J Taylor (Defence Research Agency, UK)

Abstract

This paper describes the aerodynamic and structural design of two pressurised low-speed tunnels built in the 1970's to achieve a Reynolds number of 6×10^6 and, at the same time, to enable the effects of compressibility and scale to be studied independently in tests of aircraft models in take-off and landing configurations. Despite being designed to similar specifications and providing comparable levels of flow quality, productivity and customer confidentiality, the tunnels differ significantly in several important aspects of their design. The principal features of the two designs are reviewed and a few examples of the compressibility and scale effects that have emerged from the test programmes in each tunnel are presented.

List of symbols

C_p	pressure coefficient
H	total pressure
M	reference Mach number
p	static pressure
p'	pressure perturbation, r.m.s. value
q	dynamic pressure, $\frac{1}{2}\rho U^2$
Re	Reynolds number
u	streamwise velocity component
u'	streamwise perturbation velocity, r.m.s. value
v'	lateral perturbation velocity, r.m.s. value
w'	normal perturbation velocity, r.m.s. value
U	reference velocity
\bar{U}	mean streamwise velocity component
ρ	density
λ	loss or power factor, $\Delta p/q$

Suffices:

0_{REF} reference values

1 INTRODUCTION

In the late 1960s, many voices were raised in favour of building a number of new low-speed wind tunnels. Those whose imagination had been fired by the possibility of city-centre to city-centre V/STOL transports argued for much larger atmospheric tunnels in order to reduce the wall-constraint on the path of the lifting jets. On the other hand, those who saw the future remaining with CTOL aircraft were becoming increasingly aware that the existing atmospheric wind tunnels - typically around 3m square - were unable to give reliable data on the maximum lift and stalling behaviour for the then current generation of swept-wing civil transports.¹ For these people, the results of the AGARD studies on large wind tunnels^{2,3} indicated that the most cost-effective way of achieving the desired levels of Reynolds number was by smaller pressurised tunnels. (While the concept of a

cryogenic wind tunnel had been put forward,^{4,5} the possibility of a practical implementation⁶ had not yet been considered.) Thus, while the Lockheed Aircraft Company, the Canadian Government and the German and Dutch Governments in collaboration chose to build atmospheric-pressure tunnels approximately 10m square, the UK and French Governments opted to build pressurised facilities of roughly a quarter of this size - 5m square.

With the passage of time, V/STOL city-centre to city-centre transport has been found to be impracticable due to noise and other environmental constraints. As a result, the large atmospheric facilities have been forced to diversify into non-aeronautical fields to absorb their excess capacity. In contrast, the pressurised facilities have remained in demand and have needed regular enhancement and updating. This demand stems from the continuing desire to improve take-off and landing performance: for civil transport aircraft, the rewards for achieving higher take-off weight for a given runway length, and/or lower drag levels (with one engine failed) during climb-out from an airfield, are at least as significant as improvements in the high speed portion of the flight envelope. When combined with the requirements for approach and landing, these aspects of performance translate into a range of exacting targets for lift-to-drag ratio and maximum lift coefficient. For almost all civil aircraft and many of the military CTOL aircraft designed in the last two decades, it has been necessary to employ complex systems of slatted and slotted flaps in order to meet these targets. Optimisation of the flap design and schedule continues to be beyond the capability of CFD codes.

Although the flight Mach number is low under take-off and landing conditions, the high lift coefficients involved generate high local velocities, particularly near the wing leading edge. These may result in significant compressibility effects on maximum lift. Hence, it is important that tests are conducted at the correct Mach number. Moreover, when testing scaled models, extrapolation to full-scale performance may only be made with reasonable confidence if the effects of compressibility and scale can be isolated in the test data. This requires that a pressurised wind tunnel should be used for such investigations.

In the UK, one such facility - the 8ft High Speed Tunnel at DRA (then RAE) Bedford - already existed. However, its low speed Reynolds number capability was thought to be insufficient for testing models of the larger aircraft that were emerging at the time. Moreover, this tunnel was already heavily utilised on other projects. Therefore, the case for a new low-speed pressurised facility was made. First submitted to the UK Government in 1967, approval to proceed with the design of the 5m tunnel at DRA Farnborough was originally granted in 1969. This approval was renewed in 1971 after a review necessitated by cost increases and Government re-organisations. The shell was pneumatically pressure tested in 1975 and air was driven round the circuit for the first time in November 1977. The corresponding French tunnel, the F1 tunnel at ONERA Le Fauga Mauzac, was designed between 1971 and 1973. Construction started in January 1974, as soon as approval was given. Pressure tests were conducted in May and June 1976 and the first rotation of the fan occurred on July 30th 1976. External views of the two tunnels are presented in Figure 1.

This paper describes the aerodynamic design of both tunnels, together with some of the key aspects of their structural and mechanical design.

2 DESIGN REQUIREMENTS

The main requirement for both tunnels was the same - testing of models in take-off and landing configurations, with a good representation of complex shapes, at a significant Reynolds number. In detail, this was expressed as:-

- a. At a Mach number of 0.2, the Reynolds number must be at least 6×10^6 , based on a conventional reference length of $0.1 \times (\text{test section area})^{1/2}$, a measure of the maximum

permissible mean chord for a complete model of an aircraft with wings of high aspect ratio. This is roughly a quarter of the flight Reynolds number for a typical 300-seat transport aircraft.

b. The maximum stagnation pressure must be sufficiently high as to provide a significant variation of Reynolds number at constant Mach number consistent with the needs to avoid a hydraulic over-pressure test of the shell, limit the aeroelastic distortion of the model when testing at maximum dynamic pressure and prevent excessive over-sizing of stress-critical model components like slat and flap supports.

When combined with the need to ensure that the constraining effects of the tunnel walls were small enough to be predicted with adequate accuracy on models of sufficient size to allow small but significant details of the high lift system to be properly represented, these requirements were translated into the following design parameters:

	DRA 5m	ONERA F1
Working section size	5m × 4.2m	4.5m × 3.5m
Pressure and Mach Number or speed requirements	$H_{\max} = 3\text{atm}$; $M_{\max} = 0.27$ $H_{\min} = 1\text{atm}$; $M_{\max} > 0.31$	$H_{\max} = 4\text{bar}$; $U_{\max} = 70\text{m/s}$ $H_{\min} = 1\text{bar}$; $U_{\max} = 120\text{m/s}$
Maximum temperature	35°C	<40°C

These working section sizes were large enough to permit actuators to be installed inside models, allowing adjustments to be made to certain parameters - the tail setting, for instance - remotely, without requiring direct access to the working section. For F1, the pressure of 4bar was the maximum allowed by the pressure vessel regulations. Also, although strictly speaking, a smaller tunnel would have given the specified Reynolds number - its size was increased in order to be closer to that of the UK tunnel.⁷

The following stipulations were also made:

a. The stagnation temperature should be as close as possible to ambient, without employing expensive cooling plant.

b. The flow quality in the working section should be uniform in space and stable in time, with low noise and turbulence. In order to prevent the variations in flow quality with speed and operating pressure from becoming significant (and therefore introducing additional effects that cannot be separated from the genuine effects of scale and compressibility), the following targets were set for the 5m tunnel: maximum permissible variations in dynamic pressure of $\pm 0.1\%$; zero longitudinal static pressure gradient and longitudinal turbulence levels no greater than 0.1%.

c. The time required to access the working section should be comparable with that in large low-speed tunnels operating at atmospheric pressure. (This precluded normalising the pressure throughout the circuit when operating above atmospheric stagnation conditions; in the 5m tunnel, a provisional target of 10 minutes was set.) Provision should also be made to allow for the complete preparation of the model mounting and instrumentation outside the tunnel.

d. Various model mounting arrangements should be accommodated - complete model on a sting supported by a quadrant, or on several types of struts connected to a wall balance; half model on the same wall balance - and provision should be made for future improvements.

Models should also have access to suction plant and a high pressure air supply for suction or blowing.

e. Optical access to the working section should be provided at all test conditions.

f. Control of the facility and tunnel conditions (pressure, temperature and wind speed) should be computerised and enable constant Reynolds number and Mach number conditions to be produced automatically. The data acquisition system should be versatile and capable of measuring the force and moment outputs from several balances and large numbers (>1000) of pressures simultaneously. For efficient management of the test programme by the customer, the data should be reduced and the corrected results displayed on-line.

3 GENERAL DESCRIPTION OF THE DRA 5m TUNNEL

3.1 Air circuit

A cutaway drawing of the facility is shown in Figure 2. The tunnel has a conventional closed-return circuit with $5\frac{1}{2}^\circ$ diffusers throughout, except for the passage surrounding the main drive fan and the more rapid expansion between the fourth corner and the cooler. The pressure shell, a one-piece welded steel structure with no sliding or bellows-type joints, is everywhere circular in cross-section. Internal liners are incorporated throughout the settling chamber, contraction and working section to make the air-swept surfaces rectangular with corner fillets. The fillets were introduced as a convenient means for reducing the likelihood of problems being encountered with corner-flow separations in the contraction and working section, reducing wall interference effects on model lift⁸ and, more importantly, accommodating the streamwise growth of the wall boundary layers in the working section. This is achieved by tapering the fillets in the working section. In order to reduce the possibility of secondary flows being established in the working section, the octagonal cross-sectional shape of the liners is kept almost constant from the settling chamber to the entrance of the working section.

Compressors, coolers and driers in the auxiliary plant room deliver air at 4.5bar to a manifold situated under the main drive unit. "Blowdown" valves used to control the pressure in the tunnel are connected to the other end of this manifold. Air is admitted into (or allowed to escape from) the circuit via chordwise slots in three of the straightener vanes aft of the fan. As the compressors operate at constant mass flow, their output is not always matched to the tunnel demand. Surplus compressed air, together with any exhausted from the circuit, is discharged to atmosphere via a silencer (not shown in Figure 2). Additional plant (also not included in Figure 2) provides a high pressure air supply to the working section. This may be used to provide boundary layer control, direct jet-blowing or input to TPS units on complete or half models.

The cooler, shown in Figure 3, is made from two rows of elliptic tubes with closely-spaced flat rectangular fins and can dissipate the whole power input of the fan drive whilst maintaining an air temperature of 40°C or less. The pressure drop across the cooler makes possible the use of a rapid diffuser upstream, with a consequent shortening of the return circuit and reduction in cost of the pressure shell. The transition from circular to octagonal internal cross-section is also made within this diffuser. It was originally intended that the cooler should act as a fine-mesh honeycomb which, when followed by two 1.5q screens, would enable the specified flow uniformity to be achieved within the working section. However, in this part of the tunnel, a sequence of events has produced significant changes between the initial design and what is installed in the tunnel today.

Firstly, the pressure drop of the screens was reduced from 1.5q to 1.1q for the reasons described in Section 4.2. Secondly, due to faults in the construction and assembly of the cooler bundles, it was

necessary to insert an additional conventional honeycomb between the cooler and the screens in order to meet the specified flow uniformity. Finally, after about a year of operation, severe corrosion was discovered in a large number of the brazed joints at the "crossover" points of the individual wires in the stainless steel screens, thus reducing the strength below the required safety level. To prevent future recurrence of the corrosion problem, phosphor-bronze replacement screens were chosen and, for practical reasons, these were selected to have a pressure drop of slightly less than $1.0q$ - which the investigations described in Section 4.2 show to be acceptable. These proved to be the only modifications to the circuit that had not been anticipated during its design.

3.2 Main drive system

The main drive motors are housed inside a nacelle of 6.1m diameter within the return leg of the air circuit. The drive consists of an a.c. motor of 11000kW continuous output, controlled by a liquid rheostat, together with a 1640kW d.c. motor controlled by thyristors.

The fan system, shown in Figure 4, comprises 21 cambered and twisted pre-rotation vanes, a 10-bladed single stage rotor and nine symmetrical straightener vanes. The use of a fixed-pitch fan ensures a uniform velocity distribution to the main diffuser at all tunnel speeds. The fan has an outside diameter of 10m. Each blade is 1.95m long and has a chord of 0.92m, with the thickness-to-chord ratio varying from 10% at the tip to 20% at the root. The blades are made from glass fibre reinforced Araldite and are bonded in a special way⁹ to steel root fittings. Strain gauges have been installed on three of the fan blades so that the local dynamic loading can be monitored while the tunnel is running.

3.3 Access to the working section

One of the distinctive features of the tunnel is the arrangement incorporated to ensure rapid access to the model. The basic principles of its operation are illustrated in Figure 5. Two concentric spheres surround the working section. Parts of the working section walls at the upstream and downstream ends can be rotated, so that pressure doors on the outside of the inner sphere can be swung across the air passage and closed on to the inner sphere. This can then be de-pressurised to give personnel access to the working section. A period of about 6 minutes is needed to stop the fan, move the pressure doors into position and obtain access to the model. A similar time elapses from finishing a model change to being back on-condition and ready to acquire data.

This "double-sphere" access arrangement is one of the key structural aspects of the design, because the outer pressure shell is continuous and stresses in it are not affected by access to the model. The tunnel is fixed to earth at the base of the double-sphere and all the other attachments allow longitudinal and lateral displacement due to expansion under pressure and temperature variation.

The model, together with all the instrumentation needed for the test, is mounted on a "cart" which forms the floor of the working section. The working section can be rotated about the vertical axis of the spheres until it lines up with the main access tube, as shown on Figure 6. The complete cart can then be driven electrically along a railway on to a turntable and parked in one of the four bays in the rigging area, as shown on Figure 7. In this way, the cart in the working section may be replaced and another model made ready for testing in less than an hour - although, in practice, it is rarely necessary for a model changeover time to be so short.

3.4 Outline of aerodynamic performance

The operating envelope of the tunnel is shown in Figure 8, where it is compared with that of the ONERA F1 tunnel. Here, Reynolds numbers are based on $1/10$ of the square root of the cross-

sectional area of the working section (0.46m for the 5m tunnel; 0.397m for the F1 tunnel). Complete models of transport aircraft with high aspect ratio wings may achieve values of Reynolds number about 10% greater than those shown; military aircraft models of lower aspect ratio, some 80 to 90% higher. The use of half models can increase the Reynolds number by about 50% relative to that attained with a corresponding complete model.

4 AERODYNAMIC DESIGN OF THE DRA 5m TUNNEL

Since the design was initiated in the late 1960s, it was not able to benefit from the sophisticated CFD codes that exist today. Instead, an approach utilising a combination of the empirical design rules and analytical methods available at the time was taken. As two previous low-speed tunnels designed by the then RAE had suffered from significant flow problems during commissioning, it was decided to support the design decisions with tests on 1/15th scale models of individual parts of the circuit. Some of these individual models were also assembled to form a complete model of final design of the working section leg of the tunnel - running from the start of the rapid diffuser to downstream of the first corner. A bell-mouth entry to this model was designed to produce a uniform entry flow. Alternatively, a long pipe upstream of the rapid diffuser section could be used to produce a fully-developed turbulent pipe-flow at entry.

The design methods and assumptions appropriate to each part of the tunnel circuit will now be described in some detail, alongside a selection of experimental results from the model.

4.1 Design of the rapid diffuser

The rapid diffuser, located between the fourth corner and the cooler, was employed to minimise the size (and thus the cost) of the pressure shell whilst enabling an acceptable contraction ratio to be obtained ahead of the working section. An area ratio of 1.53:1 was selected to provide an appropriate balance between the rise in air pressure associated with its diffusion and the subsequent fall in pressure resulting from its passage through the cooler so as to ensure satisfactory flow within the diffuser. The rapid diffuser was also designed to provide the desired transition in cross-sectional shape from circular to octagonal.

The initial design used a simple straight-line generation and was totally unsuccessful in model tests, the flow separating completely on entering the diffuser and proceeding to the cooler virtually unretarded. The second design was based on a scheme for diffusers at the inlet to aerodynamic coolers suggested by Küchemann and Weber.¹⁰ The profile and wall pressure distribution of a so-called "streamline" diffuser are compared with those of a more conventional "sine-wave" design in Figure 9a. Note the smaller adverse pressure gradients on the walls of the streamline diffuser. The significance of this is illustrated in Figure 9b. A recent paper by Seltsam¹¹ shows similar behaviour and supports the general shape chosen for the diffuser.

A three-dimensional diffuser shape was derived on the basis of information similar to that presented in Figure 9a. The resulting design was as close as possible to the specified variation of cross-sectional area and wall shape, whilst still providing a smooth transition from circular section at inlet to octagonal at outlet. Both square and pipe-flow inlet velocity profiles were studied during model tests of this diffuser. The cooler was simulated using a 2q screen - see Figure 10. Pitot-static traverses were made at several stations inside and downstream of the diffuser, wall static pressures were measured and the surface flow was examined with tufts. These tests indicated that the diffuser performed acceptably. However, its walls were made entirely of double-curvature plates. Therefore, in deference to future manufacturing difficulties, it was decided to modify the design to include large areas of single-curvature and to increase the size of the fillets at the diffuser exit so that the maximum angle through which the flow was required to turn was reduced from about 50° to 30°.

The results for this third design were very similar to those of the second and showed a very even distribution of dynamic pressure (and total head) downstream of the cooler for pipe-flow at inlet - better in fact than for the case of square inlet flow. This data, a sample of which is presented in Figure 11, indicated that the flow in the working section would be within the specified uniformity. (Assuming that the velocity variations in the settling chamber downstream of the cooler remain quantitatively the same whilst the velocity increases through the contraction, the maximum permissible percentage variation in the settling chamber will be approximately C^2 times larger than that in the test section, where C is the contraction ratio. For a contraction ratio of 7.64 and an allowable dynamic pressure variation of $\pm 0.1\%$, the maximum variation in velocity in the settling chamber downstream of the cooler is approximately $\pm 6\%$.)

In order to reduce the manufacturing difficulties even more, the remaining areas of double-curvature were transformed into a series of single curvature sections by utilising the surfaces of truncated cones. The resulting geometry and developed surfaces are shown in Figure 12. At the same time, the height of the settling chamber was reduced by about 2ft to suit the maximum length of continuous cooler tube which could be supplied. The attendant flattening of the roof and floor of the diffuser is clearly visible in Figure 3.

4.2 Design of the settling chamber and screen positions

The settling chamber is 15ft long and contains two smoothing screens. Following the work of Bradshaw,¹² screens with a $1.5q$ pressure drop were selected in preference to the theoretically optimum value of $2q$. In the original layout, shown in Figure 13, the second screen was placed at the exit of the settling chamber (i.e. at the start of the contraction), with the first screen 6ft further upstream. This left 8ft between the downstream side of the 1ft-wide cooler and the first screen. The rapid diffuser described above was then tested in combination with this arrangement of smoothing screens, contraction, and working section; the cooler being represented by a $2q$ screen with the addition of a honeycomb. The results indicated a total head distribution in the working section which was 2% lower in the centre than at the sides. It was quickly realised that this "dishing" was caused by the proximity of the final smoothing screen to the contraction - the flow on the centre-line starts to accelerate before the flow near the walls. Therefore, tests were undertaken with additional lengths of settling chamber inserted downstream of the second screen.

Figure 14 shows that the settling chamber would need to have been extended by 12ft in order to produce a total head variation of $\pm 0.1\%$. For the reasons outlined below, this was not an acceptable solution for the real tunnel. However, by reducing the gap between the screens to 1ft and re-positioning the first screen, it seemed possible to increase the distance between the second screen and the contraction to 6ft. With this spacing, a second investigation was conducted in which the total pressure drop of the two screens was varied - producing the results shown in Figure 15. From this figure it is clear from the results at $\Delta q=0$ that the exit flow from the cooler had a total head distribution which was high in the centre. This was to be expected since the flow at the edges of the cooler had to turn through about 50° as it passed through the cooler into the settling chamber. Thus, the variation in the total head distribution entering the working section could be controlled by arranging the "dishing" from the screens to counteract the distribution imposed by the cooler. The results in Figure 15 show that the desired variation of $\pm 0.1\%$ could be achieved by reducing the total screen pressure drop from $3.0q$ to $2.4q$ and accepting the small consequent increase in the turbulence level. Later, further re-design increased the distance between the second screen and the contraction to 7.5ft and the total pressure drop across the screens was reduced to $2.2q$. The final configuration is compared with the initial one in Figure 13.

It is quite clear from the above that the quality of the flow in the working section is largely determined by the constraint on the length of the settling chamber. This was determined by an early

decision on the length of the working section leg of the tunnel, driven by the need to constrain the constructional costs. This experience therefore provides a cautionary tale for the design of future tunnels: the overall length of the tunnel should be sufficient to allow a settling chamber of adequate length. It also points to the importance of model tests, since it is unlikely, for the foreseeable future, that CFD methods will be capable of successfully balancing the total head variations coming from the cooler and the screens. Figure 26 demonstrates that the solution derived from the model tests has been successful in the real tunnel.

4.3 Design of the contraction shape

An axi-symmetric contraction was designed by the method described by Cohen and Ritchie¹³ to have a contraction ratio of 7.64. This was then transformed, by the method described below, into an octagonal section contraction with the required dimensions.

4.3.1 Axi-symmetric design

Cohen and Ritchie propose to solve the axi-symmetric incompressible irrotational flow equation

$$\frac{\partial^2 \psi}{\partial x^2} + \frac{\partial^2 \psi}{\partial r^2} - \frac{1}{r} \frac{\partial \psi}{\partial r} = 0 \quad (1)$$

for a specified axial velocity distribution on the centre line, and then to use any streamline of this flow as a candidate contraction shape. They note that the simplest solution to (1), representing a uniform cylindrical flow, is

$$\psi = 0.5 U r^2 \quad (2)$$

and suggest that this can be generalised to give:

$$\psi = \sum_1^{\infty} f_m(x) \cdot r^{2m} \quad (3)$$

If this relation is substituted in (1) and coefficients of r^{2m} are equated, the following recurrence relationship is obtained:

$$2m(2m+2) f_{m+1}(x) = -f_m''(x) \text{ for } m > 0 \quad (4)$$

Thus, a complete solution to (3) can be generated in terms of an arbitrary function $f_1(x)$ and its successive differentials of even order. The function $f_1(x)$, which prescribes the axial velocity distribution along the centreline, needs to satisfy the following criteria:

1. as $x \rightarrow +\infty$, $2 f_1(x) \rightarrow \text{Contraction ratio, } C$
2. as $x \rightarrow -\infty$, $2 f_1(x) \rightarrow 1$
3. as $x \rightarrow \pm \infty$, $f_1^{(n)}(x) \rightarrow 0$

Cohen and Ritchie suggest that a suitable function satisfying these requirements is:

$$(u)_{r=0} = 2 f_1(x) = A + b_1 \tanh(k_1 x) + b_2 \exp(-k_2 x^2) \quad (5)$$

Within this equation, the parameters "A" and "b₁" are not entirely independent as they are both linked to the contraction ratio, C, thus:

$$A = 0.5 (C + 1) \quad b_1 = 0.5 (C - 1) \quad (6)$$

The independent parameters are k_1 , k_2 and b_2 . These can be chosen to produce a suitable shape and acceptable pressure gradients on the walls. Cohen and Ritchie found the best values to be

$$k_1 = 0.707 \quad b_2 = 0.8 \quad k_2 = 0.3 \quad (7)$$

but they limited themselves to 5 terms in the series (3) and experienced convergence problems with the shorter contraction shapes - which of course was the main interest here. For this reason, a new computer program was written, using Hosenthien's method¹⁴ for the derivation of high order derivatives of "tanh(x)". This program was able to utilise up to 32 terms of the series, if necessary, to obtain convergence, and produced a solution for the radius of the contraction by iteration. It was run with 30 different combinations of values of the three independent parameters in the ranges given below:

$$0.9 > k_1 > 0.6 \quad 0.4 > b_2 > 0.15 \quad 0.8 > k_2 > -0.2$$

The non-dimensional length, L/D , of the contractions produced is plotted against k_1 in Figure 16. The parameters yielding the shortest contraction in this study were:

$$k_1 = 0.8 \quad b_2 = 0.4 \quad k_2 = 0.2 \quad (8)$$

Therefore, the contraction was generated from the initial function:

$$2f_1(x) = (C + 1)/2 + (C - 1)/2 \cdot \tanh(0.8x) + 0.4 \exp(-0.2x^2) \quad (9)$$

4.3.2 Octagonal section design

Although the axi-symmetrical design selected produced the shortest contraction this still had an equivalent length of just over 50ft whereas the required contraction length was a little under 44.5ft. Thus, a first transform was used to reduce the axi-symmetric contraction length by 11%. A linear transform was not used as this would have increased the adverse pressure gradients on the walls at the entrance and exit of the contraction. A cosine transform was therefore constructed which reduced the contraction length mostly over the centre region.

The transformation from the original streamwise ordinates, x_i , was defined as:

$$x = x_i - 0.5(50.014 - 44.83) \{ 1 - \cos(\pi \cdot x_i / 50.014) \} \quad (10)$$

A second transformation was then used to construct an octagonal section with an area equivalent to that of the axi-symmetric design, that is

$$A(x) = ab - 2c^2 \quad (11)$$

where $A(x)$ is the area of the axi-symmetric design; "a" is the width, "b" the height, and "c" the fillet side length of the octagonal section - see Table 1.

A linear relationship, using a dummy parameter "y", was constructed between a, b and c to satisfy the end conditions, i.e.

$$a(y) = a_0 + (a_1 - a_0)y \quad b(y) = b_0 + (b_1 - b_0)y \quad \text{and} \quad c(y) = c_0 + (c_1 - c_0)y \quad (12)$$

The area $B(y)$ is then given by:

$$B(y) = a(y) b(y) - 2 [c(y)]^2$$

We require $A(x) = B(y)$. Hence for a given $A(x)$ from the axi-symmetric design we have

$$\begin{aligned} A(x) &= a(y) b(y) - 2 [c(y)]^2 \\ &= [a_0 + (a_1 - a_0)y] [b_0 + (b_1 - b_0)y] - 2 [c_0 + (c_1 - c_0)y]^2 \end{aligned}$$

i.e. a quadratic equation for y . From the resulting solution, $a(y)$, $b(y)$ and $c(y)$ can be found using Equations (12).

The dimensions of the contraction so generated are listed in Table 1. Figure 17 compares the wall shapes of the octagonal, and circular axi-symmetric, contractions and Figure 18 gives the pressure distributions on the walls and a fillet. It may be seen that there were no adverse pressure gradients on the walls. In view of this it seems probable that an even shorter contraction with acceptable pressure gradients on the walls could be generated by a modern CFD-based design method using constrained optimisation.¹⁵

4.4 Design of the corner vanes

The design of the corner vanes in the 5m tunnel follows, almost exactly, that of the vanes used successfully in the DRA 8ft High Speed Tunnel, and supported by the investigations of Dimmock.¹⁶ Dimmock's results are sufficiently interesting to justify reviewing here. Viewed as an infinite cascade, it is difficult to imagine why the vanes should be spaced in any way other than equally. However, Dimmock's results (and a little thought) reveal that the finite extent of the cascade has a major effect on the flow through it. Figure 19 shows that it requires few vanes to produce turning with low loss on the outside of the corner, but that it requires considerably more vanes to achieve low-loss turning on the inside of the corner. The concept of turning vanes whose separation increases as an arithmetic progression from inside to outside is consistent with this observation.

Dimmock's results show that vanes of a parabolic camber shape have significant advantages over circular arc vanes. Despite this, experience with the 8ft tunnel indicated that circular arc vanes would give an acceptable flow uniformity and would be considerably easier to manufacture. Hence 90° circular-arc vanes with straight trailing-edges were chosen, set with the leading- and trailing-edges aligned with the axes of the tunnel. The final design is shown in Figure 20.

In order to perform a convincing test on the performance of the corner design, it is important to provide a representative inlet flow. It was found to be difficult to do this for an isolated corner, so the tests were done by attaching the corner to the outlet of the first diffuser on the model of the complete working section leg - rapid diffuser, settling chamber and screens, contraction, working section and first diffuser.

The measurements consisted of static pressures on the walls upstream and downstream of the corner, and total head rakes placed at the "inlet" and "exit" planes defined in Figure 20. The rakes also included static probes which, although not providing a detailed exploration of static pressure, did indicate sensibly constant static pressures across the measuring planes. The total head readings could thus be converted conveniently into velocities. More detailed measurements of total head were made downstream of the corner, towards the inside, with a small boundary layer probe. Although no measurements of the flow angles were made, brief explorations with a yaw-meter showed only small angles (<5°) relative to the axial direction and so the readings of the total head rakes can be considered as the maximum values.

Figure 21 compares the velocity contours at the inlet with those recorded at the exit plane. These show two main features. Firstly there is a noticeable re-distribution of velocity downstream of the corner. Secondly the worst velocity distribution occurs between $\pm 45^\circ$ from the inside - reflecting both the difficulty of guiding the flow round the inside of the corner noted previously, but also the inelegant junctions between the vanes and the elliptic corner ring. Even here, though, there is not the loss in total head which others⁽¹⁴⁾ have found. It is possible that secondary flows occurring near the ends of the vanes are responsible for this re-energisation of the flow.

4.5 Design of the main drive, fan and pre-rotation vanes

The balancing arguments between a fixed pitch, variable speed fan, and a variable pitch, constant-speed fan are set out in Section 5.3. For the 5m tunnel, its designers came to the opposite conclusion to those at ONERA, and the 5m tunnel has a fixed pitch fan. The speed control is achieved by:

- a) an a.c. motor controlled by a liquid rheostat,
- b) a d.c. motor for fine control, which can add to or subtract from the power of the a.c. motor.

The power requirements and capabilities are set out in Figure 22.

The fan and pre-rotation vanes were designed according to the method described by Mair.¹⁸ In this method, the fan and the pre- and post-rotation vanes are treated as infinite cascades so that the effects of trailing vorticity are ignored. Simple relations based on assumptions of uniform velocity and total pressure rise through the fan are used to obtain preliminary estimates of the number of fan blades and their chord. For the 5m tunnel, the following additional constraints were imposed:

1. the tunnel power factor with a high drag model was assumed to be $\lambda = 0.42$
2. there was to be no increase of area (i.e. no diffusion) between the 2nd corner and the fan
3. the drive motor was to be inside the nacelle, thus fixing a minimum diameter for the nacelle
4. the maximum tip Mach number was to be $M = 0.50$; since the outer diameter was fixed by (2) & (3), the maximum fan speed was determined by this condition.

These preliminary assessments led to a fan design having:

Nacelle diameter	= 6.2m	Fan blade chord	= 0.924m
Fan diameter	= 10.06 m	No. of blades	= 10
Mach no. through fan	= 0.14	Max. fan speed	= 306 rpm
Design power factor	= 0.408		

Central to the method for the more detailed fan design is the "rotational interference factor", a , such that the angular velocity of the air at radius r is ωa at the fan (where ω is the rotational speed of the fan), and $2\omega a$ far downstream. The design condition for the pre-rotation vanes is then that they introduce an angular velocity to the air of $2\omega a$, in the opposite direction to that of the fan rotation, so that the velocity far downstream is axial. It then follows that the velocity of the air relative to the fan blades is :

$$W^2 = u^2 + \omega^2 r^2 (1 + a)^2 \text{ where } u = \text{axial velocity of air approaching the fan}$$

and it can then be shown that the increase in total head through the fan is given by:

$$\Delta H(r) = 2\rho\omega^2 r^2 a$$

Model tests showed that static pressure was uniform across the plane just prior to the fan, but that the axial velocity (and therefore the total head) varied approximately as shown in Figure 23. Values of a were then calculated as a function of r so that total head was constant at the fan exit. These were then used in the design of the fan and the pre-rotation vanes - as indicated above - so that the designs were consistent with each other.

Following this, a more detailed design was carried out using more realistic assumptions about the axial and circumferential velocities through the fan, and introducing the real lift and drag characteristics of the aerofoils used for the pre-rotation vanes and the fan blades. However, this detailed design process involved a degree of iteration and intuition: it is not appropriate to give a more detailed description of the method here - Mair's report¹⁸ should be consulted. However, to show the kind of variations that are likely to be encountered in future designs, the initial and final values of some of the key fan parameters are given in Table 2.

Despite this detailed design process, it was found during tests on a model of the pre-rotation vanes that:

- (a) there were significant areas of separated flow over the vanes;
- (b) the required distribution of the angle of flow downstream was not achieved; and
- (c) the fan would experience large variations of velocity as it rotated.

As a result it was decided to reduce the lift coefficient of sections towards the nacelle which exhibited regions of separated flow towards their trailing edges. Also the number of vanes was increased from 11 to 21 in order to even out the velocity variations between the vanes. The magnitude of this increase in the number of pre-rotation vanes was also selected to minimise the likelihood of fan-blade passing frequency resonance problems being encountered: 21 is one more than twice the number of fan blades (as opposed to 11, which is one more than the number of fan blades). These vanes were tested in a similar manner to the previous design and no areas of separated flow were detected. Also the circumferential variations of velocity were found to be very much smaller than previously.

4.6 Design of the nacelle and the outer passage

The design of a nacelle shape within an exterior duct severely taxed the capabilities of the designers in the late 1960s, and they went through six design iterations before a suitable pair of shapes was found. This was because they clearly wished to avoid significant adverse pressure gradients on either the nacelle or the outer passage wall and also because modifications to the geometry of one imposed significant changes in the pressure distribution on both. The initial nacelle design consisted of an elliptical nose and a straight portion followed by a parabolic tail. The diameter of the nacelle was determined by the diameter of the main drive motor which was to be housed in the nacelle. For this, a set of possible outer passage shapes was generated by directing a high-pressure water-jet at a model of the nacelle and measuring the shape of the outer, constant-pressure boundary of the perturbed jet: the length of pipe through which this jet passed before emerging was altered until the correct total head profile was obtained in the jet; the jet was aimed at both the nose and tail in order to get suitable outer profiles over the complete nacelle; the jet shapes were photographed with and without the nacelle model immersed in the jet; the resulting pictures were digitised and differences obtained. Having obtained this data, a 1/15th scale model of the nacelle and passage was made and equipped with pressure-plotting.

The pressure plotting data showed a suction peak and severe adverse pressure gradient on the nacelle where the elliptic nose joined the parallel section. It was not possible to relieve these by manipulating the shape of the outer passage without imposing unsuitable pressure gradients on the outer passage.

As a result, the nose shape of the nacelle was made more blunt and the curvature change near the maximum diameter was reduced. A new outer passage shape was also derived. Figure 24 shows the pressure distribution on the nacelle and outer passage for the final design. Whilst this is acceptable, there is little doubt that a better design could be achieved more rapidly with modern CFD-based design methods.

4.7 Other design aspects involving aerodynamics

The design of the cooler and the stressing of the pressure shell depend not only on the heat input from the power expended in the motor, but also to a significant extent on that input from the surrounding air and solar radiation. The area of tunnel surface exposed to solar radiation was estimated by photographing a model of the tunnel from a set of typical sun elevations and measuring the area of the tunnel shown on each photograph. These were then combined with estimated inputs from the surrounding air/wind and from the power input from the motor to give:-

- a) estimates of the heat load to be removed by the cooler and
- b) estimates of the longitudinal and circumferential temperature distributions for stress analysis.

Over-pressure in the working section due to an emergency shutdown of the fan is a design case for the breather slots at the aft end of the working section. The build-up in pressure is influenced by the volume into which the air is discharged through the breather slots - in this case the volume of the inner sphere. This volume is sufficient for the over-pressure to be accommodated without needing special strengthening of the working section walls.

A massive rupture of the pressure shell would cause significant damage to surrounding buildings purely due to the blast wave produced. However, there is also the probability of damage due to flying debris from pieces of the ruptured pressure shell. Estimates suggested that the maximum range of 30cm diameter pieces of pressure shell, 3cm thick, was in the region of 400m. As can be imagined, this raised some interesting obstacles that had to be negotiated during commissioning.

4.8 Aerodynamic performance of the tunnel

The final design, from the rapid diffuser through to the first corner, was implemented on the 1/15th scale model tunnel and the working section flow explored. The resulting velocity and total head variations are shown in Figure 25. On this basis the design was approved as meeting the requirements.

For the actual tunnel, a typical distribution of dynamic pressure in a cross-section of the working section at the centre of rotation of a model is shown in Figure 26. These results indicate that throughout a rectangular vertical plane of approximately 3.2m×2.0m, encompassing the central portion of the test section, the dynamic pressure varies from -0.16% to 0.06% of the value at the centreline, i.e. the variation is within $\pm 0.1\%$ of the mean value. The streamwise variations in dynamic pressure lie within similar bounds throughout the tunnel's operating envelope. The pitch of the mean flow, as judged by the integrated effect on a 1/13th scale model of an Airbus A300 sting-mounted upright and inverted on the tunnel centreline, is also very low. Routinely checked at the same time as the twice-yearly velocity calibrations, typical values of the resulting pitch correction are shown below.

REYNOLDS NUMBER	PITCH CORRECTION
6.45×10^6	-0.004°
5.00×10^6	-0.002°
2.35×10^6	-0.003°

Measurements of the turbulence have been made using a DISA miniature 'X'-probe hot wire. The results for longitudinal and lateral turbulence are shown in Figure 27. These exhibit the roughly 2:1 ratio between lateral and longitudinal turbulence that is characteristic of many tunnels and demonstrate that the desired levels have been achieved. The figure also shows that the turbulence intensity is essentially independent of Mach number at a given Reynolds number and that it varies only very mildly with Reynolds number. Thus, tests in this tunnel should be free of any spurious scale and Mach number effects arising from changes in flow quality with increasing pressurisation. The variation of turbulence intensity across the working section in Figure 28 still shows some evidence of the problems with the flow through the cooler but the average intensity is essentially constant across the span of a typical model.

Perspectives on the repeatability of the test data are presented in Figures 29 and 30. Figure 29 shows the typical repeatability of the velocity calibration, indicating an uncertainty in the region of $\pm 0.15\%$. Figure 30 shows that the repeatability between tests on the mechanical balance is better than 0.008 on the lift coefficient, C_L .

5 GENERAL DESIGN OF THE ONERA F1 TUNNEL

The general drawing of Figure 31 shows the main parts of the F1 facility.^{7,19} The air circuit is adjacent to the main building, a 300m^3 reservoir for pressurisation of the tunnel, the fan drive and the atmospheric cooling towers. Two other buildings house the compressors and the high pressure reservoir.

The pressure shell is mostly made of pre-stressed concrete, with the exception of the cart constituting part of the test section, the fan envelope and the two conical bulkheads supporting the gate valves on each side of the test section. The concrete also acts as the aerodynamic surface, except for the contraction, the test section, half of the first diffuser and some liners which cover space devoted to the (external) mechanical fixations of elements in the flow, such as honeycomb, screens, the cooler and corner vanes.

5.1 The tunnel circuit

The aerodynamic circuit is of conventional closed-return design, with 72m and 18m between the axes and the four right-angled corners. Perpendicular to these axes, the cross-sections are circular, linked to the rectangular test section by the contraction and the upwind part of the first diffuser, where shape transformations occur.

The first diffuser has a mean total angle of 5° , with a maximum of 6° in the vertical plane at the test section outlet due to the width of test section (4.5m) being larger than its height (3.5m). The surface is made up of four triangles and four quarters of a cone in the upstream metallic part and a truncated cone in the downstream concrete part. Corners 1 and 2 are of the same size, so that the first cross-leg is cylindrical; it has a catchnet for fan protection and contains the air inlet for pressurisation. The variable pitch fan is located after the second corner. A small contraction takes place between the end of Corner 2 and the plane of the fan in order to reduce flow distortion.

The second diffuser is conical with a total angle of 6.1° . The cooler uses the same type of elliptical finned tubes as the DRA 5m, but with 3 rows. It is located between the end of the diffuser and Corner 3. It provides losses at the end of the diffuser and gives a distance before the settling chamber large enough for a primary reduction of the turbulence generated by the tubes.

The cross-section is constant through Corner 3, Corner 4 and the settling chamber, which is equipped with a honeycomb and three fine screens. The shape of the channel is transformed from circular to rectangular within the contraction. For simplicity of construction, this is made of single curvature surfaces - one cone and four cylinders, as shown in Figure 32. The contraction ratio was limited to 7.2 owing to cost constraints.

5.2 Pre-stressed concrete shell

At the end of the first studies to provide an estimate of the tunnel cost, it was suggested that pre-stressed concrete should be considered as a material for the pressure shell. Experience was already available in France from the design of confinement enclosures for nuclear power plants. This kind of construction for the wind tunnel shell appeared to be much more economic than steel construction. The air tightness was sufficient not to require any metallic membrane inside the concrete and the casting process of developable surfaces in plywood moulds was able to give the shape within the required accuracy. Obviously, many steel parts had to be matched with the concrete to get a closed surface, including the fan envelope, the bulkheads and all the access holes for people, the fan shaft, pipes, wires and various internal features to be incorporated during construction.

The concrete structure, called "the tube", is a ring, the pressure end effects at the fan and the gatevalves being transmitted by horizontal beams. After the first calculations to choose the main dimensions, a finite element code was used to check the stresses and deformations under pre-stressing loads, pressure and thermal loads, for which the structure is statically indeterminate. With 320 iso-parametric volume elements and 2320 nodes, it reached the limits of one of the largest computers available in 1974. "Pre-stressing" is done in fact after the curing of the concrete, but before removal of the scaffolding supporting the formwork and the weight of concrete during construction, Figure 33, by putting under tension two sets of longitudinal and transverse cables (Figures 34 and 35). For gravity loads, the system is designed to be nearly statically determinate. Vertically, the 11000-ton structure is supported on 4000 tons of foundation. The foundations consist of three main blocks (under the working section, the Corner 2/drive area and the cooler/Corner 3 area) and four secondary blocks (under Corner 1, Corner 4 and the two diffusers). The main blocks carry most of the weight and apply a 2bar pressure on the ground. The pressure under the secondary blocks is twice this value to ensure that they follow any sinking of the main blocks. When the weight of the shell was first applied to the foundations (on removing the scaffolding), the secondary blocks sunk a little more than the main blocks. However, at Corner 1 and under the second diffuser, the secondary blocks are completed by elastic supports which are designed to supply a constant support load. This load is checked periodically with a hydraulic jack. Horizontally, "the tube" is fixed to the ground under the test section and guided under the first diffuser; everywhere else it is free to move on rubber supports.

The horizontal displacements between the tube and foundations associated with temperature, pressure and time have been measured. The separate effects are shown in Figure 36: in more than 20 years, the mean shrinkage due to the action of concrete creep under the pre-stressing loads is $300\mu\text{m/m}$ and the test leg axis has stayed straight within 2mm on 72m. Aerodynamically speaking, these deformations are negligible, the waviness is inside the tolerances and the surface is aerodynamically smooth. A thin epoxy coating, finished with paint, was used to get a good surface finish, and keep the airflow free of dust.

5.3 Drive

During the design, some major fan manufacturers were consulted. They offered either a fan with fixed blades and variable speed d.c. motor, or variable pitch blades with constant speed a.c. motor. The final choice was in favour of the latter system because:

- the speed is higher at maximum pressure, the limit of the domain being defined by :-
 $\rho V^3 \sim \text{constant}$ (proportional to maximum power) for a constant speed fan,
 $\rho V^2 \sim \text{constant}$ (proportional to maximum torque) for a variable speed fan.
- the response time of the blade pitch actuator is fast for control purposes, with the capability of a full stroke in 30s.

These arguments were balanced against:

- a lower efficiency at low air speed, and
- a less uniform speed profile at the entrance of the diffuser.

The residual rotation behind the fan was measured by the manufacturer on a model, and considered as small enough to be cancelled by the cooler and the honeycomb.

The drive system is shown on Figure 37. The 9500kW/1500r.p.m. a.c. motor is fed under 5.5kV from the 63kV grid through a transformer which limits the starting current to an acceptable value. This direct start lasts around 30 seconds. The motor, the gear reducing the speed and the bearing with rotating seal are located on a platform horizontally linked to the concrete shell and resting on the same foundation block as the fan, with the same kind of supports for horizontal displacements. The mass of concrete acts as a horizontal foundation for the fan structure, with no fixed points on the ground. The shaft goes through a short cylinder (not shown) delimiting a passage in the vanes of Corner 2.

The fan has 14 straight vanes holding the bearing of the overhung wheel, with 16 cambered and twisted blades, 1.8m long with a chord varying from 0.89m to 0.6m. Variations of camber, twist and chord were calculated to give a constant circulation across the span at the design point. A 17-blade straightener is located behind the wheel. The main dimensions (outer diameter 7.4m, inner diameter 3.8m) and speed (360r.p.m., producing a tip speed of 140m/s) were chosen from an existing family of fans with operating diagrams (pressure rise vs. flow rate) known from measurement on models or actual fans. The final selection was done by matching these diagrams with the operating points defined for the tunnel: 120m/s at 1bar, 70m/s at 4bar, with a loss factor, λ , for the tunnel with model equal to 0.49. (λ is defined as the ratio of the pressure rise at the fan, Δp , to the dynamic pressure in the test section, q .) This value is the sum of $\lambda = 0.42$ for the empty tunnel and $\lambda = 0.07$ for a large model at high incidence. The former value was defined from estimates of different sources, including tests performed on a small pressurised tunnel at CEAT (Centre d'Essais Aéronautiques de Toulouse). These tests gave an estimate of the reduction of losses with increasing pressure, but this was kept as a safety margin.

Fortunately the losses, measured by rakes of Pitot probes in front of the wheel and at the rear of the downwind fairing, were smaller than forecast. For instance, the maximum value of λ for the empty test section was 0.33 (leaving a minimum margin of $\lambda = 0.16$) - see Figure 38. For the commissioning of the fan, it was necessary to add some losses to the empty tunnel. This was done initially using a parachute mounted in the first diffuser, then by a disk of 1m diameter bolted on the quadrant perpendicularly to the wind. The margin was used for tests on models larger or at a higher incidences than forecast during the project (for example, a model of Rafale induced a $\Delta\lambda = 0.11$), and for an

extension of the domain of the tunnel, tested in 1979 after the first year of operation. Now one can reach 79m/s ($M = 0.232$) at 3.85bar, and 1.57bar at $M = 0.36$, as shown on Figure 8.

There were in fact two designs for the fan blades. For the first, the manufacturer had chosen to extrapolate his usual design of cast aluminium, with cambered profiles having a relative thickness of 13% at the root but only 2% at the tip, in order to limit the centrifugal loads. During a commissioning test in November 1976, the blades suddenly broke at 1.6bar and 20m/s. A thorough analysis was undertaken, involving the manufacturer and nearly all the departments of ONERA. The conclusions were that the failure was probably induced by the combination of several factors. The material had an acceptable ultimate strength under normal circumstances, but this had been lowered by the casting of pieces longer and thinner than usual. At low speed, the outer sections of the fan work at negative incidences and the thin profile had a strong stall, inducing high fluctuating loads. Also a harmonic of the rotation speed was not very far from a vibration mode of the wheel + blades system, in which the blades participated strongly, leading to additional vibrations and stresses.

It was then decided to build a new set of blades, made of steel, with a skin welded on a frame consisting of a longitudinal spar and transversal ribs. The thickness was increased to 16% at the root, and 12% at the tip. Several finite element calculations, confirmed by vibration tests on the blades alone, then on the complete fan at rest, predicted a better vibrational behaviour. The tests resumed in 1977 with careful monitoring of vibrations on the bearings and on the blades, one of which was equipped with strain gauges. In 1984, a spare set of blades was purchased which embodied some minor modifications deduced from the experience of SIMA wind tunnel at Modane test centre and some more refined finite element calculations.

Tests with varying pressure produced some insight into the aerodynamic loads on the blades. For example, the moment on the blades was deduced from the pressures measured in the axial hydraulic jack, carried by the wheel, which is used to set the pitch of the blades with an accuracy and stability of 2.5×10^{-4} of the range. At 1bar, the aerodynamic moment is small in comparison with the mechanical moment due to centrifugal forces. However, at 4bar, this is no longer the case and the original counterweights were not heavy enough to balance the moments: their weight was increased after the first test at 4bar.

5.4 Access to the test section and exchange of models

The main objectives of the concept were high productivity and confidentiality. It is necessary to have quick access to the test section for changes to models where many surfaces which move on the aircraft, such as slats and flaps, cannot have actuators to move them on the model. The large size of the tunnel produces times for pressurisation and de-pressurisation measured in hours - these are not acceptable for high productivity. It was decided to isolate the test section from the rest of the tunnel by two cylindrical gate valves ("the doors"), running through the beginning and the end of the test section. When they are closed, they rest on conical bulkheads. When opened, the continuity of the walls through the rectangular openings of the doors is provided by fixed wooden plates. The gaps remaining between these plates, the fixed walls and the inflatable joints required to avoid air recirculation through the plenum, were designed to have small dimensions (a few millimetres for depth and width): they do not disturb the flow. The use of fixed wooden plates in this way replaces the need for moving flaps. This feature of the design required precise machining of large components, and careful mounting and hand-fitting of the wooden plates, all of which was achieved within tight tolerances.

For model exchange, the system was designed to allow the complete preparation of a test before entering the test section and to ensure confidentiality of the tests. The system consists of a cylindrical cart, four interchangeable pallets and five closed preparation cells with protected access in the

building. The cart carries the three fixed walls forming the upper part of the test section. The bottom wall is a structural part of a pallet. The cart can move on rails perpendicular to the wind axis. In the test position, the cart is locked on a concrete beam of the circuit and sealed to the flanges of the bulkheads by inflatable joints. When the cart is in front of a preparation cell, the pallet can be transferred as shown in Figure 39. Each pallet has a different model support and a complete data acquisition unit, which allows runs for one test to be performed simultaneously with the preparation for three others. In practice, this system allows up to ten runs per day to be made at maximum pressure with manual change on the model between each run, and to change over from one test to the other in less than half a day.

6 SOME AERODYNAMIC DETAILS OF THE ONERA F1 TUNNEL

6.1 Test leg

After the contraction shown in Figure 32, the working section walls are flat plates, 11m long. The top and side walls are made of laminated wood with a plastic coating so that new windows can be easily installed when necessary. The walls are supported by the cart shell and a steel frame, with the capability to vary the divergence of the side walls. Pressure equilibrium is ensured by slots at the end of the working section. The divergence was initially set from boundary layer calculations and later slightly corrected to produce zero static pressure gradient down the working section. Figure 40 shows the static pressure distribution measured by an axial probe along the working section centre line; this does not vary with pressure. Figure 41 shows that the values of noise and turbulence in the F1 tunnel are slightly influenced by Mach number but, in common with the 5m tunnel, are unaffected by pressure. These measurements were made by Bruel & Kjaer microphones and hot wires.

Figure 42 presents the values of transition Reynolds number obtained in the F1 tunnel on a 10° cone, 1.40m long, mounted on the quadrant in the middle of the working section. Transition was detected by several means, all of which produced closely similar results:

- a) the longitudinal variation of surface temperature detected by an infra-red camera
- b) the increase in the r.m.s. value of the voltage on a hot-film produced by the increase in local velocity that occurs as the transition front crosses the film
- c) the sublimation of acenaphthene

The transition Reynolds number is seen to be essentially independent of the tunnel pressure.

Typical values of boundary layer thickness on the walls are 80mm at the start of the working section and 100mm in the middle. These values decrease slightly with increasing Reynolds number. After the working section there is a further increase in the first diffuser. Figure 43 gives the Mach number profiles at the end of the working section, at the joint between the metallic and concrete parts, and in front of Corner 1. The total head loss associated with the wall boundary layers is about 1/3rd of the total losses in the tunnel.

6.2 Corner vanes

A study of two-dimensional cascades was performed in 1971-72 by the Aerodynamic Department of ONERA, in order to determine profiles with specific constraints:-

- a) turning angle of 90°
- b) limitation of peak suction
- c) small gradients to avoid flow separation
- d) low losses

A computer version of the “hodograph” method of Legendre²⁰ was used to give the shape of the section and the pitch of the cascade corresponding to the input parameters:-

- a) Mach number at the entry to the cascade
- b) angle of the velocity vector to the plane of the cascade
- c) the required turning angle

The parameters of the conformal transformation in the method were varied in order to achieve the desired characteristics.

The pressure distributions produced were used in boundary layer calculations (laminar and turbulent) with the available criteria for transition and separation. The method gave “thick profiles”, as shown in Figure 44, with a chord/pitch ratio near 2, varying slightly with Reynolds number. These profiles have been used in F1 for Corners 1 & 2, and later in other ONERA wind tunnels. The large bending stiffness provided by the thickness avoided the need for any splitter plates to support the vanes. Some limited measurements made during commissioning are shown in Figure 45. Although not very accurate they do provide some confirmation of the study. For Corners 3 & 4, thin profiles were used for economic reasons. Initially these showed large amplitudes of vibration at the leading-edge necessitating reinforcement by steel sheet which also allowed the nose radius to be increased.

6.3 Second diffuser and cooler

The cooler is an assembly of rectangular bundles of various lengths and widths. It has an outside diameter of 13.6m, for a useful diameter of 12m. It is fitted in an annular groove in the concrete shell, with a liner downwind, but nothing upwind: a vortex flow develops in the cavity, which contributes to flow attachment at the end of the second diffuser. This groove is also a very good collector of dust after maintenance works in the circuit. The fairing of the water pipes, along the horizontal diameter, provided a support for Pitot tubes for total pressure measurement.

Pressure distributions in front of the cooler and behind it at the entrance to Corner 4, are plotted in Figure 46, showing the effect of the total head losses through the cooler. The water connections to the tubes in the cooler are such that water is admitted along the horizontal diameter of the tunnel. It is then dispersed vertically, upwards and downwards, to the outer edge of the section in half of the tubes and returned to the horizontal diameter in the other half, before being transported out of the tunnel. The mean temperature of the tubes is virtually constant, providing a temperature in the test section that is uniform within $\pm 0.5K$.

7 AERODYNAMIC RESULTS ON AIRCRAFT MODELS

As the purpose of these tunnels was to provide high Reynolds numbers, it is worthwhile to show that their design met the objectives by a brief presentation of results obtained in both tunnels.

In 1919, Gustave Eiffel²¹ wrote “it seemed to me that one cannot always extend to flight speeds the conclusions of a test at low speed”. At that time, he had already tried to build a tunnel of sufficient size and speed, knowing experimentally from tests on spheres the risks of extrapolation. A confirmation of his statement is given by the studies of maximum lift coefficient vs. Mach and Reynolds number given in Figure 47 for an Airbus A300 model (scale 1/16th) in the ONERA F1 tunnel and in Figure 48 for a BAe Hawk (scale 0.3) in the DRA 5m. tunnel. These examples show that increasing Reynolds number with Mach number held constant, leads to an increase in maximum lift, whereas increasing Mach number at constant Reynolds number gives the opposite result. Moreover the effects are non linear. These results demonstrate the impossibility of the transposition

to flight scale of measurements from a model in an atmospheric tunnel, where Reynolds number variation is concomitant with Mach number variation.

Many tests have been performed in the ONERA F1 tunnel on air intakes. A special support allows angles of attack from 0° to 90° .²² The internal flow is driven by the pressure difference between tunnel and atmosphere. Mass flow is measured in the exhaust pipe and, even at its maximum value of 75kg/s, the test duration is short enough so that total pressure variation is negligible. First tests on a 1/6th scale model exhibited an almost linear variation, with Reynolds number, of the angle of the flow separation which occurs at high incidence on the leeward lip of the intake (Figure 49). With a 1/3rd scale model, it appeared that, at high Reynolds number, a constant angle was reached, equal to the one in flight.

The research programme in the DRA 5m tunnel has been concerned over many years with identifying situations where unexpected scale effects can occur. Several mechanisms which can result in the reduction of maximum lift with increasing Reynolds number have been identified by Woodward et al.,²³ and feature strongly in a recent AGARDograph.²⁴ Another aspect of these studies is the scale effect on the lateral characteristics of aircraft - on which there is very little published data. This is surprising since Peckham and Woodward²⁵ found large effects on the rolling moment due to sideslip of a 53° sweep canard-delta (Figure 50), which could produce a very dangerous situation if the aileron power were to be determined on the basis of low Reynolds number tests.

Last but not least, a proof of the overall quality of tests in both tunnels is given by the comparison of results in the two tunnels of the same model of an Airbus A300, mounted on an identical three-strut support. This comparison²⁶ was performed within a framework of the Anglo-French Aeronautical Research Program (AFARP) at the request of Airbus Industrie. Initial comparisons had shown discrepancies on the lift coefficient (Figure 51). This led to a considerable effort from the teams of the two organisations to improve the correction methods applied for flow distortion due to wall and strut effects. The comparison of the finally corrected data (Figure 52) demonstrates that this effort was worthwhile.

8 CONCLUDING REMARKS

This paper has described the aerodynamic and structural design of two pressurised low-speed tunnels designed to address the same aerodynamic problems and to meet similar technical specifications. In spite of this, it is clear that the two tunnels differ significantly in their detailed design - quite different choices having been made for:

- a) construction material
- b) method of rapid access to the model when the tunnel is pressurised
- c) main drive and fan design
- d) maximum pressure and working section size
- e) working section layout
- f) contraction design
- g) diffuser angles
- h) corner vane design

Although these tunnels were designed 25 years ago, when CFD methods were unable to make any significant contribution to the design processes, the empirical and experimental methods used instead have produced a good quality flow in each. Furthermore, the design concepts used still have relevance today and have been employed to improve the performance of older facilities.^{27,28}

Both tunnels have made significant contributions to the low-speed performance and handling of most of the modern civil transport aircraft from both sides of the Atlantic, and will continue to be an indispensable part of the spectrum of test facilities available to designers of subsonic and supersonic²⁹ aircraft - both civil and military - for the foreseeable future.

9 REFERENCES

- 1 Isaacs, D., "Wind tunnel measurements of the low speed stalling characteristics of a model of the Hawker-Siddeley Trident 1C", RAE TR 68108, May 1968.
- 2 "The need for large wind tunnels in Europe", Report of the AGARD FDP LaWS Working Group, AGARD-AR-60, December 1972.
- 3 "A review of current research aimed at the design and operation of large wind tunnels", Report of the AGARD FDP MiniLaWS Working Group, AGARD-AR-68.
- 4 Margoulis, W., "Nouvelle méthode d'essai de modèles en souffleries aérodynamiques", *Comptesrendus Acad Sci 171*, p997, 1920.
- 5 Smelt, R., "Power economy in high-speed wind tunnels by choice of working fluid and temperature", RAE Rep Aero 2081, August 1945.
- 6 Goodyer, M.J. and Kilgore, R.A., "High-Reynolds-number cryogenic wind tunnel", *AIAA Journal*, vol.11, pp613-619, May 1973.
- 7 Pierre, M., "Soufflerie subsonique pressurisée F1 du centre du Fauga-Mauzac de l'ONERA", Paper presented at the 11th ICAS Congress, Lisbon, September 1978.
(Also ONERA TP 1978-51.)
- 8 Pankhurst, R.C. and Holder, D.W., "Wind-tunnel technique: an account of experimental methods in low- and high-speed tunnels", Pitman and Sons, London, 1952.
- 9 "Araldite fan blades for RAE wind tunnel", CIBA-GEIGY Technical Note 1/1976.
- 10 Küchemann, D. and Weber, J.A., "Aerodynamics of propulsion", pp274-276, McGraw-Hill, 1953.
- 11 Seltsam, M.M., "Experimental and theoretical study of wide-angle diffuser flow with screens", *AIAA Journal*, vol.33, pp2092-2100, November 1995.
- 12 Bradshaw, P., "The effect of wind tunnel screens on 'two-dimensional' boundary layers" NPL Aero Rpt 1085, 1963.
- 13 Cohen, M.J. and Ritchie, N.J.B., "Low-speed three-dimensional contraction design", *Journ. Roy. Aero. Soc.*, vol.66, pp231-236, April 1962.
- 14 Hosenthien, H.H., "Development of a general formula expanding the higher-order derivatives of the function 'tanh z' in powers of 'tanh z' and 'A' numbers", NASA TN D-4296, 1968.
- 15 Doherty, J.J. and Lovell, D.A., "Aerodynamic design of aerofoils and wings using a constrained optimisation method", ICAS Paper 94.2.1.2, Anaheim, September 1994.

- 16 Dimmock, N.A., "The development of a simply-constructed cascade corner for circular cross-section ducts", NGTE Memo 78, 1950.
- 17 McHarg, J.J., "Air tests on a 12 inch cascade bend", NEL Report 243, August 1966.
- 18 Mair, W.A., "The design of fans and guide vanes for high-speed wind tunnels", British ARC R&M 2435, June 1944.
- 19 Carrara, J.M. and Masson, A., "Trois ans d'exploitation de la soufflerie subsonique pressurisée F1 de l'ONERA", L'Aéronautique et l'Astronautique, No.89 (1981-4), pp75-93. Also ONERA TP 1981-105.
- 20 Legendre, R., "Tracé des Ailettes pour fluide à densité légèrement variable", ATMA 1947.
- 21 Eiffel, G., "Nouvelles recherches sur la résistance de l'air et l'aviation", Librairie Aéronautique E. Chiron, Paris, 1919.
- 22 Christophe, J., "Progrès et problèmes des grands moyens d'essais aérodynamiques", Revue Française de Mécanique No.1988-2, pp25-38. Also ONERA TP 1990-1.
- 23 Woodward, D.S., Hardy, B.C. and Ashill, P.R., "Some types of scale effect in low-speed, high-lift, flows", Paper 4.9.3, Proceedings ICAS 88, 1988.
- 24 Haines, A.B., "Scale effect on aircraft and weapon aerodynamics", AGARDograph 323, July 1994.
- 25 Peckham, D.H. and Woodward, D.S., "The importance of high Reynolds number in low-speed wind tunnel tests of canard-delta combat aircraft", RAE TM Aero 2095, February 1987.
- 26 Quémard, C. and Earnshaw, B., "Comparison of the results of tests on A300 aircraft in the RAE 5 meters and the ONERA F1 wind tunnels", Paper 3 in AGARD-CP-429 (Aerodynamic data accuracy and quality: requirements and capabilities in wind tunnel testing, Naples 12-15 October 1987). Also ONERA TP 1987-158.
- 27 Herron, R.D., Stich, P.B., Price, E.A. and Whorric, J.M., "Further improvements in cost effectiveness of wind tunnel testing at PWT", AIAA Paper 96-2258, June 1996.
- 28 Muhlstein, L., Bader, J. and Holmberg, J., "Recent productivity improvements in wind tunnel testing at Ames Research Center", AIAA Paper 96-2259, June 1996.
- 29 Armand, C., Quémard, C. and Fournier, G., "Main ONERA wind tunnels for the success of the future supersonic transport aircraft", Proceedings of the 7th European Aerospace Conference, Toulouse (France), October 25-27, 1994. Also ONERA TP 1994-163.

Distance upstream from working section x/a_0	width a/a_0	height b/a_0	fillet C/a_0
0.00000	1.00000	0.84004	0.12003
0.12560	1.00273	0.84211	0.12063
0.24833	1.00687	0.84525	0.12154
0.36828	1.01510	0.85149	0.12335
0.48557	1.02733	0.86076	0.12604
0.60035	1.04790	0.87637	0.13057
0.71285	1.07936	0.90023	0.13748
0.70139	1.12591	0.93553	0.14773
0.93201	1.19594	0.98864	0.16314
1.03927	1.29485	1.06365	0.18489
1.14542	1.43372	1.16897	0.21544
1.25083	1.62393	1.31323	0.25729
1.35586	1.86000	1.49226	0.30922
1.46089	2.10600	1.67883	0.36334
1.56630	2.31204	1.83509	0.40866
1.67245	2.46848	1.95373	0.44308
1.77971	2.59028	2.04611	0.46987
1.88841	2.68855	2.12063	0.49149
1.99887	2.76754	2.18054	0.50887
2.11136	2.82980	2.22776	0.52256
2.22615	2.87413	2.26137	0.53231
2.34344	2.90460	2.28448	0.53902
2.46338	2.92400	2.29919	0.54328
2.58612	2.93400	2.30660	0.54543
2.71172	2.93929	2.31079	0.54665

a_0 , width at end of contraction = 16.40399 ft

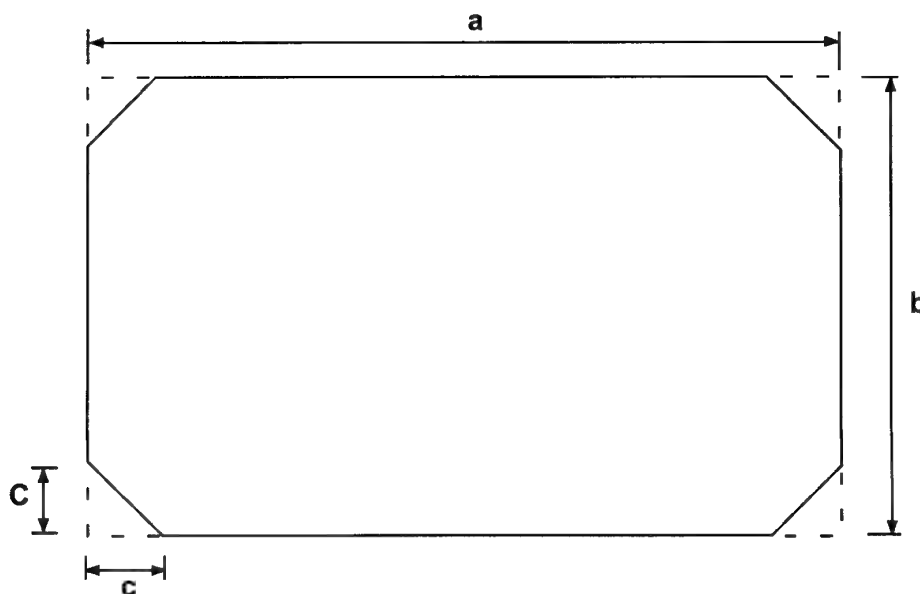


Table 1 Co-ordinates of the contraction in the DRA 5m tunnel

Non-dimensional Radius ($r-R_i/R_o-R_i$)	Inflow Factors		Lift Coefficients				Thrust Gradings (Ratios to the value at the centre)		Torque Gradings (Ratios to the value at the centre)		Blade Angle (deg)
	(a')1	(a')2	CL1	CL2	t/c	CD	(dT/dR)1	(dT/dR)2	(dQ/dR)1	(dQ/dR)2	
0.00	0.1151	0.1200	0.7745	0.7277	0.1952	0.0170	1.0000	1.0000	1.0000	1.0000	23.37
0.13	0.0994	0.1028	0.7421	0.6919	0.1733	0.0130	1.0791	1.0843	1.0825	1.0755	21.90
0.29	0.0846	0.0873	0.7063	0.6519	0.1529	0.0110	1.1764	1.1854	1.1801	1.1700	20.51
0.45	0.0730	0.0753	0.6735	0.6147	0.1368	0.0100	1.2767	1.3067	1.2771	1.2666	19.18
0.61	0.0674	0.0699	0.6829	0.6159	0.1238	0.0100	1.4654	1.4867	1.3520	1.3486	17.20
0.76	0.0623	0.0645	0.6868	0.6113	0.1130	0.0090	1.6579	1.6826	1.3988	1.3977	15.29
0.92	0.0576	0.0600	0.6858	0.6016	0.1040	0.0090	1.8519	1.8830	1.4144	1.4223	13.48
1.00	0.0554	0.0580	0.6838	0.5951	0.1000	0.0090	1.9491	1.9833	1.4100	1.4239	12.61

R_i = Inner Radius
 R_o = Outer Radius

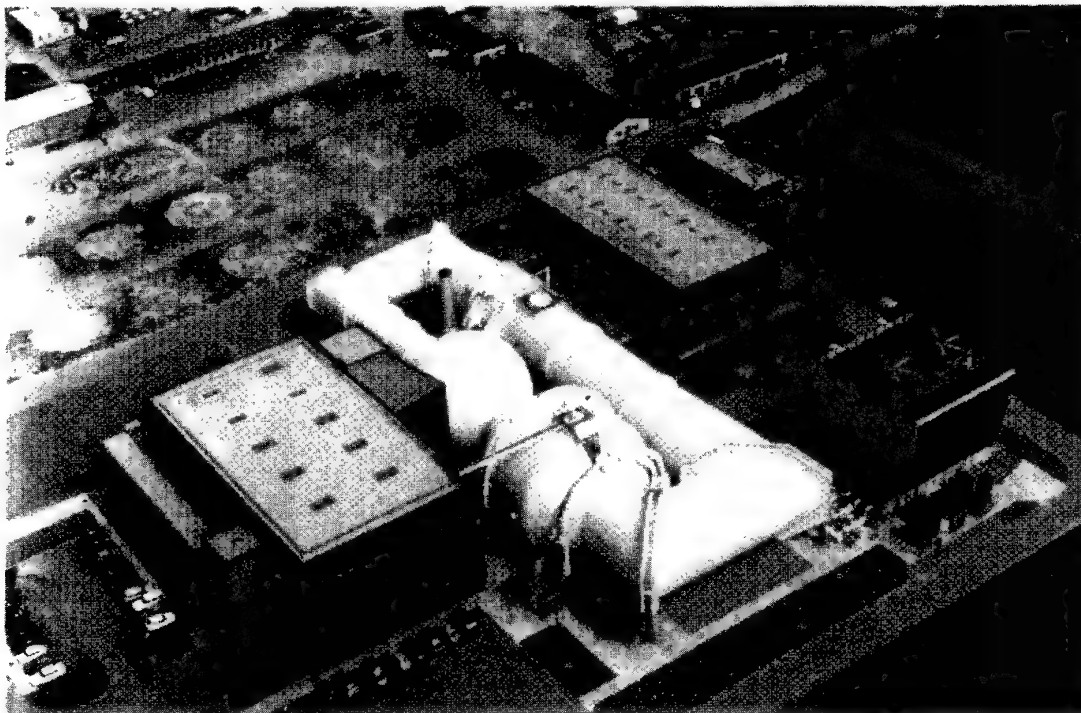
Chord = 0.924m Suffix 1 = Initial Value Suffix 2 = Final Value

a) Fan blades

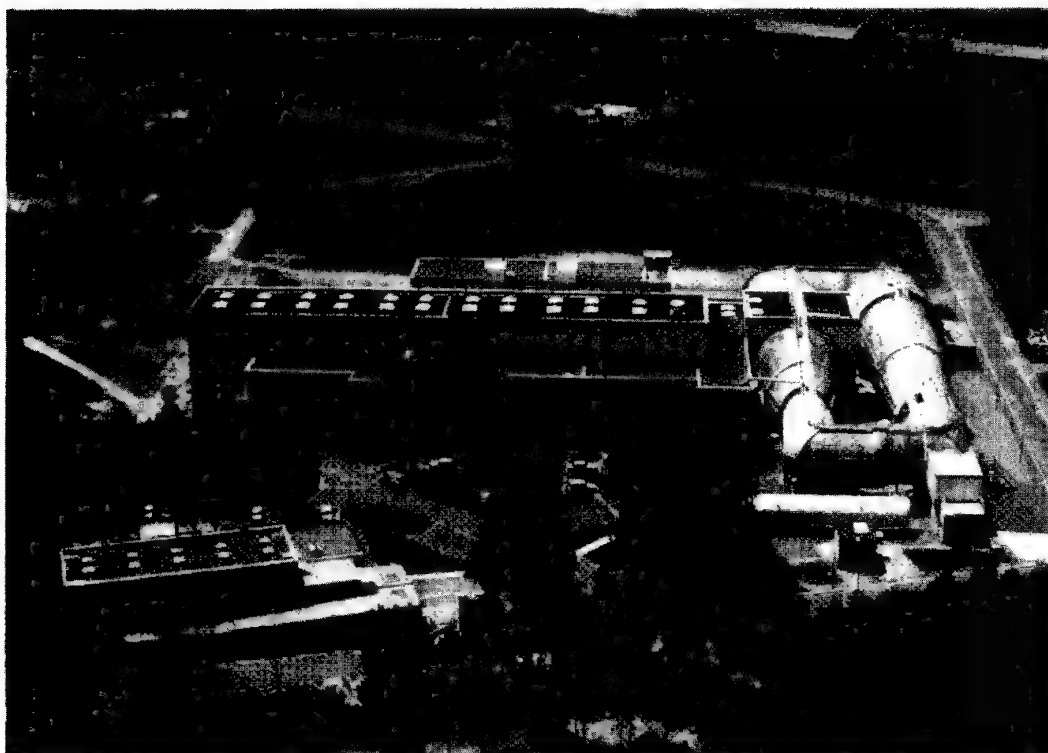
Non-dimensional Radius ($r-R_i/R_o-R_i$)	Chord (m)	Blade Angle (deg)
0.00	1.059	72.25
0.13	1.125	73.01
0.29	1.209	73.74
0.45	1.305	73.99
0.61	1.425	73.46
0.76	1.573	72.33
0.92	1.733	71.06
1.00	1.817	70.38

b) Pre-rotation vanes

*Table 2 Details of fan and pre-rotation vane design
for the DRA 5m tunnel*



a) DRA 5m tunnel



b) ONERA F1 tunnel

Figure 1 External views of the two low-speed pressurised wind tunnels

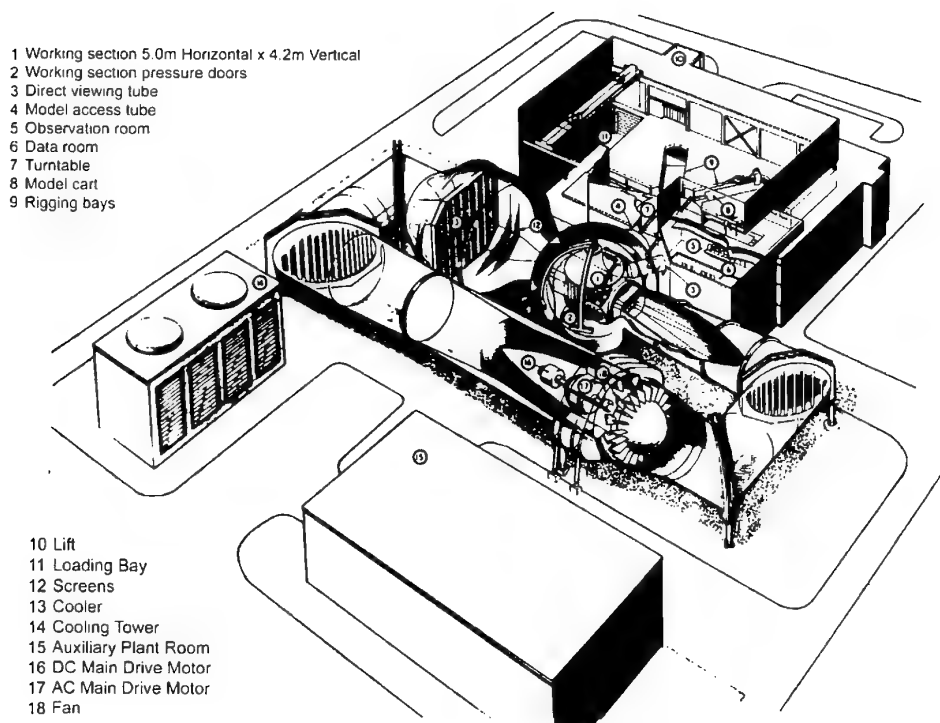
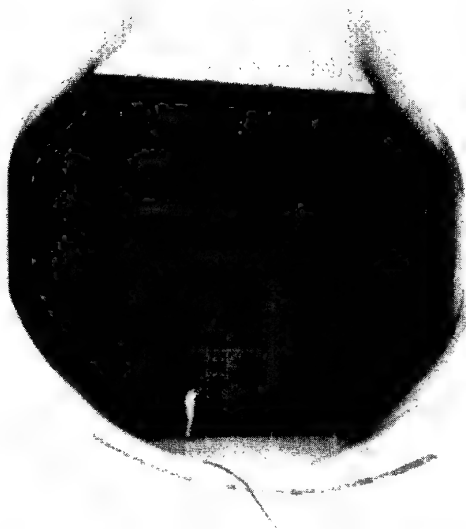
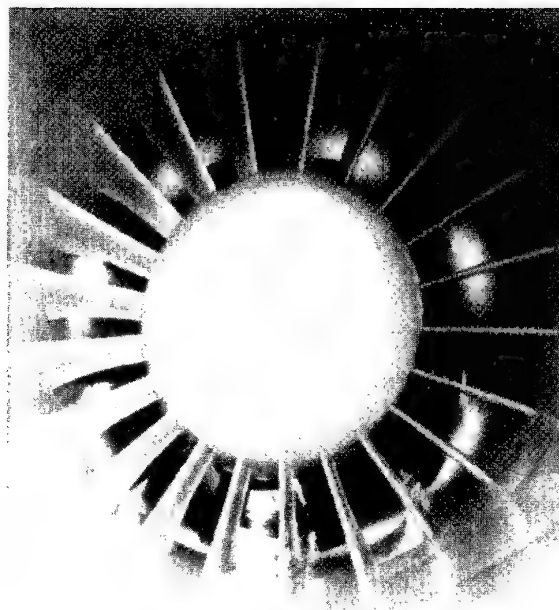


Figure 2 Cutaway drawing of the DRA 5m tunnel



*Figure 3 Cooler and rapid diffuser
in the DRA 5m tunnel
(Item 13 on Figure 2)*



*Figure 4 Fan and nacelle
in the DRA 5m tunnel
(Item 18 on Figure 2)*

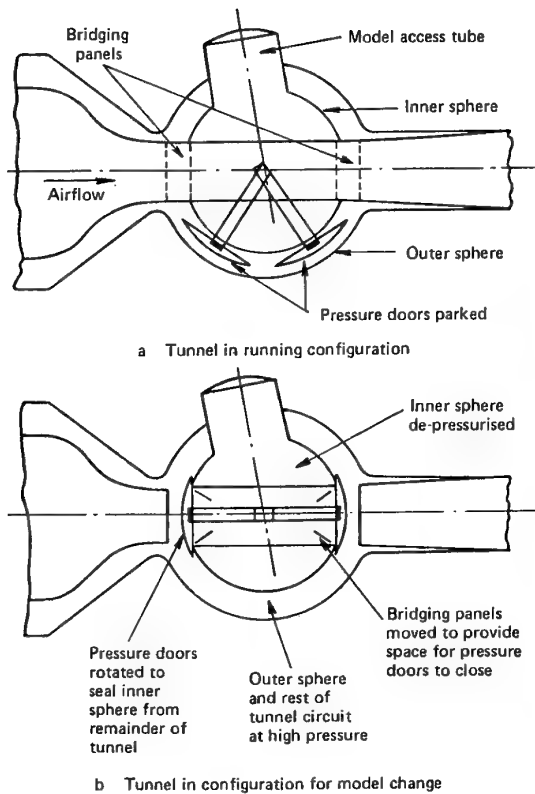


Figure 5 Schematic drawing of the operation of the model access system in the DRA 5m tunnel

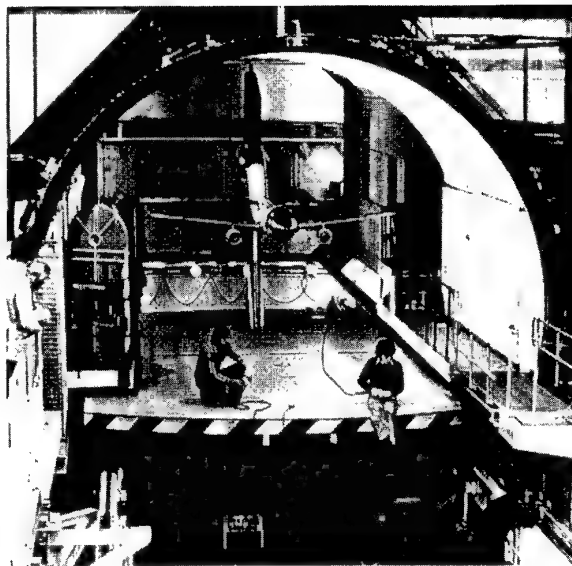


Figure 6 Working section rotated and cart emerging from access tube in the DRA 5m tunnel (Items 4 +8 on Figure 2)

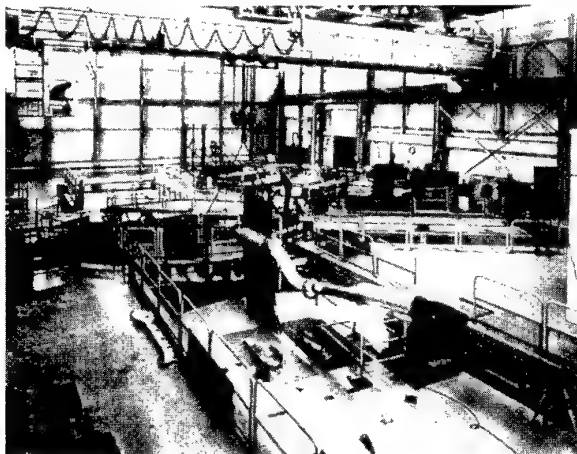


Figure 7 Rigging bay area with sting cart parked outside the DRA 5m tunnel (Items 7,8 +9 on Figure 2)

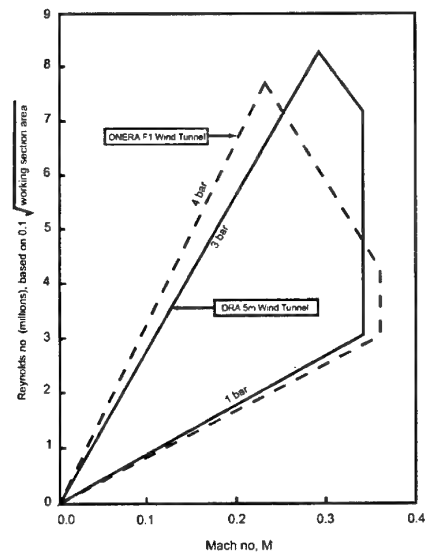
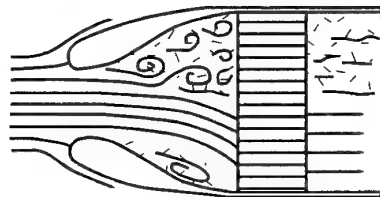
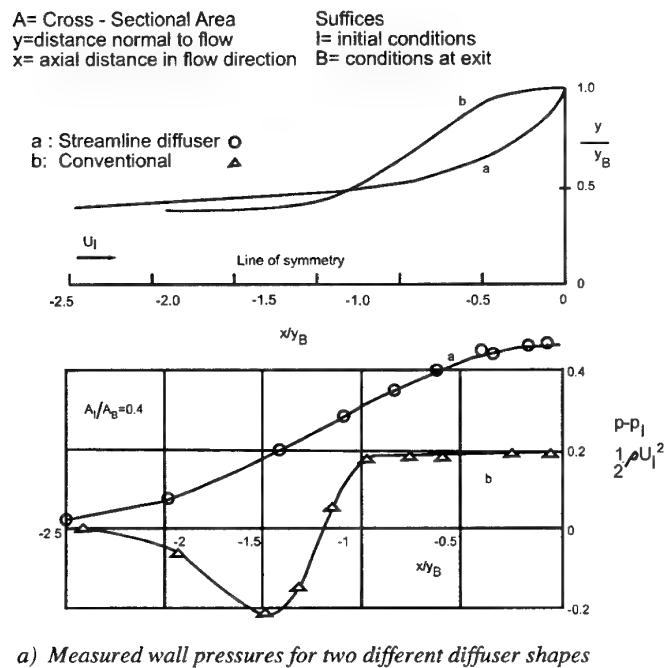


Figure 8 Operating envelopes of the DRA 5m and ONERA F1 tunnels



b) Flow pattern in the conventional diffuser from water - tunnel observations

Figure 9 Comparison of streamline and conventional diffusers (after Küchemann and Weber¹⁰)

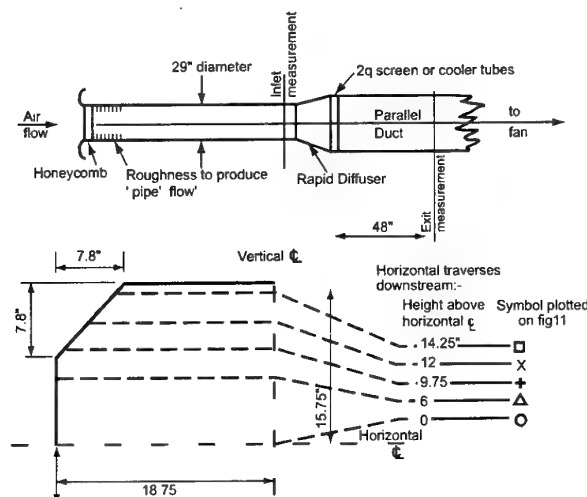


Figure 10 Test apparatus for modelling the rapid diffuser in the DRA 5m tunnel

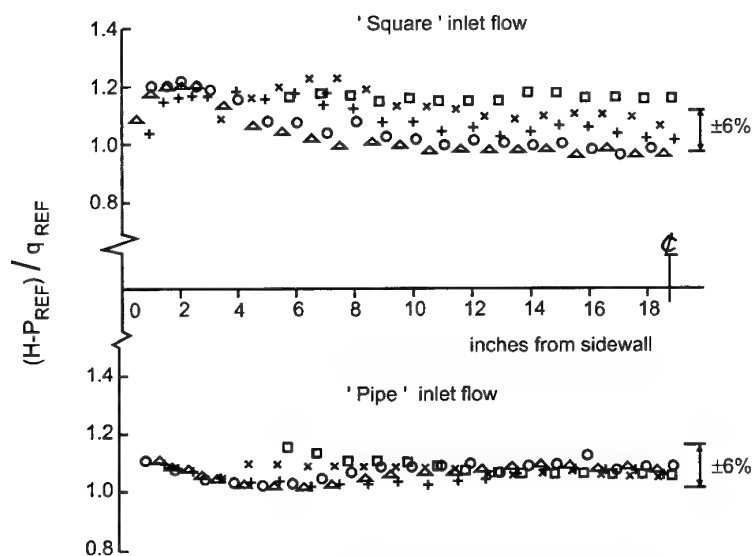


Figure 11 Total pressure distribution downstream of a model of the rapid diffuser and cooler similar to that used in the DRA 5m tunnel

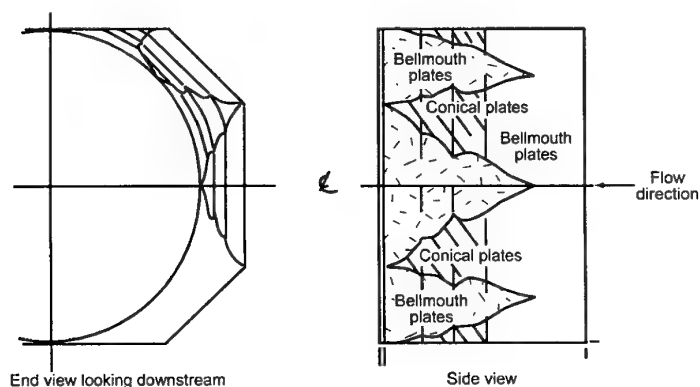


Figure 12 Final shape of the rapid diffuser in the DRA 5m tunnel

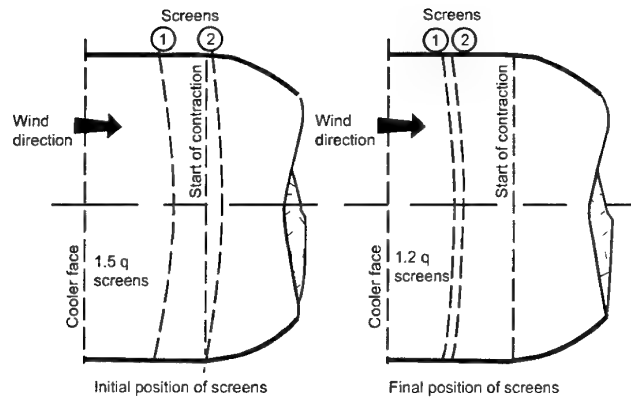


Figure 13 Development of screen layout for the DRA 5m tunnel

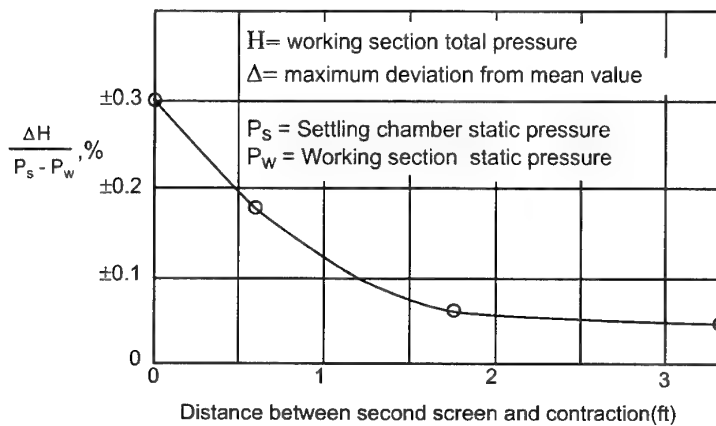


Figure 14 Effect of varying length between second screen and contraction in the model of the DRA 5m tunnel (two 1.5 q screens)

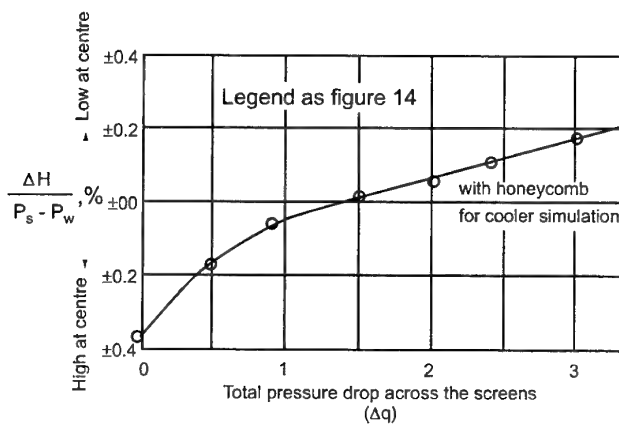


Figure 15 Effect of screen pressure drop on working section flow uniformity in the model of the DRA 5m tunnel (screens spaced 1ft apart with 6ft length before contraction)

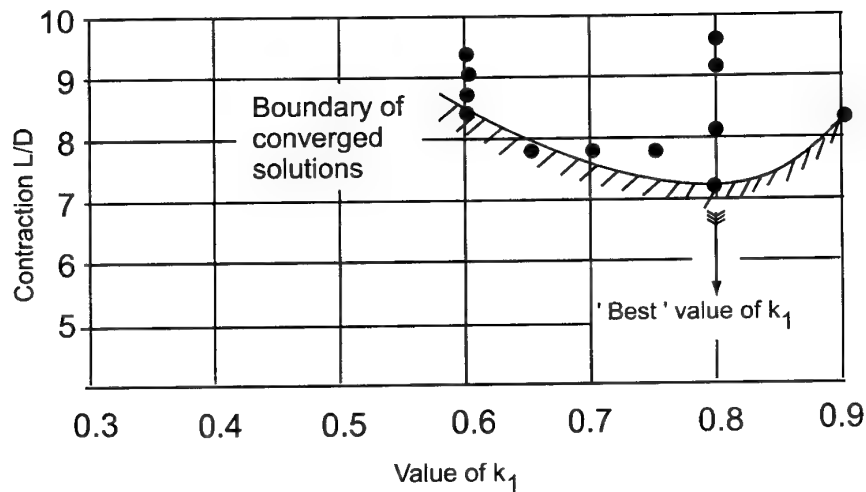


Figure 16 Variation of contraction L/D with the value of k_1

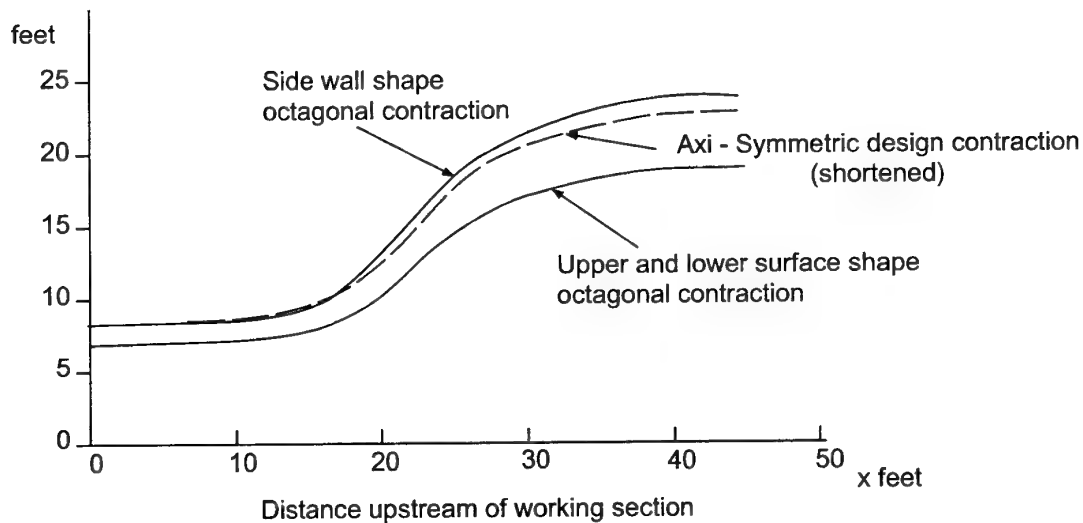


Figure 17 Contraction shape of the DRA 5m tunnel

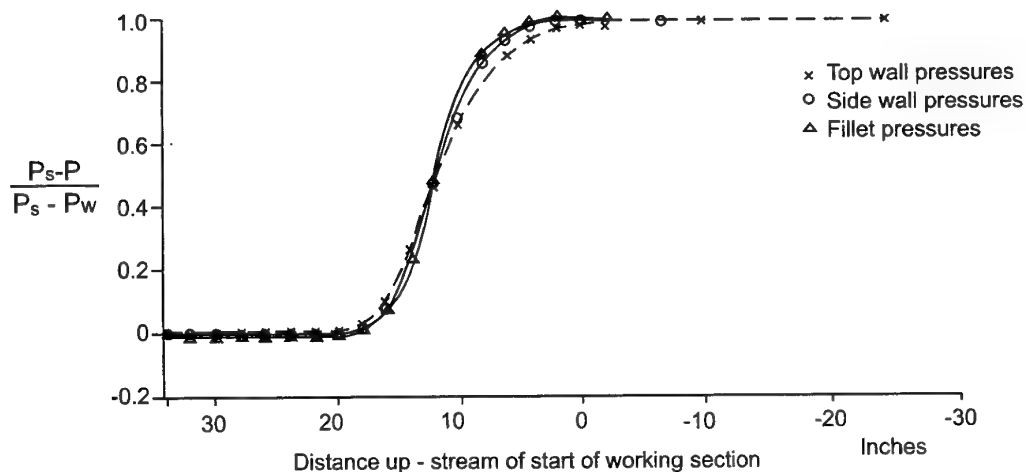


Figure 18 Static pressure on the top wall, side wall and fillet of the contraction in the model of the DRA 5M tunnel

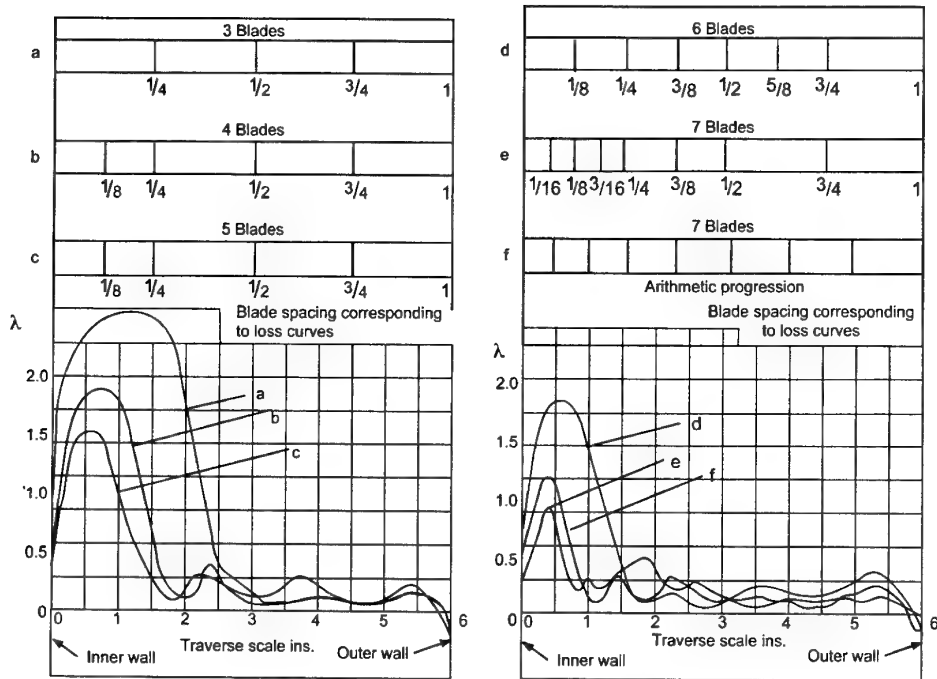
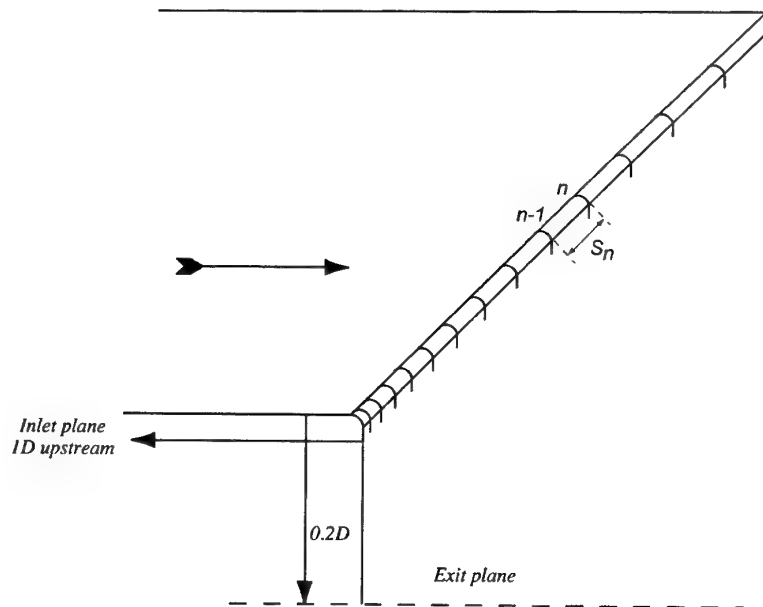


Figure 19 Variation of total head loss through various arrangements of corner vanes(Dimmock 16)

Vane Number	Vane Spacing, S_n
1	0.0400D
2	0.0465D
3	0.0529D
4	0.0549D
5	0.0658D
6	0.0723D
7	0.0787D
8	0.0852D
9	0.0916D
10	0.0981D
11	0.1045D
12	0.1110D
13	0.1174D
14	0.1239D
15	0.1303D



where D = diameter of tunnel downstream of corner

Figure 20 Turning Vane Spacings in the DRA 5m tunnel

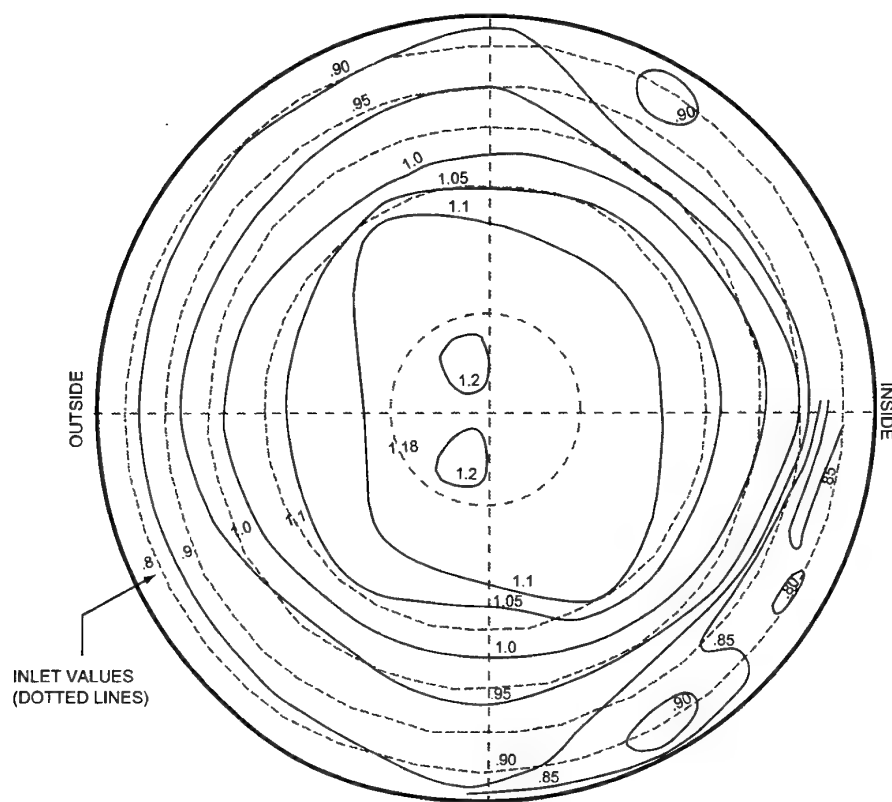


Figure 21 Comparison of inlet and exit velocity profiles $\frac{u}{U}$ of a corner in the model of the DRA 5m tunnel

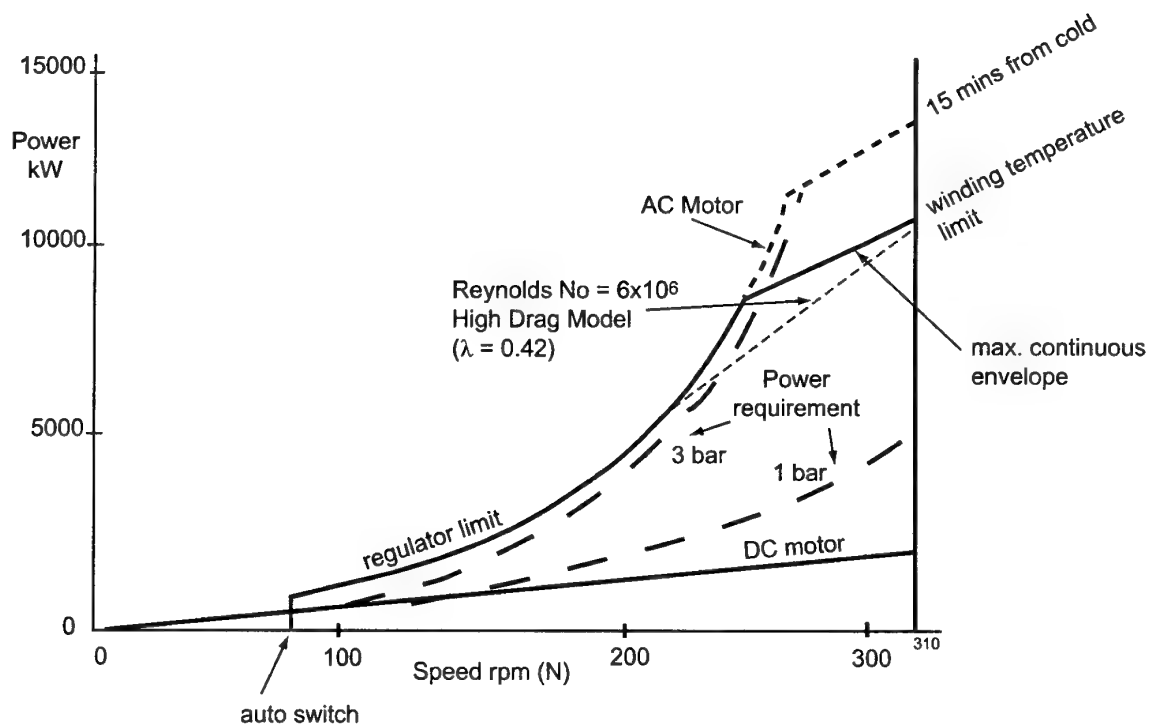


Figure 22 Designed Main Drive Power Supply for the DRA 5m tunnel

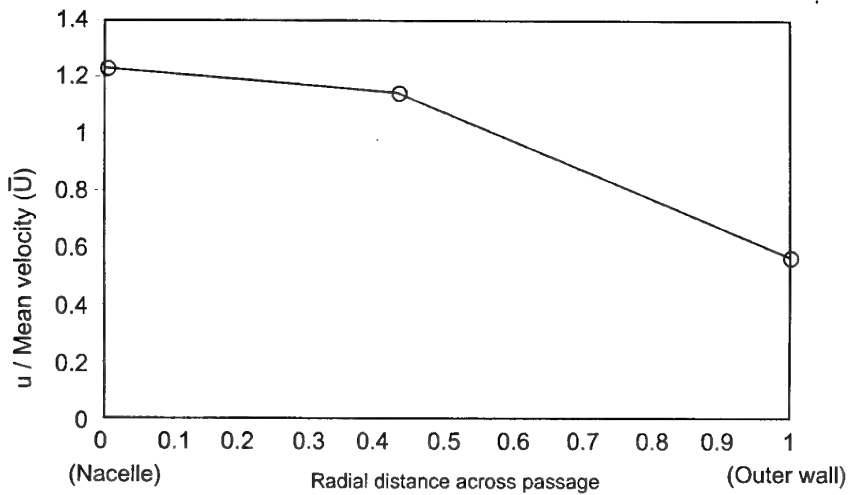


Figure 23 Velocity profile at fan entry in the model of the DRA 5m tunnel

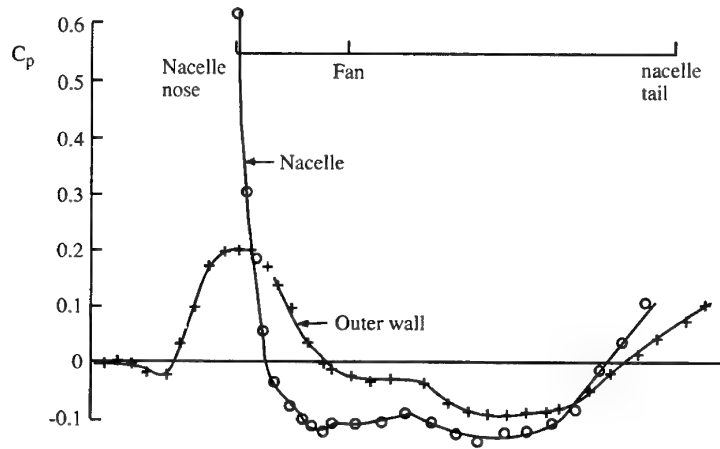


Figure 24 Pressure coefficients on walls of fan section of the DRA 5m tunnel
(Final design without pre rotation vanes or fan)

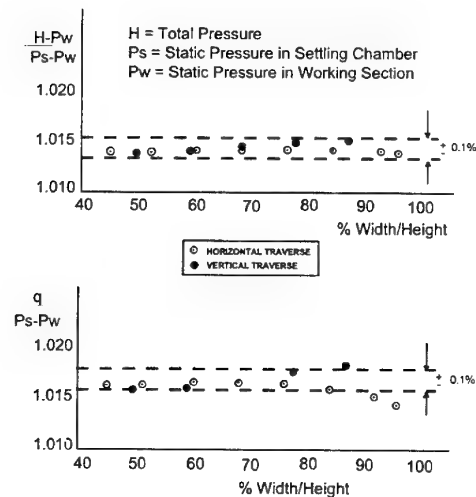
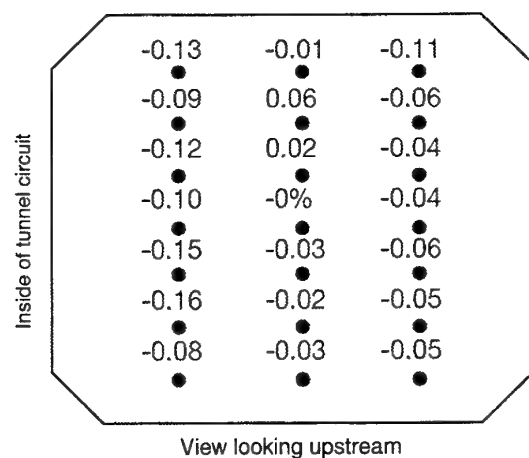
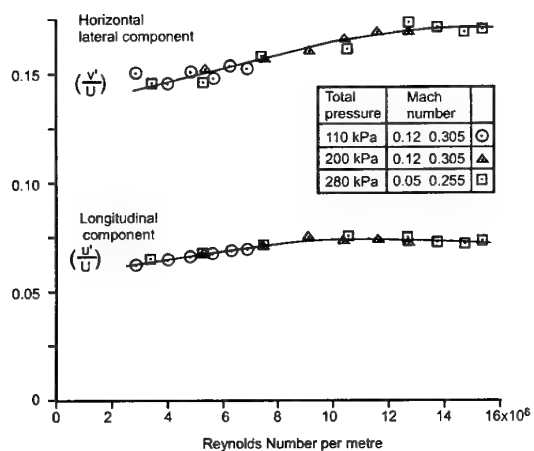


Figure 25 Distributions of total and dynamic pressure in the working section - final configuration of the DRA 5m tunnel model



Figures are mean percentage deviations of dynamic pressure
from tunnel working section centre line value

*Figure 26 Dynamic pressure distribution
in the working section of the DRA 5m tunnel*



*Figure 27 Turbulence variation with Reynolds number
in the DRA tunnel*

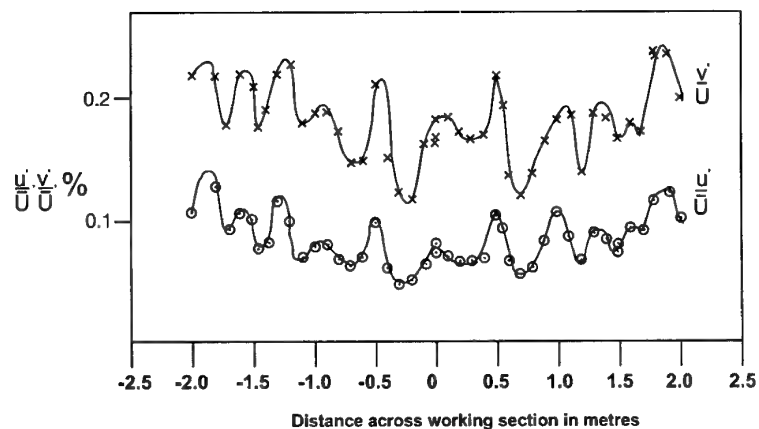


Figure 28 Spanwise turbulence variation in the DRA 5m tunnel

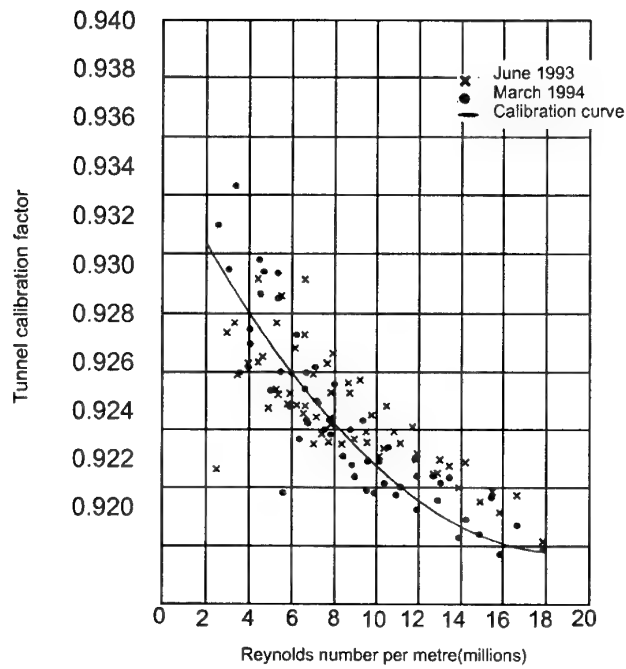


Figure 29 Repeatability of the DRA 5m tunnel calibration

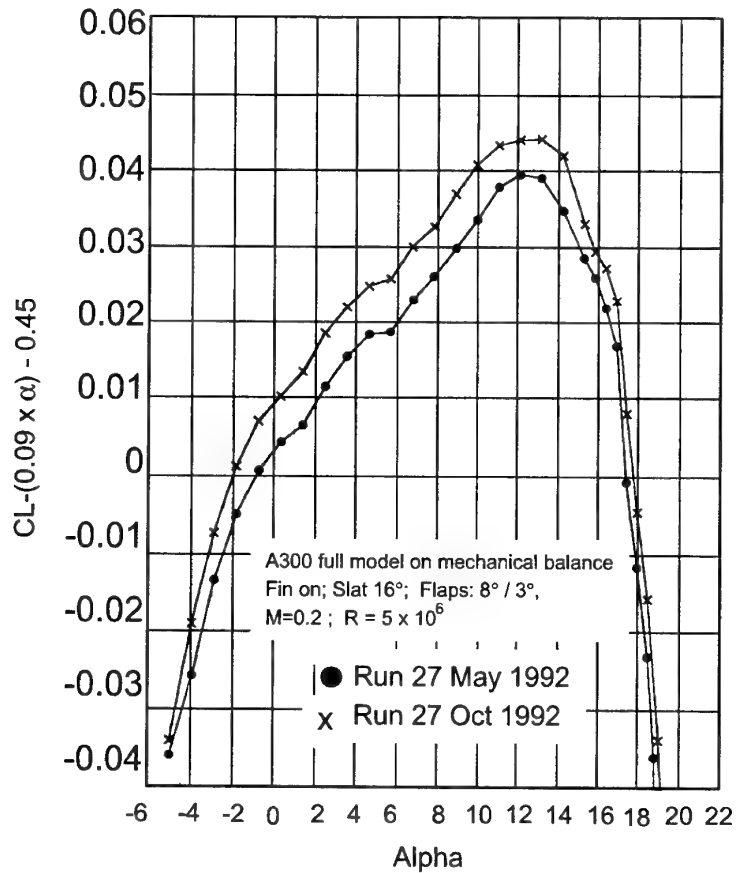


Figure 30 Overall force repeatability in the DRA 5m tunnel

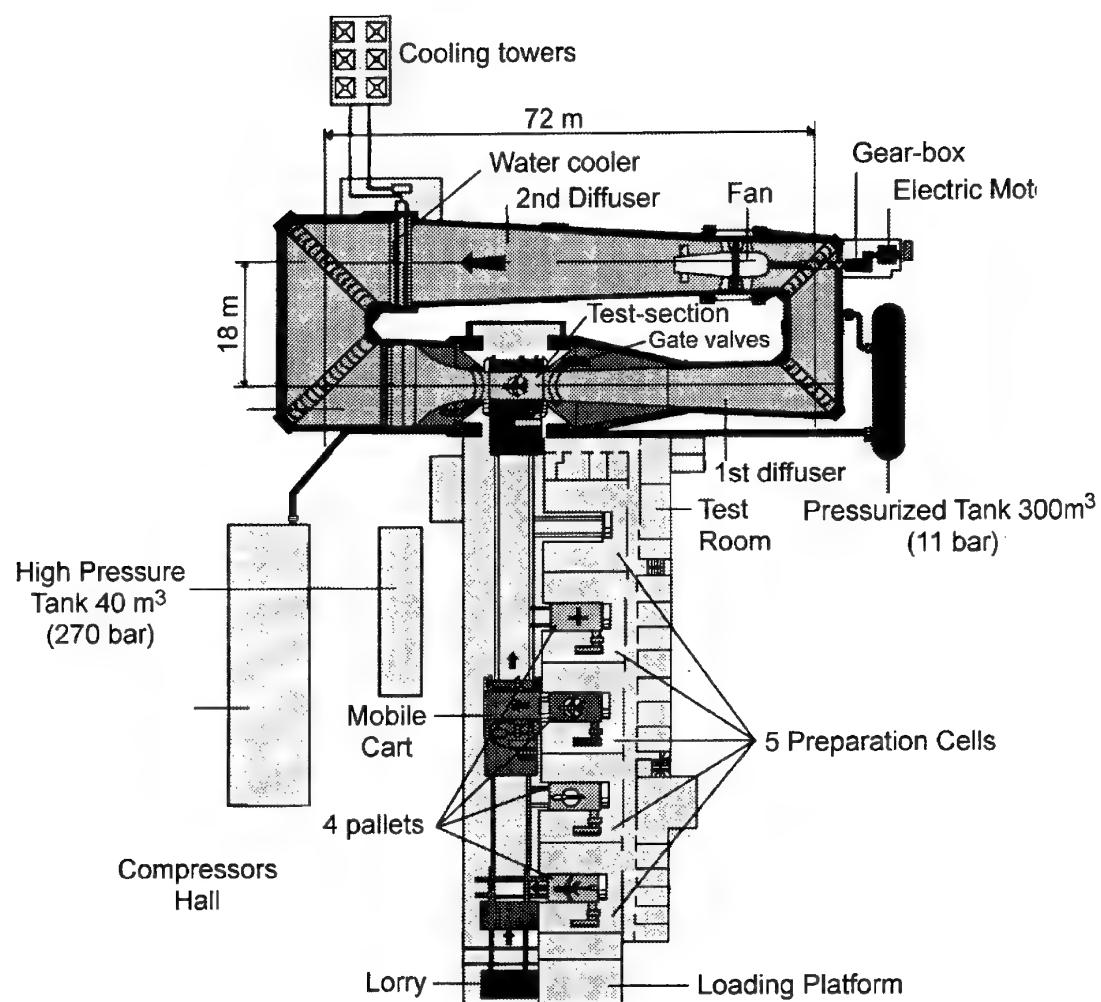


Figure 31 General drawing of the ONERA F1 facility

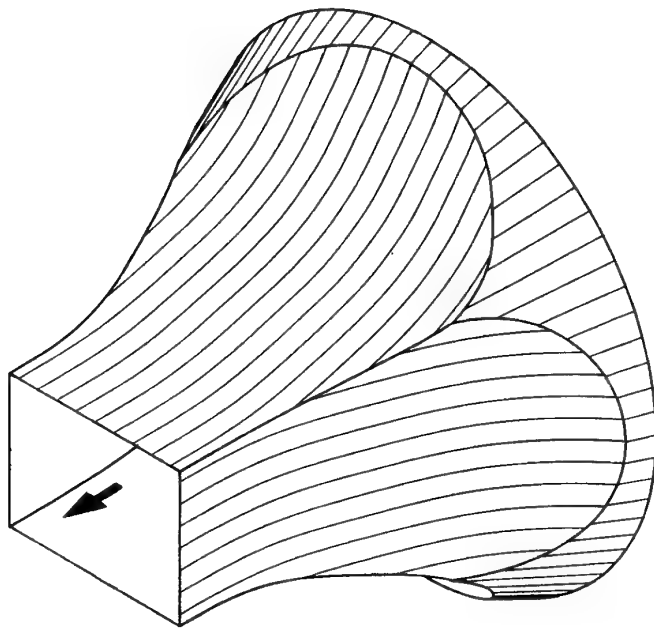


Figure 32 F1 Contraction Shape

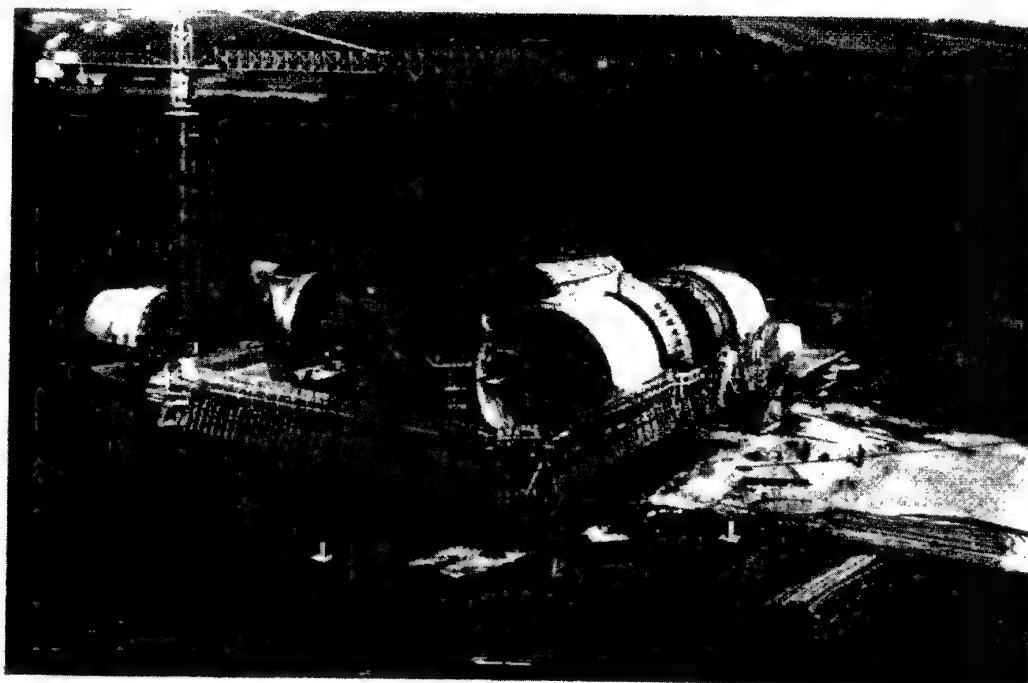


Figure 33 F1 Concrete shell during building

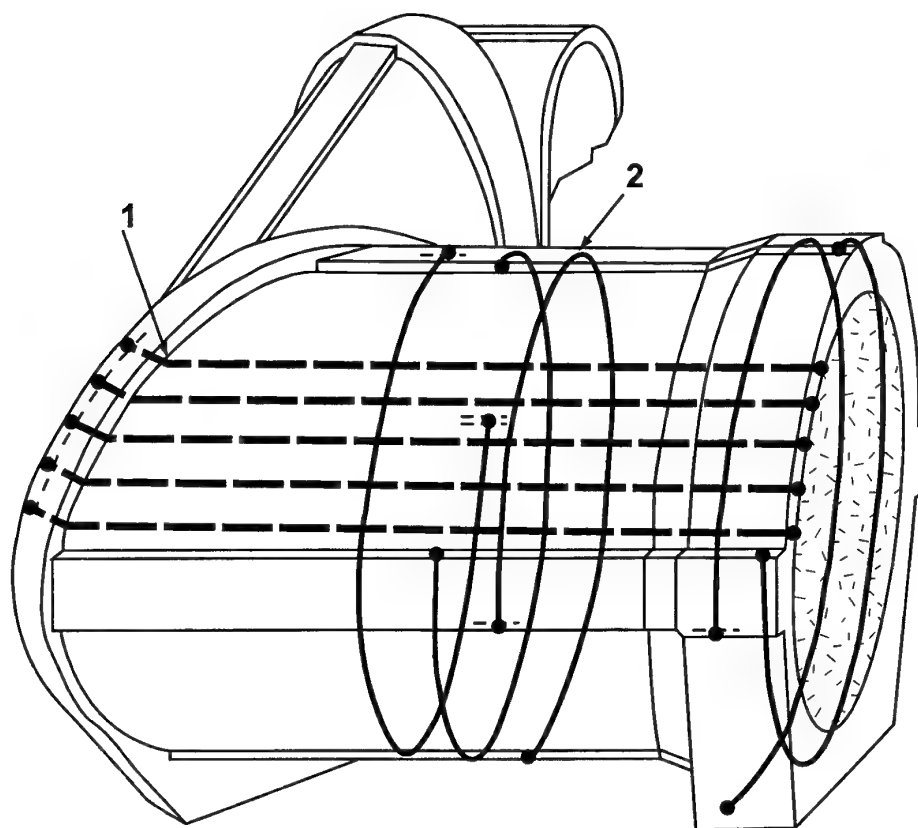


Figure 34 Pre - stressing cables in the ONERA F1 tunnel

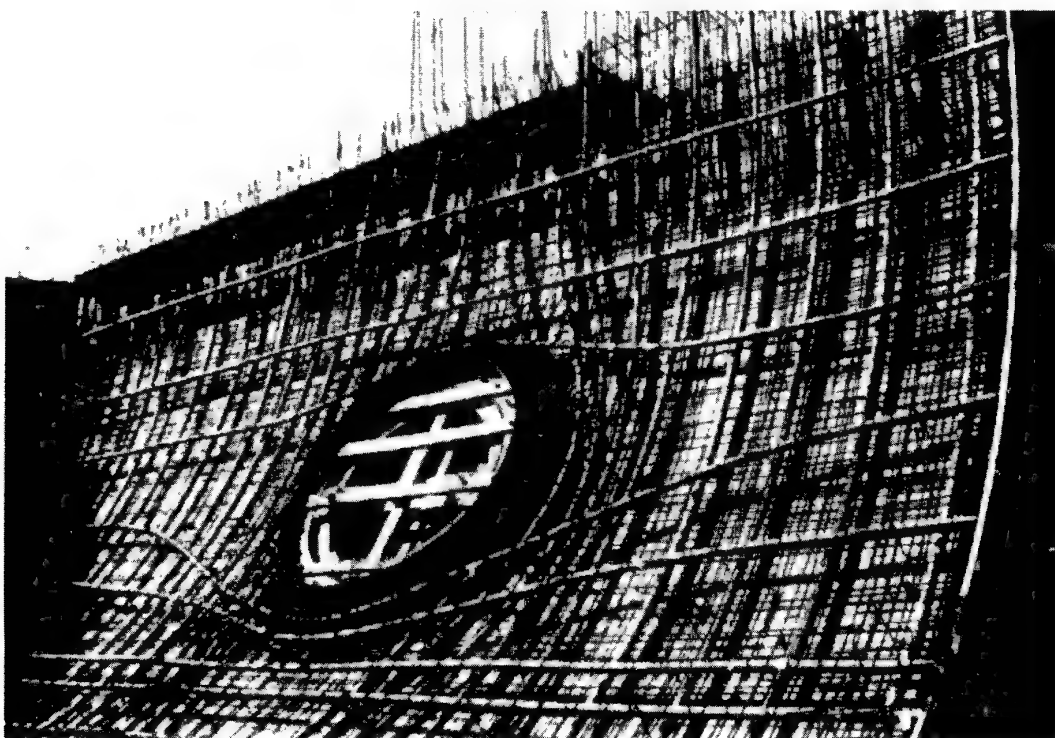


Figure 35 Sleeves of pre-stressing cables around on access door in the pressure shell of the ONERA F1 tunnel

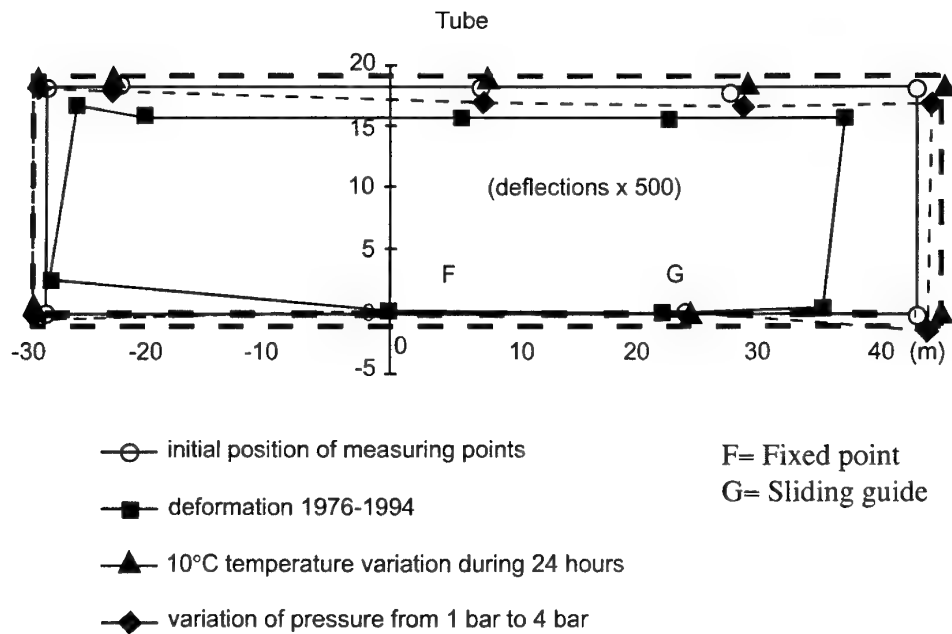


Figure 36 Horizontal displacements of F1 shell with time, temperature and pressure

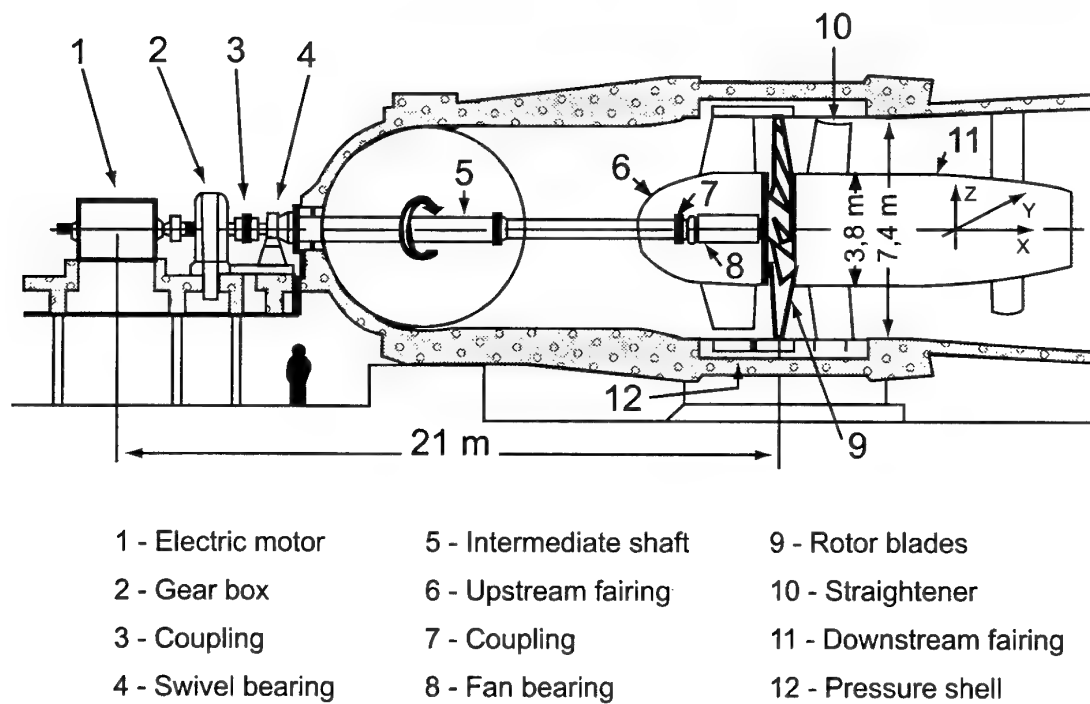


Figure 37 ONERA F1 drive system

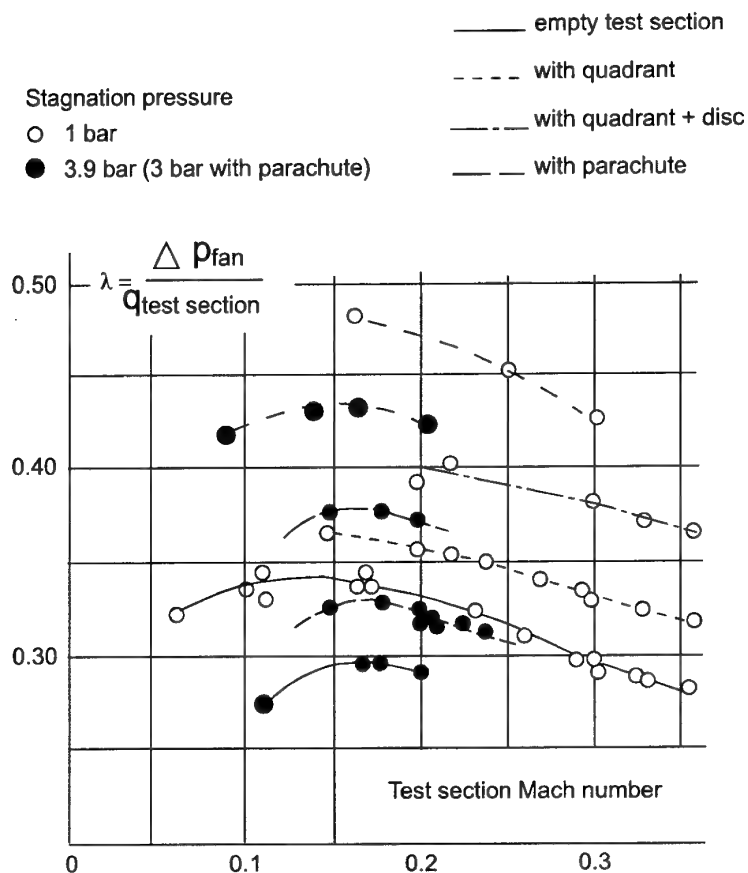


Figure 38 Variation of Total Head losses with Mach number and pressure in the ONERA F1 tunnel

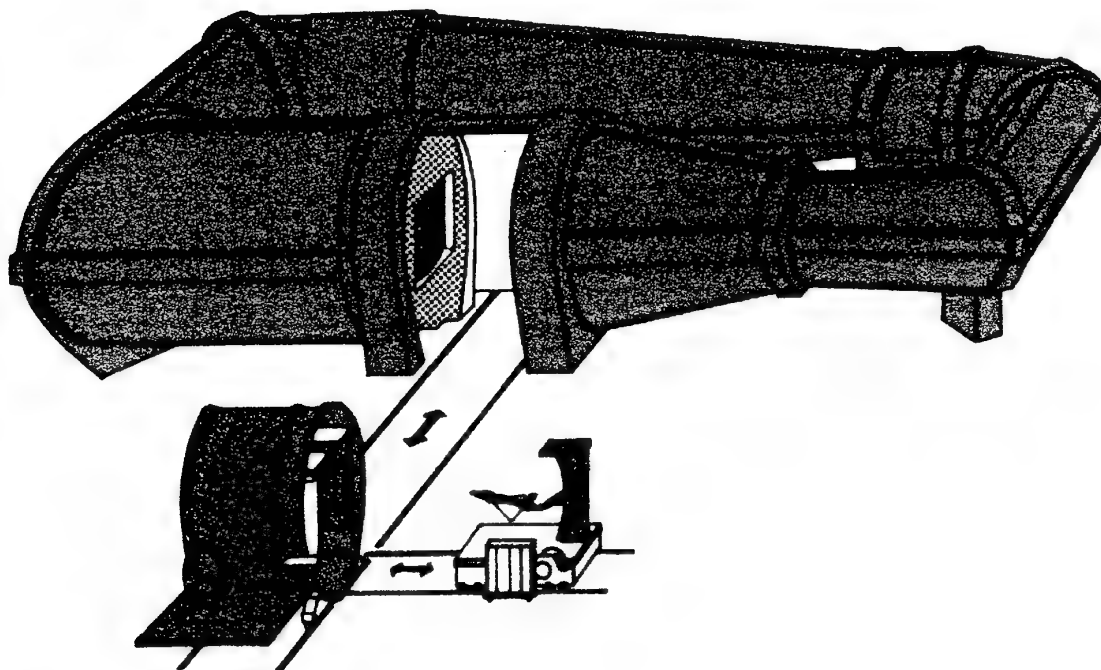


Figure 39 Access and changes of models in the ONERA F1 tunnel

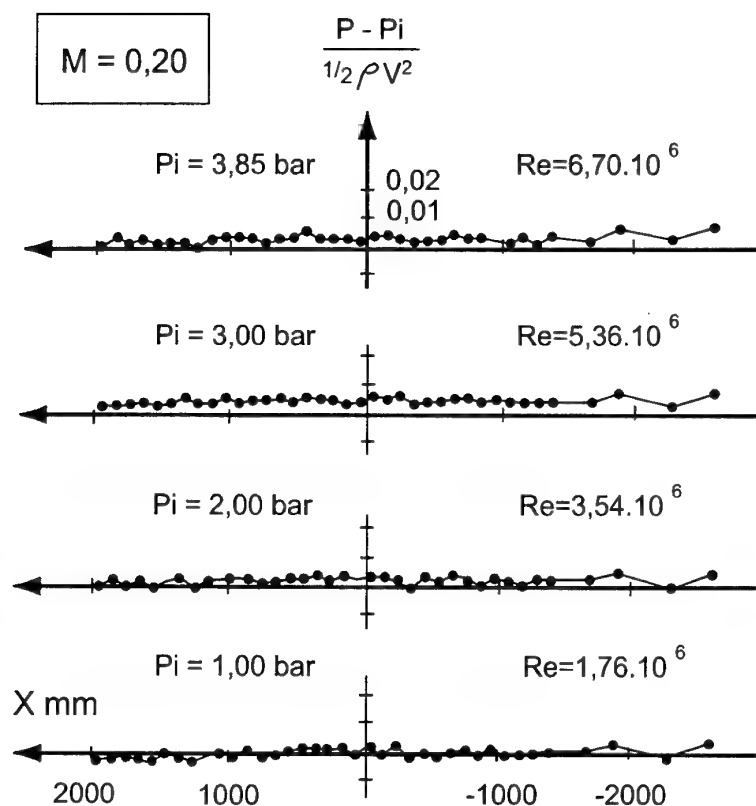


Figure 40 Static pressures along the working section centreline of the ONERA F1 tunnel

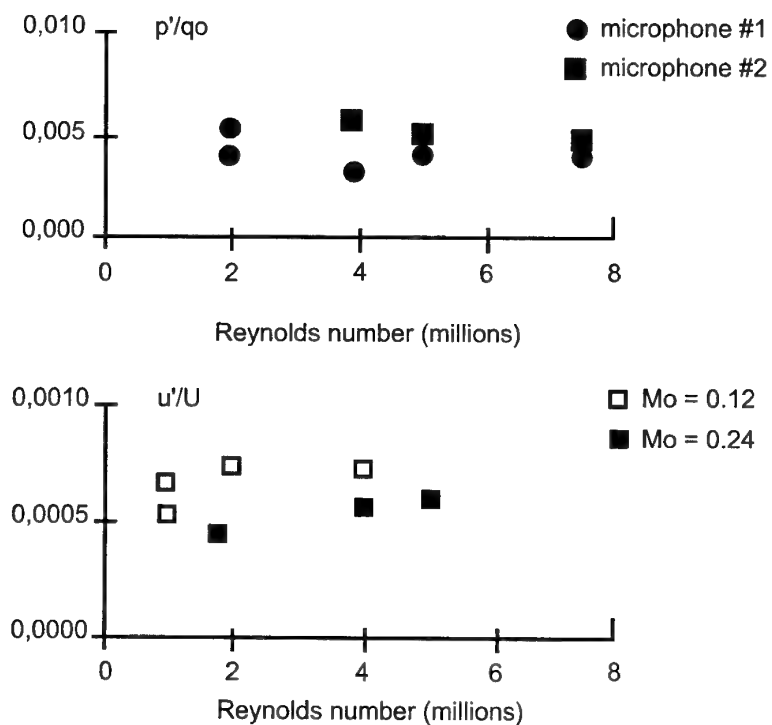


Figure 41 Noise and turbulence in the working section of the ONERA F1 tunnel

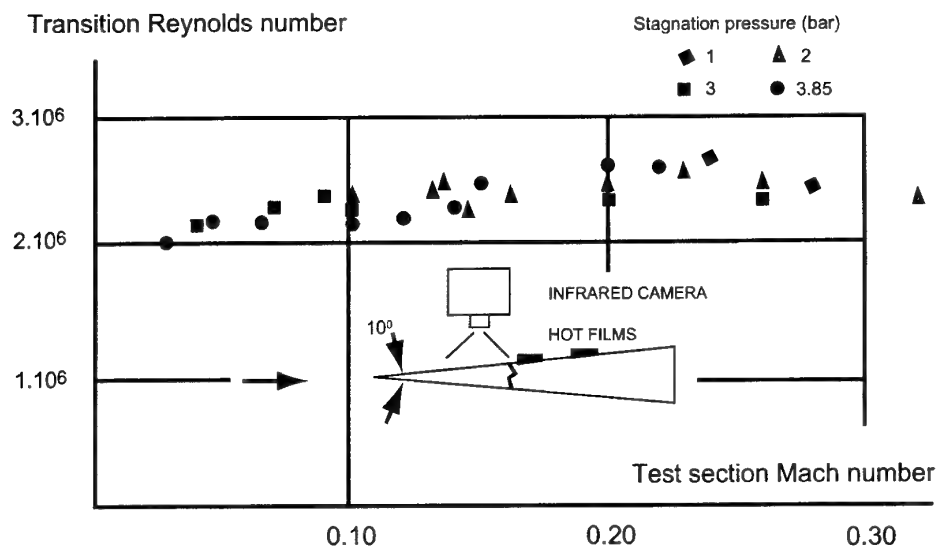


Figure 42 Measurement of transition onset on 10° cone in the ONERA F1 tunnel

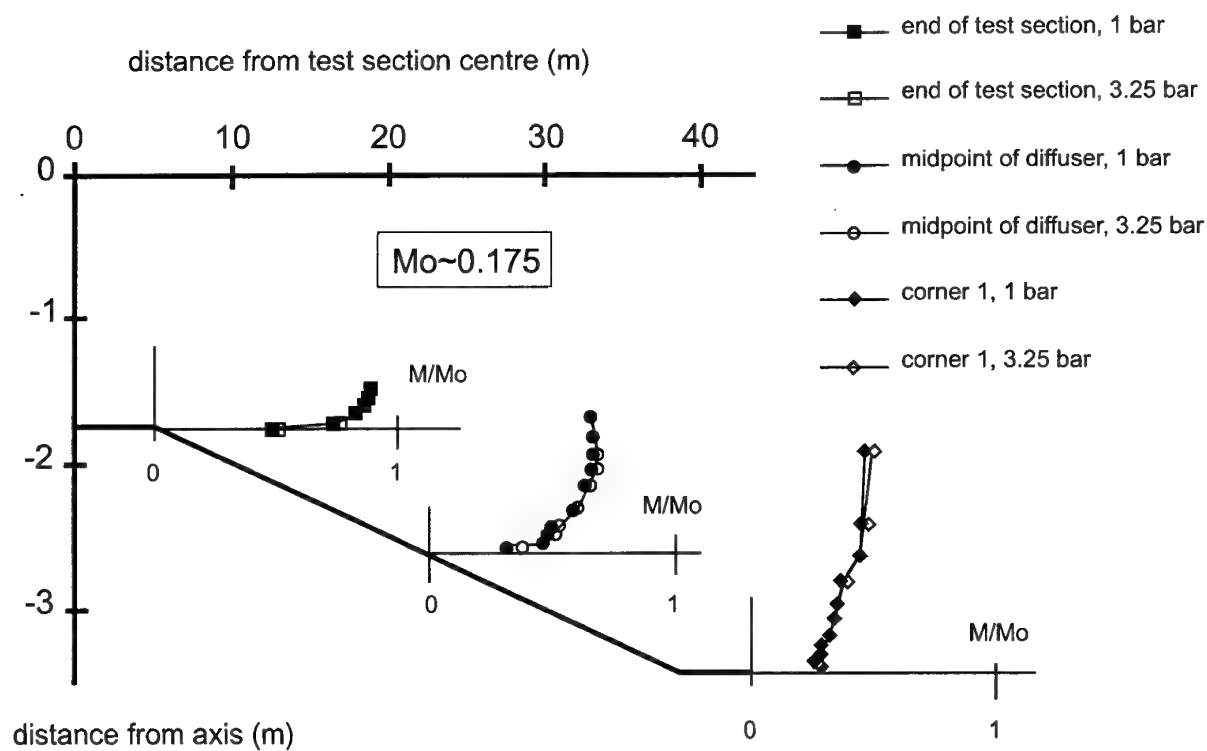


Figure 43 Wall Mach number profiles in first diffuser of the ONERA F1 tunnel

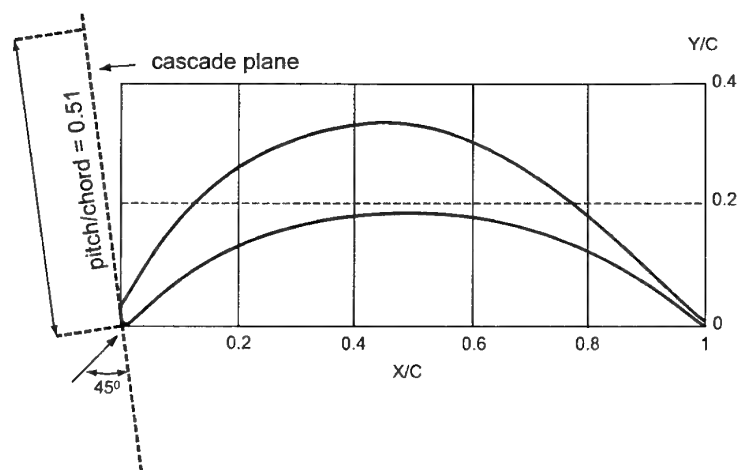


Figure 44 Profile of corner vanes for corners 1 & 2 of the ONERA F1 tunnel

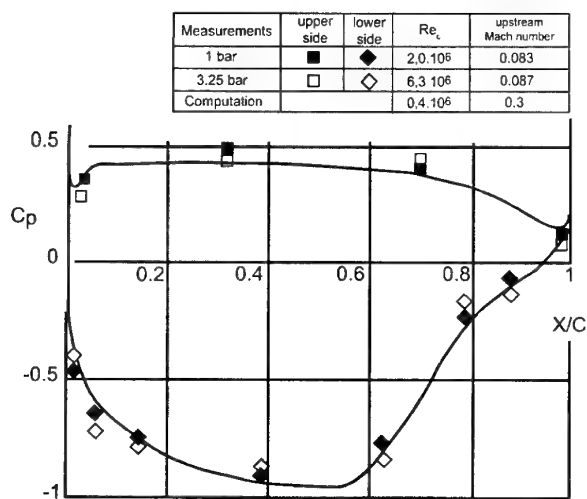


Figure 45 Pressure distribution on centre vane of corner 1 of the ONERA F1 tunnel

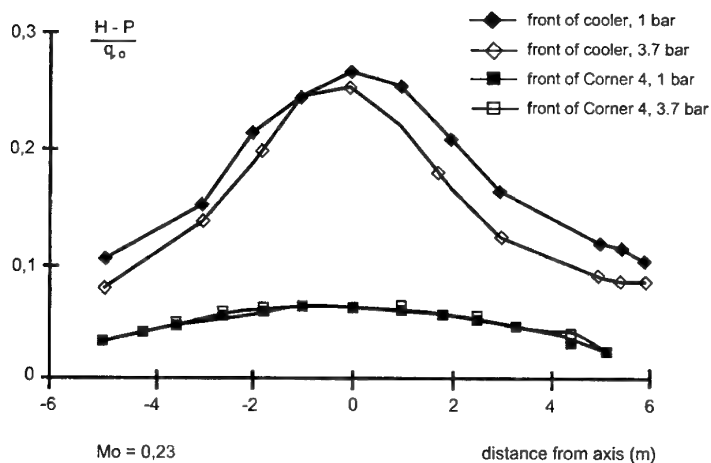


Figure 46 Total pressure distribution on both sides of cooler of the ONERA F1 tunnel

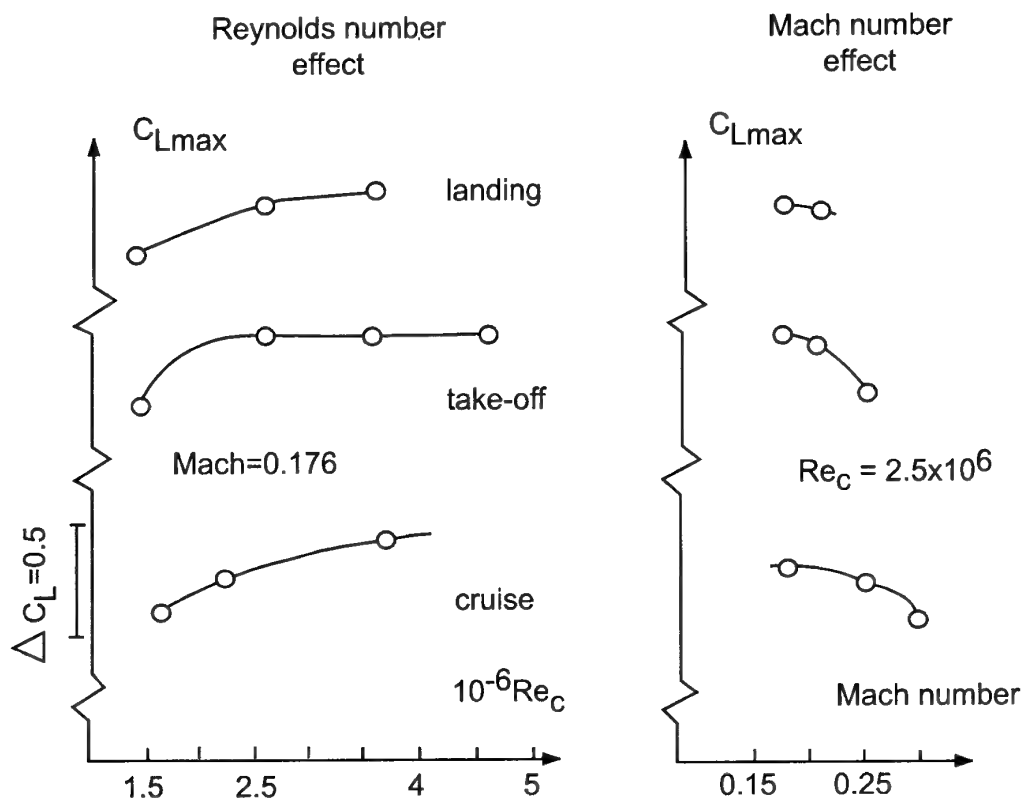


Figure 47 1/16th scale Airbus A300 results in the ONERA F1 tunnel

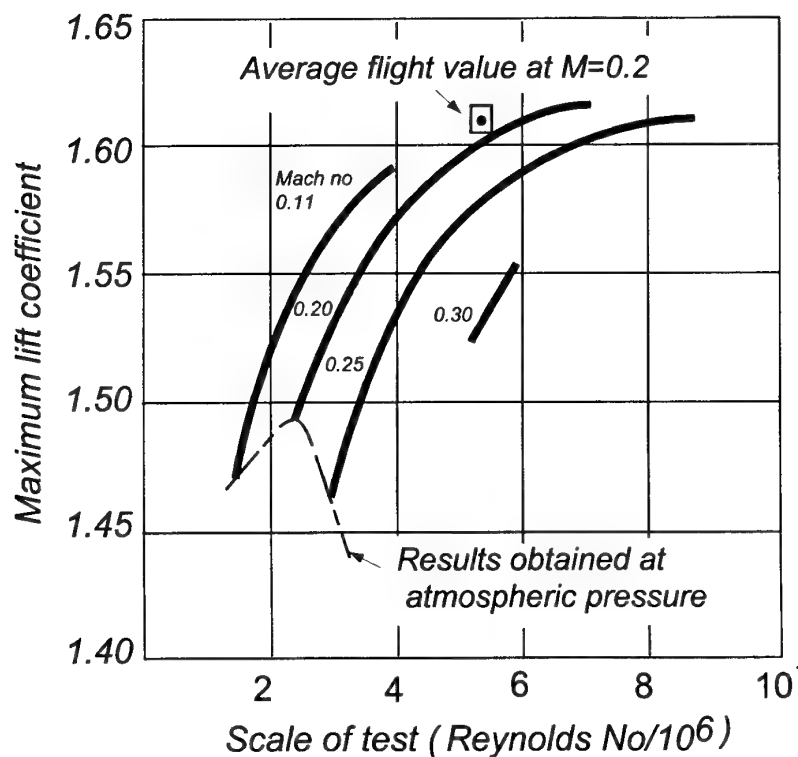


Figure 48 0.3 scale Hawk results in the DRA 5m tunnel

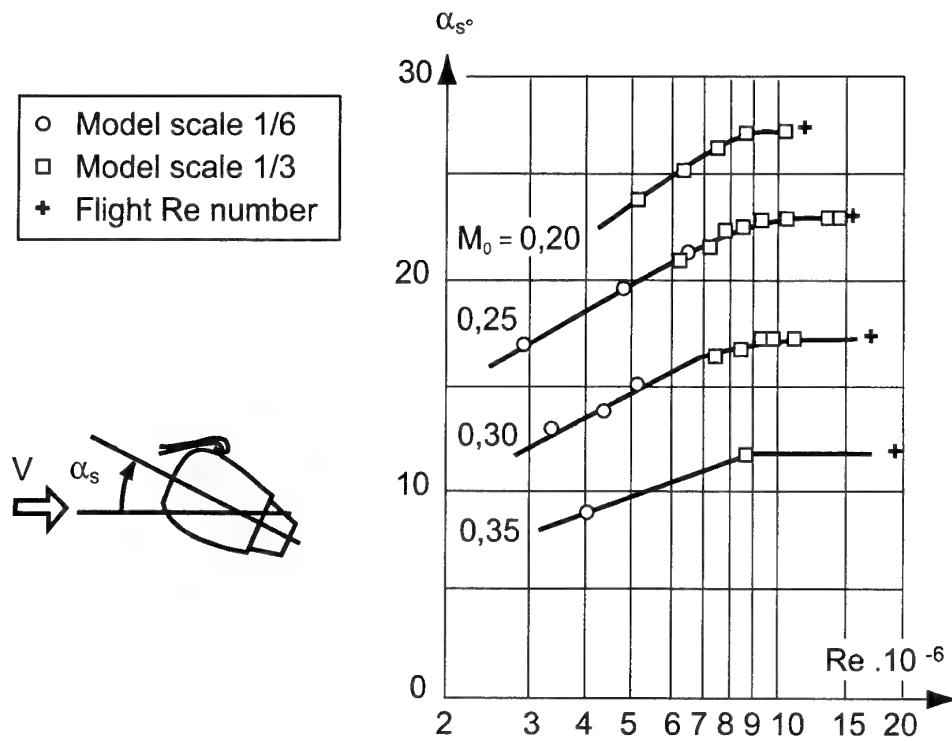


Figure 49 Scale effect on flow about a nacelle in the ONERA F1 tunnel

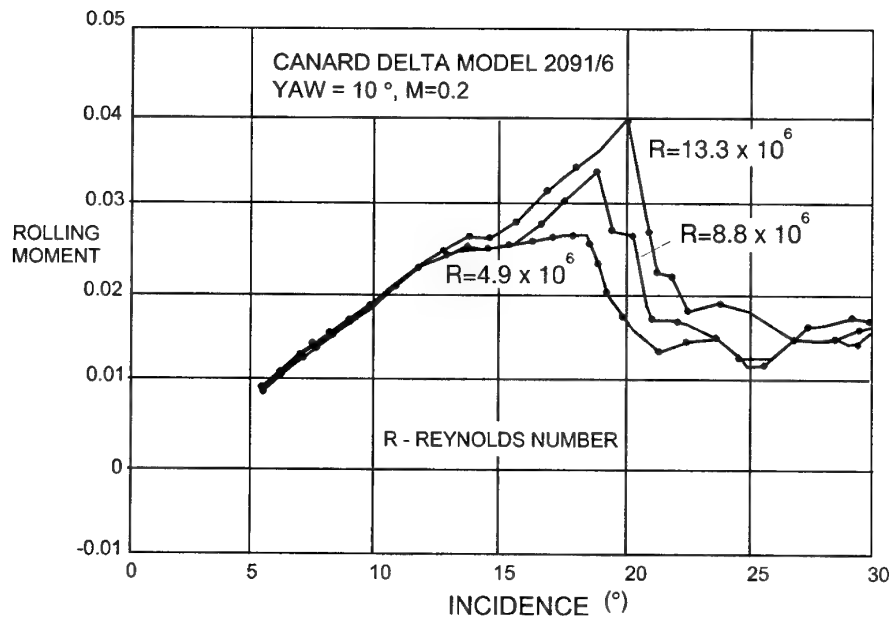


Figure 50 Scale effect on roll for canard delta model in the DRA 5m tunnel

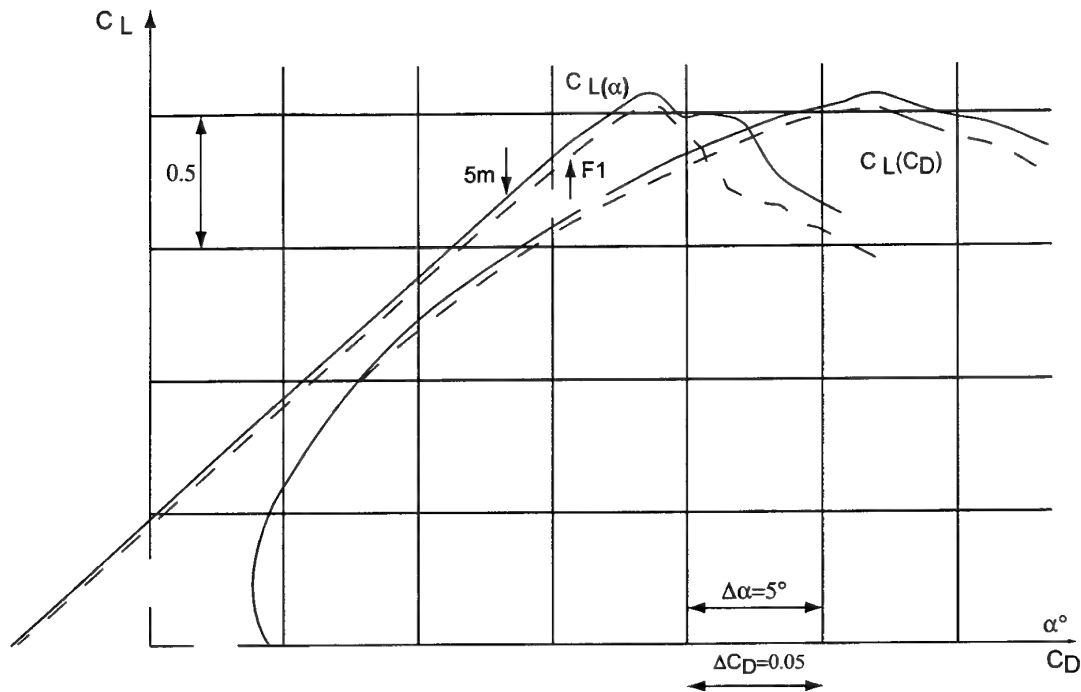


Figure 51 Initial comparison of A300B data (take off configuration) produced in the DRA 5m and ONERA F1 tunnels

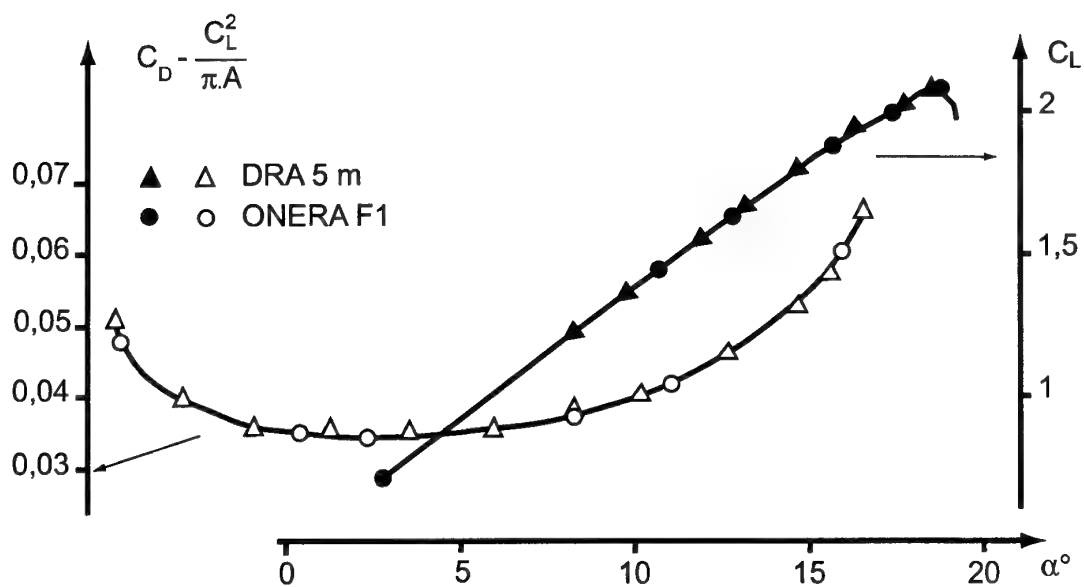


Figure 52 Final comparison of A300B data (take off configuration) produced in the DRA 5m and ONERA F1 tunnels

SUBSONIC WIND TUNNEL WITH FLOW SPEED PULSATION

M.P. Ryabokon and A.G. Malyk

Central Aerohydrodynamic Institute (TsAGI), 1, Zhukovsky Street
140160 Zhukovsky, Moscow Region, Russia

ABSTRACT

A number of calculations and experiments within the program of developing a subsonic wind tunnel with flow speed pulsation in the test section were carried out at TsAGI. The wind tunnel was designed to perform aerodynamic tests of models in regularly fluctuating flows within the Mach number range up to 0.9 with the fluctuation amplitude up to 40% of the mean flow velocity and the frequency of pulsations up to 20 Hz.

One of the possible concepts of developing a wind tunnel with flow speed pulsation was used. Speed pulsation is generated using rotating elliptic shafts located parallel in one of the wind tunnel cross sections downstream of the test section. The air is injected into the wind tunnel from the atmosphere by means of an ejector.

The results obtained were applied for designing a wind tunnel prototype with the 0.4 (W) × 0.7 (H) m test section.

Special attention in developing the wind tunnel was given to the problem of obtaining the velocity pulse shape in the test section close to the sine curve. For this purpose special correcting devices were introduced in the wind tunnel structure.

Investigation showed that shock waves can be generated in pulsing flow at transonic flow velocities. The upper velocities at which no shock waves are generated have been determined.

LIST OF SYMBOLS

a	sound speed
b	large ellipse axis
c	small ellipse axis
F	wind tunnel cross-section area
f	pulsation frequency
L	distance between the pulser and the model location
ℓ	length of the shaft
$M=V/a$	Mach number
P	pressure
S	shaft projection area onto the wind tunnel cross-section area
t	time
V	flow velocity
ΔV	velocity fluctuation amplitude
δ	relative stagnation pressure losses
α	ratio of specific heats
λ	reduced velocity
ρ	gas density
ξ	hydraulic resistance coefficient
θ	angle between the large ellipse axis and the wind tunnel axis
φ	F_2/F_3 area ratio

INDICES

1	test section area
2	pulser passage cross-section area
3	duct area downstream of the pulser
cp	mean
0	stagnation parameter
*	parameter in the critical cross-section

1. WIND TUNNEL STRUCTURE

The wind tunnel schematic is presented in Fig. 1. The wind tunnel contains a settling chamber with a honeycomb and screens, a subsonic nozzle, a test section, a short diffuser, and an ejector. The pulser – a device for generating speed pulsation – is a distinctive feature for this wind tunnel. The pulser schematic is given in Fig. 2. The pulser contains six elliptic rotating shafts in one transverse section of the wind tunnel between the short diffuser and the ejector. Four shafts are rotated at the same frequency and phase; they are designed for generating flow speed pulsation with frequency and amplitude required. The remaining two shafts are designed for pulse shape correction. Their rotation frequency is two times the rotation frequency of four shafts.

Every shaft is located in a separate channel bounded by parallel walls. At the entry of some channels, shutters for passage cross-section area variation are installed. Owing to the shutters the fluctuation amplitude or degree of correction of the pulse shape can be controlled.

Fig. 3 shows the schematic of the wind tunnel ejector. It has 16 nozzles located at the periphery. The multi-nozzle ejector was chosen owing to its capability of generating less noise than the one-nozzle ejector with a central or annular nozzle.

2. TEST SECTION FLOW CALCULATION

The test section flow was calculated on the basis of a one-dimensional model by using the flow rate and momentum equations [1]. The flow downstream of the pulser was considered as a flow in an abrupt duct expanding. The total pressure losses upstream of the pulser were assumed to be absent.

Flow rate equation

$$P_0 F_1 q(\lambda_1) = P_0 F_2 q(\lambda_2) = P_0 F_3 q(\lambda_3) \quad (1)$$

Momentum equation

$$z(\lambda_3) = z(\lambda_2) + \left(\frac{\alpha+1}{2} \right)^{\frac{1}{\alpha-1}} \frac{P(\lambda_2) (F_3 - F_2)}{q(\lambda_2) F_2} \quad (2)$$

where $q(\lambda)$, $P(\lambda)$ and $z(\lambda)$ are the gasdynamic functions.

$$q(\lambda) = \left(\frac{\alpha+1}{2} \right)^{\frac{1}{\alpha-1}} \lambda \left(1 - \frac{\alpha-1}{\alpha+1} \lambda^2 \right)^{\frac{1}{\alpha-1}}$$

$$P(\lambda) = \left(1 - \frac{\alpha-1}{\alpha+1} \lambda^2 \right)^{\frac{\alpha}{\alpha-1}}$$

$$z(\lambda) = \lambda + \frac{1}{\lambda}$$

$$\lambda = \frac{V}{a_*}$$

Upon determining the value λ_3 from Eq. (2) and substituting it into Eq. (1) we obtain relative total pressure losses in flow in the pulser.

$$\delta_1 = 1 - \frac{P_{03}}{P_{02}} = 1 - \frac{F_2 q(\lambda_2)}{F_3 q(\lambda_3)} \quad (3)$$

To determine the summary total pressure losses in the wind tunnel circuit upstream of the ejector, the drag losses are to be calculated as well; this can be made by the following equation:

$$\delta_2 = \xi \frac{P_3 V_3^2}{2 P_{03}} = \xi \frac{\pi}{2} P(\lambda_3) M_3^2 \quad (4)$$

When compared with the test data obtained in the pilot wind tunnel the value ξ can be assumed to be equal to $\xi = 0.5$. Summary total pressure losses

$$\delta = \delta_1 + \delta_2$$

calculated by Eqs. (1), (2), (3), and (4) are given in Fig. 4 as a function of the reduced velocity λ_1 in the test section at different values of parameter $\varphi = F_2/F_3$, which correspond to different values of the pulser passage area F_2 . In calculations F_1 was taken to be equal to 0.28 m and F_2 to 0.342 m

The ejector characteristics correspond to $\delta = \text{const}$ at constant ejection air pressure. Fig. 5 shows relations between λ_1 and φ corresponding to $\delta = \text{const}$. These relations are the main characteristics of the wind tunnel of the concept under study. They allow the reduced velocity λ_1 in the test section to be calculated at different pulser passage areas F_2 and within different pulser operation regimes. These relations enable also the speed pulsation shape, that is, λ_1 as a function of time t to be determined.

3. CALCULATION OF FLOW SPEED PULSATION SHAPE

The pulser passage area is specified by the pulser shafts projection onto the wind tunnel cross-section area. This projection area for the elliptic shaft is as follows:

$$s = \ell \sqrt{c^2 \cos^2 \theta + b^2 \sin^2 \theta}, \quad (5)$$

where

c, b are the small and large ellipse axes,
 ℓ is the shaft length,
 θ is the angle between the large ellipse axis and the wind tunnel axis.

Fig. 6 yields the relation between the reduced test section velocity λ_1 and the angle θ obtained by using the data in Fig. 5 and Eq. (5). The calculation was performed for $\delta = 0.1$ and $\delta = 0.15$. The ratio of the ellipse axes is as $b/c = 3$.

Analysis of these curves shows the relations to be smooth enough but their shapes to differ significantly from the sine one. In the upper part the pulsation curve becomes remarkably elongated.

In order to approximate the pulse shape to the sine curve, one of correcting pulser shafts is employed. It rotates at a frequency twice as fast as the main pulser frequency with the

shaft turned by 90° relative to the main shaft position $\theta = 0$ in the initial state. The channel, where the correcting shaft is installed, is equipped with a controllable shutter by means of which the control shaft action can be regulated.

Fig. 7 shows the reduced velocity λ_1 functions of the angle θ , obtained by using the optimum correction. The curve shape does not practically differ from the sine one.

The data in Figs. 6 and 7 correspond to the quasi-static action of the pulser, that is, according to condition $f \rightarrow 0$. At significant rotational frequencies (of about 10 Hz) of the pulser shafts wave distortions can arise in flow caused by wave motion from the pulser up to the test section upstream of the flow.

The pulser action is transferred into the test section not momentarily but with some lag. The wave transferring the disturbance moves at the sound speed a . While moving this wave is drifted by the opposing flow with the velocity v . Consequently, the real wave motion velocity relative to the duct walls is equal to $a - v$ and the time of the wave transit is

$$t = \frac{L}{a - v}$$

where L is the distance between the pulser and the model location in the test section. In the wind tunnel under consideration this distance is equal to about 1 m. Different degree of the wave lag for different pulse sections results in distorting the curve shape; the time of velocity decreasing becomes less than the time of its rising.

In order to decrease this type of distortions, the second correcting shaft of the pulser is used. Its rotational frequency is the same as this of the second shaft and in the initial position it is turned by 45° relative to the initial location $\theta = 0$ of the main shafts. Calculations carried out by authors show that in some regimes of the wind tunnel operation wave distortions can be eliminated effectively using this shaft.

Fig. 8 shows some relations between the test section flow velocities and the time with pulse frequency of about 10 Hz (rotational frequency of the main shafts is 5 Hz) and $\delta = 0.1$ with the presence of wave distortions and with the second correcting shaft operating. The velocity pulse shape was approximated to the sine curve.

Fig. 9 gives the same relations but obtained at $\delta = 0.15$. The velocity varies with an abrupt drop at some time moments. It means that shocks are generated in flow. The correcting shafts cannot improve the situation.

Investigation carried out by authors showed the shock waves to be generated at transonic flow velocities.

Fig. 10 yields data on the upper velocity region boundary, where no shock waves arise, as relations between the maximum instantaneous velocity V and the pulse frequency f at different relative pulse amplitudes, $\overline{\Delta V} = \Delta V / V_{cp}$.

4. TESTING OF THE PILOT WIND TUNNEL

An experimental study of the pilot wind tunnel with flow speed pulsation was performed to investigate wind tunnel capabilities of generating flow with regular pulses and with smoothly changing velocity. The size of the test section was 150×110 mm. The wind tunnel pulser had only one rotating shaft with 30 mm and 90 mm axes. There were no correcting elements.

Fig. 11 illustrates one of the records of velocity variation time history in the test section. The diagram shows clearly enough the nature of velocity variation and its distinctions from the sine curve.

However, the main result of this investigation is that the capability of generating stable and regular flow speed pulsation in the test section with essential frequencies and amplitudes was shown.

5. CONCLUSIONS

The main features of a subsonic wind tunnel with flow speed pulsation are presented. The pulses are generated by rotating the elliptic parallel shafts installed across the wind tunnel duct downstream of the test section. Calculations and tests

were carried out to develop a wind tunnel with a 0.4 (W)×0.7 (H) m test section. Special attention was given to development of means of correcting the velocity pulse shapes with the aim of approximating them to the sine curve.

It was also shown that shock waves can be generated in the flow. The upper velocities at which no shock waves are generated have been determined. This boundary depends on the value of the pulse frequency and relative amplitude.

6. REFERENCES

1. Abramovich, G.N., "Applied Gas Dynamics", GITTL, 1951.

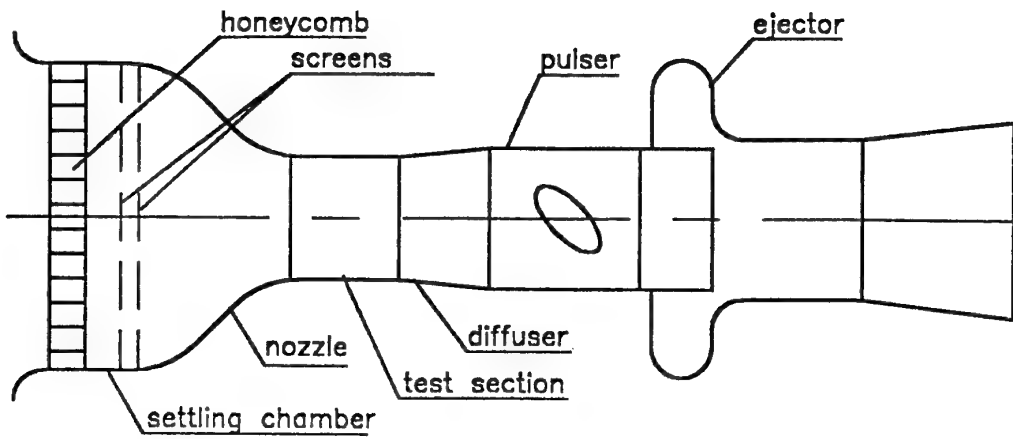


Figure 1. Schematic of the wind tunnel

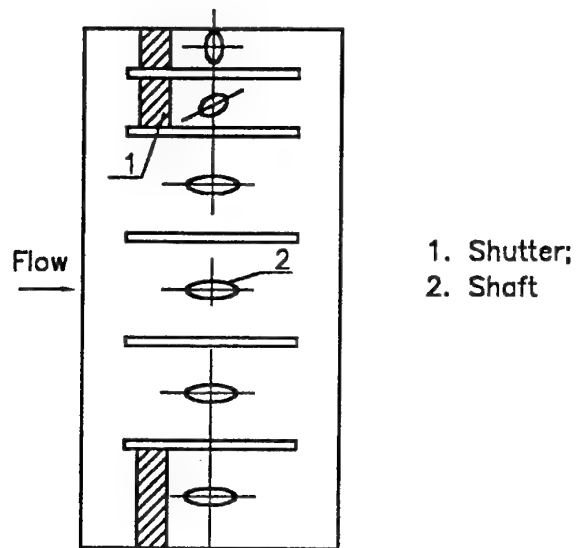


Figure 2. Schematic of the pulser.

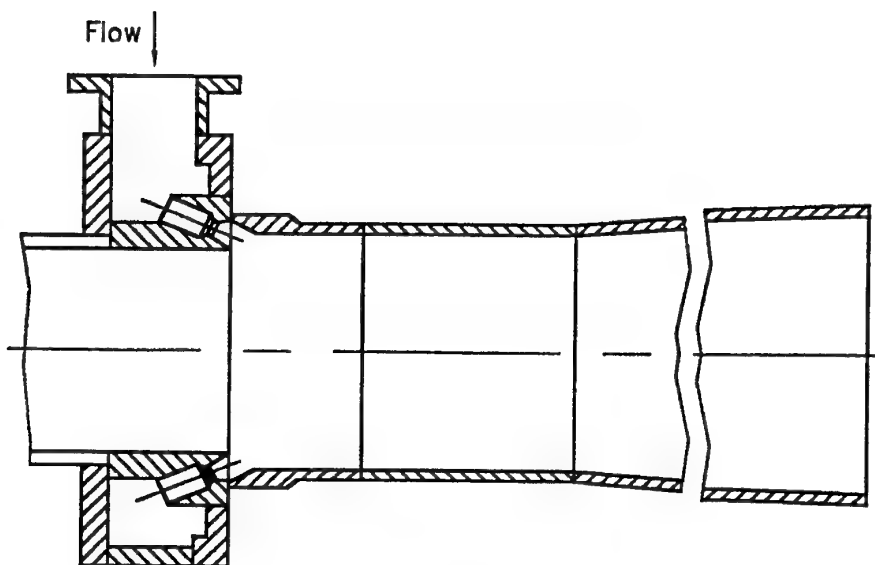


Figure 3. Schematic of the ejector

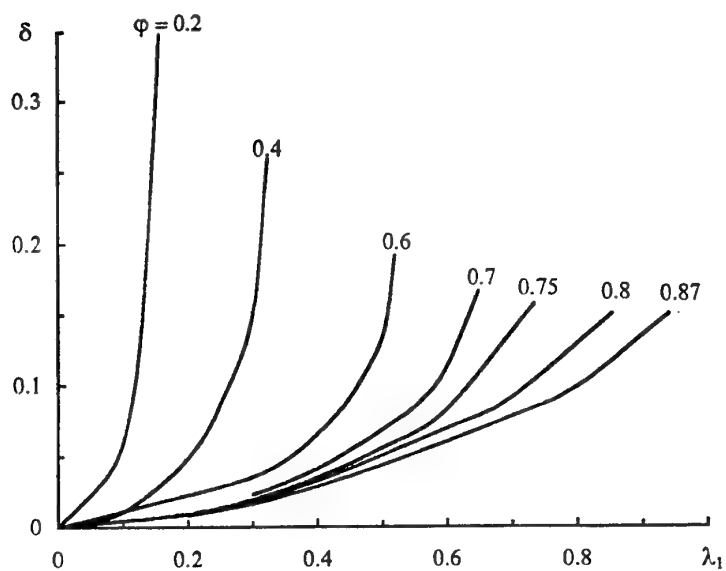


Figure 4. Stagnation pressure losses.

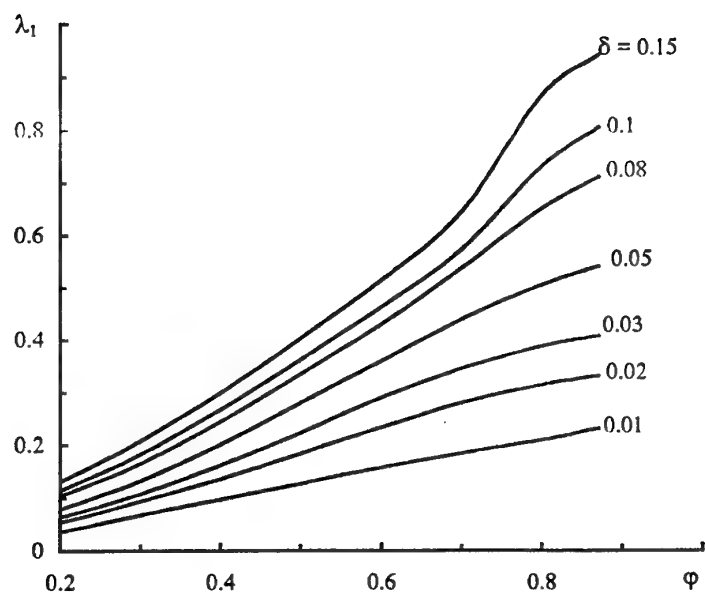


Figure 5. Influence of the pulser section area on the test section velocity.

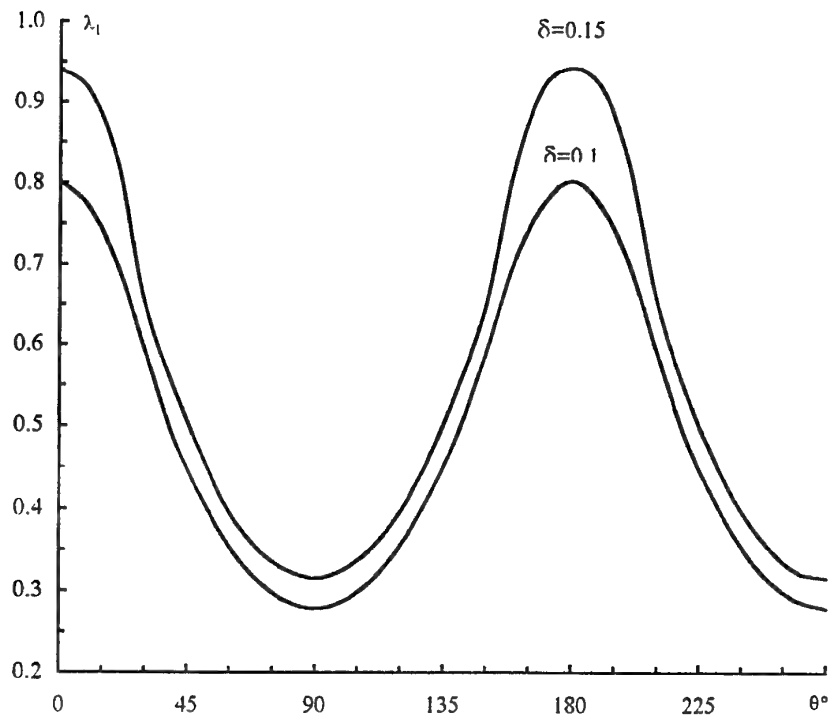


Figure 6. Velocity pulse shape without correction; $f \rightarrow 0$

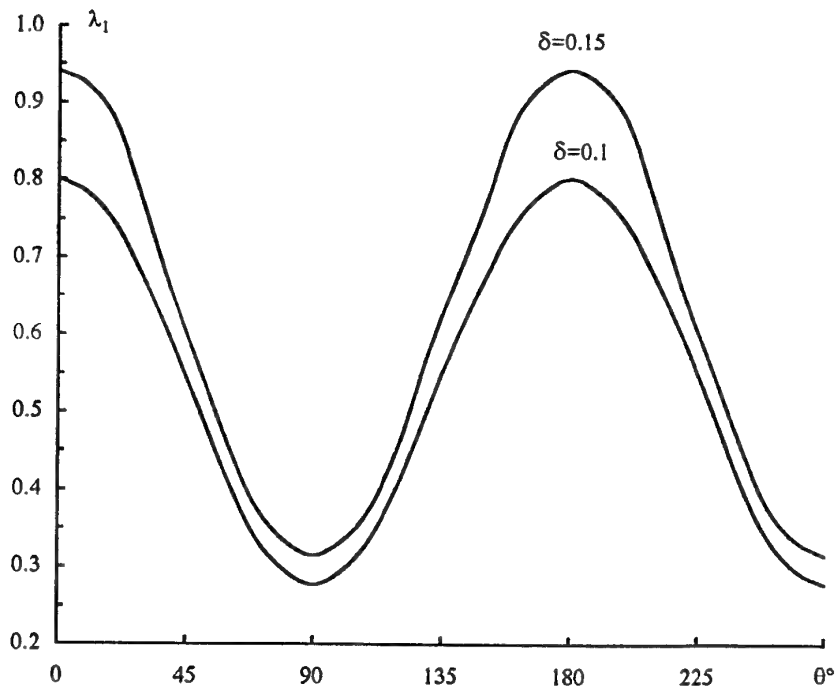


Figure 7. Velocity pulse shape with correction; $f \rightarrow 0$

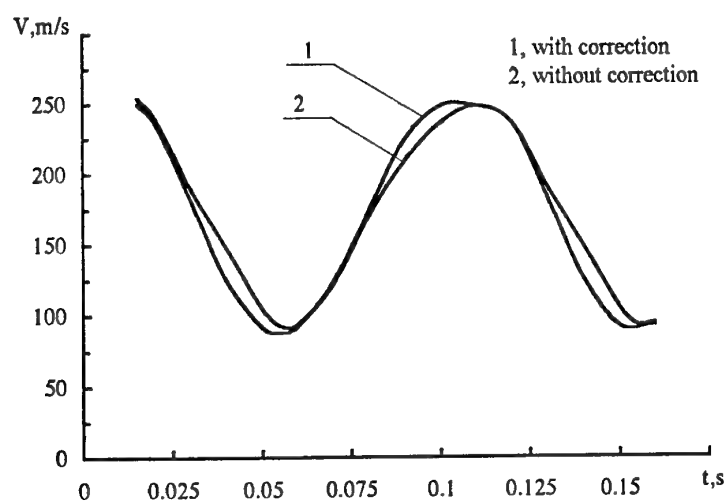


Figure 8. Velocity pulse shape; $f=10$ Hz, $\delta=0.1$.

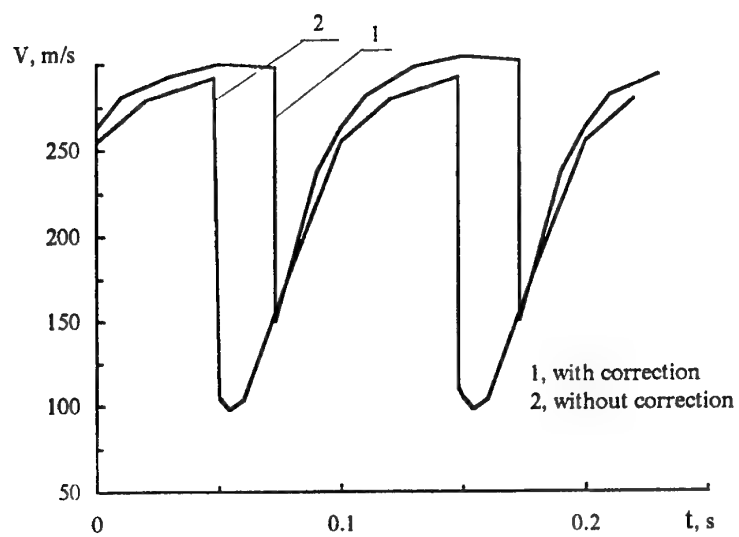


Figure 9. Velocity pulse shape; $f=10$ Hz, $\delta=0.15$

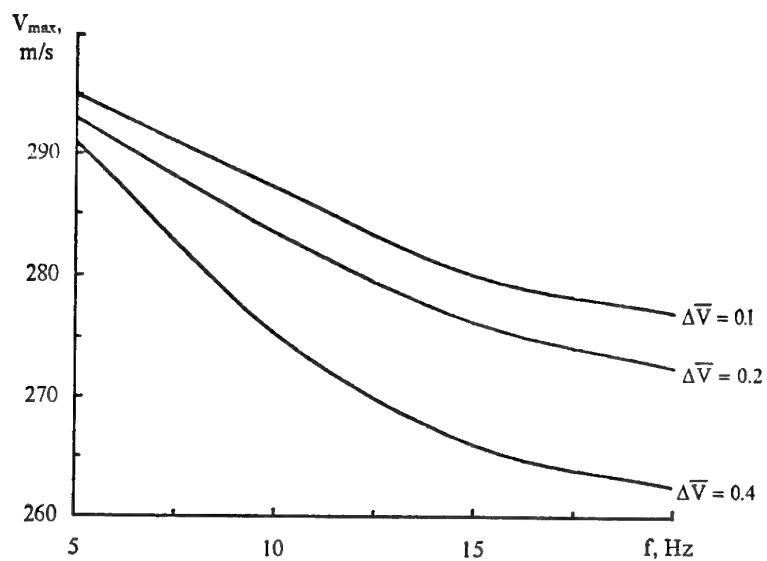


Figure 10. Upper flow velocities without shock waves

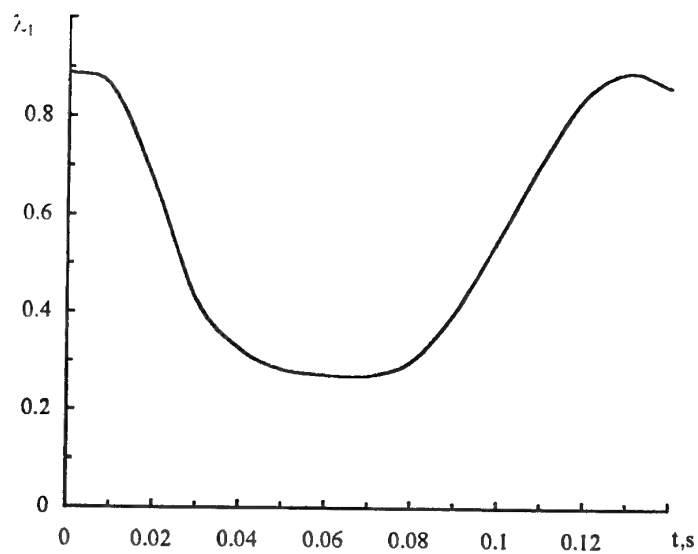


Figure 11. Velocity pulse shape. Experiment $f=10$ Hz.

Aerodynamic Design of a Civil-Aeronautical Low Speed Large Wind Tunnel

G. Gibertini and L. Gasparini

Dipartimento di Ingegneria Aerospaziale, Politecnico di Milano
via Golgi 40, 20133 Milano, Italy

A. Zasso

Dipartimento di Ingegneria Meccanica, Politecnico di Milano
p.za Leonardo da Vinci 32, 20133 Milano, Italy

SUMMARY

The new Civil-Aeronautical Low Speed Large Wind Tunnel is presented, which will be constructed in the next future at the Politecnico di Milano. This unconventional facility will allow for both civil-environmental and aeronautical researches, respectively in a very large (14x4 m) low-speed test section and in a conventional high-speed test section (4x4 m). Based on the results of preliminary tests on a 1:9 scale model the design of some critical components was reviewed. This includes the numerical optimisation of the contraction ahead of the aeronautical test section, the inverse design of a new thick section for the corner vanes and an improved configuration of the bends upstream the civil-environmental test section. Tests performed to check the effectiveness of the proposed modifications, although showing that some work is still need to fulfil the specified requirements, confirmed the feasibility of this very peculiar wind tunnel.

1 INTRODUCTION

At the Politecnico di Milano a new Civil-Aeronautical Low Speed Large Wind Tunnel (WT) will be constructed in 1997. This project is a research collaboration between the Mechanics and Aerospace Departments. The effort aims at building a single wind tunnel to be used for both aeronautical and civil-environmental purposes.

This very peculiar WT will be characterized by the presence of two test sections located on the opposite sides of the aerodynamic circuit. The first is an extremely large (14x4 m), low-speed, test section which allows for earth boundary layer simulation through conventional passive systems. This will be used for aeroelastic testing of civil structure as

well as for wind engineering and environmental applications. The second is a smaller, conventional, aeronautical test section (4x4 m) which will be especially employed for research in the fields of aeroelasticity and active control systems. These applications do not demand very high flow quality, however they do require very large test sections, particularly in the case of civil-environmental research. Once operative, the new Civil-Aeronautical WT will so provide an experimental facility presently unavailable in Italy.

Since it will be part of a new campus in the suburbs of Milan, the plant is considerably very compact, given the width of the low-speed test section and the limited size of the building in which the wind tunnel must fit. This makes the fulfilment of the project requirements a challenging task.

The general layout of the plant is first described in the following text of the paper. It results from a provisional project previously developed at Politecnico di Milano [1],[2]. The work completed up to now by the authors is then addressed: a reduced scale WT model was tested and critical points were identified in the aerodynamic circuit. An improved design was then proposed for some critical components, and the effectiveness of the new solutions was checked through further testing.

2 ORIGINAL DESIGN

The main target specifications of the Civil-Aeronautical WT are summarised in tab. 1. Here $\Delta U/U$ is the relative deviation of the flow speed from the average value, and T_{ux} is the average turbulence intensity of the longitudinal velocity component. The concomitant presence of two test sections necessarily led to a compromise solution. As a consequence, lower values of the wind speed and of the flow quality indicators in the high-speed test section

Civil-Aeronautical Low Speed Wind Tunnel		
Max. power installed 1.5 MW		
Test section	Civil	Aeronautical
Size m	13.8x3.8	4x3.8
Max speed ms^{-1}	> 14	> 50
$\Delta U/U$	< $\pm 2\%$	< $\pm 0.2\%$
T_{ux}	< 2%	< 0.2%

Table 1: General specifications.

were accepted, compared with conventional aeronautical WTs.

2.1 General layout

The WT facility will be located in the new Bovisa Campus of Politecnico di Milano, therefore the overall plant size was strictly limited to a maximum of 50x15x15 meters, not including offices, control rooms and models assembling rooms. A minimum width of about 14 meters was mandatory for the civil-environmental test section, to ensure size compatibility of aeroelastic bridge models with Danish Maritime Institute (DMI) Very Large WT facility [3]. Also, a long straight run was required upstream of the civil-environmental test section, to achieve an accurate earth boundary layer simulation. These constraints justify the unconventional design chosen in the original project [1],[2]. Its general layout is shown in fig. 1.

The plant is a closed circuit wind tunnel with vertical return duct. A very peculiar characteristic is the presence of two different test sections: one is dedicated to civil-environmental applications while the other is designed for aeronautical applications requiring moderate flow qualities and wind speed.

The array of 14 fans, each having a diameter of 1.8 meters and driven by a 100-KW a.c. electric motor, had to be placed downstairs: this was the only acceptable solution from the structural point of view. The fans are thus located on the same leg of the aeronautical test section, just ahead of bend number 1 (in the following, corners will be numbered starting from this one and going downwind). The 14 ducts continue through bend number 1 and 2, after a short transition from the circular to an almost square, constant, cross-section. The separation of the ducts was conserved, in order to allow for an active control of the flow velocity distribution in the upper test section; this will be obtained through an independent electronic variation of the rotating speed of the fans.

The heat exchanger is positioned just downstream of bend number 2 and is followed by a settling chamber with the honeycomb and the screens. It will be designed to allow for horizontal thermal stratification of the flow, thus simulating earth boundary layer conditions for environmental testing.

The limited space available did not permit to insert a contraction in front of the civil-environmental test section. A similar solution was adopted in the DMI wind tunnel too. On the contrary, a huge plant recently built in Japan [4], devoted to the aeroelastic testing of bridge models, does have a conventional contraction. Although simpler, the present solution will require more dissipative screens in the settling chamber to achieve the target smooth-flow quality in the test section. This last is 13.8 m wide by 3.8 m high and is located at the end of a 35 meters long, constant section, duct.

Downstream from bend number 3 and 4, a very short leg remained (about 35 meters long) for the second settling chamber, the contraction, the high-speed test section and the diffuser. Therefore, the settling chamber is very short (2 meters) and the two-dimensional contraction has a limited area ratio of 3.46 to 1. This gives a 4 m wide by 3.8 m high aeronautical test section which is 5 meters long. The test section will be interchangeable, allowing for out-of-the-line assembling of the models, and an open-jet test section will be provided too. Finally, in order to limit the diffusion angle and prevent flow separation, the diffuser was subdivided from the very beginning into 14 separate ducts, each running into the corresponding fan.

2.2 Preliminary assessment of the 1:9 scale model

In order to verify the feasibility of the ideas at the base of the WT project, a 1:9 scale model was constructed and thoroughly tested. Due to the limited power installed, wind speeds of about 5.5 and 19 ms^{-1} were obtained, respectively in the low-speed and in the high-speed test section. The resulting Reynolds numbers roughly correspond to the lowest possible ones for the full scale WT; infact, this will be operated at flow speeds in the civil-environmental test section as low as $0.5 \div 1 \text{ ms}^{-1}$.

A very limited selection of the measured data is reported in the following. They support the conclusion that the behaviour of the WT is promising, although the project requirements are not completely fulfilled. Therefore, the general layout of the plant may be conserved but some critical components must be improved.

Fig. 2 shows two velocity profiles measured along a vertical line in the center of the civil test section, using screens with different open area ratio in the settling chamber. The wake of the horizontal wall which partitions the duct downstream of the fans up to and including bend number 2 is clearly visible, especially in the velocity distribution that corresponds to the less dissipative of the two screens. Likewise, horizontal velocity profiles were perturbed by the wakes of the vertical dividing walls. Measurements of the average turbulence intensity, quoted in tab. 2, confirmed that the use of more dissipative screens greatly helps to achieve better flow qualities, but it significantly reduces the power efficiency. Therefore, it appears essential to improve the design

Civil test section Average turbulence intensity	
Screen open area ratio	T_{ux}
58%	1.4%
46%	0.8%

Table 2: Measured average turbulence intensity in the civil test section.

of the circuit following the fans up to the settling chamber, if the required flow uniformity is to be obtained.

A similar situation arises in the aeronautical test section where the velocity distribution was reasonably regular, as shown in fig. 3, but far enough from the specified target ($\Delta U/U \simeq 1\%$ instead of 0.2%). Here, the wakes of three vertical walls located in the bends are clearly identified. Although some structures are needed to support the turning vanes their size may and should be greatly reduced. Again, an acceptable turbulence level was measured, using just one screen with an open area ratio equal to 58% in the settling chamber.

A very important evaluation of the original project came from the measured head-loss distribution. Tab. 3 shows the measured head-losses of the individual components, $K_{0i} = \Delta h_i/q_0$, referred as usual to the dynamic head in the high speed test section, q_0 . The WT efficiency is quite low ($K_0 \simeq 1.15$) if compared with conventional aeronautical facilities, but is encouraging considering that this result comes from a first provisional project. In effect, the global figure is not so far from the value $K_0 \simeq 0.86$ declared for the low contraction conditions of DNW facility [5]. For the present plant, the necessary presence of two settling chambers almost doubles the losses due to honeycombs and screens. A heavy loss is also caused by the multi-pipe diffuser and by the short transition

Civil-Aeronautical Low Speed Wind Tunnel	
Component	Head-loss K_{0i}
Settling chamber (aeronautical test section)	0.2
Multi-pipe diffuser	0.22
Fan section, transition ducts and bend 1	0.33
Settling chamber & heat exch. (civil test section)	0.3
Others	0.1
Total	1.15

Table 3: Measured head-loss due to individual components.

ducts downstream of the fan section, as they involve a considerable diffusion too.

These observations confirmed that an improved design was needed for the ducts and bends following the fan section, and rose some questions about the efficiency of the multi-pipe diffuser. Furthermore, flow regularity in the multi-pipe diffuser was strongly influenced by the wake of models positioned in the aeronautical test section, thus suggesting the study of a new, single-duct, diffuser with flow separation control.

3 COMPONENT RE-DESIGN

3.1 Contraction optimisation

As pointed out in the description of the general layout, the unusual configuration of this WT strongly limits the length of the circuit available to the contraction, the high-speed test section and the diffuser. Thus, a short contraction is highly recommended to leave enough space for a relatively long test section and for the diffuser.

After preliminary experimental and numerical investigations of the original contraction, it appeared that some margin existed both to reduce the contraction length and to improve the flow uniformity in the test section. The design of a new contraction was therefore attempted using a numerical optimisation technique.

To obtain an efficient and costless tool, the constrained optimisation algorithm was coupled with

an incompressible, two-dimensional, vorticity based panel method and an integral, turbulent, boundary layer scheme due to Eppler [6]. The potential plus non-interacting boundary layer approximation was considered to be sufficiently accurate for the present purposes, because flow separation was neither observed on the walls of the original contraction nor expected in the re-designed one. This was confirmed comparing the predicted and measured pressure coefficients along the side and upper walls of the original contraction, as shown in fig. 4. Reference static pressure and velocity were taken at points on the axis, respectively at the inlet and outlet section.

The new contraction shape was constructed using simple linear and trigonometric functions. Three free parameters define a family of shapes ensuring slope continuity at the contraction inlet and outlet. The values of the parameters were selected by the optimisation algorithm with the object of minimizing $\Delta U/U$ at a reference station located slightly downstream of the exit section. To avoid separation along the contraction side walls, the predicted value of the boundary layer shape factor, H , was limited. However, it was found that due to the extremely thin boundary layer resulting from the accelerating flow, very low values of the shape factor were predicted near the end of the contraction. This produced unacceptable, highly curved, shapes. Therefore, a second constraint was introduced to limit the value of the velocity along the side walls, so that feasible design could be obtained.

The length of the new contraction was set to be equal to 91.5% of the original one: this is one meter less, so that the length of the aeronautical test section increased from 5 to 6 meters. The boundary layer shape factor was limited below 2.0, with separation being related to a value of $H \simeq 2.8$; also, the Reynolds number was set equal to 500000 based on the inlet diameter and the inlet velocity. This value roughly corresponds to the flow condition in the 1:9 scale model and to a wind speed of approximately 2 ms^{-1} in the aeronautical test section of the full scale facility. Therefore, a wide margin against the risk of separation should be guaranteed in the whole range of testing speeds. Relaminarisation of the turbulent boundary layer was not considered a critical issue due to the moderate area ratio, the high Reynolds number and the turbulence level of the flow. The velocity along the side walls was limited below 3.8 times the inlet velocity, i.e. below 1.1 times the outlet velocity. Approximate initial conditions were given to start the boundary layer computation: however, the final design was checked to be not very sensitive to initial conditions and Reynolds number.

The shape obtained is shown in fig. 5, where it is

compared to the original one. An interesting feature of the new design, not appreciable in the figure, is that it presents a slight over-contraction, as typical of Boerger's contractions [7]. After the new contraction was assembled and tested, the predicted pressure coefficients on the side and upper walls were compared with the measured ones: again, the agreement was satisfactory, as shown in fig. 6. The computed velocity profiles for the original design and for the new one, are compared in fig. 7. They have been computed at reference stations located just downstream of the respective exit section. It may be seen that, despite the reduced length of the new contraction, a significative improvement in the flow uniformity is to be expected. However, measured velocity profiles showed a flow uniformity much lower than predicted: very similar values of $\Delta U/U$ (up to $\pm 1\%$) were founded both for the original and for the new contraction. A check was made to exclude a significant boundary layer effect. It is now believed that such discrepancies are due to non uniform flow conditions upstream of the contraction inlet, resulting from disturbances introduced by other components of the wind tunnel circuit. It is therefore anticipated that the flow uniformity in the test section will improve significantly when all the critical components will be replaced by the re-designed ones.

3.2 Bends modification

As evidenced by the tests conducted on the 1:9 scale model a large head-loss was caused by the rapid diffusion in the short transition ducts just behind the fans, where flow separation occurred. The fact that the motor housings installed in the model were not to scale (having a much higher blockage and a very poor streamlining) surely played a significant role. Nevertheless it was decided to modify the design of the whole assembly composed by bends 1 and 2. The section transition and the diffusion were distributed along the cross leg between the two corners too; this is in contrast with the original design having constant-section cross ducts. Also, since the velocity distribution in the civil-environmental test section was clearly perturbed by the wakes of the dividing walls, these were terminated as soon as possible. They now end just upstream of bend number 2. The resulting design is much more complex than the original one, as shown in fig. 8 and 9. It should guarantee a more regular and efficient turnaround of the flow, improving the power efficiency of the plant as well as the flow quality in the upper test section.

3.2.1 Turning vanes design

Due to the very limited length of the wind tunnel circuit the flow in bends 3 and 4 may be significantly distorted by wakes generated in the upper test section. Similarly, flow in bends 1 and 2 can be disturbed by the presence of the fan-housings causing poor performance of curved-plate vanes. Therefore, a new, thick, turning vane section was designed. The object was to avoid flow separation in a range of $\pm 5^\circ$ about the nominal inflow direction, thus ensuring a complete and smooth deflection of the incoming flow.

An inverse airfoil design method, based on a vorticity panel method, has been used, which is similar to the iterative approach of Kennedy and Marsden [8]. Being based on panel method, it was readily extended to the case of an infinite cascade. It also has a multi-point design capability, in the line of the well known inverse design method originally developed by Eppler [6] and further extended by Selig and Maughmer [9]. This greatly simplifies the task of designing an airfoil section having good performance at more than one operating condition.

A major difficulty was given by the fact that the vanes may operate at very low Reynolds number, as values lower than 100000 may be reached, when performing low-speed civil-environmental tests. As a consequence, a moderate design lift coefficient was selected, $C_L \simeq 0.75$, which corresponds to a gap-to-chord ratio of 0.37. The target velocity distribution is characterized by a significative amount of aft loading. This enables a mild deceleration on the most part of the upper and lower side, resulting in a reduced risk of early separation.

The new section, which has a comfortable thickness of about 12%, is reproduced in fig. 10. In the subsequent fig. 11 the velocity distribution at the nominal incidence is shown. Numerical analyses were based on panel method and integral boundary layer with empirical transition criteria, corrected for rough air conditions as suggested in [6]. They reported no evidence of laminar separation bubbles for Reynolds number as low as 50000 in the whole desired range of inflow directions. A greater level of confidence was obtained testing a 1:9 scale model of corners 1 and 2, fitted with the new vanes. This will be described in the following text.

3.2.2 Bend testing

Since the substitution of the original corners of the scale model with the re-designed ones would have been lengthy and costly, it was decided to test the new configuration for just one of the fourteen sepa-

rate ducts. Therefore a 1:9 scale model of the WT circuit going from the fan section up to bend number 2 was built and connected to constant-section entry and exit duct, as illustrated in fig. 12. A similar model of the original configuration was also built and tested, to be used as reference. Head-losses of the individual elements were measured as well as total head distributions downstream of bend number 2 and velocity components in the vertical plane at a number of different points. Again just a very limited number of results will be presented, to document the superior performance of the new configuration.

As pointed out previously, the commercial fans used in the model produce a poor flow quality, due to a high blockage and a inefficient straightener: thus, the outcoming flow possesses a significant swirl. This fact is clearly evidenced by the velocity vectors measured inside the duct at various points on three different longitudinal planes (evenly spaced across the section), as illustrated in fig. 13 and 14 respectively for the original and for the new design. Although the resulting flow is severely perturbed it is nevertheless obvious that the new vanes turn the flow considerably better, giving a much more regular velocity distribution at the exit of the two corners and reducing flow angularity. Considering that the fans to be used in the real plant will surely deliver a smoother flow, tests were repeated inserting a long straight channel and a screen between the fan and the first corner. The resulting velocity vectors, shown in fig. 15 just for the new solution, indicate a very regular deviation of the incoming flow.

Measured head-losses confirmed that a largely dominant contribution in the aforementioned value of K_{0i} for the fan section, the transition duct and the first bend was due to the very poor fan-housing. Therefore, a much lower value should be attained in the full-scale WT. The measured head-loss for the new configuration, excluding the fan section and the first transition duct, also showed an interesting dependence on the flow speed. Comparing the results obtained in smooth flow conditions at 8.4 and 11.4 ms^{-1} inlet velocity, corresponding to chord Reynolds number of the vanes on the order of 35000 and 47000 respectively, a 20% reduction could be observed. This fact may well be related to laminar separations appearing on the vane suction side at the lower Reynolds number, as suggested by the computations. At the higher Reynolds number, which still corresponds to a very low wind speed at full-scale, the head-loss was already 15% lower than for the original configuration, confirming the superiority of the new solution.

4 CONCLUSION

The tests performed on the 1:9 scale model of the new Civil-Aeronautical Low Speed Large Wind Tunnel support the feasibility of the very unconventional solution resulting from the specific requirements. They also evidenced critical points suggesting to review the design of some major components of the aerodynamic circuit.

The new contraction, designed by numerical optimisation, is one meter shorter; it allows to extend the length of the aeronautical test section from 5 to 6 meters. It should also provide the required flow uniformity. Although this has not yet been achieved, the target should be eventually reached when the scale model will be updated with all the suggested modifications.

A new configuration has been proposed for the circuit downstream of the fan section, including the cross leg and bend number 1 and 2. The solution includes thick turning vanes, whose section was specifically designed for the present purposes. Tests of a single-motor single-duct scale model confirmed an improved flow quality at the turnaround exit as well as a reduced head-loss. It is thus anticipated that the new design will produce a more uniform velocity distribution in the civil-environmental test section and a slight increase in the power efficiency of the plant.

Finally, a completely new solution is now being pursued for the main diffuser, because the current one revealed flow stability problems triggered by the wake of models in the test section. Although not addressed in the present work, the orientation is to replace the multi-pipe arrangement with a conventional wide angle diffuser and to suppress flow separation using passive boundary layer control devices. Results so far obtained on a 1:20 scale model are encouraging.

Maritime Institute", Proc. of the 1st International Symposium on Aerodynamics of Large Bridges, Copenhagen, Denmark, 19-21 February 1992, A. A. Balkema editor, Rotterdam, Netherlands.

- [4] T. Miyata, H. Yamada, K. Yokoyama, T. Kanazaki, T. Iijima, M. Tatsumi, "Construction of Boundary Layer Wind Tunnel for Long-Span Bridges", J. of Wind Engineering and Industrial Aerodynamics, 41-44, 1992.
- [5] M. Seidel, editor, "Construction 1976-1980", DNW, Noordoostpolder, The Netherlands, 1982.
- [6] R. Eppler, "Airfoil Design and Data", Springer-Verlag, Berlin, 1990.
- [7] T. Wolf, "Improvement and Modernization of Subsonic Wind Tunnels", J. of Aircraft, 30, pp. 57-63, 1993.
- [8] J.L. Kennedy, and D.J. Marsden, "A Potential Flow Design Method for Multicomponent Airfoil Sections", J. of Aircraft, 15, pp. 47-52, 1978.
- [9] M.S. Selig, and M.D. Maughmer, "Multipoint Inverse Airfoil Design Method Based on Conformal Mapping", AIAA J., 30, pp. 1162-1170, 1992.

REFERENCES

- [1] E. Chiappella, "Una Galleria Aerodinamica", Aerospace Engineering Degree Thesis (in Italian), Politecnico di Milano, 1995.
- [2] S. De Ponte, G. Diana, M. Falco, A. Zasso, "A New Large Wind Tunnel for Civil-Environmental and Aeronautical Applications", Abstract accepted at the 2nd European & African Conference on Wind Engineering, Genova, Italy, June 22-26, 1997.
- [3] L. Wagner Smitt, M. Brinch, "A New Wide Boundary Layer Wind Tunnel at the Danish

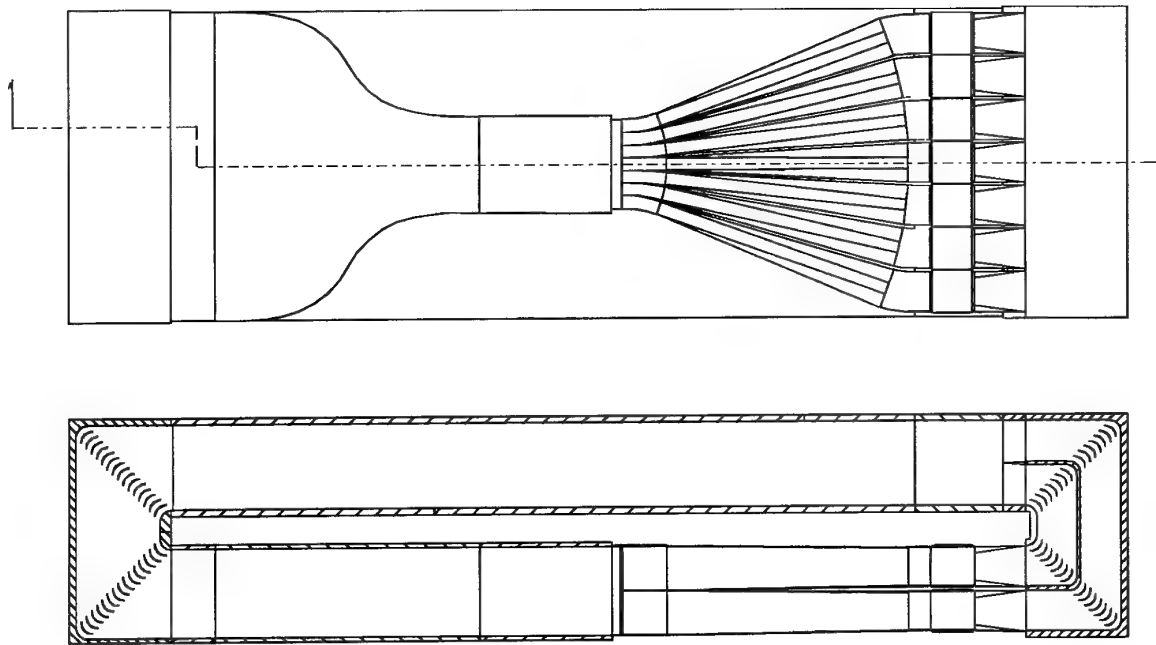


Figure 1: General layout of the Civil-Aeronautical Wind Tunnel: bottom view and longitudinal section.

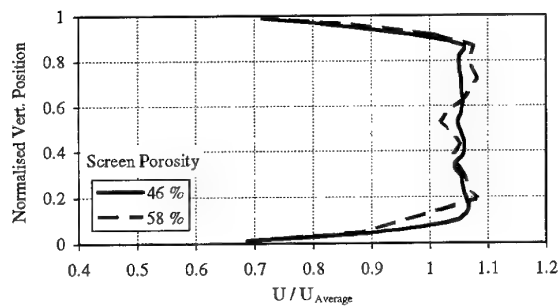


Figure 2: Velocity profile in the civil-environmental test section.

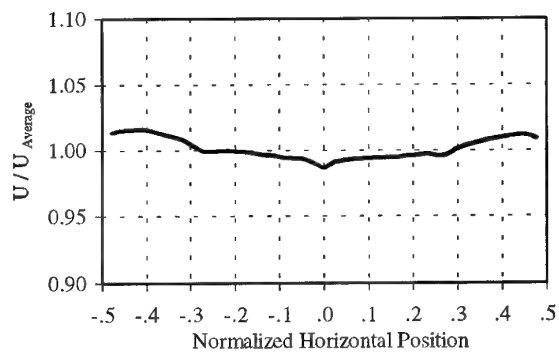


Figure 3: Velocity profile in the aeronautical test section.

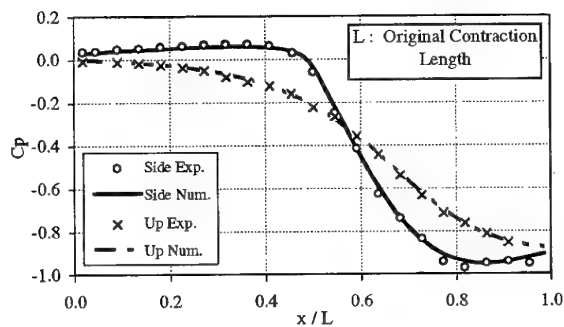


Figure 4: Measured and computed pressure coefficients on the walls of the original contraction.

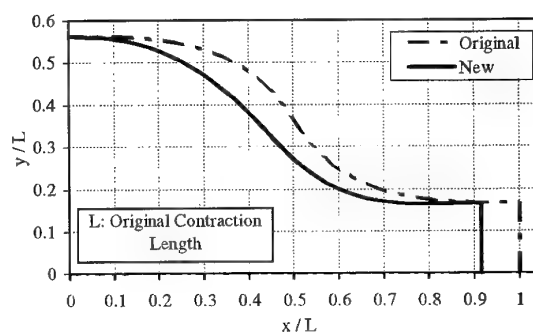


Figure 5: Original and new contraction shapes.

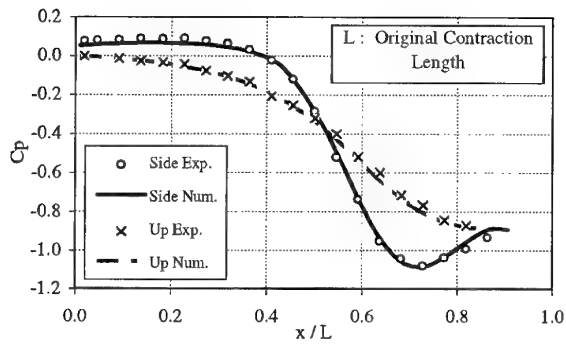


Figure 6: Measured and computed pressure coefficients on the walls of the new contraction.

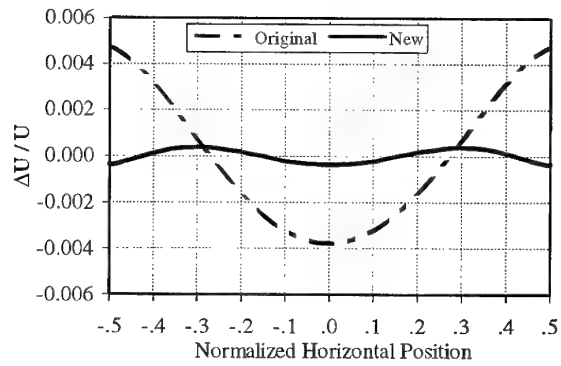


Figure 7: Computed velocity profiles in the aeronautical test section, for the original and new contraction.

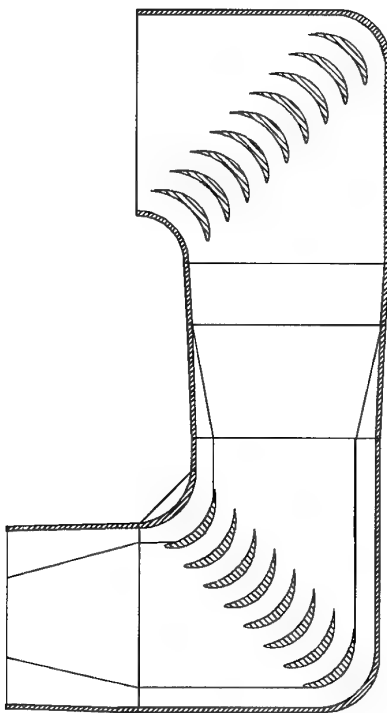


Figure 8: New configuration of bend 1 & 2: longitudinal section of one inner duct.

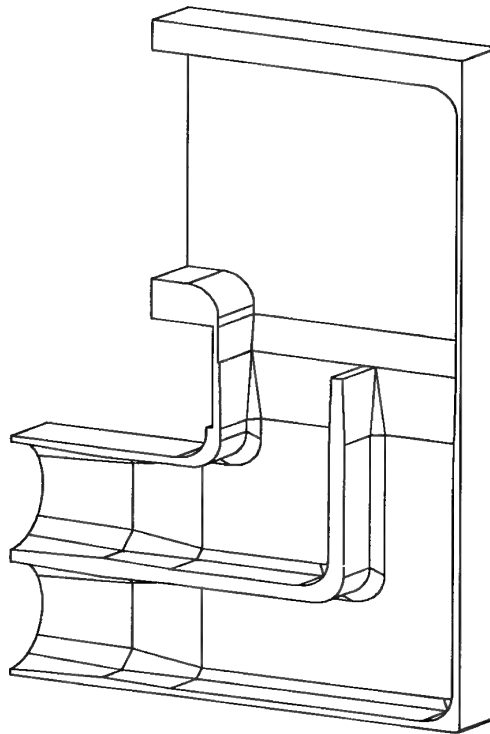


Figure 9: New configuration of bend 1 & 2: axonometric view of the two outermost ducts.

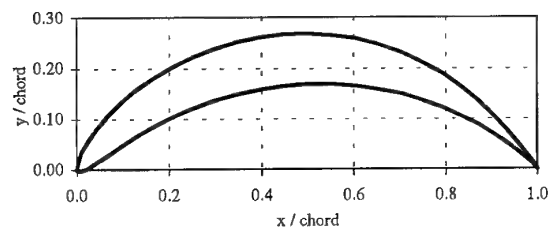


Figure 10: Turning vanes section.

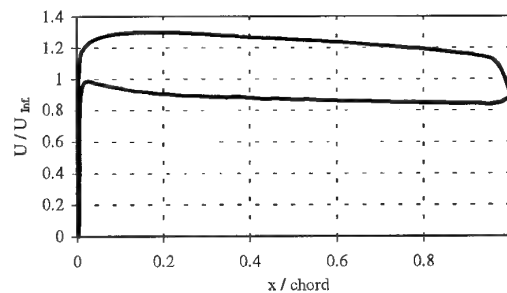


Figure 11: Turning vanes section: velocity distribution at nominal incidence.

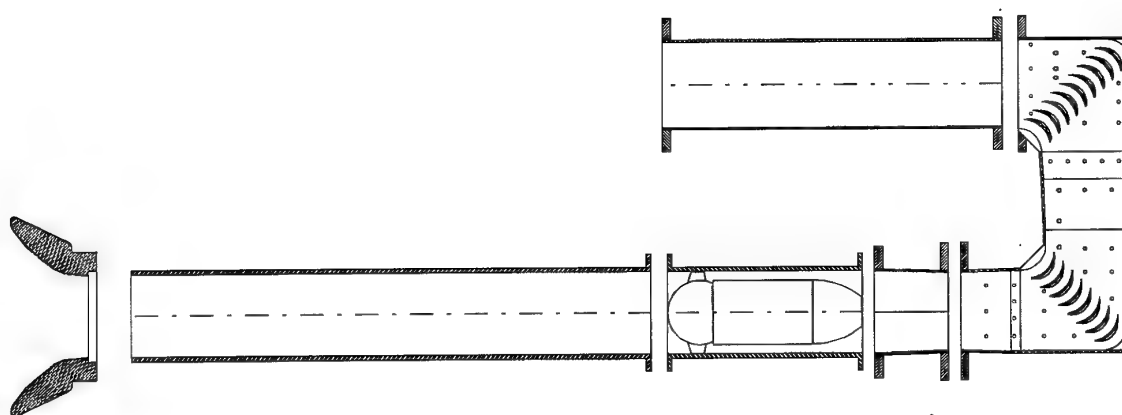


Figure 12: Experimental setup for testing new design of bends 1 & 2.

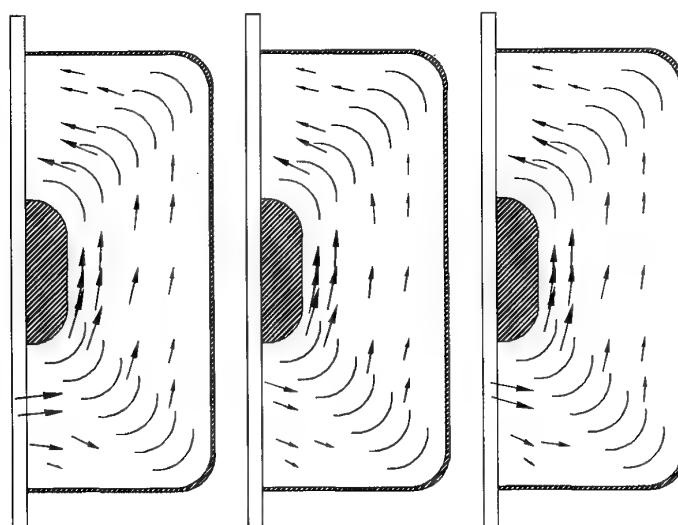


Figure 13: Measured velocity vectors: original bend design.

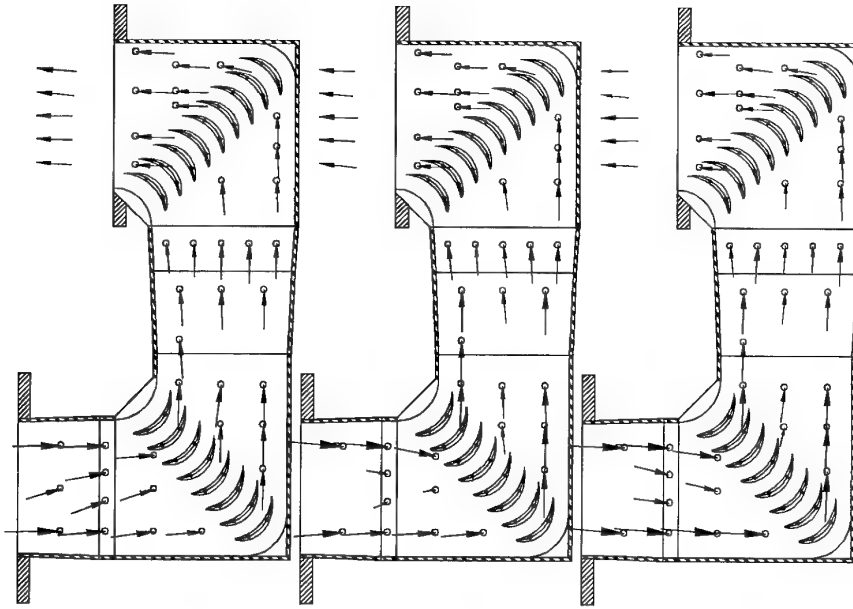


Figure 14: Measured velocity vectors: new bend design.

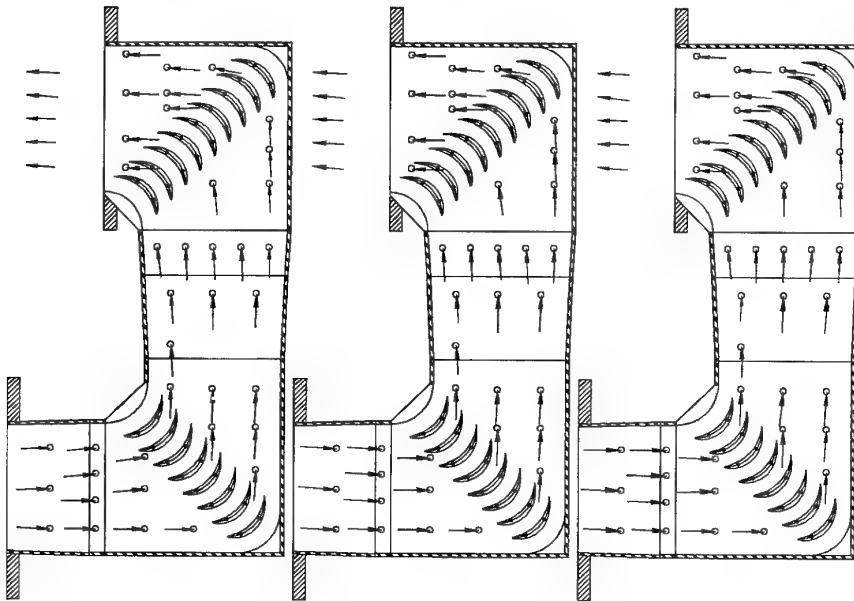


Figure 15: Measured velocity vectors with smooth inflow: new bend design.

Experimental and Computational Aerodynamics Applications for an Icing Wind Tunnel Design

F. De Gregorio, B. Esposito, G. Mingione, A. Vicini
CIRA - Centro Italiano Ricerche Aerospaziali
via Maiorise 81043 Capua (CE), Italy

Summary

The Italian Center for Aerospace Research is committed to design and build a new icing wind tunnel (IWT). The main feature of an icing wind tunnel with respect to a traditional aerodynamic one is to have an heat exchanger to cool the air flux, and a spray-bar, normally located in the settling chamber, to generate water droplets simulating the supercooled water droplets clouds that can be encountered in flight conditions. The IWT will have peculiar characteristics, such as flight altitude pressure and humidity control, and large droplets simulation (larger than those indicated in present FAA regulations). The need for these features has been identified in the preliminary design phase, and their impact on the design has thus been evaluated. In this paper a short description of the main characteristics of the CIRA IWT will be given, and some of the experimental and theoretical studies that have been carried out during the feasibility study will be illustrated.

Notation

LWC	Liquid Water Content (g/m^3)
MVD	Median Volumetric Diameter
S	droplet cross-section
S_w	droplet wetted surface
T, T_d	air, droplet temperature
L_v	water evaporation heat
a_d	droplet acceleration module
c_D	droplet drag coefficient
c_p	water constant pressure specific heat
d	droplet diameter
g	gravity acceleration
h	convective heat exchange coefficient
k	diffusivity of water vapour in air
m	droplet mass
v_r	droplet-air relative velocity
x, y, z	coordinate directions
α_i	angle between the relative velocity vector and i -th coordinate direction
β	impingement efficiency factor
ϕ	relative humidity
μ	air viscosity
ρ, ρ_d	air, water density
ρ_{vs}	saturation water vapour density
σ	water surface shear stress

1. CIRA Icing Wind Tunnel Description

The final IWT project will be realized on the basis of a feasibility study that has been carried out by CIRA. Fig.1 shows the IWT aerodynamic lay-out as developed in the feasibility study.

The IWT will have three interchangeable test sections and an open jet configuration, which performance and cloud simulation characteristics will allow:

- to support the aircraft icing certification phase according to present requirements (i.e. FAR 25 Appendix C⁽¹⁾);
- to verify the effectiveness of the aircraft anti/de-icing systems;
- to support research on ice accretion (studies for improvements of ice accretion models and scaling laws, investigations on altitude effect).

The aerodynamic and structural design of the IWT will also allow to perform icing testing under the FAA/JAA extended certification requirements which are expected to be released in 1997.

The main characteristics of the IWT test sections are summarized in the following table:

	main	secondary	additional	open jet
Height (m)	2.35	2.35	2.35	2.35
Width (m)	2.24	1.15	3.4	2.25
Length (m)	8.	6.		
Max Speed (m/s)	129	214	85	85
Blockage	20%	6%	10%	
Minimum Temperature ($^{\circ}C$)	-32	-40	-32	-32
Altitude (m)	0 to 7000			

The *main test section* will be provided with slotted side walls with fixed porosity and two turntable assemblies at the ceiling and floor walls to allow the model vertical mounting. With this test section it will be possible to simulate ice accretion on full scale aircraft components, it will be possible to reproduce flight conditions of turboprops both in holding, cruise, descent and climb phases and of jet aircraft in the flight speed regime below Mach 0.4.

The *secondary test section* is mainly devoted to bi-dimensional ice accretion tests on real parts of wings

in cruise configuration and descent phase at a maximum Mach number of 0.7. It will be provided with slotted top and bottom walls with fixed porosity, and 2 turntable assemblies on the side walls to allow the horizontal model mounting, and it will be possible to simulate test models with the ice protection system of flight instrumentation and flight sensors (Pitot and static probes, stall warning transducers, etc.).

The function of the *additional test section* is to reproduce the speed of turboprops in the holding conditions (Mach 0.25). It has slotted top and bottom walls with fixed porosity and also the possibility of a closed wall configuration, two turntable assemblies on the side walls, one floor turntable assembly.

Finally, the *open jet configuration* will be used for very large models that cannot be installed in the other test sections.

The test sections will be installed in a plenum having the function of allowing an easier configurations interchange, and an easier interface among test sections, flaps and test section diffuser. The test sections will be lowered into place through a hatch in the ceiling of the plenum by an overhead crane. The plenum will also host an external balance, a model support system, two turntables and an electrical motor (about 150 KW) for rotor testing. The plenum and the whole IWT shell will be designed to withstand the static operative pressure range from 0.39 bar (pressure altitude of 7000 m) to 1.45 bar, a temperature variation from -40°C to $+40^{\circ}\text{C}$, and will be thermally insulated.

Four large *flaps* electrically operated are located at the downstream end of the plenum; their function is to allow the flow which has entered the plenum through the slotted wall to re-enter into the test section and provide clearance for interchanging test sections.

The *fan* is driven by a 3600 kW motor located in a nacelle in the back-leg. The fan system will provide an efficiency higher than 85% for all operative points.

Flow turning vanes are located at each of the four wind tunnel corners and will have the following characteristics:

- the vanes at corners before the fan and before the test section will have the capability of adjusting the flow turning angle of ± 5 degrees to trim the characteristics of the flow;
- the total pressure loss across a corner turning vane will be less than 0.2% of the local dynamic pressure;
- the vanes profile will be designed to minimize the ice collection and the consequent drag rise;
- the vanes at the two corners after the test section will be provided with a de-icing system in order to defrost the corner vanes on demand.

As illustrated in fig. 1, a *honeycomb* panel will be located in the settling chamber upstream of the spray-bar module.

The spray bar system allows the cloud simulation in the wind tunnel, seeding water droplets in the flow at

the settling chamber location just downstream of the honeycomb. In order to meet FAA requirements two *spray bar modules* are foreseen:

- *50 μm spray bar module.* The function of this spray bar is to generate the supercooled water droplets defined in the FAR 25 Appendix C. The stratiform and cumuliform clouds conditions are generated by at least two set of nozzles. The time needed to reach steady cloud conditions at the model location are in agreement with JAR 25.103 Method 1. Each of the about 400 nozzles is supplied by pressurised hot water and compressed air. The spraying nozzles are installed in about 8 bars across the settling chamber. An anti-icing system is also provided to avoid water freezing when the nozzles are not working.
- *300 μm spray bar module.* CIRA is developing a dedicated research program including tests of nozzles in a test bench and in an icing wind tunnel with the aim of designing a new spray bar for large droplets simulation (up to 300 μm MVD).

In order to assure the best cloud distribution, the spray bars will have spray uniformity of $\pm 5\%$ at the contraction inlet. This is obtained by means of a water on/off remote control valve for each nozzle. Furthermore the aerodynamic design of the circuit will guarantee good flow quality at the spray bar location (flow angularity less than 1 degree and speed variation less than 5%).

The spray bar will have the minimum possible size and aerodynamic fairing in order to reduce the aerodynamic interference, with a local aerodynamic blockage less than 20%. The spray bar system will achieve a steady condition in less of 10 sec. for all spray conditions. Water and air flow rate and pressure will be monitored and controlled with an accuracy of 1%; control will be able to change the water and air pressure in order to simulate variable cloud conditions. When the spray bar is in function, the measurement of the inflow air temperature and humidity is monitored and controlled. At the spray bar location humidity will be controlled with an accuracy of 1%, and for a wind tunnel speed less than 80% of maximum test section speed it will be possible to adjust humidity in a range from 70% to 100% for temperatures ranging from -20°C to -15°C and at 70% for temperatures ranging from -40°C to -20°C .

For aerodynamic testing, the spray bar module can be removed and replaced with three turbulence screens.

The *heat exchanger* is mounted in the second cross-leg. The pressure drop caused by the heat exchanger will not exceed 1.35 of the local dynamic pressure per row. The cool down variation will be not less than 2 degree per minute.

An *engine flow simulation* is required to reproduce the air intake inlet flow on the nacelle. A high pressure blower will be used to extract the flow (2 to 55

Kg/sec) from the engine nacelle and inject it back into the wind tunnel circuit at a location downstream of the test section at approximately 100 m/s to minimize the impact on the main fan.

2. Altitude effect

During the preliminary design phase the possible choice to develop a pressurised facility has been considered. The main reasons of this choice can be summarized as follows:

- engine simulation tests: altitude effect allows to simulate the actual flow field (inside and outside the nacelle), accomplishing a correct simulation of ice accretion on any nacelle lip (scaled or not);
- any kind of de/anti-icing system certification;
- the capability to use static pressure as a scaling method independent parameter;
- evaluate the influence of altitude on ice accretion shapes.

Concerning last item, it has been observed that very few data about pressure effect on ice accretion are available^[2]. For this reason, CIRA and NRC (National Research Council of Canada) performed a joint research program, both theoretical and experimental, with the objective of investigating the influence of pressure on ice accretion.

2.1 Experimental studies on altitude effect

All the experimental tests were performed in NRC Altitude Icing Wind Tunnel (AIWT), which characteristics are here summarized:

- test section size (m): 0.57 (h) \times 0.57 (w)
- air velocity: 5 to 100 m/s
- air static temperature: -35°C to +40°C
- droplet median volume diameter: 10 to 35 μ m
- altitude simulation: ground to 7000 m

The test condition matrix stem from CIRA numerical investigation. All of the icing tests were performed on a NACA 0015 airfoil of 35.4 cm chord, which horizontally spanned the entire cross section of the tunnel. The model was constructed of extruded aluminum. At the velocity used for the tests, the Reynolds number based on the airfoil chord was of the order of 2.9×10^6 . Tunnel data acquisition was performed on a personal computer which recorded total and static pressures, total air temperature, fan speed, and other parameters at a 1 Hz rate. Two droplet-size spectrum measuring devices were employed to determine the characteristics of the icing spray prior to the tests (Malvern diffraction device and a forward scattering spectrometer probe (FSSP)). The LWC was determined prior to the experiments through the use of a CSIRO King probe, a hot wire device. In this exploratory set of experiments, only one spray nozzle was used. While this allowed improved test repeatability, the ice which

accreted on the airfoil was not uniform in the span-wise direction. Traditionally, ice accretion profiles are measured through the use of either a casting of the ice in place or the measurement of ice thickness using a hot knife technique. In both cases, the ice accretion is disturbed, and the experiment must be restarted from the beginning. For this study, another technique was attempted. A 20 mW helium-neon laser beam was directed through a cylindrical lens with a horizontal principal axis. This created a vertically oriented laser light sheet, which passed through one of the tunnel viewing windows and was aligned to intersect the airfoil along the centerline of the tunnel. A schematic diagram of this illumination technique is shown in fig. 2. A 35 mm camera was mounted outside the test section viewing almost parallel to the leading edge of the airfoil. With the tunnel room darkened, the camera could record either the profile of the clean airfoil or of the ice accretion. Two miniature light sources were located on the opposite wall of the tunnel and were used to ensure proper registration and thus comparison between photographs of the clean and accreted airfoil. Any possible distortion due to misalignment, i.e. camera not sighted precisely parallel to the leading edge, was removed in the post-processing of the images. The 35-mm images were scanned and the digital images which resulted were superimposed to determine the shape and thickness of the ice accretion. The leading edge of the airfoil and of the ice accretion were obtained by tracing the outlines of these shapes through the use of commercial image manipulation software. One of the advantages of this non-intrusive method of obtaining ice profiles is that experiments do not have to be interrupted in order to obtain an interim measurement of ice accretion. An example of the results obtained through this technique is shown in fig. 3a, illustrating the ice shapes obtained at pressures of 101 KPa (sea level) and 46 KPa (6200 m altitude)^[3].

2.2 Theoretical studies on altitude effect

The theoretical studies have been performed using a numerical model developed at CIRA, structured in three main modules:

- aerodynamic module;
- water droplet trajectories module;
- thermodynamic module.

The aerodynamic module is based on a potential panel method using first order singularities (sources and vortices) distribution.

The droplet trajectories calculation is obtained by using a Lagrangian approach; this module will be described in the following section.

The thermodynamic module is based on the classical Messinger model. To obtain the ice thickness the airfoil surface is divided in elementary control volumes and the ice surface temperature is calculated through a mass and an energy balance. These two balances, coupled with each other, allow the calculation of the

wall temperature and of the non-freezing water fraction; these terms, together with the total amount of water in the control volume, make it possible to evaluate the ice thickness. The terms of the mass balance are:

1. the impinging water;
2. the evaporation/sublimation mass rate;
3. the run-back from the previous volume;
4. the run-back into the following volume.

The terms of the energy balance are:

1. the convective cooling;
2. the sublimation/evaporation energy;
3. the freezing of both the impinging and run-back water;
4. the heating/cooling of both the impinging and run-back water;
5. the heat flux from the airfoil surface.

The driving terms of the energy balance are (1), (3) and (4). The convective cooling (1) is the most sensible term: very often, errors in the evaluation of the ice shape are due to a non correct evaluation of the coefficient of convective heat exchange. In this code this coefficient is calculated from the Reynolds analogy, where it is expressed as a function of the skin friction coefficient, calculated as a function of the wall sand-grain roughness^[4].

The code is able to perform ice accretion calculation on multi-element airfoils, and to evaluate the effect of a thermal anti-icing system. Fig. 3b shows the theoretical ice accretion for the same conditions of the experiment illustrated in fig. 3a. It is interesting to observe that the theoretical results show in this case a large influence of pressure on ice accretion, due to an increased collection efficiency at lower pressure^[5]; the same effect is present in the experimental results, though less evident^[3]. From the experimental and numerical tests it is not possible to derive general conclusions. The influence of altitude on ice accretion is largely dependent on the values of the icing parameters; the main effect is a change in the Ludlam limit, meaning that ice shapes that are rime at low altitudes can be glaze, for the same icing parameters, at higher altitudes.

3. Convergent design

Since the water droplets in the test section simulate the supercooled water droplets clouds that can be encountered in flight conditions, the convergent design is not only ruled by aerodynamics requirements, such as flow uniformity and boundary layer quality; in fact, an uniform spatial distribution of the water droplets in the test section must also be achieved, together with

velocity and temperature values as close as possible to the corresponding ones of the air flow.

3.1 Droplet trajectories calculation

In order to evaluate the characteristics of the droplets cloud in the test section, a droplet trajectories calculation module has been developed. The forces acting on a small droplet moving in a steady air flow are aerodynamic drag and weight; the effect of buoyancy forces is considered as negligible. The droplet temperature is also calculated, including evaporation effects; diameter variations due to evaporation are also taken into account. Therefore, the droplet equations of motion, heat and mass exchange are:

$$\begin{cases} m\ddot{x} &= \frac{1}{2}\rho v_r^2 S c_D \cos\alpha_x \\ m\ddot{y} &= \frac{1}{2}\rho v_r^2 S c_D \cos\alpha_y \\ m\ddot{z} &= \frac{1}{2}\rho v_r^2 S c_D \cos\alpha_z + m g \\ mc_p \dot{T}_d &= h(T - T_d)S_w + JL_v \\ \dot{m} &= J \end{cases} \quad (1)$$

where $J = -kS_w[\rho_{vs}(T_d) - \phi\rho_{vs}(T)]$, and the drag coefficient, c_D , is a function of the Reynolds number based on the relative velocity. The expressions adopted for the evaluation of the function $c_D(Re)$ have been obtained by experimental data^[6].

The derivation of equations (1) is based on the following assumptions:

- Quasi-steady-state approximation (i.e., at each instant and position the steady-state drag acts on the particle).
- Particles of spherical shape.
- Viscous flow effects such as thick boundary layer formation and flow separation are not considered.

The above mathematical model can be considered a valid approximation for typical icing conditions.

3.2 Convergent optimisation

The code developed has been applied to the CIRA IWT geometry. In a first phase, it has been coupled with a 3-D panel method, capable of internal flow modelling^[6].

Starting from the original IWT configuration, output of the preliminary design, a large number of possible modifications have been analysed, assuming a polynomial expression for the convergent shape (with fixed contraction ratio $r_c = 9.5$), with the inflexion point at 50% of its length. Calculations have been performed both for small diameter droplets (lower than $50 \mu m$) and for large diameter droplets (up to $300 \mu m$); in fact, though current FAA/JAA regulations limit maximum droplet diameter to $50 \mu m$ ^[1], evidence exists that droplets of larger size can be encountered during normal flight operations^[7]. For this reason, the capability of simulating large droplets seems an important feature to be considered in the tunnel design.

The tunnel leg taken into consideration comprises part of the settling chamber, the tunnel contraction itself, and the part of the test section up to the model leading edge. The air speed at the inlet is set equal to 13.16 m/sec, for a corresponding speed at the outlet of 125 m/sec. The water droplets have an initial speed of 10 m/s, and an initial temperature of 278°K. The initial temperature of the air has been set to 276°K.

To compare the different configurations, the local impingement efficiency, β , which is locally proportional to the LWC, has been used. For a given surface (a solid body, or, as in this case, the tunnel cross-section), β is locally defined as the droplet flux rate normalized to the free stream flux rate (fig. 4). For each tunnel geometry and droplet size, a number of droplets trajectories have been calculated in the vertical symmetry plane, starting from a uniform spacing at the inlet section. The distribution of β along the vertical direction in the test section has then been calculated; it must be observed that, as the droplets considered move in the vertical plane, the calculated collection efficiency doesn't take into account the contraction in the horizontal plane.

From an analysis of the results the following conclusions have been drawn:

- The impingement efficiency factor distribution in the test section is uniform with good approximation for small droplets (up to 50 μm size); for bigger droplets the distribution is distorted both by gravity effect, and by the effect of the centripetal acceleration which is imposed by the contraction (and which is proportional to the mass of the droplet).
- For a given droplet size, a longer contraction leg produces a more uniform distribution of impingement efficiency factor in the test section, as it imposes a milder gradient of centripetal acceleration to the droplets.

As a result of this investigation, an optimal configuration for the convergent has been devised.

The quality of the collection efficiency obtained in the geometry chosen as best has then been compared with that in the two largest icing wind tunnel in the world: the NASA LEWIS IRT and the BOEING BRAIT. The IRT has a test section of $1.8 \times 2.7 \text{ m}^2$, a maximum speed of 192 m sec^{-1} and a minimum temperature of -40°C . The BRAIT has three test sections: 2.63×1.64 , 1.97×1.31 and $1.64 \times 0.96 \text{ m}^2$, a maximum speed of 180 m sec^{-1} and a minimum temperature of -40°C . Both tunnels don't have altitude control. Since the actual geometries of the tunnels are not available, the calculations have been performed using geometries obtained from aerolines available in literature. In fig.s 5-7 the trajectories of 200 μm droplets in the optimised IWT, IRT and BRAIT (large test section) tunnels are illustrated. Fig.s 9-10 show a comparison of the collection efficiency in the original and optimised

CIRA IWT, IRT and BRAIT tunnels for 50 and 200 μm droplets. It is apparent that for the smaller droplet diameters all tunnels present a substantially uniform collection efficiency, whereas for larger droplets the collection efficiency in the IRT and BRAIT tunnels is greatly distorted as compared with that of the optimum IWT.

3.3 LWC distribution in the test section

In order to carry out a more detailed investigation the aerodynamic flow field has been successively computed, limitedly to the original and optimised geometries, using an Euler solver. For each diameter, about 450 trajectories have been calculated from starting points evenly distributed over the settling chamber cross section; in this way the LWC distribution over the whole test chamber cross-section has been evaluated.

The Euler solver used is characterized by a space discretization based on finite volumes and central schemes, self-adaptative explicit 2^{nd} and 4^{th} order artificial dissipation terms, and an explicit time-stepping integration scheme with multi-grid acceleration^[8].

The contour plots shown in fig.s 10, 11 illustrate the LWC distribution in the test section of the original and modified geometries for 50 and 200 μm droplets diameter; these have been obtained assuming a uniform $\text{LWC}=1$ distribution at the inlet section. Of course, in real conditions the water droplets in a cloud will have diameters distributed somehow around a mean value, with an amount of LWC associated at each diameter; the Median Volumetric Diameter (MVD) of a droplet cloud is defined as that mean diameter for which half of the total liquid water content is contained in droplets of larger size, and half in droplets of smaller size. In this case, the value of a weighted average collection efficiency, $\bar{\beta}$, can be calculated by weighting the β pertinent to each diameter with the corresponding LWC; the corresponding weighted LWC can then be obtained. After choosing the MVD of the cloud to be simulated, the Langmuir-D law has been used to determine the discrete diameter distribution representing the droplets cloud^[9] (for a MVD of 200 μm , this means to consider a minimum droplet size of 62 μm , and a maximum one of 444 μm).

The 3-D plots reported in fig.s 8,9 are the weighted LWC distributions corresponding to MVD of 50 and 200 μm , respectively. From these results it is apparent, especially for the bigger droplets, how the distribution in the modified geometry is more uniform, and covers a larger area of the cross-section. This is also evident from fig. 12, where the weighted LWC distributions are shown in the vertical symmetry plane.

3.4 Droplets characteristics in the test section

From the investigation carried out, the velocity and temperature of the water droplets in the test section result to be essentially independent from the con-

traction geometry, and uniform over the cross-section. Fig. 13 shows the temperature of the droplet moving along the tunnel axis in the optimised geometry, with and without considering the effect of evaporation (with an assumed relative humidity of 70%). Also shown in the figure is the variation of droplet diameter due to evaporation. It is apparent that small droplets have a final temperature close to the air one, whilst large droplets final temperature may be considerably higher than that of the air. By decreasing the air relative humidity it is possible to obtain a lower droplet temperature; as a drawback, a low humidity value may lead to an excessive reduction of droplets diameter, implying the complete evaporation of the smaller droplets. Fig. 14 illustrates the droplet velocity; small droplets are essentially in equilibrium with the air flow, whereas bigger ones show a velocity gap that reaches about 10 m/s in the case of 200 μm diameter. Finally, the same figure illustrates the droplet Weber and Eötvös numbers, that can be used as a criteria to verify droplet breakup. According to the Weber criterion, droplet breakup is avoided if the Weber number, $W = \rho v_r^2 d / \sigma$, is lower than 10; according to the Eötvös criterion, breakup is avoided if the Eötvös number, $E = a \rho a d^2 / \sigma$ is lower than 16.

It is clear that when droplets are injected in the settling chamber, as in the IWT case, there are no problems of droplet breakup. If droplets are injected directly in the test section, before the model, to increase spray uniformity, the large droplets may breakup due to the high air-droplet relative speed.

4 Turning vanes

The turning vanes must be designed to have the lowest ice accumulation, in order to decrease losses and tunnel de-icing time. At this stage an optimization of the turning vanes has not yet been performed, but the capability of the code for ice accretion calculation on multi-element airfoils to simulate ice accretion on turning vanes has been verified. As an example, fig.15 shows the calculation of ice accretion on the turning vanes downstream of the model; to obtain a correct result, the tunnel walls have been included in the geometry.

5 Conclusions

A general description of the CIRA Icing Wind Tunnel, as defined during the feasibility study, has been presented. The results of some experimental and numerical activities carried out during the feasibility studies have then been illustrated.

- *Altitude effect:* experimental tests and theoretical simulations have been performed to understand if pressure can influence ice accretion. Additional studies are required for a better understanding of the phenomenon.
- *Convergent design:* a droplet trajectories model, coupled to a panel method and successively to an

Euler solver, has been used to devise a convergent configuration allowing an homogeneous liquid water content in the test section, for droplets MVD up to 300 μm .

- *Droplet speed:* the difference between droplet and air speed in the test section is negligible for small droplets, whilst reaching values of the order of 10% of air speed for the bigger ones.
- *Droplet temperature:* small droplets reach a temperature close to that of the air, whilst the larger ones may have a higher difference. It is possible to decrease droplets temperature by lowering the air relative humidity, but this can imply the complete evaporation of the smaller droplets.
- *Droplet breakup:* the positioning of the spray bar in the settling chamber will prevent the droplet breakup also for large droplets.

6 References

- ¹FAA, *Aircraft Icing Handbook* (1991)
- ²Bartlett, C.S., *Icing Testing Cloud Simulation Requirements*, AIAA Paper 89-0736 (1989)
- ³Oleskiw, M.M., De Gregorio, F., Esposito, B., *The effect of altitude on icing tunnel airfoil icing simulation*, FAA Icing Conference, Washington, 1996
- ⁴Messinger, B.L., *Equilibrium temperature of an unheated icing surface as function of airspeed*, J. of the Aeron. Sci., Vol. 20, N. 1, pp. 29-42
- ⁵Amendola, A., Mingione, G., Vicini, V., *Some peculiar aspects of an Icing Wind Tunnel Design: Large Droplets and Altitude Effects*, International Icing Symposium '95, Montreal, Sept. 1995
- ⁶Vicini, A., Mingione, G., *Computation of three-dimensional droplet trajectories and temperature for the C.I.R.A. icing wind tunnel*, CIRA-TN-95-0052, Mar.1995
- ⁷Coher, S.G., Isaac, G.A., Straap, J.W., Marcotte, D., *Icing Environments Associated with Supercooled Drizzle*, International Icing Symposium '95, Montreal, Sept. 1995
- ⁸Kassies, A., Tognaccini R., *Boundary conditions for Euler equations at internal block faces of multi-block domains using local grid refinement*, AIAA 21st Fluid Dynamics, Plasma Dynamics and Laser Conference, Seattle (USA), June 1990

Acknowledgments

The authors wish to acknowledge the assistance of the National Research Council of Canada (NRC), our research partner during the joint research program performed at NRC to evaluate the effects of altitude on ice accretion. In particular, Myron M. Oleskiw and Fred Hyde for the contribution in the realization of the tests and the analysis of the results. The authors wish also to acknowledge Luigi Paparone for the assistance in the Euler computations and Paolo Leoncini for the development of the graphical module of the droplet trajectory code.

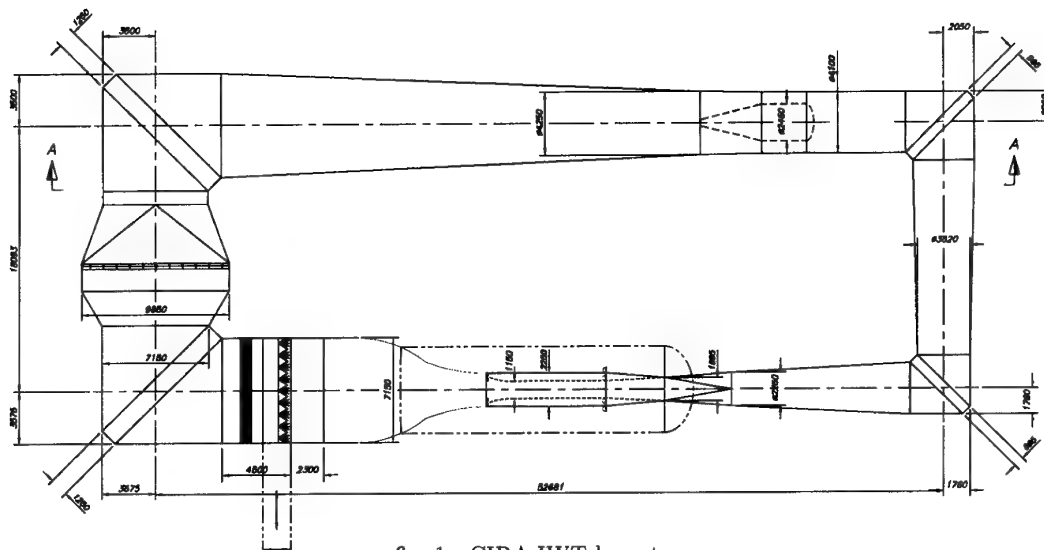


fig. 1 - CIRA IWT layout

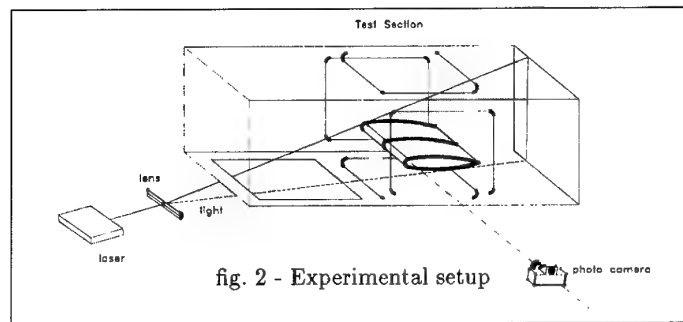
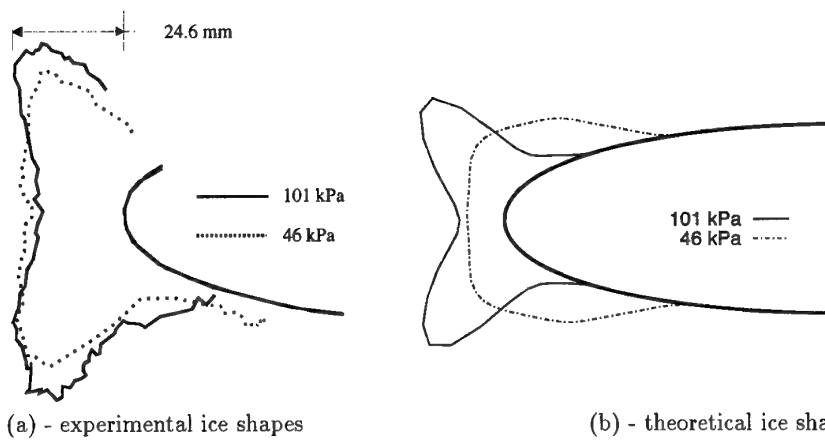


fig. 2 - Experimental setup



(a) - experimental ice shapes

(b) - theoretical ice shapes

fig. 3 - Ice accretion on a NACA 0015 airfoil: speed=95 m/s; MVD=23 μm ; LWC=1 g/m³; T=-10 °C; time=600 s

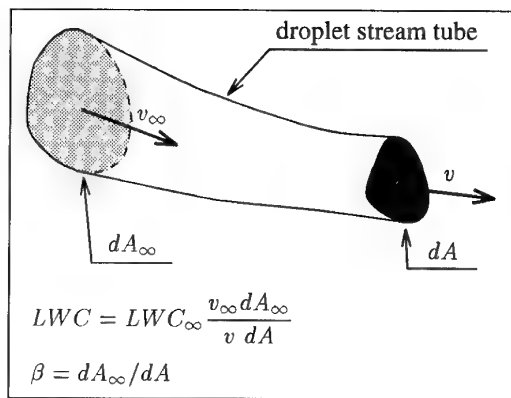
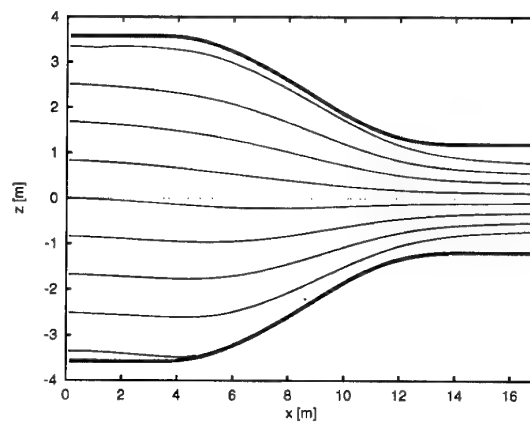
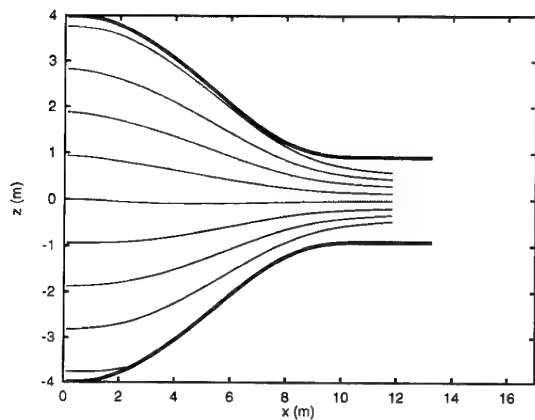
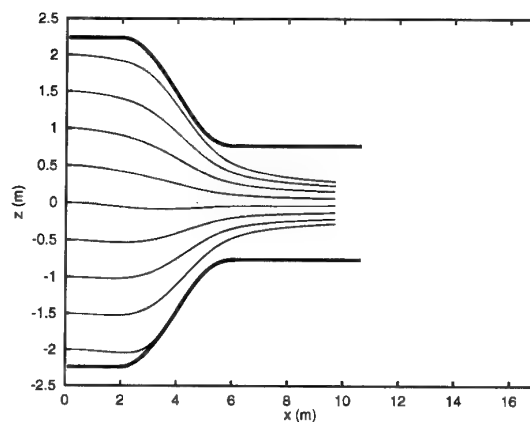
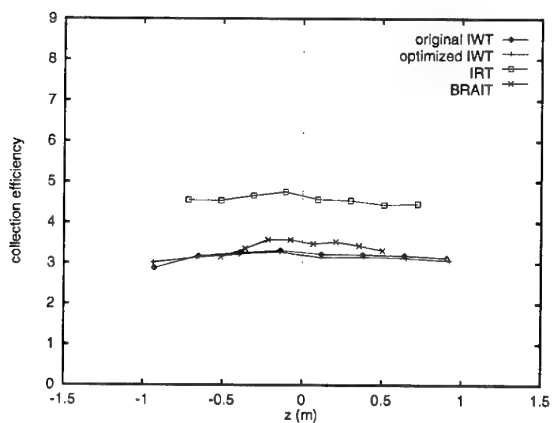
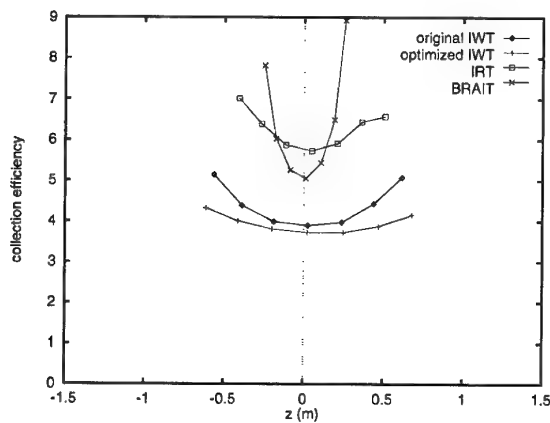


fig. 4 - Definition of collection efficiency

fig. 5 - 200 μ m droplet trajectories in the optimised IWTfig. 6 - 200 μ m droplet trajectories in the IRTfig. 7 - 200 μ m droplet trajectories in the BRAITfig. 8 - Collection efficiency in the test section for 50 μ m dropletsfig. 9 - Collection efficiency in the test section for 200 μ m droplets

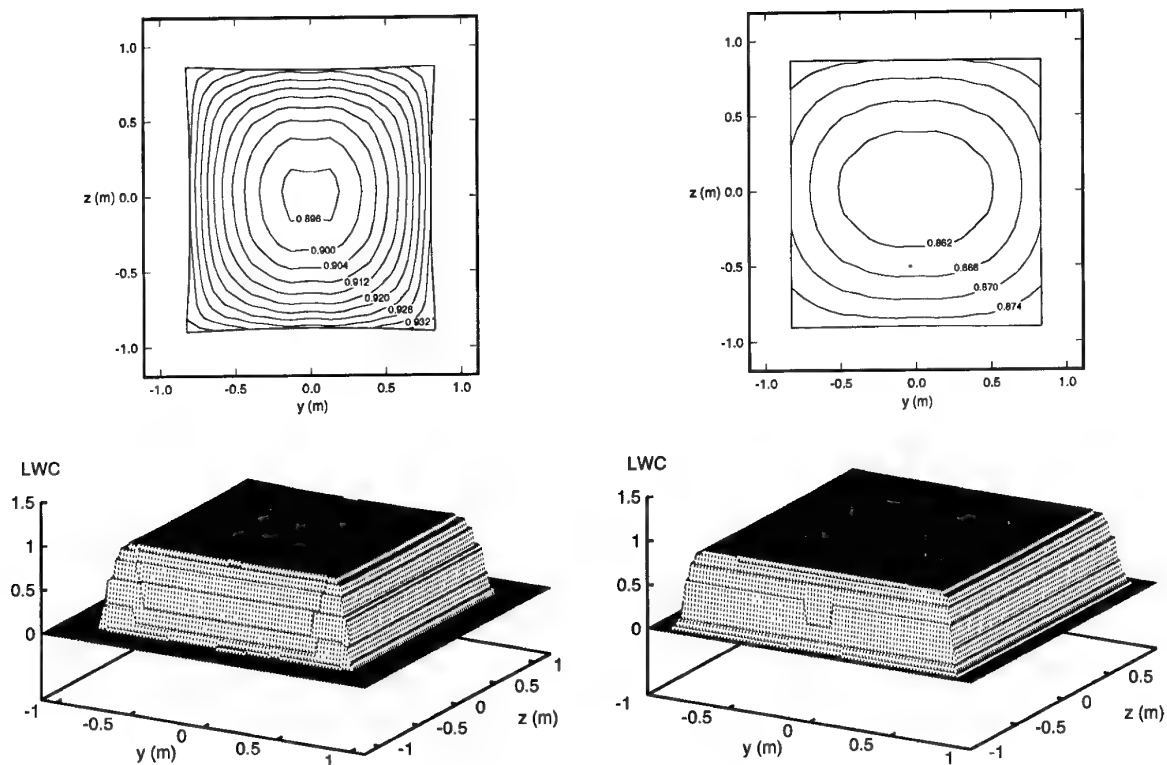


fig. 10 - LWC distribution in the test section - 50 μm droplets; original (left) and modified geometry (right)

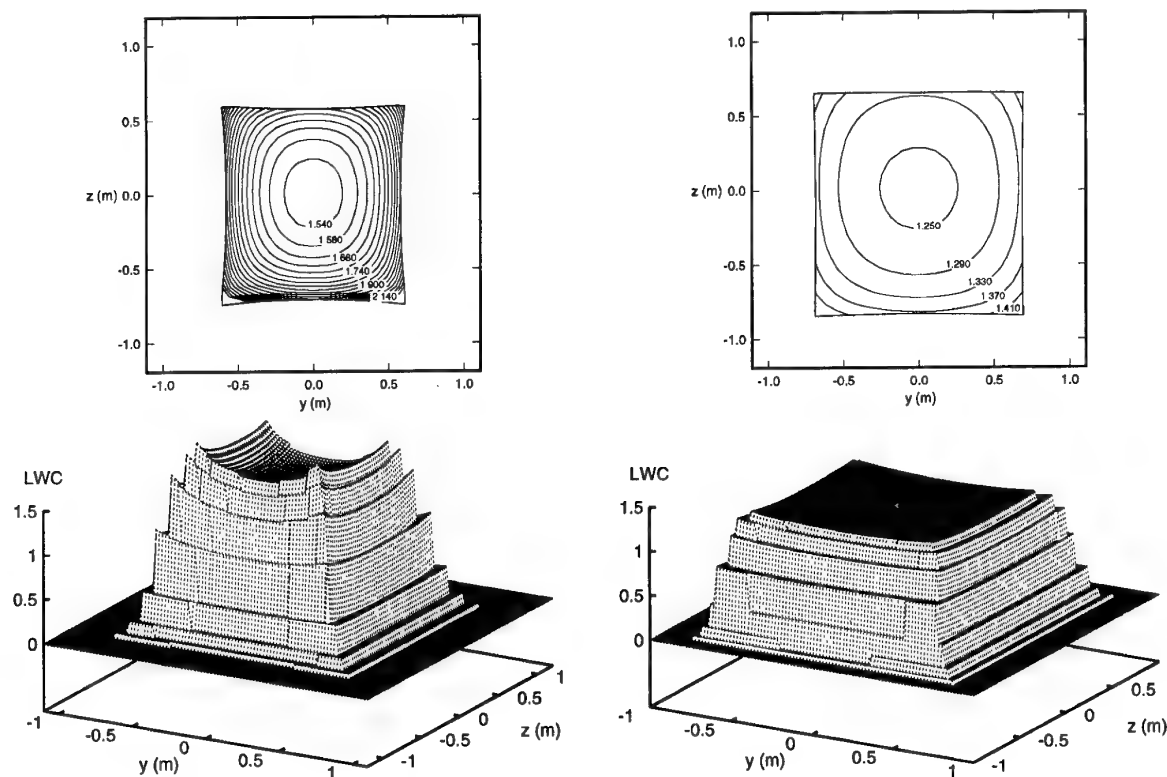


fig. 11 - LWC distribution in the test section - 200 μm droplets; original (left) and modified geometry (right)

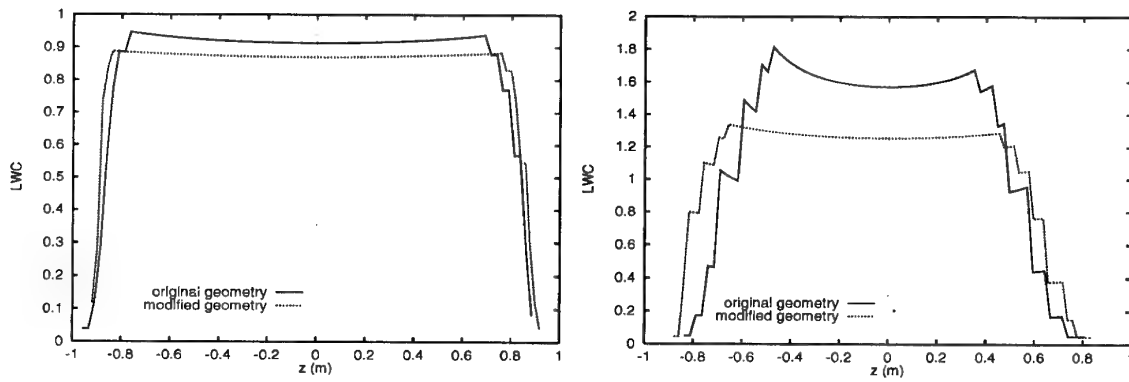


fig. 12 - LWC distribution in the test section (vertical symmetry plane) - 50 μm (left) and 200 μm MVD (right)

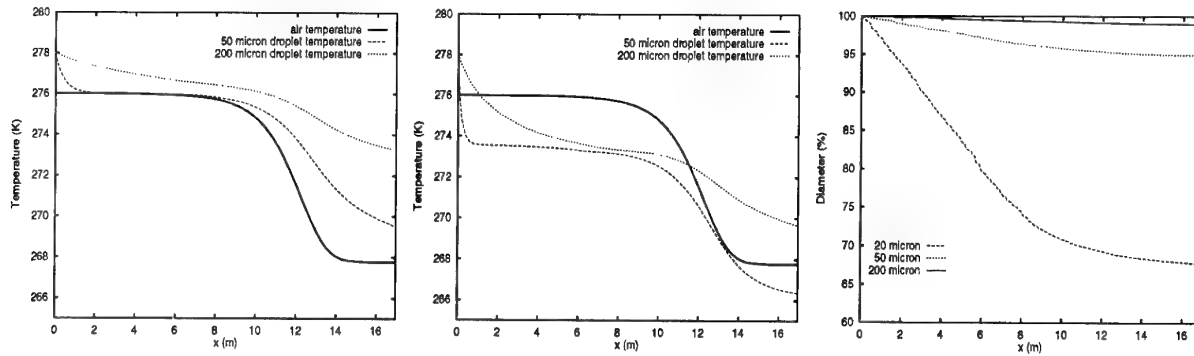


fig. 13 - Effect of evaporation: droplet temperature along tunnel axis without (left) and with evaporation (center; 70% humidity assigned); on the right, variation of droplet diameter

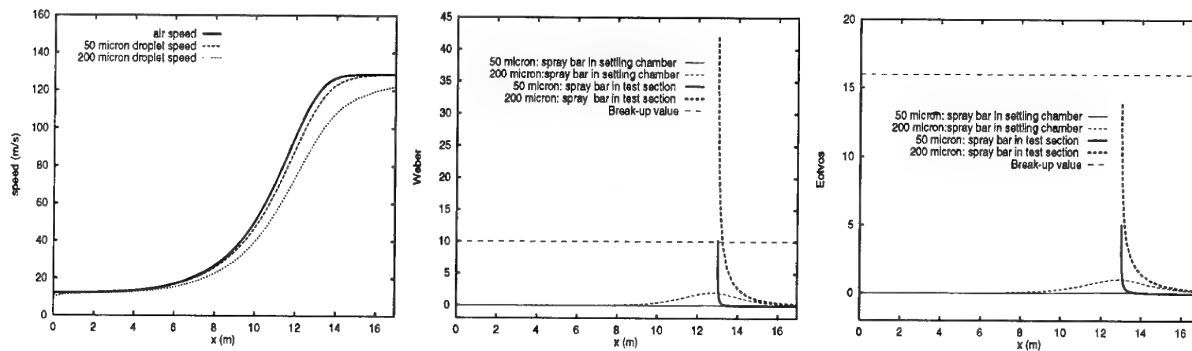


fig. 14 - Droplet velocity along tunnel axis (left); Weber and Eotvos numbers (center and right, respectively)

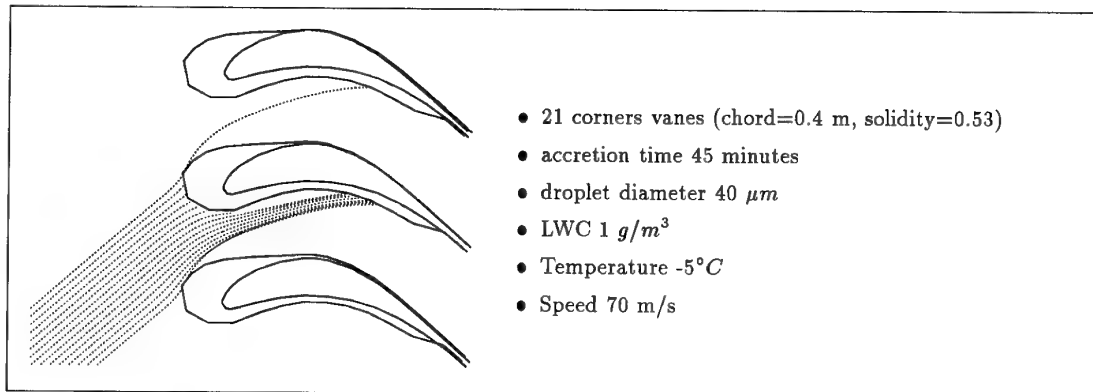


fig. 15 - Ice accretion calculation on tunnel corner vanes: impinging trajectories and ice shape

Development of Boeing Research Aerodynamic Icing Tunnel Circuit

By

Seetharam Chintamani

Danny Delcarpio

Greg Langmeyer

Boeing Aerodynamics, Noise and Propulsion Laboratory

P.O. Box 3707, M/S 1W-82

Seattle, Washington 98124-2207, USA

Abstract

There is a general understanding that aircraft design is a mature technology. All leading airframe manufacturers produce a high quality product, with a blend of sophisticated computational fluid dynamics programs and extensive wind tunnel tests. Prediction of flight characteristics and performance is usually made with previous in-house methodology backed with years of experience. On closer examination, however, there are areas where significant improvement can be made. Improvement opportunities exist for current processes in all phases of product development and manufacture. Better processes result in substantial reduction in cost and time.

One of the areas was a close examination of the certification process relating to aircraft icing. Until 1990 an airframe manufacturer was required to fly the airplane through the cloud characterized by the FAA regulation (FAR Part 25) to obtain realistic ice shapes on relevant airplane parts, such as wings, horizontal and vertical tails and ram air turbines, etc. Based on the shapes of accreted ice during flight, molds were prepared. Demonstration of handling qualities is carried out with the shapes derived from the natural icing tests, attached to appropriate locations of the airplane.

Flight testing of an airplane to extract the ice shapes in order to estimate the performance degradation and demonstration of airworthiness is a very tedious and expensive process. The Boeing Company, with the support of the FAA, proposed to simplify the airworthiness certification process on aircraft icing. The first part of the process is the extraction of the shape of ice accretion on airplane components. The FAA has issued guidelines for the development of ice shapes in the wind tunnel instead of by flight testing.

The FAA emphasized that in order to establish "certifiable" quality data, the flow qualities of the new tunnel must be equal to or superior in comparison to the NASA Lewis Icing Research Tunnel. The Aerodynamics Laboratory and Mechanical Systems Laboratory of the Boeing Company decided to modify an existing low-speed research tunnel to include icing test capability in addition to conducting basic low-speed aerodynamic research.

In order to achieve good flow quality, particularly through the modification of the existing facility, the wind tunnel designer is faced with interesting design challenges. This paper describes some unique designs of the tunnel components and the results of the calibration.

Nomenclature

b_a	Liquid water content calibration offset to determine K_a .
b_v	Liquid water content calibration offset to determine K_v .
c	Unit conversion factor equal to 49,407
C	Cloud uniformity calibration pipe ice circumference measurement in inches
ΔP	Pressure differential between spraybar water and air pressures in lbs/in^2
ΔS	Icing blade average ice accretion in inches
E_b	Icing blade efficiency
kn	Tunnel velocity in knots
K_a	Liquid water content calibration constant for constant tunnel velocity
K_v	Liquid water content calibration constant for constant spraybar air pressure.
LWC	Liquid water content in g/m^3

m_a	Liquid water content calibration slope to determine K_a
m_v	Liquid water content calibration slope to determine K_v
MVD	Median volume diameter in microns.
PSP	Static pressure measured from Super Probe II
PS_{CL}	Mean static pressure at tunnel centerline (waterline 36, buttock line 0)
P_{CL}	Mean tunnel static pressure
P_s	Probe total pressure
u'	Longitudinal turbulence normalized with respect to tunnel freestream velocity, in percentage
v'	Lateral turbulence normalized with respect to tunnel freestream velocity, in percentage
w'	Vertical turbulence normalized with respect to tunnel freestream velocity, in percentage
t	Time in seconds
ρ_{ice}	Density of ice equal to 0.88 g/cm ³
U'	Turbulence intensity
U	Mean test section velocity
V	Tunnel velocity in knots
W	Spraybar water volumetric flow in gallons/minute

Introduction

The Boeing company has recently completed the design and construction of a research wind tunnel to support aerodynamic and icing tests. This facility is a major modification to the existing 5ft by 8ft low-speed Boeing Research Wind Tunnel (BRWT). The tunnel has been operating since the late 1960s with the primary mission to support a variety of testing needs including basic aerodynamic research on high-lift systems and research and development activities of various operating divisions of the company. During 1986-87 the tunnel flow quality was substantially improved to conduct basic research on laminar flow control on large wing surfaces. This effort focussed mainly on establishing uniform turbulence intensity distribution in the test section. With a maximum test section velocity of about 200 ft/sec and excellent flow uniformity and low turbulence, the BRWT has served a variety

of testing needs. A six component external balance under the test section, which is linked to the wall mounting fixtures (also with provisions for sting mounted models with internal strain gauge balances), has provided force data to the customers. It has been very useful in fundamental work and feasibility studies on new and emerging technologies such as hybrid laminar wing design. The Mechanical Systems Laboratory organization of the Boeing Company has been involved in ice accretion testing on scale models of aircraft components in a small 15-by 20-in icing wind tunnel. In addition to this effort, several airplane project groups have been involved in testing the effectiveness of various de-icing devices in the NASA Lewis Icing Research Tunnel. The Lewis facility has been the leader in investigating the problems associated with aircraft icing for the past 45 years. Currently this facility is undergoing an extensive flow quality and cloud uniformity improvement program.

The modification of the BRWT included rebuilding a majority of the circuit to account for the increased air loads and thermal effects due to hot and cold operating modes. The rebuilt circuit retains the same dimensions as the BRWT, except for the 3rd and 4th corners which were enlarged to accommodate the heat exchanger (Figure 1). To accommodate the enhanced capability in speed, low temperature operation and relatively large blockage models (over 20% is not unusual) the rebuilt tunnel required a new fan and drive system to replace the existing 600 hp motor and 4 bladed fan. The tunnel circuit around the new fan system had to retain the same dimensions as the existing BRWT fan tunnel structure.

Tunnel Performance Objectives & Requirements

Modifications of the existing BRWT to facilitate icing tests consisted of the following basic requirements:

A) For icing tests a minimum tunnel speed of 250 kn at a tunnel temperature of 435° R was specified as a basic requirement. This condition is equivalent to flight at an altitude of about 10,000 to 15,000 ft. This is required to test airplane components exposed to ice accretion during the hold pattern. For this requirement, airplane components like wing leading edges, vertical tails ... etc. are tested. Since most of the accretion occurs around the stagnation regions of the leading edge, typically full scale models of

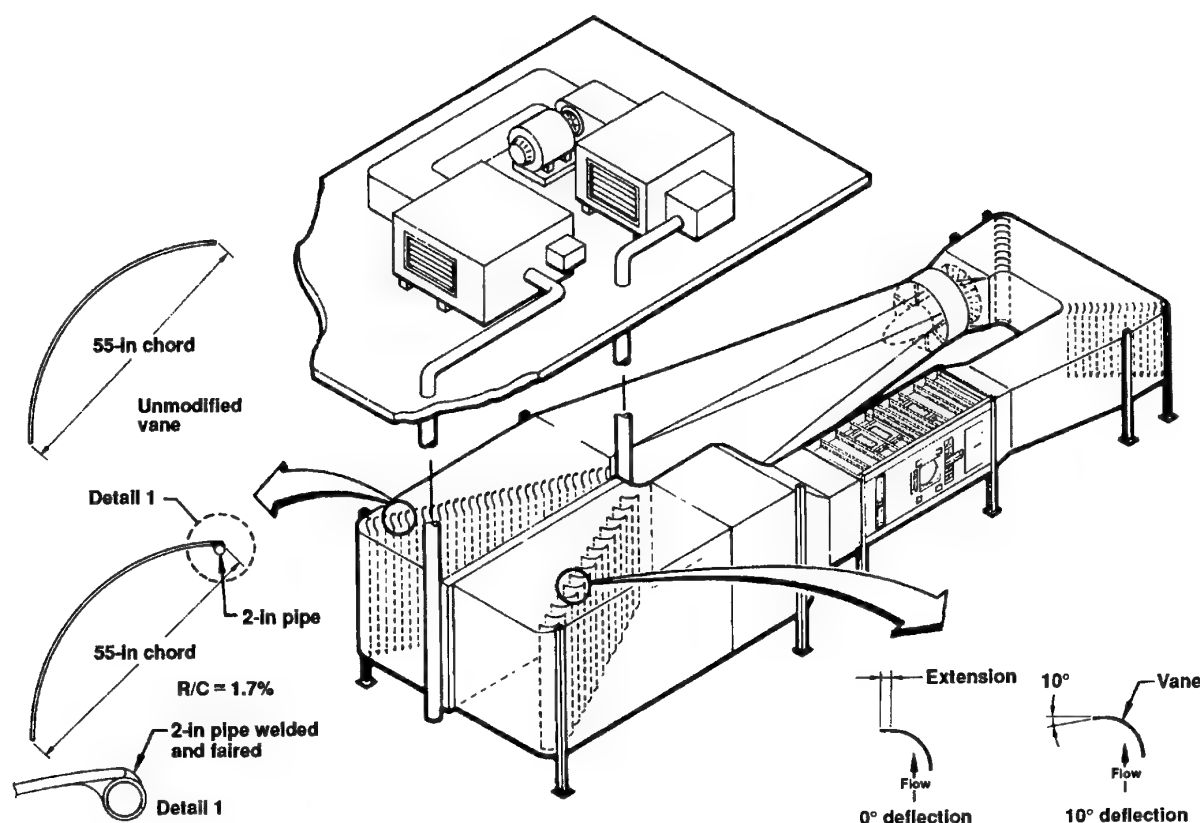


Figure 1. Boeing Research Aerodynamics and Icing Wind Tunnel.

the first 10% to 15% chord are adequate. Also, the models should have enough thickness to accommodate full scale de-icing systems near the leading edge.

B) Component testing for high lift systems, and full scale Ram Air Turbine performance during icing require a larger test section area than A, but at a lower tunnel speed of 150 kn at the same tunnel temperature of 435°R.

1. For icing tests, three test section sizes have been provided as described in the following table:

	Test Section (ft)	Velocity (kn)	Static Temperature (°R)	Flight Conditions/ Configuration
a.	5 x 8	150	435 to 520	High Lift, Ram Air Turbine
b.	4 x 6	250	435 to 520	Aircraft in hold pattern
c.	3 x 5	350	420 to 520	Probe performance and Calibration

Test Sections a and b are currently available for production and development testing.
Test Section c will be designed at a later date.

2. Spraybar capabilities:

- Liquid Water Content 0.5 to 3.0 gms/m³
- Droplet Size 15 to 40 microns

-Represents FAA specified cloud characterization in the altitude range of 10,000 to 15,000 ft.

C. In addition to the above requirements for icing tests, the basic aerodynamic features and excellent flow qualities of the original BRWT were to be retained at an increased tunnel speed.

1. Aerodynamic Tests, 5 x 8 ft Test Section

- Maximum Velocity 150 kn (275 ft/s)
- Reynolds Number /ft 1.6×10^6
- Turbulence Intensity 0.06%

In order to achieve the above test objectives the existing circuit required the following modifications:

- Area expansion of the portion of the circuit

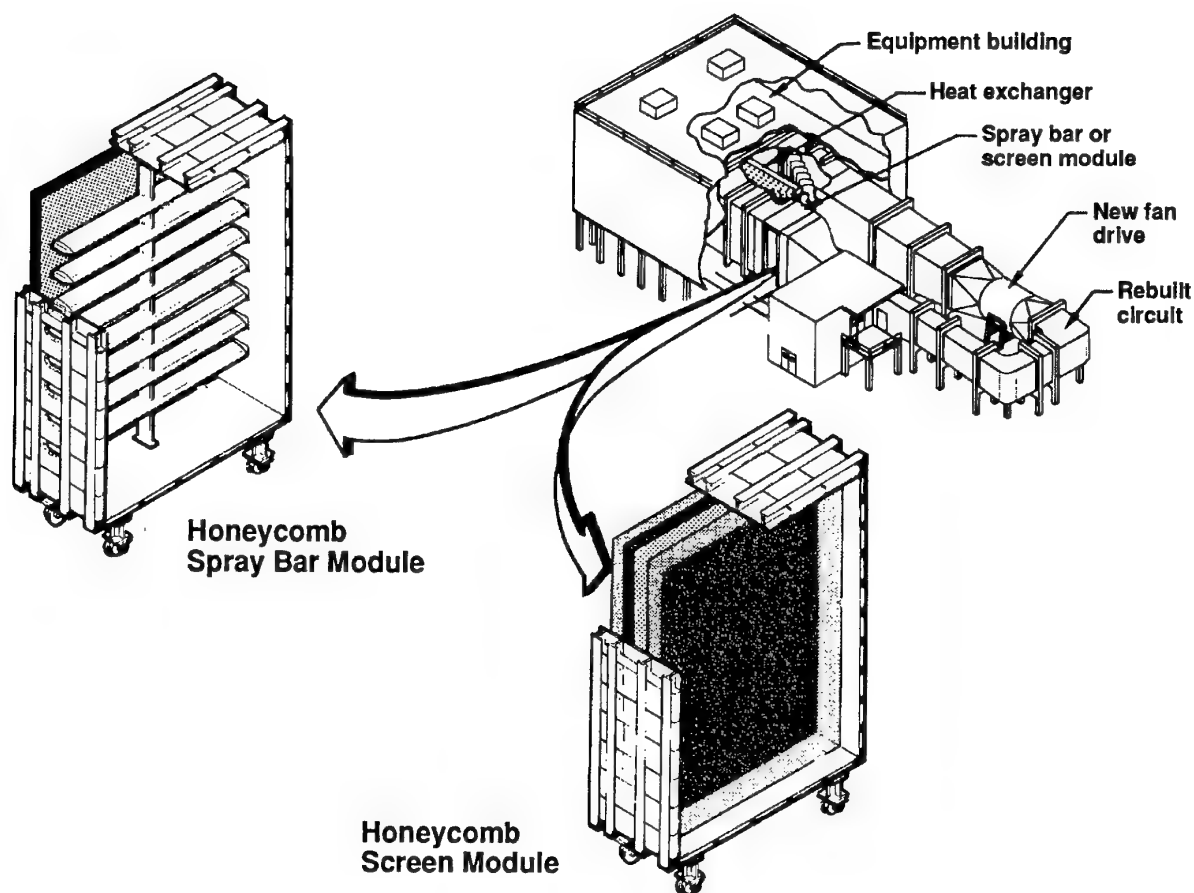


Figure 2. Honeycomb Screen and Spray Bar Modules.

enclosing the 3rd and 4th corners to accommodate a large heat exchanger (675 ft²) which is required to cool the air to sub-zero temperatures.

2. Inserts for the contraction, test section, and high speed diffuser to reduce test section size and achieve higher speed.

3. New fan and drive to provide required speed, pressure rise and power to achieve operating conditions.

Flow Quality Requirements

For aerodynamic testing, it was important to retain the flow quality of BRWT.

1. The velocity uniformity to be within 1 percent of the centerline velocity.

2. Turbulence intensity variation across the test section to be within 0.01 about center line value.

3. Flow angularity be within 0.2 deg.

For icing tests:

1. Temperature across the test section to be within ± 1 deg F.

2. Region of cloud uniformity was desired to be within $\pm 20\%$ of the test section centerline value as defined by NASA Lewis Icing Tunnel (Reference 1).

3. Velocity variation be no more than 1 Kn of the center line velocity.

Facility Description - Overview

Because of the added icing capability of the BRWT, it was renamed to the Boeing Research Aerodynamic Icing Tunnel (BRAIT). Figure 1 shows a pictorial view of the overall BRAIT as currently built. This figure also illustrates the major modifications and additions to the existing Boeing Research Wind Tunnel. The most important being the new equipment building erected above the tunnel corners 3 and 4. Most of the essential machinery and compressors necessary to the operation of the

icing tunnel air refrigeration and water spraybar systems are housed in this building. In order to accommodate a large air heat exchanger, the tunnel was expanded in the area between the third and fourth corners (figure 1).

Special interchangeable flow quality control modules are provided for either aerodynamic or icing tests. The changeover modules are illustrated in figure 2. One module is a reconstruction of the honeycomb and screens of the existing facility, used for aerodynamic testing. It is interchangeable with a second module used for icing tests. This consists of a honeycomb and water spraybar nozzles used to inject the air water mixture which will form the cloud in the test section.

In addition, the tunnel is powered with a new fan and drive system replacing the existing 600 HP motor and four bladed fan system. The rebuilt circuit retained the same dimensions except as stated above. However, the new design accounted for increased air loads and thermal effects due to hot and cold operations. In the icing mode of operation, strict criteria for temperature, velocity and cloud uniformity were emphasized.

Wind Tunnel Modifications

Four major changes were made to the existing BRWT to facilitate the requirements for icing tests. The first change is a new 2,000 HP, 900 RPM motor with a variable frequency drive and a ten bladed fan with 90% efficiency. At the maximum operating condition the blades have at least a 25% stall margin. The blade pitch is equipped with remote control capability. A bank of 7 stators limits the exit flow swirl to 5°.

The second major change from BRWT is in the test section. As stated before, the BRAIT testing envelope utilizes different sized test sections (two initially). The 4 foot by 6 foot test section is assembled through the use of insert panels which install in the floor and ceiling of the basic 5 foot by 8 foot test section. The side walls move inward to complete the formation of the 4 foot by 6 foot configuration. Fairing panels are fitted to the bellmouth, test section entry and the test section diffuser. The new test section walls and ceilings are designed to have a substantial number of optical quality heated windows for lighting, photography, and laser droplet measurement system. Figure 3 shows the details of the test section assembly.

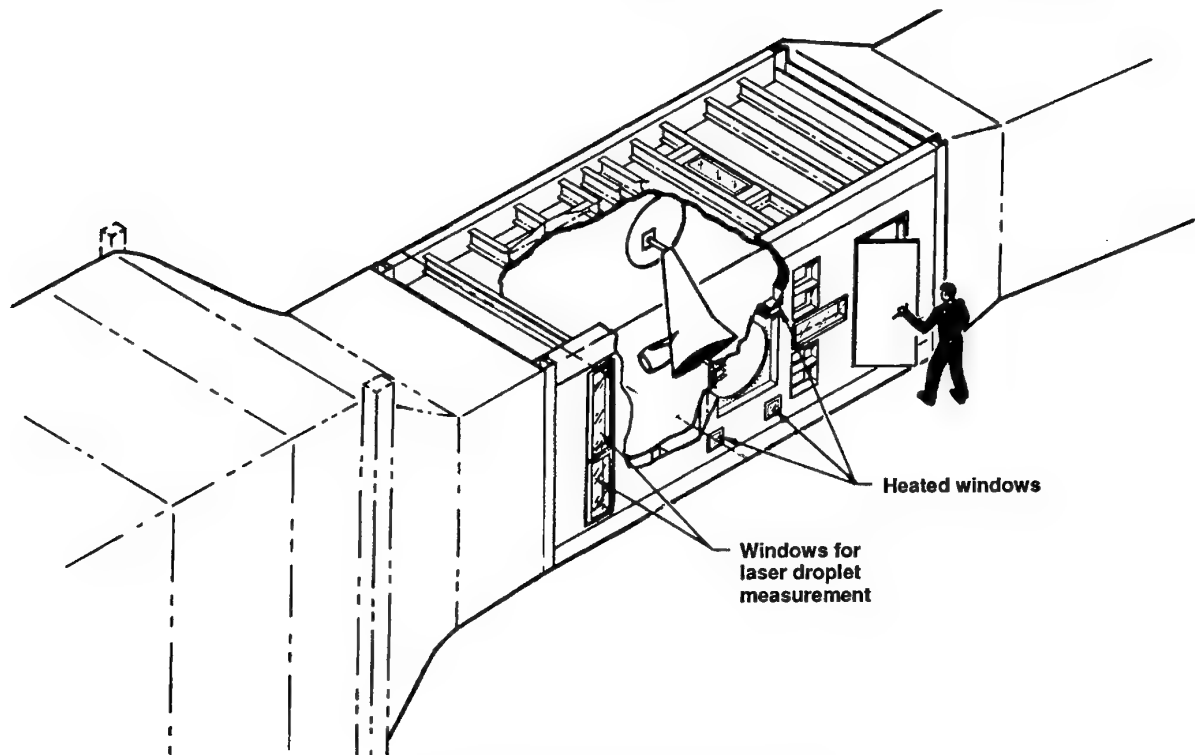


Figure 3. Test Section With Test Model.

The third modification is the removal of existing screens and honeycomb sections. In their place provisions exist for the two interchangeable modules mentioned earlier. The modules are exchanged using perpendicular rails, deployable wheels and two transport carts. An overhead guideway facilitates the removal and installation. Inflatable seals are employed to eliminate leaks around the modules.

Lastly, the majority of the tunnel circuit was rebuilt. The only exception being the contraction and turning vanes at the first and second corners. The tunnel walls are fabricated from steel, replacing mostly plywood sheet. Various tunnel components and support structure interfaces are designed to allow for thermal expansion and contraction. The entire tunnel circuit is heavily insulated in order to minimize heat transfer through the tunnel walls and maintain a constant cold temperature of operation. An ice debris catch basin and foreign object damage screen were added to protect the fan blades. The newly configured third corner consists of 30 turning vanes and the fourth has 14 vanes. Further discussion on the first corner turning vane will be discussed later.

Some of the significant features are described in the following sections.

Fan and Drive Power

The tunnel drive is provided by a 2,000 HP motor equipped with variable frequency drive. The power requirement was determined from the estimates of measured static pressure distributions along the BRWT circuit. In addition, losses due to heat-exchanger, circuit icing, and ice accreted model

were taken into account. The fan pressure rise and volumetric flow characteristics is shown in figure 4. It is readily seen from the figure that the tunnel operates in a wide range of volume flow, (400,000 to 700,000 cubic feet per minute.). This figure was developed by accounting for a 25 percent increase in the dry air circuit losses occurring during ice accretion tests (Reference 2). Detailed analysis indicated that the 4 by 6 feet test section at 250 knots and at -25 deg F would require full power (2,000 HP) to conduct ice accretion tests on a full scale model (condition 8, Figure 4).

A) In addition to the above, fan dimensions must be compatible with the wind tunnel circuit:

1. Outside diameter, overall length, and inlet and outlet dimensions are dictated by the wind tunnel geometry

2. Hub diameter must allow the motor to fit inside and must be compatible with fan diffuser geometry.

B) High efficiency (up to 90%) performance is required over a wide range of operating conditions.

C) Stall margin must be sufficient at the primary operating conditions to protect against excessive ice build-up during testing.

D) Good flow uniformity is required at the exit from the fan section for better fan diffuser performance.

E) The fan must operate under extremes of temperature and humidity.

Aerodynamic Design Philosophy

The starting point for any fan design is to select a primary operating point and, given geometric constraints, design the rotor and stator blade geometry to achieve high efficiency at practical operating speeds. For the BRAIT fan, point #8 from figure 4 was selected as the primary operating point. At this condition the fan was required to operate at 90 percent efficiency in order to successfully conduct icing tests on large models at 250 Kn. From the estimates of power requirements this condition was critical because of maximum power demand of over 2000 HP. Additional power over and above the maximum rated power is provided by 15 percent service factor of the drive motor.

A high performance single-stage axial flow fan can be expected to operate in excess of 90% efficiency at its design point. The fan design is based on conventional free vortex airfoil theory as applied to

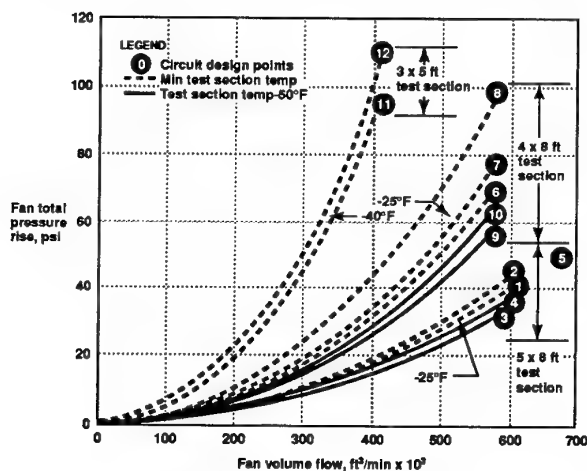


Figure 4. Circuit Operating Lines.

fan design (see References 3 and 4) to maximize efficiency at the primary design point. The rotor blade geometry selected is based on a commonly used class of blade (circular arc camber) with a thickness profile similar to the NACA 4-digit series profile. The maximum rotor blade thickness at each section is determined by strength and vibration issues. The thickness of the stators was set for structural reasons and to allow the air passages for motor cooling air. The design lift coefficients for the rotor blades are typically less than 1.0 with the heaviest loading at the hub. The loading on the stator blades is less.

The fan is based on a proprietary design by the TLT Babcock Company of Akron, Ohio. Based on their design, a maximum fan speed of 900 rpm was used. The rotor has 10 tapered and twisted blades with the chord varying from 22.4 inches at the root to 20.8 inches at the tip (profile designation TLT 91-2), aspect ratio 1.29, blade length 27.8 inches, twist 14.3°, and 7 stator vanes. The blade design provides a near uniform loading across the fan at the maximum power requirements, and has a 25% stall margin at 90% efficiency. Geometric details of the fan and stator are summarized in the following table:

Geometric Details Of Fan Blade And Stators.

	Fan	Stators
Number of Blades	10.0	7.0
Hub Diameter, in	86.6	86.6
Tip Diameter, in	144.0	144.0
Blade Chord at Hub, in	22.4	115.0
Blade Chord at Tip, in	20.8	95.3
Blade Twist, °	14.3	6.0
Max. Thickness at Hub, in	3.0	12.0
Max. Thickness at Tip, in	0.7	12.0

Off-design performance can be determined through computational methods but is more accurately determined using model or full-scale tests. The predicted performance of the BRAIT fan was based on model and full scale tests of a similar fan that was built and installed in a slightly smaller wind tunnel. The fan characteristics are summarized in figure 5 (see page 8). In this "fan map" the pressure rise is plotted against the flow rate for different blade pitch settings. The upper left boundary represents the stall line which must be avoided during normal operation.

The flow uniformity at the exit of the fan was also verified from earlier scale model tests and shown to conform to the BRAIT requirement.

When all operating points for the BRAIT fan (Figure 4) were compared to the predicted performance of the fan, it was determined that blade pitch adjustment would be necessary to handle all points. For example, operation at the design points for the 3 x 5 ft test section (Figure 4, Conditions 11 to 14) would stall the fan if run at the same blade pitch as is required to achieve high efficiency in the 4 x 6 ft test section (Condition #8). Therefore, the BRAIT fan has provisions for rotor blade adjustment in flight. The combination of adjustable pitch and variable speed allows precise control at all the required design points while ensuring maximum efficiency at critical points. An additional advantage is that if structural resonances occur at a particular fan speed, the blade pitch can be adjusted and the fan speed changed to achieve the same operating point.

In addition to the above, the tunnel velocity can be controlled to a very low value of 10 to 15 feet per second at -25 deg F through a combination of low

fan rpm of 90 and blade feathering. At this condition the tunnel temperature can be maintained at -25 deg F, while allowing access to the test section. Details of the fan evaluation are reported in Ref. 5.

High Speed Diffuser

The design of the high speed diffuser insert for the 4 by 6 feet test section proved to be a challenging problem. The problem becomes more complicated when large models with high blockage are tested. In addition, the access door to the test section was located at the end of 20 feet long test section. Immediately downstream, a pressure relief vent was

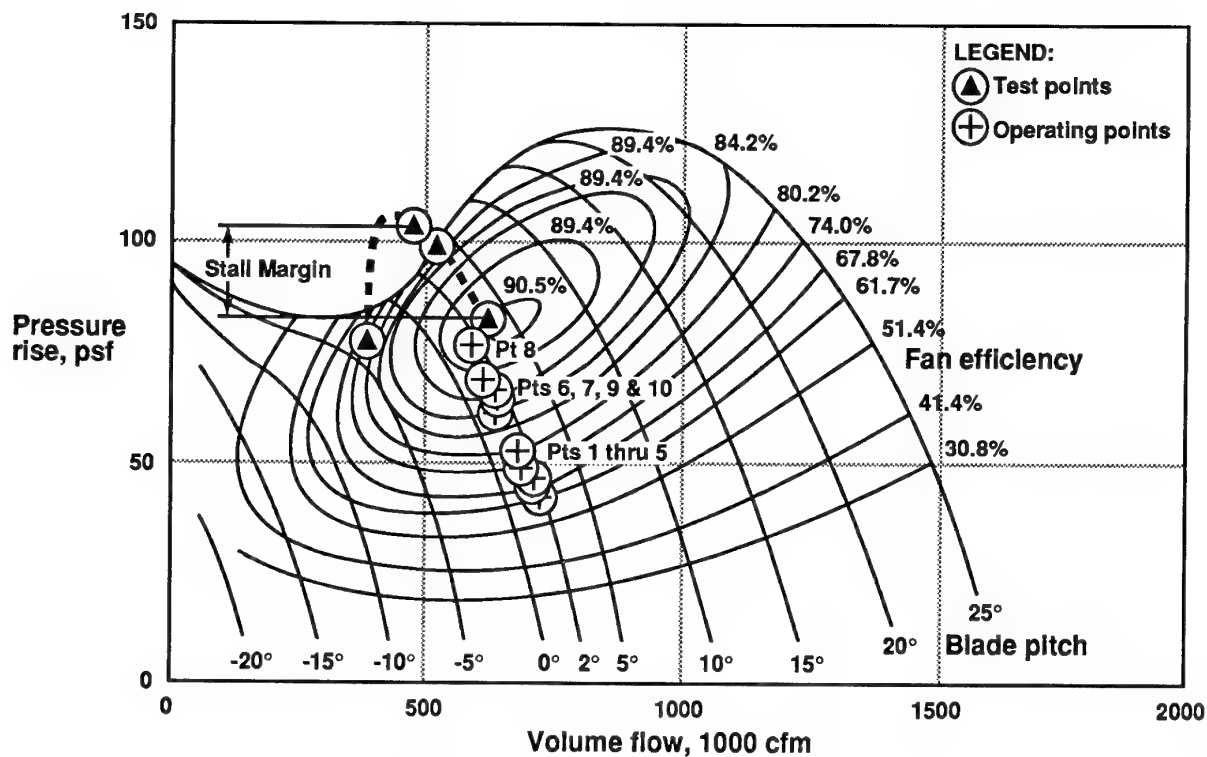


Figure 5. Fan Performance Measurements.

provided to prevent excessive wall loads which can occur during fan start up ramps. All these possibilities were thoroughly investigated through a combination of two and three dimensional potential flow code analyses. Based on the analysis it was decided to provide a 9 inch wide vent on both sides of the test section diffuser. The final compromise resulted in the diffusion half angle of 2.37 at the sidewalls and 4.4 degrees at the top and bottom walls respectively.

First Corner Turning Vanes

During the initial design phase it was strongly recommended that the first corner turning be heated to prevent excessive ice accretion. Also, the blunt leading edge (made from bent 0.375 inch sheet metal) has very high collection efficiency of about 90 percent. This was not included in the final design phase due to cost considerations. Therefore, the existing turning vanes from BRWT were used. During initial check out of the rebuilt circuit integrity and fan performance checks, a problem was discovered with the reused first corner turning vanes. After 30 hours of operation, failure of the attachment welds of the turning vanes were noticed. Diagnostic tests were conducted by using accelerometers at select locations in order to obtain the

magnitude of unsteady loads in terms of G rms. In addition to G rms measurements strain gauges at the vane support were also employed. A representative 20 percent thick symmetric airfoil (3ft chord, 4ft span) at 18 deg angle of attack was used to simulate realistic ice accretion tests. Tunnel speed was 250 kn and temperature of -25 deg F. Existing turning vanes registered a G rms value of about 16 with peak to peak value excursions of 25 G. Frequency spectrum indicated large energy concentrations at 55 and 160 Hz from the mid-span leading edge accelerometer. In view of urgency an immediate solution was desired. An effective and quick solution was readily implemented. This was accomplished by modifying the blunt leading edge into a rounded leading edge with a 1 inch diameter pipe. The concept of rounded leading edges to control and eliminate flow unsteadiness will be discussed later under the section on third corner vanes. With rounded leading edges, G rms was reduced to 4.5 indicating a substantial reduction of about 70 percent. The dominant frequency with the modified vanes was 70 Hz and the spectrum was flat at all other frequencies. The rounded leading edge geometry has been implemented in all 22 turning vanes of the first corner.

Fan Diffuser

The fan diffuser entrance has an octagonal section with a side of 61.1 inches and expands into a rectangle 176 inches wide and 236 inches high in a length of 654 inches (see figure 6). The cone angle from the concept of hydraulic diameter is about 4.75 deg and the area ratio is about 2.3. Total pressure surveys at the diffuser exit indicated pockets of separation at the outer wall at the entrance to the third corner. There was an opportunity to improve the diffuser performance by redesigning the entrance. Since this involved substantial rework and design of fan housing shell and nacelle it was not considered.

Third and Fourth Corner Turning Vanes

One of the main components of the icing tunnel is an efficient heat exchanger that will maintain the temperature uniformity within $\pm 1^\circ\text{F}$ in the test section. To ensure this goal the heat exchanger manufacturer specified the following requirement:

Approach velocity to the heat exchanger no more than 15 feet/second with maximum variation of $\pm 10\%$.

Since the conversion of the BRWT to icing capabilities was a modification of an existing circuit, the footprint available for the third and fourth corners is limited. The third corner entrance velocity was estimated to be approximately 35 feet/second for an area of 288 square feet. In order to achieve the approach velocity of 15 feet/second at the heat exchanger, which is located between the third and fourth corners, the third corner must have an area expansion ratio of 2.34. Design of efficient turning vanes in an expanding corner is not within the realm of conventional wind tunnel design. The problem was complicated by the imposition of the stringent constraint on velocity uniformity. Various approaches invoking a combination of computational fluid dynamics and empirical methods were used to select candidate designs for 1/5-scale model tests. These tests demonstrated that simple cambered flat plate 90° turning vanes offered nearly the desired flow qualities, but they suffered from a dramatic periodic stall. Only after a unique vane leading edge treatment (Figure 1) was added was the stall eliminated and the requirements met. The velocity and turbulence intensity distributions are illustrated in figures 7 and 8 (reference 6). The tests also

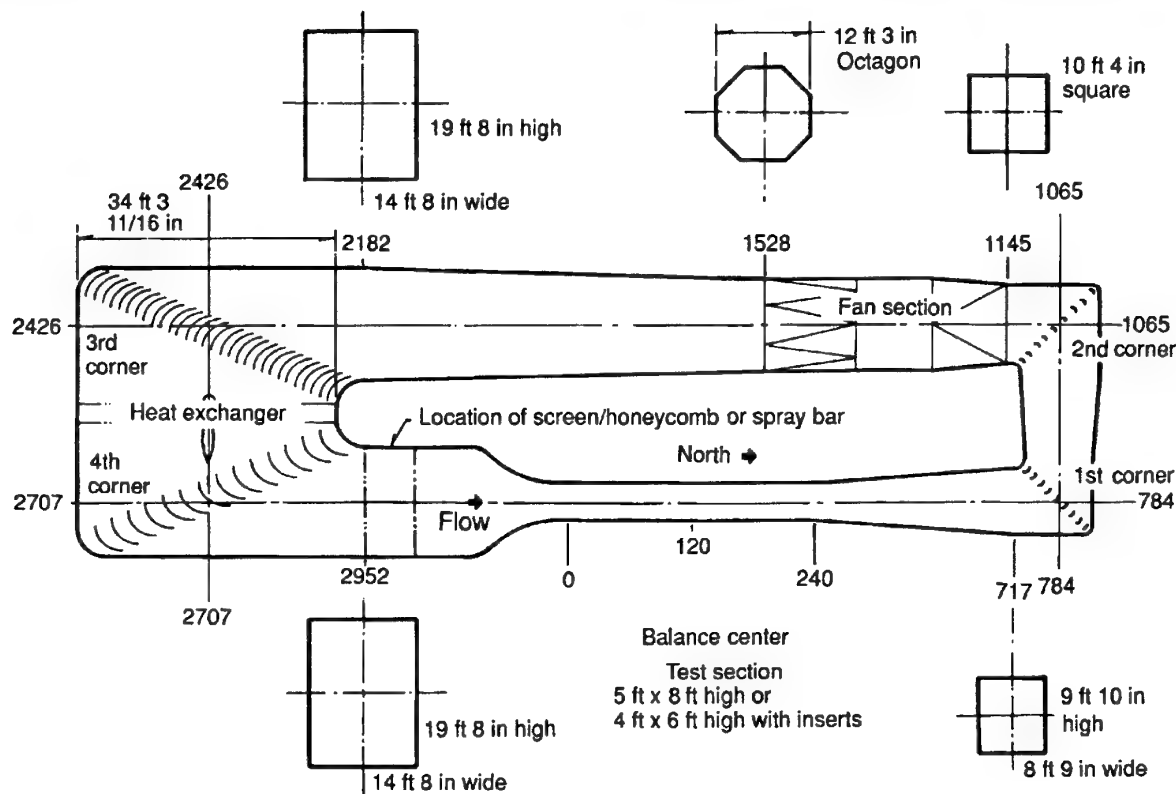


Figure 6. Boeing Research Aerodynamic Icing Tunnel (BRAIT).

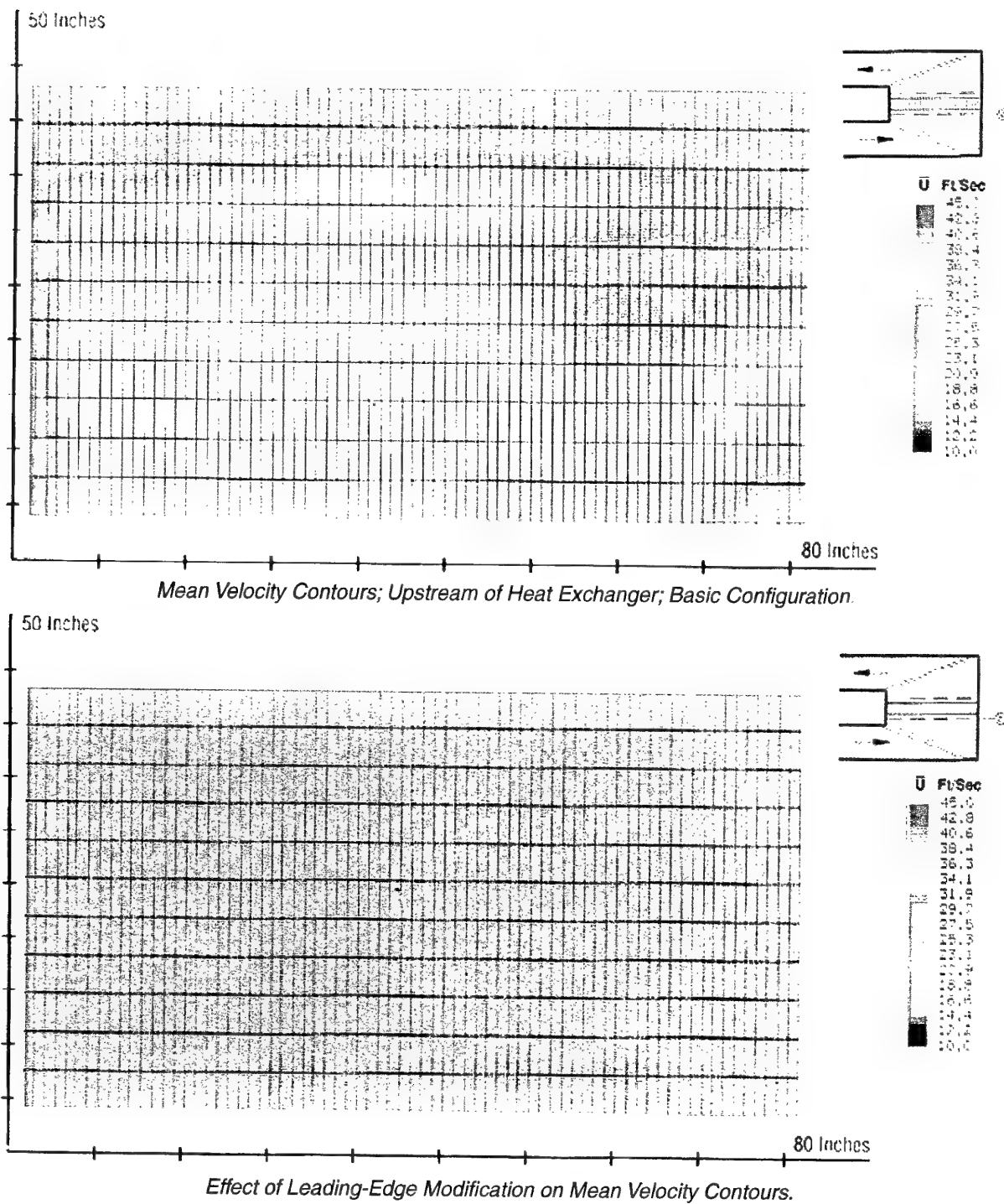


Figure 7. Velocity Contours.

revealed that the modified vanes are reasonably tolerant of inlet flow distortions and do indeed demonstrate the desired robustness. (U.S Patent no 5,405,106, April 11, 1995).

The fourth corner turning vane design is relatively simple since it is a converging corner. Scale model test results indicated that by providing adjustability in the vane trailing edge, the velocity profile exiting the corner can be trimmed to be reasonably uniform.

The downstream flow conditioning and the contraction will aid in delivering the necessary flow uniformity in the test section. Figure 1 shows the final configuration of the turning vane geometry with 10 inch trailing edge extensions deflected 10 degrees.

Heat Exchanger

A conventional flat configuration which is used in several industrial and domestic applications was used. Fin spacing was an important consideration, particularly for closed return icing tunnels. While normal heat exchangers have 8 to 10 fins per inch,

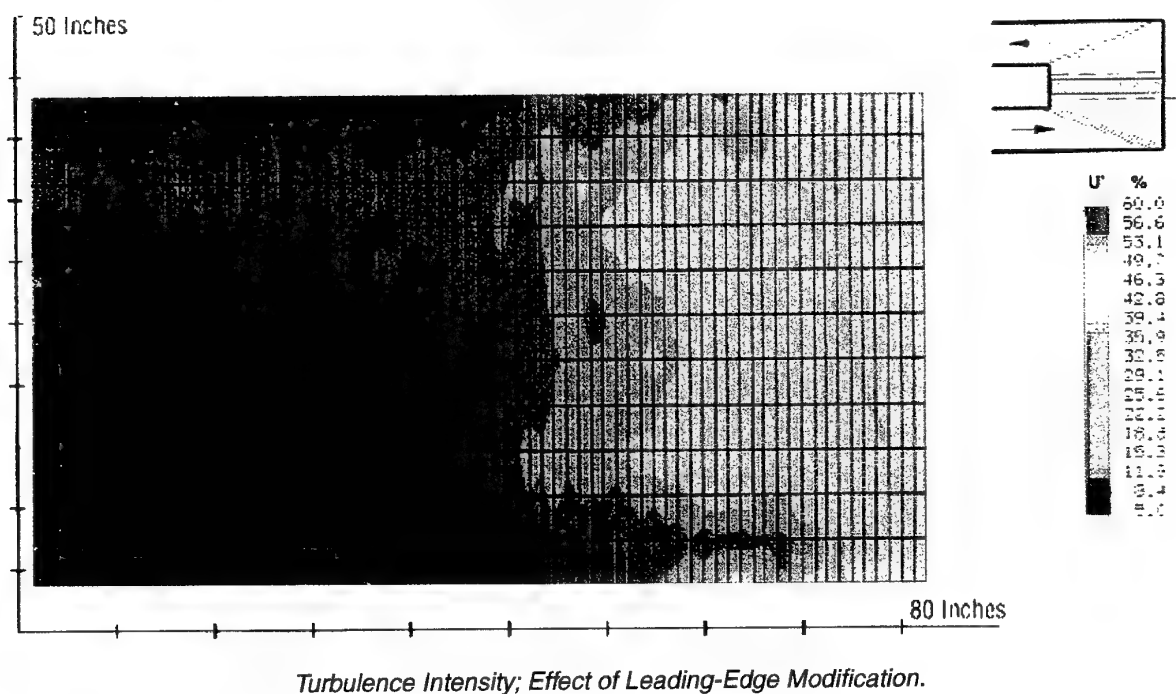
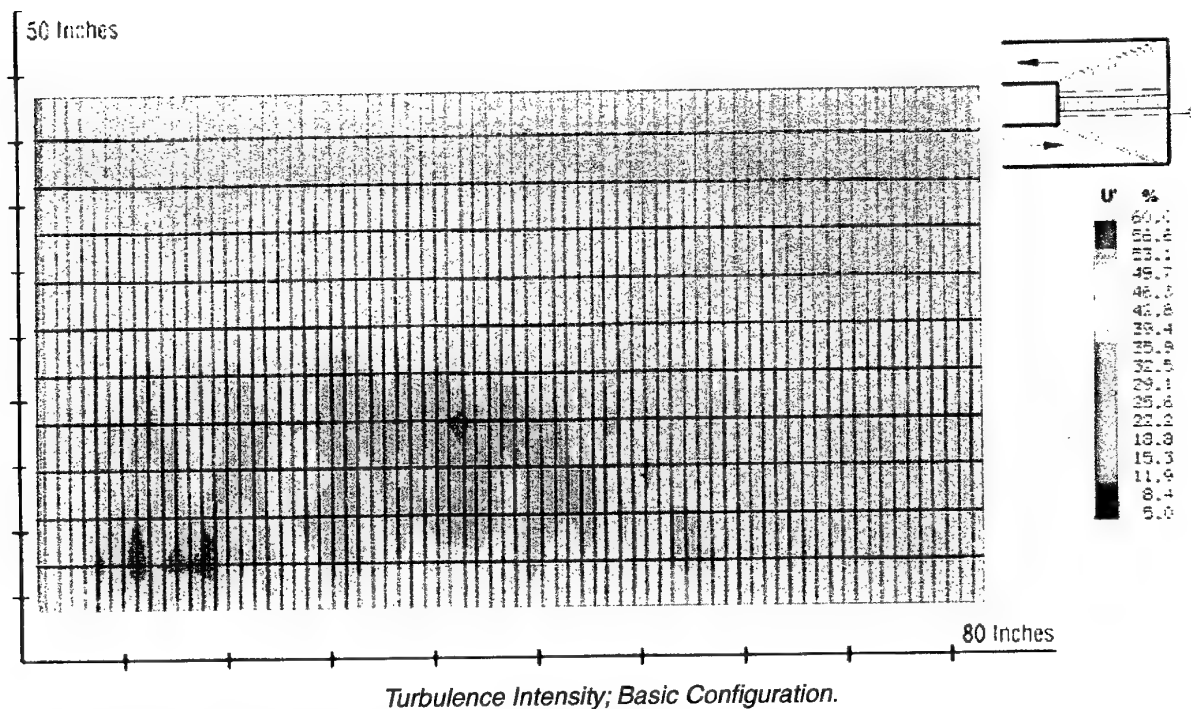


Figure 8. Turbulence Intensity.

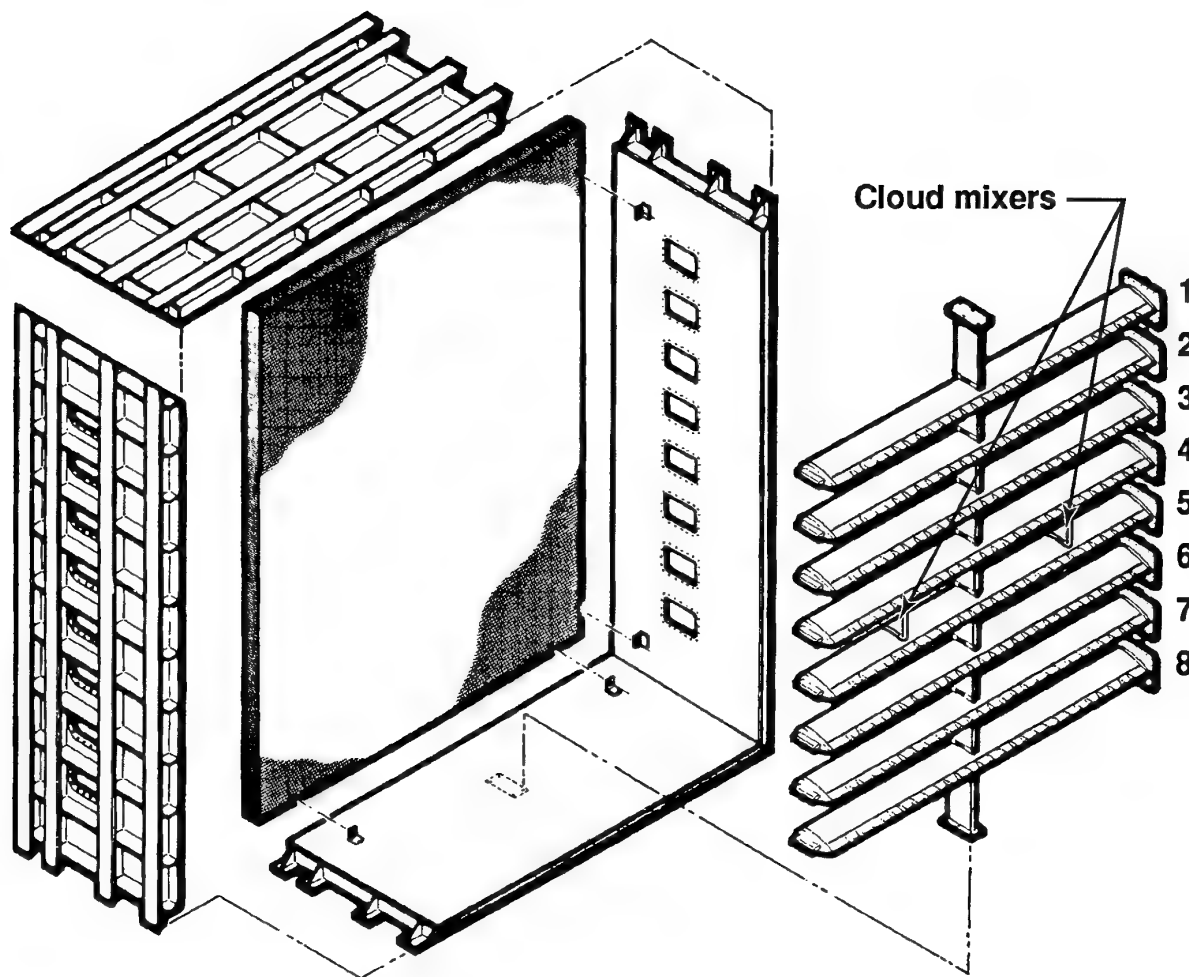


Figure 9. Spraybar/Honeycomb Tunnel Section (Exploded View).

BRAIT has 4 fins per inch. Wider spacing of fins minimizes the possibility of frosting and icing on the fins. Final configuration of the heat exchanger has the following dimensions:

Fins: 4 fins per inch, 0.015 inch aluminum

Coils: 1 inch dia aluminum.

Surface Area : 675 sq feet

Maximum Volumetric flow: 1000 cubic ft/minute.

Refrigerant: 22000 lb of R-22 liquid freon at -52°F is delivered to the coils by means of 1250 and 900 hp screw compressors.

The heat exchanger is 2 feet deep and is arranged in six sections. Freon flow can be controlled in individual sections to obtain good exit flow temperature uniformity (within $\pm 1^\circ\text{F}$).

The heat exchanger supplier made an estimate of the pressure loss across the heat exchanger based upon experience. In order to determine a better estimate, the actual pressure loss across the sample piece provided by the supplier was measured. This experiment was conducted during the development of turning vanes for the third corner. Measured pressure losses were 40 percent lower than the estimate.

Spraybar System

The water spray system is comprised of a water spraybar assembly, a water heater and an air heater that provides conditioned air to the individual spraybars. The water spraybar assembly consists of eight (8) individually controlled spraybars each containing twenty seven (27) spray nozzles (Figure 9). The nozzles are modified designs of the NASA Lewis Icing Tunnel nozzle. Air and water control to each nozzle and activation and deactivation is

accomplished electronically. A spray air heater provides 75°F to 300°F conditioned air to the spraybars. The spray water heater provides 35°F to 200°F conditioned water to the spraybars. This water spray system is predicted to provide stabilized spray conditions in less than fifteen (15) seconds after initiating spray. Operational tests have demonstrated that this is achieved. Rapid stabilization is critical for icing testing. Figure 10 shows the details of the spraybar system assembly.

In addition to the refrigeration and water spray system, a thermal anti-ice air system was also installed in the BRAIT facility. This auxiliary air system will allow simulation of engine bleed air in the airfoil/wing models to be tested. It provides up to 25 pounds/minute of 1000°F air at up to 75 psig.

Aerodynamic Module

Extensive pilot testing was done before the modification to improve the flow qualities of the Boeing Research Wind Tunnel. This was initiated due to pressure by the user community, particularly the laminar flow research group working on Natural and Hybrid Laminar flow wings. The flow manipulator array of the existing configuration consisted of five

screens and a honeycomb. Two 0.0065 inch diameter, 38 mesh screens were used upstream of the honeycomb. The 0.375 inch cell honeycomb section was assembled in 12 sections with 0.25 inch seams. Two fine 38 mesh screens followed by a 20 mesh, 0.0017 inch diameter screen was used downstream of the honeycomb. These fine mesh screens also had seams of 0.25 inch. Hot wire traverses in the test section indicated a non uniform turbulence distribution across the cross section. This was traced to the signatures from the seams. This was undesirable for the laminar flow wing tests. Therefore, the honeycomb was replaced by a single piece seamless 0.75 inch cell 10 inch deep configuration. The five original screens were eliminated. They were replaced by a high porosity 10 mesh, 0.02 inch diameter screen 2.5 inches downstream of the honeycomb. Two 20 mesh 0.017 inch diameter screens were also used, one located 20 inch upstream of honeycomb and the other 17 inches downstream of the high porosity screen (Figure 11). This configuration resulted in a very uniform turbulence distribution. This module is not yet tested in the BRAIT.

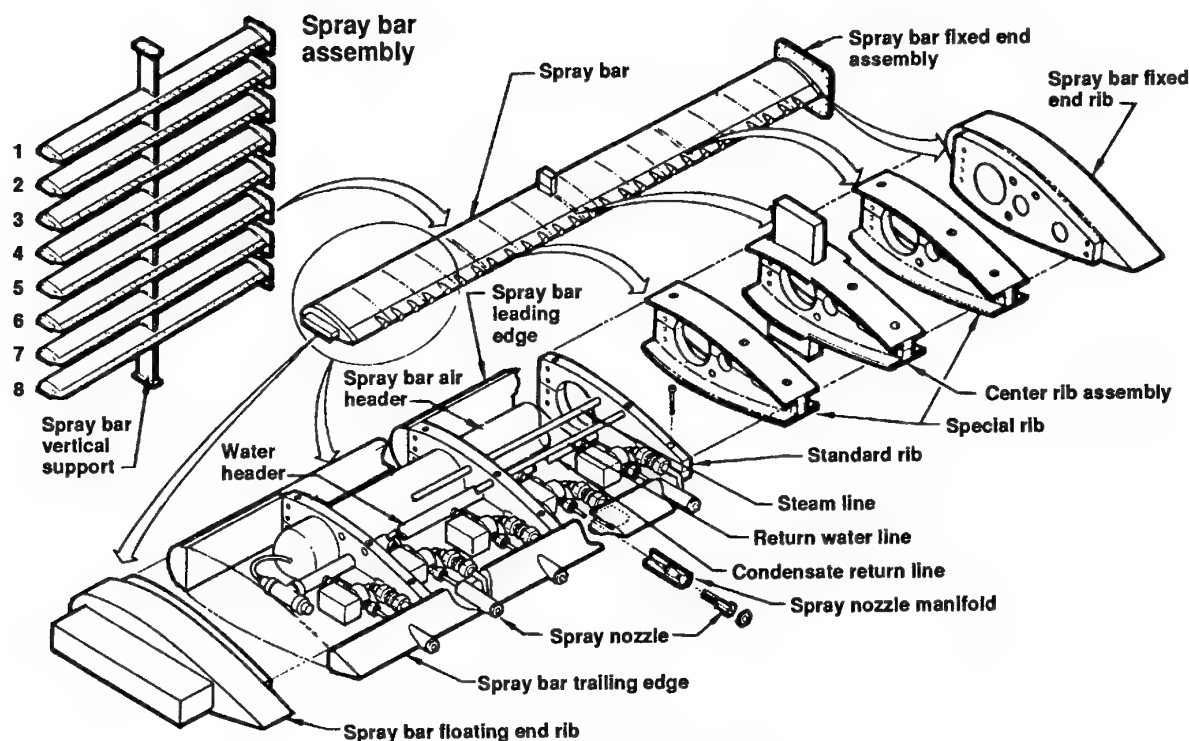


Figure 10. Spraybar Assembly.

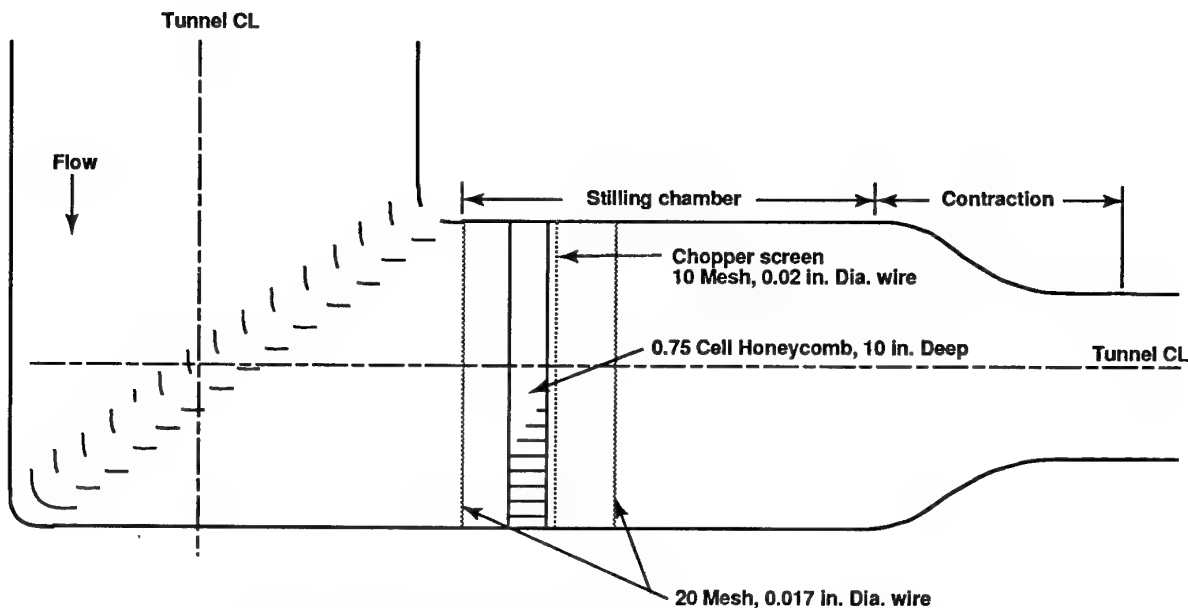


Figure 11. Flow Manipulator System for Aerodynamic Testing.

Contraction

The original contraction for the 5 by 8 ft. test section was retained. The contraction shape was developed for the 4 by 6 ft. test section. Care was taken to ensure smooth longitudinal acceleration throughout the length of the contraction. One main concern was to ensure that ice does not accrete on the contraction walls.

TUNNEL CALIBRATION

The BRAIT calibration was carried out in the 4 foot x 6 foot test section configuration which was immediately required for icing tests of the 777 airplane program. In this configuration the tunnel circuit was fitted with the spraybar honeycomb module. The calibration program was carried out in two phases. The first phase concentrated on the determination of basic flow qualities of the clear tunnel in the dry mode without water injection. The second phase determined the calibration of the BRAIT in the icing mode. In the dry mode of running, the effect of air injection for a preselected combination of nozzles on the flow qualities was also included in the calibration. The calibration was made at the center plane of the test section, Tunnel Station 120 (Figure 6) in order to determine the following flow parameters: A) Centerline static pressure correction, B) Velocity uniformity, C) Turbulence Intensity distribution, D) Temperature uniformity, E) Clear tunnel upflow and crossflow, F) Boundary layer thickness.

The original aerodynamic calibration was conducted in March 1993 (Reference 7). Calibrations for centerline static pressure corrections, velocity uniformity, flow angularity and turbulence surveys were made. Turbulence intensity and flow angle profiles exhibited regions of high turbulence intensity and crossflow angles. This was traced to the discontinuous vertical strut supporting the spraybars. A gap between spraybars 4 and 5 of about 14 inches was intentionally provided in the design to accommodate thermal effects. This gap was filled in and limited calibrations were done to determine centerline static pressure corrections, velocity and temperature uniformity. Results of 1993 and 1995 calibrations are presented in the later sections.

AERODYNAMIC CALIBRATION

Test Conditions

The calibration was made in the following range of tunnel operating conditions:

Velocity Range	150 to 250 Knots
Temperature Range	435° R to 485° R (- 25° to 25° F)

Turbulence measurements were made at a nominal temperature of 500° R (40° F).

Instrumentation

Velocity and pressure surveys were made with the use of Super Probe II, figure 12. Super Probe II is a 1 inch diameter five-hole probe designed to measure

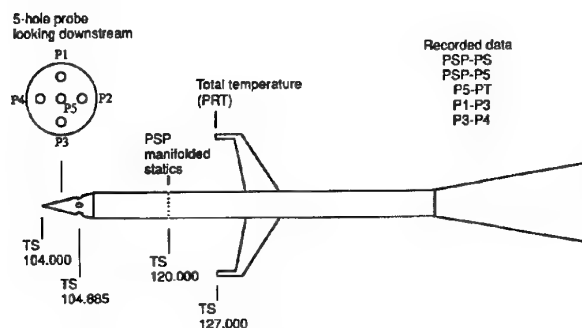


Figure 12. Super Probe II Instrumentation.

total and static pressures, with four pressure taps located 90° apart on the conical portion used to measure the clear tunnel upflow and crossflow. In addition to pressure measurements, the probe is equipped with two temperature measuring platinum resistance thermometers. The Super Probe II is extensively used in the calibration of several Boeing facilities and the NASA Ames 11 foot transonic tunnel. Super Probe II was fixed to the tunnel traversing mechanism, capable of horizontal and vertical travels. The traverse range in the horizontal direction was ± 12 inches from the tunnel center and in the vertical direction from Water Lines 18 to 68.

Turbulence measurements were obtained using hot wire anemometers. Three hot wire probes of 0.00015 inch diameter (one single wire and two cross wires) were assembled 0.5 inch apart on a frame holder which could be fixed to the traversing mechanism. In addition to the hot wires, two accelerometers were used to correct the hot wire data for support system vibrations as needed. Figure 13 shows the arrangement of hot wire probes and accelerometers.

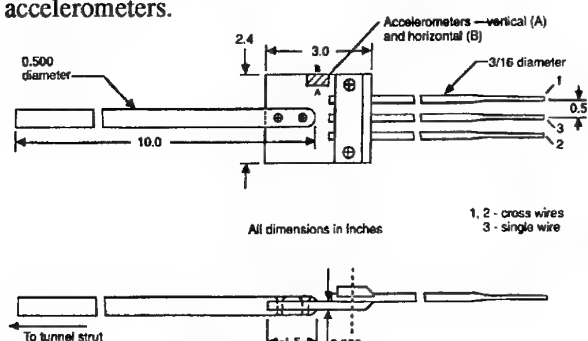


Figure 13. Hot Wire Diagram.

Two, 3 inch boundary layer rakes were used to measure the clear tunnel boundary layer thickness.

They were positioned 8 inches above the tunnel horizontal center line (Water Line 44) on the test section sidewalls at Tunnel Station 120. The rakes were made from 19, 0.043 inch diameter stainless steel tubes arranged with closer pitch near the wall to obtain a good definition of boundary layer profile, a static pressure probe was included on the rake at a height of 3 inches.

The hot wire and anemometer data was recorded on a magnetic tape for spectral analysis of the unsteady loads and fluid flow. The root mean square value of the three component turbulence was recorded in a frequency bandwidth of 2 Hz to 10 kHz and King's Law method was used to compute all three components of turbulence.

RESULTS AND DISCUSSION

Tunnel Centerline Static Pressure Correction

This test was conducted by positioning the Super Probe at the tunnel center line, Tunnel Station 120 and Water line 36, which is the balance center reference. The vertical spraybar support was continuous with no 14 inch gap in the center of the tunnel. This test was made to establish the relation between the static pressure input to the tunnel velocity controller and the test section center line static pressure measured by the Super Probe in the velocity range of 50 to 250 knots. The ratio of the center line static pressure to the test section static pressure (PSCORR) is used to compute the corrected free stream tunnel velocity (Figure 14). This data is compared to the 1993 data with the 14 inch gap in the vertical spraybar support. Note the significant change in the centerline static pressure

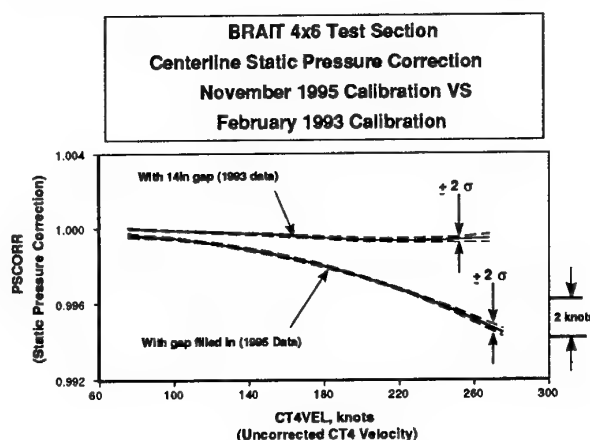


Figure 14. Tunnel Centerline Static Pressure Correction.

correction for the 1995 data. A $\pm 2\sigma$ band for 95.4 percent confidence level is shown for comparison for each set of data. This confidence level was determined from four repeat runs. No total pressure corrections are made for either case since the Super Probe total pressure agreed well with the measured tunnel total pressure.

Velocity Distribution: The velocity distribution was reevaluated by performing Super Probe vertical traverses. The traverses were made at five buttock lines including tunnel center line, with and without spraybar blowing. The results are shown in figure 15 for a free stream velocity of 250 knots and are

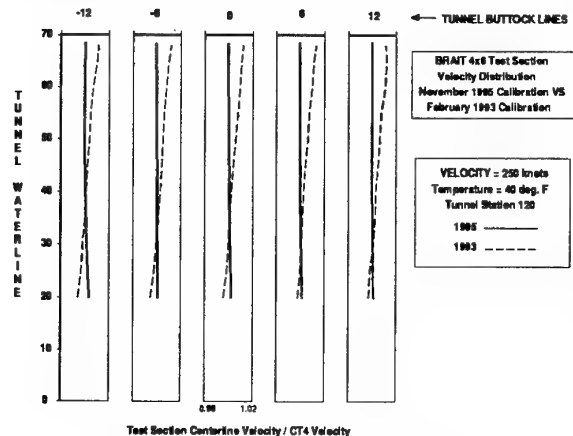


Figure 15. Velocity Distributions.

compared to the 1993 calibration in which the vertical strut had a 14 inch gap. Local velocity is normalized with respect to the tunnel velocity. The results indicate a steady gradient of about 0.4 percent per foot with free stream velocity reaching test section velocity at tunnel Water Line 30 for the discontinuous vertical strut data. The continuous vertical strut data indicates nearly no velocity gradient except near the floor at Water Line 20. Velocity is practically uniform across all buttock lines. At a tunnel velocity of 250 knots the maximum variation is within ± 1 knot. However, the velocity variation is within ± 0.25 knots in an area of ± 1 foot about the tunnel center plane where most models are tested. The velocity distribution is excellent and shows a marked improvement over the 1993 data.

Temperature Distribution: Temperature surveys were carried out with the Super Probe II and a special probe holder to cover the areas not covered by the traverse mechanism. The results indicate an

excellent temperature uniformity over the entire cross section of the test section at Tunnel Station 120. Figure 16 shows that at a tunnel temperature of 0°F, temperature uniformity is within $\pm 1^\circ$ F except for a small region above Water Line 25 at 150 Kn.

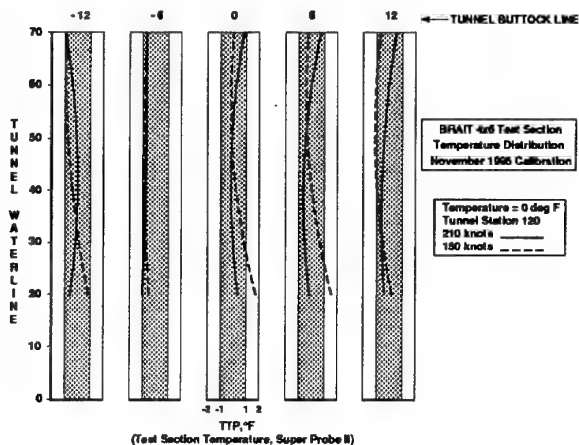


Figure 16. Test Section Temperature Distribution.

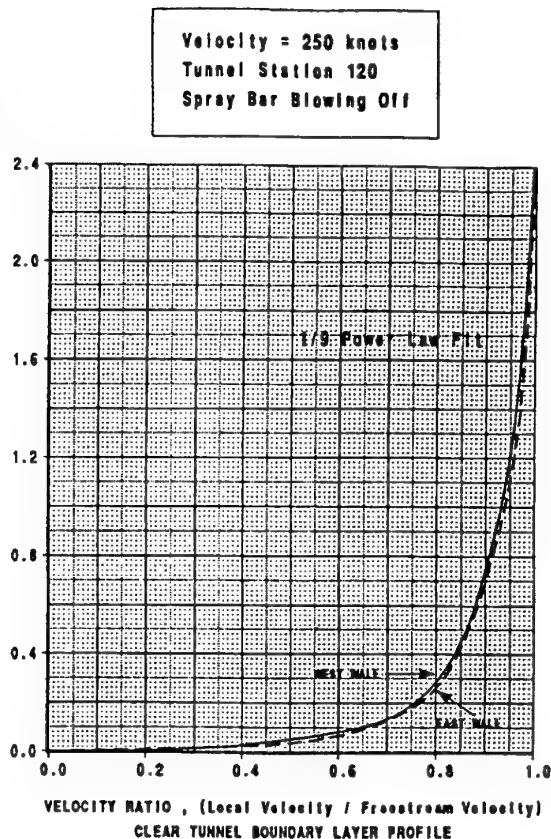


Figure 17. Boundary Layer Profiles.

Boundary Layer Measurements: The boundary layer thickness was not reevaluated in 1995 because the vertical spraybar support strut gap change would have no effect on the boundary layer thickness of the tunnel. Total pressure measurements obtained in 1993 from the boundary layer rakes were normalized with the outer edge velocity; these are shown in figure 17. The physical thickness of the boundary layer at 250 knots is 2.3 inches at a velocity ratio of 0.995. Further analysis of the profile indicated a power law fit of $1/9$. The displacement thickness for this power law profile is 0.23 inch. At 150 knots the boundary layer thickness is about 2.5 inches indicating a slight increase as expected. Also, the spray nozzle blowing did not alter the boundary layer characteristics.

Flow Angle Measurements: Flow angle measurements were not repeated in 1995 due to time constraints and the fact that the data was not important for ice accretion testing. Figures 18 and 19 show clear tunnel upflow and crossflow profiles at several buttock lines, at two velocities of 150 and 250 knots respectively. Since all icing tests are done with spraybar blowing, flow angularity

distributions are presented for that condition. At the tunnel velocity of 150 knots (Figure 18) the upflow and crossflow distribution is well within $\pm 0.2^\circ$ and uniform. Whereas at 250 knots (Figure 19) the flow angularity distribution is substantially non-uniform. Also the maximum crossflow is more than 0.4° . This was rather surprising since the flow conditions were the same except for the 67 percent increase in the approach velocity to the spraybar. However, the following explanation is proposed. At 150 knots the momentum in the approach flow and the jet momentum from the spray nozzles appear to be well balanced such that the down stream flow and the wakes from the spraybars and support structure mix well resulting in a fairly uniform flow angle distribution in the test section. For the case of 250 knots, because of higher approach momentum at the spraybar, and with the same jet momentum, the mixing process is incomplete. This results in relatively higher flow angularity with non-uniform profiles. Also, the discontinuous vertical spraybar support could cause excessive crossflow due to wakes shedding off the ends of the spraybars in the center of the stilling chamber. With a continuous

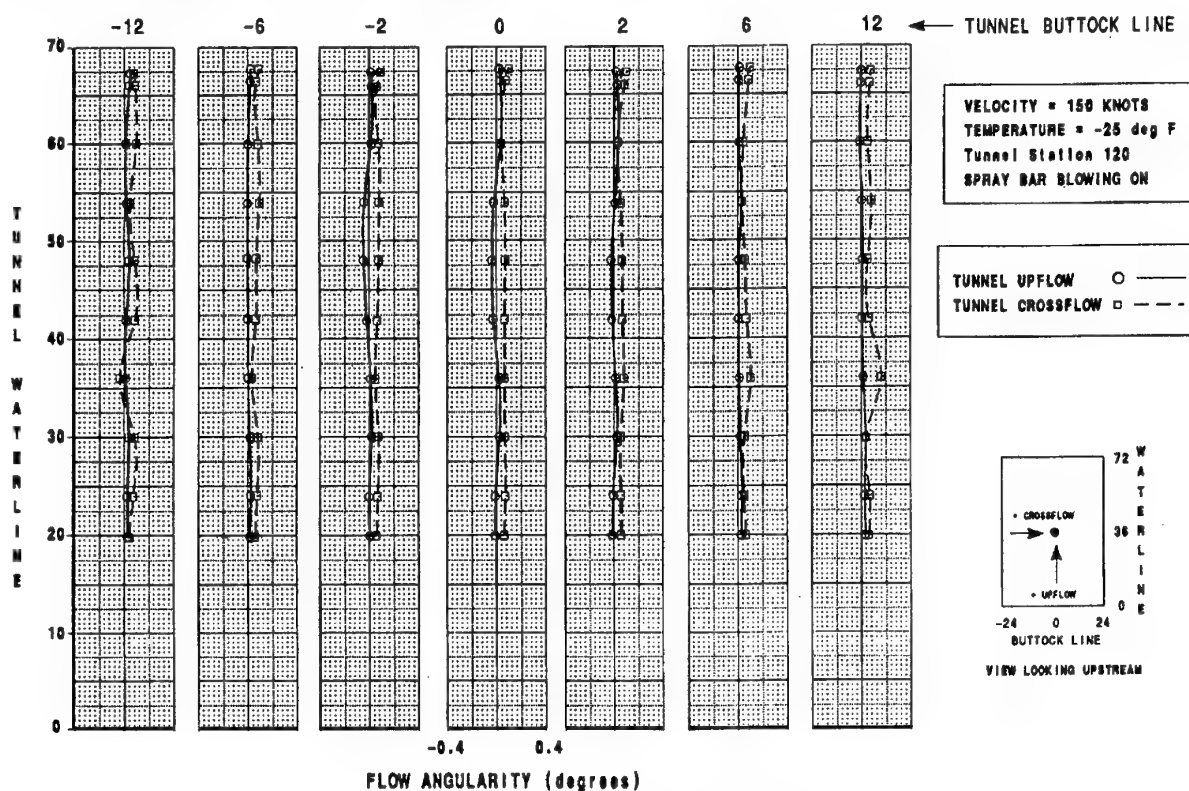


Figure 18. Flow Angularity (degrees).

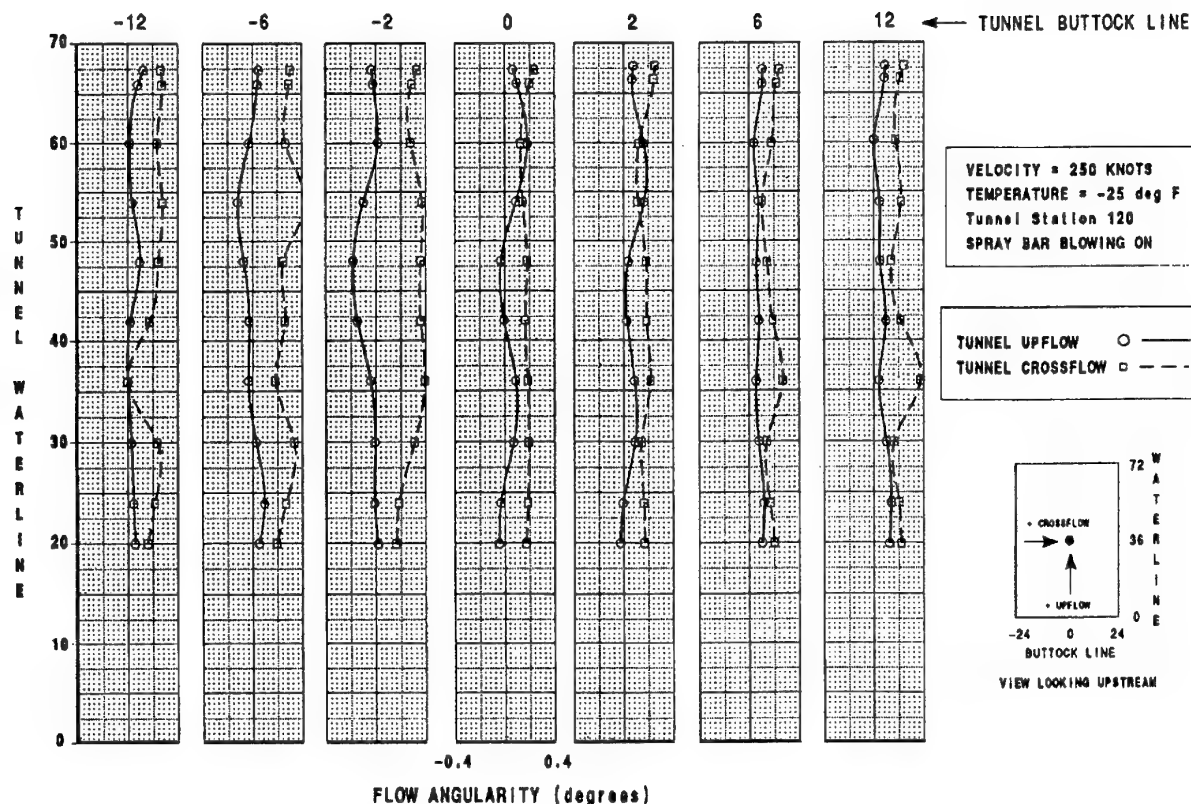


Figure 19. Flow Angularity (degrees).

vertical spraybar support, improved crossflow distributions is expected.

Turbulence Measurements: Data shown is from the 1993 calibration with the discontinuous vertical spraybar support. Turbulence measurements were obtained at a tunnel temperature of 40°F, with and without spraybar blowing. Attempts to obtain the data at lower temperatures proved unsuccessful since the tunnel was not completely dry. Small ice crystals formed at sub-zero temperatures damaging the hot wires.

The output from the hot wires was carefully analyzed and compared with the accelerometer signals. This comparison was made from frequency spectra, coherence plots of accelerometer and anemometer signals. Detailed analysis indicated a very weak dependence on the mounting system vibrations, but the turbulence data was not affected by more than 0.005. Therefore, the final data does not include this correction. Figure 20 shows the distribution of turbulence intensity at 250 knots without spraybar blowing. The turbulence intensity is defined as follows:

$$U' = \sqrt{1/3 (u_{av}^2 + v_{av}^2 + w_{av}^2)} \quad \text{Eq. (1)}$$

where u_{av}^2 = average of longitudinal turbulence measurements.

Note the high regions of turbulence intensity on either side of the horizontal center plane (Water Line 36). The center line turbulence intensity is about 0.8 to 0.9 percent. This is due to the discontinuous vertical strut supporting the spraybars. As stated before, with spraybar blowing, the turbulence profiles tend to flatten as seen in figure 20. It is also seen from the figure that overall mean turbulence level is about 1.1 percent.

The role played by turbulence on the ice accretion process is not clearly understood. As such, there is no specific recommendation on the desired level of turbulence intensity by the icing test community. However, intuitively it is necessary to obtain a reasonable turbulence intensity uniformity in the test section. Uniform turbulence results in enhanced regions of cloud uniformity.

Overall Flow Qualities: The flow qualities are qualitatively compared with the NASA Lewis Icing Research Tunnel (IRT) calibration data reported in Reference 1.

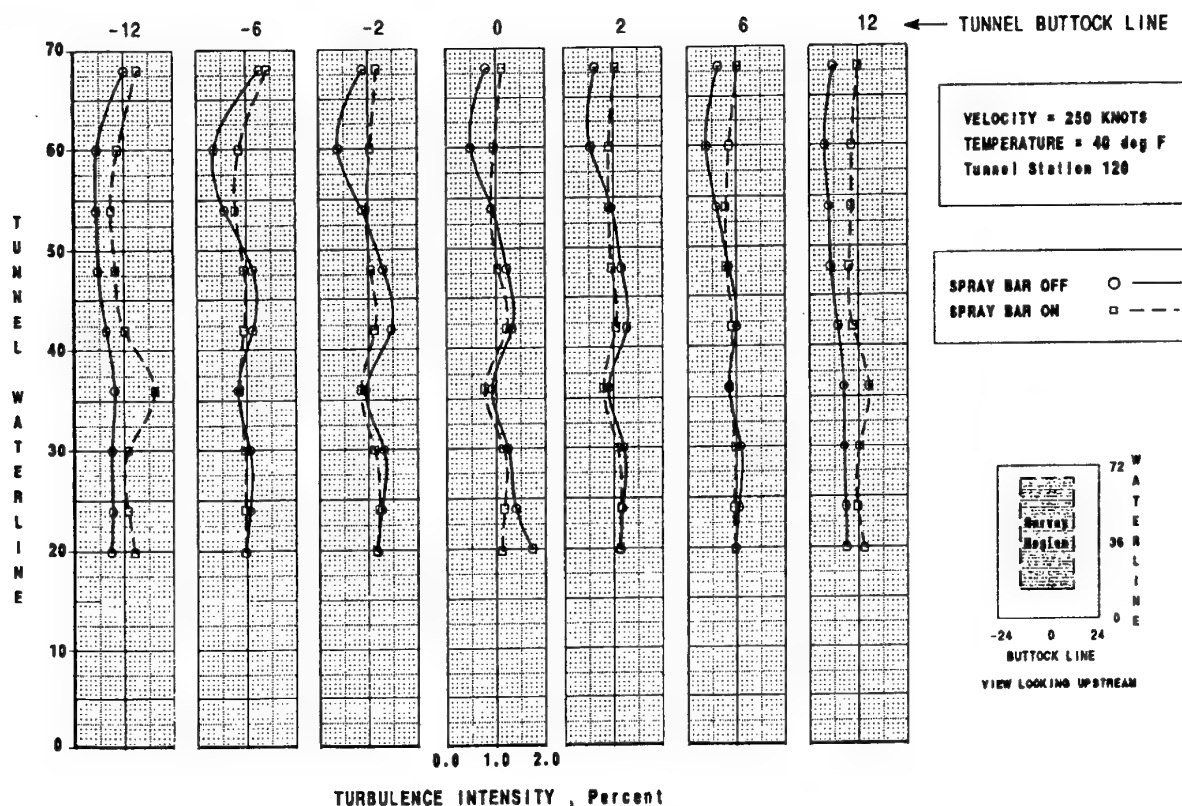


Figure 20. Turbulence Intensity.

1. Clear tunnel velocity uniformity is superior to IRT. For most of the test section, the velocity is within ± 1 percent of the free stream velocity. Velocity distribution is not affected by spraybar blowing.
2. Temperature uniformity is excellent, with a uniformity of $\pm 1^\circ\text{F}$ for all tunnel temperatures.
3. Mean turbulence intensity is about 1 percent which is higher than IRT. However, at the center line the value is comparable to IRT.

The dry air flow qualities demonstrate much better characteristics compared to IRT. Higher level of turbulence and homogeneity has helped in achieving the desired cloud uniformity in the test section.

ICING CALIBRATION

The icing calibration was initially conducted in 1993 and repeated in 1996 in the 4 foot x 6 foot test section. The calibration procedures followed NASA Lewis IRT procedures very closely. Icing calibration in the BRAIT is accomplished by cooling the air to 0°F and injecting water droplets into the airstream via the spraybar system (figure 10) to

simulate natural icing conditions encountered during flight. Temperature has negligible effect on icing cloud quality and hence, the icing calibration can be conducted at a fixed temperature. The icing calibration was completed in order to determine the following: A) Individual nozzle calibrations, B) Droplet size calibration, C) Cloud uniformity, D) Liquid water content.

Test Conditions

The calibration was made in the following range of tunnel operating conditions:

Velocity Range	50 to 250 Knots
Temperature Range	442° R (0° F)
Droplet sizes	Varying
Liquid Water Content	Varying

Instrumentation

The Laser Droplet Measurement System (LDMS) being used in the BRAIT facility is mounted externally to the tunnel circuit for fixed point drop size measurements during normal icing runs. The laser being used is an Aerometrics Phase Doppler Particle

Analyzer (PDPA). It simultaneously measures the size and velocity of spherical particles that pass through the sample volume formed by the intersection of two argon-ion laser beams. The fringe pattern is reflected back to the receiver aperture. The method for measuring the particle velocity is based on the laser Phase Doppler velocimeter principle. The PDPA is used in the off-axis back-scatter mode of operation and the typical diameter range is from 0.5 to 8,000 microns.

Nozzle Calibrations

Prior to conducting an icing calibration, the individual nozzles which inject water into the tunnel must be calibrated. This is done to determine nozzle selection and optimum spacing. There are two sizes of nozzles used in the BRAIT, MOD-1 and Standard nozzles which are similar to the nozzles used in the NASA Lewis IRT. The MOD-1 nozzles are used for the low liquid water content range (0.5 to 1.0 g/m³) and have a water tube internal diameter of 0.0155 inch. The Standard nozzles are used for the high liquid water content range (0.8 to 2.5 g/m³) and have a water tube internal diameter of 0.0250 inch.

Individual nozzle calibrations are accomplished by the use of a spray rig which uses high pressure air to atomize a water jet. The droplet size and liquid water content are set by adjusting the water and air pressure delivered to each nozzle. Each nozzle is installed in the spray rig and a predetermined schedule of water and air pressures tested on each individual nozzle to determine a flow coefficient which is defined as follows:

$$C_f = W / \Delta P^{0.5} \quad \text{Eq. (2)}$$

where W is the water flow rate in gallons/min and ΔP is the differential pressure between the water and air supplied to the nozzle in pounds per square inch (psi). For most nozzles, the flow coefficient remains relatively constant over the entire water and air pressure schedule. A total of 139 MOD-1 and 209 Standard nozzles were tested.

The nozzles used in the BRAIT spraybar system were selected based upon the consistency of the flow coefficients over the test conditions and then grouped with other nozzles that varied no more than $\pm 5\%$ from the average of the nozzles calibrated for that type of nozzle. The average flow coefficient for the MOD-1 nozzles was 0.004873 and for the Standard nozzles, 0.0113. A total of 63 MOD-1 and 106 Standard nozzles were used in the final BRAIT

configuration. The total number of nozzles to be used is determined by calculating the range of water weight flows needed for a given range of liquid water contents. Given the average flow coefficient for each type of nozzle, one can determine the number of that type of nozzle needed.

Droplet Size Calibration

The Laser Droplet Measurement System described earlier measures a Median Volume Diameter (MVD) which is the droplet diameter at which half the liquid volume has smaller diameters. It is calculated by integrating a histogram of volume weighted diameters and determining the 50% point. The Laser Droplet Measurement System was used to map the droplet sizes as a function of air pressure and the differential pressure between the water jet and air pressure (ΔP). This was done for both the MOD-1 and Standard nozzles. The droplet sizes were recorded in the middle of the tunnel only.

Cloud Uniformity

Liquid water content cloud uniformity testing was conducted for each set of nozzles. It was done in three phases. In the first phase, a 6 inch square mesh grid with 0.188 thick horizontal and vertical members was installed in the tunnel. Testing began by installing the 63 MOD-1 nozzles in a uniform pattern in the spraybars. Using a nominal tunnel setting, spray was initiated until approximately 0.5 inch of ice was accreted on the grid. Initial studies were to determine where individual nozzles accreted on the grid. This was accomplished by activating only a few of the MOD-1 nozzles at a time and recording where the ice accretion occurred until all the nozzles had been activated and their respective ice accretion locations recorded. It was shown that the nozzle spray followed the contraction ratio of the tunnel bellmouth to a reasonable extent. This allowed the determination of which nozzles to move when the local ice accretion was deficient or too high.

The second phase of cloud uniformity testing involved using the 6 inch mesh grid to move spray nozzles to obtain a uniform ice accretion over the entire grid. The determination of uniformity was done visually due to the difficulty in measuring the ice accretion on the grid. For areas of low ice accretion, the nozzle accretion map described above was used to determine which nozzle to exchange with a nozzle which had a higher flow coefficient.

Likewise, for areas of high ice accretion, the suspect nozzle was identified using the map, and that suspect nozzle was exchanged with a nozzle with a lower flow coefficient. In addition, nozzles were activated or deactivated for areas of low or high ice accretion. This process was repeated until a reasonable cloud uniformity was obtained.

The third phase of cloud uniformity testing involved using a series of 1.5 inch diameter pipes to quantitatively assess the cloud uniformity. There are two sets of pipes, one horizontal and one vertical. The horizontal pipes consist of 7 pipes located at Water Lines 6, 16, 24, 36, 48, 56, and 66. The vertical pipes consist of 5 pipes located at buttocklines ± 18 , ± 9 , and 0.

Initially, the horizontal pipes were installed with the MOD-1 nozzles, nominal test conditions set, and spray initiated. Ice was allowed to accrete on the pipes until approximately 0.25 inch of ice had accumulated in the center of the test section. The circumference of the ice accretion was then measured at two inch intervals along each pipe. The recorded measurements were normalized to the test section center value using the following equation:

$$\frac{\text{LWC}_{(x,y)}}{\text{LWC}_c} = \frac{C_{(x,y)} - C_{\text{pipe}}}{C_c - C_{\text{pipe}}} \quad \text{Eq. (3)}$$

Current NASA Lewis IRT guidelines define an acceptable cloud uniformity as being within $\pm 20\%$ of the test section center value. For the above equation this equates to values between 0.8 and 1.2. To get an acceptable cloud uniformity condition, several iterations of nozzle exchanging were completed until a reasonable cloud uniformity was established. These nozzle changes were made using the data from the horizontal pipes. Once an acceptable cloud uniformity was established using the horizontal pipes, the vertical pipes were installed and identical test conditions run. Because the vertical pipes measure the cloud uniformity at different points in the test section than the horizontal pipes, it became necessary to change nozzles on the basis of the vertical pipe cloud uniformity data also. Once the nozzles are changed on the basis of vertical pipe results, the horizontal pipes must be re-installed to check the cloud uniformity at the horizontal stations. Thus, it becomes an iterative process to achieve an acceptable cloud uniformity. Once an acceptable cloud uniformity has been

established for both the horizontal and vertical pipes, the data is algebraically merged together and a contour plot is created for each calibration condition.

Using the above procedures, reasonable cloud uniformity levels were achieved with Standard nozzles. However, close examination of Figure 21a revealed that pockets of low levels of ice accretion were present in the regions adjacent to the vertical centerline. This was traced to the continuous vertical spraybar support wake. It was deduced that the now

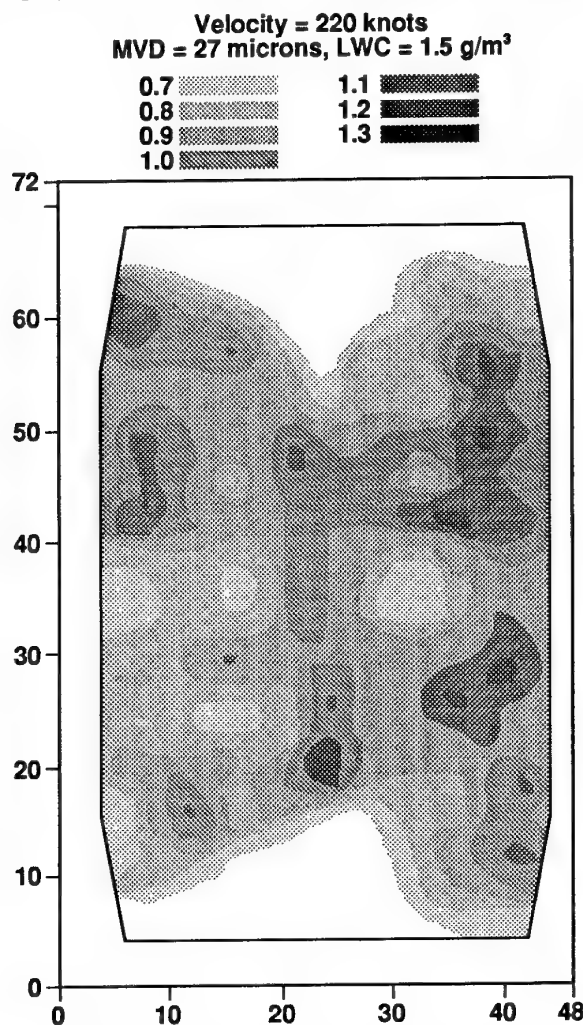


Figure 21a. Cloud Uniformity Plot Without Spraybar Mixers.

continuous vertical spraybar support was creating a wake which propagated into the test section. It is believed this wake caused the spray from other nozzles to be entrained into it causing a large concentration of water directly downstream of the vertical support. In the interest of improving the

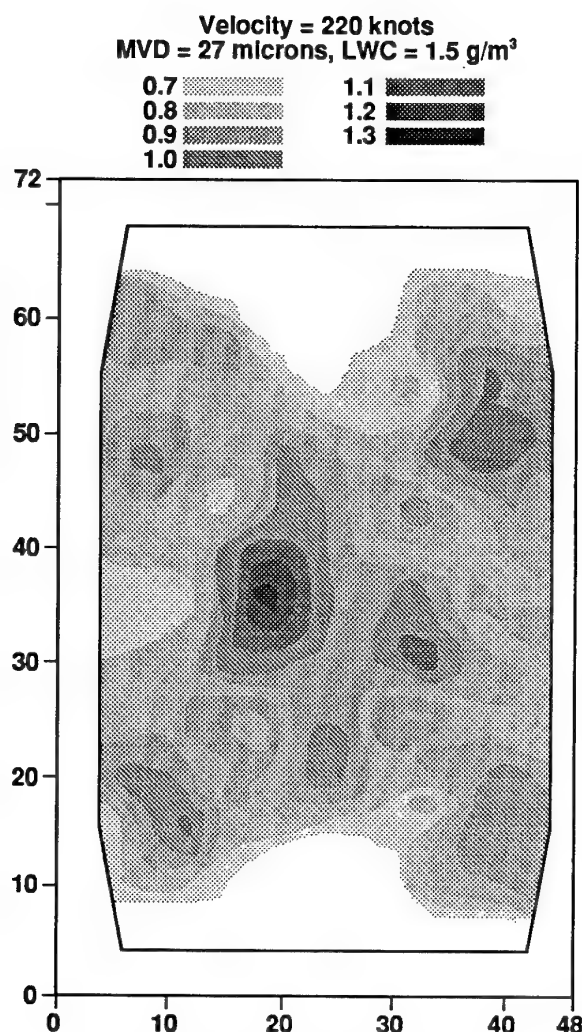


Figure 21b. Cloud Uniformity Plot With Spraybar Mixers.

cloud uniformity further, two vertical airfoil sections were installed between spraybar numbers 4 and 5 midway between the stilling chamber wall and the spraybar vertical support (Figure 9). These two sections are identical in shape to the airfoil shaped spraybar vertical support. These two airfoil sections served the purpose of enhancing the mixing process by creating wakes which enhances the mixing of the water cloud prior to entering the contraction. Figures 21a and 21b show the cloud uniformity with the two airfoil sections removed and installed, respectively. This clearly illustrates the improvement in cloud uniformity with the airfoil cloud mixers installed. The resulting data shows remarkable improvement in the spread of the icing cloud across the center of the test section. This would indicate that the turbulence uniformity across the

test section has improved with the addition of the two airfoil cloud mixers similar to the improvement seen with the closure of the 14 inch gap in the vertical spraybar support. The improved turbulence uniformity due to these cloud mixers caused an overall improvement in the icing cloud homogeneity.

Much discussion has occurred in the icing community about the effect of turbulence levels and turbulence homogeneity on the icing cloud. The correlation between flight turbulence intensity and ice accretion is an unknown factor in the industry. Likewise, the effect of turbulence on the icing cloud and ice accretion in a wind tunnel environment is unknown and much study remains to find a correlation between the two, if any.

It was found that tunnel velocity and LWC impacted cloud uniformity the most. Decreasing velocity or increasing LWC improves the cloud uniformity dramatically. Droplet size and tunnel temperature had little or no effect on cloud uniformity. Figures 22 and 23 show typical MOD-1 nozzle cloud uniformity contour plots. Figure 22 shows the cloud uniformity at a nearly constant LWC with different velocities. The 130 knot velocity map clearly shows a superior cloud uniformity than that of the 235 knot case demonstrating that cloud uniformity improves with decreasing velocity. Similarly, figure 23 shows the cloud uniformity at a constant velocity of 220 knots and different liquid water contents. The .75 g/m³ map clearly shows a superior cloud uniformity than that of the .45 g/m³ map, demonstrating that cloud uniformity improves with increasing liquid water content.

Liquid Water Content Calibration

The liquid water content (LWC) of an icing run is defined as the amount of water delivered into a volume of air. It is defined in units of grams per meter cubed and is a function of tunnel velocity, test section size, number of spray nozzles, and nozzle water and air pressure. Liquid water content was determined using the NASA Lewis IRT icing blade method. An icing blade installed in the center of the test section was used to measure the liquid water content over a range of velocities and nozzle air and water pressures. The blade is made of aluminum and is 6 inch long, 2 inch wide and 0.125 inch thick. Spray time was adjusted for each condition to allow approximately 0.125 inch of ice to accrete on the blunt leading edge of the blade (Figure 24). The

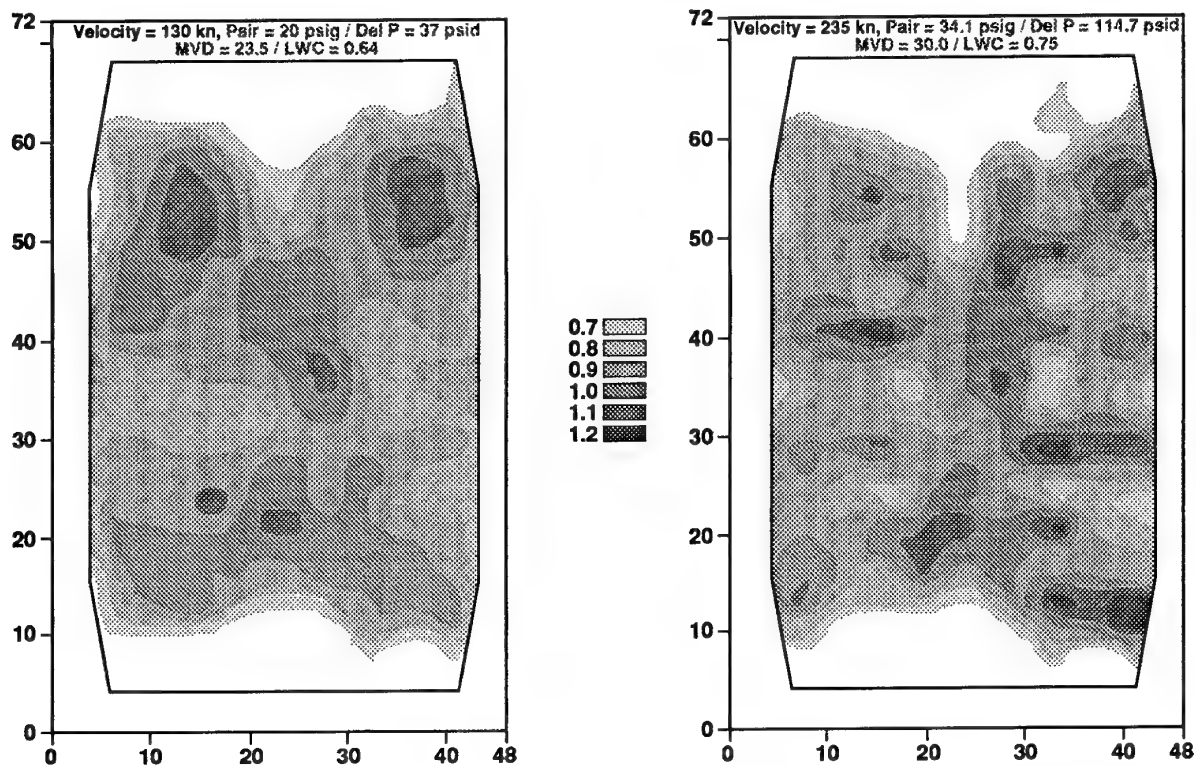


Figure 22. Effect of Velocity On Cloud Uniformity.

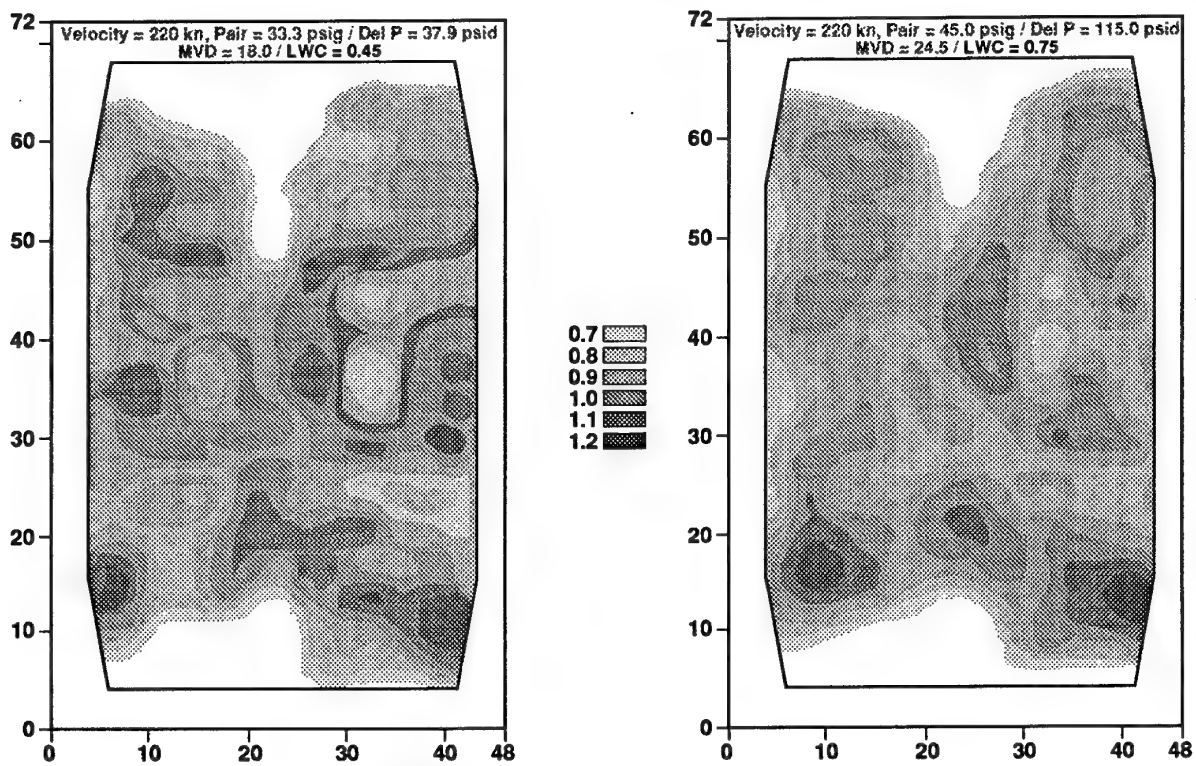


Figure 23. Effect of Liquid Water Content On Cloud Uniformity.

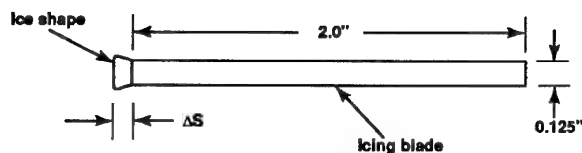


Figure 24. Liquid Water content Icing Blade.

thickness of the ice on the blade was measured at 5 stations spaced 1/2 inch apart using chilled calipers. The average ice thickness and the time of exposure were used in the following equation to calculate LWC:

$$\text{LWC} = c * \rho_{\text{ice}} * \Delta S / (E_b * V * t) \quad \text{Eq. (4)}$$

where c is a unit conversion factor, ρ_{ice} is the ice density (0.88 g/cm^3), ΔS is the average ice accretion in inches, E_b is the blade collection efficiency, V is the freestream velocity in knots, and t is the blade exposure time in seconds. A blunt blade is used to maximize blade efficiency. The blade efficiencies range from 0.90 to 0.99. The blade efficiency data is provided by NASA Lewis IRT and is expressed as a function of tunnel velocity and droplet size. It should be noted that the blade is covered by a sheath until the spraybar air and water pressure stabilize. Once the spraybar air and water pressure stabilize, the sheath is pulled from in front of the blade and the blade exposure to the icing cloud begins.

To predict liquid water content based upon spraybar pressure settings and tunnel velocity, the following equation is used:

$$\text{LWC} = K * \Delta P^{0.5} / V \quad \text{Eq. (5)}$$

It has been determined that the calibration constant K is best defined as a function of air pressure and test section velocity. This relationship takes the form:

$$K = K_a * K_v / K_0 \quad \text{Eq. (6)}$$

where K_0 is a reference constant. For calibration purposes, K_a and K_v are calculated at any given tunnel condition by equating Eqs. (4) and (5) resulting in the following:

$$K = C * \rho_{\text{ice}} * \Delta S / (E_b * \Delta P^{0.5} * t) \quad \text{Eq. (7)}$$

K_a and K_v are linear functions of their respective independent variables. K_a is determined by holding velocity constant and varying the spraybar air pressure. K_v is determined by holding spraybar air pressure constant and varying the tunnel velocity. Figures 25 and 26 show plots of K_a versus spraybar air pressure for Standard and MOD-1 nozzles,

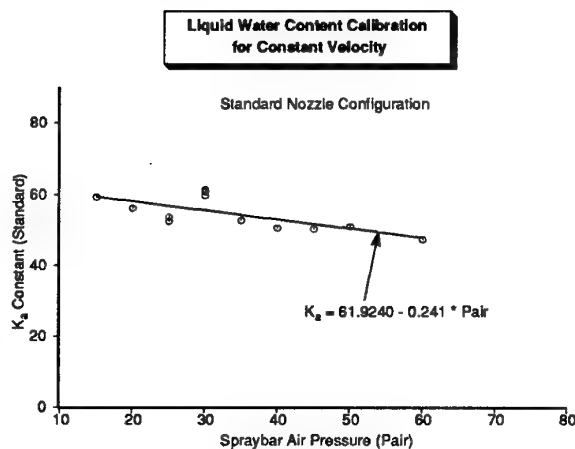


Figure 25. LWC K_a Calibration for Standard Nozzles.

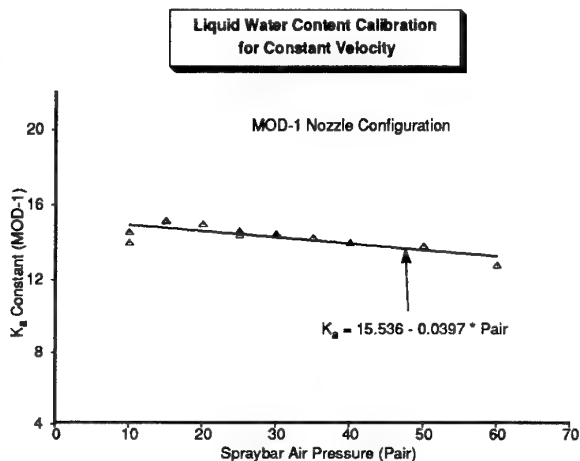


Figure 26. LWC K_a Calibration for MOD-1 Nozzles.

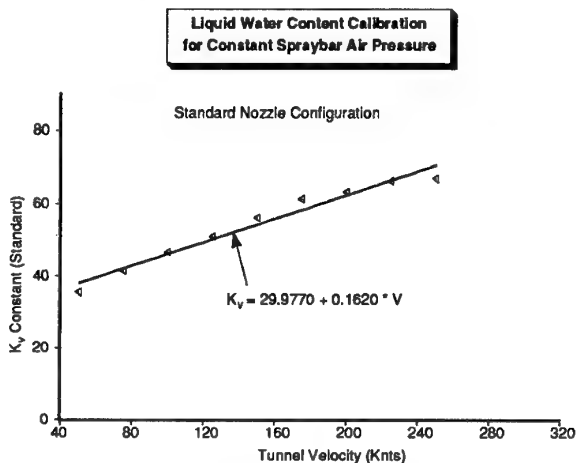


Figure 27. LWC K_v Calibration for Standard Nozzles.

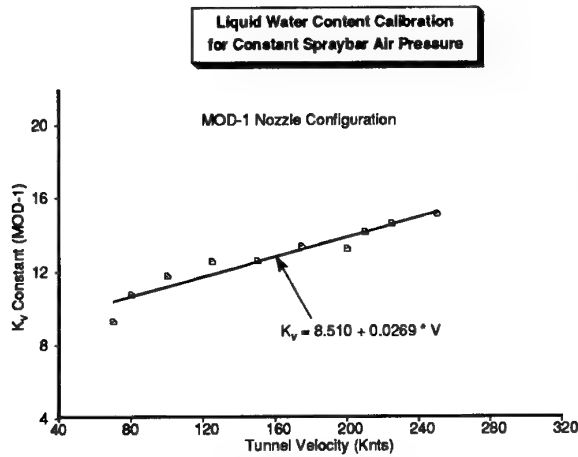


Figure 28. LWC K_v Calibration for MOD-1 Nozzles.

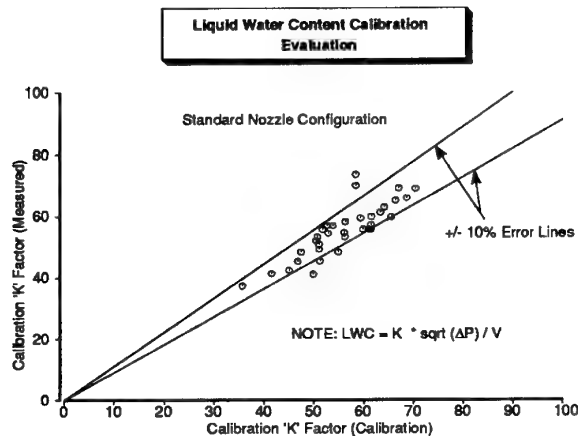


Figure 29. LWC Calibration Evaluation for Standard Nozzles.

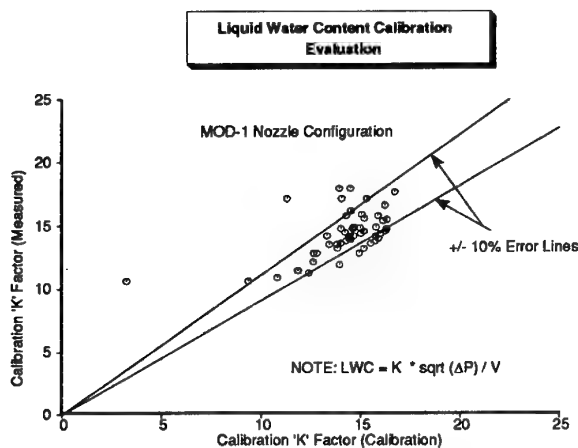


Figure 30. LWC Calibration Evaluation for MOD-1 Nozzles.

respectively. Figures 27 and 28 show plots of K_v versus velocity for Standard and MOD-1 nozzles, respectively. The following equations show the linear relationships for both K_a and K_v :

$$K_a = m_a * P_{\text{air}} + b_a \quad \text{Eq. (8)}$$

$$K_v = m_v * V + b_v \quad \text{Eq. (9)}$$

To check the validity of the calibration, the calibration data was reduced using Eq. (5) for both the Standard and MOD-1 nozzles. The results are presented in figures 29 and 30, respectively. The two lines on this plot represent the $\pm 10\%$ error bands to illustrate the validity of the calibration. As these figures illustrate, the majority of the calibration data points lie within the $\pm 10\%$ error bands. The $\pm 10\%$ error bands are the current industry standards based on using icing blade methodology to measure liquid water content.

Concluding Remarks

Since the commissioning in 1993, the BRAIT has demonstrated impressive flow quality and substantial regions of good cloud uniformity distribution in the test section. The results presented in this paper illustrate further improvement efforts which were possible.

- Velocity variation is within 0.40 percent in the area covered by ± 1 foot from the center plane. However, at the tunnel center, (Buttock Line 0, and Water Line 36) the local velocity is within 0.20 percent of the calibrated velocity which is excellent. The addition of the vertical strut between the spraybars resulted in a marked improvement in the velocity distribution over the 1993 tests.
- The boundary layer thickness at Tunnel Station 120 is 2.3 inches and the corresponding displacement thickness is 0.23 inches.
- At 150 knots with the spraybar blowing, the flow angularity (upflow and crossflow) is within $\pm 0.2^\circ$. At 250 knots the tunnel upflow is also within $\pm 0.2^\circ$, but the crossflow increases to levels approaching 0.4° . These values are typical of most low speed wind tunnels.
- The tunnel free stream temperature uniformity is excellent. The tunnel temperature uniformity is within $\pm 1^\circ\text{F}$ throughout the test section at Tunnel Station 120.
- Cloud uniformity improves with increasing liquid water content and decreasing velocity.

- Cloud uniformity for the BRAIT is better than the NASA Lewis IRT, however, improvements in the MOD-1 nozzle cloud uniformity could be achieved with airfoil cloud mixers.
- Incorporating improved cloud mixing methods will improve cloud uniformity.
- The calculated liquid water calibration is generally accurate to within 10% of the measured value which is the current industry standard.
- The tunnel is currently being used as a major certification tool in the determination of ice shapes on sensitive airplane components such as the wing, horizontal tail, engine nacelles and air data probes.

The tunnel has been operating since 1993. Extensive certification tests were conducted relating to the 777 program. Demonstration of ice shapes, deicing systems, engine nacelle intake ice shapes at significant thrust level conditions and ram air turbine power assessment under icing conditions were successfully accomplished. Very few flight tests were made to confirm the results of the wind tunnel tests. Substantial time and cost savings were realized. During 1996, we completed the tests on the deicing system evaluation of the 737-800 engine nacelle. We have completed the test requirements of national and international customers with great success. We are closely working with NASA Lewis on their Icing Research Tunnel upgrade program for the proposed development of large droplet nozzles.

Recommendations

It should be noted that although some minor improvements to the BRAIT circuit have been undertaken, this does not invalidate any previous testing done in the BRAIT.

- The effect of turbulence intensity and homogeneity on ice accretion in both the wind tunnel and flight needs to be more closely investigated.
- The addition of airfoil cloud mixers between the spraybars improved the overall cloud homogeneity. However, further optimization could be realized with additional testing.
- With the addition of airfoil cloud mixers in the BRAIT, the level of turbulence intensity and turbulence distribution needs to be determined.

Acknowledgements

The authors would like to sincerely acknowledge the support and suggestions from the following:

- G. E. Cain and B. D. Thompson of the Boeing Mechanical Systems Laboratory.
- D. J. Holler of the Boeing Aerodynamics Laboratory.
- J. E. Holland of the Boeing Aerodynamics Instrumentation Laboratory.

References

1. Soeder, R. H. and Andrachio, C. R., "NASA Lewis Icing Research Tunnel User Manual", NASA Technical Memorandum 102319, June 1990.
2. Newton, J. E., and Olsen, W., "Study of Ice Accretion on Icing Wind Tunnel Components", NASA Technical Memorandum 87095, January 1986.
3. Eck, B., "Fans - Design and Operation of Centrifugal Axial Flow and Cross Flow Fans", Pergamon Press, Oxford, 1973.
4. Wallis, R. A., "Axial Flow Fans and Ducts", Wiley and Sons, New York, 1983.
5. Chintamani, S. H., Belter, D. L., McCormick, M M., and Templin, J. T., "Fan Drive System for the Boeing Research Aerodynamic Icing Tunnel", AIAA-94-2490, June 1994.
6. Chintamani, S. H., and Sawyer, R. S., "Experimental Design of the Expanding Third Corner for the Boeing Research Aerodynamic Icing Tunnel", AIAA-92-0031, January 1992.
7. Chintamani, S. H., and Belter, D. L., "Design Features and Flow Qualities of the Boeing Research Aerodynamic Icing Tunnel", AIAA-94-0540, January 1994.
8. Cain, G. E., and Yurczyk, R. F., Belter, D. L., Chintamani, S. H., "Boeing Research Aerodynamic Icing Tunnel Capabilities and Calibration", SAE 940114, February, 1994.

NEW TEST CELL DESIGN METHODS BASED ON INTEGRATED USAGE OF CALCULATED AND EXPERIMENTAL RESEARCHES

I.I. KABAKOV, A.N. TIMOSHIN

Central Institute of Aviation Motors, 12/30 Naberezhnaya Str.
140061 Lythkarina, Moscow Region, Russia

SUMMARY

The results of integrated usage of mathematical and physical models to develop aerodynamic lay-outs of altitude and sea-level test cell components to test aviation engines are presented in the report. Performances of dissipative layer in the intake manifold are investigated. New scheme of effective gas flows mixing is developed. The method for pressure control by inducing jets in the pressure cell is given. The basic principles for engine simulators creation are shown.

LIST OF SYMBOLS

P_k	air pressure in the altitude chamber
P_1, P_2	total gas pressure in the inner and outlet profiles of the jet nozzle
P_c	total pressure of the induced air
π_1, π_2	pressure ratio decreasing in the jet nozzle
G_k	relative flow rate of ventilating air
G_m, G_f	air mass flows through the simulator and full-scale engine intake
G_{1m}, G_{2m}	gas flow rates in the Core & Fan jet nozzle profiles of the simulator engine
G_{1f}, G_{2f}	gas flow rates in the Core & Fan jet nozzle profiles of the full-scale engine
$T_{1m} = T_{2m}$	air temperature in the jet nozzle and simulator profiles
T_{1f}, T_{2f}	gas temperature in the inner and outlet full-scale engine profiles

1. INTRODUCTION

During construction of new test cells and during reconstruction of the existing ones to test large - thrust $R = 40\ 000 \dots 50\ 000$ H turbofan engines and turbojet with reheating engines at cyclic and transient modes, it is necessary to pay great attention to aerodynamic perfection of the test cells under construction.

The following procedure of test cells aerodynamic design is widely used in CIAM for a few tens of years:

- preliminary mathematical modelling using rather simple and practically approved calculated models;
- physical modelling using aerodynamic models of test cell and its components manufactured in the scale $M = 1/12 \dots 1/30$;
- final mathematical modelling using the results of experimental research.

Result analysis of experimental research of full-scale test cells showed good coincidence with the designed ones.

It should be mentioned that during the aerodynamic test, very often we are successful to simplify the configuration and to improve the aerodynamic performances of different test cell components. Close combination of calculated and experimental researches allows to perfect aerodynamic performances of the test cell components and the test cell itself. It is also possible to achieve reliable aerodynamic test cell performances during the process of the test cell designing excluding even the smallest risk of error in aerodynamic performances.

In the given report the development results of some test cell components are stated. Of course, it is not possible to cover the whole test cell, but the presented components are the basic ones and they give us idea about the integrated usage of mathematical and physical modelling.

The following components are considered in the report:

1. intake manifold;
2. different temperature air flows mixer;
3. thermal vacuum chamber;
4. ejector device for pressure control inside the thermal vacuum chamber;
5. engine simulator for aerodynamic researches.

2. INTAKE MANIFOLD

In practice of aviation engine testing both in sea-level test cells and in altitude test cells the intake manifold is widely and frequently used with the gap of a profile realized when the intake manifold has a smooth profile. Such a profile has been introduced into the practice out of engine tests in unrestricted space or in large-size sea-level test cells.

At present due to the increase of engine sizes, that is with the increase of relative dimension of the intake manifold (d/D) the problems associated with the separated flow in the circulation zone upstream the intake manifold arise. The preliminary calculations showed the increase of the dissipative layer in the manifold. But for more reliable determination of the dissipative layer thickness, experimental researches using a model were carried out (See Fig.1). To determine the influence of relative manifold diameter, one manifold and 4 settling chamber models were manufactured. Constant M number value and correspondingly Re number were kept up in the manifold. It gave an opportunity to obtain the dependence of dissipative layer thickness only of the relative diameter at constant M and Re numbers.

Fig.1 shows the velocity profile in the manifold at the distance equal to two diameters of the manifold from its entrance. As it is seen in Fig.1, at the increase of the relative manifold diameter, the dissipative layer thickness increases. The velocity profile in the boundary layer changes, it becomes less filled out. It takes place because the dissipative layer in the manifold is a part of mixing layer in front of the manifold which interacts with the manifold walls. As a result of this interaction, a very complicated dissipative layer appears the thickness and the filling of which depends on the relative manifold diameter and the distance from the entrance to the manifold. As it is seen in Fig.1, the intake manifold with the profile gap is expedient to use at relative manifold diameter < 0.3 . At larger values of relative manifold diameter, it

is expedient to use the manifold profile without any gap - like Vitoshinsky nozzle type.

3. DIFFERENT TEMPERATURE GAS FLOWS MIXER

To control air temperature at the engine face, cold air and hot air mixers are used. The basic performances of such mixers are:

- Temperature field uniformity.
- Temperature time lag.
- Coefficient of hydraulic resistance.

A great deal of different types of gas flow mixers do exist, including petalled, jet, vortical, etc.

To decrease the mixing chamber length, the jet split-up for a great number of jets is used. But in this case a number of problems associated with ensuring the uniform flow distribution by small jets arise. In case of a non-uniform distribution of flow rates by jets, the global non-uniformity appears; its smoothing takes place on a length which is proportional to the mixing chamber diameter. Besides, if the global non-uniformity already exists, some problems connected with the decrease of the non-uniformity arise.

On the basis of numerous experimental researches "S"-shape mixers were designed by CIAM specialists. This type of a mixer is two reversible elbows joined in series. The twin vortex is formed in the elbow and because of this the temperature profile downstream the elbow changes nearly on the contrary one. In the second elbow the twin vortex with a very high turbulence intensity is also formed. As a result, downstream the two reversible rotatable elbows the uniform velocity field with 0.8% of non-uniformity takes place. On the same length in the straight-line channel the temperature field non-uniformity is 12%, but downstream one rotatable elbow it is 7%. The schematic of "S"-shape mixer and the temperature field in different type mixers are presented in Fig.2. It should be mentioned that due to a decrease of mixing chamber length, the temperature time lag and the mixer hydraulic resistance coefficient decreases.

The coefficient of the mixer resistance is approximately equal to the resistance coefficients sum of the two rotatable elbows and it makes 1 (according to dynamic pressure in the mixer).

Performances comparison of "S"-shape mixer with other mixer types demonstrates

the advantage and the design simplicity of "S"-shape mixer. These type of mixers ("S"-shape) are widely used in the test cells for aviation engine tests.

4. ALTITUDE CHAMBER AND EXHAUST DIFFUSER INFLUENCE ON THE JET NOZZLE PERFORMANCES

One of the basic demands presented to the test cell when altitude engine tests are carried out is elimination of altitude chamber and exhaust device influence on engine performances. For this purpose in the whole altitude chamber out of the jet bounds it should be one and the same pressure and low velocity of the air flow inside the altitude chamber. It is only possible at definite area ratio of the jet nozzle, altitude chamber and the exhaust diffuser. Moreover, the increased pressure fluctuations inside the altitude chamber should not take place.

During the aviation engine tests at altitude conditions inside the altitude chamber with delivery of the ventilated air, the air mass flow of which is $G_k = 0.05 \dots 0.10$ (5...10%) of the air mass flow through the engine to the altitude chamber, the circulating flow appears as a rule. Its nature and intensity depend upon the relative area F_d of the exhaust diffuser, the distance l_c from the nozzle section to the exhaust diffuser, relative altitude chamber area F_k and engine operation mode, where F_d and F_k is a relation of the exhaust diffuser area and the altitude chamber to the area F_c of the jet nozzle exit section.

Investigations of jet nozzle models for turbojet engines in the altitude chamber with the exhaust diffuser showed that the most favourable geometric parameters are the parameters when the whole jet with the mixing layer enters into the exhaust diffuser. The reverse flow which appears in the diffuser at its wall induces the secondary vortex. When the part of the mixing layer does not enter the exhaust diffuser, but flows around its outer wall, several vortexes may appear in the altitude chamber. The pressure fluctuations inside the altitude chamber is greater by several fold if we compare with the first case, and the pressure along the altitude chamber wall becomes variable. That is why it is expedient to specify small distances l_c but in addition it should not be an influence on pressure along the outer surface of the jet

nozzle. The investigations showed, to exclude the altitude chamber and the exhaust diffuser influence on the jet nozzle it is enough to arrange the jet nozzle section at the distance $l_c = (0.5 - 0.7)d_c$, where d_c is a diameter of jet nozzle exit section.

The investigations showed that the pressure along the altitude chamber wall is practically constant for a wide range of change of engine operation mode if $F_k > 15 - 20$. For high by-pass ratio engines and large thrust engines (like "Trent", GE-90) it is a problem to create altitude chambers with the relative area $F_k = 15-20$. Russian altitude test cell chambers can have the relative area $F_k = 3.5 \dots 5$ to test similar engines. Due to this it is necessary to study the altitude chamber and the exhaust device influence on the performances of by-pass ratio jet nozzle. For this purposes the model installation and the jet nozzle model was designed. It simulated the jet nozzle for HK-93 engine the by-pass ratio of which is 16. The schematic diagram of the model installation is presented in Fig.3. The diffuser with the punched and optimal configuration gas intake was used in the model installation. During the tests the coefficient of flow rates for inner and outer profiles of the engine model was determined as well as distribution of pressure along the surfaces of the jet nozzle when the article was tested without any altitude chamber (reference conditions) and with the altitude chamber. The investigations showed that at $F_k = 5$ with the optimal configuration of a diffuser the flow rate coefficients of the inner and outer profiles for test reference conditions and for tests in the altitude chamber practically coincide.

It is shown that the altitude chamber with the exhaust diffuser does not also influence the distribution of pressure along the engine nacelle and the flow over the inner profile in the investigated range $\Pi c_2 = 1.2-1.7$.

The scheme and velocity fields in the altitude chamber for section I are given in Fig.3. The section I agrees with outlet nozzle section of the outer profile and for section II located in the zone of circulating flow. The measurements were performed for $G_k = 0; 0.06$ and 0.11 . At $G_k = 0$ in the section I the reverse flow in the altitude chamber takes place and it disappears when $G_k = 0.06 \dots 0.11$. Pressure distribution along the altitude chamber wall is a result of inner

flow in the altitude chamber. Investigations showed the pressure on the altitude chamber wall on the length of its front end to the section 1 is practically constant.

In the zone of the inner profile nozzle positioning the pressure slightly differs from the pressure in the section 1; the greatest difference of the static pressure is observed in the circulating zone downstream the jet nozzle. During the experiment it was obtained that with the increase of the relative flow rate of ventilating air G_k up to 0.06...0.10, pressure distribution on the altitude chamber wall in circulating zone becomes more uniform.

5. PRESSURE CONTROL IN THE ALTITUDE CHAMBER DURING ENGINE TESTS AT TRANSIENT MODES

At transient modes of engine tests such as engine response, rotational frequency release, increase of rotational frequency just after engine response, it is necessary to maintain constant pressure inside the altitude chamber. The task becomes more complicated because with rotational speed change the exhaust diffuser efficiency changes. For example, with engine rotational frequency increase at constant pressure downstream the exhaust diffuser the pressure inside the altitude chamber will decrease. In order not to have such situation, during the transient mode it is necessary to compensate the efficiency of the exhaust diffuser. Such problem might be solved by mechanical throttle installation downstream the exhaust diffuser. But because of high temperature of the exhaust gases (2300 K) it is difficult to realize. That is why the throttle is usually installed downstream the test cell gas cooler.

Altitude test cells as a rule have large dimensions (1000 - 3000 m³) from the exhaust diffuser up to the throttle that predetermines the pressure control system time lag in the altitude chamber even in case if the throttle is a quick-acting one.

Calculation researches of possibility to control the pressure in the altitude chamber by additional air delivery downstream the exhaust diffuser demonstrated low efficiency of this procedure.

Introduction of ventilating air to the altitude chamber will be effective only during the exhaust diffuser operation at critical

modes, that is very seldom at altitude test cell conditions. The exhaust diffuser operates mainly at subcritical modes when the ventilating air influence on the exhaust diffuser performance is not significant.

A new procedure to maintain pressure inside the altitude chamber during engine transient mode is worked. The procedure consists in the following: different effectiveness compensation of the exhaust diffuser is performed by exhaust gases ejection at small rotational frequencies up to the pressure made by the exhaust diffuser at maximal or reheated modes, but not with the help of counterpressure downstream the diffuser.

Schematic diagram of the altitude test cell with pressure ejector control system is depicted in Fig. 4.

To control pressure in the altitude chamber, to the initial section of the exhaust diffuser inducing air is delivered through the nozzles; so the exhaust diffuser is used as a mixing chamber. At engine rotational frequency the inducing air is mixed with engine exhaust gases and ventilating air of the altitude chamber. As a result pressure increases from P_k in the altitude chamber up to pressure P_3 downstream the diffuser. Air mass flow through the ejector nozzle is controlled by a throttle.

At large air volume of the exhaust system pressure P_3 will change slightly and this pressure approximately can be maintained unchangeable with the help of the test cell throttle.

During the transient mode, for example, engine response from idle to maximal mode to achieve $P_k = \text{Const.}$, it is necessary at all the rotational frequencies of engine transient modes to have constant pressure ratio in the combined system "exhaust diffuser - ejector" and to have it equal as well to the pressure ratio of the exhaust diffuser at maximal mode. The largest air mass flow of the inducing air will be at idle mode; with rotational frequency increase the above air mass flow will be decreased and at the maximal mode it will be equal to the zero. Hence, the inducing air is delivered only during the transient mode, that is it is delivered in the shot run. That is why it is expedient to deliver the inducing air from high pressure tank system.

To choose optimal parameters of the inducing jet, gasdynamic calculations were performed. Well known ejection equations

[1,2] for slightly complicated diagram presented in Fig.4 were used.

These calculations showed that in case the exhaust diffuser is used as a mixing chamber, the supersonic nozzle for the inducing air practically does not improve the ejector performances in comparison with the sonic nozzle.

On the other hand it is more simple to manufacture a convergent nozzle. That is why the further calculations and designing were carried out for $\lambda = 1$. Test mode (altitude and Mach number) influences the required air mass flow of the inducing air as well as transient mode type and its nature. In order to design the system it was necessary to choose the nondimensional area value Fe as the relation of the nozzle exit area for the inducing air to the exhaust diffuser area.

Calculations for different Fe values were done. It should be mentioned that the area of the critical section for the ejector nozzle is only some percents of the exhaust diffuser area and the choice of Fe value was determined by pressure Pe . As the area Fe was not large, 24 axisymmetrical nozzles were used in the altitude chamber for pressure control system. The nozzles arrangement was uniform along the circumference, nearby the exhaust diffuser walls. Gas parameters calculations in the exhaust system and in the ejector nozzles were performed for different engine transient modes.

The calculations showed there is a possibility to use the procedure to control pressure in the altitude chamber by introduction of inducing jets to the initial section of the exhaust diffuser.

6. BASIC PRINCIPLES OF ENGINE SIMULATOR MODELLING

For aerodynamic researches to determine optimal nozzle blockage for aerodynamic test cell with external flow around the test engine and for investigation of closed sea-level test cells performances the engine simulator is required. Flow parameters of this simulator at its inlet and outlet are similar to the realistic ones. It is more simple to manufacture the engine simulator at aerodynamic modelling when the air flow at the outlet of the simulator jet nozzle is originated with ejector.

- The initial modelling condition is geometric similarity of the intake entrance section and the jet nozzle passage.

- Another modelling condition is achievement of two flows with Mach numbers similar to the full-scale engine both at the intake inlet section and at the jet nozzle exit section. It means that the air mass flow through the intake should be determined by the following relation: $G_m = G_f/M^2$ where M is the modelling scale.

Equality of Mach numbers at the jet nozzle exit section of the model and the full scale engine demands the equality of pressure ratio decrease in the jet nozzle. Hence, pressure in the simulator jet nozzle should be higher than the pressure at the inlet as it has place in the full-scale engine.

Flow rate in both flows of the jet nozzle should be equal:

- for the Fan

$$G_{2m} = G_{2f}/M^2 * \sqrt{T_{2f}/T_{2m}} \quad (2)$$

- for the Core

$$G_{1m} = G_{1f}/M^2 * \sqrt{T_{1f}/T_{1m}} \quad (3)$$

From relations (2,3) it follows that in the engine simulator the total air mass flow through the jet nozzle is higher than the air mass flow through the intake. With high by-pass ratio "m" increase the difference in the air mass flows through the jet nozzle and the intake decreases. The fact that the air mass flow through the jet nozzle of the simulator is higher than the air mass flow through the intake gives the possibility to introduce to the engine model the compressed air, thereby to increase the air pressure in the ejector channel upstream the jet nozzle.

The calculations showed at large "m" values the ejection coefficients are high and it is not always possible to provide the required pressure ratio.

To achieve the prescribed parameters of the engine simulator jet with high by-pass ratio, we are to perform a separate partial suction of air which passes through the intake. With this the flow rate of the induced air increases and the ejection coefficient of the ejector decreases that gives precondition to achieve the prescribed pressures in the jet nozzle. With "m" increase the relative flow rate of the suction air becomes higher and with relative pressure increase of the induced air it decreases. Pressure increase of the compressed air is also expedient on constructional considerations as well because at higher pressure it is easier to solve the problems dealing with the induced air distribution along the mixing chamber section. Engine simulator

length should correspond to the length of the full-scale engine at the accepted modelling scale and during the development of the simulator the problem about the mixing chamber length arises. For ejector efficient operation it is necessary to have the length of the mixing flows sufficient to achieve uniform flow in the jet nozzle. It can be only obtained by splitting of the mixing flows for small jets the relative length of which should be 10-15. All this requires the application of multinozzle ejector with the delivery of the compressed air to the nozzles through the pylons located along the profile sections. The simulator with 264 supersonic inducing nozzles is described in work [3].

The optimal parameters of the ejector for engine simulators PW - 2037, GE - 90 and HK - 93 with high by-pass ratio corresponding to 6,8 and 16 were determined. PW - 2037 engine model was manufactured in the scale 1 / 12. GE - 90 engine model scale was 1 / 15,6 and the scale of HK - 93 engine model was 1 / 30. Aerodynamic configuration of engine simulator is shown in Fig.5. Air from the engine simulator was extracted through the punched section located between the entry manifold and the screen of the ejector nozzles, and through the annular channel inside the simulator the extracted air was delivered to the pylons and further into the exhausters. All the models have multinozzle design with 60 - 210 ejector nozzles. Ejecting nozzles were located uniformly along the mixing chamber section. Compressed air pressure was $(12 - 14) \cdot 10^5 \text{ Pa}$. Different prescribed pressures P1 and P2 in the simulator flows were achieved by choice of corresponding geometric ejector parameters.

Testing of aerodynamic simulators for PW - 2037, GE - 90 and HK - 93 showed good agreement of calculated and experimental flow parameters at the simulator inlet and outlet and the possibility of operation modes change to simulate taking - off, cruise and idle modes of the simulated engines.

7. CONCLUSIONS

It is seen from the report that for successful development and selection of aerodynamic test cell and its components configuration, integrated application of mathematical and physical models is required.

- It is shown that in conditions of relatively large inlet manifold diameters a thick dissipative layer is formed on the manifold

walls. It is expedient to use the profile with the gap in the inlet manifold at relative manifold diameter, up to 0,3, but at larger values of relative diameter the inlet manifold without a gap is preferable.

- 'S' - shape configuration of the mixer suggested in the report provides temperature field with 0,8% of non-uniformity at the length less than 7 mixing chamber diameters. This mixer allows to reduce non-uniformity in the channels with high global temperature non-uniformity.
- Flows in the altitude chamber can influence the performances of the engine nozzles at relative altitude chamber area less 0.15 and small distances between the nozzle section and the inlet exhaust diffuser ($l < 0.15$). The possibility to test large - thrust engines at relative altitude chamber area with selection of optimal exhaust diffuser providing ventilation air mass flow 0.06...0.10 of air mass flow through the engine is presented in the report.
- Schematic diagram suggested in the report to control pressure in the altitude chamber at transient modes provides pressure steadiness in the altitude chamber by introducing induced jets into the front section of the exhaust diffuser.

On the basis of the suggested concepts to simulate large - thrust engines, engine models GE - 90, PW - 2037 and HK - 93 were designed and investigated. Investigations showed good performances matching between the model engines and full-scale engines.

8. LITERATURE

1. Yu.N. Vasiliev Theory of Supersonic Gas Ejector With Cylindrical Type Mixing Chamber. Collected Book: Blade-Type Machines And Jet Vehicles. Issue -2M; Machinostroenie. 1967
2. G.N. Abramovich Applied Gas Dynamics. M. 1976.
3. A.I. Karamanlis, J.S. Sokhey, T.C. Dunn, D.C. Bellomy "Theoretical And Experimental Investigation of Test Cell Aerodynamics for Turbofan Applications" AIAA - 86 - 1732, 1986.

Fig.1 Boundary Layer In Intake Manifold

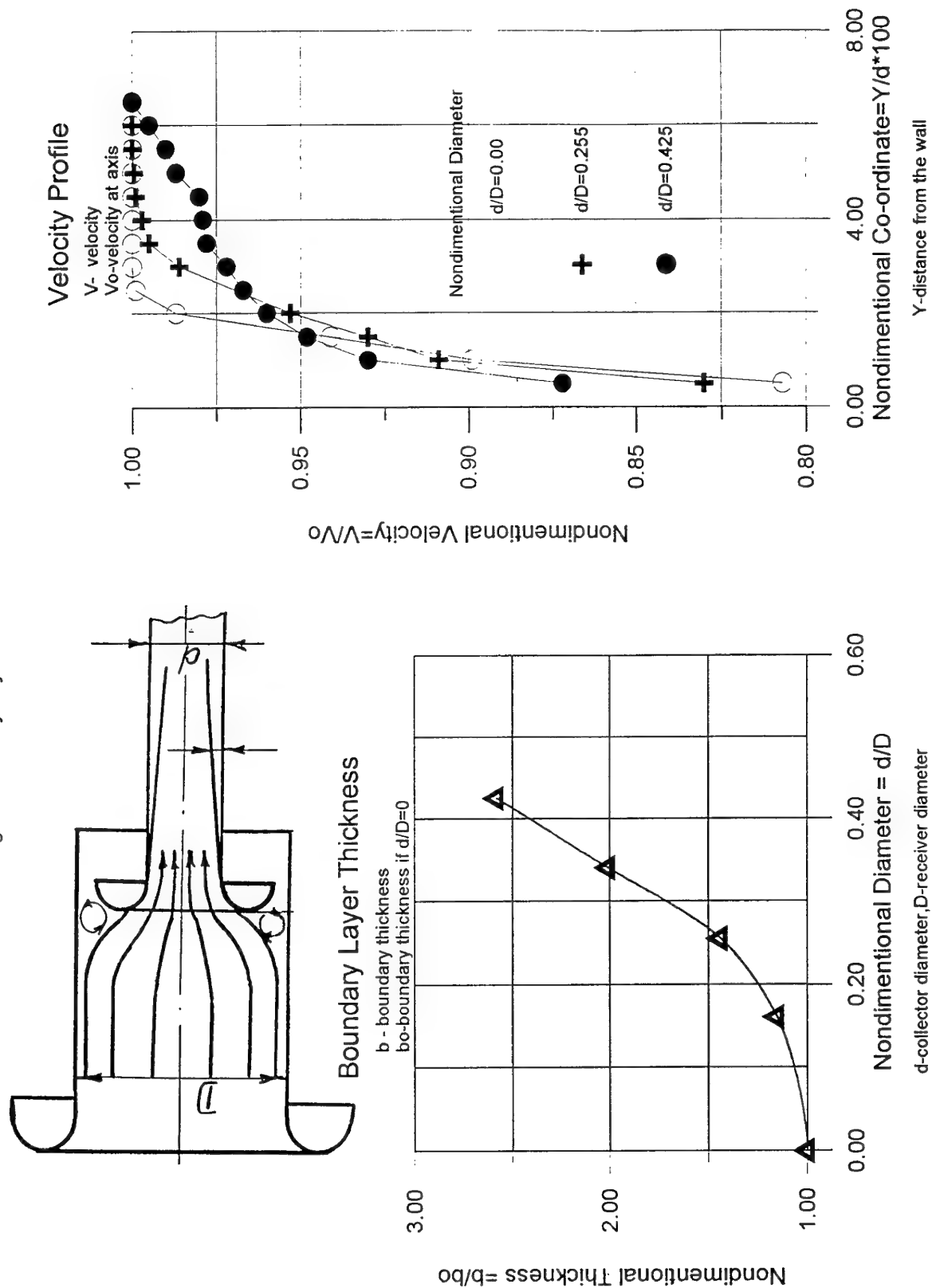


Fig.2 S-Shape Mixing Chamber

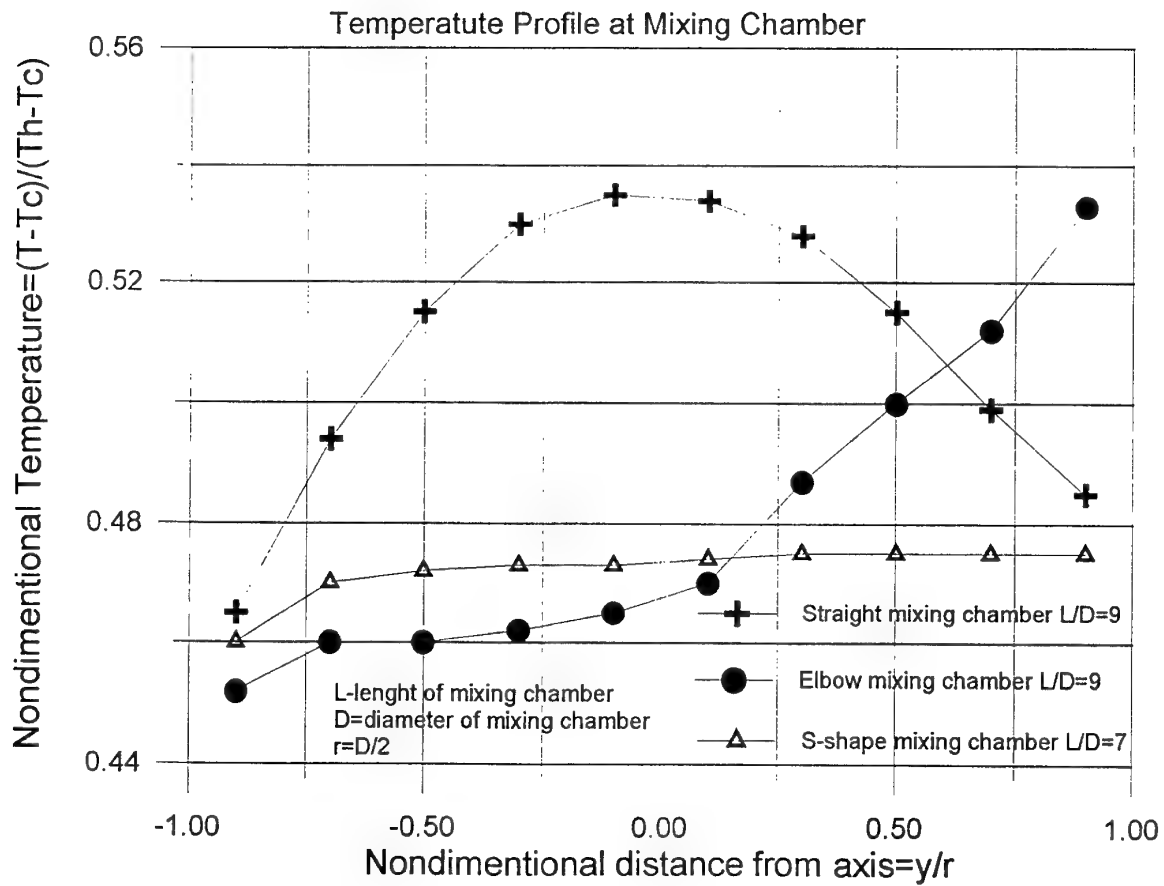
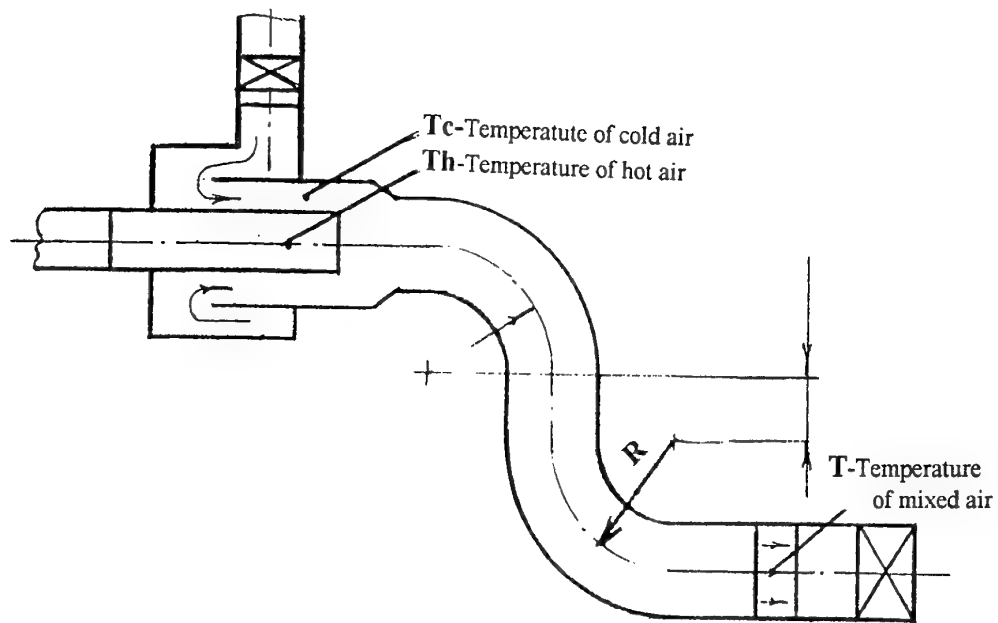
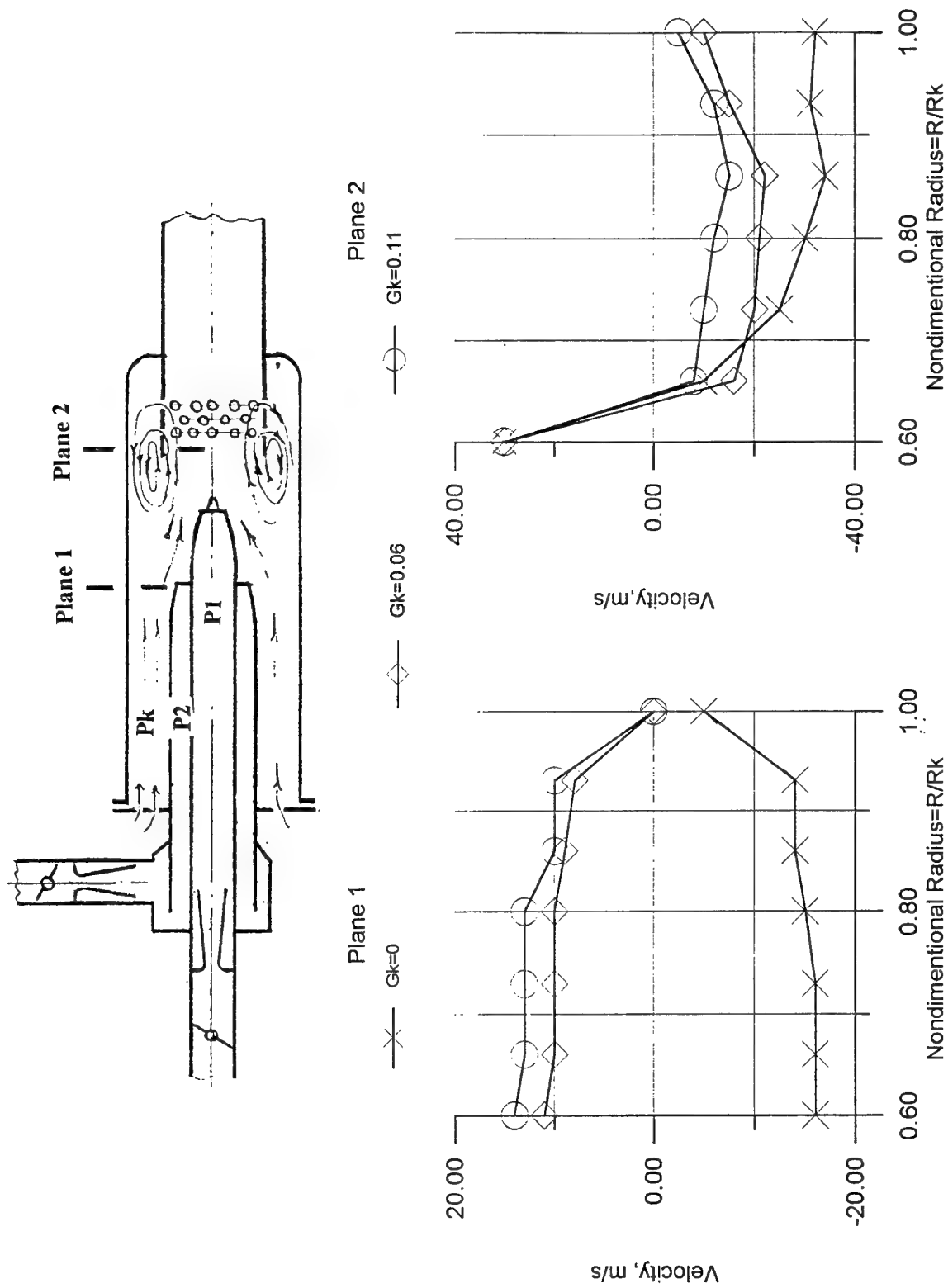


Fig.3 Velocity Profile In Test Cell



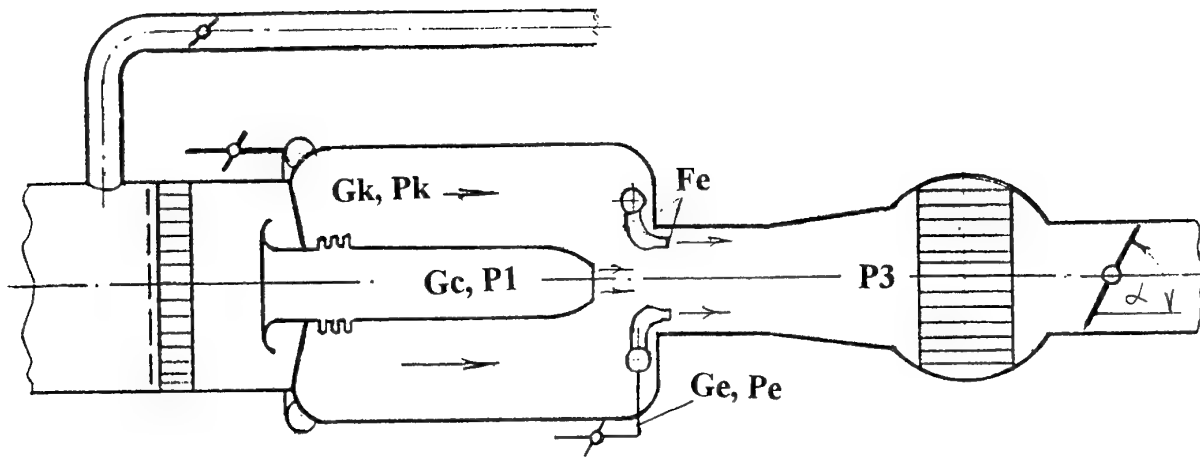


Fig.4 Ejector system for Test Cell pressure control

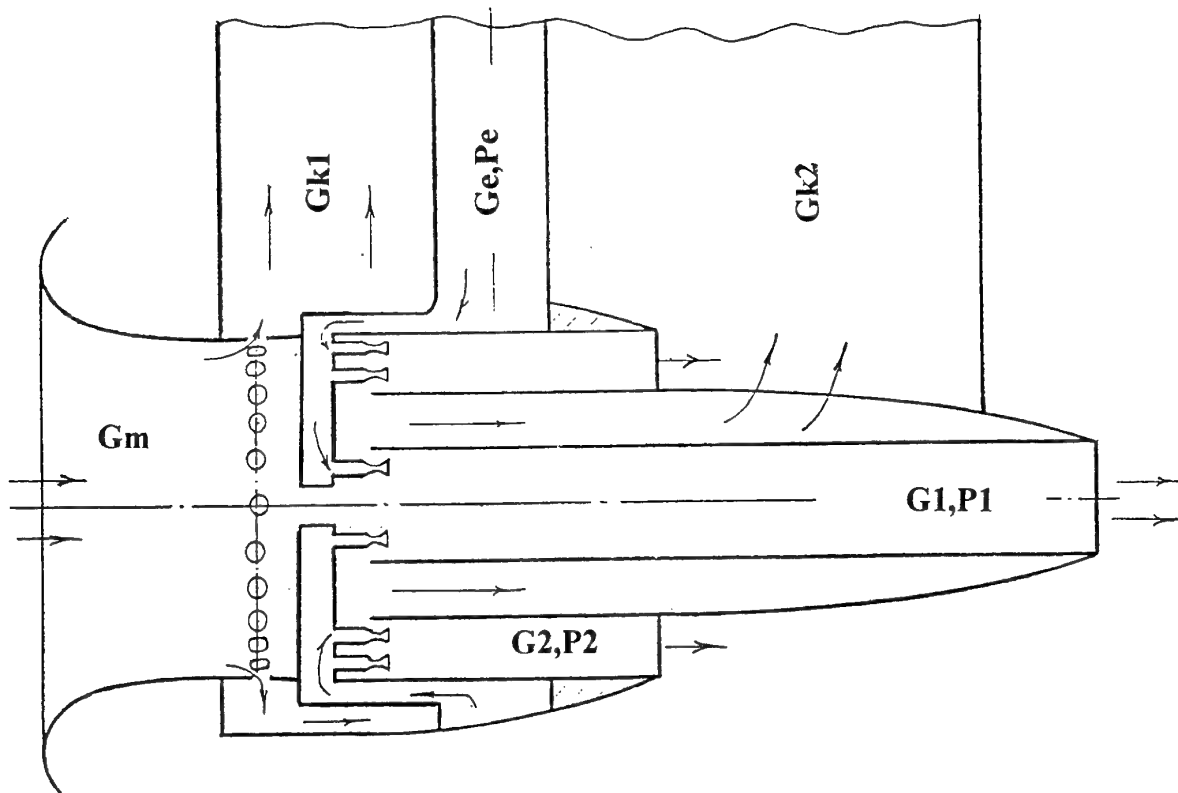


Fig.5 Engine Simulator

ETW Aerodynamic Design -A Case Study-

X. Bouis

J. Prieur

Office National d'Etudes et de Recherches Aéropatiales
BP n° 72-92322 Châtillon Cedex (France)

J. A. Tizard

Elswick Lodge, Lodge Lane,
Elswick, Nr. Preston,
Lancashire, PR4 3ZJ (England)

G. Hefer

ETW GmbH
Postfach 90 61 16
D 51127 Köln 90 (Germany)

Summary

The European Transonic Windtunnel, ETW offers flight/near flight Reynolds numbers. This paper addresses the definition of the basic specification and the expansion of this basic specification into an overall aerodynamic design and concept of control of the facility. The rationale used in the definition of various tunnel components is explained and an overview of some of the studies and calculation methods employed to achieve the design of different sections of the tunnel are given.

The need of test rigs is discussed and some details of the use of the pilot facility PETW in the development of the design are presented. The calibration methods and calibration results showing that the design was successfully implemented are outlined and show the excellent quality that is currently being achieved and demonstrate that the design concept works up to full flight Reynolds numbers.

budget one of the most demanding wind tunnel projects ever realised, ETW designers had to deal with a "real world's situation" where difficulties were not only technical:

- since the construction of a first major generation of wind tunnels in the 50 and 60's, much of the relevant hands on experience had been lost
- aerodynamic testing quality and associated wind tunnel requirements had increased substantially over the 70 and 80's especially for high Reynolds number simulation
- minimisation of operating costs and cryogenic operations were adding serious challenges
- the many deferments of the final "go ahead" and the large number of funding partners could have led to non-desirable situations. "designing by committee" syndrome etc.

List of Symbols

A	Area
$C_{p_{ms}}$	Broadband noise level
$F(n)$	contribution to $C_{p_{ms}}$ in reduced frequency band Δn
f	frequency
GN_2	gaseous nitrogen
K_t	total pressure loss coefficient
LN_2	liquid nitrogen
M	Mach number
n	reduced frequency = $f \cdot w/U$
P_s	static pressure
P_t	total pressure
S	test section cross sectional area
T_t	total temperature
U	mean axial velocity
u	axial pressure fluctuation
v	lateral pressure fluctuation
w	test section width
ϵ	turbulence intensity
θ_k	wall angle relative to tunnel centerline
η	static pressure recovery efficiency

Introduction

Much has already been published on ETW, the European Transonic Wind Tunnel, little however on the way its design actually proceeded. Indeed, before achieving in time and within

Fortunately, three factors considerably helped to the final success:

- the long time, more than eight years before final design really started, could be used judiciously and whilst the spending rate was kept low, it allowed time to look at numerous options, to run pilot facilities, to learn from other's experiences: hence to pave the way for quick decisions in the next phase. The few engineers who stayed all through these years and the main engineering consultant helped in saving the project's memory
- shortly after the start of final design i.e. late 1985, the main specifications were definitely frozen and limited to the most essential goals
- the new ETW team was then given adequate authority to manage all aspects of the project, technically and commercially, by the four share holders: DLR, DRA, NLR and ONERA. This team brought up to date practical experience into the project and could easily access any relevant information or advise in the four above European establishments.

Following AGARD's request to present a "case study" the paper reviews item by item how the aerodynamic design developed. It can be seen that some concepts and shapes were frozen very early whilst others had to be reconsidered at a time where machining was already going on! Some of the results of the calibration of the tunnel and of early model tests which demonstrate the success of the design are also presented.

Basic Specification

The need for a high Reynolds number wind tunnel was identified as long ago as 1968 by the Fluids Dynamic Panel of AGARD. In 1969 the Large Wind Tunnel Working Group (LaWs) proposed a basic specification of the transonic wind tunnel. In 1971 the NATO Defence Research Group (DRG) established an ad-hoc group called the AEROTEST Group that in 1973 recommended to build a high Reynolds number transonic wind tunnel, to be jointly constructed and operated by several European countries. In 1975 a Project Group (PG7) also under the aegis of the DRG was tasked with selecting the power drive system for the tunnel and to develop a plan for its realisation. After looking at a number of concepts of drive systems the cryogenic transonic tunnel was adopted.

The LaWs group recommendations related to a facility that was based on different concepts to that finally adopted, the cryogenic concept. The main stipulations of the LaWs group, relevant to this paper, was that the maximum Mach number was to be 1.35, the design Mach number should be 0.9, and at the design Mach number, it should have a Reynolds number range of 25 million to 40 million at constant dynamic pressure.

In 1976 the Project Group PG.7 defined the flow quality necessary for a high Reynolds number wind tunnel, reference 1.

After the adoption of the cryogenic option in 1977 the test section size of 1.95m x 1.65m was chosen as the minimum at which the required model detail could be adequately represented and to minimise capital investments. Furthermore the conservative assumption was made that the model local flow saturation would take place at a local flow Mach number of 1.7. This, together with the given test section dimensions and the required Reynolds number of 40×10^6 , leads to a maximum stagnation pressure of about 450kPa. The operating envelope for $M=0.9$ is shown in figure 1.

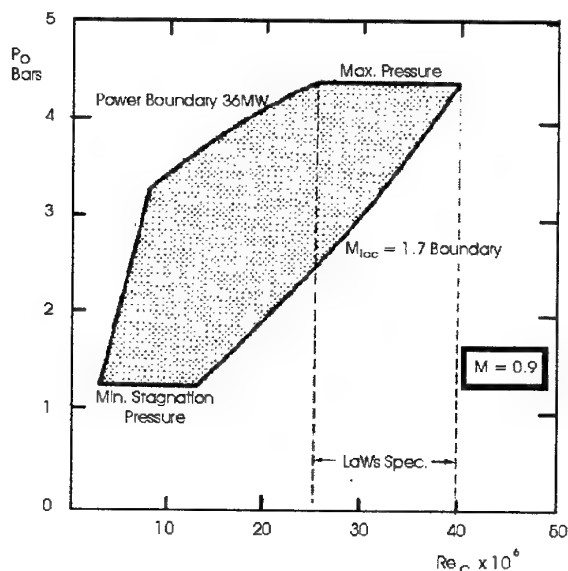


Figure 1: Early ETW Operating Envelope

Specification Development

An Airline Optimisation Study, ref. 2, was conducted by DSMA of Canada to define the most economical circuit configuration based on the combination of capital and operating costs consistent with flow quality, test spectrum and operational flexibility requirements.

The main parameters considered in the optimisation study were the basic geometrical circuit features: contraction ratio, area ratio of the 1st cross leg and the transonic diffuser angle, fan power, fan diffuser angle and area ratio of the 2nd cross leg.

As the circuit losses have a direct impact on the fan power and therefore on the LN_2 consumption, a loss prediction program was developed and validated against HST (of the NLR) test results. It was determined that the main circuit losses are distributed in the test section diffuser (28%), the model and its support strut (24%), the nozzle and test section (14%), the 2nd corner (13%), all other components accounting for the remaining 21% of the total circuit loss.

By tuning the circuit geometrical parameters and checking the sensitivity of the optimum configuration to these parameters, an optimised circuit was arrived at, with the following features:

- optimum contraction ratio: 8 to 12
- optimum 1st cross leg area ratio: 2.25 with a test section diffuser angle 2θ of 4.25 deg.
- optimum 2nd cross leg area ratio: 5, with a fan diffuser angle 2θ of 2.75 deg.

The results of the above study and the flow quality requirements of PG7 were an input to the Preliminary Design performed by Sverdrup Technology of the USA.

Later, it became apparent that the overall tunnel optimisation had to take more into account the demanding requirements from potential users concerning the productivity and flexibility of tunnel operation, especially in terms of set point changes. The consideration of these dynamic aspects led to the development of a dynamic model (see section Control Aspects of ETW) which was a powerful tool in the overall optimisation throughout final design and construction stages.

The flow quality requirements were continuously reviewed during the development of the facility and finalised in 1988 as construction began. These flow quality goals for the test section are given in Table 1.

Mach Number Uniformity	Subsonic ± 0.001 Supersonic ± 0.008
Mach Number Stability	± 0.001 during polar
Temperature Uniformity and Stability	± 0.25 K
Flow Angularity	± 0.1 degree (repeatability and measurability ± 0.01 degree)
Pressure Stability and low frequency fluctuations	$\Delta P/P < 0.002$ during polar $\Delta P/P < 0.001$ between 0.2 and 5 Hz
Turbulence	< 0.05 %
Noise	$C_{p_{max}} \leq 0.004$ $\sqrt{n}F(n) \leq 0.001$ for $n < 1$ ($n = fw/u$)
Dew Point Temperature	≤ 210 K

Table 1 Flow Quality Goals

Test Section and Re-Entry

As mentioned previously the test section size of 1.95 x 1.65 m was initially defined by PG.7 as being the minimum at which model detail could be represented for high Reynolds numbers. The slotted wall with re-entry flaps configuration was also selected at this time. This decision was made with the expectation that the subsonic region of testing was of prime importance and the associated slot noise should be kept to a minimum.

With the flexible nozzle on the top and bottom walls, the best supersonic flow quality (smallest Mach number deviation) will occur when the top and bottom wall angles match the nozzle exit angles, reference 3. Remotely adjustable wall angle capability was provided for the sidewalls, allowing a 0 to 0.25 deg divergence on each wall for control of axial Mach number gradients in the test section. Using simple Prantl-Meyer angle theory, the resulting supersonic Mach number deviations were calculated to be:

M	θ_k	ΔM (wall)	ΔM (centerline)
1.20	-0.132	0.00032	0.00065
1.40	-0.147	0.00024	0.00048

Since these deviations were less than the goal flow quality ($|\Delta M| \leq 0.001$) and the transitional effects of the slots could be considered of a similar magnitude, the test section was considered satisfactory at that time.

Six slots were provided on both the top and bottom walls and two slots were provided on each sidewall. Subsequent analyses showed that slot tone resonance occurred with the first fundamental blade passing frequency with the 5 percent open-area ratio. By reducing the slot open-area ratio to 3.8 percent, the resonance problem could be eliminated.

The European industry, by means of the AECMA-CIPS committee (Association Européenne des Constructeurs de Matériel Aéronautique - Comité International Permanent des Souffleries), requested that the test section size be increased to 2.4m x 2.0 m. to give a higher Reynolds number capability and to be compatible with existing European transonic tunnels.

In 1986 an International Working Group was set up to review the test section configuration. With guidance from this group the following decisions were made:

- to adopt the size recommendation of the AECMA-CIPS committee
- test section length $\geq 3\sqrt{S}$ (S = test section cross sectional area) plus the re-entry area
- 6 slots on top and bottom walls and 4 slots on side walls, for the initial build the side wall slots should be closed and the top and bottom walls have a ventilation of 6.25%
- wall porosity to be variable between 0 and 12% per wall by manually changing slot inserts
- top and bottom wall angle to be remotely adjustable from 0.5 degree inwards to 1 degree outwards and the sidewalls fixed
- as a retrofit, the top and bottom walls to be capable of being replaced with flexible walls providing a 2D wall adaptation.

For the subsonic and low supersonic Mach numbers, with the nozzle set on the sonic contour, the axial Mach number uniformity and gradient can be controlled by careful slot shape design and top

and bottom wall angle variation. The initial slot shape is of extreme importance if the flow is expanded to supersonic conditions by flow removal through the slots. The development of slot shapes to achieve smooth supersonic Mach numbers without over-expansion or waviness in the axial distribution from a sonic contour, or to increase the level above a supersonic nozzle exit value, has until recently been largely an experimental iteration process. An analytical approach, Ref. 5 that is directly applicable to two-dimensionally slotted tunnels (top and bottom slots) provides an explanation of the flow mechanism causing the over-expansion found for simple linearly tapered slots and confirms the value of the "pinched" slots seen in several transonic tunnels. Since the achievement of smooth flow for $1.0 \leq M \leq 1.1$ with the ETW nozzle was uncertain, a slot shape determined from the methods in Ref. 5 should be considered to allow this Mach regime to be optionally achieved with a sonic nozzle contour. The slot width in the model test location should also be selected to avoid slot tone resonance with the first fundamental blade passing tone.

For supersonic Mach numbers, the axial Mach number uniformity is primarily a function of the flow quality in the nozzle first rhombus with secondary influence of slot shape, particularly if the test section Mach number is made to deviate from the nozzle exit value.

For the initial build of ETW the top and bottom wall slots start as close to the exit of the nozzle as possible and expand over a length of 383mm to a width of 25mm. The slots are kept parallel for the full length of the slots. A contoured slot will be developed as more is known of the characteristics of the tunnel.

Test Section Slot Noise: The largest spectral component contribution anticipated over and above the turbulent boundary layer sound field is the aerodynamic noise caused by vortex interactions in the longitudinal slots. The transverse sectional shape of the slot edge was rounded and bevelled to minimise this acoustic disturbance.

Re-entry Flap Region:

The length of the re-entry section is significantly shorter than that considered in the Airline Optimisation Study. This was primarily a result of the model handling scheme adopted. Design of the re-entry flaps was based primarily on experience by NASA with a tapered flap configuration referred to as finger flaps. The NASA 8-Ft Transonic Tunnel, reference 4, uses this flap configuration. This tunnel required a compressor pressure ratio of only 1.09 at $M = 1.0$, which made it, at that time, one of the most energy efficient wind tunnels for which data are available. It was believed that the unique finger-flap design for the re-entry area was responsible for the low circuit losses. Although an analytical explanation for the benefits provided by the finger flaps was not available, it was believed that it was associated with a reduced boundary layer blockage in the re-entry area.

In ETW the model support sector is located in the re-entry region with the sector penetrating the top and bottom walls of the re-entry. Area compensation for the sector and sting boss is incorporated into the sidewalls. During design, 2-d calculations led to a modification of the shape of this area. Figure 2 indicates the changes in supersonic flow patterns as a consequence of the changes. Tests in PETW have confirmed the effectiveness of these modifications.

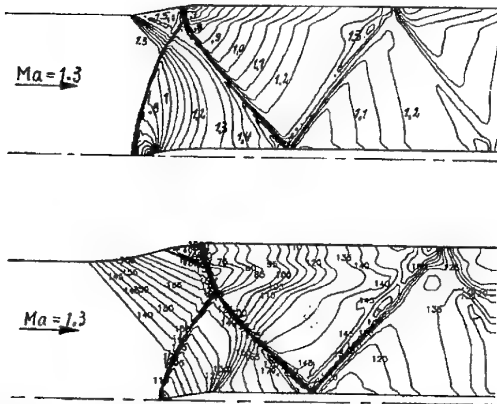


Figure 2: Supersonic Flow Pattern of Original (top) and Modified (bottom) Re-entry Configuration

A view of the test section and re-entry is shown in the photograph of figure 3.

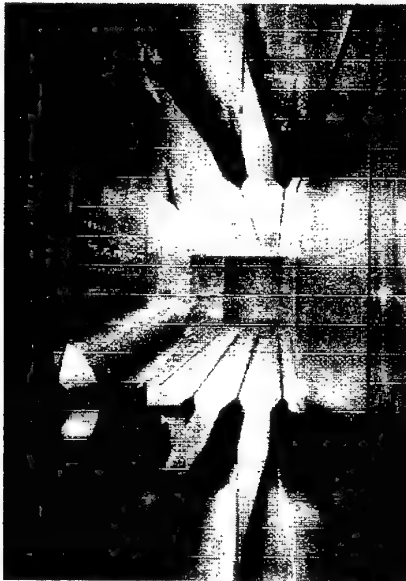


Figure 3: View of Test Section and Re-entry looking Upstream

Second Throat and High Speed Diffuser

The Airline Optimisation Study was based on a simple fixed diffuser downstream of the test section. However, it was anticipated, at that time, that a variable diffuser would be incorporated at a later date.

The loss in total pressure was calculated from the static pressure recovery efficiency, η , where:

$$\eta = \frac{(\Delta P_s)_{Actual}}{(\Delta P_s)_{Ideal, \Delta Pr=0}}$$

A correlation between η and the blockage at the diffuser entrance was used, where blockage was defined as the area reduction due to the boundary layer displacement thickness and the plenum re-entry

flow. The boundary layer thickness at diffuser inlet was calculated from the last screen in the stilling chamber to the test section exit plane. The contribution of the plenum re-entry flow to the test section diffuser inlet blockage is related to the mass flow and velocity of the plenum flow re-entering the circuit.

A two-piece transition section was defined to provide an area distribution that matches a constant half angle as the cross-section changes from rectangular to circular.

Once the test section geometry was clear a number of studies on the inclusion of a variable second throat was undertaken. In 1985 the decision was made to incorporate a second throat in ETW. The selected concept is shown in figure 4.

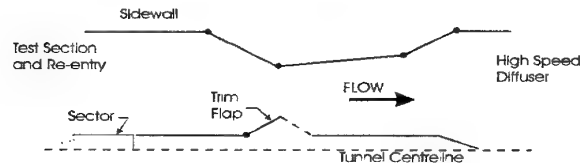


Figure 4: Schematic of ETW Second Throat

The second throat is situated at the high speed diffuser inlet. It consists of moveable sidewalls operating through a three hinge system and a centrebody situated directly behind the model support sector in which a Mach controller (trim flaps) is located. The purpose of the second throat is to:

- reduce disturbances propagating upstream from the high speed diffuser and downstream areas
- provide faster Mach number control during model traverses
- stabilise terminal shock in the supersonic regime and maintain plenum suction.

A contract was placed with Dornier GmbH to conduct a detailed parameter study of the flow through the second throat. The flow was assumed to be inviscid and two-dimensional as well as symmetrical to the centreline of the centrebody. A finite volume code was used for solving the Euler equations in full conservation form.

Two test cases were considered, one with a uniform inlet profile, the other with a non-uniform inlet profile to simulate re-entry flow conditions, caused by finger flaps. Figure 5 showing the total pressure loss calculated as mean values at the diffuser exit section versus the sidewall shock position for uniform and non-uniform flows revealed that the difference in loss was less than 0.25%. The re-entry deficit was 2.2%. The ETW target value for the shock face Mach number was 1.15, see figure 6. For this condition the total pressure loss equals 2.5% for a uniform inlet profile with a shock position 0.4m downstream of the first moveable hinge. The non-uniform inlet profile gives 3.5% total pressure loss and a shock position at 0.7m downstream of the throat.

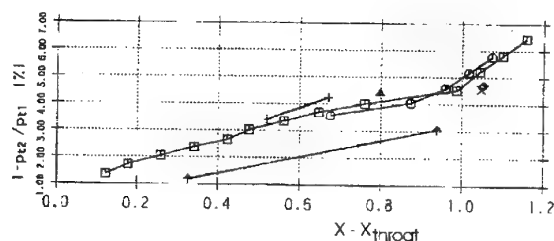


Figure 5: Total Pressure Loss vs Sidewall Shock Position

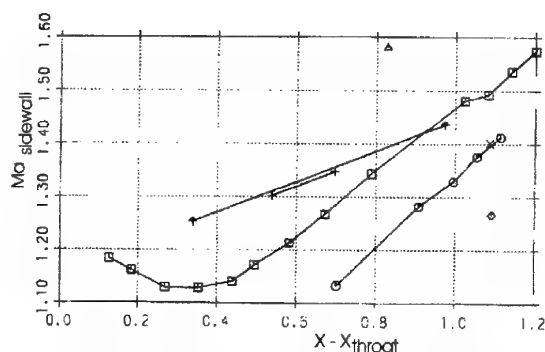


Figure 6: Sidewall Mach Number vs Sidewall Shock Position

Legend for figures 5 and 6:

	trim flap position	trim flap angle
□ uniform	1.940m	15°
○ non-uniform	1.940m	15°
△ uniform	1.700m	15°
+ non-uniform	1.700m	15°
x uniform	2.190m	15°
◇ non-uniform	2.190m	15°
⋈ uniform	1.940m	9°

For a uniform inlet profile, the most upstream position of the shock corresponding to a completely choked flow was at $X - X_{throat} = 0.15m$. With nonuniform inlet profiles however, the shock can only be moved up to $X - X_{throat} = 0.6m$. For values below $0.6m$ the flow was unchoked. Due to the re-entry deficit the sonic line is not emanating from the 1st movable hinge (geometrical throat) but approximately $0.5m$ downstream showing a highly curved form in this region. This configuration should be avoided with respect to the following reasons:

- the total pressure losses are high
- the allowable displacement of the shock is confined to a small region at the aft part of the second ramp resulting in poor controllability
- a sonic line emanating from the flat plate may influence the Mach controllability during a polar.

Shifting the trim flap down stream of its normal position had a negative effect because it supports the above mentioned negative drawbacks.

Shifting the trim flap upstream gives positive effects, the drawbacks of point 2 and 3 above are now eliminated. The shock controllability was increased.

Fan Inlet

During Preliminary design further analysis of the circuit losses was undertaken. It was found necessary to increase the flow area of corner 2 to reduce the velocity in that area and hence reduce the losses. Deletion of the compressor nose cone extension through corner 2 and a crossleg diffuser was adopted. An aerodynamic fairing was provided to cover the compressor shaft to reduce shaft wake effects on the compressor inlet profile. Figure 7 shows the corner 2 layout at that time.

In 1986 a number of studies were undertaken by prospective compressor suppliers which revealed the need to further increase the size of corner 2 in order to provide some contraction to improve the flow velocity distribution at the inlet of the

compressor. A larger corner 2 has the additional advantage to further reduce the pressure losses through the corner and the catch net.

Increasing corner 2 size without changing corner 1 size would increase the cross leg diffuser angle beyond acceptable limits (5.6 degree half angle). It was therefore recommended to increase corner 1 size in the same proportion as corner 2. Again, corner 1 losses would decrease as a result of this modification.

It was clear that the high speed diffuser, fitted between an extended second throat and an enlarged corner 1 would not be adequate. It was therefore recommended to lengthen the high speed diffuser, keeping the same wall angle, until the exit diameter reaches the enlarged corner 1 diameter. Obviously this extra length had to be compensated for by an equivalent lengthening of the low speed leg of the circuit.

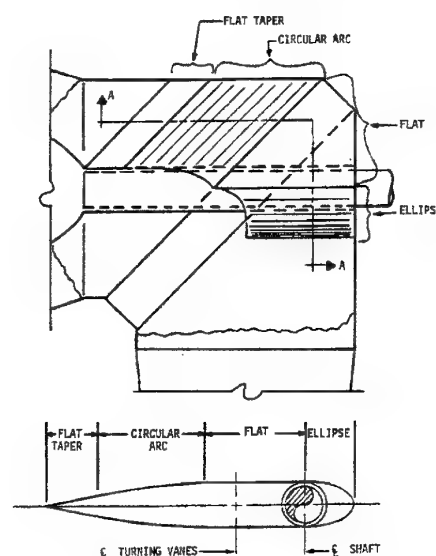


Figure 7: Layout of Corner 2

The above proposed change, alone, would result in a circuit volume increase. This volume increase would impact not only the construction cost but also the operating cost of the facility: as the volume increases, the response time of the circuit would increase and therefore the transient times between set points would increase accordingly. It was necessary to consider additional circuit changes in order to minimize or if possible balance out the above volume increase. In order to improve the performance of the compressor tailcone diffuser without increasing its length, it was desirable to reduce the exit diameter. This, in itself, contributes to a slight volume reduction. Further, the low speed diffuser had a very conservative design and could, without any significant adverse effect, be replaced by a constant diameter tube followed by a 2 degree half angle conical diffuser connected to the third corner. The resulting volume reduction could be further extended by reducing corner 3 diameter. This corner size reduction has a large beneficial effect on volume and a minor adverse effect on the pressure losses, as the flow velocity in that area is very low. Corners 3 and 4 would then be connected by a diffuser. The diffuser performance was improved by the GN_2 blow off section located there. The rest of the circuit from the inlet of corner 4 down to the test section would not be modified.

The consequences of the proposed changes on the flow quality aspects of the facility were considered to be nil, as these aspects are primarily determined by the circuit configuration and internals between corner 4 and the test section and this part of the circuit was not affected by the proposed changes.

Wide Angle Diffuser

The Airline Optimisation study indicated an area ratio of 2 for the wide angle diffuser with a contraction having a ratio of 10. In the Preliminary Design the contraction ratio was increased to 12 to give a safety margin on the test section turbulence level which resulted in the wide angle diffuser ratio being increased to 2.4. The wide angle diffuser contour was modified at this time to be formed by two conical sections of 12.5 and 25 degree half angles respectively. It is fitted with two filling screens, one at the junction of the two conical sections and the other at the outlet of the diffuser. The placement of the spherically-shaped screens, their size and fabrication geometry were selected to satisfy both structural and aerodynamic considerations. The aerodynamic criteria for the screens followed the classic experimental findings of Ref. 6. The criterion equation of Ref. 6 specified a pressure loss coefficient of 1.306 for the screen locations and a spherical geometry was chosen to equalize this factor. To be on the conservative side, and to insure complete diffuser filling with minimal intermittent separation, the loss factor finally selected was 1.447. The screen geometry for this coefficient follows:

Screen	Mesh wires/m	Wire Dia.(mm)	K_t
1	118.1	2.34	1.447
2	118.1	2.34	1.447

Tests in the DLR test rig demonstrated the adequacy of the design of the diffuser and screen location and the absence of any separation.

Stilling Chamber

The stilling chamber design has changed very little from that developed during the Preliminary Design.

The stilling chamber inserts include one honeycomb and two screens, not taking into account the wide angle diffuser screens. The constant diameter part of the settling chamber is 1.3 times its radius, which is more than sufficient according to reference 7. Consistent with Bradshaw and Pankhurst, reference 7, it was assumed that the turbulence level at the exit of corner 4 was 5% and is isotropic.

The tunnel specification originally called for a turbulence level of 0.1% and was later modified to a maximum level of 0.05%. The turbulence level was defined as:

$$\epsilon = \frac{1}{U} \sqrt{\frac{u^2 + 2v^2}{3}}$$

where U is the average axial velocity and $\sqrt{u^2}$ and $\sqrt{v^2}$ are the time averaged (RMS) values of the axial (u) and lateral (v) velocity fluctuations. It was considered that based on axial velocity fluctuations alone

$$\frac{\sqrt{u^2}}{U} \leq 0.05\%$$

would be difficult to achieve, while $\epsilon \leq 0.05\%$ was a realistic goal.

Although initial calculations were performed for a specification of $\epsilon \leq 0.1\%$, it was shown that with the assumptions made, $\epsilon \leq 0.00044$ was achieved, thus meeting the new specification of 0.0005.

For the suppression of turbulence a curve fit of experimental data provided in ref. 7 was used to predict the effect of screens. This curve fit is similar to the simple turbulence attenuation factor $\sim (1 + K)^{1/2}$ for a screen given in ref. 7 for the lateral turbulence component. This simple expression shows that using multiple screens is more effective than using a single screen of the same overall resistance. Based on the above formulae and experimental data the attenuation factors correlate well with:

$$\text{for axial component} \quad 1.62\sqrt{1+K}$$

$$\text{for lateral component} \quad 1.13\sqrt{1+K}$$

thus showing that the lateral component is more difficult to suppress than the axial one. In order to achieve their turbulence suppression the screens have to feature a fine mesh for the turbulent wake of the wires to decay and a spacing of about 500 wire diameters to allow this decaying process to take place before the next screen. For ETW two anti-turbulence screens with a loss factor (K) of 1.2 are provided with a provision of a third if required.

For the honeycomb a large length to diameter (L/D) ratio with fully developed flow in the cells, lateral component annihilation can be achieved reference 8. The adequacy of the 0.5 m honeycomb with 20mm cells ($L/D = 25$) to generate fully developed flow has been compared to Lumley's criterion in figure 8 and an adequate margin is available even at minimal Reynolds number conditions.

The alignment of the honeycomb to the stilling chamber centerline is critical for its performance. For the transverse steady-state component it was assumed that the downstream perturbation is a direct function of the tangent of the two-sigma cell alignment tolerance. Results of the application of the calculations through the various elements are shown in Figs. 9 and 10 for a Mach number of 0.90.

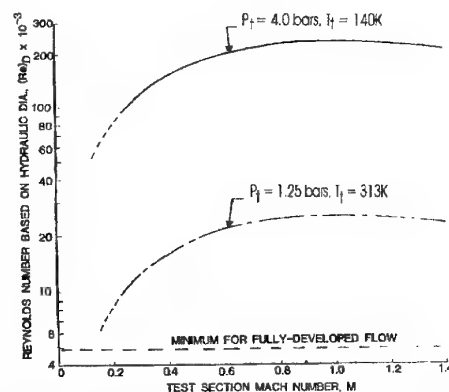


Figure 8: Adequacy of $L/D = 25$ Honeycomb to Generate Fully Developed Flow

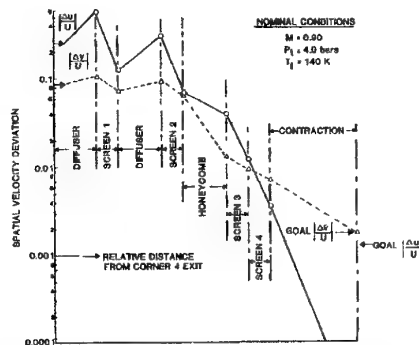


Figure 9: Schematic of Calculation Algorithm for Test Section Spatial Velocity Deviations

The $\Delta v/U$ curve (Fig. 9) through the honeycomb is for an assumed honeycomb alignment of 0.75 degrees relative to the tunnel centerline. With this alignment, the flow quality goal on this parameter is marginally met at this Mach number. The $\Delta u/U$ goal is easily met, as is the turbulence intensity goal of 0.0005 (See Fig. 10).

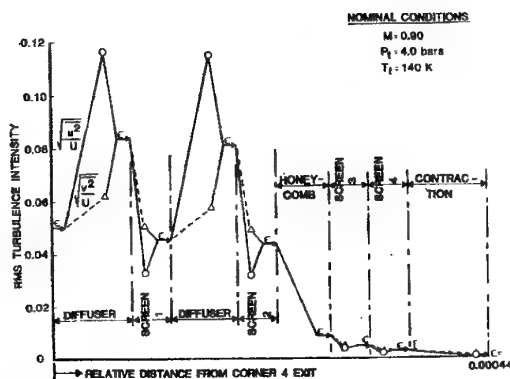


Figure 10: Schematic of Calculation Algorithm for Test Section RMS Turbulence Intensities

Figure 11 shows that achievement of the flow angularity goal at the lower Mach numbers will require a honeycomb alignment of near 0.5 degrees. If this alignment accuracy cannot be achieved, the addition of another screen may be necessary.

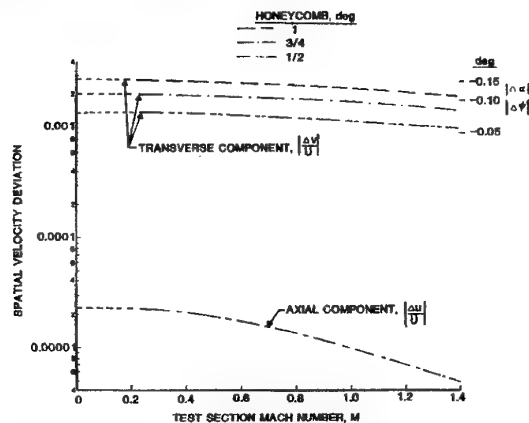


Figure 11: Predicted Test Section Steady-State Velocity Deviations ($P_t = 4.0$ bars, $T_t = 140$ K)

In ETW, for structural reasons, a honeycomb length of 400mm was installed giving a L/D of 20 to an alignment accuracy of better than 0.5 degrees. Further analysis was done to confirm the adequacy of this change.

The final layout of the ETW stilling chamber is shown in figure 12.

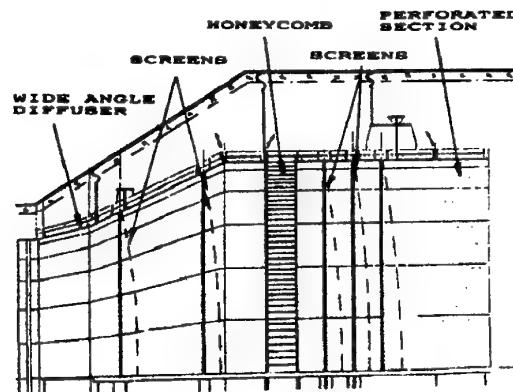


Figure 12: Layout of ETW Stilling Chamber

Contraction

The initial contraction configuration was based on a one dimensional criterion that the second derivative of the velocity versus axial distance should be a sine function. Further analysis indicated that this configuration gave an adverse pressure gradient in the inlet region. The area distribution resulting from this analysis is shown in figure 13 as the solid line. This rather rapid area change near the inlet was deemed partly responsible for the magnitude of the adverse pressure gradient and the risk of boundary layer separation. A "cosine" area distribution was developed which, as can be seen by the dashed line of figure 13, relaxed the rapid area reduction over the region 1m to 6m whilst retaining the required inlet and outlet radii.

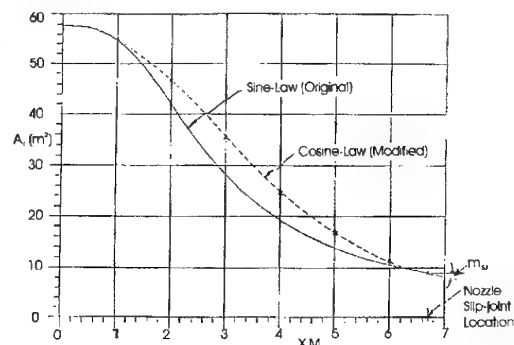


Figure 13: Parametric Curves for Three Dimensional Contraction

The effect of this redistribution of area change is shown in figure 14 which illustrates the calculated wall pressure and Mach number as a function of axial distance along the first 1.5 m of the contraction for both the original and modified geometries. The equivalent axisymmetric flowfield was computed using an inviscid analysis based on a compressible stream function formulation of the Euler equations for irrotational flow. A simple sonic contour was added downstream of the contraction exit to permit the

computation of the entire contraction/nozzle flowfield. The computations shown in figure 14 were made using an inlet Mach number of 0.047 which yielded a test section Mach number of approximately 0.83 which represents a typical contraction operating condition.

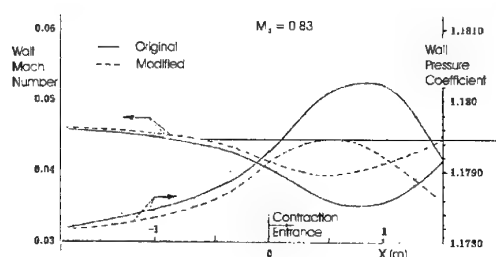


Figure 14: Inviscid Wall Mach Number and Pressure Distributions

Based on this analysis figure 14 also illustrates the degree of improvement in reducing the adverse pressure gradient. Figure 15 gives the computed distributions of skin friction resulting from the pressure distributions shown in figure 14 for the lowest expected Reynolds number at $M_{TS} = 0.83$. The computations were made using an improved version of the integral turbulent boundary layer code reported in reference 9.

It is evident that the modified geometry causes a smaller drop in skin friction thus reducing the chance of boundary layer separation compared to the original geometry. Check computations undertaken by DLR confirm these improvements to the contour.

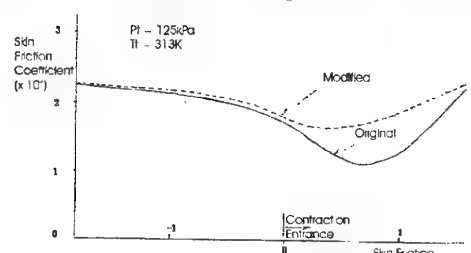


Figure 15: Contraction Flow Characteristics - Skin Friction

Flexible Nozzle

After the tunnel was upsized the specification of the nozzle was reviewed and the maximum Mach number requirement was relaxed from the original 1.4 to 1.3. Based on the revised geometry new aerodynamic contours were defined for Mach 1.0, 1.1, 1.2 and 1.3. Viscous corrections were applied to the inviscid aerodynamic contours at a design point based upon the area with the highest percentage of operating time as a function of temperature and pressure from the predicted test spectrum of the facility. To correct the inviscid contours for boundary layer growth, an initial estimate was made of the boundary layer characteristics at the junction between the contraction and the flexible plate. These characteristics were established using the Shear Work Integral Method (SWIM) documented in reference 9. The calculations to start the computations were begun at the last screen in the stilling chamber just upstream of the contraction region.

Once the starting viscous layer properties were determined at the contraction/flexible plate junction, viscous corrections were determined for the inviscid aerodynamic contours. The viscous

correction procedure involved the iteration of the boundary layer growth characteristics with the inviscid contours adjusted in such a way that the physical contour maintains the proper slope and position characteristics both at the upstream and downstream ends of the nozzle. The resulting viscous corrected aerodynamic contours for wall position and local wall angle are shown in figures 16 and 17 respectively.

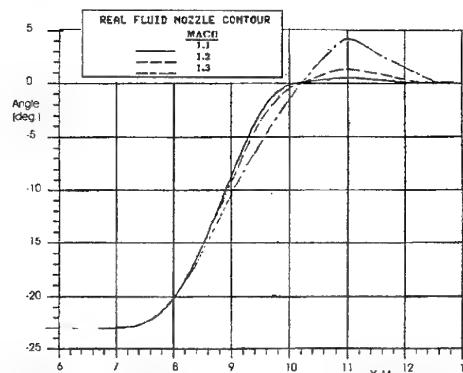


Figure 16: Supersonic Nozzle Contour Wall Angle Corrected for Viscous Effects

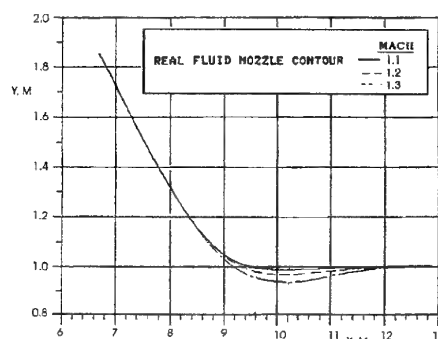


Figure 17: Supersonic Nozzle Contours Corrected for Viscous Effects

Test Development Facilities

Two test facilities were built in the early stages of the evolution of ETW to develop the design and to evaluate the flow quality attained. Both facilities, the test rig and the pilot ETW (PETW) have demonstrated their usefulness for the detail design and construction of ETW.

Test Rig

Towards the end of the preliminary design phase of ETW it became evident that results from the pilot facility PETW would not be available in time to sufficiently confirm the ETW aerodynamic circuit before the start of the final design phase. It was decided to build a test rig operating under near ambient flow conditions, well aware of the deficiency that Reynolds number in such a rig would be about 2 orders of magnitude lower than that in ETW. Nevertheless there was hope to get valuable information not only for test section flow quality but also for high speed leg and cross-leg diffuser operation.

The predictive computational methods in use was examined by these results at low Reynolds numbers applying them to special test rig geometry in order to give better confidence in the extrapolation

to the higher Reynolds numbers of ETW. Likewise any component of the circuit endangered by flow separation could be investigated in order to look for possible changes to avoid these effects at least at low Re-numbers. Other parameters such as local flow angularity and Mach number distribution in the test section may be less influenced by Reynolds number effects so these results give direct information on the flow quality.

Flow visualization techniques are very advantageous in these investigations. Therefore the material for the tunnel tube was selected rendering this possibility combined with sufficient strength to withstand the aerodynamic loads and with a very smooth surface to avoid flow effects induced by additional roughness. Further the material was required to be machined easily and exactly to guarantee for the high geometrical accuracy specified.

All these considerations led to the choice of plexiglass except for the corner vanes, which, because of the complicated form and for timesaving fabrication, have been made out of metal. A schematic of the rig is given in figure 18 and a photograph in figure 19.

Tests were conducted to investigate:

- the flow quality in the test section and pressure losses of major components of the circuit and to compare these with the theoretical design approach
- high speed diffuser performance and its improvement by boundary layer blow-off
- the second throat configuration and noise measurements at various locations around the circuit
- compressor inlet flow quality and possible improvement by a contraction.

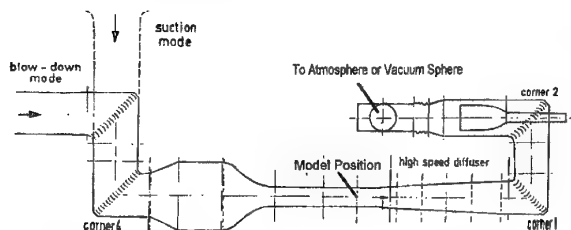


Figure 18: Schematic of Test Rig

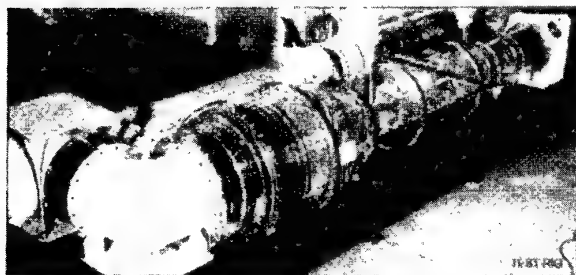


Figure 19: Test Rig

Pilot Facility - PETW

In 1978, early in the Preliminary Design phase of the project the decision was made to build a pilot version of ETW - PETW. Originally, based up on the initial ETW configuration, its scale was 1/8. The scale factor for the present sized ETW is 1/8.8 with test section dimensions of: 270.8mm wide x 229.2mm high. Initial tests

using the original configuration were to:

- confirm flow quality
- loss measurement - validate static model
- validate centerbody second throat
- loss measurement - offset sting
- assessment of the noise spectrum in the test section
- supersonic testing
- gain experience of the operation of a cryogenic transonic wind tunnel.

In 1988 the PETW test section was updated to meet the ETW flow quality specifications. Tests undertaken included:

Noise measurements: checking improvements from slot profile changes and the effect of fairings on windswept regions of the plenum structure. To assess noise contributions from the strut, re-entry flaps, plenum, etc.

Supersonic Tests: initial tests indicated that PETW was unable to achieve supersonic Mach Numbers. Modification to the re-entry area was made to increase the Mach number previously limited by natural choking of the re-entry. Tests confirmed the success of the change.

Dynamic Measurements: for control purposes.

Flow quality: measurements of turbulence, temperature fluctuations, effect of wall divergence and finger flaps on Mach number uniformity.

A schematic of the PETW is shown in figure 20.

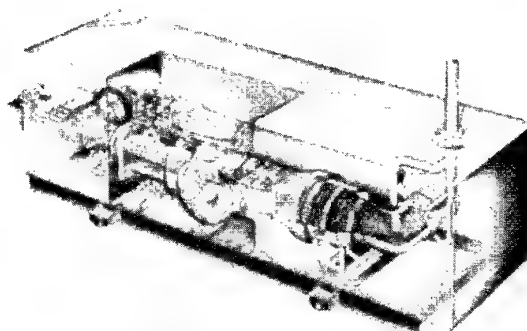


Figure 20: PETW Schematic

Control Aspects of ETW

This paper only touches the control aspects of the tunnel as it directly affects the aerodynamic performance. For a more comprehensive discussion of the control system see the paper, ref 10, presented later at this meeting.

Whilst it is important to be able to operate the tunnel under static test conditions it is also important to the aerodynamicist to be able to move from one test condition to the next and to be able to stabilise the new condition as quickly as possible. During the Preliminary Design Phase of ETW a general computer model of the tunnel was developed as part of the control studies. A simplified dynamic model, developed separately, was implemented and compared with the general model during that phase. Intermediate results of these studies exposed a number of problems. The main problem areas relate to the loss of physical significance of the equations after the various modifications and manipulations of the

model over the years, the lack of proper documentation of these modifications, the increasing mathematical complexity of the code, the discrepancies between the model and the static loss program results, the rather unbalanced combination of overdetailed calculations and crude assumptions in the model and the insufficient consideration given to the consequences of the change to internal insulation and to the effects of the metallic internals of the tunnel. These difficulties surfaced when the model failed to predict reasonable set point changes.

Hence in 1986 the build up of a new dynamic model was undertaken. The goal of the which was to represent the dynamic behaviour of the wind tunnel process using a computer program and to make it flexible enough so that it could be used in quasi-real time and easily modified to accommodate future developments. For that purpose two solutions can usually be used :

- Develop a model based on physical considerations.
- Develop a model of representation using test results.

As ETW was not yet built only the first solution could be used at this time.

The first step was established by developing a computerized mathematical model able to represent the dynamic behaviour of the wind tunnel process. The second step was to develop a set of simple control laws in order to drive the dynamic model in closed loop.

Using the dynamic model and the control algorithms, it has been possible to run simulations of wind tunnel operations in order to determine the required performances for all subsystems (compressor/drive, LN2 injection system, Blow-off) and particularly to study and check the designs of the LN2 injection and blow-off systems.

From the beginning, solutions requiring large amounts of computation and therefore super computers were dismissed. This led to a compromise between optimization and simplicity. In addition a dedicated program running in real time in the control computer monitors permanently the behaviour of the overall system (wind tunnel + subsystems + control system).

As it was obvious that the aerodynamicists would want to use the wind tunnel as soon as possible for aerodynamic tests and that time for tuning the control system would be short, the algorithms needed to be easy to be tuned. One year before starting commissioning of the tunnel a new set of algorithms able to learn and tune themselves was developed and successfully tested in simulation mode.

The model inputs are the control parameter :

- Compressor rotational speed (RPM)
- Injected LN2 massflow rate (mLN2) and enthalpy (HLN2)
- GN2 Blow-off valve setting (CV)
- Second throat geometry

These are the parameters which are under the direct control of the control system.

The outputs calculated by the model are the state variables :

- Total pressures (upstream and downstream of compressor)
- Static pressure in the plenum chamber
- Static pressures in the second throat

- Total temperatures at various places around the circuit
- Internals temperatures, for aluminum liner and steel structures at various locations around the circuit.

The ETW control is very much a multi-disciplinary operation. The basic methodology of the ETW dynamic model consists of dividing the wind tunnel circuit into a number of volumes and black boxes as shown on Fig. 21 and 22. A black box, in the present context, represents a physical phenomena which determines the state of the gas (temperature and/or pressure and/or massflow) at the output of the box as a function of the state of the gas at the input. The black boxes simulate locations in the circuit where the control parameters are active (test section/second throat, compressor, LN2 injection, and GN2 Exhaust).

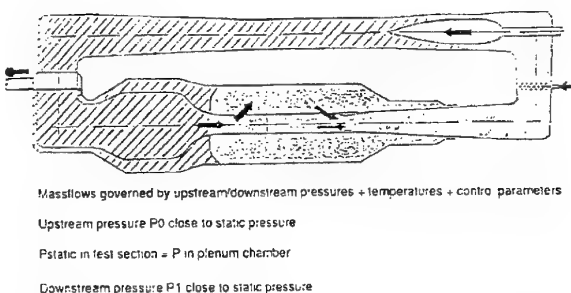


Figure 21: Dynamic Model - Pressures and Massflows

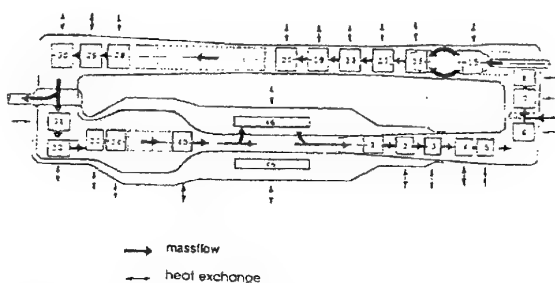


Figure 22: Dynamic Model - Temperatures and Heat Exchanges

The calculation scheme consists basically in resolving volume equations and black box equations in sequence around the circuit. The black box equations provide the values of the state variables resulting from the control parameters and the volume equations provide the time derivatives of these state variables. Once the circuit loop is completed, the time derivatives are used to update the state variables before starting the next circuit loop. A clear separation between spatial integration around the circuit and time integration is maintained. The definition and ordering of the black boxes and volumes is such that the equations have an explicit solution and therefore are kept simple.

At an early stage the model has been improved to simulate more accurately the aerodynamic phenomena in the test section, the plenum chamber and the re-entry area. For that purpose an additional black box has been added with a new input variable which is the incidence of the aircraft model in the test section. The added state variables are the static pressure, the gas temperature and the temperature of the internals in the plenum chamber.

Calibration Test Results

The calibration of the tunnel is not yet complete. Calibration test runs have been carried out in close connection with commissioning activities and model tests in order to gain information on performance of the facility as well as experience in operation at the same time. The very ambitious specifications have been checked in calibration runs on:

- tunnel circuit losses
- temperature distribution
- pressure distribution
- turbulence and noise level

Model tests have been carried out to get realistic information on the performance of the control system, the data acquisition system, and the productivity of the tunnel, i.e. in terms of measured quantities.

- change and stability of flow conditions
- data quality

These tests have been performed over the complete subsonic and transonic Ma , Re -envelope which is shown in figure 23, the symbols indicate the calibration conditions.

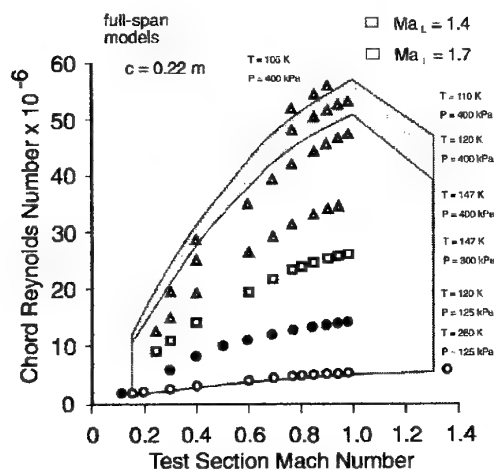


Figure 23: Covered Ma , Re - envelope

For the determination of the circuit losses, pressure data from 22 pitot probes upstream and downstream of the compressor have been taken and compared with theoretical predictions. The results are given in figure 24. The term "low Re " refers to tunnel conditions of $T_t = 280$ K and $P_t = 125$ kPa, the term "high Re " refers to 180 K and 300 kPa. In the Mach number region between 0.65 and 0.95 the control of the Mach number can be done by the second throat which causes higher losses than given in the diagram.

For a cryogenic wind tunnel, the temperature distribution in the test section is of great importance. The tuning of the injection nozzles for a uniform test section temperature distribution has been performed by measuring the temperature at 45 points in the stilling chamber covering the whole cross section area as shown in figure 25. Comparisons with measurements in the test section using probes on a rotating rake proved the uniformity of temperature within ± 0.25 K emanating from non-uniformities in the stilling chamber of less than ± 0.6 K. In addition, the tests showed that the flow is free of twist as the pattern of non-uniformity stays unchanged between the stilling chamber and the test section.

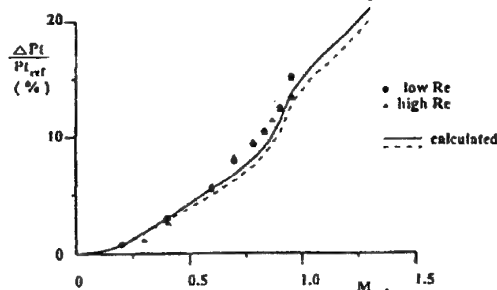


Figure 24: Preliminary Results of ETW Circuit Loss Measurements

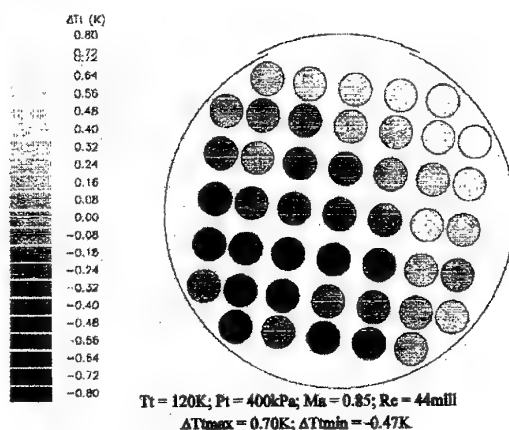


Figure 25: Temperature Distribution at Stilling Chamber Exit

The total pressure has been measured in the test section at the model location by means of pitot probes mounted on the rotating rake. Using high accuracy, small range differential pressure transducers, a uniformity of better than $\pm 0.15\%$ (i.e. ± 600 Pa) has been demonstrated for the test section Reynolds number of 42 million ($P_t = 400$ kPa, $T_t = 120$ K, $Ma = 0.78$). On the centerline, there is no pressure loss between the settling chamber and the test section. The distribution of the static pressure along the empty test section walls is plotted in figure 26. Over the model volume, indicated by the centred line near the bottom of the diagram, the scatter is in the order of $\Delta c_p = \pm 0.005$ which is equivalent to $\Delta Ma = \pm 0.002$ at the given Mach number. This value includes the scatter caused by the individual pressure taps signature.

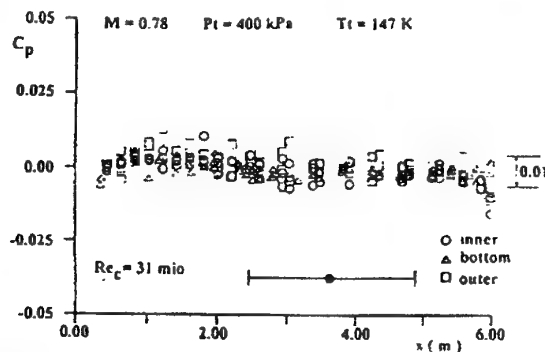


Figure 26: Pressure Distribution along Empty Test Section Walls

Turbulence measurements at high Reynolds number transonic flow conditions mean a challenge for the measurement technique applied. At ETW, hot film and hot wire probes have been used in the settling chamber and in the test section up to Reynolds numbers of about 40 million and Mach numbers of 0.9. At the same time, noise measurements with wall and rake mounted Kulite pressure transducers have been performed. From figure 27 the beneficial effect of the second throat being active can be seen. The data have been taken with an auxiliary instrumentation grid installed in the settling chamber.

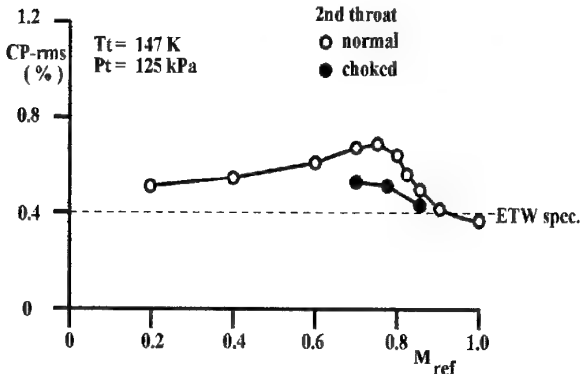


Figure 27: Pressure Fluctuation Level in the Test Section

The excellent control capability of ETW has been verified by measurements on set point changes and set point maintaining stability. For these tests, the flow reference system and a special "check out probe", mounted on the centerline of the test section, have been used. Figure 28 gives a plot of Mach number versus time, the Mach number being changed stepwise with periods of "set point maintaining" in between. The difference in Mach number by the different measurement systems is due to the upstream influence of the check out probe support. As can be seen, a Mach number step of $\Delta M = \pm 0.02$ can be achieved in about 25 seconds and the stability is better than $\Delta M = \pm 0.001$.

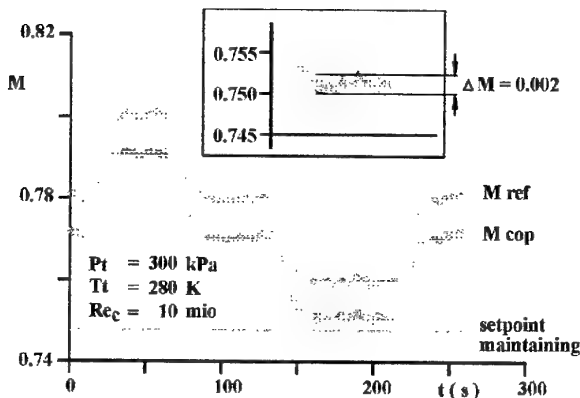


Figure 28: Mach Number Control Capability

These properties of the control system are the prerequisites for the high productivity and the outstanding data quality of ETW. In general, polars are taken in a continuous mode, and a fast reaction of the control system is required for the high pitch rate applied. A large number of model tests have been carried out until now, all of them showing a high data quality documented by a very good repeatability. The following table lists up typical results obtained at tests with the ETW reference model as well as clients models.

Parameter	Calibration Result
Mach Stability: T > 200 K T < 200 K	± 0.0005 ± 0.001
Pressure Stability: $\Delta P_t / P_t$	< 0.002
Temperature Stability: T > 200 K T < 200 K	± 0.3 K ± 0.1 K
Flow Angularity : α	$= 0.02$ deg.
Flow Curvature Tail off: ΔCM	$= 0.0003$
Repeatability: short term long term	< 0.5 drag count $= 1$ drag count

Table 2: Typical Model Results during Test Campaigns

Acknowledgements

The authors would like to express thanks to all the companies, especially the four National Establishments (the four share holders of ETW: DLR, DRA, NLR and ONERA) and the many engineers that assisted the ETW team in the development of the facility.

References

1. Hartzuiker, J.P., On the Flow Quality Necessary for the Large European High-Reynolds-Number Transonic Windtunnel LEHRT, AGARD-R-644, March 1976.
2. DSMA Ltd., Airline Optimisation Study of the ETW Facility, Report 4004/R19, November 1978.
3. Gunn, J.A., The Standard Deviation Method for Defining Mach Number Distribution in Transonic Wind Tunnels, Sverdrup Inc., Presentation to STA Meeting, September 1969.
4. Anonymous, A Description of the Langley Eight Foot Transonic Pressure Tunnel, NASA User's Manual, October 1979.
5. Dougherty, N.S., A Study of Acoustic Disturbances and Means of Suppression in Ventilated Transonic Wind Tunnel Walls, AEDC TR-77-67, October 1977.
6. Schubauer, G.B. and Spangenberg, W.G., Effect of Screens in Wide Angle Diffusers, NACA Report 949, 1949.
7. Bradshaw, P. and Pankhurst, R.C., The Design of Low Speed Wind Tunnels, Progress in Aeronautical Sciences, Vol. 5, Pergamon Press, 1964.

8. Lumley, J.L., Passage of a Turbulent Stream through Honeycombs of Large Length-to-Diameter Ratio, Transactions of ASME, June 1964.
9. Whitefield, D.L., Integral Solutions of Compressive Turbulent Boundary Layers Using Improved Velocity Profiles, AEDC-TR-78-42, 1978.
10. Gobert, J. L. Control and Mathematical Models of Transonic Wind Tunnels, AGARD FDP Symposium: Aerodynamics of Wind Tunnel Circuits and their Components, Moscow, September, 1996

Control and Mathematical Model of Transonic Wind Tunnels. Modélisation et pilotage des souffleries transsoniques.

J.L. Gobert

CERT-ONERA, 2 av. Ed. Belin, 31055 Toulouse Cedex

SUMMARY :

Presently, a large part of wind tunnel testing concerns the subsonic and transonic ranges for civil transport aircraft; one particular topic in such type of tests is that the flow parameters (Mach number, pressure, temperature) require to be controlled with a high level of accuracy.

Then, today's wind tunnels shall be equipped with an efficient control system capable to take the best of their performances. During the acquisition of data on the model, the flow parameters shall be maintained within small tolerances, leading to a restricted number of tests performed with a high level of quality in very well defined conditions. The operations of interpolation to be carried out during data post-processing are minimized and the task of the aerodynamicists while scaling up the results to the actual flying conditions shall be easier. On another hand, dead times during the transition periods when going from one set point to another one shall be reduced to keep the running costs as low as possible.

This document presents a control technic which was originally developped at ONERA and then adapted, improved and implemented in a recently built and large facility, the European Transonic Wind tunnel ETW erected in Cologne (Germany). During the first years of the ETW design, a computer dynamic model of the facility has been developped to support the control activities. This model, based on the knowledge of the aerodynamic phenomena present in the wind tunnel circuit, simulates the effects of heat transfers and temperature propagation along the circuit as well as the breathing of the Plenum Chamber. It performs a time simulation of the wind tunnel physical phenomena; at each time step, the parameter variations are integrated using the thermodynamics equations. In a following stage, control laws have been studied to drive the dynamic model; then careful checking and tuning have been performed before to implement them

into the wind tunnel control system in order to drive the actual process. Results of tests recorded on the actual plant are included in the document.

At the present time, a task is undertaken to enhance the performances of the ONERA S1 and S2 wind tunnels. The way this technic can be adapted to existing wind tunnels in order to trace the possible weaknesses of the facility, to correct them and improve the overall behavior are quickly discussed and supported by results of simulation.

It is demonstrated that this type of dynamic model can be used to design or redesign, set up and tune a transonic wind tunnel control system in an efficient and economical way as well as to improve the overall performances. Use of this technic enabled to run the ETW facility almost from the first days in automatic mode minimizing considerably the time required to tune the control system and providing quickly satisfactory results.

INTRODUCTION

Les souffleries aérodynamiques contribuent de manière décisive au développement des projets aéronautiques. Complémentaires des puissants ordinateurs, elles sont restées et resteront encore l'outil principal des aérodynamiciens. Durant les dernières décennies, les avions ont considérablement évolué par leur taille et leurs performances et les industriels ont fait apparaître un besoin en installations permettant une meilleure simulation des conditions de vol et une maîtrise plus fine des conditions d'essais. Ceci s'est traduit soit par la modernisation de souffleries existantes, soit par la construction de nouvelles installations telles que la soufflerie transsonique européenne ETW érigée à Cologne. Dans un cas comme dans l'autre, un point important est la nécessité d'un pilotage très précis des paramètres de l'écoulement, ce qui a entraîné l'introduction de calculateurs performants dans les boucles de contrôle-commande ainsi que la mise en œuvre de nouvelles méthodes.

Avant de chercher à mettre en place des lois de commande permettant de tirer le meilleur profit des capacités globales de l'installation, il est important de veiller à la bonne intégration des différents composants (compresseur, système de refroidissement,...) et principalement à l'homogénéité de leurs performances dynamiques. Dans un même ordre d'idée, lors de la remise à niveau d'une installation existante, il sera très intéressant et même nécessaire de vérifier que les performances globales ne sont pas dégradées de façon inacceptable par certains points faibles possibles de l'un ou l'autre de ces composants, auquel cas une reconsidération du composant incriminé sera souhaitable préalablement à l'étude et l'installation d'un nouveau système de contrôle.

Ce document décrit brièvement un modèle mathématique simulant le comportement dynamique d'une soufflerie transsonique. Il montre comment sa mise en œuvre permet de résoudre de façon sûre et économique les problèmes évoqués ci-dessus.

Cette technique, développée initialement vers 1975 pour la soufflerie R1Ch de l'ONERA (France) [ref.1], a été reprise sous une forme plus élaborée durant les années 80 lors de la transformation de la soufflerie T2 du CERT-ONERA (France) pour fonctionner à température cryogénique [ref.2 et 3]. L'augmentation des performances des calculateurs a rendu possible une évolution appréciable de cette technique par adjonction d'identification en temps réel au début des années 90 pour les besoins de la soufflerie ETW [ref.4] où elle donne des résultats très satisfaisants tant du point de vue de la précision du pilotage des paramètres d'essais (nombre de Mach, température et pression génératrices) que du point de vue de l'efficacité (coût et productivité).

En 1995, la direction des Grands Moyens d'Essais de l'ONERA a demandé une étude concernant les souffleries S1 et S2 du centre de Modane-Avrieux [ref.5]. L'objectif essentiel de cette étude est la réduction du coût moyen des essais réalisés à S1 et S2. Quelques résultats de simulation sont donnés dans ce document.

1- OBJECTIFS

Le système de contrôle d'une soufflerie transsonique doit satisfaire des spécifications très strictes concernant trois points essentiels qui sont la précision, l'efficacité et la robustesse.

- **Précision** : Le but primordial est d'obtenir et surtout de maintenir les paramètres de l'écoulement avec une excellente précision. Cette précision est étroitement liée aux possibilités matérielles de l'installation et aux performances intrinsèques de ses organes de pilotage. Les précisions couramment recherchées sont les suivantes:

. **Nombre de Mach** : $\pm 0,001$, une valeur de $\pm 0,002$ est parfois suffisante

. **Température** : $\pm 0,25$ K si un moyen d'action efficace est existant, ce qui est le cas dans les souffleries cryogéniques. Cette valeur peut être retenue pour les souffleries conventionnelles équipées d'un dispositif de réglage efficace du débit d'eau dans le réfrigérant.

. **Pression** : $\pm 0,1\%$ à $\pm 0,2\%$ en valeur relative dans le cas où un dispositif de pilotage efficace de la pression équipe l'installation, ce qui est le cas des souffleries cryogéniques ainsi que de quelques souffleries pressurisées conventionnelles.

- **Efficacité** : Devant les restrictions croissantes de budget, une réduction du coût d'exploitation des souffleries est apparue nécessaire. Dans le cas de la soufflerie ETW, cette nécessité de faible coût s'accompagne d'un souci de productivité élevée, les spécifications d'ETW prévoient en effet 3000 polaires par an. Pour cela, le système de contrôle doit maintenir les valeurs des paramètres avec la précision demandée pendant la phase d'acquisition des données intéressant les aérodynamiciens; mais il doit aussi être capable de changer les conditions d'écoulement d'un point de fonctionnement à un autre le plus rapidement possible. A titre d'exemple à S2, une réduction de la durée des transitoires d'un facteur 2 (ce qui est tout à fait envisageable) permettrait une réduction de consommation totale d'énergie proche de 40%.

- **Robustesse** : Compte tenu du coût des installations et des maquettes utilisées dans les souffleries, il est évident que le système de pilotage doit assurer un très haut niveau de sécurité matérielle. Pour cela, tout risque de divergence des lois de contrôle doit être totalement évité et l'évolution des paramètres doit être parfaitement maîtrisée pour ne pas sortir du domaine admissible qui peut éventuellement être restreint en fonction du type d'essai réalisé. Il sera également nécessaire de tenir compte de la fatigue des actionneurs et de la réduire autant que possible en évitant toute oscillation inutile, ceci permettra d'allonger la durée de vie de ces actionneurs et d'en réduire la maintenance.

2- DESCRIPTION DU CIRCUIT TYPE

Les circuits des souffleries transsoniques présentent des points communs; dans ce document, nous utiliserons le circuit type décrit sur la fig. 1. Il s'agit d'un circuit fermé où l'écoulement est entraîné par un compresseur installé dans le circuit retour. Ce compresseur peut être entraîné de façons diverses; à ETW, il est entraîné par un moteur électrique à vitesse variable (Puissance = 50 MW); à S1 et S2, il est entraîné par des turbines mues par l'eau provenant d'une conduite forcée. Il est à noter que pour la soufflerie T2 de l'ONERA, l'écoulement n'est pas entraîné par un compresseur, mais par un système à induction injectant de l'air comprimé à grande vitesse dans les aubes du coude numéro 2.

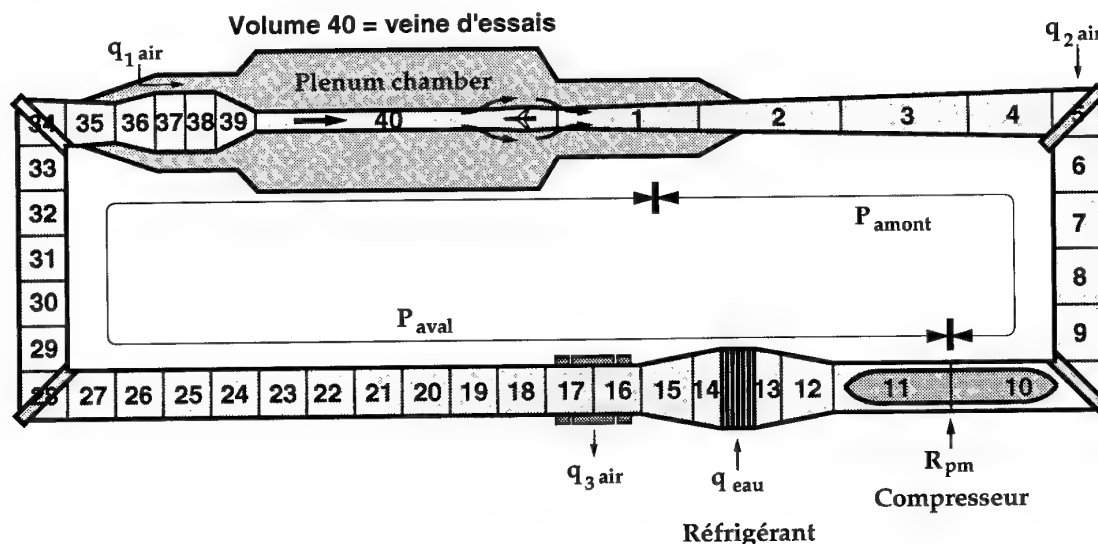


Fig. 1: Circuit type de soufflerie transsonique à compresseur

Un système de refroidissement disposé en amont ou en aval du compresseur (en aval sur la fig.1) permet de compenser l'élévation de température due à la dissipation de puissance de ce dernier; un moyen d'action sur la température du gaz est ainsi disponible. Dans le cas d'une soufflerie conventionnelle, le système de refroidissement est généralement un réfrigérant à circuit d'eau (soufflerie S2 par exemple); il peut également se matérialiser sous la forme d'entrées d'air atmosphérique comme sur la soufflerie S1. Sur les souffleries cryogéniques, le système de refroidissement est constitué d'une injection d'azote liquide (ETW, NTF aux U.S.A ou T2 en France).

Les souffleries pressurisées sont équipées de dispositifs permettant d'injecter et d'extraire les masses de gaz nécessaires au pilotage de la pression, ces dispositifs peuvent être situés en divers points du circuit. L'injection d'azote liquide des souffleries cryogéniques, en plus de son rôle de refroidissement, joue le rôle d'une entrée de gaz, le liquide étant immédiatement évaporé; il est à noter qu'il en est de même du système d'entraînement à induction de la soufflerie T2. La veine d'essais est très souvent entourée d'un caisson appelé aussi Plenum Chamber qui communique avec le circuit par l'intermédiaire de fentes ou de perforations situées sur les parois de la veine d'essais, la "respiration" de ce caisson avec la veine d'essais a une forte influence sur les "constantes de temps" du circuit lors de changement de nombre de Mach.

Les limites du domaine de fonctionnement sont variables d'une installation à une autre, les valeurs suivantes peuvent être retenues (restriction au domaine transsonique):

$$0,1 < \text{Mach} < 1$$

275 K < Température < 320 K pour les souffleries conventionnelles

100 K < Température < 320 K pour les souffleries cryogéniques

Pression atmosphérique pour les souffleries conventionnelles

1,1 b < Pression < 4,5 b pour les souffleries pressurisées; jusqu'à 9 bars à NTF [ref.6 et 7]

Certaines souffleries comme S2MA sont équipées de dispositifs (sphères à vide) qui permettent de diminuer la pression à des valeurs largement en dessous de la pression atmosphérique (jusqu'à 0,15 b à S2).

3- MODELE MATHEMATIQUE

Les systèmes de contrôle des souffleries R1ch et T2 ont été développés en utilisant des modèles de représentation très simplifiés. Pour la soufflerie ETW, un modèle mathématique mono-dimensionnel de simulation numérique plus sophistiqué a été développé pour deux raisons:

Les études du système de contrôle ont commencé alors que la soufflerie n'était pas encore construite, donc aucune information concernant son fonctionnement n'était alors disponible.

Ce modèle était également destiné à évaluer des scénarii de fonctionnement incluant les durées et les temps dans la phase d'étude préliminaire d'ETW.

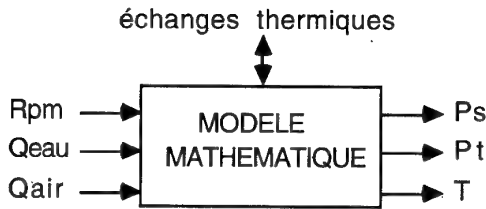


fig.2 : Entrées-sorties du modèle mathématique

Le but du modèle mathématique est de représenter le comportement dynamique de l'installation; la fig.2 donne un diagramme schématisant sa fonctionnalité. Ses entrées principales sont les paramètres qui sont normalement sous le contrôle direct de l'utilisateur, soit :

- La vitesse rotationnelle du compresseur Rpm ou son équivalent.
- Les réglages du système de refroidissement (débit d'eau du réfrigérant ou d'azote liquide,...)
- Les réglages du système de pressurisation.
- Certains éléments de la géométrie (tuyère, second col, ...)

Bien que n'étant pas un moyen de pilotage des paramètres de l'écoulement, l'incidence de la maquette installée dans la veine d'essais ainsi que la géométrie du circuit sont, *du point de vue mathématique*, des entrées du modèle.

Les sorties calculées par le modèle sont les grandeurs observables:

- Pressions totales en amont et en aval du compresseur.
- Pression statique dans la Plenum Chamber.
- Températures du gaz le long du circuit.
- Débits en divers points du circuit.
- Températures de nombreux éléments du circuit (éléments mécaniques situés à l'intérieur du circuit et enveloppe du circuit)

La méthode de base consiste à décomposer le circuit de la soufflerie en un certain nombre de volumes et de fonctions de transfert (boîtes noires), représentant les organes de contrôle; le schéma de la fig.1 montre un découpage en 40 volumes du circuit de S2.

Les fonctions de transfert simulent les endroits où les paramètres de contrôle sont appliqués (compresseur, réfrigérant,...). Une fonction de transfert, dans ce contexte, représente un phénomène physique qui détermine l'état du gaz (températures et/ou pressions et/ou débits) à la sortie en fonction de son état à l'entrée et des commandes qui sont appliquées.

Un exemple est donné par la fonction de transfert du compresseur (fig.3) qui sert à déterminer le débit masse Q_c et la température de

sortie T_{sortie} à partir de lois f et g représentées par des réseaux de polynômes fournissant une approximation de la caractéristique du compresseur; on a:

$$Q_c = f(Rpm, \lambda, T_{\text{entrée}})$$

$$T_{\text{sortie}} = g(\eta, \lambda, T_{\text{entrée}})$$

où η représente l'efficacité et λ le rapport de pression.

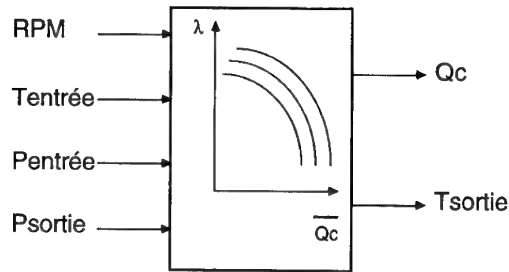


Fig.3 : Fonction de transfert du compresseur

Dans le cas d'un réfrigérant, on considère que toute l'énergie de refroidissement de l'eau est entièrement transférée à l'air suivant l'équation:

$$Q_{\text{air}} \cdot C_p \cdot \Delta T_{\text{gaz}} = 4183 \cdot Q_{\text{eau}} \cdot \Delta T_{\text{eau}}$$

Pour un système d'injection d'azote liquide, on aura:

$$Q_{\text{air}} \cdot C_p \cdot \Delta T_{\text{gaz}} = 120000 \cdot Q_{\text{ln2}}$$

A l'encontre des fonctions de transfert, les volumes sont utilisés pour déterminer non pas les variables d'état, mais pour calculer les valeurs de leurs dérivées premières. Les hypothèses suivantes sont faites:

- Les variations de pression sont instantanées dans les volumes; ce qui revient à considérer que le temps de propagation de l'onde de pression est négligé.
- Les pertes de charge sont concentrées dans la partie haute vitesse du circuit (veine d'essais, second col, diffuseur aval). Ceci entraîne que la pression est constante de la veine d'essais au compresseur ($P_{\text{entrée}}$) et du compresseur à la veine d'essais (P_{sortie}); il est donc à noter que seulement deux pressions totales sont calculées.

Les équations des volumes sont essentiellement basées sur les équations de conservation de l'énergie et de la masse en tenant compte des flux de chaleur entre le gaz et les éléments situés dans le circuit ainsi que ceux entre le gaz et l'enveloppe. Les échanges entre l'enveloppe et l'air extérieur sont également

calculés sauf si la soufflerie est équipée d'une très bonne isolation interne (ETW par exemple).

La veine d'essais, la Plenum Chamber et le col aval sont simulés par une fonction de transfert. Ce cas est beaucoup plus complexe. L'hypothèse est faite que le débit rentrant dans cette zone se divise en deux parties, l'une allant dans la veine d'essais et l'autre dans la Plenum Chamber, de la maquette installée dans la veine d'essais. Un calcul itératif permet alors de déterminer le débit sortant de la Plenum Chamber et entrant dans la veine d'essais dans la zone aval appelée réentrée. A l'équilibre, ces deux débits sont égaux, mais ils peuvent être très différents pendant les changements de régime du compresseur ainsi que pendant les changements de pression. Une fois ce débit calculé, les autres grandeurs en découlent. Les échanges thermiques à l'intérieur de la Plenum Chamber sont également pris en compte.

La méthode de calcul utilisée dans le modèle dynamique consiste à résoudre en séquence les équations des fonctions de transfert et des volumes le long du circuit. Les fonctions de transfert fournissent les valeurs des variables d'état à leur sortie, les volumes donnent les dérivées premières de ces variables d'état. Une fois ces calculs effectués, les valeurs sont intégrées avant de démarrer l'itération suivante. Une nette distinction entre calcul spatial et calcul temporel est faite.

4- LOIS DE CONTROLE

Le contrôle d'une soufflerie présente de nombreuses difficultés parmi lesquelles nous pouvons citer :

- La non-linéarité des relations entrées-sorties; celles ci sont en effet extrêmement liées au point de fonctionnement.
- Les couplages très serrés entre les paramètres. Chaque entrée agit sur tous les paramètres et non pas sur un seul à la fois.
- Le temps de propagation de la température d'un endroit du circuit à un autre. A ETW ce temps peut atteindre 15 secondes à basse température et faible nombre de Mach. Ce temps de propagation introduit un retard pur avec toutes les difficultés connues que cela implique sur le contrôle.

Le modèle mathématique a permis d'avoir une meilleure connaissance des phénomènes physiques présents dans un circuit de soufflerie. Il a donc été décidé de tenir compte de cette connaissance pour simplifier le problème et d'essayer d'adapter des algorithmes de contrôle classiques.

Le comportement du système est linéarisé à chaque instant autour de son point de

fonctionnement, les effets des couplages sont annulés par des termes correcteurs ou en choisissant des variables réduites mieux appropriées. L'effet du temps de retard pur introduit par la propagation de la température est éliminé en prenant en compte le fait que le gaz recircule en permanence dans le circuit.

Le contrôle du compresseur utilise une représentation simplifiée du premier ordre linéarisé du type:

$$\tau \dot{M}(t) + M(t) = C + G \cdot \omega(t - \tau_r)$$

τ = constante de temps

τ_r = retard pur

ω = vitesse rotationnelle du compresseur.

Une loi de contrôle optimale basée sur le principe du maximum de Pontryagin [ref.8, 9 et 1] est alors utilisée, cette loi consiste à minimiser une fonction de coût; dans le cas présent la fonction de coût choisie J rend minimum une pondération du carré de l'erreur ε et de sa dérivée $\dot{\varepsilon}$, elle s'écrit:

$$J = \sum (\varepsilon + k \dot{\varepsilon})$$

avec $\varepsilon = M_0 - M$

et $\dot{\varepsilon} = \frac{d\varepsilon}{dt}$

M est le nombre de Mach mesuré.

M_0 est le nombre de Mach de consigne.

Il est à noter que le même type d'algorithme est utilisé pour une soufflerie russe du TsAGI [ref.10], la fonction de coût choisie étant un critère de temps minimum pour atteindre le nombre de Mach de consigne.

En ce qui concerne le contrôle des autres paramètres (débits d'eau, air, azote liquide ou gazeux,...), ils utilisent des lois de type proportionnel, intégral et dérivée auxquelles de nombreux termes correcteurs ont été ajoutés afin de s'affranchir des effets de couplage et des non linéarités.

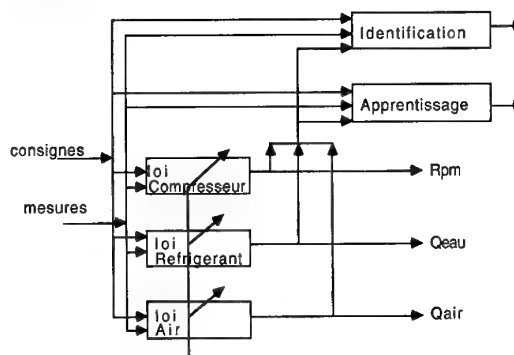


Fig. 4 : structure des lois de contrôle utilisées à ETW.

La fig. 4 montre deux particularités des lois de contrôle utilisées pour la soufflerie ETW.

La première est l'adjonction dans le logiciel de parties destinées à mémoriser de manière automatique les informations nécessaires à la linéarisation des paramètres des lois de contrôle (boîte apprentissage de la fig.4). Ce dispositif a permis de démarrer ETW en mode entièrement automatique dès les premiers jours de rotation acquérant progressivement les connaissances nécessaires pour piloter l'installation dans l'ensemble du domaine de fonctionnement.

La seconde particularité est la détermination de certains paramètres par une identification en temps réel utilisant la méthode du gradient. Cette identification permet en particulier de déterminer des constantes de temps et des temps de retard.

5- SIMULATION

Le modèle, comme la soufflerie qu'il représente, doit être piloté; ceci peut être réalisé de diverses façons et particulièrement en lui adjoignant un jeu de lois de contrôle.

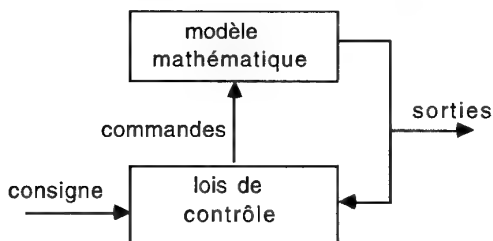


fig.5: utilisation du modèle dynamique en mode simulation

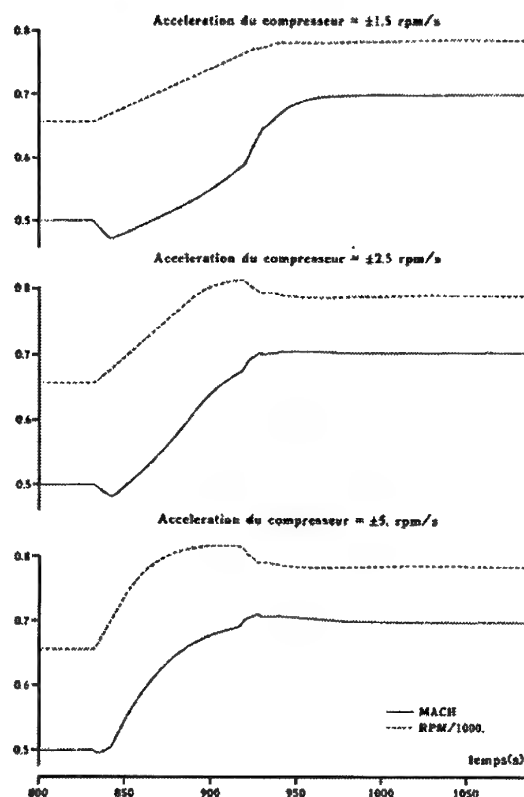
Une configuration telle que celle décrite sur la fig.5 réalise un simulateur sur lequel diverses idées de lois de contrôle peuvent être essayées à un coût très faible comparé à celui d'essais en soufflerie. Le modèle peut être modifié à la demande en ajoutant du bruit, de l'hystérésis, des non-linéarités,... sur les actionneurs et capteurs afin de procéder à des études de sensibilité. Dans le même ordre d'idée, des modifications dans les caractéristiques des composants (compresseur, système d'entraînement, réfrigérant, circuit d'air, ...) peuvent être testées.

Durant la phase de construction de la soufflerie ETW, ce type de simulateur a permis de vérifier le comportement des lois de contrôle sur tout le domaine de fonctionnement de l'installation. Il a été en particulier possible de s'assurer que les systèmes d'apprentissage et

d'identification étaient capables d'exécuter leurs tâches correctement. Mais, le simulateur a également été utilisé pour fixer les spécifications d'accélération, de résolution et de précision nécessaires pour les sous-systèmes (Compresseur, système d'injection d'azote,...) ainsi que les tolérances acceptables sur l'hystérésis et la stabilité de façon à garantir que les performances globales de l'installation seraient en accord avec celles souhaitées. Le logiciel de contrôle de la soufflerie installé sur le site dans sa version et sa configuration finales sur le matériel définitif a pu être complètement testé pendant les six mois qui ont précédé la mise en service d'ETW en fonctionnant en mode simulation avec le modèle dynamique. Ceci a permis de passer au contrôle réel de la soufflerie en mode totalement automatique en un temps très court, en toute sécurité et avec un coût de mise au point très réduit.

6- RESULTATS

6-1 Résultats de simulation



M=0,5 -->0,7 ; Pt=2,27 b -->1,356 b ; T=300 K
Nombre de Mach et RPM en fonction du temps

Fig.6: Changement de point de consigne à S2 simulé avec trois valeurs d'accélération du compresseur

La figure 6 donne un exemple typique de ce que le modèle, fonctionnant en mode simulation, peut apporter dans le cas d'une remise à niveau d'installation. Il s'agit ici de simulations qui ont été faites pour la soufflerie S2 de l'ONERA. Le but de cette phase de l'étude consistait à voir quel serait l'effet d'une amélioration des capacités d'accélération des turbines entraînant le compresseur sur le temps d'établissement du nombre de Mach. Pour cela, plusieurs changements de point de consigne en nombre de Mach ont été simulés avec trois valeurs de l'accélération maximale du système compresseur/turbines, une de ces simulations est présentée sur la figure 6.

La figure 7 donne la synthèse de quatre changements de point de consigne différents, l'essai 2 correspond aux courbes de la figure 6.. L'essai 1 correspond à un changement de $M=0,7$ à $M=0,9$; $P=1,35b$ à $P=1b$ à T constante (300K) et l'essai 3 à un changement de $M=0,9$ à $M=0,95$; $P=1b$ à $P=0,95b$ à T constante (300K). L'essai 4 correspond à un démarrage de $M=0$ à $M=0,95$; $P=0,9b$ à $P=0,95b$ à $T=300K$. L'analyse des résultats montre qu'il serait illusoire de penser qu'une augmentation des capacités d'accélération du compresseur diminuerait de façon très sensible les temps nécessaires aux changements du nombre de Mach dans tous les cas. Seul l'essai 4 qui correspond à un démarrage de l'installation est très affecté par la valeur de ce paramètre. Le gain escompté en exploitation ne permet pas de justifier la dépense très élevée que nécessiterait une telle modification. Sans l'utilisation d'un modèle dynamique, il aurait été très difficile, voire impossible de faire cette évaluation.

Essai	$\pm 1,5$ Rpm/s	$\pm 2,5$ Rpm/s	± 5 Rpm/s
1	120 s	120 s	140 s
2	170 s	120 s	120 s
3	120 s	120 s	120 s
4	500 s	300 s	200 s

Fig.7: Effet de l'accélération du compresseur sur les performances globales de S2

6-2 Résultats sur soufflerie

Les résultats obtenus à ETW permettent une comparaison objective entre simulation et réalité, puisque le système de contrôle a été entièrement élaboré à l'aide du modèle dynamique d'ETW puis installé sur la soufflerie elle-même où il est utilisé quotidiennement depuis plus de 3 ans.

Grâce à l'auto-adaptation des lois de pilotage, le système de contrôle d'ETW a fonctionné dès les premiers jours en mode totalement automatique. La fig. 8 montre un changement de point de consigne typique en nombre de Mach et température; ce changement de $M=0,8$ à $M=0,6$ et de $T=290K$ à $T=275K$ est effectué en moins de 50 s.

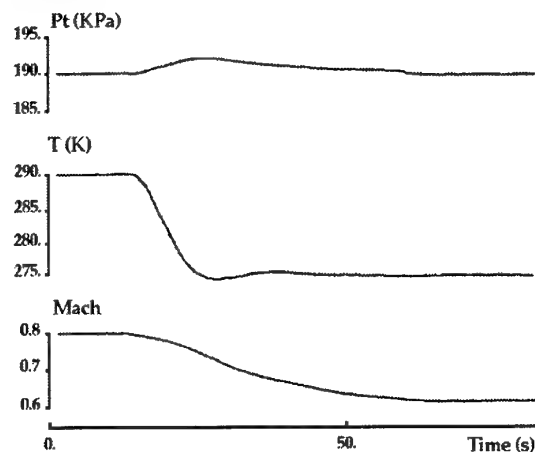


Fig.8: Changement de point de consigne à ETW (Résultat réel)

La fig. 9 donne les valeurs des paramètres enregistrés pendant une polaire, on peut voir que les trois grandeurs (Mach, pression et température) sont maintenues dans des fourchettes meilleures que les spécifications de la soufflerie.

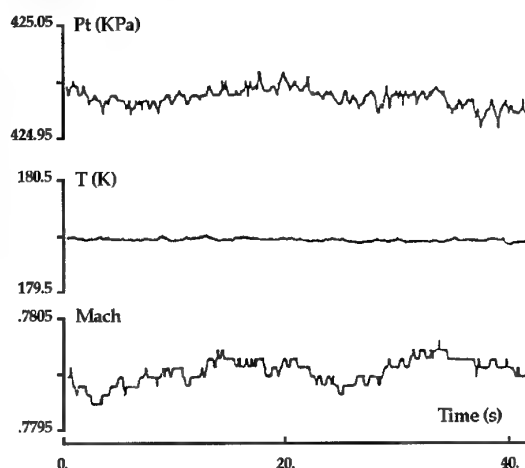


Fig.9: Maintien des valeurs de consigne à ETW en phase stabilisée

Les résultats présentés pour ETW sont tous des résultats d'essais enregistrés sur l'installation elle-même. Les écarts de durées de transitoires relevés généralement entre le modèle dynamique (non représenté dans ce document) et la

réalité sont inférieurs à 10%, les résultats obtenus sur l'installation sont sensiblement meilleurs que ceux obtenus en simulation concernant ce point.

CONCLUSION

Un modèle mathématique permettant la simulation dynamique de souffleries transsoniques est disponible. Ce modèle utilise les équations simplifiées de la mécanique des fluides. Il est suffisamment détaillé pour représenter fidèlement des phénomènes tels que la respiration de la Plenum Chamber et la propagation de la température du gaz dans le circuit qui sont des points particulièrement cruciaux pour le pilotage des paramètres d'essais d'une soufflerie. Mais il est également suffisamment simple pour s'exécuter rapidement sur un ordinateur de performances relativement modestes, des simulations en temps réel sont possibles sur un PC équipé d'un processeur 486 fonctionnant à 100 MHz. Il représente donc l'outil idéal pour l'étude d'un système de conduite et pour l'élaboration de ses lois. Son utilisation pour la soufflerie ETW a montré qu'il est possible de passer directement de la simulation à la conduite du processus réel réduisant considérablement les coûts de mise au point. Le logiciel de contrôle-commande avec tous ses éléments incluant l'interface homme-machine a été testé en simulation pendant plusieurs mois dans toutes les configurations possibles et sur tout le domaine de fonctionnement de la soufflerie. De ce fait, seul un nombre très restreint d'erreurs logicielles a été recensé après trois années de fonctionnement.

REMERCIEMENTS:

Une grande partie de ce travail a été effectué dans des conditions excellentes sous la responsabilité de Mr. Bouis, aujourd'hui Directeur des Grands Moyens d'Essais à l'ONERA; je tiens à le remercier ici très vivement. Mes remerciements vont également à Mr. T.B. Saunders, Directeur Général d'ETW GmbH, qui m'a autorisé à utiliser des résultats obtenus sur la soufflerie ETW.

REFERENCES

- Ref. 1 :** J.L. Gobert :
Commande en temps réel du nombre de Mach dans une soufflerie transsonique à rafales
Document ONERA Octobre 1975
Thèse de 3^e cycle Université Paris VI
- Ref. 2 :** J.L. Gobert, A. Mignosi :
Studies on the cryogenic induction driven wind tunnel T2
ETW cryogenic Technology Review Meeting
NLR-Amsterdam 15-17 Sept. 1982

- Ref. 3 :** J.L. Gobert :
Data acquisition and process control in the ONERA/CERT T2 wind tunnel
11th International Congress on Instrumentation in Aerospace Simulation Facilities
(IEEE) Stanford University 1985

- Ref. 4 :** J.L. Gobert :
ETW Control System - Design and first results
18th AIAA Aerospace Ground Testing Conference
Colorado Springs 20-23 Juin 1994

- Ref. 5 :** J.L. Gobert :
Contrôle des paramètres d'écoulement dans les souffleries transsoniques
AAAF- 32^eme colloque d'aérodynamique appliquée
Lyon (France) 25-27 Mars 1996

- Ref. 6 :** Bruce, W.E., Jr
The U.S National Transonic Facility
AGARD-FDP/VKI Special Course on Cryogenic Technology for Wind Tunnel Testing.
Rhode-St Genèse Apr. 22-26 1985

- Ref. 7 :** Balakrishna, S.
Modeling and Control of Transonic Cryogenic Wind Tunnels.
NASA CR-163588 Oct 1980

- Ref. 8 :** Pontryagin L.S., Boltyanskii V.G., Gamkrelidze R.V and Mishchenko E.F. :
The mathematical Theory of Optimal Processes.
Interscience Publishers Inc.,
New York 1962

- Ref. 9 :** Athans M., Falb P.L. Optimal Control
McGraw-Hill Book Comp., New-York

- Ref. 10 :** Koudrin N.A., Petronjevitch V.V. :
Optimal Mach number control in a fan driven wind tunnel.
Document TsAGI.

ELABORATION OF CRYOGENIC TRANSONIC SHORT-DURATION WIND TUNNEL AT ITAM

V.I.Zvegintsev, A.I.Omelaev

Institute of Theoretical and Applied Mechanics,
Siberian Branch of Russian Academy of Sciences,
Novosibirsk, 630090, Russia

ABSTRACT

The research program directed to the transonic cryogenic wind tunnel creation have been carried out at the ITAM. Two variants of short-duration cryogenic wind tunnel have been worked out as a paper projects. One of them is constructed as a classic blow-down wind tunnel. Here the cold air (or nitrogen) is collected within thermoinsulated storage vessels at a pressure up to 20 MPa and temperature 190 K. During a run the gas is flowing into the settling (plenum) chamber wherein its pressure falls down to 1 MPa and temperature to 120 K due to throttling effect. The cold gas flowing out is accompanied by a high pressure and ambient temperature air flowing into the accumulator thus practically constant stagnation parameters of flow will be kept during the run. Another variant is constructed as a modified Ludwig tube tunnel. The modification consists in the using of an additional reservoir attached to the high-pressure tube with a perforated baffle (wall) between them. Such device allows one to eliminate reflected rarefaction wave and to prolong useful running time.

An experimental program has been initiated at short-duration impulse gasdynamic facility where the first mentioned variant of transonic wind tunnel was checked out. A transonic flow with a good uniformity after throttling device was brought off during these tests. The experiments carried out at TsAGI (Moscow) allow one to establish the conditions when the reflected wave is eliminated for the second version of the tunnel.

1. INTRODUCTION

At the Institute of Theoretical and Applied Mechanics of the Siberian Branch of the Russian Academy of Sciences the investigations directed to the creation of a transonic cryogenic wind tunnel are carried out. Such tunnel as assumed essentially expands the Institute's experimental possibilities while performing of physical and industrial aerodynamic investigations. At the same time, it can be regarded as model set for new design solutions checking out while creating large-size transonic tunnels.

At the beginning, the studies were concentrated on the development of a steady-operation compressor-type wind tunnel known as "T-334". The scheme of gasdynamic contour of this tunnel was worked out at the Central Aerohydrodynamics Institute (TsAGI, Moscow). The tunnel is of closed type designed for the pressures of air up to 0.8 MPa with a temperature of 100 K. The test section has cross section of 0.625 by 0.625 m. During the process of this tunnel development an extensive research program on the problems of injection, mixing and evaporation of the liquid-nitrogen jets was carried out [1].

Further, the complexity of the of such tunnel design and high cost of its construction and operation have resulted in the necessity of alternative variants studying.

2. THE PROBLEMS OF TRANSONIC FLOW SIMULATION

It has been relatively easy to duplicate flight Mach number in the ground facilities. However, the ability to simulate the flight Reynolds number is conditioned by two main peculiarities of transonic flows that result in the necessity of huge consumption of air and energy. First, the flow at $M = 1$ has maximal value of specific density. Hence, it has the maximal value of flow mass rate in comparison with the flow that has an equal cross section, but differs in Mach number (see Figure 1, curve 1). Second, acceptable sizes of the model which can be tested without a flow field distortion decrease theoretically up to zero at $M = 1$ (practically by factor 3 to 5 compared to usual model sizes tested in supersonic tunnels). Reduction of tested model sizes means that attainable value of Reynolds number will decrease too. Moreover, the fabrication and handling of a small sizes model become very complicated. If one should try to use the model of normal sizes it leads to an additional flow rate growth (see Figure 1, curve 2). It can be seen from the Figure 1, the total increase in required air consumption at $M = 1$ is 8 times more in comparison with $M = 2$, 21 times more compared with $M = 3$ and 50 times more compared with $M = 4$.

It is well-known the decrease of the flow temperature T increases Reynolds number Re and simultaneously decreases the drive power N (see Figure 2). Based on this pointed out consideration, at present time, the most perspective direction is considered a flow temperature lowering up to air condensation. An investigation and development of the cryogenic transonic wind tunnels are under consideration in different countries now [2].

Characteristics of cryogenic wind tunnels under consideration at the ITAM

Wind tunnel index	Test section sizes, m	Pressure MPa	Reynolds number millions	Running time s
T - 334	0.6 * 0.6	0.8	24	1800
T - 335	0.4 * 0.4	1.0	20	3 - 5
T - 336	0.4 * 0.4	1.0	20	1

The general acknowledged leader among of this type tunnels is NTF (USA) [3].

In our opinion one of the attractive method of air and energy economy consists in a run duration decreasing. During two decades the experience of short-duration wind tunnel design and operation has been accumulated at the ITAM. So, the possibilities of short-duration facilities for transonic flow creation were examined. It was supposed that future short-duration transonic tunnel must preserve the main advantages of classic (usual) steady flow transonic wind tunnel, as well as to provide a cost reduction and realizable parameters range expansion.

3. SHORT-DURATION BLOW-DOWN WIND TUNNEL. GENERAL DESCRIPTION

The variant of short-duration transonic wind tunnel with a title "T-335" is represented in Figure 3. In this scheme, working gas (nitrogen or air) at pressure up to 20 MPa comes from the supply system flowing via special refrigerator (1) filled by evaporating liquid nitrogen. The working gas is cooled in the refrigerator to the temperature 180 to 190 K. Depending on the refrigerator efficiency from 0.4 to 0.8 kg of liquid nitrogen is required to cool 1 kg of working gas. Cold working gas is collected in the accumulator (2) which consists of standard high-pressure storage vessels. The number of storage vessels depends on the sizes of creating flow and on the desired run duration. In the scheme considered, 16 storage vessels are used with a total volume 6.4 m³ and having up to 2430 kg of cold working gas.

To start the tunnel, fast-acting valve (3) is opened. The gas from the accumulator (2) begins to flow into the plenum chamber (5). A non-regulating constrictor (4) is placed between the valve and plenum chamber, where the pressure of working gas is reduced by approximately a factor of 20. After that, the stagnation pressure in the plenum chamber doesn't exceed 1 MPa. Simultaneously, at the expense of the effect of Joule-Tompson, while adiabatic throttling, the stagnation temperature of the working gas decreases up to 110 or 120 K. In the plenum chamber, we use well-known methods aimed on the flow equalization and its level of turbulence reduction before entering the nozzle such

as: assembling of screens, boundary-layer suction and high degree of flow contraction ratio (from 7 to 10). After the plenum chamber, the working gas flows into the nozzle (6), then to the test section (7) with the sizes 0.4 by 0.4 m, then it is pushed via diffuser (8) into the (dump tank) exhaust reservoir (9) with volume 220 m^3 . The test section has perforated walls and is surrounded by a pressure chamber from which gas suction takes place.

Another fast-acting valve (10) is located between the diffuser and the exhaust reservoir. During the run this valve allows us to control a flow Mach number in the test section, as a sonic-throat adjustable diffuser when subsonic regimes are realized. When the test is completed the valves (3) and (10) are closed. The cold gas from the test section is quickly discharged into the atmosphere. After that the access to the model for readjustment is possible. Some part of this gas is used for accumulator (2) cooling.

One of the advantages of the tunnel T - 335 is that it doesn't need a thermal insulation of the contour walls because of short time of low-temperature flow influence on them. Besides, the high-pressure storage vessels of the accumulator (2) will be working at comparatively small cryogenic temperatures (180 to 190 K). It sufficiently simplifies their operation and decreases the cooling expenses.

4. POSSIBLE OPERATION MODES

On the base of quasistationary mathematical model, three possible operation modes of tunnel T-335 work were analyzed [4].

1. Cold operating gas at a temperature 190 K flows out the accumulator via plenum chamber and nozzle. The time of flow maintaining in nozzle is 0,6 s. After that, the gas flowing down with smooth quasistationary decreasing of flow pressure and temperature takes place as it happens in a hot-shot tunnel (see Figure 4, curve 1). The duration of operating regime, in this case, continues about 3 - 4 s, and it is limited by pressure increasing inside exhaust reservoir. During this time, pressure in the flow decreases approximately by the factor 2. We should note that the comparatively low rate of pres-

sure change allows us to apply a controlled constrictor (4) which could maintain constant pressure in the plenum chamber.

2. The cold gas flowing out from accumulator is accompanied by flowing in of high-pressure ambient temperature air from the existing at the ITAM pressurized air supply with volume of 100 m^3 . In this case, the air flow works as a gas piston. It pushes out cold working gas during 4 - 5 s practically at constant pressure. Pressure drop during the run doesn't exceed 5 % (see Figure 4, curve 2).

3. Air of ambient temperature flowing out the accumulator and from the air supply system, mentioned above, is used. With that the operating regime duration as well as the velocity of pressure drop are preserved as in the previous case, but the resulting Re numbers are smaller by a factor of 4 to 5 (see Figure 4, curve 3). Such regime of the work is simply realized and it is useful for comparative and adjusting experiments.

The principle of cryogenic transonic tunnel T - 335 operation provides the possibility of increasing in the sizes of the test section. Thus, for test section sizes 1 by 1 m, it is necessary to increase the accumulator volume up to 32 m^3 and the volume of exhaust reservoir should be increased up to 2000 m^3 . Then the duration of operating regime remains about 5 s. As to the Re number value, it will be increased by a factor 2.5.

5. MODIFIED LUDWIEG TUBE TUNNEL. GENERAL DESCRIPTION

This innovative short-duration transonic tunnel, known as "T-336", was designed on the base of gasdynamic scheme suggested at the TsAGI [5]. A general view of this tunnel is given in Figure 5. As a classic Ludwig tube the tunnel T-336 consist of a high pressure channel (1). The diameter of the channel is 0.8 m and the length is 40 m. The channel serves as a plenum chamber for a transonic nozzle (2) attached to the ventilated test section (3) with sizes 0.4 by 0.4 m. The flow contraction ratio in the plenum chamber is 3.14.

The modification of usual scheme lies in additional reservoir (4) which is connected to the opposite end of the cylindrical channel via the perforated baffle (5). The volume of the reservoir is 8 m^3 . The main starting valve (7) is located down-stream of the test section and includes the changeable sonic throat for a Mach number control. The valve (7) has a diameter 950 mm and a moving mass 584 kg. The working gas, after flowing over the model in the test section, is pushed into the exhaust (dump tank) reservoir (8) with volume of 220 m^3 .

Before the run, the volume of tunnel contour from the perforated baffle (wall) (5) to starting valve (7) is filled by a cold working gas (nitrogen at a pressure 1 MPa and temperature from 100 to 120 K) from the supply system (9). The problem of insulation of the tunnel walls is not analyzed at this step. The maximal gas consumption for one run is 850 kg. The attached reservoir (4) is filled by usual air at the same pressure. Ambient pressure is maintained in the exhaust reservoir (8).

When the fast-acting valve (7) is opened, the rarefaction (expansion) wave starts to extend along the test section. Behind the wave there appears flow moving with the required speed. The Mach number of the creating flow is defined by opening degree of pass cross-section of the valve (7). The perforated baffle (wall) (5) and reservoir (4) allows us to eliminate reflected rarefaction wave almost completely and to increase useful operating time by the factor of 3 to 5 at the expense of choosing of corresponding wall perforation degree which consist 10 to 20%. With that, a warm air flowing out from the attached reservoir (4) into the channel (1) via perforation represents, by itself, a gas piston which is pushing out a cold working gas. The main advantage of the tunnel T-336 is low expected turbulence level of creating flow.

6. TUNNEL RUN DURATION

The useful time interval of operating regime of tunnel T-336 begins after the valve (7) is opened and nozzle (2) is started. The end of this interval is defined by the moment of approaching (arrival) of contact surface separating warm pushing-out gas (gas piston) to the nozzle. The time of acting of the

starting valve (7) is between 0.09 to 0.105 s. The duration of a nozzle starting process is 0.22 to 0.24 s. Valid duration of tunnel run is minimal at $M = 1$ and it lasts from 0.9 to 1.0 s. For comparison it may be pointed out that, while operating of given facility in Ludwig tube mode (regime) (without attached reservoir and with rarefaction wave reflection), valid useful run duration will be only 0.04 s. If the length of the high-pressure tube is increased to 80 m then useful running time rows to 2.1 to 2.3 s. The Ludwig tube of the same sizes have the useful running time from 0.40 to 0.44 s.

7. TRANSONIC FLOW IN A SHORT-DURATION FACILITY

The experimental program aimed on check-out of the transonic flow in a short-duration facility creation was carried out. Tests were conducted in the innovative small sizes impulse wind tunnel [6]. Layout of the tunnel is presented in Figure 6a. The facility is equipped by the set of changeable contoured nozzles that gives us a possibility to create the flow with Mach number from 1 to 7. The diameter of the flow is 100 mm. A typical run duration - 0.1 s.

For transonic testing a modification of the facility was made out (see Figure 6b). An additional (auxiliary) plenum chamber with volume 6.4 cubic dm was mounted next to the main plenum chamber (volume 6.7 cubic dm). The main chamber is closed by a fast-acting valve and filled by pressurized air before the run. After the valve is switched on (opened) a working gas flows via the throttling device into the additional chamber and then through the contoured sonic nozzle (with diameter 100 mm) to the atmosphere. High pressure of air in the main chamber drops within an additional chamber due to throttling effect. In much the same way the flow density and mass flow rate are decreased. This modification allows us to achieve a running time up to 0.15 s at $M = 1$ and at the mentioned above geometry [7].

Some results of the pressure measurements in the both chambers during the run are shown in Figure 7. As it is usual for the hot-shot wind tunnel a pressure in the main plenum chamber is smoothly decreasing after the starting valve is opened.

In a steady state a pressure in the additional chamber must follow it thus their ratio will be equal to this chamber entrance and exit area ratio (that is 1 : 15 in our case). In the reality the process of chamber filling becomes at the run beginning so the pressure is raising here. According to experimental results a transition to a steady state lasts approximately 20 ms. The total (Pito) and static pressures were measured at the nozzle exit plane during the tests. With using of these results a Mach number variation at the different points of the flow was calculated. As it is seen from the Figure 7 after a short transition process the quasistationary transonic flow established. When the run is over a flow static pressure becomes equal to the ambient pressure. Since the total pressure is decreasing the flow Mach number is decreasing from this moment up to full stop ($M = 0$).

One of the key problems for the wind tunnel of proposed scheme is a flow quality (uniformity) at the test section. This problem arises with a strong distortion of the flow after throttling device at the entrance of additional plenum chamber. In our facility the flow velocity profile is equalized by: the entering flow breaking into a number of jets; air jets turning out from a longitudinal axis; a large volume of the additional chamber and high contraction ratio using; proper sonic nozzle contouring. The results of Mach number measurement at the nozzle exit during the quasisteady period of the run show that the spatial and temporal average value of Mach number obtained in this experiment is $M = 1.04$. The root-mean-square deviations from this value are not more than 2 % and are located within the measurement errors.

8. REFLECTED RAREFACTION WAVE ELIMINATION

The method of a Ludwieg tube run duration enlargement (increasing) is based on the well-known principle: a rarefaction wave reflects from the hard surface as another rarefaction wave and from the free surface as a shock wave. When we are using a certain combination of the hard and free surfaces (as a perforated wall, for example), we can obtain the situation when the rarefaction wave does not reflect in any way.

The possibilities of reflected wave elimination have been investigated at the TsAGI [8]. Sketch of the experimental setup arrangement is given in Figure 8. The main part of the facility consists of two coaxial steel tubes, filled by pressurized air. When the diaphragm 1 is destroyed the rarefaction wave begins to move along the smaller tube and reflects from the perforated baffle 3. The nature of reflection is related to the initial wave intensity (or Mach number M of moving gas) and level of a baffle perforation.

The results on reflected wave intensity measurements are shown in Figure 9. It is seen from this figure, when the level of perforation (a number of holes with diameter of 3 mm in the baffle) is raised the reflection as a rarefaction wave ($dP/P < 0$) transforms into the reflection as a shock wave ($dP/P > 0$). The value $dP/P = 0$ means the reflected wave is eliminated at that level of perforation.

The same experiments were conducted with different temperatures of gas from both sides of the baffle [9]. These results are shown in Figure 10 as a required level of perforation against the temperature ratio. The solid lines in the Figure 9, 10 represent theoretically predicted values that are in a good agreement with the experimental results. In whole, the required level of the baffle perforation account for 15 - 20 % of the high-pressure tube area.

9. CONCLUSION

The analyses of developed versions of the wind tunnels show that cryogenic transonic short-duration wind tunnels may provide rather high parameters of creating flow with sufficient reduction in design and operating cost. Short-duration facilities are distinguished by the simplicity, wide range of flow parameters, high level of Reynolds number. They provide a possibility of gradual increasing of working characteristics at the expense of modularity of the main units.

10. LITERATURE

1. Omelaev, A.I., "Simulation and Flow Structure Study in Wind Tunnels at Cryogenic Temperatures"

in "Recent Advances in Experimental Fluid Mechanics", Proceedings of the 1-st International Conference on Experimental Fluid Mechanics, Chengdu, China, 1991, p 563-569.

2. Kilgore, R.A., "Cryogenic Tunnels: Past, Present and Future", Proceeding of International Conference on the Methods of Aerophysical Research, Novosibirsk, 1992, pp 70-75.

3. Fuller, D.E., Williams, M.S., "Testing Experience with National Transonic Facility", AIAA 14th Aerodyn. Test. Conf., 1986, pp 110-120.

4. Zvegintsev, V.I., Elaboration of Transonic Cryogenic Short-Duration Wind Tunnel", International Conference on the Methods of Aerophysical Research, Novosibirsk, 1992, pp 203-206 (in Russian).

5. Grodzovsky, G.L., "Interaction of nonstationary shock waves with perforated plates", Uchenye

zapisky TsAGI, v. VI, N2, 1975, pp 7-15 (in Russian).

6. Zvegintsev, V.I., "Short-Duration Wind Tunnel at $M < 8$ ", Izvestija Sibirskogo Otdelenija, Novosibirsk, N5, 1990, pp 129-134 (in Russian).

7. Zvegintsev, V.I., "The Gasdynamics of Working Process in the Impulse High Reynolds Number-Wind Tunnel", Proceeding of International Seminar "Problems of Simulation in Wind Tunnels", Novosibirsk, 1989, pp 219-228 (in Russian).

8. Khvostov, N.I., Zaika, V.I., "The Study of Rarefaction Wave Interaction with Perforated Plate", Trudy TsAGI, N2306, 1983, pp 24-36 (in Russian).

9. Khvostov, N.I., Zaika, V.I., "The Study of Rarefaction Wave Interaction with Perforated Plate at Different Temperatures before and after it", Trudy TsAGI, N2600, 1986, pp 83-88 (in Russian).

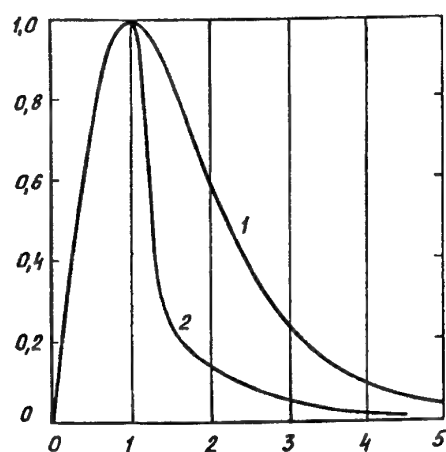


Fig. 1 Transonic peak in flow mass rate.

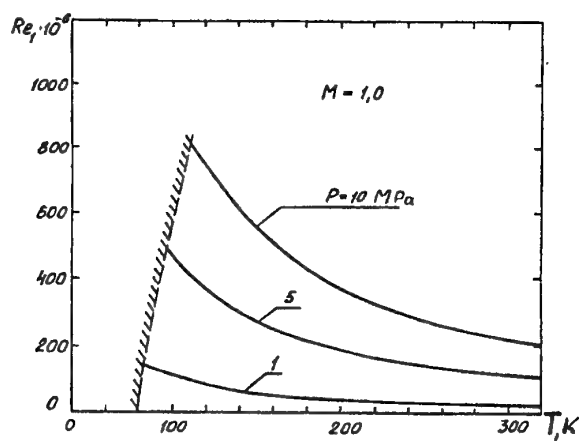


Fig. 2 Variation in Re number with static temperature.

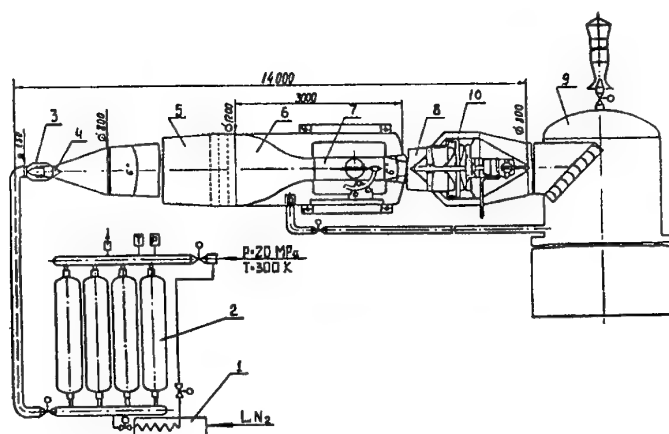


Fig. 3 Schematic layout of transonic wind tunnel T - 335.

1 - refrigerator; 2 - accumulator; 3 - starting valve; 4 - throttling device; 5 - plenum chamber; 6 - nozzle; 7 - test section; 8 - diffuser; 9 - exhaust reservoir; 10 - fast-acting valve.

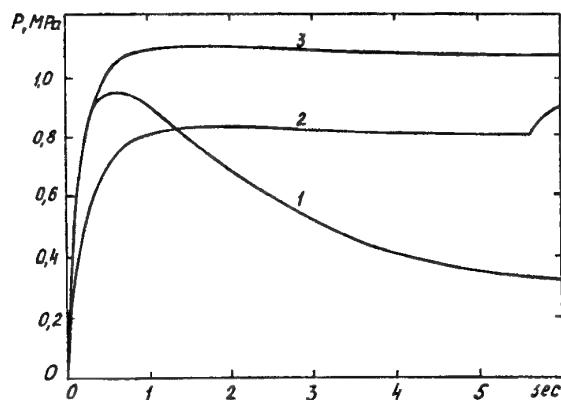


Fig. 4 Stagnation pressure as function of time. 1 - gas flows out from the accumulator; 2 - gas is pushed out by a "gas piston"; 3 - ambient temperature gas is pushed out by a "gas piston".

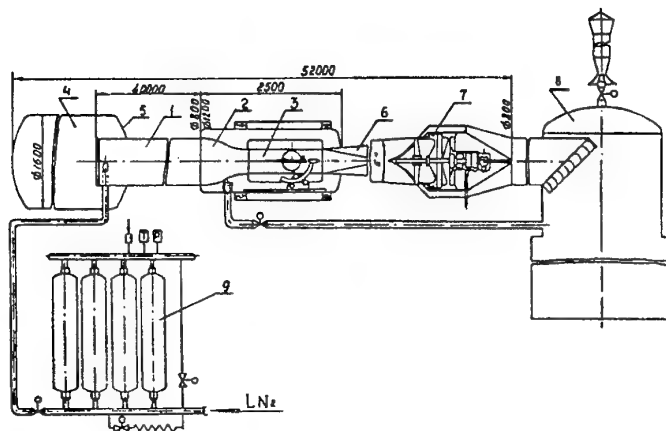


Fig. 5 Schematic layout of transonic wind tunnel T - 336. 1 - high-pressure tube; 2 - nozzle; 3 - test section; 4 - additional reservoir; 5 - perforated baffle; 6 - diffuser; 7 - starting valve; 8 - exhaust reservoir; 9 - cold nitrogen accumulator.

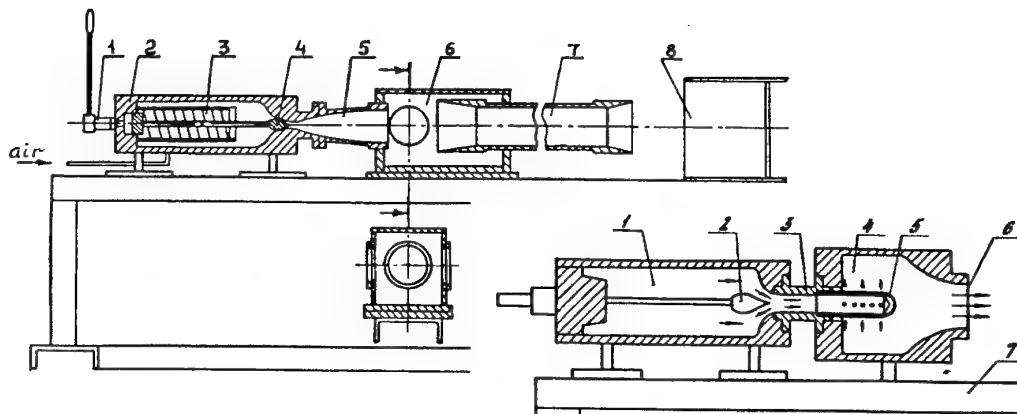


Fig. 6 a) Short-duration wind tunnel. 1 - driving piston; 2 - plenum chamber; 3 - electric heater; 4 - plug valve; 5 - nozzle; 6 - test section; 7 - diffuser; 8 - exhaust deflector. b) Transonic assembly. 1 - main plenum chamber; 2 - plug valve; 3 - insert; 4 - additional plenum chamber; 5 - throttling device; 6 - sonic nozzle; 7 - basement.

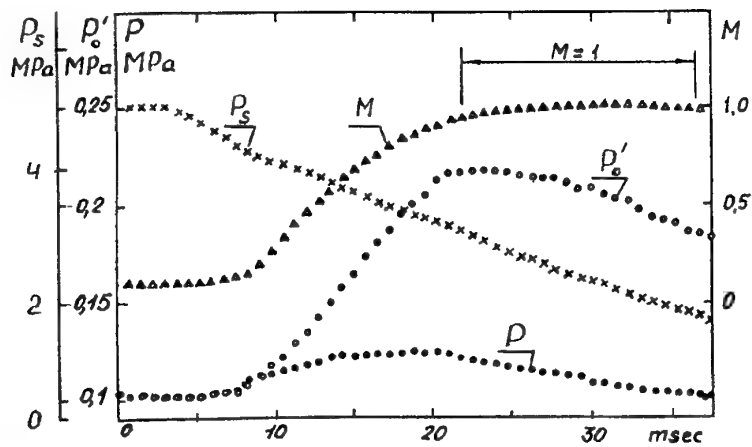


Fig. 7 Typical pressure records during the running time
Mach number from Pito and static pressure measurements.

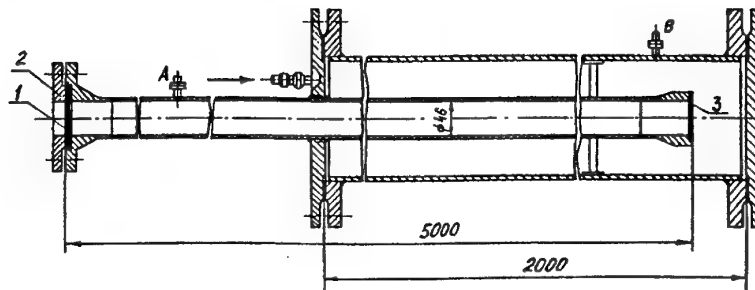


Fig. 8 Experimental facility set-up. 1 - diaphragm; 2 - flange; 3 - perforated baffle.
A, B - pressure gages.

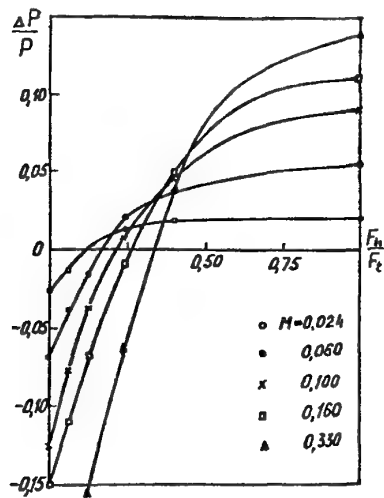


Fig. 9 Variation in reflected wave
intensity with level of perforation.

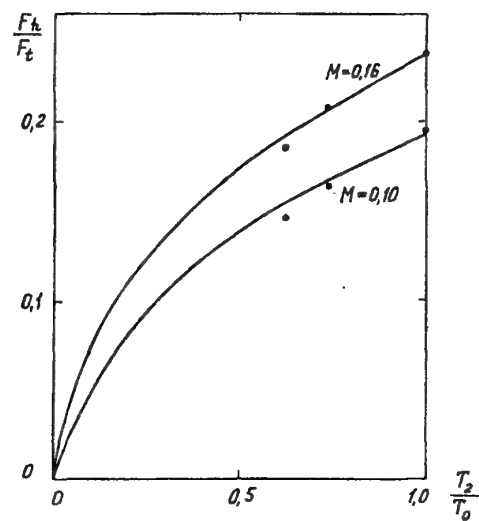


Figure 10 Required level of perforation.

14. The Impulse Transonic Wind Tunnel U-11. New effective technology for generation of sub-, trans- and supersonic gas flow.

V.V.Kislykh *), V.V.Koudriavtsev, O.V.Petrova, V.V.Puchkov

Central Research Institute of Machine Building
(4, Pionerskaya st, 141070 Korolev, Moscow region, Russia)

Abstract

New technology for generation of sub-, trans-, and supersonic gas flows along with based on this technology impulse transonic wind tunnel ITT U-11 (nozzle dia 0.8) operated at TSNIIMASH are presented.

The most important units and systems of the wind tunnel, test results on flow parameters in the working section and also their comparison with the same parameters for usual intermittent wind tunnels are described. The comparison has shown that suggested technology and the wind tunnel design, which allow to reduce essentially wind tunnel dimensions and power consumption, may be used for development of special rigs for complex investigation of aerogasdynamic and acoustic characteristics of flight vehicle models with engine jets simulation.

P_o - total pressure
 ΔP - pressure difference in two neighbouring points of the flow
 p' - pressure fluctuations
 P_b - base pressure
 P_s - static pressure
 q_∞ - dynamic head
 ρ - gas density
 u' - velocity fluctuations
 $\overline{u'^2}$ - mean value of velocity fluctuation
 U_∞ - flow velocity
 $\sqrt{(\overline{u'})^2}$ - relative intensity of turbulent velocity fluctuations
 V - vacuum chamber volume

Indices

o - stagnation parameter
 ∞ - oncoming flow parameter

List of symbols

C_p - pressure coefficient
 d_{hole} - perforation hole diameter
 D_{flow} - gas flow diameter
 ε (%) - turbulence intensity
 $F^{-1/2}$ - non-dimensional spectral density of velocity fluctuation
 G - flow rate per second
 G_{mod} - jet rate for model
 G_{veh} - jet rate for vehicle
 K_G - jet rate coefficient
 L_Σ - noise level
 L - distance from perforate plate to downstream
 m - model scale

1. Introduction

In the last years requirements imposed on ground experimental facilities, used for developing new types of flight vehicles, have become more severe. In particular it is necessary to create cost-effective transonic wind tunnels which allow to provide investigations on relatively large-scale models at high values of Reynolds number Re_∞ . As a result of analysis existing transonic wind tunnel designs and investigations the

*) Head, PGU Department,
Member AIAA

concept of an impulse transonic wind tunnel (ITT) was developed in TSNIIMASH for generation of sub-, trans-, and supersonic flows with Mach number $M \sim 0.1-2$.

One of the variants of ITT was realized on the basis of the large-scale multi-purpose piston unit PGU-11 TSNIIMASH which is widely used for simulation of hypersonic flows [1], investigation of supersonic combustion [2], and also as a generator of high temperature jets with various composition exhausted into vacuum chamber [3]. Wide use of PGU is explained by the unique properties of piston gasdynamic units based on multi-cascade compression technology [4] for a generation of different gas flows with pressure up to 250 MPa and temperature in the range 300 - 3500 K - for diatomic gases, and up to 10000 K - for monatomic gases, its operation time is about 1 sec and more.

In 1980s a problem of influence of heavy launch vehicle "Energia" engine jets on aerogasdynamic and acoustic characteristics of joint craft "Energia - Buran" had arisen. Multi-purpose PGU-11 operation regimes, if it is used as gas generator, comply with requirements for simulation of flight parameters of "Energia" engine jets, in particular their ejecting and acoustic effect on "Energia-Buran" aerodynamic characteristics [5]. Several interchangeable modules for PGU-11 were manufactured in order to provide simulation of flow over vehicle up to Mach number $M = 2$. This variant of the facility was named "Impulse transonic wind tunnel U-11 (ITT - U-11)".

2. ITT operation and scheme.

The scheme of ITT is shown in Fig. 1. The wind tunnel includes vessels for accumulation of high pressure working gas (i. 1,2), impulse shutoff- starting valves for forechamber (SSV_f, i.3) and for gas supply line (SSV_m, i.4), throttle-expanding nozzle (i.5), vacuum chamber (i.6) with silencer (i.7), diffuser (i.8) with system for adjustment of pressure under perforated walls (i.9), buffer vessel (i.10), impulse

adjusting exhaust valve (AEV, i.11), and vacuum vessel as exhaust channel (12).

ITT performance is based on accumulation of working gas in high pressure vessels, pumping of vacuum vessels and setting initial pressure in vacuum chamber prior to a run. The wind tunnel starts, depending on a specific task of a run starting of the wind tunnel occur by programmed opening either both impulse valves SSV_f and SSV_m through time interval ≤ 1 sec, or one of them. Working gas flows to the throttle-expanding nozzle where its cross-section area increases while throttling. Compression wave, arisen during formation of jet and then uniform flow, reaches AEV and affects the latter, the valve is opened according to prescribed program, and then required gas flow regime is set in the vacuum chamber.

The flow with given parameters is formed by the throttle-expanding nozzle. Schemes of two such type nozzles for generation of sub-, trans-, and supersonic gas flows [6] are shown in Fig. 2,3. The nozzle I (Fig. 2) is used for generation of air flows and incorporates perforated plate (i.1) and silencer (i.2). The nozzle II (Fig.3) comprises perforated plates in series (i.1) and is used for formation of air, nitrogen, carbon dioxide flows while simulating atmospheres of Mars and Venus, and also of methane and other gases flows for simulation of other planets' atmospheres. Provision is made for preliminary gas (for instance, carbon dioxide) heating, while supplying the nozzle II, or for gas cooling to obtain maximum Reynolds numbers.

Throttle-expanding nozzles include one or several thick perforated plates for generation of a flow with prescribed parameters. The last perforated plate have a decisive effect on flow structure. Flow parameters in vacuum chamber are defined by a ratio $d_{\text{hole}}/D_{\text{flow}}$, by a drag and a permeability of the last plate and a set of wire meshes placed just before the plate are selected to provide in a place of a model location acceptable levels of flow uniformity; flow turbulence; acoustic disturbances (background noise), low-frequency pressure fluctuations; temperature fluctuations, etc.

Gas supply system for ITT nozzle is done in such a way that it excludes powerful noise at low frequency, and high frequency noise caused by jet flows is reduced in the vacuum chamber using noise-absorbing coating of the facility circuit.

As it is indicated in [7], lattices of contoured axisymmetric supersonic nozzles were used in Germany to reduce the length of a supersonic nozzle. At a certain distance from the nozzle lattice exit a flow uniformity was satisfactory, but this distance is comparable with the length of equivalent customary nozzle, thus the aim - to reduce a nozzle length - was not obtained.

In our case by using transonic throttle-expanding nozzles, which incorporate thick perforated plate with cylindrical channels (Fig 1, i.13; Fig.2,3, i.1), it is unnecessary to have a bulky stilling chamber with corresponding pipes and relatively long customary nozzle. So dimensions of facility essentially reduce..

Duration of ITT run is defined by volumes of high pressure chambers, vacuum vessel and a time interval of transient process in the facility circuit. For given crosswise size of a flow in ITT, which in fact set a vacuum chamber volume, the time interval required for transition to a steady state flow is:

$$\tau \sim V \cdot \rho / G \ll 1 \text{ sec.}$$

Since ITT has no forechamber, shutoff-starting valves are placed in the immediate vicinity of the throttle-expanding nozzle and a working gas with a given flow rate are supplied at high pressure ($\sim 5.0\text{--}15.0$ MPa), a time interval required for the flow in the facility to become steady depends mainly on a speed of opening impulse valves SSV_f , SSV_m and AEV. Calculations of transition with use of quasi-one-dimensional analysis have shown that this time interval is about $\tau \leq 1$ sec for impulse valves designed at TSNIIMASH.

Impulse regime of ITT operation has allowed to devise a method for increasing Reynolds number which use a cooling of gas in the facility without some problems and disadvantages inherent to usual intermittent wind tunnels. The basic idea

of this method is an application of positive effect of Joule-Tompson during gas throttling from ITT accumulating high pressure chambers from initial temperature which on the one hand is less than temperature of inversion and on the other hand its level is high enough to exclude influence of low temperature on structural materials' strength. The analysis has shown that throttling of working gas from pressure $\sim 15 - 20$ MPa to pressure $0.3\text{--}0.5$ MPa in vacuum chamber allows to vary working gas temperature in the vacuum chamber in the range $100 \text{ K} - 200 \text{ K}$. Short action of low temperature flow on the facility design is analogous to effect of high temperature flow in PGU where, due to a short run duration, temperature of PGU elements surface does not reach a level when materials' strength starts to reduce noticeably.

3. ITT U-11 operation and main units for conducting tests in air at Mach number $M \leq 0.6 - 0.7$ with jet simulation.

External view of the facility is shown in Fig. 4, and Fig.5 presents its gasdynamic scheme for calculation. PGU U-11 power part (i.1) is used in this scheme as jet generator. Model gases (air at $T_0 \sim 300 \text{ K}$, nitrogen at $T_0 \sim 380\text{--}400 \text{ K}$, helium at $T_0 \sim 500\text{--}600 \text{ K}$) flow through collector (i.18) from PGU forechamber to hollow sting (i.19) where 1:50-scaled model of "Energia-Buran" was mounted on. Run duration was defined by the volume of model gas for jets simulation. When the model gas was nitrogen, the duration was $\sim 1.5\text{--}2.5$ sec, and for helium - $\sim 0.8\text{--}1$ sec. The facility includes some units which allow to modify it for tests of various types. For instance a nozzle with exit diameter 800 mm for PGU operation as hypersonic facility can be placed instead of interchangeable modules of vacuum chamber (i.8).

The throttle-expanding transonic nozzle with maximum exit cross section

800 mm is done according to the scheme I (Fig.2). The main element of the nozzle is a perforated plate with thickness 60mm, holes' diameter $d_{\text{hole}} = 4$ mm and permeability 22 %.

The design of ITT U-11 vacuum chamber with diameter 1.4 m permits to locate tested model at any its cross section. Vacuum chamber working zone proper is at a distance $L = 3.0-3.5$ m from the nozzle exit (the last perforated plate).

Fig. 4 presents most of the above mentioned ITT units including collector for high pressure air supply (20 MPa) with shutoff-starting valve (SSV_m) with diameter of pass cross section 200 mm (i.5) and pipes (i.4) for supplying of throttle-expanding nozzle (i.6) with high pressure air.

The system for formation of axisymmetric air flow in vacuum chamber includes cylindrical shell made from wire mesh and fixed on elements of slot perforation manufactured from circular rods with total permeability about 20% and noise-adsorbing cover placed between circular rods and vacuum chamber walls with thickness 200÷300 mm. Cylindrical diffuser with diameter 800 mm (i.11) adjoin to permeable walls of the facility is mounted in exit cross section of the vacuum chamber. There is an annular channel between the diffuser walls and vacuum chamber which diameter in this place is equal to 1000 mm, the channel area at the exit is adjusted by special device. The vacuum chamber has exhaust into vacuum vessel with volume ~1000 m³ through impulse adjusting exhaust valve (AEV).

4. Flow parameters in ITT U-11

Jet flow in ITT ahead of perforated plate is highly nonuniform. Required uniformity of the flow parameters in test section is obtained by equalizing action of the perforated plate and subsequent alignment of the flow field formed by mixing of jets exhausting from the plate holes with diameter $d_{\text{hole}} = 4$ mm.

In order to examine efficiency of the process on the flow field alignment, total

pressures have been measured in cross sections at distances $L = 3180$ mm and 4400 mm from the plate using a rake with total pressure heads. Pressure transducers have been connected with the heads through differential scheme. Such technique permits to determine a pressure difference between two near by points ΔP . Besides 2 transducers in the central head of the rake measure absolute value of total pressure P_0 .

Static pressure was measured on vacuum chamber walls between cross sections $L = 1200$ mm to 3100 mm.

Particular attention has been given in the last years to such characteristic of flow quality as turbulence intensity :

$$\varepsilon (\%) = [\sqrt{(\bar{u}')^2} 100 \%] / U_{\infty}.$$

For conventional wind tunnels oncoming flow turbulence depends on air supply system, flow contraction in forechamber and so on. Some special wind tunnels are known for which ε is a fraction of a percent, but usually it is equal to 1÷3%. In ITT U-11 pressure difference up to 15 MPa is realised at perforated plate and behind the plate powerful jet flow forms with high turbulence intensity ε which decay downstream due mixing. A study of ITT U-11 flow parameters included measurements of flow mean velocity U_{∞} , turbulence intensity ε , frequency spectrum of velocity fluctuations, and mean flow temperature.

Measurements of mean velocity and intensity of turbulence were conducted at a distance $L = 3000$ mm from perforated plate by thermoanemometer of constant temperature. Average flow temperature was measured also by thermoanemometer probe when it operates as thermometer of resistance. Relative error for mean velocity measurements was $\leq \pm 3\%$, for turbulence intensity $\leq \pm 4\%$, for mean flow temperature $\leq \pm 1\%$ and for Mach number $\leq \pm 4\%$.

Some results of the measurements are presented in Fig. 6, and fig. 7 shows results of spectral measurements ($F \bar{u}'^2 = \bar{u}'^2(f) / \bar{u}'^2$).

Nonuniformity of P_0 field in cross sections ($L = 3000 \div 3500$ mm from the plate) is $0.6 \div 0.7\%$ in the flow core. Nonuniformity of P_∞ along the vacuum chamber length at the indicated interval does not exceed 1%.

In particular it should be noticed that values of turbulence intensity in the flow at $L = 3000$ m is lower comparing with data for more close distance from the plate.

As it is seen in Fig. 6, value of ε depends on Mach number. In the region where models are placed in ITT U-11 value of ε at Mach number $M \sim 0.6$ is lower than in test sections of conventional intermittent wind tunnels (U-3 - ejector type transonic wind tunnel at TSNIIMASH).

M	ITT U-11	U-3	References
0.6	1.42 - 1.49	1.6 - 2.4	1 - 4

The next important flow feature is level of background noise. From this point of view ITT differs from conventional wind tunnels by gas supply system and perforated plate as the facility nozzle. As it is mentioned above, gas supply system is designed in such a way that appearance of intensive low frequency noise, which may arise during throttling of compressed air from pressure 20 MPa to $1 \div 5$ MPa, is excluded. High level of flow noise reduces in a cavity before perforated plate using noise-absorbing coating, Fig. 2 (i.2). In turn, jet flow behind the plate is noise source where maximum intensity with frequency $10 \div 20$ kHz takes place at sonic flow in the plate holes.

Analysis of the results has shown that the main source of noise is the unit for generation of sub-, trans-, and supersonic flows, including perforated plate. Noise level measured near the plate ($L = 480$ mm) is equal to ~ 160 dB, that is in agreement with preliminary evaluations. Noise level in the flow downstream from the plate reduces due to attenuation and

effect of noise-absorbing coating in vacuum chamber. At the distance $L = 3500$ mm from the plate noise level L_Σ [dB] is lower than at the distance $L = 480$ mm by $13 \div 20$ dB.

As it follows from the comparison of background noise for different Russian conventional wind tunnels U-3, ST-5, T-109 and for ITT U-11 (Fig. 8) at $M \sim 0.6$ background noise level for ITT U-11 lays practically in region inherent to conventional wind tunnels even for conditions far from the optimal for used noise-absorbing material. Fig. 9 shows

$C_p = \frac{\sqrt{\bar{p}^2}}{q_\infty}$ dependency downstream from the nozzle.

Investigation which has been carried out confirmed main principles of ITT design.

ITT U-11 were used for investigation of engine jet influence on gasdynamic and acoustic characteristics of "Energia-Buran". Results of this investigation are a specific theme. Here we only note that in case of identical tests of "Energia-Buran" models in conventional intermittent wind tunnels and in ITT U-11 when compressed air at temperature $T \sim 300^\circ$ is used for engine jet simulation, results agree well.

The influence of jet composition on base pressure was examined in ITT U-11, and the method for selection of working gas and its parameters for model jets was confirmed [8]. Fig. 10 presents reduced base pressure $\bar{P}_b = P_b / P_s$ plotted against jet flow rate coefficient $K_G = G_{\text{mod}} / m \cdot G_{\text{veh}}$ ($m = 1/50$ - model scale) at $M_\infty \sim 0 \div 0.3$ and $M_\infty \sim 0.6$. As expected, ejection properties of heated helium jet are the most close to real jet properties.

Fig. 11 presents appearance of "Energia-Buran" model mounted in ITT U-11 as viewed from the throttle-expanding nozzle. The model against a background of the nozzle (perforated plate) during its arrangement before test is shown in Fig. 12.

5. Conclusion.

Suggested concept and technology of ITT are promising for creation of new experimental facilities.

It should be noticed that ITT U-11 designed and built at TSNIIMASH is the first example of such kind facility which performance may be improved essentially optimising its elements and systems. The concept is of special importance for creation large-scale facilities with nozzle diameter $\sim 5\div 10$ m. With the same size of perforation (and hence jet flow behind a perforated plate) ~ 4 mm and increased diameter of the plate (by an order) influence of jet flow on flow parameters rather reduces in a zone of the model location.

It is interesting that the main element of ITT, namely thick perforated plate with required dimensions is in production and used, for instance, in timber industry.

Acknowledgements.

Present work had been carried out during "Energia -Buran" program realization.

Literature.

1. Kislykh V.V. " The Efficacious PGU Multicascade Compression (MCC) Method for Aerothermodynamic Ground Testing of a New Generation of Aerospace", J.C.E.F.M. 94, Proceedings of the 2nd International Conference on Experimental Fluid Mechanics, July 4-8, 1994, Torino, Italy, Edited by M. Onofrio, Levrotto e Bella, Torino, p.p. 538-546.

2. Erdos J.I., Kislykh V.V., Orth R.C., " Results of the First Hypersonic Combustion Tests in the TsNIIMash PGU-11 Facility", AIAA, Sixth International Aerospace Planes and Hypersonic Technologies Conference, April 3-7, 1995, Chattanooga, T.N

3. Kislykh V.V., Reshetin I.A., " Methods for complex investigations of loads on the vehicle stern in PGU with engine jets simulation", The News of SD AS USSR, vol. 5, scientific and technical series, 1990, p.p.141-144(in Russian).

4. V.V. Kislykh, O.V. Petrova, V.V. Puchkov, "Method of compression in aerodynamic unit", patent 972 931 of 01.01.82. , Bulletin of state Inventions Committee, vol. 29, 1989 (in Russian).

5. Kislykh V.V., Reshetin I.A., "Methods for simulation of the jets in aerodynamic tubes", Gagarin's Scientific reading cosmonautics and aviation, 1989", M, 1990r(in Russian).

6. Veremiev E.S., Zorin E.V., Kislykh V.V., Tsaregorodtsev L.A., Shestakov Y.N., "A Mean of Conducting Gas of a Transonic Tube", patent № 356 687 of 07.08.87, Bulletin of state Inventions Committee, vol. № 20, 1982r.(in Russian).

7. Pankhurst R.C., Holder D.W., "Wind-Tunnel Technique. An Account of Experimental Methods in Low-and High-Speed Wind Tunnels", London, 1952.

8. Kislykh V.V., Reshetin I.A., "Afterbody Effects Study on Energia Reusable Launcher Models. Selection of Jet Propulsive Masses Parameters Within Jet Streams Ejecting Model", International Union of Theoretical and Applied Mechanics, Separated Flow and Jets, Edited by V.V. Kozlov, V. V. Dovgal, IUTAM - Symposium, Novosibirsk, July 9-13, 1990.

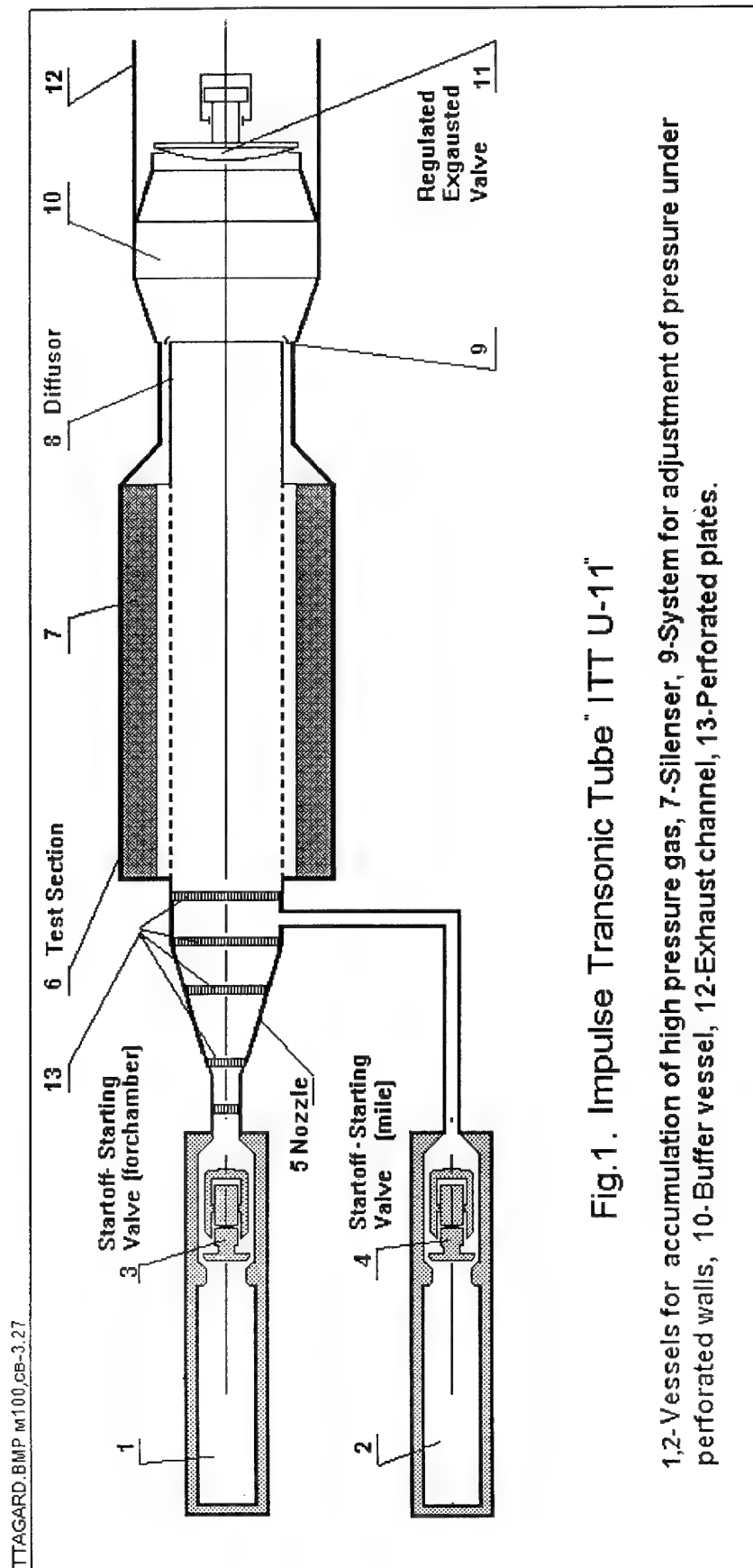


Fig.1. Impulse Transonic Tube "ITT U-11"

1,2-Vessels for accumulation of high pressure gas, 7-Silencer, 9-System for adjustment of pressure under perforated walls, 10-Buffer vessel, 12-Exhaust channel, 13-Perforated plates.

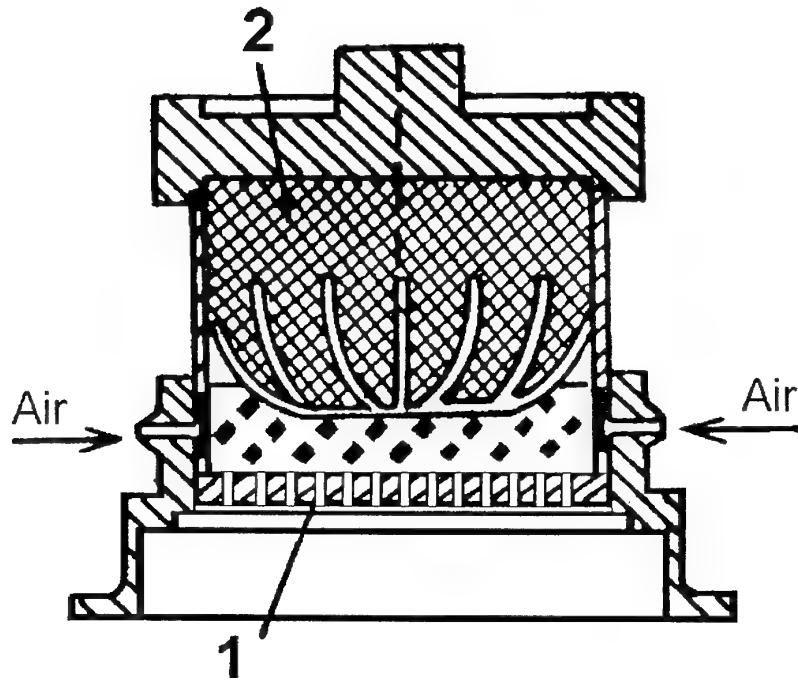


Fig.2 Nozzle I

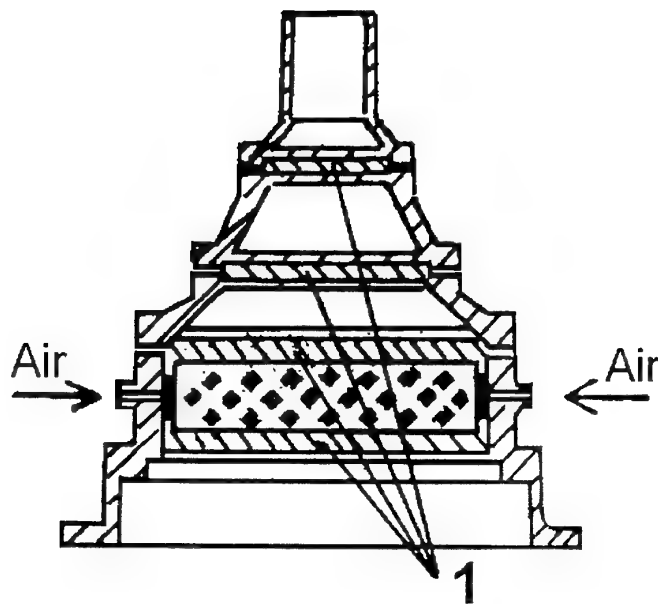


Fig.3 Nozzle II

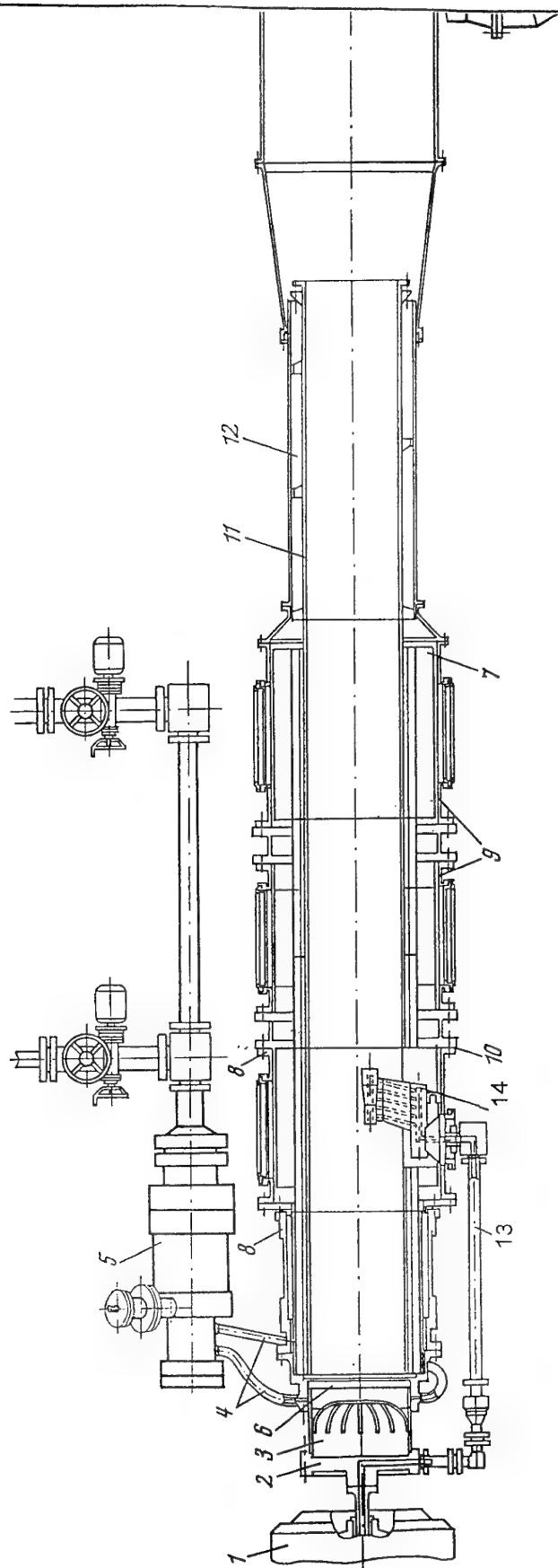


Fig. 4. Impulse Transonic Tunnel "ITT U-11".

1-power part, 2-gas collector, 3-silencer, 4- air collector, 5 -startoff-starting valve(mile), 6-perforated plate, 7- silencer, 8-separable modules of test section, 9-stationary modules of test section, 10-mounting seat of test section modules, 11-diffuser, 12-internal diffuser channel, 13-gas collector for supplying model, 14-hollow sting.

ITT CX.BMP M100,cb-3.27

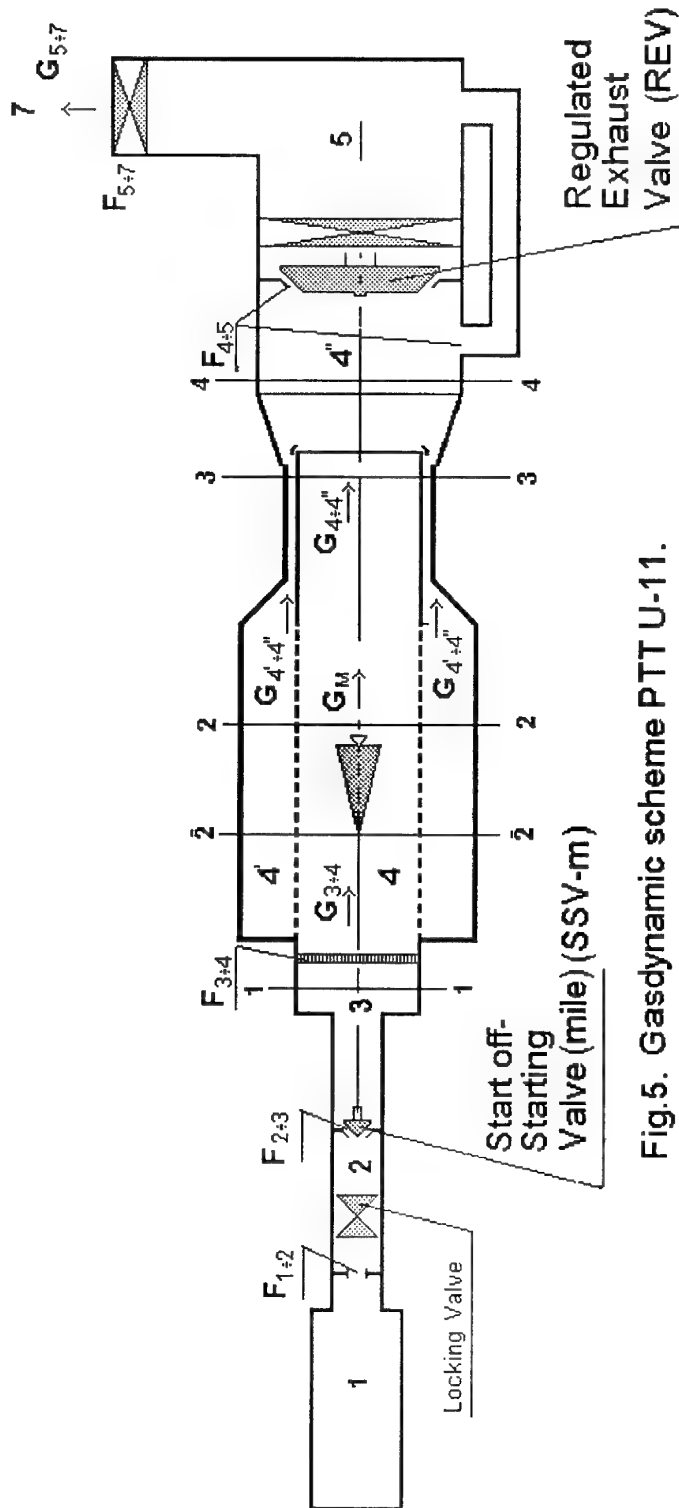


Fig. 5. Gasdynamic scheme PTT U-11.

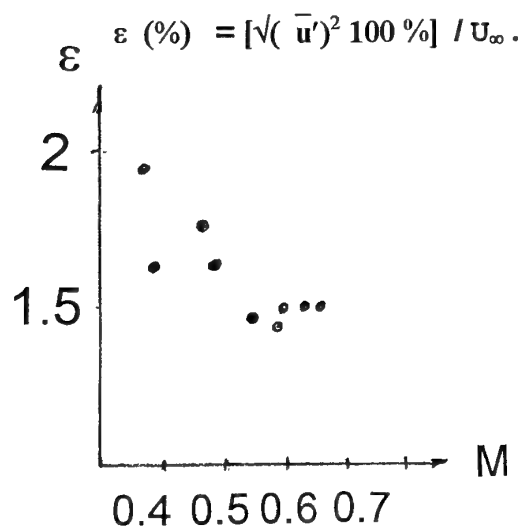


Fig. 6.

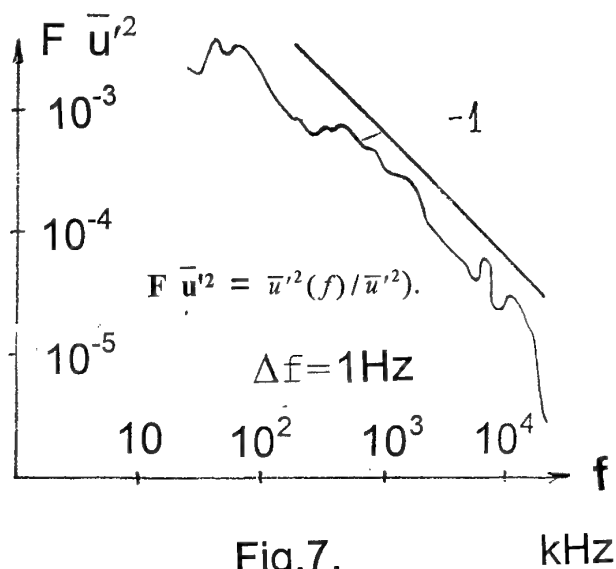


Fig. 7.

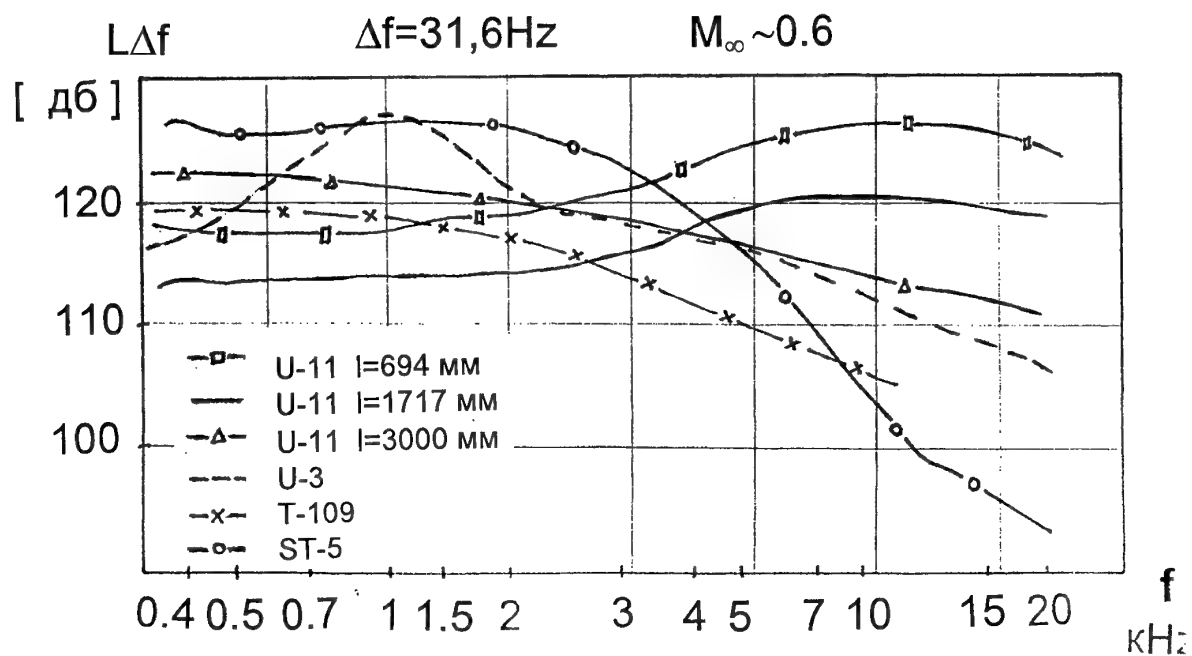


Fig. 8.

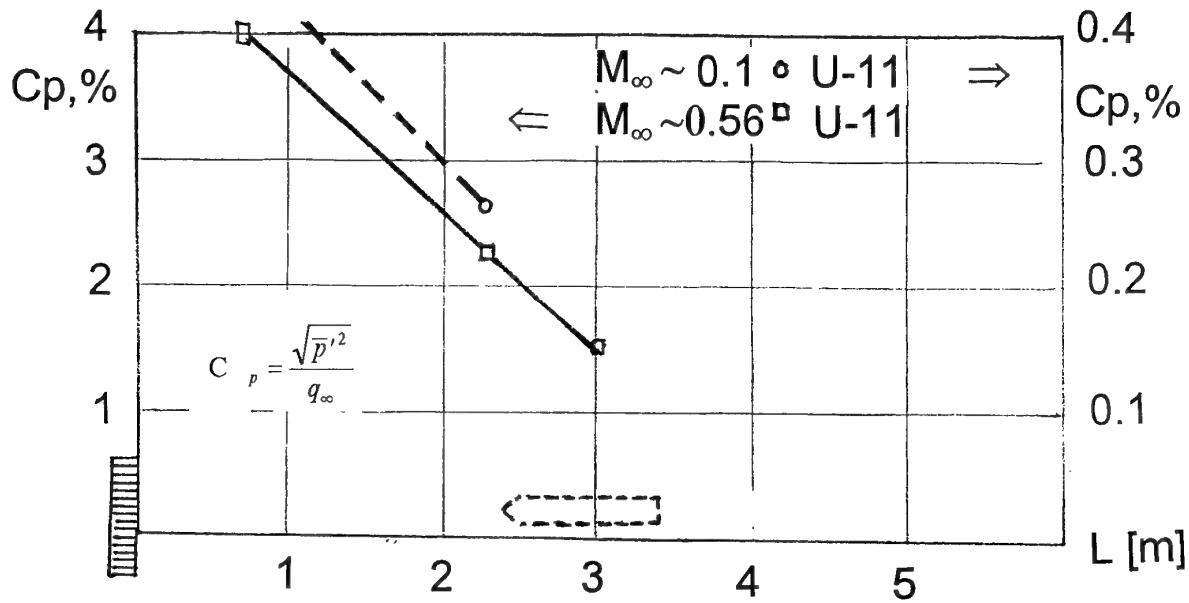


Fig.9.

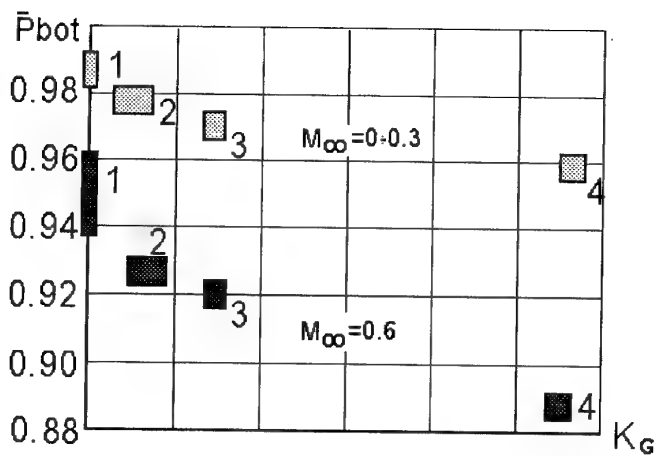


Fig.10. Relative bottom pressure $\bar{P}_{bot} = P_{bot} / P_{st}$ as function of model jets expenditure coefficient dependence $K_g = G_{mod} / m G_{nat}$, in wake (m-model scale)

1-FT data, 2- ITT U-11, jets He, $T_o \sim 600$ K,
 3- ITT U-11, jets N₂, $T_o \sim 400$ K,
 4-T-109, air jets, $T_o \sim 290$ K.

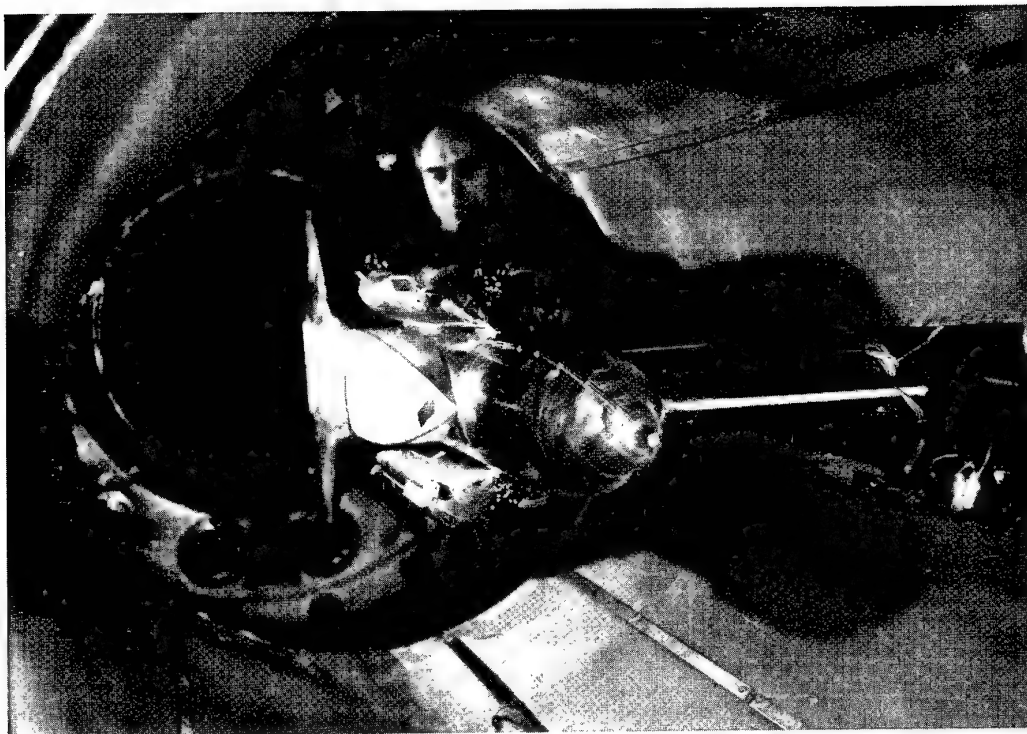


Fig. 11. Front View of Model.

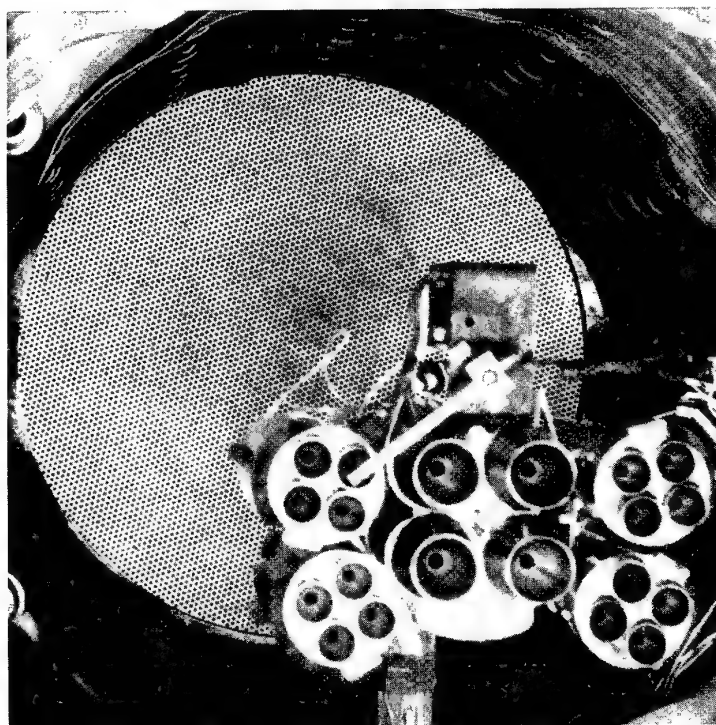


Fig. 12. View of Nozzle from back Model.

A NEW TOOL FOR SCREEN INTEGRATION IN INTERNAL FLOW SYSTEMS AND ITS APPLICATION TO WIND TUNNEL DESIGN

M. M. Seltsam

Deutsche Forschungsanstalt für Luft- und Raumfahrt
Bunsenstrasse 10, D-37073 Göttingen, Germany

Summary

To consider mesh screens in internal fluid flow a numerical method is modified. A Navier-Stokes method with the standard k - ϵ turbulence model is employed. The new extended numerical method is applied to wide-angle diffuser flow. The comparison of calculated diffuser flows with experimental results yields the requisite correspondence. The numerical and experimental investigations lead to a modification of the actual windtunnel. After realization of the modification a remarkable reduction of spatial velocity disturbances is achieved. The capability of screens to suppress turbulence is displayed by comparison of turbulence level distributions before and past the optimization of the settling chamber.

List of Symbols

c_μ	constant of k - ϵ turbulence model
b	width
d	diameter
H	height
K	pressure drop coefficient
k	turbulent kinetic energy
l	length scale
m	exponent
p	pressure
p_0	stagnation pressure
r	radius coordinate
Re_S	screen Reynolds number
S	source term
Tu	turbulence level
u, v, w	velocity components
u', v', w'	turbulent velocities
U	velocity
U_m	mean velocity
x, y, z	cartesian coordinate
α	deflection coefficient
β	screen porosity

ϵ	dissipation rate
Θ	angle between screen normal and upstream flow
μ	dynamic viscosity
μ_k, ν_k	damping factor in longitudinal, lateral directions
μ_t	eddy viscosity
ν	kinematic viscosity
ρ	density
$\sigma_k, \sigma_\epsilon$	constants of k - ϵ turbulence model
Φ	angle between screen normal and downstream flow

Subscripts

i, j, k	grid indices
K	related to the pressure drop
sc	screen
x, y, z	direction of cartesian coordinates
Θ	dependent on Θ
1,2	before, past the screen

1 Introduction

The main task of every wind tunnel design is to provide uniform flow conditions in the test section. That means every component of the wind tunnel circuit has to be evaluated concerning its generation of disturbances. Sections which tend to contain flow separation like diffusers are especially critical. Therefore, proper design of diffusers is essential for attaining the desired flow quality in the test section. The problems arise, if employment of a wide-angle diffuser is unavoidable. Wire screens or similar installations are necessary to prevent flow separation. However, the treatment of screens in the design of internal flow systems and their use in wide-angle diffusers or in stilling chambers comprise a lot of unsolved questions. Some of these questions concern the characteristics of screens and its mechanism of turbulence generation. For de-

signers of wind tunnels flexible tools must be available to account for screens computing ducted flows.

Up to now wide-angle diffuser design is carried out by simple empirical means. Support is provided by design charts, e.g. given by the ESDU [1] or by the data collection of Mehta [2]. Some attempts were made to calculate ducted screen flow - in every case with limited success, respectively with limited practicability.

Investigations on wide-angle diffuser flow were prompted by demands of flow quality improvement during the modernization of the Transonic Windtunnel Göttingen (TWG). An appropriate modification had to be found to remove the flow separation in the wide-angle diffuser and to reduce flow disturbances.

In this paper a method to perform a complete computation of internal flows with integrated screens is presented. Its application to the wind tunnel leads to a distinct flow quality improvement.

2 Properties of Wire Screens

A detailed description of fluid flow through screens comprising every effect becomes an expensive venture. Each wire causes small scale flow separation in its wake. The complexity increases if spatial distribution and interaction of wakes is considered. There exist attempts to explain wake development past screens: Böttcher [3] presents investigations on vortex structures past screens obtained from water towing tank tests under laminar flow conditions. A different point of view is considered by Morgan [4]: Fluid emerges from the plane of the screen as a pattern of jets. They tend to stick together in random groups and form typical structures. Bradshaw [5] shows an expressive picture of coalescing jets past a grid.

A screen can be regarded as a device to generate or alterate turbulence. There are many useful papers which deal with screens as turbulence generators, like Cenedese et al. [6] and many others. Suppression of turbulence by screens in wind tunnels is investigated by Dryden & Schubauer [7] and Schubauer et al. [8, 9]. In each contribution screens and their influence on ducted flows are regarded from a global point of view. The lack of a 'high resolution' model of screen effects enforces employing existing global relations.

The various influences of screens on fluid flow can be reduced to two basic effects: The screen causes a pressure drop Δp and an alteration of the turbulence, expressed by the turbulent kinetic energy k and the dissipation rate ϵ .

2.1 Pressure Drop

Global relations are transferred to local conditions. So, the local pressure drop across the screen plane is defined as

$$\Delta p_j = K_j \frac{1}{2} \rho U_j^2 \quad (1)$$

The pressure drop coefficient K_j is calculated by the formula of Wieghardt [10]. This formula is derived from the resistance of a single cylinder. It is the best validated approximation among all existing attempts to correlate pressure drop and screen porosity:

$$K_j = 6 \frac{1-\beta}{\beta^2} Re_S^{-1/3} \quad (2)$$

This formula is valid in the range of the screen Reynolds number, $Re_S = (ud)/(\nu\beta)$, from 60 to 600. The screen porosity β is defined as the fraction of the open area based on frontal projection; d is the wire diameter, and u is the upstream velocity. Above $Re_S=600$ the pressure drop remains almost constant according to Cornell [11], i.e. $K_j = 6(1-\beta)/\beta^2 600^{-1/3}$.

The pressure drop diminishes with increasing inclination angle Θ :

$$K_\Theta = K \cos^m \Theta \quad (3)$$

Mehta [12] presents proper data for the definition of the exponent m dependent on screen porosity β . For usage in a numerical method the following analytical relation is defined [13]:

$$m = 2 - \sqrt{\frac{5}{3}\beta} \quad (4)$$

Screens are also used for changing flow direction. For small angles between the screen and the up and downstream flows, Θ and Φ , and for a moderate porosity ($\beta \cong 0.6$) Mehta [12] gives the empirical relation:

$$\alpha \cong \frac{\Phi}{\Theta} = 0.66 + \frac{0.31}{\sqrt{1+K}} \quad (5)$$

This is a modification of Dryden & Schubauer's relation presented by Taylor & Batchelor [14]. It is only applied for the calculation of change in turbulence, eqn. (11). In the numerical procedure streamline deflection is practically the only result due to screen pressure drop.

2.2 Alteration of Turbulence

The most important task of screens in windtunnels is to damp turbulence. Big oncoming eddies are destroyed and smaller, soon dissipating eddies are generated. After a short distance flow turbulence becomes

isotropic. Depending on screen geometry screens also work as turbulence generators. As screen porosity decreases so does the influence of upstream turbulence on the downstream turbulence. Longitudinal motions are generally more damped than lateral ones. The damping factors in longitudinal and lateral direction, μ_k and ν_k , are defined from turbulent velocities before and past the screen:

$$\mu_k = \frac{u'_2}{u'_1} \quad \text{and} \quad \nu_k = \frac{v'^2_2 + w'^2_2}{v'^2_1 + w'^2_1} \quad (6)$$

The mean energy of turbulence upstream is:

$$k_1 = \frac{1}{2} (u'^2_1 + v'^2_1 + w'^2_1) \quad (7)$$

The turbulent energy of the downstream flow is determined by the damping factors μ_k and ν_k :

$$k_2 = \frac{1}{2} (\mu_k u'^2_1 + \nu_k (v'^2_1 + w'^2_1)) \quad (8)$$

The assumption of isotropic turbulence at the screen plane simplifies the relation between the upstream and downstream turbulent energies:

$$k_2 = \frac{1}{3} k_1 (\mu_k + 2\nu_k) \quad (9)$$

Taylor & Batchelor [14] derive damping factors μ_k and ν_k for steady and unsteady disturbances. Because steady disturbance relations better approximate experimental finding, they are used in this study.

$$\frac{u'_2}{u'_1} = \frac{1 + \alpha - \alpha K}{1 + \alpha + K} = \mu_k \quad (10)$$

This equation for longitudinal motion is an universal relation including the more restrictive theories of Prandtl [15] ($\alpha=0$) and Collar [16] ($\alpha=1$): Lateral disturbances are damped by the factor ν_k , which is equal to the screen deflection coefficient α (equation (5)):

$$\nu_k = \alpha \quad (11)$$

The alteration of the length scale l generated by a screen is also calculated by an equation given by Taylor & Batchelor [14]. Independent of the isotropy of the turbulence the length scale alteration is:

$$\frac{l_K}{l_{K=0}} = \frac{(1 + \alpha - \alpha K)^2}{\mu_k (1 + \alpha + K)^2} \quad (12)$$

For high Reynolds numbers the dissipation rate ϵ relates to the length scale l and the turbulent kinetic energy k :

$$\epsilon = \frac{k^{3/2}}{l} \quad (13)$$

According to equation (12) alteration of the dissipation rate at the screen plane becomes:

$$\epsilon_{2j} = \epsilon_{1j} \left(\frac{k_2}{k_1} \right)^{3/2} \left(\frac{l_{K=0}}{l_K} \right)_j \quad (14)$$

3 Numerical Method

To obtain complete information on the flow field a numerical method has to be applied. Diffuser flow, and particularly wide-angle diffuser flow is dominated by viscous effects, flow separation often occurs. To calculate appropriate diffuser flows the complete Navier-Stokes equations must be solved.

By integrating extensions in an existing finite volume method the computation of internal fluid flow with screens becomes possible. The computational method is based upon the assumption of incompressible flow. It employs the k - ϵ turbulence model with the standard constants according to Launder & Spalding [17]. A detailed description is published by Perić et al. [18] and by Kessler et al. [19]. The viscous sublayer near the walls is bridged by the wall functions which assume that the velocity profile near the walls is logarithmic. While the k - ϵ turbulence model has a number of well known limitations, the proposed computational method is not intended for extreme accuracy, but rather for guiding a proposed change in design. It has the requisite accuracy to demonstrate general effects of screens on ducted flows. Future improvements using refined turbulence models should be easy to integrate.

3.1 Governing Equations

Direct representation of a close-meshed screen in a numerical method requires an unacceptable effort. It is not feasible with today's computers. Therefore the screen is considered as a local discontinuity. The numerical method is modified merely by introducing the effects of screens.

Dependent on upstream flow, the determining values of p , k and ϵ are altered in the screen plane. The momentum equation is:

$$\frac{\partial(\rho U_j U_i)}{\partial x_j} - \frac{\partial}{\partial x_j} \left((\mu + \mu_t) \frac{\partial U_i}{\partial x_j} \right) = \rho S_{U_i} \quad (15)$$

Pressure drop across the screen plane is represented as an additional source term:

$$S_{U_i} = \frac{\partial}{\partial x_j} \left[(\nu + \nu_t) \frac{\partial U_j}{\partial x_i} \right] - \frac{1}{\rho} \frac{\partial p}{\partial x_i} + S_{sc,j} \quad (16)$$

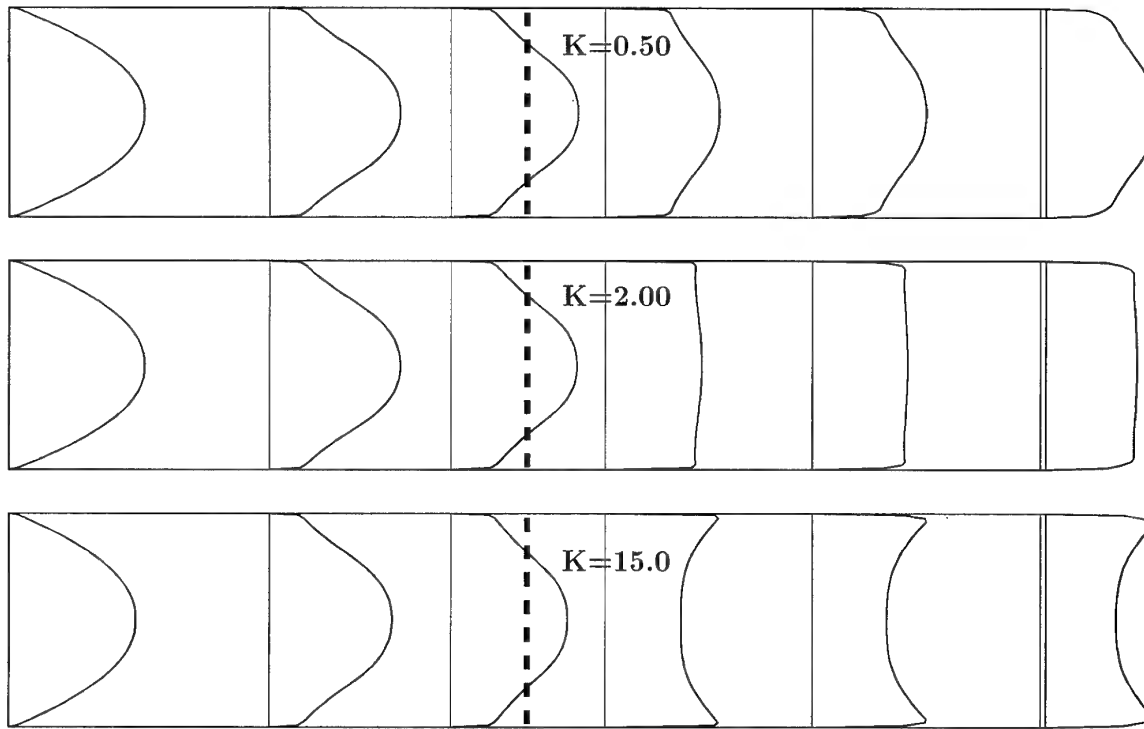


Figure 1: Influence of different screen resistances on velocity profiles: straight duct, $l=4.00\text{m}$, $b=0.40\text{m}$.

The screen source term is defined as:

$$S_{sc,j} = -\frac{1}{\rho} \frac{\partial(\Delta p_j)}{\partial x_j} \quad (17)$$

The values of k and ϵ produced by a screen are represented in the transport equations of the k - ϵ model in a similar way:

k -equation:

$$\frac{\partial(\rho U_j k)}{\partial x_j} - \frac{\partial}{\partial x_j} \left(\left(\mu + \frac{\mu_t}{\sigma_k} \right) \frac{\partial k}{\partial x_j} \right) = S_{k,j} \quad (18)$$

ϵ -equation:

$$\frac{\partial(\rho U_j \epsilon)}{\partial x_j} - \frac{\partial}{\partial x_j} \left(\left(\mu + \frac{\mu_t}{\sigma_\epsilon} \right) \frac{\partial \epsilon}{\partial x_j} \right) = S_{\epsilon,j} \quad (19)$$

The source terms S_k and S_ϵ at the screen plane are replaced by screen-determined source terms, depending on the upstream turbulence values:

$$S_{k,j} = \frac{\partial(\rho U_j k_{2,j})}{\partial x_j}, \quad S_{\epsilon,j} = \frac{\partial(\rho U_j \epsilon_{2,j})}{\partial x_j} \quad (20)$$

3.2 Straight Duct with Screens

The screen representation in the numerical method is examined by calculating the screen effects on the flow

of a straight duct. The alteration of the velocity profiles by the screen is emphasized. Effects of different screen resistances and damping potentialities are investigated. Plane, two-dimensional flow is calculated using cartesian, non-uniform computational grids. Grid-lines are concentrated near the screen location in x -direction and near the walls in y -direction. Pressure drop at the screen is added to the source terms of three grid cells behind each other in the ratio of 25%/50%/25%, in order to smooth the screen influence and to avoid difficulties concerning numerical instability. The development of the turbulent quantities is of minor interest in this study.

To simulate highly non-uniform inlet flow conditions, a parabolic velocity profile at the entrance plane is defined. Test calculations were carried out with three different supposed screen resistances. As the most essential results the developments of the velocity profiles across the screen plane are displayed in figure 1:

The rather low pressure drop $K=0.5$ is accomplished by a screen with high porosity, $\beta \approx 0.75$. Such a screen is typically applied in settling chambers of windtunnels to damp flow disturbances. This screen slightly reduces velocity nonuniformities.

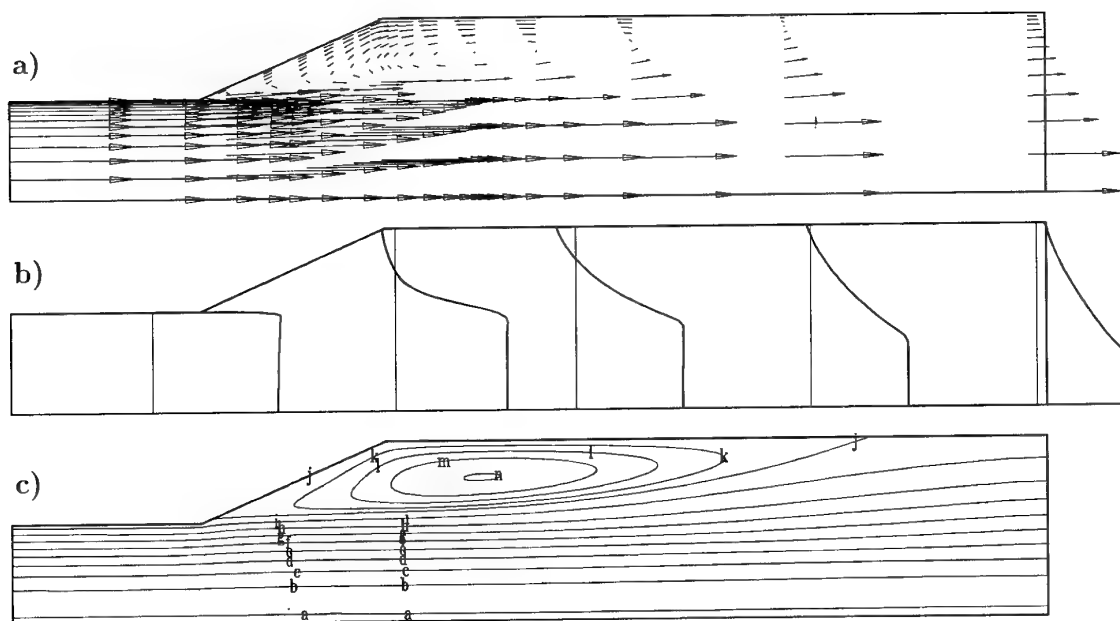


Figure 2: Axisymmetric diffuser flow, no screen: a) flow vectors, b) longitudinal velocity profiles, c) streamlines; inlet velocity $u(x=0)=65\text{m/s}$.

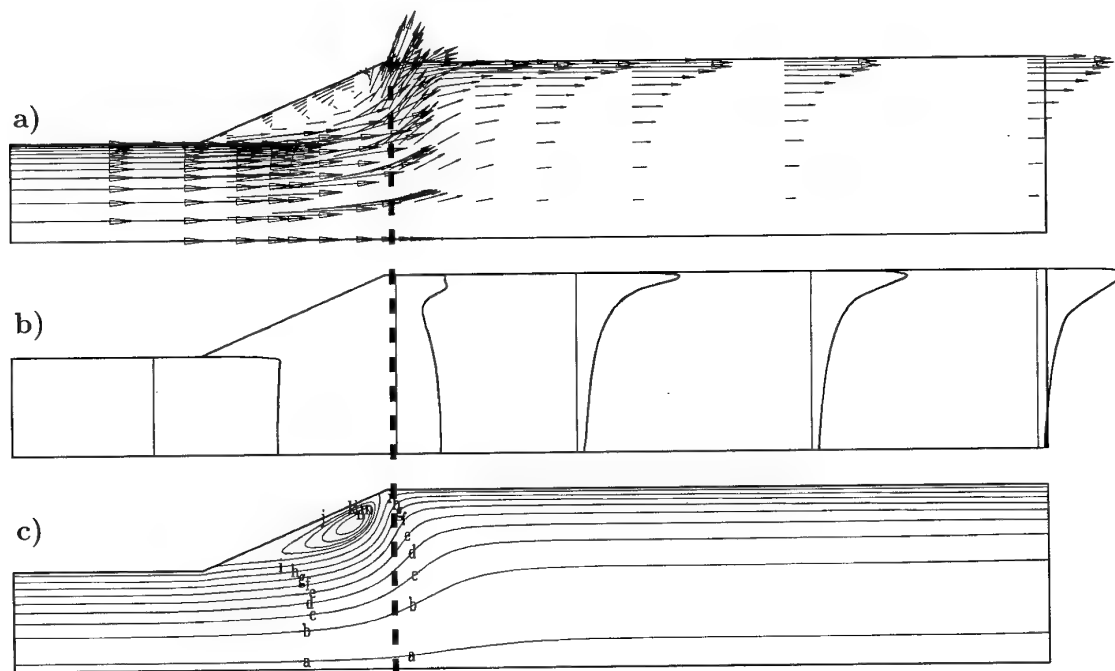


Figure 3: Axisymmetric diffuser flow, with screen (terminal resistance, $K=15$, $x=392\text{mm}$): a) flow vectors, b) longitudinal velocity profiles, c) streamlines; inlet velocity $u(x=0)=65\text{m/s}$.

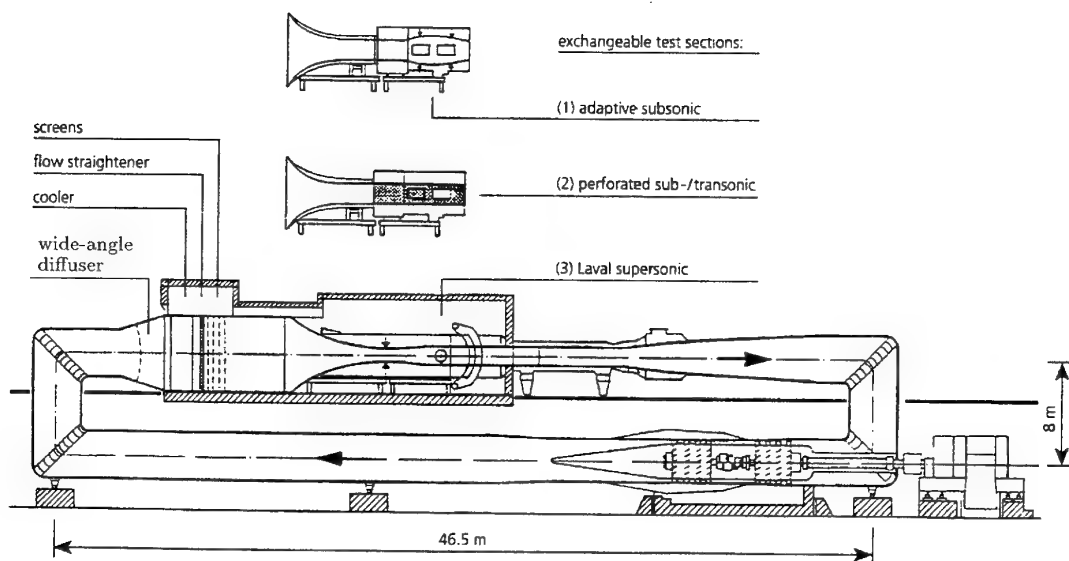


Figure 4: Transonic wind tunnel at DLR in Göttingen (TWG).

This screen simulation is compared with calculations of two different screen resistances. The resistance coefficient of $K=2.0$ corresponding to the porosity $\beta \approx 0.53$ generates an almost completely homogeneous axial velocity profile. Although they produce a high degree of homogeneity, these screens are rarely used due to higher losses and an increased possibility of instability generation, a phenomenon which is supposed to be observed during the experiments presented later in this paper.

Further increase in screen resistance does not produce a more uniform velocity profile. Inverted velocity profiles are obtained past a very high pressure drop ($K \approx 15$ corresponding to $\beta \approx 0.20$). The streamline deflection takes place before the screen due to the 'filling effect' and past the screen due to an 'acceleration effect'. The latter is caused by different local static pressures due to different local pressure drops. Increased upstream velocity leads to reduced local static pressure past the screen and to decelerated flow downstream. Conversely, reduced upstream velocity generates accelerated flow. This 'inversion effect' is surprising for the present. Nevertheless it corresponds to experimental findings presented in the next section. Some earlier investigators obtained similar experimental results, e.g. Mehta [12], who detected the 'overshoot' in the boundary layer flow past a screen.

3.3 Diffuser Flow with Screens

The numerical method is applied to the flow of a diffuser. In fig. 2 the results of a diffuser flow with an area ratio of 3.26 and a cone half-angle of 23.3° is shown. This is analogous to the geometry of the model diffuser introduced in the next section. Without screen resistance at the exit plane of the diffuser the flow separates near the diffuser entrance; a large separation bubble is generated. Results of calculations for a screen at the diffuser exit are presented in fig. 3. The resistance coefficient of $K=15$ is equal to the cooler resistance of the actual windtunnel. The separation is removed at the screen location but a separation bubble remains in front of the screen. A remarkable change in the velocity profiles is generated by the screen resistance due to the streamline deflection. The enormous increase of the velocities past the screen near the wall corresponds to the results obtained for a straight duct.

4 Wind Tunnel Application

4.1 Transonic Wind Tunnel

The numerical method was employed for investigations at the transonic wind tunnel at DLR (TWG), fig. 4. Before the modernization, which took place in 1991/92

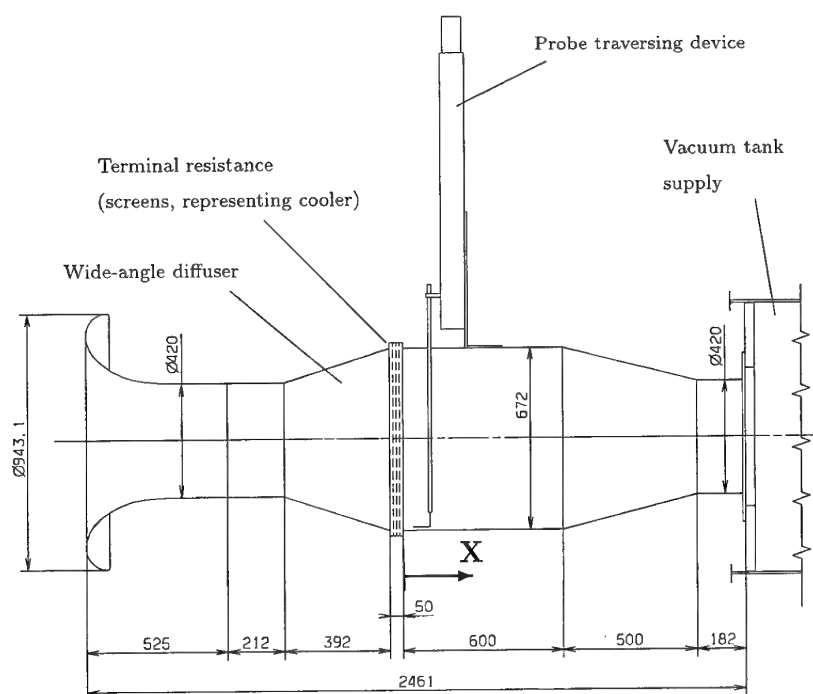


Figure 5: Model diffuser test rig (measuring units in mm).

[20], the flow in the wide-angle diffuser was separated. This wind tunnel has a test section area of $1\text{m} \times 1\text{m}$. It operates in a Mach-number range from $M=0.50$ to 2.20 and in a stagnation pressure range of $p_0=30$ to 145 kPa. The settling chamber contains a cooler, a honeycomb flow straightener and four screens. The diffuser, located upstream, has a mean half-angle of 23.3° and accomplishes the cross-sectional transition from circular to quadratic by an area ratio of 3.26 . No screen was installed in the diffuser. The flow separation in the diffuser reduces the efficiency of the wind tunnel cooler located immediately behind the diffuser and causes non-uniform temperature distribution. Velocity inhomogeneities that affect the flow in the test section downstream may also result.

The investigations on TWG flow quality were carried out in four steps:

- A model diffuser was built in order to test modifications at the diffuser and to obtain data sets for comparison with theoretical results.
- The model diffuser flow with integrated screens was calculated by the extended numerical method. The numerical method was validated by the experimental results.
- The flow of the TWG wide-angle diffuser was calculated and the best screen arrangement was found.

- The results were transferred to the actual wind tunnel and the success of the modification was examined.

4.2 Model Diffuser

Existing analytical methods to improve the flow of the TWG diffuser are thought not to be reliable enough. Therefore a test rig (fig. 5) at a scale of $1:5.95$ has been built to test various modifications in the diffuser. With a traversing Prandtl probe past the screens representing the wind tunnel cooler the most interesting data was recorded. The velocity is determined using the local total pressure and the local static pressure. It is related to the mean velocity in the section plane and plotted against the tunnel-height.

The results at the center line for the empty diffuser (fig. 6 top) show increased velocities in the center and also increasing velocities near the walls. Several types of guide vanes are tested in the diffuser, as well as several screens and screen combinations. Best results are achieved using a screen of $K=1.90$ at $x=130\text{mm}$. The velocity distribution (fig. 6 bottom) with this moderate additional loss is more uniform, although a slight increase near the walls persists.

Experimental values for the middle measuring line of the downstream duct at various distances from the outlet plane the diffuser, with and without a screen, are compared with numerical results plotted for differ-

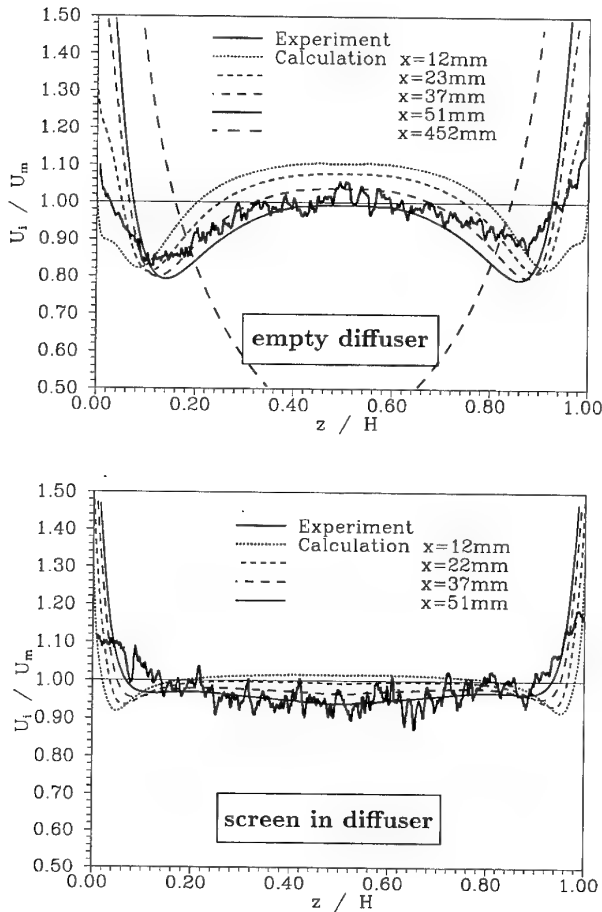


Figure 6: Comparison calculation - experiment: velocity distribution past the terminal resistance; calculated velocity profiles at different distances past the screen.

ent distances from the screen (fig. 6). The traversing probe has been about 50mm away from the screen. Agreement is quite remarkable, though the geometries are different. The tested diffuser performs the transition from circular to quadratic cross-section area in contrast to the axisymmetric design of the calculated diffuser. A large computed increase in velocity near the walls occurs because of the absence of the wind tunnel nozzle in the computational representation, because of three-dimensional effects in the tested diffuser and because of deficiencies in the representation of the screen in the numerical method. The screen is considered in a very narrow region, i.e. over three grid cells. The simulation of the cooler shows that the velocity profiles become more uniform with a distributed pressure drop. Therefore, more about the generation of the pressure drop and its local distribution should be known to achieve an even more realistic consideration

of screens.

4.3 Wind Tunnel Diffuser Flow

The TWG wide-angle diffuser flow was analyzed by the extended numerical method. For proper determination of the diffuser flow the pressure drop of the cooler, which is located at the exit as terminal resistance, must be considered in an appropriate way. That means the pressure drop must be distributed in x-direction. The arrangement of the actual settling chamber installations with cooler, flow straightener, and four screens is displayed in fig. 7. Fig. 8 displays the resulting flow for the dimensions of the transonic wind tunnel of DLR, TWG. Still a separation persists in the diffuser. Nevertheless, the outlet velocity profiles show increased homogeneity. Nearly uniform velocity profiles are obtained by adding a screen in the diffuser (fig. 9). Integration of a screen ($K=1.90$) into the wind tunnel diffuser leads to nearly optimal diffusion. This modification was put into practice at the TWG.

The results of both, the numerical and the experimental investigations, lead to a modification of the actual wind tunnel. The velocity profiles of the flow downstream of all stilling chamber installations, taken before and past installing the specified screen into the diffuser, show remarkable reduction of disturbances (fig. 10).

5 Flow Quality

5.1 Screen Flow

The measured velocity profiles past screens presented in this paper are highly non-uniform. The data for each line seems to be noisy and scattered. Measurements for several of the different versions were repeated under the same conditions and almost exactly the same results were always obtained. This is exemplified by fig. 10 presenting overlapping velocity distributions taken four times for each configuration. That means, these small-scale disturbances are local non-uniformities and not time dependent. These steady structures can only be obtained by measuring techniques with high spatial resolution. Mutual coalescence of the jets emerging from a screen with low porosity is responsible for that typical phenomenon. This effect, also called 'instability' [4, 5], was not expected past the employed screen with a porosity of $\beta=0.59$.

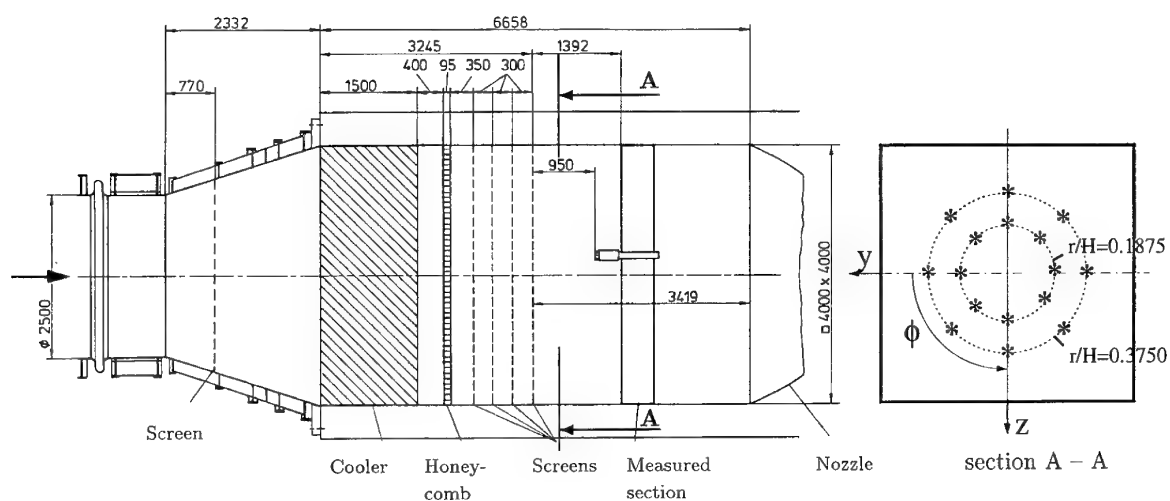


Figure 7: Settling chamber of the TWG (measuring units in mm).

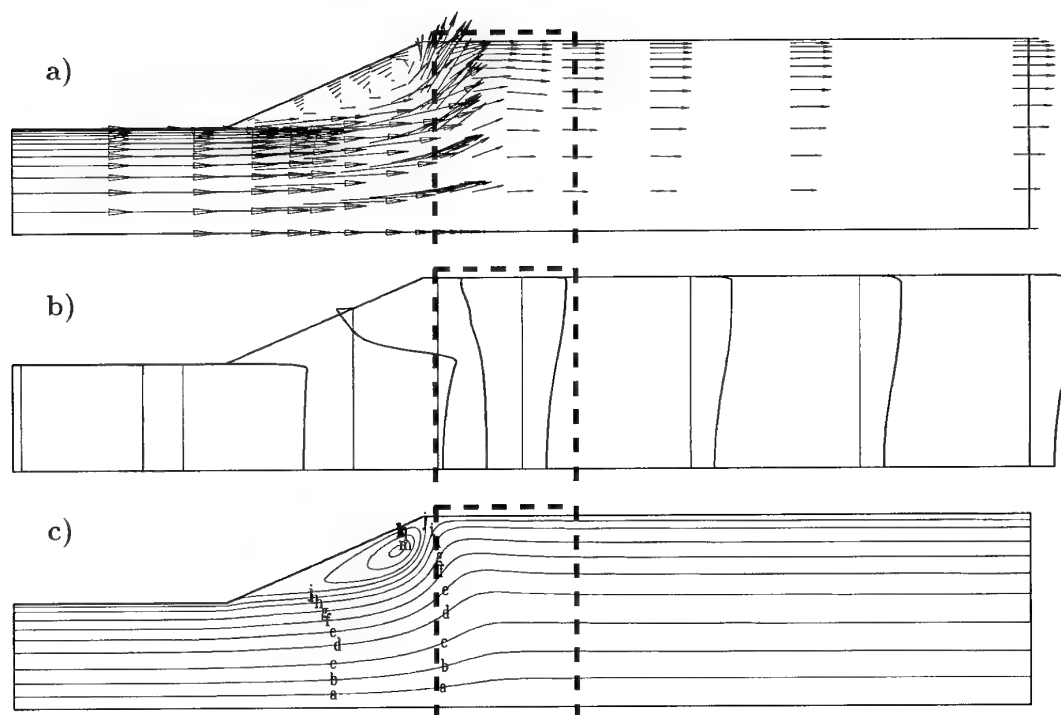


Figure 8: Axisymmetric diffuser flow, cooler at the end, no screen. (TWG-Configuration): a) flow vectors, b) longitudinal velocity profiles, c) streamlines; inlet velocity $u(x=0)=37.35\text{m/s}$.

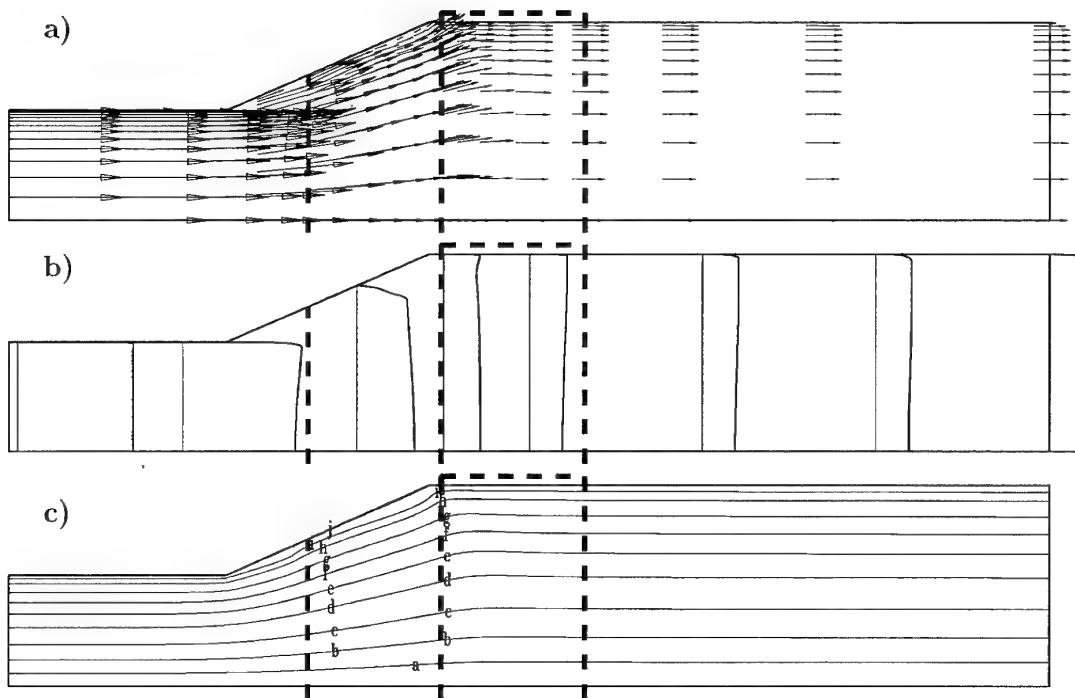


Figure 9: Axisymmetric diffuser flow, cooler at the end, with screen. (TWG configuration after modification): a) flow vectors, b) longitudinal velocity profiles, c) streamlines; inlet velocity $u(x=0)=37.35\text{m/s}$.

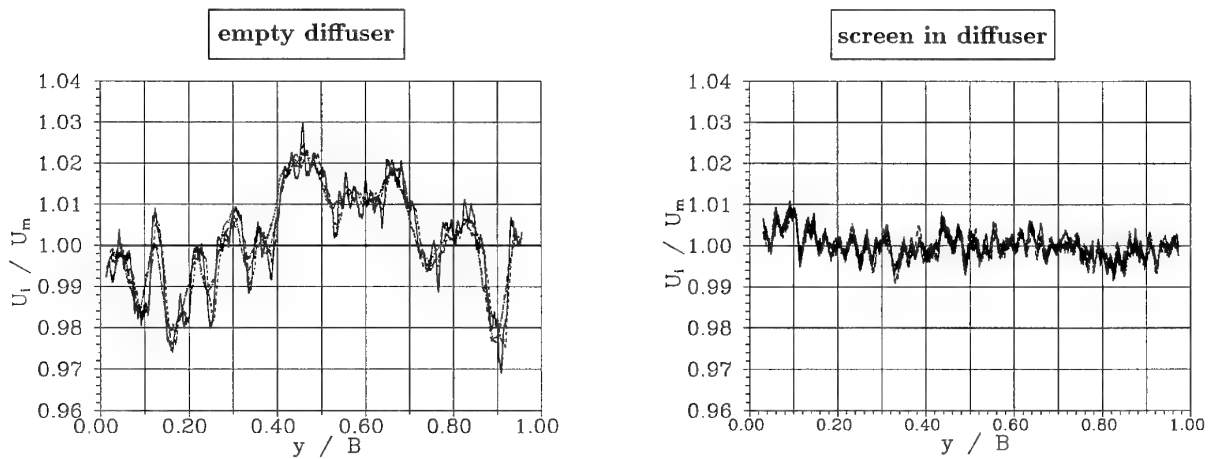
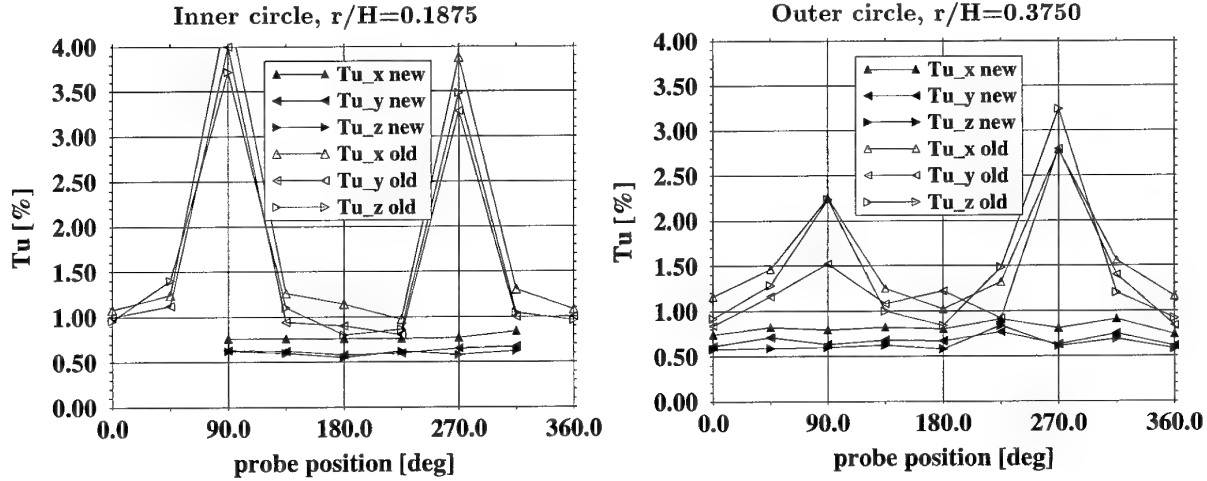


Figure 10: Measured velocity distribution in the settling chamber of the TWG (four measuring lines of the same flow situation overlap each other).

	Wide-angle Diffuser	Cooler	Honeycomb	Screens	$Tu_x = u'/u$
pre- modernization	empty	circular tubes	$d/l=0.13$	$2^* d=1.20\text{mm}, \beta=0.41$	$1.0 \dots 4.0\%$
past modernization	with screen $d=0.40\text{mm}, \beta=0.37$	elliptic tubes	$d/l=0.10$	$2^* d=0.40\text{mm}, \beta=0.59$ $2^* d=0.60\text{mm}, \beta=0.59$	$\cong 0.75\%$

Table 1: Settling chamber of TWG pre- and past modernization

Figure 11: Local turbulence level at the downstream end of the TWG settling chamber: $Tu_x=u'/u$, $Tu_y=v'/v$, $Tu_z=w'/w$, before modernization ('old'), and past modernization ('new').

5.2 Turbulence Level

The turbulence level in a wind tunnel test section is mainly governed by the turbulence generated in the stilling chamber. The turbulence here is usually dominated by screens, used as the last downstream installations. Their ability to eliminate disturbances is responsible for flow homogeneity in the test section. Proper stilling chamber design is therefore substantial for attaining the desired high flow quality.

Measured data from the wind tunnel calibration of TWG show the result of an improved stilling chamber and screen arrangement. The turbulence levels before and past wind tunnel modernization taken in a cross-sectional plane past the last settling chamber screen are compared. In fig. 11 the achieved turbulence reduction is displayed, presenting the local relative fluctuation velocities in each direction on two circles (compare fig. 7, section A-A) around the tunnel centre axis. This is achieved by settling chamber installations listed in tab. 1.

A major difference between old and new settling chamber is found in the design of struts for the wind tunnel cooler and the honeycomb flow straightener. Past the modernization less struts are inserted and the

strut cross-section profiles are improved. The change of the cross section of the cooler tubes from circular to elliptic should diminish the wake turbulence. Before the modernization the two screens in the settling chamber were not capable to remove disturbances caused by the wakes of the blunt struts of cooler, flow straightener, and screens.

Additionally the screens of the 'old' wind tunnel made of four pieces with soldered seams and a framework on each upstream side had of course no perfect structure. The one-piece cantilever screens of the new wind tunnel provide a uniform surface and meet the requirements for full homogeneous fluid flow.

6 Conclusion

Extensions on a numerical method permit to account for screens in internal fluid flow systems. The application of this method is demonstrated in the calculation of a wide-angle diffuser with screens. The result of theoretical and experimental investigations was used to optimize a wind tunnel wide-angle diffuser flow. Convincingly better uniformity of the downstream velocity profile is demonstrated. The presented procedure can

be used to design new facilities as well as to improve existing flow systems.

Detected patterns in measured velocity profiles downstream of meshed screens lead to new considerations of screen effects and come along with new questions for future investigations. Stilling chamber design must be done carefully regarding screen generated turbulence. Improved arrangement and mounting of settling chamber installations may reduce the turbulence level dramatically.

References

- [1] Engineering Sciences Data Unit, ESDU 73024, London. *Performance of Conical Diffusers in Incompressible Flow*, 1973. ISBN 0 85678 048 6.
- [2] R.D. Mehta. The aerodynamic design of blower tunnels with wide-angle diffusers. *Prog. Aerospace Sci.*, 18, 1977.
- [3] J. Böttcher. Die Strömung im Nachlauf von Sieben und die Entstehung von Längswirbeln in der Staupunktströmung. Bericht FB 87-27, DFVLR, 1987.
- [4] P.G. Morgan. The stability of flow through porous screens. *Journal of the Royal Aeronautical Society*, 64:359–362, 1960.
- [5] P. Bradshaw. The effect of wind-tunnel screens on nominally two-dimensional boundary layers. *Journal of Fluid Mechanics*, 22:679, 1965.
- [6] A. Cenedese, S. Iannetta, P. Mele, and M. Morganti. Turbulence management by means of grids. *Archiwum Mechaniki Stosowanej*, 32(5):633, 1980.
- [7] H.L. Dryden, G.B. Schubauer, W.C. Mock, and H.K. Skramstad. Measurements of intensity and scale of wind-tunnel turbulence and their relation to the critical Reynolds number of spheres. NACA Report TR 581, NACA, 1937.
- [8] G.B. Schubauer and W.G. Spangenberg. Effect of screens in wide-angle diffusers. NACA Report TN 1610, 1948.
- [9] G.B. Schubauer, W.G. Spangenberg, and P.S. Klebanoff. Aerodynamic characteristics of damping screens. NACA Report TN 2001, 1950.
- [10] K.E.G. Wieghardt. On the resistance of screens. *The Aeronautical Quarterly*, 4:186–192, 1953.
- [11] W.G. Cornell. Losses in flow normal to plane screens. *Transactions of the ASME*, 80:791–799, 1958.
- [12] R.D. Mehta. Turbulent boundary layer perturbed by a screen. *AIAA Journal*, 23(9), 1985.
- [13] M. Seltsam. Theoretische und experimentelle Untersuchung der Strömung in Weitwinkel-Diffusoren mit Sieben. Technical Report FB 95-03, DLR, 1995.
- [14] G.I. Taylor and G.K. Batchelor. The effect of wire gauze on small disturbances in a uniform stream. *Quarterly Journal of Mechanics and Applied Mathematics*, 2:1–29, 1949.
- [15] L. Prandtl. *Herstellung einwandfreier Luftströme (Windkanäle)*. Akademische Verlagsgesellschaft mbH, Leipzig, 1932.
- [16] A.R. Collar. The effect of a gauze on the velocity distribution in a uniform duct. Technical Report R.M. 1867, RAE, 1939.
- [17] B.E. Launder and D.B. Spalding. The numerical computation of turbulent flows. *Computer methods in applied mechanics and engineering*, 3:269–289, 1974.
- [18] M. Perić, R. Kessler, and G. Scheuerer. Comparison of finite-volume numerical methods with staggered and colocated grids. *Computers and Fluids*, 16:389–403, 1988.
- [19] R. Kessler, M. Perić, and G. Scheuerer. Solution error estimation in the numerical predictions of turbulent recirculating flows. In *Validation of Computational Fluid Dynamics*, number 437. AGARD, 1989.
- [20] B. Binder, L. Riethmüller, S. Tusche, and R. Wulf. Modernisierung des Transsonischen Windkanals in Göttingen. Technical report, Jahrbuch der Deutschen Gesellschaft für Luft- und Raumfahrt e.V. (DGLR), 1992.

ADAPTIVE-WALL PERFORATED TEST SECTION FOR TRANSONIC WIND TUNNELS

Neyland V.M., Ivanov A.I., Semenov A. V., Semenova O.K., Amirjanz G.A.
Central Aerohydrodynamic Institute (TsAGI), 1, Zhukovsky Street
140160 Zhukovsky-3, Moscow Region, Russia

ABSTRACT

The review will be presented on the experimental study of using of variable wall porosity for the methodical and productive wind tunnel testing of the aircraft models. Except for brief discussion of present state in this area the main reported results are based on the experience of exploitation of different porous wall test sections of TsAGI T-128 wind tunnel.

This facility has 4 interchangeable test sections, each of them equipped with the specially designed variable porous walls according to the testing specialty. For example, test sections N1 and N2 have each 128 controlled sections designed as overlapping porous surfaces with the open area ratio variation from 0 to 18%. Test section N3 is equipped with longitudinally- variable slots, open area ratio changing from 0 to 13%. This test section is used for 2-D airfoil testing and has all the necessary instrumentation: controlled wall boundary layer suction upstream the model, 2-degree of freedom wake survey mechanism, pressure measurement system for 1200 points on the basis of electronic modules etc.

Test section N5 serves for aeroelastic model testing. Adjustable wall porosity is designed only in model location area. It is used not only for wall interference reduction but also as an flow excitation source.

As the example of different adaptive-wall test sections using the data are presented at two geometrically-similar A4 airfoil models testing in the test section N3; reference model AEDC-2 testing in the test section N1 as compared to the 16-T wind tunnel testing of the same model; "flying" strut testing in the test section N5.

1. INTRODUCTION

In the near future wind tunnels will remain the decisive instrument when developing new flying vehicles. And every time the desire will appear to test the largest possible model in a given wind tunnel. One of the means to achieve this target is adaptive walls of test section.

History of the development of the adaptive-wall wind tunnel is well known primarily due to the studies of Dr. S. Wolf and Dr. H. Goodyer [1]. They found out publications describing the experiment carried out in such facility as early as in the pre-war years. However, the second and true birth of the concept of the adaptive boundaries of the flow is tightly related to the names of Sears [2] and Ferry and Baronti [3]. They have based their idea on well-known principle of solid stream lines.

Therefore, the first technical implementation of this concept was also realized in most obvious way, i.e. flexible adaptive walls. Since that time and up to now this type of self-adaptive flow boundaries remains most popular in the world, though neither of these facilities was used for industrial purposes.

First non-classified Russian papers in this direction [4] were published soon after the pioneer works [2], [3] appeared, so their independent development and implementation is quite obvious.

In the end of 60-s TsAGI began to develop project of large industrial wind tunnel T-128 with perforated adaptive panels on the test section walls. The facility was put into service in 1982. The new configuration of test section walls was aimed at minimization of harmful effect of flow boundaries on the flow past model by optimum adjustment of local perforation. This adjustment should be performed automatically by the controlling computer. During years of its operation certain advantages (rather significant) as well as drawbacks (which can be eliminated) were found out [6, 7].

The present paper contains brief description of T-128 wind tunnel and all its sections having different variable porosity design depending on experiment requirements.

Nomenclature

M	Mach number
Re	Reynolds number
Cp	dimensionless pressure coefficient
f	porosity coefficient = (S orifices) / (S wall)
x	coordinate along the tunnel axis
R	mathematical porosity parameter
α	angle of attack
C _L	lift
b	airfoil chord
h	wind tunnel width (height)

2. T-128 wind tunnel is a closed-circuit facility (Fig. 1) with variable density (total pressure varies from 0.3 to 4 atm). Mach number range is 0.2 - 1.7, dimensions of the test section are 2.75x2.75m. Reynolds number range of T-128 is compared with Re numbers of other facilities of analogous size in Fig. 2. The facility is equipped with 5 interchangeable test sections designed for various experiments:

- N 1: tests of full models installed on the tail sting;
- N 2: tests of half-models;
- N 3: test of airfoil models;
- N 4: (is not completed yet); simulation of jets; optical/physical studies
- N 5: aeroelasticity tests.

Interchangeable test sections allow enhancing the productivity of the facility because the time required for the model installation in the tunnel circuit is reduced considerably.

All the test sections are equipped with perforated wall panels of different configuration. Test section N1 and N2 have similar design of variable perforation.

The walls of either of these test sections consist of 128 independent panels the porosity of which may vary from 0 to 18%. Porosity level is varied by overlapping the perforation holes by external plates moving along the fixed frame. Schematic of the wall panels as well as conventional locations of models are presented in Fig. 3.4.

By the moment of putting the facility into operation no one had clear understanding of what should be the algorithm for wall porosity control. The investigations showed that the classical scheme of Sears matching the flow in the tunnel with the imaginary flow outside the circuit was not good because of the lack of super-fast techniques of computing 3-D transonic flows which allow to control the experiment in the on-line mode. On the other hand, it was technically difficult to measure the flow velocity component normal to the wall. For these purposes a non-intrusive method of measurements is desirable for transonic regimes, but at present this problem remains unsolved for the facilities of this size.

To cope with these difficulties a simplified approach was adopted which was based on the following considerations. It is known that in a purely subsonic potential flow the internal region is fully governed by a single velocity component given on its boundaries. In this case, maintaining the given pressure distribution on the boundary corresponding to free stream conditions around a model shall ensure interference-free tests. There are two factors that distinguish the tunnel conditions from the above assumptions: viscous layer near the walls and local supersonic regions in the flow.

Account of the first factor may be taken with the help of traditional (though rather complicated) methods. As for the second factor, it deteriorates the assumption of harmonicity of the functions defining the flow in the internal region. So, generally speaking, the above consideration becomes inapplicable. And the problem of errors induced by the local supersonic regions is still waiting in-depth analysis if the wall

adaptation procedure is based on the given pressure distribution.

So, the strongly simplified version of boundary conditions adaptation up to the wall interference elimination looks as follows (Fig. 5). The viscosity effect correction is applied to the measured wall pressure, and the resultant figure is compared with the designed value of free stream conditions near the model. The value of the mismatch permits us to correct the local wall porosity.

In fact, practical application of a theoretical concept even in such an over-simplified version causes a lot of problems. First of all, to calculate the reference far field one should choose the proper schematizing of the model. In subsonic case a set of singularities is quite adequate. Proper choice of schematizing is validated by comparison of the computed pressure with the measured pressure distribution on the walls at the given wall boundary conditions.

In transonic flows at low angles of attack and side-slip angles the far field is governed by the transonic area rule. For high-lift models one may use the transonic lifting line theory. However, one should bear in mind that the both cases correspond to the test section size which is much larger than the size of a model. As a rule, in wind tunnel conditions the width of the test section is close to the length of the model. To predict the reference field for these conditions the calculations of a flow past a real configuration shall be done by the known numerical methods.

Re-calculation of pressure measured on the tunnel walls to the edge of the potential flow core is done by computation of the boundary layer development on a porous surface at the measured $C_p(x)$ [5]. Fortunately, in the majority of cases the optimum porosity level of the walls is very small, so the corrections applied to C_p due to mass flow through the wall are small too. The alternative approach is measuring of C_p at some distance from the wall, for example, with the rails tapped by static pressure holes.

The adaptation procedure presented in Fig. 5 is an iterative process the convergence of which depends on the choice of the initial approximation. At transonic regimes it is asymptotic transonic theory [6] that can help us to understand what is the initial porosity level. In accordance with this theory

$$f_{opt} \sim \sqrt{1 - M_\infty^2}, \text{ i.e. the porosity } f \text{ is close to}$$

zero at $M_\infty \sim 1$. It will be shown below that this conclusion is proved experimentally.

3. Let us present some experimental data based on the above considerations.

3.1 In test section N 2 of T-128 the two geometrically-similar half-models of a civil aircraft were tested which differ in their size by a factor of

1.75 (schematic of the large model installation is shown in Fig. 4). Blockage ratio was 1.03% and 3.16%, respectively. The models were installed on the external 5-component strain gage balance on the test section ceiling. Simultaneously with load measurements the pressure distributions were measured in 8 wing sections and along the 4 walls of the test section.

When testing large half-model, pressure distribution C_{pt} along 6 rails, located outside of wall boundary layer was measured to provide data for wall adaptation in on-line mode.

For the large model tests the wall adaptation was done at $M=0.88$, $Re_c = 7 \cdot 10^6$, $\alpha = 0^\circ$ and -4° . The interference free pressure field was determined by the linear subsonic theory.

The wall porosity was adjusted to the optimum value by maintaining the measured pressure $C_{pt}(x)$ close to the predicted value of $C_{pf}(x)$.

To find $f_{opt}(x)$ the technique of coordinate-by-coordinate retrieval was used. The resultant table of the functions f_{opt} for each of the four walls and dependencies versus M and α were input in the computer controlling the porosity of the walls.

Fig. 6 shows the rail pressure distribution obtained for the optimum porosity values in comparison with predicted free flow value C_{pf} . One can see that we managed to achieve rather good agreement of pressure profiles near the left wall where the pressure amplitude was maximum, and, consequently, its contribution of the interference effect should be maximum, too. On bottom wall C_p is close to 0 and is not sensitive to the porosity variations.

3.2 The wall adaptation procedure is quite time-consuming one and in many cases it can be substituted by less expansive approach - wall interference correction method. The original method was developed in T-128 based on its variable porosity implementation [7]. It consists of: a) a few runs with constant porosity value varying from min. to max. and showing the scatter in aerodynamic characteristics due to this variation; b) wall interference corrections obtained with CFD method being applied to given porosity value should collapse all data to a single curve, representing interference free results.

The example of such an approach is given in Figs. 7, 8 for AEDC-2 reference model. It was tested in T-128 test section N1 at different porosity value $f = 2\% - 10\%$. (Left curve show scatter in $C_L(\alpha)$ due to f variation). Then it was tested in AEDC 16-T wind tunnel of much large size, so that AEDC data can be considered as interference free ones. The comparison of T-128 corrected for wall interference $C_L(\alpha)$ (right curves) not only collapse to a single

curve but also coincide with AEDC data. The last were obtained a few month later, when fully corrected results of T-128 were issued.

3.3 Wind tunnel T-128 has special test section N3 destined to airfoils testing which are placed between side walls. Model is attached to two rotating discs which provide given angle of attack.

Airfoil drag is measured as total pressure deficit in the wake profile as determined by Pitot tube. The automatic 2-degree of freedom survey mechanism provides with the profiles of total pressure. All pressure measurements in the wake and on the model surface are executed by electronic modules and gages collected into single measuring system.

Test section walls are designed as variable longitudinal slots with porosity value change from 0 to 13%. Slots are longitudinally segmented in such a way that each part of about 1 m length can vary its porosity independently. In the model location area only horizontal walls are perforated, while side walls are solid, downstream of the airfoil all 4 walls are perforated. Along centerlines of test section walls more than 1000 static pressure taps are located.

One of the most valuable features of test section N3 is that controllable suction from side walls upstream of the model provides perfect 2-D flow.

Some results of two geometrically-similar models of A4 airfoil of Boeing company are presented in Figs. 9, 10. Lift curves $C_L(\alpha)$, obtained at T-128 and corrected for wall interference by very sophisticated CFD approach [8] gave good coincidence for two models of different blockage parameter $b/h = 0.17$ and $b/h = 0.29$. These data are in good agreement with IAR wind tunnel data obtained earlier.

3.4 Test section N5 is used for aeroelastic testing, for example, so called flying strut (Fig. 11) was tested here at transonic M number to prove stability and safety of the design. Wall porosity variation in this case served as excitation source to produce acoustic disturbances in the flow.

Typical examples of digital waveforms recording 2 sec. long in the frequency range up to 200 Hz for 4 sensors outputs, obtained by means of spectrum analyzer, are depicted at Fig. 12. These pictures are for $M=0.9$ and two values of porosity factor - 2% and 18% (for $P = 1$ atm).

The signals from bending and torsional gauges, exhibits stochastic irregular character with random changes of amplitude. It means these elastic oscillations are pure forced ones due to tunnel turbulence, but not self-excited oscillations.

Therefore, the system is far from loss of dynamic stability in frequency range of main vibration modes, i.e. it is far from flutter.

4. CONCLUSIONS

4.1 15 years of T-128 exploitation has shown that variable adaptive porosity is very valuable tool for wall interference reduction/elimination

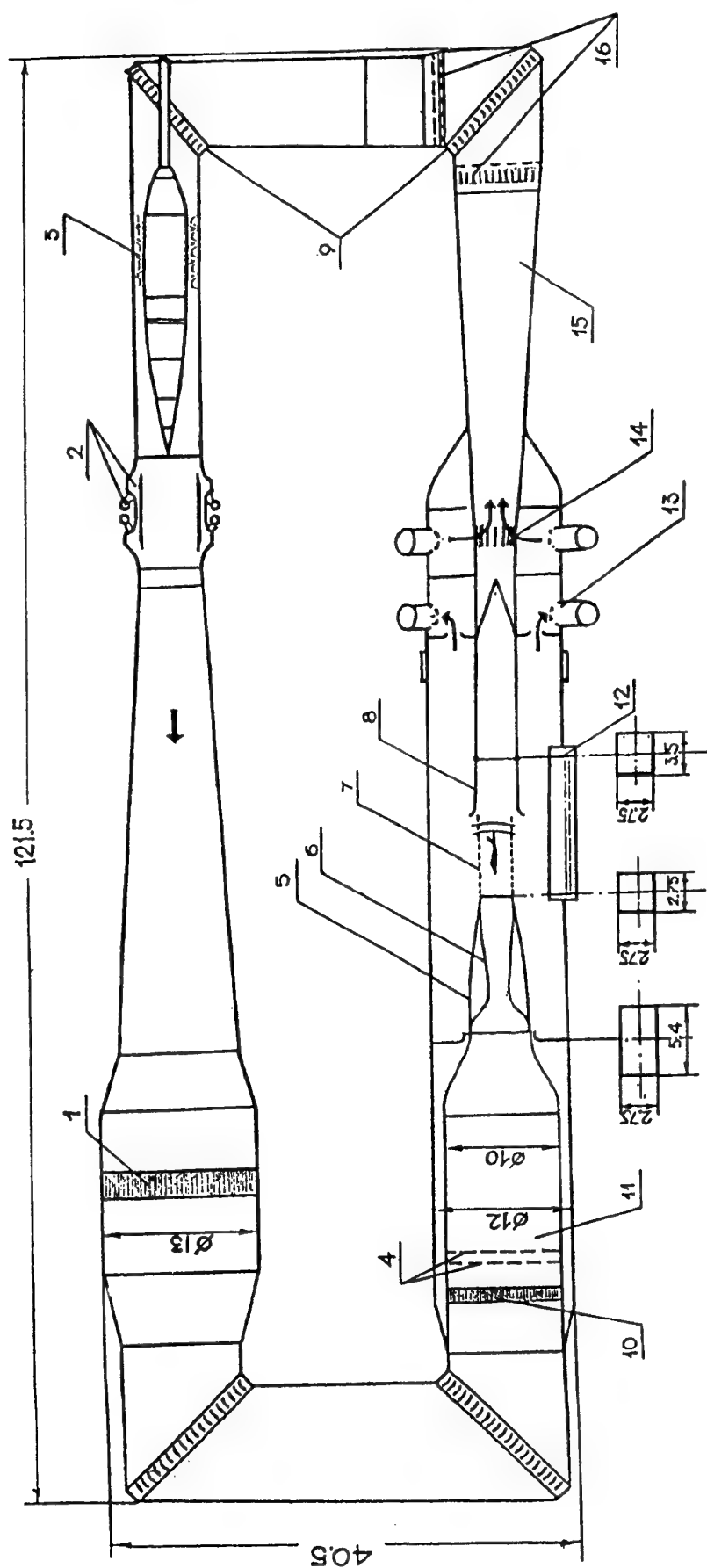
4.2 The variable porosity could be used in two ways:

- non adaptive (relatively cheap) mode, giving data for wall interference corrections on the base of CFD/experiment matching.
- adaptive (quite expensive) mode, eliminating wall interference in on-line regime.

4.3 Some improvements of adaptive variable porosity design should be done when repeating this approach in a new or modified transonic wind tunnel.

5. BIBLIOGRAPHY.

1. Adaptive Wall Newsletter. N6, Nov. 1987.
2. Sears W.R.
"Self Correcting Wind Tunnels". The Sixteenth Lanchester Memorial Lecture. May, 3, 1973. (published in the Aeronautic Journal vol. 78, Feb./Mar. 1974).
3. Ferri A., Baronti P.
"A Method for Transonic Wind Tunnel Corrections". AIAA journal, vol.11 N1, Jan. 1973 pp. 63-66.
4. Sychev V.V. Fonarev A.S.
"Interference - free Wind Tunnels for Transonic Research". Science Notes of TsAGI, N5 1975.
5. Ivanov A.I.
"An Experimental Study of Gas Flow Near the Perforated Walls of a Transonic Wind Tunnel". Fluid Mechanics - Soviet Research vol. 17 N4, Jul.-Aug. 1988.
6. Neyland V.M.
"Optimum porosity of Wind Tunnel Walls at Small Supersonic Speeds". Mechanics of Fluid and Gas, Soviet Academy of Science News, N4, 1989 pp. 187-189.
7. Neyland V.M. Semenov A.V., Semenova O.K., Glazkov S.A., Ivanov A.I., Khozyaenko N.N.
"Testing Technique Features of the Experiments in the Wind Tunnel with Adaptive Perforated Walls" Preprint TsAGI N 47, 1991.
8. Velichko S.A., Lifshits Yu.B., Neyland V.M., Solntsev I.A., Sorokin A.M. Numerical Modeling of Transonic Flow Past an Airfoil in a Wind Tunnel. Comp. Maths. Math. Phys. vol. 35, N10, pp. 1221 - 1235, 1995.



- | | | | |
|--|----------------------|-----------------------------------|------------------------|
| 1. Refrigerator | 5. Subsonic nozzle | 10. Honeycomb | 13. Suction |
| 2. Pressure up and down inside the tunnel shell. | 6. Supersonic nozzle | 11. Setting chamber | 14. Blowing up |
| 3. Compressor | 7. Test section | 12. Hatch for test section change | 15. Diffuser |
| 4. Deturbulising screens. | 8. Movable leaves | | 16. Protection screens |
| | 9. Turning blades | | |

Fig. 1

Re referred to 0.1 sq.root of
test section cross area (mln.)

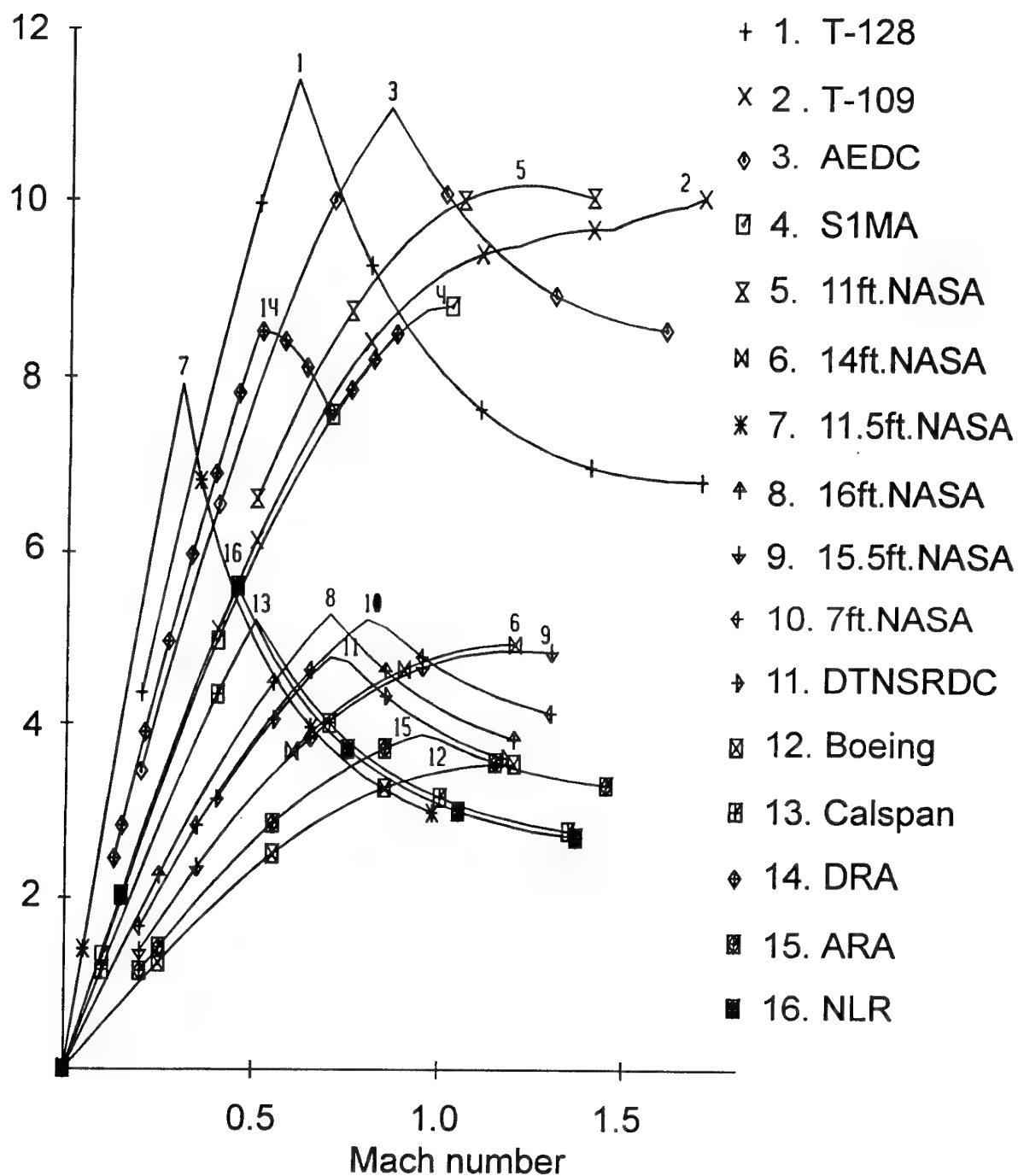
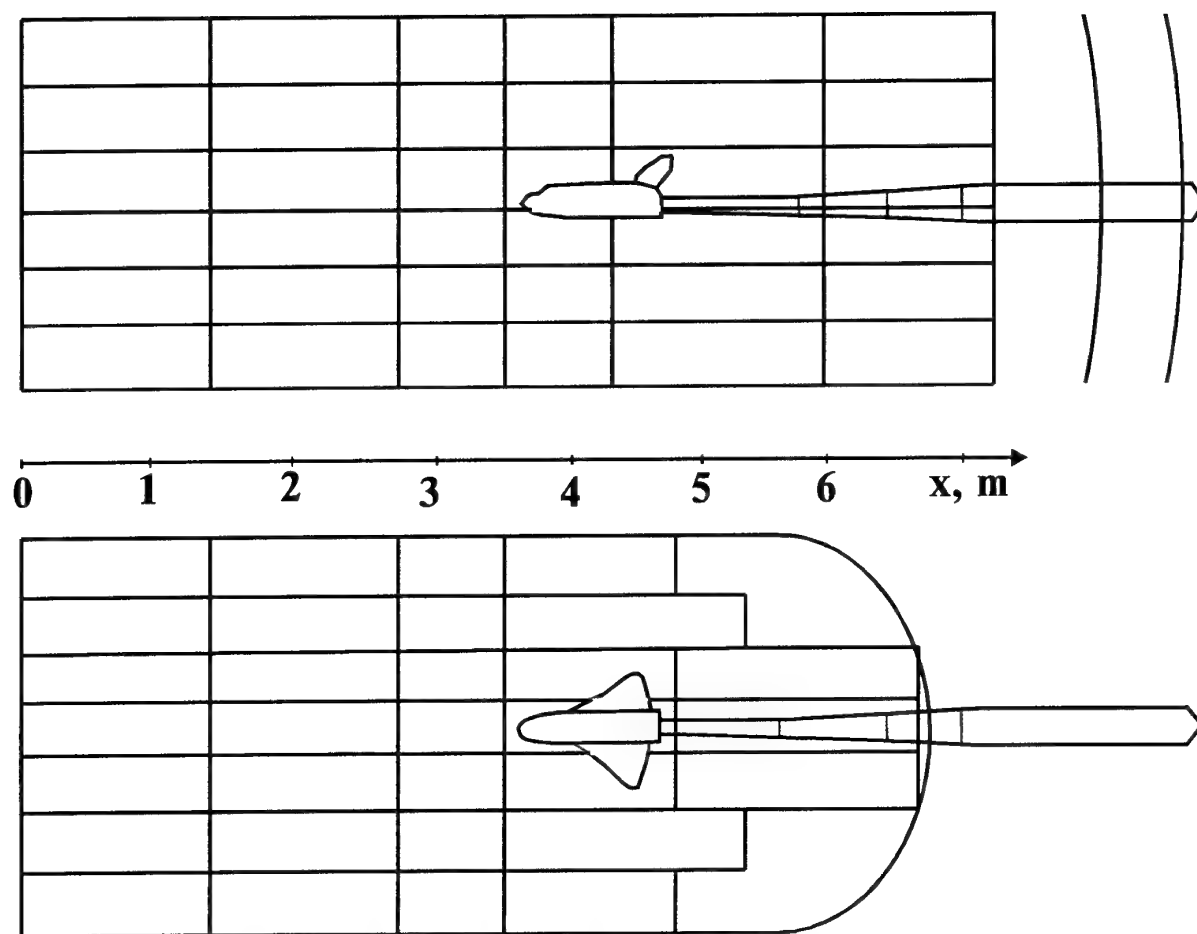


Fig. 2



**Walls surface segmentation of test section N1
(each rectangle corresponds to independent unit).**

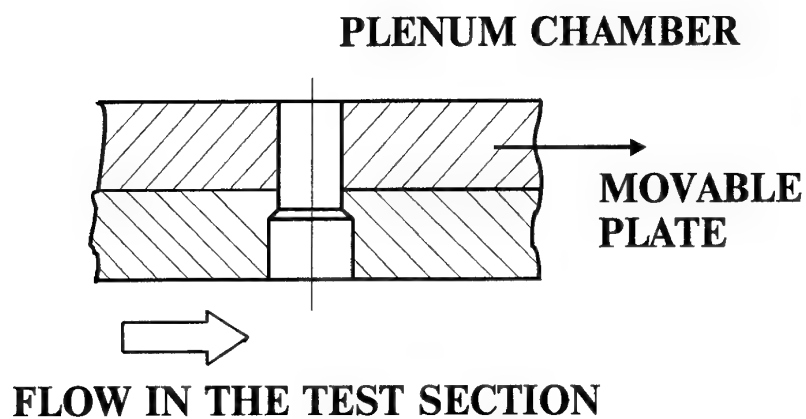


Fig. 3 Porosity variation scheme

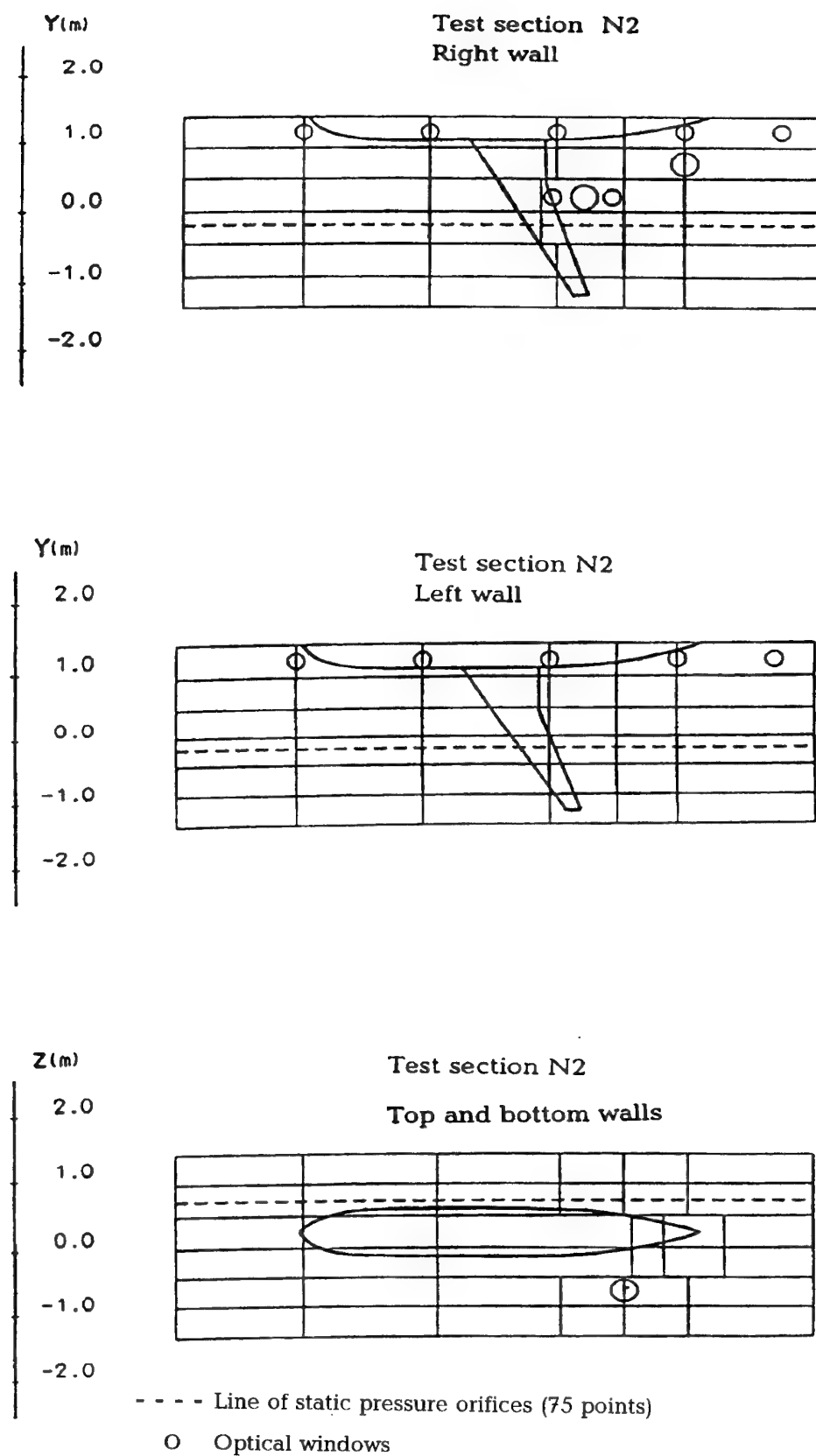
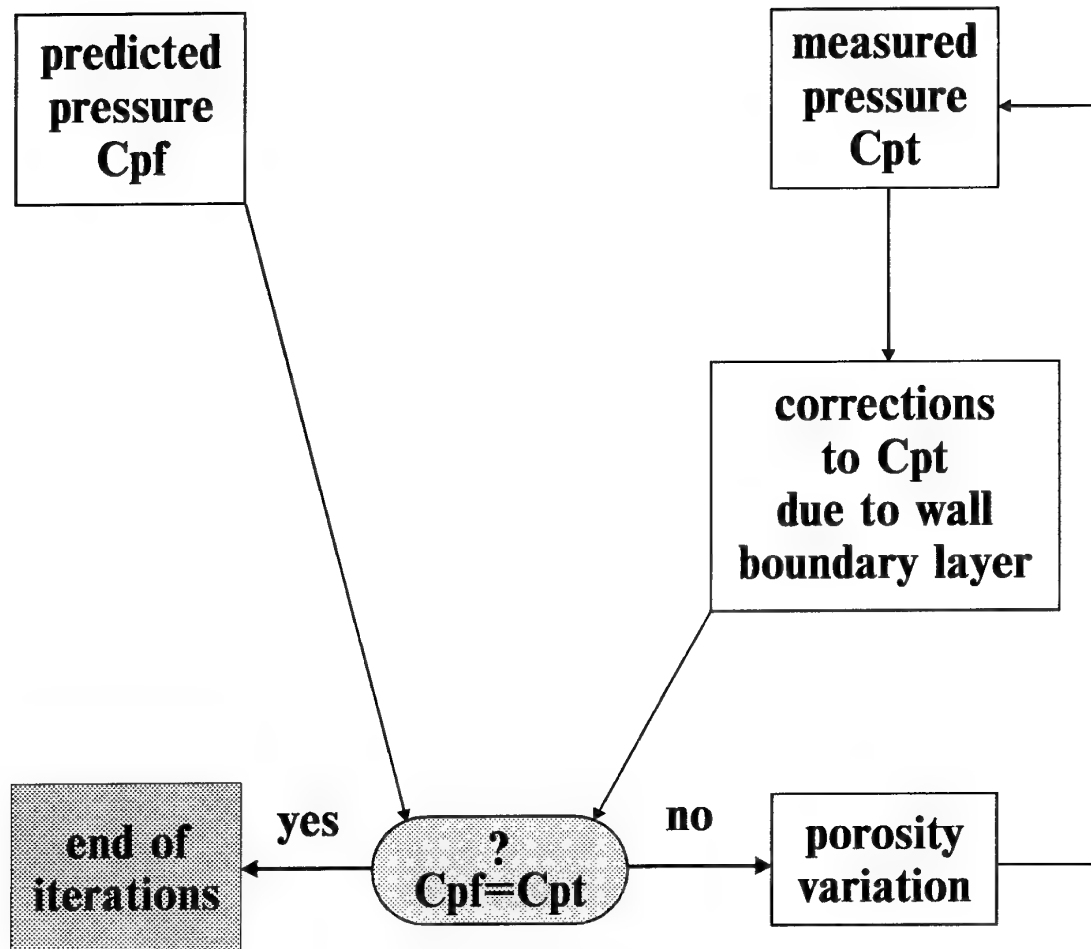
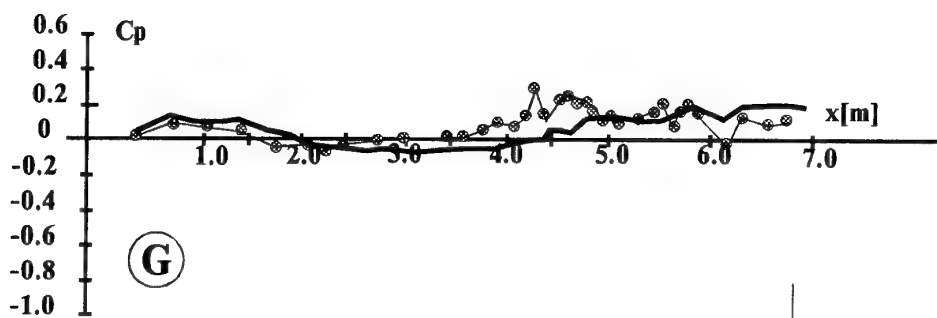
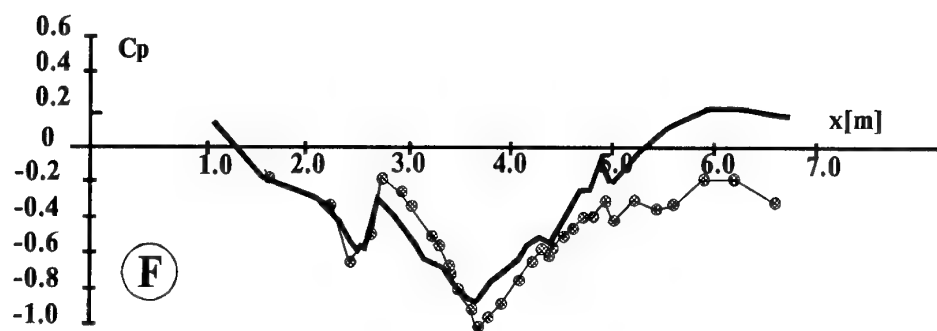
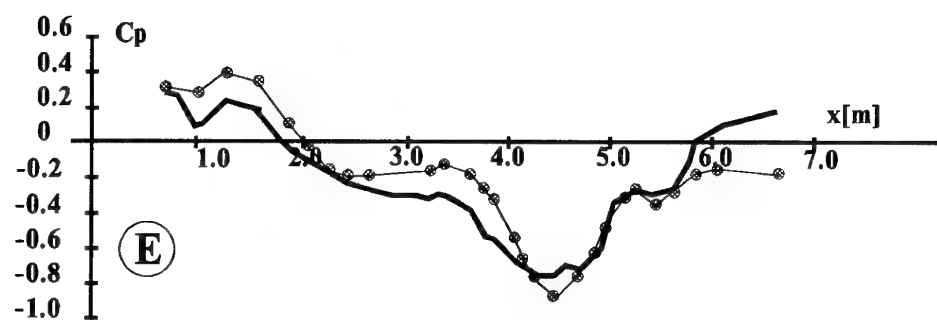


Fig. 4

**Fig. 5**



free-air calculation
+ empty WT
experimental data
(adaptation)

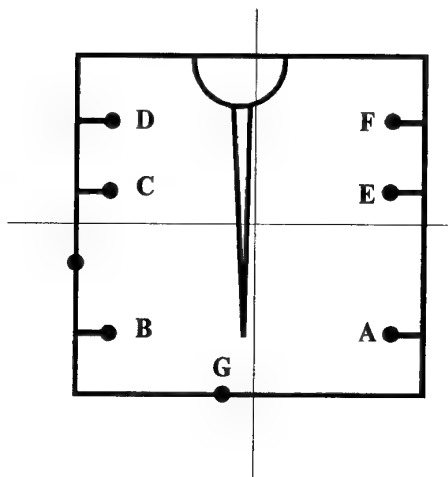


Fig. 6

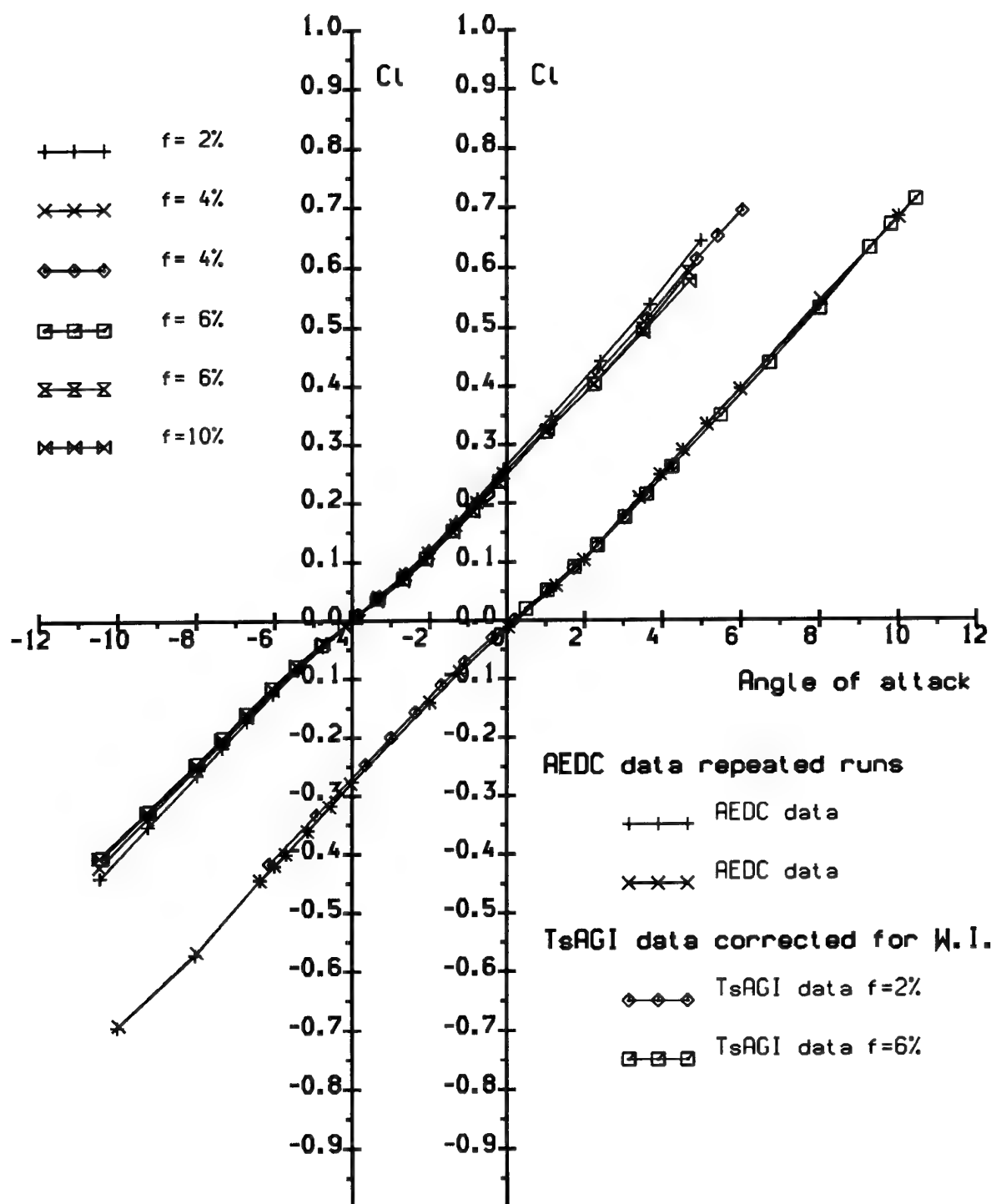
$M=0.95$


Fig.7 AEDC and TsAGI data comparison

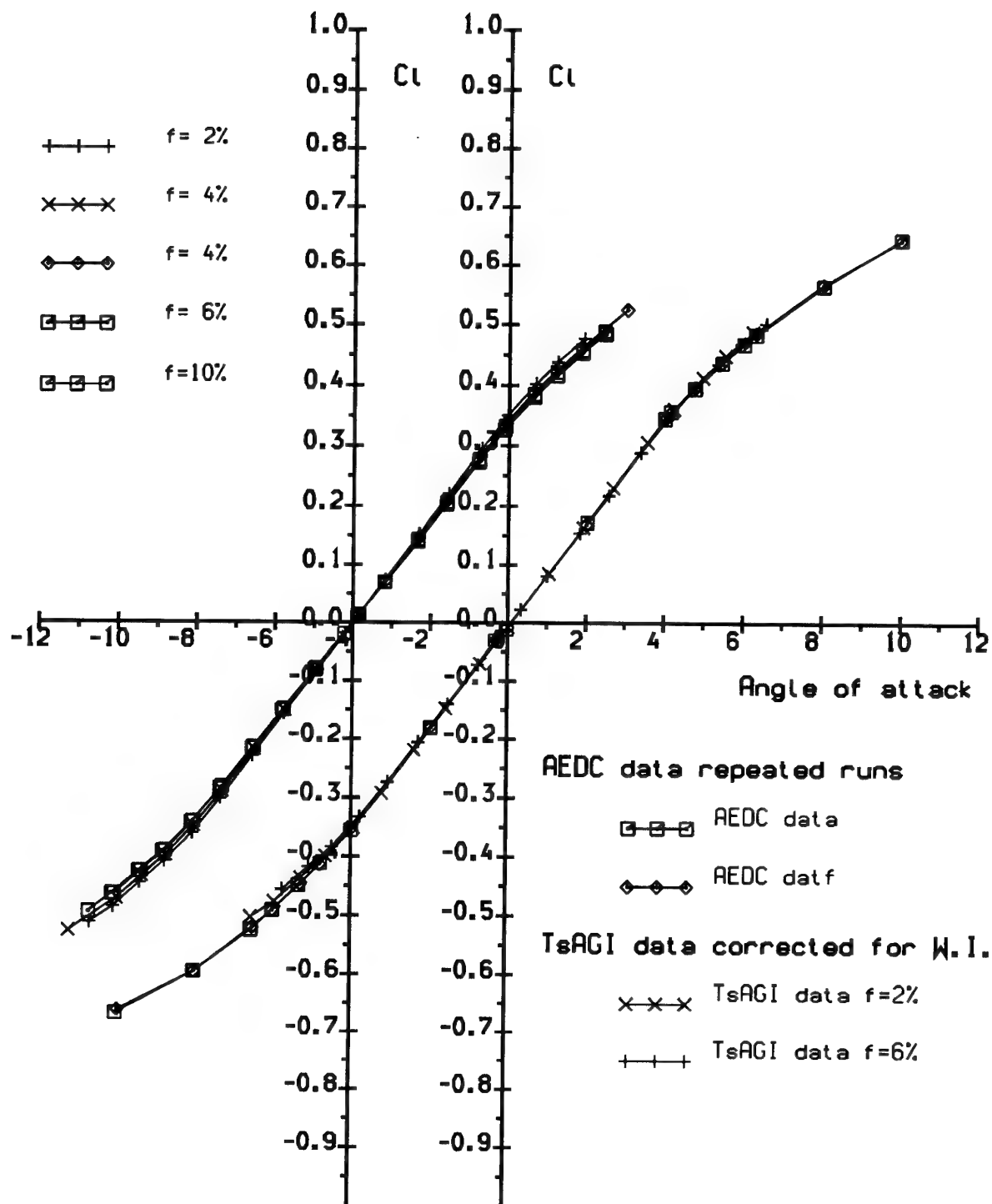
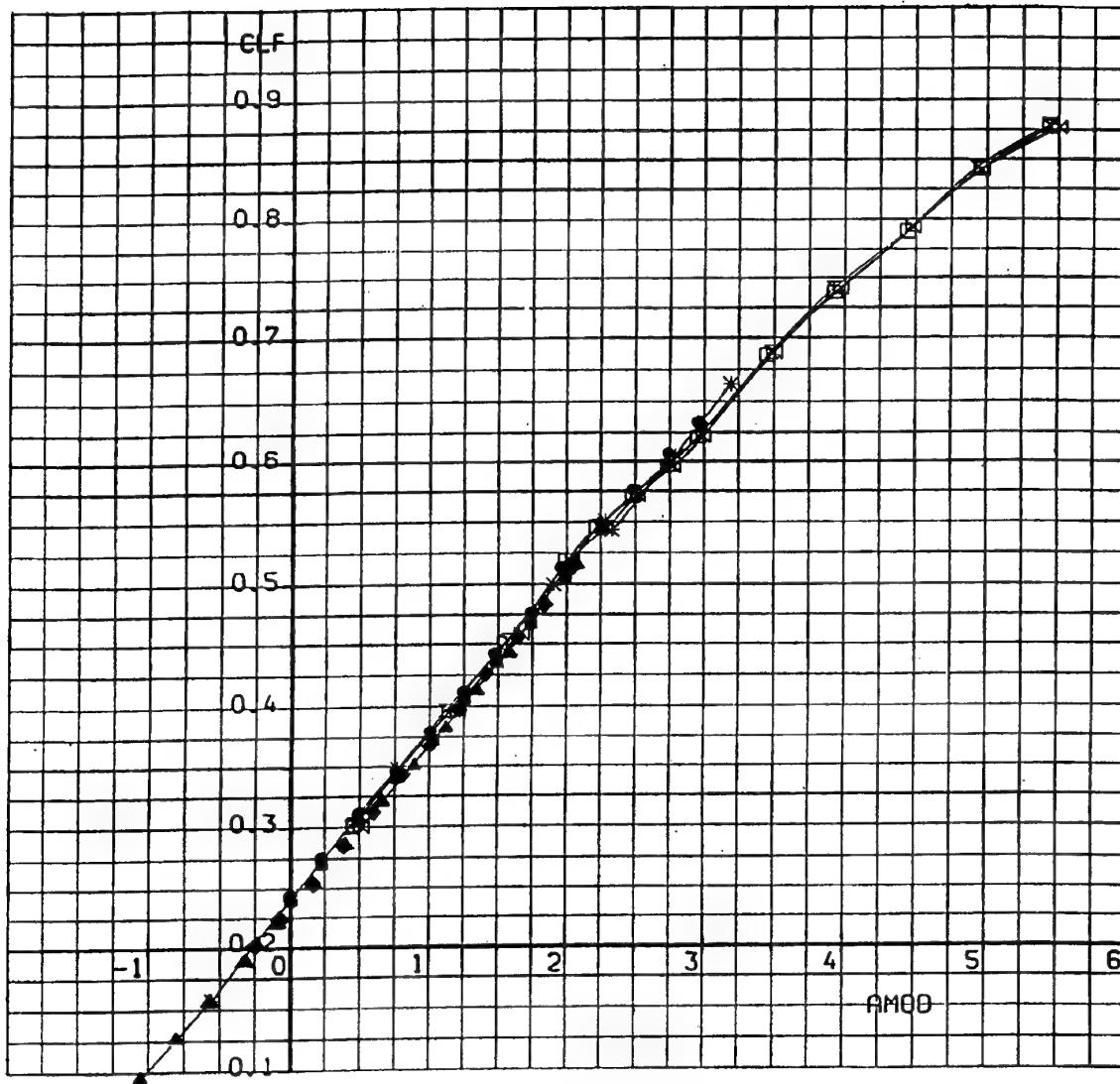
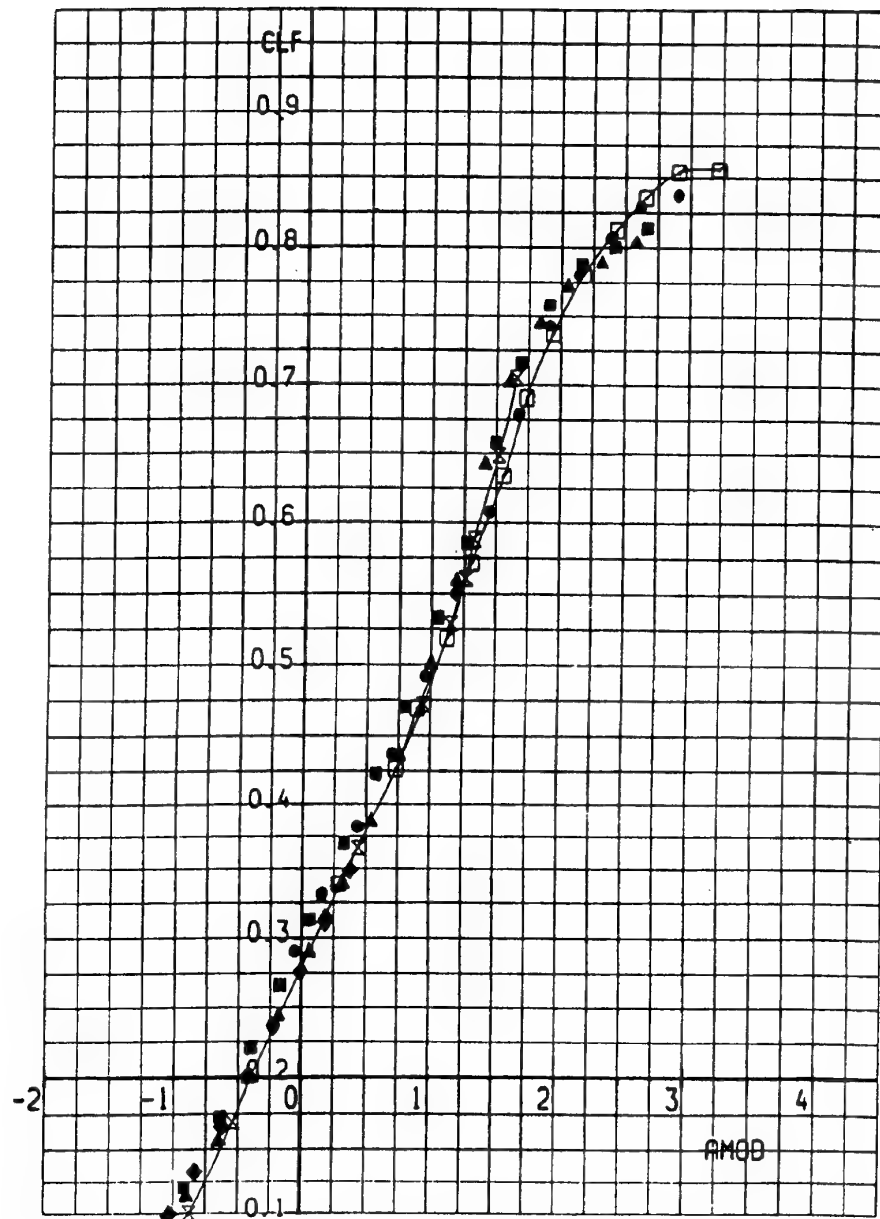
$M=0.85$


Fig.8 AEDC and TsAGI data comparison



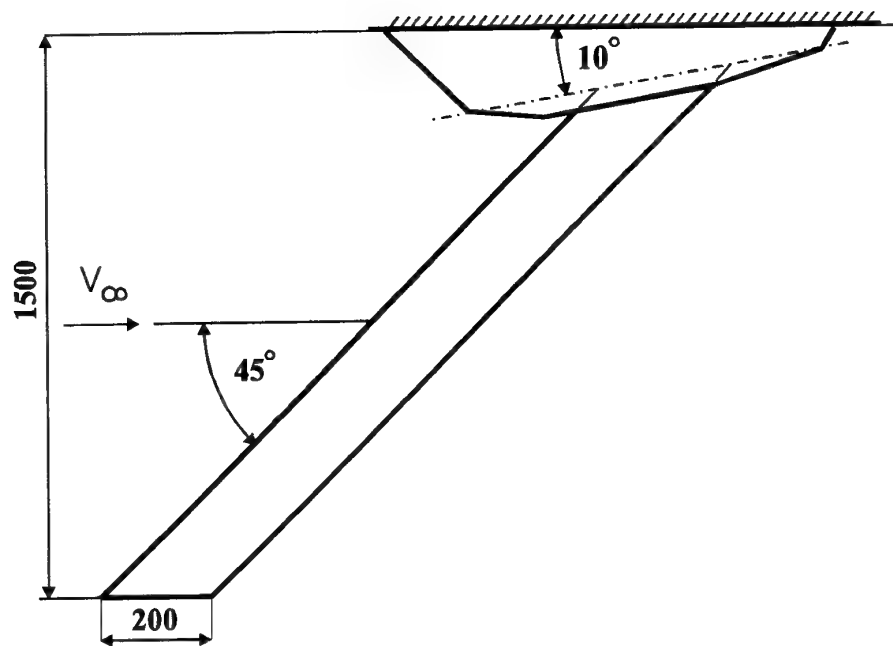
	Run #	Mach	f %	b/h	R _b (mln)	Comment
□	2249	.602	3	0.17	13.99	T-128 1995, corrected
⊗	2251	.601	3	0.17	13.98	T-128 1995, corrected
⊗	2256	.601	3	0.17	14.02	T-128 1995, corrected
*	-	.599	-	-	14.26	IAR data
●	8966	.600	0	0.29	10.68	T-128. 1993, corrected
■	8987	.600	2	0.29	10.74	T-128. 1993, corrected
▲	9027	.599	4	0.29	10.73	T-128. 1993, corrected
◆	8976	.601	6	0.29	10.69	T-128. 1993, corrected

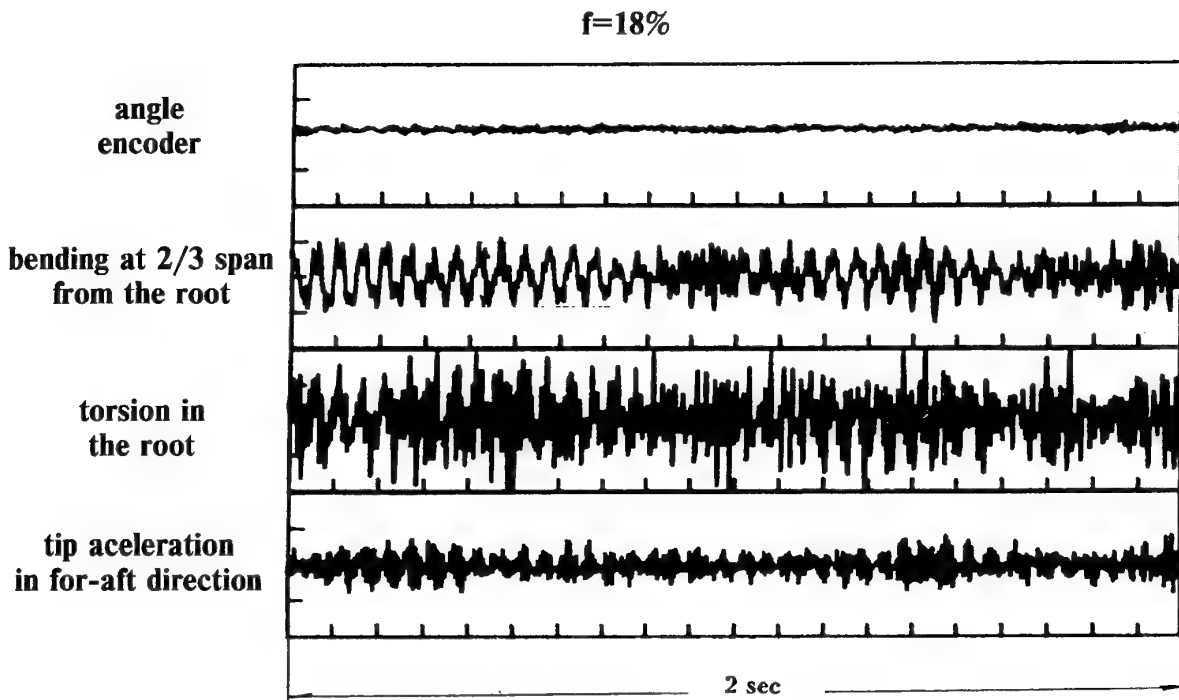
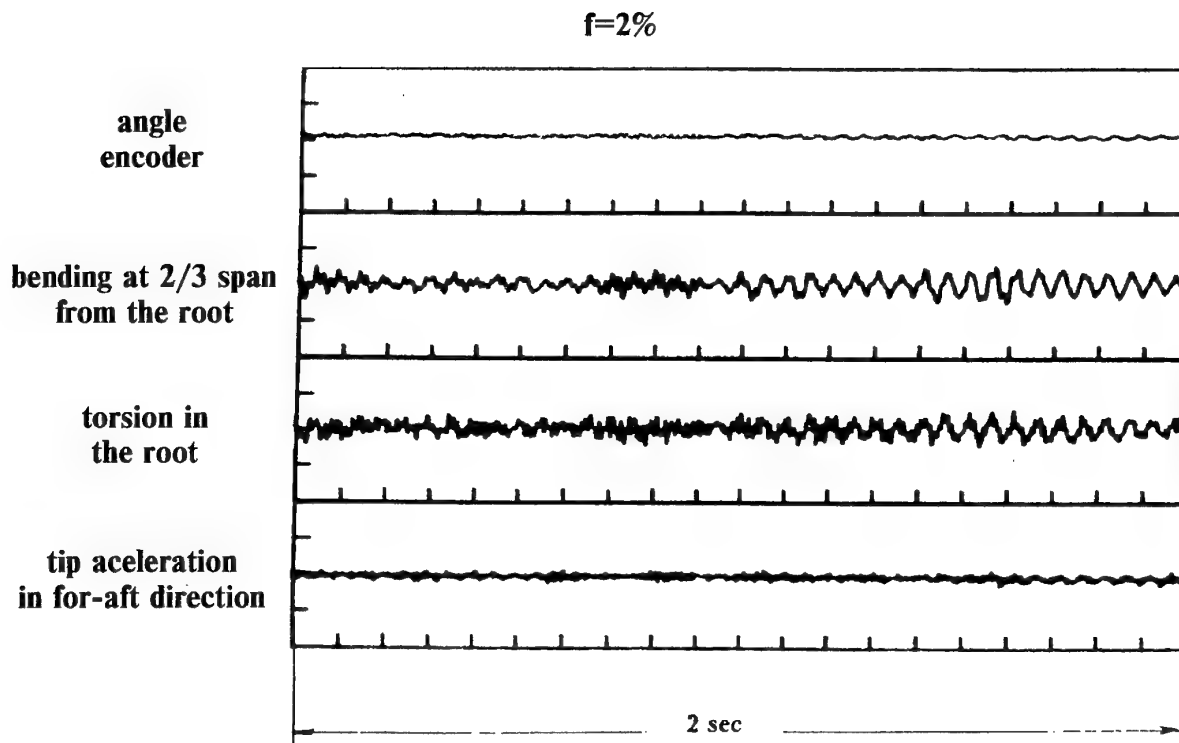
Fig. 9 Comparison of T-128 and IAR data for model A4



	Run #	Mach	f %	b/h	R _b (mln)	Comment
□	2255	.780	3	0.17	14.03	T-128 1995, corrected
×	-	.777	-	-	14.15	IAR data
●	8994	.780	0	0.29	12.80	T-128. 1993, corrected
■	9028	.779	2	0.29	12.78	T-128. 1993, corrected
▲	9026	.779	4	0.29	12.79	T-128. 1993, corrected
◆	9029	.780	6	0.29	12.69	T-128. 1993, corrected

Fig. 10 Comparison of T-128 and IAR data for model A4

**Fig. 11**



Output waveforms. $P_o=1$ atm. $M=0.9$

Fig. 12

Alleviation of Axial Static Pressure Gradients in 2D Perforated Test Section of IAR Blowdown Wind Tunnel

F.C. Tang and Y.Y. Chan
Aerodynamics Laboratory
Institute for Aerospace Research, National Research Council Canada
Montreal Road, Ottawa, Ontario, K1A 0R6
Canada

SUMMARY

The complicated flow mechanism in the empty, porous IAR 2D test section including the plenum chamber and downstream diffuser section was studied and postulated. The forward-facing inclined holes in the test section top and bottom walls resulted in the plenum pressure being higher than the test section static pressure. The original test section side walls were too short and a big opening was formed between the test section and the downstream diffuser. The plenum air mass was readily entrained through this opening by the free jet flow formed downstream of the test section. The removal of the plenum air mass from this opening effectively lower the plenum pressure resulting in the outflow phenomenon in the test section. With the presence of a long side wall extension, the opening between the test section and the downstream diffuser section would be shortened. The plenum mass flow was greatly reduced as entrainment was decreased due to a shorter free jet flow. A pressure equilibrium condition between the plenum and the test section was thus established resulting in a constant pressure distribution along the test section. This paper presents the results obtained during the commissioning of this extended side wall configuration and the subsequent modifications made to it. A close to optimum configuration for the IAR 2D test section extension has been found.

1. INTRODUCTION

During commissioning of the IAR 1.5m Trisonic Wind Tunnel with inter-changeable test sections in 1989 (Ref. 1), an adverse static pressure gradient in the axial direction was observed in the 2D test section. The side walls of the test section (Fig. 1) are solid and form a 0.38m (15") wide channel. The top and bottom walls feature variable porosity having slanted holes with splitter plates (Fig. 2) as opposed to the old test section with normal holes perforation. The forward-facing, 60° inclined holes are more effective in inducing flow from the test section to the plenum chamber. The plenum pressure for this type of wall configuration is always higher than the test section static pressure. There is an equilibrium plenum pressure with which the mass flow from the test section into the plenum chamber through the perforations and the discharge of air mass from the plenum chamber to the downstream diffuser is matched. Once the plenum pressure deviates from this equilibrium value, either an out-flow or in-flow situation will develop at the walls, resulting in static pressure gradient changes in the test section.

The static pressure gradient observed in the 2D test section is found to be Mach number dependent and its magnitude varies from $1.4 \times 10^{-2}/m$ at $M = 0.2$ to $5.5 \times 10^{-3}/m$ at $M = 0.9$ in terms of C_p . In the quest for ongoing improvement of wind tunnel flow quality, the presence of this adverse static pressure gradient, even though its magnitude is quite small, is undesirable. Recently there have been attempts to alleviate this adverse pressure gradient (Ref. 2). The preliminary findings indicated that by installing side wall extensions to the wind tunnel test section (Fig. 3), flat axial static pressure distributions could be achieved for a wide

range of Mach number. The success was attributed to the control of the re-entry flow from the plenum chamber into the downstream diffuser section. The side wall extensions used were of ordinary steel plates and measurements could only be carried out at low Reynolds number, up to $26 \times 10^6/m$, due to safety concerns.

A structurally durable set of side wall extensions was designed and manufactured based on findings of this preliminary investigation. This paper presents the results obtained during the commissioning of this extended side wall configuration and the subsequent modifications made to it.

2. 2D TEST FACILITY

As mentioned before, the 2D test section featured porous top and bottom walls and solid side walls. The solid side walls terminated about 0.56m (22") ahead of the downstream diffuser section. This large opening was originally designed to avoid the possibility of choking the channel at higher Mach number due to the blockage of the 3D model support and at the same time avoid excessive transient loading of the side wall structure during tunnel start-up and shut-down. Both concerns were eventually discarded. Settings of the Side Entry Flap (SEF), "L" and Contraction Joint (CJ), "D" in the downstream diffuser section were adjustable and were usually set wider than the test section width (Figs. 3, 5).

At the IAR 1.5m wind tunnel, top and bottom walls static pressure measurements were routinely made when operating in the 2D mode. The measurements were used in determining corrections to the measured data due to wind tunnel wall interference (Ref. 3). The present set of measurements were made in the empty test section in the Mach number range of 0.2 to 0.9. Unit Reynolds number varied from 6.6 to $98 \times 10^6/m$. Top and bottom walls tubes were used to measure static pressure distribution in the axial direction (Fig. 4). Each tube had 40 static pressure orifices but only 32 were measured using the 32-port Scanivalve 15 psid ZOC-22 module. For calibration purposes, a centreline static pressure tube, having 29 ports, was available. However, when side wall extensions were in place, measurements from the static pressure tubes were found to be influenced by the position of the 3D model strut. The downstream mounting mechanism of the centreline tube interfered with the "NAE Sting Support" of the 3D model support strut at its normal centreline position. The strut had to be re-positioned to either below or above the tunnel centreline. This off-centre position produced an asymmetry in the static pressure distributions on the wind tunnel top and bottom walls. Eventually, the centreline static pressure tube was removed and only the results obtained from the top and bottom walls static pressure tubes were used to evaluate the static pressure distributions in the test section.

Various configurations of side wall extensions were tested to investigate their effects on test section static pressure gradients.

3. FLOW MECHANISM

It is well known that for a test section with forward facing inclined holes, the plenum chamber pressure tends to be higher than the test section static pressure. When an equilibrium pressure is established in the plenum chamber, there is no in-flow or out-flow and the ideal flat static pressure gradient is achieved in the test section (Ref. 4). The large openings at the downstream end of the original 2D test section allowed unrestricted plenum flow to be entrained by the free jet formed downstream of the test section (Fig. 5). This excessive mass flow from the plenum chamber lowered the plenum pressure below the equilibrium value and induced flow out of the test section. The resulting out-flow led to the adverse static pressure gradient observed in the test section (Fig. 6).

The placement of the solid side wall extensions as well as the blanking plates in the downstream diffuser section were intended to eliminate the communication between the plenum chamber and the diffuser exit flow (Fig. 3). By adjusting settings of the Side Entry Flap (SEF) and the Contraction Joint (CJ) of the diffuser section (Fig. 5), it was hoped that an effective control of the plenum exit flow could be achieved, and consequently the control of the static pressure gradient. Preliminary results from Reference 2 do support this hypothesis.

Results from the present investigation provides additional information about the flow mechanism in the exit of the test section and the downstream diffuser section. It was found that the control of plenum exit flow by adjustment of settings of the Side Entry Flap and the Contraction Joint of the diffuser section was marginal at best. The test section exit configuration had to be very close to the optimum case for the control to be effective. The pressure at the test section exit location (P_e) and subsequently at the downstream diffuser section (P_d) may have a more profound effect on the plenum pressure and in turn the test section static pressure distribution than previously anticipated. Tufts flow visualization showed that the flow direction at the channels formed by the flow restraining walls and the downstream diffuser walls could be either upstream or downstream, which further complicated the flow mechanism at this region.

4. RESULTS

Figure 6 shows the static pressure distributions in coefficient form as measured by the ceiling tube in the original test section for a wide range of Mach number. The unit Reynolds number was kept constant at $49 \times 10^6/\text{m}$ ($15 \times 10^6/\text{ft.}$). Only results from the ceiling tube are shown as there is hardly any differences between the top and bottom walls data. The static pressure gradients are found to be Mach number dependent and their magnitude varied from $1.4 \times 10^{-2}/\text{m}$ ($3.6 \times 10^{-4}/\text{in.}$) at $M = 0.2$ to $5.5 \times 10^{-3}/\text{m}$ ($1.4 \times 10^{-4}/\text{in.}$) at $M = 0.9$ in terms of C_p .

The 2D side wall extension as used in Reference 2 is quite simple in design. The schematic of the final configuration of extension used in that preliminary study is shown in Figure 7. Basically the extension was made up of three pieces of 15.8mm (5/8") thick carbon steel plate for each side wall, staggered as shown. The overall length was 0.56m (22") and angle irons were used as reinforcement at the back. The improvement to the static pressure gradients is quite dramatic. Figure 8 shows the results obtained with this preliminary side wall extension in place during the present test programme. The static pressure distributions in the test section are flat for all Mach numbers investigated. The SEF and CJ settings of the downstream diffuser allowed for a 0.254m

(10") gap between the side wall extension and the flow restraining wall laterally (Fig. 5). The flow restraining wall formed a 1.5° half angle diffuser as well. The blanking plates in the downstream diffuser were not used. It should be noted that due to safety concerns, measurements were made at a very low stagnation pressure (25 psia) for this extension configuration.

The very encouraging improvements to the 2D test section static pressure distributions by such a simple modification prompted the design of structurally-sound "permanent" side wall extension to the facility. The schematic of this test section extension is shown in Figure 9. More elaborate reinforcement of the 15.9mm (5/8") thick carbon steel plate is incorporated. The overall length of the extension is 0.55m (21.5"). Mounting brackets for the extension are designed such that upon installation in the tunnel circuit, the test section extension formed a 2° half angle diffuser. This configuration retained approximately the same exit area of the preliminary extension as described before and at the same time eliminated the steps which are not very practical in the wind tunnel routine operation. Upon commissioning of this "permanent" side wall extension, it was found that the tunnel flow characteristic had been changed from that of out-flow to that of in-flow (Fig. 10). The subject length of this solid extension almost closed the opening between the test section and the downstream diffuser. The control of plenum exit flow by adjustment of settings of the Side Entry Flap and the Contraction Joint of the diffuser section was marginal at best and insufficient to alter the gross negative static pressure gradients with or without the blanking plates in the diffuser section. Schemes to change the extension exit conditions such as installing forward facing steps of various heights worked well but were highly Mach number dependent.

Quite a number of conjectures were put forward as to the reasons why the very crude preliminary side wall extension appeared to work well in the initial investigation but not at all with the more refined configuration of the "permanent" side wall extension. The most plausible one being that small gaps were created in forming the steps in the preliminary side wall extension. These gaps allowed some plenum flow to leak through (as confirmed by flow visualization). The "permanent" extension with smooth surface is a far more effective diffuser and the solid section effectively restricted the outflow of the plenum air mass. Notably, it was found that a very small change in the plenum pressure, in the order of 0.001 in C_p , was sufficient to alter the static pressure gradients in the test section.

Modifications had to be made to the "permanent" side wall extension in order to make it functional and practical for routine wind tunnel operation. Several parameters of the test section extension were investigated, among them the extension length, the extension configuration and the extension's diffuser angle.

4.1 Effects of Length

With the "permanent" extension in place, the plenum pressure was found to be higher than the desirable equilibrium value and resulted in the "in-flow" phenomenon. It was thought that by reducing the length of the extension, the restriction to the plenum flow to be entrained by the free jet flow would be reduced. The preliminary extension used in the initial trial was suitable for such an investigation. There were sufficient adjustments in the set up to allow one of the three plates to be moved back and forth (Fig. 11) to form extensions with lengths of 0.4m (16"), 0.43m (17") and 0.46m (18"). The test section static pressure distributions as obtained from these various

extended lengths extensions are shown in Figure 12. The pressure distribution from the original test section (designated by 0") is included for comparison as well. It can be seen that the static pressure distribution obtained with the 0.43m (17") extension in place is the best. With the test section shortened by just 2.54cm (1") from the 0.43m long extension, the opening between the test section and the downstream diffuser became bigger and allowed more plenum mass flow to exit. Lower than equilibrium plenum pressure was established resulting in the "out-flow" situation. With the test section lengthened by 2.54cm (1") from the 0.43m (17") long extension, the opening between the test section and the downstream diffuser became smaller and allowed less plenum mass flow to exit. Higher than equilibrium plenum pressure was established resulting in the "in-flow" situation. The results from this Figure further substantiate the hypothesis that there is an optimum opening between the test section and the downstream diffuser to allow an equilibrium value of plenum pressure to be established. However, this is not the only parameter that has an effect on the test section static pressure distribution as is shown below.

4.2 Effects of Extension Configuration

Having established the most appropriate side wall extension length to use, the effects of various extension configurations were investigated. The preliminary extension which was made up of three separate pieces as described before were arranged in various combinations. Five extension configurations resulted, all of the same length (0.43m, 17"), and are shown in Figure 13. Configuration (a) is just a parallel extension of the existing test section. Configuration (b) has a 0.35m (14") long parallel section followed by a 0.08m (3") long parallel section with a 15.9mm (5/8") step. Configuration (c) features a 0.23m (9") long parallel section followed by a 0.2m (8") long parallel section with a 6.4mm (1/4") step. Configuration (d) has a 0.23m (9") long parallel section followed by a 0.2m (8") long section with a 2° half angle. Configuration (e) has a 0.23m (9") long parallel section followed by a 0.2m (8") long section with a 6.4mm (1/4") step and a 2° half angle.

The results obtained are shown in Figure 14. The simple parallel extension, Configuration (a), and Configuration (b) still have features of the out-flow situation. Configuration (e) with the 6.4mm (1/4") step and a 2° half angle over the last 0.2m (8") of the extension shows features of the in-flow phenomenon. Configuration (d) with the 0.23m (9") long parallel section followed by a 0.2m (8") long section with a 2° half angle resulted in the most desirable static pressure distribution in the test section among the five configurations investigated.

4.3 Effects of Extension Diffuser Angle

Spacers of different thickness were used with the side wall extension brackets to form extension of the same length but with various diffusion angles. The investigations were carried out only at low Mach number and low dynamic pressure ($M = 0.26$, $q = 1$ psia) for safety concerns.

Figure 15 shows that for the side wall extension with length of 0.44m (17.5"), a diffusion angle of approximately 1° half angle would provide the flattest static pressure distribution in the test section. With the side wall extension diffusion angle at 2° half angle, the pressure at the exit of the extension would be higher than that of the extension with diffusion angle of 1.1° half angle. It is believed that the higher pressure at the test section exit would provide more resistance for the plenum mass flow to be entrained into the main flow. The higher exit pressure would eventually

communicate with the plenum pressure via the channels formed by flow constraining walls and the downstream diffuser section side walls. As expected, the lower test section exit pressure from the 0.67° half angle diffuser would provide less resistance for the plenum mass flow to be entrained by the freestream flow. No pressure measurement at the test section exit location was taken, however a rough estimate based on ideal isentropic relations suggest that the pressure difference at the test section exit between the 2° half angle extension and the 1.1° half angle extension would be approximately 0.08 in C_p . This small difference in test section exit pressure does have a large effect on the wind tunnel test section static pressure gradient as can be seen in Figure 15.

4.4 Final Extension Configuration

Modifications were made to the "permanent" side wall extension based on results reported above. The length of the extension was reduced to 0.44m. An aluminum plate with a 2° wedge angle followed by a constant thickness section was attached to the surface of each side wall extension (Fig. 16). After installation in the wind tunnel, the extension would be a 0.22m long parallel section followed by a 0.2m long section with a 2° half angle, very similar to Configuration (d).

The test section static pressure distributions obtained with this extension are shown in Figure 17 for a wide Mach number range of 0.2 to 0.9. The unit Reynolds number is constant at $49 \times 10^6/\text{m}$ ($15 \times 10^6/\text{ft.}$). The settings of Side Entry Flap and Contraction Joint are the same for all cases. The pressure distributions are very flat for all Mach numbers. Figure 18 shows the results as expressed in $\Delta M (M_{\text{local}} - M_{\text{ref}})$ distributions. There is hardly any gradient in the test section for all Mach numbers of interest. This particular extension configuration works for the higher, more realistic Reynolds numbers as well. Figure 19 shows the pressure distributions obtained for unit Reynolds number of $49 \times 10^6/\text{m}$ ($15 \times 10^6/\text{ft.}$) and $98 \times 10^6/\text{m}$ ($30 \times 10^6/\text{ft.}$) for the $M = 0.9$ case. The pressure distributions are very flat for both Reynolds numbers.

5. CONCLUSIONS

The complicated flow mechanism in the empty, porous IAR 2D test section including the plenum chamber and downstream diffuser section was postulated. The forward-facing inclined holes in the test section top and bottom walls resulted in the plenum pressure being higher than the test section static pressure. There is an equilibrium plenum pressure where no in-flow or out-flow situation occurs at the walls. The original test section side walls were too short and a big opening was formed between the test section and the downstream diffuser. The plenum air mass was readily entrained by the free jet flow through this opening. The removal of the plenum air mass from this opening effectively lower the plenum pressure resulting in the out-flow phenomenon in the test section. With the presence of a solid side wall extension, the opening between the test section and the downstream diffuser section was reduced. The plenum mass flow was greatly reduced as entrainment was decreased due to a shorter free jet flow. A pressure equilibrium condition between the plenum and the test section was thus established resulting in a constant pressure distribution along the test section.

Some of the more important parameters having an effect on the IAR 2D test section static pressure distributions have been identified. They are:

size of opening between test section and

downstream diffuser section (extension length):

- test section exit area configurations and
- test section exit pressure.

A close to optimum configuration for the IAR 2D test section extension has been found. The extension features a 0.22m long parallel section followed by a 0.2m section with a 2° half angle. The addition of this extension has proved to be insensitive to Mach number and Reynolds number variations. The empty test section static pressure distributions have been improved. There is no need to make run to run fine adjustment to the wind tunnel which makes it a very practical addition to the test facility.

REFERENCES

1. Öhman, L.H. et al, "New Transonic Test Sections for the NAE 5FT X 5FT Trisonic Wind Tunnel", NAE-AN-62, NRC No. 31216, Jan. 1990, National Research Council Canada
2. Medved, B.L., "Alleviation of Adverse Axial Static Pressure Gradients in the Two-Dimensional Test Section of the IAR 1.5m Wind Tunnel", ICAS-93-3.3.3, Proceeding of 19th Congress of the ICAS Conference, Anaheim, California, U.S.A., September 1994
3. Mokry, M., "Subsonic Wall Interference Corrections for Finite Length Test Sections Using Boundary Pressure Measurements", AGARD-CP-335, Paper No. 10, Sept. 1982
4. Goethert, B.H., "Transonic Wind Tunnel Testing" - Edited by Wilbur C. Nelson, Pergamon Press, 1961, pp 283-296.

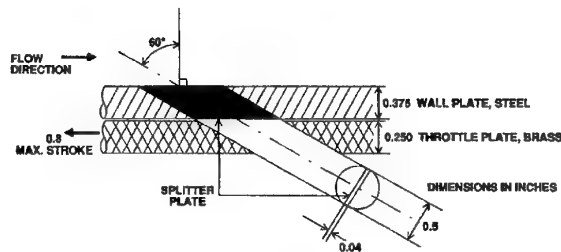


Figure 2 Variable Porosity Wall Hole Geometry

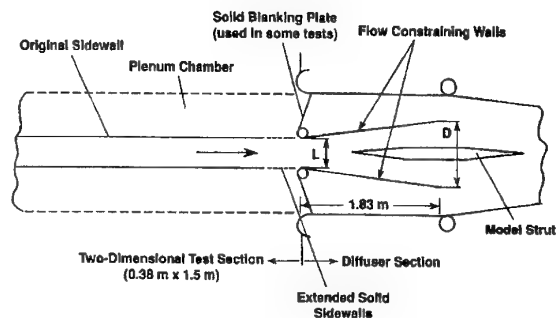


Figure 3 2D Test Section Configuration with Modifications

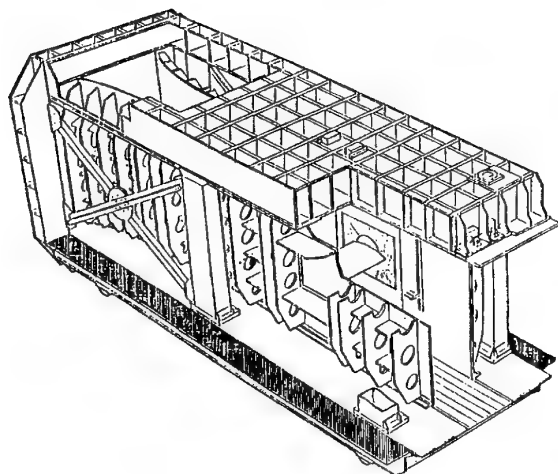


Figure 1 IAR 0.38mX1.5m 2D Test Section

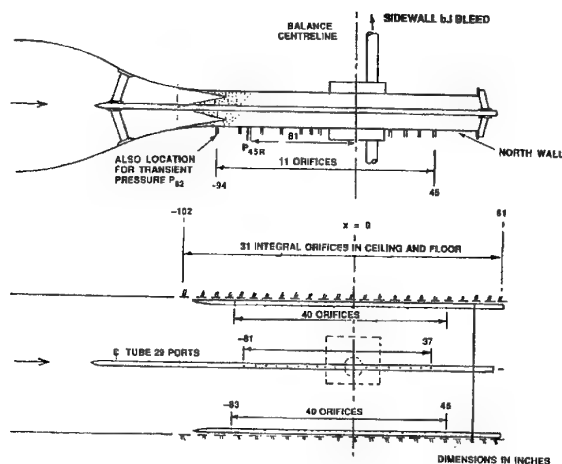


Figure 4 2D Test Section Static Pressure Calibration Arrangements

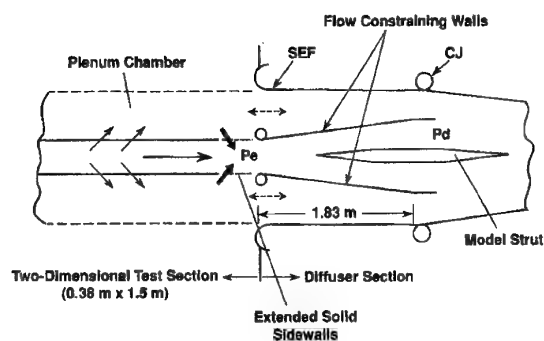


Figure 5 Flow Mechanism in 2D Test Section and Diffuser Section

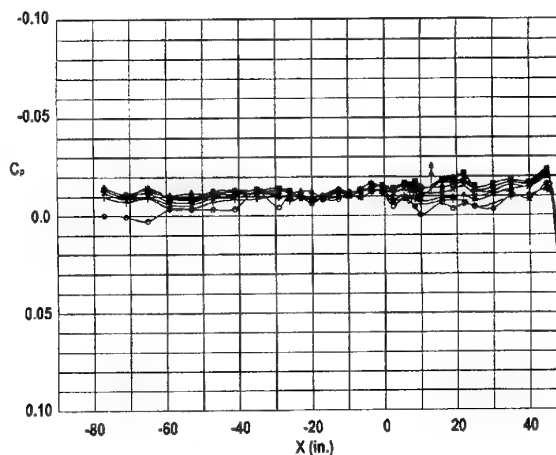


Figure 8 Ceiling Static Pressure Distributions (with Preliminary 2D Test Section Extension)
 $Re = 2 \text{ to } 9 \times 10^6/\text{ft.}$, $M = 0.2 \text{ to } 0.9$

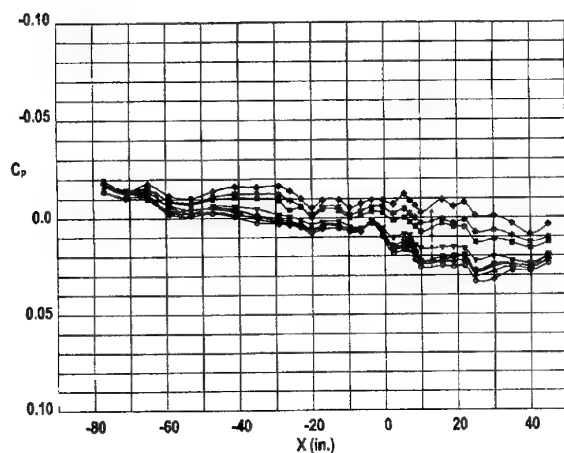


Figure 6 Ceiling Static Pressure Distributions (Original 2D Test Section)
 $Re = 15 \times 10^6/\text{ft.}$, $M = 0.2 \text{ to } 0.9$

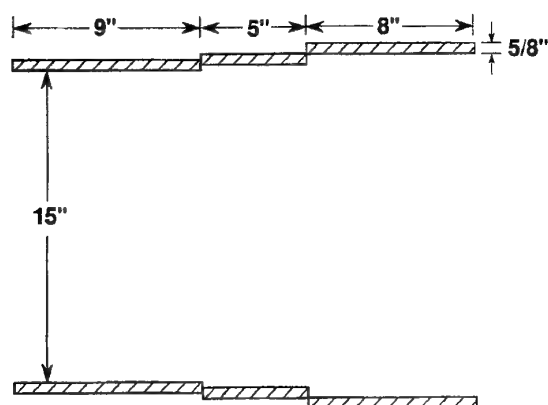


Figure 7 Schematic of Preliminary 2D Test Section Extension Configuration

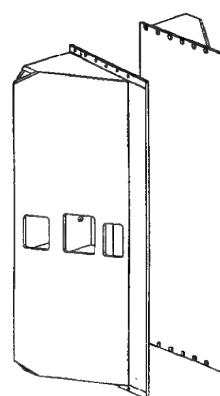


Figure 9 Schematic of "Permanent" 2D Test Section Extension Configuration

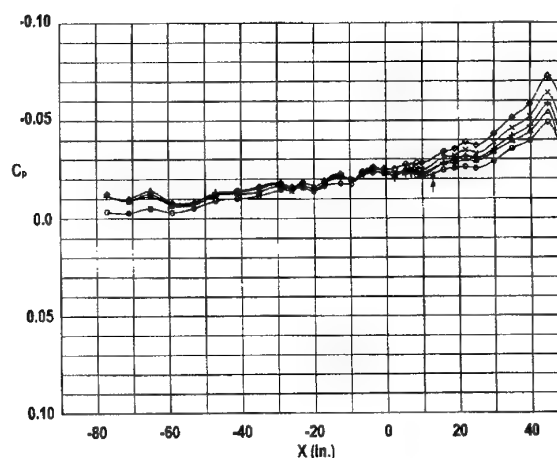


Figure 10 Ceiling Static Pressure Distributions (with "Permanent" 2D Extension)
 $Re = 2 \text{ to } 7 \times 10^6/\text{ft.}$, $M = 0.2 \text{ to } 0.7$

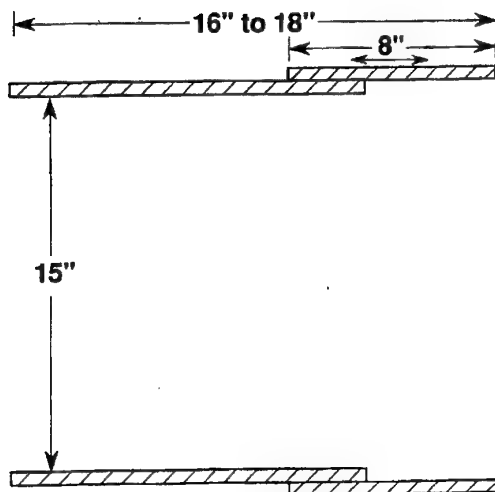


Figure 11 Schematic of 2D Test Section Extension Configuration with Adjustable Length

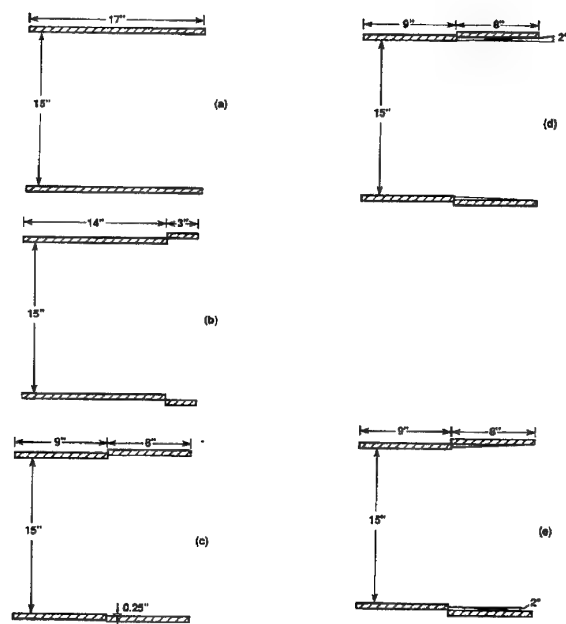


Figure 13 Schematics of Various 2D Test Section Extension Configurations

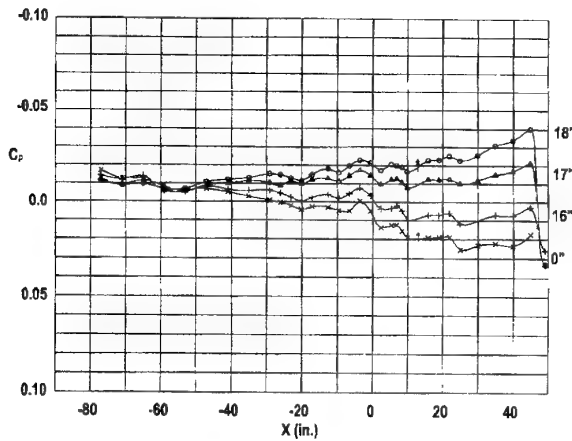


Figure 12 Effects of Extension Length to Test Section Static Pressure Distributions
 $Re = 5 \times 10^6/ft.$, $M = 0.5$

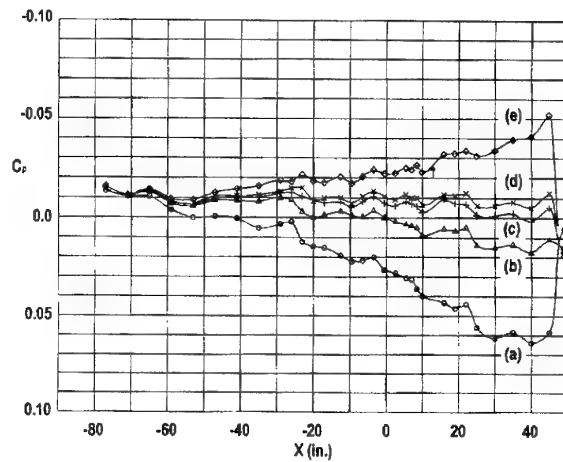


Figure 14 Effects of Extension Configurations to Test Section Static Pressure Distributions
 $Re = 8.6 \times 10^6/ft.$, $M = 0.8$

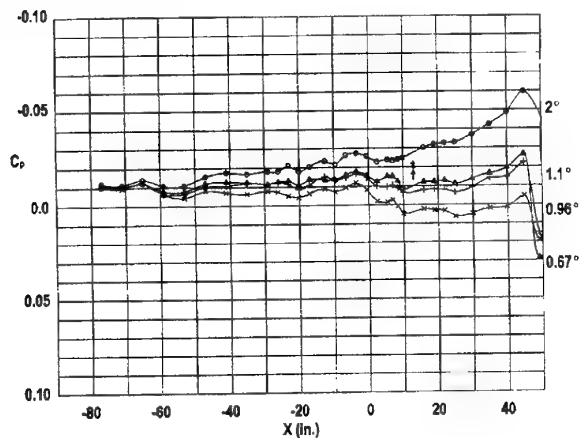


Figure 15 Effects of Extension Diffuser Angles to Test Section Static Pressure Distributions

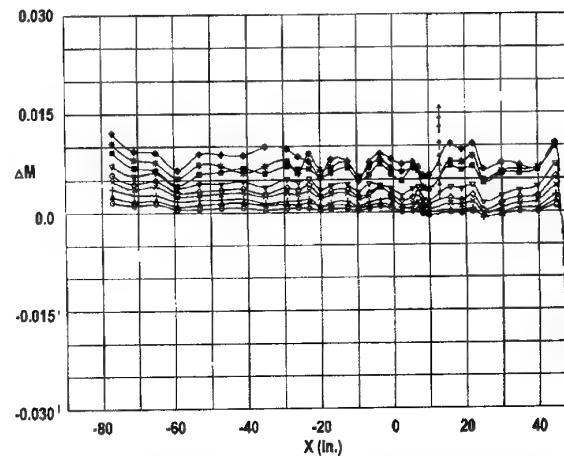


Figure 18 Ceiling Mach Number Distributions (with Final 2D Test Section Extension Configuration)
 $Re = 15 \times 10^6 / ft.$, $M = 0.2$ to 0.9

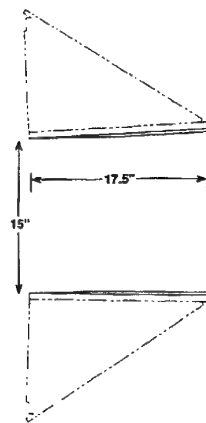


Figure 16 Schematic of Final 2D Test Section Extension Configuration (Top View)

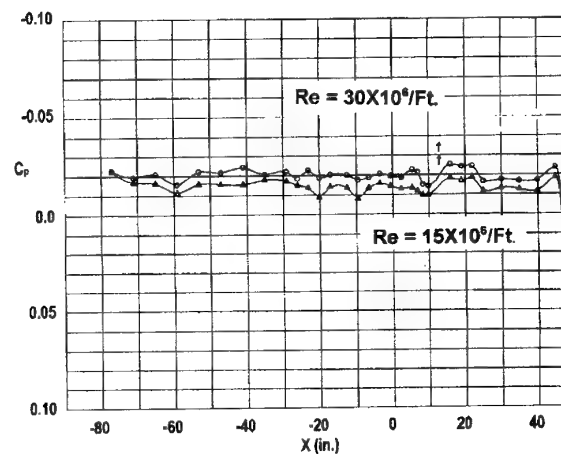


Figure 19 Ceiling Static Pressure Distributions (with Final 2D Test Section Extension Configuration)
 $Re = 15$ and $30 \times 10^6 / Ft.$, $M = 0.2$ to 0.9

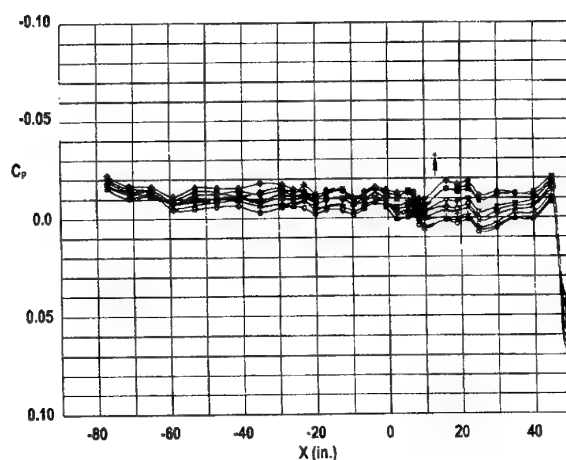


Figure 17 Ceiling Static Pressure Distributions (with Final 2D Test Section Extension Configuration)
 $Re = 15 \times 10^6 / ft.$, $M = 0.2$ to 0.9

EVALUATING ANALYTICALLY AND EXPERIMENTALLY THE GAS DYNAMICS OF TRANSONIC WIND TUNNELS WITH DEVICES FOR AIR EVACUATION FROM PLENUM CHAMBER

V.P. Verkhovsky

O.V. Lyzhin

Z.G. Pasova,

Central Aerohydrodynamic Institute (TsAGI), 1, Zhukovsky Street
140160 Zhukovsky, Moscow Region, Russia

ABSTRACT

The report provides results of experimental evaluation of flow in a transonic wind tunnel with forced suction from the plenum chamber surrounding a perforated test section. It is shown that the test section exit part features an air outflow into the plenum chamber; this decelerates flow, increases pressure, and decreases the Mach number at the entry into the main subsonic diffuser of the wind tunnel. In this case, total pressure losses become notably less.

Also reported are results of experimental investigation into operation of a large wind tunnel with the suction system which extends the ranges of Mach and Reynolds numbers and reduces total pressure losses.

Nomenclature

G_{suc}	suction system flowrate
G_{ts}	test section flowrate
$K = G_{suc}/G_{ts}$	suction flowrate factor
L	length of the "suction diffuser"
M	Mach number in test section
M_{exit}	Mach number at the test section exit
P_0	stagnation chamber pressure
P_{0d}	total pressure at the exit section of subsonic diffuser
$\nu = P_{0d}/P_0$	total pressure recovery coefficient
σ	permeability coefficient of test section walls

INTRODUCTION

When operating a transonic wind tunnel and/or making a wind tunnel with subsonic nozzle reach a Mach number of over 1, the process is accompanied with penetration of a certain fraction of the working gas through perforated walls into the plenum chamber surrounding the test section. This fraction may be either returned into the main stream through an end slot at the test section exit (the self-adjusting suction) or removed from the plenum chamber by using a special system (the suction).

The total pressure losses at a certain test section Mach number can be characterized in terms of the total pressure recovery coefficient ν . In the design with self-adjusting suction the function $\nu = f(M)$ is completely governed by the wind tunnel geometry – in particular, by the height of an end slot downstream of the test section. In a wind tunnel with suction the value of ν depends not only on M but also on the suction flowrate factor K .

The ν values attainable with the suction system are higher than those in the case of self-adjusting suction; this reduces the compression required (thus, the power of the main fan). However, removing the gas from the test section requires extra power. Nevertheless, the theory predicts that resorting to suction is beneficial at certain operation conditions. Moreover, suction becomes notably profitable when test

section pressure is higher than atmospheric and the removal does not require power.

1. EXPERIMENTAL EVALUATION OF "SUCTION DIFFUSER"

The experiments were mounted in a blow-down wind tunnel with a 180 mm by 180 mm test section; it is supplied with the air from bottles with pressure of up to 1 MPa. Nozzles in the wind tunnel are planar, with fixed geometry. All four walls of the test section are perforated, with the wall permeability coefficient ranging from 0% to 30%. Side walls are parallel to the test section axis, whereas the upper and lower walls are set at 30° to the axis (in order to compensate for boundary layer displacement). Downstream of the test section is the section with controllable flaps that provide for operation with both self-adjusting suction and forced suction. The test section is surrounded by the chamber from which the air may be sucked by a single-stage supersonic ejector.

Figure 1 represents the experimentally obtained relation of the total pressure losses to the suction flowrate factor, $\nu = f(K)$, for test section Mach numbers 0.8, 1.0, and 1.2 (at $\sigma = 1 - 13\%$). With Mach number fixed, the value of ν notably increases with the suction flowrate factor, while not depending on the wall permeability degree.

For comparison's sake, Figure 2 depicts the function $\nu = f(M)$ for operation with self-adjusting suction. One can see that forced suction ensures much greater ν values than the self-adjusting suction.

Figure 3 shows the pressure distribution along the test section at $M=1$ and various values of the suction flowrate factor (the wall permeability σ is approximately 13%); and Figure 4 represents the Mach number profile along the test section with different permeability degrees at $K=0.14$. It is seen from Figure 3 that a major part of the test section features an almost constant pressure which is equal to the plenum pressure. At the exit of the test section there exist an elevated pressure zone. It is in this zone that the gas does run from the test section into the plenum chamber, thereafter into the suction system. The measured values of P/P_0 may be utilized to evaluate Mach number profiles along the test section, refer to Figure 4. It is seen that pressure does rise in going to the test section exit, while Mach number gets significantly less. This test section zone with higher pressure may be called "a diffuser due to suction", or "a suction diffuser", because gas is decelerated here due to gas flowing out into the plenum chamber, whereas at $M=\text{const}$ the Mach number at the test section exit, M_{exit} , is only governed by the gas removal rate (the K factor).

Figure 5 demonstrates how the test section end Mach number M_{exit} depends on K at $M=0.6, 0.8, 1.0$. For all values of σ the test points for each M value are on common curves. The experimental data obtained at Mach numbers 0.6 and 0.8 may very accurately be described by a simple relation $q(M_{exit}) = q(M)(1-K)$ where $q(M)$ is a function of a relative flowrate of the nozzle. Some discrepancy between the test

points and the theoretical curve at $M=1.0$ seems to be due to inadequate compensation for boundary layer in the test section under these conditions.

The length L of the "suction diffuser" at $M=\text{const}$ depends on the suction flowrate factor and the test section wall permeability: $L=f(K, \sigma)$. The length increases if the suction flowrate factor increases and/or the permeability degree is decreased. In the case of low permeability (say, $\sigma \leq 5\%$) and $K=0.1$ the "suction diffuser" may be as long as the test section (Figure 6).

Dependence of the "suction diffuser" relative length $\bar{L}=f(K, \sigma)$ ($\bar{L}=L/L_0$) for $M=1.0$ may be seen in Fig. 7.

All the points obtained experimentally at $K=\text{const}$ are on smooth curves. With Mach number and K being maintained, for most conditions (especially at $\sigma=10\% - 30\%$) the \bar{L} value is inversely proportional to σ . This function $\bar{L}=f(K, \sigma)$ is of practical significance since it enables determining the test section exit value σ necessary for the "suction diffuser" being downstream of the test model. From the relation $\bar{L}=f(K, \sigma)$ it follows that the "suction diffuser" length is 0.15 for $K=0.1$ and $\sigma=30\%$. It may be assumed that if permeability σ of walls in the test section exit section of length $\bar{L} \approx 0.10$ is 40% (with some kind of extrapolation from the data available) then the flow deceleration zone will be strictly downstream of the test model, regardless of the permeability degree over the main part of walls. Test results demonstrated in Fig. 8 have been the decisive validation of this assumption. Resorting to perforation with $\sigma_x=40\%$ does almost eliminate the effects of plenum chamber suction on quality of the stream in the domain for installing a test model.

In a wind tunnel with "suction diffuser" the Mach number M_{exit} of the stream outflowing into a subsonic diffuser is less than the test section Mach number. In this situation the recovery of total pressure in the main diffuser depends on M_{exit} only. Plotting the dependence of ν on M_{exit} for M values not exceeding 1.0 shows that experimental points fall on a common curve (Fig. 9). Test data for the facility with forced suction are slightly over the curve for tests with self-adjusting suction. This can be explained taking into account the fact that the main diffuser with forced suction has a thinner boundary layer at the entry.

2. RESULTS OF STUDYING THE PERFORMANCE OF TRANSONIC WIND TUNNEL WITH SYSTEM FOR AIR EVACUATION FROM PLENUM CHAMBER

The experimentally validated theoretical principles for a wind tunnel with a suction system have been embodied in the fan-driven T-128 wind tunnel with a 2.75 m by 2.75 m test section for a Mach number range 0.2 to 1.7. A schematic of the suction system is depicted in Fig. 10. The system includes a separate fan, heat exchanger, and control components.

An important problem was to develop subsystems for controlling the suction operation and protecting the wind tunnel in emergency. Special experiments for determining the characteristics of the suction subsystem were carried out to create suction subsystem control algorithms and computer software. These envisage

- monitoring the condition of shut-off/control components,
- flow monitoring,
- controlling the suction flowrate, and
- shutting down the subsystem in emergency situations.

The suction flowrate is controlled by means of suction/bypass throttles. The maximum flowrate depends on the suction subsystem fan drive power (≈ 20 MW) and may be as great as 110 kg/s. The maximum suction flowrate factor K depends on a rated Mach number and a stilling chamber pressure. Figure 11 represents the maximum suction flowrate factor K as a function of the test section Mach number M at the stilling chamber pressure $P_0=0.1$ MPa.

The suction system has made it possible to extend the M and Re ranges available. For example, the Reynolds number has been increased by 9% - 28% for $M=0.87 - 1.0$. As well, Mach number of 1.4 - 1.7 has been reached, while ensuring a uniform flow in the model installation domain - without the suction system the maximum Mach number is 1.4.

The extension of capabilities has earlier been said to be due to reduction of total pressure losses. With this in mind, Fig. 12 demonstrates the experimentally obtained relation of the total pressure recovery coefficient to M in the wind tunnel with forced and self-adjusting suction. In these evaluations the test section contained an airplane model with a relative wing area of 0.07, the angle of attack being as high as 20 degrees.

The suction system was also used to remove boundary layer from test section side walls in front of an airfoil. Because of extremely low gas flowrate required ($K \sim 1\%$) the suction system control options have been modified. Sucking the boundary layer enabled reducing the boundary layer displacement thickness by 75% - 80% of the value for the wind tunnel with no suction system; this ensured high-quality "two-dimensional" flow around the model.

The present suction system was also employed to evacuate the main channel of the wind tunnel. In this case the time to pressure of 30 kPa has been 3 minutes instead of 40 to 50 minutes with vacuum pumps.

REFERENCE

1. O.V.Lyzhin and Z.G.Pasova. Experimental study of transonic wind tunnel with "suction diffuser". - Uchenyye Zapiski TsAGI, vol. 10, no. 4, 1979.

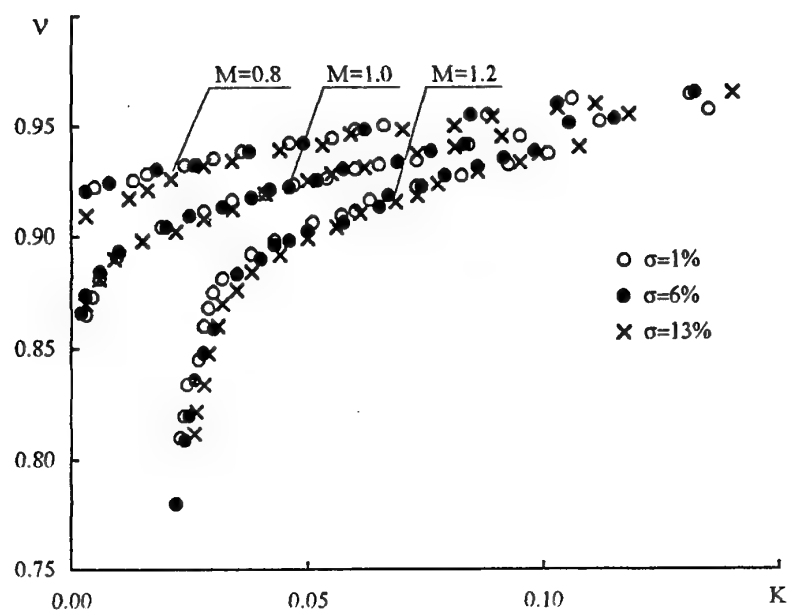


Figure 1. Total pressure recovery coefficient v as a function of suction flowrate factor K at certain Mach numbers M .

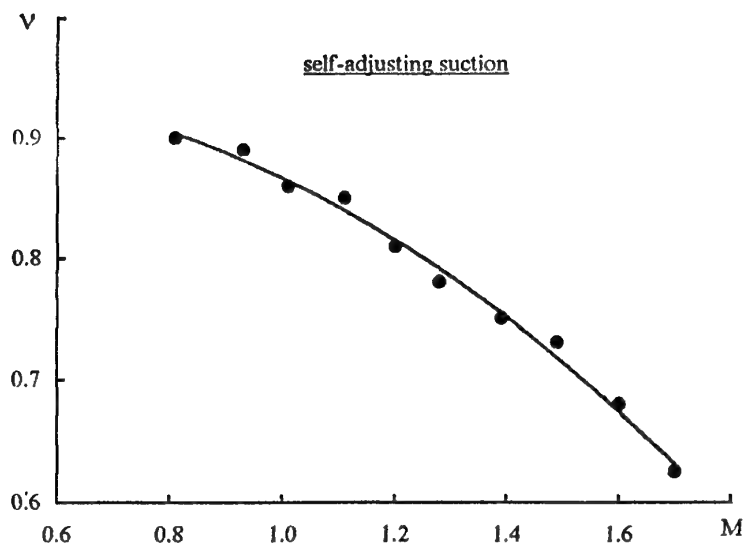


Figure 2. Total pressure recovery coefficient V vs. Mach number M .

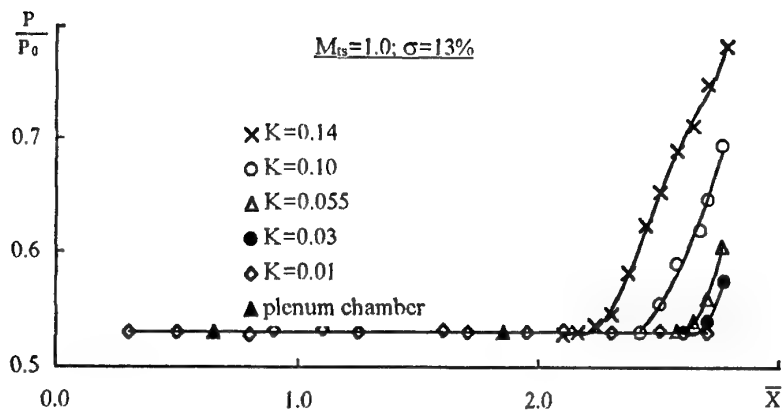


Figure 3. Pressure profile (P/P_0) along the test section (\bar{X} coordinate)

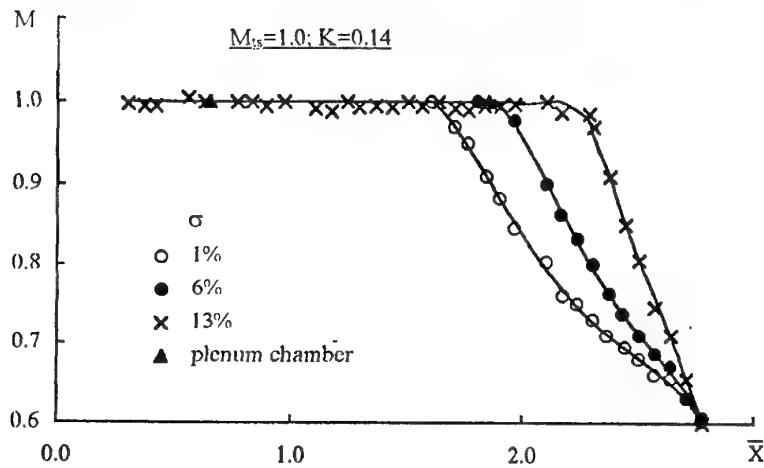


Figure 4. Mach number profile along the test section (\bar{X} coordinate).

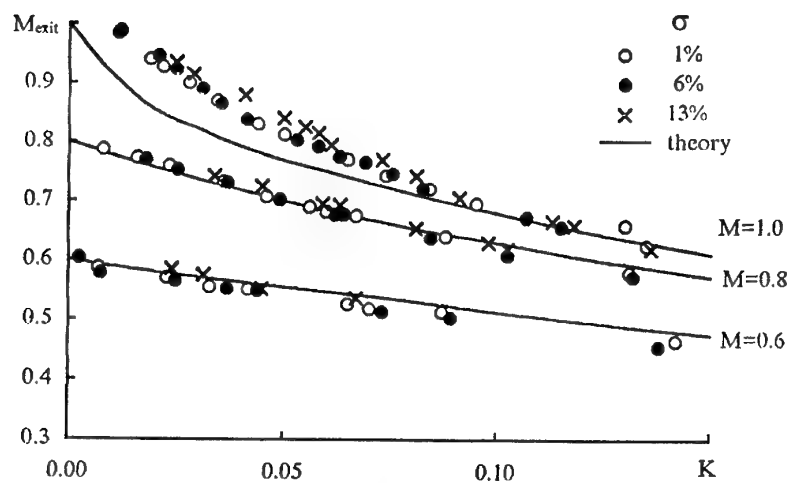


Figure 5. Dependence of test section-exit Mach number M_{exit} on suction flowrate factor K for flows with $M=0.6, 0.8, 1.0$.

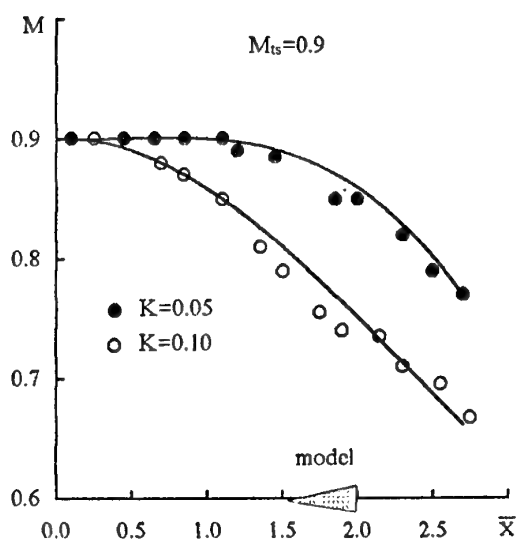


Figure 6. Mach number profile along the test section with wall permeability coefficient σ of 5%

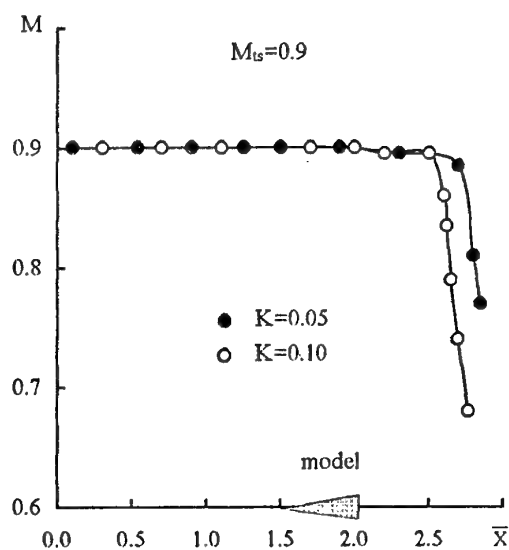


Figure 8. Mach number profile along the test section with wall permeability coefficient $\sigma = 5\%$ at $\sigma_k = 40\%$.

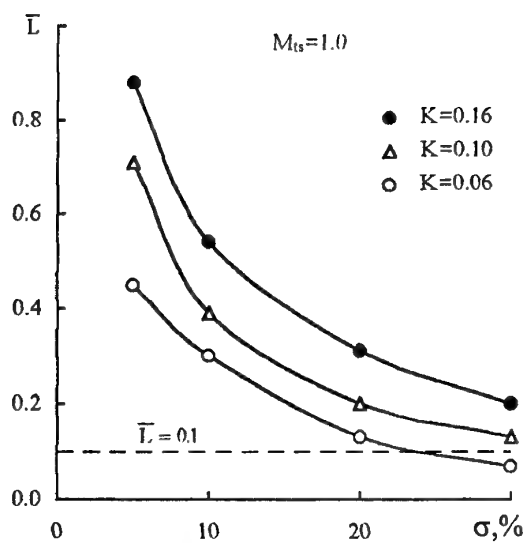


Figure 7. Relative length of "suction diffuser", \bar{L} , as a function of wall permeability coefficient σ for certain values of suction flowrate factor K .

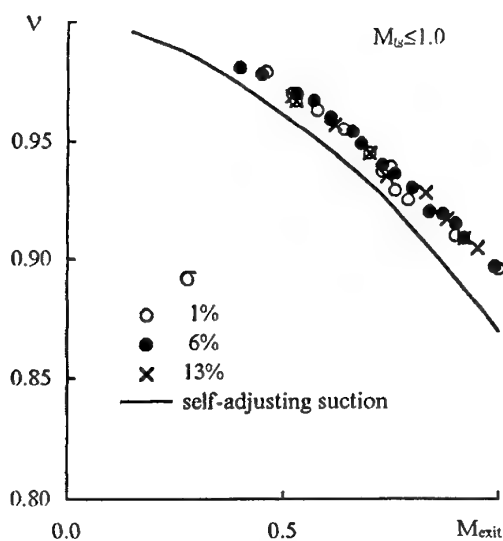


Figure 9. Total pressure recovery coefficient v vs. test section exit Mach number M_{exit} .

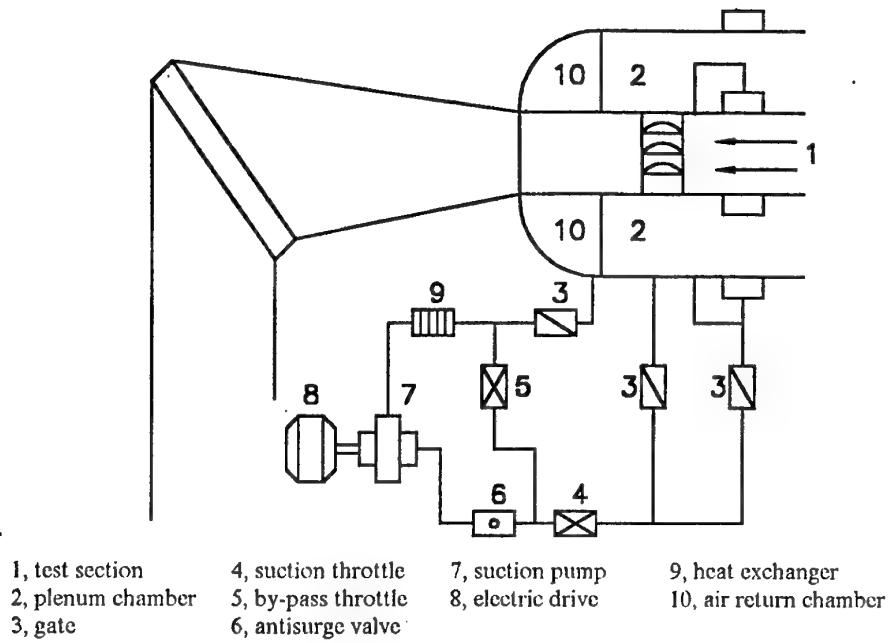


Figure 10. Schematic of TsAGI T-128 wind tunnel air section system

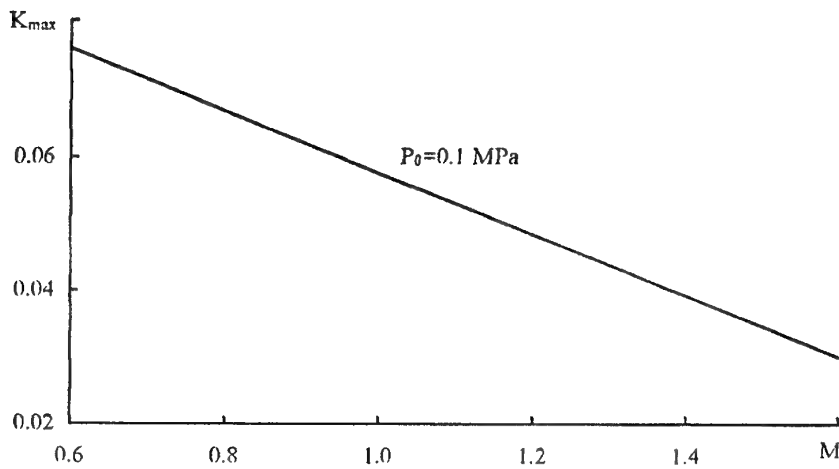


Figure 11. Dependence of maximum suction flowrate factor K on test section Mach number

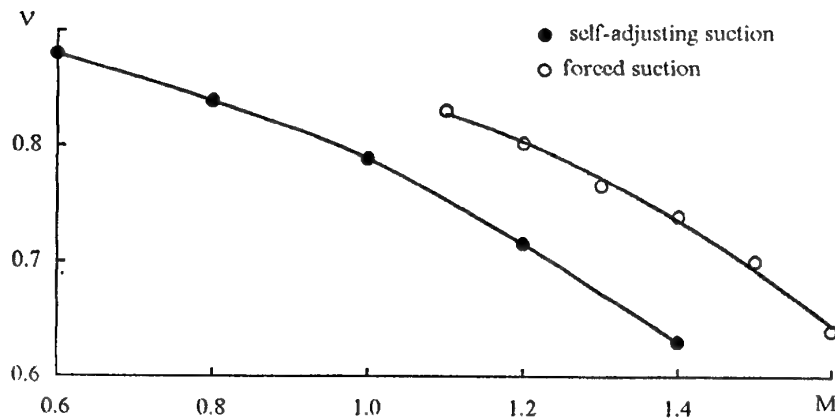


Figure 12. Total pressure recovery coefficient v as function of Mach number M in test section with self-adjusting suction and forced suction from plenum chamber.

ADAPTIVE SLOTS: AN ALTERNATIVE CONCEPT TO REDUCE WALL INTERFERENCE

J. Quest
ETW GmbH
Ernst - Mach - Str.
D - 51147 Köln, Germany

W. Nitsche
Technical University of Berlin
Marchstr. 12
D - 10587 Berlin, Germany

A. Mignosi
Centre d'Etudes et de Recherches de Toulouse
2, avenue Edouard Belin
F - 31055 Toulouse cedex, France

SUMMARY

An alternative concept to reduce wall interference in wind-tunnel testing by means of adaptive slots is presented and its benefits are highlighted by means of experimental as well as numerical investigations. The qualification of the 3d-NAVIER-STOKES code employed for the parametric numerical investigations is demonstrated by comparison with Laser 2-focus and surface pressure measurements.

The effectiveness of a single central adaptive slot is proved for a convex profile as well as for a body of revolution by referencing the results to 2d wall adaptations.

For a simplified 3d slot adaptation featuring 6 slots on top and bottom wall each, better agreement with the freestream solution than for the 2d wall adaptation was achieved.

1. INTRODUCTION

The benefit of the adaptive wall technique for the reduction of wall interference in wind-tunnel testing has been impressively and successfully demonstrated since more than a decade [1, 2]. Nevertheless, its application is nowadays still restricted to small size test-sections, mainly of research facilities.

Hence, it was obvious that adaptive wall aspects should also be considered during the design phase of the European Transonic Windtunnel (ETW). But the test-section dimensions of $9 \times 2.4 \times 2$ m (length x width x height) combined with the tunnel operation limits of 450 kPa in pressure and down to 100 K in temperature would have required large flexible plates and powerful actuators with high load capabilities and suitable for cryogenic operations. Consequently, only an option for a future retrofit of adapted walls was set up at that time.

The present design of ETW consists of a slotted wall test-section with six slots in the floor and ceiling and four on each side-wall, the latter currently closed for full

model testing. Machined inserts define the slot shape providing a low flexibility for an individual adaptation. The half model test capability at ETW (available in 1998) will require the models to be attached to the top wall. Thus, wall adaptations would preferably be provided on the side-walls of the test-section. In the light of these aspects and the additional request to generate fast and easily a solid wall configuration a new adaptation concept employing adaptive slots instead of adaptive walls has been developed.

2. THE ADAPTIVE SLOT PRINCIPLE

The basis of the so called 'Adaptive Slot' concept is closely allied to the 'adaptive wall' principle. The principle is sketched in fig. 1.

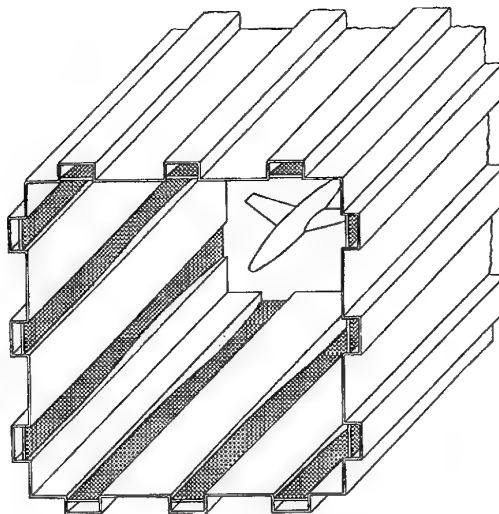


Fig. 1 Sketch of a test-section with adaptive slots

As opposed to the 'Adaptive Wall', where due to the streamlining process additional cross-section area is provided by a deflection of a complete wall, the 'Adaptive

Slot offers the capability to adjust the floor of each slot individually, hence, allowing a three dimensional adaptation by reducing the residual effects over the span of lifting models. Referring to a slotted rectangular test-section as in ETW, the slot channels (i.e. the region behind the gaps in the walls which is typically open to the surrounding plenum) may be bounded by the backup structure of the walls while the floor of each channel consists of a flexible plate. Small size hydraulic, pneumatic or electric actuators manage the longitudinal deflection of each plate to achieve the required shape being requested for the specific model and its test condition to minimize wall interference. A use of sliding seals on the plates will protect against lateral gas exchange between two adjacent channels and render the plenum superfluous.

With respect to a possible modification of existing slotted tunnels cost for implementation or retrofit will be lower than for adaptive walls because the main supporting structure of the test-section can be kept. The resulting cancellation of classical high energy slot flow should also cause a reduction in circuit losses and aerodynamic noise.

3. THE VALIDATION CONCEPT

3.1 The Strategy

Attempting to demonstrate that a concept for 3-dimensional adaptation works satisfactory for any test-object and tunnel configuration would be unrealistic. Even after the introduction of major simplifications and restrictions there are too many parameters left which might have an influence on the final solution (e.g. number of slots, longitudinal slot shape, slot width to depth ratio, slot spacing, slot / wall or slot / slot interference). Consequently, the majority of parametric investigations had to be carried out by means of a qualified Navier - Stokes code. While the flow solver itself is validated by comparison with wind-tunnel measurements, calculations for adapted slot configurations are referenced to results obtained for 2d adaptive wall solutions.

Future work is planned to modify the test-section of a research facility by an implementation of 'adaptive slots' to perform the final experimental proof.

3.2 The Tool

The presence of complex 3 dimensional flow fields clearly favoured the use of a 3d Navier Stokes Code. The Department of Aeronautics and Astronautics at the Technical University of Berlin in Germany, which performed all numerical calculations on the presented subject, operates the flow solver TASCFLOW3d. Generally, it solves the time-averaged Navier-Stokes equations by application of a simultaneous treatment of pressure and velocity terms. For turbulent flow quantities a standard k- ϵ turbulence model is used.

The numerical grid generation is favourably of the elliptical type offering the application of block-structured non-orthogonal grids with embedding and attaching

functions. Storing all dependent variables at each grid node this single cell storage simplifies the implementation of the discretization scheme and provides a strong conservation of momentum. The discretization of the calculation domain is performed by a finite element (FEM) based finite volume (FVM) method combining their individual advantages of high geometrical flexibility (FEM) with accurate conservation property (FVM).

A fully implicit, incomplete lower / upper factorization solver manages the relaxation scheme employing an unstructured grid data structure. Acceleration capacity for the solution process is available from an algebraic multigrid method, which is capable of generating automatically adequate equations for grid crudeness without requiring any information about local grid geometry or structure.

4. THE VALIDATION PERFORMANCE

4.1 Validating the numerical Code

The numerical flow solver was considered to be suitable for the analytical purpose if the static pressure distribution calculated on a test model and its surrounding test-section walls was in acceptable agreement with the relevant measurements. It was also expected that the development of flow in the environment of slot(s) could be simulated correctly to understand the aerodynamic background.

4.1.1 The experimental Setup

The experimental basic investigations and the 2d tests were carried out in the transonic wind tunnel of the Technical University of Berlin. Taking the benefit of the adapted wall capability of the quadratic test section sized 150 x 150 mm, the floor was modified to form a single central slot 40 mm wide and framed by two identical slats as presented in figure 2. For the model tests a convex profile with 100 mm chord and a thickness of $d/2 = 6$ mm (alternatively $d/2 = 10$ mm) was attached to the ceiling at test section centre.



Fig. 2 Test -Section of TU - Berlin tunnel with single slot

Longitudinal rows of pressure taps on each slat, on the bottom of the slot as well as on the ceiling provide wall pressure distributions.

While the slot width is always kept constant over the length

of the test-section, the depth contour follows a cosine function generating zero deflection at both ends and a maximum of 25 mm at the centre. To compensate for the boundary layer growth and to achieve a zero axial pressure gradient, top and bottom wall were set to a slight divergence. The resulting test-section geometry used for numerical and experimental basic investigations is given in figure 3. At five axial positions local flow field measurements were performed with a Laser 2-focus anemometer indicated by 'Plane', whereas 'BL' stands for the locations of boundary layer surveys to determine the velocity profiles.

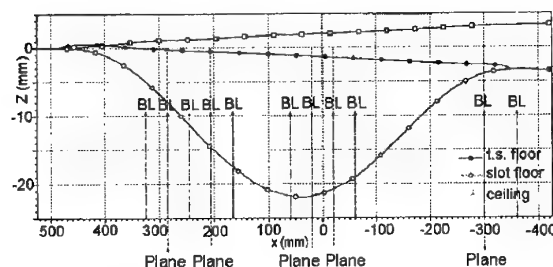


Fig. 3 Basic test-section geometry and location of L2F surveys

Realistic boundary conditions for the flow field calculation were provided by the Mach number distribution in the wind tunnel nozzle and the turbulence profile at test-section inlet.

4.1.2 An empty test-section with a single slot

The single slot configuration described was numerically simulated by about 70000 control volumes representing half the test-section. At the downstream boundary of the calculation domain a homogeneous static pressure distribution was assumed.

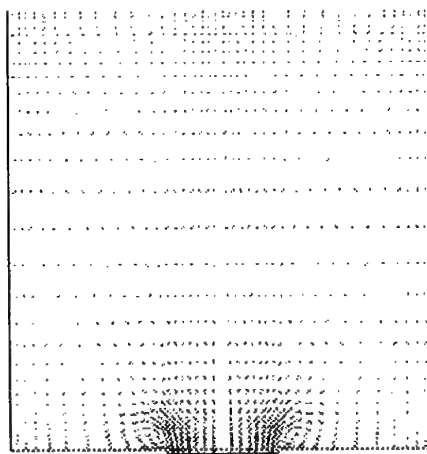


Fig. 4 Vector plot of calculated velocities for returning slot flow

Having achieved a stable converged solution when running the code on an IBM-RS 6000/370 computer,

calculation and measurements were in excellent agreement and allowed a study of the development of slot flow. This is characterized by an inflow into the slot in the first half of the test-section followed by an outflow downstream of the location of maximum slot depth. While the entering flow only slightly affects the environmental main flow, two strong counterrotating vortices are generated by the returning slot flow as seen in figure 4 by means of a vector plot. The strong vortex shifts the region of low turbulence towards the test-section side walls. Resulting major disturbances of the main flow are traceable up to about 20% of test-section height ($z = 25$ mm).

A comparison between the measured and calculated relevant Mach number distributions at the same axial position is given in figure 5. It has to be pointed out that due to the limited availability of windows no L2F measurements could be performed within the slot. Additionally, due to the 2-focus principle no information about the third (the lateral) velocity component can be provided.

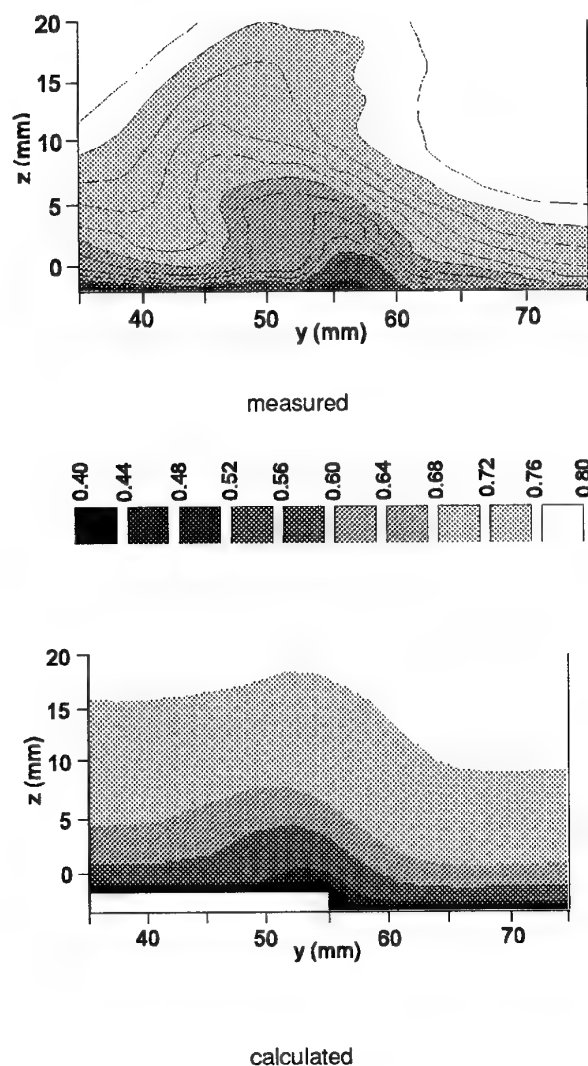


Fig. 5 Mach number comparison L2F measurement - NS calculation for a slot region

Despite these restrictions a qualitatively good agreement can be stated. The Iso-Mach lines in the segments presented are based on an L2F survey at about 250 locations while the numerical results, showing smoothed and laterally more stretched constant Mach areas, rely on 860 volumes representing the test-section and about 100 volumes for the slot itself.

4.1.3 A convex profile being attached to the roof

After acceptable agreement was achieved between experimental and numerical results for an empty test-section configuration with and without a slot, the comparative work was extended to more practical test cases including a model. Beside the objective of validation of the numerical code also for more complex configurations it was aimed at an investigation of mutual interference between slot and test object. To start with a simple case, a symmetrical 2d convex profile (max. thickness $d/2 = 6$ mm) was attached to the top wall. Further studies were carried out using a similar profile with $d/2 = 10$ mm, but operated at a reduced freestream Mach number of 0.7 to avoid supersonic flow areas.

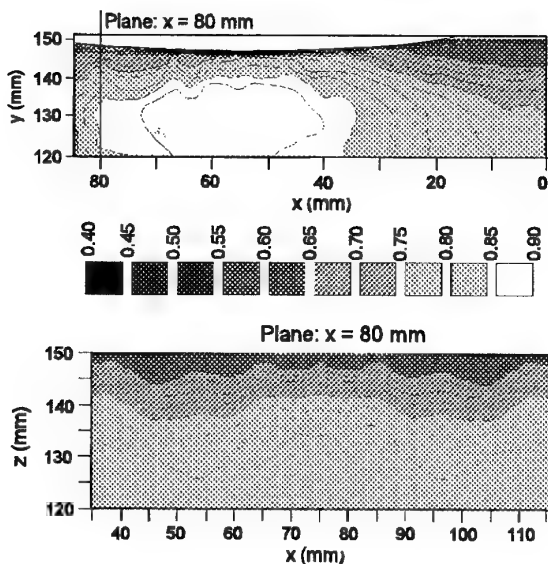


Fig. 6 Measured Mach number distribution around a convex profile ($d/2=6$ mm) for a floor with a single slot (Mach = 0.78)

The Iso-Mach lines based on L2F measurements are presented in figure 6 and document the 2d flow character in the vicinity of the profile. There seems to be a slight slot generated effect at $y = 55$ mm (and $y = 95$ mm), but it should be noted that for the configuration considered here the emphasis is on numerical / experimental comparison for code validation and, therefore, the slot depth was not adapted for interference free flow around the profile.

Such comparative results for measured (by pressure taps) and calculated surface pressures in the vertical plane of symmetry are given in figure 7.

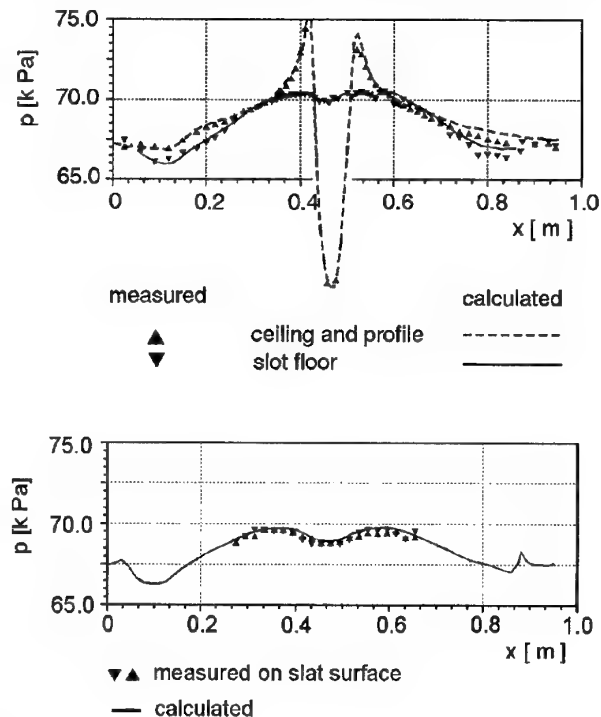


Fig. 7 Measured versus calculated surface pressure distributions

An agreement in static pressure of better than 1% is achieved everywhere. The largest discrepancies exist at the beginning and end of a slot where the geometry is complex and in the separated flow region close to the leading edge of the profile. Local grid refinement which was applied at a later stage led to remarkable improvement of results in these areas. The very satisfying accordance on the slot floor and on the profile surface was considered to qualify the numerical code as suitable for the intended analytical investigations.

4.1.4 Side - wall effects

One aspect not yet considered is the possible interference between slot generated effects and the test-section side walls. It is obvious that with justifiable expenditure such a configuration could only be investigated numerically. Figure 8 documents the outcome of a parametric study for a non adapted slot of increased depth. A deeper slot should provide additional area for compensation and, hence, cause conditions to be expected from an overcompensation by an adaptive wall. In fact, a stronger vertical Mach number gradient is generated in the test-section and the returning slot flow develops more distinct vortices. Nevertheless, even at this sensitive cross section area just below the maximum thickness of the profile and at the deepest location of the slot, all 3d effects are rapidly cancelled out in the vicinity of the slot and do not affect the profile environment. It clearly turns out that the three dimensional flow behaviour in the test - section is introduced by the side-walls and not by the slot.

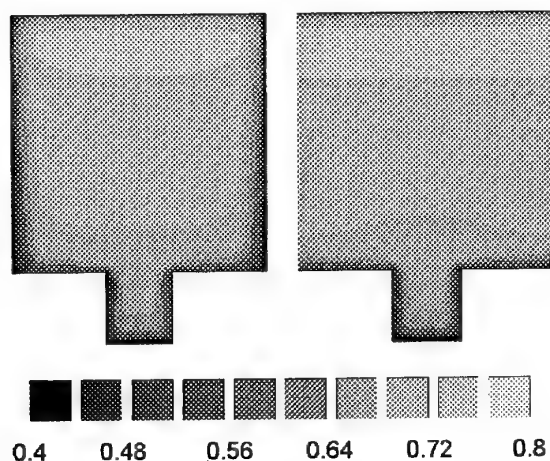


Fig. 8 Side-wall effects on Mach no. distribution ($Ma_{\infty} = 0.78$)

4.2 Single Slot Adaptation for a 2d convex profile

The adaptive wall techniques for two dimensional aerofoil testing rely on the principle of wall streamlining. In our particular case for a profile being attached to the top wall, bottom wall interference should be eliminated by adjusting the flexible bottom wall in a curvature so that the effective contour follows a streamline in the infinite flowfield. This is achieved by driving the flexible wall to a shape where its static pressure distribution (measured inside the test-section) matches the one computed along the flexible wall boundary of imaginary (exterior) flow which completes the infinite flowfield.

Contouring the wall, a process usually referred to as wall streamlining or wall adaptation, is made by reference to the test-section alone, hence, independent of any knowledge of the model geometry of the flow around it. In practice the adaptation is often achieved by iterative wall adjustment [3]. Each iteration then requires test-section measurements combined with theoretical calculations to ascertain whether the desired flow conditions have been reached and to determine necessary adjustments to the shape of the flowfield.

An alternative adaptation procedure was proposed by AMECKE [4] known as single step method. Based on a solid wall test-section measurement the required wall shape for interference free conditions is now calculated and subsequently adjusted in one step. From a comparison of the two measurements the remaining interferences (residua) can be calculated and used for final corrections. In this way 2d wall adaptation is performed for 2d models in the tunnel of TU Berlin.

After a comparison of non adapted empty tunnel measurement and calculation which showed excellent agreement, the theoretically required 2d - shape for the test-section floor was calculated. For the resulting geometry the Navier Stokes flow solver was applied. In

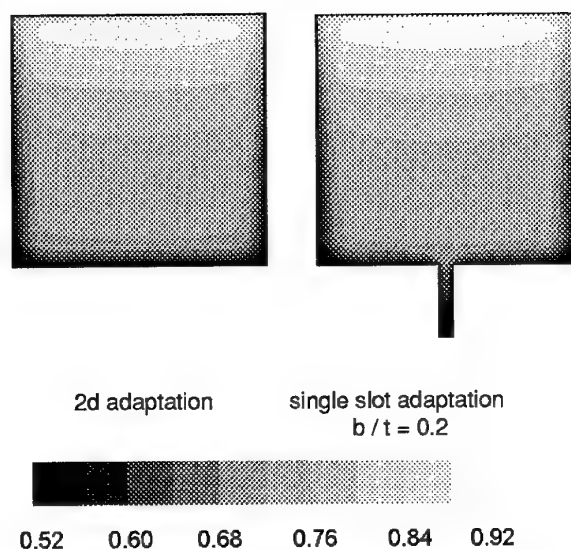


Fig. 9 Mach number distribution in the cross-section at maximum profile thickness ($Ma_{\infty} = 0.7$)

the upper part of figure 9 the relevant Mach number distribution is presented for the cross section at the maximum thickness of the convex profile.

As outlined above the static pressure distributions on the floor and profile surface are essential for the judgement of remaining interference. In case of a slot adaptation the lateral static pressure distribution will be different on the test-section floor and within the slot. Therefore, a transfer function has to be developed to convert local or laterally averaged static pressure into relevant slot floor deflection or adequate slot depth if the slot width is kept constant. As no suitable rule is available from theory it was decided to apply an area rule for the first approach which is effectively redistributing the deflection of the 2d adapted floor at each axial position into a slot with given and constant width. Thus, the resulting axial slot depth distribution is proportional to the vertical elongation of a 2d wall.

Calculated Mach number distributions in the central cross section as well as the plane of symmetry of the test-section are presented in figures 9 and 10.

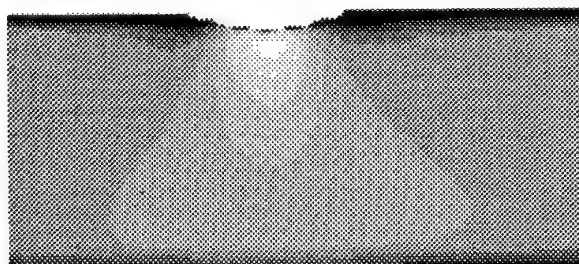


Fig 10a

2d adaptation

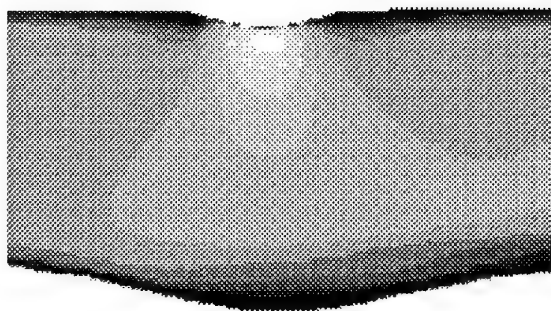
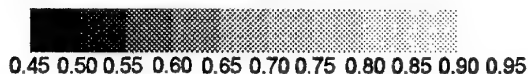
Fig 10b single slot adaptation $b/t = 0.2$ 

Fig. 10a,b Mach number distribution in the plane of symmetry of the test-section

In the vicinity of the profile the Mach number contours show no significant difference between the 2d adapted wall and the adapted slot configuration. Obviously, low energy material is concentrated on the floor of the narrow deep slot but all individual slot generated effects on speed seem to be cancelled out at a test-section height of less than 10%. Figure 9 gives even the impression of a reduced low speed area in the lower corners of the test-section.

A more sensitive indicator for finding differences is the profile surface pressure distribution. Hence, the relevant calculated distribution in the plane of symmetry is given in figure 11.

In the upper part of the figure the convex profile is sketched, indicating the location of maximum thickness at station $x = 0.465$ m.

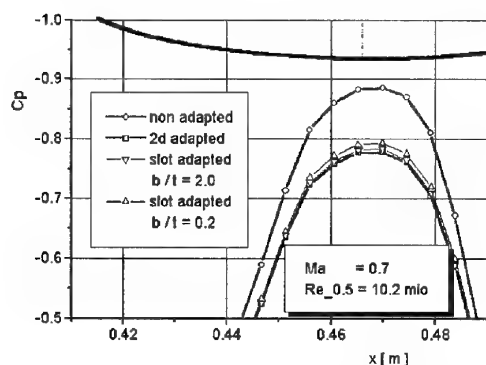


Fig. 11 Pressure distribution on the convex profile (plane of symmetry)

Where the C_p -distribution peaks, the agreement for all considered types of adaptation is better than 0.015 which is equivalent to a difference in Mach number of $\Delta M \approx 0.005$. For comparison the non adapted case (top bottom wall slightly divergent for boundary layer compensation and zero axial pressure gradient and no slot) is also presented. Related to the 2d adaptation a Mach number increase of $\Delta M = 0.04$ is to be implied.

The basic investigations were performed with a relatively wide slot generating a maximum width to depth ratio (b/t) of about 2 (see fig. 2). It was natural to check the effect of this parameter on the level of achievable wall interference cancellation and whether a lower limit exists in practice. Also in the light of possible modifications of existing slotted wall facilities it is more reasonable to consider low ratios to make allowance for existing constraints in the test-section structure. ETW has the capability to realize a maximum slot width of 90 mm only by removing inserts. Combined with the backup structure of the top / bottom walls deep channels with ratios down to values of 0.2 can be formed.

The calculated effect of a simple variation of slot geometry is visible in figure 11. Referring to the solution for the adapted wall, narrowing the slot causes a deterioration of the adaptation. This may be explained by the fact that the slot is generated by a redistribution of the individual axial cross-section area whereas the flow reacts on an effective area. Entering a slot a jet contraction takes place comparable to the development around an orifice. The introduction of a suitable contraction-coefficient in the slot design and consequently an increase in slot cross-section area might remove the existing discrepancies.

4.3 Single slot adaptation for a 3d model

To extend the validation to three dimensional test objects a body of revolution was selected. A suitable candidate was found in the "ETW Transition Body" (ETB), a model which is designed to study the shift of the boundary layer transition location over a wide Reynolds number range.

4.3.1 Experimental efforts

While the ETB was undergoing being tested for design validation in the T2 cryogenic wind-tunnel of ONERA - CERT in Toulouse, France, an excellent opportunity was given to obtain body surface pressure distributions for comparison with numerical calculations. As T2 is a 2d adaptive wall facility with a test-section of 0.4×0.4 m, the transition body with its maximum diameter of 100 mm generates a blockage of about 5 %, hence, representing conditions to demonstrate the benefit of the adaptive wall / slot technology to reduce wall interference. The experimental setup showing the ETB mounted in the test-section of T2 is given by figure 12.

In T2 the required wall setting for an adaptation is achieved by an iterative procedure. Based on a comparison between calculated and measured static pressure distributions the final wall shape is approached step by step until the requested accuracy is obtained. The starting configuration always reflects the empty test-section with zero axial pressure gradient which is achieved by a top and bottom

wall divergence of 0.17 deg, while both side walls are non flexible and parallel. Hence, it was natural to select this configuration for the so called "non adapted" case.

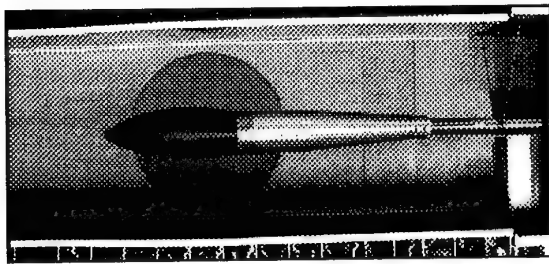


Fig. 12 ETW Transition Body (ETB) in the test-section of T2 wind-tunnel (ONERA - CERT)

For the numerical representation this test-section geometry including the upstream nozzle and the downstream second throat area was transmitted to TU Berlin. Additionally, striving for high quality results the turbulence distribution and the boundary layer profiles at test-section inlet were also provided. The strut and the suspension wires for model support and attachment which are visible in figure 12 have been neglected in the application of CFD. Taking the benefit of the top / bottom and right / left symmetry of the considered arrangement the calculation domain was reduced to a quarter of the test-section allowing a finer numerical grid and a better representation of the individual geometry.

Of course, the experimentally determined wall shape of the T2 tunnel could also be used as input for the NS - calculation of the 2d adapted wall case. But it was decided to take the challenging opportunity to perform theoretical calculations prior to a test for subsequent comparisons. More difficulties were caused by the fact that TU Berlin operate a different procedure for 2d wall adaptation in their tunnel. Here, a single step method developed by HOLST [5] is usually applied to determine the wall setting to minimize interference. The method allows the calculation of the required final wall shape in one step based on the measured or calculated wall pressure distribution obtained for the non adapted test-section. Remaining interferences can be estimated from comparison of the measurements of the adapted and non adapted configuration. Consequently, the flow field for the ETB installed in T2 was at first calculated for the non adapted case. The resulting pressure distribution was fed into the HOLST code to determine the wall shape. The obtained contour defined subsequently the top / bottom wall shape for the numerical simulation of the transition body installed in T2 with a 2d wall adaptation.

A comparison of measurements with calculations is presented in figure 13 for the static pressure distributions on the ETB surface. The body starts at $x = 0$ reaching its maximum thickness at $x = 0.175$ m and intersects with the cylindrical sting at $x = 0.248$ m. A perfect agreement between measured and calculated pressures can be seen up to the point of

maximum surface velocity. The deviation at $x = 0.171$ m is due to an imperfection on a pressure tap. Approaching the joint between body and sting, the existing disagreements might be due to numerical boundary layer treatment.

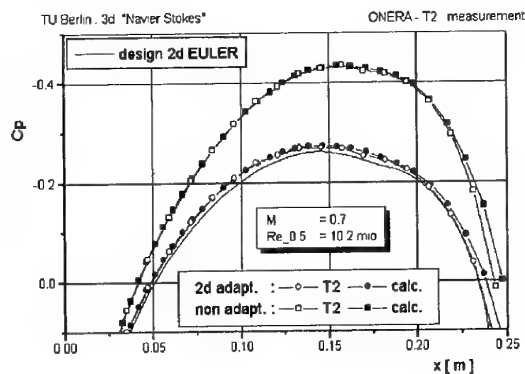


Fig. 13 Comparison of measured / calculated body surface pressure distribution

4.3.2 A single Slot versus 2d Wall Adaptation

In the same way as for the convex profile the axial 2d wall deflection was transformed into the relevant depth of a single central slot on the top and bottom wall by applying the area rule (see chapter 4.2). A slot width to depth ratio of 0.2 was selected for this numerical test case. By applying the flow solver on the isolated ETB, i.e. all walls removed, the interference free condition could be included in the considerations and used as a reference for subsequent parametric studies.

An extract from the resulting body surface pressure distribution is provided in figure 14. In the environment of maximum diameter a nearly 100% agreement is achieved between 2d - design and the fully 3d viscous solution. Here, the 2d wall adaptation results in a C_p - drop of 0.012 (equivalent to $\Delta M = 0.004$) whereas about twice this value is achieved for the single slot.

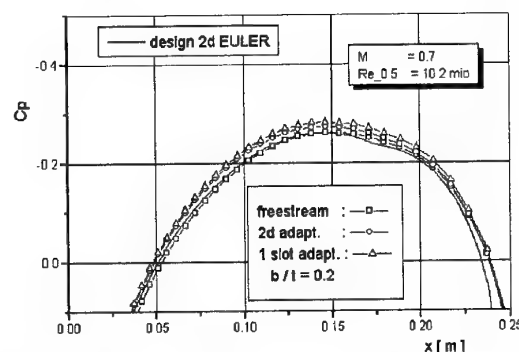


Fig. 14 calculated body surface pressure distributions for different configurations

Referring to chapter 4.2 it is assumed that the narrow slot does not provide sufficient effective cross section area due to an increased internal low energy flow development. The

outlined flow situation is clearly visible in figure 15 which presents Mach number contours in the cross section at station $x = 0.175$ m.

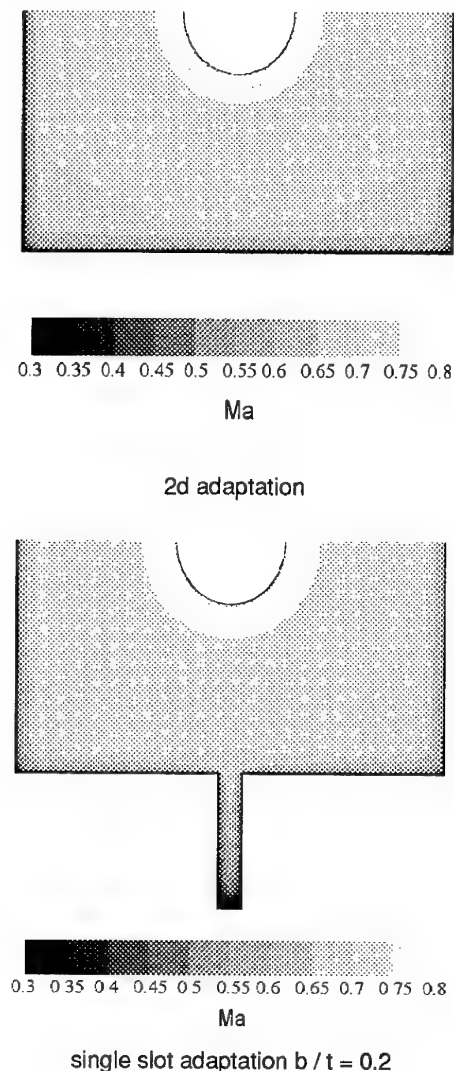


Fig. 15 Mach contours for the ETB in T2 in the cross section at $x = 0.175$ m

An extended low energy flow region can be identified in the lower part of the slot offering less effective area for the compensation of the body in the test-section. The individual slot generated effects are limited to the vicinity of the slot and do not reach the main flow and even less the region around the test object.

4.4 Multislot Arrangements

For a demonstration of the full advantage of the adaptive slot concept it would be desirable to see the capability of individual slot adaptation in a multislot test-section configuration. Increasing the number of slots means at first the creation of additional variable parameters concerning the geometry of an individual slot and its arrangement in a test-section. For the numerical representation fine grids have to be

generated leading to extended computer CPU-times to achieve converged solutions.

As the origin of the adaptive slot concept is in close relation to ETW, it was natural to select a configuration which might be similar to a possible realization by retrofit in the existing test-section of the facility. Based on the maximum slot width of ETW the bottom wall was scaled down to the dimension of the T2 test-section floor. Consequently, the relevant slot width to depth ratio of 0.2 was also kept. With the ETB on the centreline generating about 5 % test-section blockage, two different slot arrangements were numerically considered.

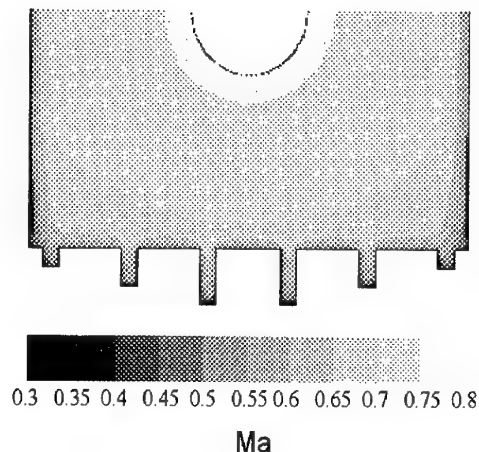


Fig. 16 Mach Number Contours in the Cross section at $x = 0.175$ m for a multislot arrangement with slot arrangement with linear slot depth distribution

At first, a configuration with 6 identical slots on floor and ceiling was investigated. At each axial position the total cross-section area of all slots reflects the wall elongation being calculated and experimentally determined for the case of 2d adapted walls. Secondly, the latter total slot cross section area was kept but this time the slot depth was varied laterally in a linear way. The resulting configuration per wall is characterized by two deep slots ($b/t = 0.33$) in the middle of floor and ceiling while the two slots with minimum depth ($b/t = 1$) are located close to the side walls of the test-section.

The calculated Mach number contours and the test-section configuration for the latter multislot (12 slots) arrangement are presented in figure 16.

It is worth noting that now there is no central slot anymore just below the body. The selected "random" distribution of slot depth over the test-section width causes quite different aerodynamic loading to the individual slots. High speed flow penetrates deeper into the more central channels but boundary layers seem also to grow faster over there. No slot generated effect on the flowfield around the test object is to be seen.

The calculated surface pressure distributions on the transition body are presented in figure 17. Assuming that the freestream solution reflects the interference free condition, the largest deviation in Mach number at peak

velocity location ($x = 0.15 \text{ m}$) is of about $\Delta M = 0.008$ for the 2 slot (central slot on top and bottom) configuration. Maximum speed determined for the classical 2d wall adaptation is higher by 1.5 m/sec compared to the reference case. The best agreement was achieved with six slots on floor and ceiling each, the test-section setup given in figure 16. The calculated deviation of $\Delta M = 0.002$ is equivalent to a difference in flow speed of less than 1 m/s for a freestream velocity of 243 m/s, i.e. 0.3 %.

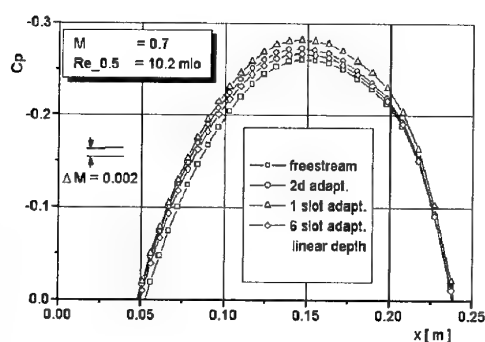


Fig. 17 Calculated body surface pressure distributions for 2d and 12-slot adaptation

Some checks have been performed to ensure the independency of the numerical solutions from grid generation and refinement. Accepting some inaccuracy in CFD which is natural, it has to be pointed out that the given objective was the validation of the adaptive slot concept mainly by comparisons to a classical 2d wall adaptation. This target is successfully met.

5. CONCLUSIONS AND FUTURE WORK

Numerical investigations using a 3d Navier-Stokes code have successfully demonstrated the validity of the adaptive slot concept for reduction of wall interference. The method offers the additional capability for an individual 3d-adaptation if a sufficient number of slots can be provided.

No significant influences from the slots onto the flow field around the test object could be detected. Variations of the slot width to depth ratio over the range of $0.2 < b/t < 2$ have been analyzed. The use of deep narrow slots seems to require more specific consideration to take into account jet contraction and viscous effects.

For practical application, the simple area rule must be replaced by a suitable transfer function to correlate the pressure distribution on the walls and on the bottom of the slot floors with the relevant deflection of each floor to achieve interference free flow around the test object. Alternatively, a modified single step method might be applicable.

An experimental validation of the adaptive slot concept by modifying the test-section of a suitable research

facility is under consideration.

6. ACKNOWLEDGEMENTS

The authors have pleasure in acknowledging the helpful support of Mr. I. Wallbruch and Dr. M. Swoboda of TU Berlin for performing and postprocessing of the numerical investigations.

Appreciation is also expressed to Mr. D. Caruana of ONERA - CERT for his technical assistance and helpful discussions on the experimental work on the transition body.

7. REFERENCES

- [1] "Adaptive Wind Tunnel Walls: Technology & Applications", AGARD - AR - 269, 1990
- [2] S.W.D. Wolf, "Adaptive Wall Technology for Improved Wind Tunnel Testing Techniques - A Review", Prog. Aerospace Sci., Vol. 31, pp. 85-135, 1995
- [3] U. Ganzer, Y. Igeta, J. Ziemann, "Design and Operation of TU - Berlin Wind Tunnel with Adaptive Walls", ICAS paper 84 - 2.1.1, 1984
- [4] J. Amecke, "Direct Calculation of wall Interferences and Wall Adaptations for 2d-flows in wind tunnels with solid walls" (in german), DFVLR - FB - 85 - 62, 1985
- [5] H. Holst, "Verfahren zur Bestimmung von 3d Windkanalinterferenzen und Wandadaptationen mit Hilfe gemessener Wanddruecke bei kompressibler Unterschallstroemung", DLR - FB 90 - 46, 1990
- [6] ETW GmbH, "Windtunnel", Patent Application P 42 14 991.6 - 51, 1993 and German Utility Application G 92 18 804.4, 1995
- [7] J. A. Tizard, "ETW User Guide", Feb. 1995
- [8] E. Wedemeyer, L. Lamarche, "The Use of 2d-adaptive Wall Test-Sections for 3d-Flows, AIAA-paper 88 - 2041, May 1988

PROGRESS IN DETERMINING WALL-INDUCED INTERFERENCE IN SLOTTED-LINER WIND TUNNELS USING MEASURED WALL CONDITIONS

by
M.M. Freestone and D.M. Sykes
City University, Northampton Square
London EC1V 0HB
United Kingdom

SUMMARY

Further work and analysis relating to a previously proposed scheme for determining slotted-liner wall-induced interference at subsonic speeds are presented. The scheme utilises measurements of wall (slat) pressures and values of the velocity-component normal to the liner measured in the plane of the liner along a slot centre line. This flow component is measured by a probe, and longitudinal distributions of the normal velocity are obtained both from traverses and multiple point measurements. With a three-dimensional test configuration, measurements would be made on each slat and slot, but in the present tests with a two-dimensional aerofoil the slats and slots in each wall (roof and floor) are assumed to behave equally. Assessment of the results of utilising the scheme is based on comparisons of aerofoil pressures at corrected conditions of Mach number and (three-quarter chord) incidence. More detailed assessment by other means is suggested. The scheme appears reliable for the range of test conditions undertaken, and these more than adequately cover conditions likely to be found in the large three-dimensional test facilities for which the method is intended.

1. NOTATION

a	slot width over parallel portion of slot
C_L	lift coefficient
C_{Lc}	corrected lift coefficient = (Lift per unit span) / $\left(\frac{\gamma}{2} p_c M_c^2\right)$
C_p	pressure coefficient = $(p - p_{ref}) / \left(\frac{\gamma}{2} p_{ref} M_{ref}^2\right)$
C_{pc}	corrected pressure coefficient = $(p - p_c) / \left(\frac{\gamma}{2} p_c M_c^2\right)$
c	aerofoil chord
d	lateral spacing between slots in roof and floor
H	working section height, at model mid-chord
h	slot depth
k	vortex strength used in two-dimensional theory
L	slot length
M_c	average of M_{cl} over aerofoil chord
M_{cl}	local Mach number, corrected for wall interference, on test section centre-line
M_{probe}	local Mach number indicated by three-hole probe
M_{ref}	reference Mach number - related to p_{ref} and p_0

Copyright

©

City University
1996

M_∞	Mach number in undisturbed flow (relates to VGK calculations of free-air flows)
p	local static pressure
p_c	static pressure corresponding to M_c and p_0
p_{ref}	static pressure at reference pressure tap
p_0	wind-tunnel total pressure
R	Reynolds number based on aerofoil chord
s	distance of probe centre-line from plane of floor
U_{ref}	axial velocity corresponding to M_{ref}
u	velocity component in x -direction
v_n	velocity normal to plane of floor, positive into the test section
v	velocity component in y -direction
x	axial coordinate along test section centre line, with origin at leading edge of aerofoil
y	coordinate normal to x , positive upwards
α_c	aerofoil incidence, corrected for wall interference, evaluated at aerofoil three-quarter-chord position
α_g	aerofoil geometric incidence (angle relative to x direction), positive nose-up
α_i	value of α_{il} at aerofoil three-quarter chord position
α_{il}	local induced aerofoil incidence, due to wall interference
β	$(1 - M_c^2)^{1/2}$
γ	ratio of specific heats
ρ	local density of air
ρ_{ref}	density of air at reference pressure and temperature

2. INTRODUCTION

Earlier work carried out at City University with the object of establishing a method for the accurate determination of the interference velocity field in a slotted-liner transonic wind tunnel has been reported in Refs. 1-3. This earlier work developed a method of utilising wall pressure measurements and slot flow measurements to yield the conditions of the effective inviscid-flow (EIF) at the test section boundary, and then used these conditions with the Ashill and Weeks method (Ref. 4) to find the wall-induced interference flow. It was shown that the proposed method could be both feasible and accurate for two-dimensional and three-dimensional tests. By avoiding the need for specific model-flow representation, and also by avoiding the need to represent the slot-flow by either an analytic or empirical scheme, the proposed approach based on boundary measurements has several attractions. It is essentially a post-test method of interference determination, which may readily be automated and incorporated into the wind-tunnel analysis software, so as to be used on-line. With results established from a number of typical cases, the method could also be used predictively, prior to testing.

A major reservation associated with the introduction of the procedure to large slotted-liner facilities is perceived to be a doubt about the universal validity of relating the local EIF normal velocity to the slot-flow normal velocity in the way that would be appropriate and accurate in inviscid flows. (The relation used is actually applied to normal mass flux rather than normal velocity.) This doubt arose from the work of Refs. 2 and 5, which showed that in certain situations, where slot flow was passing from the plenum chamber back into the working section (inflow), relatively large disturbances in the near-wall flow could result, and that these disturbances would not be accounted for by use of the simple (*i.e.* direct) approach proposed. In Ref. 2 it was shown that this returning flow could be effectively amplified by a factor of about 4, in terms of the disturbance it generated in the EIF. In Ref. 3, where steps were taken to avoid strong returning flow, the direct (inviscid) relationship between measured slot normal velocity and EIF normal velocity was entirely adequate, and no difficult-to-determine amplification factor was needed.

To resolve the doubt about using the simple relationship between the slot-flow normal velocity and EIF normal velocity, it is necessary to demonstrate that there are cases with returning flow for which it is adequate, and, ideally, to show that these cases include all situations of potential interest. The consideration that this might be possible is based on the observation that the only cases so far identified where the direct approach proved inadequate occurred with two-dimensional tests where there was exceptionally large wall interference, due either to the relatively large model chord or to relatively high lift.

In the present work, a number of two-dimensional test cases are studied, and the approach is somewhat similar to that reported in Ref. 2. The same small induced-flow transonic wind-tunnel is used, and the aerofoil section employed is again the well-documented NACA0012, but in the present case the chord is smaller, being 4 inch (101.6mm), rather than the 5 inch (127mm) chord used in the earlier tests, see Figure 1. There are also a number of other important differences. In the present tests, great care was taken to make the slot-flow probe measurements

as free of aerodynamic interference as possible, and to this end the traverse system previously employed was rejected, for the majority of the tests, in favour of a number of fixed-position probe measurements. (Incidentally, fixed-position probes would be utilised in any large-scale application.)

A further new development is in the form of the three-hole flow probe employed for the slot-flow measurements. This has a geometry (see Figure 2) enabling the local (pitch) flow inclination angle to be found accurately even in flows with large rates of shear normal to the plane of the wall-liner. The probe is also relatively insensitive to yaw. Another significant enhancement is provided by measurements made with the flow probe within the test section flow, see Section 5.1.

The following Sections describe in outline the current work, and present the conclusions that may be drawn so far.

3. OUTLINE OF APPROACH FOR ASSESSING SCHEME FOR DETERMINING SLOTTED-LINER INTERFERENCE

3.1 Appropriate Range of Pressure Variations

It is important to note that the work is intended to be applied to three-dimensional testing at high subsonic speeds in large slotted-liner wind tunnels. Consequently, levels and gradients of pressure coefficient in the locality of the slotted liners of the present tests should be comparable with those likely to arise in the large facilities. A good indication of these large facility C_p levels and gradients is given in Ref. 6, where data from tests conducted on two transport aircraft configurations in the National Transonic Facility at the Langley Research Center are reported. It would appear from these tests that wall-liner C_p variations, $(C_p)_{max} - (C_p)_{min}$, of about 0.05 could be expected, with associated pressure gradients corresponding to these C_p variations occurring over a streamwise distance of about half the test section height or width. Expressed in terms of corresponding variations in p/p_0 , these amount to variations of about 0.017 in this parameter at high subsonic test Mach numbers. More extreme tests could be expected to generate variations and gradients possibly twice as high as these. These levels will be referred to again in the discussion of the present results.

3.2 Methods of Assessment

The method of assessment adopted in Ref. 2 was based on comparisons of aerofoil pressure distributions at corrected conditions with pressure distributions considered to represent free-air conditions accurately. The comparisons were made utilising the proposed scheme to correct the Mach number and incidence of the slotted-liner data. Determining what constitute reliable yardstick pressure distributions at the test Reynolds numbers and flow conditions is not a simple matter, but may be done by combining information provided by a well-established free-air aerofoil code (VGK, see Refs. 7 and 8) with test data obtained from solid-liner tests for which the wall-induced interference and corresponding corrections can be found highly reliably. This method of assessment is again utilised.

In the present work, a further assessment of the slot flow influence

on the test section flow is provided from data obtained from traverses made with the three-hole probe along a slot. These traverses were made at two different values of s (distance from the liner plane), in each case centrally along a slot. They revealed data for the 'decay' of normal velocity (or, more precisely normal mass-flux) with s , both for regions of outflow (flow passing into the plenum chamber) and inflow (flow passing into the test section), which can be compared with the decay expected on the basis of inviscid crossflow-theory.

In principle, a more detailed assessment of the present scheme of determining slotted-liner wall interference could be made by utilising a method similar to that of Capelier, Chevallier and Bouniol (Ref. 9, see also Ref. 10). In this approach, the free-air flow about the model, at conditions appropriate to those of a test, would be represented, and, together with measured wall pressures, could be used to provide the distributions of EIF normal velocity along the test section boundaries – at least within an arbitrary constant normal velocity. This approach is under investigation, but no data from it are given here.

4. DESCRIPTION OF EXPERIMENTS

4.1 Test Section, Aerofoil and Test Procedure

The test section of the induced-flow wind tunnel, T5, which is constructed in steel to a high standard of accuracy, is shown in Figure 1. It has slotted roof and floor wall-liners (each with four slots) and solid sidewalls. The roof and floor liners are each set at a divergence angle to the tunnel centre-line of 0.67 deg. The plenum chambers above and below the slotted liners are 80 mm deep. At the rear of the roof and floor (the re-entry section) the walls diverge rapidly and the slots widen, so providing the means by which fluid is extracted (sucked) from the plenums. Each of the slotted liners has 23 pressure taps located along a slot centre-line, and 14 pressure taps near a slot edge (along the length of the slot) on the plenum chamber side.

The aerofoil used in the current tests has a chord of 101.6 mm and has the NACA0012 profile. It is equipped with 43 pressure taps. Boundary-layer transition at about 7 per cent chord was ensured, on both upper and lower surfaces, by means of roughness strips. Tests at geometric aerofoil incidences of 0 deg, ± 2 deg, ± 4 deg were conducted. Pressures from the reference tap, contraction pitot tube, aerofoil, roof- and floor-liners, and plenum chambers were recorded by means of three 48-port Scanivalves. For runs utilising the Scanivalves, the wind tunnel would be run up to the desired reference pressure, the pressure lines would be clamped, and the tunnel then shut down. Scanning of the lines would then be carried out. Repeated scanning was employed to detect leaks. Reservoir volumes were employed in the pressure lines to ensure that the process of scanning clamped lines introduced no perceptible error.

A traverse mechanism is mounted in the lower plenum, consisting of two end supports, two guide bars, a lead-screw and a traversible block. A probe could be attached to this block, and arranged so as to traverse most of the length of one of the floor slots. Unfortunately, the traversible block presents some degree of obstruction to the lower plenum flow, and despite the use of fairings attached to the block, it was found that the flows in the

wind tunnel were slightly affected by the position of the block. For most of the tests, therefore, the traverse block was left in a fixed position (parked most forward), and the slot flow was investigated by means of the probe attached to a low-interference mount. This mount could not be traversed, but had to be re-positioned between tunnel runs. For tests employing the flow probe, Scanivalves were not used. Instead, pressures from the three tubes of the probe, and the reference pressure tap, and one other pressure tap were logged during a run, using five pressure transducers and associated 14-bit logging channels. Logging at a rate of about 15 per second for each of the five channels was done. For these tests a Mach sweep procedure was used, with the tunnel being gradually run through the desired Mach number range. For tests where the traverse was employed, the tunnel reference pressure was held as near constant as possible for the duration of each traverse.

4.2 Three-Hole Probe and Calibration

The form of the three-hole probe is shown in Figure 2. By having the inclined tubes mounted in line abreast, rather than displaced vertically, the probe is made insensitive to vertical variations in speed (*i.e.* in local pitot pressure). Inclining the faces of the outer tubes at 30 deg to the probe axis ensures that the probe can be utilised effectively at inclination angles up to 20 deg or more.

The three-hole probe was first calibrated, using the Mach sweep procedure, by holding it in a mount at a number of different inclination angles to the flow in an otherwise empty test section. The probe was calibrated both upright and inverted, thus permitting absolute flow inclination angles to be found. Some tests were made with the probe yawed, and these showed that the probe was relatively insensitive to yaw, with 5 deg of yaw producing comparable pressure changes to those produced by 1 deg of pitch. The calibrations involved measuring pressures from each of the three probe tubes individually.

It was desired to use the three-hole probe to provide data for local pressure, local Mach number and local flow (pitch) angle. Individual measurement of the absolute pressure from each of the three probe tubes provides sufficient information, when used with the calibration data, to permit these parameters to be found. The actual process of determining the parameters is not particularly simple, and involves iteration, but once the process is programmed the required parameters can be found from the measured ones very rapidly. It was estimated that the flow inclination angle could be generally be found within about 0.2 deg, with the limit of accuracy being set by the tunnel steadiness. Once local pressure, Mach number and inclination are found it is a simple matter to find other parameters, such as $\rho v_n / \rho_{ref} U_{ref}$, provided some reasonable assumption relating to the local static temperature is made. When mounted in a slot, the probe introduces some disturbance, although this is thought to be small. Clearly a smaller probe in relation to the slot width would be desirable. Work on determining the levels of disturbance produced by the probe would be of value.

4.3 Test Series

The test series conducted were as follows.

- (a) Three-hole calibration runs in empty tunnel.
- (b) Slot traverses using three-hole flow probe with aerofoil mounted.
- (c) Solid-liner aerofoil tests, in which aerofoil and liner pressures were measured. The solid liners comprised the slotted liners with the slots sealed with tape.
- (d) Slotted-liner aerofoil tests, in which aerofoil, liner and plenum pressures were measured.
- (e) Slot flow measurements with the three-hole probe mounted at a number of different positions.

In Test Series (c) to (e), reference Mach numbers in the range 0.55 to 0.8 were covered, for aerofoil incidences of $0, \pm 2, \pm 4$ deg. Only a very few tests were made in Series (b).

4.4 Accuracy of Measurements

Accuracy of the use of the flow probe has already been referred to. Errors in measurement of the pressures arise from a number of sources. It is estimated that pressures are generally measured to within ± 100 Pa. Consequently C_p is measured generally within ± 0.002 . Occasionally, because of the nature of the operation of the wind tunnel (by induced flow), pressure fluctuations arise which result in slightly anomalous values of C_p being evaluated, possibly as a result of different response rates of the pressure lines. These anomalies rarely exceed ± 0.03 in C_p .

5. TYPICAL RESULTS

In this Section some typical results from the Test Series are presented.

5.1 Traverse Tests

Figure 3 shows results from Test Series (b) for the normal mass-flux parameter $\rho v_n / \rho_{ref} U_{ref}$, for two traverses of the flow probe, one for $s = 0$ and the other for $s = 10$ mm. For these flows corresponding to $\alpha_g = 2$ deg, there is outflow over the whole of the slot length, with v_n remaining negative. The magnitude of the normal mass-flux parameter decreases rapidly as s increases from 0 to 10 mm, declining to about 25 per cent of the $s = 0$ values, although the decline is not uniform along the length of the slot. (A uniform decline would only be expected in inviscid flow if the streamwise pressure was uniform.) The inviscid crossflow theory indicates a decline in v_n to about 27 per cent of the mean slot normal velocity as s changes from 0 to 10 mm (a change in s equal to $1.25 \times$ slot width, i.e. $1.25a$). The rapid decline of mass-flux parameter with s points to the desirability of making routine measurements at or close to the plane $s = 0$, as this moderates the absolute accuracy requirements placed on the probe measurement technique.

In Figure 4, results for a case where $\alpha_g = -2$ deg are shown. Here there is a portion of the slot where the flow returns to the test section. The probe Mach number decreases markedly in this region. The traverse at $s = 10$ mm again shows the decrease in Mach number, although it is less marked, as would be expected. A similar decline in the magnitude of normal mass-flux as s increases from 0 to 10 mm is again found, even in regions where v_n is positive, suggesting that no significant disturbances are produced by the degree of returning flow present in this case.

The variation in the value of C_p as indicated by one of the aerofoil pressure taps during the course of a traverse is shown in Figure 5. The variation is seen to amount to about 0.05, and indicates that there is a degree of aerodynamic interference generated by the traverse block in the lower plenum which it would be unwise to ignore.

5.2 Solid-Liner Tests

Typical results from this Test Series are shown in Figures 6 to 10. Data for pressures on the aerofoil, roof and floor are given, expressed in terms of p/p_0 .

5.3 Slotted-Liner Tests

Typical results from this Test series are shown in Figures 11 to 15. Relative to the solid liner tests the wall pressures show significantly less variation.

5.4 Slot Flow Measurements

Results from Mach sweeps with the flow probe located at two different positions are shown in Figures 16 and 17. The relatively complex nature of the variation of the slot flow for values of M_{ref} above 0.75 is noted. The data for $\rho v_n / \rho_{ref} U_{ref}$ plotted against x are shown in Figures 18 to 22. It is not known at present if the rather odd behaviour indicated at $\alpha_g = 2$ deg is genuine or spurious, but it appears likely to be spurious. Investigation showed that the uncertainty associated with these data had a negligible impact on the calculated interference levels.

A very limited number of tests with the probe mounted in a roof slot at $x = 0$ showed closely comparable results at $\alpha_g = -4$ deg to those from a floor slot at $x = 0$ and $\alpha_g = 4$ deg. This is taken as justification for relying on data from the floor slot to provide results relevant to the roof slots also.

6. ANALYSIS OF RESULTS

6.1 Solid-Liner Tests

The first object is to apply the method of Ashill and Weeks (Ref. 4) to derive the wall-induced interference for these tests. The measured wall pressures provide the distributions of the x -component of normalised velocity (u/U_{ref}) in the EIF at the test section boundary – by use of the small-disturbance relationship. The normalised y -component is set to zero for a parallel-wall section, and to the relevant wall inclination angle in the case of a divergent or convergent section. The effect of the tunnel boundary-layer displacement-thickness variation (estimated or measured) may also be allowed for through

adjustment of the v component.

Results of applying the method of Ref. 4 to give the interference velocities on the test section centre-line are shown for two test runs in Figure 23. As expected, positive blockage is obtained. The upwash distributions are seen to compare very well with the distributions obtained from inviscid two-dimensional theory, in which the effects of the walls are represented by a series of image vortices, the strength of each vortex being $k = C_{Lc} c U_{ref}/2$. Such good comparisons give confidence that the approach of Ref. 4 yields the interference velocities accurately for the solid-liner tests.

It has been shown (Ref. 11) that, so far as the aerofoil lift is concerned, the effects of a stream with wall-induced upwash varying with x are very close to those of a uniform stream inclined at α_c , the value of the incidence (in the non-uniform stream) at the three-quarter chord position. On this basis, the lift-curve slopes, $dC_{Lc}/d\alpha_c$, may be compared with the carefully assessed results given by McCroskey (Ref. 12) for the NACA0012 aerofoil. For the lift parameter that remains almost constant with M_c (up to M_c about 0.65), namely $\beta dC_{Lc}/d\alpha_c$, the present tests yield values around 0.092 per deg, whereas Ref. 12 indicates that the best results at the relevant Reynolds numbers for this parameter are close to 0.103 per deg. The differences are probably due to the combined effects of a number of factors, including the relatively small span to chord ratio of the present model (which may result in a significant influence from the different rates of sidewall boundary-layer growth above and below the aerofoil), some influence of the roof and floor boundary layers, and effects of the transition-fixing trips. Such factors similarly affect the slotted-liner tests except for the roof and floor boundary layers which will be affected by the slot flows, so comparisons of corrected lift curves from the solid and slotted liner tests, may still be used to assess the accuracy of the corrections determined for the latter.

In Figure 24, a comparison is given between an observed pressure distribution, and the distribution predicted by the VGK code for the NACA0012 aerofoil at the corresponding (corrected) Mach number, lift coefficient and Reynolds number. The good agreement suggests that any influence of wall-induced camber on aerofoil pressure distributions (not accounted for by the use of α_c) is slight.

6.2 Slotted-Liner Tests

Again the method of Ashill and Weeks is used to determine the wall-induced interference. For the slotted-liner tests the normalised v -component at the wall liners allows for the normal velocity through the liner slots. This is done in the present analysis simply by factoring the normal flux parameter at a particular x -position (as measured by the three-hole probe at the slot centre-line in the plane of the floor liner) by the ratio of slot-width to 'slat-plus-slot' width – with allowance as appropriate for variation of this factor over the region where the slots are tapered – thus providing the laterally averaged EIF normal velocity as required by the method. Previous work (Refs. 1 and 3.) indicated that this procedure is accurate for a range of low-speed tests.

Results of applying this procedure to some of the slotted-liner test cases are shown in Figure 25. The slot normal velocity has a

significant influence on the blockage. The slots also influence upwash, but the major effect is indirect, in terms of changes that the slots produce in the wall (slat) pressures.

The corrected slotted-liner tests yield for the lift-curve parameter, $\beta dC_{Lc}/d\alpha_c$, values within a few per cent of those obtained from the corrected solid-liner tests (i.e. about 0.092 for $M_c < 0.65$), suggesting that the scheme utilised for determining the slotted-liner corrections provides upwash angle, α_i , at least reasonably accurately, and probably better than 0.1 deg for most of the tests.

Comparison of slotted-liner aerofoil pressures, at corrected conditions, with VGK calculations corresponding to the (corrected) lift coefficient (see Figure 26) also suggests that the slotted-liner corrections are being accurately evaluated by the scheme.

7. DISCUSSION AND CONCLUSIONS

In the foregoing Sections some of the test data have been presented and analysed. Further examination of the data obtained should be done, and some more tests are called for to improve upon some of the present incomplete or uncertain results. Further analysis of the data should, for example, indicate how static pressure in the slot differs from that on the slat, and allowance for this difference could be incorporated into the scheme. Roof, floor and sidewall boundary-layer effects should also be examined.

The main evidence that blockage and upwash are being accurately obtained by the proposed scheme is indirect but quite strong. Further evidence provided by traverse measurements, which relates to the nature of the slot flow, indicates that for the slotted-liner cases of the present tests, the slot flows are well-behaved, and are compatible with the simple inviscid relationship between slot normal velocity and EIF normal velocity. The flows certainly encompass most slot flow conditions likely to be encountered in three-dimensional tests, since the pressure variations of the present tests well exceed those shown in Ref. 6, with the wall p/p_0 variations even at $\alpha_g = 2$ deg exceeding 0.02. More direct evidence of the error levels with which the EIF normal velocity are being determined would however clearly be desirable, and one possible suggestion for providing this evidence (using the approach of Ref. 9) has been given. Another way is to use an aerofoil flow calculation scheme in which the (measured) wall pressure distributions could be imposed as an outer boundary condition. The wall normal-velocity distributions would then be among the quantities capable of being accurately calculated, and these could be compared with the corresponding normal velocities deduced from the probe measurements of the present work. In all such investigations it would appear to be important first to check that the procedure deals reliably with the well-established solid-liner data.

In terms of the practical application of the method to large-scale facilities, one has to note that additional probes (and corresponding calibrations) and measurements would need to be provided over and above those normally utilised. However, once a 'library' of detailed results was available for a particular test section configuration, it would almost certainly be possible to

simplify the approach, and reduce the number of individual probes required to provide an adequate definition of the slot flows. Furthermore, it seems that for solid-liner tunnels the wall-pressure technique is becoming more widely used, and the proposed scheme for slotted-liner sections may be seen as a parallel development.

8. ACKNOWLEDGEMENTS

Support for the present work has been provided by City University, and this is gratefully acknowledged. Earlier support from the DTI should also be mentioned. The authors wish to record their particular thanks to Mr M Smith of the Centre for Aeronautics for his assistance.

9. REFERENCES

1. FREESTONE, M.M. MOHAN, S.R. LOCK, R.C. Interference corrections in wind tunnels with slotted walls. Paper 16, Wind tunnels and wind tunnel test technique, Royal Aeronautical Society, 1992.
2. FREESTONE, M.M. MOHAN, S.R. Interference determination for wind tunnels with slotted walls. Paper 19, AGARD CP 535, 1993.
3. MOHAN, S.R. FREESTONE, M.M. Interference determination for three-dimensional flows in slotted-liner wind tunnels. ICAS Paper 94-3.3.1, ICAS 1994
4. ASHILL, P.R. WEEKS, D J A method for determining wall-interference corrections in solid-wall wind tunnels from measurements of static pressure at the walls. Paper 1, AGARD CP 335, 1982.
5. FIRMIN, M.C.P. COOK, P.H. Disturbances from ventilated tunnel walls in aerofoil testing. RAE Tech Memo. AERO 1971, 1983.
6. AL-SAAD, J.A. Wall interference and boundary simulation in a transonic wind tunnel with a discretely slotted test section. NASA Technical Paper 3334, September 1993.
7. COLLYER, M.R. An extension to the method of Garabedian and Korn for the calculation of transonic flow past an aerofoil to include the effects of boundary layer and wake. RAE Technical Report 77104, 1977.
8. ASHILL, P.R. WOOD, R.F. WEEKS, D.J. An improved, semi-inverse version of the viscous, Garabedian and Korn method (VGK). RAE Technical Report 87002, 1987.
9. CAPELIER, C. CHEVALLIER, J.P. BOUNIOL, F. Nouvelle methode de correction des effets de parois en courant plan. La Recherche Aerospaciale, Jan-Fev 1978.
10. OHMAN, L H (Ed) Two-dimensional wind tunnel wall interference. AGARDograph No. 281, 1983.
11. ASHILL, P.R. GOODYER, M.J. LEWIS, M.C. An experimental investigation into the application of wind tunnel wall corrections. ICAS Paper 96-3.4.1, September 1996.
12. McCROSKEY, W.J. A critical assessment of wind tunnel results for the NACA 0012 airfoil. Paper 1, AGARD CP 429, 1988.

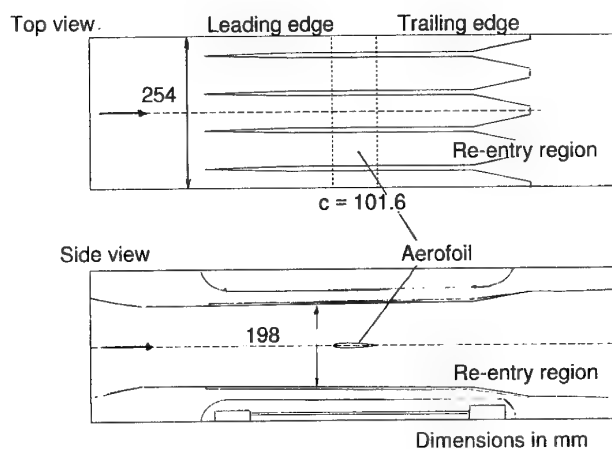


Figure 1 T5 wind tunnel test section

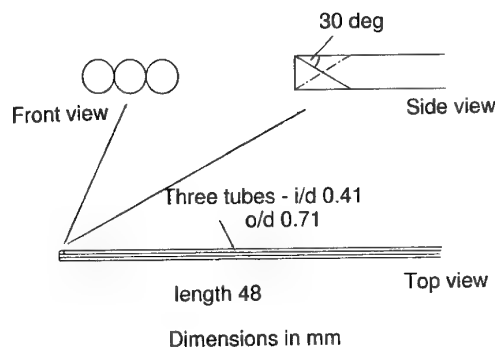


Figure 2 Three-hole flow probe

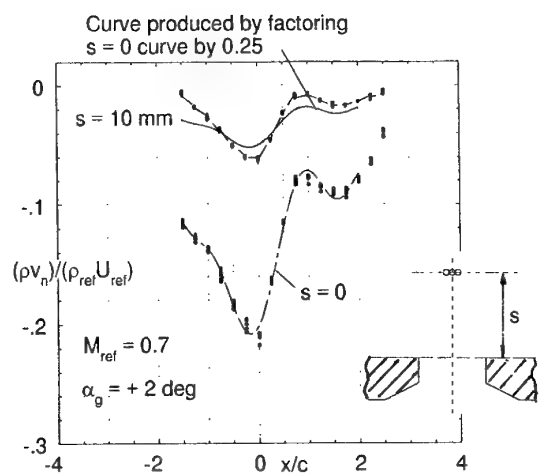
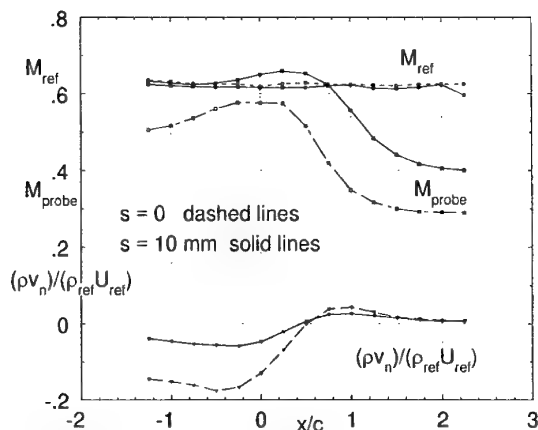
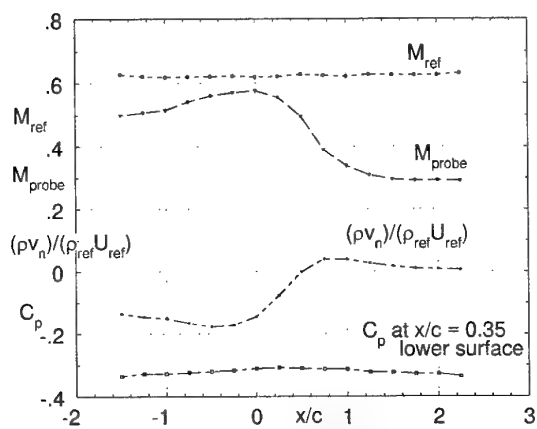
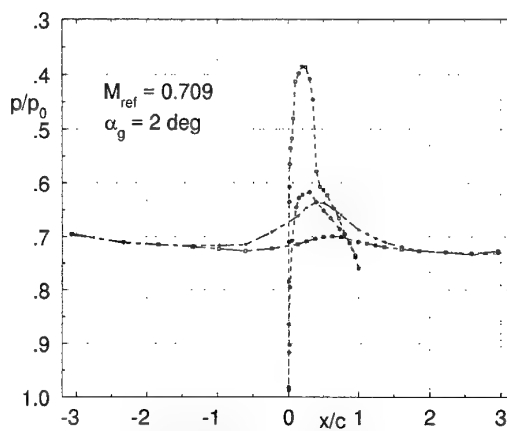
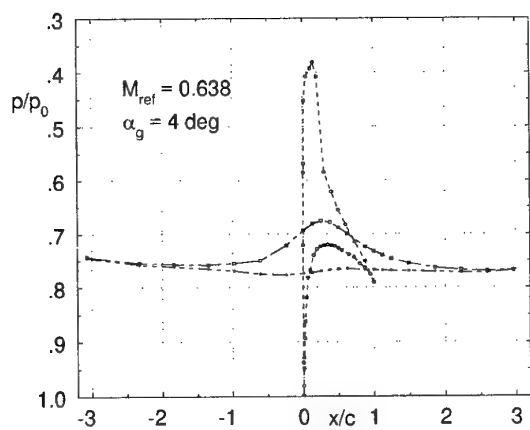
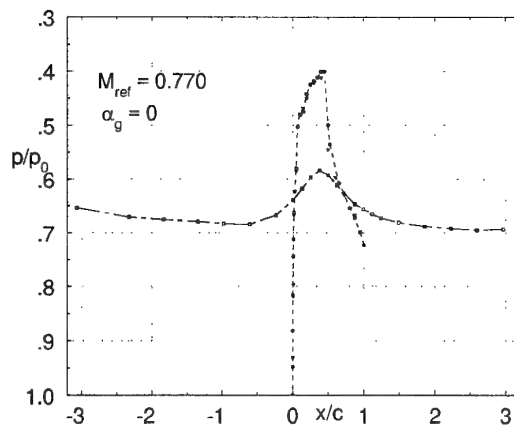


Figure 3 Normal mass flux parameter from two slot traverses

Figure 4 Variations of mass flux and Mach number parameters from two slot traverses, $\alpha_g = -2 \text{ deg}$ Figure 5 Traverse data including aerofoil C_p , showing effect of traverse block positionFigure 6 Aerofoil, roof and floor pressures - solid liners
 $M_{\text{ref}} = 0.709$, $\alpha_g = 2 \text{ deg}$ Figure 7 Aerofoil, roof and floor pressures - solid liners
 $M_{\text{ref}} = 0.638$, $\alpha_g = 4 \text{ deg}$ Figure 8 Aerofoil, roof and floor pressures - solid liners
 $M_{\text{ref}} = 0.770$, $\alpha_g = 0$

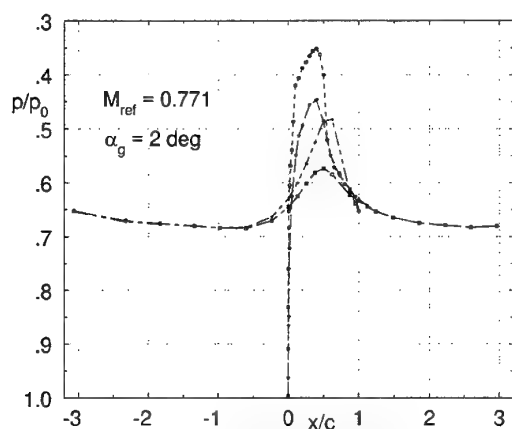


Figure 9 Aerofoil, roof and floor pressures - solid liners
 $M_{ref} = 0.771, \alpha_g = 2 \text{ deg}$

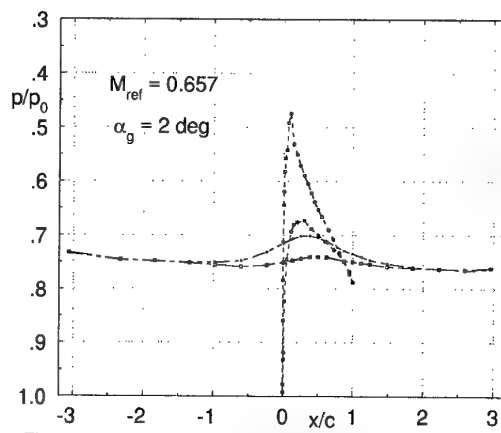


Figure 10 Aerofoil, roof and floor pressures - solid liners
 $M_{ref} = 0.657, \alpha_g = 2 \text{ deg}$

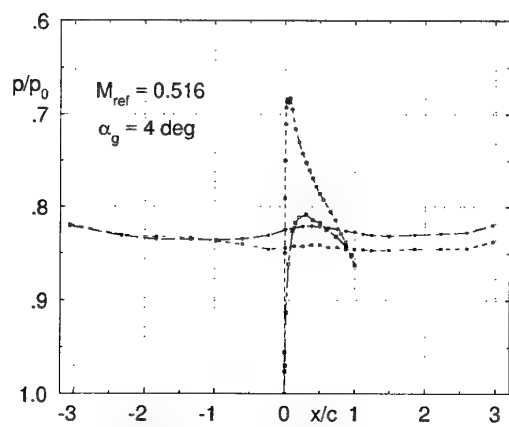


Figure 11 Aerofoil, roof and floor pressures - slotted liners
 $M_{ref} = 0.516, \alpha_g = 4 \text{ deg}$

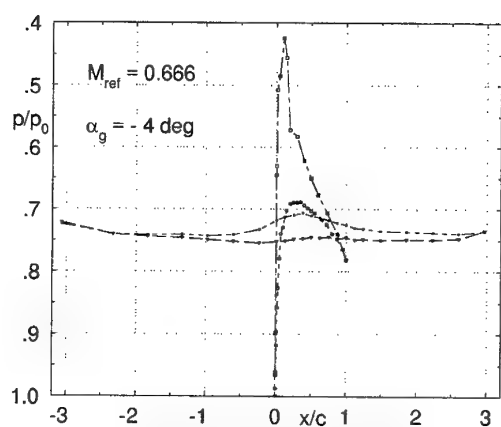


Figure 12 Aerofoil, roof and floor pressures - slotted liners
 $M_{ref} = 0.666, \alpha_g = -4 \text{ deg}$

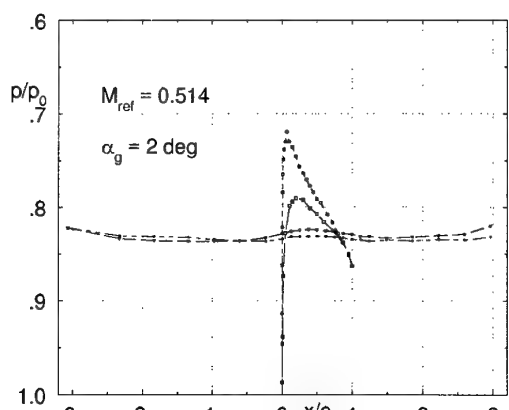


Figure 13 Aerofoil, roof and floor pressures - slotted liners
 $M_{ref} = 0.514, \alpha_g = 2 \text{ deg}$

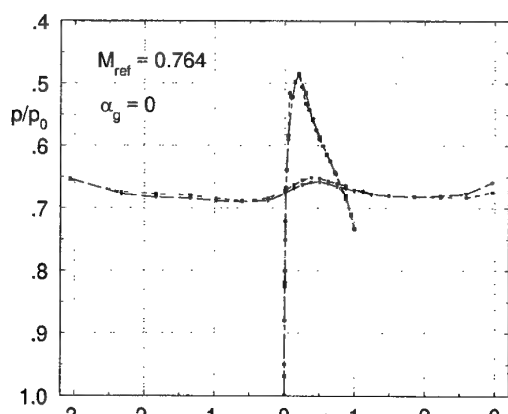


Figure 14 Aerofoil, roof and floor pressures - slotted liners
 $M_{ref} = 0.764, \alpha_g = 0$

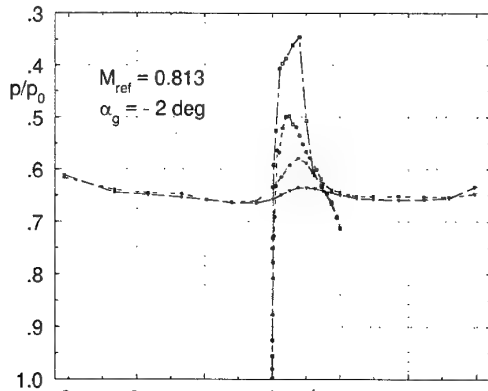


Figure 15 Aerofoil, roof and floor pressures - slotted liners
 $M_{ref} = 0.813$, $\alpha_g = -2$ deg

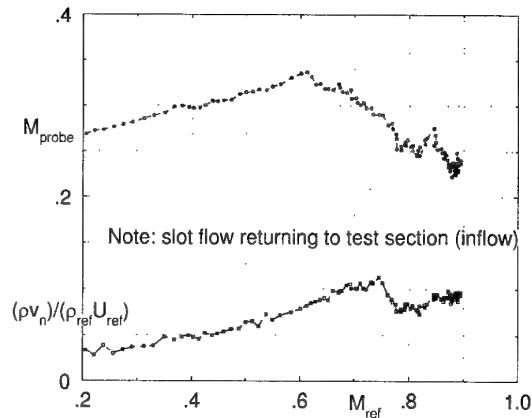


Figure 16 Mach number sweep - probe at $x/c = 1$, $\alpha_g = -4$ deg

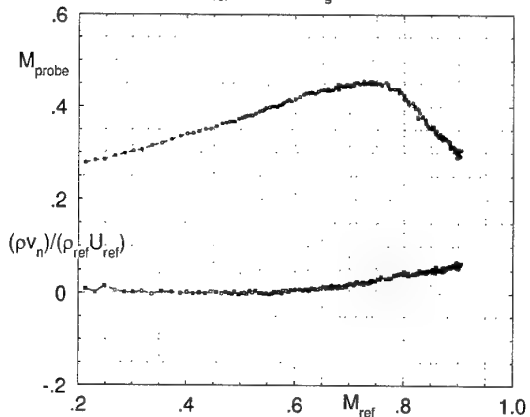


Figure 17 Mach number sweep - probe at $x/c = 1$, $\alpha_g = 0$.

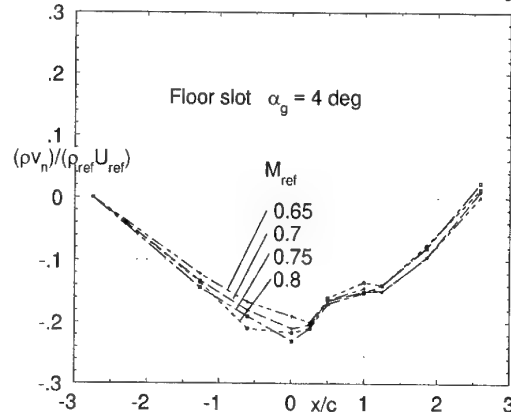


Figure 18 Variation of mass flux along slot, $\alpha_g = 4$ deg

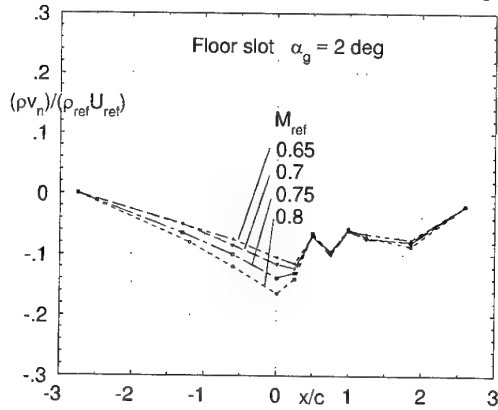


Figure 19 Variation of mass flux along slot, $\alpha_g = 2$ deg

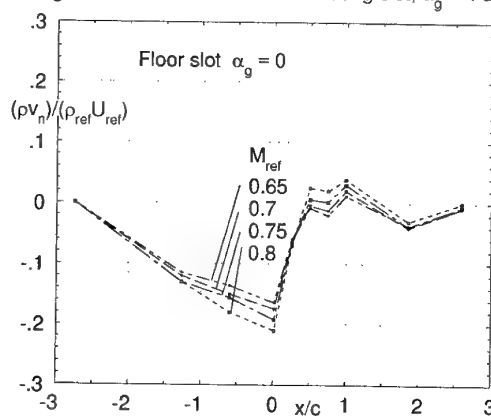


Figure 20 Variation of mass flux along slot, $\alpha_g = 0$

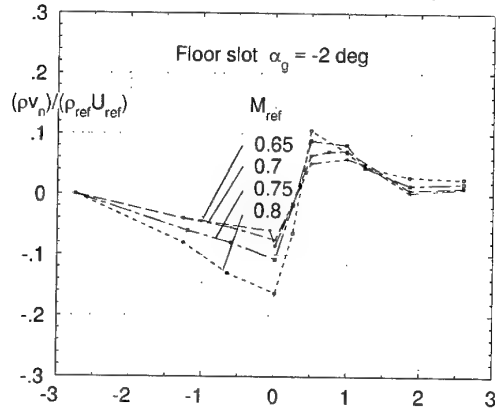


Figure 21 Variation of mass flux along slot, $\alpha_g = -2$ deg

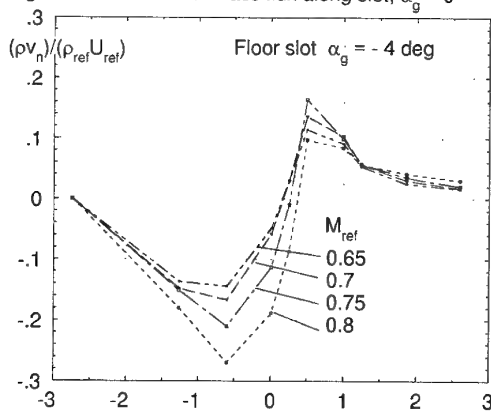


Figure 22 Variation of mass flux along slot, $\alpha_g = -4$ deg

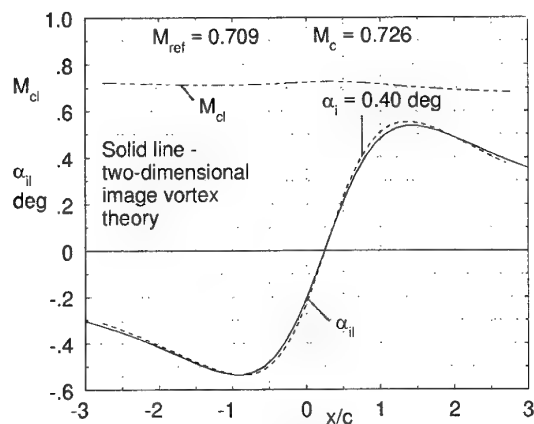


Figure 23 Wall-induced interference by method of Ref. 4
 $M_{ref} = 0.709$, $\alpha_g = 2$ deg

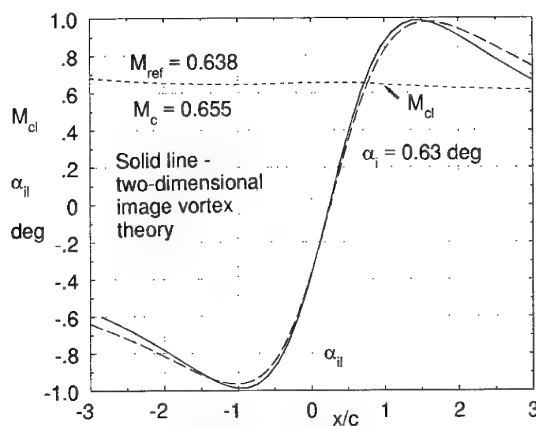


Figure 23 (concluded) Wall-induced interference
 $M_{ref} = 0.638$, $\alpha_g = 4$ deg

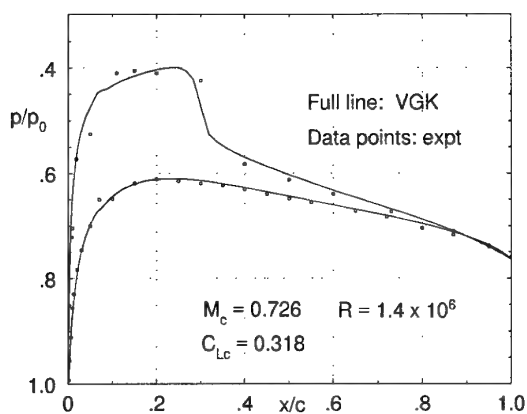


Figure 24 Comparison of computed and measured pressures
 - solid liners

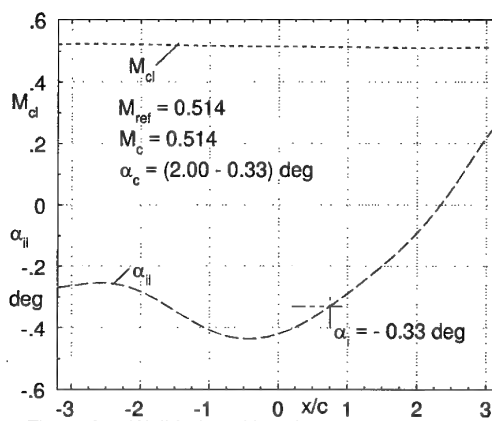


Figure 25a Wall-induced interference on slotted liners
 $M_{ref} = 0.514$, $\alpha_g = 2$ deg

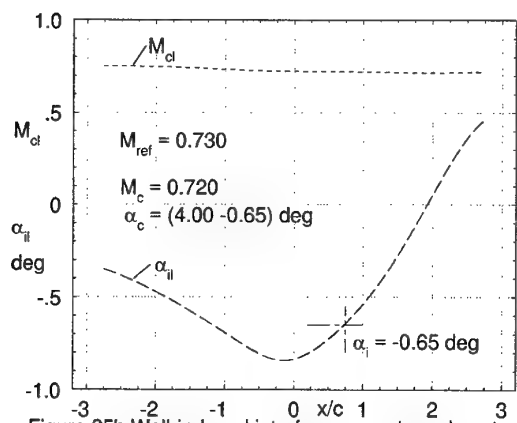


Figure 25b Wall-induced interference on tunnel centre line
 - slotted liners, $M_{ref} = 0.730$, $\alpha_g = 4$ deg

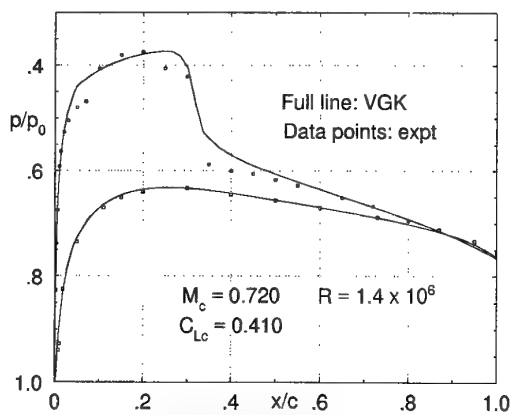


Figure 26 Comparison of computed and measured pressures
 - slotted liners

AERODYNAMIC DESIGN OF AXIAL-FLOW FANS FOR SUBSONIC WIND TUNNELS

GOSNITs TsAGI named after Prof. N.E.Zhukovsky, Moscow, Russia

Prof. I.V.Brusilovsky, Principal Research Scientist
17, Radio Street, 107005 Moscow, Russia

ABSTRACT

The report highlights features of wind tunnel fans with axial annular diffusers, as well as relations for defining fan parameters (including the total pressure loss factor) with the aid of the equivalent diffuser length and the total pressure loss coefficient of a planar diffuser. Test data on planar and annular diffusers (including data on the annular diffusers tested with fans) are compared. Foundations of fan aerodynamic design are provided; this is subdivided into two principal stages: 1) determining the basic parameters (volume-averaged axial flow-speed coefficient, theoretical pressure coefficient, and two new parameters: the prewhirl upstream of an impeller and the residual whirl downstream of an outlet guide vane) as well as the fan hub diameter; 2) shaping the guide vanes and impeller blading. The operational envelope is outlined; taking parameters in this domain ensures creating a fan with really separation-free flow about blades both at a rated regime at a maximum possible efficiency and over a certain domain around the rated regime. The design parameters are selected, and efficiency evaluated, in the general form for a complete fan configuration comprising an inlet guide vane (IGV), the impeller, and an outlet guide vane (OGV). Results for configurations without one or two guide vanes are the corresponding particular cases. Expressions for optimizing the design parameters and the respective efficiency are derived. Theoretical and experimental values of the two new parameters of flow whirl are compared. The shaping procedure (i.e., defining the airfoil setting angle, shape, curvature, the blade array spacing, rated airfoil angle of attack, total number and shapes of the blades) is based on generalized test-data; the relations allow for radial blading-variation and the "distance" to the maximum pressure on the fan characteristic curve. Airfoil setting angles and radial variation of airfoil curvature are proposed to be defined from theoretical data on airfoil arrays on the basis of a unified method for all bladed components with arbitrary array density. This aerodynamic design method developed at GOSNITs TsAGI is being used and improved for more than 45 years and has been comprehensively verified.

BASIC NOMENCLATURE

C_J and C_x – Joukowski circulation force coefficient and profile drag coefficient, respectively

C_a and C_u – flow axial and tangential speeds [m/s], respectively

C_{a0} – volume-averaged axial flow-speed [m/s]; in obvious situations the C_{a0} is replaced with C_a

$\bar{C}_a = C_a/U$;
 $\bar{C}_u = C_u/U$ – flow axial and tangential speed coefficients, respectively

D – fan diameter [m]

d – hub diameter [m]

L – diffuser length [m]

l_{pl} – planar diffuser generatrix length [m]

l_{equiv} – equivalent diffuser length [m]

$F = \pi D^2/4$ – characteristic area [sq.m]

N – fan wattage [W]

$n_1 = c_{1u}/(c_{2u} - c_{1u})$ – prewhirl upstream of impeller

$n_2 = c_{3u}/c_{2u}$ – residual whirl downstream of outlet guide vane

P – static pressure at a stream point [Pa]

P_{0i} ($i = 1, 2, 3$) – total pressure at a stream point [Pa]

P_V – total fan pressure rise [Pa]

P_V' – total fan pressure [Pa] (for example, for an impeller with a diffuser)

$P_{TV} = P_V/\eta$ – theoretical fan pressure [Pa]

P_{dv} – fan dynamic pressure [Pa]

Q – fan throughput [cu.m/s]

$R = D/2$ – impeller radius [m]

r – a current radius [m]

$\bar{r} = r/R$ – relative radius

s – diffuser wet surface area [sq.m]

U – peripheral speed at the radius R [m/s]

γ_1 and γ_2	- inclination angles of the internal and external cones of the diffuser [degree]
ζ	- pressure loss coefficient
η	- fan efficiency
$\tilde{\eta}$	- relative efficiency
η'	- fan diffuser efficiency
$\mu = C_x/C_f$	- drag-to-lift ratio of an airfoil in blading
$v = d/D$	- hub relative diameter
ρ	- gas density [kg/cu.m]
$\varphi = Q/F$	- fan throughput coefficient
$\varphi_a = C_{a0}/U = \varphi/(1-v^2)$	- volume-averaged speed coefficient
$\psi = 2P_V/\rho U^2$	- pressure coefficient
θ_e	- local diffuser divergence angle, equivalent diffuser divergence angle [degree].

ABBREVIATIONS AND INDEXES

<i>IGV, I, OGV</i>	- outlet guide vane, impeller, inlet guide vane, respectively
<i>a</i>	- axial component
<i>H, K</i>	- inlet and outlet sections, respectively
<i>u</i>	- tangential component
<i>opt</i>	- optimum
1, 2, 3	- upstream of impeller, downstream of impeller, downstream of outlet guide vane, respectively
(')	- (the prime sign), for parameters of fan with diffuser.

1. SOME FEATURES OF MATING THE FAN WITH A DIFFUSER. OPTIMEZATION OF DIFFUZER

Consideration hereafter is given to a fan with an attached diffuser. This is because the diffuser pressure losses depend on fan geometry (for example, on the fan hub relative diameter) and flow parameters at the fan exit section. Initial data for design include the required air flowrate (the fan throughput Q) and the total pressure P_V . Normal operation of a fan requires a fan entry air speed field to be rather uniform, especially well axisymmetric. This is important in

order to improve vibratory characteristics of the very wind tunnel, fan shaft bearings, and fan blading. It is often that a fan diameter D is prescribed within a wind tunnel design. Also specified are usually a fan rotational speed n and an electric drive power N . A wind tunnel configuration may be seen in Fig. 1.

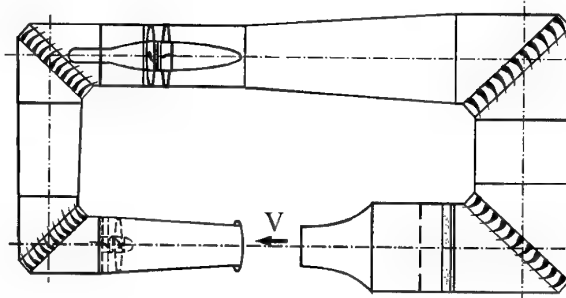


Figure 1. Conventional wind tunnel flow path

A particular recommendation is to reject the configurations in which the fan entry is immediately downstream of an exit section of a diffuser, however perfect, or the fan efficiency may get less by at least 5%. An annular axial diffuser downstream of a fan needs to be highly efficient. The GOSNITs TsAGI have generalized considerable amounts of experimental data for reasonably specifying the multiple parameters of such diffusers (and some other types). One should bear in mind that the fan itself, placed into a wind tunnel, is often "in the fourth quadrant", i.e., has negative static pressure, in which case the drag of the entire wind tunnel is overcome by transforming the fan dynamic pressure into static pressure in the diffuser. Straight annular diffusers may be designed by using the plot in Fig.2 that relates the optimum loss factor ζ_t^* to diffuser geometry.

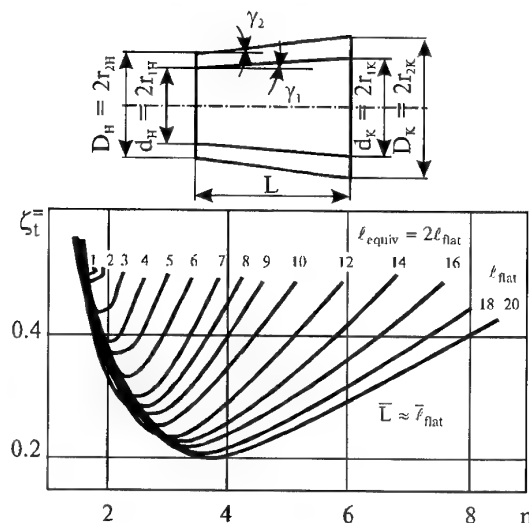


Figure 2. Nomogram for determining the annular diffuser total pressure loss factor ζ_t^* on the basis of data for planar diffusers (ζ_t^*)

In the plot the reduced length of a diffuser is as follows:

$$l_{equiv} = \frac{2\bar{L}}{1 - \bar{d}_H^2} \left(\frac{1 + \bar{D}_K}{\cos \gamma_2} + \frac{\bar{d}_H + \bar{d}_K}{\cos \gamma_1} \right);$$

$$\bar{L} = \frac{L}{D_H}; \quad \bar{D}_K = \frac{D_K}{D_H};$$

$$\bar{d}_H = \frac{d_H}{D_H}; \quad \bar{d}_K = \frac{d_K}{D_H};$$

$$n = \frac{F_K}{F_H} = \frac{r_{2K}^2 - r_{1K}^2}{r_{2H}^2 - r_{1H}^2};$$
(1)

(subscripts H and K identify the outlet and inlet sections, respectively). When working within the one-dimensional theory, one of the most reasonable methods for defining diffuser parameters uses the so-called equivalent length l_{equiv} and the local divergence angle θ_e . According to the proposal in [3], the equivalent divergence angle of an arbitrarily shaped diffuser is described by using.

$$\sin \frac{\theta_e}{2} = \frac{n-1}{l_{equiv}} \quad (2)$$

Here, $n = F_K/F_H$ is a diffuser expansion ratio and $l_{equiv} = s/F_H$. The physical meaning of the angle θ_e is that the value of $\sin(\theta_e/2)$ represents a pressure difference to be overcome by the stream, with the difference being referred to the dynamic pressure at a particular cross section of the diffuser. Thus the local angle shows the ability of flow to move against positive pressure gradient. For planar diffusers we have $l_{equiv} = 2L/(h_H^* \cos \gamma)$; here, $l_{pl} = L/\cos(\gamma/2)$ (the planar diffuser generatrix length). Comprehensive testing of insulated straight annular diffuser that are most widely employed in fan installations (especially in wind tunnels) was conducted; also, Reference [4] provides results of test evaluation of planar straight diffusers; these data enable designing and evaluating the annular diffusers by proceeding from characteristics of planar diffusers. The results of [4] were utilized to draw the plots of total pressure loss coefficient ζ_t^* for planar diffusers; two values of a relative boundary layer displacement thickness at the diffuser upstreammost section: $\Delta_H^* = \delta_H^*/h_H^* = 0.015$ and 0.03 (here, h_H^* is the diffuser upstreammost section height). Note that generally $\zeta_t = \zeta_{t^{intern}} + \zeta_K$, where

$$\zeta_{t^{intern}} = \frac{1}{N_H \rho C_{Ha0}^2 / 2} \cdot \left[\frac{1}{F_H} \int_{F_H} P_0 \frac{C_a}{C_{a0}} dF - \frac{1}{F_K} \int_{F_K} P_0 \frac{C_a}{C_{a0}} dF \right];$$

$$\zeta_K = \frac{1}{n^2} \frac{N_K}{N_H} \quad (3)$$

$$N_H = \frac{1}{F_H} \int_{F_H} \left(\frac{C_a}{C_{a0}} \right)^3 \frac{dF}{\sin^2 \delta_H}$$

$$N_K = \frac{1}{F_K} \int_{F_K} \left(\frac{C_a}{C_{a0}} \right)^3 \frac{dF}{\sin^2 \delta_K}$$
(4)

In these expressions, we use $n = F_K/F_H$, $\sin \delta_H = C/C_{Ha}$, and δ_H the angle between the velocity and the diffuser axis. Figure 2 depicts computed results, $\zeta_t^-(n)$, for various values of l_{pl} at

$$\Delta_H^* = \delta_H^* / h_H^* = 0.015.$$

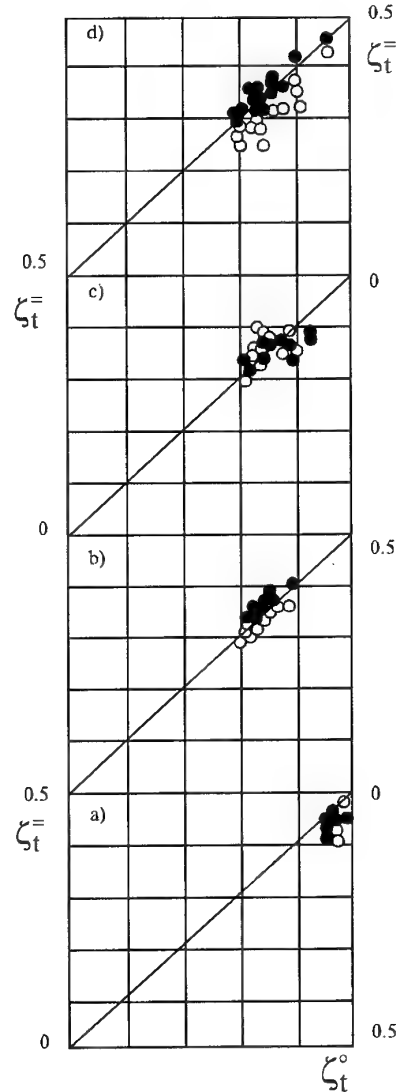


Figure 3. Comparing the annular diffuser total pressure loss factor ζ_t^+ and the planar diffuser total pressure loss factor ζ_t^- .

Figure 3 compares the planar diffuser total pressure loss coefficient ζ_t^- with the annular diffuser loss

coefficient ζ_t^* as obtained in [6]. In this Figure, the circles (o) in parts a) and b) correspond to $\Delta_H^* = 0.015$ and filled circles, to $\Delta_H^* = 0.03$; part c) is for diffuser tested in [7], with open circles corresponding to $\tilde{C}_{Ha} = 0$ and the filled ones, to $\tilde{C}_{Ha} = 0.03$. Reference [7] provides the following formula:

$$\tilde{C}_{Ha} = \frac{2}{1 - \bar{d}_H^2} \int_{\bar{r}_b}^{\bar{r}_H} \left(\frac{C_{Ha}}{C_{Ha0}} - 1 \right) \bar{r} d\bar{r} \quad (5)$$

In the latter, the symbols r_b and r_H correspond to the \bar{r} values at which the axial speed (C_a) is equal to the volume-averaged flow-speed (C_{Ha0}). The part d) in Fig. 3 compares loss coefficients ζ_t^* and ζ_t^o of annular diffusers experimentally evaluated with fan. Also, here circles (o) correspond to $\Delta_H^* = 0.015$, and black points, to $\Delta_H^* = 0.03$; note that the value ζ_t^o ($= \zeta_t^*$) for the maximum-efficiency regime of the fan with the diffuser was determined by using $\zeta_t^* = 1 - \xi_D$ (here, ξ_D is the coefficient of transformation of dynamic pressure downstream of the fan into static pressure in the diffuser); in this case,

$$\xi_D = \frac{P_{sV}' - P_{sV}}{N_H \rho C_{Ha0}^2 / 2}$$

Here, P_{sV}' and P_{sV} is the static pressure of the impeller with and without the diffuser, respectively, as measured immediately in a suction chamber of a test setup (see [9]); C_{Ha0} is a volume-averaged axial flow-speed downstream of the fan, at the diffuser entry. The value of N_H is set to 1. From Fig. 3 it is seen that the total pressure loss coefficient for annular diffusers installed downstream of axial-flow fans in wind tunnels may well be determined from total pressure loss plots such as those in Fig. 2 which were obtained by testing a planar diffuser with a rectilinear axis.

2. FUNDAMENTALS OF AERODYNAMIC DESIGN OF FANS.

Consider a general single-stage fan with a complete configuration incorporating the inlet guide vane (IGV), the impeller, and the outlet guide vane (OGV) (the "inlet guide vane + impeller + outlet guide vane" configuration). This breakdown simplifies analysis of particular combinations in a wind tunnel: "impeller alone," "impeller + outlet guide vane," and "inlet guide vane + impeller." A similar approach has been prepared for developers of

- axial fans with meridional acceleration of flow in all blade wheels,
- fans with counterrotating impellers, and
- multistage fans.

The fan aerodynamic design includes two main phases: (1) determining the necessary values of parameters and (2) shaping the blading. In the general case the following four aerodynamic parameters are considered:

- the coefficient of volume-averaged axial velocity $\bar{C}_a = C_a / U$,
- the coefficient of theoretical pressure $\psi_T = 2P_V / \rho U^2 \eta$,
- the prewhirl parameter $n_1 = c_{1u} / (c_{2u} - c_{1u})$,
- the residual whirl parameter for flow downstream of the outlet guide vane, $n_2 = c_{3u} / c_{2u}$

and the relative hub diameter $v = d/D$ which is an aerodynamic and structural parameter simultaneously. Here, u is a circumferential fan speed at the impeller blade tip; $P_V = P_{02} - P_{01}$ is a fan total pressure rise; P_{01} and P_{02} are total pressures upstream and downstream of the fan, respectively; ρ is an air mass density (consideration is given to fans in which air compressibility may be neglected, i.e., when $M = U/a < 0.5$); η is a fan efficiency ($\eta = QP_V / N$); c_{1u} is a flow tangential speed in the inlet guide vanes; c_{2u} is a flow tangential speed downstream of the impeller; c_{3u} is a residual tangential speed downstream of the outlet guide vane. The efficiency of the complete configuration ("inlet guide vane + impeller + outlet guide vane") with a cylindrical passage is expressed as follows:

$$\begin{aligned} \eta' = 1 - \frac{\Phi_a}{\bar{r}} \left[\mu_I + n_1 \mu_{IGV} + \right. \\ \left. (1 + n_1)(n_2 - 1) \mu_{OGV} \right] - \\ - \frac{1}{\bar{r} \Phi_a} \left\{ \mu_I \left[\bar{r} - \frac{(1 + 2n_1)\psi_T}{4\bar{r}} \right]^2 + \right. \\ \left. + n_1 \mu_{IGV} \left(\frac{n_1 \psi_T}{4\bar{r}} \right)^2 + (1 - n_1)(n_2 - 1) \cdot \right. \\ \left. \mu_{OGV} \left[\frac{(1 + n_1)(1 + n_2)\psi_T}{4\bar{r}} \right]^2 \right\} - \\ - \frac{1}{4} K_{JU} n_2^2 (1 + n_1)^2 \psi_T - \frac{\zeta \Phi_a^2}{\psi_T}. \end{aligned} \quad (6)$$

Here, $\Phi_a = \bar{C}_a$, $\bar{r} = \sqrt{(1 + v^2)}/2$ is a mean geometric radius of a blading; $\mu = C_x / C_J$ is a drag-to-lift ratio of the relevant blading (with C_x taking into account both the profile drag and secondary

losses); C_J is a Joukowski circulation force coefficient; ζ is a diffuser pressure loss factor; K_{JU} is a coefficient of losses related to the dynamic pressure determined on the basis of the tangential speed downstream of the fan. For various types of blading the value of μ ranges from 0.04 to 0.055; its sign is the blading circulation sign. Circulation of an impeller is positive. If $\zeta = 0$, we have $\eta' = \eta$, that is, the efficiency of the fan itself. With $n_1 = 0$ the relation (6) describes the efficiency of the fan in the "impeller + outlet guide vane" configuration; with $n_2 = 1$, the efficiency of the "inlet guide vane + impeller" configuration; with $n_1 = 0$ and $n_2 = 1$, the efficiency of the "impeller" configuration (with no vanes); and equalities $n_1 = -1$ and $n_2 = 0$ correspond to axial outflow in "inlet guide vane + impeller" and "impeller + outlet guide vane" configurations, respectively. Initially, the variable ψ_T is determined on the basis of the efficiency η of a previously known design. Thereafter, equation (6) is utilized to evaluate efficiency. Usually, two iterations are enough. The theory suggests that the "inlet guide vane + impeller" configuration may be described by a relation for establishing n_{1opt} and the "impeller + outlet guide vane" configuration, by a relation for establishing n_{2opt} ; experiments confirmed this statement. It is interesting to note that implementing these values increases the fan efficiency and decreases the mass and the longitudinal size (see Fig. 4).

Optimum values, n_{1opt} and n_{2opt} , are determined from equations $\partial\eta'/\partial n_1 = 0$ and $\partial\eta'/\partial n_2 = 0$.

In this case the value of n_{1opt} can be obtained from the equation (7)

$$an_{1opt}^2 + bn_{1opt} + c = 0 \quad (7)$$

As for the "IGV + Impeller" configuration, we may write

$$n_{1opt} \approx c/b$$

(7')

The latter include coefficients

$$\begin{aligned} a &= 3 \left[\mu_{IGV} + (1 + n_2^2)(n_2 - 1)\mu_{OGV} \right] \\ b &= 8 \left[\mu_I + \frac{3}{4}(1 + n_2^2)(n_2 - 1)\mu_{OGV} + \frac{K_{JU}n_2^2\bar{r}^3\varphi_a}{\psi_T} \right] \\ c &= 4 \left[\mu_I + \frac{3}{4}(1 + n_2^2)(n_2 - 1)\mu_{OGV} \right] - \\ &\quad - \frac{16r^2\mu_I}{\psi_T} + 4 \left(\frac{2\bar{r}\varphi_a}{\psi_T} \right)^2 \left[\mu_{IGV} + \right. \\ &\quad \left. + (n_2 - 1)\mu_{OGV} \right] + \frac{8K_{JU}n_2^2\bar{r}^3\varphi_a}{\psi_T} \end{aligned} \quad (8)$$

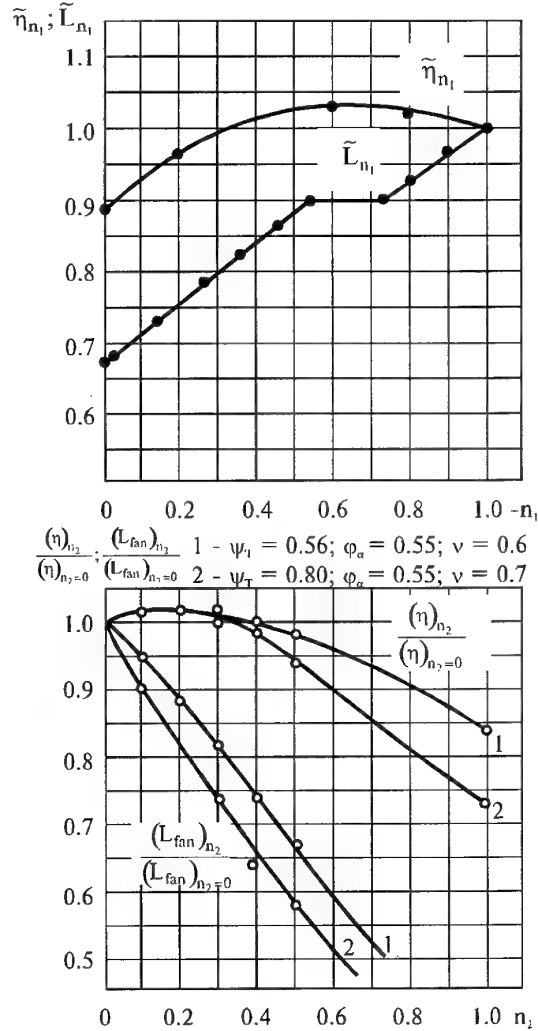


Figure 4. Experimental data on dependence of efficiency and dimensions on inflow prewhirl parameter n_1 (for "IGV + Impeller" configuration) and outflow residual whirl parameter n_2 (for "Impeller + OGV" configuration)

Behaviour of Equation (7) in the vicinity of n_{1opt} is thoroughly analyzed in [1]. Figure 4 demonstrates an example of experimentally determining the relative efficiency $\tilde{\eta}_{n_1} = \eta_{n_1}/\eta_{n_1=-1}$ as a function of n_1 and the "IGV + Impeller" configuration linear dimension $\tilde{L}_{n_1} = L_{n_1}/L_{n_1=-1}$. Equation (7') was employed to evaluate n_{1opt} for "IGV + Impeller" configuration with $\varphi_a = 0.55$, $\psi_T = 0.56$, $v = 0.6$; this gives -0.7 which is very close (refer to Fig. 4) to the experimental estimate. The n_{2opt} is to be found from the relation.

$$An_{2opt}^2 + Bn_{2opt} + C = 0 \quad (9)$$

The corresponding expressions for coefficients A , B , and C are provided in [1]. Each of these incorporates terms with $[(1+n_1)\psi_T/2r]^2$. If the latter are allowed to be neglected, we arrive at the following expression:

$$n_{2opt} \approx -\frac{2\mu_{OGV}\Phi_a}{K_{JU}\bar{F}(1+n_1)\psi_T} \quad (10)$$

Values obtained from (9) and (10) differ very insignificantly. Figure 4 represents results of experimental study on the influence of the n_2 parameter on the relative efficiency $(\eta)_{n_2}/(\eta)_{n_2=0}$ and the relative length $(L_{fan})_{n_2}/(L_{fan})_{n_2=0}$ of blading in the "Impeller + OGV" configuration; treated were two "Impeller + OGV" fans. Computed values of n_{2opt} do not almost differ from experimental results. It should be noted that the advantage in respect of efficiency of the fans designed for n_{1opt} and n_{2opt} is held in rather wide vicinities of the optimal condition. The advantage in respect of efficiency of fans with optimal residual whirl takes also place in some arrangements with diffusers downstream of them, see [6]. Comprehensive experiments were summarized to outline the domain Σ from which the aerodynamic parameters of various types of fans should be taken (see Fig. 5). Adopting aerodynamic parameters ψ_T , Φ_a , n_1 , and v from this domain

ensures the development of a fan with a high efficiency and almost separation-free flow in blading. If the fan diameter D is not specified, the formula $\partial\eta'/\partial\Phi_a = 0$ is employed to determine the optimum value $(\Phi'_a)_{opt}$ for the installation with a diffuser, and then the diameter is determined:

$$D_{opt} = 2.9 \cdot \sqrt[3]{\frac{Q}{n\Phi_{opt}}}; \quad \Phi_{opt} = (\Phi'_a)_{opt}(1-v^2).$$

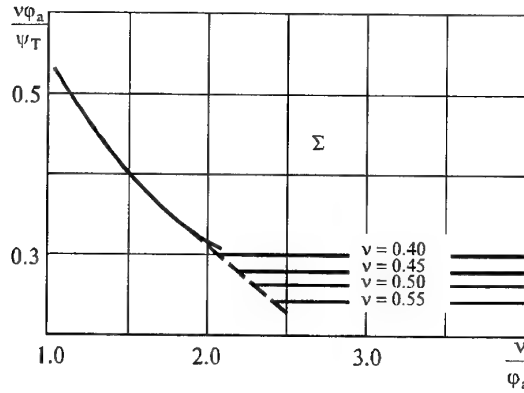


Figure 5. Operational envelope Σ for "Impeller + OGV" configuration

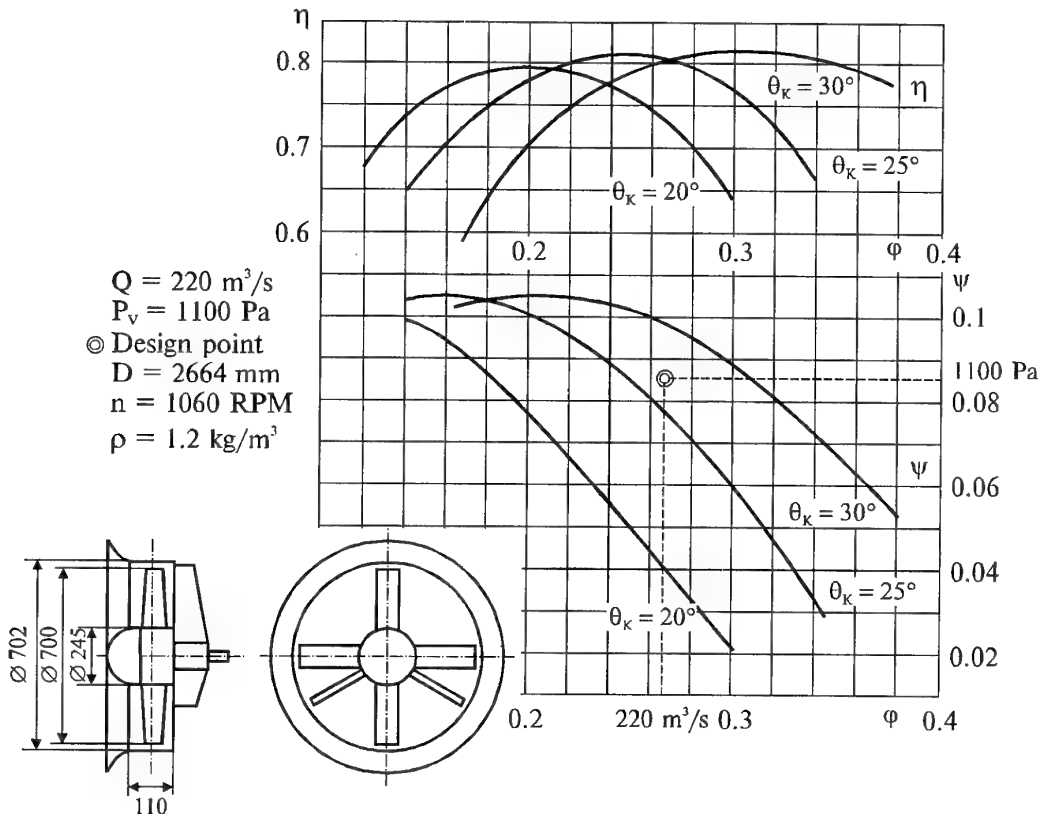


Figure 6. Characteristics of TsAGI T-102 wind tunnel model with differing impeller blade setting angles θ_K .

It is usual that the extreme is shallow for small values of $\zeta/\psi T$; so the diameter can be reduced by selecting φ_a in excess of $(\varphi'_a)_{opt}$. For this situation the respective expressions have been derived that evaluate losses in efficiency η' . At GOSNITs TsAGI the software programs are available that solve the aforementioned problems of establishing the aerodynamic design parameter, including the case with no specification of the diameter and/or the circumferential speed. The next phase is to compute the radial profiles of flow speeds in gaps between blade rows – the so-called velocity triangles. It is conventional to assume circulation and the axial speeds to be constant. Software programs have been prepared to calculate flows in devices where these parameters vary with radius under different laws. Having determined the velocity triangles, other programs are utilized to shape the blade rows, i.e., to define radial blade solidity, angles of attack, airfoil geometry (and camber), thickness-to-chord ratio, the total number of blades and their shape; requirements to acoustic characteristics and vibration intensity are

taken into account. The shaping is based on generalized experimentally obtained relations that define the blade row solidity and angles of attack and allow for a position along a blade and for a margin to the pressure maximum on the fan characteristic curve. Specification of blade setting angles and camber as functions of the position radius is based on theoretical characteristics of airfoil rows. Methods and programs for adjusting the wind tunnel fans by re-setting the inlet guide vane and impeller blades have been developed. The wind tunnel fan aerodynamic design method (i.e., determining the necessary values of parameters and shaping the blading) is versatile for all configurations of the axial fans and takes into account customer's requirements in each case. This method has been comprehensively validated and is being used and improved for more than 45 years. The tremendous database concerning the fans and their performance, as compiled at GOSNITs TsAGI, simplifies definition of a point $\{\varphi, \psi\}$ with a high efficiency, in order to modify blading in compliance with customer requirements and to define the fan diameter and rotational speed:

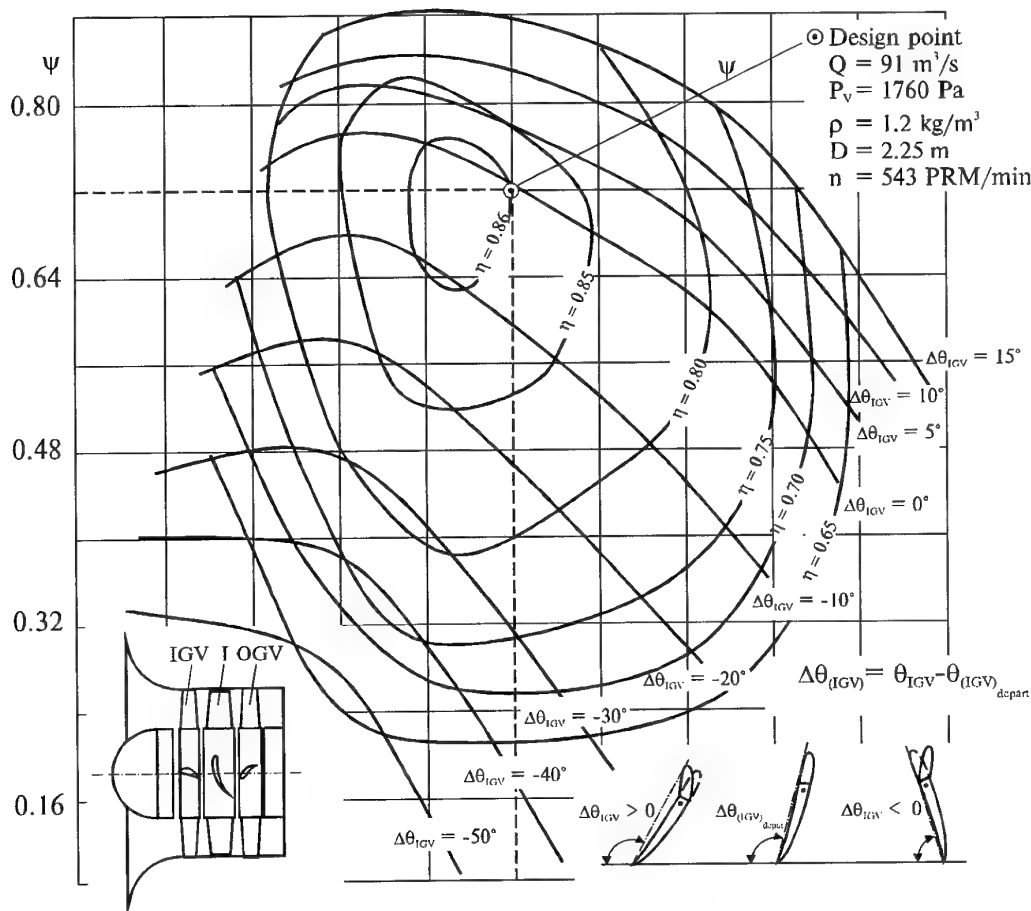


Figure 7. Characteristics of TsAGI T-124 wind tunnel model with differing inlet guide vane blade setting angles

$$D = 0.56 \left(\frac{Q}{\varphi} \right)^{1/2} \left(\frac{\psi}{P_V} \right)^{1/4} \text{ (m)}$$

$$n = 138 \left(\frac{Q}{\varphi} \right)^{1/2} \left(\frac{P_V}{\psi} \right)^{3/4} \text{ (RPM)}.$$

Presented as examples in Figures 6 and 7 are aerodynamic characteristics of fans developed at GOSNITs TsAGI for T-102 and T-124 wind tunnels of TsAGI.

The author confirms that there are no restrictions on presentation and publication of the paper described in the abstract.

I.V.Brusilovsky

3. REFERENCES

1. Brusilovsky I.V. Aerodynamic performance prediction for axial-flow fans. - Mashinostroyeniye, Moscow, 1986, 284 pp.
2. Brusilovsky I.V. Optimizing the diffusers of axial-flow fans and evaluating their energy characteristics on the basis of test data. - TsAGI, "Industrial aerodynamics", issue 2 (34), Mashinostroyeniye, Moscow, 1987, pp.118-133.
3. Dorfman A.Sh., Saykovsky M.I. Approximate determination of losses in curvilinear diffuser with separated flow. - TsAGI, "Industrial aerodynamics", issue 28, Mashinostroyeniye, Moscow, 1986, pp.98-120.
4. Reno, Djonston, Klayn. Characteristics and evaluation of planar diffuser with rectilinear axis. - Theoretical foundations of engineering analyses, 1967, no. 1, Russian translation by Mir.
5. Mitrofovich V.V. Determining the limiting parameters of axial fans with high static efficiency. - TsAGI, "Industrial aerodynamics", issue 4 (36), Mashinostroyeniye, Moscow, 1991, pp.260-280.
6. Dovzhik S.A., Kartavenko V.M. Experimental study on effects of flow whirl on efficiency of annular channel and outlet nozzles in axial turbomachinery. - TsAGI, "Industrial aerodynamics", issue 31, Mashinostroyeniye, Moscow, 1974, pp.94-109.
7. Dovzhik S.A. The influence of flow radial nonuniformity on efficiency of annular diffusers. - TsAGI, "Industrial aerodynamics", issue 32, Mashinostroyeniye, Moscow, 1975, pp.5-28.
8. Brusilovsky I.V. Aerodynamic configurations and characteristics of TsAGI-developed axial fans. Handbook. - Nedra, Moscow, 1978, 198 pp.
9. Brusilovsky I.V. Aerodynamics of axial-flow fans. Concepts. - Mashinostroyeniye, Moscow, 1984, 240 pp.

EJECTOR-DRIVEN WIND TUNNELS

Yu. K. Arkadov, V. P. Roukavets
Central Aerohydrodynamic Institute (TsAGI), 1, Zhukovsky Street
140160 Zhukovsky, Moscow Region, Russia

1. ABSTRACT

The experience accumulated at the Central Aerohydrodynamic Institute for many years in calculating, designing, and running wind tunnels in which pressure difference is produced by a jet ejector-compressor, is analyzed. Theories for optimal gas ejectors and their systems are given, new schemes of gas ejectors of improved performance are discussed, and problems of improving economic efficiency of the "wind tunnel-gas ejector" system are considered. Examples of a successful use of ejectors as a major drive of subsonic, trans-, and hypersonic wind tunnels are presented.

2. Nomenclature

p, ρ, T, w	pressure, density, temperature, velocity
p_0, ρ_0, T_0	pressure, density, stagnation temperature
a_*	critical velocity
$\lambda = w/a_*$	equivalent velocity
$q(\lambda) = \rho w / \rho_* w_*$	equivalent mass flow
κ	adiabatic exponent
f	jet cross-section area
$a = f_1 / f'$	ratio of areas of high- and low-pressure gas jets
G	gas mass flow
$K = G_1 / G'$	ejecting-to-ejected gas mass ratio
$\sigma = p_0' / p_{01}$	ratio of pressures of high- and low-pressure gas
$\epsilon = p^*_0 / p_{01}$	pressure ratio
$p_{0 \text{ still}}$	wind tunnel stilling chamber pressure
p_a	ambient air pressure
M	Mach number
\bar{f}	blockage factor
\bar{h}	ratio of diffuser throat area to test section.

Parameters of the ejecting gas are denoted by the symbols with a prime (for example, p_0'); Parameters of the ejected gas are denoted by the symbols with the index "1" (for example, p_{01}); The mixture parameters are denoted by the symbols with a double prime (for example, p_0'').

3. INTRODUCTION

Russia and TsAGI are pioneers in developing industrial wind tunnels in which the main flow is generated by a jet compressor-ejector. Currently, TsAGI has more than twenty sub-, trans-, super- and hypersonic wind tunnels where single-stage and multi-stage ejectors can be used. It goes without saying that of interest is the experience of development of such wind tunnels. Abroad they have not practically used the ejector drive for a long time, except for the facilities designed for engine testing. They became interested in such a drive about 15 years ago in connection with the problems of developing transonic high-Reynolds-number wind tunnels. Currently, such tunnels are being or have been developed in Sweden, China and other countries.

When developing a wind tunnel the most complicated thing is to develop a compressor and for a closed-circuit wind

tunnel it is the development of the system for flow cooling. When reaching supersonic speeds and large dimensions of wind tunnels and compressors these problems become hard to solve. The ejector drive provides solution of many problems, but at the same time generates a number of the specific ones. The major disadvantage of the ejector drive is its low efficiency which is due to a specific operating process in the drive, namely: nonelastic collision of the ejecting and ejected jets. The other essential disadvantage is the noise which is also due to the operating process in it, that is jet mixing. However, the ejector drive has several advantages. Besides simplicity, reliability, and large service life the possibility to accumulate energy in the high pressure bottles for a rather long time as well as reduction of transient time while running the wind tunnel and changing its operating conditions can be added to the advantages.

When developing the wind tunnel with such a drive the problems of the ejector optimization are usually solved. The currently developed theories for an optimal gas ejector allow it to be done rather successfully for different operating wind tunnel conditions. Currently difficulties arise in those cases when many operating conditions with respect to Mach numbers, blockage factor, Reynolds number range, and dynamic pressures are wanted to combine in one wind tunnel. In this case optimization is a difficult problem and extremely important one.

4. THEORY FOR OPTIMAL EJECTOR

A simple and widely used theory for the gas ejector is based on solving the equations of conservation (mass, energy, and momentum) for inlet and exit sections of a cylindrical mixing chamber with regard to the total pressure losses in the exhaust diffuser. This theory allows the device optimality criteria to be determined by using the variational calculus methods. It turns out that these criteria [1] are different for high and low pressure ratios. At low pressure ratios ($\epsilon < 1.05$) the ejector with a low equivalent velocity of the low-pressure gas is the optimal one (Fig. 1) and at high pressure ratios ($\epsilon > 1.1$) it is the device with a high almost sonic speed of the low-pressure gas at the mixing chamber inlet (Fig. 2).

The former of these optima is really achievable and there are examples of its realization in the practice of development of transonic wind tunnels and gas-filling systems of inflatable life rafts and escape slides. The latter optimum (at sonic speed of low-pressure gas) requires to fulfil contradictory criteria and is not really achievable. To approach to it (and thereby to improve ejector efficiency) the multi-stage designs were conventionally used whose limiting possible characteristics were investigated in detail by Uryukov and Christianovich in [2]. A certain approach to this optimum is also possible in the single-stage designs with a specific generation of flow in the mixing chamber [3].

5. HIGH PRESSURE RATIO EJECTORS WITH IMPROVED LIMITING CHARACTERISTICS

5.1. Ejector with offset nozzles. There exist many versions of ejectors with two nozzles for high-pressure gas. At a supersonic outflow of improper pressure ratio the

high-pressure gas jets have a shape of divergent and convergent cones. With location of all nozzles in a single initial cross-section the area maximums of all jets are in a single cross-section as well. In case with one offset nozzle in the flow direction this coincidence does not take place and as a result a passage section and ultimate mass flow of low-pressure gas increase. Figure 3 shows a flow pattern in the planar "sonic" ejector with the offset nozzle and Figure 4 presents the results of the experimental investigation of such a device. It is seen that the offset increases the ejecting-to-ejected gas mass ratio by a factor of 1.5-2.

5.2. Ejector with helical nozzle arrangement. In the axisymmetric gas ejector the offset of the wave maximums of the adjacent jets can be obtained with the high- and low-pressure nozzles of a helical arrangement (Fig. 5). The experimental investigation confirmed the possibility of improving the limiting characteristics although it was observed in the reduced operating envelope: $0 < q(\lambda) < 0.8$

(Fig. 6)

5.3. Ejector with perforated nozzle. It was discovered that perforation with longitudinal slots was the most effective way to change choking conditions for the gas ejector and improve its limiting characteristics at the initial section of the mixing chamber (Fig. 7). A perforated wall facilitates a rapid jet mixing already before the section of choking the ejector in the mixing chamber. The experiments show that this way allows some limiting characteristics to be improved by several times (Fig. 8). For example, a maximum pressure ratio of one of the tested ejectors has increased by a factor of 6.

The devices considered above have the improved limiting characteristics in case of inequality of the static mixed gas pressures at the inlet of the mixing chamber, i. e., in case of $q(\lambda) < 0.8$. Further it was suggested the scheme which allowed the ejector characteristics to be improved throughout the operating envelope, this was the ejector with a noncylindrical wall perforated at the boundary of the mixed jets. The experiments have shown that in the operating envelope of high equivalent mass flow of the low-pressure gas $q(\lambda) = 0.8 - 1$ characteristics can be improved by a factor of 2-3. The wall profile in the longitudinal section can be linear (conical) or curvilinear.

An example of a successful use of the ejectors of the new schemes is upgrading the TsAGI SVS-2 wind tunnel. This wind tunnel is mainly designed for investigations of aircraft inlets at trans-, super- and hypersonic speeds. The wind tunnel has a variable nozzle of the 500×516 mm exit section and changeable round nozzles of 565 mm exit diameter. The variable nozzle is designed for Mach numbers of up to 5 (without heating) and round nozzles are used at $M > 5$ with flow heating. To achieve high Mach numbers a single-stage ejector was installed in the exhaust duct of the SVS-2 wind tunnel. For the purpose of increasing a maximum Mach number achievable at a low pressure in the stilling chamber (up to 10 at) the above-said ejector was twice upgraded by means of installation of the wall with longitudinal slots in it.

In 1968 the use of a 1700 mm long perforated nozzle with 16 slots of 20 mm width allowed the ejector pressure ratio to be doubled from 5 to 10. In 1995 this nozzle was replaced by a new and longer one ($l = 2350$ mm) with 6 slots of 46 mm width. As a result of the second modernization the pressure ratio in the main operating wind tunnel conditions at Mach

numbers of 5 - 6 became two times greater (Fig. 9) this provided the opportunity to run the wind tunnel at 2 - 4 at. At the same time this allowed the Mach number range to be increased up to 7.5 - 8.

5.4. Compact gas ejector of high pressure ratio with helical nozzle arrangement. Schematic of this device is presented in Figure 10. The device comprises: mixing chamber 1, high-pressure gas stilling chamber 2, set of active supersonic nozzles 3, low-pressure convergent nozzle 4, and diffuser 5. The design suggested is simpler and easier to control than a multi-stage ejector system. However, from the point of view of gasdynamics it is more complicated than the ejector system because all its 9 independent geometric parameters are connected with each other through the process in the mixing chamber and have to be of a higher reliability. When developing the given ejector these parameters were experimentally specified.

An experimental characteristic of the investigated ejector with a helical nozzle arrangement (line 1) is presented in Figure 11 in the form of a pressure ratio-mass ratio curve. At zero mass ratio such an ejector provides a pressure ratio of 546. With increasing the mass ratio the pressure ratio decreases up to 50 at $K=0.01$.

To compare efficiency of such an ejector with the other versions, characteristics of the 4-stage ejector (line 2), the ejector with longitudinal slots (line 3), and the conventional single-stage ejector (line 4) are also presented in Figure 11. It is seen that the ejector with the helical nozzle arrangement provides higher pressure ratios and is more economic among the given devices. In comparison with the single-stage ejector to which it is similar in terms of structural parameters (small length, one stilling chamber, one controlling element) the characteristics of the ejector with the helical nozzle arrangement are several times higher. In comparison with the 4-stage ejector the pressure ratio and mass ratio gain is 20 - 30% and plus structural advantages.

This gas ejector is the first operating jet compressor of a high pressure ratio, in which the active gas supply distributed over the length is fulfilled as in a single-stage device. The positive result obtained in experiments evidences that development of jet ejectors without stages along with multi-stage well-proven systems is reasonable.

6. IMPROVING ECONOMIC EFFICIENCY OF WIND TUNNEL-EJECTOR SYSTEM

The economic ejector-driven wind tunnel efficiency mainly depends on the drive quality and the ejector cross-section. The less is the inlet ejector area, the greater is the economic efficiency of the system, however one can encounter the problem of attaining low Mach numbers (if wind tunnel is designed for many operational modes) or at high blockage factor. In the present chapter possibilities of meeting these conflicting requirements in one wind tunnel design are considered.

6.1. Gas cooling behind test section. In many wind tunnels the gas ahead of the nozzle is heated. Downstream of the test section there is no need for such an increased temperature and the high-pressure gas flow rate is proportional to the square root of the low-pressure gas temperature. From this follows that one of the possible ways of reducing operational costs is cooling of the gas sucked ahead of the ejector.

number of the main flow heated up to the condensation boundary and then cooled down to the previous temperature was carried out. The calculations have shown that at Mach numbers over 5, cooling the main flow can essentially reduce the high-pressure gas mass flow through the ejector, particularly, at $M=10$ almost by a factor of 2.

6.2. Supersonic variable diffuser. Use of a supersonic variable diffuser in the induction blowdown wind tunnels has a number of singularities. In particular, the invariable ejector located behind the variable diffuser demands almost the permanent compressed air mass flow irrespective of the diffuser throat dimension. That is why, there exists an opinion that a supersonic variable diffuser is ineffective in the ejector-driven wind tunnel. In fact, the situation is ambiguous. If the ejector of the variable cross-section area would be located behind the variable diffuser then reducing simultaneously the supersonic diffuser throat and the ejector cross-section could decrease the compressed air mass flow.

Starting and working heights of the diffuser throat sections of one of the TsAGI wind tunnels are presented in Figure 12. It is seen that at $M=5-10$ the starting height values in the wind tunnel with and without a model constitute about 0.5 of the test section height and the working height ones were up to 0.1. If the ejector dimensions can vary within a wide range then savings of the compressed air spend by the ejector could be 50 - 90% of the usual quantity. To confirm these assumptions an experiment with running the hypersonic ($M=5-10$) wind tunnel model having the diffuser throat-to-test section cross-section area ratio of 0.49 and essential blockage factor equal to 4-7% for a conical model; with regard for the model support the blockage factor was about 10 - 11% (Fig. 13).

Figure 14 shows the dependence of the starting and stalling conditions in such a wind tunnel on the Mach number of the cold flow (without heating). It is seen that the wind tunnel easily runs at all specified Mach numbers and a considerable flow contraction in the supersonic diffuser does not prevent from running the wind tunnel even with a large model. The flow heating somehow changes these values, but apparently it has no effect on the qualitative flow pattern. The experiments were performed with the model of the compact ejector described above and they are applicable to any ejector-driven wind tunnel. As a whole, this experiment has confirmed the possibility of further essential improvement of the efficiency of the supersonic wind tunnel ejector drives.

6.3. Use of parallel ejectors. The above-described ways for improving the economic efficiency encounter the obstacle which is due to the fact that the majority of wind tunnels are designed for many operating modes. The economic ejector cannot provide all operating modes. The solution of the problem may be in using into operation parallel ejectors: the wind tunnel can be equipped with several ejectors and involve them, if necessary. This will give an opportunity to realize more economic operating versions in all operating modes.

7. TRANSONIC EJECTOR-DRIVEN WIND TUNNELS

7.1. TsAGI T-109 wind tunnel. The TsAGI T-109 wind tunnel is one of the first and largest transonic ejector-driven wind tunnels. This wind tunnel is equipped with two ejectors: upstream and downstream ejectors (a supplier-ejector and suction-ejector). At transonic modes only the upstream ejector operates, it takes a dry air from the tunnel exhaustor and supplies it the stilling chamber together with the active air coming from gasholders. The mass ratio at $M=1$ attains 1, i. e., in comparison with a straight-through wind tunnel air savings constitute up to 50%. The T-109 wind tunnel was constructed in the 50s and at that time it was a great achievement.

7.2. Modern transonic ejector-driven wind tunnels. Currently many transonic ejector-driven wind tunnels are in operation and under construction. Since 1970 the T-2 transonic ejector-driven wind tunnel has been operating in Toulouse (France). Since 1988 a large 1.5×1.5 m transonic ejector-driven wind tunnel has been successfully operating in Sweden. In China a greater 2.4×2.4 m transonic ejector-driven wind tunnel has been constructing. This growth in construction of such wind tunnels is caused by two reasons. The first one is connected with aspiration to achieve higher Reynolds numbers at $M=1$; this essentially increases the required fan power and makes the wind tunnel design more complicated. The other reason is such that at high Reynolds numbers and high pressures in the test section the inner drag of the ejector-driven wind tunnel can be essentially reduced in comparison with a fan version by means of gas suction at the stagnation point of the working flow. This improves the efficiency of the wind tunnel-ejector system and makes its operational cost similar to the operational cost of the fan-driven wind tunnel and therewith we have a simple and reliable design.

There are several operating transonic model wind tunnels at TsAGI. In the T-02 facility the problem of an optimal suction of the air supplied by the ejector is studied with a special attention and for this purpose the tunnel has five suction units with the appropriate control devices. The T-02 proving wind tunnel characteristics are given in Figure 15. The Mach numbers obtained are in the range 0.2 - 1.35. The mass ratios at transonic speeds are 4 - 5.

REFERENCES

1. Yu. K. Arkadov, Optimal Gas Ejector with Diffuser, *Uchenye Zapiski TsAGI*, vol. XI, no. 2, 1980.
2. B. A. Uryukov, Theory for Differential Ejector, PMTF, no. 5, 1963.
3. Yu. K. Arkadov, On possibility of Improving Gas Ejector Characteristics by Varying Choking Conditions, Session on Mechanics, Abstracts, *Izvestiya AN SSSR*, 1968.
4. Yu. K. Arkadov, Compact Gas Ejector of High Pressure Ratio, *Uchenye Zapiski TsAGI*, vol. XV, no. 6, 1984.

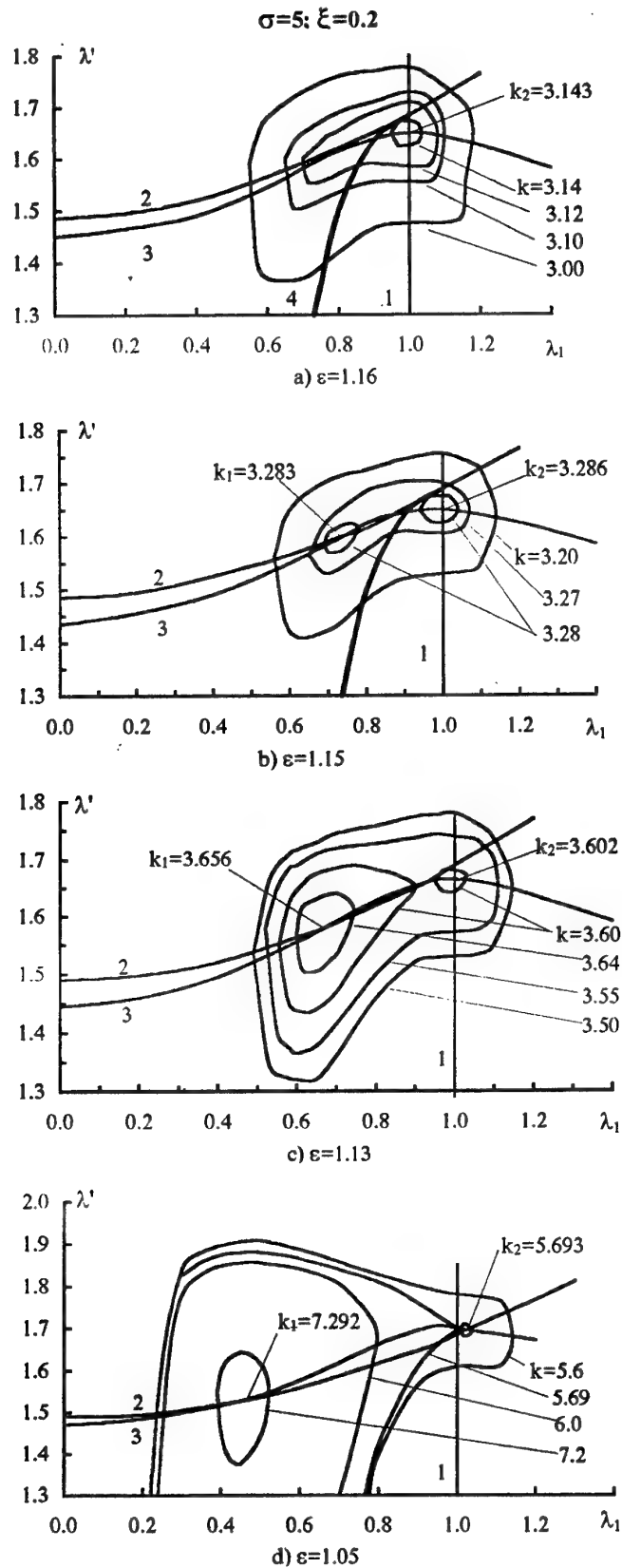


Figure 1. Locations of mass ratio maximum k at various calculated pressure ratios ($k=\text{const}$ are level lines)

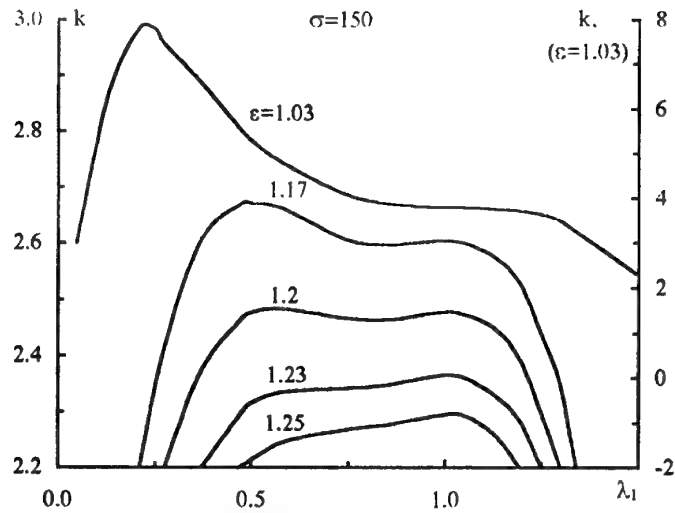


Figure 2. Variation of mass ratio k with equivalent velocity λ_1 for ejectors of different pressure ratios ϵ

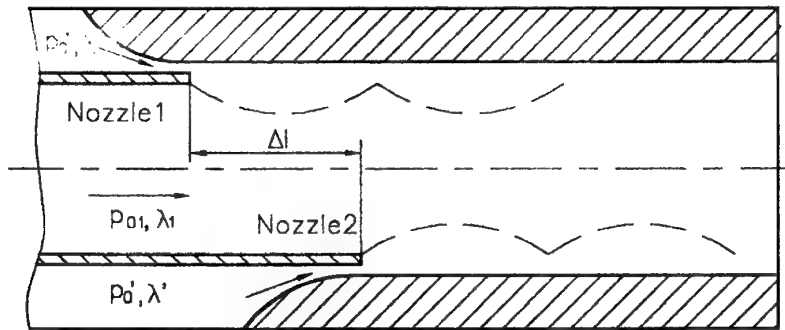


Figure 3. Jet flow pattern in planar ejector with offset nozzle

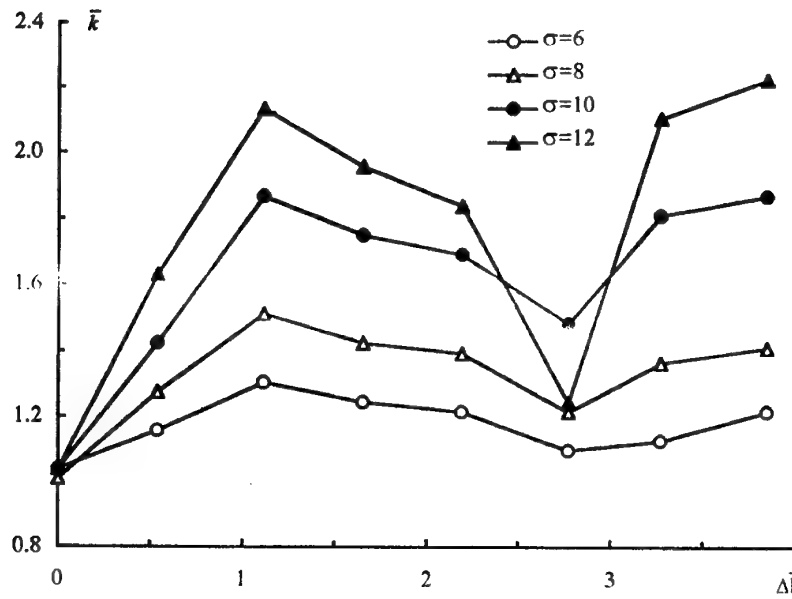


Figure 4. Gain in mass ratio \bar{k} depending on relative nozzle offset $\Delta \bar{l}$.

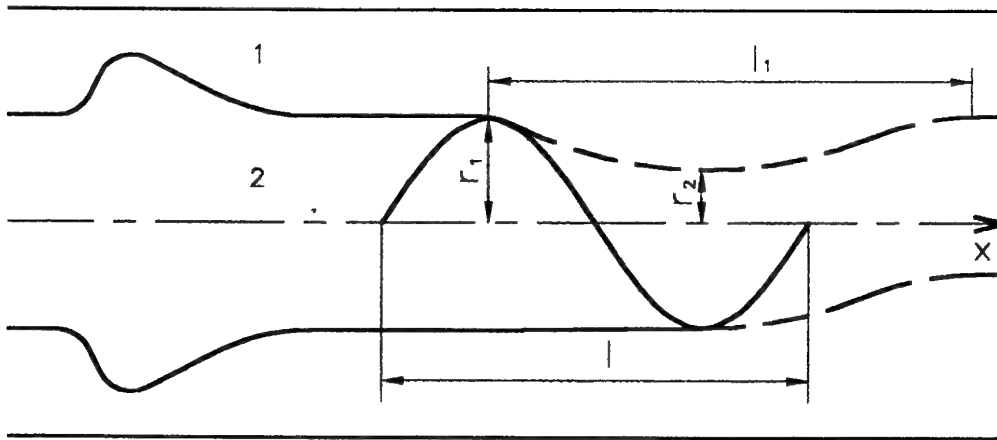


Figure 5. Schematic of ejector with helical nozzle arrangement

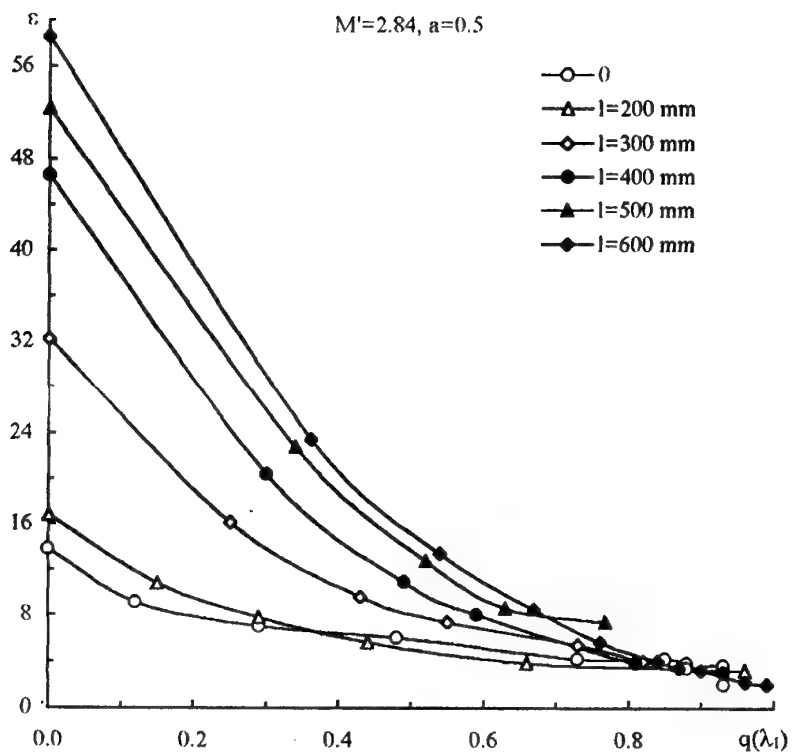


Figure 6. Dependence of ultimate pressure ratio ε on equivalent low-pressure gas mass flow $q(\lambda_1)$ at different lengths of helical line

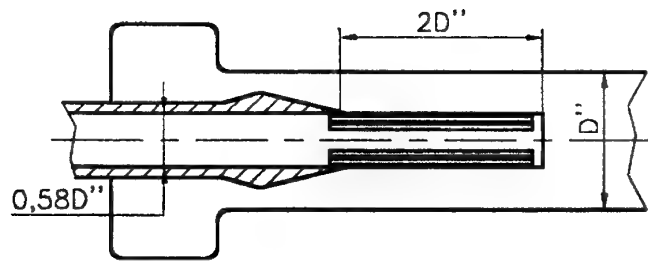


Figure 7. Schematic of ejector with perforated nozzle

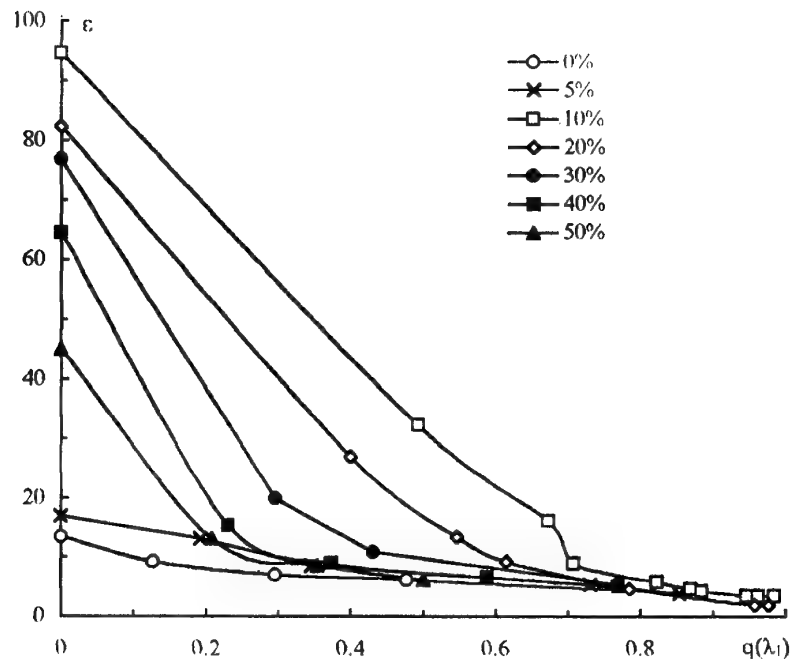


Figure 8. Characteristics of ejector with perforated nozzle at different ratios of slot area to cylindrical side wall surface area (%)

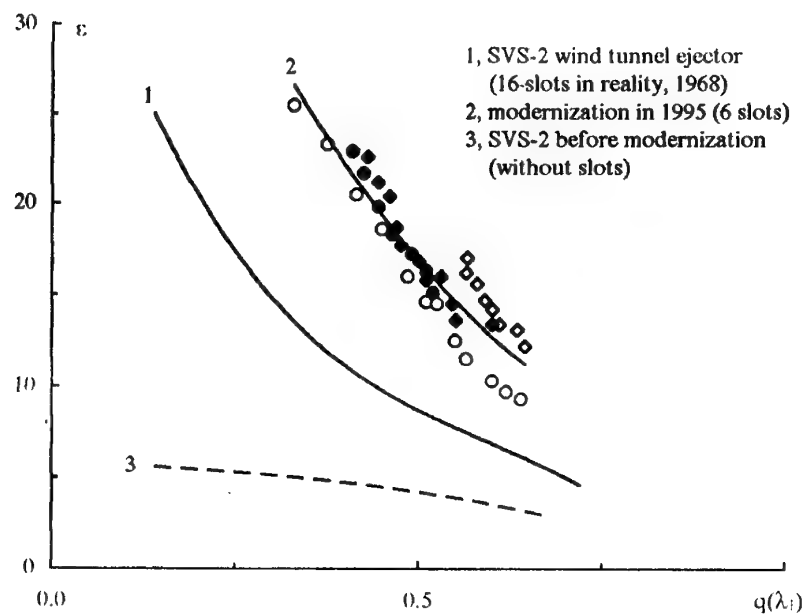
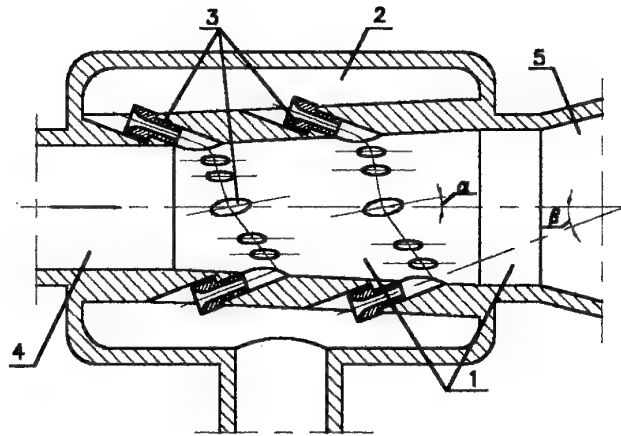


Figure 9. Characteristics of SVS-2 wind tunnel ejector of classical scheme (without slots) and with 16 slots (1968) and 6 slots (1995)



- 1, mixing chamber 3, set of active supersonic nozzles 5, diffuser
 2, high-pressure gas stilling chamber 4, low-pressure convergent nozzle

Figure 10. Schematic of compact ejector with many nozzle

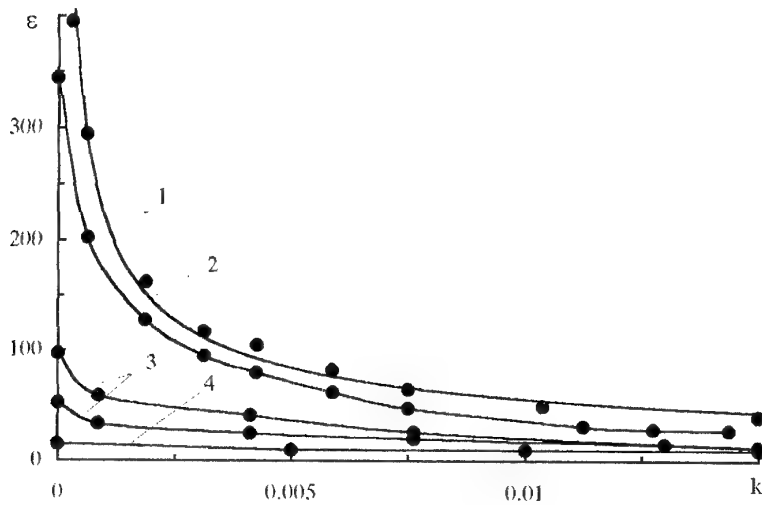


Figure 11. Characteristics of compact ejector (1), 4-stage ejector (2), ejector with perforated nozzle (3), conventional ejector (4).

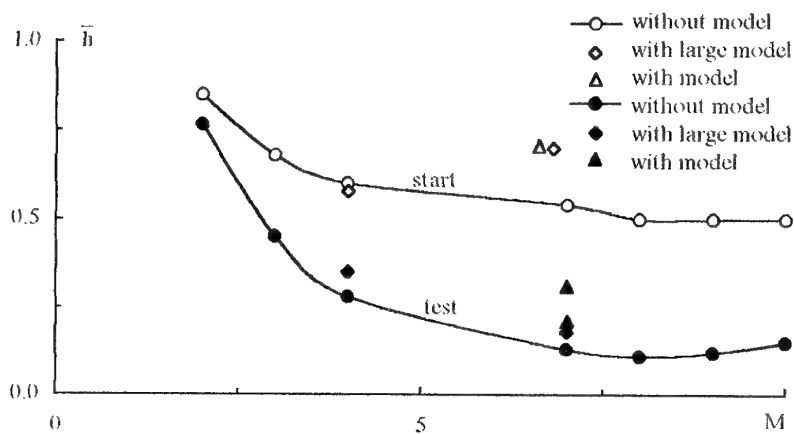


Figure 12. Experimental dependencies of minimum relative diffuser throat height on flow Mach number with and without models in test section for starting and operating wind tunnel modes.

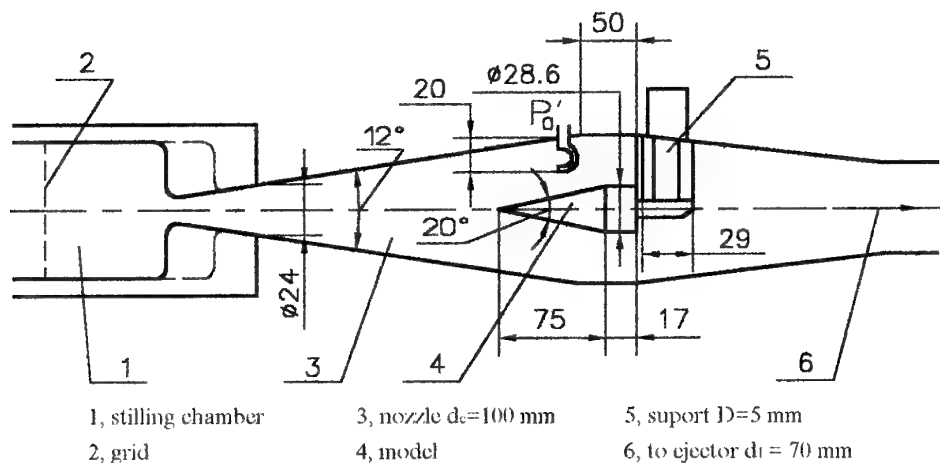


Figure 13. Schematic of hypersonic ejector-driven wind tunnel with high flow contraction downstream of test section $\Gamma=0.49$

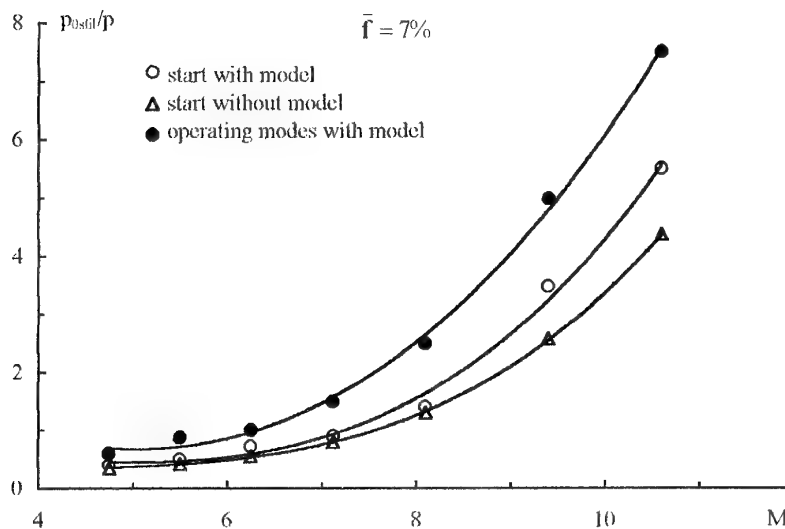


Figure 14. Pressures in stilling chamber, corresponding to starting and operating hypersonic wind tunnel modes flow contraction $\bar{F}=0.49$

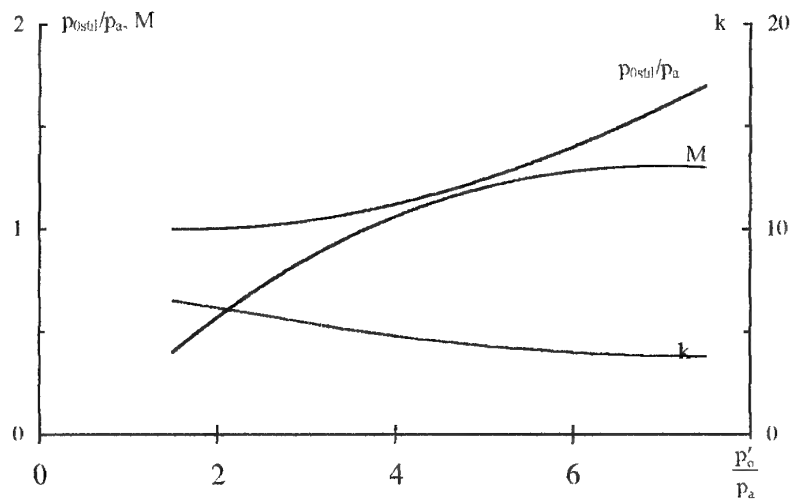


Figure 15. Experimental characteristics of T-02 transonic ejector-driven wind tunnel model.

IMPROVING TRANSONIC WIND TUNNEL COMPRESSOR OPERATION BY MEANS OF GUIDE VANE ANGLE OPTIMIZATION

A.G. Kukinov, G.E. Dyadchenko,
A.A. Lunyov and V.S. Panasenko,
Central Aerohydrodynamic Institute (TsAGI), 1, Zhukovsky Street
140160 Zhukovsky, Moscow Region, Russia

SUMMARY

The implementation of adjustable guiding vanes (AGV) angle of setting optimization for the transonic wind tunnel's compressor characteristics' improvement is considered. Experimental research results of gas dynamic characteristics of T-128 wind tunnel's compressor and dynamic stress in its blades are presented.

Necessity of monitoring the operation point position in the compressor operating envelope for providing its stable operation is shown.

NOMENCLATURE

π	compressor total pressure ratio
$G_c = G\sqrt{\theta}/\delta$	corrected air flow
$N_c = N/\sqrt{\theta}$	corrected rotor rotational speed
θ	ratio of compressor inlet total temperature to standard condition
δ	ratio of compressor inlet total pressure to standard condition
$\pi_d, G_{c,d}, N_{c,d}$	designed values of π , G_c and N_c
$\bar{\pi} = \pi/\pi_d$	rated total pressure ratio
$\bar{G} = G_c/G_{c,d}$	rated corrected air flow
$\bar{N} = N_c/N_{c,d}$	rated corrected rotor rotational speed
M	Mach number in wind tunnel test section
η	compressor adiabatic efficiency
η_d	compressor adiabatic efficiency at designed pressure ratio
$\bar{\eta}$	compressor rated adiabatic efficiency
$\Delta\theta$	vane turn angle (vane setting angle increment)
i	blade incidence angle
σ	vane dynamic stress

ABBREVIATIONS

GV	guide vanes
IGV	inlet guide vanes
OGV	outlet guide vanes
CW	compressor wheel

1. INTRODUCTION

We shall note some features of the compressor operation in the sub- and supersonic wind tunnel, which has fixed dimensions of the test section. These features are connected to matching of increase of a total pressure, required for operation of a wind tunnel and available increase of total pressure, produced by the compressor. In particular, an axial compressor has high efficiency only in the narrow area within its operating envelope: compressor total pressure ratio π versus corrected air flow G_c . In the case of sub- and supersonic wind tunnel only the regimes of compressor

operation take place in this area, which correspond to maximum Mach numbers in the test section.

At the supersonic regimes of the wind tunnel operation, if the Mach number decreases from maximum to $M = 1$, the required compressor total pressure ratio decreases under near-fixed air flow and the working point on the compressor characteristic (π versus G_c curve) is brought into compressor low efficiency area. Low required values of compressor total pressure ratio are still retained also at subsonic speeds in the wind tunnel test section. Because of this compressor efficiency has very low values in the whole range of subsonic speeds. This case takes place even in the wind tunnel, which is designed for moderate values of maximum Mach number (~ 1.6). For illustration in Fig. 1 the characteristics of the compressor, curves of the equal efficiency values and design curves of the required total pressure ratio are presented; Mach number values in the test section of the wind tunnel are also depicted on the last curves.

The low values of efficiency are not the only negative property of the transonic wind tunnel compressor. The low values of the required total pressure ratio at subsonic speeds result in flow past the blade rows at off-designed incidence angles that along with the efficiency decrease causes increase of blade dynamic stresses.

In the present report by the example of the T-128 wind tunnel compressor, which aided by AGV, some opportunities of its operation improvement are considered. A double control of the compressor is applied in the wind tunnel: by changing the rotor rotational speed and setting up the AGV. Such a control noticeably improves the operating conditions of the compressor; in particular, it excludes the necessity of a long operation close to resonant speeds of rotation and provides necessary fast-action of a control system. However, at original control of AGV (when the blades of all AGV turn through the same angle), mentioned above matching features of the compressor and wind tunnel characteristics are not eliminated.

Design parameters of 4-stage compressor of T-128 wind tunnel are follows:

- compressor total pressure ratio $\pi = 1.56$,
- corrected blade tip velocity $U/\sqrt{\theta} = 212$ m/s,
- corrected axial flow velocity in front of compressor $C_{A1}/\sqrt{\theta} = 124$ m/s,
- hub/tip ratio $\bar{a}_h = 0.68$.

The model of the T-128 wind tunnel compressor was constructed for testing of design characteristics and simulation of possible operation regimes of the compressor. The given below gas dynamic characteristics of the compressor was obtained as a result of the model tests.

2. SUBSONIC SPEEDS IN THE WIND TUNNEL TEST SECTION

An attempt was made to increase the compressor efficiency at subsonic speeds in the wind tunnel test section through the application of optimization of vanes turn angle. For this purpose the nonlinear programming problem of choice of vane turn angle values, ensuring maximum efficiency at the given point in the compressor operating envelope (at π -vs.- G_c plot) was solved [1].

The solution of the problem will allow to design the optimized program for compressor AGV control, which is intended to operate at subsonic speeds in wind tunnel test section. The optimized program was checked of the model of wind tunnel compressor. Results of the model tests demonstrated, that compressor efficiency increased on approximately by 10% when it was controlled by the optimized program in comparison with the case, when it was controlled by the original control program. The aforesaid may be illustrated in Fig. 2 where the efficiency values, referred to its value at the designed total pressure ratio, as a function of the rated corrected air flow \bar{G} at various values of the rated corrected rotor rotational speed \bar{N} .

The compressor efficiency increase by optimization of vane turn angle is the result of a flow improvement past the blade rows. Thus non-uniformity of flow parameters distribution through the blade rows, in particular blade incidence angles, decreases. Figure 3 demonstrates the designed results of blade incidence angles distribution through the blade rows, when the compressor is operated by the original and optimized AGV control programs at $\bar{N} = 0.55$ and two values of \bar{G} .

As in the considered case operational total pressure ratio of the compressor is distinctly less than its maximum value at the given rotor rotational speed, the blade incidence angles through all blade rows (except inlet guide vanes - IGV) become negative. For the original control program the maximum blade incidence angle in magnitude is achieved at last blade rows. During the optimization of AGV control program these values decrease noticeably, that owing to the nonlinear dependence of pressure loss coefficients versus blade incidence angles results in essential reduction of overall losses of total pressure in the compressor.

Another important outcome, obtained due to application of the optimized the AGV control program, was the resonant dynamic stresses decrease in the rotor blades of the full-scale compressor at the subsonic operation regimes of wind tunnel. As this takes place, dynamic stresses in the blades of 4-th compressor wheel have decreased noticeably. These stresses were detected at blades vibrations under the third mode on frequencies equal $f = 34 N$ (at $\bar{N} \sim 0.55$) and $f = 24 N$ (at $\bar{N} \sim 0.814$), where N is the rotor rotational speed. In the first case the vibrations were caused by the influence of the guide vanes GV, located in front of the compressor wheel; in the second case - by the influence of GV located behind it. The calculation analysis showed, that reduction of stresses took place at the expense of decreasing the variable aerodynamic forces which excite vibration of the blades. The values of dynamic stresses are determined by measurement results, which was performed in 6 blades (of the 4-th compressor wheel) depending on the designed estimation of the exciting aerodynamic force are shown in Fig. 4 (where \bar{Y} is nondimensional exciting aerodynamic force;

$\bar{\sigma} = (\sigma / p_1^*) \cdot 10^{-2}$, where p_1^* is total pressure in front of compressor).

For estimation of the variable aerodynamic force, acting on the compressor wheel (CW) blade and which is induced by the upstream GV vortex wake, a simplified physical model [2] was used, in which this force was connected with the flow velocity in the wake by the same equations as for an undisturbed stream. According to the model the flow velocity decrease in the wake is considered to be proportional to the profile loss coefficient in the GV cascade. The guiding vanes placed downstream of CW creates a circulatory non-uniformity of pressure and axial velocity distributions behind the compressor rotor cascade. For a quantitative estimation of the non-uniformity the jet streamlining of flat plates cascade theory [3] was used. As it is shown in Fig. 4, optimization of the AGV control program results in an essential decreasing of the variable aerodynamic forces, acting on the compressor wheel blades. It turned out that the dynamic stresses in the blades were near-proportional to the variable aerodynamic force at application of both AGV control programs.

3. SUPERSONIC SPEEDS IN THE WIND TUNNEL TEST SECTION

The mentioned above optimized control program cannot be used for compressor control in the supersonic operation regimes of the wind tunnel. In this case the problem of maximum Mach number attainment in the test section comes into being. Thus the AGV control program should provide the highest possible position of compressor stall boundary in the operating envelope.

To create such control program, due by the authors solution of the problem of maximum value of the compressor total pressure ratio at the given rotational speed and air flow, was used. Figure 5 compares the compressor stall boundaries (based on the compressor model test results) for the AGV various control programs. Here also designed connections between π and \bar{G} are shown, which should be realized in the wind tunnel at various values of the model aerodynamic drag, which may be installed in the test section. It can be seen from Fig. 5, that the optimized control program essentially rises up the compressor stall boundary in comparison with original control program. The subsonic control program gives the lowest position of the compressor stall boundary.

At supersonic speeds in the wind tunnel test section the required total pressure ratio depends on the tested model aerodynamic drag. As this drag is not known beforehand, the operation points on the compressor characteristic can appear near the compressor stall boundary. Therefore there is a necessity to supervise a compressor stall margin:

$$\Delta K = \left(\frac{\pi^* G_c^*}{\pi G_c^*} - 1 \right) \cdot 100\%, \text{ (where } \pi^* \text{ and } G_c^* \text{ are the values}$$

at stall boundary), when the wind tunnel operates in the supersonic regimes. For this purpose the reduced air flow and total pressure ratio are measured during tests on the full-scale compressor, basing on these values the stall margin ΔK is calculated. In doing so, compressor operation regimes are limited by a certain minimum value ΔK .

Figure 6 shows the compressor characteristic as superposition with designed curves of ΔK equal values and operation curves, which are drawn by the test points, realized in the test of a certain aircraft model. Each operation curve corresponds to a constant value of Mach number in test section at various

model angles of attack. Here is also depicted the compressor stall boundary for a subsonic control program case. It can be seen from this curves, that the considered regimes of compressor operation cannot be obtained completely through the use of this program.

In conclusion it should be noted, that at supersonic velocities of flow in test section, the wind tunnel is operates at design rotational speed of the compressor. The transfer from subsonic AGV control to supersonic one (and backwards) is accomplished at this compressor rotational speed. Because of absence of blades resonant frequency in the vicinity of the compressor design rotational speed, problems of blades' dynamic stresses have not takes place at supersonic regimes of wind tunnel operation and at transfer from the control program to another one.

REFERENCES

1. Kukinov, A.G., Lunyov, A.A. and Romashkin, I.K., "On Choice of Optimal Adjustable Guiding Vanes Turn Angles for Axial-Flow Compressor", Trudy TsAGI, issue 1785, 1976 (in Russian).
2. Samoilovich, G.S., "Nonstationary Flow Around and Turbomachine Cascades Aeroelastic Vibration", Nauka, Moscow, 1969 (in Russian).
3. Stepanov, G.Yu., "Hydrodynamics of Turbomachine Cascades", Fizmatgiz, Moscow, 1962 (in Russian).

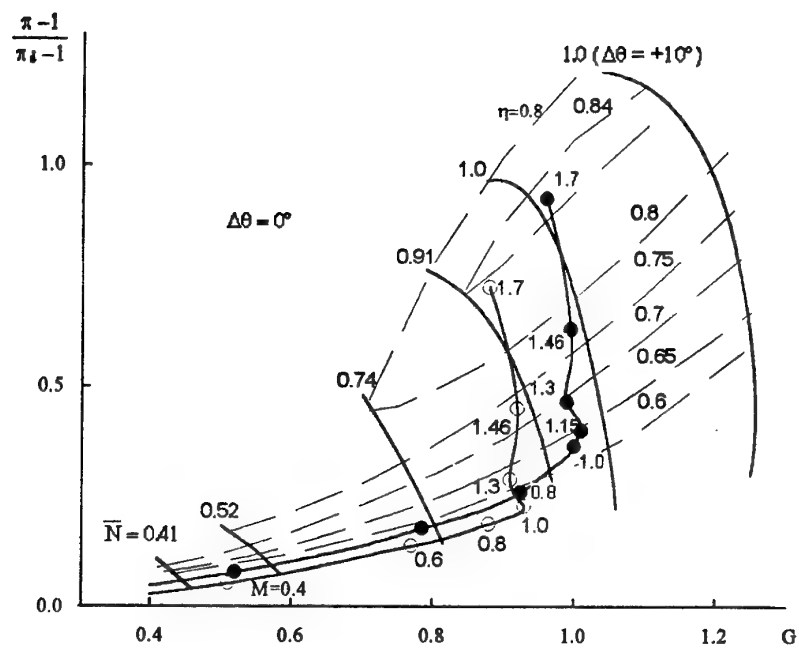


Figure 1. Compressor performance characteristics and operating lines

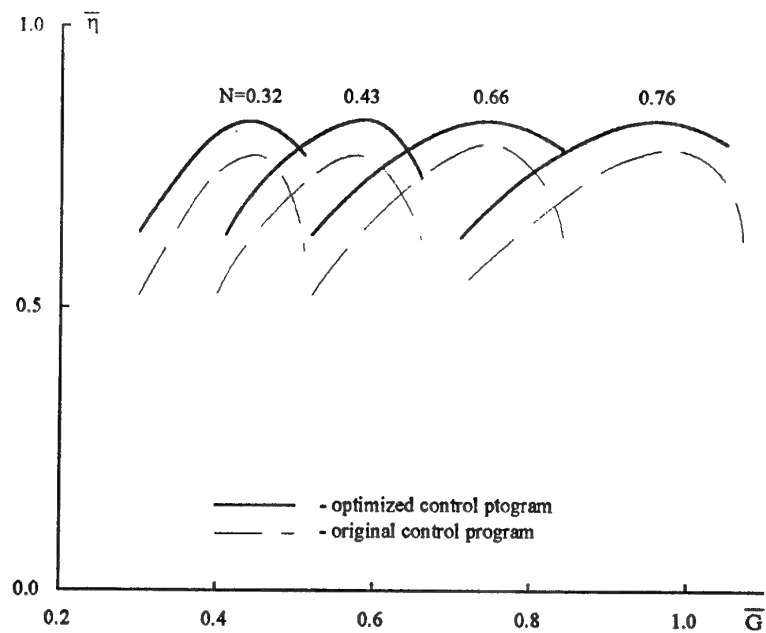


Figure 2. Compressor efficiency under two AGV control program

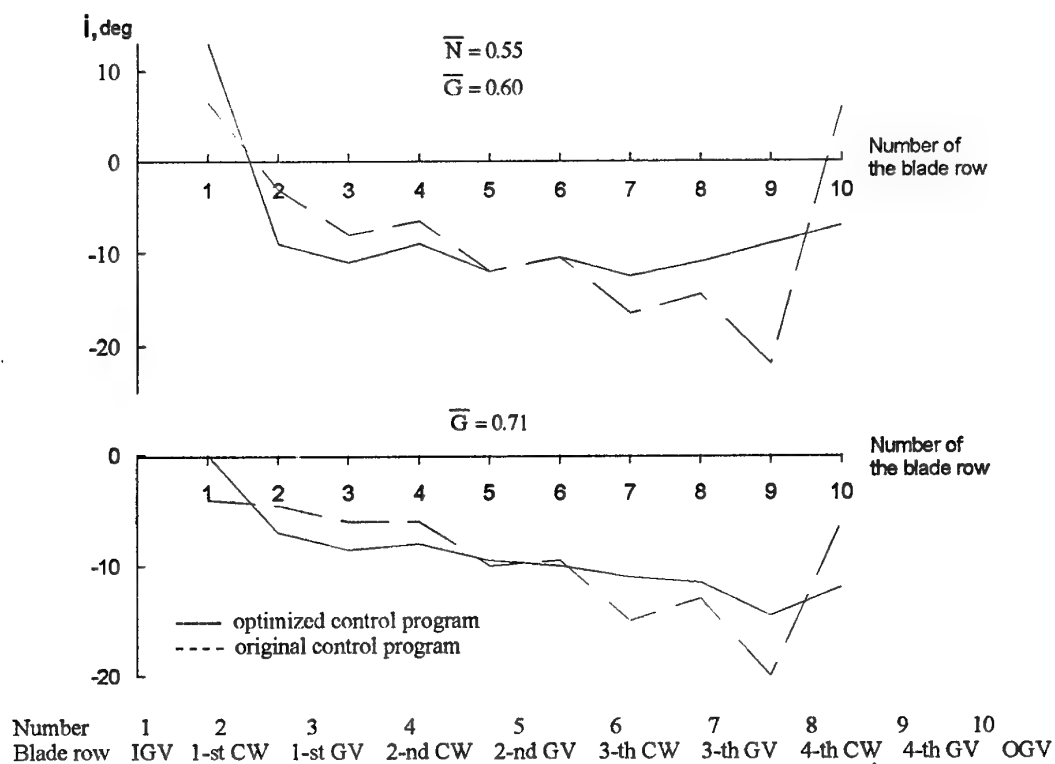


Figure 3. Incidence angles profile along blade rows

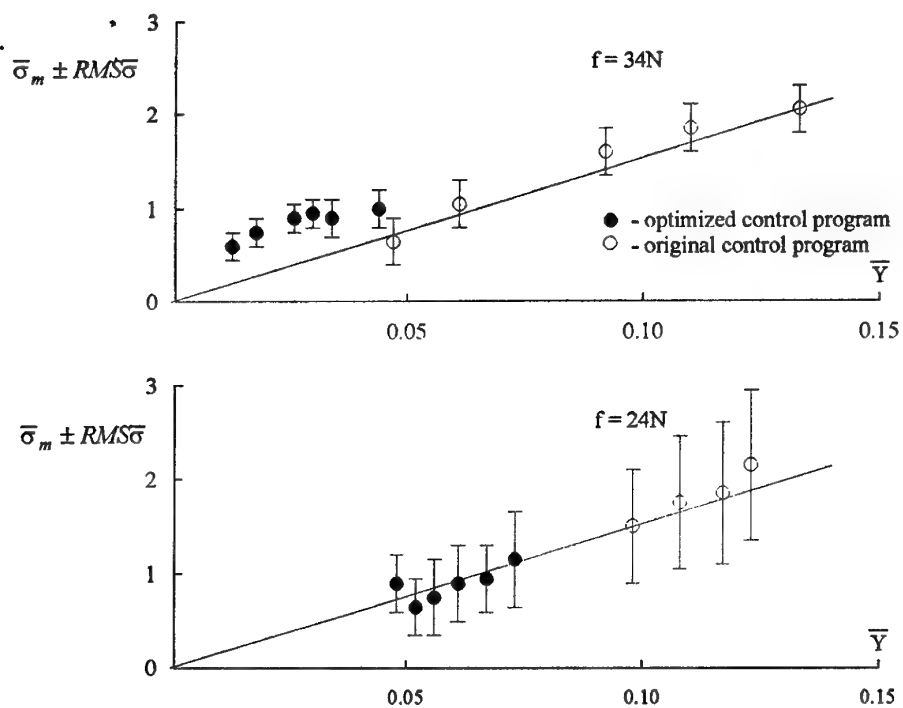


Figure 4. Dynamic stresses in blades of 4-th rotor wheel in depends on variable aerodynamic force

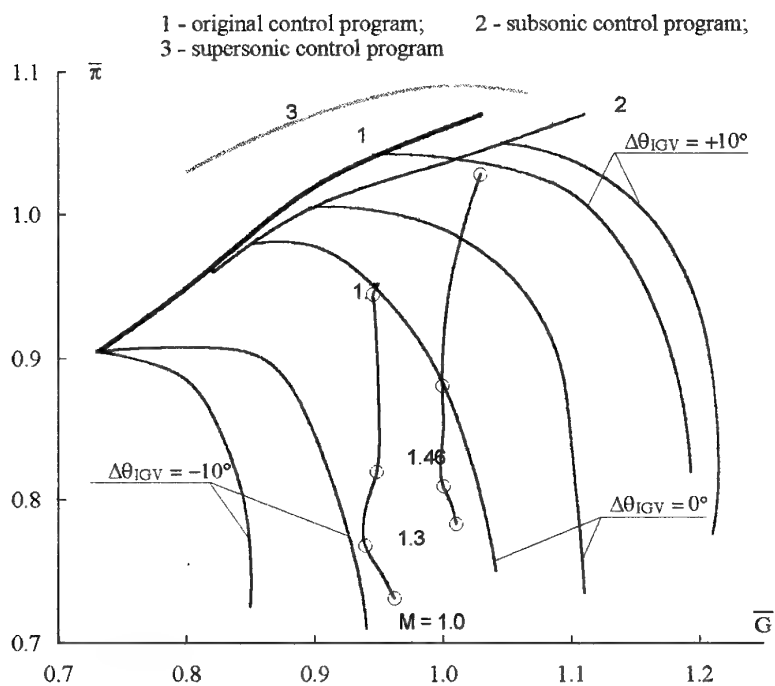


Figure 5. Compressor performance characteristics under different control program

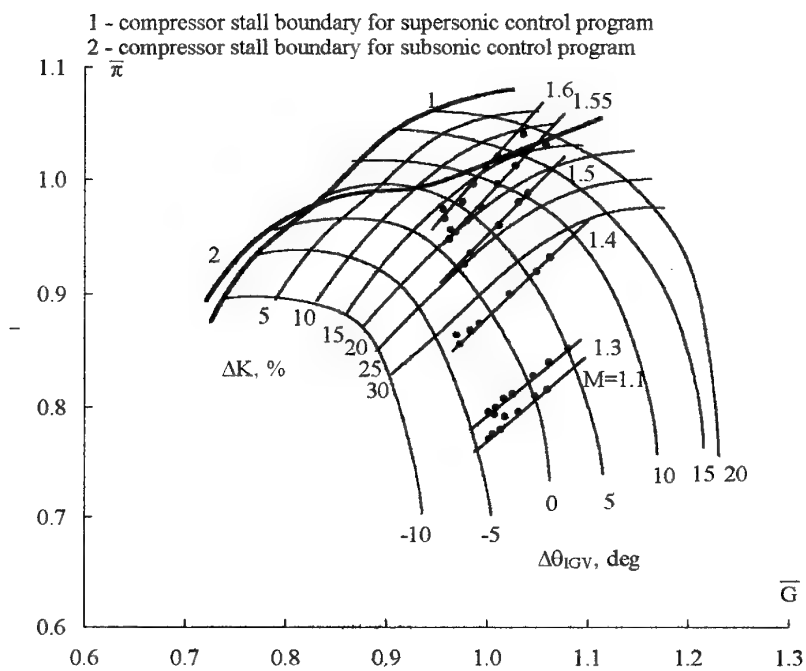


Figure 6. Compressor map at various Mach numbers in wind tunnel test section

Development of Closed-Circuit Subsonic Wind Tunnel with Diametral Fan.

Korovkin A.G.*, Savchuk V.D., Kuroles V.K.

Raduga Machine-Building Design Bureau
2a, Zhukovsky Str, Dubna, 141980 Moscow Region, Russia

* Scientific-research Centre of TsAGI
17, Radio Str, 107005 Moscow, Russia

SUMMARY

In this paper the features of air flow in a diametral fan (DF) contour and its aerodynamic characteristics are reported. The field of application for the DF in the wind tunnels is determined. The results of experimental investigations of DF geometrical parameters effect on DF aerodynamic parameters are given.

The performance data of the MBDB Raduga compact subsonic wind tunnel and the Laboratory Training Aerodynamic Complex (ULAK) for Technical Schools which is developed on its base are offered.

The method of approximate simulation of following a body contour with a liquid with free surface in a wide range of F_z numbers for subsonic wind tunnels is proposed, and the possibility of DF use in the installations of this type is considered.

SYMBOLS

b	working wheel length, m;
$\bar{b} = b/D$	relative length of the working wheel;
D, D_1	working wheel diameter acc. to inner and outer blade edges, m;
$D_{med} = (D+D_1)/2$	
F	fan characteristic area, m^2
for DF	$F = D \cdot b$,
for AF	$F = \pi D^2/4$;
$Fr^2 = V^2/(gL)$	Froude number;
f	blade profile deflection;
L	characteristic dimension of the WT-tested model;
l	blade profile chord, m;
M	Mach number;
N	working wheel shaft horsepower, W;
n	wheel rotation frequency, 1/min;
p_v	total fan pressure, Pa;
$Re = UD/v$	Reynolds number;
Q	fan capacity, volumetric air consumption, m^3/s ;

$q = \rho V^2/2$	velocity head, Pa;
$U = \pi D n / 60$	wheel tip speed, m/s;
V	air flow velocity, m/s;
z	number of wheel blades;
β_1, β_2	blades angle acc. to inner and outer blade edges;
δ	radial clearance rate;
$\eta = Q p_v / N = \varphi \cdot \psi / \lambda$	DF overall efficiency;
θ	angle of casing cowling opening, or wheel circular coordinate;
$\lambda = 2N/(\rho F U^3)$	fan consumed power coefficient;
ν	kinematic viscosity coefficient, m^2/s ;
ξ	wind tunnel hydraulic resistance coefficient related to velocity head in the wind tunnel working section;
ρ	air density, kg/m^3 ;
$\tau = l_s z / \pi D_{med}$	chord spacing ratio of wheel blade cascade;
$\varphi = Q/(D \cdot b \cdot U)$	DF capacity coefficient;
$\psi = 2 p_v / (\rho U^2)$	DF total pressure coefficient.

INDICIS:

sh	shaft
w.s	working section
x	in x-direction
y	in y-direction

I. INTRODUCTION

The wind tunnel (WT) design work is to be performed with regard to the following requirements:

- obtaining the conditions of uniform stationary flow in the WT working section;
- providing a small degree of turbulence;
- meeting the similarity criteria;
- convenience in testing (access to the working section, working section capacity, noise, etc.);
- high aerodynamic efficiency;

- simplicity of structure and small dimensions (compactness).

The basic components of the closed-circuit subsonic WTs are: nozzle, working section, diffuser, fan unit, elbows with swinging blades, return channel and prechamber with flow straightening and aligning devices. The fan type and correlation between its aerodynamic characteristics and WT air network characteristics are of first importance in selection of WT configuration and its geometric dimensions.

At the present time, creating a subsonic wind tunnel does not present to serious scientific or technical difficulties because of a great experience gained in many countries concerning its design, development and manufacturing. Both the configurations of such a wind tunnel and the use of the axial-flow fans (AF) in its structure are conventional.

In this paper we consider ability of the use of DFs in the subsonic wind tunnels, which, even if less efficient than the AFs, are more simple in their structure that allow us to reduce the WT dimensions and enhance WT capabilities for working-section flow control.

It is known that these proposals have been offered before but we do not know any publications about the existing wind tunnel designs of this type, much less about their realization.

This paper contains the results of:

- conducting parametric and physical aerodynamic studies of all main components of the working wheel (rotor) and DF casing as well as of their inside flow pattern;
- choosing the aerodynamic layout and designing optimal DF dimensions for the subsonic WT with flow velocities in its working section of 10 to 60 m/s, and analysis of aerodynamic control methods;
- detailed design, manufacturing, adjustment and experimental operation of the Laboratory Training Aerodynamic Complex (ULAK-1) with the subsonic WT designed for R&D works and efforts of applied character on vehicle and industrial aerodynamics for production and training purposes.

2. DF FEATURES AND POTENTIALITY OF USE FOR SUBSONIC WIND TUNNELS.

The diametral flow in bladed turbomachines (in technical literature they are designated as diametral, tangential or cross-flow ones) is characterized by two-fold flow about the common vaned circular cascade. The mechanism of initiation of the flow is as follows.

When placing the uniformly rotating wheel with a cascade of forward-curved vanes in gas or fluid space unbounded with walls and in so doing eliminating

the possibility of medium motion along the axis, a circulatory motion of a medium appears, a "vortex" with the rotation axis coincident with the wheel's one. The major condition for initiation of diametral flow in the wheel is the availability of an asymmetry about the rotation axis. In this case the axisymmetric flow is transformed so that the vortex axis transfers to a new position - to the wheel periphery. Independently of a nature of flow-transforming elements the axis of the new vortex position in distorted, non-axisymmetric velocity field does not go beyond the circle boundaries with a diameter on outer tips of the wheel's blades. And the vortex itself is generally located near the non-axisymmetric elements.

The so-called lateral (diametral) flow which is formed under these conditions doubly intersects the circular cascade of the same wheel, turns through availability of the vortex zone about its axis and envelopes the vortex (Fig.1). In fact, the DF is a two-stage bladed machine with the one operating wheel. The first stage operates as in a centripetal fan, and the second one - as in a centrifugal fan.

To obtain a diametral flow through creating an axial unsymmetry we can use:

- a) an outer (side) flow, such as a plane one, created through another machine;
- b) an unsymmetric casing, such as a bend-shaped one, or variously shaped bodies located outside the wheel's circular cascade (Fig.1);
- c) plate- or profile elements as well as the bladed system (the interior guiding device) located inside the wheel, i.e. in the space which is bounded by a contour of the vaned circular cascade.

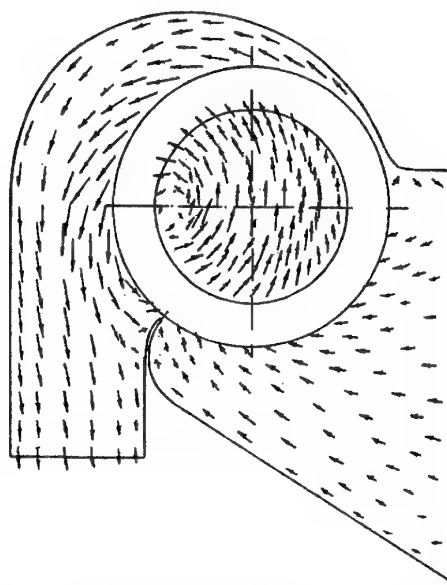


Fig.1. Vector diagram of absolute velocities in the diametral fan flow section

Using the above-outlined wheel flow model as the base we have developed a great set of DF configurations with various aerodynamic and energy parameters (Fig.2). The DF principal structural configuration consists of the operating bladed wheel with an arbitrary extension, which is mounted in the casing with an inlet branch pipe and a delivery one (diffuser).

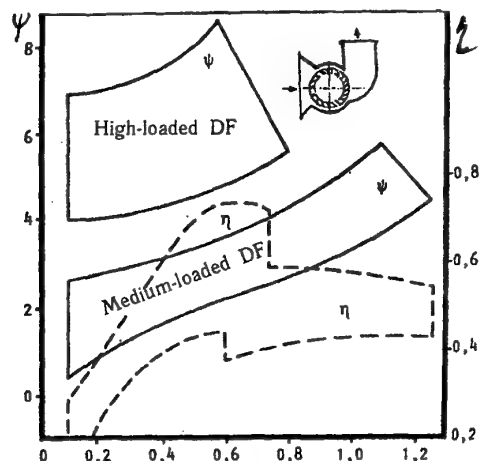


Fig.2. Areas of nominal parameters at the regime of diametral-fan maximum efficiency.

Compared to the AF, the wheel (rotor) design is considerably simple. Furthermore, the flow in the DF can be rotated through 90...180 degs, allowing the WT structure to be simplified.

The different types of fans can be compared between each other using the accepted fan-building performances and parameters, like capacity and pressure coefficients, specific velocity and overall dimensions.

To compare aerodynamic facilities with different types of fans, it is necessary to work out an integrated criterion which will include both the fan and WT performances.

To assess an area of DF application in the WT we use the relation

$$\psi = \xi \varphi^2 / \bar{F}^2 \quad (1)$$

derived from the following expressions

$$\psi = \frac{2 \cdot p_v}{\rho U^2}, \quad \varphi = \frac{F_{ws} \cdot V}{F \cdot U}, \quad p_v = \xi \frac{\rho V^2}{2}$$

At designated ratio of working section area to the fan characteristic one and at the known values of WT hydraulic resistance we obtain the relationship of necessary values $\psi = f(\varphi)$. A comparison of this relationship with the aerodynamic characteristic of any type of a fan defines the area of its working points.

In Fig.3 we present the comparison of characteristics of the particular DF/AF types.

Let us introduce K_ψ , K_φ , K_ξ , K_F , K_D , K_n coefficients as ratios between homogeneous characteristics and parameters of WT with DF and those of WT with AF, corresponding to operating points values.

The following ratios are recorded for these coefficients:

$$K_\psi = K_\xi \cdot K_\varphi^2 \cdot K_F^2 \quad (2)$$

$$K_D = \frac{0.886 \cdot K_F^{0.5}}{\bar{b}^{0.5}} \quad (3)$$

$$K_n = 1.128 \frac{\bar{b}^{0.5}}{K_\varphi \cdot K_F^{1.5}} \quad (4)$$

With reference to Fig.3, it can be seen that DF operation area as compared with AF one is defined by $K_\varphi > 3.0$ and $K_\psi > 10$ coefficients. In addition it is seen that for DF operation in nominal conditions the WT should have high values of ξ , and thus aerodynamic efficiency of the WT with DF will always be less than that of the WT with AF, with regard to lower efficiency of DF.

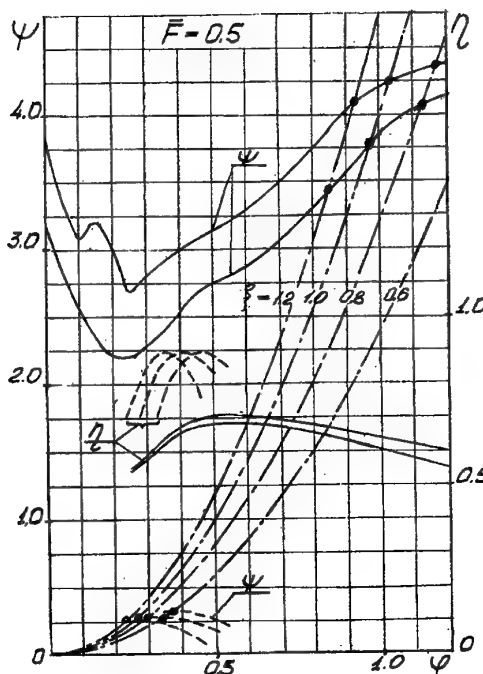


Fig.3. Chart for determination of fan's nondimensional coefficients depending on the WT hydraulic resistance.

On the other hand, from (3), (4) expressions it follows that DF will be smaller in diameter and have lesser r.p.m. as compared with AF, and consequently the overall dimensions of the WT with DF can be considerably smaller than those of the WT with AF, with regard to structural features.

Fig.4,5 demonstrate aerodynamic configurations of the WT with AF with working section of $D=0.6$ m and the WT with DF with working section of 0.6×0.4 sq.m.

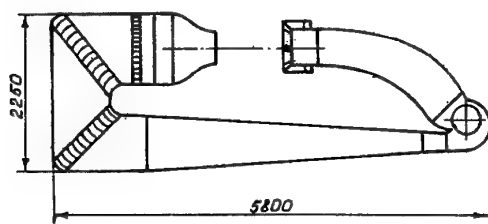


Fig.4. Scheme of the WT with DF (working section of 0.4×0.6 sq.m).

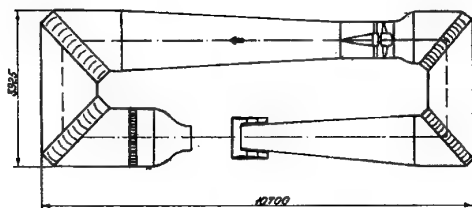


Fig.5. Scheme of the WT with AF (working section of $D=0.6$ m).

3. PARAMETER INVESTIGATIONS OF DF AERODYNAMIC CONFIGURATION.

In theoretical and experimental investigations of DF aerodynamics geometrical parameters of the wheel vane cascade and contours of the casing flow ele-

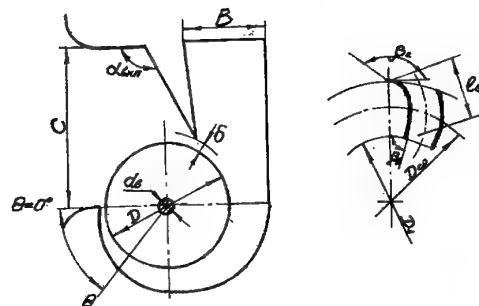


Fig.6. Scheme and designations of the main optimizing geometrical parameters of the working wheel and fan casing.

ments, given at the diagram in Fig.6, were optimized.

It has been found that the vane channel of the wheel must be of a diffuser-confuser shape, and inner (β_1) and outer (β_2) edge blade pitch optimum angles are: $\beta_2 = 150^\circ \pm 5^\circ$ and $\beta_1 = 80^\circ \pm 3^\circ$. The vane channel bending is to be of $f = 0.2$.

To acquire high values of ψ and η and reduce the noise level solidity and number of blades in the vane cascade are to be in the range of $\tau = 1.6 \dots 2.7$, and $z = 20 \dots 32$.

Tip loss reduction increases ψ and ϕ values by a factor of 1.2 with increasing of the rotor relative length from $\bar{b} = 0.2$ to $\bar{b} = 1.0$.

If $\bar{b} > 1.0$ its impact on ψ and ϕ is insignificant.

The impact of \bar{b} on η is limited by $\bar{b} < 0.5$ area.

An inner shaft mounted in the rotor causes considerable losses of the fan efficiency and reduction in pressure coefficient ψ . So in nominal rating conditions at $d_{sh} = 0.1$ the efficiency decreases by 20% and ψ_{sh} decreases by 25%. Thus, to ensure better aerodynamic and energetic characteristics of DF, rotors should be performed without an inner shaft.

The impact of the relative values of inlet and outlet flow wise sections on DF aerodynamic characteristics is defined

$$\bar{c} = C/D \quad \text{and} \quad \bar{B} = B/D.$$

The resulting optimum values of these parameters are: $\bar{c} = 1.25 \dots 1.75$ and $\bar{B} = 0.4 \dots 0.5$.

The main element of DF flow section contour is the so-called "tongue" shape and δ value of the relative clearance between the "tongue" and DF rotor. In nominal rating conditions of DF operation the tongue turned back to the delivery branch pipe is optimum. At $\phi' > \phi_N$ the tongue turned to the opposite direction is more advantageous, thus, the tongue optimum shape selection is eventually to be determined by the operating point position on DF aerodynamic characteristic.

Relative clearance δ impact is shown in Fig.7.

The fact that structural variation of the clearance between the rotor and tongue can be realized by tongue translation offers strong possibilities of WT characteristics regulating as well as non-stationary flows creating in the WT with specified characteristics.

During DF parameter investigations, a scale effect evaluation was also carried out (see Fig.8). It has been followed from the experimental investigations that the automodel operating envelope of DF was at $Re > 10^5$. At the lower values the pressure coefficient ψ and η tend to considerable reduction.

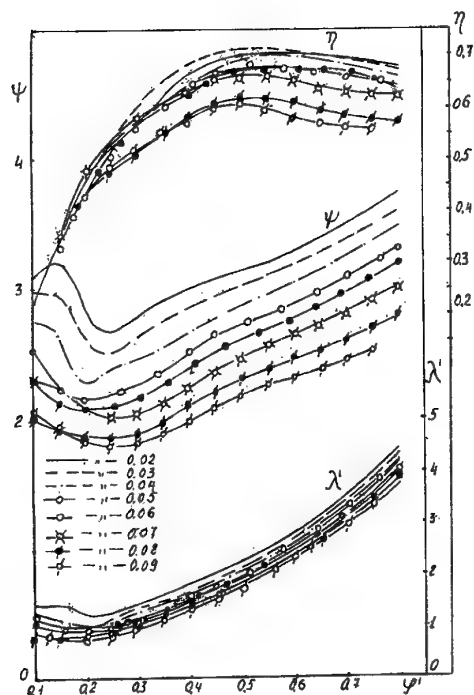


Fig. 7. DF aerodynamic characteristics for WTs with different radial clearances (model of $b=0.5$ m; $D=0.3$ m).

Parameter investigations results have made it possible to develop the wide range of the medium-loaded ($\psi = 3.2 \dots 4$) and high-loaded ($\psi = 6.0 \dots 8.5$) DFs.

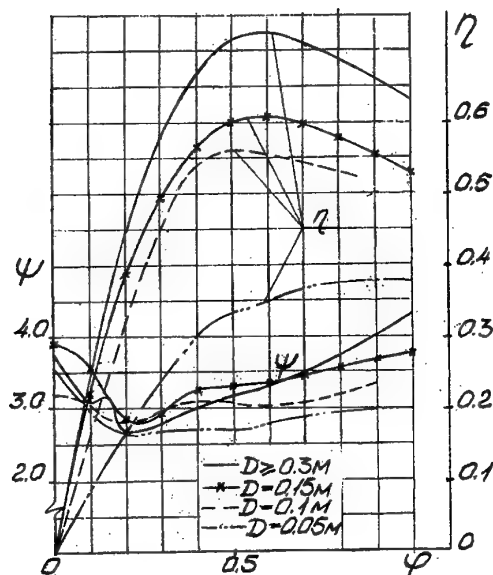


Fig. 8. The action of scale effect on DF aerodynamic characteristics.

DFs with devices for deep aerodynamic control of operating conditions and suppression of discrete components in the acoustic spectrum are designed. Developed DF configurations can be used not only in the WTs but also in the different production equipment, conditioners, laser units, aircraft, air-cushion vehicles, etc.

4. DEVELOPMENT AND MANUFACTURING OF A COMPACT SUBSONIC WIND TUNNEL AND ULAK.

When working at the compact closed-circuit subsonic wind tunnel (WT) (Fig. 9) we have developed its airflow channel with four swinging elbows, and a diametral fan with optimized flow layout and dimensions (rotor diameter $D=0.46$ m, rotor length $b=1.1$ m) has been placed in the second swinging elbow flowwise, the fan casing, in which the flow makes a 90-degree turn, functioning as the second WT swinging elbow and the rotor rotation axis being normal to the tunnel plane of symmetry, placed outside the tunnel outlines.

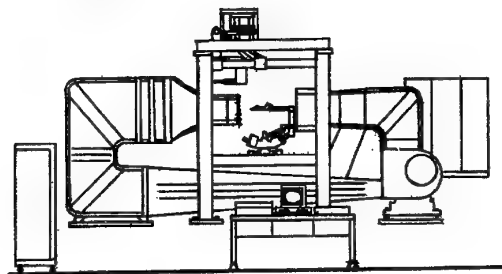


Fig. 9. The general view of the ULAK-1.

The above WT layout made possible to eliminate the employment of an angle gearbox or a long drive shaft, passing through the tunnel outlines. In the WT airflow channel developed, the diametral fan with the design pressure-flow characteristics delivers the flow into the diffuser with the vane guiding device and further through the third and fourth swinging elbows forces the flow into the prechamber with the honeycomb and the grid placed inside, and then, into the nozzle and the WT open working section. Passing through the working section, the flow slows down in the inlet diffuser with the mouth and, passing the first swinging elbow, appears directly in the DF intake that makes possible to substantially simplify the tunnel construction, make it more compact and improve the tunnel flow quality.

The designed compact subsonic WT with DF has the following technical characteristics:

Wind tunnel dimensions

length 5,800 mm

width	2,000 mm
height	2,500 mm
Flow velocity	10 to 60 m/s
Working section	open
Working section length	1,000 mm
Working cross-section	600 x 400 mm ²
Model length	up to 400 mm

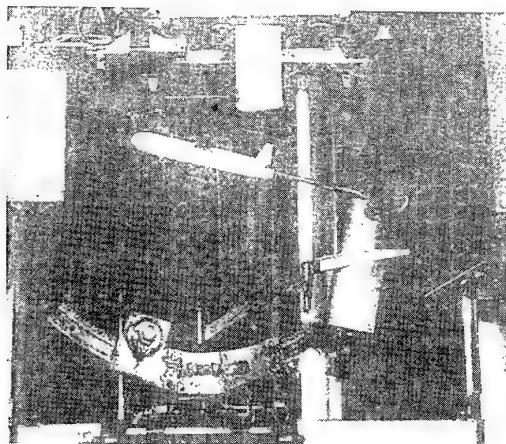


Fig. 10. ULAK-1 working section.

On the basis of the developed WT the test complex ULAK-1 (Fig.9) has been created proving the following advantages:

complex compact installation;
automatic movement of a model under study;
automatic measuring of aerodynamic parameters.

The ULAK-1 complex consists of the following components:

compact wind tunnel;
model angular movement mechanism;
control - manual and automatic;
measurement range at:

angle of attack -10° to $+20^\circ$
slip angle -90° to $+90^\circ$;

fitting precision for :

angle of attack $\pm 0.1^\circ$
slip angle $\pm 0.25^\circ$;

model motion limit speed 5 °/s;

mechanism of sting motion along X, Y and Z axes;

control - manual and automatic;
sting motion:

along X axis 600 mm
along Y axis 600 mm
along Z axis 400 mm;

motion speed 25 mm/s;

six-component strain gage;

pressure gages and a sting;

measuring units;

program package to provide experiments.

5. AN EXAMPLE OF DF USE IN THE SUBSONIC WT TO SIMULATE BODY MOTION IN A LIQUID WITH THE FREE BOUNDARY.

Owing to the above-mentioned features, the DF could be used not only as a WT power unit but also as an auxiliary equipment. As an example, we consider DF possible use to simulate body motion in the WT in a liquid with the free boundary. As a rule, this task is decided by means of pulling the body models through the flow channels. In addition, this example is of interest because it gives a clear interpretation of effect of the working-section walls to aerodynamic characteristics of the model under study.

It has been known that in uniform body motion in a liquid, in parallel with it's free surface, the wave is initiated on the liquid's surface and moves together with the body. When the flow moves in the opposite direction, the wave becomes steady, and the so-called low waves condition is fulfilled on the free surface, that may be written as

$$\frac{dV_x}{dx} = \frac{V_y}{Fr^2} \quad (5)$$

We consider gas two-layer flow in the closed working section of the subsonic wind tunnel, where h_1 - height of the main flow and h_2 - height of gas layer, with $h_2 < h_1$ (see Fig.11). The gas parameters as it leaves the nozzle: P_1, ρ_1, V_1 - in the main flow and P_2, ρ_2, V_2 - in the layer. The relation among such a flow has been developed in one of the works of Neyland V.M.

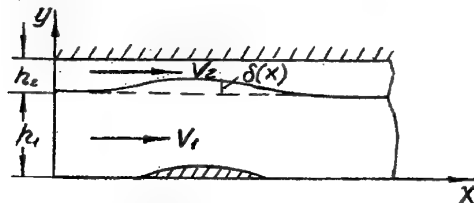


Fig.11. Scheme of two-layer flow in the WT working section.

A line of demarcation between two flows under disturbances caused by a body which is placed into the main flow is off a straight line by $\delta(x)$, with

$$\frac{d\delta}{dx} = \frac{V_{ly}}{V_{lx}} \quad (6)$$

where V_{ly} , V_{lx} - nondimensional components of basic flow velocity on a line of demarcation.

The gas motion in h_2 layer has the continuity and energy equations

$$h_2 \cdot \rho_2 \cdot V_2 = (h_2 - \delta)(\rho_2 + \rho_2')(V_2 + V_2') \quad (7)$$

$$\frac{\gamma}{\gamma-1} \frac{p_2}{\rho_2} + \frac{V_2^2}{2} = \frac{\gamma}{\gamma-1} \frac{(p_2 + p_2')}{(\rho_2 + \rho_2')} + \frac{(V_2 + V_2')^2}{2} \quad (8)$$

In this case, under the assumption that the process is adiabatic:

$$\frac{p_2}{\rho_2^\gamma} = \frac{p_2 + p_2'}{(\rho_2 + \rho_2')^\gamma} \quad (9)$$

Providing infinitesimal of P_2 as compared to P_2 and using expressions (6) - (9), we derive a nondimensional equation

$$\frac{dV_{lx}}{dx} = \frac{h_1 q_2}{h_2 \cdot q_1 (1 - M_2^2)} \frac{Vy}{Vx} \quad (10)$$

It follows from a correlation between (5) and (10) that these equations are identical, if

$$Fr^2 = \frac{h_2}{h_1} \frac{q_1}{q_2} (1 - M_2^2) \quad (11)$$

So, when creating an additional plane gas flow with the height h_2 , the velocity head q_2 and the Mach number M_2 along one of the walls of the subsonic WT closed working section, we can approximately simulate the free heavy-liquid surface; an analogue of such a surface is the surface of demarcation of two gas flows. At given relation h_2/h_1 and velocity head value q_1 in the WT working section, the "heaviness" of a liquid is primarily defined by additional gas flow velocity head q_2 .

An instance of $Fr \rightarrow 0$ corresponding to very heavy liquid corresponds in our interpretation to the case when $q_2 \gg q_1$.

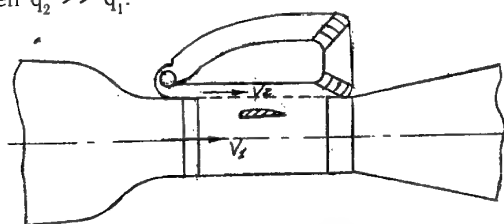


Fig. 12. The application of the DF to design the WT with two-layer flow in the working section.

An instance of $Fr \rightarrow \infty$ corresponding to body motion in weightless liquid corresponds to the case $q_2 \rightarrow 0$.

It can be noted that both cases bring closer to the cases achieved during aerodynamic experiments: the first - in the tunnel with rigid non-perforated walls, and the second - in the Eiffel chamber.

The unit which allows an approximate simulation of Froude number action in the wind tunnel can be implemented using the DFs (see Fig. 12).

6. NOTES

1. Korovkin A.G., etc. Diametral Fan. Certificate of authorship, N 1767234. Bulletin of inventions, N 37, 1992.
2. Savchuk V.D., etc. Closed-Circuit Subsonic Wind Tunnel. Certificate of authorship, N 1821664. Bulletin of inventions, N 22, 1993.

EXPERIMENTAL STUDY OF A LOW-SPEED WIND TUNNEL TEST SECTION WITH A FREE JET

V. P. Roukavets, A. P. Byrkin

A. L. Iskra, A. P. Filatov

V. V. Troitsky, V. C. Ponomaryova

TsAGI, Central Aerohydrodynamic Institute, Zhukovsky, RU

D. Holzdeppe

Turbolifttechnik, Zweibrücken, Germany

H. D. Papenfuss

Ruhr-Universität Bochum, Germany

D. Barbagallo

CIRA, Centro Italiano Ricerche Aerospaziali

Via Maiorise, 81043 Capua, Italy

1. ABSTRACT

Results of experimental study of various configurations of the subsonic wind tunnel test section with a free jet and Eiffel chamber are presented in order to determine its optimum variant corresponding to minimum values of velocity and pressure pulsation, hydraulic losses and flow non-uniformity in the model location zone. At a given reduced jet length the parameters of the test section configuration were provided by varying the relation of the diffuser entry section area to the nozzle exit section area and by variations of the collector placed in front of the diffuser. Different forms of the collector were studied: one-piece contracting collector, contracting collector adjusted along the angle and collector with parallel walls. From the collectors investigated the best in the aggregate of the flow efficiency criteria is the one-piece contracting collector with an angle of inclination of walls $\alpha \approx 14^\circ$ and an optimum relative value of the gap between it and the diffuser ≈ 0.2 .

2. NOMENCLATURE

A	section area
ΔA	parameter expressed by areas of the nozzle exit section, diffuser entry section and ideal area of the collector exit section
H	cross section height
W	cross section width
S	side of the cut angle of the octagonal cross section
$D_{n \text{ hyd}}$	hydraulic diameter of the nozzle cross section
L	length, noise level
L_0	microphone proper noise
δ	width of the wall
x, y, z	Cartesian co-ordinates
$\bar{x} = x / L_{\text{jet}}$	
$\bar{y} = y / H_n$	relative current coordinates
$\bar{z} = z / W_n$	
R	radius
α	wall inclination angle toward the flow axis
U	flow velocity
U	root-mean-square value of velocity pulsations
ρ	air density
μ	air dynamic viscosity
p	pressure
p'	root-mean-square value of pressure pulsations
$Re = \rho D_{n \text{ hyd}} U_0 / \mu$	Reynolds number
C_p	static pressure coefficient
q	dynamic pressure

Δp	difference of mean static pressures in two points
K	coefficient of hydraulic losses
$E = U/U$	turbulence level (intensity of velocity longitudinal pulsations)
f	frequency of oscillations
n	rotational frequency of the fan rotor.

Subscripts

b	breathers in the collector walls
c	collector
cx	cross section at the collector exit
cl	inlet edge of the collector
cn	collector entry
d	diffuser entry
g	gap between the collector and diffuser
n	nozzle exit
p	plenum chamber
sc	settling chamber
wt	wind tunnel duct
jet	free jet
an	nozzle attachment
f	fan
0	mean flow parameters at the nozzle exit
f_1	fan entry
f_2	fan exit
a	atmosphere.

3. INTRODUCTION

To study flows over aircraft and other industrial objects (automobiles, buildings, special facilities) wide use is made of the wind tunnels of small subsonic velocities both with a closed (perforated walls included) and an open test section. The advantage of the last is a free access to the model and apparatus, simplicity of construction, possibility of creating a low-noise or anechoic test section to perform acoustic tests.

It is known [1-5] that in the closed-circuit wind tunnels with an open test section there appear, over certain velocity ranges, auto-oscillations bringing about a noticeable growth of low-frequency pulsations of the longitudinal velocity and pressure through the whole duct of the wind tunnel. Formation of low-frequency perturbations is associated with resonance phenomena appearing in the test section (Eiffel chamber) and in the return circuit of the wind tunnel. The circular vortices, that shed from the nozzle edges and envelope the jet, also turbulize the flow in the free jet of the test section.

This paper presents the material on the experimental investigation of various configurations of the test section with a free jet in the plenum chamber with an aim of choosing a variant with minimum pulsations of velocity and pressure and

hydraulic losses and also non-uniformity of the flow along the axis of the free jet and in the cross section at the mid of its length.

4. EXPERIMENTAL FACILITY AND OBJECTS OF TESTING

The aerodynamic diagram of the TsAGI T-03 wind tunnel that served to perform the tests is shown in Fig. 1. The diagrams of the test section with the investigated collectors located in front of the diffuser are presented in Figs 2 and 3.

A one-piece contracting collector was investigated, known by papers [6, 7], with the setting angles of the walls to the axis $\alpha_c = 12; 14.5; 16; 25; 45^\circ$ at the presence of a gap with an area of A_g between the collector exit section (area A_{cx}) and the diffuser entry section (A_d) to bypass air from the plenum chamber to the flow at the diffuser entry (Fig. 2). All parameters given below were varied at each value of α_c .

The parameter A_d/A_{cx} was equal to 0.9; 1.0; 1.05.

The second variable parameter was the value determined by relation,

$$\Delta \bar{A} = \frac{A_d - A_n}{A_{cx, id} - A_n}$$

where $A_{cx, id}$ is an ideal section area at the collector exit calculated as part of the area of the free jet cross section at its end with the gas rate being equal to the rate through the nozzle [8]. In the experiment this parameter had the values: 0.85; 1.00 and 1.30.

The third variable parameter was the radius of the collector entry edge R_{cl} . Its value as related to the collector half-width at the entry $W_{cn}/2$, $\bar{R}_{cl} = 2R_{cl}/W_{cn}$ was equal to 0.05; 0.12 and 0.36; the indicated values \bar{R}_{cl} were realized only for the collector with the parameters: $\alpha_c = 14.5^\circ$, $A_d/A_{cx} = 0.9$ and $\Delta \bar{A} = 0.85; 1.00; 1.30$ ($\bar{L}_{jet} = L_{jet}/D_{n, hyd} = 2.5 - 2.8$). For these radii ($R_{cl} = 20; 50$ and 150 mm) the thickness of the collector walls δ was 2.5 mm, while with variation of the parameters α_c and A_d/A_{cx} the collectors had thick walls ($\delta = 2R_{cl} = 40$ mm).

The fourth parameter actively affecting the resonance phenomena in the wind tunnel was the total relative area of the gap between the collector and the diffuser A_g/A_{cx} . For all variants of the test section configuration in the experiment it varied from 0 to about 0.5 to determine the optimum value of $(A_g/A_{cx})_{opt}$, under which pulsations of pressure in the plenum chamber p_p/q_0 would be minimum over the flow velocity range considered (at the nozzle exit) U_0 from 30 to about 62 m/s and at that there would be no resonance at $U_0 \approx 50 - 60$ m/s.

As a particular case of a contracting collector an adjustable collector was investigated, the flaps of which were set at an angle to the collector axis $\alpha_c = 4; 8$ and 12° . This collector is characterized by the fact that it had four longitudinal wedge-type gaps between the adjustable flaps. The width of the gaps varied as a function of the angle α_c . For this collector the parameters of the test section were $A_d/A_{cx} = 1.0$, $A_g/A_{cx} = 0$, $R_{cl} = 20$ mm and $\Delta \bar{A} = 0.85; 1.00$ and 1.30 .

Apart from the contracting collector, a collector with parallel walls was also studied, that for the ultimate case had 14 rectangular longitudinal breathers (see Fig. 3). The relative total area of the breathers A_b/A_{cx} varied and was equal to 0;

0.2 and 0.4 at $A_g/A_{cx} = 0$. This collector was also investigated for a combination of breathers with a gap between the collector and the diffuser: $A_b/A_{cx} = 0.2$ and $A_g/A_{cx} = 0.2$. In this case the other parameters of the collector were as follows: $A_d/A_{cx} = 1.00$; $R_{cl} = 20$ mm ($\bar{R}_{cl} \approx 0.05$) and $\Delta \bar{A} = 0.85; 1.00$ and 1.30 .

The length of the free jet as related to the nozzle hydraulic diameter varied over the range $\bar{L}_{jet} = 2.5 - 3.0$.

All the above mentioned parameters of the test section configuration were provided only by variations of the collectors and three shaped attachments (see Fig. 1) for the base nozzle of the T-03 wind tunnel. The other elements of the wind tunnel, including the diffuser, were unchanged. The principal dimensions of the T-03 wind tunnel, the investigated types of collectors and the attachments for the nozzle studied are presented in Figs. 1 - 3.

5. METHODOLOGY AND TECHNIQUES OF THE EXPERIMENT

For each configuration of the test section, characteristics of the flow efficiency in the free jet were determined: noise level and pulsations of pressure in the plenum chamber over the range of velocity variations from 30 to about 62 m/s; distribution of static pressure, velocity and turbulence level E by the jet axis x and by the axis z (along the width of the jet) in the mid cross section at the flow velocity ~ 50 m/s, coefficient of hydraulic losses in the wind tunnel duct at the flow velocities from 30 to ~ 62 m/s. For the collector with parallel walls ($\alpha_c = 0$) and with parameters $A_b/A_{cx} = 0$, $\Delta \bar{A} = 1.00$ and 1.30 the coefficient of hydraulic losses in the free jet was measured for the flow velocities 30 and 40 m/s.

Measurements of the flow efficiency characteristics, carried out at constant velocity, were performed at practically stable values of the flow parameters at the nozzle exit. For instance, for the averaged in time velocity $U_0 \approx 50$ m/s its value deviated from the mean value by $\pm 1\%$; the flow temperature varied within a run of duration of 7-15 minutes not more than by $\sim 3K$, remaining somewhat higher than the atmospheric one (by 5-15K).

The flow stability was provided by a constant rotational frequency of the fan rotor n ($\Delta n \leq 0.2\%$) and heat-mass exchange of the test air and the atmospheric one through four windows in the duct of the wind tunnel (two upstream and downstream of the corner, see Fig. 4).

Figure 4 shows a diagram of measuring the static pressure in the flow using a precision measurement system based on two vibration-frequency converters of pressure, and static pressure on the walls of wind tunnel elements using a system measurements with electro-inductive converters of pressure. The error of measuring the difference of static pressures $p(\bar{x}) - p(0)$ by the transducers of the first type for the time of averaging ~ 20 s does not exceed 1.2 Pa. For the transducers of the second type the error of measurement attains ~ 10 Pa.

The errors of measuring the air temperature in the settling chamber using a copper thermometer and the atmospheric air temperature (in the hall where the T-03 wind tunnel is located) using a mercury thermometer does not exceed 0.2 K. The error of measuring the atmospheric pressure using a mercury barometer does not exceed 10 Pa.

The noise level in the plenum chamber (beyond the free jet, near floor) was measured by a Bruel & Kjer 4133-type condenser microphone of diameter 1/2" with the proper noise $L_p \leq 65$ dB at the recorded level of the acoustic signal $L = 108 - 122$ dB. The pressure pulsations p'_p/q_0 were based on the measured noise level in the plenum chamber.

The averaged in time flow velocity $U(x)$ and $U(z)$ and its pulsations U/U were measured by a hot-wire anemometer. The system of measurements with the help of hot-wire anemometer consists of:

- two hot-wire anemometers with a tungsten filament 5 μ m in diameter, 2 mm long with practically equal values of electrical resistance;
- hot-wire anemometers ETAM-17 and DISA 55M01;
- digital voltmeter for measuring the difference signal of two hot-wire anemometers;
- conditioner with a coefficient of amplifying the hot-wire anemometer signal $k=10$ and the signal frequency pass band limited by the filters of low and high frequencies (bandwidth) $\Delta f = 1$ Hz - 10 kHz;
- data acquisition system.

6. FLOW EFFICIENCY CRITERIA

The influence of variables of the geometric parameters on the flow efficiency in the test section and coefficient of hydraulic losses in the wind tunnel duct were evaluated using a family of criteria. The following flow parameters were assumed to serve as the flow efficiency criteria:

- p'_p/q_0 , the value of the pressure pulsations in the plenum chamber;
- $dC_p/d\bar{x}$ (at $U_0=50$ m/s), gradient of the pressure coefficient on the jet axis $C_p = [p(\bar{x}) - p(0)]/q_0$, (see Fig. 1);
- $K_{wt} = \Delta p/q_0$, coefficient of hydraulic losses in the wind tunnel duct, the free jet included ($\Delta p = p_n - p_0$);
- $E = U/U$, velocity pulsations on the flow axis at the nozzle exit ($\bar{x} = 0$) and in the mid part of the jet ($\bar{x} = 0.5$);
- $2|\bar{z}|_{\max}$, width of the flow core in the mid part of the jet at $\bar{y} = 0$.

The comparable values of these criteria over the range of variation of the flow velocity from 30 to 60 m/s are given in Table 1.

7. RESULTS OF THE EXPERIMENT

7.1. ONE-PIECE COLLECTOR

Table 1 represents the best magnitudes of the flow efficiency criteria obtained at established in these investigations optimum values of the relative gap value $(A_g/A_{cx})_{opt}$ for the considered parameters α_c , A_d/A_{cx} , \bar{R}_{cl} and the two values of the parameter $\Delta \bar{A}$: 1.00 and 1.30, most realistic during the design of the wind tunnels.

Analysis of these results leads to conclude that by the majority of the criteria of the flow efficiency the best results were obtained for the collector with thick walls to compare with the collector with thin walls for the similar parameters: $\alpha_{c, opt} = 14.5^\circ$; $(A_d/A_{cx})_{opt} = 0.9$; $\bar{R}_{cl} = 0.05$; $\Delta \bar{A} = 1.00$ and 1.30. The following geometric parameters of one-piece collectors (considering the use of a wind tunnel with a model in the test section) were taken to be optimum by the majority of the flow efficiency criteria:

$$\alpha_{c, opt} = 14.5^\circ; (A_d/A_{cx})_{opt} = 1.0; \bar{R}_{cl, opt} = 0.12; \\ (A_g/A_{cx})_{opt} \approx 0.2; \Delta \bar{A}_{opt} = 1.30.$$

The value of the optimum inclination angle of the collector walls toward the axis, being equal to 14.5° , was confirmed by additional (check) tests of collectors with the angles $\alpha_c = 25^\circ$ and 45° . The flow efficiency criteria in this case were worse than at $\alpha_{c, opt} = 14.5^\circ$.

The diagrams with the flow structure characteristics for the case of one-piece collector for optimum parameters are represented in Figs. 5-10.

7.2. ADJUSTABLE COLLECTOR

With an increase of the setting angle of the collector flaps α_c from 4 to 12° the intensity of the pressure pulsations p'_p/q_0 , the velocity pulsations $E(\bar{x})$ at $\bar{y} = \bar{z} = 0$, $E(\bar{z})$ at $\bar{x} = 0.5$, $\bar{y} = 0$, the coefficient gradient C_p and the coefficient of hydraulic losses K_{wt} decreases. Their minimum values obtained at $\alpha_c = 12^\circ$ and $\Delta \bar{A} = 1.3$ are equal or somewhat higher than the same for the case of one-piece rigid collector with its optimum parameters. For the sake of comparison Figs. 11 and 12 show diagrams of the dependencies $E(U_0)$ at $\bar{x} = \bar{y} = \bar{z} = 0$ and $E(\bar{x})$ at $\bar{y} = \bar{z} = 0$ and $U_0 = 50$ m/s.

7.3. COLLECTOR WITH PARALLEL WALLS

The only advantage of the collector with parallel walls without breathers and gap ($A_b/A_{cx} = 0$, $A_g/A_{cx} = 0$) to compare with the collector with breathers is only larger length of the free jet with practically constant coefficient $C_p(\bar{x})$. All other flow efficiency criteria are worse than in the case with breathers. An increase in the relative area of breathers from $A_b/A_{cx} = 0.2$ to 0.4 also worsens the flow efficiency. The best flow efficiency was obtained for the combination of breathers with gap: $A_b/A_{cx} = 0.2$, $A_g/A_{cx} = 0.2$. However, in this case the accepted criteria of the flow efficiency are not better than for the optimum parameters of the one-piece collector. For example, it is seen from comparison of the diagrams of dependencies $E(U_0)$ ($\bar{x} = \bar{y} = \bar{z} = 0$) and $E(\bar{x})$ ($\bar{y} = \bar{z} = 0$) at $U_0 = 50$ m/s shown in Figs. 11 and 12. The value of the coefficient of hydraulic losses in the free jet $K_{jet} = 0.37$.

CONCLUSIONS

1. From the investigated types of collectors of the test section with a free jet (one-piece contracting collector, contracting collector adjustable along the angle and collector with parallel walls) the best in the aggregate of the flow efficiency criteria is the one-piece contracting collector with an optimum relative value of the gap between it and the diffuser being equal to ~ 0.2 .

2. The optimum parameters of the one-piece collector are:

- inclination angle of walls toward the axis $\alpha_c \approx 14^\circ$,
- relation of area of diffuser entry to area of collector exit $A_d/A_{cx} = 1.0$,
- parameter $\Delta \bar{A} = 1.30$.

3. For the range of velocities at the nozzle exit $U_0 = 30 - 60$ m/s at Reynolds numbers $Re = 9.2 \times 10^5 - 1.9 \times 10^6$ that correspond to the hydraulic diameter of the nozzle the following data were obtained for the optimum one-piece collector in the TsAGI T-03 wind tunnel:

- pressure pulsations in the test section $p'_p/q_0 = 1.1 - 0.8\%$;

- turbulence level on the flow axis in the mid part of the jet $E(\bar{x}=0.5) = 0.88\%$ for the turbulence level at the nozzle exit $E(\bar{x}=0) = 0.3\%$ ($U_0=50$ m/s);
- gradient of the pressure coefficient C_p along the jet on the path $\bar{x}=0.05 - 0.3$ $dC_p/d\bar{x} \approx 0$ and on the path $\bar{x}=0.3 - 0.7$ $|dC_p/d\bar{x}| \leq 0.017$ ($U_0=50$ m/s);
- total coefficient of hydraulic losses in the wind tunnel K_{wt} falls down from ~ 0.56 at $Re \approx 9.2 \times 10^5$ to ~ 0.52 at $Re \approx 1.9 \times 10^6$;
- width of the flow core $2|\bar{z}|_{\max} = 0.8$ at $\bar{x} = 0.5$ and $\bar{y} = 0$ ($U_0=50$ m/s).

4. The adjustable collector with a variable angle of inclination of flaps toward the axis and four longitudinal wedge-type gaps between the flaps and also the collector with parallel walls and beathers in the walls and a gap between the collector and the diffuser for the optimum geometric parameters have the same or worse flow characteristics to compare with the optimum one-piece collector.

REFERENCES

1. E. Jacobs. NACA Reports, N 322, 1929.
2. O. Schrenk. Technische Mechanik und Thermodynamik, 1.s.158, 1930.
3. K. K. Baulin, S. T. Astabatyanyan, and F. N. Krasheninnikov. Investigation of Wind Tunnels with Open Test Section, Trudy TsAGI, vip. 140, M.-L., 1932 (in Russian).
4. C. P. Strelkov, G. A. Bendrikov, and N. A. Smirnov. Pulsations in the Wind Tunnels and Means of their Damping. Trudy TsAGI, vip. 593, 1946 (in Russian).
5. Sumio Nishikawa. Low Noise and Multi-mission Wind Tunnel. HONDA Report, vol. 46, N1, 1992.
6. Haussammann W. Die Windkanalanlage der Kriegstechnischen Abteilung in Emmen (Luzern). Schweizerische Bauzeitung, N 39. Sonderheft zur 48. Generalversammlung der G.E.P., Luzern, 25/27. September, 1948.
7. J. Wiedemann and G. Wickern (AUDI AG), B. Ewald and C. Mattern (Technische Hochschule Darmstadt). Audi Aero-Acoustic Wind Tunnel. SAE TECHNICAL PAPER SERIES, 930300, 1995.
8. G. H. Abramovich. Theory of Turbulent Jets, M., Fizmatizdat, 1960 (in Russian).

The best test section parameters and values of criteria at

$$(A_d/A_{cx})_{\text{opt}} \text{ and } \bar{L}_{\text{jet}} \approx 2.5 - 2.8$$

Table 1

Parameters and criterion values		Criterion name					
		$(p'_p / q_0)_{\min}, \%$ $U_0=30-60$ m/s	$ dC_p/d\bar{x} _{\min}$ $U_0=50$ m/s	$K_{wt \min}$ $\bar{x} = \bar{y} = \bar{z} = 0$ $U_0=30-60$ m/s	$E_{\min}, \%$ $\bar{x} = 0.5$ $\bar{y} = \bar{z} = 0$ $U_0=30-60$ m/s	$E_{\min}, \%$ $\bar{x} = 0.5$ $U_0=50$ m/s	$ \bar{z} _{\max},$ (flow core) $\bar{x} = 0.5, \bar{y} = 0$ $U_0=50$ m/s
α°_c	$\Delta \bar{A} = 1.00$	12	12; 14.5; 16	12; 14.5; 16	12	12; 14; 15; 16	14.5
	$\Delta \bar{A} = 1.30$	14.5	12; 14.5; 16	12; 14.5; 16	12	16	12
Criterion value	$\Delta \bar{A} = 1.00$	1.1 — 1.2	-0.007 — +0.03	0.60 — 0.56	0.23 — 0.31	0.78	0.42
	$\Delta \bar{A} = 1.30$	1.2 — 0.8	-0.007 — +0.03	0.56 — 0.52	0.24 — 0.32	0.78	0.42
A_d/A_{cx}	$\Delta \bar{A} = 1.00$	1.05	0.90; 1.00; 1.05	0.90; 1.00	0.90; 1.00	1.00	1.00
	$\Delta \bar{A} = 1.30$	1.05; 1.00	0.90; 1.00; 1.05	0.90; 1.00	0.90; 1.00	1.00	0.90
Criterion value	$\Delta \bar{A} = 1.00$	0.4-0.8	-0.007 — +0.03	0.28 — 0.32	0.28 — 0.32	0.78	0.42
	$\Delta \bar{A} = 1.30$	0.6-1.2	-0.007 — +0.03	0.33 — 0.38	0.33 — 0.38	0.88	0.42
\bar{R}_d	$\Delta \bar{A} = 1.00$	0.36	0.12	0.12	0.12	0.36	0.12
	$\Delta \bar{A} = 1.30$	0.36	0.12	0.12	0.12	0.36	0.05; 0.12; 0.36
Criterion value	$\Delta \bar{A} = 1.00$	1.3-1.0	-0.005 — +0.02	0.28-0.31	0.28 — 0.31	0.63	0.41
	$\Delta \bar{A} = 1.30$	1.5-1.2	-0.008 — 0.00	0.32 — 0.36	0.32 — 0.36	0.76	0.41

Three attachments to the nozzle

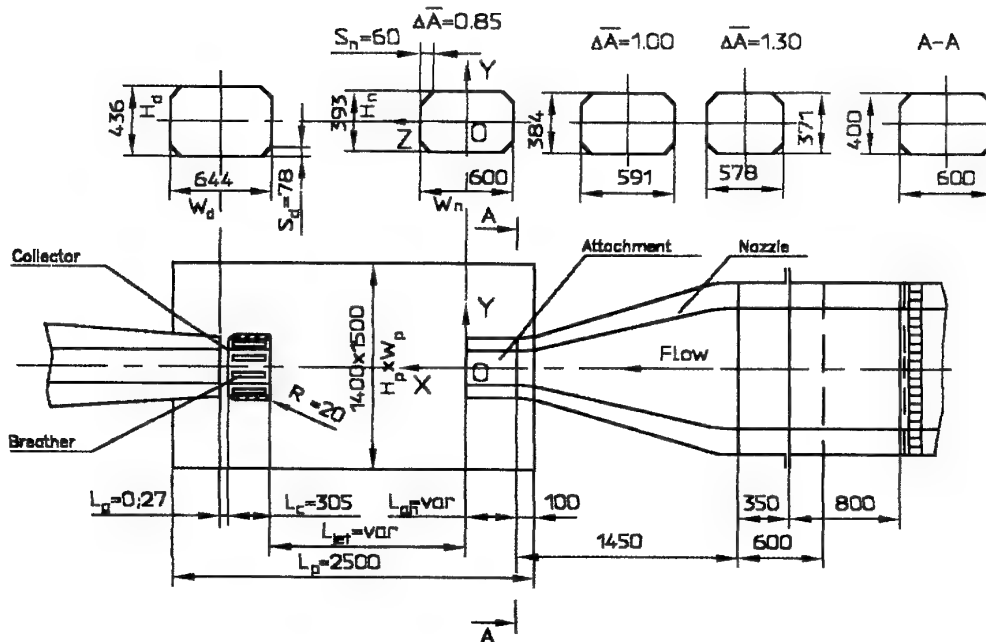
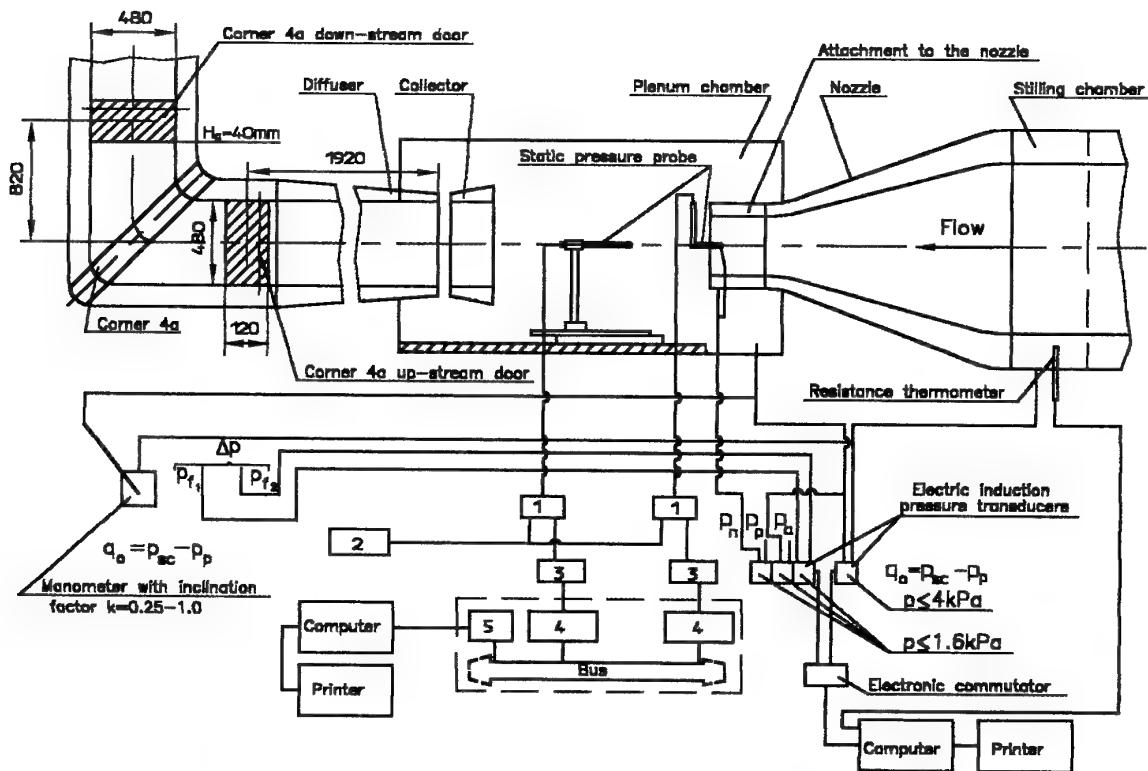


Figure 3. Collector with flaps with breathers



- | | |
|---------------------------------|----------------------------------|
| 1, Pressure-frequency converter | 4, Frequency-to-number converter |
| 2, Power supply | 5, Controller |
| 3, Normalizer | |

Figure 4. Pressure measurement system

OPTIMUM ONE - PIECE COLLECTOR:

$$\alpha_c = 14.5^\circ, \frac{\Lambda_d}{\Lambda_{cx}} = 1.0, \frac{\Lambda_f}{\Lambda_{cx}} = 0.2, \Lambda\bar{\Lambda} = 1.3$$

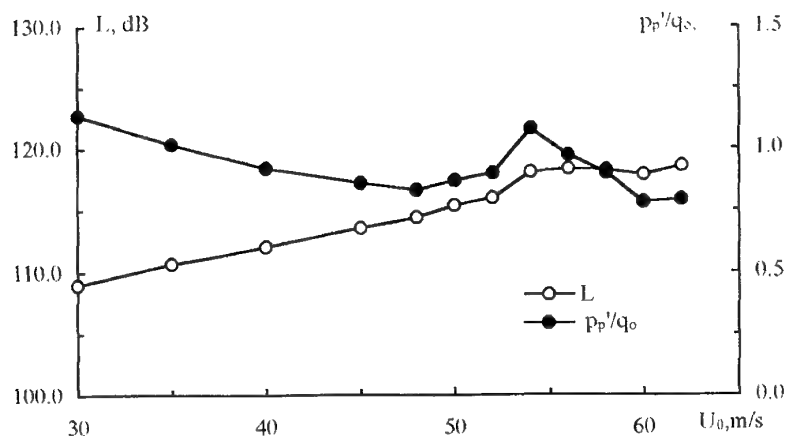


Figure 5. The noise level (L) and pressure fluctuations (p_p'/q_0) as a function of the flow velocity

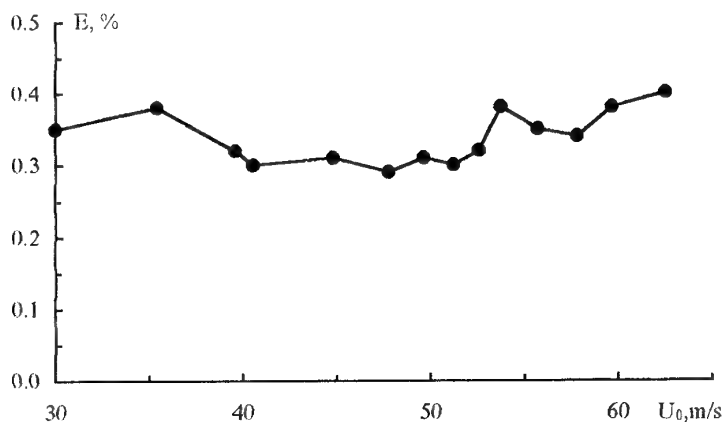


Figure 6. The turbulence level at $\bar{x} = \bar{y} = \bar{z} = 0$ as a function of the flow velocity

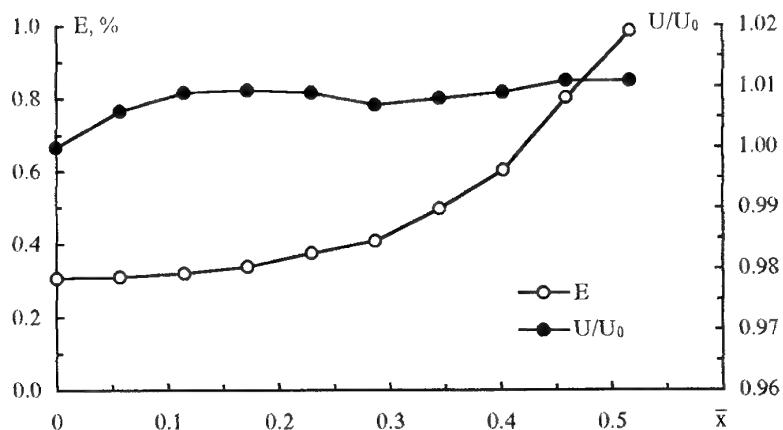


Figure 7. Turbulence level $E(\bar{x})$ and relative velocity $U/U_0(\bar{x})$ distributions along the jet center line ($\bar{y} = \bar{z} = 0$) at $U_0 = 50$ m/s

OPTIMUM ONE - PIECE COLLECTOR:

$$\alpha_c = 14.5^\circ, \frac{\Lambda_d}{\Lambda_{cx}} = 1.0, \frac{\Lambda_g}{\Lambda_{cx}} = 0.2, \overline{\Lambda} = 1.3$$

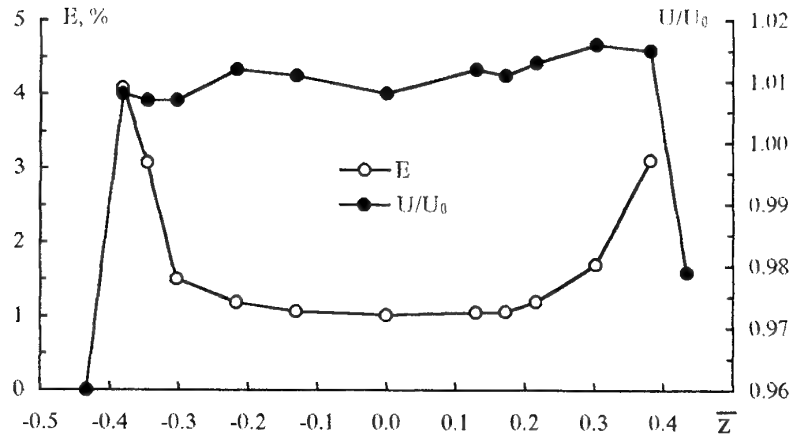


Figure 8. Turbulence level $E(\bar{z})$ and relative velocity $U/U_0(\bar{z})$ distributions over the z axis at the jet mid-point $\bar{x}=0.5$, $\bar{y}=0$ and $U_0=50$ m/s

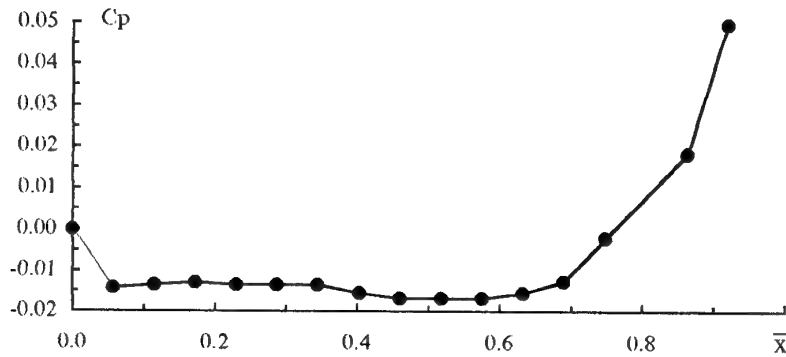


Figure 9. Static pressure profile along the free jet

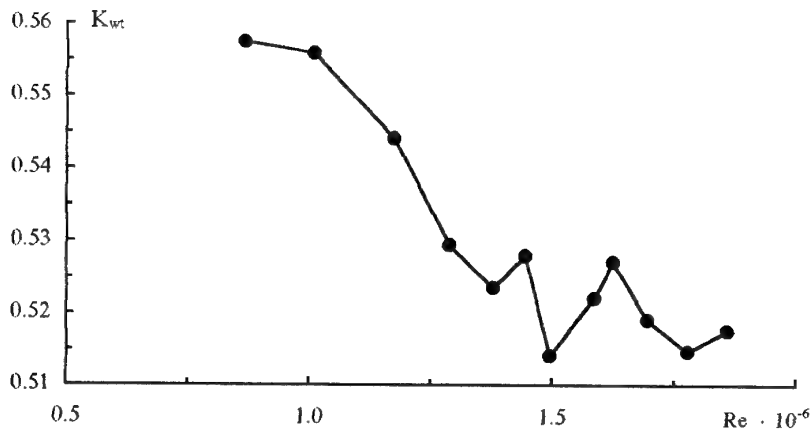


Figure 10. The total pressure loss factor for the wind tunnel dependence on Re ($D_{n,hyd} = 0.471$ m)

VARIOUS TYPES OF COLLECTORS AT OPTIMAL PARAMETERS

- one-piece collector: $\alpha_c = 14.5^\circ$; $\frac{A_d}{A_{cx}} = 1.0$; $\frac{A_g}{A_{cx}} = 0.2$; $\Delta\bar{A} = 1.3$
 ● variable position flaps collector: $\alpha_c = 12^\circ$; $\frac{A_d}{A_{cx}} = 1.0$; $\Delta\bar{A} = 1.3$
 ▲ collector with parallel flaps and breathers: $\frac{A_d}{A_{cx}} = 1.0$; $\frac{A_b}{A_{cx}} = 0.2$; $\frac{A_g}{A_{cx}} = 0.2$; $\Delta\bar{A} = 1.3$

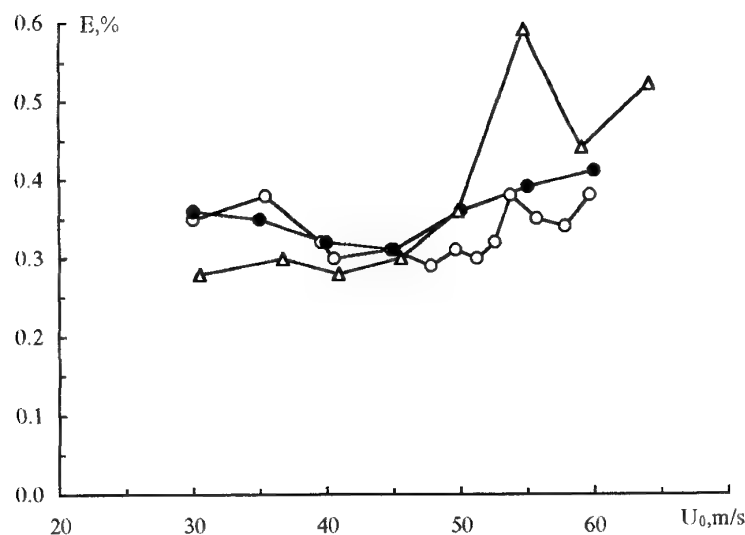


Figure 11. Turbulence level at $\bar{x} = \bar{y} = \bar{z} = 0$ as a function of the flow velocity.

- one-piece collector: $\alpha_c = 14.5^\circ$; $\frac{A_d}{A_{cx}} = 1.0$; $\frac{A_g}{A_{cx}} = 0.2$; $\Delta\bar{A} = 1.3$
 ● variable position flaps collector: $\alpha_c = 12^\circ$; $\frac{A_d}{A_{cx}} = 1.0$; $\Delta\bar{A} = 1.3$
 ▲ collector with parallel flaps and breathers: $\frac{A_d}{A_{cx}} = 1.0$; $\frac{A_b}{A_{cx}} = 0.2$; $\frac{A_g}{A_{cx}} = 0.2$; $\Delta\bar{A} = 1.3$

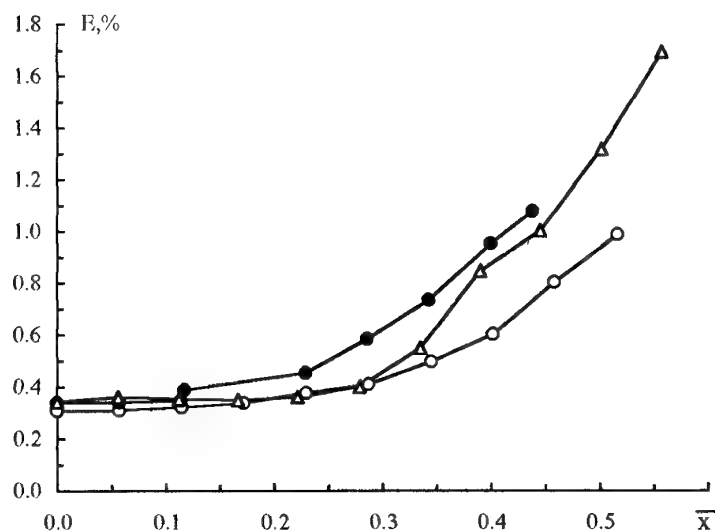


Figure 12. Turbulence level distributions along the jet center line ($\bar{y} = \bar{z} = 0$) at $U_0 = 50$ m/s.

LOWERING THE TURBULENCE LEVEL IN AN OPEN-JET WIND TUNNEL BY NOVEL ADJUSTABLE JET-EXIT VANES

H.D. Papenfuss¹, D. Holzdeppe², W. Lorenz-Meyer³, V.P. Roukavets⁴ and A.P. Filatov⁴

¹Ruhr-Universität Bochum, Germany; ²Turbo-Lufttechnik GmbH, Zweibrücken, Germany;
³Ingenieurbüro, Göttingen, Germany; ⁴TsAGI, Zhukowsky, Russia

SUMMARY

A new design of jet-exit vanes has been used to study the effect on wind tunnel turbulence in an open-jet test section. The new device offers the possibility to adjust its geometry to the specific situation. The most effective elements of the device are triangular teeth which protrude from the nozzle rim into the flow. By shifting these elements into the direction normal to the flow an optimum with regard to the turbulence reduction could be achieved.

LIST OF SYMBOLS

b	nozzle width
Re	Reynolds number, based on nozzle width
Tu	streamwise turbulence intensity (in percent)
u	local time-averaged streamwise velocity
U_∞	wind tunnel speed
y	coordinate, transverse direction
z	coordinate, vertical direction

1 INTRODUCTION

The most effective way to reduce self-excited flow pulsations in open-jet wind tunnels is the proper design of the collector in combination with an optimized gap between the collector and the diffuser. If flow pulsations still occur, jet-exit vanes mounted along the periphery of the nozzle can be a useful tool to reduce this problem. The classical vanes of the Seiferth type developed in the forties in Germany (Ref 1) are simple inclined rectangular wings which point alternately into and out of the flow. The mechanism of the Seiferth wings is usually explained as interaction between generated longitudinal wing-tip vortices and vortex rings periodically shed from the nozzle exit. The vortex interaction leads to partial destruction of the otherwise very stable vortex rings so that the collector rim is no longer hit by this periodic flow structure.

An improvement over the rectangular Seiferth wings are swept-back wings (Ref 2) or triangular shaped jet-exit vanes (Ref 3) which generate longitudinal vortices of higher intensity. On principal, jet-exit vanes are accompanied by adverse side effects which cannot be avoided. The border between the potential flow and the surrounding free shear layer is shifted inward so that the utilizable potential flow core is reduced in size. In addition, noise is generated and the efficiency of the wind tunnel is slightly reduced. However, in

most cases the positive effects prevail, and the adverse effects are tolerated.

Jet-exit vanes of design mentioned above have in common that they are fixed in geometry and, as soon as they are mounted, cannot be adjusted to match specific situations. In the present study a new type of adjustable jet-exit vanes has been used in a wind tunnel located at the University of Kassel (Germany). First of all the gap between the collector and the diffuser and additional breathers had been optimized so that long-waved flow pulsations were essentially eliminated. The question to be studied was if and to what extent additional jet-exit vanes would help to further reduce the remaining turbulence in the test-section.

2 GEOMETRY OF THE JET-EXIT VANES

The jet-exit vanes used in the present study are the result of a development at the TsAGI (Russia). The device consists of three elements:

- 1) Pyramidal wedges of triangular cross-section mounted flat onto the interior nozzle wall. Their tips point upstream, and their bases are in alignment with the nozzle flange.
- 2) Triangular end plates screwed to the base of the wedges with their tips pointing into the flow ("shark teeth").
- 3) Inclined round flaps pointing out of the flow.

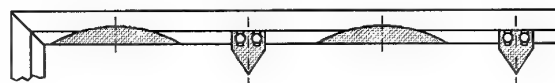


Figure 1: Arrangement of jet-exit vanes along periphery of nozzle exit. View from test section

The first two elements, since they are screwed together, form a unit. Such units alternate with the inclined round flaps along the periphery of the nozzle exit; see Fig. 1. The triangular end plates can be shifted parallel to the wedge bases and normal to the flow direction. Consequently, defined sections of these triangular end plates project into the flow with their tips and leading edges.

3 WIND TUNNEL AND EXPERIMENTAL SETUP

The experiments were carried out in a recently built

wind tunnel of the University of Kassel (Germany), Department of Civil Engineering (Prof. Thiele). The wind tunnel is of the Göttingen type with open test section. The nozzle has a quadratic cross-section of 0.886 m width at its exit. The test section length is 1.8 m. The tunnel provides a maximum test section velocity of 70 m/s which corresponds to a Reynolds number of $4 \cdot 10^6$ based on the nozzle width.

Three cross-sections of the test section have been examined at well defined grid points. The cross-sections were located 0.4 m, 0.9 m and 1.4 m downstream of the nozzle exit, in the following denoted as plane 1, plane 2 and plane 3, respectively. Plane 2 corresponds to the center of the test section. Three positions of the triangular teeth have been studied in order to determine their effect on the turbulence intensity. The minimum position of the triangular teeth is reached when their edges coincide with the wedge-base edges. The maximum position is reached when the tips of the triangular teeth rise above the wedges by 5.6 mm.

Three wind tunnel speeds have been used in the study, i.e. 14 m/s, 35 m/s and 50 m/s. Measurements of time-averaged local velocities and instantaneous streamwise velocity fluctuations have been carried out using constant-temperature hot-wire anemometry (single normal-wire probe).

4 EXPERIMENTAL RESULTS

The baseline configuration is the original nozzle without jet-exit vanes which serves as reference for comparisons. The optimum configuration is characterized by the most effective turbulence reduction in the test section. In the present case, the optimum is reached when the triangular teeth rise above the wedges by 2.5 mm. This optimum value must be seen in context with the thickness of the oncoming boundary layer in the nozzle.

Fig. 2 shows the spanwise distribution of the time-averaged axial velocity component for the three cross-sections mentioned above. The results are for a wind

tunnel speed of $U_\infty = 35$ m/s which corresponds to a Reynolds number of $2 \cdot 10^6$. The velocity profiles in the region of the shear layer assume the typical error-function shape. The effect of the jet-exit vanes is that the thickness of the turbulent shear layer at its origin (nozzle exit) is increased depending on how far the triangular teeth protrude into the flow. However, the downstream growth of the shear layer remains the same so that its interior border is displaced inward. Consequently, the utilizable cross-section of the jet characterized by the plateau of the velocity profile is reduced, in the optimum case by approximately 10% in width.

Fig. 3 shows the distribution of the turbulence intensity along the (transverse) centerline of the three test planes. The turbulence intensity, Tu , is defined as the root mean square of the streamwise velocity fluctuations normalized with the wind tunnel speed, expressed in percent. The reference case (nozzle without jet-exit vanes) shows clearly that high values of the turbulence intensity are not restricted to the shear layer whose interior edge is commonly defined via the mean velocity profile. The cross-sectional area of the central core with relatively low and constant turbulence intensity is considerably smaller than the corresponding area of the central jet characterized by the plateau of the mean velocity profile. This property is preserved when jet-exit vanes are used.

In plane 1 which is adjacent to the nozzle exit, the turbulence intensity could be reduced by almost 50% by means of the jet-exit vanes. This reduction was achieved when the triangular teeth were in optimum position. The favourable effect of the jet-exit vanes decreases downstream but is still recognizable in planes 2 and 3. There, the turbulence level is still reduced by approximately 15%. A side-effect of the jet-exit vanes is that the origin of the drastic growth of the turbulence intensity adjacent to the shear layer is slightly shifted inward and that the growth rate is increased. However, this effect is unimportant since this outer region of the jet is usually not used for experiments.

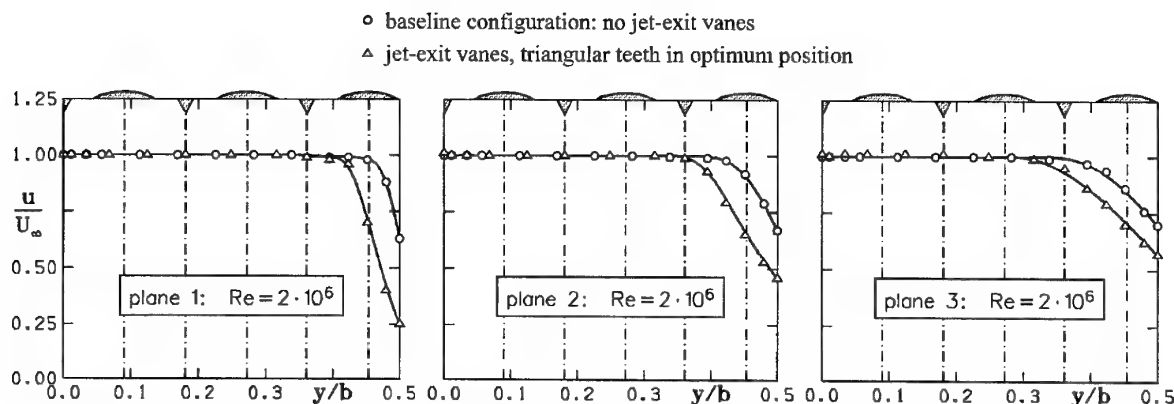


Figure 2: Spanwise distribution of time-averaged streamwise velocity component in three planes of test section

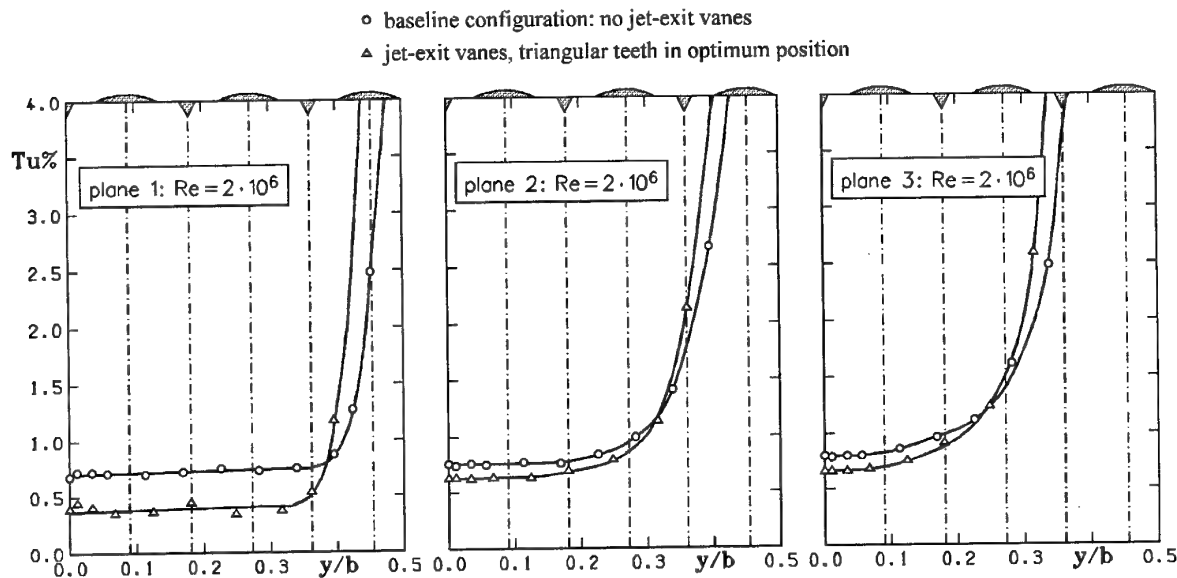


Figure 3: Spanwise distribution of turbulence intensity in three planes of test section

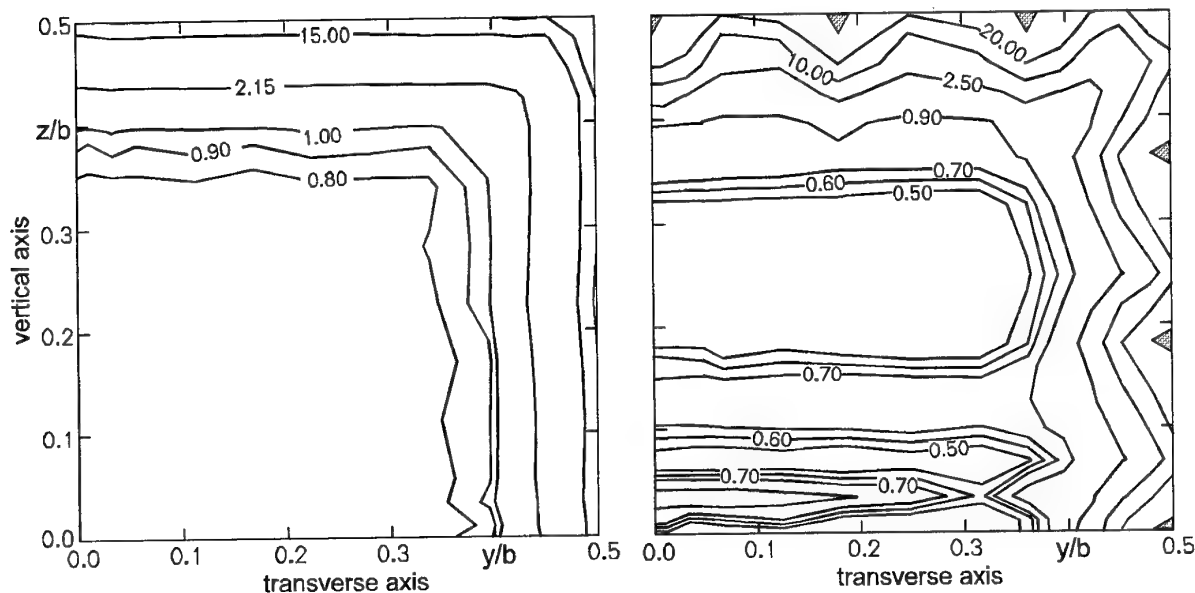


Figure 4: Distribution of turbulence (in percent) in quadrant of plane 1: $Re = 2 \cdot 10^6$.
 Left panel: baseline configuration. Right panel: triangular teeth in optimum position

Shifting the triangular teeth beyond their optimum position is accompanied by an increase of the turbulence level in the test section. In the case of very large displacements this increase becomes extremely high and non-uniform and is, therefore, not tolerable.

Fig. 4 shows as an example the complete distribution of the turbulence intensity in a quadrant of the first cross-section (plane 1). The results demonstrate the effect of the jet-exit vanes, i.e. lowering the turbulence level in the central core as compared with the baseline configuration. The corrugation of the turbulence intensity in the outer region of the jet is clearly induced by the triangular teeth. This phenomenon, however, is unimportant for most experiments since

models should not be placed in this outer region of the jet.

5 CONCLUSIONS

It was demonstrated that jet-exit vanes of the type used in the present study are successful devices to lower the turbulence level in the utilizable core of the jet in an open test section. A turbulence reduction up to 50% could be achieved. In an additional investigation whose details are not reported here a further favorable effect of the new jet-exit vanes has been found, i.e. a remarkable reduction of the noise level as compared with the classical Seiferth wings.

REFERENCES

Seiferth, R.: Vorausberechnung und Beseitigung der Schwingungen von Freistrah-Windkanälen. *Monographien über Fortschritte der deutschen Luftfahrtforschung seit 1939*. Ed.: A. Betz. AVA Göttingen 1946.

Schulz, G. und Viehweger, G.: Der Unterschall-

windkanal der DVL in Porz-Wahn (Teil II): Verbesserungen und Entwicklungen an den Eigenschaften und Einrichtungen). *DLR Forschungsbericht 65-56 (1965)*.

Sellers III, W.L., Applin, Z.T., Molloy, J.K. and Gentry, G.L.: Effect of jet exit vanes on flow pulsations in an open-jet wind tunnel. *NASA TM86299 (1985)*.

MODEL AND FULL SCALE INVESTIGATIONS OF THE LOW FREQUENCY VIBRATION PHENOMENA OF THE DNW OPEN JET

H. Holthusen

J.W. Kooi

German-Dutch Wind Tunnel (DNW), Emmeloord, The Netherlands

Abstract

The German-Dutch Wind Tunnel DNW is a large low speed wind tunnel with three different sized closed and one open test section (Open Jet). Already during the first calibration phase of the Open Jet in 1981, it soon became clear that the maximum jet velocity was not limited by the available fan power, but by the maximum allowable vibrations of the Test Hall which surrounds the Open Jet. Due to low-frequency pressure fluctuations generated by the Open Jet, the vibrations reached levels which could become critical for the Test Hall structure. In order to be able to increase the maximum velocity beyond this 80 m/s an extensive research programme was executed in the 1:10 scaled pilot wind tunnel of DNW. The objective of this programme was to find the sources of the observed low frequency pressure fluctuations and to verify different configurations for their potential to reduce the vibration level. The tested configurations included a number of well-known nozzle modifications as well as a new configuration with so-called tetrahedrons. The effect of modifications of the collector geometry and the effect of extra bleeding was also investigated. After completing the tests in the pilot wind tunnel, the most promising solutions were tested in the DNW. It turned out that the results found in the two wind tunnels correlated very well. A surprising outcome was that in both tunnels the tetrahedrons increased the jet speed without a noticeable reduction of the usable cross-section of the Open Jet and without increasing the acoustic background noise level.

1. INTRODUCTION

In the initial phase of the development of the German-Dutch Wind Tunnel (DNW) the wind tunnel was designed with closed-wall test sections. The design included three different sized test sections: one with a cross section of 6 m x 6 m, one with a cross section of 8 m x 6 m and one with a cross section of 9.5 m x 9.5 m. A complete test section configuration consisted of a nozzle, a parallel test section and a transition. During the development it gradually became clear that besides the need for a new, large low-speed wind tunnel, there was an arising need for acoustic testing capability. The idea was to use the exchangeable components of the closed test section to build an open test section for acoustic testing.

A feasibility study was done using DNW's 1:10 scaled model wind tunnel PLST (Pilot Low Speed Tunnel). From this study it turned out that a combination of the 8 m x 6 m nozzle together with the 9.5 m x 9.5 m transition could be a workable Open Jet configuration (Figures 1 and 2). To optimise the acoustic performance of the DNW Open Jet, the transition had to be modified. Therefore, the internal walls of the transition were lined with acoustically absorbent material. On the leading edge of the transition an elliptical shaped collector was added, also lined with acoustical absorbent material. These modifications had no negative influence on the functionality of the closed 9.5 m x 9.5 m test section. Between the ending of the transition and the beginning of the first diffuser a gap of 0.25 m was left to give the transition the possibility to breathe.¹ To achieve anechoic conditions the room around the Open Jet test section (the so-called 'Test Hall') was treated with acoustically absorbent wedges and liner material. Above 200 Hz the sound absorption in this room is better than 99%.² With its dimensions

of $b \times w \times h = 47.1 \text{ m} \times 28.2 \text{ m} \times 18.7 \text{ m}$ it is one of the biggest anechoic chambers in the world.

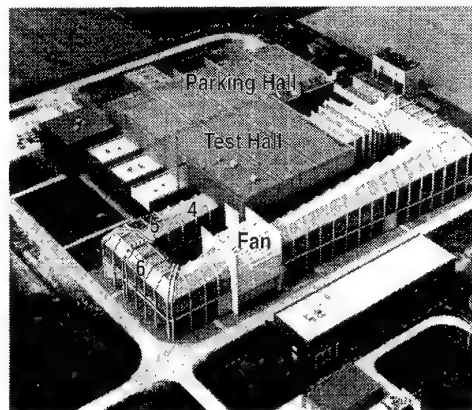
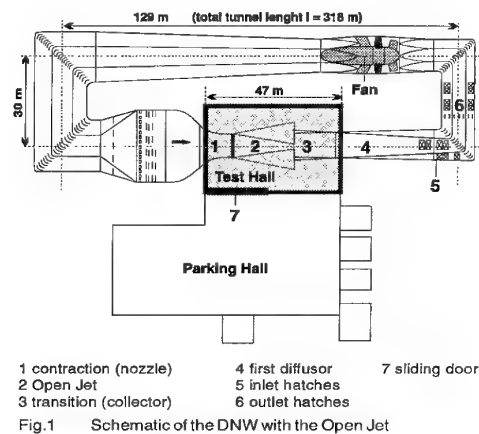


Fig.2 Aerial photograph of DNW (see also Fig. 1)

In the PLST it is possible to run the open jet without any problems to the highest possible speed of rotation of the fan ($\text{RPM}_{\text{max}} = 225$, which is equal to a maximum velocity of about 95 m/s). Therefore it was an unexpected surprise that in 1981 during the first calibration run of the DNW Open Jet a strong vibration problem occurred. Starting from a velocity of 60 m/s the side walls and the ceiling of the Test Hall shook at a noticeable level. At a velocity of 80 m/s (which is equal to a RPM of 187 min^{-1} , for the empty test section) the vibrations had reached a critical level. Finally parts of the structure broke from the ceiling at a velocity of 84 m/s ($\text{RPM} = 198$), so the calibration run had to be stopped. The maximum displacement of the ceiling, measured by a number of accelerometers, was about 20 mm peak to peak.³ Until today the maximum velocity in the DNW Open Jet is limited for safety reasons to 80 m/s ($\text{RPM} = 191$, with a model in the test section). Despite this limitation in speed, the DNW Open Jet is world wide the biggest open jet with the highest possible velocity of 80 m/s. Although this velocity is high enough for most of the tests in the Open Jet, for some it would be an advantage to measure at velocities up to 95 m/s (e.g. take-off and landing configurations of aircrafts).

2. PRE-INVESTIGATIONS IN THE PLST

In order to be able to increase the maximum velocity by using the maximum available fan RPM an comprehensive research programme was executed in the PLST (starting in 1989).^{4,5,6} The objective was to find the sources of the observed low frequency pressure fluctuations and to verify different configurations of the test section for their potential to reduce the critical vibration.

Generally low frequency vibrations occur in most wind tunnels with large open test sections. So it is not surprising to find descriptions of a lot of possible excitation and resonance mechanisms in the literature.^{7,8,9,10}

There are also many different solutions documented to reduce the vibrations. But often these solutions are more or less very specific for the different wind tunnels. The solutions to reduce the vibrations can mainly be divided into two groups of modifications. The first group contains modifications at the nozzle. The main goal is thereby to break up the ring vortex which is created at the trailing edge of the nozzle and travels downstream in the shear layer of the open jet towards the collector. The second group contains modifications of the geometry of the collector and the transition. Most of these modifications found in the literature were tested in the PLST.

To the first group belong different types of Seiferth wings and vortex generators placed inside the nozzle or at the leading edge of the nozzle.⁹ Results from tests in the PLST showed that these modifications did not solve the vibration problem (the situation had become even worse with the Seiferth-wings). Very promising results were obtained by mounting small tetrahedrons at the inner side of the leading edge of the nozzle (see Figure 4). The velocity in the open jet is increased with about 6% (for a fixed RPM) without a noticeable reduction of the core width of the jet. But the price for this speed increase is a strong negative pressure gradient behind the nozzle, caused by

a post contraction. The width of the shear layer was significantly smaller than for the standard nozzle (the width of the shear layer with the Seiferth wings in the nozzle was about 3 times wider than normal!). No increase of the background noise level could be detected. At the same velocity the vibration level was lower than with the standard nozzle configuration. Until now the mechanisms of these effects are not exactly known.

The transition was modified by adding ring gaps or breather hatches on a number of different locations. Even the inlet area of the collector was changed over a wide range. The inlet and outlet hatches of the tunnel circuit were also opened (Figure 1). The length of the open jet was shortened and the geometry of the Test Hall was changed by removing some side walls.

As mentioned before it is possible to run the Open Jet in the PLST up to a velocity of 95 m/s without any signs of critical vibrations of the Test Hall. One explanation for this phenomenon is that the displacement s caused by an acceleration a decreases with the second power of the acceleration frequency f .

$$s = \frac{a}{(2 \pi f)^2} \quad (1)$$

The scale factor of 1:10 is the reason why most of the frequencies created by aerodynamic or room resonance effects are ten times higher in the PLST than in DNW. Therefore, the displacement of a structure in the PLST at a fixed acceleration level is always 100 times smaller than in the DNW.

The second reason is that the construction of the Test Hall of the PLST is significantly stiffer than the construction at DNW. Only with special data acquisition and processing techniques was it possible to detect the low frequency vibrations in the PLST. Therefore, one important task of the investigations in the PLST was to find out measurement techniques and criteria to compare the efficiency of the tested modifications. More details on this can be found in Holthusen.¹¹

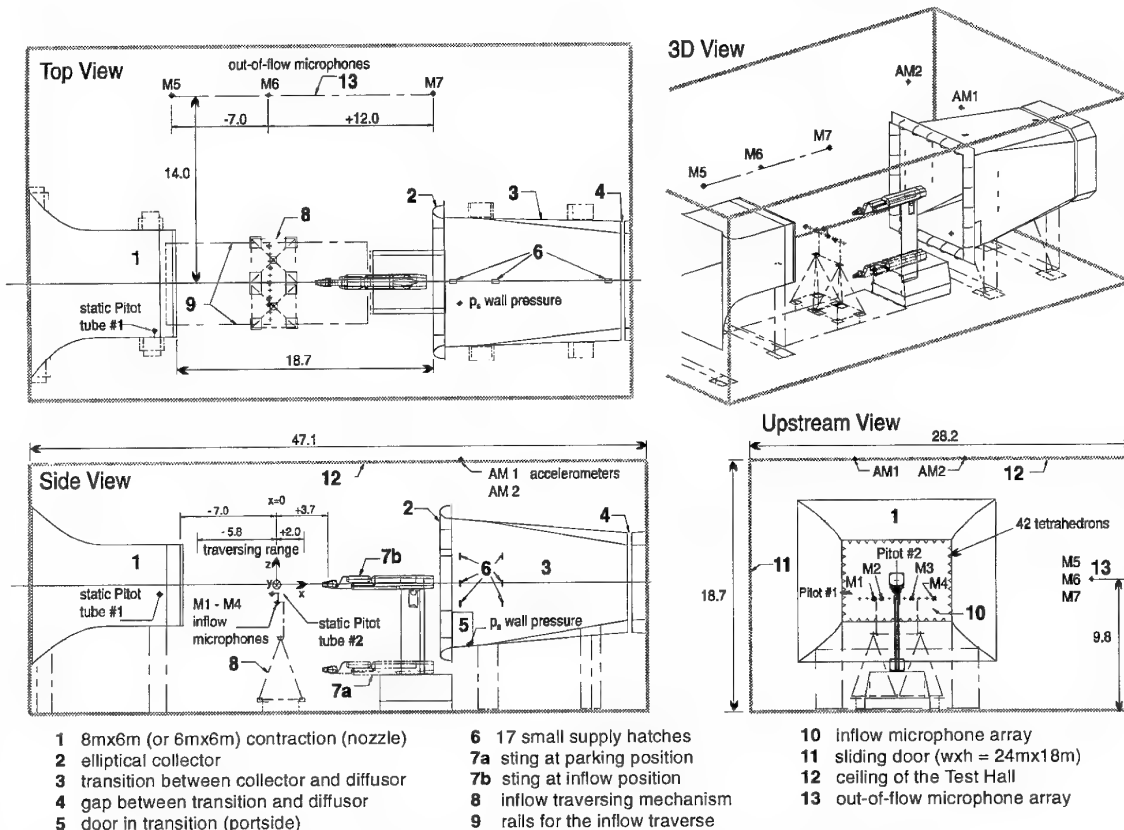


Fig.3 Test section and instrumentation set-up for the low frequency noise and vibration investigation in DNW (all dimensions in meters)

3. INVESTIGATIONS OF THE DNW OPEN JET

3.1 Wind tunnel test set-up

Figure 3 shows the test set-up of the Open Jet and the position of the different sensors for the investigations, which were executed in 1993.¹¹

The following configurations were investigated:

- the Open Jet 'standard configuration'
- the sliding door of the Test Hall opened
- the transition with some extra bleeding openings
- the inlet- and outlet hatches open
- 42 tetrahedrons in the 8m x 6m nozzle
- the 6m x 6m nozzle

Figure 4 shows a close-up of the nozzle with the tetrahedrons and some details of the horizontal inflow microphone wing.

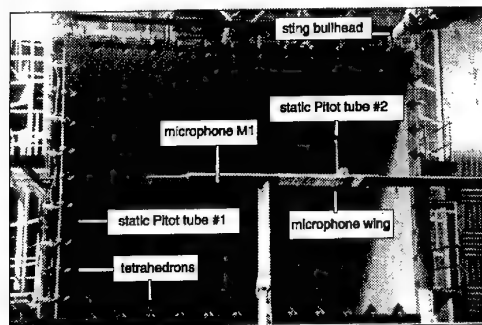


Fig.4 View from the Open Jet into the 8mx6m nozzle with the 42 tetrahedrons

3.2 Data acquisition

The standard steady state wind tunnel parameters were measured with the Static Data Acquisition system (SDA). For the measurement of the instationary data the 12-channel Dynamic Data Acquisition system (DDA) was used. The acquisition hardware of DDA is based on three 16-bit DIFA SCADAS II frontends and a HP755 UNIX workstation. The acquisition software is based on CADA-X software from LMS. All measured time signals are digitised and stored to hard disk. The total amount of time signal data of the measurement at DNW was about 600 MB. From these data about 8400 narrow-band spectra were calculated.

The following signals were measured during the test in DNW (Figure 3):

- the wind tunnel reference system (SDA)
- 1 static Pitot tube in the 8m x 6m nozzle (SDA & DDA)
- 1 static Pitot tube on the inflow traverse mechanism (SDA & DDA)
- 1 static pressure sensor on the wall of the transition (SDA)
- 4 microphones on the horizontal wing of the inflow traverse mechanism (DDA)
- 3 microphones on the out-of-flow traverse mechanism (DDA)
- 2 accelerometers on the ceiling of the Test Hall (DDA)

All signals measured with DDA were sampled over a time of about 120 s with a bandwidth of 200 Hz (sample frequency 400 Hz). For acoustic investigations some measurements were additionally done with a bandwidth of 10 kHz (and also 40 kHz) and a sample time of 2 seconds per data point.

3.3 Data reduction

The static data were reduced and presented with the standard software package on the VAX-computer system of DNW. The dynamic data were processed and presented on DDA with a

software package developed by DNW.

From the time signal data autopower spectra were calculated with the FFT procedure. To find the highest vibration amplitude during a 120 s sample, the low frequency spectra (bandwidth = 200 Hz, $\Delta f = 0.1$ Hz) were averaged with the peak hold method. From these spectra RMS (root mean square) values were calculated over different frequency ranges. Because the frequency range between 0 and 30 Hz is the important one for the vibration phenomena, this frequency range was chosen for the standard RMS-plots. For an easier comparison these RMS-values are made non-dimensional by dividing them by fixed reference values. As reference values the RMS-values are chosen, which are measured with the standard configuration of the Open Jet at a velocity of 80 m/s.

For another form of normalised presentation the amplitudes of the autopower spectra were divided by the dynamic pressure q . Equation (2) gives the transformation for the pressure signals, the transformation for the acceleration signals is given in equation (3).

$$L_p^{\wedge} = 10 \log \left(\frac{p}{q_t} \right)^2 \quad (2)$$

$$L_a^{\wedge} = 10 \log \left(\frac{a}{a_0} \frac{p_0}{q_t} \right)^2 \quad (3)$$

with L_p^{\wedge} = normalised pressure fluctuation level [dB]
 L_a^{\wedge} = normalised fluctuation level of the acceleration [dB]
 p = RMS-value of the pressure fluctuation [Pa]
 a = RMS-value of the acceleration [m/s^2]
 p_0 = reference pressure $2 \cdot 10^{-5}$ Pa
 a_0 = reference acceleration $1 m/s^2$
 q_t = dynamic pressure in the core of the open jet [Pa]

The frequencies f are transferred into a non-dimensional Strouhal-number St by dividing them by the velocity v_t (v_t = velocity in core of the open jet; for a handy scaling the characteristic length d was set to 100 m).

$$St = \frac{f d}{v_t} \quad (4)$$

The high frequency spectra (bandwidth 10 kHz, $\Delta f = 2.4$ Hz) were averaged with the standard linear averaging method. From the sound pressure level L_p of these spectra also some OSPL's (overall sound pressure level) over different frequency ranges are calculated (reference pressure $p_0 = 2 \cdot 10^{-5}$ Pa).

$$L_p = 10 \log \left(\frac{p}{p_0} \right)^2 \quad (5)$$

3.4 Results of the static data measurements

3.4.1 Velocity calibrations

Figure 5 shows the result of the velocity calibration of the standard configuration in comparison with three other test section configurations. With the tetrahedrons a velocity of about 85 m/s could be reached. This result is identical to the result from the PLST. It might be even possible to go to higher velocities, however for some technical and safety reasons this was not done. With the 6m x 6m nozzle the velocity could not be set to more than 80 m/s because the vibration level was already higher than with the standard configuration. In the PLST the maximum velocity with this nozzle configuration was about 110 m/s. With all the opened inlet and outlet hatches in the tunnel circuit only a maximum velocity of about 45 m/s could be reached. A further increase of the velocity was too risky due to decrease of pressure lower than atmospheric in the Test Hall. This could lead to critical loads for the walls and the ceiling of the Test Hall. This effect also occurred in the PLST.

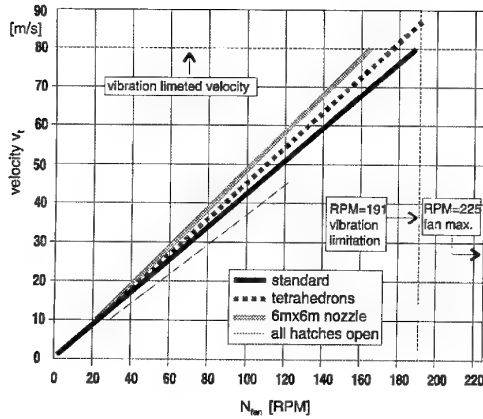


Fig. 5 Velocity v_t as function of the fan RPM for 4 different configurations

3.4.2 Static pressure distribution in the jet

The distribution of the static pressure $p_{s,2}$ at the centre line of the Open Jet was measured using the Pitot static tube #2 between the positions $x = -5.8$ m and $x = +2.0$ m. The pressure coefficient $c_{p,trans}$ was calculated from the difference of $p_{s,2}$ and the barometric pressure p_b divided by the dynamic pressure q_t (which was also measured with the Pitot static tube #2).

$$c_{p,trans} = \frac{p_{s,2} - p_b}{q_t} \quad (6)$$

The barometric pressure p_b was chosen, because a stable reference pressure was necessary for the dynamic measurements of the pressure signals of the Pitot static tubes #1 and #2.

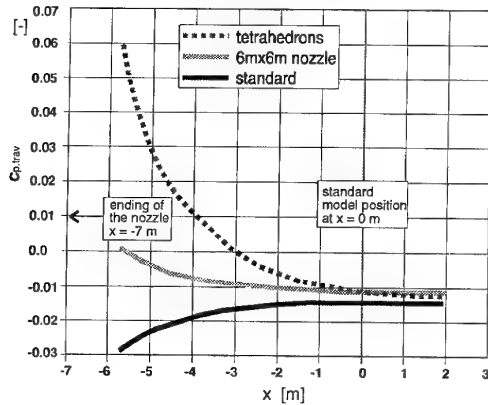


Fig. 6 Non-dimensional static pressure $c_{p,trans}$ on the centre line of the Open Jet as function of x for 3 different nozzle configurations

For the standard Open Jet configuration, the nozzle configurations with the tetrahedrons, and the 6 m x 6 m nozzle the results are given in Figure 6. The strong positive pressure gradient behind the nozzle shows a shape identical with the gradient measured in the PLST. The gradient indicates a post contraction produced by the tetrahedrons, which is responsible for the speed increase. From a comparison with the pressure distribution for the standard configuration the conclusion can be drawn that from the x -position $x = -2$ m on the gradient can be neglected. For short wind tunnel models, such as propulsion models, this pressure gradient is acceptable.

The additional pressure gradient caused by the 6 m x 6 m nozzle is significantly smaller than for the tetrahedrons.

3.4.3 Static pressure in the transition

Due to the entrainment in the shear layer of an open jet, the

volume flow grows with the length of the jet. For the DNW Open Jet some calculations of the shear layer development, the velocity profiles and the volume flows were done, using a model from Regenscheit.¹² Some of the results are shown in Figure 7. The figure shows that the volume flow V_t which flows into the transition would be 25% greater than the volume flow V_c out of the nozzle. This violation of the law of continuity is corrected by the open jet by building up a positive static pressure gradient in front of the collector (transition). As the ratio of V_t/V_c grows the gradient also gets stronger. For a ratio smaller than one the gradient change from positive to negative shape. These theoretical conclusions were verified in the PLST by changing the inlet area of the transition. The results of the calculations agreed very well with the experimental results.

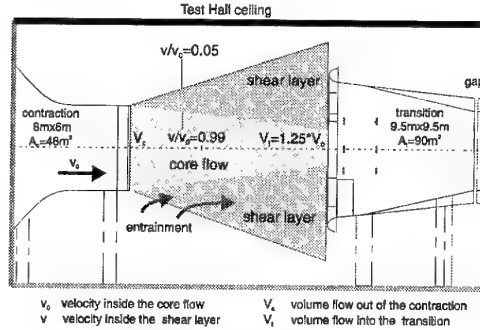


Fig. 7 Schematic of calculated shear layer and volume flows of the DNW Open Jet¹²

As already mentioned, the width of the shear layer with the tetrahedrons is smaller than without. This is the reason why the growth of the volume flow are smaller, and the pressure gradient in front of the transition smaller.

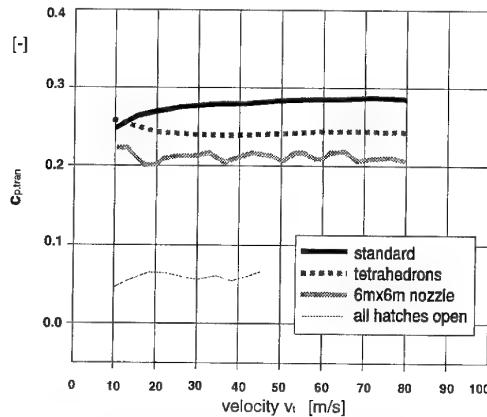


Fig. 8 Non-dimensional static wall pressure $c_{p,tran}$ on the centre line at the inlet of the transition

This explains, why in Figure 8 the static pressure in the transition with the tetrahedrons is somewhat lower than with the standard nozzle.

For the configuration with the 6 m x 6 m nozzle the static pressure is lower because the total volume flow of the open jet is smaller than with the 8 m x 6 m nozzle (the total shear layer area is smaller).

With the inlet and outlet hatches opened the static pressure is so low because a considerable part of the extra volume flow of V_t is breathed out of the hatches.

The static pressure $p_{s,wall}$, measured at the wall of the transition, was converted to the pressure coefficient $c_{p,tran}$ similar to eq. (6).

$$c_{p,tran} = \frac{p_{s,wall} - p_b}{q_t} \quad (7)$$

3.5 Results of the dynamic data measurements

3.5.1 Excitation and resonance mechanisms

As vibration occurs two different phenomena are to be considered. On the one hand the excitation mechanisms, which supplies (periodically or permanently) the energy for the vibrations, and on the other hand the resonance mechanisms which react to the excitations and amplify the vibrations.

From the literature a number of these mechanisms are known to be responsible for vibrations in wind tunnels with open jets. Hereafter a short description of the most important mechanisms follows. At first the excitation mechanisms.

Due to the rotation of the wind-tunnel fan periodical pressure fluctuations are created, which can be found back in the whole wind tunnel circuit. Generally known is the so-called blade passing frequency f_{bpf} of a fan, which is described by (8):

$$f_{bpf} = \frac{\text{RPM}_{fan} R}{60} \quad (8)$$

with f_{bpf} = blade passing frequency of the fan [Hz]
 R = number of rotor blades of the wind tunnel fan (at DNW $R=8$)
 RPM_{fan} = speed of rotation [min^{-1}]

For instance at a velocity of $v_t = 80$ m/s ($\text{RPM}_{fan} = 187$) f_{bpf} is equal to 25 Hz. But also higher- or sub-harmonics of this frequency can function as excitation sources. At DNW the fan revolution frequency ($R = 1$) can be found back as a peak in the frequency of the measured pressure.

Another special excitation mechanism found in open jets, is the periodical separation of eddies from the nozzle. The transportation speed of the eddies is about half the velocity in the core of the open jet. The shedding frequency f_{sle} can be described by equation (9), which was derived by Michel based on measurements in the Open Jet of DNW in 1985.¹²

$$f_{sle} = \frac{0.48 v}{d_D} \quad (9)$$

with f_{sle} = shear layer eddy shedding frequency [Hz]
 v = velocity in the core of the open jet [m/s]
 d_D = characteristic length (diameter) of the DNW 8 m x 6 m nozzle, $d_D = 7$ m

The eddies created at the nozzle are transported downstream in the shear layer. As they hit the collector a special feed-back mechanism can arise. At certain combinations of velocity and distance between the nozzle and the collector so-called edge tone noise can be created. In this case the sound waves, created by the periodic impact of the eddies on the collector trigger the generation of eddies at the nozzle.¹⁴

$$f_{cet} = \frac{0.85 v}{d_L} \quad (10)$$

with f_{cet} = collector edge tone noise frequency [Hz]
 v = velocity in the core of the open jet [m/s]
 d_L = free length of open jet, which is defined by the distance between the nozzle and the collector; at DNW is $d_L = 19$ m

All the excitation mechanisms have one thing in common: they create a sharp frequency, which rises linear with the velocity. For the velocity range of the DNW Open Jet all these frequencies lie below 30 Hz. Nothing can be said about the relationship between the velocity v_t and the amplitude of these frequencies. Some of them occur exclusively at very special velocity and geometric conditions.

Quite different from the other excitation mechanisms is the characteristic of the excitation caused by broad-band 'noise'. This 'noise' can be created by the vortices in the turbulent shear layer. Is it difficult to decide for these low frequencies (below 30 Hz), whether these 'noise' is caused by pure hydrodynamic pressure fluctuations or by pure sound waves or by a combination of the two mechanisms. To find out, what the real nature of these pressure fluctuations is, it is necessary to measure the phase speed of the pressure fluctuations. Therefore, the cross-correlation between some pressure sensors positioned at a well defined distances has to be measured. For a given frequency the phase speed could than be calculated from the phase information from the cross-correlation. Such an analysis of the measured data is not yet done. But it is planned to do this in the future. A typical spectrum of the 'noise' of these vortices shows a broad peak at very low frequencies and a continuous decrease in amplitude with increasing frequencies. The amplitude of such a spectrum grows continuously with an increase of the velocity.

An important resonance mechanism is the resonance of an air column inside a fixed volume. The different natural frequencies of an air column in a rectangular volume, such as the Test Hall, can be calculated from equation (11).

$$f_{fr} = \frac{c}{2 \sqrt{\left(\frac{l_x}{n_1}\right)^2 + \left(\frac{l_y}{n_2}\right)^2 + \left(\frac{l_z}{n_3}\right)^2}} \quad (11)$$

with f_{fr} = natural frequency of an air column [Hz]
 c = speed of sound in air $c = 340$ m/s
 $l_{x, y, z}$ = geometric dimensions of the enclosed air column [m]
 $n_{1, 2, 3}$ = modulus of the natural frequency, with n_i an integer greater or equal one

The whole wind tunnel circuit or some sub-parts of the circuit can function as an organ pipe. The resonance of such an organ pipe can be calculated by equation (12).¹⁵

$$f_{opt} = \frac{c}{2 l_{op} \left[1 - \frac{(d_a - d_e)^2}{\pi^2 n^2 d_e d_a} \right]} \quad (12)$$

with f_{opt} = frequency of an organ pipe [Hz]
 l_{op} = length of the organ pipe [m]
 n = modulus, integer $n \geq 1$
 d_e = parameter for the ending condition at the beginning of the pipe
 d_a = parameter for the ending condition at the ending of the pipe

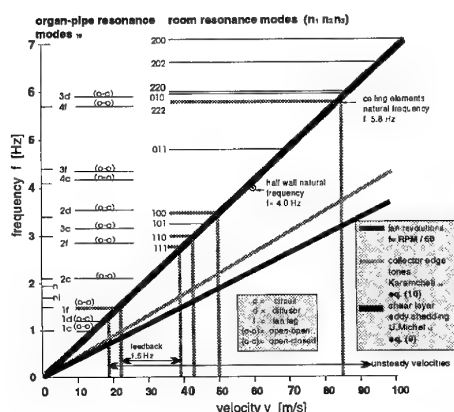


Fig.9 Survey of excitations and resonance modes for the DNW Open Jet

The natural frequency of a plate or a wall can also be calculated from the dimensions, the material and the kind of assembly. In this way the calculated natural frequency of the ceiling elements of the Test Hall is 5.8 Hz, the natural frequency of the walls of the Test Hall is about 4.0 Hz.

Figure 9 gives a survey of the relationship between the frequencies and the velocity for the described excitation and resonance mechanisms for the DNW Open Jet.¹⁶

3.5.2 Acceleration spectra

Figure 10 shows typical narrow-band spectra for the acceleration of the ceiling of the Test Hall at a velocity of 80 m/s (Open Jet standard configuration). The accelerometers AM1 and AM2 were placed at the centre of two different ceiling elements near the collector (see also Figure 3). The two spectra show that the maximum amplitude of the vibration is a function of the location at the ceiling. This result is supported by subjective observations which were done while standing on the ceiling. A kind of nodal and antinodal patterns of the ceiling elements could easily be recognised. This pattern was slightly changed in time and location. The spectra also show that the highest amplitude are at frequencies around the calculated natural frequency ($f = 5.8$ Hz). Another strong peak lies at 7.0 Hz. Furthermore below a frequency of about 3 Hz no vibrations can be detected. Because the accelerometer can detect even DC-signals, the acceleration data were also processed with a finer frequency resolution of $\Delta f = 0.01$ Hz, but still no lower frequencies could be detected. This was an important piece of information, because from the subjective impressions it was thought, that the vibration frequency was significantly lower than the measured frequencies. The expected vibration frequencies were estimated between 0.1 Hz and 1 Hz. The explanation for this can be found in a comparison of the spectra and the time signal of the acceleration.

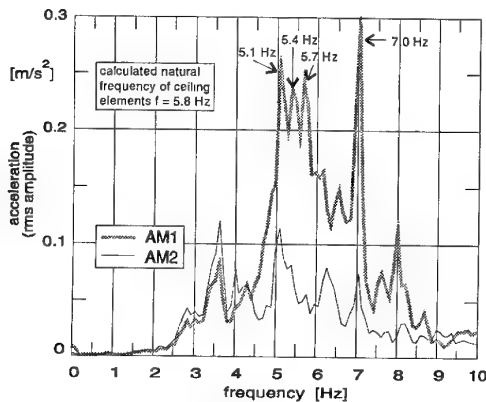


Fig. 10 Typical narrow-band spectra of the acceleration of the Test Hall ceiling ($v_t = 80$ m/s, Open Jet standard configuration, $\Delta f = 0.1$ Hz, integration time 120 s)

The peaks around 5 Hz in Figure 10 lie very close together (about $\Delta f = 0.3$ Hz). When two or more frequencies lie close together the phenomenon of beating can occur. In this case an excited structure not only vibrates with the excitation frequencies but also with the beating frequency, which is defined by the difference of the excitation frequencies. In this case the beating frequency is about 0.3 Hz. For the accelerometer AM1 is the corresponding time signal for the spectrum in Figure 10, shown in Figure 11. Of the total recorded 120 seconds only an extract of about 10 s is shown. The time signal also shows a pattern of this low frequency. The subjective recognised vibrations can therefore be explained by beating.

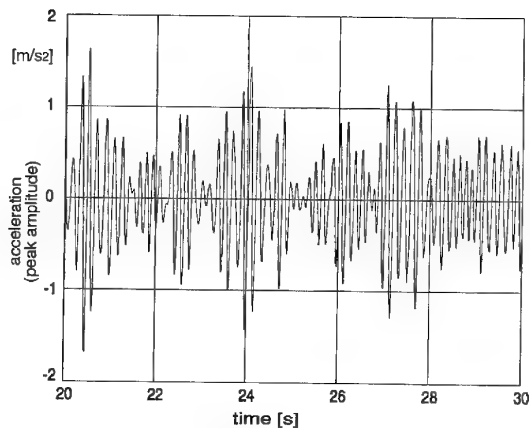


Fig. 11 Typical acceleration time signal (signal of sensor AM1, see also Fig. 10)

3.5.3 Normalised spectra

For three different velocities (40, 60 and 80 m/s) Figure 12 shows the normalised spectra of the total pressure fluctuations $p_{t,2}$, measured with the static Pitot tube #2 mounted on the inflow microphone wing. For all velocities the amplitudes of the spectra are nearly identical. Because all amplitudes of the spectra are normalised by the dynamic pressure q_t , the conclusion can be drawn that the amplitude of the fluctuation grows proportionally with the dynamic pressure (or with the square of the wind velocity in the core of the open jet).

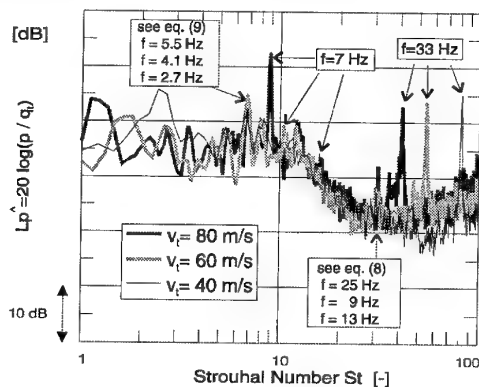


Fig. 12 Normalized pressure fluctuation $Lp^$ of the total pressure $p_{t,2}$ as function of the Strouhal number St . $p_{t,2}$ measured with the Pitot tube #2. Open Jet standard configuration

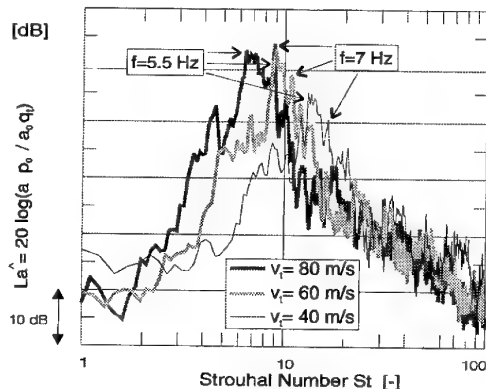


Fig. 13 Normalized acceleration level $La^$ as function of the Strouhal number St . Accelerometer AM1. Open Jet standard configuration

The frequencies of the spectra were normalised with the velocity v_t by transferring them into Strouhal numbers. In the figure two types of peaks can be recognised. The peaks of the first type increase the Strouhal number proportionally to the increasing velocity v_t . This type of frequencies can be described with the equations (8), (9) and (10). For instance the peaks caused by the blade passing frequency eq.(8) and the peaks of the shear layer eddy shedding eq.(9) can be identified. The peaks of the second type stay fixed at a constant Strouhal number, they are caused by resonance frequencies which are not changing with the velocity. The peak at $f = 33$ Hz is caused by a pipe resonance in the static Pitot tube #2; (the transfer characteristics of the Pitot tubes were especially measured). The origin of the strong peak at 7 Hz is not known yet.

Figure 13 shows the normalised acceleration levels, which were measured with the accelerometer AM1 on the ceiling of the Test Hall. Here it can be seen, that the amplitudes increase proportionally with the increase of the dynamic pressure. In these spectra only the peaks of the second type can be found (fixed frequencies at 5.5 Hz and 7 Hz). Therefore we come to the conclusion, that the vibrations of the ceiling elements are dominated by resonance mechanisms which are triggered by broad-band excitation.

3.5.4 RMS-values

Figure 14 shows the RMS-values measured with 5 different sensors as a function of the velocity v_t for the standard configuration of the Open Jet. The RMS-values at $v_t = 80$ m/s were used as reference values, therefore the relative RMS-values at this velocity are equal to one. Up to a velocity of 55 m/s a step of $\Delta v_t = 1$ m/s was used and above this point the velocity was increased in steps of $\Delta v_t = 5$ m/s. The shape of the plots also shows that there is a distinct relationship between the increase of the RMS-levels and the square of the velocity (or the dynamic pressure).

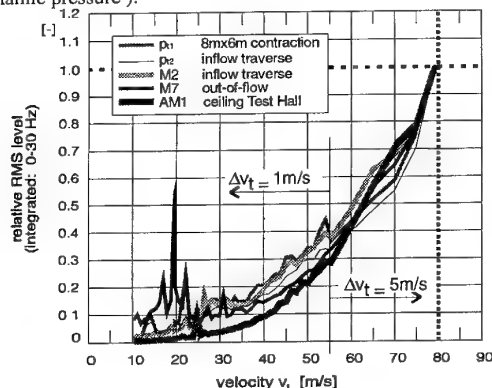


Fig.14 Non-dimensional RMS-levels as function of the velocity v_t . Open Jet standard configuration

Only for the lower velocities ($v_t < 55$ m/s) some resonance situations occur, e.g. at $v_t = 17, 19, 22, 28, 32$ or 54 m/s. But above that velocity the RMS-levels increase continuously with the velocity. An interesting result is, that just at a velocity of 60 m/s the RMS-levels reach half of the maximum level reached at 80 m/s. By further increasing the velocity the RMS-levels rise very fast. This probably explains why most wind tunnels with large open jets operate only up to a maximum velocity of 60 m/s.

Figure 15 shows the RMS-levels for the nozzle configuration with the tetrahedrons. At a velocity of 80 m/s the RMS-values were from 20% up to 45% lower than with the standard nozzle at the same velocity. The maximum velocity was about 84 m/s and the RMS-values were at this velocity still between 12% and 27% lower than at the reference situation. For a short acoustic measurement a maximum velocity of 87 m/s was reached.

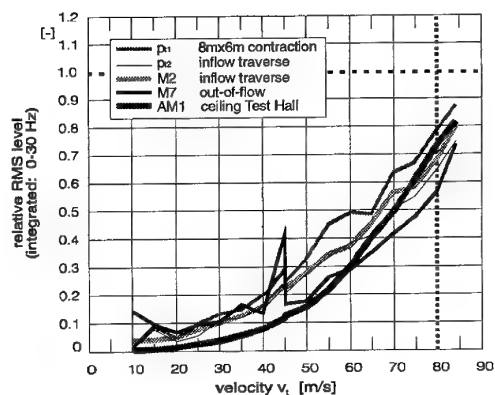


Fig.15 Non-dimensional RMS-levels for the nozzle configuration with 42 tetrahedrons ($\Delta v_t = 5$ m/s, max. velocity $v_t = 84$ m/s)

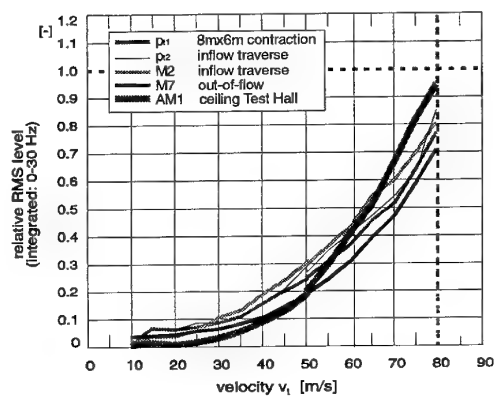


Fig.16 Non-dimensional RMS-levels as function of the velocity v_t for the configuration with the opened sliding door of the Test Hall, standard nozzle and transition. ($\Delta v_t = 5$ m/s, max. velocity $v_t = 80$ m/s)

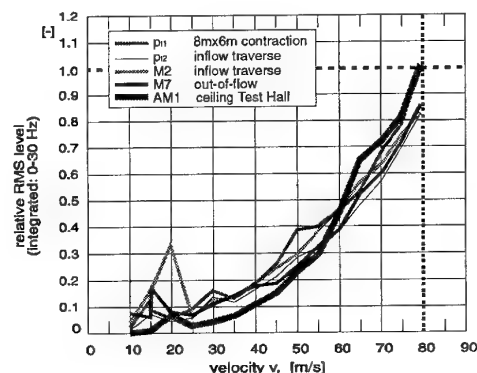


Fig.17 Non-dimensional RMS-levels as function of the velocity v_t for the configuration with the maximum opened transition (17 supply hatches and door opened) and the standard nozzle, ($\Delta v_t = 5$ m/s, max. velocity $v_t = 80$ m/s)

The RMS-values for the configuration with the opened sliding door are shown in Figure 16. Due to change of the resonance characteristic of the air column enclosed in the Test Hall it is possible to reduce the RMS-levels. But the RMS-value of the acceleration can only be decreased a little bit. For acoustic research in the Open Jet it is necessary to close the sliding door to achieve anechoic conditions.

Figure 17 shows, that the vibration of the ceiling can not be efficiently reduced by opening the small supply hatches in the transition.

3.5.5 OSPL-level

Measurements with the inflow microphones M1 to M4 show that the OSPL of the low frequency pressure fluctuations, integrated between 0 and 200 Hz, inside the Open Jet increase continuously with an increasing distance between the microphones and the nozzle. The measured level also increases by decreasing the distance between the microphone to the shear layer. Microphone M4 was nearest to the shear layer. Therefore the conclusion can be drawn that the shear layer is the source location of the low frequency pressure fluctuations (Figure 18). For the frequency range 200 Hz the OSPL (0.2 - 10 kHz) is nearly constant at every x position on the centre line (Figure 19).

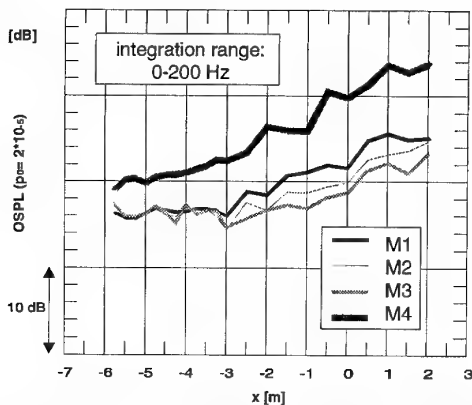


Fig.18 Overall sound pressure levels (OSPL) measured with 4 inflow microphones as a function of x . Open Jet standard configuration, $v_t = 60$ m/s

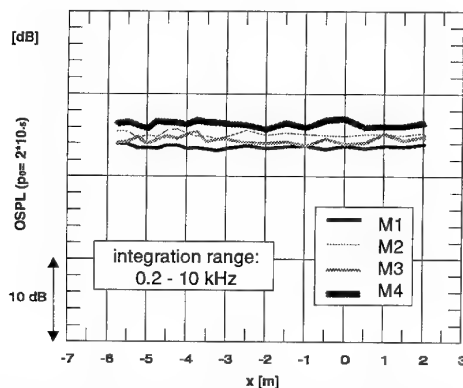


Fig.19 Overall sound pressure levels (OSPL) (conditions see Fig. 18)

4. CONCLUSIONS

An experimental programme was executed to obtain a better understanding of the low frequency pressure fluctuations generation by the Open Jet of the DNW. This low frequency pressure fluctuations and the associated vibrations of the walls and the ceiling of the Test Hall currently limit the maximum speed of the Open Jet to 80 m/s. It was hoped that by understanding the sources better, modifications could be designed which allowed an increase of the velocity up to the initial design speed of about 95 m/s. Pre-investigations were performed in the scale 1:10 pilot wind tunnel of the DNW. The investigations have led to the following conclusions:

- Results from the pilot wind tunnel (PLST) correlate well with the results from the DNW.

- Due to the difference in stiffness and the ten times higher frequencies because of the scaling, the PLST walls and ceiling do not show the same large vibration as the walls and ceiling of the DNW Open Jet.
- Of all tested nozzle modifications only the tetrahedrons reduced the vibration. The Open Jet with the tetrahedrons installed has a thinner shear layer and it has a six per cent higher velocity at the same RPM. The tetrahedrons create directly downstream of the nozzle a steeper longitudinal pressure gradient. Tetrahedrons reduce the broad band (in the range up to 30 Hz) pressure fluctuations of the Open Jet. This is acceptable for testing with shorter models as used for example in propulsion testing.
- None of the modifications of the collector, the transition and the opening of hatches in the diffuser reduced the vibrations at higher velocities. A reduction occurred only at some special low resonance velocities, where the vibrations were not at a critical level.
- The Open Jet can be excited by pressure fluctuations caused by the fan, by organ-pipe resonance's, by collector edge tones and by shear layer eddy shedding. However, it is not a resonance, but the broad-band low frequency pressure fluctuations in the shear layer vibration which drives the vibration of the walls and ceiling at higher velocities. The level of these broad-band pressure fluctuations is proportional to the dynamic pressure.
- Extrapolation of the vibration levels indicates a maximum velocity for the installed tetrahedrons of 90 m/s.

5. REFERENCES

- 1 "Construction" 1976-1980, DNW, 1982
- 2 K.J. Schultz, K.H. Spiegel, "Acoustic calibration of the German-Dutch Wind Tunnel anechoic quality of the DNW Test-Hall", DFVLR Braunschweig IB-128-81/7, 1981
- 3 J.K.v. Fucht, F.A.R.v. Ewijk, J.E. Sunter, "Vibration Measurements during the 'open jet' calibration of the DNW", NLR Memorandum IE-81-024 L, 1981
- 4 H. Holthusen, "Beeinflussung des Freistrahls in der offenen Meßstrecke des 1:10 Modellkanals des DNW und Prüfung der Übertragbarkeit der Ergebnisse auf den Großwindkanal", (in German) 1990
- 5 S. Keye, "Maßnahmen zur Verbesserung der Stabilität des Freistrahls in der offenen Meßstrecke des DNW 1:10 Modellkanals (PLST)", (in German) DNW-MP-91.05, 1991
- 6 H. Holthusen, "Übersicht über die Versuche im 1:10 Modellkanal zur Erhöhung der Geschwindigkeit der Freistrahlmessstrecke", (in German) DNW-PA-93.20, 1993
- 7 A.J.Slijkhuis, "Onderzoek van een kleppensteel in de contractietuit ter vermindering van snelheidsfluctuaties in de kleine windtunnel van het N.L.L.", (in Dutch) NLL-TM A.1466, 1957
- 8 G.Schulz, G.Viehewer, "Der Unterschallwindkanal der DVL in Porz-Wahn" DVL Forschungsbericht (Teil II) (in German) 65-56, 1965
- 9 F.W.Scholkermeier, "Untersuchungen über Luftstrahlpulsationen und deren Beseitigung im Niedergeschwindigkeits-Windkanal der DFVLR in Braunschweig", (in German) DFVLR Braunschweig IB 157-75 A 02, Dezember 1975
- 10 G.S. Manuel, J.K. Molloy, "Effect of Collector Configuration on Test Section Turbulence Levels in an Open-Jet Wind Tunnel", NASA Technical Memorandum 4333, 1992
- 11 H. Holthusen, "Untersuchungen von niederfrequenten Schwingungen in der Freistrahlmessstrecke des DNW", (in German) DNW-TR-94.02, 1994
- 12 B. Regenscheit, "Isotherme Luftstrahlen, Ki Klima+Kälte ingenieur extra 12", (in German) ISBN 3-7880-7067-6, Verlag C.F.Müller Karlsruhe 1981
- 13 U. Michel, E. Froebel, "Turbulence at Far Downstream Positions in the Open Working Section of the German-Dutch Wind Tunnel DNW", DLR IB-22214-85/B10, Dez. 1985
- 14 K. Karamcheti, A.B. Bauer, W.L. Shields, G.R. Regen, J.P. Wolley, "Some Features of an Edge Tone Flow Field. Basic Aerodynamic Noise Research" NASA SP 207, 1969.
- 15 G.K. Batchelor, "Sound in Wind Tunnels", ACA-18, 1945.
- 16 J.C.A. van Ditshuizen, H. Holthusen, "Review and prospects for aeroacoustic testing at DNW", DNW-MP-92.40, May 1992

SELF-OSCILLATION FLOW CONTROL IN FREE-JET WIND TUNNELS

A.S.Ginevsky

Central Aero-Hydrodynamic Institute
State Scientific Research Center
TsAGI, 17, Radio Str., Moscow 107005, Russia

SUMMARY

In wind tunnels with the open test section strong self-oscillations arise at certain flow velocities which are accompanied by a sharp increase of pressure and velocity pulsations in the test section. Traditional methods of self-oscillation control do not provide their complete suppression. In the work presented the acoustic methods of self-oscillation control (their suppression or generation), based on the coherent jet structure response to periodic excitation have been investigated. The experiments were carried out in four wind tunnels with different outer diameters of the exhaust nozzle $d = 0.15\text{--}2.2$ m.

LIST OF SYMBOLS

x, r - cylindrical coordinates

d - outer diameter of the nozzle

u_0 - velocity in x -direction

f -frequency

$St = fd / u_0$ -Strouhal number

$\varepsilon_u = \frac{\langle u'^2 \rangle^{1/2}}{u_0}$ -intensity of velocity fluctuations

$\varepsilon_p = \frac{\langle p'^2 \rangle^{1/2}}{(\rho u_0^2 / 2)}$ - intensity of pressure fluctuations

L - noise level

ρ - air density

u', p' -velocity and pressure fluctuations

Indices

s - applied to acoustical excitation

1.INTRODUCTION

In return-circuit wind tunnels with open test section the strong self-oscillations arise at certain flow velocities which lead to essential increase of pressure and velocity fluctuations in all wind tunnel sections. This self-oscillations [1] are due to interaction of periodic hydrodynamic oscillations of flow in mixing layer of free jet and acoustic oscillations in return-circuit channel (standing acoustic waves). The presence of hydrodynamic oscillations in a jet mixing layer lead to the situation when intensity of velocity fluctuations in main flow core of open test section exceeds corresponding fluctuations in wind tunnel with closed test section [2].

The most widespread means for damping oscillations of such kind come either to suppress regular vortex structure in mixing layer of a free jet or to suppress an influence of the oscillations in free jet on oscillations in return-circuit channel. The first one is achieved through introducing of azimuthal heterogeneity in boundary layer at

initial jet cross-section; in the finite account it weakens or destroys ring vortexes; the second one is achieved with use of holes in diffuser walls near its input edge. The character of self-oscillation in wind tunnel is determined by two branches of acoustical feedback: along the flow through return-circuit channel and against the flow through test section. The last type of feedback corresponds to the case [3] when round jet impinges on coaxial ring (it is known as edge tone). In the work the acoustical methods of suppression and generation of self-oscillations in wind tunnels with open test section are investigated; the methods are based on an sensibility of jet coherent structures to periodic excitation [4]. At the high-frequency excitation when Strouhal number $St_s = f_s d / u_0 = 2-5$, they are weakened; at the low-frequency excitation at $St_s = 0.3-0.8$ they are increased. The most sensible place of jet to periodic excitation is the thin mixing layer in direct vicinity from nozzle edge. At the acoustical excitation it is the same place where vortex disturbances are generated; they are the reason for an increasing or weakening of coherent quasi-periodic structures.

The experiments were conducted in four wind tunnels having different diameters of nozzle exit cross-section $d = 0.15, 0.44, 1.2$ and 2.2 m; moreover in the tunnel there were the devices for weakening of self-oscillations which however have not suppressed it completely. In process of the experiment the fields of mean velocity and pressure, velocity and pressure fluctuations, their spectra, and also space correlation

coefficients of velocity and pressure fluctuations were measured. The resonant frequencies of return-circuit channel were determined in conditions without flow using a loudspeaker connected to generator of sinusoidal oscillations, and microphone placed in return-circuit channel.

It has studied the two variants of acoustical excitation:

- 1) the loudspeaker is placed in return-circuit channel; in this case the frequency of excitation is chosen so that it coincided with the one of the resonant frequency return-circuit channel; the known deficiency of the method consists in generation of pressure fluctuations at the wind tunnel test section [5,6];
- 2) the acoustical disturbances are introduced in boundary layer of nozzle through a narrow slot, and as a result there is realized periodic blowing/suction [7]. Such way of excitation has the two important advantages in comparison with the first variant.

In the first, for control of coherent structures in mixing layer it is excited only thin boundary layer near the nozzle edge, but not all volume of return-circuit channel and not flow core in test section. In the second, as the thin slot is very noneffective sound generator, so it may hope that significant pressure fluctuations will not arise in wind tunnel test section.

2. RESULTS OF THE EXPERIMENTAL INVESTIGATION

2.1. In fig.1 are presented variations of the longitudinal velocity fluctuations intensity vs. flow velocity on the axis of wind tunnel

test section in the point $x/d = 1$ for four wind tunnels having diameters $d = 0.15, 0.44, 1.2$ and 2.2 m when electrodynamic radiator was located in return-circuit channel.

In these cases Strouhal numbers of acoustic radiation with frequency f_s were $St_s = 2-5$. From fig.1 it may conclude that such radiation leads to the practically full suppression of self-oscillations. More full data are presented (fig.2) for wind tunnel having diameter $d = 1.2$ m. It should be mentioned that radial velocity fluctuations retain practically invariable both in presence of and without self-oscillations.

In forementioned four wind tunnels the initial boundary layer on nozzle exit was laminar for little tunnels (formparameter $H = 2.3-2.5$), transitional and turbulent - for large tunnels ($H = 1.3-1.4$). The velocity profiles in the boundary layer on nozzle exit cross-section retain practically invariable at acoustic excitation; the variations of longitudinal velocity fluctuation profiles were not significant also. The electrical power of sound radiator always was smaller than 0.1% from wind tunnel drive power for such way of excitation. Acoustic power of the sound radiator was smaller because the used loudspeakers had efficiency about 2-4 %.

The investigation of turbulent flow statistical characteristics in wind tunnel test section have shown that at high-frequency excitation there are sharp reduction of velocity fluctuations on self-oscillating regimes (by 2-12 times) and a certain reduction on nonselfoscillating regimes. In these cases it was achieved the visible

noise reduction in the room of test section - in jet near field (up to 12 dB).

The space correlation measurement of velocity fluctuations $R_{uu}(r)$ in test cross-section $x/d = 1$ have shown that after arising self-oscillations there was plane hydrodynamic wave in test section core, that the correlation is very closed to unity. The correlation coefficient decreases at suppression of the self-oscillations, and the coefficient increases at its generation (fig. 3). Also in fig. 3 is shown the space correlation coefficient of velocity fluctuations on the test section axis and pressure fluctuations in return-circuit channel $R_{up}(x/d)$ at self-oscillating regime ($u_0 = 16$ m/s) and at the regime of acoustical suppressing of self-oscillations at $St_s = 2.87$.

In fig. 4 are presented the spectra of velocity and pressure fluctuations in wind tunnel test section at nozzle diameter $d = 0.44$ m, velocity $u_0 = 40$ m/s in the point $x/d = 1$, $r/d = 0$ both without ($St_s = 0$) and in presence of high-frequency acoustical radiation ($St_s = 3.3$). We may see the change of spectra at suppression of self-oscillations. In the case when the spectrum of velocity fluctuations has the essential peak on the frequency excitation, the contribution of sound radiation to velocity fluctuations on the radiation frequency at self-oscillating regimes is not essential.

At the high-frequency excitation it is realized self-oscillation suppression when amplitude of pressure fluctuations generated by external acoustical field becomes comparable with the amplitude of pressure fluctuations at self-oscillations of flow. That is why

it is reasonable to include the external acoustical radiation before than the self-oscillation will reach the steady state regime, and some more better - until arising of self-oscillations. For example, the sound radiation is included at low flow velocity, and after that a flow velocity may increase. This way was used for large wind tunnels ($d = 1.2$ and 2.2) where the radiation power was deficit.

2.2. Let us see the second way of an influence on jet by realization of periodic blowing/suction through a narrow slot near nozzle edge (fig. 5,a).

In fig. 5,b it is demonstrated the changes of longitudinal velocity fluctuations intensity at the self-oscillating regime ($u_0 = 15$ m/s) in the point $x/d = 1$, $r/d = 0$ in dependence from frequency of excitation f_s . Also there are represented data for the case when a loudspeaker was located in return-circuit channel, where 1 corresponds to initial value of ϵ_u without excitation, 2 corresponds to the case of jet excitation by radiator located in wind tunnel stilling chamber (electrical power of the radiator is 5 W), 3 and 4 correspond to the cases of periodic blowing/suction through the slot in nozzle wall (electrical power 50 and 3 W accordingly). In fig. 5,c also are shown the oscillograms of longitudinal velocity fluctuations in the point $x/d = 1$, $r/d = 0$ both in presence of self-oscillations and in the case its suppression. It should attract an attention on different character of the dependences $\epsilon_u(St_s)$ at the cases 2 and 3,4. In the case 2 the high-frequency excitation has resonant character, but in cases 3 and 4 that is not so, while the dependences $\epsilon_u(St_s)$ have smooth character.

The dependences of longitudinal velocity fluctuations intensities from flow velocity u_0 in wind tunnel test section at $x/d = 0$, 0.5 and 1.0 both in presence of ($f_s = 358$ Hz) and without high-frequency excitation are presented in fig. 6. In the figure there are also the dependences of noise levels $L(u_0)$ outside test section in the point $x/d = 0$, $r/d = 1.3$ both in presence of and without the acoustical excitation.

Also it have been studied the influence of wind tunnel test section blocking up on effectiveness of acoustical radiation leading to suppression of self-oscillations. For this purpose in test section of the two wind tunnels with nozzle output diameter $d = 0.15$ and 0.44 m there were placed cross-flowed cylinders having various diameter and length. It was found that the dependence of self-oscillating regimes from velocity and intensity of self-oscillations has been changed in some extent when a value of test section blocking up was changed from 1.5 to 6.5 %. At the same time high-frequency radiation have suppressed the self-oscillations at indicated values of the blocking up.

2.3. The excitation of sinusoidal longitudinal velocity fluctuations in wind tunnel test section may be achieved by low-frequency acoustic radiation with frequencies corresponding to Strouhal numbers $St_s = 0.3-0.8$. Such method of self-oscillations generation may apply only for little wind tunnels having nozzle output diameter $d < 0.5$ m as there are no low-frequency radiators.

In fig. 7 are shown initial and maximal r.m.s. values of velocity fluctuations excited by sound at

$St_s=0.3-0.8$ on wind tunnel test section axis ($x/d=1$). The curves 1 and 2 determine the range of longitudinal velocity fluctuations which may be reached at generation of self-oscillations. At flow velocity corresponding to self-oscillation regimes the generation of self-oscillations permits to increase the intensity of longitudinal velocity fluctuations in some times. Almost sinusoidal longitudinal velocity fluctuations are excited, and their amplitudes are determined with sound radiation power.

At the end of this section let us draw attention on wind tunnel aerodynamic characteristics. So, at low-frequency excitation ($St_s=0.3-0.8$) a track drag is reduced in some extent and flow velocity in test section is risen. On the contrary, at high-frequency excitation ($St_s=2-5$) a track drag is risen in some extent, and flow velocity in test section is reduced.

2.4. Let us mention here also the so-called resonant method of acoustic field's suppression in return-circuit channel by exciting of compensating field in it with using additional sound source [8,9]. The scheme of the experiment is shown in fig.8,a. Transducer 1 transforms the acoustical oscillations in return-circuit channel 5 into electrical signal which through the phase-inverter 2 and amplifier 3 enters to radiator 4 and excites acoustical oscillation in return-circuit channel having the given phase shift. The experiments were carried in wind tunnel with open test section having square cross-section of nozzle and diffuser with dimension 0.3 m.

In fig.8,b is shown the dependence of velocity fluctuations

level at the nozzle exit from flow velocity both without suppression of self-oscillations (1) and at conditions of optimal self-oscillation suppression (2) which was reached with selection of optimal phase shift. The authors [8] have shown that the electric power of radiator has not exceeded 1 W at the regime of full self-oscillation suppression.

3. ACKNOWLEDGEMENTS

This work has been completed under financial support of the Russian Foundation on Fundamental Investigations (Grant 96-O2-19577).

4. LITERATURE

1. Strelkov S.P., Bendrikov G.A., Smirnov N.A. "Pulsations in wind tunnel and means for its damping."- Proc. of TsAGI, 1946, N593, 57 pp. (in Russian).
2. Michel U. "Influence of shear layer induced fluctuations on the velocity unsteadiness in free-jet wind tunnels."-Adv.Turbulence 2: Proc.2nd Eur.Turbulence Conf., Berlin, Aug.30-Sept.2, 1988. Berlin etc., 1989, p.480-483.
3. Curasava H., Yamanoue K., Obata T. "Self-excited oscillation in an axisymmetric jet with a coaxial circular pipe."- Mem.Nagano Techn.Coll., 1987, N18, p.21-30.
4. Vlasov Ye.V., Ginevsky A.S. "Coherent structures in turbulent jets and wakes."- Achievements in Science and Technic. Ser. Fluid and Gas Mechanics, vol.20. Publ.by VINITI, 1986, p.3-84 (in Russian).
5. Bojarchikova M.Yu., Vlasov Ye.V., Ginevsky A.S., Zosimov A.V. "Self-oscillation suppression in wind tunnel with

open test section."- News of Academy of Sciences USSR, Fluid and Gas Mechanics, 1982, N 1, p.126-132 (in Russian).

6. Zosimov A.V. "Acoustic method of velocity and pressure pulsations control in wind tunnel with open test section."- Proc. of TsAGI, 1986, N2292, 38pp.(in Russian).

7. Moskvina M.Yu. "Oscillation suppression in wind tunnel with open test section by periodic blowing/suction in

boundary layer of nozzle."- Engineering-Physical J., 1990, vol.59, N1, p.115-119 (in Russian).

8. Ffowcs Williams J.E. "Anti-sound."-Proc. Roy. Soc. London, 1984, A395, p.63-68.

9. Gromov P.R., Zobnin A.B., Kijashko S.V., Sushchik M.M. "Pulsation level reduction in a wind tunnel using active sound control.- Acoustical J., 1988, vol.34, N 2, p.349-350 (in Russian).

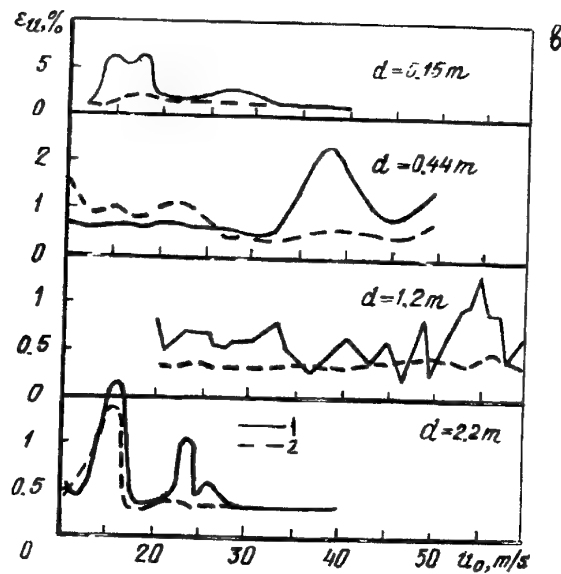
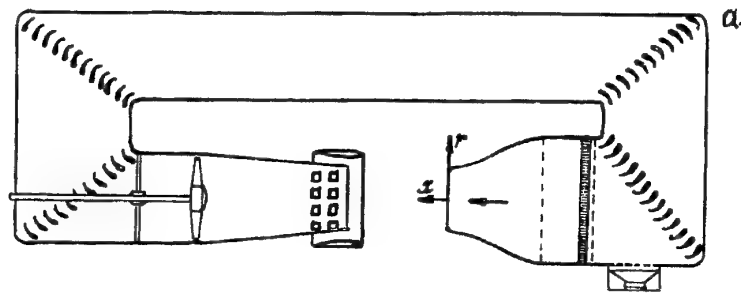


Fig. 1. a) The return-circuit wind tunnel with open test section.
b) The intensity of longitudinal velocity fluctuations ε_u vs. flow velocity u_0 in wind tunnels at $d = \text{var}$ in presence of and without acoustic excitation; 1- $St_s = 0$, 2- $St_s = 2-5$.

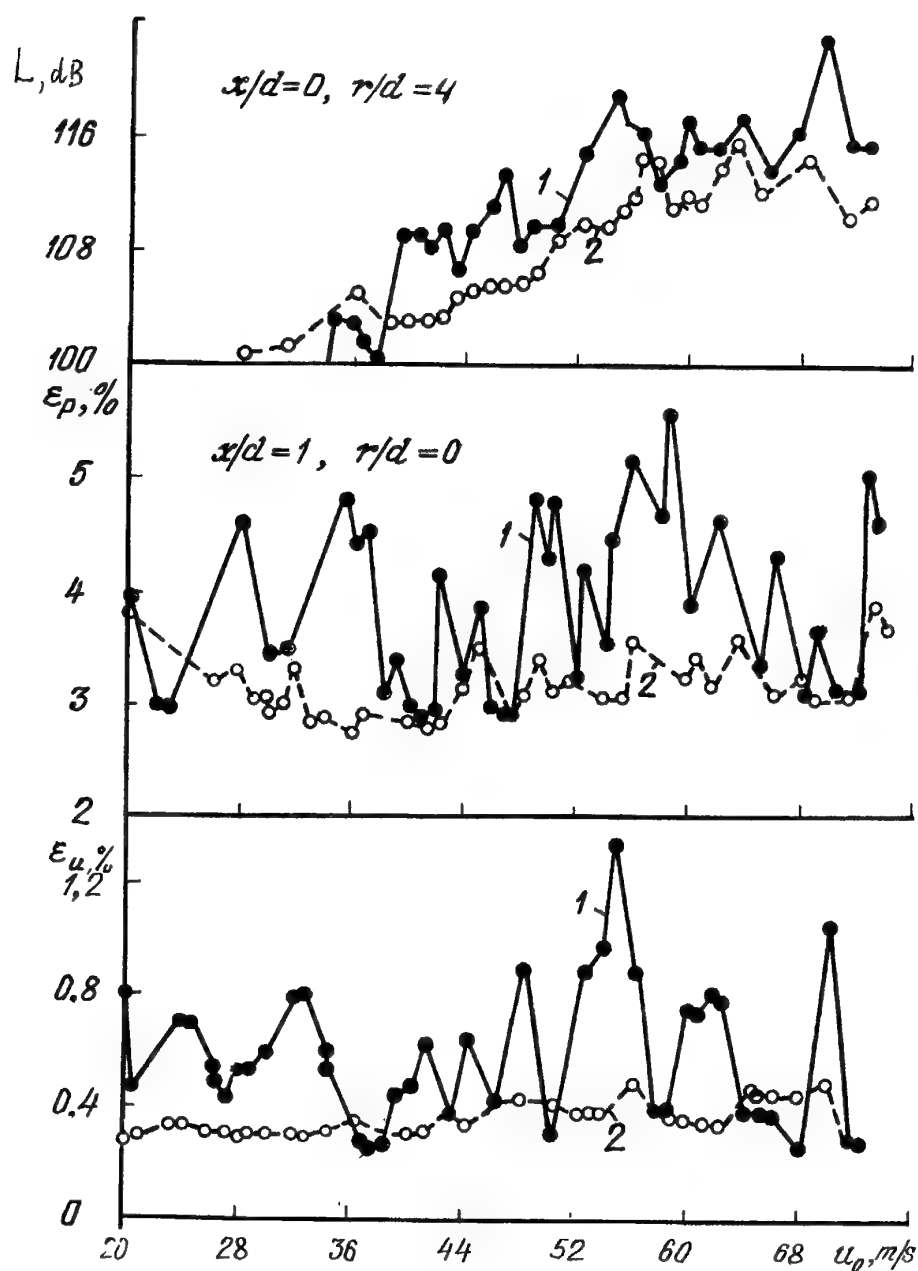


Fig. 2. Noise levels outside of jet L, pressure and velocity fluctuations on jet axis ($x/d=1$) vs. flow velocity in wind tunnel test section at the nozzle diameter $d=1.2$ m in presence of acoustic excitation at frequency corresponding $St_s = 2-5$; 1- $St_s = 0$, 2- $St_s = 2-5$.

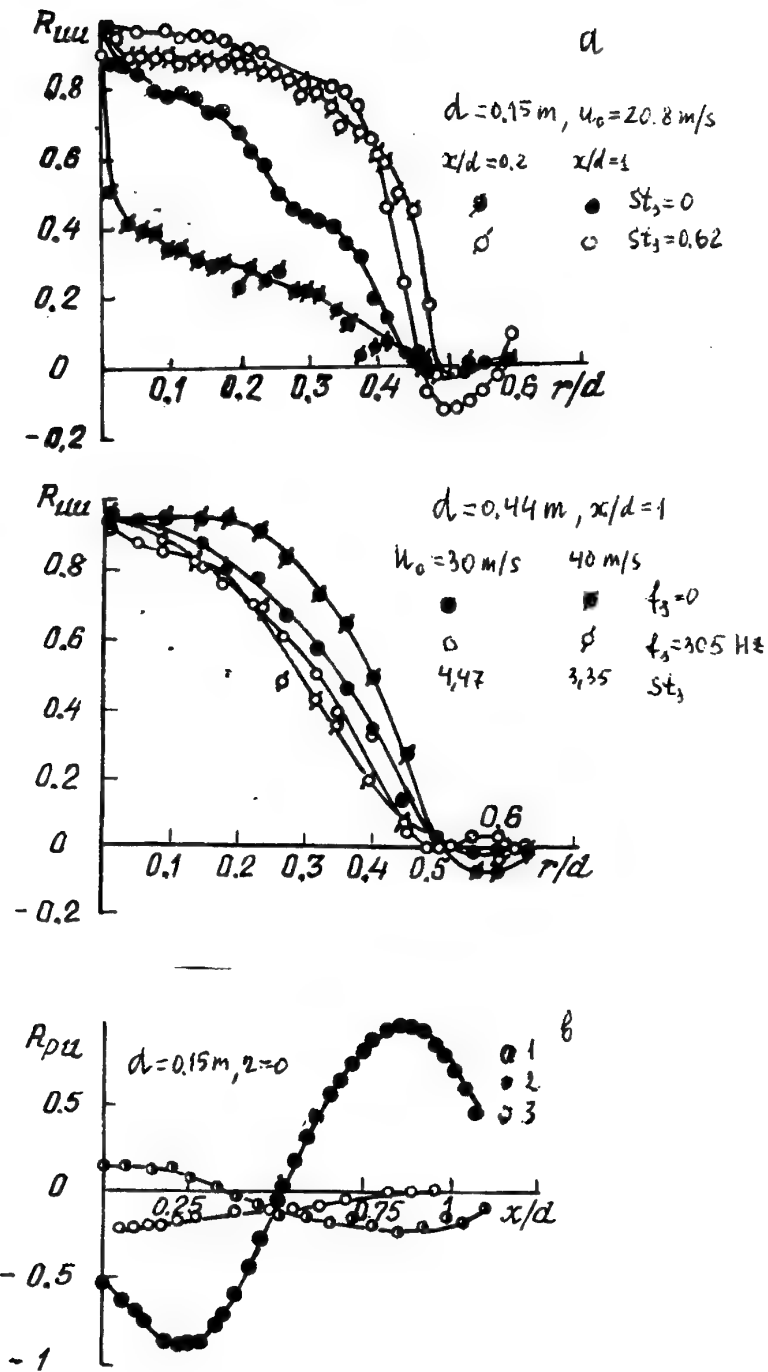


Fig. 3. a) Variation of space correlation coefficients $R_{uu}(r/d)$ in wind tunnels at $d = 0.15 \text{ m}$ and $d = 0.44 \text{ m}$ both in presence of and without acoustic excitation. b) $R_{pu}(x/d)$ both in presence of and without acoustic excitation: 1- $u_0 = 40 \text{ m/s}$, $St_s = 0$; 2- $u_0 = 16 \text{ m/s}$, $St_s = 0$; 3- $u_0 = 16 \text{ m/s}$, $St_s = 2.87$.

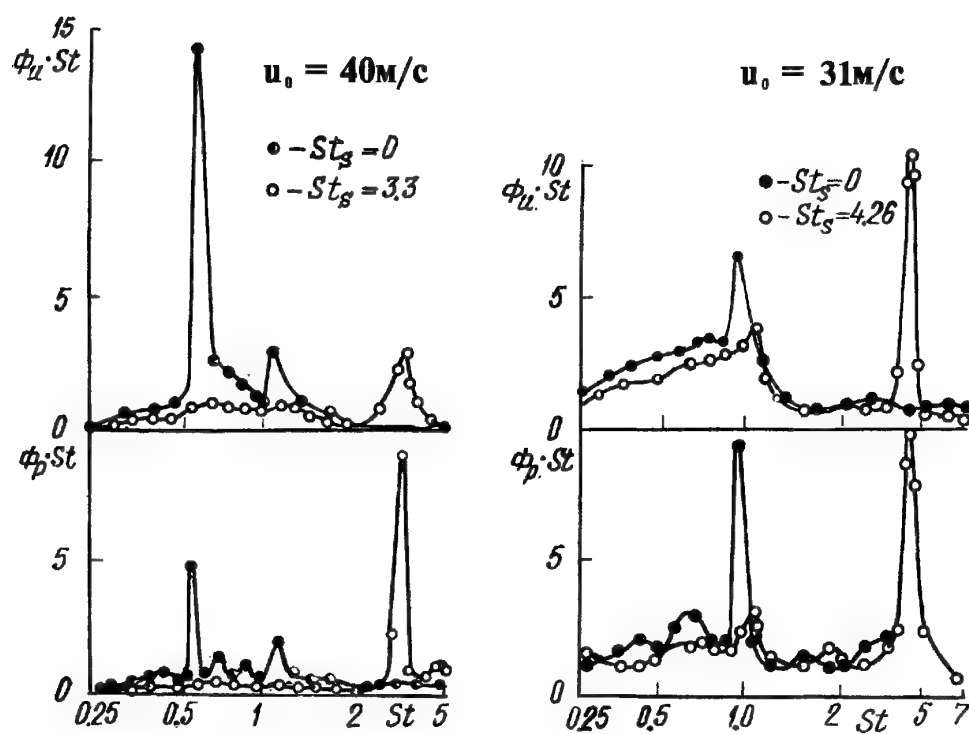


Fig. 4. The spectra of velocity and pressure fluctuations in wind tunnel test section ($d = 0.44$ m, $x/d = 1$, $r/d = 0$) in presence and without acoustic excitation both at self-oscillational and non-self-oscillational modes.

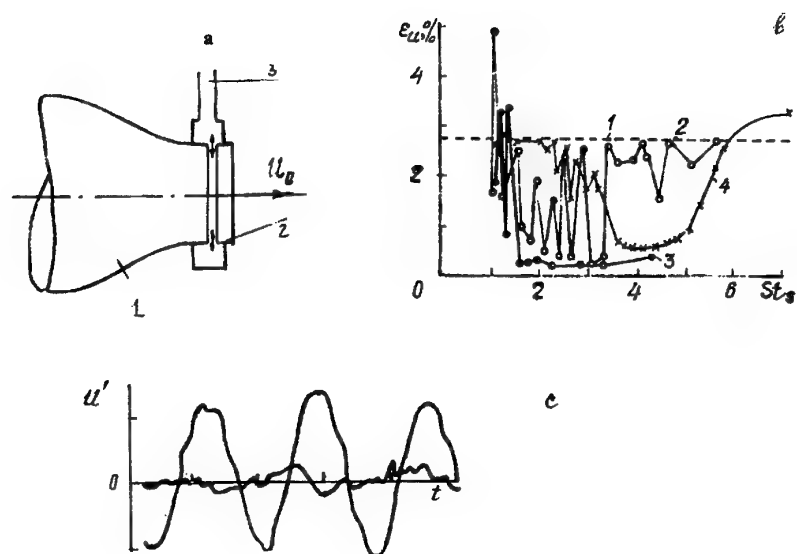


Fig. 5. a) The scheme of the nozzle with a slot: 1- nozzle, 2- alternating blowing/suction, 3- waveguide from loud speaker. b) Action on nozzle boundary layer by periodic blowing/suction ($d=0.15$ m). Function $\varepsilon_u(St_s)$ in the point on axis ($x/d=1$) at the self-oscillational mode: 1-regime of self-oscillations ($u_0=15$ m/s), 2- loud speaker in the return-circuit channel ($N=5W$), 3- alternating blowing/suction through the slot ($N=50W$), 4- alternating blowing/suction through the slot ($N=3W$). c) Oscillograms of velocity fluctuations.

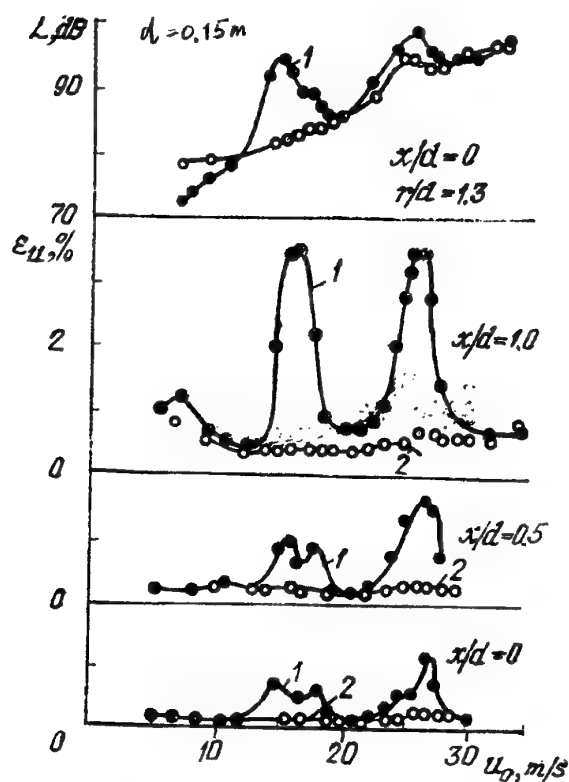


Fig. 6. Functions $\varepsilon_u(u_0)$ at $x/d=0, 0.5$ and 1.0 and $L(u_0)$ outside of test section in presence of alternating blowing/suction through the slot; 1- $f_s=0$, 2- $f_s=358$ Hz ($St_s=3.58$ by $u_0=15-28$ m/s).

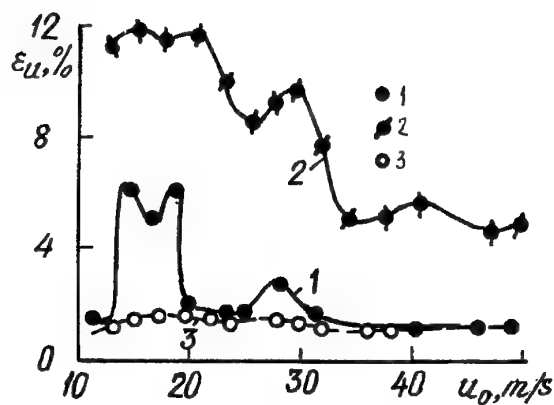


Fig. 7. The excitation of self-oscillations in the wind tunnel for the purpose of generation the sinusoid-shaped flow in function of time ($d=0.15$ m/s, $x/d=1$, $r/d=0$). Functions $\varepsilon_u(u_0)$ without excitation, and also at low-frequency and high-frequency excitation: 1- $St_s=0$, 2- $St_s=0.3-0.8$, 3- $St_s=2-5$.

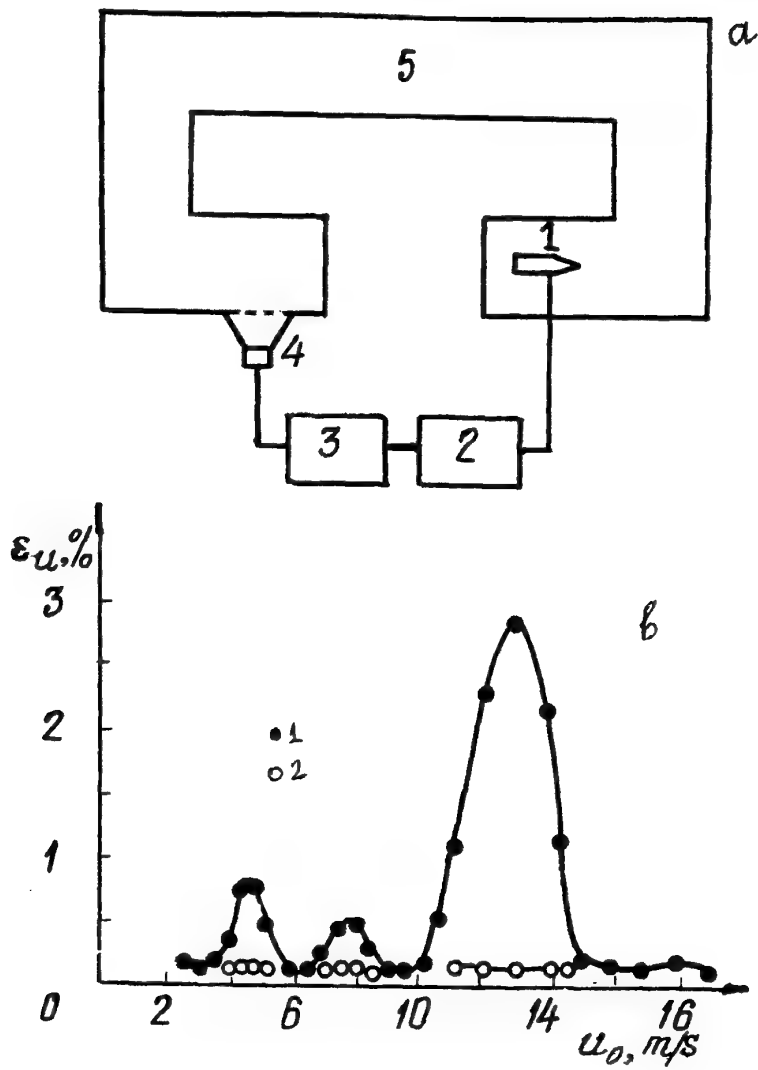


Fig. 8. Suppression of self-oscillations by antisound. a) The scheme of the experiment: 1- transducer, 2- phase inverter, 3- amplifier, 4- loud speaker, 5- return-circuit channel. b) Functions $\epsilon_u(u_0)$ in wind tunnel both in the presence of self-oscillation (1) and at its suppression (2).

Turbulence and Noise Criteria and their Implementation in NWTC-Type Wind Tunnels

Eli Reshotko

Mechanical and Aerospace Engineering
Case-Western Reserve University
Cleveland Ohio 44106

William S. Saric

Mechanical and Aerospace Engineering
Arizona State University
Tempe, Arizona 85287-6106

Hassan M. Nagib

Fluid Dynamics Center
Armour College
Illinois Institute of Technology
Chicago Illinois 60616

1 INTRODUCTION

This paper considers the establishment of turbulence and noise criteria as a function of Mach number and total pressure for utilitarian low-speed and transonic wind tunnels of the National Wind Tunnel Complex (NWTC) class facilities such that boundary-layer transition models likely to be tested in them will not be contaminated by the flow environment. Aside from the NWTC tunnels themselves, the ideas in this paper apply to upgrades and revisions of existing tunnels such as the NASA-Ames 11-foot Unitary Tunnel and the AEDC 16T tunnel.

1.1 Need for Turbulence and Noise Criteria

Test-section turbulence and noise can trigger a "bypass" transition such that the transition from laminar to turbulent flow on model surfaces occurs upstream of its location in an environment where freestream turbulence and noise are *below* some threshold value. Since some future aircraft may well rely on large regions of laminar flow to achieve performance goals the tunnels addressed herein must, as a minimum, be designed to achieve these threshold values in order to conduct meaningful development tests.

Since the tunnel turbulence and noise generation and suppression mechanisms are different, it is important to separate the criteria for the two phenomena. Since much of the environmental data that have been obtained to

date use hot-wire systems that inherently react to both noise and turbulence, the criteria must be determined from those experiments that have carefully distinguished between acoustic (noise) and vortical (turbulence) disturbance fields.

1.2 General Ideas of Turbulence Management Schemes

The recommendations made in this section are based on extensive experience in the design and modification of wind tunnels for the purpose of achieving high flow quality in their test sections. This experience started with small-scale subsonic wind tunnels at IIT (Loehrke and Nagib 1972, 1976; Nagib and Marion 1984; Tanatichat et al. 1982; Wigeland et al. 1978, 1981), continued through interactions with industry and government laboratories (Morel 1975; Nagib 1993; Harvey et al. 1980; Steinle and Rose 1982) over a period of 20 years, and culminated in the design, construction and evaluation of the National Diagnostic Facility (NDF) at IIT (Nagib 1992; Hites and Nagib 1994; Nagib et al. 1994; Nagib and Hites 1995). Several innovative concepts have been introduced and investigated through this effort and several traditionally accepted practices were found to be problematic. In particular over the last five years the design of the NDF (4x5-foot cross section with speeds of up to Mach 0.4) has allowed us to confirm several general guidelines that are recommended for the design of low-disturbance-level

wind tunnels. These guidelines can be summarized as follows:

- Control separation in all diffusers by using small angles (less than 3 degree. half angle) or with aid of pressure-drop generating screens and grids.
- If necessary, remove all major (larger than few percent) mean-velocity nonuniformities before the last turn, upstream of settling chamber; via coarse medium-solidity screens (approx. 40%).
- Allow a minimum wake-decay distance of two to three chords downstream of the inside turning vane.
- Use a honeycomb with a cell size approximately 10% of the turning-vane separation and a length of 12-20 times the honeycomb mesh.
- Use 5 to 7 low solidity screens (approx. 35%) with a mesh from 5 to 15 times finer than the honeycomb mesh. Allow adequate separation between screens; 250 meshes or larger.
- Use a contraction with area ratio between 6 and 9, a profile with largest area change in central section (like a fifth-degree polynomial) and a length of approx. 1.25 the larger entrance dimension.

In Section 4 we discuss means of establishing the characteristics of extremely low turbulence levels in wind tunnels and to separate them from non-vortical disturbances and electronic noise. With the aid of these techniques, $u'_{rms}/U_{\infty} \approx 0.03\%$ to 0.05% in the test section of the NDF over the speed range of the facility. Moreover, most of the vortical fluctuations have frequencies less than 100 Hz. Comparable performance can be expected from the design of the NWTC if the above guidelines are followed. In the following sections each of these guidelines will be briefly discussed.

It is important at the outset, however, to clarify a few important strategies behind the implementation of these guidelines. These strategies are based on the physical understanding of the various components contributing to wind-tunnel noise. First, one must prevent the generation of any separated or low-frequency unsteady flows in all components of the wind tunnel. Often this can only be achieved at the cost of a lower efficiency of the wind tunnel. However, one cannot afford the generation of such disturbances since they are nearly impossible to remove. The reduction of low-frequency

disturbances has the additional important benefit of improving the time required to acquire data for a given test case because the averaging time for statistical convergence is reduced. This cost benefit can often outweigh the increased cost of operating the wind tunnel at a lower efficiency.

Next, all mean velocity and temperature nonuniformities need to be minimized prior to the final suppression of turbulence. In fact, it is sometimes advisable to introduce moderate-intensity large-scale turbulence to eliminate these nonuniformities. The scale of the newly generated turbulence needs to be comparable to the scale of the mean-velocity and temperature nonuniformities. Then, turbulence reduction can be achieved with the aid of a single honeycomb, multiple screens, and a moderate area-ratio contraction.

Concurrent with these turbulence-reduction techniques, one must also take steps to reduce high-amplitude acoustic noise generated by the fan. One recent successful technique utilized sound-absorbing foam embedded in the turning vanes upstream of the test section (Nagib 1993; Hites and Nagib 1994; Nagib et al. 1994; Nagib and Hites 1995).

1.3 Outline

In addition to providing threshold criteria for turbulence, turbulence management schemes (combinations of honeycomb sections and screens) are suggested that can implement the criteria taking into account the properties of the wind-tunnel contractions. Once the tunnels are constructed, it is important to confirm that the test-section noise and turbulence are within the established criteria. A protocol will be described based on two adjacent hot-wire measurements and an optimal filtering scheme that distinguishes between the noise and the turbulence. Finally, based on having seen drawings of the tunnel circuits of both the low-speed and the transonic NWTC tunnels, we shall offer comments that can result in improvements in the mean flow as well as the disturbance flow.

2 TURBULENCE & NOISE CRITERIA

The turbulence criteria for the wind tunnels are determined by the boundary layer response to T-S instabilities. Crossflow and Görtler instabilities do not require separate criteria.

There are two additional points to be raised before criteria are proposed:

The first is that criteria will be given separately for velocity fluctuations, u'_{rms}/U_∞ , and for pressure fluctuations, p'_{rms}/q_∞ . This is because techniques are now available to separately measure these quantities. An example of a technique will be described in Section 4. Raw hot-wire measurements of velocity fluctuations as done to date contain unseparated contributions from both the turbulence and the noise. It is suggested that for an interim period, the data be quoted both "separated" and "unseparated" so that a transition can be made from existing data bases.

The second point is that for the compressible flows of transonic tunnels, hot-wire data are reduced properly to mass-flow and total-temperature fluctuations rather than velocity fluctuations. The discussion that follows is nevertheless in terms of velocity fluctuations since the stated criteria are established primarily by our experience with low-speed tunnels. A deeper consideration of this point is an action item for later work.

2.1 Turbulence Criterion

The suggested limit for u'_{rms}/U_∞ is 0.05% based on separated signals and considering frequencies above 0.1 Hz. This has been readily achieved in a number of facilities. For example, Figures 1 and 2 show data from NDF (Nagib et al. 1994), Figure 3 shows data from the NASA-Langley 8-foot Transonic Pressure Tunnel (TPT) for Mach numbers up to 0.38 (Wlezien et al. 1994) and Figure 4 shows data from the NASA-Langley Low Turbulence Pressure Tunnel (LTPT) at Mach numbers up to 0.3 (Wlezien et al. 1994).

For unseparated measurements, the suggested limit for u'_{rms}/U_∞ is 0.07% which corresponds roughly to the e^9 transition Reynolds number of 3.6×10^6 . This is reflected also in the unseparated LTPT data shown in Figure 5 (Wlezien et al. 1994). Generally, u'_{rms}/U_∞ tends to increase with Mach number but decrease as tunnel total pressure is increased as shown in Figures 3 and 4 (Wlezien et al. 1994).

It must be emphasized that these criteria are for the total signal above 0.1 Hz. The portion of this signal in the T-S band is immeasurably small; so the total signal must be within the suggested limits in order to insure that the amplitude in the T-S band is acceptably small.

2.2 Pressure Fluctuation Criterion

The suggested limit for p'_{rms}/q_∞ is 0.3% based on separated signals. Here p'_{rms} is the rms static pressure fluctuation level and q_∞ is the freestream dynamic pressure. This criterion has been achieved on the AEDC transition cone in flight (Dougherty and Fisher 1980) as well as in NDF as shown in Figures 6 and 7 (Nagib et al. 1995) and at low unit Reynolds numbers in the 8-foot TPT as shown in Figure 8 (Wlezien et al. 1996). It is shown in Figure 7 that p'_{rms}/q_∞ can be affected by fan-blade pitch angle.

The criterion is expressed in terms of p'_{rms}/q_∞ rather than sound pressure level (*SPL*) in dB since *SPL* can be shown to vary significantly with both total pressure and Mach number for constant p'_{rms}/q_∞ . Generally p'_{rms} decreases with increase in tunnel total pressure (Figure 8). Even so, *SPL* will increase. The relationship between *SPL* and p'_{rms}/q_∞ can be derived from the definition of *SPL*:

$$SPL(\text{dB}) = 20 \log_{10} (p'_{rms}/p_{ref}) \quad (1)$$

where $p_{ref} = 20 \mu\text{Pa}$

It can then be shown that

$$SPL(\text{dB}) = 20 \log_{10} \left(\frac{p'_{rms}}{q_\infty} \right) \left(\frac{\gamma}{2} \right) \left(\frac{p}{p_{atm}} \right) \left(\frac{p_{atm}}{p_{ref}} \right) (M^2) \quad (2)$$

The second and fourth terms on the right side of Equation (2) are constants. At a given p'_{rms}/q_∞ and Mach number, in going from a tunnel total pressure of 0.25 atm to 5 atm, *SPL* increases by 26 dB. For constant p'_{rms}/q_∞ and p_t , increasing the Mach number from 0.1 to 1.0 increases *SPL* by 40 dB. If the experimental increases in *SPL* are less than expected from total pressure or Mach number change alone, the implication is that p'_{rms}/q_∞ is decreasing.

2.3 Turbulent Spectra

The measured spectra should be "decent" over the T-S frequency range. By "decent" is meant that the amplitudes should be monotonically decreasing with frequency following a somewhat flat low-frequency region. An "indecent" spectrum tends to show a peak at

intermediate frequencies. A few examples of indecent spectra are given below.

Despite the LTPT being a low-turbulence tunnel to total pressures of 2 atm, the spectrum of Figure 9 shows about a 10-15 dB peak in the 50-90 Hz range (Wlezien et al. 1994). Note that LTPT has a short 17.6:1 contraction. Similarly the spectrum of Figure 10 from the 8-foot TPT (20:1 contraction ratio) has about a 10 dB peak centered at 100 Hz (Wlezien et al. 1994). It is conjectured that the vortex stretching in high-contraction-ratio tunnels is nonuniform across the spectrum and these examples are included in order to illustrate the need to keep the contraction ratio down (below 9) to avoid problems with the turbulence structure.

2.4 T-S Frequency Band

The T-S frequency band is expressed in dimensionless form by the reduced frequency, F , defined by

$$F = \frac{2\pi f\nu}{U_\infty^2} \quad (3)$$

where f is the physical frequency in Hz, ν is the kinematic viscosity at the tunnel static temperature and static pressure, and U_∞ is the freestream speed. For a tunnel static temperature of 100°F

$$f = 0.116[F \times 10^{10}][p_t(\text{atm})]M^2 \quad (4)$$

M	$p_t(\text{atm})$	F	f
0.3	5	30×10^{-6}	15.7 kHz
0.6	3	30×10^{-6}	37.6 kHz
0.8	5	25×10^{-6}	92.8 kHz
1.0	5	20×10^{-6}	116.0 kHz

The chosen values of F are in the middle of the T-S bands. Thus low-speed wind tunnels (to $M \sim 0.6$) should have good spectra to 70 kHz at their high total pressure limits, and the transonic tunnels to 200 kHz. Note the strong influence of total pressure on the frequency range. Temperature has a very weak influence. For a tunnel static temperature of 120°F, the coefficient in the above relation is 0.113.

2.5 Test Matrix

A facility should be evaluated for turbulence and noise at low, intermediate and high values of Mach number, and at low, intermediate and high total pressures for the chosen Mach numbers. This is a matrix of nine points.

3 TURBULENCE MANAGEMENT CRITERIA

3.1 Separation Control in diffusers

The control of separation in all diffusers can be achieved by using small angles (less than 3° half angle) or with the aid of screens and grids. The low-frequency disturbances generated by diffuser separation are typically the most difficult to remove. Downstream of the test section and upstream of the fan, diffusers utilizing splitter plates such that the $< 3^\circ$ condition is met, will work as well. However, downstream of the fan, screens positioned at various stations within the diffuser will act to prevent transient separation; i.e., diffusers in high-quality wind tunnels cannot be used effectively for large pressure recovery. This is the only means by which a wide-angle diffuser can be used between the fan and test section. The design of the screens or grids within the diffusers can be based on the requirement that the associated pressure drop is intended to balance most of the pressure recovery.

3.2 Mean Velocity and Temperature Nonuniformities

It is best to remove all major mean velocity and temperature nonuniformities which are greater than a few percent before the last turn into the settling chamber and test section via coarse to medium-solidity screens (approx. 40%). Once the flow passes through the honeycomb, large-scale *turbulence* will be sufficiently suppressed and any remaining large-scale *mean* temperature and velocity nonuniformity will be nearly impossible to remove. In addition, these nonuniformities will lead to generation of new turbulence and to amplification into concentrated vortical structures within the stagnation regions of the flowfield of the models being tested. Screens downstream of the honeycomb are intended for reducing the turbulence level and scale (low-solidity screens) and will not be effective in reducing any mean-velocity nonuniformities larger than a few percent. The most

effective means to reduce mean-flow nonuniformities is to utilize moderate pressure-drop devices that generate moderate (3-10%) turbulence with scales larger than the dimensions of the nonuniformities.

Honeycombs are also most the effective manipulators to remove flow angularities. Criteria developed by Tanatichat et al. (1982) have consistently resulted in test-section flowfields without any significant flow angularities. This has been achieved in the modification of wind tunnels by the addition of a honeycomb (e.g., the Boeing transonic wind tunnel and NASA Langley 4x7 m wind tunnel).

3.3 Turning Vanes

To eliminate disturbances caused by the turning vanes, one should allow a minimum distance of two to three vane chords downstream of the inside turning vane. Turning vanes with an aerodynamic cross section designed near the optimum pressure-drop solidity (spacing) condition, have been found to consistently produce wakes that decay significantly within the first two to three chord lengths downstream. Recent attempts to optimize the aerodynamic cross section of the turning vanes (at the Swedish Royal Academy) have resulted in only a small incremental gain in flow quality over simpler aerodynamic designs such as the double circular arc with a trailing flap used in the NDF.

In addition, turning vanes have been effectively used in the NDF as heat exchangers in the turns upstream and downstream of the fan and to reduce the fan noise by 7 to 10 dB in the turn upstream of the test section. The latter was accomplished by embedding acoustic foam beneath a flush-mounted perforated surface on the suction side of the turning vane.

3.4 Honeycomb Selection

It is recommended to use a honeycomb with a cell size (Mesh m) that is 10% of the separation between adjacent turning vanes and a length, L , 12-20 times the honeycomb mesh. An L/m around 12 is most effective for turbulence reduction while an L/m of 15-20 is most effective for removing flow angularity. The mesh should have a scale which is less than half of the width of the vane wakes. The honeycomb should be located three chord lengths downstream of the turning vanes.

Often the honeycomb length is controlled by structural limitations. Earlier work, which suggested that the length of the honeycomb be based on achieving fully-

developed flow conditions within the cells, has proven to be non-effective in turbulence reduction in addition to its excessive pressure-drop contribution. Therefore, the maximum length of the honeycomb should be dictated by structural (including minimizing deflection) requirements and maintaining the ratio of L/m between 12 and 20. If necessary the material selection and mesh size may have to be altered to achieve this goal (Nagib 1993).

3.5 Screen Selection

The first screen should be located a distance equal to 20 to 40 honeycomb mesh sizes downstream of the honeycomb to allow for adequate turbulence decay. Recent work has concluded in favor of this over the earlier suggestions by Loehrke and Nagib (1976). Use of 5 to 7 low-solidity screens (approx. 35%) with a mesh from 5 to 15 times finer than the honeycomb mesh size is now recommended. The 35% solidity requirement [developed by Steinle and Rose (1982)] must be adhered to in order to render the screens effective in turbulence suppression. While screens with a solidity greater than 35% are more effective in reducing mean velocity and temperature nonuniformities, they are less effective in reducing the turbulence level. In fact, their increased effectiveness in reducing nonuniformities is coupled to their generation of new turbulence scales immediately downstream. The role of screens should be dedicated to reducing turbulence intensity, and as stated earlier, the nonuniformities should be removed well upstream of the settling chamber and honeycomb position.

One must allow adequate separation between the screens: on the order of 250 mesh sizes or larger to achieve maximum turbulence reduction. The screen mesh can be made finer for the same solidity to achieve better strength. Again, the screen solidity should be between 30 and 35 %. A gradual moderate area-ratio contraction may start soon after the last screen.

3.6 Contraction Area Ratio

The use of a contraction with an area ratio between 6 and 9 is highly recommended. It is important to choose a profile which has the largest area change in the central section (e.g., a fifth-degree polynomial) and a length of approximately 1.25 the larger entrance dimension. An $L/D = 1.25$ avoids separation in contractions with area ratios between 6 and 9. Zero slope and zero curvature at

the inlet to a fifth-degree contraction also helps in avoiding separation, even at low speeds. Zero slope and zero curvature conditions at the exit of the contraction provides good boundary-layer and turbulence conditions near the test-section inlet. Contractions with area ratios larger than 9 produce test-section conditions with several problems in the structure and development of freestream turbulence. Moreover, large growth of Görtler vortices are a source of low-frequency unsteadiness.

Among the many problems with a higher area-ratio contraction (Nagib and Marion 1984) are the mismatched turbulence intensities and scales between the streamwise and lateral components. This results in, not only artificial anisotropies, but also in a test section with a rapidly evolving turbulence condition. Both of these characteristics are unlike flight conditions encountered by aircraft. Therefore, the only real gain achieved by a higher area-ratio contraction is to increase the test-section speed. Optimization of the design of the fan within the tunnel circuit can result in a higher test-section speed through the use of a larger-diameter fan capable of higher flow rates at lower pressure drop performance.

The above design philosophy was used successfully in the NDF in order to achieve the design requirements. The use of a large diameter, lower RPM fan has the additional advantages of reducing the acoustical disturbances in the wind tunnel. Any remaining blade-passing frequency harmonics can easily be suppressed with the aid of various sound-reduction elements (e.g., acoustically treated turning vanes).

4 ISSUES OF SEPARATING TURBULENCE AND SOUND

Because of the different criteria used to specify the flow-quality limits of u'/U_∞ and p'/q_∞ , unambiguous measurements of these quantities should be made. Moreover, in compressible flows, u' must be separated from $(\rho u)'$. These are not matters of academic interest since the strategy of reducing u' is different from reducing p' . This separation of fluctuating quantities has been neglected in the past and has led to confusion and misinterpretation of the data.

4.1 Straightforward Separation Technique

A serviceable technique for separating the two signals utilizes a cross correlation between two probes that are

widely separated. A typical scale is the width of the tunnel.

A measured fluctuating property $X(t)$, which can be either $p'(t)$ from a microphone or $u'(t)$ from a hot wire, is made up of a rotational (turbulence) component, $T(t)$, and an irrotational (noise) component, $S(t)$. Measurements at two points in the flow field can be represented by the following:

$$X_1(t) = T_1(t) + S_1(t) \quad (5)$$

$$X_2(t) = T_2(t) + S_2(t) \quad (6)$$

If points 1 and 2 are separated by a distance that exceeds the turbulent integral length scale and are in the same plane, then T_1 and T_2 are uncorrelated while S_1 and S_2 are correlated. Because of the great disparity in length scales, there is no cross-coupling term in Equations 5 and 6. Moreover, for relatively uniform acoustic fields,

$$S_1 = S_2 = S \quad (7)$$

With this idea, the turbulent fluctuations, T_1 , can be extracted from the total signal, X_1 , by subtracting the noise field, S . Ideally, S is the *cross correlation* of X_1 and X_2 , defined by $\langle X_1, X_2 \rangle$. Thus, the turbulence levels are given by:

$$T_1 = X_1 - \langle X_1, X_2 \rangle \quad (8)$$

Equation (8) expresses the so-called *differencing technique* that has been used in the past in a number of different experiments (Corke and Nagib 1979; Saric et al. 1988; Wlezien et al. 1994). The limitations of Equation (8) are well known. Essentially one is limited to uniform flow and uniform noise fields. Because one cannot always separate the probes by a sufficient distance, the cross correlation, $\langle X_1, X_2 \rangle$, can contain the correlated parts of the turbulent field. By defining the fraction of $\langle X_1, X_2 \rangle$ that contains correlated turbulence by σ , then the amplitude and spectrum of T_1 is reduced by $(1 - \sigma)$.

$$u'_{rms}|_{measured} = (1 - \sigma)u'_{rms}|_{actual} \quad (9)$$

Typically this produces unacceptable errors. Moreover, the application of (8) can only be done in transform space which limits the technique to rms amplitudes and spectra. The correct time series cannot be recovered.

4.2 Optimal Filtering

In order to reduce the errors associated with Equation (9) obtained from the straightforward technique, it is suggested that optimal filtering be utilized. The basic ideas are found in Widrow et al. (1975) and a direct application to wind tunnels has recently been implemented by Naguib et al. (1995). This technique permits a more accurate evaluation of rms turbulence but can recover the time-series information as well.

The objective is to subtract the noise (i.e. the sound field) from the signal $X(t)$. The noise signal, $y(t)$, obtained from $X(t)$, should "look like" a *reference* signal $d(t)$. A set of filter coefficients, $f(n)$, where $n = 1, 2, 3, \dots, N$, are established in such a way that f operating on X produces y . Thus y is the part of X correlated with d .

The error signal is defined by:

$$e(t) = d(t) - y(t) \quad (10)$$

The thrust of optimal filtering is that $f(n)$ are chosen to minimize e in the *least-squares* sense. If $e = 0$, then $y = S$. For $e \neq 0$, the spectrum is reduced by $(1 - \sigma^2)$ and Equation (9) becomes:

$$u'_{rms}|_{measured} = (1 - \sigma^2) u'_{rms}|_{actual} \quad (11)$$

Equation (11) can be easily implemented in a real-time measurement of u' or p' . Thus, optimal filtering is a *second-order* accurate scheme compared to the first-order accurate straightforward technique. Moreover, the time-series of the turbulence signal can be recovered.

4.3 Limitations and Areas of Development

Near Mach 1, the T-S wavelengths and turbulent integral scales are not that much shorter than the acoustic wavelengths. This makes the straightforward technique of Section 4.1 completely useless and puts a premium on the use of optimal filtering to recover something.

In supersonic flows, perhaps the Laufer and Vrebolovich assumption that p' is more or less constant in the boundary layer for $M < 3.0$ can be used to separate u' and p' .

For near transonic flows, it is necessary to separate ρ' and u' from a measurement $(\rho u)'$. Without further work, it is not clear how much more difficult the optimal-filtering technique will become.

5 SUGGESTED NWTC DESIGN CRITERIA

The following suggestions apply to both the low-speed and the transonic tunnels:

The settling chamber should have an aspect ratio of the order of one to provide the length needed for the turbulence management schemes to be sufficiently effective to satisfy the suggested criteria. Although screen separations and honeycomb placement are suggested in terms of mesh lengths, for the number of screens needed, the required overall length will be of the order of the cross-sectional dimension and so the layout should plan on an aspect ratio of one.

The contractions should have a length of about 1.25 times the larger entrance dimension. For the contraction shape, use fifth-degree polynomials with zero slope and zero curvature at the entrance and exit.

Put the heat exchanger into the turning vanes. This eliminates the bulbous heat exchanger in the tunnel circuit. This type of arrangement is used successfully in the National Diagnostic Facility (NDF) at Illinois Institute of Technology.

Go from circular cross section to rectangular cross section downstream of the compressor. The circuit should be basically rectangular especially in the corners to simplify the turning vane structures as well as allow their use as heat-exchanger elements.

The 5-foot fillets being considered for the corners of the LSWT test section are not essential, especially if the circuit and in particular the contraction is rectangular. This has been shown in the NDF at IIT. Figures 11 and 12 (Nagib and Hites 1995) show uniform rectangular core flows in the tunnel at the beginning and end of the test section respectively. There is no evidence of corner vortices in these figures nor in the NDF experience.

Screens should have a solidity no greater than 35%, except perhaps for a 40% solidity screen upstream of the

honeycomb if needed. The honeycomb scale should be 5-15 times the wire separation of the screens. Screen and honeycomb considerations are treated in greater detail in Section 3.

For the transonic speed wind tunnel (TSWT), although the contraction shape is not yet specified, the contraction ratio of nearly 12:1 is excessive. The contraction ratio should be no larger than 9:1. Otherwise, because of the large turning of the flow in the contraction, there are problems with the uniformity of the test section mean flow and the structure of the turbulence in the test section (Tan-atichat 1980; Nagib and Marion 1984).

ACKNOWLEDGMENTS

The authors' wish to acknowledge discussions with Travis Binion and Frank Steinle of the NWTC Program Office and Dr. Jeffrey Crouch of Boeing. These discussion have helped in clarifying numerous issues considered in the paper.

REFERENCES

- Corke, T.C. and Nagib, H.M. Large Signal-To-Noise Technique for Unsteady Pressure Measurements. *AIAA J.*, Vol. 17, pp. 114-6.
- Dougherty, N.S. Jr. and Fisher, D.F. 1980 Boundary Layer Transition on a 10-Degree Cone. *AIAA Paper 80-0154*.
- Harvey, W. D., Stainback, P.C., and Owen, F.K. 1980 Evaluation of Flow Quality in Two Large NASA Wind Tunnels at Transonic Speeds. *NASA Tech. Paper 1737*.
- Hites, M. and Nagib, H.M. 1994 Measurement of Disturbance Levels in the National Diagnostic Facility. *AIAA Paper 94-0770*.
- Loehrke, R.I. and Nagib, H.M. 1972 Experiments on Management of Free-Stream Turbulence. *AGARD Report 598*.
- Loehrke, R.I. and Nagib, H.M. 1976 Control of Free-Stream Turbulence by Means of Honeycombs: A Balance Between Suppression and Generation. *J. Fluids Eng.*, Vol. 98, pp. 342-53.
- Morel, T. 1975 Comprehensive Design of Axisymmetric Wind Tunnel Contractions. *J. Fluids Eng.*, Vol. 97, pp. 225-33.
- Nagib, H. 1992 A National Low Disturbance Subsonic Tunnel. *AIAA Paper 92-3911*.
- Nagib, H. 1993 Review of Turbulence Reduction System Design. NASA Ames Consultant Report.
- Nagib H. and Hites, M. 1995 High-Reynolds-Number Boundary-Layer Measurements in the NDF. *AIAA Paper 95-0786*.
- Nagib, H.M., Hites, M., Gravante, S. and Won, J. 1994 Flow Quality Documentation of the National Diagnostic Facility. *AIAA Paper 94-2499*.
- Nagib, H.M. and Marion, A. 1984. On the Design of Contractions and Settling Chambers for Optimal Turbulence Manipulation in Wind Tunnels. *AIM Paper 84-0536*.
- Naguib, A.M., Gravante, S.P. and Wark, C.E. 1995 Extraction of Turbulent Wall-Pressure Time-Series Using an Optimal Filtering Scheme. submitted *Exp. Fluids*.
- Saric, W.S., Takagi, S. and Mousseux, M.C. 1988 Fundamental Requirements for Freestream Turbulence Measurements. *AIAA Paper No. 88-0053*.
- Steinle, F.W. and Rose, W.C. 1982 The Effect of Various Proposed Slot Baffle Configurations on Test Section Flow Quality in the NASA-Ames 11-Foot Transonic Wind Tunnel. *57th Semiannual STA Meeting*, Seattle, Washington.
- Tan-atichat, J. 1980 Effects of Axisymmetric Contractions on Turbulence of Various Scales. PhD Thesis, Illinois Institute of Technology (NASA Contractor Rep. 165136).
- Tan-atichat, J., Nagib, H.M., and Loehrke, R.I. 1982 Interaction of Free-Stream Turbulence with Screens and Grids: A Balance Between Turbulence Scales. *J. Fluid Mech.*, Vol. 114, pp. 501-28.
- Widrow, B., Glover, J.R., McCool, J.M., Kaunitz, J., Williams, C.S., Hearn, R.H., Zeidler, J.R., Dong, E. and Goodlin, R.C. 1975 Adaptive Noise Cancelling: Principles and Applications. *Proc. IEEE*, Vol. 63, No. 12, pp. 1692-716.
- Wigeland, R.A., Ahmed, M., and Nagib, H.M. 1978 Management of Swirling Flows with Application to Wind Tunnel Design. *AIAA J.*, Vol. 16, pp. 1125-31.
- Wigeland, R.A., Tan-atichat, J., and Nagib, H.M. 1981 Evaluation of a New Concept for Reducing Freestream Turbulence in Wind Tunnels. *J. Aircraft*, Vol. 18, pp. 528-36.
- Wlezien, R.W., Spencer, S.A. and Grubb, J.P. 1994 Comparison of Flow Quality in Subsonic Pressure Tunnels. *AIAA Paper 94-2503*.

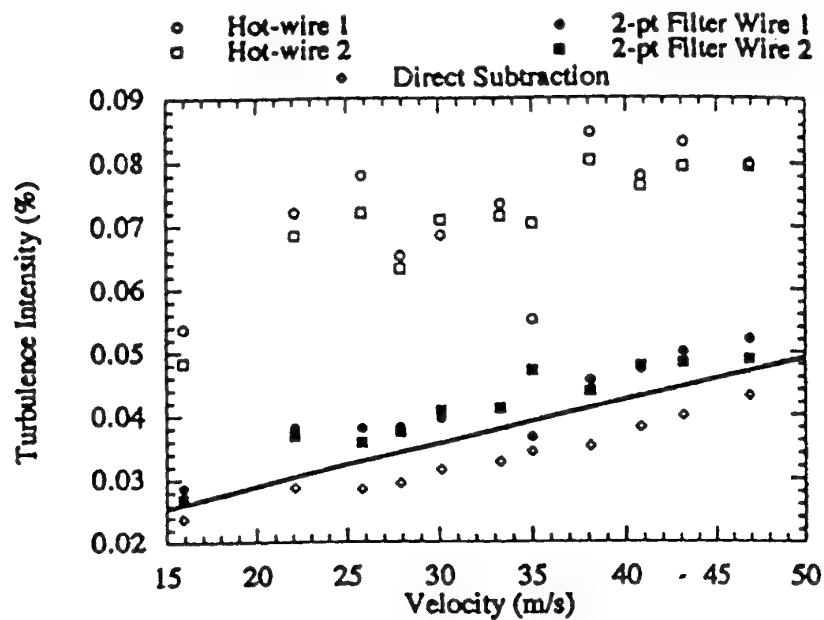


Figure 1. Turbulence intensity, $(u'/U_\infty) \times 100$, calculated from a long timeseries at location "A" ($x = 79$ cm, 31") for various freestream velocities using different signal processing techniques; from Nagib et al. (1994).

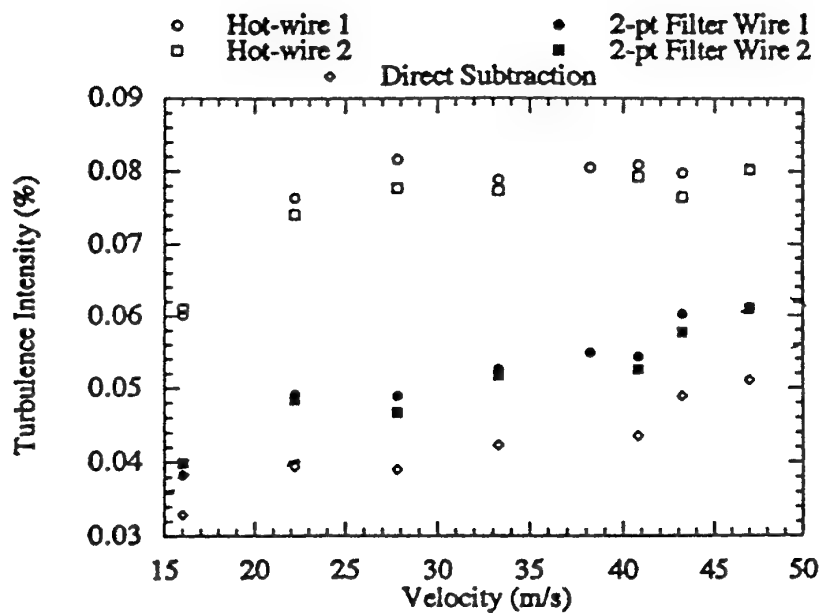


Figure 2. Turbulence intensity, $(u'/U_\infty) \times 100$, calculated from a long timeseries at location "B" ($x = 409$ cm, 13'5") for various freestream velocities using different signal processing techniques; from Nagib et al. (1994).

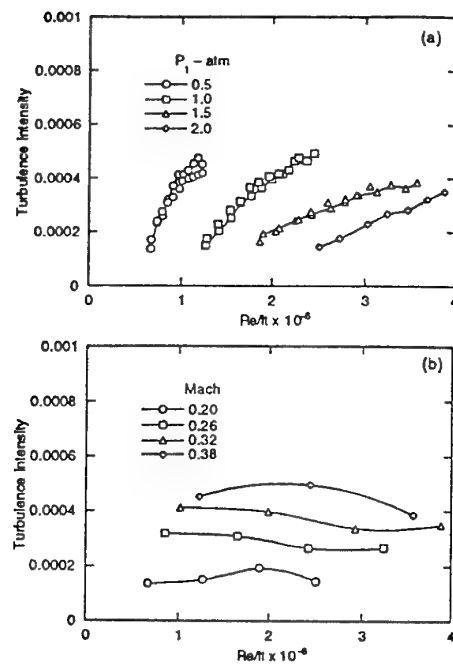


Figure 3. 8-ft TPT turbulence intensity at constant a) pressure and b) Mach number; from Wlezien et al. (1994).

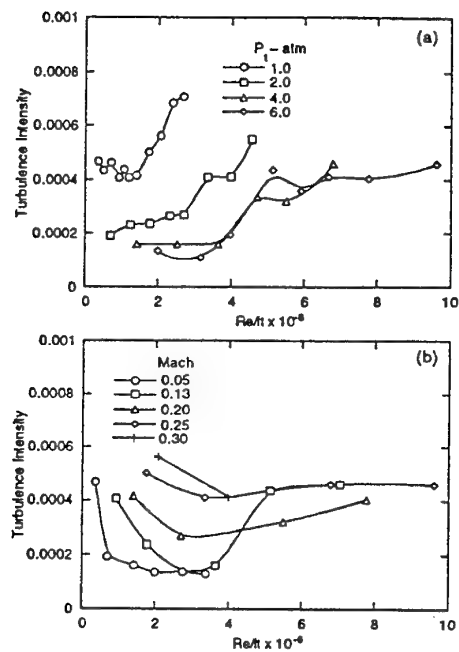


Figure 4. LTPT turbulence intensity at constant a) pressure and b) Mach number; from Wlezien et al. (1994).

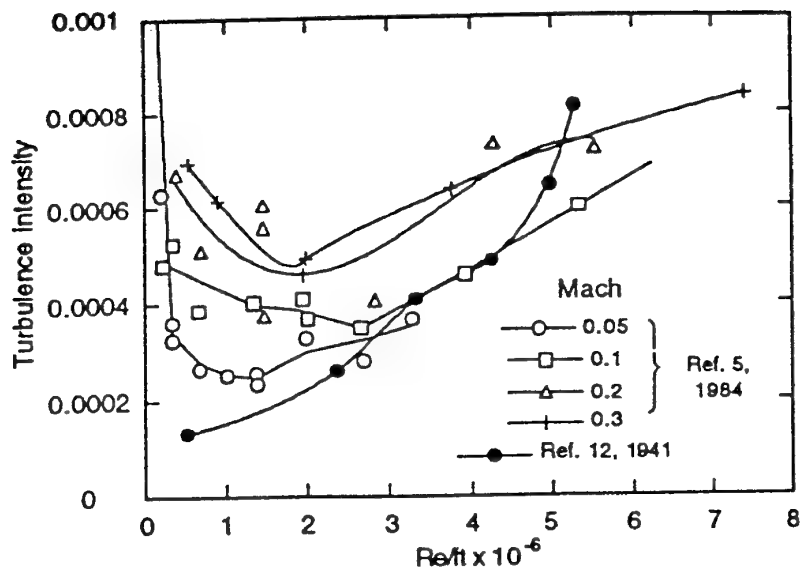


Figure 5. LTPT turbulence intensity data; from Stainback et al. (1984).

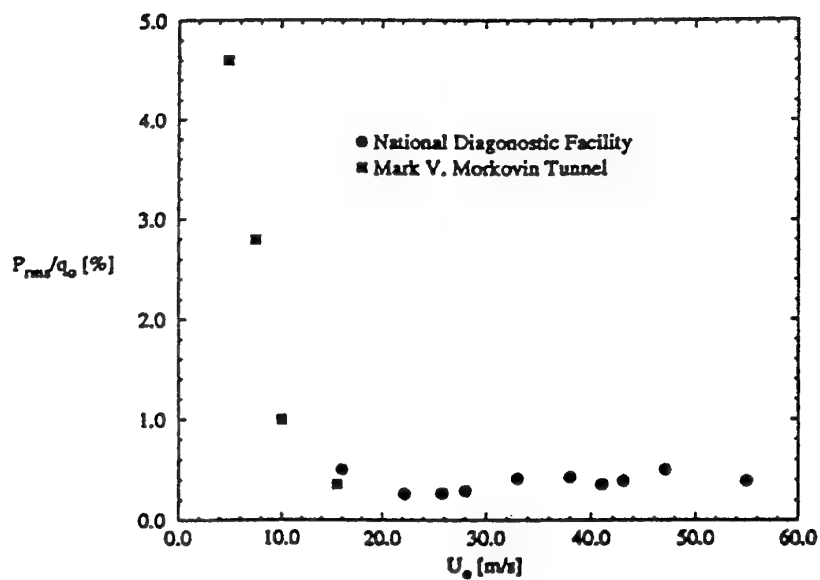


Figure 6. Fluctuating pressure intensity at various freestream velocities; from Nagib et al. (1994).

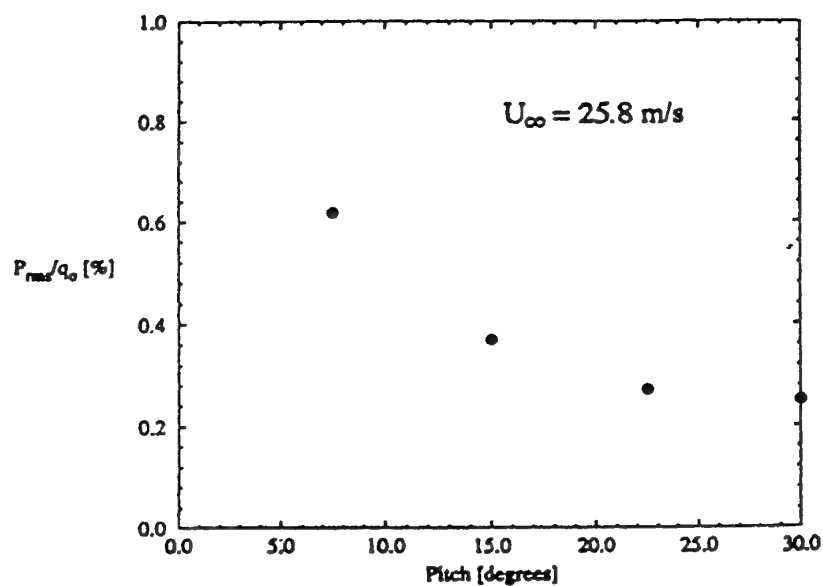


Figure 7. Fluctuating pressure intensity for various blade-pitch settings at 25.8 m/s; from Nagib et al. (1994).

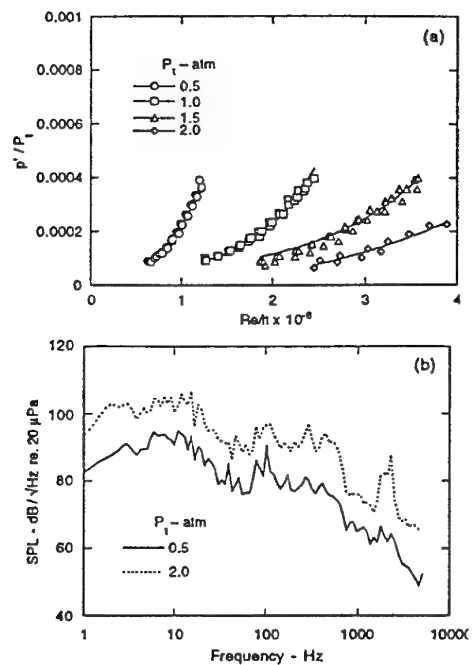


Figure 8. 8-ft TPT a) normalized acoustic data and b) acoustic spectra at Mach 0.24; from Wlezien et al. (1994).

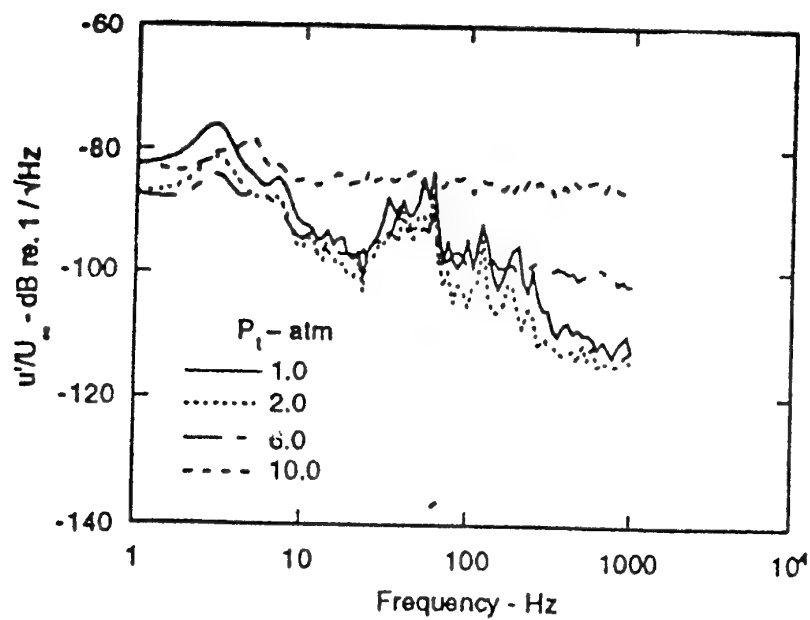


Figure 9. LTPT velocity spectra at Mach 0.24; from Wlezien et al. (1994).

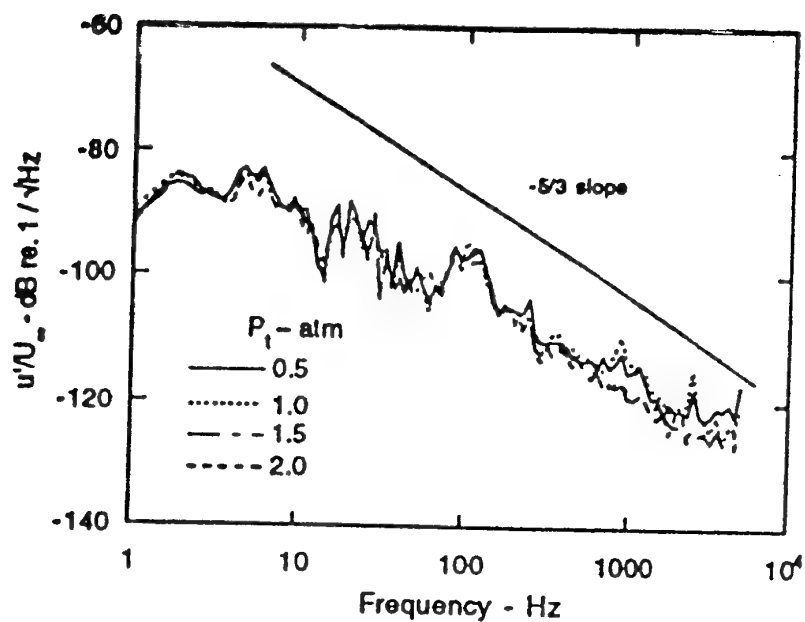


Figure 10. 8-ft TPT velocity spectra at Mach 0.24; from Wlezien et al. (1994).

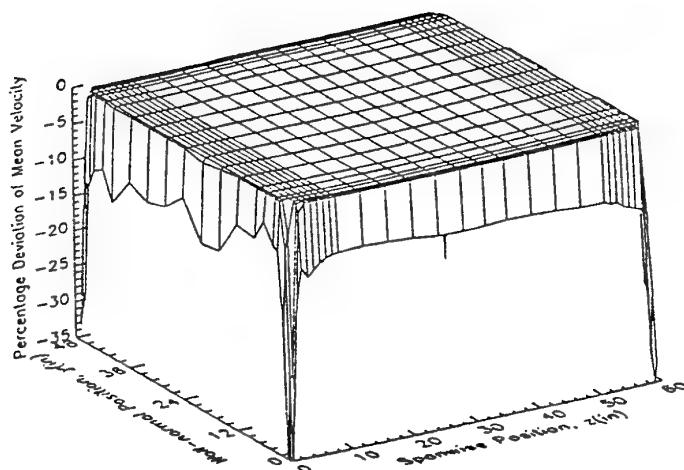


Figure 11. Mean velocity uniformity across the test section at a location 8 in. from the contraction exit. Freestream velocity is 40 m/s; from Nagib et al. (1994).

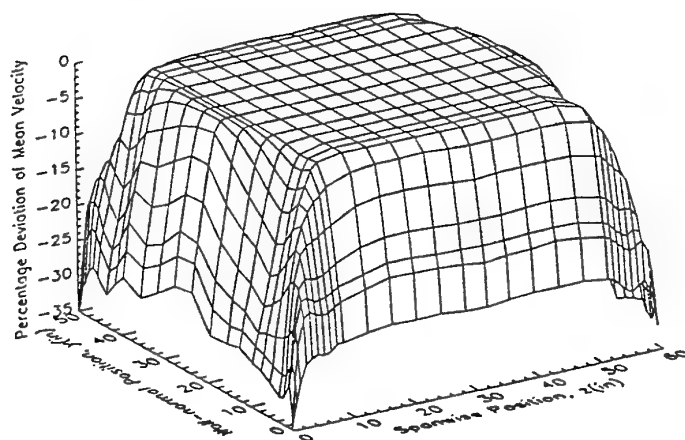


Figure 12. Mean velocity uniformity across the test section at a location 26 ft. from the contraction exit. Freestream velocity is 40 m/s; from Nagib et al. (1994).

CONCEPTION ET QUALIFICATION DE LA SOUFFLERIE SILENCIEUSE R1Ch DE L'ONERA

(DESIGN & VALIDATION OF A QUIET SUPERSONIC WIND TUNNEL)

O. Papirnyk, G. Rancarani, J. Détery

Office National d'Études de Recherches Aérospatiales (ONERA)
8 rue des Vertugadins, 92190 Meudon, France

D. Arnal

Centre d'Études et de Recherches de Toulouse (ONERA/CERT)
2, Avenue Edouard Belin, 31055 Toulouse Cedex 4, France

ABSTRACT

The R1Ch blow down wind tunnel was recently converted into a quiet supersonic wind tunnel at Mach 3.

In order for the boundary layers on the nozzle wall to remain laminar, the following tasks were accomplished : noise minimization coming from the upstream circuit, realization of suction upstream of the throat to eliminate the boundary layer in the contraction, optimization of the nozzle shape calculated in order to reduce Görtler vortex, realization of a surface quality to avoid triggering of transition due to the roughness.

The theoretical, numerical and technological works resulting in the realization of the wind tunnel, are presented with the description of the facility.

A preliminary validation of the wind tunnel was done with : measurement of pressure fluctuations in the stilling chamber, probing of boundary layer upstream of the nozzle throat, probing of pitot pressure and flux measurement on plane plate in the test section, and probing of boundary layer in the nozzle exit plane.

RÉSUMÉ

La soufflerie à rafale R1Ch a été transformée récemment en soufflerie supersonique "silencieuse" à Mach 3.

Pour que les couches limites sur les parois de la tuyère puissent rester laminares, l'effort a porté sur : la minimisation du bruit provenant de la partie amont du circuit, d'une aspiration destinée à éliminer la couche limite du convergent, l'optimisation de la forme de la tuyère pour réduire le développement des tourbillons de Görtler, l'obtention d'un état de surface suffisamment soigné pour éviter les déclenchements de transition par effet de rugosité. La description de l'installation ainsi que les travaux théoriques, numériques et technologiques aboutissant à la réalisation de la soufflerie sont présentés.

Une qualification préliminaire de l'installation a été effectuée avec : des mesures de fluctuations de pression dans la chambre de tranquillisation, des sondages de couche limite en amont du col de la tuyère, des sondages de pression d'arrêt et des mesures de flux sur une plaque plane dans la veine d'expérience ainsi que des sondages de couche limite dans le plan de sortie de la tuyère.

1. INTRODUCTION

L'établissement de l'ONERA situé à Chalais-Meudon, en Ile-de-France, comprend un complexe de souffleries couvrant une large gamme de nombres de Mach. Ces souffleries sont utilisées en partie pour des besoins industriels, mais surtout pour des études fondamentales destinées à élucider des phénomènes complexes et à valider les codes de calcul mis au point à l'ONERA ou ailleurs.

L'établissement de Chalais-Meudon s'est ainsi fait une spécialité en matière d'analyse fine d'écoulements décollés grâce à la mise en oeuvre de techniques de mesures avancées (sondes de pression multi-trous, vélocimétrie laser).

Trois de ces souffleries, R2Ch, R3Ch et R5Ch, fonctionnent à des nombres de Mach élevés. Ce sont des installations à rafales qui, dans un passé récent, ont été largement employées pour des études liées au projet HERMES. Elles sont utilisées aujourd'hui pour des

problèmes qui intéressent les applications aéronautiques et spatiales dans le domaine du vol à grande vitesse (missiles, lanceurs de satellites, avions supersoniques, corps de rentrée). Une opération de rénovation de ces souffleries a été effectuée de 1989 à 1993. Le paragraphe 2 sera consacré à une description succincte de ces installations et de leurs performances actuelles.

À l'époque où les souffleries précédentes ont été rénovées, une autre soufflerie à rafales, R1Ch (nombre de Mach nominal égal à 3), a été reconditionnée et remise en service après une période d'inactivité. Les travaux ont revêtu un caractère spécifique puisqu'ils avaient pour objectif de transformer R1Ch en soufflerie "silencieuse", afin de reproduire au mieux l'environnement existant dans les conditions de vol.

Le besoin de disposer d'une installation offrant un faible niveau de bruit a été motivé par l'intérêt porté aux études de transition laminaire-turbulent en écoulement

supersonique. On sait, en effet, que les perturbations extérieures à la couche limite (bruit, turbulence résiduelle) accélèrent les mécanismes de transition et réduisent la longueur du parcours laminaire. Or, les souffleries supersoniques conventionnelles sont très bruyantes : les fluctuations de pression rayonnées par les couches limites turbulentes se développant sur les parois de la tuyère "excitent" la couche limite laminaire de la maquette, donnant sur cette dernière des nombres de Reynolds de transition bien plus faibles qu'en vol. Le problème est illustré sur la figure 1, qui compare les nombres de Reynolds de transition R_{x_T} mesurés sur des cônes sans incidence en soufflerie et en vol [1].

Pour réduire le niveau de bruit rayonné, il faut maintenir sur les parois de la tuyère des couches limites laminaires, beaucoup moins bruyantes que les couches limites turbulentes. Partant de ce principe, les ingénieurs de la NASA Langley ont conçu un "quiet tunnel" à Mach 3,5 ; la référence [2] en donne une description détaillée. Dans cette installation, le niveau des fluctuations de pression est un ou deux ordres de grandeur plus faible que celui mesuré dans les souffleries conventionnelles. Des études fondamentales de transition sur cône ou plaque plane [3], sur cylindre en flèche [4] ou sur aile delta [5] ont fourni des résultats parfois très différents de ceux connus jusqu'alors ; ce qui démontre, si besoin était, que la qualité d'écoulement peut influencer sur les phénomènes aérodynamiques. On voit par exemple sur la figure 1 que les nombres de Reynolds de transition sur plaque plane s'approchent de ceux mesurés en vol. D'autres installations à des nombres de Mach plus élevés ont été conçues à la NASA Langley ; certaines d'entre elles ont été réalisées et testées [6].

Pour que les couches limites sur les parois de la tuyère du "quiet tunnel" puissent rester laminaires, l'effort a porté sur quatre points essentiels : minimisation du bruit amont, aspiration de la couche limite en amont du col, état de surface soigné, forme de la tuyère calculée pour réduire le développement des tourbillons de Görtler [6]. Ces mêmes principes ont été adoptés pour diminuer le bruit dans la soufflerie R1Ch. On donnera au paragraphe 3 une description des travaux effectués, puis les premiers résultats à caractère préliminaire seront présentés.

2. LES SOUFFLERIES A RAFALES DE L'ONERA A CHALAIS-MEUDON

Les souffleries à rafales R1Ch, R2Ch, R3Ch et R5Ch, construites au cours des années 60, viennent d'être rénovées récemment et leurs performances ont été améliorées. Elles sont destinées à couvrir un domaine de nombres de Mach supersonique et hypersonique compris entre 3 et 10 et une plage étendue de nombres de Reynolds unitaire (Re/m compris entre 2×10^6 et 2×10^7) grâce à une large variation de la pression génératrice ($2 \times 10^5 \text{ Pa} < P_o < 170 \times 10^5 \text{ Pa}$). Le temps de rafale varie, suivant les souffleries, de 10 s à 60 s. Le diamètre de sortie des tuyères se situe entre 0,190 m et 0,350 m.

La soufflerie R1Ch, qui fait l'objet de la présente étude,

a été construite à l'emplacement d'une ancienne soufflerie transsonique qui avait comme particularité d'être équipée pour son alimentation d'une vanne silencieuse. C'est l'une des raisons pour laquelle le site a été choisi pour la réalisation d'une soufflerie silencieuse.

La soufflerie R2Ch est une soufflerie à jet libre qui peut être équipée de tuyères interchangeable Mach 3 et 4 de 0,190 m de diamètre ou de tuyères Mach 5, 6 et 7 de 0,326 m de diamètre. La pression génératrice peut atteindre $80 \times 10^5 \text{ Pa}$. Le réchauffeur, de type conventionnel à accumulation, a été rénové récemment, ainsi que les circuits d'alimentation, pour fournir un air non pollué d'un débit maximal de 40 kg/s à une température de 800 K. L'amorçage étant progressif, un dispositif spécial permet d'introduire rapidement les maquettes dans l'écoulement. La durée de la rafale peut atteindre 60 s.

La soufflerie R3Ch est aussi une soufflerie à jet libre avec une tuyère en forme Mach 10 de 0,350 m de diamètre. Il est maintenant possible d'obtenir un niveau de pression génératrice variable entre 12×10^5 et $120 \times 10^5 \text{ Pa}$. La température génératrice de l'écoulement atteint 1100 K à l'aide d'un réchauffeur instantané à effet Joule. Le débit maximal est de 2 kg/s. L'amorçage de l'écoulement est obtenu en quelques millisecondes à l'aide d'une vanne spéciale à 3 voies. La durée de la rafale est de 10 s. Le nombre de Reynolds unitaire atteint $2 \times 10^6/m$.

La soufflerie R5Ch est une soufflerie hypersonique Mach 10 à basse densité et également à jet libre. Sa tuyère en forme a un diamètre de 0,355 m. Elle est destinée à étudier les phénomènes liés aux effets simultanés des grands nombres de Mach et des faibles nombres de Reynolds en régime continu (analyse des phénomènes de forte interaction visqueuse et des écoulements décollés laminaires). La pression génératrice est de $2,5 \times 10^5 \text{ Pa}$. Un réchauffeur à effet Joule permet d'obtenir une température de 1100 K. La durée de la rafale peut dépasser la minute.

3. LA SOUFFLERIE SILENCIEUSE R1Ch

3.1 Conception de la soufflerie

Comme on l'a signalé en introduction, améliorer la qualité d'écoulement d'une soufflerie supersonique nécessite d'agir sur quatre points :

- minimisation du bruit provenant de la partie amont du circuit ;
- application, un peu en amont du col, d'une aspiration destinée à éliminer la couche limite du convergent, afin d'obtenir au col une couche limite de très faible épaisseur ;
- optimisation de la forme de la tuyère pour retarder la transition sur la paroi ;
- obtention d'un état de surface suffisamment soigné pour éviter les déclenchements de transition par effet de rugosité.

Le premier point, purement technologique, sera abordé

au paragraphe 3.2. Les trois autres, qui se sont appuyés sur des travaux théoriques et numériques, sont discutés ci-dessous. On en trouvera une description plus complète dans [7].

3.1.1 Convergent et système d'aspiration

Dès le début de l'étude, il a été décidé d'équiper la soufflerie d'un convergent existant, axisymétrique et long de 0,4 m. Le diamètre de sortie est de 0,146 m, pour un rapport de contraction voisin de 13. Il a en outre été convenu d'installer le système d'aspiration à 0,135 m en amont du col (nombre de Mach local = 0,35 ; diamètre local du convergent = 0,196 m). A partir de la couche limite, afin de connaître les caractéristiques de celle-ci au niveau de l'aspiration ; la connaissance de l'épaisseur physique δ , par exemple, devait permettre de définir la hauteur de la lèvres d'aspiration.

La distribution de vitesse extérieure à la couche limite a été déterminée en supposant un écoulement par tranche. La figure 2 montre les évolutions théoriques de δ obtenues pour plusieurs calculs effectués en supposant le convergent précédé d'une plaque plane longue de 1,5 m. Sur cette figure, X représente l'abscisse curviligne le long de la paroi ; l'origine X = 0 est située au bord d'attaque de la plaque, et l'emplacement du système d'aspiration est repéré par une flèche. La pression génératrice est de 10^6 Pa. Quatre hypothèses ont été adoptées : la couche limite est toujours laminaire, la transition se situe à X = 1 m, la transition se situe à X = 0,5 m, la couche limite est turbulente depuis le bord d'attaque de la plaque.

On observe, bien entendu, un amincissement important de la couche limite, provoqué par la forte accélération de l'écoulement dans le convergent. Au niveau de l'aspiration, δ varie d'une valeur quasiment nulle à plus de 5 mm suivant les hypothèses adoptées. Devant cette incertitude, des sondages de couche limite ont été réalisés dans le collecteur ; on a trouvé, pour des pressions génératrices comprises entre 5×10^5 et 15×10^5 Pa, une épaisseur δ de l'ordre de 1 mm ; mais le faible nombre de points de mesure dans la couche limite n'a pas permis de savoir si elle était laminaire ou turbulente. Quoiqu'il en soit, la hauteur de la lèvres d'aspiration a été fixée à 1,5 mm.

3.1.2 Calcul de la forme de la tuyère

En supposant que la couche limite au col est laminaire et que l'état de surface de la tuyère est "parfait", il faut maintenant faire en sorte que la transition au régime turbulent s'effectue le plus en aval possible. Deux types d'instabilité peuvent provoquer cette transition : les ondes du type Tollmien-Schlichting et les tourbillons de Görtler. Ces derniers les plus dangereux dans le cas présent, sont des tourbillons longitudinaux, contrarotatifs, qui prennent naissance sur les parois concaves, qui s'amplifient, dans la direction de l'écoulement principal, ils déforment la couche limite laminaire et la déstabilisent de façon telle que la turbulence finit par apparaître. Des mesures réalisées à la NASA Langley ont révélé que ces tourbillons étaient effectivement

responsables de la transition sur les parois des tuyères supersoniques.

Sur le plan théorique, les tourbillons de Görtler peuvent être étudiés à l'aide d'une théorie linéarisée. On suppose que les perturbations de vitesse longitudinale u' engendrées par ces tourbillons sont de la forme :

$$u' = u(y) \exp(\sigma X) \sin(2\pi Z/\lambda)$$

où y désigne la normale à la paroi et Z la direction selon l'envergure (écoulement plan) ou la direction azimutale (écoulement de révolution). Lorsque l'écoulement moyen est connu, la résolution des équations de stabilité linéarisées fournit, pour un tourbillon de longueur d'onde λ fixée, l'évolution du taux d'amplification σ en fonction de X. L'amplification totale $I(\lambda)$ de ce tourbillon est ensuite calculée en intégrant σ dans la direction X. On appelle facteur N la valeur maximale de $I(\lambda)$ à une abscisse donnée (maximisation par rapport à λ). La règle empirique dite du e^N , proposée par Smith en 1955 [8], consiste à supposer que la transition se produira lorsque ce facteur N atteindra un seuil critique, que l'on prend généralement égal à 9 ou 10.

La détermination du point de transition sur la paroi de la tuyère se déroulera donc en trois étapes :

- calcul de l'écoulement potentiel dans la tuyère par la méthode des caractéristiques ;
- utilisation de la distribution de pression à la paroi pour calculer le développement de la couche limite laminaire, dont l'origine sera supposée au col ;
- calcul de stabilité linéaire sur l'écoulement visqueux déterminé précédemment, et application du critère du e^N . On a en fait utilisé trois approches légèrement différentes pour ces calculs : une approche dite locale, une approche dite parabolisée et une méthode simplifiée. On en trouvera une description dans [7]. Il n'est pas nécessaire de préciser les différences entre ces méthodes puisque, comme on va le voir, elles aboutissent à des résultats très voisins.

Comme les tourbillons de Görtler naissent sur des parois concaves, on peut espérer, en repoussant la partie concave de la tuyère vers l'aval et en limitant sa courbure, retarder la transition et obtenir un rhombe "silencieux" de longueur suffisante pour pouvoir y placer des maquettes. C'est dans cette optique qu'a été développée une méthode pour créer des profils de tuyère comportant une partie rectiligne. La procédure suivie est la suivante. Le col, dont la forme circulaire est imposée par le code basé sur la méthode des caractéristiques, est prolongé par une paroi rectiligne. L'angle que fait cette paroi avec l'axe de la tuyère fixe les limites de la zone circulaire autour du col. Le raccord entre ces deux zones respecte la continuité du profil ainsi que celle de sa dérivée première. La longueur de la partie rectiligne est telle que le nombre de Mach sur l'axe produit à l'extrémité de cette zone soit celui désiré en sortie de tuyère. A partir de ces deux premiers tronçons de paroi,

le code déduit la forme de la paroi concave à ajouter pour produire un écoulement uniforme. On a ainsi testé numériquement différentes formes de tuyère en faisant varier trois paramètres : la géométrie (plane ou de révolution), la longueur de la partie rectiligne et sa pente.

Pour rester dans les limites des dimensions imposées par les autres installations, la hauteur (ou le diamètre) de sortie de la tuyère a été fixée à 0,3 m, pour un nombre de Mach nominal égal à 3. Au niveau du calcul, aucune différence fondamentale n'est apparue pour guider le choix entre une tuyère plane ou une tuyère de révolution. Chaque solution présentait des avantages et des inconvénients. Toutefois, il a semblé que l'usinage et l'installation d'une tuyère de révolution étaient plus aisés, ce qui a conduit en fin de compte à opter pour l'option axisymétrique.

Il restait à optimiser les deux autres paramètres : longueur et pente de la partie rectiligne. Dans ce but, un balayage systématique a été effectué en mettant en oeuvre, pour chaque géométrie, la succession des trois calculs décrits plus haut. Le profil retenu, ainsi que le réseau correspondant de caractéristiques descendantes, sont tracés sur la figure 3. L'interruption des caractéristiques marque le début de l'écoulement uniforme. Celui-ci débute à $X_u \approx 1$ mètre (distance mesurée à partir du col). On remarquera la longueur importante de la tuyère, nécessaire pour minimiser les parties concaves générant des tourbillons de Görtler. On a reporté sur la figure 4 la variation des nombres de Mach sur l'axe et à la paroi ; les deux courbes sont très voisines. Notons que la forme finale de la tuyère a été corrigée de l'effet de déplacement de la couche limite, supposé laminaire.

En ce qui concerne les résultats des calculs de stabilité linéaire, la figure 5 montre l'évolution du facteur N calculé pour une pression génératrice 10^6 Pa. On a considéré ici les tourbillons de Görtler les plus amplifiés, associés à une longueur d'onde d'environ 0,7 mm. Les trois méthodes utilisées donnent des résultats presque identiques. En fixant à 9 la valeur du facteur N critique, on trouve une abscisse de transition théorique à $X \approx 1$ m. Ensuite, en parcourant la caractéristique descendante passant par ce point, on définit l'extrémité aval de la zone "silencieuse" sur l'axe, qui, dans le cas présent, se situe à $X_s \approx 1,45$ m. La longueur du rhombe utile (nombre de Mach constant et écoulement silencieux) serait ainsi égale à $X_t - X_u \approx 0,45$ m, ce qui est suffisant pour placer des maquettes de taille raisonnable.

3.1.3 Etat de surface de la tuyère

La minceur de la couche limite dans la région du col est telle qu'une aspérité de très faible hauteur risque de déclencher la transition et d'annihiler les efforts déployés par ailleurs pour retarder la transition. De ce fait, il est impératif que la surface de la tuyère soit parfaitement polie, du moins tant que la couche limite n'a pas une épaisseur suffisante pour résister aux imperfections de la paroi. Cet aspect du problème a été abordé par Beckwith et al. en 1988 [9]. Ces auteurs proposent un critère pour estimer la hauteur de rugosité k admissible. Ce critère

est basé sur le nombre de Reynolds R_k défini par :

$$R_k = \rho_k U_k k / \mu_k$$

où ρ_k , U_k et μ_k sont la masse volumique, la vitesse moyenne et la viscosité moléculaire prises à l'altitude $y = k$.

Les expériences montrent que la hauteur maximale de rugosité ne déclenchant pas la transition correspond à $R_k = 10$.

La figure 6 montre, pour une pression génératrice de 10^6 Pa, l'évolution de la hauteur de rugosité admissible le long de la tuyère. Le calcul présenté débute au col, alors qu'en réalité, la couche limite laminaire a son origine au niveau de la lèvre d'aspiration à 0,135 m en amont. On estime donc que la hauteur maximale tolérée est d'environ 2 μ m. Il semble que la qualité d'usinage de la tuyère soit compatible avec cette contrainte.

3.2 Description de l'installation

Lors du reconditionnement de la soufflerie R1Ch, opération lancée en 1989, un soin particulier a été pris pour la rendre complémentaire des deux autres installations voisines R2Ch et R3Ch. Ces trois souffleries disposent maintenant de caissons d'essais identiques et de tuyères dont les noyaux sains sont également identiques et voisins de 0,3 m. Dans ce contexte, R1Ch (voir Fig. 7) est destinée à servir pour des nombres de Mach supersoniques faibles ou modérés (2 à 5) et des débits élevés à basse température génératrice.

Les deux souffleries R1Ch et R2Ch utilisent un circuit commun d'alimentation en air comprimé alimenté à 230×10^5 Pa par le réseau général du centre de Chalais-Meudon dont la capacité de stockage est de 30 m³ (voir Fig. 8). En tête des installations, se trouve un poste de détente réglant la pression de l'air à la valeur souhaitée pour les rafales dans les souffleries. L'utilisateur sélectionne de un à trois des détendeurs disponibles, capables de délivrer jusqu'à 70 kg/s de débit total. L'air est ensuite dirigé vers un réchauffeur à accumulation si une température génératrice élevée est désirée (800 K maximum pour R2Ch) ou bien directement vers les souffleries ; des vannes de mélange air froid-air chaud permettent des valeurs plus basses de température (en général autour de 400 K pour R1Ch). R1Ch peut fonctionner soit directement à l'atmosphère, cas courant pour une utilisation à Mach 3, soit vers la sphère à vide de 500 m³ commune pour R1Ch, R2Ch et R3Ch. Cette possibilité permet des rafales à très basse pression génératrice ($0,5 \times 10^5$ Pa) ou facilite l'amorçage en cas de forte obstruction du montage d'essai. Le circuit proprement dit de la soufflerie R1Ch comporte une vanne d'arrêt immédiatement suivie de la vanne silencieuse qui débite dans la chambre de tranquillisation. Sur la bride aval de cette chambre se monte l'ensemble tuyère-col relié au caisson d'essai par un compensateur de dilatation. R1Ch est une soufflerie du type à jet libre avec, à l'aval de la tuyère, une canalisation de reprise. Les principaux organes vont être maintenant détaillés.

Vanne silencieuse :

Cette vanne a été récupérée sur la version précédente de la soufflerie R1Ch. Le principe d'une telle vanne est de détendre l'écoulement à travers des labyrinthes radiaux usinés dans des disques de métal empilés (voir Fig 9). L'air arrive au centre et en s'écoulant vers l'extérieur suit une série de coudes tout en voyant sa section de passage augmenter. Un piston central découvre une plus ou moins grande portion des disques assurant ainsi un ajustement de la pression détendue. Ce type de vanne est dit "silencieux" car le bruit généré voit son spectre déplacé vers des fréquences élevées, alors que la plupart des organes de laminage produisent du bruit à basse fréquence. Comme ce bruit à haute fréquence est mieux absorbé dans les structures métalliques, il s'en suit un niveau de bruit plus faible. Si une part importante du bruit se situe dans les ultrasons elle n'est pas perçue par l'oreille humaine.

Chambre de tranquillisation :

C'est une enveloppe cylindrique en acier de 0,54 m de diamètre intérieur et de 0,08 m d'épaisseur, longue de 2,775 m. Elle contient tous les éléments disposés entre la vanne silencieuse et la tuyère.

Filtre à cartouches :

Juste derrière la vanne silencieuse est installée une batterie de 102 cartouches filtrantes en acier inoxydable fritté. Ces cartouches ont un seuil de filtration de 6 microns afin de retenir les particules présentes dans l'écoulement, essentiellement produites par l'oxydation des tuyauteries et bouteilles d'air comprimé de distribution.

Éléments anti-turbulence :

L'intérieur de la chambre comporte un filtre nid d'abeille d'une épaisseur de 0,185 m avec des alvéoles de 6,5 mm. Viennent ensuite quatre grillages en acier inoxydable à maille de 1,5 mm et fil de 0,5 mm.

Parois absorbantes :

L'ensemble des grillages est monté sur des viroles en tôles minces garnies de mousse alvéolaire de 10 mm d'épaisseur sur la face en contact avec l'écoulement. Cette mousse est destinée à atténuer le bruit à haute fréquence.

3.3 Qualification de la soufflerie silencieuse

3.3.1 Méthodes de qualification

La qualification d'une soufflerie silencieuse comporte deux phases : une phase de mesures stationnaires effectuées comme pour une soufflerie classique et une phase de mesures stationnaires et instationnaires destinées à évaluer l'effet des différents dispositifs ayant pour but de réduire le niveau de bruit et de turbulence à l'intérieur du rhombe de Mach.

La première de ces phases consiste à explorer la veine d'expérience pour en obtenir une cartographie du nombre de Mach. La phase des essais propres à la conception de la soufflerie silencieuse comprend d'une part, des mesures directes de la qualité de l'écoulement

(détermination des niveaux de bruit et de turbulence de l'écoulement dans la chambre de tranquillisation et dans la veine d'expérience) et d'autre part des mesures indirectes qui permettent de juger de la qualité de la soufflerie silencieuse (ce sont des mesures effectuées au voisinage de la paroi de la tuyère et sur des maquettes dans la veine d'expérience).

Parmi les mesures à effectuer à la paroi de la tuyère, le sondage de la couche limite, dans le plan de sortie de la tuyère, peut permettre d'observer l'effet dû à l'aspiration de la couche limite en amont du col de la tuyère (voir Fig 10).

L'autre technique consiste à essayer de détecter la zone de transition à l'intérieur de la tuyère. On peut utiliser des films chauds collés à la paroi. Ceux-ci sont difficiles à mettre en place et peuvent aussi provoquer des perturbations locales susceptibles de déclencher une transition prématurée.

Les diagnostics qui peuvent être faits sur des maquettes sont basés sur la détection de la zone de transition. Les plaques et les cônes sont les maquettes les plus utilisées avec des mesures de flux comme technique de détection.

La quasi-totalité de ces mesures a été programmée à ce jour. Ainsi ont été effectués :

Dans la veine d'expérience :

- des sondages de pression d'arrêt

Dans la chambre de tranquillisation :

- des mesures de fluctuations de pression,
- des sondages de couche limite en amont du col de la tuyère.

Dans la tuyère :

- des sondages de couche limite dans le plan de sortie,
- des mesures de flux sur une plaque plane.

Une partie de ces essais a été exécutée avec aspiration de la couche limite en amont du col.

3.3.2 Premiers résultats d'essai

Sondages de pression d'arrêt dans la veine d'expérience

Sondages longitudinaux :

Ces essais ont eu lieu avant la mise en place du système d'aspiration de la couche limite en amont du col. Un peigne équipé de 7 prises de pression d'arrêt a été monté sur un dispositif de déplacement suivant l'axe longitudinal de la tuyère (voir Fig. 11). La longueur explorée est voisine de 0,250 m. Le peigne a été placé verticalement, horizontalement et à 45° comme indiqué Fig. 12a. Un exemple de résultats de cartographie du nombre de Mach obtenus avec le peigne à l'horizontale est montré Fig. 12b. Les résultats dans les autres plans sont identiques. La distribution du nombre de Mach est homogène et voisine de Mach 3 à $\pm 0,01$ près dans toute la veine d'expérience, sauf sur l'axe longitudinal où elle oscille de $\pm 0,05$ du fait de la focalisation des ondes de Mach.

Sondages transversaux :

Des sondages transversaux de la veine d'expérience ont été effectués en même temps que les sondages de couche limite dans le plan de sortie de la tuyère. Pour cela il a été utilisé un peigne à deux sondes de pression d'arrêt distantes de 0,1 m. Les deux exemples de résultats montrés Figs. 13a et 13b confirment les observations précédentes.

Mesures de fluctuations de pression dans la chambre d'alimentation

Ces mesures ont été effectuées dans l'ancienne soufflerie (en 1975), avec un capteur piézo-électrique protégé des vibrations et placé à la paroi de la chambre d'alimentation au niveau de la vanne silencieuse. Les analyses spectrales présentées Fig. 14 montrent que le bruit émis par la vanne silencieuse est du domaine ultrasonore avec un maximum de niveau autour de 40 kHz. Il a été montré que le bruit émis est proportionnel au niveau de pression moyenne P_0 dans la chambre ; c'est la raison pour laquelle les fluctuations sont présentées en \tilde{P}/P_0 pour comparer le bruit émis pour différents réglages d'ouverture de la vanne silencieuse et différentes vitesses moyennes dans la chambre. Ce rapport \tilde{P}/P_0 sera aussi utilisé pour comparer le bruit émis par les souffleries silencieuses.

Mesures de fluctuations de pression dans la chambre de tranquillisation

Les fluctuations de pression ont été mesurées avec plusieurs types de capteur et différents montages. Ces mesures sont difficiles à faire pour les raisons suivantes :

- les fluctuations de pression sont faibles (inférieures au 1/1000 de la pression moyenne),
- le niveau moyen de la pression à l'intérieur de la chambre de tranquillisation est élevé (de 2×10^5 à 15×10^5 Pa),
- le temps de montée en pression de la chambre est court (# 0,5 seconde),
- le temps d'essai est bref (de 10 à 20 secondes),
- il n'existe pas de capteur capable de mesurer à la fois les basses et les hautes fréquences, et de mesurer directement de faibles pressions avec un niveau moyen aussi élevé.

La technique utilisée a donc été la suivante :

- Pour les basses fréquences (jusqu'à environ 100 Hz), il a été utilisé un capteur différentiel de faible étendue de mesure mais capable de fonctionner avec une pression de ligne élevée (de l'ordre de 35×10^5 Pa). Ce

capteur (Druck PDCR 10/L) a été placé au plus près de la paroi de la chambre. Pour éviter sa destruction au moment de la mise sous pression, un dispositif particulier de communication entre les prises de pression a été réalisé à l'aide d'une électrovanne à 3 voies (voir Fig. 15).

- Pour les fréquences plus élevées et les hautes fréquences (de 100 à 100 000 Hz), il a été utilisé un microphone 1/8" et 3 capteurs piézoélectriques de différents types. Ces capteurs ont été placés en membrane affleurante à la paroi de la chambre de tranquillisation.

Deux exemples d'analyses spectrales obtenues avec le capteur différentiel et l'un des capteurs piézoélectriques sont montrés Figs. 16a et 16b. L'intégration des domaines spectraux sains, c'est-à-dire hors des zones de résonance de capteur ou de cavité, permet d'obtenir un niveau global des fluctuations de pression dans un domaine spectral comparable aux résultats obtenus dans les autres souffleries silencieuses, notamment celles de la NASA Langley (voir Fig. 17) [10].

Sondages de couche limite en amont du col

Ces sondages ont été effectués avant la mise en place du système d'aspiration de la couche limite. Des exemples de profils de vitesse sont tracés Figs. 18a à 18c. Elles montrent que la couche limite a une épaisseur d'environ 1 mm.

Sondage de couche limite dans le plan de sortie de la tuyère

Ces essais ont eu lieu avec et sans aspiration de la couche limite en amont du col de la tuyère. Cette dernière configuration a été réalisée avec la plus grande ouverture du dispositif d'aspiration. Parallèlement à ces sondages, on a relevé les pressions pariétales dans le collecteur jusqu'à l'intérieur du système d'aspiration dont le schéma, ainsi que la position des prises de pression, sont donnés Fig. 19.

Les résultats des mesures de pression montrés Figs. 20a et 20b font apparaître l'amorçage du col lors de l'aspiration de la couche limite.

Les sondages de couche limite dans le plan de sortie de la tuyère, effectués avec et sans aspiration de la couche limite en amont du col et présentés Figs. 21a et 21b pour la pression d'alimentation de 2×10^5 Pa et Figs. 21c et 21d pour une pression de 8×10^5 Pa, ne montrent pratiquement aucune différence. Cela est confirmé par le tableau de résultats suivant :

N° Essai	Aspiration de la couche limite	P_0 [Pa]	δ (mm)	δ^* (mm)	θ (mm)	facteur de forme H
564	sans	2×10^5	18,057	5,142	1,081	4,756
571	avec	2×10^5	17,748	5,103	1,070	4,768
580	sans	8×10^5	15,431	4,523	0,951	4,755
581	avec	8×10^5	15,506	4,408	0,929	4,741

Les paramètres de forme incompressibles sont voisins de 1,3 ; ce qui montre que la couche limite est turbulente.

Mesures de flux sur une plaque plane

Une plaque plane à bord d'attaque effilé, équipée de thermocouples de type peau épaisse, a été placée à l'intérieur de la tuyère, comme indiqué Fig. 22. Elle a été essayée avec et sans aspiration de la couche limite en amont du col et pour une pression d'alimentation voisine de 8×10^5 Pa et une température de 340 K.

Les résultats d'essais, présentés Fig. 23, ont été comparés avec un calcul correspondant aux deux états - laminaire et turbulent - de la couche limite.

Les résultats correspondent à une couche limite turbulente ; la transition a eu lieu en amont du premier thermocouple. Des sondages de couche limite effectués vers le milieu de la plaque plane confirment effectivement ces résultats (voir Figs. 24a et 24b).

4. CONCLUSION

Il semble à peu près certain que la qualité d'écoulement dans la soufflerie R1Ch n'est pas encore suffisante pour obtenir des conditions favorables au maintien du régime laminaire sur une maquette. Mais il ne faut oublier que ces résultats sont préliminaires. Dans un avenir proche, on essayera des positions intermédiaires du dispositif d'aspiration ; la qualité de surface de la tuyère et l'état de la lèvre d'aspiration seront également vérifiés. D'autres formes de lèvres d'aspiration sont à l'étude.

Au cours des prochaines campagnes d'essais, de nouvelles techniques de mesure de la qualité de l'écoulement sont programmées :

- sondage axial avec mesure des fluctuations de pression sur l'axe de la tuyère à l'aide d'un cône effilé équipé d'une prise de pression statique instationnaire à large bande passante,

- sondage axial avec mesure de fluctuations de vitesse sur l'axe de la tuyère à l'aide d'un film chaud sur cône,

- mesure de turbulence avec fil et film chaud dans la chambre de tranquillisation,

- détection de la zone de transition à la paroi de la tuyère à l'aide de films chauds collés à la paroi ou par thermographie infrarouge.

L'effort de développement de la version silencieuse de R1Ch va donc être poursuivi activement de façon à se doter d'un outil bien adapté - et indispensable - aux études sur la laminarité.

Remerciements

Les auteurs remercient Michèle Ledoux de la Division d'Aérodynamique Appliquée pour la mise à leur disposition du code de définition de la tuyère par la méthode des caractéristiques, ainsi que Lucien Morzenski et son équipe des Souffleries à Rafales pour les travaux réalisés à la soufflerie R1Ch.

REFERENCES

- [1] Beckwith I.E. "Development of a high Reynolds number quiet tunnel for transition research". AIAA Journal, Vol 18, N° 8, 1980.
- [2] Beckwith I.E., Creel T.R., Chen F.J., Kendall J.M. "Free stream noise and transition measurements on a cone in a Mach 3.5 pilot low-disturbance tunnel". NASA Technical Paper 2180, 1983.
- [3] Chen F.J., Malik M.R. "Comparison of boundary layer transition on a cone and flat plate at Mach 3.5". AIAA Paper 88-0411, 1988.
- [4] Creel T.R., Beckwith I.E., Chen F.J. "Transition on swept leading edges at Mach 3.5". J. of Aircraft, Vol 24, N° 10, 1987.
- [5] Cattafesta L.N., Yyer V., Masad J.A., King R.A., Dagehart J.R. "Three-dimensional boundary layer transition on a swept wing at Mach 3.5". AIAA Journal, Vol. 33, N° 11, 1995.
- [6] Beckwith I.E., Chen F.J., Wilkinson S., Malik M.R., Tuttle D. "Design and operational features of low-disturbance wind tunnels at NASA Langley for Mach numbers from 3.5. to 18". AIAA Paper 90-1391, 1990.
- [7] Hennequin Y. "Etude numérique de l'instabilité de Görtler : application à la définition d'une soufflerie supersonique silencieuse". Thèse soutenue à l'ENSAE, Toulouse, septembre 1993.
- [8] Smith A.M.O. "On the growth of Taylor-Görtler vortices along highly concave walls". Q. Appl. Mech., Vol 13, N° 3, pp. 233-262, 1955.
- [9] Beckwith I.E., Chen F.J., Malik M.R. "Design and fabrication requirements for low noise supersonic/hypersonic wind tunnels". AIAA Paper 88-0143, 1988.
- [10] Piatt M. J. "An experimental investigation of a large ΔP settling chamber for a supersonic quiet tunnel". NASA report 3436, 1981.

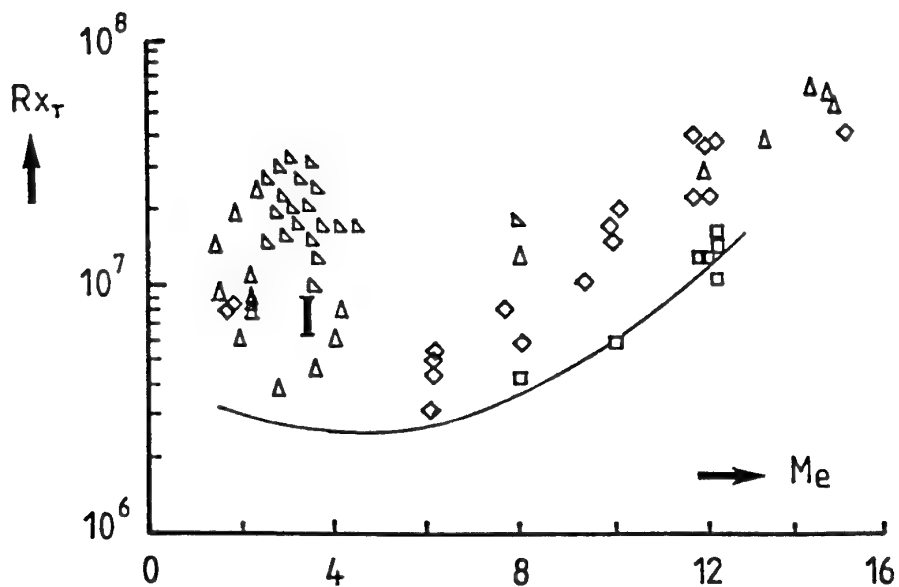


Fig. 1 Nombres de Reynolds de transition sur cônes mesurés en vol (symboles) et en soufflerie (ligne). Trait vertical à $M = 3.5$: résultats du "quiet tunnel" de la NASA Langley.

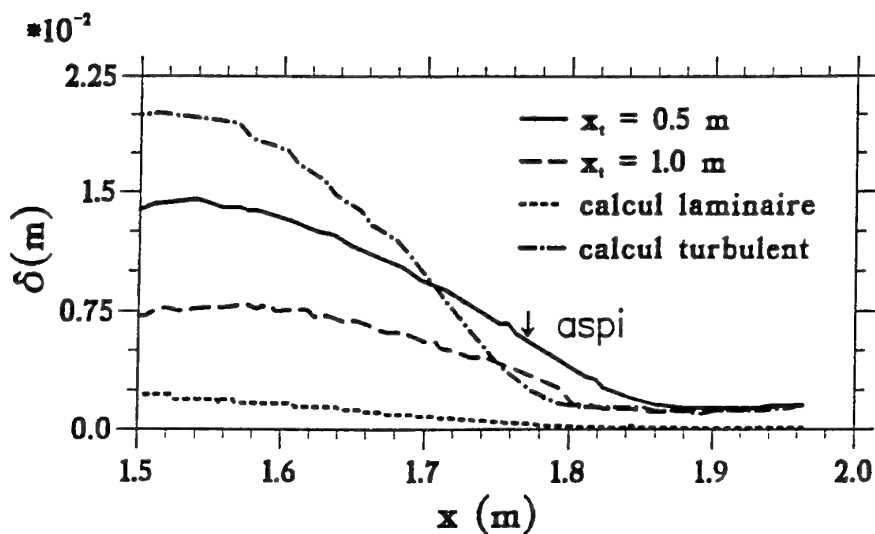


Fig. 2 Epaisseur de couche limite dans le collecteur.

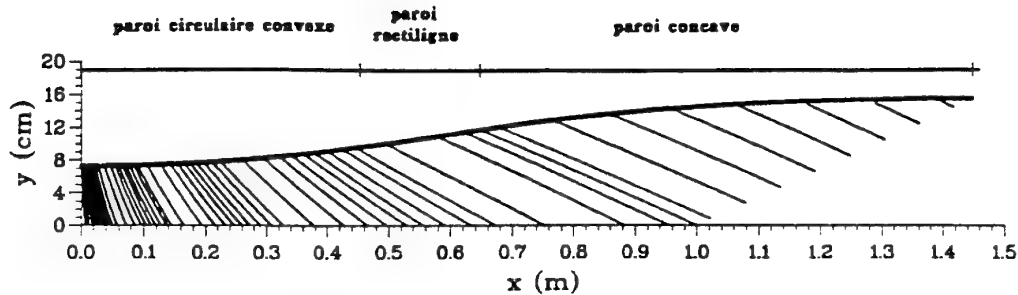


Fig. 3 Forme de la tuyère de la soufflerie R1Ch.

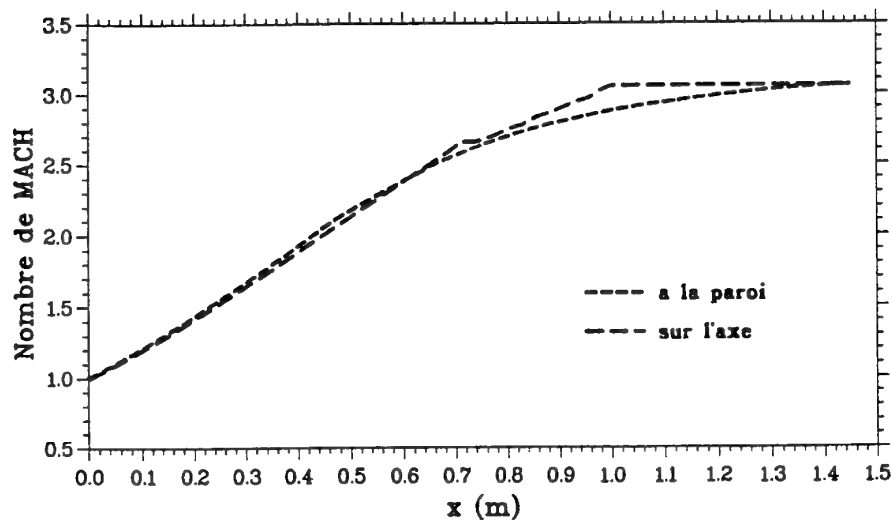


Fig. 4 Nombre de Mach sur l'axe et à la paroi de la soufflerie R1Ch.

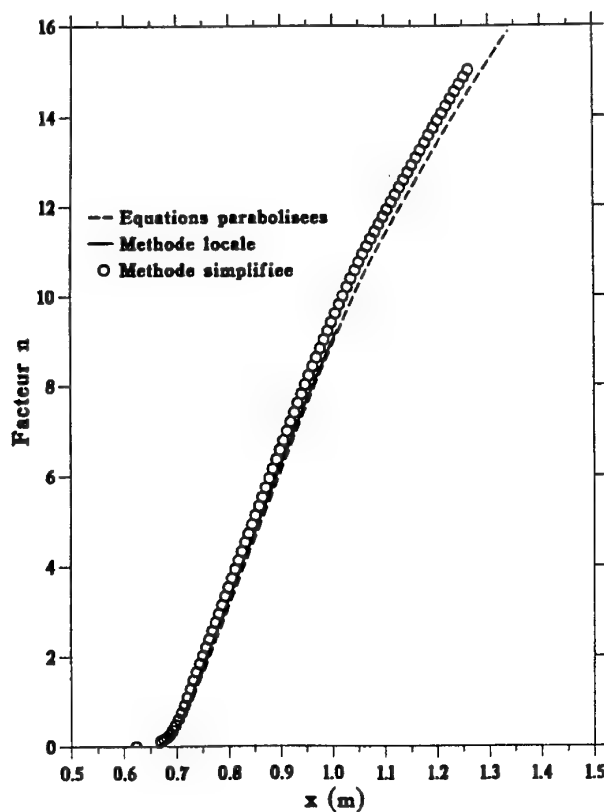


Fig. 5 Facteur N des tourbillons de Görtler pour une pression génératrice de 10×10^5 Pa.

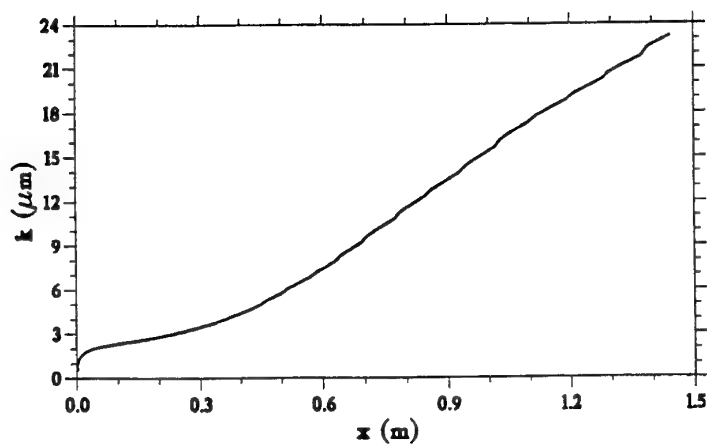


Fig. 6 Rugosité admissible pour une pression génératrice de 10×10^5 Pa.

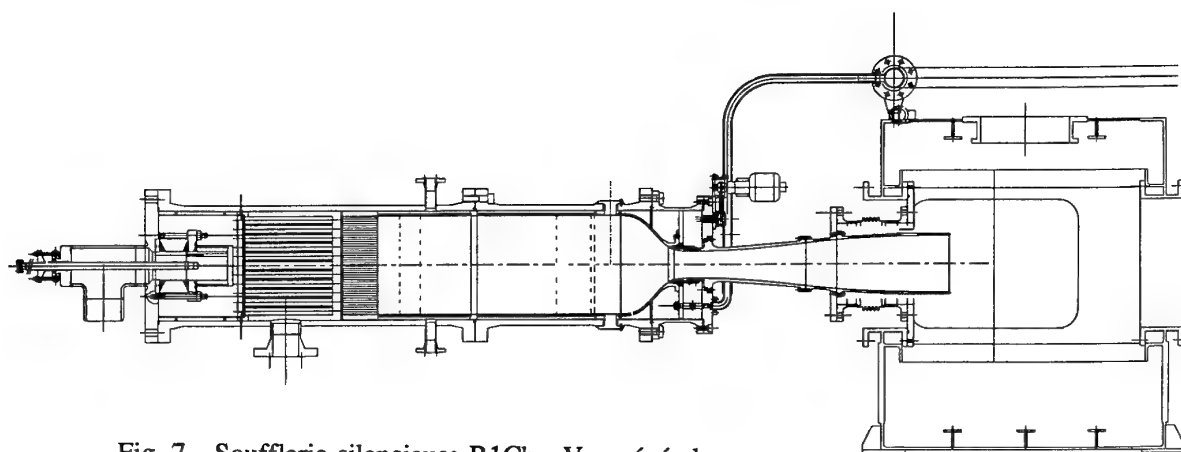


Fig. 7 Soufflerie silencieuse R1Ch - Vue générale

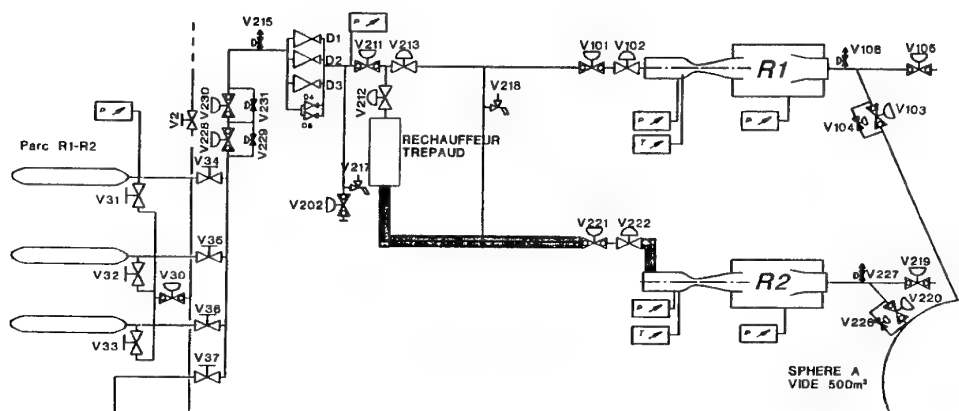


Fig. 8 Circuit d'alimentation en air comprimé

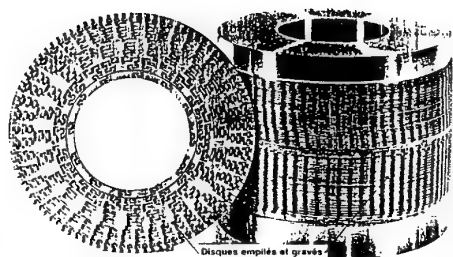


Fig. 9 Disques de laminage de la vanne silencieuse "Control Component"

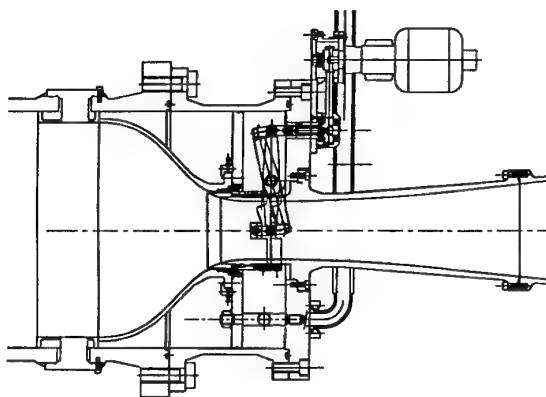


Fig. 10 Mécanisme de réglage de l'aspiration de la couche limite

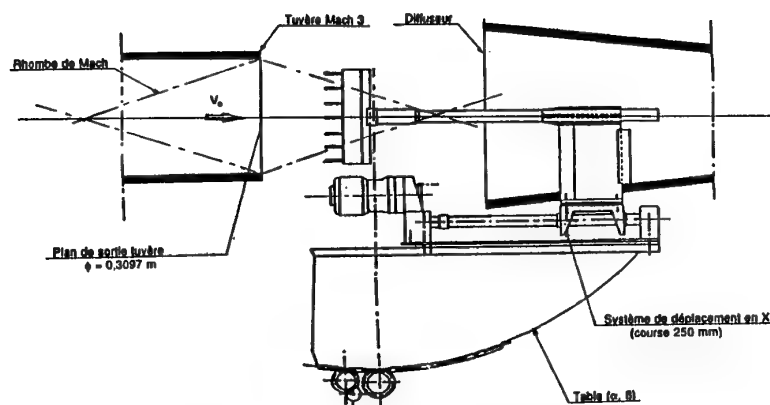
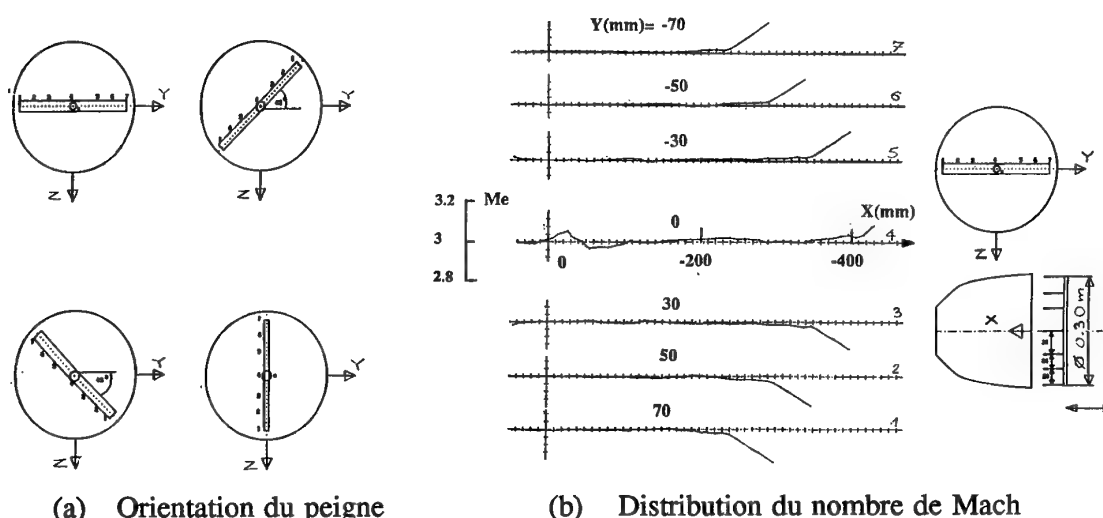


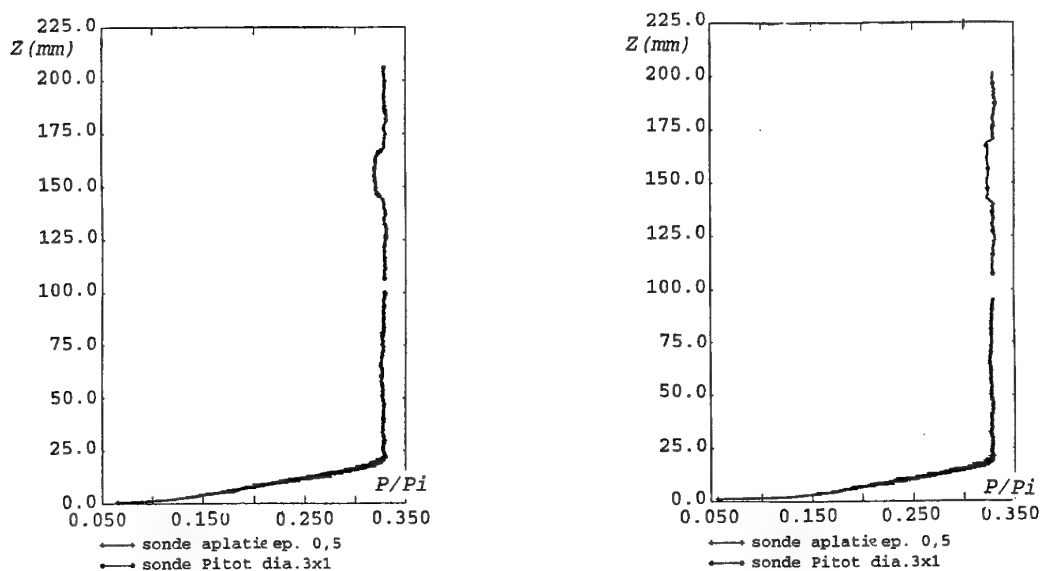
Fig. 11 Sondage de pression d'arrêt dans la veine d'expérience.
Dispositif de déplacement longitudinal



(a) Orientation du peigne

(b) Distribution du nombre de Mach

Fig. 12 Qualification de la veine d'expérience



(a) $P_o = 2 \times 10^5$ Pa ; sans aspiration

(b) $P_o = 8 \times 10^5$ Pa ; avec aspiration

Fig. 13 Sondage transversal de pression d'arrêt

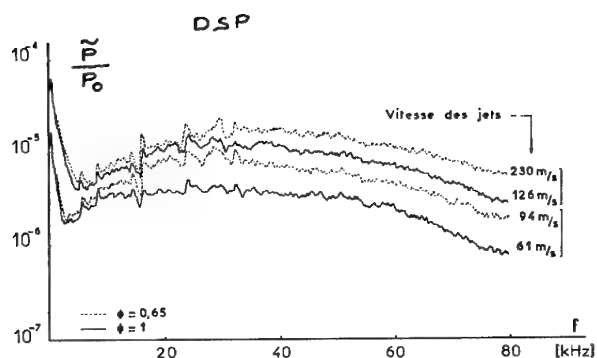


Fig. 14 Fluctuations de pression dans la chambre d'alimentation

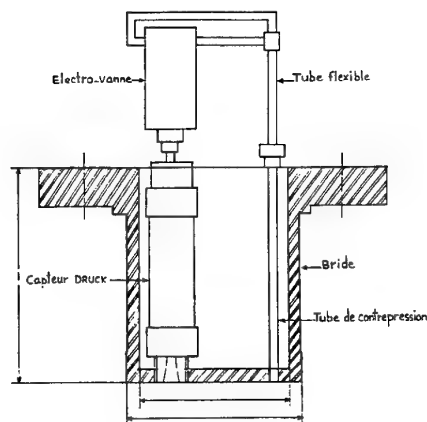


Fig. 15 Dispositif de mesure des fluctuations de pression basses fréquences avec capteur différentiel Druck

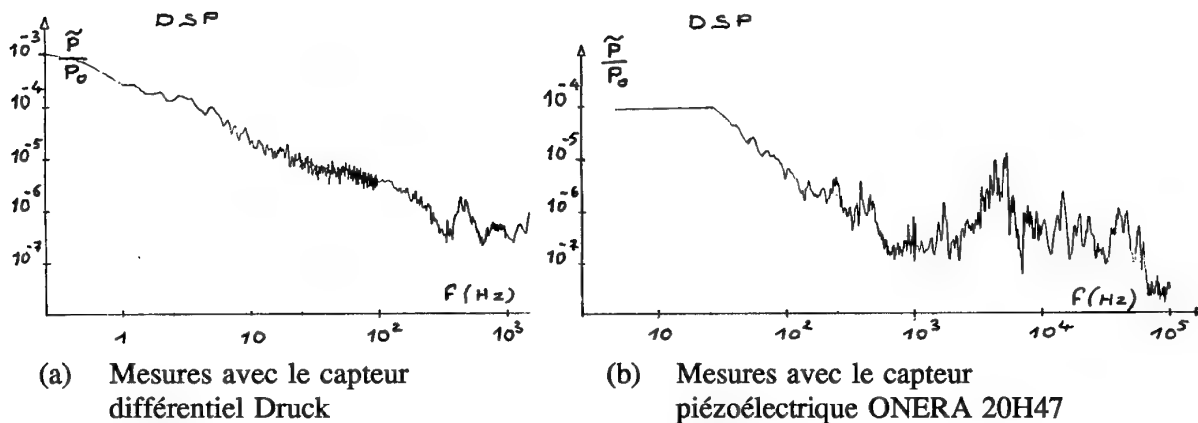
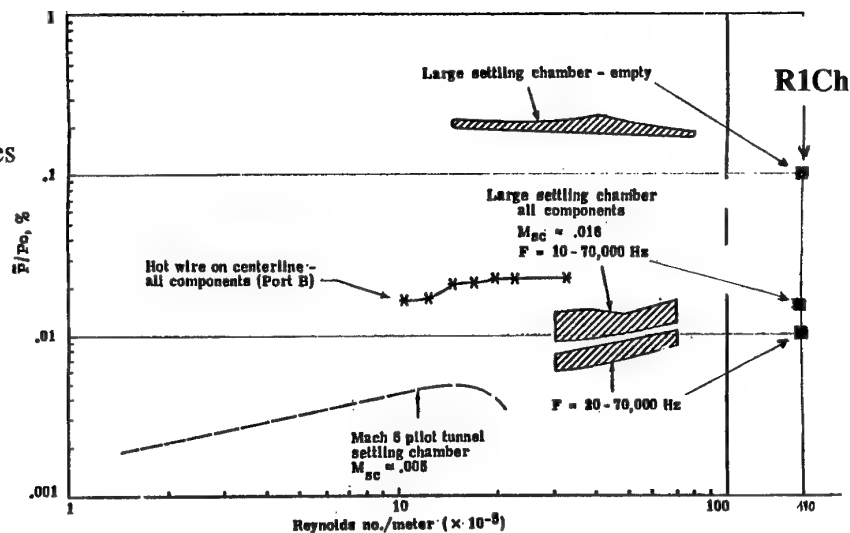


Fig. 16 Fluctuations de pression dans la chambre de tranquillisation

Fig. 17 Comparaison des niveaux de bruit entre les souffleries R1Ch et la Supersonic Pilot Quiet Tunnel (NASA Langley) [réf. 10]



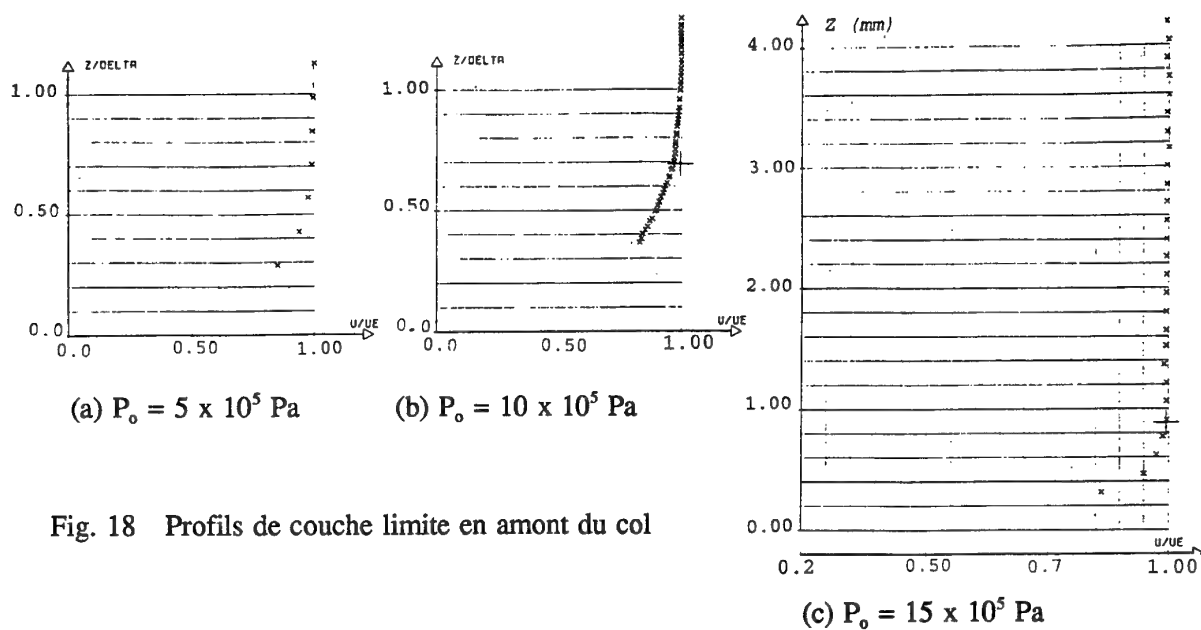


Fig. 18 Profils de couche limite en amont du col

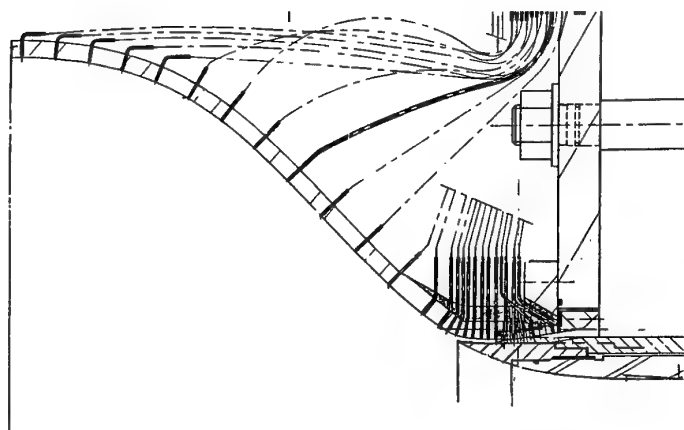
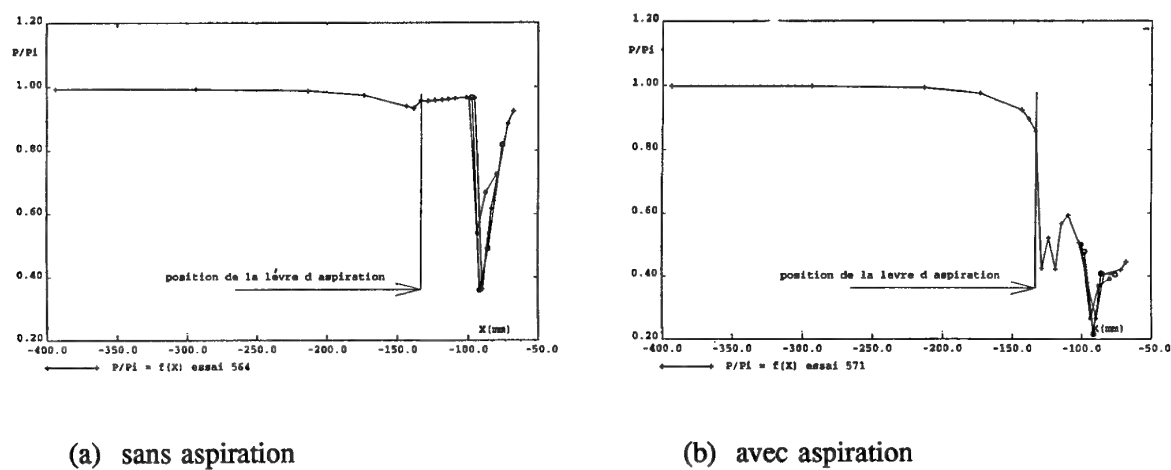


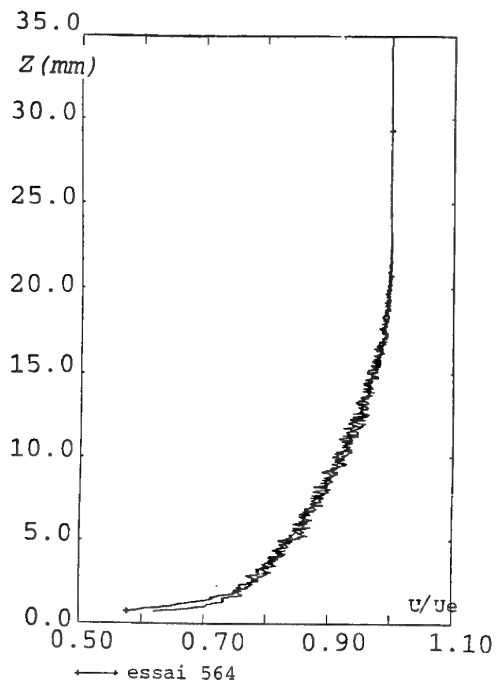
Fig. 19 Implantation des prises de pression dans le collecteur et la fente d'aspiration



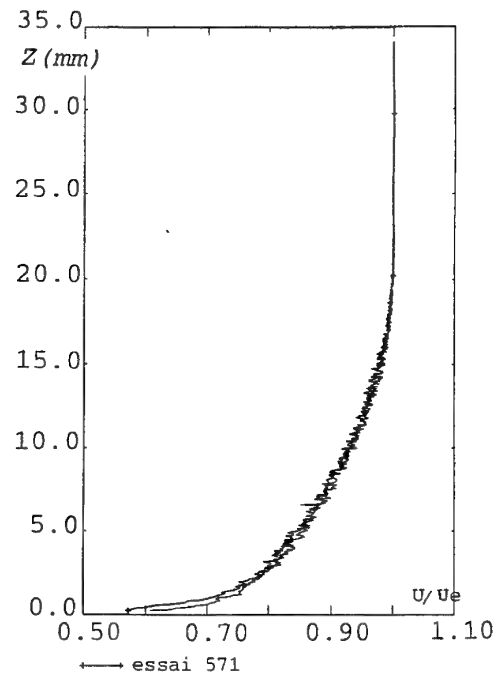
(a) sans aspiration

(b) avec aspiration

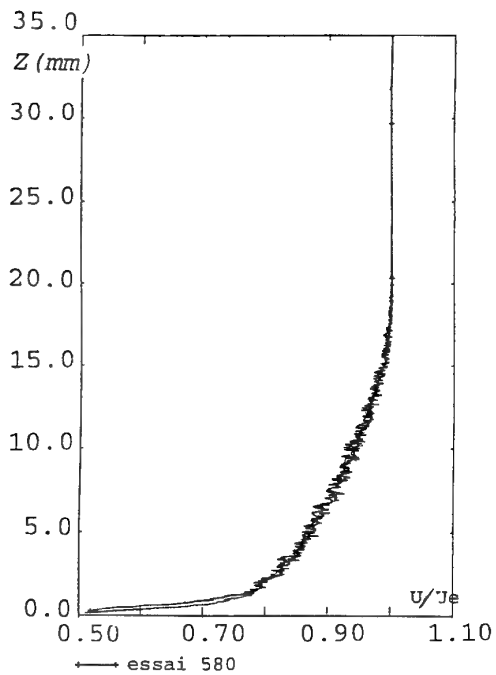
Fig. 20 Pressions pariétales dans le collecteur et la fente d'aspiration



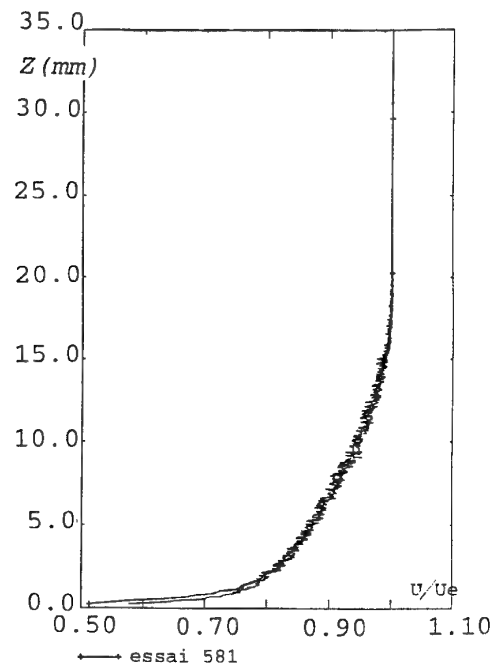
(a) $P_o = 2 \times 10^5$ Pa
sans aspiration



(b) $P_o = 2 \times 10^5$ Pa
avec aspiration



(c) $P_o = 8 \times 10^5$ Pa
sans aspiration



(d) $P_o = 8 \times 10^5$ Pa
avec aspiration

Fig. 21 Profils de couche limite dans le plan de sortie de la tuyère

Fig. 22 Implantation dans la tuyère de la plaque plane équipée de fluxmètres

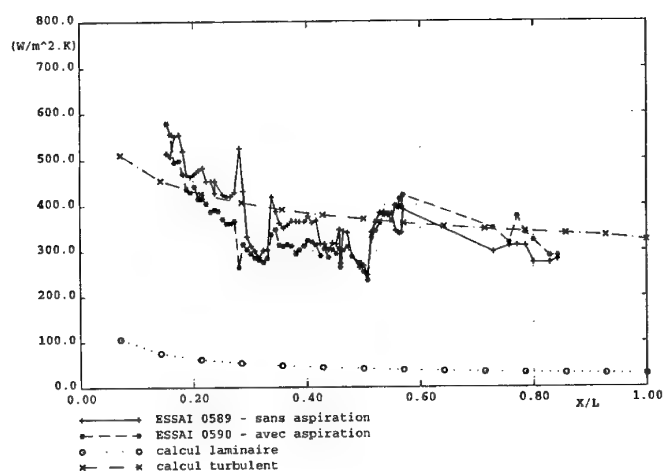
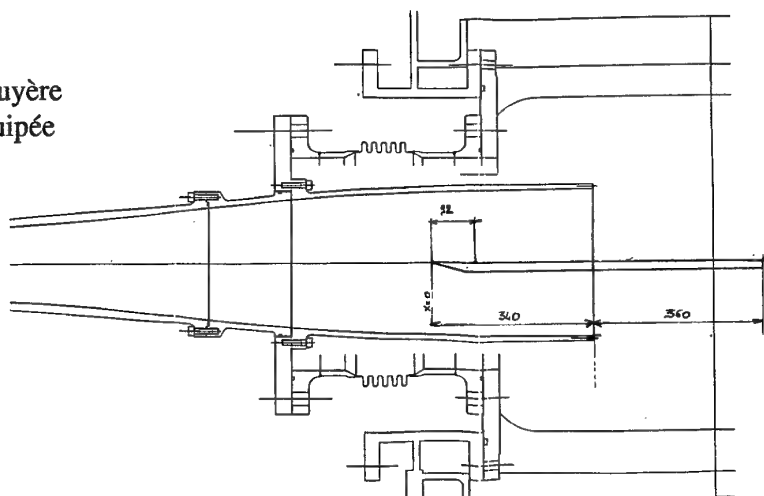
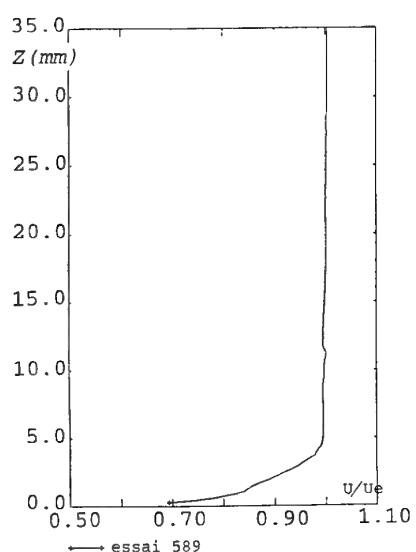
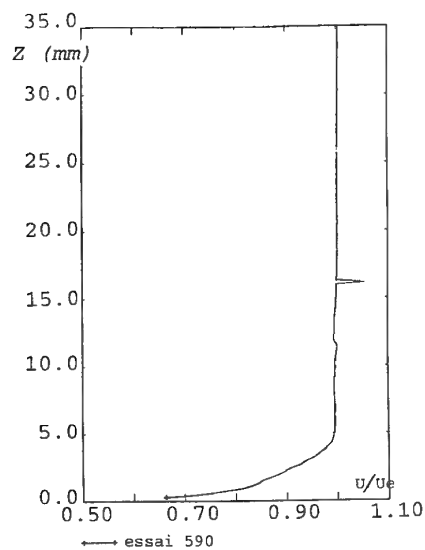


Fig. 23 Distribution de flux sur la plaque plane (comparaison calcul - expérience)



(a) $P_o = 8 \times 10^5$ Pa
sans aspiration



(b) $P_o = 8 \times 10^5$ Pa
avec aspiration

Fig. 24 Profils de couche limite sur la plaque plane (à mi - longueur)

CHARACTERISTICS OF THE NASA-AMES LAMINAR FLOW SUPERSONIC WIND TUNNEL FOR UNIQUE MACH 1.6 TRANSITION STUDIES

Stephen W.D. Wolf* and James A. Laub**

Fluid Mechanics Laboratory Branch

Mail Stop 260-1

NASA Ames Research Center

Moffett Field, California 94035-1000, USA

1. SUMMARY

Flow quality measurements have been performed in the unique Laminar Flow Supersonic Wind Tunnel (LFSWT) to examine both mean and dynamic characteristics. The intent was to provide the necessary flow information about this ground test facility, to support meaningful transition research at Mach 1.6 and flight unit Reynolds numbers. This paper is intended to assist other experimentalists with similar goals of characterizing low-supersonic test environments. An array of instrumentation has been used to highlight the importance of proper selection of pressure instruments and data acquisition procedures. We conclude that the test section is low-disturbance (based on classical standards of pressure disturbances less than 0.1% with no specified data bandwidth), and has uniform flow. This is confirmation that the quiet design features of the LFSWT are effective. However, characterization of the test section flow over a 0.25k-50k bandwidth shows that the disturbance levels can be greater than classical standards particularly for stagnation pressures < 9.5 psia (0.65 bar) with low stagnation temperatures. Variability of the flow disturbances in the settling chamber and test section is contained in a narrow frequency bandwidth below 5k Hz, which is associated with resonant frequencies from the pressure reduction system. So far, these disturbances have not impacted transition along the tunnel walls or a 10° cone. However, continual vigilance is required to maintain a known low-disturbance environment for transition research in the LFSWT. Furthermore, the formation of standards for flow quality measurements is strongly recommended, so that transition research can be better isolated from tunnel disturbances.

2. LIST OF SYMBOLS

α Angle of attack, incidence
 M_∞ Free stream Mach number
 P_o Tunnel stagnation pressure
 P_{rms} Total pressure rms

P_t Free stream total pressure
 P_∞ Free stream static pressure
 Re Unit Reynolds number per foot
 T_o Tunnel stagnation temperature
 T_w Tunnel wall temperature
 u' Velocity perturbation
 U_∞ Free stream velocity
 X Streamwise station relative to nozzle throat station (positive downstream) - in inches
 Y Vertical station relative to centerline (positive up) - in inches
 Z Spanwise station relative to centerline (positive right looking upstream) - in inches

3. INTRODUCTION

An unique, low-disturbance (quiet) supersonic wind tunnel was commissioned at the NASA-Ames Fluid Mechanics Laboratory (FML) in 1994 to support Supersonic Laminar Flow Control (SLFC) research. Known as the Laminar Flow Supersonic Wind Tunnel (LFSWT), this tunnel is designed to operate at potential cruise Mach numbers and unit Reynolds numbers (Re) of the High Speed Civil Transport (HSCT). The need to better understand the transition phenomena on the leading edge region of swept (HSCT) wings has provided the impetus for building this tunnel.

Low-disturbance or "quiet" wind tunnels are now recognized as an essential part of any meaningful boundary layer transition research. In particular, the receptivity of supersonic boundary layers to wind tunnel disturbances can significantly distort the transition phenomena under investigation. This factor has added much confusion to transition research in the past.

The definition of quiet flow, as we currently know it, is based on achievable and measurable levels of low disturbances. Ultimately, this definition must be linked to the range of actual atmospheric disturbances at HSCT supersonic cruise altitudes (47,000 to 60,000 feet), and a better understanding of transition receptivity to different

* Senior Research Scientist, MCAT, Inc.

** FML Facility Operations Manager

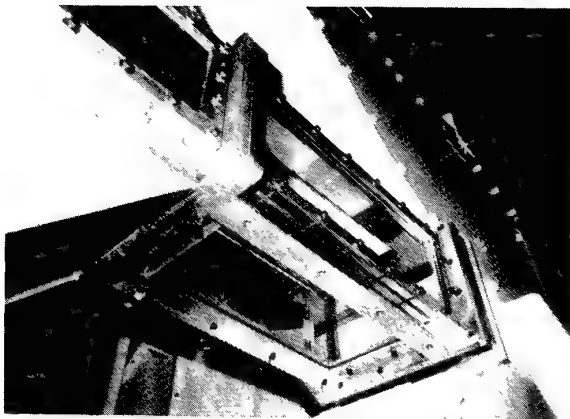


Fig. 1 - LFSWT test section viewed from below to show that windows are fitted to all four walls.

disturbance characteristics. Currently, the consensus is that flow is "quiet" if the free stream is spatially and temporally uniform with acoustic and convected disturbances (ratio of total pressure rms to total pressure - P_{rms}/P_t) less than 0.1%. This consensus forms the basis of what we can now call a classical standard, albeit with no reference to disturbance bandwidth.

This standard is typically met with laminar boundary layers on the supersonic nozzle and test section walls, and pressure disturbance levels in the settling chamber (P_{rms}/P_o) less than 0.2% and velocity (vortical) fluctuations (u'/U_∞) less than 1%. Additionally, the potential adverse effects of wall vibrations in the nozzle and test section, and shock movements in the supersonic diffuser need to be minimized, in the absence of known acceptable levels.

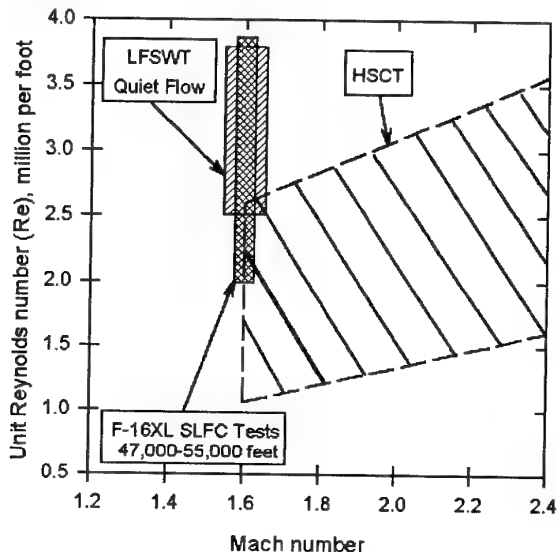


Fig. 2 - Comparisons of LFSWT Reynolds number envelope with flight at HSCT cruise conditions.

The LFSWT design is based on the concept behind the Jet Propulsion Laboratory (JPL) 20-inch supersonic tunnel, which is recognized as the first quiet supersonic tunnel used by Laufer for pioneering transition research starting in the mid-1950s.¹ The LFSWT has an 8 inch (20.32 cm) high, 16 inch (40.64 cm) wide and 32 inch (81.28 cm) long test section, designed with all-round optical access (as shown on Figure 1).

The LFSWT is the first low-supersonic wind tunnel purpose built for quiet operation.² The quiet features of the LFSWT are different from those of the NASA-Langley quiet wind tunnels, which operate at Mach 3.5 and above with much higher test Reynolds numbers.³ The distinctive aerodynamic features of the LFSWT are a low-disturbance settling chamber, laminar boundary layers on the nozzle and test section walls, vibration isolation of the test section/nozzle/settling chamber, and steady supersonic diffuser flow. Furthermore, the LFSWT runs continuously at unusually low stagnation pressures using an indraft injector drive system², with uniquely low compression ratios (less than unity). This test envelope provides a unit Reynolds number (Re) range from 2.5 to 3.8 million per foot (8.2 to 12.5 million per meter), which encompasses flight conditions at Mach 1.6 (as shown on Figure 2).

Flow measurements have been made in both the test section and settling chamber of the LFSWT to document if the tunnel meets or exceeds the classical standards for quiet flow. A special 3-axis traverse mechanism was built for these measurements in the test section (See Figure 3).⁴ A full range of instruments (miniature pressure transducers, hot-wires, thermocouples, five-hole probes, and Schlieren/shadowgraph flow visualization) were used for these measurements. We consider that the use of all available measurement

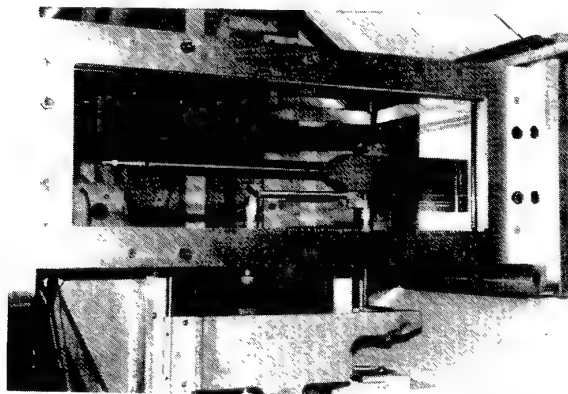


Fig. 3 - View of 3-axis traverse mechanism installed in the LFSWT test section. The Y and Z drive motors can be seen mounted below the test section.

techniques is the best means of mapping and quantifying the quality of the tunnel test core. Furthermore, we have identified significant differences between repeat measurements made using different pressure instrumentation, as discussed later.

A subjective test of the LFSWT flow quality, using a 10° cone, is reported. This test represents an international pseudo-standard for wind tunnel flow quality. There is a wealth of transition data on the 10° cone in flight and large-scale wind tunnels. Hence, the 10° cone test offers an opportunity to compare the LFSWT flow quality with other data sources, provided that adequate precautions are taken to avoid transition bypass due to roughness and nose bluntness.

The normal wind tunnel mean-flow calibration parameters: Mach number uniformity, flow angularity, and stability of controllable test parameters have been found to be within acceptable limits.⁴ Furthermore, time-averaged pressures on a swept wing have been used to confirm the quality of the LFSWT mean flow against CFD predictions.⁴

This paper provides a synopsis of the flow quality measurements made in the LFSWT thus far. This work is intended to help identify those tunnel design parameters which are most important to achieving a quiet test environment at low supersonic speeds. Furthermore, the characterization of the LFSWT flow disturbances (being fed into a model's boundary layers) forms part of the boundary conditions for each experiment. In this way, future transition research will be performed in a better known and controlled test environment, with the possibility of boundary layer receptivity to unknown disturbances minimized.

4. LFSWT DESCRIPTION

A detailed description of all tunnel components is contained in Reference 2. A schematic of the settling chamber components is shown on Figure 4. For completeness, this section contains details of the pressure reduction elements, contraction, nozzle and test section.

4.1 Pressure Reduction Elements

The pressure reduction elements form the pressure reduction system at the inlet to the settling chamber. The elements are necessary to provide a suitable back pressure in the inlet piping when supplying up to 27 lbs/sec (12.25 kg/sec) of air to the tunnel. This back pressure minimizes the pipe size required to prevent flow choking, which reduces cost and complexity. The elements also provide a reasonable means of spreading the flow from the inlet piping to the settling chamber (a 38:1 expansion ratio), and some noise isolation of the settling chamber from inlet piping noise (valves, turns etc.).

The pressure reduction system consists of up to three concentrically mounted cans, as found in a typical muffler (silencer) (See Figure 4). The elements are made of perforated plate with solid endplates on all but the third (downstream) element. The second and third elements are lined with sheets of porous sintered filter material (call Rigimesh). The Rigimesh used is Type-J, which is 0.006 (0.15 mm) thick and has a pore size of approximately 234 micro-inches (6 micron). The flow out of the third element remains predominantly orthogonal to the tunnel centerline, since the ratio of the flow area around the cylinder to the flow area of the endplate is 9.8:1. This situation assists the inlet flow to expand through the 3.28:1 area ratio, between the settling chamber and the third element.

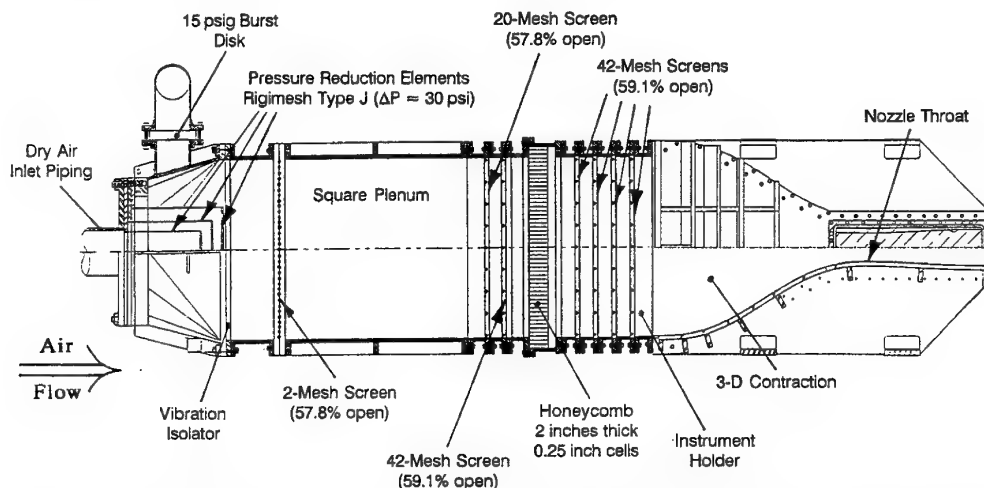


Fig. 4 - Schematic layout of the LFSWT settling chamber, with flow from left to right (to scale).

During the course of these experiments, the pressure reduction system was operated with and without the first (upstream) element, to alter the inlet conditions. The pressure drop associated with the elements was approximately 2.5 times P_o with the first element removed. This pressure drop increased to approximately 3.2 times P_o with the first element installed.

4.2 Contraction and Nozzle

The nozzle and contraction are fabricated as one component out of 6061-T6 aluminum, as shown on Figure 5. This material was chosen to take a fine polish and also for its corrosion resistance. The complete assembly is 75.38 inches (1.91 m) long, consisting of 48 inches (1.22 m) of three-dimensional contraction and 27.38 inches (69.54 cm) of nozzle, from throat to exit.

The shape of the 3D contraction was calculated using fifth-order polynomials. Since the settling chamber is 39.24 inches (0.99 m) square, the contraction ratio based on the throat dimensions is 6.2:1 vertically and 2.45:1 horizontally, which combine to give an overall high contraction ratio of 15.25:1. (The overall contraction ratio based on the test section dimensions is 12:1, which is above average). The ratio of contraction length to unit area change is 0.86:1 horizontally, and 1.46:1 vertically. Ratios of one or greater are preferred, but design compromises led to a less than optimum sidewall contraction.

The corners between the contraction walls are near sharp, since the floor and ceiling were made separately and fit between the sidewalls. No radius was introduced in the corners to delay or modify corner flows, but this is an option for the future.

The nozzle is 2D, fixed-block type designed according to the methodology of Riise⁵ (as used on the JPL-SWT

nozzle) with allowance for laminar boundary layer growth on all four walls. Consequently, the nozzle has an 1.267:1 area ratio which is larger than the theoretical value (1.25:1) for Mach 1.6 flow. The nozzle has a relatively long expansion section (compared to other design methodologies⁶) with surface curvature minimized. The maximum Görtler number along the nozzle walls is about 7 (safely below the accepted transition threshold of 10.4), at a location some 19 inches (47.5 cm) from the throat.

Both the nozzle and contraction flow surfaces were hand finished to an achievable 10L standard (roughness height 10 micro-inches - 0.25 micron), which is a mirror-like finish (See Figure 5). This roughness corresponds to a maximum roughness Reynolds number of 3.3 at the nozzle throat, which is below the generally accepted limit of 12 for laminar flow.³ The 10L standard is an rms roughness, which could hide 100 micro-inch peaks (ten times the rms value according to Beckwith).

The weight of the nozzle and contraction is supported by Korfund vibration isolators. Since the settling chamber has vibration isolation from inlet piping, and the test section has vibration isolation from the injectors, the nozzle and contraction structure experiences minimal vibration. A capacitive-type accelerometer mounted on the nozzle sidewall has recorded accelerations of only 0.02 g over a frequency range up to 1000 Hz, with the tunnel running. Of course, the large mass of the nozzle and contraction (2,354 lbs - 1,068 kg) also helps eliminate vibration due to radiated noise.

4.3 Test Section

The test section is 8 inches (20.32 cm) high, 16 inches (40.64 cm) wide at its entrance, and 32 inches (81.28 cm) long. The design consists of four windows and a frame. Like the nozzle, a rectangular cross-section was chosen for the test section to move the flow corners away from the tunnel centerline. The general-purpose windows are made of 2.0 inches (5.08 cm) thick optical quality Plexiglas (UVT grade), and account for 61% of the test section surface area (as shown on Figure 1). The frame is fabricated from 6061-T6 aluminum. To minimize steps and gaps, the windows are manufactured with an interference fit to their frames at room temperature. A 5° taper is provided on the joint between window and frames, to simplify window removal and replacement.

The test section floor and ceiling diverge at a total angle of 0.5° downstream as an allowance for boundary layer growth on all four walls. The sidewalls are parallel. The test section is cantilevered from the nozzle contraction, and the critical joints with the nozzle are hand finished to

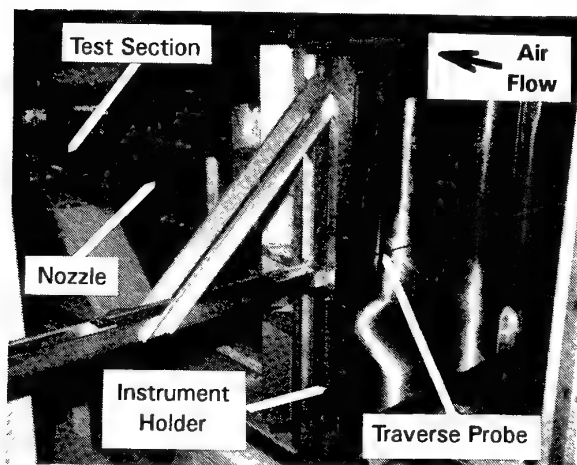


Fig. 5 - LFSWT contraction exposed during the fitting of the settling chamber traverse.

the same 10L standard applied to the nozzle and test section flow surfaces.

The downstream end of the test section is attached to the supersonic diffuser/injectors by a rubber isolator, to prevent conduction of injector vibration into the test section/nozzle structure. A capacitive-type accelerometer mounted on the test section sidewall frame has recorded horizontal accelerations of 0.015 g over a frequency range up to 1000 Hz, with the tunnel running.

5. LFSWT INSTRUMENTATION

The instrumentation used in our flow quality measurements includes the following: pitot and five-hole probes for steady-state measurements; hot-wires plus miniature pressure transducers (Kulites) for dynamic measurements; thermocouples for temperature distributions; and schlieren/shadowgraph for flow visualization. More details can be found in References 2 and 4.

A custom-built single 5-micron (200 micro-inch) Tungsten wire was used in the test section probe, and a Dantec single 5-micron (200 micro-inch) platinum-coated Tungsten wire in the settling chamber. Both hot-wires were powered by the Fluid Mechanics Laboratory's own constant-temperature bridge circuits. Tuning of the circuits was completely manual using a square wave signal. Optimum tuning was achieved with the tunnel running, such that a hot-wire response of 80k Hz was possible in the settling chamber and 25k Hz in the test section. The output signals from the hot-wires were fed to a Tektronix 2642A Fourier Analyzer system, which can analyze up to 4 simultaneous inputs. The Fourier Analyzer usually samples each input signal at 400k Hz (with 16-bit resolution) using a Hanning window and anti-alias filtering. The Analyzer also provides averaged 4096-point real-time Fast Fourier Transforms (FFTs), data capture and display. Twenty FFTs were averaged for each power spectra discussed here. However, the operator acquired several averaged power spectra at each test condition to determine the 'best' average. All data were then collected on a PC computer for data archiving, post processing and data presentation. A bandwidth of 0.25 to 50k Hz was chosen to remove low frequency noise and high frequency roll-off from our measurements.

The settling chamber hot-wire was calibrated in-situ by varying P_o during tunnel operation, which corresponded to changing only the flow density (since the LFSWT nozzle throat is fixed). A simple King's law relationship defines the wire's response very well. However, the calibration does rely on the assumption that the hot-wire's response to density changes is the same as the hot-wire's response to velocity changes. This is a reasonable

assumption for the range of settling chamber conditions encountered. Fluctuating flow quantities were obtained from the sensitivity of the mean hot-wire voltage to mass flow changes (the product of density times velocity) after subtracting a wind-off rms voltage. The wire sensitivity was computed from mean data recorded at the same time as the fluctuating data.

Various miniature dynamic pressure (Kulite) transducers were used with frequency responses beyond 150k Hz. These transducers varied in diameter from 0.050 inch (1.27 mm) up to 0.093 inch (2.36 mm). The 0.050 inch (1.27 mm) diameter Kulite had no screen to protect the pressure sensor. Larger Kulites were fitted with a Kulite M-type screen. Kulite excitation voltages were manufacturer recommended unless otherwise stated.

The Kulites were powered by high-frequency response signal conditioners (Dynamic 8000s with a 3dB drop-off at 500k Hz). The output signals were fed to the previously described Fourier Analyzer for capture, analysis and display, as for the hot-wire signals. The Kulites are sensitive to changes in stagnation temperature (T_o), so in-situ calibrations were made for each run. Fluctuating pressures were obtained using the transducer sensitivity (DC output voltage verses mean pitot pressure) for each run. This sensitivity was calculated from the steady-state data, recorded with the fluctuating data.

6. FLOW QUALITY MEASUREMENTS

6.1 Settling Chamber

Settling chamber flow measurements were made to determine pressure, velocity and temperature fluctuations. For the duration of these measurements, the pressure reduction system mounted at the inlet to the settling chamber was fitted with only two elements (see Figure 4). During the course of the test section measurements, it became necessary to change the number of pressure reduction elements to three in an attempt to minimize disturbances, as described in the next sub-section.

The settling chamber probes were supported from both sidewalls, 1 inch (2.54 cm) downstream of the last screen ($X=-51.5$) at the contraction entrance/instrument holder (see Figures 4 and 5). The probes could be traversed across the entire span of the settling chamber.² The XCS-093 Kulite was used to measure pressure fluctuations, a 5-micron (200 micro-inch) platinum coated tungsten hot-wire was used for the velocity fluctuations, and a type-T thermocouple pitot was used for the temperature distributions.

The pressure fluctuations on the centerline of the settling

chamber are summarized on Figure 6, over the bandwidth 0.25-50k Hz. We observed that the pressure fluctuations are at a minimum when stagnation pressure $P_o = 7.5$ psia (0.52 bar). However, the pressure fluctuations remain below 0.2% over the entire P_o range. It is interesting to see that the signal to noise ratio drops to unity at low P_o values, which serves to highlight the difficulty of low-disturbance measurements.

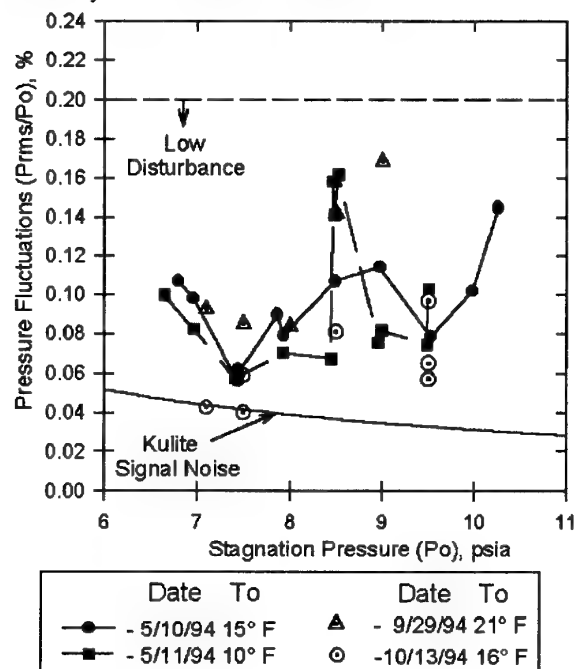


Fig. 6 - Comparison of settling chamber pressure fluctuations data sets taken at different T_o ($X=-51.5$; $Y=0$; $Z=0$; Bandwidth 0.25-50k Hz).

Post-test examination of the data repeatability shows that an unstable flow condition existed in the settling chamber, which was centered around $P_o = 8.5$ psia (0.58 bar). This instability is contained within a variable 1.85k Hz spike in the Kulite spectra (as shown on Figure 7 for the measured $Prms/P_o$ extremes). Furthermore, this instability tended to be more prevalent when the stagnation temperature was low (i.e. the unit Reynolds number was higher for a given P_o), as found in Winter testing with low T_o values.

The variations of pressure fluctuations across the settling chamber are shown on Figure 8 for two values of P_o . These streamwise measurements confirm that the flow is low-disturbance (fluctuations < 0.2%), but the left side appears to have higher disturbances than the right side. The data show that the mean pressure fluctuation is 0.087% at $P_o = 7.1$ psia (0.49 bar), and a lower 0.073% at $P_o = 9.5$ psia (0.65 bar). The standard deviation of the pressure fluctuations is also less at the higher P_o .

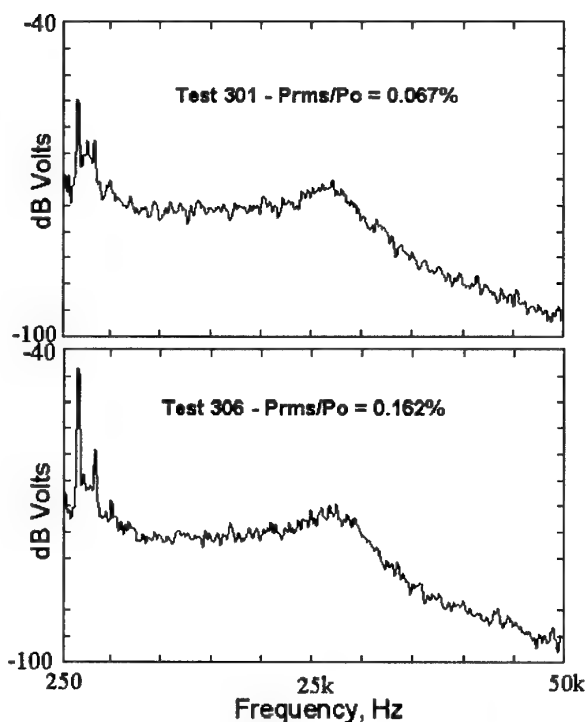


Fig. 7 - Effect of low frequency settling chamber flow instabilities on pressure fluctuation power spectra ($P_o = 8.5$ psia - 0.58 bar; $X=-51.5$; $Y=0$; $Z=0$; $T_o \sim 7^\circ F$ - 259 K).

Velocity fluctuations across the settling chamber are shown on Figure 9 for $P_o = 7.5$ and 8.5 psia (0.52 and 0.58 bar). There are significant differences. The $P_o = 7.5$ psia

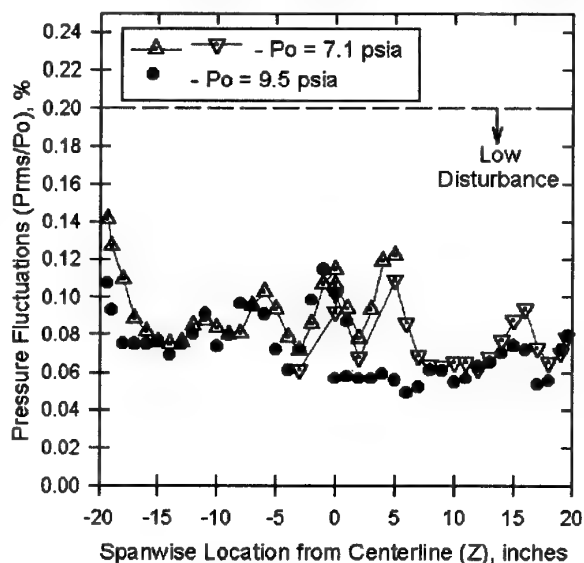


Fig. 8 - Spanwise distribution of pressure fluctuations in the settling chamber for two values of P_o , at near constant T_o ($X=-51.5$; $Y=0$; $T_o \sim 21^\circ F$ - 267 K; Bandwidth 0.25-50k Hz).

(0.52 bar) data show a mean velocity fluctuation of 0.648%, while the $Po = 8.5$ psia (0.58 bar) data show much more variation with a mean value of 1.06% (above the low-disturbance boundary). The data sets were taken from consecutive tests with only a small variation in the low Winter To from 1° to 3° F (256 to 257 K). The increased velocity fluctuations at $Po = 8.5$ psia (0.52 bar) are associated with the instability present in the pressure fluctuations (See Figure 7) at the same Po value. The hot-wire power spectra on the tunnel centerline clearly indicate that again disturbances below 2k Hz are responsible for variation in the measured velocity fluctuations.⁴ Consequently, we have found an interesting correlation between pressure transducer and hot-wire spectra in the settling chamber. The disturbance variations are at low frequencies in both cases, with a frequency shift between instruments.

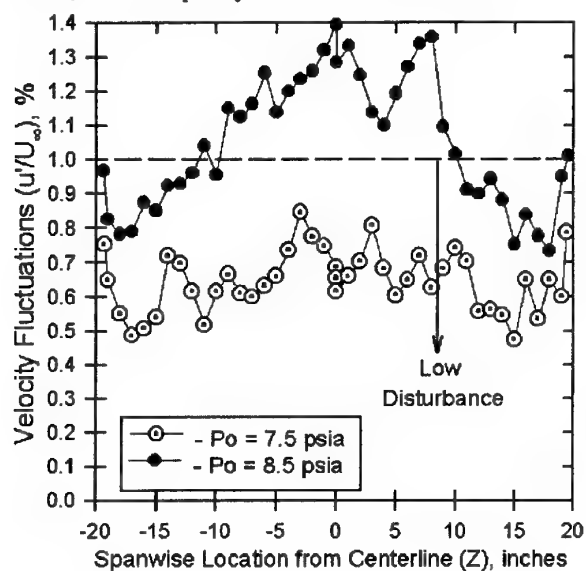


Fig. 9 - Spanwise variation of velocity fluctuations in the settling chamber at two values of Po , at low To ($X=-51.5$; $Y=0$; Bandwidth 0.25-50k Hz).

Interestingly, the $Po = 8.5$ psia (0.58 bar) velocity fluctuations indicate that 50% of the settling chamber flow (in one horizontal plane $Y=0$) is above the classical low-disturbance criteria for vortical disturbances ($<1\%$). However, the bandwidth of the rms calculation is a critical factor in this assessment, and is not specified in the classical criteria for low-disturbance flow. It is also noteworthy to observe that the distributions of velocity fluctuations are relatively symmetrical compared with the asymmetry of the pressure fluctuation distributions (See Figure 8). Variability in the performance of the pressure reduction system is certainly a possible explanation.

Temperature measurements across the settling chamber clearly show there is a thermal boundary layer on the relatively hot walls of the settling chamber. This thermal layer is typically about 2 inches (5.08 cm) thick. The temperature variation across the settling chamber (excluding the thermal boundary layers) is less than 0.9° F (0.5° C), which is within the resolution of the thermocouple used. More details are contained in Reference 4.

The temperature rise across the sidewall thermal boundary layer was found to be typically 16° F (8.8° C) in Winter ($T_w/To \approx 104\%$).⁴ Since, this temperature rise is dependent on the inlet air and tunnel wall temperatures (which are determined by ambient conditions), we can expect the rise to be less in the Summer. However, the walls of the tunnel will always be hot relative to the free stream, unless the inlet air can be heated.

6.2 Test Section

6.2.1 Free Stream Pressure Fluctuations

The flow quality measurements in the test section were made with different combinations of pressure reduction elements at the inlet to the settling chamber (See Figure 4). These changes were intended to minimize disturbances found during the course of our flow quality measurements, as discussed later.

With two elements in the pressure reduction system (as for the settling chamber measurements), flow characteristics in the test section were measured at three streamwise locations, $X = 29.88, 43.38$ and 54.38 . These locations correspond to the entrance-, mid- and exit-regions of the test section. A sidewall-mounted traversable pitot probe was used in this instance, mounted on the tunnel vertical centerline, at one streamwise location per run. The probe was fitted with an XCS-093 Kulite for pressure fluctuation measurements. The traverse could be fitted to either sidewall, allowing measurements over the entire 8 inch (20.32 cm) mid-span of the test section. Data measured from each sidewall overlapped by 2 inch (5.08 cm) to demonstrate repeatability between runs.

Pressure fluctuations (the ratio of total pressure rms to the mean pitot pressure - $Prms/P_t$) were computed over a similar frequency bandwidth to the settling chamber measurements (0.25k to 50k Hz). Centerline measurements are shown on Figure 10 over a range of Po . The worst disturbances appear in the mid-region of the test section, and are just above the quiet boundary (0.1%). It is interesting to note that the pressure fluctuations do not increase linearly with streamwise distance. Tunnel unstart occurred when a Po of 6.8 psia (0.47 bar) was

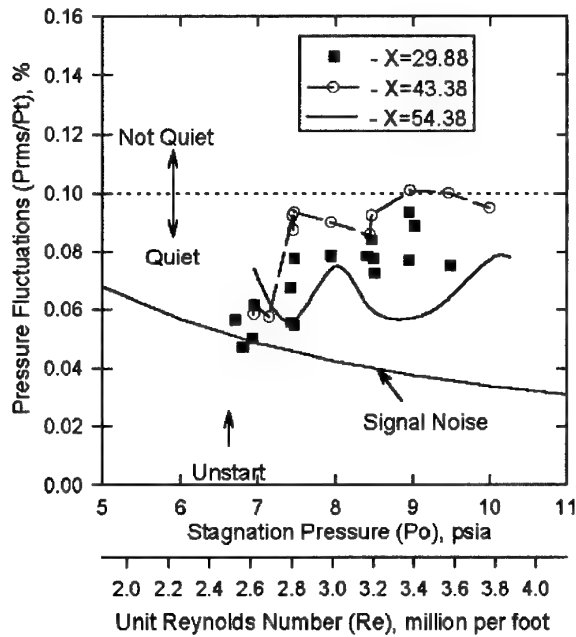


Fig. 10 - Test section (XCS-093 Kulite) pressure fluctuations on the tunnel centerline ($Y=0$; $Z=0$) over a range of P_o at three different streamwise locations ($T_o \approx 18^\circ \text{F} - 265 \text{K}$).

approached, with an empty test section. The unstart was easily detected by the erratic (flashing) and growing pressure fluctuations measured in the test section.

Spanwise pressure fluctuations are shown on Figure 11 near the test section entrance ($X=29.88$) for two different free stream disturbances, at $P_o = 7.5 \text{ psia}$ (0.52 bar). The settling chamber traverse was actually used as a disturbance generator to provide the case with above normal free stream turbulence. In effect a 0.25 inch (6.35 mm) diameter cylinder was stretched horizontally across the contraction entrance, with a pitot attachment placed on the tunnel centerline (See Figure 5). Interestingly, the wake of the pitot was observed in the test section 80.38 inches (2.04 m) downstream. The wake caused the pressure fluctuation non-dimensional quantity to reduce, despite a total pressure drop. The fact that the settling chamber cylinder and the test section traverse are in the same plane exaggerates the situation and more studies are required off the vertical centerline. Nevertheless, a small change in free stream turbulence in the settling chamber is seen to clearly destroy quiet flow away from the pitot wake. This finding again highlights the strong influence of free stream disturbances on flow quality in low-supersonic testing.

Repeat pressure fluctuation surveys were made at $X=29.88$ (in plane with the upstream edge of the sidewall

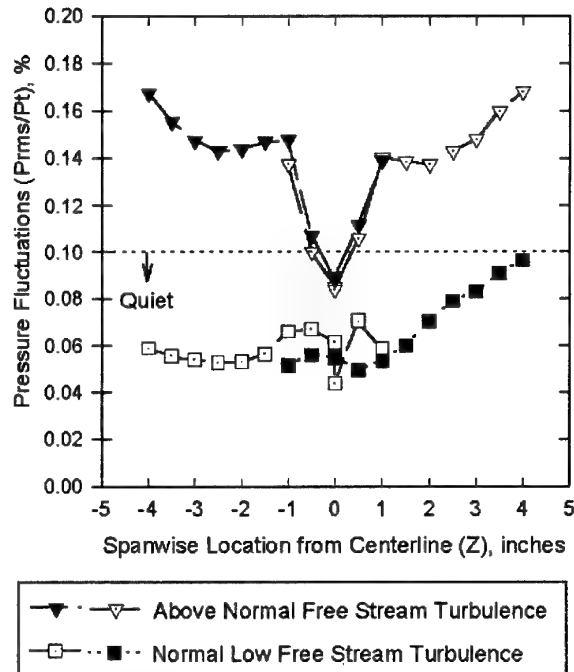


Fig. 11 - Spanwise distributions of XCS-093 pressure fluctuations near the test section entrance ($X=29.88$) with normal and above-normal free stream disturbances ($P_o \approx 7.5 \text{ psia} - 0.52 \text{ bar}$).

windows for ease of position sighting) using the 3-axis traverse, fitted with a smaller XCS-062 Kulite. The pressure fluctuation data across the test section are summarized on Figure 12. Clearly, the flow has

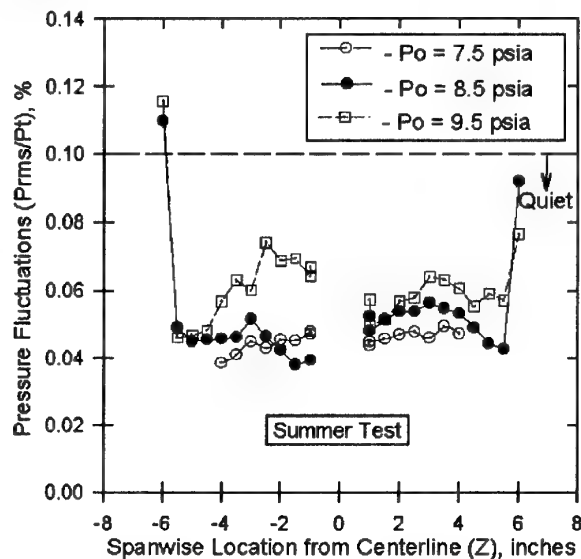


Fig. 12 - Spanwise variation of (XCS-062 Kulite) pressure fluctuations at the test section entrance, over a range of P_o ($X=29.88$; $Y=0$; $T_o \approx 17^\circ \text{F} - 265 \text{K}$; Bandwidth 0.25-50 kHz).

remained low-disturbance except for $-5.5 > Z > +5.5$, and the measurements indicate a flow field more uniform in the streamwise direction than previously found.²

Interestingly, the rise in pressure fluctuations at $Z = \pm 6$ can be attributed to the influence of the normal unstart shock (as shown in the schlieren picture on Figure 13) near the traverse probe tip. This effect occurred when the normal shock was positioned less than 3 inches (7.62 cm) downstream of the probe tip (by adjusting the traverse blockage). This finding serves as a reminder that disturbances can still be fed upstream in a supersonic flow through a boundary layer. However, in this case, this upstream influence is quite localized. The unsteadiness of the normal shock (which was small amplitude) was apparently unaffected by the probe or nose cone position relative to the shock. Both horizontal and vertical observations confirmed that the unstart shock was indeed normal in two dimensions, with lambda feet on the probe body (as shown on Figure 13).

Normal Shock

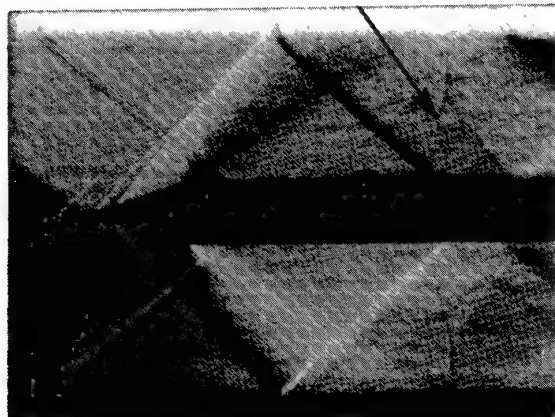


Fig. 13 - Schlieren visualization of Mach 1.6 flow round the 3-axis traverse with a normal shock present.

During repeat pressure fluctuation measurements made during Winter months (with the XCS-062 Kulite), we observed significant changes from our Summer data. The T_o varied from 17° to 1° F (265 to 256 K) for these two data sets. Examination of the Kulite power spectra has revealed that all the seasonal variations were contained at low frequencies (< 2 kHz) over the entire P_o range. This is the same frequency band which contains the variation in our spatial Kulite measurements in the test section and settling chamber. A typical comparison of Summer and Winter power spectra for $P_o = 8.5$ psia (0.58 bar) is shown on Figure 14. The energy spikes at 1.75 kHz and the associated harmonics in the Summer test can be seen to shift down to 1.12 kHz in the Winter test. This frequency shift and increased amplitude of the

noise spikes correspond to a 62% increase of the pressure fluctuations from Summer to Winter.

The signal to noise ratio for the test section pressure fluctuation data from the 3-axis traverse was a minimum of 8. A much higher value than obtained with the larger XCS-093 Kulite used in previous tests.² Also, the in-situ calibration of the XCS-062 Kulite was very stable despite the uncontrollable T_o changes. So, we had no concerns about the Kulite performance during the acquisition of the Winter and Summer sets of traverse data.

Winter spanwise variation of pressure fluctuations near the test section entrance ($X=29.88$; $Y=0$; $T_o \sim 1^\circ$ F - 256 K), are summarized on Figure 15. The pressure fluctuations are low-disturbance for $P_o < 8.5$ psia (0.58 bar) but are less uniform than before (See Figure 12). At $P_o = 9.5$ (0.65 bar), the Winter pressure fluctuations have grown above the 0.1% low-disturbance/quiet criteria over the entire span of the test section. The raw Kulite signals show that the variation across the tunnel span continued to be contained in a narrow frequency band below 2 kHz. Based on settling chamber and test section observations (like the near-centerline measurements shown on Figure 14), the spanwise variations are mostly likely temporal rather than spatial.

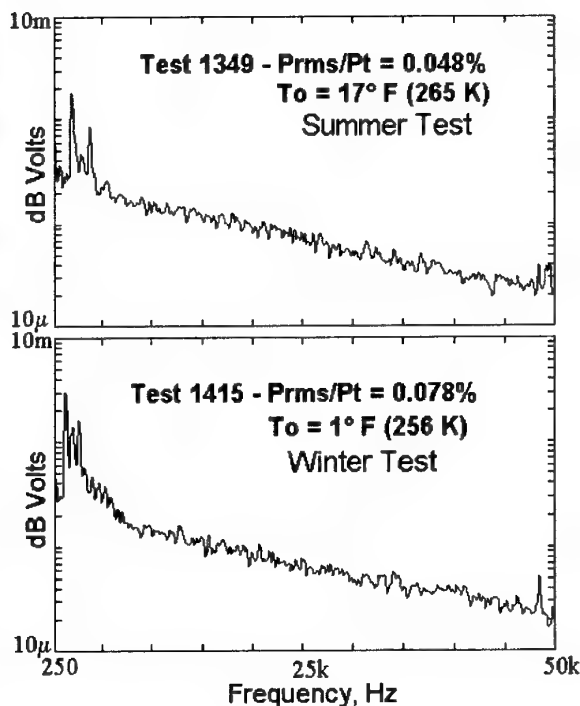


Fig. 14 - Comparison of XCS-062 pressure fluctuation power spectra at the same location and P_o , with different T_o test conditions ($X=29.88$; $Y=0$; $Z=+1$; $P_o=8.5$ psia - 0.58 bar).

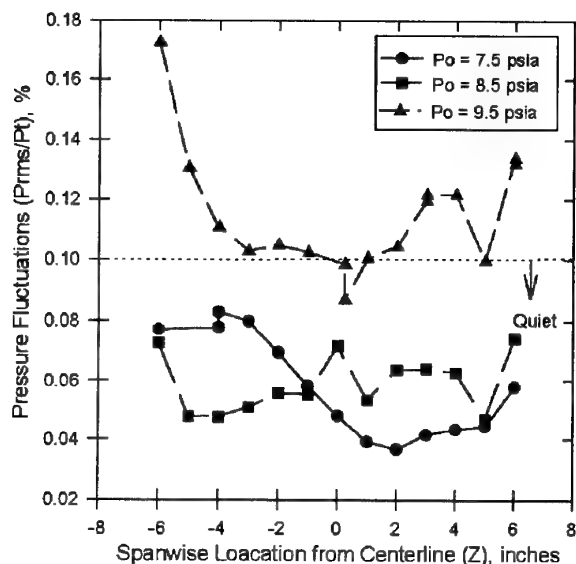


Fig. 15 - Winter spanwise variation of XCS-062 pressure fluctuations near the test section entrance at three values of P_o ($X=29.88$; $Y=0$; $T_o \approx 1^\circ F - 256 K$; Bandwidth 0.25 - 50k Hz).

In an effort to minimize seasonal variation, test section Kulite measurements were also made with three elements fitted to the pressure reduction system (since this was prime candidate for the source of seasonal noise changes). A comparison of centerline data, over the P_o range, is shown on Figure 16, for back-to-back tests with two and three elements fitted in the pressure reduction system. The three element data indicate a marked

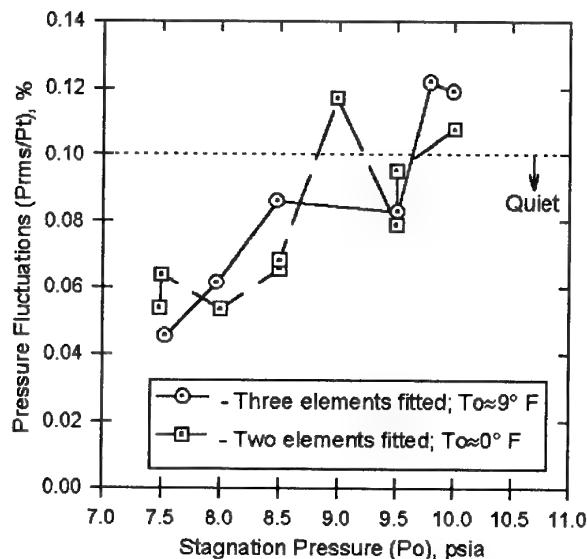


Fig. 16 - Comparison of centerline XCS-062 pressure fluctuations with two and three elements in the pressure reduction system ($X=35.0$; $Y=0$; $Z=0$; Bandwidth 0.25-50k Hz).

improvement in the stability of the pressure fluctuations for $P_o < 9.5$ psia (0.65 bar) during Winter testing. The onset of the flow instability appears to have been delayed, allowing quiet flow to be achieved at higher values of P_o , when T_o is low in the Winter.

Detailed examination of the Winter Kulite signals sampled at both the normal (400k Hz) and a lower (40k Hz) sampling rate showed no significant differences (see Figure 17).⁴ So, we are confident that our signal processing is not concealing any information, and no additional disturbance spikes were discovered.

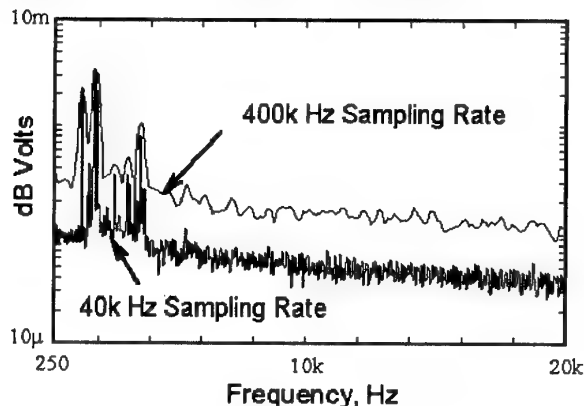


Fig. 17 - Effect of changing the sampling rate from 400k Hz to 40k Hz on the power spectra of XCS-062 Kulite signals ($X=35.0$; $Y=0$; $Z=0$; $P_o=8.5$ psia - 0.58 bar; $T_o=7^\circ F - 259 K$).

Furthermore, signal processing was performed over different bandwidths (for both sampling frequencies considered previously), which confirmed our observation that all the pressure disturbances and harmonics were contained below 5k Hz (as shown in Figure 18 for one sampling frequency). There is no noticeable effect of changing sampling rate, except for the inevitable frequency cut-off. Clearly, this study demonstrates the importance of bandwidth choice to the detection or not of flow disturbances. Of course, pressure transducer signals are more susceptible to noise contamination when low frequencies (near 0 Hz) are included in the signal processing. This is a primary reason for the general practice of ignoring low frequency spectra. In our case, low frequency is taken to mean below 250 Hz, and is based on actual study of the wind tunnel signals for the different instruments used.

6.2.2 Boundary Layers

Since we have found some quiet flow present in the test section, the nozzle and test section boundary layers must be laminar according to Laufer.¹ Tests were performed with the wall boundary layers tripped to turbulence to confirm this assertion. Transition was achieved with

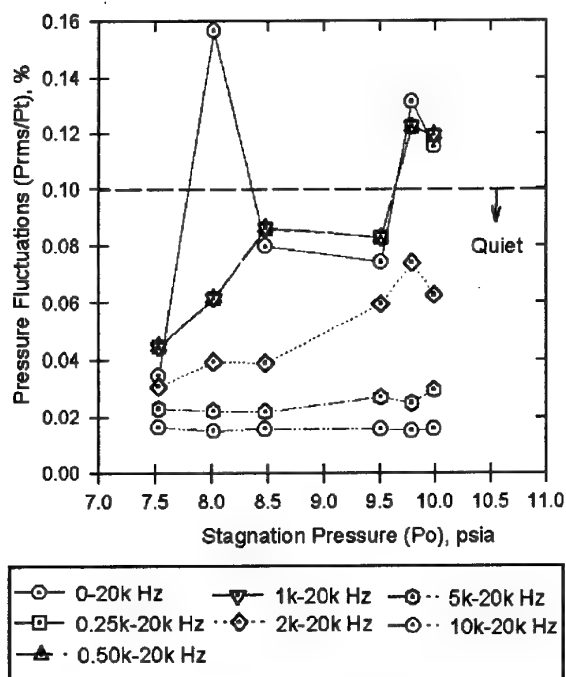


Fig. 18 - Variation of pressure fluctuations with P_o , using different data bandwidths for signal processing at a normal 400k Hz sampling rate ($X=35.0$; $Y=0$; $Z=0$; $T_o \approx 9^\circ \text{F} - 260 \text{K}$).

trips (approximately 0.5 inch - 12.7 mm wide strips of 80 grit sandpaper) applied to each of the four walls at the test section entrance. The total height of the trips was measured as 0.023 inch (0.584 mm). Centerline pressure fluctuations (using an XCS-093 Kulite) in the mid-region of the test section are shown on Figure 19, for the normal and tripped conditions. The centerline pressure fluctuations are significantly higher for the tripped case (order 0.25%), and were observed not to vary spanwise.

Examination of the power spectra of these Kulite signals (as shown on Figure 20 for the $P_o \approx 7.5$ psia - 0.52 bar case) reveals a broad band increase of signal power over the 0.25k-50k Hz bandwidth, which is indicative of noise radiating from a turbulent boundary layer. Interestingly, this difference was not evident in the spectra variations observed spanwise and streamwise in the test section with no trips fitted (See Figure 14).⁴

In parallel with these Kulite measurements, a hot-wire probe was used to assess the state of the floor and ceiling boundary layers directly. Hot-wire measurements were made at $X=43.38$ with and without the wall boundary layer trips, and with and without the settling chamber traverse installed. The hot-wire data are summarized on Figure 21 over the range of P_o . The hot-wire was mounted on the tunnel centerline 0.025 inch (0.635 mm)

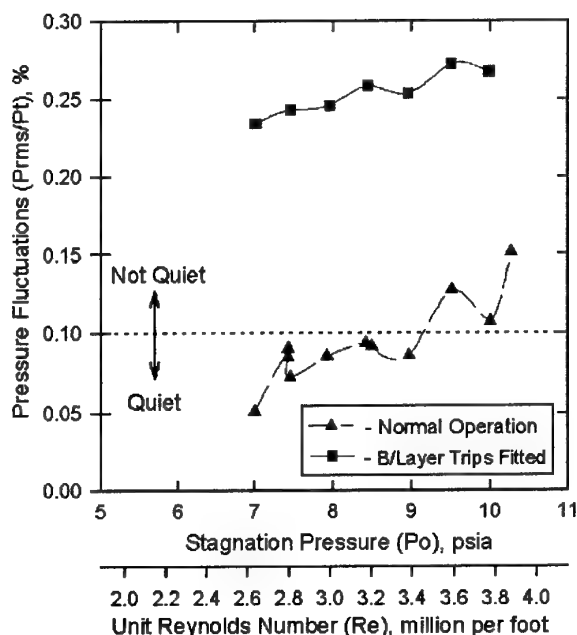


Fig. 19 - Kulite XCS-093 pressure fluctuations measured in the middle of the test section ($X=43.38$; $Y=0$; $Z=0$) over a range of P_o , with and without wall boundary layer trips fitted.

away from the floor. A standoff distance roughly equal to a third of the minimum estimated boundary layer thickness at that streamwise location.²

The hot-wire data are presented as raw signal rms here because the instrument cannot be calibrated in the LFSWT supersonic flows. Nevertheless, the raw hot-wire data has been shown to be useful in determining qualitatively the state of the boundary layer at Mach 1.6.⁷ During normal tunnel operation, the hot-wire rms was order 60 mV. With the wall trips fitted, the hot-wire rms rose to order 150 mV.

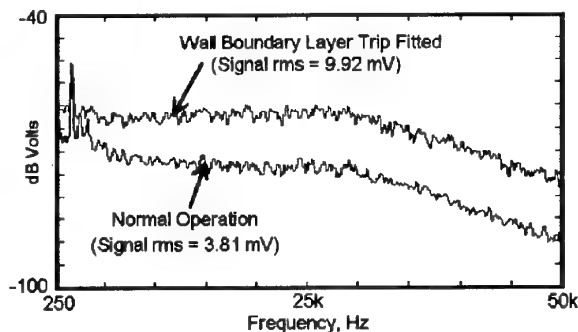


Fig. 20 - Kulite XCS-093 signals measured in the mid-region of the test section ($X=43.38$, $Y=0$; $Z=0$) with and without wall boundary layer trips fitted at $P_o \approx 7.5$ psia (0.52 bar).

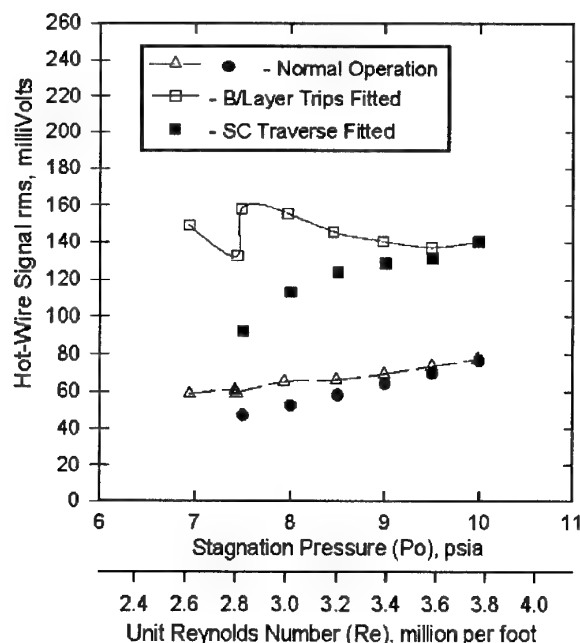


Fig. 21 - Hot-wire signal rms over the Po range, show the effects of boundary layer trips and the settling chamber traverse ($X=43.38$; $Z=0$; 0.025 inch - 63mm above floor; Bandwidth 0.25-50kHz).

Examination of the associated hot-wire power spectra (shown on Figures 22) reveals known boundary layer characteristics. With the boundary layer tripped, the hot-wire measured random disturbance surges, which increased the power of the signal spectra mostly at the low frequencies. This situation is indicative of a turbulent boundary layer. With no wall trips, the signal spectra is relatively flat, which is indicative of a laminar boundary layer. It is interesting to note that the floor boundary layer is receptive to increased levels of settling chamber disturbances. At $Po = 10$ psia (0.69 bar), we

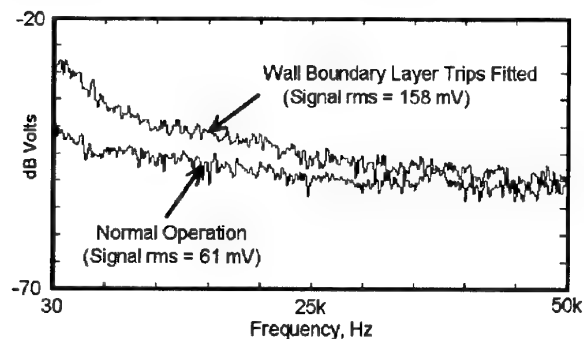


Fig. 22 - Hot-wire power spectra measured above the floor in the mid-region of the test section ($X=43.38$; $Z=0$) with and without boundary layer trips fitted at $Po \approx 7.5$ psia (0.52 bar).

observed no difference between the tripped wall boundary layer case and the introduction of settling chamber disturbances. This finding again highlights the importance of settling chamber flow quality in low supersonic testing.

Centerline hot-wire measurements made near the exit-region of the test section ($X=54.38$) are summarized on Figure 23 over the Po range. ($X=54.38$ corresponds to 27 inches - 0.68 m downstream of the test section entrance and 5 inches - 12.7 cm from the test section exit). The signal to noise ratio was 3.5 and greater for these data. The hot-wire height (standoff distance) above and below the floor and ceiling respectively appears to only be critical when greater than 0.060 inch (1.52 mm). There is good agreement between the floor and ceiling data for the lower values of hot-wire height. The data taken 0.090 inch (2.29 mm) above the floor show the effects of moving the hot-wire into the free stream.

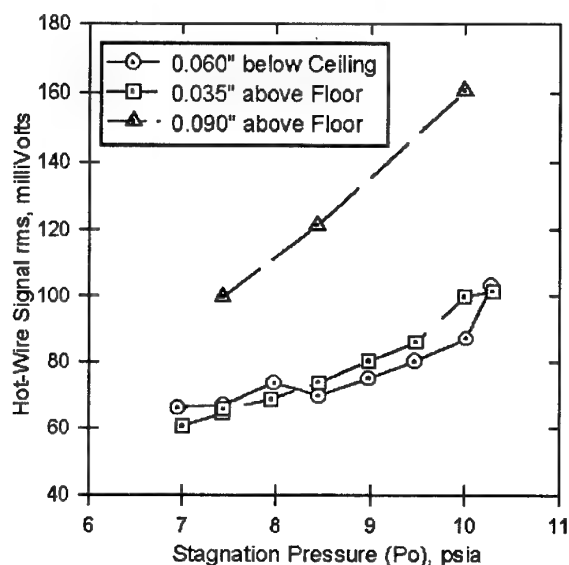


Fig. 23 - Variation of hot-wire signal rms with Po , at different heights from the test section walls in the exit-region ($X=54.38$; $Z=0$; $T_o \approx 20^\circ F$ - 266 K; Bandwidth 0.25-50kHz).

Examination of the hot-wire power spectra shows a relatively flat frequency response over the 0.25-50k Hz bandwidth (as shown on Figure 24). This response is identical to the spectra found further upstream (as shown on Figure 22). Furthermore, there is no significant change in the hot-wire spectra over the Po range. These observations confirm that the floor and ceiling boundary layers are still laminar at $X=54.38$. So, the laminar run lengths are > 102 inches (2.59 m) along the LFSWT walls, and are unaffected by the low frequency disturbances discovered in the settling chamber and test section.

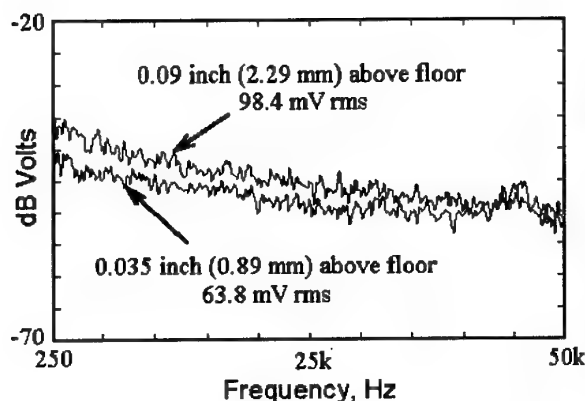


Fig. 24 - Comparison of hot-wire spectra at $P_o \approx 7.5$ psia (0.52 bar) at two heights above the test section floor ($X=54.38$; $Z=0$; $T_o \sim 20^\circ\text{F} - 266\text{K}$).

It is also apparent that the presence of a relatively hot tunnel structure does not promote transition on the tunnel walls, in the low Re operating environment of the LFSWT. The wall temperature ratio (T_w/T_o) in the test section is order 103%. However, a thick thermal layer has been found (see the flow visualization on Figure 13) which has severely compromised our ability to perform meaningful boundary layer traverses on the tunnel walls.

7. THE 10° CONE TEST

The 10° cone test is a widely accepted indirect measurement of flow quality in wind tunnels and the atmosphere (a pseudo-standard it might be said). A large database exists about the measured locations of transition in quiet and noisy flow fields.^{8,9} Alas, at the LFSWT test conditions, the position of transition recorded in flight was at distances from the tip beyond the length of the LFSWT cone. However, the relatively small LFSWT test section brings the model much closer to the tunnel walls than in larger facilities. Therefore, any wall generated noise is likely to be less attenuated than in a large wind tunnel.¹⁰ So, the LFSWT test provided a critical assessment of the state of the wall boundary layers.

To provide an objective comparison with other data sets, the surface quality of the cone was maintained in a state of high polish with a 2L finish. Also, the nose tip was validated with a less than 0.001 inch (0.025 mm) tip flat radius, and the tip was checked concentric with the base.

A simple cone support design was chosen utilizing an existing LFSWT window blank (See Figure 25). We placed particular emphasis on the accurate positioning of the cone, and stiffness of the support to minimize vibrations, to further reduce the possibility of extraneous effects on the transition phenomena. Predicted cone resonate frequencies for different support lengths were compared with test section vibrations. These

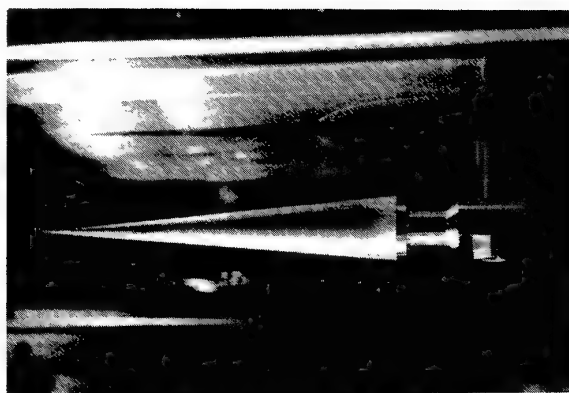


Fig. 25 - The 10° cone installed in the middle of the LFSWT test section.

comparisons were then used to select the best support length to avoid excitation.

An array of 106 type-K thermocouples was mounted inside the 15-inch (38.1 cm) long cone, equally spaced along two rays placed in the horizontal plane for these tests. The cone is made of 17-4 stainless steel. It is hollow with a nominal skin thickness of 0.030 inch (0.762 mm).

The heat transfer properties of laminar and turbulent flow are such that the skin temperatures of the cone, for a given total temperature, vary depending on the boundary layer state (whereby turbulent boundary layers induce warmer skin temperatures). Adequate skin temperature accuracy was obtained experimentally by developing a suitable data acquisition procedure to eliminate data channel differences, and minimization of cold junction drift.¹¹ Typically, the model was allowed to cold soak during the first 20 minutes of each tunnel run, and then averaged measurements were made at each test condition with no specific time delay. The temperatures measured using this data analysis procedure showed good repeatability, order $\pm 1^\circ\text{F}$ ($\pm 0.55^\circ\text{C}$).

Flow disturbance levels in the LFSWT test section were again varied by tripping the wall boundary layers at the test section entrance, as previously reported in our flow quality measurements. The associated skin temperature variations are plotted on Figure 26, for the 8 inches (20.32 cm) of cone ahead of the bow shock reflection (See the schlieren picture on Figure 27). These temperature distributions show the strong effect of pressure turbulence (of the order 2.5%) on the cone boundary layer, as found in conventional noisy tunnels. The initial skin temperature rise is order 4°F (2.2°C) in noisy flow, which is very similar to that found with a boundary layer trip (transition) fitted to the cone.¹¹ This confirms that we have detected transition on the cone (ahead of the bow shock reflection) due to increased flow disturbances. The

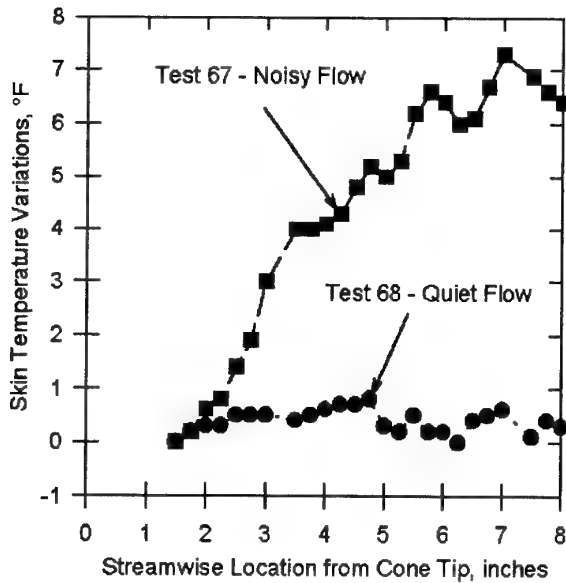


Fig. 26 - Cone skin temperature variations, ahead of the bow shock reflection, for two flow conditions with different free stream disturbances ($P_o \approx 7.5$ psia - 0.52 bar; $T_o \approx 10^\circ\text{F}$ - 261 K; $\alpha = 0^\circ$).

estimated transition Reynolds numbers were order 0.2 million in noisy flow, and 6 million in quiet flow.¹⁰ We observed transition only in noisy flow at Reynolds numbers between 0.3 and 0.6 million.

Repeat tests confirmed our observation that transition did not occur naturally on the 10° cone in the LFSWT (at near zero pitch). This finding adds further proof to our claim that the LFSWT flow is indeed low-disturbance.

Impinging Bow Shock Reflection



Fig. 27 - Schlieren visualization of the 10° cone at Mach 1.6. Weak Mach lines can be seen in the flow, which originate from the hand-finished window and test section joints. Thick thermal layers on the test section walls are also noteworthy.

8. PRESSURE TRANSDUCER SELECTION

An array of Kulite pressure transducers were tested in the LFSWT during our flow quality studies. The smallest was a 0.050 inch (1.27 mm) diameter transducer (the XCS-050), which is now the tiniest ultra-miniature pressure transducer commercially available. This Kulite is supplied with one option, a differential pressure range of 100 psi (6.89 bar) or greater.

The XCS-050 sensitivity was found to have a direct correlation with the probe temperature. Typically, the probe temperature varied from -9°F (250 K) down to -25°F (241 K) during our tests. Since, stagnation temperature (T_o) and the probe temperature were uncontrollable from run to run, we had to measure the Kulite's temperature and correct the Kulite calibration by estimating temperature effects.

The pressure fluctuations from the XCS-050 were compared with repeat measurements made with the largest transducer used, a 0.093 inch (2.36 mm) diameter Kulite (XCS-093) with a 15 psi (1.03 bar) range. The XCS-050 pressure fluctuations were found to be typically over 50% smaller (as shown on Figure 28 for the $P_o \approx 7.5$ psia - 0.52 bar case).

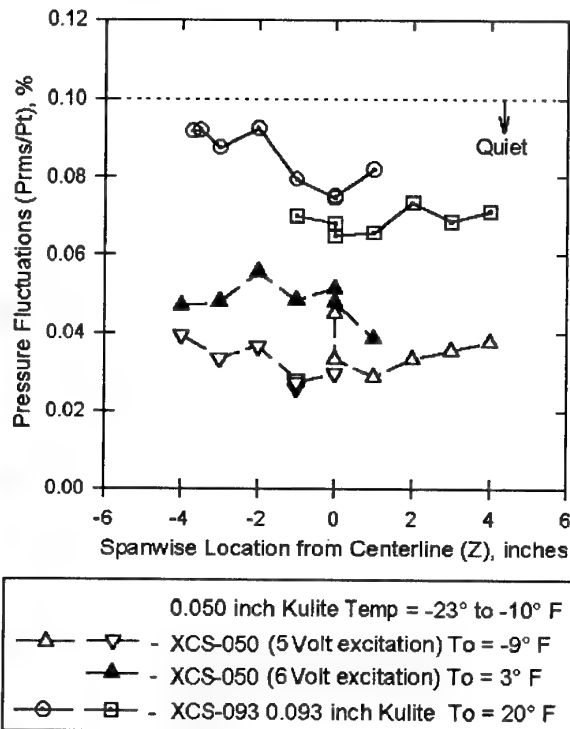


Fig. 28 - Comparison of pressure fluctuations measured with different Kulite transducers and excitation voltages ($X=54.28$; $Y=0$; $P_o \approx 7.5$ psia - 0.52 bar; Bandwidth 0.25-50k Hz).

All the pressure fluctuation measurements shown on Figure 28 indicate that the LFSWT flow is low-disturbance. However, this finding clearly shows the difference the size and type of pressure transducer can make to flow quality measurements. We can identify two factors which are responsible for this difference. First, the pressure sensitivity is 700% greater for one Kulite relative to the other. Second, the reduced transducer sensitivity necessitates increased data acquisition gain, which amplifies signal noise and reduces the signal-to-noise ratio. We found that increasing the electronic gain for the XCS-050 Kulite from 500 to 2000 did not significantly change the pressure fluctuations measured. However, when we raised the excitation voltage from 5 Volts (the manufacturer's recommended level) to 6 Volts, the XCS-050 pressure fluctuations appeared to increase only by a small amount, insufficient to provide a better comparison with the larger Kulite data.

We can conclude that ultra-miniature Kulite transducers are not sensitive enough for quiet wind tunnel calibration at near ambient stagnation conditions. This knowledge led to the acquisition of the 0.062 inch (1.57 mm) diameter (XCS-062) Kulites, with a 15 psi (1.03 bar) range, for use in our 3-axis traverse. These transducers combine small size, with good pressure sensitivity. In addition, we have experienced excellent repeatability and reliability with the XCS-062 Kulite.

9. FURTHER DISCUSSION OF RESULTS

We have overcome numerous difficulties associated with the injector drive system, and instrumentation to present the LFSWT characteristics in this paper. Our two-years of studies have shown that the flow in the test section is low-disturbance in the classical sense, if a suitable data bandwidth is chosen. Furthermore, we have demonstrated that the free stream in the settling chamber and the wall boundary layers are critical to quiet flow at low-supersonic speeds.

The pressure reduction system has become the only source of significant disturbances discovered in the LFSWT, thus far. These disturbances are only significant in the sense that the levels are large compared with the low background noise. Over the 0.25k-50k bandwidth, the LFSWT flow quality is only quiet for stagnation pressures (P_o) < 9.5 psia (0.65 bar) when T_o is low. The disturbances are persistent and variable with dependence on T_o , P_o and accumulated tunnel run-time. The containment of the primary disturbances in a narrow frequency band between 1k-2k Hz is indicative of flow resonance within the pressure reduction system. The pressure reduction system was designed with research flexibility in mind, so modifications are planned to

geometrically change flow chambers. In fact, the option remains to make the pressure reduction system a tunable disturbance generator for future receptivity research.

Currently, we have not observed any detrimental effect of these variable disturbances on LFSWT transition research with swept wings⁴, a cone¹¹, and swept cylinders.¹² Furthermore, the boundary layers along the tunnel wall have been documented as laminar in the exit-region of the test section, and are unaffected by seasonal flow disturbance variations. This is further confirmation that the quiet design features applied to the LFSWT are working well.

The model tests have provided an independent confirmation of our dedicated flow quality measurements. The cone temperatures indicate repeatable laminar boundary layers ahead of the bow shock reflection, at zero angle to the flow. This situation is only possible with good flow quality in the LFSWT at Mach 1.6, as demonstrated by the significant effect on transition of artificially created noisy flow.

Our detailed and repetitive flow quality measurements have characterized the LFSWT test environment more thoroughly than any predecessor. The relatively straightforward measurement of the pressure fluctuation ratio (P_{rms}/P_t) is not sufficient to define flow quality today, and should only be used as a means to detect flow anomalies. Analysis of individual pressure transducer (Kulite) signals allows characterization of the pressure fluctuations to be all encompassing, to address receptivity issues now and in the future.

In the settling chamber, we found conflicting information which indicates the free stream does not satisfy the classical requirement for low-disturbance vortical flow at $P_o > 8.5$ psia (0.58 bar), while satisfying the pressure disturbance requirement. Nevertheless, the test section flow can be low-disturbance over the same data bandwidth. The seasonal variation in disturbances found in the test section must co-exist in the settling chamber. Consequently, the fact that the settling chamber data sets for pressure and velocity fluctuations were taken in the Summer and Winter respectively probably explains the differences. However, by serendipitous selection of the data bandwidth all the settling chamber data could be made to satisfy the classical standards for low-disturbance flow. This point serves as a reminder that the classical standards need to be re-evaluated in the light of new knowledge about receptivity and measurement techniques.

Our testing of various pressure transducers has led us to conclude that the XCS-062 Kulite is the most accurate,

electrically stable, and low-noise device for use over a 15 psia (1.03 bar) range. Transducers with large gains (>20) are not recommended due to the resulting near unity signal to noise ratio. Clearly, the selection of transducer is critical to the correct characterization of the test section flow. As yet, no standardization of instrumentation exists despite repeated recommendations (over the last 20 years at least) that this needs to be done.¹⁰

Of equal importance to the flow quality issue is the signal processing and the ability to calibrate instrumentation at tunnel operating conditions. Regular in-situ calibration is recommended, because this provides a check of the transducer integrity at tunnel operating conditions. Checks made wind-off are insufficient to detect all possible failure modes.⁴ It is interesting to note that the manufacturer's calibration of our XCS-062 Kulite was almost double the sensitivity we measured in the tunnel. This can be attributed to the low temperatures associated with LFSWT operations.

The discovery of flow instabilities and disturbances originating in the pressure reduction system explains the discrepancies in our previously reported flow quality measurements.² These data showed variability that could not be traced to upstream or downstream propagation of disturbances. Furthermore, the pressure fluctuations were only observed to change in frequencies below 2k Hz, where we now know that the pressure reduction system is producing a resonate disturbance. We can therefore assume that all the variability in our (normal operation) traverse data, thus far, was due to temporal variations in the flow through the pressure reduction system. The indications are that the spatial variations of flow quality in the LFSWT are very small over a broad bandwidth.

LFSWT mean flow studies⁴ have shown that Mach number and flow angularity are within current international standards of flow quality for supersonic tunnels.¹³ However, a more complete mapping of the test section cross-section is still required to characterize the weak disturbances due to window and test section joints. These weak disturbances appear not to impact the transition processes we have investigated so far. However, we need to document the similarity between these Mach lines and canopy/inlet shocks found in flight.

The inability to control T_o remains an obstacle to providing repeatable test conditions at any given time. A situation that has significantly complicated and exaggerated our problems with the pressure reduction system. This uncontrolled variability of test conditions adds uncertainty to all our measurements, by affecting both the tunnel flow and the instrumentation. We have found that continual vigilance is necessary, by LFSWT

operators, to maintain quiet flow. Instances of flow quality changes due to T_o variations and accumulated tunnel run-time are well documented.

In general, standardization of flow quality measurements would greatly improve the quality of transition research. Our experience has shown that different instruments can give misleading results, which complicate the task of minimizing disturbances. Currently, transition research needs to be isolated from tunnel disturbances as much as possible (until a better understanding of boundary layer receptivity to disturbances is known). Standardization of flow quality measurements would go a long way to providing an objective assessment of tunnel disturbances fed into the transition process under investigation. As an interim measure, these authors suggest that flow quality measurements should at least be accompanied by instrument, signal processing and data bandwidth information, as provided in this paper.

10. CONCLUSIONS

- 1) Pressure fluctuations in the LFSWT test section are low-disturbance and satisfy the classical standard for quiet flow when no bandwidth is specified.
- 2) Characterization of the LFSWT test section flow over a 0.25k-50k bandwidth shows that the disturbance levels can be greater than classical standards, particularly for stagnation pressures (P_o) < 9.5 psia (0.65 bar) with low T_o .
- 3) Variability of the flow disturbances in the settling chamber and test section is contained in a narrow frequency bandwidth below 5k Hz, which is associated with resonant frequencies from the pressure reduction system.
- 4) Laminar boundary layers have been detected on the tunnel walls near the exit of the test section, with no perceived receptivity to seasonal variations of LFSWT free stream disturbances.
- 5) The pressure reduction system is the only source of significant flow disturbances discovered in the LFSWT. The lack of spatial variation of disturbances in the test section indicate that the quiet design features of the LFSWT are working.
- 6) Mean flow measurements and a wing test indicate that the LFSWT flow meets current international standards of Mach number uniformity and flow angularity for supersonic tunnels.

- 7) Selection and in-situ calibration of miniature (Kulite) pressure transducers is critical to the accuracy of flow quality measurements. The 0.062 inch (1.57 mm) diameter Kulite, with a 15 psi (1.03 bar) range, is the best type for the LFSWT.
- 8) We have found that (Kulite) pressure transducers can fail in modes undetectable in intermittent wind tunnels with no in-situ calibration capability.
- 9) The lack of natural transition on a 10° cone (at zero angle to the flow) has provided further proof that the LFSWT flow is low-disturbance or quiet.
- 10) Characterization of low-disturbance flow quality requires careful selection of instrumentation, proper data acquisition procedures, and detailed signal analyses. Classical standards are not sufficient to fully characterize supersonic flow for transition research.
- 11) The formation of standards for flow quality measurements is strongly recommended, so that transition research can be better isolated from tunnel disturbances.

11. REFERENCES

1. Laufer, J.: **Aerodynamic Noise in Supersonic Wind Tunnels**, *Journal of the Aerospace Sciences*, vol. 28, no. 9, September 1961. pp. 685-692.
2. Wolf, S.W.D.; Laub, J.A.; and King, L.S.: **Flow Characteristics of the NASA-Ames Laminar Flow Supersonic Wind Tunnel for Mach 1.6 Operation**. AIAA Paper 94-2502. Presented at the 18th AIAA Aerospace Ground Testing Conference, June 1994, Colorado Springs, Colorado. 18 pp.
3. Wilkinson, S.P.; Anders S.G.; Chen, F.-J.; and Beckwith, I.E.: **Supersonic and Hypersonic Quiet Tunnel Technology at NASA Langley**. AIAA Paper 92-3908. Presented at the AIAA 17th Aerospace Ground Testing Conference, July 1992. 25 pp.
4. Wolf, S.W.D.; and Laub, J.A.: **Low-Disturbance Flow Measurements in the NASA-Ames Laminar Flow Supersonic Wind Tunnel**. AIAA Paper 96-2189. Presented at the 19th AIAA Advanced Measurement and Ground Testing Technology Conference, June 1996, New Orleans, Louisiana. 19 pp.
5. Riise, H.N.: **Flexible-Plate Nozzle Design for Two-Dimensional Supersonic Wind Tunnels**. JPL Report 20-74, June 1954. 41 pp.
6. Wolf, S.W.D.: **Supersonic Wind Tunnel Nozzles - A Selected, Annotated Bibliography to Aid in the Development of Quiet Wind Tunnel Technology**. NASA CR-4294, July 1990. 84 pp.
7. Wolf, S.W.D.; and Laub, J.A.: **Development of the NASA-Ames Low-Disturbance Supersonic Wind Tunnel for Transition Studies at Mach 1.6**. AIAA Paper 94-0543. Presented at the AIAA 32nd Aerospace Sciences Meeting & Exhibit, January 10-13 1994, Reno, Nevada. 12 pp.
8. Dougherty, N.S.; and Fisher, D.F.: **Boundary Layer Transition on a 10-Degree Cone: Wind Tunnel/Flight Data Correlation**. AIAA Paper 80-0154. Invited paper presented at the 18th AIAA Aerospace Sciences Meeting, January 1980, Pasadena, California. 16 pp.
9. Fisher, D.F.; and Dougherty, N.S.: **In-Flight Transition Measurement on a 10° Cone at Mach Numbers from 0.5 to 2.0**. NASA TP-1971, June 1982. 143 pp.
10. Westley, R.: **Problems of Noise Measurement in Ground-Based Facilities with Forward-Speed Simulation (High-Speed Windtunnel Noise)**. In: *A Further Review of Current Research Aimed at the Design and Operation of Large Wind Tunnels - Appendix 5*, AGARD AR-83, September 1975. pp. 75-100.
11. Wolf, S.W.D.: **NASA-Ames Laminar Flow Supersonic Wind Tunnel (LFSWT) Tests of a 10° Cone at Mach 1.6**. February 1996. NASA TM to be published. 15 pp.
12. Coleman, C.P.; Poll, D.I.A.; Laub, J.A.; and Wolf, S.W.D.: **Leading Edge Transition on a 76° Swept Cylinder at Mach 1.6**. AIAA Paper 96-2082. Presented at the 27th AIAA Fluid Dynamics Conference, New Orleans, Louisiana, June 17-20, 1996. 12 pp.
13. Morris, D.E.; and Winter, K.G.: **Requirements for Uniformity of Flow in Supersonic Wind Tunnels**. RAE TN Aero.2340, September 1954. 9 pp.

Fluctuation Characteristics of Flows in Test Sections of High-Speed Wind Tunnels

V.A. Lebiga, V.N. Zinoviev

Institute of Theoretical and Applied Mechanics
Russian Academy of Sciences
630090, Novosibirsk, Russia

SUMMARY

The results of fluctuation structure study in test sections of wind tunnels in the wide range of velocity (from large subsonic up to supersonic) are presented in this paper. A correlation between characteristics of the boundary layer on the test section walls of the supersonic wind tunnel with fluctuations in the flow core is shown. Detailed characteristics of fluctuations in ventilated test sections are given for different types of walls (perforated, slotted, smooth rigid). The constant current hot-wire anemometer and developed at ITAM technique have been used for fluctuation measurements and interpretation of the results.

LIST OF SYMBOLS

M	Mach number
Re	Reynolds number
Sh	Strouhal number
α, β	Mach number functions
m	mass flow
u	velocity
ρ	density
p	pressure
T	temperature
e	voltage across a wire
F	mass flow sensitivity coefficient
G	temperature sensitivity coefficient
r	relative sensitivity coefficient
R	correlation coefficient
χ	the angle between flow and wave propagation directions
χ'	the angle of Mach wave inclination
ϕ	the angle between flow direction and line connecting a probe and a source of fluctuations
$(\)'$	fluctuations
$< >$	dimensionless RMS value

SUBSCRIPTS

o	stagnation parameter
u	velocity
ρ	density
m	mass flow

1. INTRODUCTION

Adequacy of modeling of flight conditions in wind tunnels is largely determined by the level of flow fluctuations and their characteristics.

Because of small temperature inhomogeneity and acoustic background, "the turbulence level" (as a result of fluctuation intensity of three velocity components) gives rather objective information on the flow quality in test section of a low speed wind tunnel. But, as a rule, there are no parameters on flow fluctuation characteristics among those describing the flow quality in the test section of a high speed wind tunnel. A reference model test allows one to obtain only a level of reliability of data in a wind tunnel but not information on the fluctuation level. However this means that the fluctuation influence is in a certain permissible frame.

An interest to flow fluctuations has been increasing from time to time. The ability of high level turbulence to provide an effect like the Reynolds number increase results in more correct testing of relatively small models. For a long time the attention of researchers has been paid to so-called "unit Reynolds number effect". It was clear from the very beginning that this effect is a result of flow fluctuations. A plenty of experimental data have been obtained. However, up to now there are no well grounded and reliable methods to calculate transition location on models under testing. There are now at least two problems where it is necessary to reduce fluctuations in the test section of the high speed wind tunnel. The first one is associated with basic problems, the other corresponds to applied ones.

First, it is important to achieve a very low level of fluctuations in the test section for pure experiment when controlled disturbances have to be introduced into the flow to study stability, transition or receptivity problems. This problem is successfully solved at least for quiet subsonic wind tunnels, there is some progress for supersonic wind tunnels [1, 2].

The second problem arises when the test Reynolds numbers are close to the flight ones, especially in

cryogenic transonic wind tunnels because the state of the turbulent boundary layer on models in this case does not correspond to natural condition. It is especially important in modeling the flight Reynolds number when the advantages of high Reynolds numbers can disappear because disturbances can change essentially the boundary layer state, location of separation zones, the aerodynamic characteristics of models, etc.

However, these problems correspond to different kinds of wind tunnels. The first one arises in supersonic wind tunnels due to the noise of the turbulent boundary layer on the walls of nozzle and test section. The second one is associated with transonic wind tunnels because the test section has, as a rule, perforated or slotted walls. Therefore, relatively high level of fluctuations is an attribute of transonic wind tunnels and advantages of flight Reynolds number modeling can be brought to minimum due to influence of fluctuations on the boundary layer separation, transition location, heat transfer, etc.

Different types of fluctuations are dominating in low-velocity and high-velocity wind tunnels. Intensity, structure and spectral characteristics of fluctuations are determined by the size and design peculiarities of wind tunnel circuit. The main source of fluctuations in test sections of supersonic wind tunnels is turbulent boundary layer on the walls. The main source of fluctuations in ventilated test sections is perforation of the walls. Boundary layers on the walls radiating acoustic disturbances are sources of fluctuations in test sections of supersonic wind tunnels. Temperature nonuniformities carried from settling chamber should be taken into account for wind tunnels with working gas heating.

It is also important to measure fluctuations in the place of model installation, because the fluctuations near a test section wall can differ from those in the flow core for two reasons: (i) because of influence of acoustic fluctuations of the boundary layer on the wall, and (ii) due to different distribution of fluctuations across the test section, since sources, producing disturbances in different points of flow, are various.

In order to take into account the influence of fluctuations properly it is necessary to determine a minimum set of characteristics which identifies these fluctuations. It is coming to determine a minimum set of necessary and sufficient parameters to specify adequately the fluctuations.

First of all, it is the intensity of all three types of fluctuations (velocity, acoustic, and temperature) as well as the spectral composition of each type of these disturbances.

Fortunately, there are no wind tunnels where the intensity of three types of fluctuations are considerable

simultaneously. It is well known that velocity fluctuations are dominating in low speed wind tunnels, temperature inhomogeneity exists in wind tunnels with a closed circuit due to bringing energy to the flow by a fan, in wind tunnels with flow heating, in cryogenic wind tunnels. Acoustic fluctuations are determinative in transonic and supersonic wind tunnels

However, due to frequency selective influence of fluctuations on the flow near a model and on boundary layer characteristics a part of disturbance spectrum can be important. Sometimes these disturbances are rather small compared with total intensity but big enough within certain frequency range.

Measuring equipment must satisfy to many requirements. It is desirable to use a universal instrument to measure all these characteristics, however there are no methods satisfying all requirements. The most popular instruments for fluctuation measurements are pressure transducers, hot-wire anemometers, and devices based on the LDA principles. Microphones are least suitable, they are sensitive to pressure pulsations provided both by acoustic fluctuations and by pseudosound due to velocity fluctuations. Laser-Doppler method is a non-intrusive one, it is possible to measure all three velocity components of fluctuations and other factors (density and temperature), however in this case the cost of equipment grows rapidly. Moreover, it is difficult to make all necessary places accessible for measurements.

The advantage of hot-wire is that practically all characteristics of fluctuations (velocity, pressure, temperature) in the required flow area can be obtained with its help while a microphone gives only pressure fluctuations on the model surface or on a wall of the test section, and a thermocouple gives only temperature fluctuations.

The hot-wire method has been used in these investigation because it guarantees the obtaining of the most complete data on flow fluctuation structure in wind tunnels [3]. The use of hot-wire for fluctuation measurement at high subsonic and transonic speeds is effective due to the presence of fluctuations of different types in the flow. The detailed inspection to check characteristics of disturbances, obtaining the detailed information on a fluctuation structure in a transonic test section, study of correlation of fluctuation with disturbance sources become possible due to developed fluctuation measurement techniques for transonic flow velocities.

2. EXPERIMENTAL EQUIPMENT AND TECHNIQUE

2.1 Facility

The experiments were carried out in T-325 and MT-325 wind tunnels of the Institute of Theoretical

and Applied Mechanics of Siberian Division of Russian Academy of Sciences with 20 cm × 20 cm and 4 cm × 4 cm test sections, respectively. A limited number of experiments has been carried out in supersonic wind tunnel T-313 with 60 cm × 60 cm test section.

Supersonic wind tunnel T-325 was designed as a quiet wind tunnel. To provide a low turbulence level in the test section a set of measures was foreseen, namely: a honeycomb; up to ten screens; noise reducing system; smooth nozzle surface and side walls made as the whole without any joints; large contraction (the ratio of settling chamber cross-section area to test section one is about 20).

There are two test sections for T-325. One has supersonic Laval nozzles for fixed Mach numbers $M = 1.5 \dots 4.0$ and the other is a transonic ventilated test section. The transonic test section has either perforated or slotted upper and lower walls. The perforated walls with holes 6 mm in dia provide porosity coefficient $\xi = 26\%$, where ξ is a ratio of hole area to wall surfaces. Slotted walls with permeability $\xi = 23\%$ have 4 mm width longitudinal slots.

Wind tunnel MT-325 has four replaceable test sections with solid walls for design Mach numbers $M = 1, 2, 3, 4$ and ventilated test section with replaceable walls. For MT-325 perforation was formed by holes of variable diameter 1...2 mm distributed over upper and lower walls. To provide a gradual increase of velocity along the test section the wall slots of MT-325 are of variable width simulating slots of real big wind tunnels. Several variants of slots disposition have been used during experiments (2 or 4 slotted walls, 4 or 6 slots for upper and lower walls). Special diaphragm with controlled cross-section was placed behind the test section. The use of this diaphragm together with injectors and changing pressure in the settling chamber allows one to vary flow density and, as a result, the Reynolds number within a broad range at constant flow velocity.

2.2 Equipment for fluctuation measurements

Constant current anemometers TPT-2 and TPT-4 designed at ITAM and hot-wire probes with tungsten sensitive elements $6 \cdot 10^{-6}$ mm in dia and 1.2 mm length have been used. The frequency range of anemometers is 200 kHz at all overheat parameters. Anemometer TPT-4 has an automatic compensation of probe thermal lag.

Spectrum measurements have been provided with the help of the Bruel & Kjaer equipment for frequency analysis (Analyzer 2010 and Recorder 2307).

2.3 Technique

As a rule, eight overheats have been used at hot-wire

measurements to obtain one fluctuation diagram. Sensitivity coefficients of the probes have been determined using both direct in-flow calibrations and semi-empirical correlations. The details of calibration and measurement procedures are described in [4]. A possibility of measuring the anemometer's noise makes available the measuring of low level of fluctuations.

Due to the presence of different types of fluctuations it is impossible to use an approach to hot-wire data interpretation similar to incompressible flows when only velocity fluctuations are present in a flow and the hot-wire probe voltage fluctuations are proportional to velocity fluctuations unambiguously: $e' = F_u \cdot u'$, where F_u is the velocity sensitivity coefficient. Therefore, the fluctuation diagram approach for hot-wire data interpretation has been used in this work.

2.3.1. Supersonic velocities

At supersonic flow velocities a hot-wire probe output e depends on mass flow m and total temperature T_0 fluctuations [5]:

$$e' = F m' + G T_0', \quad (1)$$

where F and G are sensitivity coefficients to mass flow and total temperature. After ordinary transformations for RMS hot-wire output,

$$\mathcal{Q}^2 = r^2 \langle m \rangle^2 - 2r R_{mT_0} \langle m \rangle \langle T_0 \rangle + \langle T_0 \rangle^2 \quad (2)$$

$$\text{where } \mathcal{Q}^2 = \frac{\langle e \rangle^2}{G^2}, \quad r = \frac{F}{G}, \quad R_{mT_0} = \frac{\langle m T_0 \rangle}{\langle m \rangle \langle T_0 \rangle}$$

According to Kovasznay [6], three modes of fluctuations can exist in a compressible flow:

Vorticity mode:

$$\mathcal{Q} = |\beta - r| \langle u \rangle \quad (3)$$

Entropy mode:

$$\mathcal{Q} = (r + \alpha) \langle T \rangle \quad (4)$$

α and β are the Mach number functions:

$$\alpha = \left(1 + \frac{\kappa - 1}{2} M^2\right)^{-1}, \quad \beta = \alpha(\kappa - 1) M^2 \quad (5)$$

Acoustic mode

For Mach waves with inclination χ

$$\cos \chi = -\frac{1}{M} \quad (6)$$

the fluctuation diagram is

$$\mathcal{Q} = r \left(1 - \frac{1}{M^2}\right) \langle \rho \rangle \quad (7)$$

One or some modes can exist in supersonic flows simultaneously. In this case it is necessary to use Eq.2. However, in many cases and under certain assumptions separation of fluctuations according to the type is possible.

2.3.2. High subsonic velocities.

The use of a hot-wire at high subsonic and transonic velocities is questionable due to the problem of determination of the law of heat transfer between a probe and a flow when the probe sensitivities to density ρ and flow velocity u are different and dependence on the Mach number appears in the heat transfer law. However, this effect is perceptible in a rather narrow Mach number range. Grounding on experimental data it was supposed in the present work that density and velocity sensitivities are equal [7].

Special approaches have to be used for interpretation of the hot-wire measurements at high subsonic speeds when, similar to supersonic ones, velocity, temperature, acoustic disturbances are present [8...9]. Therefore, some questions must be answered, namely: (i) up to what velocities it is permissible to neglect compressibility effects, (ii) what method has to be employed for hot-wire anemometer output interpretation at high subsonic velocities since an effect of compressibility becomes considerable, (iii) is it possible to use Kovasznay's mode diagram method proposed for supersonic velocities?

For special cases of vorticity and entropy modes, none of the assumptions specific for supersonic velocities have been made; thus, Eqs.(3) and (4) are valid for subsonic cases, too. It is necessary to determine the corresponding velocity limits and to estimate the order of terms in these equations for possible simplifications. It is well known that if velocity and temperature fluctuations are present in a low speed flow, small overheats have to be used to measure temperature fluctuations and high overheats have to be used to measure velocity fluctuations. However, this is not correct for supersonic and high subsonic speeds. Fluctuation diagrams for acoustic disturbances in subsonic flows are a subject of special study [10...11].

Vorticity mode

The diagram of fluctuations for vorticity mode looks similar to the diagram for supersonic velocities and is of V-shape. According to (3), the diagram consists of two segments of straight lines and is equal to zero at $r = \beta$. At low flow velocities ($M < 0.3$), β tends to zero and $\vartheta \approx r < u >$.

Entropy mode

There are no principle differences in the entropy mode diagram at sub- and supersonic speeds. In general, the value of α at subsonic velocities is comparable with r ($\alpha > 5/6$, see Eq.5), thus in all cases the presence of temperature fluctuations in the flow requires the use of Eq.4 without any simplification:

Acoustic mode

This sort of fluctuations exists in test sections of transonic wind tunnels due to wall perforation,

resonance phenomena, noise from ejectors, etc.

The diagram for acoustic fluctuations at subsonic speeds in the general case is a hyperbola with parameters depending on the nature of sources and their actual distribution. There are some special cases very important for practice when the diagram is linear, or looks like the letter "V", or is a hyperbola with perfectly determined characteristics.

1. For plane acoustic waves propagating at an arbitrary angle χ about the flow, instead of Eq.(7) corresponding to special case Eq.(6) the general equation can be written as follows

$$\vartheta = \left[\alpha(\kappa - 1) \left(1 + M \cos \chi_0 \right) - r \left(1 + \frac{\cos \chi_0}{M} \right) \right] < \rho > \quad (8)$$

2. The similar equation can be used for acoustic disturbances radiated by a single source. In this case it is possible to use the equation establishing the relationship between angles χ and φ corresponding to the inclination of the vector from the source to the place of measurements.

3. For the sources of acoustic disturbances equispaced along the flow over a rectangular area, the equation of fluctuation diagram is a hyperbola with the coefficients depending only on the Mach number.

The ground for hot-wire application at transonic velocities is given in Annex A.

3. EXPERIMENTAL RESULTS AND DISCUSSION

3.1. Supersonic Speeds.

Investigation of fluctuations in supersonic wind tunnels were performed in a wide range of Mach numbers M and unit Reynolds numbers Re_1 . Fluctuation diagrams and spectrums of fluctuations were obtained for all wind tunnels. An example of fluctuation diagrams at $M = 3$ and $Re_1 \approx 30 \cdot 10^6 \text{ m}^{-1}$ is shown in Fig.1.

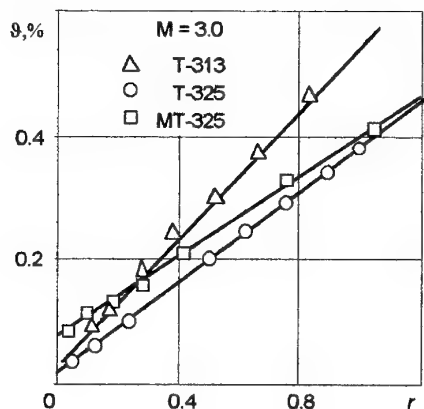


Fig.1

The intensity and characteristics of acoustic fluctuations have been calculated from the fluctuation

diagrams. The results of calculations for data presented in Fig.1 are given in Table 1.

Table 1

Wind Tunnel	$\langle m \rangle$, %	$\langle T_0 \rangle$, %	$\langle p \rangle$, %	$\langle u \rangle$, %	c/u	χ'
T-313	0.51	0.03	0.60	0.09	0.26	27°
T-325	0.35	0.04	0.43	0.08	0.40	34°
MT-325	0.30	0.08	0.41	0.11	0.58	53°

Figure 2 presents the intensity of acoustic fluctuations versus Re_1 for T-325. It was found that behavior of fluctuation characteristics obtained in T-325 at supersonic speeds differs from analogous known data when the intensity of fluctuations decreases with Re_1 increasing. (The data for T-313 corresponds to these conventional well-known results). Nonmonotonous dependences of fluctuation intensity on Re_1 for T-325 (see Fig.2) were confirmed by measurements with the help of microphones flush mounted at a flat plate placed under zero angle of attack in the flow core. But the pressure fluctuation measurements with the microphone built into the test section wall have given ordinary monotonously decreasing dependences at all Mach numbers. Additional investigations and analysis allow to explain the discovered unusual behavior.

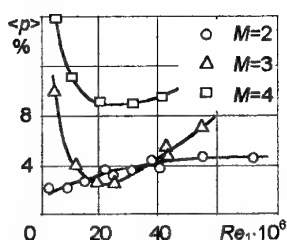


Fig.2

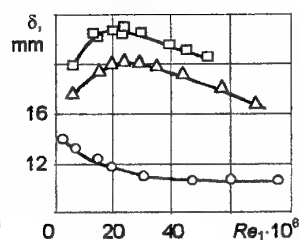


Fig.3

It was found that the dependences shown in Fig.2 are a result of undertaken measures to reduce the fluctuations in T-325. Thanks to these measures, the disturbances convected from the settling chamber are small enough. (Measurements of disturbances upstream the supersonic part of the Laval nozzle in T-325 has shown that the level of fluctuations at the Laval nozzle inlet does not exceed 0.02%. This means that the contribution of fluctuations generated in the settling chamber to the total fluctuation level in the test section is negligibly small and fluctuations generated by the boundary layer on test section walls to acoustic disturbances in the flow core is prevailing.) In addition, high quality of nozzle surfaces ensures a delayed transition in the boundary layer downstream the throat. The results of measurements of the boundary layer thickness on the walls of T-325 approximately at the end of the nozzles shown in Fig.3, serve as indirect confirmation of this assumption because nonmonotonous changing of the

boundary layer thickness can be explained as a result of the transition zone travel. It is known that the transition zone is a source of high level acoustic fluctuations radiated from the boundary layer into the flow core. Comparison of dependences of the fluctuation level and boundary layer thickness on Re_1 (Fig.2 and Fig.3) indicates a correlation of these two parameters.

Using the fluctuation diagram method, it is possible to determine the velocity c of disturbance sources generated acoustic fluctuations and inclination of radiated sound waves. Calculated relative source velocities c/u are given in Fig.4. These data are in good agreement with the data obtained by Laufer both using the fluctuation diagram method and correlation measurements [12].

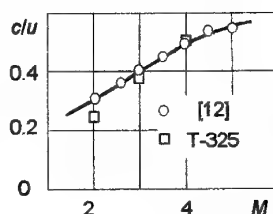


Fig.4

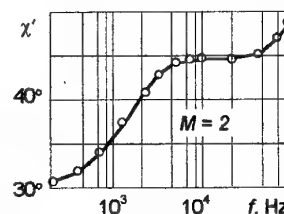


Fig.5

The value of the relative velocity of sources of acoustic fluctuations gives some information on the nature of acoustic fluctuations. As it follows from Table 1, c/u is different for all wind tunnels. The low value of c/u for T-313 points to considerable contribution of the Mach waves to acoustic fluctuations. This is a consequence of small imperfections of the nozzle surface.

The highest value c/u corresponding to the smallest wind tunnel MT-325 is owing to prevailing contribution of moving sources of acoustic fluctuations because on the one hand comparatively big value of $\langle T_0 \rangle$ cannot be explained by a high level of entropy or vorticity fluctuations convected from the settling chamber due to large contraction ratio and high quality of the flow before the nozzle, and on the other hand the correlation coefficient $R_{mT_0} \approx -1$.

The dependences of relative velocity of the sources of sound waves on fluctuation frequency were obtained applying the same approach to the fluctuation spectrums. It was found that at low frequencies the inclination tends to that corresponding to the Mach waves ($\chi' = 30^\circ$ at $M = 2$) when the source velocity tends to zero at low frequencies and increases with the frequency of fluctuations. An example of the acoustic wave inclination versus frequency is shown in Fig.5. The angle of the wave inclination changes from that corresponding to the Mach waves and tends to $\pi/2$ for high frequencies.

3.2. High Subsonic Speeds

Results on fluctuations structure in transonic test sections of wind tunnels have been obtained using developed hot-wire technique for subsonic compressible flows. The experiments were carried out both in T-325 and in MT-325.

In transonic test sections of wind tunnels can exist both disturbances similar to those in test sections of supersonic wind tunnels and propagated upstream. The presence of perforated or slotted walls is the reason for appearance of additional acoustic fluctuations. Several types of such fluctuations are possible due to jets in the perforation holes, the resonance phenomena, steps and jets injected along the walls at the end of ventilated test section, etc.

The fluctuations convected from a settling chamber are comparatively small in transonic wind tunnels because of honeycombs, screens and high contraction especially. However for cryogenic wind tunnels the contraction ratio cannot be chosen too large due to reducing of the flow velocity in the settling chamber and the danger of flow temperature stratification.

The fluctuation diagrams obtained in the transonic test section of T-325 at several Mach number values are shown in Fig. 6 for perforated (a) and slotted (b) walls.

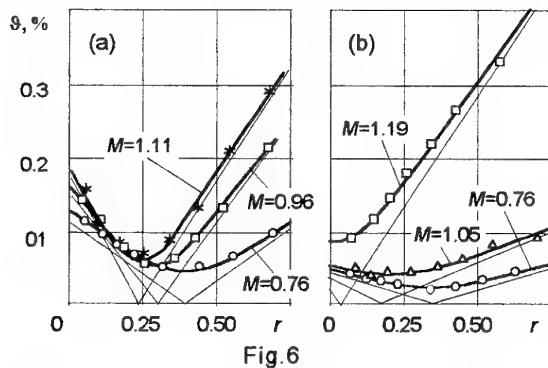


Fig. 6

Calculated values of the fluctuation parameters are given in Table 2.

Table 2

Walls	M	$\langle m \rangle, \%$	R_{mT0}	r_{\min}
Perforated	0.76	0.31	0.96	0.38
	0.96	0.63	0.97	0.28
	1.11	0.72	0.91	0.24
Slotted	0.76	0.12	0.90	0.35
	1.05	0.16	0.62	0.17
	1.19	0.59	0.07	0.01

The spectrums of hot-wire output at the maximum overheat coefficient for various flow conditions and different walls are shown in Fig. 7.

High values of the correlation coefficient are typical for the diagrams in the case of the perforated walls.

Some decreasing of R_{mT0} to 0.91 at $M = 1.11$ can be explained by the presence of two types of acoustic fluctuations - moving plane waves due to resonance phenomena and the Mach waves. Both these types can be visualized using spark Schlieren photograph or high speed cinema techniques. The presence of two sorts of acoustic fluctuations leads to a growth of mass flow fluctuations with the Mach number. Qualitatively, it is confirmed by the spectrum of hot-wire output obtained at the highest overheats of the probe, see Fig. 7, where a growth of low frequency fluctuations typical for Mach waves is clearly seen. The increase in intensity of fluctuations at high frequencies is connected with acoustic wave generation by holes.

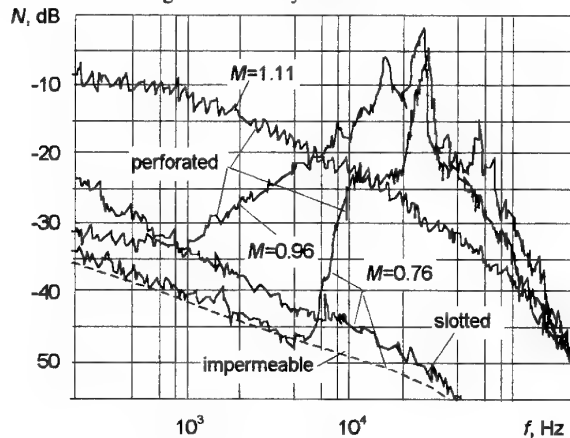


Fig. 7

The mass flow fluctuations are increasing with the Mach number and corresponding shift of the minimum of fluctuation diagrams for slotted walls is more marked in comparison with perforated walls. A possible reason for it is an increasing role of fluctuations caused by appearance of unsteady Mach waves. The spectrums shown in Fig. 7 confirm this because they do not contain maximums or discrete tones typical of local sources.

Analogous experiments have been performed in MT-325. Both average and spectrum data on fluctuation structure were obtained for perforated, slotted, rigid test section walls as well as with jet as well as with jets at the end of adaptive borders. The fluctuation diagrams appear qualitatively similar to those for T-325. It was shown that the highest level of disturbances takes place in the test section with perforated walls. An example of fluctuation spectrum for perforated walls is given in Fig. 8. The frequency spectrum of fluctuations for this case contains a maximum in the range of medium frequencies, while for slotted and smooth walls the amplitude of fluctuations monotonously decreases with frequency. The type of disturbances at certain frequencies is determined according to parameters of fluctuation diagrams obtained with help of narrow-band filters.

Typical Strouhal numbers calculated with respect to hole diameter and frequency corresponding to the maximums of spectrums for both wind tunnels are close enough, $Sh = 0.30$ for T-325 and $Sh = 0.34$ for MT-325.

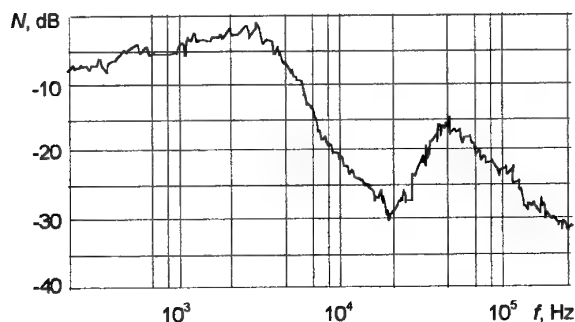


Fig. 8

The correlation coefficient $R_{uT_0} = 0.71$ for MT-325 is smaller than those for T-325. It can be explained by a larger contribution of fluctuations produced by the boundary layer on test sections walls.

It was obtained also that diagrams at low frequencies are of non-acoustic type in contrast to high frequency fluctuations which are of acoustic nature. The source of the latter fluctuations is the boundary layer on the test section walls. A good agreement of the spectrums with those for smooth walls serves to confirm this fact, see Fig. 7. The results for the smooth walls can be used also to estimate fluctuations in test sections with adaptive non-porous walls when the main source of fluctuations is the boundary layer on the walls

5. CONCLUSIONS

Adequacy of modeling of flight conditions in wind tunnels depends on the information about the flow fluctuations and their characteristics. The obtaining of the most complete data on flow fluctuation structure in the test sections is an urgent requirements of modern experiments both in supersonic and in transonic wind tunnels.

At high flow speeds, when disturbances of different nature (velocities, density, pressure, temperature, etc.) are present, the use of the hot-wire technique together with the methods of mode diagrams makes sure a possibility of obtaining data on detailed structure of fluctuations.

Results of measurements carried out at ITAM shows that both total level of fluctuations and spectral distribution of the modes of fluctuations are very important to provide controlled conditions of experiments in high speed wind tunnels.

6. REFERENCES

1. Wilkinson, S.P., Anders, S.G., Chen, F.-J., Beckwith, I.E. "Supersonic And Hypersonic Quiet Tunnel Technology at NASA Langley", AIAA Paper 92-3908, July, 1992, 25p.
2. Wolf, S.W.D., Laub, J.A. "Development of the NASA-Ames Low-Disturbance Supersonic Wind Tunnel for Transition Studies at Mach 1.6", AIAA Paper 94-0543, January, 1994, 12p.
3. Lebiga, V.A., "Experimental Investigation of Turbulence in a Supersonic Flow". *Izvestia Akademii Nauk SSSR, Mekhanika Zhidkosti i Gasa*, (in Russian) 1989, 3, p.119-124.
4. Lebiga, V.A. "On Measurements of Turbulence of Compressible Flows". *Metody i Tekhnika Aerofizicheskikh Issledovaniy*, Novosibirsk, (In Russian), ITAM, 1978, p.44-56.
5. Kovasznay, L., "The Hot-Wire Anemometry in Supersonic Flow" *J.A.S.*, 1950, Vol.17, p.565-572.
6. Kovasznay, L., "Turbulence in Supersonic Flows", *J.A.S.*, 1953, Vol.20, p.657-674.
7. Lebiga, V.A., Zinovjev, V.N., "Hot-Wire Measurements at High Subsonic Velocities", *Proceedings, International Conference on Aerophysical Research, ICMAR'92, Part 1, Russia, Novosibirsk*, 1992, p.79-82.
8. Horstman, C., Rose, W., "Hot-Wire Anemometry in Transonic Flow", *AIAA Journal*, 1977, Vol.15, p.396-401.
9. Stainback, P.C., Johnson, C.B., Basnett, C.B., "Preliminary Measurements of Velocity, Density and Total Temperature Fluctuations in Compressible Subsonic Flow", *AIAA 21st Aerospace Scientific Meeting*, 1983, Reno, Nevada.
10. Lebiga, V.A., "Hot-Wire Anemometer in a Compressible Subsonic Flow". *Izvestiya Akademii Nauk SSSR, Mekhanika Zhidkosti i Gasa*, 1991, No 6. p.160-167.
11. Lebiga, V.A., Zinoviev, V.N., "Acoustic Measurements with Hot-Wire Anemometer at High Subsonic Velocities". *DANTEC Information*. 1991.- No 10.- p.14-16.
12. Laufer, J. "Some Statistical Properties of the Pressure Field Radiated by a Turbulent Boundary Layer", *Physics of Fluid*, 1964, Vol. 7, No 8, p.1191-1197.

Annex A.

FLUCTUATION DIAGRAM FOR ACOUSTIC MODE AT SUBSONIC FLOW VELOCITY

A1. Plane Acoustic Waves

Denoting by χ the angle between the normal to the wave front and the flow velocity vector an equation similar to Eq.(8) for elementary sound wave can be written as

$$\delta\theta = \left[\alpha(\kappa - 1)(1 + M \cos \chi) - r \left(1 + \frac{\cos \chi}{M} \right) \right] \delta \langle \rho \rangle \quad (A1)$$

Unlike supersonic velocities any orientations of acoustic waves are possible at subsonic speeds:

$$-1 < \cos \chi < 1 \quad (A2)$$

For moving plane acoustic waves in test sections of transonic wind tunnels (being visualized with flash photography they resemble a set of Mach waves with spacing and inclination depending on the flow parameters, test section sizes, etc.) $\chi = \chi_0 = \text{const}$, and Eq.(A1) transforms into Eq.(8).

As it follows from Eq.(A1), the fluctuation diagram intersects axis r at

$$r_0 = \beta \frac{M^{-1} + \cos \chi_0}{M + \cos \chi_0} \quad (A3)$$

Thus, there are combinations of probe overheats and angles of sound wave propagation when the hot-wire is insensitive to acoustic fluctuations. For each Mach number, there is a range of r_0 unrealizable at any inclination χ_0 and limited by

$$|r_0| = \frac{(\kappa - 1)M}{1 + \frac{(\kappa - 1)}{2}M^2} \quad (A4)$$

It is important that depended only on the Mach number the intersection of vorticity mode diagram with the abscissa at $r = \beta(M)$ always is close to the origin.

The following special cases of orientation of plane waves should be noted.

1. Plane waves are propagating downstream at $\cos \chi_0 = 1$. Hot-wire output is zero at $r_0 = \alpha(\kappa - 1)M$.
2. Plane waves are propagating upstream at $\cos \chi_0 = -1$, $r_0 = -\alpha(\kappa - 1)M$.
3. Plane waves are propagating across the flow at $\cos \chi_0 = 0$, $r_0 = -\alpha(\kappa - 1)$.
4. As it follows from Eq.(A3), at $\cos \chi_0 = -M$ the denominator vanishes, and r_0 tends to infinity.

Calculated fluctuation diagrams corresponding to cases (1...4) are shown in Fig.A1 for 1% density fluctuations. All the diagrams intersect themselves at $r = \beta$ when the terms containing $\cos \chi_0$ cancel each other, see Eq.(8), and for these conditions the hot-wire

output does not depend on orientation of acoustic waves:

$$\vartheta(\beta) = \langle \rho \rangle \beta \left(\frac{1}{M^2} - 1 \right) \quad (A5)$$

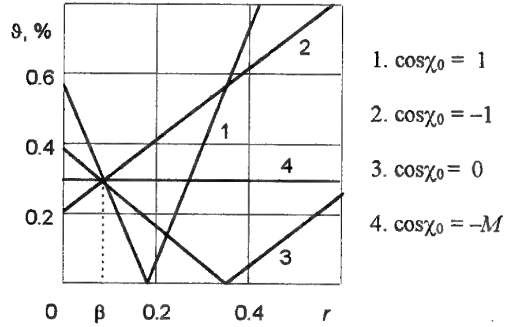


Fig.A1

Therefore, the intensity of plane acoustic disturbances can be found from the measurements at single overheat, if it is chosen such that $r = \beta$. The intensity of the entropy mode must be fairly low, the vorticity mode does not have any effect, since the sensitivity of a probe to that mode is equal to zero at $r = \beta$.

A2. Point Source

This is the cases when the sound source is localized and may be regarded as point source, for instance, the sound generated by a hole when the relative distance from finite sources to the probe is large.

Consider the response of a probe, placed at a point $P(0, y, 0)$, to acoustic fluctuations whose source is located at $S(x, 0, z)$. The notation is clear from Fig.A2.

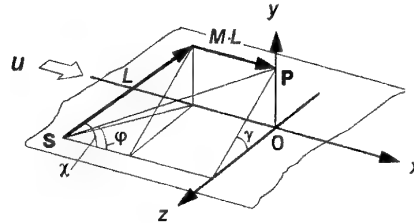


Fig.A2

The flow velocity is directed along x , and the probe wire is in (y, z) plane. Only those disturbances departing from the point S arrive to the point P , which propagate at a certain angle χ ($0 < \chi < \pi$) with sound velocity and are carried by the flow with velocity u . From geometric constructions:

$$\cos \chi = \cot \varphi \sin \chi - M \quad (A6)$$

The angle φ ($0 < \varphi < \pi$) governs the direction from the source to the probe. Solving Eq.(A6) for $\cos \chi$, we find

$$\cos \chi = -\frac{M^2}{1 + \cot^2 \varphi} + \frac{M^2}{\sqrt{(1 + \cot^2 \varphi)^2 + \frac{\cot^2 \varphi - M^2}{1 + \cot^2 \varphi}}} \quad (A7)$$

The second solution (with the minus sign in front of the radical) can be discarded, since it does not satisfy the condition $\sin \chi > 0$. Clearly, for a single-point source the fluctuation diagram also consists of two segments and is V-shaped, as that is in the previous case of a plane wave. Calculated from Eq.(A7), the values of $\cos \chi$ make it possible to determine r_0 using Eq.(A3).

A3. Distributed Sources

More general case corresponds to acoustic fluctuations produced by the sources distributed over a certain surface in the flow. Let us consider the response of hot-wire to acoustic fluctuations generated by sources S located in the plane (x, z) in a subsonic flow. The probe is placed at the point P , see Fig.A2.

Let $Q = Q(x, 0, z)$ be the intensity of the source of acoustic disturbances at a point S in the direction L forming an angle χ with the velocity vector. Assuming that the intensity of acoustic fluctuations varies inversely with distance L , for the fluctuations arriving to P from an element $dx dz$, using Eq.(A1) we have

$$d\mathcal{G}^2 = \frac{Q^2}{L^2} \left[\alpha(\kappa - 1)(1 + M \cos \chi) - r \left(1 + \frac{\cos \chi}{M} \right) \right]^2 dx dz$$

Taking into account $L = y/(\sin \chi \sin \gamma)$, we obtain

$$\mathcal{G}^2 = \iint_s \frac{Q^2 \sin^2 \chi \sin^2 \gamma}{y^2} \left[\alpha(\kappa - 1)(1 + M \cos \chi) - r \left(1 + \frac{\cos \chi}{M} \right) \right]^2 dx dz \quad (A8)$$

Replacing the variables (x, z) with (χ, γ) :

$$x = L/(M + \cos \chi), \quad z = y \cot \gamma, \quad d\chi d\gamma = d\sigma:$$

$$\iint_s F(x, z) dx dz = \iint_\sigma F(\chi, \gamma) \frac{\partial(x, z)}{\partial(\chi, \gamma)} d\chi d\gamma$$

where Jacobian:

$$\frac{\partial(x, z)}{\partial(\chi, \gamma)} = \begin{vmatrix} \frac{\partial x}{\partial \chi} & \frac{\partial x}{\partial \gamma} \\ \frac{\partial z}{\partial \chi} & \frac{\partial z}{\partial \gamma} \end{vmatrix} = \frac{\partial x}{\partial \chi} \frac{\partial z}{\partial \gamma} - \frac{\partial x}{\partial \gamma} \frac{\partial z}{\partial \chi}$$

$$\frac{\partial x}{\partial \chi} = -\frac{y(1 + M \cos \chi)}{\sin^2 \chi \sin \gamma}, \quad \frac{\partial z}{\partial \chi} = 0$$

$$\frac{\partial x}{\partial \gamma} = \frac{y(M + \cos \chi) \cos \gamma}{\sin \chi \sin^2 \gamma}, \quad \frac{\partial z}{\partial \gamma} = -\frac{y}{\sin^2 \gamma}$$

After substitutions and calculations instead of Eq.(A8) we have

$$\mathcal{G}^2 = \iint_\sigma \frac{Q^2(\chi, \gamma)}{\sin \gamma} (1 + M \cos \chi) \times \left(\frac{\beta - rM^2}{M^2} + \frac{\beta - r}{M} \cos \chi \right)^2 d\chi d\gamma \quad (A9)$$

Equation (A9) is the equation of acoustic mode diagram for the fluctuations generated by sources distributed over a plane in a subsonic flow. If the intensities of source generation are equal and do not depend on direction i.e. $Q(\chi, \gamma) = Q = \text{const}$, the variables can be separated:

$$\mathcal{G}^2 = Q^2 J_\chi J_\gamma \quad (A10)$$

$$\text{where } J_\gamma = \int_{\gamma_1}^{\gamma_2} \frac{d\gamma}{\sin \gamma},$$

$$J_\chi = \int_{\chi_1}^{\chi_2} (1 + M \cos \chi) \left(\frac{\beta - rM^2}{M^2} + \frac{\beta - r}{M} \cos \chi \right)^2 d\chi$$

For sources of disturbances equispaced over a wall and when measurements are made by a probe mounted on the axis of the test section the limits of integration for J_γ are $-\pi/4 \leq \gamma \leq 3\pi/4$ and

$$J_\gamma = \int_{-\pi/4}^{3\pi/4} \frac{d\gamma}{\sin \gamma} = \frac{1}{2} \ln \frac{1 + \cos \gamma}{1 - \cos \gamma} \Big|_{-\pi/4}^{3\pi/4} \approx 1.76$$

The limits of integration for J_χ can be defined as $0 \leq \chi \leq \pi$ assuming that the contribution from distant sources is not significant:

$$\begin{aligned} J_\chi &= \int_0^\pi \left[\left(\frac{\beta - rM^2}{M^2} \right)^2 + 2 \frac{\beta - rM^2}{M^2} \frac{\beta - r}{M} + \frac{(\beta - rM^2)^2}{M^3} \right] \cos \chi + \\ &+ \left(\frac{(\beta - r)^2}{M^2} + 2 \frac{(\beta - rM^2)(\beta - r)}{M^2} \right) \cos^2 \chi + \\ &+ \frac{(\beta - r)M^2}{M^2} \cos^3 \chi \Big] d\chi = \\ &= \pi \left[\frac{(\beta - rM^2)^2}{M^4} + \frac{1}{2} \frac{(\beta - r)^2}{M^2} + \frac{(\beta - rM^2)(\beta - r)}{M^2} \right] \end{aligned} \quad (A11)$$

Finally, after transformations and calculations, Eq.(A11) becomes

$$\mathcal{G}^2 \approx 553 \frac{Q^2}{M^2} \left[\frac{r^2}{2} (4M^2 + 1) - r\beta(4 + M^2) + \beta^2 \frac{2 + 3M}{2M^2} \right] \quad (A12)$$

This is an equation of hyperbola with a minimum at the point $(r_*, 0)$

$$r_* = \beta \frac{4 + M^2}{4M^2 + 1} \quad (A13)$$

The correlation coefficient R_{mT_0} between the mass flux and total temperature fluctuations depends only on the Mach number:

$$R_{mT_0} = \frac{(4 + M^2)M}{\sqrt{2 + 3M^2} \sqrt{4M^2 + 1}} \quad (A14)$$

and at high subsonic velocities it tends to unity.

AERODYNAMIC DESIGN OF NOZZLES FOR SUBSONIC AND TRANSONIC WIND TUNNELS

Byrkin A.P., Ponomaryov S.P.,
Ponomaryova V.S., Filatov A.P.
Central Aerohydrodynamic Institute (TsAGI), 1, Zhukovsky Street
140160 Zhukovsky, Moscow Region, Russia

1. ABSTRACT

This report gives results of theoretical considering and experimental researching of gas flows in axisymmetric nozzles of sub- and transonic wind tunnels. Two classes of nozzle transverse contours were investigated at test section flow velocities corresponding to Mach numbers of $M_\infty=0.1-1.0$. Cross-section shapes for the first class of contours were calculated using the Witoszinski equation [1], and for the second class they were determined by the equations considered in the present report.

It is shown that the flow pattern which takes place in the considered nozzles, especially at nozzle entries, is not one-dimensional. It is found, that the Witoszinski contour is unacceptable for a practical implementation of representative contraction factor and nozzle length-to-diameter ratio values; the reason is unacceptable negative longitudinal velocity gradient value on the wall near the nozzle entry, which can lead to boundary layer separation.

Similar results are given for a gas flow in the nozzles having rectangular, circular and octagonal transverse contours and also in the nozzle having circular transverse entry contour and octagonal transverse exit contour.

2. NOMENCLATURE

x, y, z	rectangular coordinate system
x, r, φ	cylindrical coordinate system
u, v, w	velocity components in coordinate systems mentioned above
$V = \sqrt{u^2 + v^2 + w^2}$	resultant velocity
a	speed of the sound
$M=V/a$	Mach number
$\psi(x, r)$	stream function
y_w, z_w, r_w	ordinates of nozzle transverse contour in coordinate systems mentioned above
l	length of curvilinear part of nozzle contour
d	nozzle diameter
$c=F_1/F_2$	nozzle contraction factor
F	cross-section area
L	shape factor of turbulent boundary layer
ε	turbulence intensity

Subscripts

1	nozzle entry
2	nozzle exit
0	nozzle axis
w	nozzle wall
∞	uniform flow
sc	stilling chamber

3. INTRODUCTION

The function of wind tunnel nozzle is to shape uniform gas flow at nozzle exit. The mean velocity in nozzle increases

from small values (in nozzle entry) up to the values, at which researches in a wind tunnel will be carried out.

One of the nozzle characteristics is the nozzle contraction factor i.e. the ratio of the entry section area to the exit section area.

An important requirement imposed to a nozzle is the absence of flow separation on the wall, because of the positive pressure gradient along the wall at a strongly curved contour [2-3]. Flow separation is undesirable, as it promotes the flow turbulence intensity increase. One of the ways of reducing the positive wall pressure gradient is to increase the nozzle length, but it is unacceptable, because viscosity effect reduces the uniform flow core in the test section, which is of particular importance for large wind tunnels.

In the present report, the technique for designing of an axisymmetric nozzle contour is described, in which such positive pressure gradient is allowed along the wall that the boundary layer separation does not occur. In the line of this technique the velocity fields in the nozzle were calculated assuming that the flow was inviscid; numerical integration of the stream function equation is performed by a relaxation method. The nozzle contour of the contraction factor $c=12$ was designed under the suggested technique; an experimental research was performed with the purpose to determination of longitudinal distribution of gas velocities on the nozzle axis and wall over the range of Mach numbers of $M_\infty=0.3-1.0$ at a nozzle exit. The design and test results are in satisfactory agreement.

The results of theoretical and experimental investigations of gas flow through the nozzle having a quasi-rectangular cross-sections are also considered in the report.

Furthermore, the principles and results of designing of the T-134 cryogenic wind tunnel nozzle, having a circumferential entry and octagonal exit cross-sections, are considered in the report.

4. CALCULATION OF INVISCID GAS FLOW IN SUBSONIC AXISYMMETRIC NOZZLES. COMPARISON WITH THE EXPERIMENT

The equation for stream function [4] is used for description of the subsonic potential compressed gas flow in the nozzle having specified contour $r_w(x)$,

$$\left[1 - \left(\frac{u}{a}\right)^2\right] \frac{\partial^2 \psi}{\partial x^2} - 2 \left(\frac{u}{a}\right) \left(\frac{v}{a}\right) \frac{\partial^2 \psi}{\partial x \partial r} + \left[1 - \left(\frac{v}{a}\right)^2\right] \frac{\partial^2 \psi}{\partial r^2} - \frac{1}{r} \frac{\partial \psi}{\partial r} = 0.$$

In this case it is assumed, that the function $r_w(x)$ has asymptotes of $r_w(x)=\text{const}$ at $x \rightarrow \pm\infty$.

This equation is solved in the internal area, limited by the nozzle contour (a typical nozzle contour is shown on Fig. 1) under appropriate boundary conditions. By the use of independent variable transformation,

$$\xi = x, \quad \eta = \frac{r}{r_w(x)}$$

the original region of integration is reduced to the rectangular strip of width of $\eta=1$ and the equation to determine the function ψ take the form,

$$\frac{\partial^2 \psi}{\partial \xi^2} = A \frac{\partial \psi}{\partial \eta} + B \frac{\partial^2 \psi}{\partial \eta^2} + C \frac{\partial^2 \psi}{\partial \xi \partial \eta},$$

where A, B and C are the changeable coefficients, which are determined by value of Mach number in the design point, the nozzle wall coordinate $r_w(x)$ and also values of first- and second-order derivatives of the coordinate x ($r'_w(x)$ and $r''_w(x)$ respectively).

The calculation of a inviscid gas flow in nozzle was carried out on the basis of numerical integration of the equation for stream function ψ by the relaxation method [5].

As an example design of subsonic gas flow in nozzle was executed by authors; a curvilinear part of the nozzle contour being defined by the Witoszinski formula,

$$r_w(x) = \frac{r_{w2}}{\sqrt{1 + \left[\left(\frac{r_{w2}}{r_{w1}} \right)^2 - 1 \right] \frac{[1 - 3(x/s)^2]^2}{[1 + (x/s)^2]^3}}}, \quad (1)$$

$(0 \leq x \leq s/\sqrt{3}),$

where s is the parameter, related to the length of curvilinear part l by the equation $s = \sqrt{3}l$.

We will note that the Witoszinski formula was used earlier in the practice of designing nozzles for wind tunnels in Russia.

The Witoszinski nozzle contour with the contraction factor of $c=(r_{w2}/r_{w1})^2=5.4$ is depicted in Fig. 1. The reduced length of $l=4.2$ is chosen for this factor c according to the recommendation of Ref. [6]. Here and below all the linear dimensions are related to the radius of the nozzle exit section r_{w2} , except as otherwise noted. The coordinate of the contour interflexion point x_i is indicated on the plot.

Calculation of the stream in the above-outlined nozzle was carried out for uniform flow at nozzle exit section at Mach number of $M_\infty=0.3$. The distributions of nondimensional resultant velocity ($V = \sqrt{u^2 + v^2}$) on the nozzle axis (V_0/V_∞) and on the nozzle wall (V_w/V_∞) against nondimensional coordinate x/d_1 are shown in Fig. 2. It is seen that zones of negative longitudinal velocity gradient on the nozzle wall take place in the vicinity of initial and final portions of the nozzle curvilinear part, which can result in a boundary layer separation and thereby in an increased flow turbulence intensity.

Besides, calculations of gas stream in the Witoszinski nozzle are performed at Mach numbers of $M_\infty=0.5$; 0.8 and 1.0. Distributions of Mach numbers on the nozzle axis ($M_0(x)$) and on the nozzle wall ($M_w(x)$) along nondimensional coordinate x/d_1 at Mach numbers of 0.5 and 1.0 are shown in Fig. 3. Under all considered Mach numbers M_∞ the distributions of nondimensional velocity on the nozzle wall are V_w/V_1 presented in the vicinity of a initial portion of the nozzle curvilinear part (V_1 is the velocity of uniform flow at nozzle entry section) and distributions of values of $V_w/V_\infty(x)$ in the vicinity of the final portion of the nozzle curvilinear part are also presented. It is seen that the Mach number M_w along the nozzle wall vary non-monotonically. We will note

that the function V_w/V_1 practically does not depend on Mach number M_∞ . Non-monotonicity of Mach number M_w (or V_w/V_∞) distribution along the x axis is minimal in the vicinity of the exit section at $M_\infty=1.0$.

It is possible to make the conclusion on the basis of the obtained results of the calculations that there will be no deterioration of the flow quality near nozzle exit section at transonic velocities in comparison with the case of small subsonic velocities.

The calculated distributions of velocities and Mach numbers along the Witoszinski nozzle axis are compared with the test data. The test nozzle had the diameter of nozzle entry section of $d_1=232$ mm, the diameter of exit section of $d_2=100$ mm and length of curvilinear part $l=210$ mm. The equalizing wire screen were mounted in the stilling chamber at a distance of ~ 200 mm from a junction line of the stilling chamber and the nozzle; drag coefficient of the screen $\zeta=2.0$. The cylindrical test section with the diameter of 100 mm was jointed to the nozzle exit.

The following characteristics were measured during the tests: static pressure distributions along the stilling chamber, nozzle and test section walls; static pressure distributions along the axis of symmetry; total pressure distributions across area of the test section.

Comparison of calculated data on gas velocity and Mach number distributions on the nozzles wall and axis along the nozzle length with the same test result demonstrated (see Figs. 2 and 3), that the satisfactory correlation takes place in the Mach numbers range from $M_\infty=0.3$ to $M_\infty=1.0$. Besides, the comparison is testifies, that viscosity effect on flow nature is weak and by this reason the presented results can be used for wind tunnels with essentially larger linear dimensions.

For conditions which are adequate to the above mentioned test conditions (total pressure is close to atmospheric one; velocity $V=50-100$ m/s) calculation of shape factor L for turbulent boundary layer on the wall of nozzle entry part was performed using the technique given in Ref. [7]. It turns out, that the magnitude L exceeds in absolute value its critical magnitude. It means, that the boundary layer separation should occur at the vicinity of nozzle entry.

The presence of the boundary layer separation indirectly proves to be true by flow pattern visualization on the inner surface of nozzle wall with use of oil flow technique. The film gets characteristic "scaly" structure under the action of gas flow in the vicinity of calculated maximum negative velocity gradients. Upstream and downstream from this place "beam lines" are inherent in visualized pattern of flow. When soot-oil medium was applied on the wall in the form of points, the points remained unchanged at the place of the calculated maximum negative velocity gradients but upstream and downstream of this place the points were transformed to longitudinal "strokes".

5. CHOICE OF THE ACCEPTABLE NOZZLE TRANSVERSE CONTOURS FOR WIND TUNNELS. CALCULATION OF FLOW FIELDS AND FLOW SEPARATION CRITERIA

Lengthening of the nozzle is one of the ways for decrease of a velocity negative gradient on the nozzle wall for the purpose of prevention of a boundary layer separation at nozzle entry. However this approach is undesirable because of flow

inviscid core reduction in the test section and wind tunnel extension. To attain this purpose, other approaches are used (see e.g. [2, 3]). The dominant content of the work [2] is to find the nozzle contour of finite length, along the wall of which monotonous increase of velocity is realized. The Ref. [3] is devoted to finding the required nozzle contour (within of an examined class of contours) wherein negative velocity gradient can be realized on the wall, but boundary layer separation does not occur. Using the technique of [3] in a simplified form, we can write there the second-order derivative of contour curve $r_w''(x)$ in the form (see Fig.1),

$$r_w''(x) = -\alpha \sin\left(\frac{x}{x_i} \pi\right) \quad 0 \leq x \leq x_i,$$

$$r_w''(x) = \beta \sin\left(\frac{x-x_i}{l-x_i} \pi\right) \quad x_i \leq x \leq l,$$

where α, β are the positive constants and x_i is the coordinate of the inflexion point.

Then, after reiterate integration and using the condition $r_w'(0)=0$ and given value $r_w(0)$ we obtain,

$$r_w(x) = r_w(0) + \alpha \frac{x_i}{\pi} \left[\frac{x_i}{\pi} \sin\left(\frac{x_i}{\pi} - x\right) - x \right], \quad 0 \leq x \leq x_i,$$

$$r_w(x) = r_w(0) - \alpha \frac{x_i^2}{\pi} - 2\alpha \frac{x_i}{\pi} (x - x_i) + \beta \frac{l-x_i}{\pi} (x - x_i) - \beta \left(\frac{l-x_i}{\pi} \right)^2 \sin\left(\frac{x-x_i}{l-x_i} \pi\right), \quad x_i \leq x \leq l. \quad (2)$$

Values of constants α and β for the given contraction factor c , length of curvilinear part l and coordinate of inflexion point x_i are determined by the condition of $r_w'(l)=0$ and constant value $r_w(l)$,

$$\alpha = \frac{r_w(0) - r_w(l)}{x_i l} \pi, \quad \beta = \frac{x_i}{l - x_i} \alpha.$$

Contrary to Ref. [3] Eqs. (2) provide a possibility to represent the nozzle contour $r_w(x)$ at an analytical form. Due to introduction of the additional parameter i.e. coordinate of an inflexion point x_i into the Eqs. (2), this formulae give the family of nozzle contours, in contrast with the Witoszinski formula; these contours have the same values of contraction factors and length-to-diameter ratio. At fixed values of parameters c and l , we obtain nozzles contours more flatter (steeper) in the initial portion of the curvilinear part and, on the contrary, more steeper (flatter) in final portion of this part by changing coordinate x_i .

The curvilinear contours $r_w(x)$ calculated under the Witoszinski formula (for $c=12$ and $l=8$) and Eqs. 2 (for $c=12$, $l=8$ and $x_i=2.65$), are presented in Fig. 4. The nozzles, corresponding to the contours above mentioned will be designated as "1" and "2". It is seen in Fig. 4, that the entry part of nozzle "2" is flatter than one of nozzle "1".

Here results of flow pattern calculation in the mentioned nozzles at Mach number of $M_\infty=0.1$ are presented in the form of distributions V_0/V_∞ , V_w/V_∞ along longitudinal coordinate x . It is possible to see that flatter distributions of $V_w/V_\infty(x)$ take place in the nozzle "2" entry part, that decreases the probability of flow separation on the wall. At the same time, some increase of flow non-uniformity near the wall in a vicinity of $x=l$ decreases quickly along wall in comparison with nozzle "1".

Note also that in case of nozzle "2", being preferable for the above reason, velocity perturbations of uniform flow (up to 0.5 %) take place at nozzle entry at a distance of $\Delta x \approx 3$ upstream of the initial portion of the curvilinear part. It means, that last equalizing screen in stilling chamber should be mounted in front of nozzle at a distance, not smaller than calculated value of Δx .

Calculations of gas flows in the nozzle "2" were carried out for Mach numbers of $M_\infty=0.3$; 0.5; 0.8 and 1.0; some results of the calculations are shown in Fig. 5 (similar to Fig. 3) and are compared with the experimental results.

The tested nozzle had the contraction factor of $c=12$, entry diameter $d_1=232$ mm, exit diameter $d_2=67$ mm and length $l=268$ mm. The technique of the test was the same, as in the test of Witoszinski nozzle with contraction factor of $c=5.4$. Comparison of the calculation and test results testifies their satisfactory conformity.

Calculation of the turbulent boundary layer form factor L at the entry part nozzle "2" was performed for test conditions. Despite flatter distributions of reduced velocity V_w/V_∞ along the wall in comparison with nozzle "1" case, the maximum values of L proved to be just below the critical value of the factor; in the case of nozzle "1" magnitude of L exceeds critical value.

The flow pattern visualization at the entry part using oil-soot film has shown, that under the action of gas flow the film gets more uniform structure in comparison with the pattern, described in Part 3. It does not allow, however, to make conclusion about completely unseparated flow on the nozzle wall.

On the basis of estimations of the form factor L it may be considered that unseparated flow conditions can be realized in case of nozzle "3" (see. Fig. 4), which has the length of the curvilinear part of $l=10$ at the same contraction factor $c=12$. In comparison with the nozzle "2" location of the inflexion point x_i does not change, and the increase of l from $l=8$ up to $l=10$ is achieved at the expense of a part of the stilling chamber so that the distance from last equalizing screen downstream up to the nozzle exit section was remained the same as in the case of nozzle "2".

6. RESEARCH OF GAS FLOW IN NOZZLE OF RECTANGULAR CROSS SECTION WITH CUT CORNERS

Experimental research of gas flow was carried out in a rectangular cross section nozzle installed in the wind tunnel model [8] at $V_\infty=70$ m/s. The nozzle contraction factor was of $c=6.4$; shape and dimensions of nozzle entry and exit cross-section of curvilinear parts are shown in Fig. 6. Nozzle length $l=1100$ mm was chosen on the basis of the recommendation of work [6]. Considering that the greatest longitudinal positive pressure gradients can occur in right corners of nozzle cross-section the corners were fabricated oblique at 45° . The nozzle walls contours $y_w(x)$ in the plane of $z=0$ and $z_w(x)$ in the plane of $y=0$ are shown in Fig. 6. All linear dimensions are related here to the half-height of nozzle y_{w2} at the exit section.

We note, that the contours $y_w(x)$ and $z_w(x)$ agree close to the contours calculated by the Eqs. (2) at $x_i=1.5$ and above specified the nozzle linear dimensions.

The flow characteristics in nozzle were estimated by its quality in the test section and by longitudinal pressure distribution along the nozzle axis and axes of symmetry of three surfaces (see Fig. 6): upper, lateral and angular (obliqued surface). So, a uniform flow was obtained in the test section with reduced static pressure non-uniformity (related to dynamic pressure) of $\leq \pm 0.2\%$. Flow turbulence intensity ϵ calculated through the use of measured values of longitudinal velocity components is equal to $0.075 - 0.090\%$; the measurements were made in cross section, located in half way along solid wall test section. These data testify to rather high flow quality in the wind tunnel test section, and it can be assumed that a flow separation on walls at nozzle entry part did not arise. As the tests results show [6], when flow separation occurs in nozzle, it makes flow quality in nozzle exit worse.

Distributions of values V/V_∞ were calculated on the basis of the longitudinal pressure distributions along of nozzle axis and along axes of symmetry of the upper, lateral and angular walls; results of calculation are given in Fig. 6. Here subscript "j" refers to the characteristic cross section points which are marked by digits "0", "1", "2" and "3". As can be seen from the Fig. 6 increased spread of test points take place at the nozzle exit section which can be explained by some departures of real nozzle contour coordinates in this section from the designed contour due to nozzle fabrication.

The test results are compared with the results of calculation, performed by analogy to work [10]. The presence of cut corners of the rectangular nozzle contour was not taken into account.

It can be seen graphically in Fig. 6 that on the largest part of the nozzle length the calculated data agreed satisfactorily with experimental results on the nozzle axis and on the axes of symmetry of the upper and lateral walls. The experimental distributions of $V_3/V_\infty(x)$ differ from the calculated one on the angular panel. They have appeared close to the distributions on the upper ($V_1/V_\infty(x)$) and lateral ($V_2/V_\infty(x)$) walls. Thus, flow pattern in the rectangular nozzle with cut right corners comes nearer to the axisymmetric stream.

The final flow equalizing occurs in the test section at a distance of half of its caliber. The tests have confirmed the obtained earlier theoretical deduction that the nozzle contour affects the flow in stilling chamber upstream at a distance up to $0.5 d_{sc}$.

7. DESIGN OF ADAPTING NOZZLE WITH CIRCUMFERENTIAL ENTRY CROSS-SECTION AND RECTANGULAR EXIT CROSS SECTIONS WITH CUT RIGHT CORNERS. EXPERIMENTAL RESEARCH OF THE NOZZLE

The nozzle is one of critical elements of the 625×625 mm cryogenic transonic wind tunnel T-134 designed of TsAGI. The nozzle function is acceleration of gas flow from Mach number of $M_\infty=0.05$ (in the stilling chamber) to design velocity in the test section up to the sound speed ($M_\infty=1.0$) inclusive.

Besides common requirements, that can be imposed to the nozzle (the provision of flow uniformity and unseparated stream), additional condition of wind tunnel design optimization was laid down in this case: the stilling chamber should have a circumferential cross-section, and the wind tunnel test section should have a rectangular cross-section with cut right corners. By this means, the nozzle should carry

out a service of the "distance adapter", (hereinafter we shall use the term "adapting nozzle") which cross-section shape changes from circumferential to octagonal; simultaneously the nozzle should carry out its general aerodynamic service. The main part of nozzle, contiguous to the wind tunnel test section represents a part of original nozzle with octagonal shape of cross section. The other and smaller part of nozzle, beginning from stilling chamber, is designed as the adapting nozzle; for the decision of the problem of adapter designing specialized computer graphic system was used. The configuration of adapting nozzle of wind tunnel T-134 is shown on Fig. 7.

In the basis of development of the nozzle adapter the following principles were fixed:

- The surface of a through-flow part of the adapting nozzle should consist of four wide and four narrow surfaces single (longitudinal) curvature, i.e. cylindrical surfaces, being upstream extensions of wide and narrow sides of octagonal test section. The eight double curvature surfaces should be placed between them.
- The double curvature surfaces should connect wide and narrow single curvature surfaces in the nozzle cross sections by arches of a circle under the radius of r variable along length of the adapter: from $r = r_{sc}$ at the nozzle inlet to $r=0$ at the nozzle exit.
- Values of first-order derivatives r'_w at $\varphi=\text{const}$ for surfaces of single and double curvature should be equal to each other on the lines of their connection.
- The distribution of the cross sections areas $F(x)$ of an adapter should be the same as to the designed (original) octagonal nozzle.

Calculation of the coordinates $y_w(x)=z_w(x)$ of the original octagonal nozzle with chosen contraction factor of $c=12.7$ and reduced length $l/r_{sc}=2.3$, are calculated under the Eqs. (2); this nozzle was the basis for the designing the adapter. Projections of the change lines between wide and narrow nozzle sides onto the plane of yz (see Fig. 7) are straight lines. The narrow side width at the nozzle exit, related to the test section height, was set to be equal to 0.1; width of narrow side at nozzle entry was determined from the condition, that the original nozzle area at the nozzle entry is equal to the area of stilling chamber cross-section.

Stipulated above conditions allow to determine a three-dimensional geometry of a through-flow part.

Longitudinal contouring the adapter surface was performed through the use of two-dimensional spline functions ensuring continuity of the coordinates and their first-order derivatives at nodal points. The latter ensured smooth easement of connection between round cylindrical stilling chamber and the octagonal contour of the original nozzle.

The 1/5-scale adapting nozzle wood model of the wind tunnel T-134 was fabricated and then it was tested in a gas-dynamic test bench.

The test longitudinal distributions of Mach numbers (M_w vs. $-x/r_{sc}$) on the nozzle wall at values of coordinate of $\varphi=0$ and 45° and Mach number in uniformly stream of $M_\infty=0.5$ are shown in Fig. 8. Mach numbers M_w are calculated under the measured ratio between static pressure on the nozzle wall and the total pressure in the stilling

chamber. The calculated and experimental curves of Mach numbers M_∞ distributions coincide practically and they are of monotonic type of curves at $\varphi = 0^\circ$ and 45° .

The satisfactory experimental data obtained on the nozzle model suggest to apply above mentioned principles of designing of the adapting nozzle in case large-scale wind tunnels.

REFERENCES

1. Witoszinski, C., "Über Strahlerweiterung und Strahlablendung. Vorträge auf dem Gebiete der Hydro- und Aerodynamik (Insbruck, 1922)", Berlin, 1924.
2. Twaits, B., "On the Design of Contractions for Wind Tunnels", ARC R & M, 1949, No. 2278.
3. Mikhail, M.N., "Optimum Design Wind Tunnel Contractions", AIAAJ, vol. 17, No. 5, 1979.
4. Fabricant, N.Ya., "Aerodynamics. Part 1", Moscow, 1972.
5. Marchuk, G.I., "Methods of Computing Mathematics", Izd. SO AN SSSR, Novosibirsk, 1972 (in Russian).
6. Juska, J.A., Diedrich, J.H., Claugh, N., "Lewis 9-by 15-Foot V/STOL Wind Tunnel", NASA TM X-2305, 1975.
7. Schlichting, H., Gersten, K., "Berechnung der Strömung in rotationssymmetrischen Diffusoren mit Hilfe der Grenzschichttheorie", Zeitschrift für Flugwissenschaften, v. 9, 4/5, 1961.
8. Ponomarev, S.P., "Aerodynamic Configuration and Aerodynamic Characteristics of Model of TsAGI's Subsonic Wind Tunnel T-03", Trudy TsAGI, issue 2306, 1986 (in Russian).
9. Klein, A., Ramjee, V., Ventkataramani, K.S., "An Experimental Study of the Subsonic Flow in Axisymmetric Contractions", Zeitschrift für Flugwissenschaften, v. 21, No. 9, 1973.
10. Byrkin, A.P. and Yakusheva, V.L., "Numerical Calculation of Three-Dimensional Gas Flows through Low Speed Wind Tunnel Contractions (Nozzles)", Uchyonnye Zapiski TsAGI, vol. XI, No 5, 1980 (in Russian).

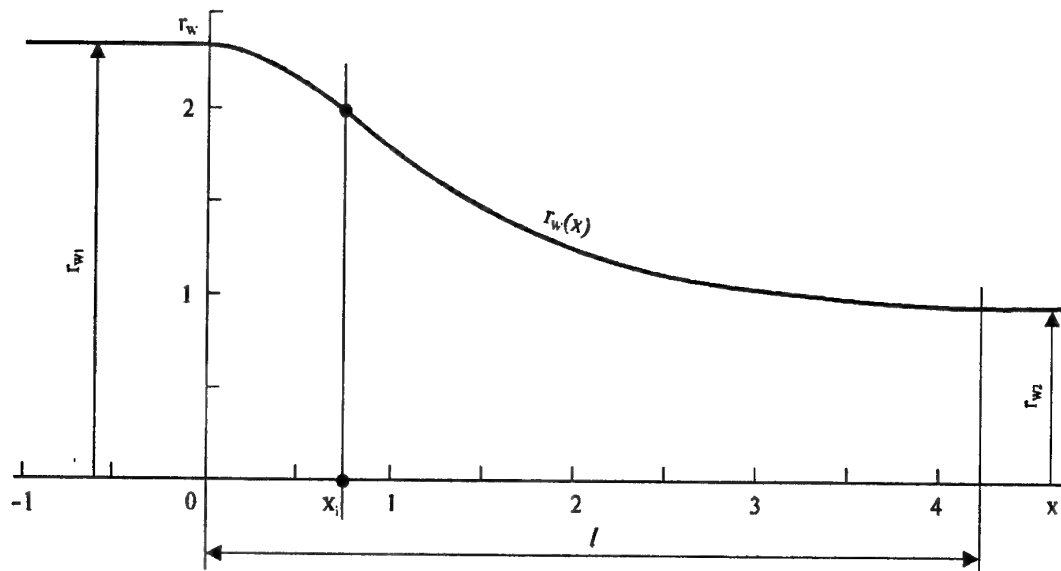


Figure 1. Contour of Witoszinski nozzle: $r_w(x)$, $c = 5.4$.

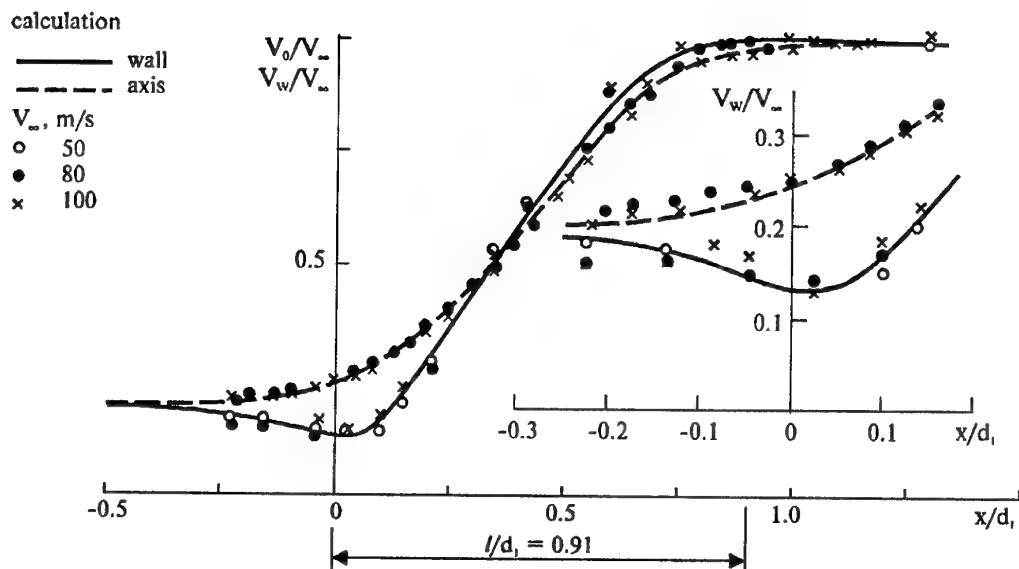


Figure 2. Reduced velocities profile V_0/V_∞ and V_w/V_∞ along x coordinate in Witoszinski nozzle, $c = 5.4$.

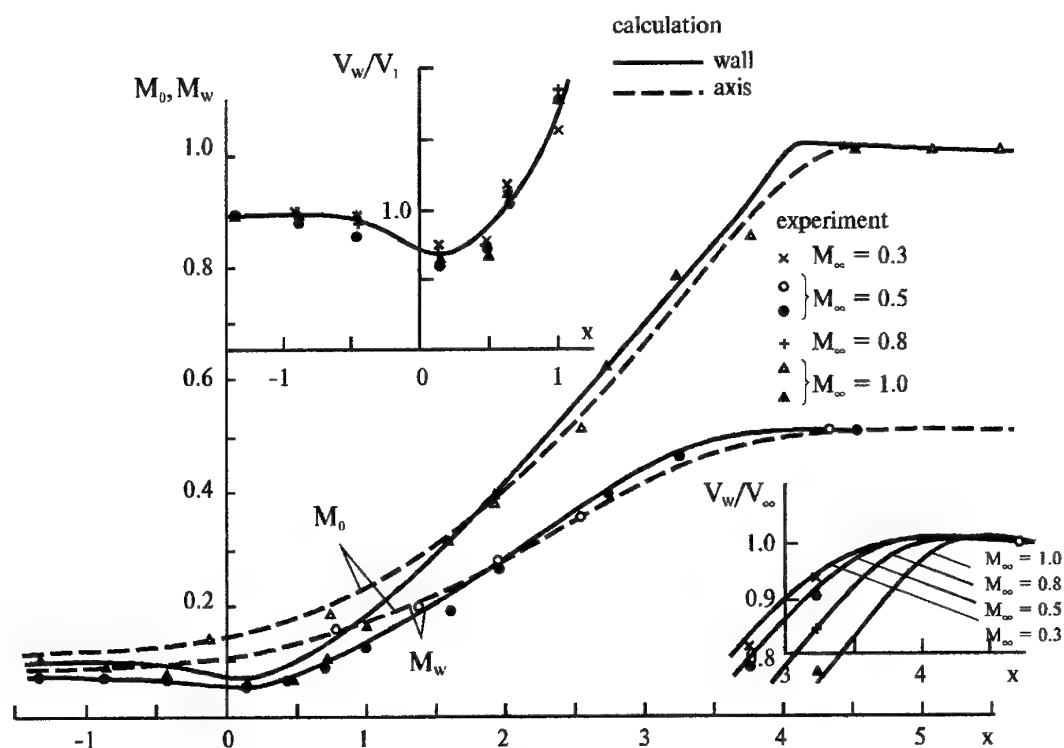


Figure 3. Mach numbers profile M_0 , M_w and reduced velocities V_w/V_1 , V_w/V_∞ along x coordinate in Witoszinski nozzle ($c = 5.4$) at $M_\infty = 0.3$; 0.5; 0.8 and 1.0.

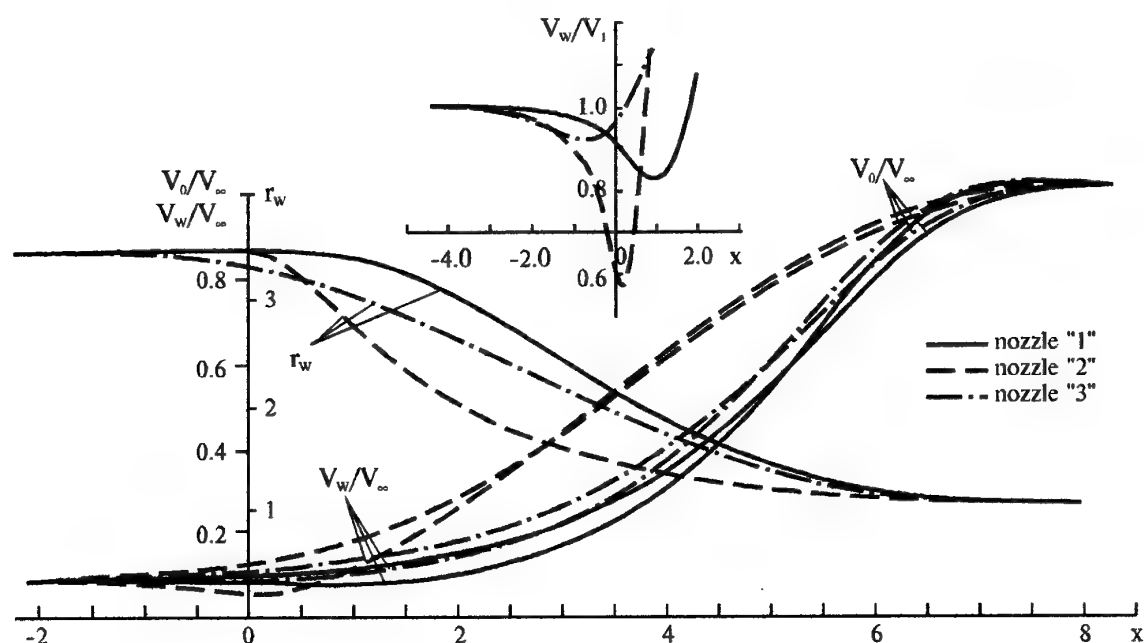


Figure 4. Contours of Witoszinski nozzle (nozzle "2") and recommended contours (nozzles "1" and "3") at $c=12$. Reduced velocities profile V_0/V_∞ and V_w/V_∞ along x coordinate at $M_\infty=0.1$.

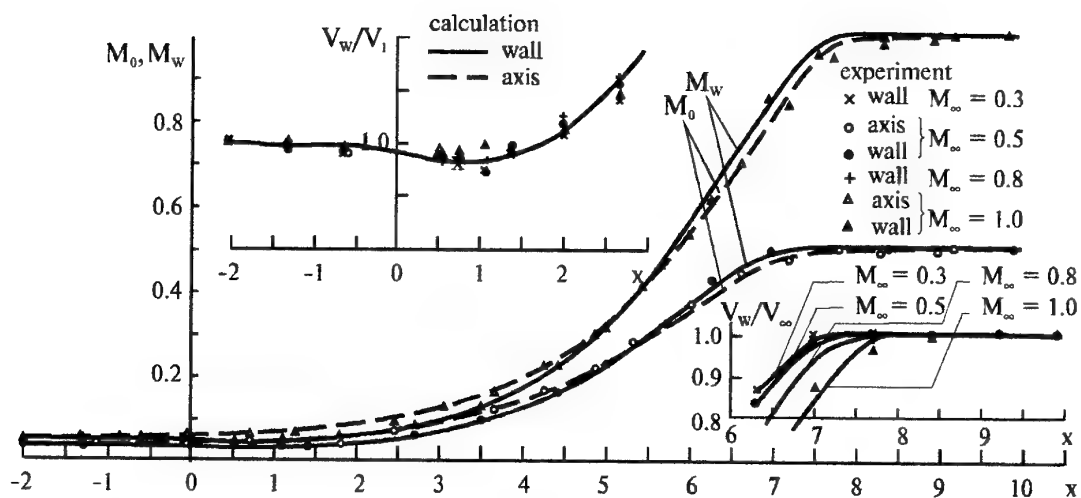


Figure 5. Mach numbers profile M_0 , M_w and reduced velocities profile V_w/V_1 and V_w/V_∞ along x coordinate in nozzle "1".

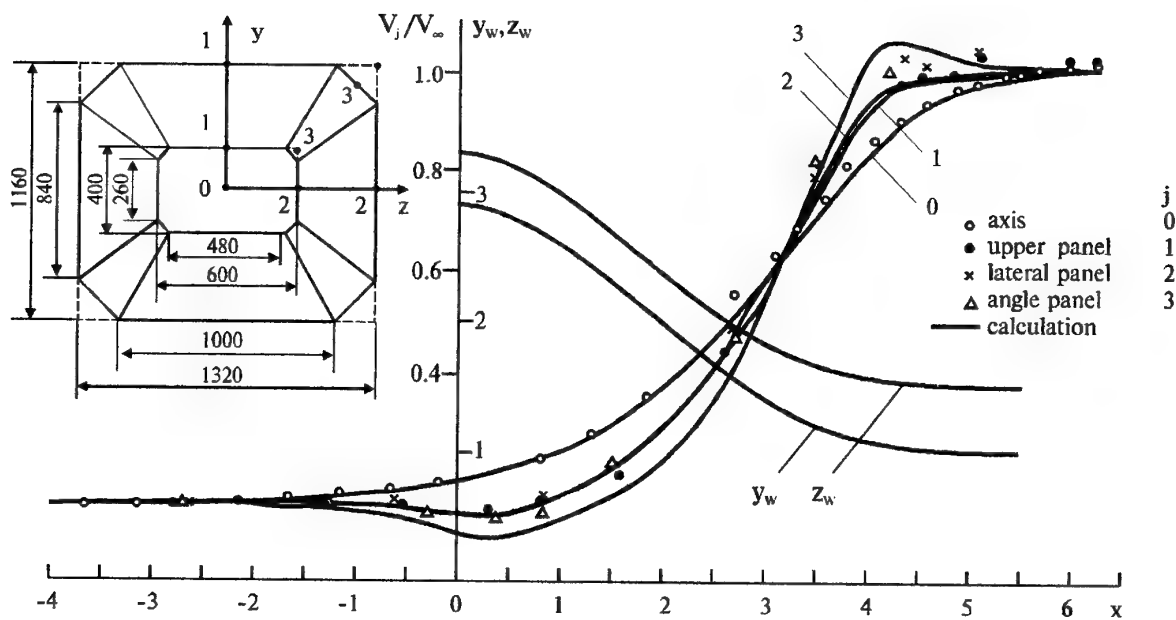


Figure 6. Contours of octagonal cross-section nozzle $y_w(x)$ and $z_w(x)$. Reduced velocities profile V_j/V_∞ along x coordinate.

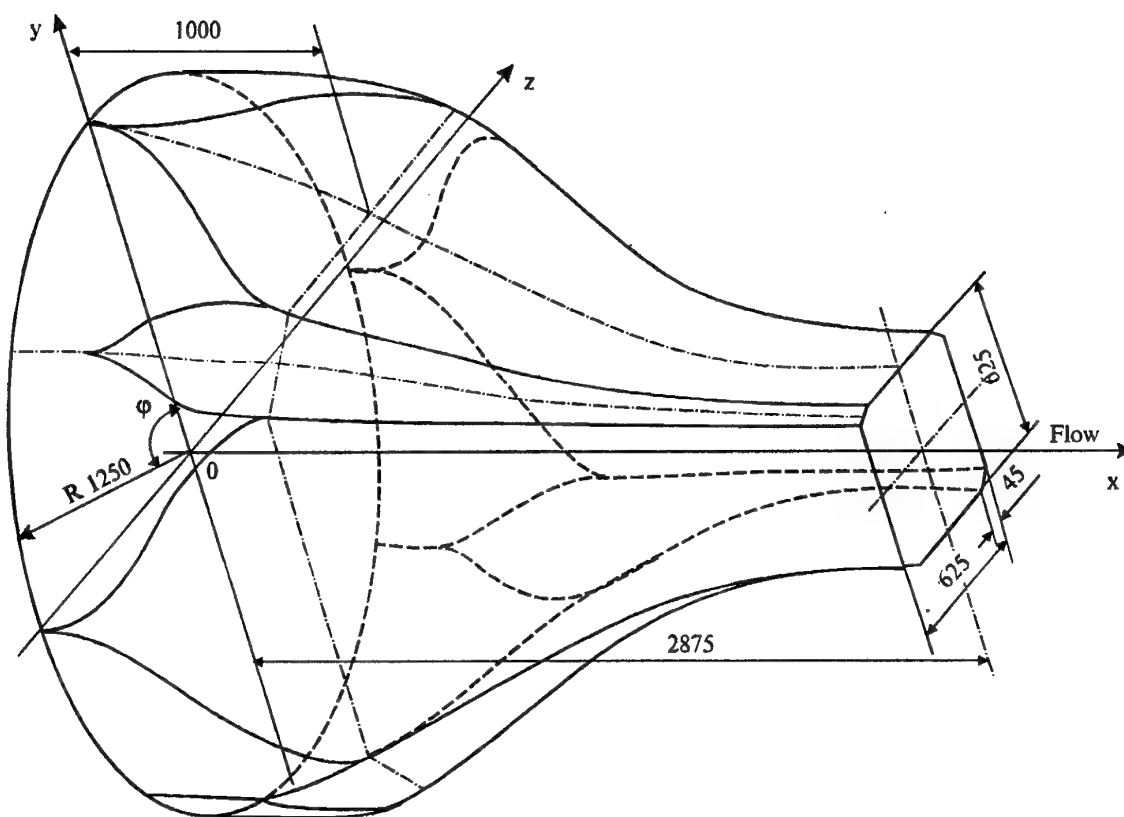


Figure 7. Geometric characteristics of nozzle adapter.

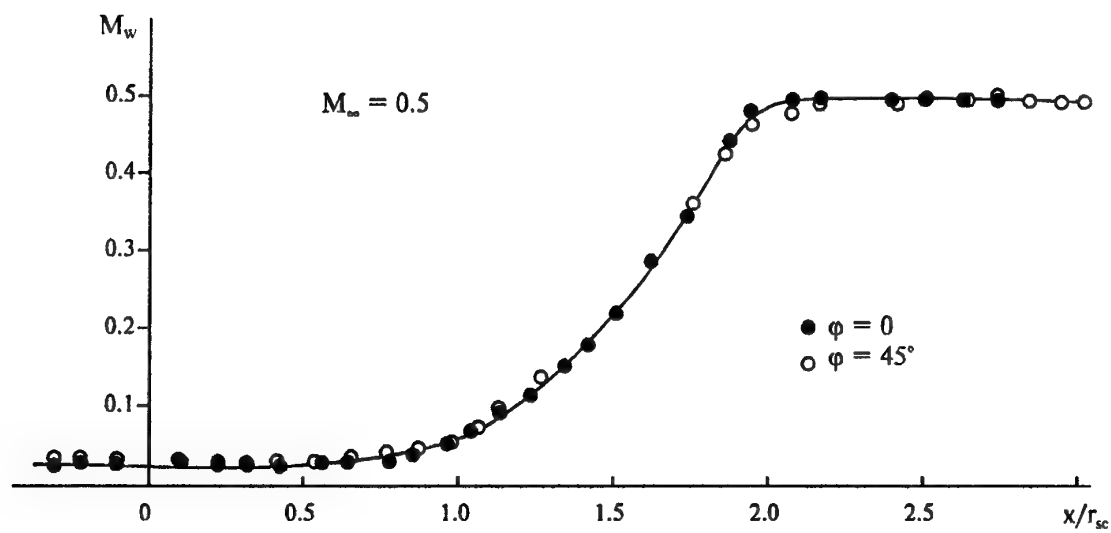


Figure 8. Mach number profile M_w along x/r_{sc} coordinate in nozzle adapter at $\phi = 0$ and 45° ($M_\infty = 0.5$).

METHOD FOR THE CALCULATION OF 2D SUPERSONIC VARIABLE NOZZLE CONTOURS

V.P. Verkhovsky
Central Aerohydrodynamic Institute (TsAGI), Zhukovsky, RU

ABSTRACT

The report considers a supersonic adjustable nozzle including a rigid acceleration-section and a flexible smoothing-section. These are proposed to be designed by the method that ensures a Mach number field uniform (within 1% error) in the characteristic rhomb for a certain Mach number range, while requiring only a few adjustment points (where hydraulic actuators are attached). The method is based on numerical analysis of flow in a nozzle whose flexible section is described by a cubic spline.

Consideration is given to nozzles with a maximum angle of the acceleration section of 10 through 18°, which are intended to provide the exit Mach number of 1.2 to 4.0. It is shown that using three or four adjustment points in nozzles with inclination angles of less than 12° ensures the characteristic-rhomb flow nonuniformity of no greater than 0.5%, and for angles less than 17° the flow nonuniformity does not exceed 1%.

In order to allow for air viscosity in nozzles designed to $M < 5.0$, a general relation between the boundary layer displacement thickness and the Mach number is proposed.

NOMENCLATURE

$D_{y_{opt}}$	optimum setting (the vertical coordinate) of drive # III
h_*	semi-height of the nozzle throat
H	semi-height of the nozzle exit section
L_1, L_2	lengths of shaped and straight portions of rigid acceleration section, respectively
L_3	length of flexible wall
L_4	length of rigid portion at the nozzle exit
L_{H1}	hinge lever length
L_s	length of supersonic portion of nozzle
M	Mach number
M_i	nozzle exit Mach number
M_p	nozzle design Mach number
R_0	nozzle profile curvature radius at the nozzle throat
Re	Reynolds number
x, y	Cartesian coordinates (x is measured from the throat; and y , from the nozzle axis)
θ_0	angle of setting the straight acceleration portion (measured from the x axis) as required for attaining the design Mach number M_p
θ_{opt}	optimum angle of acceleration portion of wall
θ_{0i}	angle of acceleration portion for a Mach number M_i
δ^*	boundary layer displacement thickness
$\delta_0^* = 2\delta^*$	"effective" boundary layer displacement thickness
$\Delta\theta_0$	additional angle to compensate for boundary layer
$\Delta M/M = (M_{max} - M_{min})/2M_{mean}$	mean flow nonuniformity in the characteristic rhomb at the nozzle axis.

1. INTRODUCTION

There exist a number of wind tunnels in which use is made of planar supersonic adjustable nozzles that have rigid acceleration portions and flexible smoothing portions, see [1 - 5]. These nozzles ensure gas flow with acceptable amount of nonuniformity, $\Delta M/M < 1\%$, while employing a few (1 - 7) adjustment points. In the nozzles whose movable walls are composed entirely of flexible plates the amount of driven points is as large as 10 through 30. Decreasing the number of the points does notably simplify the nozzle control system and improves its operational reliability. As a rule, the maximum inclination angles of an acceleration portion in such designs does not exceed 12°. It is often necessary to make an adjustable nozzle shorter, for which reason the acceleration portions are set to greater angles θ_0 . The present article studies gas flow in an adjustable nozzle with inclination angle $\theta_0 = 10 - 18^\circ$, designed for $M_p = 4$.

2. COMPUTATION PROCEDURE

Figure 1 schematically represents the adjustable nozzle. Movable walls include a rigid acceleration-section and a flexible smoothing-section. The rigid section in the vicinity of the throat (over a length L_1) may be described by a fourth-order polynomial that is continued in the downstream direction as a straight line with the length L_2 . Installed at the rigid section is the drive # I intended to specify the throat height. At the exit of the rigid section is the drive # II for setting the acceleration-section inclination angle θ_0 . The smoothing portion of the nozzle is a constant-thickness flexible strip whose length is L_3 . The flexible wall is attached to correction drives. Figure 1 represents the drive # III only; if necessary, the total number of the drives may be increased. At the exit from the nozzle there is a rigid straight portion of length L_4 which is used to set (by means of the drive # IV) the inclination angle at the right-hand side of the flexible portion in order to moderate the boundary layer effects. Here, H is a semi-height of the nozzle exit section.

At the initiatory stage, the main geometric parameters (θ_0 , H , and L_1) that ensures flow at the exit with a design Mach number M_p . The computation is carried out within the assumption of radial flow along the closing characteristic AB in the acceleration portion (refer to Fig. 1). The effort produces all geometric characteristics: h_* (semi-height of the nozzle throat), L_2 (length of straight portion), L_3 (length of flexible wall), $L_s = L_1 + L_2 + L_3 + L_4$ (length of supersonic portion of nozzle), R_0 (nozzle profile curvature radius at the nozzle throat), shaped part end coordinates (x_1, y_1) and acceleration section end coordinates (x_2, y_2). In this analysis, x is measured from the nozzle throat. The flexible wall is described by a cubic spline function:

$$y = \sum_{i=0}^3 a_i (x - x_2)^i + \sum_{j=1}^k b_j (x - x_j)^3 U(x - x_j).$$

Here, k the total number of correction points; x_j the abscissae of the drive attachment points; a_i and b_j the spline coefficients; $U(x - x_j) = 0$ or 1 for $x < x_j$ and $x > x_j$, respectively.

When identifying the spline coefficients, use is made of conditions imposed on ends of the flexible strip and on the x_j points of application of concentrated loads, where ordinates of the nozzle are prescribed.

The optimal contour of an adjustable nozzle is outlined in the following way. Calculated at the first stage is the gas flow in the nozzle having three drive points I, II, and IV (the correction drives are not involved). For each Mach number $M_i < M_p$ we should determine the optimum acceleration-section angle θ_{opt} at which the flow nonuniformity in the characteristic rhomb is at minimum. This calculation provides the optimum angle as a function of M for the entire range: $\theta_{opt} = f(M_i)$. Analyses show that the function $\theta_{opt} = f(M_i)$ may without notable degradation in nozzle flow quality be approximated by a function $\theta_{opt} = f(M_i)$ for an adjustable nozzle whose acceleration section rotates about a point C . Such contours can be implemented by using two simpler structural concepts in which the nozzle is controlled via two actuators I and IV. The first concept is to install a hinge at the point C and rigidly link the acceleration section with the hinge. The second concept is to make the actuator I move two points I and II, thereby specifying the throat height (h_t) and the acceleration-section inclination (θ_{0i}). Displacements of the points I and II must be proportional to a certain constant value and make the acceleration section be rotated around an equivalent hinge at the point C .

To additionally improve nozzle flow the option is to employ correction drives attached to the flexible strip. Assuming one drive, two drives, etc., their coordinates are sought for so as to minimize the rhomb flow nonuniformity measure ($\Delta M/M$). Calculation shows that in nozzles with $\theta_0 < 18^\circ$ for $M=1-4$ the value $\Delta M/M < 1\%$ may be attained by installing one drive in the interval from $L_3/3$ to $L_3/2$.

Flows in the nozzles were computed by the method of characteristics for inviscid ideal gas with adiabatic exponent of 1.4. Isentropic nozzle profiles are formed by decreasing the nozzle ordinates by the boundary layer displacement thickness δ_0^* which may be assumed to vary linearly: $\delta_0^* = \Delta\theta_0 x$ ($\Delta\theta_0$ is an angular correction). This means also that the boundary layer is present at the throat. The value δ_0 depends on Mach number: $\Delta\theta_0 = 0.0017M_i$; for more information refer to section 5 below.

Flow in the nozzle was computed starting from the throat, assuming a straight characteristic that corresponds to $M=1.005$. The total number of points on the characteristic was 30. In this case the gas flowrate along secondary characteristics is constant within 0.05%.

3. COMPUTATION RESULTS; COMPARISON WITH TEST DATA

Figure 2 represents theoretical and experimentally obtained flow fields in the available adjustable nozzle that offers $M_i=0.4-3.5$. The nozzle exit semi-height H is 1125 mm, and the maximum inclination angle of the straight acceleration-section at $M_p=3.5$ is equal to 10.5° .

The nozzle was manufactured before accomplishment of the present study. Therefore the rigid acceleration-section was a circular arc with a radius $R_0=4000$ mm matched with a straight line whose length L_2 was 2265 mm. The flexible strip length L_3 was 6023 mm. The profile has been optimized by using the above technique. The profiles of the nozzle with an optimum angle θ_{opt} (without involving the correction drive III) ensure a rather high quality of nozzle flow: the flow

nonuniformity in the rhomb does not exceed 1.1% for Mach number $M_i=1.1-3.5$. Correcting the shape by the drive III improves the nozzle flow: $\Delta M/M < 0.7\%$.

Figure 2 represents theoretical and real distributions of Mach number along the symmetry axis for three shapes which were designed to be operated at M_i of 1.7, 2.0, and 2.5 (note that $\bar{x} = x/H$, and the coordinate is originated at the exit section; hereafter, all dimensions are referred to the exit section semi-height H). The lower part of Fig. 2 depicts the $M=1.7$ nozzle shape and the characteristic lines of flow. In the experiments, the Mach number fields were obtained by measuring the total pressure in a stilling chamber and the static pressure at side walls (through pressure orifices in the nozzle symmetry plane). In general, the theoretical and experimental Mach numbers along the nozzle axis may be said to coincide. Nonuniformity of experimental fields in the rhombs are within tolerance: $\Delta M/M < 1\%$. The function $M(x)$ shows breakpoints caused by discontinuity in curvature at the point where the circular arc makes contact with the rigid straight section; the disturbance propagates downstream along the characteristics. Calculations show that eliminating the acceleration-section curvature discontinuity may reduce the nozzle flow nonuniformity to below 0.5%.

Figures 3 through 5 demonstrate results of parametric analysis of flow in the nozzles with the acceleration-section inclination angle $\theta_0=10-18^\circ$ for $M_i=1.2-4.0$; $H=1000$ mm. The problem was to optimize the shape in order for flow in the characteristic rhomb to be uniform (in terms of $\Delta M/M$) within 1%.

Computation showed that nozzles without correction actuators offer flow with nonuniformity of over 1%. By correcting the contour through the use of the drive III installed at the distance of $0.4L_3$ from the upstreammost point of the flexible strip the nozzle flow quality gets improved notably, see Fig. 3.

Nonuniformity in nozzles with inclination angle θ_0 of 10° and 12° is 0.5%. Increasing the angle does degrade flow, and the nonuniformity reaches the tolerance value (1%) at $\theta_0=17^\circ$.

Figure 4 demonstrates how Mach number influences the optimal correction (Dy_3) to the shape of the flexible strip driven by the actuator III. The correction is of significance for flows with $M>2$; in the case of lesser Mach numbers it is useless because flow nonuniformity is insignificant.

Figure 5 represents the supersonic part length L_s and the flexible strip length L_3 as functions of the acceleration-section inclination angle θ_0 . Note that the supersonic part length notably decreases with the angle θ_0 , whereas the flexible strip length decreases only slightly. Mainly, the nozzles get shorter due to shortening of the rigid acceleration-section.

4. ALLOWANCE FOR GAS VISCOSITY

Viscosity is taken into account in considering the movable walls only (as the flat side walls remain parallel). The approach is to decrease the derivatives by a constant angle correction θ_0 . The upper wall ordinates are decreased by the "effective" boundary layer displacement thickness (which is double the boundary layer displacement thickness, i.e., $\delta_0^*=2\delta_0^*$); it is calculated by using, $\delta_0^*=\Delta\theta_0 x$. The angular corrections may be established from either the theory or experiments. For instance, Reference [1] suggests an empirical relation $\Delta\theta_0=0.0028M+0.0002$; Reference [6]

proposes $\Delta\theta_0=0.0037(M_i-1)$ for a two-dimensional supersonic nozzle with a square exit section. The experimental studies in [1] showed that these formulas provide overestimated values of $\Delta\theta_0$ when $M_i>3.0$.

The present approach has been to generalize the test data on turbulent boundary layer displacement thickness δ^* in planar and axisymmetric supersonic nozzles for various numbers M and Re . As a result, the following relation is suggested:

$$\frac{\delta^*}{L_s} Re^{0.2} = \begin{cases} 0.04 \cdot M_i & 1 \leq M_i \leq 5 \\ 0.04 & 0 \leq M_i \leq 1. \end{cases}$$

It does well approximate the available test data for $M=0-5$. With this, the angle correction is computed as,

$$\Delta\theta_0 = \frac{\delta_0^*}{L_s} = \frac{0.08 \cdot M_i}{Re^{0.2}}.$$

In particular, a simplified formula is $\Delta\theta_0=0.0017 \cdot M_i$ if Reynolds number is computed assuming the 300 K stagnation temperature. The Pitot pressure P_0 at $M_i=1.0$ is equal to 150 kPa and varies linearly:

$$P_0=150+87.5(M_i-1) \text{ kPa}$$

(thus reaching 0.5 MPa at $M_i=5$).

5. STRENGTH, FORCES AND MOMENTS

With the nozzle profile optimized, the thickness h of the flexible wall should be defined and the actuator forces estimated.

The thickness of the flexible wall is computed by,

$$h = \frac{2(1-\mu^2) \delta}{E \sup |y''(x, M_i)|}.$$

Here, σ the allowable tensile stress, μ the Poisson's ratio of the structural material, E the Young's modulus, $\sup |y''(x, M_i)|$ the maximum value of the second-order derivative of the profile curve of the nozzle with the exit Mach number M_i .

The bending moment $M_{\text{bend}}(x)$ is calculated as

$$M_{\text{bend}}(x) = D_b y''(x, M_i)$$

where $D_b = Eh^3B/12(1-\mu^2)$, B is the width of the flexible wall. Concentrated loads for the ends of the flexible wall (at $x=x_2$ and $x=x_4$) and for $x=x_3$ are estimated using

$$P(x_2) = D_b y'''(x_2, M_i); P(x_4) = D_b y'''(x_4, M_i); P(x_3) = P(x_4) - P(x_2).$$

The forces applied to the rigid part of the adjustable nozzle are computed on the basis of equilibrium conditions for the rigid section.

Analyses indicate that the second-order derivative of the profile is maximum in the nozzle intended for the design Mach number ($M_i=M_p$); the respective point is at the joint of rigid and flexible parts. The value of $y''(x_2)$ is $30 \times 10^{-6} \text{ 1/mm}$. With this, the strip thickness h may be as great as 50 – 100 mm. The maximum force from the correction drive, $P(x_3)$, does not exceed 100 kN.

6. IDENTIFYING THE INFLUENCE FUNCTION

To correct the Mach number field, one should know the influence functions that show how deviations of actuator attachment points affect the Mach number in the characteristic rhomb. These functions are also necessary to define the tolerable errors in drive installation when preparing the automatic control system for the adjustable nozzle. The influence function for each correction drive may be obtained by calculating the flow in the nozzle with

- the profile for Mach number prescribed and
- the profile in which the drive attachment point ordinate is deflected by an increment Δh (the unit deflection – for example, $\Delta h=10 \text{ mm}$). The flexible wall shape, $y_b(x)$, can be described by the relation,

$$y_b(x) = y(x) \pm \Delta h \bar{\varphi}(\bar{x}, \bar{x}_j),$$

where x_j is an abscissa of a drive attachment point (in the example computations it is taken to be x_3);

$$\bar{\varphi}(\bar{x}, \bar{x}_j) = \varphi(\bar{x}, \bar{x}_j) / \varphi(\bar{x}_j, \bar{x}_j), \quad \bar{x} = (x - x_2) / L;$$

$$\bar{x}_j = (x_j - x_2) / L; \quad L = x_4 - x_2,$$

$$\begin{aligned} \varphi(x, x_j) = & -(1 - \bar{x}_j)^2 (1 + 2\bar{x}_j) (\bar{x})^3 + \\ & + 3(1 - \bar{x}_j)^2 (\bar{x}_j) (\bar{x})^2 + (\bar{x} - \bar{x}_j)^3 U(\bar{x} - \bar{x}_j). \end{aligned}$$

Calculation provides Mach number fields for original flow, $M_0=f_1(x)$, and disturbed flow, $M_{0b}=f_2(x)$. A difference between these is just the influence function $\Delta M=f_3(x)$ for the drive point (x_j) after deflecting the ordinate by Δh . Dependence of the nozzle axis flow nonuniformity on the nozzle deformation may also be obtained by employing the linear relation of the local flow nonuniformity parameter $\Delta M/M$ to a local nozzle angular deviation $\Delta \text{tg} \theta$.

$$\Delta M/M = C(M_i) \Delta \text{tg} \theta$$

where $C(M_i) = 2(1 + (\alpha - 1)/2M_i^2) / \sqrt{M_0^2 - 1}$, $\Delta \text{tg} \theta = \bar{\varphi}(\bar{x}, \bar{x}_j)$.

This relation does not allow for interference of disturbances from the nozzle profile. For taking these into account the following formula is recommended:

$$\Delta M/M = C(M_i) \sum_{g=1}^k \varphi_g(\xi, x_j),$$

Here, $\varphi_g(\xi, x_j)$ is a function derived from the function $\bar{\varphi}(\bar{x}, \bar{x}_j)$ over an interval $[x_{g-1}, x_g]$ by means of a substitution which refers the function to the interval $[0, \xi]$; k is the total number of acts of reflection of the disturbance from the wall. Calculation shows that the linearized theory provides the nonuniformity extent very close to prediction by exact methods.

Let us determine the allowable error in the correction drive III installation ordinate; here, use can be made of the linear dependence between the flow nonuniformity and the local angular defects. Evaluate the maximum flow nonuniformity in the case of the correction drive installation ordinate deviating by Δh . The maximum value, $(\Delta M/M)_{\text{max}}$, depends on the maximum angular defect: $(\Delta M/M)_{\text{max}} = C(M_i) \bar{\varphi}'_{\text{max}}(\bar{x}, \bar{x}_3)$. The correction drive is at the distance of $0.4L_3$ from the upstreammost end of the flexible wall; therefore, the maximum is close to the case of the correction drive being at the center of the flexible wall:

$$\overline{\phi'}_{\max} = \pm \frac{3}{2} \frac{\Delta h}{L}$$

where $L=L_3/2$.

For the Mach number range from 2 to 4 the function $C(M_i)$ is approximately 2. So the maximum nonuniformity may be evaluated as

$$(\Delta M/M)_{\max} \approx \pm 3 \Delta h/L$$

Numerical analyses show that, if $M_i \geq 2.5$, the maximum nonuniformity extents computed by the present equation and the exact methods are almost identical. If $M_i < 2.5$, the maximum nonuniformity extent from the present equation is half the real value; this is because the equation does not take into account interference of disturbances from the flexible wall.

By fixing the allowable nonuniformity, the allowable error in drive III installation is

$$(\Delta h)_{\text{alwbl}} \approx \pm \frac{L}{3} (\Delta M/M)_{\text{alwbl}}$$

For the nozzle under study (with the exit height $2H=2000$ mm) the length L is 3000 mm. If the allowable nonuniformity is 0.002, then the allowable error is 2 mm for $M_i > 2.5$ and is twice this value (i.e., 4 mm) for $M_i < 2.5$. Note that the greater the number of correction drives, the tighter the drive installation ordinate tolerance. For example, if two correction elements are used ($L=2000$ mm), the allowable value $(\Delta h)_{\text{alwbl}}$ is only 1.3 mm.

To determine the allowable error in drive II installation ordinate, we can use the linear relation between the flow nonuniformity extent $\Delta M/M$ and the angular defect $\Delta \theta$ of the rigid acceleration-section. We may assume that the drive II is at the end of the acceleration-section (at the point x_2); also, variation of the drive ordinate is related to the angular defect by $\Delta h \approx L \Delta \theta$ ($L=y_2/\sin \theta_0$, the distance from the source to the acceleration-section end); in this case the drive II installation ordinate tolerance is:

$$(\Delta h)_{\text{alwbl}} \approx \pm \frac{L}{2} (\Delta M/M)_{\text{alwbl}}$$

A minimum value of the allowable deviation is for $M_i=4.0$; it depends on the acceleration-section inclination angle θ_0 specified. For example, if $\theta_0=10^\circ$ and the nonuniformity tolerance $(\Delta M/M)_{\text{alwbl}}=0.002$, then drive II installation

ordinate tolerance Δh_{alwbl} is 3 mm; for a nozzle with $\theta_0=18^\circ$ the tolerance is 1 mm.

Let us address the drive I installation ordinate tolerance. It mainly influences the nozzle throat height setup and the exit Mach number M_i deviation. Flow nonuniformity in the characteristic rhomb is varied insignificantly in this case. Therefore, the drive I installation ordinate deviation Δh_i may be replaced by a throat height deviation Δh_* . A relationship between Δh_* and the nozzle exit Mach number M_i deviation is found by proceeding from the gas flowrate conservation for the throat and the exit section:

$$\Delta h_* = H[G(M_i + \Delta M) - G(M_i)],$$

Here, $G(M_i)$ is the gas dynamic function for the equivalent flowrate. Computations show that, in a nozzle for $M_i=1.5$, a throat semi-height deviation by $\Delta h_*=\pm 1$ mm implies exit Mach number error $\Delta M \approx \pm 0.002$ (i.e., $\Delta M/M \approx 0.0013$) - whereas at $M_i=4.0$ the deviation ΔM is ± 0.013 (with $\Delta M/M$ being ± 0.003).

In general, the nozzles under study (with $H=1000$ mm and $M_i=1.1 - 4.0$) can tolerate a drive installation ordinate error Δh_* of 1 - 3 mm.

REFERENCES

1. Verkhovsky V.P., Lysak I.V. Numerical optimization method for designing the planar supersonic adjustable nozzles by means of spline functions. - *Uchenyye Zapiski TsAGI*, vol. 13, no. 4, 1982.
2. AVA Taetigkeitsbericht, 1968, X.
3. Kawasaki Toshio, Ando Hisashi, Kinoshita Hideo. Variable nozzle design for supersonic blow-down tunnel. - *Proc. Eleventh Japan Nat. Congress for Appl. Mech.*, Tokyo, 1962.
4. Trisonic tunnel FFA-TVM. - *FFA wind tunnel facilities - Part 2: Transonic-supersonic tunnels*, 1969.
5. Erdmann S.F. A new economic flexible nozzle for supersonic wind tunnels. - *J. Aircraft*, vol. 8, no. 1, 1971.
6. Ryabinkov G.M. Experimental evaluation of supersonic nozzles. - *Uchenyye Zapiski TsAGI*, vol. 1, no. 1, 1970.

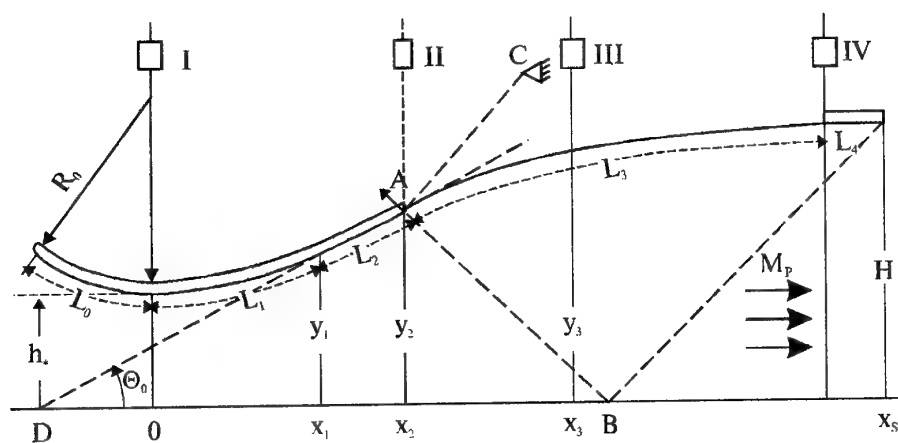


Figure 1. Schematic of a nozzle

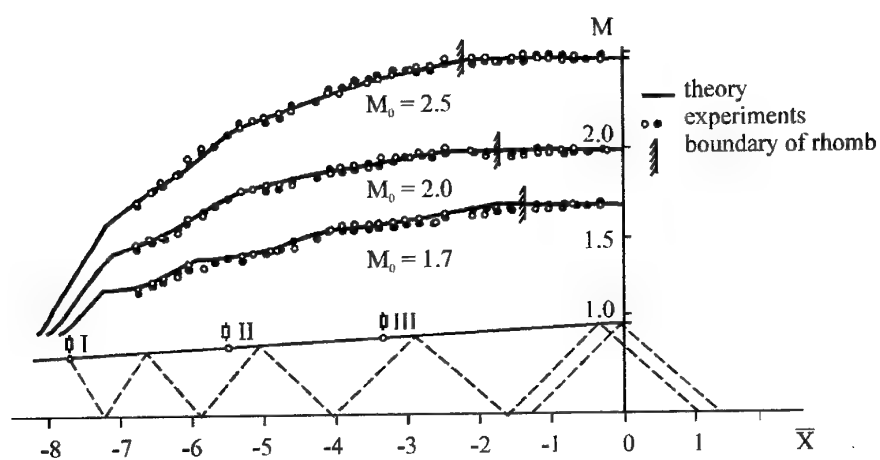
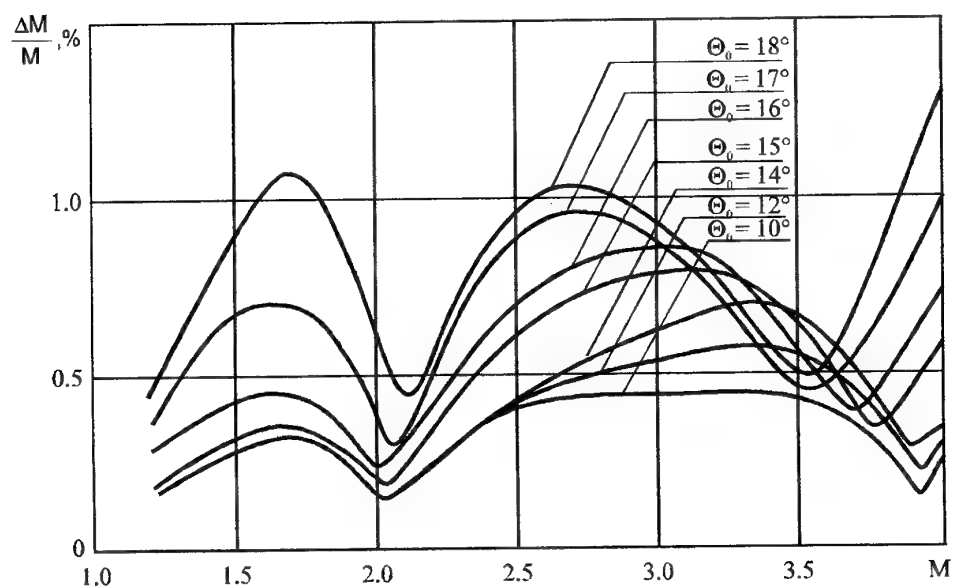


Figure 2. Comparing results from theory and experiments

Figure 3. Flow nonuniformity $\Delta M/M$ vs. Mach number M in nozzles with angle $\Theta_0 = 10^\circ - 18^\circ$

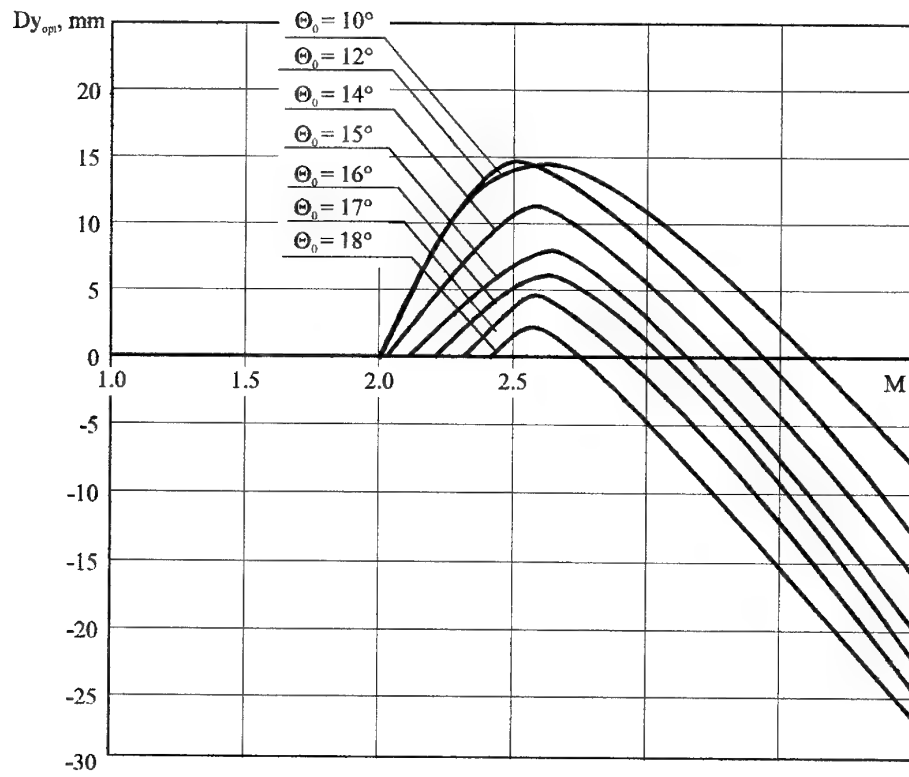


Figure 4. Dependence of correction Dy_{opt} on M for nozzles with $\Theta_0 = 10^\circ$ – 18°

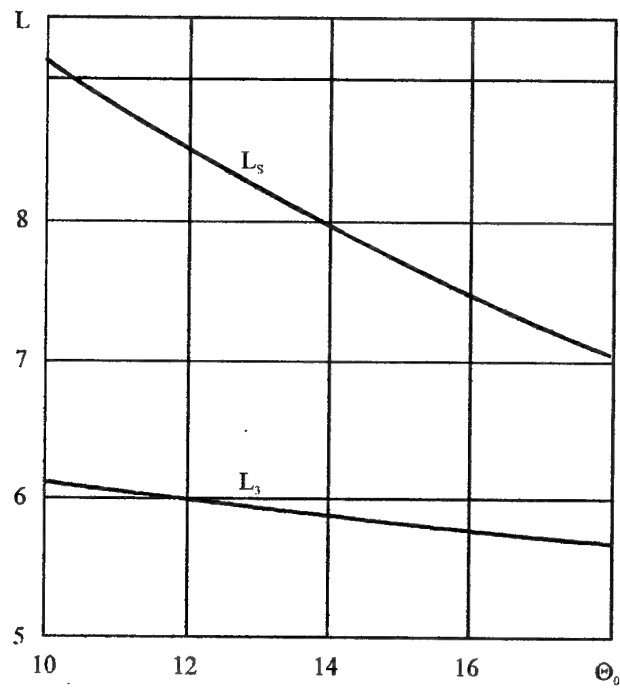


Figure 5. Relationship between angle Θ_0 , length L_3 of flexible wall, and nozzle supersonic portion length L_s

GENERAL DISCUSSION

FDP Fall Meeting in Moscow, Russia

R. Bengelink, Boeing Company, U.S.A.

This is the final session of this Symposium. I think most will agree that this has been a very historic meeting. It is also unique because we had very close to 50% participation from both Russian and Western contributors. We also had two Technical Evaluators. It is the practice of AGARD to have a Technical Evaluator sit through all of the sessions and then give his opinions at the end as to the content of what was heard and how it matched what we were trying to accomplish with the symposium. In this case we have asked two people to do that, one from Russia and one from the West. I would like to begin this session by asking for the reports of those Technical Evaluators, and we will start with Dr. Vasily Roukavets, from TsAGI.

Dr. Roukavets was also a member of the Program Committee and contributed significantly to the success of this meeting. Now he will give us his evaluation of the content of the meeting.

V. Roukavets, TsAGI, Russia

Dear Ladies and Gentlemen, before I start my short analysis, I would ask your permission not to name the authors. While analyzing the reports, I will refer only to the numbers of the reports as they are presented in the program. The reports representing the 79th Symposium of AGARD confirmed very well that the topics that we discussed today are up-to-date and they are actual. By now we have about 500 air wind tunnels in the world, and they are still continuously being designed everywhere. The creation of new wind tunnels, as a rule, is based upon the known prototypes with consideration of the experience of their operation. At the same time, the evolution in the creation of the aircraft requires the upgrading of the existing wind tunnels, especially concerning the full-scale configurations, at the same time maintaining the low cost of the new developments. The analysis of the presented reports shows that all of them have been aimed at resolving this task, and in some aspects we have quite good achievements of several groups of researchers. It is quite natural that a big importance is placed on the upgrading of the existing wind tunnels and for building the new ones. This is the experience shown in the reports 4, 8, 11, 16, 18, 19, 20, 21, 23, 25, 26 and in some others. Out of these reports, I would like to mention specifically report Nos. 16, 19, and 20 which

were aimed at resolving the problem of interference of the walls of the test sections which showed the different approaches of how they achieved good results. The results of investigations shown in Nos. 18, 21 and 22 reports contain specific recommendations on expanding experimental possibilities of aerodynamic wind tunnels, considering their safety and reliable operation. Information which is contained in report No. 26 confirms the well-known truth, how risky it is to create big structures without detailed preinvestigation of not very well-known phenomenon processes. Report No. 27 shows a possible solution of the problem described in Report No. 26. Many reports have been aimed at achieving high quality of the flow which would correlate in the level of turbulence and uniformity of parameters to the flight experience.

Positive estimation in these aspects were given in Nos. 15, 28, 33 and 31. No. 17 was a very good report; unfortunately it was aimed at the partial problem, some specific configuration of the test section, and it did not give us global recommendations. But knowing that similar facilities exist in other places, we can follow some of the results of this investigation. Considering the increased interest of the use of the wind tunnel to the test sections with the free flow, which simplifies the access to the tested object significantly, I would like to mention the report which was aimed at the improvement of the flow quality and improving the geometrical parameters. Nos. 13 and 24 are of interest regarding new methods of creating airflows of good quality, but we think that more investigations are required for the implementation. I feel a great respect for the investigators of paper No. 11, the ETW wind tunnel. Unfortunately, the ways of achieving the high quality of the flow and efficiency of the wind tunnel and other parameters are not very well known in the world practice, and it may have a determining effect as to giving recommendations for new wind tunnel designs. In general, all the presented reports have a lot of useful information which will serve the future evolution and progress in the creation of modern air wind tunnel technology, and the authors of the articles have my acknowledgment and respect. I would like to say a big thank you to everybody; to those who made the presentations and to those who listened to them. I would like to wish you success in the practical implementation of the information achieved.

As a result, I would like to point out one more aspect of today's Symposium. In some reports it was seen, we are talking here about the international character of the investigations, we can talk about the integration between the scientists of different countries to resolve different aspects of the problems, I would see it reasonable and useful for expanding this integration, to hold similar symposia on this subject; to hold them once every 4 or 5 years, regularly. Thank you very much for your attention.

R. Bengelink, Boeing Company, U.S.A.

Thank you Dr. Roukavets. The other Technical Evaluator is Dr. Frank Steinle, who worked at NASA, Ames, for many years as an experimentalist and as the administrator responsible for these wind tunnels. He is currently associated with support to the AEDC wind tunnels at Tullahoma, Tennessee.

F. Steinle, AEDC, U.S.A.

Mr. Chairman, Members of the Fluid Dynamics Panel, Colleagues, Ladies and Gentlemen. I thank you for the honor of serving as one of the Evaluators of this historic Symposium. I am awed by the scope of the material presented and the accomplishments of the authors.

Consequently, I believe that it will be far easier to overlook or underappreciate an important point or concept than it will be to give an evaluation that captures the spirit of this Symposium.

Nevertheless, I will try. This Symposium, for its historic significance alone, is an unqualified success for it signifies the potential unity in a technical community of those who are about the business of developing, operating, and utilizing experimental ground test facilities. We are scientists, but we are also artists, for much of what we are about is an art. And, as artists, for a time we can forget that we are also competitors, on occasion, and we can come together to appreciate and to assist each other in the practice of our art. And, as the product of artists, the papers presented stand on their own merits. Consequently, it is not my intention to march through the Agenda giving a paper by paper assessment. The approach I plan to follow is to highlight some of the challenges that we face both now and in the future and then relate what we have learned here to those challenges. Further, I hope to highlight issues that will lead to discussion and ultimately will serve to improve both our art and our science. The first challenge that is seen is the assurance of a continuation of scientists and engineers who are artists in our craft. The topic of this Symposium is, "Knowledge and ongoing research on the aerodynamic design and evaluation of ground test facilities, focusing primarily on wind tunnels, in order to provide to the designers of experimental facilities an opportunity to exchange information, ideas and vision". It is my contention that without the people who know how to use the facilities well, the answers produced are more likely to be a hindrance than a help. The concept being suggested is a classic one in the systems engineering sense, namely, that the personnel (that would be not only their persona, but their intellect and their knowledge) are a subsystem of what should be the proper systems definition of a ground facility. A hint of this concept was found in paper No. 2, by Lynch and Crites, where in the summary portion it is noted that "The need to have a

thorough knowledge of the important flow physical features...", and also "to adequately understand and identify wind tunnel flow quality requirements and effects on data quality, accuracy and adequacy" are very important. Well, what is then required of the people who are to carry on? What skills and experience are required? What working relationships must they develop between their peers, their customers, their suppliers, managers, subordinates, and also their competitors? You will note that this list transcends technological issues, which really was the focus of this conference. It isn't enough to be able to compute from first principles or to comprehend and improve on something that has been done before. How do we help the critical transfer that must take place to prevent a repeat of past mistakes and to assure continued advances in the years to come? That is the real challenge of continuity. You can look at the age of all of us in this auditorium and you can think about who is going to carry on. It is getting harder.

Moving on the second challenge. In the text, the first paper by Prof. Bedrzhitsky and Dr. Roukavets, it was noted that, "the experience of the development of the wind tunnels for the Chaplyguin's Laboratory has shown that the best results are achieved under close cooperation and reciprocity between the customers, designers and operators". Well, that laboratory was completed, according to the paper, in 1931 and ever since then TsAGI has followed this philosophy in the continuous improvement of their facilities. There are two key words mentioned here: cooperation and reciprocity. The achievement of optimal cooperation and reciprocity to meet the future's challenges won't happen without focus. This is our second great challenge, but it is also related to the first one.

From an integrated perspective, what do we need from each other? That is the reciprocity part. How best should we cooperate? Dr. Roukavets has just recommended to you that we should get together every four or five years. I think that is a wonderful idea, but we may decide that the problem is so compelling that it should be sooner. I don't know what the optimum is, or what kind of protocol we should follow in getting together, but that is certainly a topic for the Panel to discuss.

On the international level, it is suggested that exchange of information in our art is the key element, as we have learned from this conference. I will say this, the papers that have been presented whet the appetite for additional details to maximize the usefulness of the data that has been presented. The presumption that I am under is that if a reference is cited, that it would be made available if someone wished it so. I hope that this is the case.

The third challenge seen is the forecasting of the technological requirements of the future with sufficient certainty that support for

enabling technology development can be argued. We haven't had any papers on forecasting of needs; although Dr. Reshotko's, Saric's, and Nagib's paper on requirements for natural laminar flow gave us sort of a framework for that piece. Think of the lead time of what it takes. If you go on the history of the ETW, nearly a decade of technology work prior to entering detailed design, then nearly a decade to commissioning and operation, and add to that the lead time for product development and certification, and one has on the order of a quarter of a century to be looking ahead if a major new facility is to be developed. This is extremely difficult when modern business managers controlling funding have enormous difficulty in seeing past three years. The arguments for sustaining technology development must be compelling. To do so, they must be cast in such a way that the impact on product risk, cost and return are understood by others than ourselves. The development of the forecast and the measure of importance of the enabling technology vs. its cost in a language that will be well received by those controlling what is done is our challenge. Here the close cooperation indicated in the second challenge is vital to success.

The fourth challenge is, having identified what is needed for the future, how do we go about accomplishing it? What changes in design, philosophy, and methodology are needed to provide ground test based information that is of the quality necessary to satisfy the requirements of the customer. Putting this another way and relating this question to this Symposium, if each of us were to be involved all over again in developing our respective facilities, but with today's tools and knowledge, how would we approach the task? We have heard descriptions of facilities, the design of elements of those facilities, flow quality results, problems, solutions, attempts to understand the flow physics, facility performance, efforts to improve performance, progress in correcting for wall interference, and more.

Over 30 facilities, pilot tunnels and the like have been introduced these past four days. They cover the speed range from low speed to hypersonic and operate continuously or for short durations or intermittently. Each of these facilities represented a local optimum solution at the time, based on the host of constraints, that is: time, resources, technology, and requirements. In the work reported here, either in progress or has been done, that is a clear indication that the initial solution turned out not to be an optimum for all time. What was the impetus for our making changes in the past and what is the impetus for our wanting changes now? Those particular elements didn't come through very clearly in this Symposium as a whole, although there was a hint of it in many cases.

The paper by Frank Lynch and Roger Crites, Paper No. 2, outlined the framework for user requirements concerning reliable and meaningful data obtained that would be cost effective and obtained in a timely

fashion. Although it is essential to understand the effects of flow quality imperfections and both wall and support interference, industry prefers to not have to test in an environment with those effects present. These sentiments were also represented in the requirements for the United States National Wind Tunnel Project which Dr. Reshotko pointed out has been postponed for an indefinite time. It may really be for an indefinite time. It had very ambitious requirements for flow quality, low wall interference, high test productivity, high information quality, flexibility to accommodate tests of all kinds at Mach numbers ranging from very low speed to Mach 1.5, and also to do it at low cost. As part of that project the work reported by Reshotko, Saric and Nagib addressed the turbulence and noise requirements required to perform natural laminar flow technology development. Other requirements led to open-jet test capability up to speeds of Mach 0.6, or alternatively, to come up with phased-array technology to be brought to a sufficient state of maturity with a closed jet to eliminate the need for a new open-jet test cart with these characteristics.

Information quality placed additional requirements on data acquisition systems, instrumentation systems, optical access for the instrumentation in the test section, accommodation of instrumentation and wall characteristic control to minimize wall and support interference, balances (both external and internal) tunnel calibration, metrology, and control of tunnel conditions. Productivity, cost of operations and model size accommodations had significant impact on the design of the compressor, plenum evacuation system, airplant and model transportation and installation systems - what does that have to do with us, now that that project is dead? These same pressures of information quality, productivity and cost are being felt everywhere in our business. Other problems concern supporting and improving facilities which are not now in demand, but will again be in demand if our quest for higher atmospheric speed flight or efficient manned space launch and recovery is renewed. Either status or progress in attacking some of these problems have been represented in this Symposium. Let me enumerate some of the overview principles. We have seen application of computational fluid dynamics to improvements in the design of facility elements, we have heard guidelines for developing low speed tunnels, we have had reported how the design of components was carried out in the past with some recommendations on how it could be done differently using constrained optimization. We have been presented with test results showing flow quality, circuit loss performance, compressor performance, plenum exhaust performance, attempts to stabilize open-jet flows, heard how computational fluid dynamics has shown that integrated design for turbulence reduction systems and wide angle diffusers is needed. We have heard about utilization of computational fluid dynamics to optimize locations for icing spray

systems and improved dispersion by reshaping the contraction. We have seen some different methodology for separating velocity, pressure and temperature fluctuations from hot wire measurements. We have been treated to compressor design methodology, new approaches to alleviating wall interference. We have seen a solution for obtaining oscillating subsonic flow to support helicopter rotor technology. We have seen an approach to engine and nozzle testing and nozzle design methodology. We have heard recommendations for noise and turbulence criteria for laminar flow testing, and we have seen the results of attempts to develop quiet supersonic flow. There must be others that I have forgotten, but those are the ones that come to mind. In addition to the technical papers, we have been well received and well entertained at the reception. We have been hosted to excellent tours, we have made personal contact for the first time with outstanding colleagues. Overall, as stated at the beginning of this presentation, this Symposium has been a success. What should we work on next? Of course, those four challenges that I mentioned and all of their subsidiaries. Aside from those first three, which can be the topic for a Round Table Discussion as to how to approach or maybe even a symposium, I think the fourth topic deserves a symposium of its own.

The issue is not the design of singular elements, but the integrated design. The experience that I have gained working on the National Wind Tunnel Complex Project convinced me that one had to look at the entire design. We have heard some recommendations from others about how screen placement and so forth had to be integrated with the shape of the contraction, etc. That is really true. In closing, I will try to relate some of these issues to some of these things that we have heard here. In the area of turbulence and noise, when dealing with high Reynolds number, there are questions of screen deflection, if screens are to be used. One would prefer not to have a screen deflection, for then that gives flow turning and that's not planar flow entering into the contraction. One can calculate a contraction with an Euler code, which we have had examples of in this conference, and it looks really good from a high quality flow standpoint, but when a Navier-Stokes solution is run, the secondary flows caused by the boundary layer create stream angles that are outside the realm of what you would like to have. We need to start with what we have heard today, but to go beyond that to an integrated methodology that uses rather sophisticated computational fluid dynamics for a better design. Also, the low noise requirement implies that you have to do sound absorption where you cannot do sound elimination. We had an excellent paper concerning the civil Aeronautical Low Speed Wind Tunnel under development at Politecnico di Milano where they used an inverse method and came up with rather thick guide vanes. We have had a paper on the DRA 5 meter and ONERA F-1 tunnels nonlinear spacing of the turning vanes was discussed. It is critical to put

sound absorptive material in the vanes. That doesn't do the entire story, because the cutoff frequency at which decent sound absorption in turning vanes is realized is around 80 hertz. So, one has to do something else to reduce the magnitude of the acoustic disturbance below 80 hertz. This gets at compressor/fan design. We heard some good papers on the design of compressors, but none that were related to how one designs the compressor system for low noise as well. The sound absorptive material that is put in guide vanes creates structural problems as well because, as everyone knows, at the first set of corner vanes downstream of the test section, the flow is extremely rough, and it is a very tough structural problem to get a good set of vanes that will last and not fail. When you have to accommodate acoustic material as well, the problem is harder. Of course, cost of operations is a strong concern and there is a tradeoff between plenum evacuation and main drive compressor power and capital cost; and we have heard an excellent paper on plenum exhaust systems as well. For reducing wall interference, there are several solutions that have been posed: flexible solid walls, solid walls with flexible strips, slots, porous slots (not mentioned at this conference). But you also have to have an astounding amount of optical access. When you integrate all that together, what would be the optimal solution? What design process would we have to go through? This is what I would like to see in the next symposium in order to arrive in an optimal solution that addresses all of those particular issues.

As far as the open-jet capability is concerned, the low noise question is really tough. The NWTTC requirement to go to 0.6 Mach number was based on part of the mission requirements for a high speed commercial transport. I believe that this will one day become a reality, in which case relaxing the noise requirements don't seem to be appropriate. So, the question is how to obtain the proper certification and development for that type of a problem. Perhaps you can't do it with an open-jet. So this argues that phased-array technology must be worked. In summary, let me say that this conference gave much food for thought, it gave many reports on what has been accomplished in the past, but the challenges of the future require considerably more than what we have seen today, which includes a fair amount of enabling technology work. I hope that we can step up to the challenge.

R. Bengelink, Boeing Company, U.S.A.

We now have an opportunity to hear from the audience. Frank touched on it, but I would like to remind you that we really had a two-fold purpose in this conference. The first was to share our experiences and our understanding of the aerodynamic design of wind tunnel circuits, such that we all can leave with a better understanding than

when we began. Then secondly, we intend to demonstrate the value of a cooperative symposium between two groups of engineers who have not previously communicated to this level. We should start out the discussion by asking the question, "do you think we have achieved our purposes?". I would also welcome comments to the challenges that Frank put before us.

Dr. A.D. Khon'kin, TsAGI, Russia

I would like to say thank you to AGARD and the foreign scientists who found it possible to come to Russia and tell us about their achievements. It is no secret that Russian scientists have problems with going abroad. That is why we are very, very thankful to you for this opportunity given to us to get acquainted with the status of your investigations. At the same time, I would like to say thank you for listening to our reports and achievements. I would like to tell you a few words about those achievements which were not included in the program. My discussion won't be as global as the previous presentation, but I think it may be of interest, not only to myself.

First of all, I would like to tell you that at TsAGI, besides those wind tunnels which we have discussed today, in the Bedrzhitsky and Roukevets reports, we have low noise and low turbulence, subsonic and supersonic wind tunnels. Similar tunnels are also in Novosibirsk in the Institute of Theoretical and Applied Mechanics which was touched upon in one of the presentations today. In these wind tunnels, they obtained unique results on the transition, the development of the disturbances, turbulence structure in the boundary layers. These achievements are well known also abroad. I would like to tell you that in these wind tunnels we could conduct a lot of interesting investigations. Right now, due to the lack of financing, these types of research have been slowed down. I would like to tell you about one which was conducted, and I participated in it, concerning the research on the possibilities of studying the laminarization problem in transonic speeds. Right now, due to the development of the SST supersonic passenger aircraft, we have a problem. The LFC (laminar flow control) was expected to be done there due to the suction from the boundary layer. There was a problem encountered to investigate this phenomenon at transonic speeds. Before we studied the problem of LFC in perforated walls in large wind tunnels, we decided to see how this effect will take place in a low noise, low turbulence air wind tunnel with cross section 20 x 20 cm using a plate. We installed the plate inside the test section with solid walls, and also we used a circular holes perforation test section. We expected that the transition would be moved forward because we have the same plate, but it did not happen. The Reynolds number of the transition was even higher. We didn't have time or money to investigate it further. Maybe perforation did not effect the transition due to the

fact there was some overflow due to the redistribution of pressure gradient, but we were not able to go into details with this investigation. The transition was even delayed. That fact was interesting, and we thought it may be of interest to some of our colleagues, and we could conduct cooperative research on that.

One more thing, some time ago, at TsAGI, we had some programs on cryogenic wind tunnels. Also, in the United States, we thought a cryogenic wind tunnel was built. I didn't attend all the presentations, but I didn't think anybody paid much attention to this problem. For the future symposiums, I would like somebody to be invited who is well acquainted with this problem so that they would share their achievements with us in this area. Also, I would like to make another comment. We would like to listen to some invited report concerning the accuracy provided by the measurements in the wind tunnels, computational fluid dynamics methods used - what is their accuracy? How is it possible to apply them at the experimental wind tunnels?

R. Bengelink, Boeing Company, U.S.A.

In subcommittee this morning, we talked about possible future symposia topics, and I think we have heard two or three so far this afternoon.

Ir. B. Elsenaar, NLR, Netherlands

There are a few remarks I would like to make. I feel that from what has been presented here, we got to know a lot of new facilities with new possibilities, and it would be very interesting to learn from each other what kind of things have been achieved. My recommendation would be for the next conference, rather not to look at wind tunnels again, but to look at what has been achieved in the wind tunnels and to learn more about the applied aerodynamics side of it.

The other point is that I think this exchange of information has been extremely useful. I talked with some people, and I got the impression that in some aspects in the design of wind tunnels, it is a different culture between Russia and the Western world. Many of the wind tunnels that we witnessed were driven to solve a particular problem and to really go back to an aerodynamic problem. I think that has opened up our eyes and whetted our appetite from what was going on in these tunnels. One of the problems though, is communication. I don't know how to go around it. If you don't speak Russian it is difficult to speak with a Russian, and vice versa. What has been very helpful is that all the proceedings were on the table before the meeting such that you could read it and could think

about it, and if possible could ask questions with an interpreter and find out what was going on.

Dr. E. Reshotko, Case Western Reserve University, U.S.A.

I think we all learned a lot at this Symposium about how wind tunnels have been built over the last few decades, and improvements in wind tunnel design following these traditional lines. However, in looking at wind tunnel components for the future, we have to take more account of the possibilities provided by emerging instrumentation techniques. Frank Steinle hinted at that when he said that there is demand for more optical access in the design of the test section, enabling greater use of pressure-and shear-sensitive paints, etc. Another emerging technology is MEMS (Micro-Electro-Mechanical Systems) sensors. These devices having characteristic sizes of about 100 microns are fashioned from silicon by the same techniques as used in integrated circuit technology. Pressure sensors, wall-shear-stress sensors, heat flux gauges and hot-wires are presently under development and test. This technology also provides the opportunity for integrating processing electronics on the same chip with the sensor, and in the longer term allowing for the telemetering of data directly to a remote receiver. One can envision arrays of such devices not only for wind tunnel models but also in a flight test and perhaps even in flight operations. The implementation of telemetering would require that the wind tunnels would have to operate in a quiescent electromagnetic environment. This may be difficult to achieve in large complexes where all kinds of electrical power supplies are present. But I think that we should start considering such matters in looking at wind tunnel components for future application.

There is one other topic that is not directly related to this Symposium on aerodynamics of Wind Tunnel Components. It concerns the intelligent use of the wind tunnel toward estimating the results for flight. In other words, how do we translate the results from wind tunnels into the needed information for flight conditions. This was not addressed here. It was addressed a decade ago by Working Group 09 of the FDP Panel. The final report (AGARD Report AR-224) was published and no doubt sits on shelves in people's libraries. But I very little in the way of further development of the methodologies for the intelligent use of wind tunnels. I would appreciate seeing more so that the wind tunnel results can provide for even further confidence in our flight predictions.

Prof. V. Neyland, TsAGI, Russia

My views of wind tunnels have two almost opposite aspects. On one hand, I am the Director of the organization that possesses wind

tunnels. On the other hand, I am a customer who makes use of their produce - in order first of all to develop various flight vehicles. Therefore, I would like to note three features concerning wind tunnel development ideology and data usage.

Let us address the simplest factor. A significant figure of merit of each test facility is the cost of information it generates. So the important area in test procedure improvement is associated with the necessity to offer options for evaluating fields of pressure, temperature, etc. not only discretely, but also continuously in terms of both space (the pressure sensitive paints, the temperature sensitive coatings and so on), and time (when we vary test parameters such as Mach number and/or angles of attack and sideslip). In dealing with these matters TsAGI has acquired a considerable experience.

More challenging is the second feature, the challenge of test errors and measurement correction techniques. It has been very recently that I attended the AIAA conference where a long session was dedicated to these issues. Regretfully, almost all the time was spent considering random errors and test repeatability. Of course, these aspects of the problem may be treated in the simplest way, by proceeding from repeatability. Good results may be derived when studying a model that is very similar to a previously known art which has been evaluated comprehensively, especially in flight.

However, special efforts are required if we must investigate into systematic disturbances such as effects from transonic flow boundaries, model support devices, and air dissociation in hypersonic flow/model interaction. Otherwise, the considerably new aircraft would be developed under too great a threat to feasibility including technical data validity and financial figures.

These features are closely associated with the third one to which I would like to separately draw the attention of colleagues. This is the challenge of developing the test facilities. The attempts to obtain extreme values of major parameters such as Mach and Reynolds numbers seem to me to be ungrounded in many cases. Best understood is the situation with Mach number and flow stagnation parameters. The experience in work on hypersonic aircraft of various types taught certain lessons to researchers. For example, it is simpler and less expensive to evaluate aerodynamics in the wind tunnels where thermodynamic characteristics of stream about a model are determined better. These are mainly the test facilities in which stagnation temperature only ensures oxygen not condensing in the test section. It is well known that very hot flows with dissociation in a test section and/or with nonequilibrium processes in the nozzle make it difficult to extrapolate test data to real flight conditions. So it

becomes better (and more reliable, in particular) to have a set of inexpensive specialized installations for treating the thermal protection problems (especially with catalytic surfaces), evaluating aerodynamics in rarefied gases, etc. Generally speaking, a hypersonic wind tunnel is a component in an all-round methodology involving Computational Fluid Dynamics (CFD) options and, sometimes, in-flight measurements.

Last (but not least) is the problem of attaining high Reynolds number and resorting to cryogenic test setups. The latter are known to show certain disadvantages including costly experiments, low productivity, and considerable complexities in test procedures. However, this area had been assigned much money and effort. Did this make sense, and should we hope to obtain results paying off the costs? The questions are not easy to answer since at values of Reynolds number over 50 million the laminar-to-turbulent transition is notably influenced by factors not immediately related to Reynolds number; those factors are acoustic disturbances, aircraft skin vibrations (which differ for the model in a wind tunnel and the airplane in flight) and surface roughness. One knows various sources of disturbance: Tollmien-Schlichting waves, transverse instability, etc. Therefore, the results obtained in cryogenic wind tunnels are very difficult to interpret and relate to a respective flying vehicle. The use of these installations is clearly challenged.

Prof. I.V. Brusilovsky, TsAGI, Russia

In the program of the present Symposium which we got before it started its work in order to prepare reports, by separate line there were suggested reports on flow fans for wind tunnels. I join your very high evaluation of the Symposium, which impressed me very much. Almost every report applied to test sections, collectors, settling chambers and nozzles for wind tunnels. However, only two reports from GosNITs TsAGI were devoted to the fans proper and one report from TsAGI to optimal adjusting of guide vanes by turning of blades of multistage compressor. One report, my invited report, was devoted to aerodynamic design of axial fans which, because of a lack of time, went theoretically and experimentally into details of only one new, but in my opinion, important in aerodynamic and constructive plan feature of axial fans. Another report was devoted to the unique project of a wind tunnel with diametrical fan. I know that many speakers who delivered very interesting reports represented countries with very high level of aerodynamic design of fans. These are the U.S.A., England, Germany and so on. I would like to have a response to why these countries did not present a single report on aerodynamic design of fans. I would like to apologize, but I got only one single question to my report, and it was from TsAGI. I understood that among my listeners from western countries there were no specialists

in fans. There was no discussion or questions on fans - obligatory part of wind tunnel, and I was not satisfied with that. I dare say that GosNITs TsAGI developed absolutely unique method of aerodynamic design of axial fans not only for wind tunnels, theoretically and experimentally well-founded and widely tested. I would like to discuss it with specialists. I would like to see more detailed discussion of aerodynamic and constructive-technological investigation and design of axial fans in the future Symposia of this kind. Perhaps, it would be useful to arrange Symposium on fans, compressors and turning vanes.

R. Bengelink, Boeing Company, U.S.A.

Maybe I can give a little bit of an explanation to those of you who are not familiar with how we run our Symposium. We put together a call for papers that tries to describe all of the areas that we think fit under the topic. Then the people who receive the call for papers decide whether or not they want to respond at this time. We do try to do some invited papers, especially if we want a particular person to address a specific topic. We probably did more of those in this Symposium than we do in most. But, at the same time, the Program Committee is faced with the fact that, for some subjects, no one responds, for various reasons. The meeting might not fit their schedule, they have no time to prepare, etc. I think your suggestion that this is an area that ought to be emphasized, is certainly one that we will take seriously as we contemplate future symposia.

D. Woodward, Defense Research Agency, U.K.

I would like to take slight issue with Professor Neyland about his comments about Reynolds number, and then in the end, possibly to slightly agree with him. Certainly as far as the low speed area is concerned in our 5 m tunnel, we find that the Reynolds numbers that we can achieve, although much higher than can be achieved in atmospheric facilities, are by no means large enough to be confident that a good prediction of the maximum lift will result. We have identified transition mechanisms which will result in the maximum lift decreasing between the Reynolds number we can achieve in the 5 m tunnel and in flight. Therefore, there is a trap there for the unwary, and that would suggest that the ability to get even higher Reynolds numbers would lead to a significant increase in confidence in the prediction of the full-scale maximum lift. This situation, I have to admit, applies mainly to transport airplanes, and high performance military airplanes in general do not display such a sensitivity to Reynolds number. But the type of airplane which is used for training pilots displays a very significant sensitivity to Reynolds number and some of those are exceedingly dramatic. However, whilst we have expended a lot of money on the development of high

Reynolds number facilities, and the ETW is a typical example, we do not seem to be expending a similar amount of money on the solution of the problem of wall and support interference. None of these major facilities have made any attempt to draw upon the increasing amount of experience on adaptive walls. We still persist with the conventional solid walls for low speed tunnels and either perforated or slotted walls for transonic tunnels. It was Frank Lynch, I think, who highlighted this as one of the key problems that are going to come in the future. So, it may well be that I agree with you Professor Neyland that we don't need to push ahead any more with increasing Reynolds number, but we do need to push ahead with the solution of the problem of the wall interference.

N. Malmuth, Rockwell, U.S.A.

I strongly agree with Dave Woodward. There has been much wall interference and adaptive wind tunnel research. In view of the progress, we should use this technology in the design of new wind tunnels. In this connection, three-dimensional transonic wall interference corrections and accurate static pressure measurements near ventilated walls remain as challenges. This is not a trivial problem. Furthermore, new developments in control theory and genetic optimization algorithms should be investigated for adaptive wall applications.

D. Stanniland, ARA, U.K.

We have talked extensively about the use of wind tunnels for aircraft configurations as though we are representing the geometry which is actually flying in the skies. We need to bear in mind that aircraft have very fine geometric details on them which significantly affect the flow, but which are not represented on the model. There are also elastic phenomena which are present in both the tunnel and in flight, but are different in each case.

R. Bengelink, Boeing Company, U.S.A.

We are about out of time and ready to go into the closing ceremony. In closing, I would just like to say that I really appreciate all the effort that has been made by all of the participants to make this a very successful meeting. The authors all responded very well in getting us text ahead of time to do the extra translations: the Russian authors especially worked hard to get the English versions ahead of time which, as has been stated before, has been very valuable to improved communication. To all of you I would like to say thank you very much. I now would like to turn the meeting over to the Fluid Dynamics Panel Chairman, Professor Ciray.

Dr. Ciray, Middle East Technical University, Turkey

Ladies and Gentlemen, as the Chairman of the Fluid Dynamics Panel of AGARD, I have the honor and privilege and the responsibility to bring this meeting to a close. We came to the end of the Symposium on Aerodynamics of Wind Tunnel Circuits and their Components. During this week many papers have been presented and a number of discussions have taken place within this room. My judgment is that this Symposium was a good one, was a successful one. I hope that you also found this Symposium to your expectations. It takes some time to prepare a Symposium. For this Symposium it took perhaps a bit more.

More than a couple of years ago, we were on our way to Crete for another Symposium of this kind. We had been told by AGARD authorities that it was possible to have an AGARD panel activity in Moscow, and that we could consider it seriously. During the Crete meeting, and also in the following ones, to my recollection in Berlin, Ankara, Trondheim. Then AGARD, the Russian authorities, the Fluid Dynamics Panel have all done their work to realize this meeting - and it is realized. After being here for one week, seeing the interactions, seeing the quality of the papers, listening to the discussions that have taken place just a few moments ago; it is my judgment, and I repeat once more, that this Symposium is realized with success. I would like to thank the AGARD authorities of NATO and the Ministry of Defense Industries of the Russian Federation for their leadership in the first place to help to promote this meeting.

I would like to thank TsAGI for its help in organizing this meeting and also the technical tour to visit the impressive TsAGI facilities.

Similarly, I would like to extend my thanks to Moscow State Institute of Aviation for allowing us to visit the highly reputed Institute. I want also to extend our thanks to the Airforce Engineering Academy for the wonderful reception on Monday night at Peter's Palace (minus my speech). Well, let us show our appreciation to TsAGI, to MAI, and the Airforce Academy for their kindness and for their help.

I would like also to thank Mr. Anatoli Bratoukhin from the Ministry of Defense Industries; Dr. Jurgen Wild, Director of AGARD; Professor Valdimir Neyland, Director of TsAGI; Professor General Valdimir Koutahov from the Airforce Engineering Academy; Professor Alexander Matveyenko, Rector of MAI; Dr. Vasili Roukavets, Head of the Aerodynamic Division for coming and welcoming us the first day at the Opening Ceremony.

Now, to make this meeting some people worked very hard. This group of people have been responsible for the organization and some technical problems of this meeting. Mr. Bengelink, as the Chairman, Mr. Elsenaar, Mr. Bouis, Prof. Ewald, Ms. Krymasova, Dr. Malmuth, Prof. Matveyenko, Mr. Monge, Mr. Muylaert, Professor Onorato, Mr.

Roukavets, and Dr. Woodward. They have been very active in the Technical Program Committee, but for overall organization they have been helped by Colonel Kauw, Dr. Molloy and Ms. Danielle Pelat. I would like these people to stand up. We appreciate your zealous work and thank you very much.

Our special thanks go to some people without whom this room would have been silent. These are the authors and the speakers who have arduously prepared their papers and bravely came and presented their work in this audience. We thank you for the endeavor and the work you have done for these presentations. I would like to thank especially the Technical Evaluators, Dr. Roukavets and Mr. Steinle for their preparation and the difficult job they had. Any other person could leave this room, but these two gentlemen didn't have that possibility. They had to sit, to listen, to take notes, to assimilate everything and they made a short, neat, concise presentation here to induce the discussions. Indeed, both of them were very successful, and we thank them very much.

There are some unseen, but noticed warriors behind the screens - the interpreters. They have done a marvelous job, and we owe them a lot.

If you really feel in your heart that this was a success, that you have heard something, either it was presented in Russian or it was presented in English and you got something from it, we have to thank the interpreters. I think that we owe them a special ovation. There were also other people behind the scenes. We had some technicians who helped the systems work properly, and there were ladies outside who were helping us with our problems. We thank all these ladies and gentlemen again for their help.

We come to another part of a group of people who are very, very important - the audience. You have been surely a wonderful audience according to what I have heard from those who have been able to attend various sessions; because unfortunately, personally I didn't have much chance to be in this room, but I did some spying, and the attendance was very good, very responsive and discussions after the presentations were lively. Most of you have come from long distances and some of you came from short distances. You exchanged views, you listened to papers and apparently the performance of the audience was at the same level as that of the authors and speakers. Without a good audience, no meeting is a good one. If we say that it was a good one, this means that we also had a good audience. We thank you all.

I told you at the very beginning that this has been an AGARD activity. It is our custom also to give an outlook to the programs of AGARD in the future. First of all, in April 1997 we are going to have a spring symposium in Paris. This is a unique event. This is a

symposium where all the panels of AGARD are participating. The six panels plus the Aeromedical Panel, and the Aerospace Applied Studies Committee are joining their efforts to make this symposium. 1997 is also going to be the forty fifth anniversary of AGARD. This is the first time that all Panels are coming together to make a single symposium. I think that this is going to be a very exciting event. The title of it is, "Future of Aerospace Technologies in Service to the Alliance". As you know, AGARD is also undergoing some changes; we are in a transition period, and who knows, this event in Paris may also mark the rebirth of a new AGARD mentality, and I hope that it is going to be so. Before the Paris meeting, we are having a workshop on Hypersonic Experimental and Computational Capabilities, Improvement and Validation. This is a specific topic for the Fluid Dynamics Panel. This is not a part of the general symposium I mentioned earlier. It is going to take place prior to the symposium. In Fall 1997 we will go to Seattle, U.S.A. for the "Advanced Measurement Technologies Symposium". You know that the AGARD Fluid Dynamics Panel is in close connection with the von Karman Institute of Fluid Dynamics to collaborate on issues related to our interests.

Now, there are going to be two special courses at VKI. One of them is "The Effect of Rain Icing and De-Icing on Wing Performance". This is going to take place in February at VKI. The other one is a special course on "Turbulence in Compressible Flows", which will take place in June at VKI and, if I am not mistaken, also at NASA Langley. I think that with this program, we are going to close the 1997 year. Ladies and Gentlemen, I am coming to the end of my remarks. Here in Moscow during this meeting we have seen and found a warm hospitality, impressive facilities, a profoundly deep culture that we knew to exist, but now we have witnessed with our own eyes. We have, I believe, created new friendships; AGARD and the Russian authorities, the Minister of Defense Industries, have been instrumental in all of this. I hope that all this activity will help to create a better world in the future.

I wish you all, a safe return home, and I hope to meet you at another AGARD meeting. I thank you very much.

REPORT DOCUMENTATION PAGE

1. Recipient's Reference	2. Originator's Reference AGARD-CP-585	3. Further Reference ISBN 92-836-0042-8	4. Security Classification of Document UNCLASSIFIED/ UNLIMITED		
5. Originator Advisory Group for Aerospace Research and Development North Atlantic Treaty Organization 7 rue Ancelle, 92200 Neuilly-sur-Seine, France					
6. Title Aerodynamics of Wind Tunnel Circuits and their Components					
7. Presented at/sponsored by The 79th Fluid Dynamics Panel Symposium held in Moscow, Russia, 30 September - 3 October 1996.					
8. Author(s)/Editor(s) Multiple			9. Date June 1997		
10. Author's/Editor's Address Multiple			11. Pages 446		
12. Distribution Statement There are no restrictions on the distribution of this document. Information about the availability of this and other AGARD unclassified publications is given on the back cover.					
13. Keywords/Descriptors <table style="width: 100%; border: none;"> <tr> <td style="width: 50%; vertical-align: top;"> Wind tunnels Test facilities Aerodynamics Design Circuits Evaluation Wind tunnel tests Data processing </td> <td style="width: 50%; vertical-align: top;"> Walls Unsteady flow Aerodynamic characteristics Turbulence Fluid dynamics Laminar flow Wind tunnel nozzles Interference analyzers </td> </tr> </table>				Wind tunnels Test facilities Aerodynamics Design Circuits Evaluation Wind tunnel tests Data processing	Walls Unsteady flow Aerodynamic characteristics Turbulence Fluid dynamics Laminar flow Wind tunnel nozzles Interference analyzers
Wind tunnels Test facilities Aerodynamics Design Circuits Evaluation Wind tunnel tests Data processing	Walls Unsteady flow Aerodynamic characteristics Turbulence Fluid dynamics Laminar flow Wind tunnel nozzles Interference analyzers				
14. Abstract <p>The papers prepared for the AGARD Fluid Dynamics Panel (FDP) Symposium on "Aerodynamics of Wind Tunnel Circuits and their Components", which was held 30 September - 3 October 1996 in Moscow, Russia are contained in this Report. A Technical Evaluator's Report aimed at assessing the success of the Symposium in meeting its objectives, and an edited transcript of the General Discussion held at the end of the Symposium, are also included. It should be noted that 50% of the papers presented were by Russian authors.</p> <p>Papers presented during the sessions addressed the following subjects:</p> <ul style="list-style-type: none"> — Circuit Design - Low Speed and High Speed — Ventilated & Adaptive Test Sections — Drive Systems — Open Jet Test Sections — Laminar/Turbulent Flow Considerations — Nozzles 					

Aucun stock de publications n'a existé à AGARD. A partir de 1993, AGARD détiendra un stock limité des publications associées aux cycles de conférences et cours spéciaux ainsi que les AGARDographies et les rapports des groupes de travail, organisés et publiés à partir de 1993 inclus. Les demandes de renseignements doivent être adressées à AGARD par lettre ou par fax à l'adresse indiquée ci-dessus. *Veuillez ne pas téléphoner.* La diffusion initiale de toutes les publications de l'AGARD est effectuée auprès des pays membres de l'OTAN par l'intermédiaire des centres de distribution nationaux indiqués ci-dessous. Des exemplaires supplémentaires peuvent parfois être obtenus auprès de ces centres (à l'exception des Etats-Unis). Si vous souhaitez recevoir toutes les publications de l'AGARD, ou simplement celles qui concernent certains Panels, vous pouvez demander à être inclu sur la liste d'envoi de l'un de ces centres. Les publications de l'AGARD sont en vente auprès des agences indiquées ci-dessous, sous forme de photocopie ou de microfiche.

CENTRES DE DIFFUSION NATIONAUX

ALLEMAGNE

Fachinformationszentrum Karlsruhe
D-76344 Eggenstein-Leopoldshafen 2

BELGIQUE

Coordonnateur AGARD-VSL
Etat-major de la Force aérospatiale
Quartier Reine Elisabeth
Rue d'Evere, 1140 Bruxelles

CANADA

Directeur - Gestion de l'information
(Recherche et développement) - DRDGI 3
Ministère de la Défense nationale
Ottawa, Ontario K1A 0K2

DANEMARK

Danish Defence Research Establishment
Ryvangs Allé 1
P.O. Box 2715
DK-2100 Copenhagen Ø

ESPAGNE

INTA (AGARD Publications)
Carretera de Torrejón a Ajalvir, Pk.4
28850 Torrejón de Ardoz - Madrid

ETATS-UNIS

NASA Center for Aerospace Information (CASI)
800 Elkrige Landing Road
Linthicum Heights, MD 21090-2934

FRANCE

O.N.E.R.A. (Direction)
29, Avenue de la Division Leclerc
92322 Châtillon Cedex

GRECE

Hellenic Air Force
Air War College
Scientific and Technical Library
Dekelia Air Force Base
Dekelia, Athens TGA 1010

ISLANDE

Director of Aviation
c/o Flugrad
Reykjavik

ITALIE

Aeronautica Militare
Ufficio del Delegato Nazionale all'AGARD
Aeroporto Pratica di Mare
00040 Pomezia (Roma)

LUXEMBOURG

Voir Belgique

NORVEGE

Norwegian Defence Research Establishment
Attn: Biblioteket
P.O. Box 25
N-2007 Kjeller

PAYS-BAS

Netherlands Delegation to AGARD
National Aerospace Laboratory NLR
P.O. Box 90502
1006 BM Amsterdam

PORTUGAL

Estado Maior da Força Aérea
SDFA - Centro de Documentação
Alfragide
2700 Amadora

ROYAUME-UNI

Defence Research Information Centre
Kentigern House
65 Brown Street
Glasgow G2 8EX

TURQUIE

Millî Savunma Başkanlığı (MSB)
ARGE Dairesi Başkanlığı (MSB)
06650 Bakanlıklar-Ankara

Le centre de distribution national des Etats-Unis ne détient PAS de stocks des publications de l'AGARD.

D'éventuelles demandes de photocopies doivent être formulées directement auprès du NASA Center for Aerospace Information (CASI) à l'adresse ci-dessous. Toute notification de changement d'adresse doit être faite également auprès de CASI.

AGENCES DE VENTE

NASA Center for Aerospace Information
(CASI)
800 Elkrige Landing Road
Linthicum Heights, MD 21090-2934
Etats-Unis

The British Library
Document Supply Division
Boston Spa, Wetherby
West Yorkshire LS23 7BQ
Royaume-Uni

Les demandes de microfiches ou de photocopies de documents AGARD (y compris les demandes faites auprès du CASI) doivent comporter la dénomination AGARD, ainsi que le numéro de série d'AGARD (par exemple AGARD-AG-315). Des informations analogues, telles que le titre et la date de publication sont souhaitables. Veuillez noter qu'il y a lieu de spécifier AGARD-R-nnn et AGARD-AR-nnn lors de la commande des rapports AGARD et des rapports consultatifs AGARD respectivement. Des références bibliographiques complètes ainsi que des résumés des publications AGARD figurent dans les journaux suivants:

Scientific and Technical Aerospace Reports (STAR)
publié par la NASA Scientific and Technical
Information Division
NASA Langley Research Center
Hampton, Virginia 23681-0001
Etats-Unis

Government Reports Announcements and Index (GRA&I)
publié par le National Technical Information Service
Springfield
Virginia 22161
Etats-Unis
(accessible également en mode interactif dans la base de données bibliographiques en ligne du NTIS, et sur CD-ROM)



AGARD holds limited quantities of the publications that accompanied Lecture Series and Special Courses held in 1993 or later, and of AGARDographs and Working Group reports published from 1993 onward. For details, write or send a telefax to the address given above. *Please do not telephone.*

AGARD does not hold stocks of publications that accompanied earlier Lecture Series or Courses or of any other publications. Initial distribution of all AGARD publications is made to NATO nations through the National Distribution Centres listed below. Further copies are sometimes available from these centres (except in the United States). If you have a need to receive all AGARD publications, or just those relating to one or more specific AGARD Panels, they may be willing to include you (or your organisation) on their distribution list. AGARD publications may be purchased from the Sales Agencies listed below, in photocopy or microfiche form.

NATIONAL DISTRIBUTION CENTRES**BELGIUM**

Coordonnateur AGARD — VSL
Etat-major de la Force aérienne
Quartier Reine Elisabeth
Rue d'Evere, 1140 Bruxelles

CANADA

Director Research & Development
Information Management - DRDIM 3
Dept of National Defence
Ottawa, Ontario K1A 0K2

DENMARK

Danish Defence Research Establishment
Ryvangs Allé 1
P.O. Box 2715
DK-2100 Copenhagen Ø

FRANCE

O.N.E.R.A. (Direction)
29 Avenue de la Division Leclerc
92322 Châtillon Cedex

GERMANY

Fachinformationszentrum Karlsruhe
D-76344 Eggenstein-Leopoldshafen 2

GREECE

Hellenic Air Force
Air War College
Scientific and Technical Library
Dekelia Air Force Base
Dekelia, Athens TGA 1010

ICELAND

Director of Aviation
c/o Flugrad
Reykjavik

ITALY

Aeronautica Militare
Ufficio del Delegato Nazionale all'AGARD
Aeroporto Pratica di Mare
00040 Pomezia (Roma)

The United States National Distribution Centre does NOT hold stocks of AGARD publications.

Applications for copies should be made direct to the NASA Center for AeroSpace Information (CASI) at the address below.

Change of address requests should also go to CASI.

SALES AGENCIES

NASA Center for AeroSpace Information
(CASI)
800 Elkridge Landing Road
Linthicum Heights, MD 21090-2934
United States

The British Library
Document Supply Centre
Boston Spa, Wetherby
West Yorkshire LS23 7BQ
United Kingdom

Requests for microfiches or photocopies of AGARD documents (including requests to CASI) should include the word 'AGARD' and the AGARD serial number (for example AGARD-AG-315). Collateral information such as title and publication date is desirable. Note that AGARD Reports and Advisory Reports should be specified as AGARD-R-nnn and AGARD-AR-nnn, respectively. Full bibliographical references and abstracts of AGARD publications are given in the following journals:

Scientific and Technical Aerospace Reports (STAR)
published by NASA Scientific and Technical
Information Division
NASA Langley Research Center
Hampton, Virginia 23681-0001
United States

Government Reports Announcements and Index (GRA&I)
published by the National Technical Information Service
Springfield
Virginia 22161
United States
(also available online in the NTIS Bibliographic
Database or on CD-ROM)



Printed by Canada Communication Group Inc.
(A St. Joseph Corporation Company)
45 Sacré-Cœur Blvd., Hull (Québec), Canada K1A 0S7